Thermal(Photo) Induced Selective C–H Bond Functionalization/Oxidative Cyclization in Di-Nitrogen Benzenoid Heteroarenes

A dissertation submitted in partial fulfilment for the degree of
Doctor of Philosophy

Submitted by

SUBHENDU GHOSH

Roll No. – 166122017

Department of Chemistry

Indian Institute of Technology, Guwahati

February, 2024

TH-3369_166122017

TH-3369_166122017

DEDICATED

TO

MY WELL-WISHERS

TH-3369_166122017

TH-3369_166122017

INDIAN INSTITUTE OF TECHNOLOGY GUWAHATI

Department of Chemistry

STATEMENT

I do hereby declare that the matter embodied in this thesis is the result of investigations carried out by me in the Department of Chemistry, Indian Institute of Technology Guwahati, India, under the guidance of Prof. Bhisma K. Patel. This thesis has been submitted by me to the Department of Chemistry, Indian Institute of Technology Guwahati for the award of the Doctor of Philosophy.

In keeping with the general practice of reporting scientific observations, due acknowledgments have been made wherever the work described is based on the findings of other investigators. I further declare that this work has not been submitted anywhere else for any degree, diploma, associateship or membership etc. of any Institute or University to the best of my knowledge.

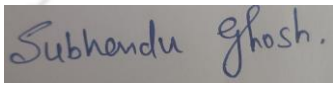

February 2024 **Subhendu Ghosh**

IIT Guwahati

TH-3369_166122017

TH-3369_166122017

INDIAN INSTITUTE OF TECHNOLOGY GUWAHATI

Department of Chemistry

CERTIFICATE

This is to certify that Subhendu Ghosh has been working under my supervision since August 2016 as a regular Ph.D. student. His thesis entitled "**Thermal(Photo) Induced Selective C–H Bond Functionalization/Oxidative Cyclization in Di-Nitrogen Benzenoid Heteroarenes**" is an authentic record of the results obtained from the research work in the Department of Chemistry, Indian Institute of Technology Guwahati, Assam, India. I am forwarding his thesis to submit for the Ph.D. (Science) degree from this institute. I certify that he has fulfilled all the requirements according to the rules of this institute regarding the investigations embodied in his thesis and this work has not been submitted elsewhere for a degree.

February 2024

Prof. Bhisma K. Patel
(Thesis Supervisor)
Department of Chemistry
IIT Guwahati

TH-3369_166122017

TH-3369_166122017

ACKNOWLEDGEMENT

With an extreme sense of gratitude and excitement, I take this opportunity to thank all the individuals who have helped and encouraged me during my Ph.D. journey. I thank IITG for the friendly environment it has provided which helped me enormously. I thank everyone from the bottom of my heart. I can say in tag line "Manush manusher jonne…".

Firstly, I extend my sincere and immense gratitude to my Guru, Prof. Bhisma K. Patel sir. It was an inestimable privilege for me to have the opportunity to work under his supervision. I will always be grateful for his guidance, scientific ideas, support, encouragement, and motivation throughout my journey at IITG. I thank him for everything and for trusting me which gave me strength to work efficiently and responsibly. I will be happy if I can give him "Guru Dakshina" (in the form of a good publication). "Guru Brahma Gurur Vishnu Guru Devo Maheshwaraha Guru Saakshat Para Brahma Tasmai Sree Gurave Namah"

I would like to express my deepest gratitude to my doctoral committee members, Prof. Bhubaneswar Mandal sir, Prof. Subhas Chandra Pan sir, Dr. Shyam Prasad Biswas sir, and Dr. Dipankar Srimani sir for their continuous guidance in every step of my Ph.D. work. It is my pleasure to thank them for their valuable suggestions which added towards the improvement of my thesis. I also thank Prof. Siddhartha Sankar Ghosh sir (BSBE, IITG) and Dr. Sugumar Venkataramani sir (IISER Mohali) for the collaborative work done with them for my two project works. I am extremely thankful to Sugumar sir for the valuable discussions and suggestions during my last project work.

I would also like to express my special and profound thanks to the Department of Chemistry, CIF IITG for all the instrument facilities without which the work included in this thesis would not have been possible. Together with this, I would also like to thank all the instrument operators including my batch mates for their carefulness and patience which led to swift and correct analysis of the samples. I would like to thank Dr. Babulal Das for helping me with Single Crystal XRD studies. I also thank all the other staff members of the Chemistry department and IITG for their help whenever I was in need.

I have been indeed fortunate enough to work with very experienced lab mates. I would like to thank my seniors Dr. Suman Pal, Dr. Suresh Rajamanickam, and Prakash Ranjan Mahanta

TH-3369_166122017

for their valuable guidance and support in every step of my Ph.D. work. I also thank my juniors (Priti, Raju and Deepjyoti) and friends (Mihir, Kanu, Debasish, Deepanjan, Bijoy, Tanumoy, Rabindranath and others) for their helping hand. I am extremely thankful to my junior Tamanna she helped me a lot in her capability. Also thankful to her for the financial loan during my non-fellowship days. I express my gratitude to all my friends in IITG for making the journey memorable.

A very special thanks to my close person cum best friend Satarupa "Didimoni". During my hard times, she stood with me and became a supportive system to eliminate the negativity, which helped me a lot to fight my battle. Without her continuous encouragement and motivation, probably I would not have achieved this. Also thankful to her for the financial support during the non-fellowship journey. I promise you one day I will shine definitely.

Finally, my Ph. D. endeavour could not have been completed without the endless love, unending support, tolerance, and blessings from my family. My deepest gratitude especially to my 'BABA and MAA' who stood against all odds just to support me. They are the pillars of my achievements. Their enormous sacrifices and unconditional love in every stage of my life motivated me to overcome all the challenges and I owe my entire life to them.

Finally, I thank the super-powerful GOD for blessing me during this Ph.D. journey and for everything I achieved. I will just pray please stay with me and give me positive energy, it's enough to fight for victory. Om Namah Shivay....

At the last, my keywords: "Belief in God..Believe in yourself..Work hard..Love your research & also fight for…Meet the problems with a cup of black COFFEE, Try to solve them with a chilled mind like MSD..Do Good with good people..Help the poor/needy person; they are the real God on Earth..Never think about negative particles..If you think you can let's do it.. Explore the opportunities..To create a new way, sometimes you have to walk alone...Never say it's over; keep rolling...."

Subhendu Ghosh

TH-3369_166122017

TH-3369_166122017

Abstract

The research work described in this thesis has been divided into five chapters based on the results of experimental works performed during the research period. The introductory **Chapter I** of the thesis mainly features a brief description of the C–H functionalization/oxidative annulation reactions onto di-nitrogen heteroarenes under transition metal and photocatalysis.

Chapter II demonstrates a Ru(II) catalyzed oxidative annulation of diversely substituted quinoxalines with internal alkynes. The *N*-directed site-selective strategy offers simultaneous C–C/C–N bond formations to access a library of annulated fluorescent quaternary salts in excellent yields. Further, the synthesized annulated products are explored towards their multifunctional real-world applications. Annulated adducts serve as AEEgens in DMF/water solvent systems owing to their restricted intramolecular motions (RIM) of donor–π–acceptor architecture. The detailed theoretical and experimental study elucidates the actual mechanism. In addition, the AEEgens are portrayed as reversible mechanochromic, latent-fingerprint detecting, and cellular-imaging probes.

Chapter III describes a sustainable Mn(I)-catalyzed solvent-switched regiodivergent *ortho* and C3-H maleimidation of imdazopyridines under oxidant/silver-free protocol. Herein, apolar aprotic solvent THF offers exclusive *o*-chelation-aided proximal C–H functionalization whereas, polar protic TFE promotes electrophilic distal C–H alkylation at C3–H of imidazopyridines.

Chapter IV portrays Mn(I)-catalyzed site-selective non-directed C3-maleimidation of quinoxalines. The electrophilic C3-metalation competes with the easily accessible *N*-directed strategy to deliver variably substituted quinoxaline-embed succinimides. The maleimidated adducts undergo PIFA-promoted $C(sp^2)$–$C(sp^3)$ spirocyclization *via* π-electrons drifting from aryls and Selectfluor-mediated dehydrogenation of succinimide at room temperature.

Chapter V illustrates visible light-driven singlet oxygen capturing C3-maleimidated quinoxalines to provide quaternary oxygenated tertiary C–H hydroxylation and intramolecular spiro-etherification *via* a photosensitizer-free reagent-less approach. Detailed experimental evidence and theoretical insights firmly supports the proposed mechanism.

New Findings and Future Perspective:

Part-I summaries a Ru(II)-catalyzed substrate-controlled divergent metalation leads to *ortho* bis-hydroalkenylation and [2+2+2] annulation reaction of quinoxalines with internal alkynes under oxidant/silver-free protocol.

Part-II discusses a photo-induced triplet-energy transfer (E_nT) enabled exploration of bis-alkenylated quinxalines for intramolecular oxidative cleavage and cyclization of quinoxaline-tethered alkenes.

TH-3369_166122017

CHAPTER I: *A Concise Overview*

This chapter outlines the thermal(photo) induced C–H functionalization and oxidative cyclization of functional di-nitrogen heteroarenes. This chapter is divided into two section, (i) metal catalysis under thermal condition and (ii) photocatalysis.

I.1. Metal Catalysis Under Thermal Condition

C–H bond activation is one of the common processes in nature. For several billion years' nature has evolved specific enzymes such as cytochrome P450 and methane monooxygenase for metal-based C–H activation. Currently, C–H activation has become a powerful tool for constructing organic frameworks *via* directed C–H functionalization and oxidative annulation or cyclization.

Directed C–H Functionalization:

The idea of using C–H bonds as starting points for chemical synthesis comes with two major challenges: sufficient inertness for the cleavage of the strong C–H bond and the control of site selectivity. In this regard, directing group-assisted C–H bond cleavage has shown great promise. The lone pair of electrons bearing directing groups (DGs) facilitates C–H functionalization through chelation. In general directing groups first coordinate with the metal center through the donation of a alone pair of electrons bringing the metal closer to the proximity of C–H bonds to form chelated five or six-membered metalacycle to achieve the fixed point C–H activation and functionalization (Scheme.I.1). In this context, versatile directing groups have been employed for the catalytic C–H functionalization. Mainly *N*-containing DGs are more efficient for offering strong chelating behavior for site-selective C–H functionalization.

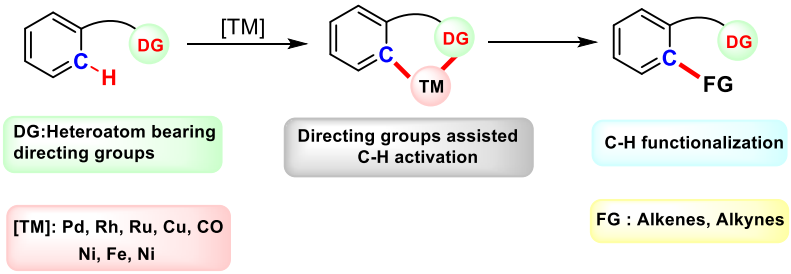

Scheme I.1. *Site-selective C-H functionalization*

TH-3369_166122017

Oxidative Annulation/Cyclization:

Transition-metal-catalyzed C−H activation followed by oxidative annulation has been a straightforward and versatile tool for the construction of various π conjugated poly-heterocyclic and carbocyclic luminogens. It provides a step and atom economical route for the elaboration of simple arenes to diversely substituted poly-heterocyclic compounds thereby improving the overall efficiency of the desired transformation. Such annulation reactions mainly involve metal-catalyzed C−H activation, migratory insertion, and reductive elimination to give the oxidative annulated adducts (Scheme.I.2).

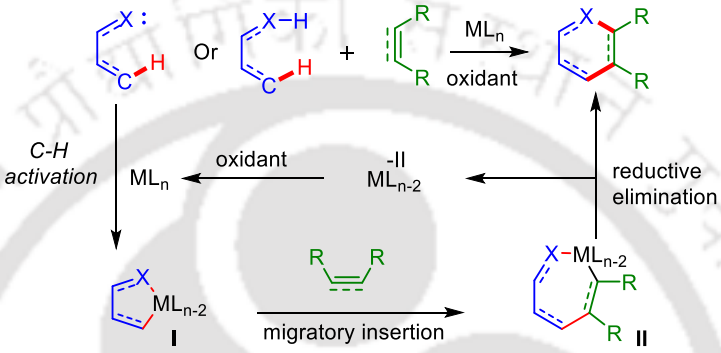

Scheme I.2. *Site-selective oxidative cyclization via C-H activation*

I.2. Photocatalysis

In the recent era of contemporary organic synthesis, photo-catalysis appeared as a powerful synthetic itinerary. Nowadays it is evolving rapidly to offer sustainable eco-friendly synthetic routes for the synthesis of various medicinal drugs, natural products and agrochemicals. On the basis of working principles photo-catalysis is classified into four parts- (i) photoredox catalysis, (ii) energy transfer catalysis, (iii) EDA complexation-enabled catalysis, (iv) direct-photo-induced catalysis.

Photoredox Catalysis:

This section of photo-chemistry is catalyzed by metal or metal-free photo-catalysts. In photoredox catalysis, photo-catalyst (PC) first absorbs light and excites to PC*. Then two consecutive single electron transfers (SET) take place between donor components (D) and acceptor component (A). If these two consecutive SET starts by gaining electrons from the donor (D), it is termed reductive quenching; if it starts with a release of electrons, it is termed oxidative quenching (Figure.I.1).

TH-3369_166122017

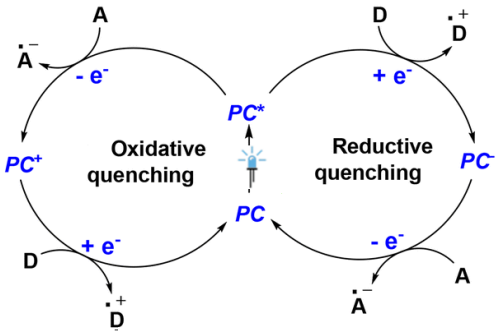

Figure I.1. *Photo-induced redox catalysis*

Energy Transfer (EnT) Catalysis:

In EnT catalysis, the photo-induced excited photo-sensitizer transfers the energy to the substrate, which is not able to absorb the light at ground state (Figure.I.2).

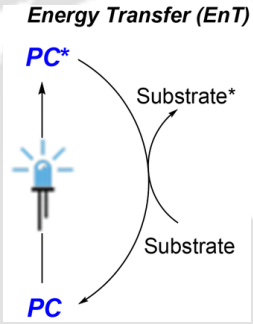

Figure I.2. *Photo-induced energy transfer catalysis*

Electron Donor-Acceptor Complexation-enabled Catalysis:

Researchers have recently shown immense interest in photo-induced electron donor-acceptor (EDA) complex-enabled photochemical approaches. In this strategy, a good electron donor (D) and a good electron acceptor (A) substances aggregate together to form a colored molecular aggregation in the ground state which is known as an electron donor−acceptor (EDA) complex. Surprisingly, both substances may not absorb visible light before complexation individually, but their aggregated EDA complex does. Upon visible light irradiation on the EDA complex, an intramolecular electronic charge transfer occurred from donor to acceptor to deliver radical ion pair as D+• and A−•. Then the coupling of these radicals gives the complex organic molecules (Figure.I.3).

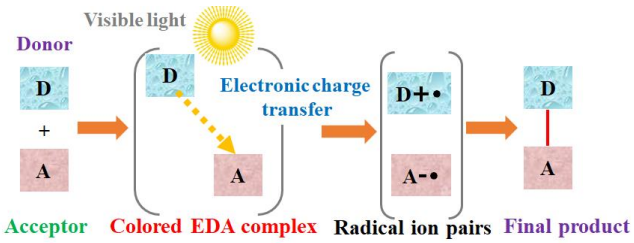

Figure I.3. EDA complexation-induced photocatalysis

TH-3369_166122017

Direct Photo-induced Catalysis:

In this part of photo-catalysis, the substrate itself activated to an excited state without the requirement of any photo-sensitizer or EDA complexation. The excited substrate undergoes hemolytic cleavage to facilitate the reactive free radical intermediates.

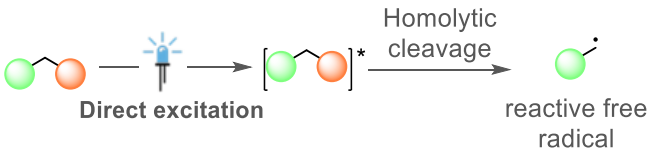

Figure I.4. Direct photo-induced catalysis

CHAPTER II: Access to Multifunctional AEEgens via Ru(II)-Catalyzed Quinoxaline-Directed Oxidative Annulation

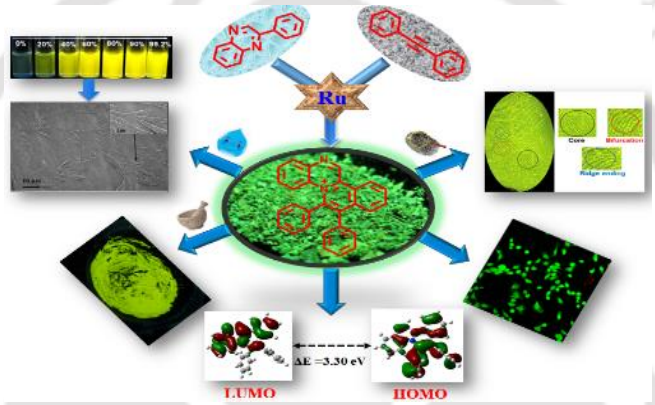

Abstract: *This chapter gives the outline of Ru(II) catalyzed oxidative annulation of quinoxalines with alkynes. While the synthesized compounds exhibit emissions in the green-to-yellow region with large Stokes shifts and reasonable quantum yields, their DFT calculations display a 3D twisted conformation bearing a donor−π−acceptor (D-π-A) configuration where the two phenyl moieties could serve as the donors and the extended quinoxaline core as the acceptor. Single-crystal analysis of the quaternary salt depicts multiple intermolecular noncovalent and weak π−π interactions that are possibly responsible for the luminescence behavior. Further, the synthesized annulated adducts possess multifunctional AEEgens in DMF/water solvent systems. Such AEEgens are explored towards mechanochromism, latent fingerprint detection and cellular bio-imaging.*

Transition-metal-catalyzed C−H bond functionalization/ annulation has emerged as a step- and atom-economical strategy to forge diversely substituted cyclized complex molecular entities. The last decades have witnessed numerous advances in this field, among which chelation-aided oxidative *N*-annulation with a large spectrum of unsaturated systems *via* C−H

TH-3369_166122017

activation for constructing π-extended nitrogen-containing polyaromatic salts has received noteworthy attention. Ru has gained significant importance among various transition-metal catalysis due to its ready availability, stability, selectivity, and low cost compared to Pd or Rh. However, despite the emergent applications of *N*-heterocyclic salts, Ru(II)-catalyzed C−H bond activation-enabled synthetic routes are less investigated. After considering all these aspects herein, we are interested in couple 2-aryl (hetero)aryl quinoxalines with internal alkynes under ruthenium catalysis. But this directing group-aided C–H activation proposal faces two possible critical site-selectivity issues (i) oxidative annulation through the dual activation of C3-H and *ortho*-H of 2-aryl quinoxalines and (ii) participation of one nitrogen atom and *ortho*-C-H of 2-aryl quinoxalines with internal alkynes. To see which of these possibilities occur, a reaction was carried out between 2-phenyl quinoxaline (**1**) and diphenylacetylene (**2**) with the aid of $[RuCl_2(p\text{-cymene})]_2$ (5 mol%), $Cu(OAc)_2.H_2O$ (1.2 equiv) and triflic acid (TfOH) (1.5 equiv) in 1,2-dichloroethane (DCE) at 85 °C for 20 h. Pleasingly annulated *N*-quaternary salt was isolated in 56% yield, which was highly fluorescent active.

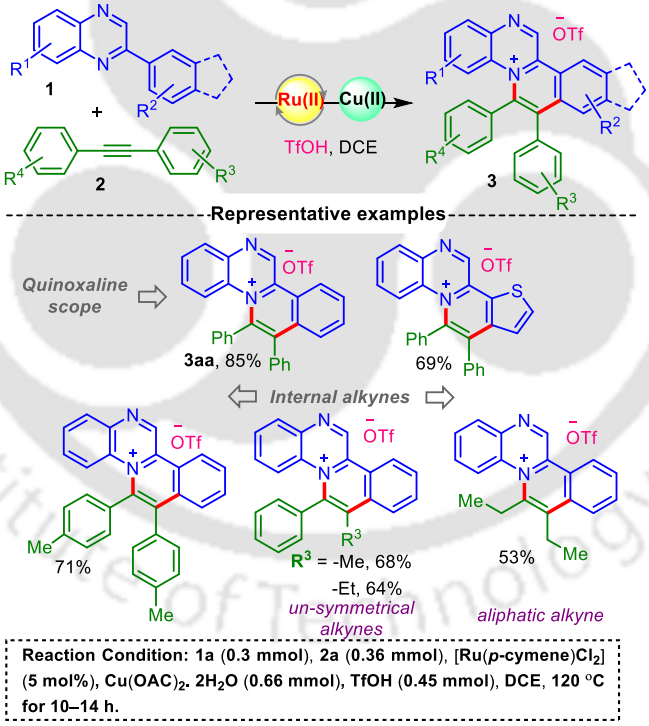

Scheme II.2. *Representative scope of oxidative annulation*

Further, the structure was confirmed by NMR and X-ray crystallographic analysis. After a series of optimizations in terms of catalyst, oxidants, additives, solvents and reaction temperature, the use of 2-phenyl quinoxaline (**1a**, 0.3 mmol), diphenylacetylene (**2a**, 0.36 mmol), $[RuCl_2(p\text{-cymene})]_2$ (5.0 mol %), $Cu(OAc)_2.H_2O$ (0.66 mmol), triflic acid (TfOH)

TH-3369_166122017

(0.45 mmol) in dichloroethane at 120 ^{o}C was established as the optimized reaction protocol with 85% isolated yield. Under the optimized condition, the oxidative annulation reaction scope was extended by varying diversely substituted quinoxalines and internal alkynes (Scheme II.2).

A possible mechanism for this annulation reaction is proposed in Scheme II.3 based on literature precedence on Ru(II) catalyzed oxidative annulations. An active ruthenium catalyst (B) is initially generated through anion exchange with copper acetate monohydrate. The coordination of the nitrogen atom of quinoxaline (**1a**) to the ruthenium acetate species (**B**) and subsequent *ortho*-metalation afforded a five-membered ruthenacycle intermediate (**C**). Then the regioselective coordination and migratory insertion of alkyne **2a** into the Ru-carbon bond of intermediate (**C**) generates the seven-membered intermediate (**D**). Reductive elimination of intermediate (**D**) in the presence of TfOH delivers the product **3aa**.

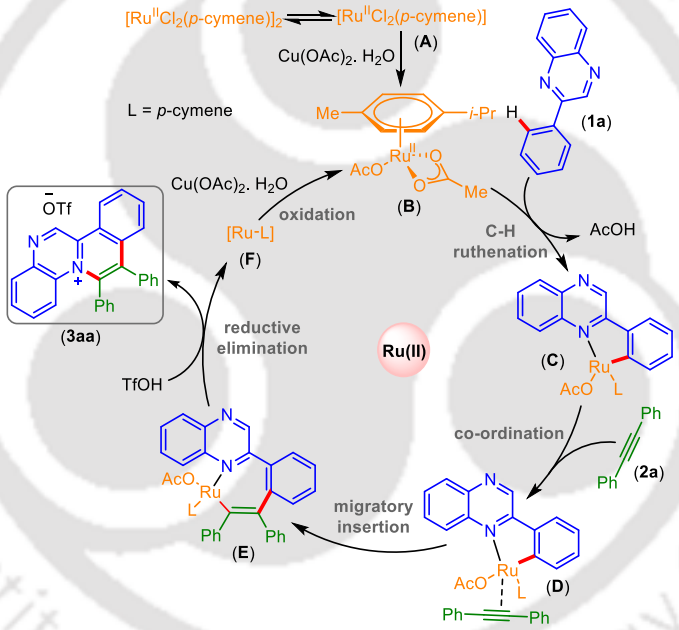

Scheme II.3. *Ru(II)-Catalyzed oxidative annulation*

On the other hand, one major focus of synthetic chemists is to design and develop new luminescent materials with diverse functionalities. The development of extended π–conjugated polycyclic and heterocyclic fluorescent materials is noteworthy owing to their versatile real-world applications. Based on DFT calculation the synthesized annulated adduct have twisted donor-π-acceptor configuration where quinoxaline ring act as the acceptor and the alkyne section act as the donor. They serve as AEEgens in DMF/water mixed solvent, further their utilization in reversible mechanochromism, latent-fingerprint detection and cellular imaging were explored.

TH-3369_166122017

In conclusion, a series of multifunctional AEEgens are developed *via* quinoxaline *N*-directed Ru(II)-catalyzed oxidative annulation of 2-aryl quinoxalines with internal alkynes to access diversely substituted annulated quaternary ammonium salts in the presence of $Cu(OAc)_2.H_2O$ as the oxidant. Restriction of intramolecular motion (RIM) shows AEE behavior of the AEEgens having donor–π–acceptor (D–π–A), where two phenyl moieties could act as a donor while the extended quinoxaline core as the acceptor. The compounds are easy to prepare, possessing stable structures, tunable emission and displayed strong luminescent with large Stokes shift and aggregation-enhanced emission (AEE) with moderate quantum yields. Such AEEgens having mechanochromic property can be utilized for latent fingerprints for possible forensic investigation. The compounds have anti-cancer effects, where cellular uptake can be monitored by luminescent imaging. Thus, the synthesized AEEgens have multifaceted application potential for forensic and biomedical research.

CHAPTER III: Solvent Switched Manganese(I) Catalyzed Regiodivergent Distal vs Proximal C-H Alkylation of Imidazopyridine with Maleimide

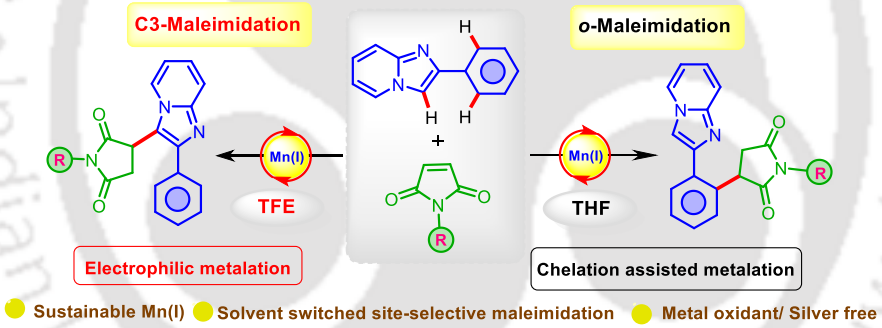

Abstract: *This chapter outlines solvent-switched regeiodivergecy in C–H maleimidation of imidazopyridine under sustainable Mn(I) catalysis without silver and metal oxidants. In light of mechanistic investigation, polar protic TFE solvent offers exclusive distal C3-H maleimidation via an electrophilic metalation whereas apolar aprotic THF solvent promotes proximal o-C–H maleimidation via direction-aided strategy. This simple ease protocol delivers a library of succinamide adducts of imidazopyridine with good yields. This present method shows its applicability to functionalize the zolimidine drug candidate.*

The transition metal-catalyzed regio and site-selective C–H bond activation opens up a new paradigm for the development of various functional molecules and their late-stage diversifications. Several groups have made remarkable contributions towards selective C–H

TH-3369_166122017

bond functionalization, through the controlled choice of catalysts, oxidants, additives, and solvents to achieve the region-selectivity over the indiscriminate possibilities (Scheme III.1.a). Past decades have witnessed notable contributions using precious 4d- and 5d-metals. However, the high cost, toxicity, and low abundance are some of the major impediments to their usage. Successfully many of these are replaced with more Earth-abundant, cost-effective, sustainable, and environmentally benign 3d-metal catalysts. Further, Mn, the third most abundant metal in Earth's crust, has gained greater acceptability due to its low cost, lesser toxicity, and biocompatibility in homogeneous catalysis. Despite the significant advances in C–H bond activation, utilizing Mn as a catalyst for controlled regio and site-selective manner is highly desired. Among various *N*-containing heterocyclic scaffolds, imidazo[1,2-*a*]pyridine is unique due to its presence in a plethora of natural products and pharmaceutical feedstock.

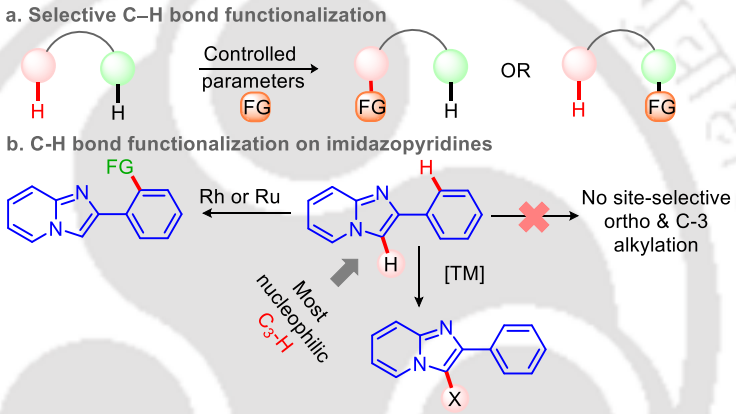

Scheme III.1. *Site-selective C-H functionalization*

Various research groups have devoted themselves to C–H bond functionalization on imidazopyridine, most of which revolve around the active nucleophilic C-3 site. Selective *o*-functionalization without protecting the active C-3 site is quite stimulating. As a result, there is no report on site-selective alkylation at the *ortho* and C-3 position of imidazo[1,2-*a*]pyridine using a single catalytic system (Scheme III.1.b).

TH-3369_166122017

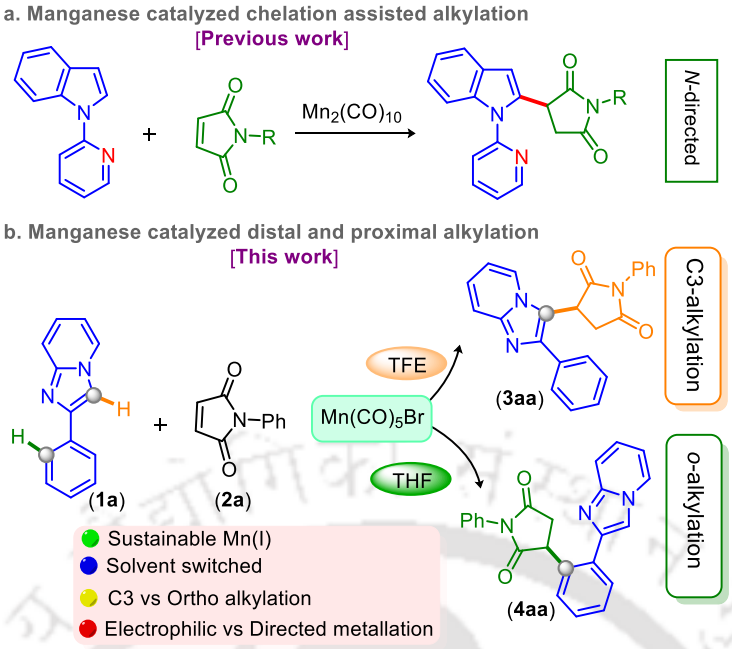

Scheme III.2. *Mn-catalyzed C-H alkylation*

Whereas in the last few years several metal-catalyzed alkylation of maleimides in various other scaffolds have been reported with the aid of 4d and 5d metals in the presence of other metal oxidant and Ag salt. Thus a sustainable regioselective (*ortho* C–H vs C3–H) alkylation in 2-aryl imidazopyridine using 3d-metal without silver and oxidant is highly appreciable. Manganese catalyzed C–H functionalization of acrylates with heteroarenes is well documented, but the functionalization of maleimides is confined to a single report of $Mn_2(CO)_{10}$ catalyzed *N*-directed alkylation of 1-(pyridin-2-yl)-1*H*-indole (Scheme III.2.a). Herein, we unveiled a solvent switched selective *ortho* and C-3 alkylation of 2-arylimidazopyidines under Mn(I) catalysis to access 1-phenyl-3-(2-phenylimidazo[1,2-*a*]pyridin-3-yl)pyrrolidine-2,5-dione (**3aa**) and 3-(2-(imidazo[1,2-*a*]pyridin-2-yl)phenyl)-1-phenylpyrrolidine-2,5-dione (**4aa**) (Scheme III.2.b).

TH-3369_166122017

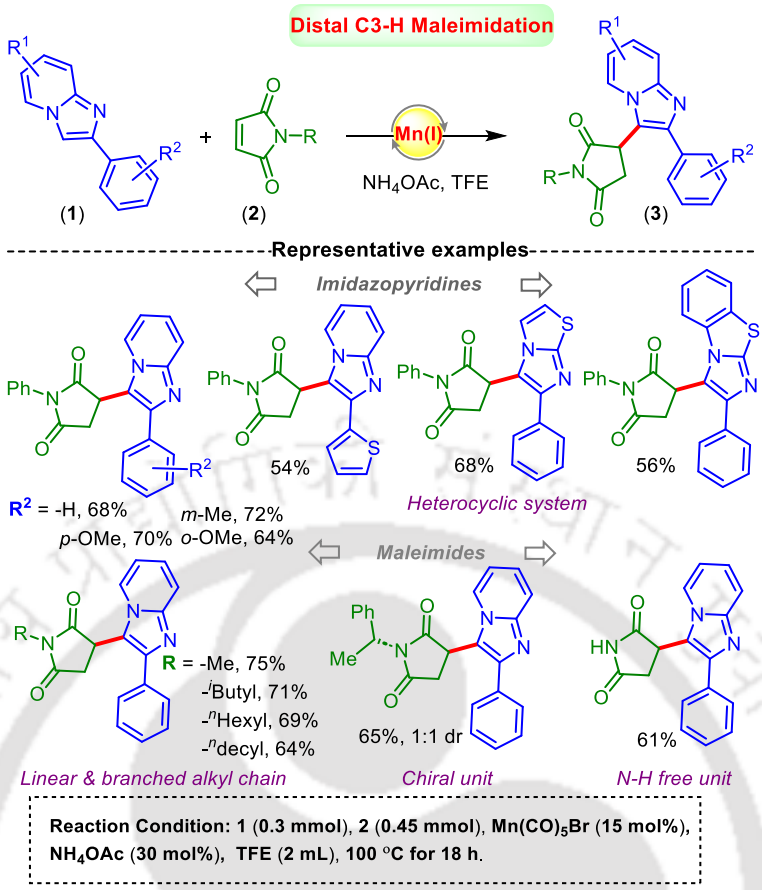

Scheme III.3. *Representative scope of C3-H maleimidation*

The optimization study was commenced by tuning various reaction parameters. Notably during the solvent optimization, it was found that the use of polar protic TFE solvent provided exclusive alkylation at the C3-H of imidazopyridine through an electrophilic distal metalation whereas an apolar aprotic THF solvent yielded exclusive o-alkylation through proximal chelation assisted metalation. Finally, the optimal condition for the C3-maleimidation was the use of (**1a**, 0.3 mmol), (**2a**, 0.45 mmol), $Mn(CO)_5Br$ (15 mol%) and NH_4OAc (30 mol%) in TFE (1.5 mL) at 100 °C for 18 h. Similarly, for the *o*-maleimidation the best condition was: (**1a**, 0.3 mmol), (**2a**, 0.45 mmol), $Mn(CO)_5Br$ (15 mol%) and NH_4OAc (30 mol%) in THF (1.5 mL) at 100 °C for 18 h.

TH-3369_166122017

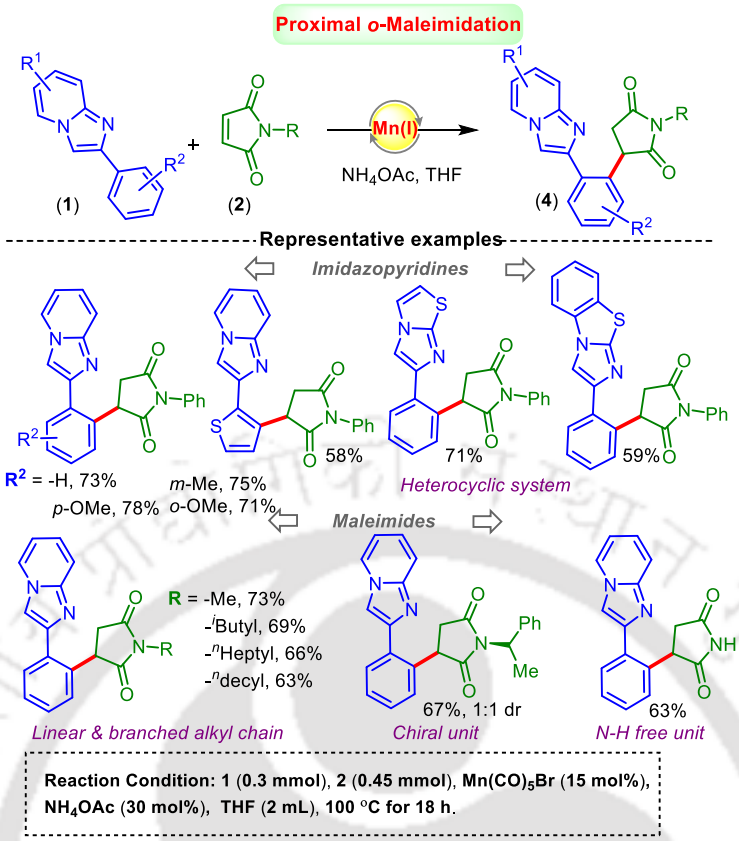

Scheme III.4. *Representative scope of ortho-maleimidation*

After arriving at the optimized reaction condition, including heterocyclic system various electronically varied substituents at para, meta and ortho position of the aryl ring of 2-substituted imidazopyridines were coupled in TFE solvent with *N*-phenyl maleimides to access diversely substituted C3-maleimidated products in decent yields (Scheme III.3). Similarly, various *N*-substituted maleimides including long alkyl chain, chiral unit and N-H free skeletons all were successfully coupled with 2-phenyl imidazopyridines to afford the corresponding C3-maleimidated products in good yields. Whereas, naphthoquinone, *p*-benzoquinone, diethyl maleate, maleic anhydride and cumarine system were found to be inactive to this protocol. In a similar fashion, the scope of the *o*-maleimidation of imidazopyridines in THF solvent was demonstrated by varying the substituents on imidazopyridines and maleimides to deliver the corresponding o-maleimidated adducts in good to excellent yields (Scheme III.4). Furthermore, the reported protocol was extended towards the maleimidation of Zolimidine drug. The bis-maleimidation of bis-imidazopyridines was obtained under the optimized protocol in THF solvent (Scheme III.5).

TH-3369_166122017

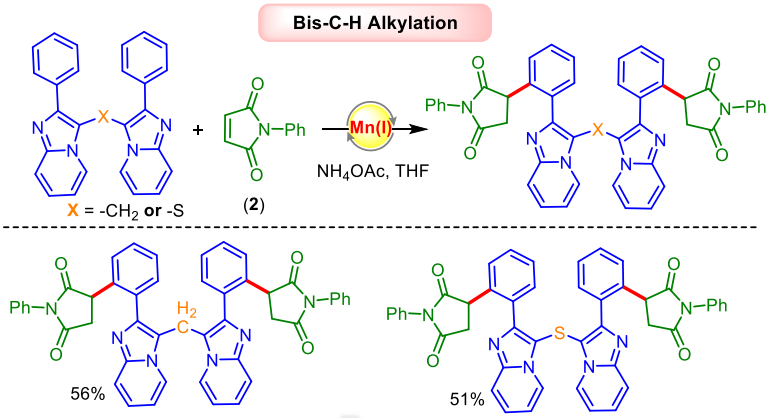

Scheme III.5. *Bis-C-H maleimidation of bis-imidazopyridines*

Based on the experimental results obtained from control reactions and previous reports, a plausible catalytic cycle for this regiodivergent alkylation in TFE and THF is depicted in (Scheme III.6). Initially, $Mn(CO)_5Br$ reacts with NH_4OAc, to provide the active $Mn(CO)_5OAc$ species (**I**). In polar protic TFE solvent, the substrate (**1a**) undergoes electrophilic metalation with the Mn complex assisted by H-bonding interaction of TFE with the C3-H to give a metallated species (**A**), detected in ESI-MS. This is followed by the coordination of *N*-phenyl maleimide (**2a**) and subsequent insertion to the Mn–C bond to generate an intermediate (**C**). Then a proto-demetalation in the presence of AcOH delivered the C3-alkylated product (**3aa**) along with the regeneration of the active catalyst by recombination of CO. On the other hand, in THF, **1a** undergoes *N*-directed chelation-aided cyclometalation of Mn at the *ortho* C–H to give a five-membered cyclometalated complex **A'**, detected in ESI-MS. This is followed by the coordination of *N*-phenyl maleimide (**2a**) and subsequent insertion to Mn–C bond. Finally, the proto-demetalation in the presence of AcOH and CO leads to an *o*-alkylated product (**4aa**) with the regeneration of the active (Scheme III.6).

In summary, a sustainable Mn(I) catalyzed solvent switched C3 (in TFE) and *o*-alkylations (in THF) of various imidazopyridines with *N*-substituted maleimides are developed. This metal oxidant and silver salt-free regiodivergent alkylation protocol was successfully explored for the functionalization of zolimidine drug. Here, the polar protic solvent TFE prefer electrophilic metalation whereas polar aprotic solvent THF went for *N*-chelation assisted metalation under the same catalytic scenario.

TH-3369_166122017

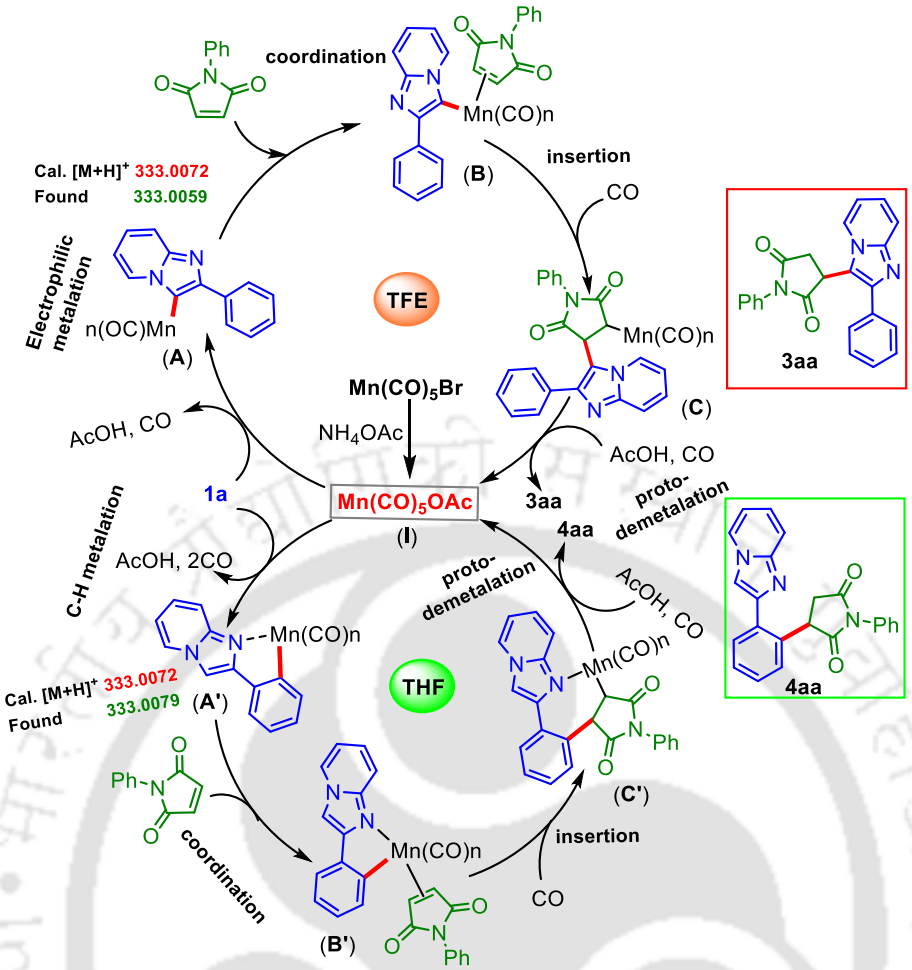

Scheme III.6. Mn-catalyzed regiodivergent C-H alkylation

CHAPTER IV: Mn(I) Catalyzed Preferential Electrophilic C3-Maleimidation in Quinoxaline Leading to Spiro-cyclization and Dehydrogenation of Succinimides

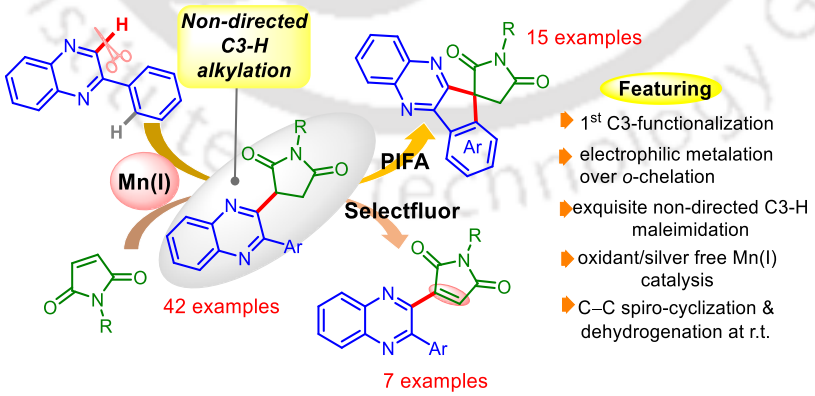

Abstract: *This chapter illustrates Mn(I) catalyzed preferential electrophilic metalation over N-directed chelation to access C3-maleimidated quinoxalines under Ag/oxidant free protocol. Herein, at room temperature, the maleimidated adducts undergo PIFA-promoted*

TH-3369_166122017

$C(sp^2)$–$C(sp^3)$ spiro-cyclization via an electron drifting from aryl ring to electron-deficient succinimide core and Selectfluor-mediated dehydrogenation through the quaternary fluorinated intermediates.

Quinoxaline is a privileged *N*-containing fused heterocycle, found in natural products, pharmaceuticals, and material sciences. In 2-aryl substituted quinoxaline core as well, the DG strategy invariably leads to *o*-C–H functionalizations (Scheme IV.1.a). However, regioselective functionalization at the non-directed C3-position on quinoxaline is unexplored, as it requires challenging electrophilic metalation over favorable *N*-directed *o*-chelation (Scheme IV.1.a). The use of 3d-metal catalysts to achieve such metalation is advantageous, among which Mn is the most promising one, which offers selective electrophilic metalation over DG enabled strategies. Thus, we envisioned a C3–H maleimidation of quinoxaline over the DG-assisted *o*-functionalization under Mn(I) catalysis. Previously *o*-maleimidation and spiro-cyclization of 2-aryl quinoxalines had achieved under Ru(II) catalysis using Cu/Ag additives. The spiro-cyclization proceeds via nucleophilic attack of the diffused quinoxaline π-electrons to the *o*-functionalized C–C bond of maleimide (Scheme IV.1.b). To validate our proposition, a reaction was conducted between 2-phenyl quinoxaline (**1a**) and *N*-phenyl maleimide (**2a**) in the presence of $Mn(CO)_5Br$ (10 mol %) and NH_4OAc (20 mol %) in DCE at 100 °C (Scheme IV.2). Delightfully, an exclusive C3–H maleimidated quinoxaline (**3aa**) was isolated in 52% yield.

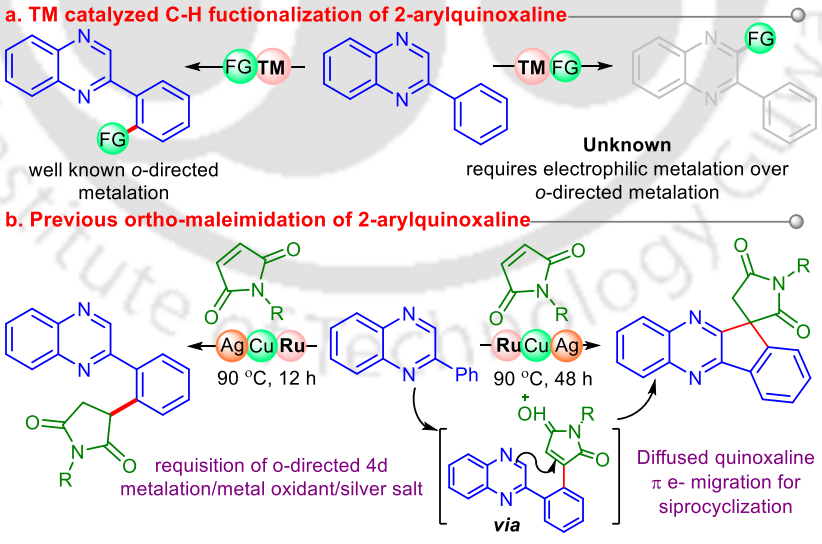

Scheme IV.1. *Prior C-H functionalization of quinoxaline*

TH-3369_166122017

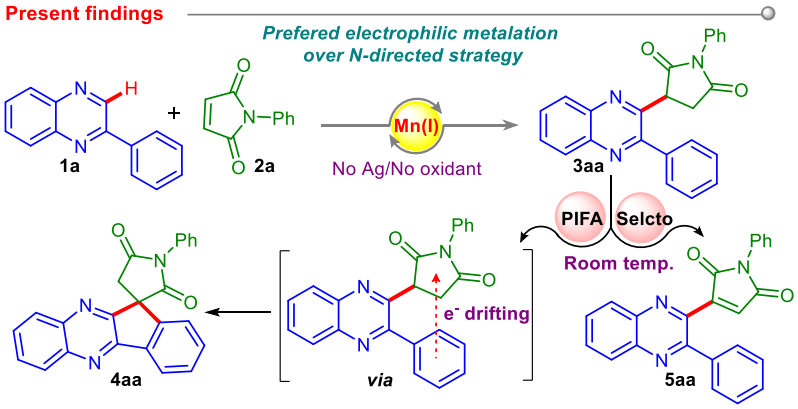

Scheme IV.2. *Present strategy*

Now, to further improve the yield, various solvents (TFE, $CHCl_3$, EtOAc, MeCN) and other reaction parameters were tuned and the optimized reaction condition was achieved as 2-phenyl quinoxaline (**1a**, 0.2 mmol), *N*-phenyl maleimide (**2a**, 0.28 mmol), $Mn(CO)_5Br$ (10 mol %) and NH_4OAc (30 mol %) in ethyl acetate (0.1 M) at 100 ^oC for 9 h. The scope and generality of non-directed C3-maleimidation were extended by varying diversely electronically varied substituents on the ortho, meta, and para of the aryl ring and the quinoxaline skeleton (Scheme IV.3). Similarly, various substituents were introduced on the *N*-site of maleimides and successfully coupled with 2-phenyl quinoxalines to give their corresponding C3-maleimidated products in excellent yields. Notably, the maleimides derived from chiral amine, tryptamine, aminopyrene were well responded to this present protocol. Further (-)-borneol and *L*-menthol appended quinoxalines were also smoothly reacted with maleimides to give desired products in decent yields.

TH-3369_166122017

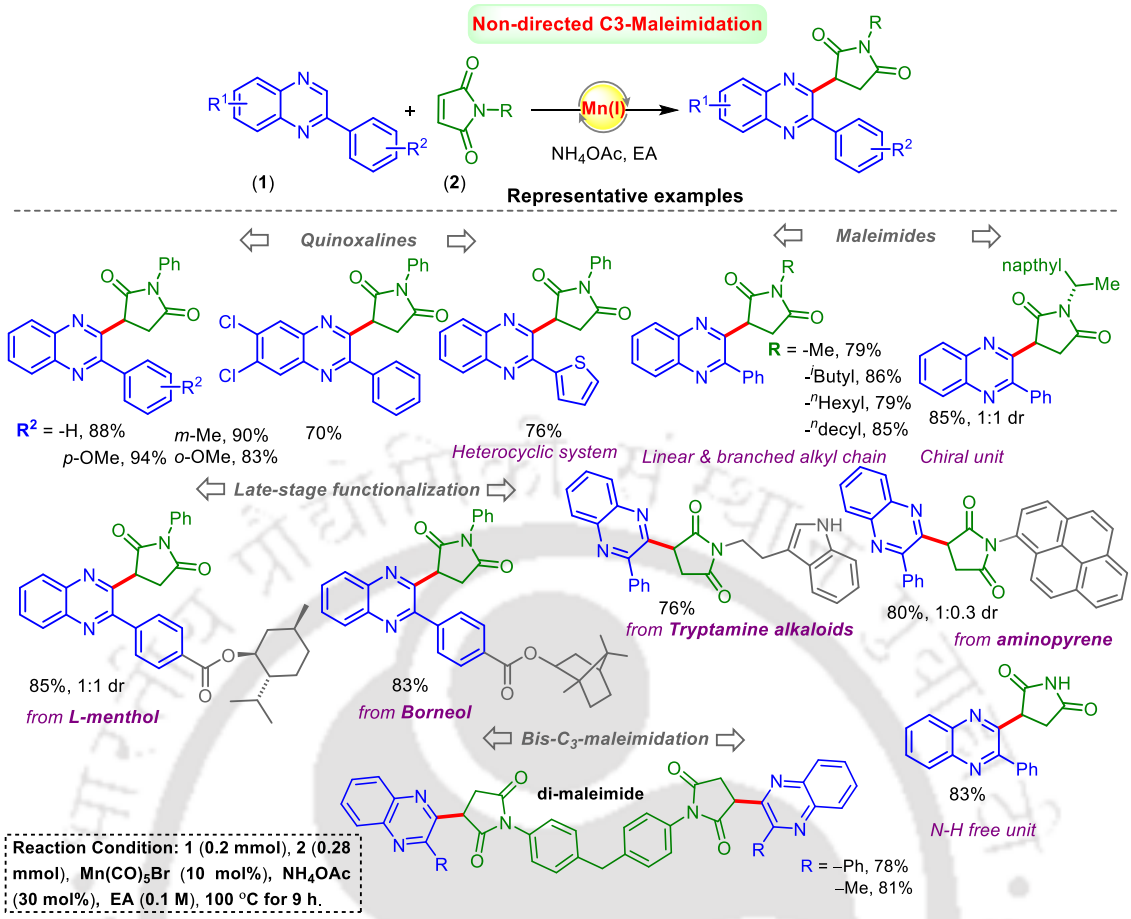

Scheme IV.3. *Representative scope of C3-H maleimidation*

The product **3aa** possesses a 2-aryl ring and a succinimide in proximity, can there be an π–electron drifted spiro-cyclization from the aryl ring to an electron-deficient succinimide in the presence of hypervalent-iodine? To execute the envisioned strategy, the C3-maleimidated product (**3aa**) was reacted with *bis*(trifluoroacetoxy)iodobenzene (PIFA) in DCM at room temperature. As anticipated, an intramolecular spiro-cyclized product **4aa** was isolated in 85%. Pleasingly, this is the first report where unperturbed phenyl π electrons offer C(sp^2)–C(sp^3) spiro-cyclization at room temperature *via* dearomatization-rearomatization process (Scheme IV.4). While attempting fluorination at the quaternary C–H site on the succinimide **(3aa**) using fluorinating agent selectfluor®, it underwent de-hydrogenation providing C3-alkenylated quinoxaline (**5aa**) in MeCN at room temperature possibly *via* a quaternary fluorinated intermediate (Scheme IV.4). This is a unique illustration of selectfluor® serving as a de-hydrogenating agent in succinimide system. This protocol may serve as an alternative to de-hydrogenation in succinimides, where *β*-hydride elimination is unfavorable under metal catalysis.

TH-3369_166122017

On the basis of literature precedents and control experiments, a plausible mechanism for C3-maleimidation, spiro-cyclization and de-hydrogenation has been proposed in Scheme IV.5. Initially, $Mn(CO)_5Br$ reacts with NH_4OAc, to provide the active $Mn(CO)_5OAc$ (**I**). Then 2-phenyl quinoxaline (**1a**) undergoes electrophilic metalation with the Mn-complex **I** to give C3-metalated species (**A**) (confirmed by HRMS) along with the elimination of AcOH. This is then followed by coordination of *N*-phenyl maleimide (**2a**) which undergoes subsequent insertion to Mn–C bond to generate intermediate (**C**). Then a proto-demetalation in the presence of AcOH, provided the C3-maleimidated product **3aa** and the regeneration of active catalyst **I** by recombination of CO. Further in DCM **3aa** undergoes keto-enol tautomerization at room temperature and in the presence of PIFA it provides the iodo-complex **B'**. Then an electron-drifting from 2-aryl ring towards C3-appended succinimide provides a radical intermediate **C'**, which has been trapped by BHT and the adduct was confirmed by HRMS. Then this radical intermediate **C'** undergoes re-aromatization to afford the spiro-cyclized product **4aa**. On the other hand, acetonitrile **3aa** undergoes electrophilic fluorination at the α-position of C3-appended succinimide to give a quaternary fluorinated species **B"**, which has been confirmed by NMR and HRMS analysis of the reaction aliquot. The intermediate **B"** provides the de-hydrogenated succinimides **5aa** *via* the elimination of HF (Scheme IV.5).

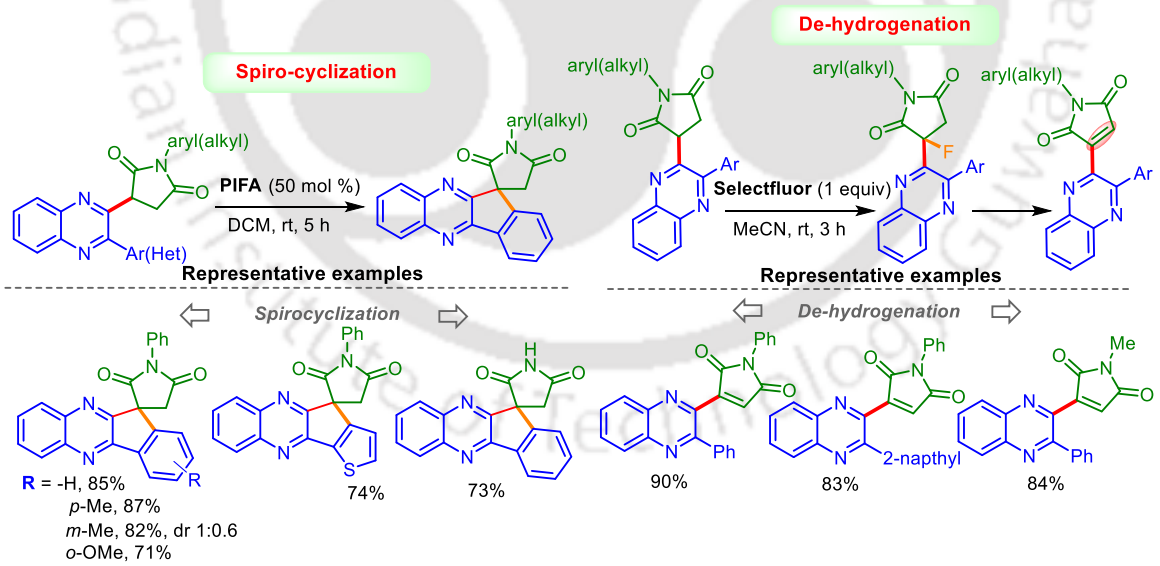

Scheme IV.4. *Representative scope of spiro-cyclization and de-hydrogenation*

TH-3369_166122017

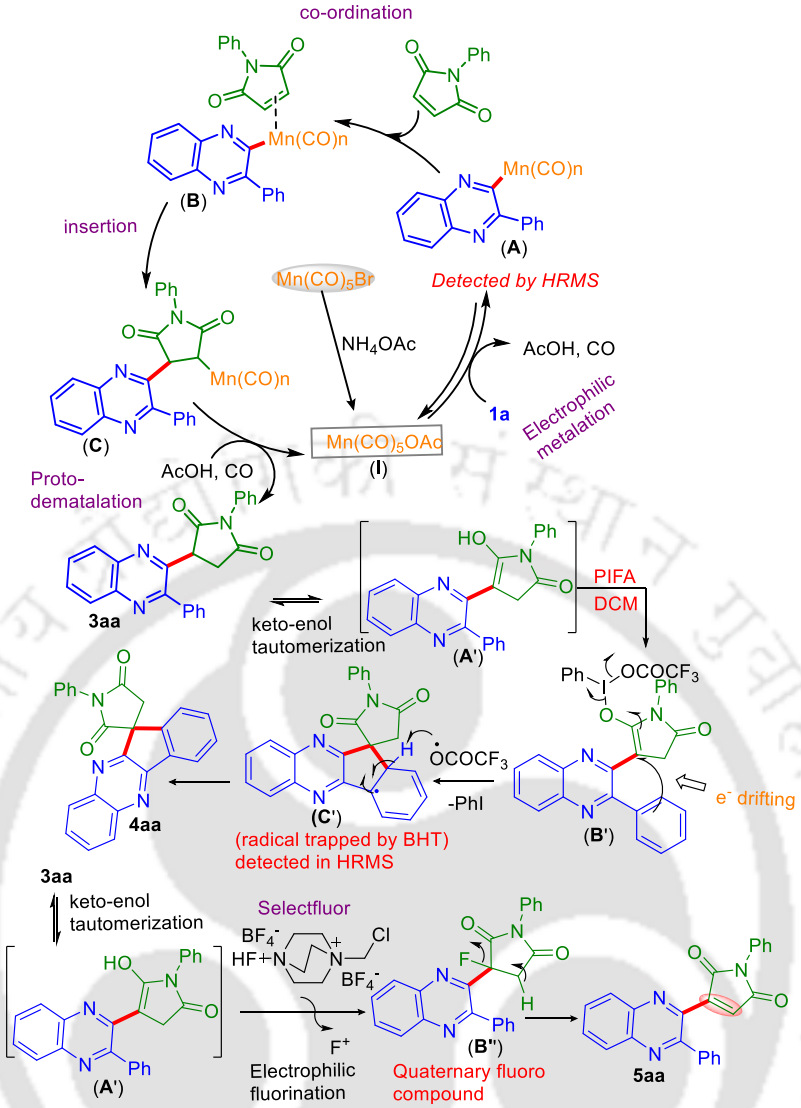

Scheme IV.5. *Plausible mechanism for C3-maleimidation/spiro-cylization/dehydrogenation*

In summary, a Mn(I)-catalyzed site-selective non-directed C3-H maleimidation of quinoxaline has been introduced under oxidant/silver-free protocol. This methodology offers a preference for electrophilic C3-metalation over the easily accessed o-directed metalation in ethyl acetate. Interestingly C3-maleimidated product undergoes PIFA-promoted C(sp^2)–C(sp^3) spiro-cyclization and selectfluor® mediated dehydrogenation of succinimides at room temperature. In the spiro-cyclization, the unperturbed 2-phenyl π–electrons are utilized to construct the spiro-cyclized product. A broad range of substrates including natural products *L*-menthol and borneol, good functional group tolerance, and simple protocol are the salient features of this report.

TH-3369_166122017

CHAPTER V: Photo-Induced Generation of Oxygenated Quaternary Centers *via* EnT Enabled Singlet O_2 Addition to C3-Maleimidated Quinoxaline: A Reagent-Less Approach

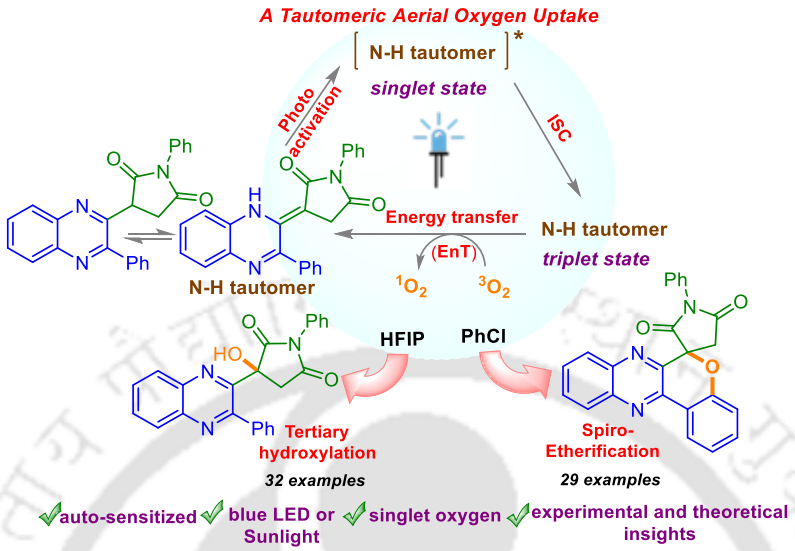

Abstract: *This chapter describes the brief outline of solvent-switched photo-induced triplet-energy transfer(EnT) enabled singlet oxygen driven tertiary C(sp^3)-H hydroxylation and intramolecular spiro-etherification of photo-responsive C3-maleimidated quinoxalines leading to C–O bond formations under a photosensitizer-free condition. This protocol represents broad substrate scope with very good functional group tolerance and is also extended toward some functional molecules tethered C3-maleimidated quinoxaines. Further radical and spin-trapping experiments confirm the radical pathway of this protocol. Along with a series of control reactions including singlet oxygen trapping supports the plausible mechanism. Moreover, detailed theoretical calculations firmly validate the mechanistic aspects.*

The selective C(sp^3)–H oxygenation reactions offer a strategy to install C–O bonds into the aliphatic organic scaffolds. The oxygen-containing scaffolds including cyclic and acyclic tertiary alcohols have shown their existence in numerous drugs, and natural products and play a key role in organic synthesis. Thus, introducing hydroxyl functionality to the aliphatic C(sp^3)–H site became a contemporary research topic. Traditionally, Barbier-type nucleophilic addition to the carbonyl system provides the tertiary alcohols, but the utilization of a stoichiometric reactive organometallic system encounters side reactions and suffers low functional group tolerance (Scheme V.1a). In the contemporary approach, the tertiary alcohols

TH-3369_166122017

are accessed by functionalizing the C–H bonds *via* DG-enabled metal catalysis, using stoichiometric oxidant and expensive enzymatic oxidations (Scheme V.1a).

Aryl-alkyl ether linkages are widely distributed in a large spectrum of pharmaceuticals, and medicinally pertinent natural products. In particular, hindered α-tertiary ethers have useful contributions in pharmaceuticals, agrochemicals and functional materials and fuel additives. Traditionally such linkages were accomplished by Williamson ether synthesis, but this protocol is limited to primary and secondary etherification. In addition, the well-studied transition metal-catalyzed Buchwald-Hartwig, Ullman cross-couplings are also confined to the requisition of the pre-functionalized substrates (Scheme V.1b). Whereas contemporary photo-catalyzed intermolecular dehydrogenative couplings became an attractive synthetic itinerary. To date, the photo-induced intramolecular α-tertiary spiro-etherification is yet to be established. Over the past decades, photo-redox catalysis has gained enormous appreciation in the preparation of fine chemicals, medicinal drugs, and many more functional groups installed to organic molecules.

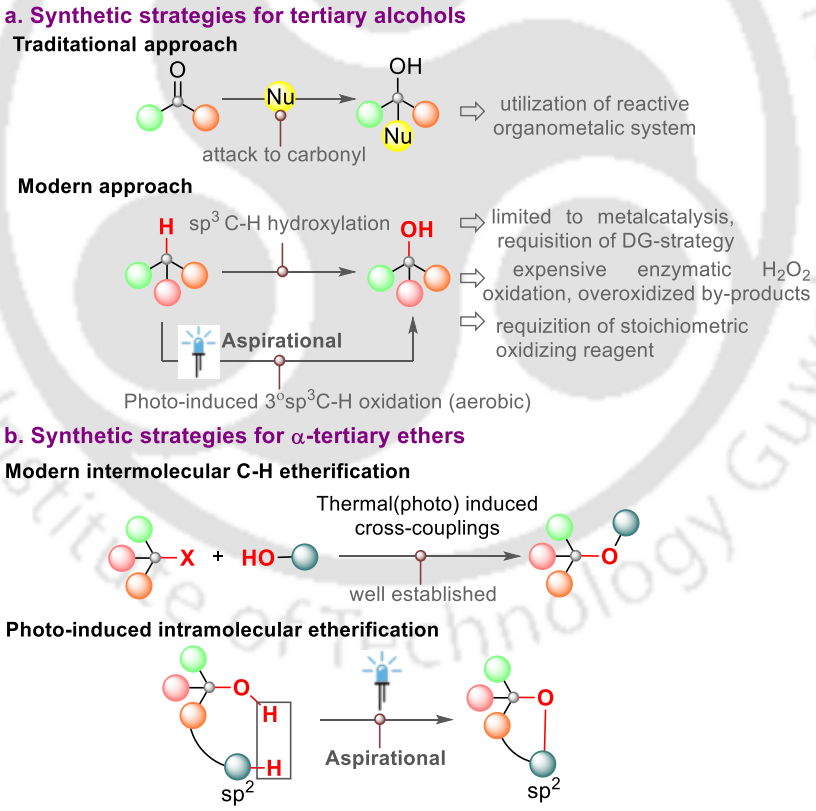

Scheme V.1. *Synthetic routes to tertiary alcohols and ethers*

Mainly photo-redox catalytic operations are based on transition metal-based photo-catalysts (Ru, Ir etc.) and some metal-free organic dyes (Eosin Y, Rose bengal, Methylene blue etc.). Herein we have demonstrated a solvent-switched sustainable photo-catalyst-free aerobic

TH-3369_166122017

tertiary C(sp^3)–H hydroxylation and intramolecular spiro-etherification of photo-responsive C3-maleimidated quinoxalines *via* the generation of sterically hindered tertiary-alkoxy radical (Scheme V.2). The spiro-etherification is supposed to proceeds *via* an electronic attack from alkoxy radical towards electron-rich 2-aryl ring of C3-maleimidated quinoxaline. It is a unique illustration of polarity-mismatched radical addition (Scheme V.2).

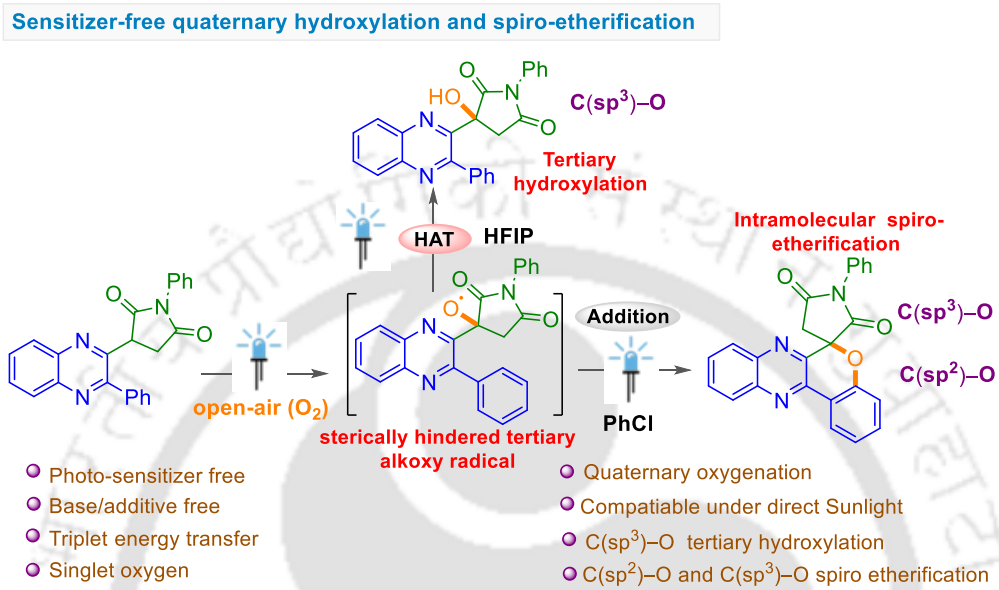

Scheme V.2. *Our findings*

Under the optimized condition, the scope and generality of tertiary hydroxylation and intramolecular spiro-etherification were demonstrated by tuning electronically varied substituents on quinoxaline and maleimide scaffolds of C3-maleimidated quinoxaline adducts (Scheme V.3 and V.4). Notably, in both the cases maleimides derived from functional amine molecules are well responded to this protocols. Similarly, natural product tethered quinoxaline bearing maleimidated adduct also well-reacted to the optimized protocol.

TH-3369_166122017

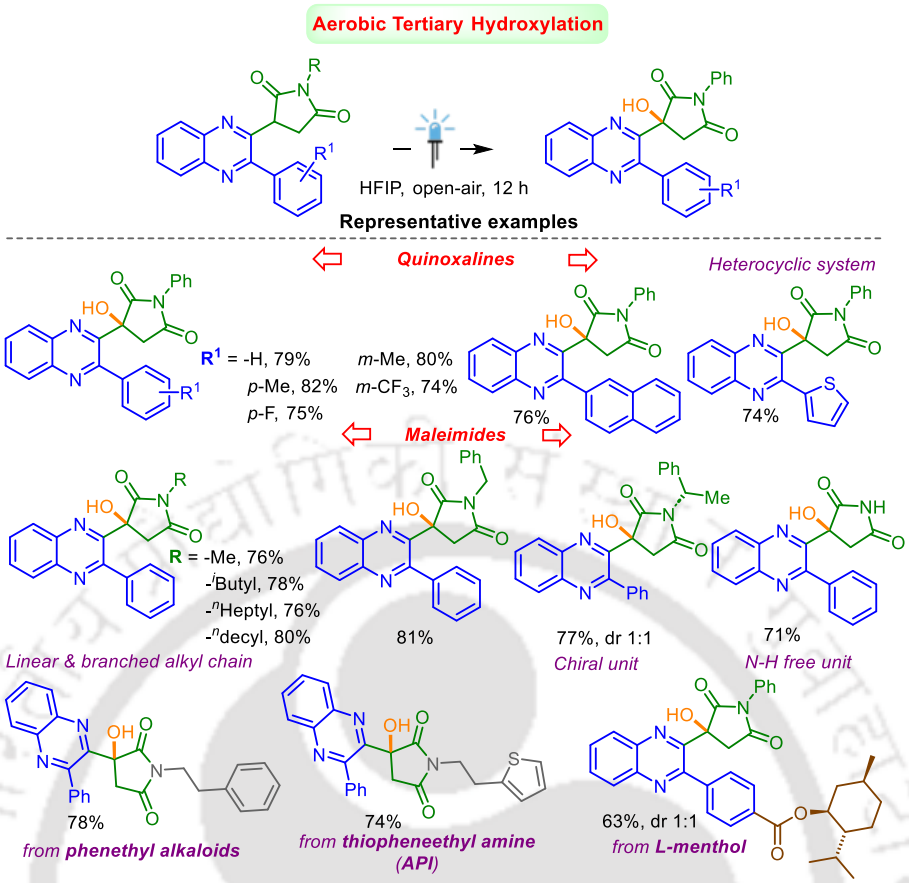

Scheme V.3. *Scope of tertiary C-H hydroxylation*

Based on the mechanistic studies and theoretical calculations, plausible mechanisms for both these reactions are depicted in Scheme V.6. Due to the fact that the longer wavelength absorption is computationally predicted only for the N-H tautomer, possibly the tautomer **A_0'** of C3-maleimidated quinoxaline (**1**) upon photo-irradiation gets excited to its singlet state (**$^1A_0$'**), followed by an ISC to triplet state (**$^3A_0$'**). This triplet species (**$^3A_0$'**) then transfers its energy to a triplet oxygen ($^3O_2$) generating singlet oxygen ($^1O_2$) and returns to the ground state (**A_0**) (path-I). This auto-sensitized photocatalytic cycle generates sufficient reactive singlet oxygen ($^1O_2$) for further reaction. The singlet oxygen produces a *tert*-radical species (**B**) and HOO$^\bullet$ *via* an ene-type reaction with (**A_0**). The formation of *tert*-radical species (**B**) has been confirmed by ESI-MS analysis of its radical trapped adduct with scavenger TEMPO and BHT. Subsequently, the *tert*-radical (**B**) combines with HOO$^\bullet$ to provide a hydroperoxylated (**C**) intermediate, the formation of which has been confirmed by ESI-MS. The photochemical homolytic-cleavage of the peroxy-bond in intermediate (**C**) produces a hindered *tert*-alkoxy radical (**D**) and a hydroxyl radical HO$^\bullet$. Recombination of two such hydroxyl radicals generates H_2O_2. The formation of H_2O_2 has been confirmed by $KMnO_4$ and iodometric tests.

TH-3369_166122017

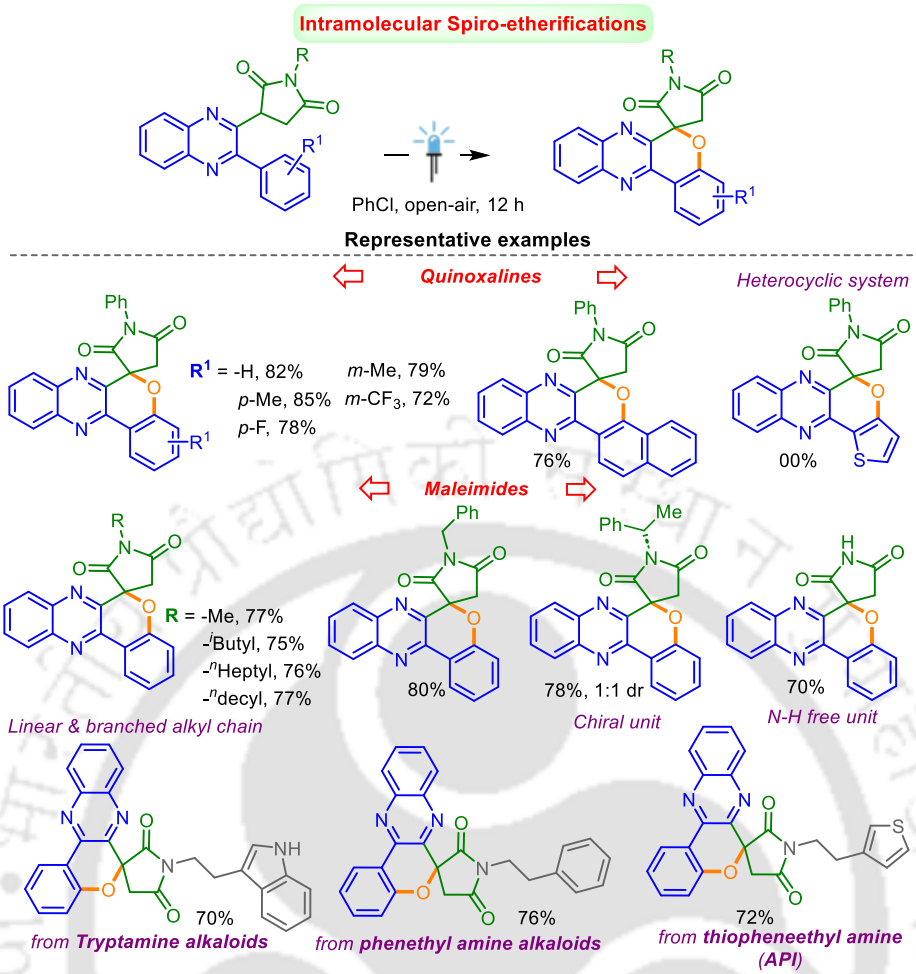

Scheme V.4. *Scope of intramolecular spiro-etherification*

The strongly hydrogen-bonded protic solvent, HFIP transfers a proton *via* hydrogen atom transfer (HAT) to produce a hydroxylated product (**1a**). On the other hand, in an aprotic solvent PhCl, this alkoxy radical **D** underwent a polarity-mismatched radical addition at the *ortho*-position of the C2-phenyl ring to generate a spirocyclic de-aromatized radical intermediate (**E**). Now, abstraction of the adjacent *tert*-hydrogen from the intermediate (**E**) by $HOO^{\bullet}$ radical provides the spiro-ether (**1b**) with the release of H_2O_2. This is an excellent illustration of solvent-dependent selectivity. Despite this, the possible involvement of an O-H tautomer ($\mathbf{A_0}$) in the above process, cannot be completely ruled out (path II).

TH-3369_166122017

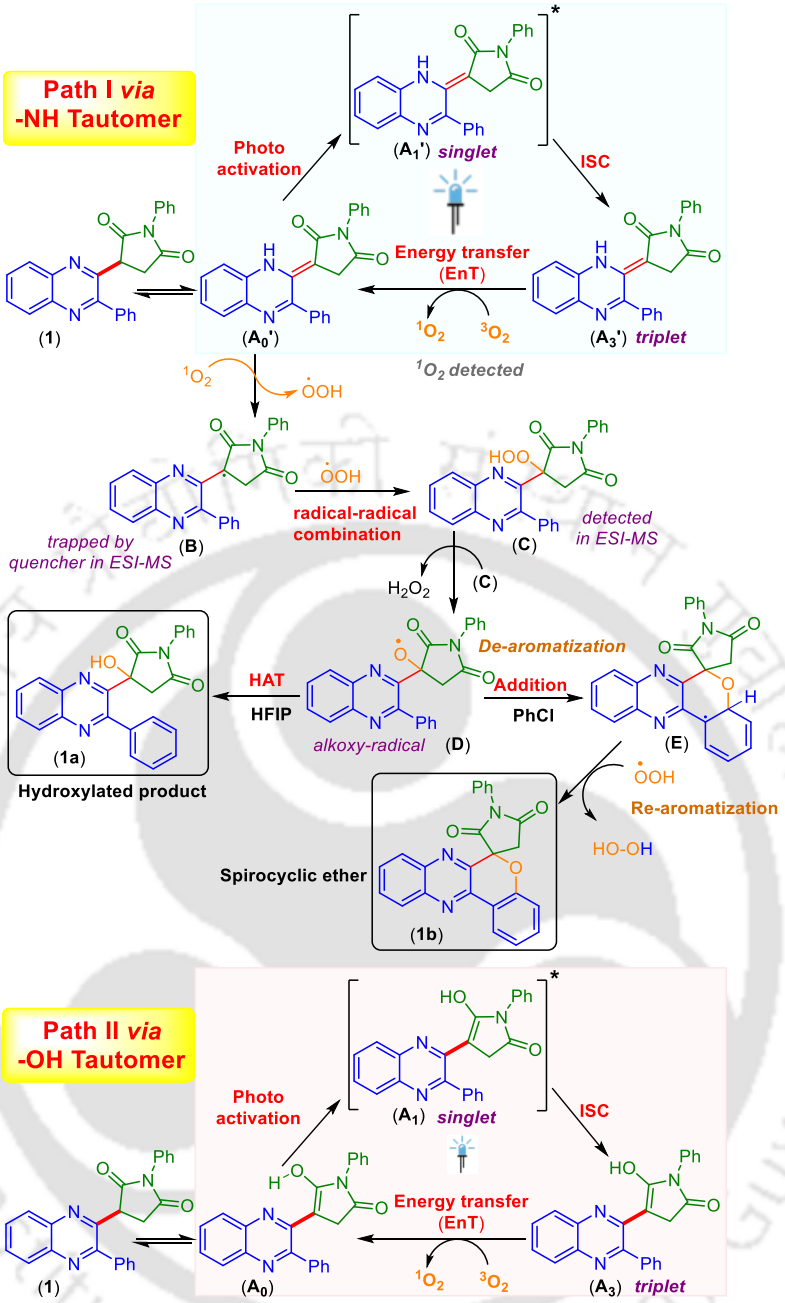

Scheme V.6. *Plausible mechanism for hydroxylation and spiro-etherification*

In summary, a solvent-switched photocatalyst free α–tertiary C–H hydroxylation and intramolecular spiro-etherification of photo-responsive C3-maleimidated quinoxalines were demonstrated. Here in the highly π-conjugated N–H tautomer of C3-maleimidated quinoxalines allows the substrate to get excited by irradiation at longer wavelengths of light, and subsequently, it attains the triplet state *via* intersystem crossing (ISC). This excited triplet-state sensitized molecule then transfers its energy to a triplet-state oxygen ($^3O_2$) generating reactive singlet oxygen ($^1O_2$) for hydroxylation and spirocyclization depending on the solvent used. The

TH-3369_166122017

detailed mechanistic elucidation, broad substrate scope, good functional group tolerance, and an overall sustainable methodology are the fruitful outcome of this investigation.

NEW FINDINGS and FUTURE PERSPECTIVE OF THESIS (UNDERGOING)

PART-I: Preferential Bis-alkenylation and [2+2+2] Annulation of Quinoxaline with Alkyne: A Substrate-Controlled Dual C-H Activation

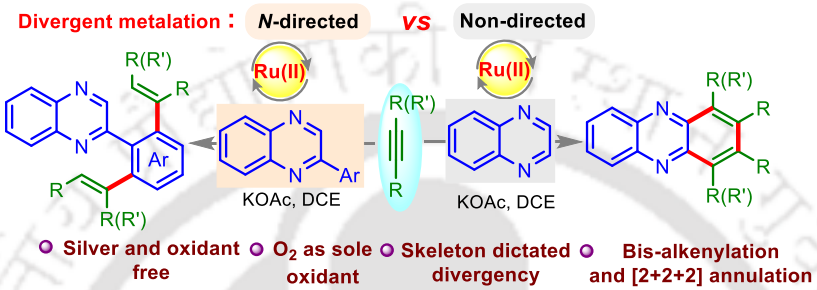

This section demonstrates a Ru(II) catalyzed substrate-controlled divergent access of bis-ortho alkenylation and [2+2+2] annulation of diversely substituted quinoxalines with various symmetrical and unsymmetrical internal alkynes to afford a library of bis-alkenylated and annulated extended quinoxalines. Herein, for 2-aryl quinoxaline system, the N-directed ruthenation was observed whereas for non-arylated quinoxalines, a non-directed ruthenation facilitates the annulation reaction under an identical set of conditions. Furthermore, the detailed mechanistic studies for fruitful implantation of the mechanism are currently undergoing.

PART-II: Intramolecular EnT Dictated Divergent Access of Oxidative Olefin Cleavage/Intramolecular Cyclization of Photochromic Bis-alkenylated Quinoxaline

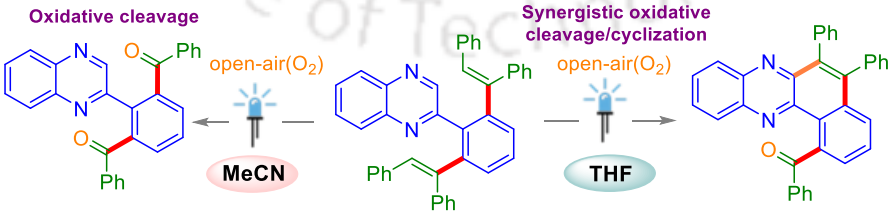

This section portrays a bis-alkenylated quinoxaline possess an intramolecular n-π^* charge-transfer mediated triplet energy transfer to facilitate the intramolecular oxidative cleavage and cyclization process of the appended olefins. Further, a set of control reactions along with derivations are currently being pursued.

TH-3369_166122017

CONTENTS

Chapter I: ***A Concise Overview of Thermal(Photo) Induced C–H Functionalization and Oxidative Annulation (Cyclization)*** 01

IA. Overview of thermal induced metal catalysis 02

IA.1. Introduction 02

IA.1.1. Transition-metal Catalyzed C–H Activation/C–H Functionalization 02

IA.1.2. Transition-metal Catalyzed Oxidative Annulation/Cyclization 08

IA.1.2.1. Classification of Annulation Reaction (based on no. of reacting atoms) 09

IA.1.2.2. Annulation Strategies Involving Various Bond Activations 13

IA.1. References 19

IB. Overview of Photocatalysis 23

IB.1. Introduction 23

IB.2. Classification of Different Modes of Photo-Catalytic Strategies 23

IB.2.1. Photoredox Catalysis 23

IB.2.2. Energy Transfer (EnT) Catalysis 28

IB.2.3. Electron Donor-Acceptor (EDA) Complexation-enabled Catalysis 34

IB.2.4. Direct Photo-Excitation of Photochromic Substrate 43

IB.3. References 46

Chapter II: ***Access to Multifunctional AEEgens via Ru(II)-Catalyzed Quinoxaline-Directed Oxidative Annulation*** 51

II.1. Introduction 52

II.2. Prior Strategies for Forging Various N-Heterocyclic Quaternary Salts 53

II.3. Present Strategy 57

TH-3369_166122017

II.4. Multifaceted Application 62

II.5. Experimental Section 86

II.6. References 92

II.7. Spectral Data 104

II.8. NMR Spectra 117

Chapter III: ***Solvent Switched Manganese(I) Catalyzed Regiodivergent Distal Vs Proximal C-H Alkylation of Imidazopyridine with Maleimide*** 119

III.1. Introduction 120

III.2. Prior Strategies of Metal-Catalyzed Controlled Regiodivergent C−H Functionalization 120

III.3. Prior Strategies of Metal-Catalyzed C−H Functionalization of Imidazopyridne 133

III.4. Present Strategy 138

III.5. Experimental Section 150

III.6. References 166

III.7. Spectral Data 172

III.8. NMR Spectra 206

Chapter IV: ***Mn(I)-Catalyzed Preferential Electrophilic C3- Maleimidation in Quinoxaline Leading to Spirocyclization and Dehydrogenation of Succinimides*** 209

IV.1. Introduction 210

IV.2. Prior Strategies of Metal-Catalyzed Synthesis of Succinimide Scaffolds 210

IV.3. Prior *ortho*-Directed C−H Functionalization Strategies of Quinoxaline 212

IV.4. Present Strategy 214

IV.5. Experimental Section 225

IV.6. References 240

IV.7. Spectral Data 244

TH-3369_166122017

IV.8. NMR Spectra 277

Chapter V: ***Photo-Induced Generation of Oxygenated Quaternary Centers via EnT Enabled Singlet O2 Addition to C3- Maleimidated Quinoxaline: A Reagent-Less Approach*** 279

V.1. Introduction 280

V.2. Modern Tertiary Hydroxylation Strategies 281

V.3. Modern Etherification Strategies 284

V.4. Present Strategy 286

V.5. Experimental Section 305

V.6. References 346

V.7. Spectral Data 351

V.8. NMR Spectra 388

Future Perspective and Concluding Remarks 527

Publications and Conferences 534

Copyrights 536

TH-3369_166122017

CHAPTER I

Introduction: A Concise Overview of Thermal(Photo) Induced C–H Functionalization and Oxidative Annulation (Cyclization)

TH-3369_166122017

CHAPTER IA

IA.1. Introduction

The C–H bond activation is one of the common processes in nature. For several billion years' nature evolves specific enzymes such as cytochrome P450 enzymes and methane monooxygenase for metal-based C–H activation. Currently, C–H activation become a powerful synthetic tool for the construction of valuable organic frameworks *via* a directed C–H functionalization and oxidative annulation or cyclization to construct various C–C and C–heteroatom bonds.

IA.1.1. Transition-metal Catalyzed C–H Activation/C–H Functionalization

Transition metal catalyzed C–H bond functionalization *via* unreactive C–H bond activation has brought a revolution in the scenario of synthetic methodologies towards the development of versatile pharmaceuticals, natural products, polymers.[1] Over the traditional approaches this strategy has offered direct conversion of C–H bonds into C–C and C–heteroatom bonds through an atom-step economical pathway.[2]

The C–H functionalization in chemical synthesis comes with two major challenges: sufficient inertness for the cleavage of the strong C–H bonds (Figure IA.1.1.1)[3] and the control of site-selectivity and chemo selectivity issues. In this regard, directing group-assisted C–H bond functionalization has shown better efficiency. The lone pair of electrons bearing directing groups (**DGs**) facilitates C–H functionalization through σ-chelation. In general, directing groups first coordinate with metal centers through the donation of a lone pair of electrons bringing the metal closer to the proximity of C–H bonds and forming chelated five or six-membered metalacycle to achieve the site-selective C–H activation and functionalization (Scheme IA.1.1.1). In this context, versatile directing groups including pyridines, oxazolines, imines, amides, anilides, amines, carboxylic acids, ketones, esters etc. have been employed for the catalytic C–H functionalization.

TH-3369_166122017

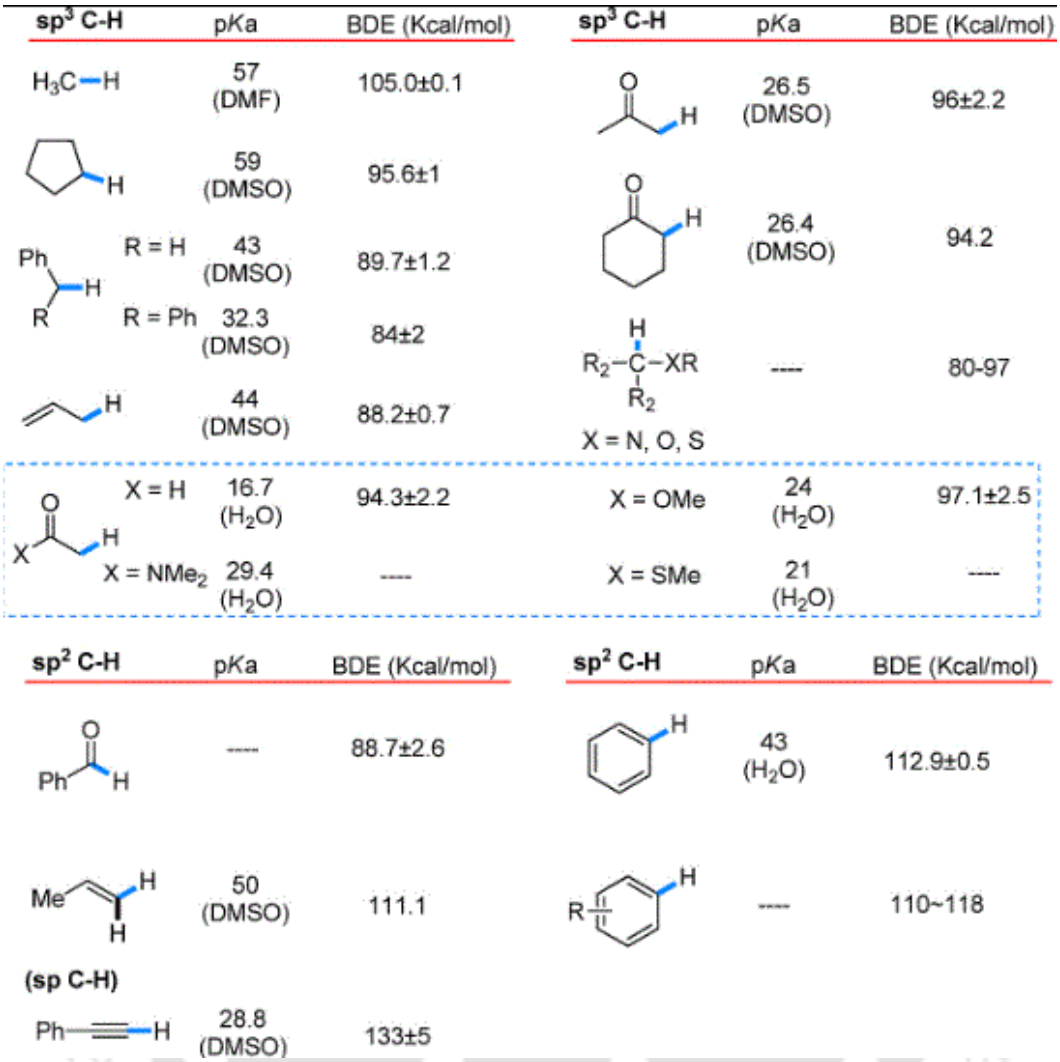

Figure IA.1.1.1. *pKa and Bond Dissociation Energy of major C–H Bonds. Reproduced with permission from ref (3). Copyright 2017 American Chemical Society*

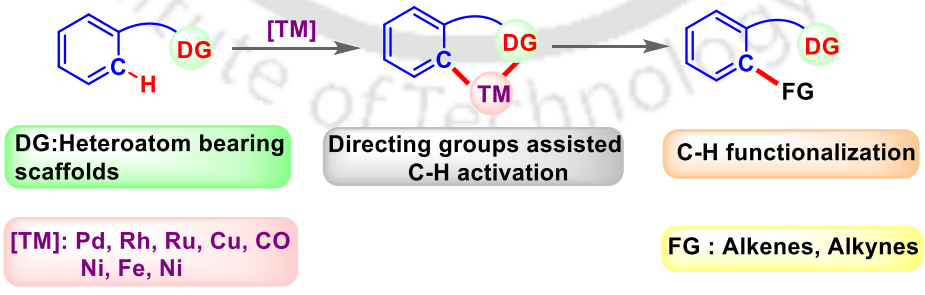

Scheme IA.1.1.1 *Site-selective directed C–H functionalization*

TH-3369_166122017

The directed C–H functionalization reaction are also classified based on the nature of directing groups (DG). Some representative examples of each section are illustrated below.

❖ Mono-dentate DG Strategy

The *N*-atom based heteroarenes are extensively studied in directed C–H functionalization, as they offered strong σ-donation towards the metal salts. These type of DGs are termed as strong-directing groups. Beside this, several weak mono-dentate DGs including amides, carbonyls, thio-ethers and alcohols are also well elaborated in literature.[4] Some of these are depicted below.

Twentieth-Century Edition

In the year 2001, the rhodium-catalyzed C–H alkenylation of 2-phenylpyridine was reported by Lim and Kang, in which PPh_3 was indispensable to keep the activity of the Rh(I) catalyst (Scheme IA.1.1.2).[5]

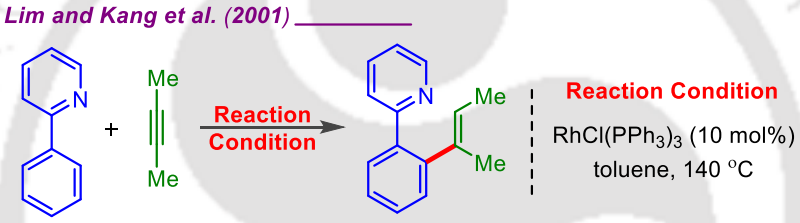

Scheme IA.1.1.2. *Rh(I)-catalyzed ortho-directed hydroalkenylation of 2-phenyl pyridine*

Leeuwen and co-workers demonstrated a *ortho*-olefination of anilides with acrylates by the palladium-catalyzed oxidative coupling reaction at room temperature in 2002 (Scheme IA.1.1.3).[6]

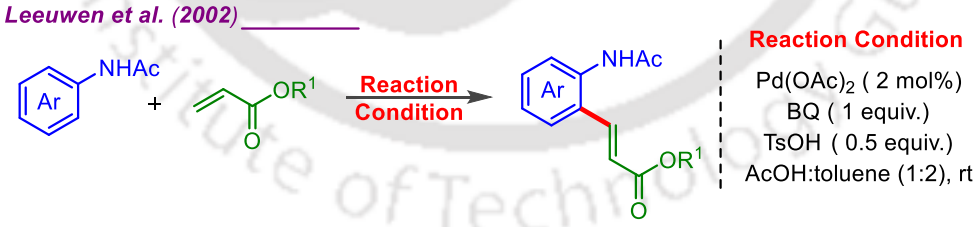

Scheme IA.1.1.3. *Pd(II)-catalyzed ortho-directed C–H olefination*

❖ Bidentate DG Strategy

The utilization of bidentate DGs offers strong coordination with metal salts along with tuneable coordination properties making this strategy popular over mono-dentate DG strategy. The last decades have witnessed several reports on heteroatom-based bidentate DG-directed C–H functionalization.[7] Some of them are summarized in Figure IA.1.1.2.

TH-3369_166122017

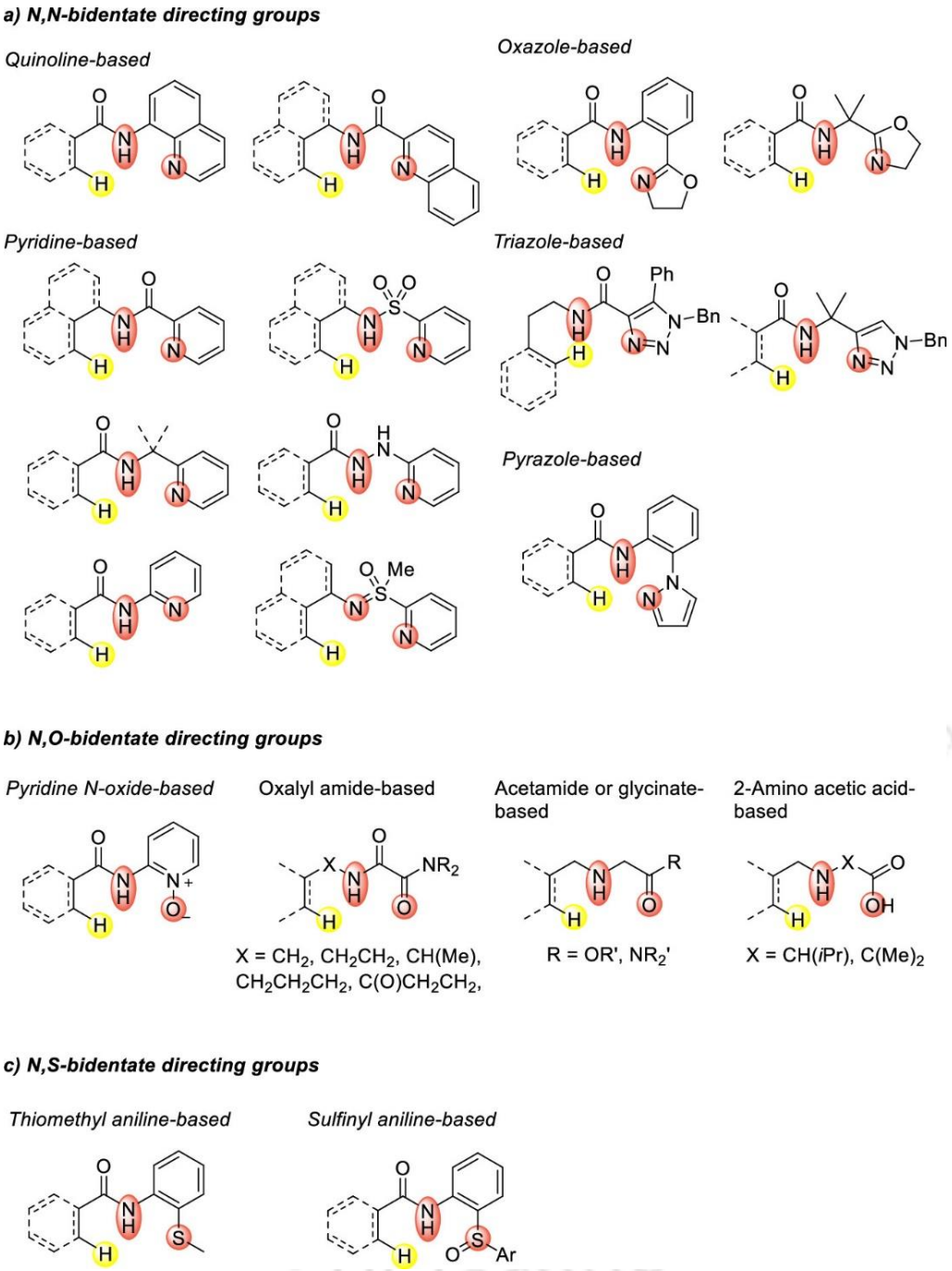

Figure IA.1.1.2. *Common examples of heteroatom-based bidentate directing groups. Reproduced with permission from ref (7). Copyright 2020 American Chemical Society*

Among the available bidentate DGs, the most familiar one carries the *N*, *N*-bidentate sites and thus well documented in literature.

TH-3369_166122017

Daugulish *et al.* reported a Pd(II)-catalyzed C(sp^2)–H and C(sp^3)–H arylation of aromatic and aliphatic amides (Scheme IA.1.1.4).[8] Here in, 8-amino quinolone auxiliary serves as a *N*, *N*-bidentate directing group.

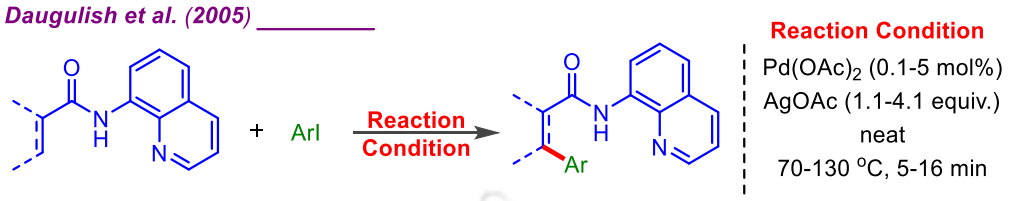

Scheme IA.1.1.4. *Pd-catalyzed C(sp^2)–H and C(sp^3)–H arylation using bidentate DG*

In 2018, Van der Eycken and co-workers described a Ru(II) catalyzed C–H/N–H annulation of with alkenes to construct substituted isoquinolines (Scheme IA.1.1.5).[9] In this reaction α-amino acid esters serves as a bidentate directing group.

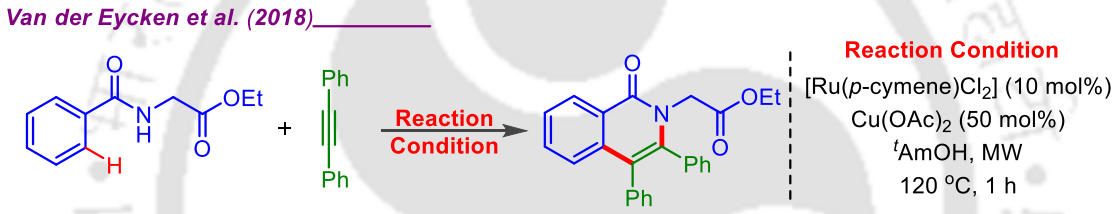

Scheme IA.1.1.5. *Ru-catalyzed C(sp^2)–H annulation using bidentate DG*

❖ Transient DG Strategy

In transient DG strategy, the directing groups are installed and removed *in situ*. The most common transient DGs are imines, prepared from the condensation of amines and carbonyl compounds. In the year 1997, Jun *et al.* introduced a transient imine-directed hydroacylation of terminal alkenes under Rh(I)-catalysis (Scheme IA.1.1.6).[10] In this reaction, a catalytic amount of 2-amino-3-picoline was utilized for the *in situ* generation of transient imine DG from the corresponding aldehydes.

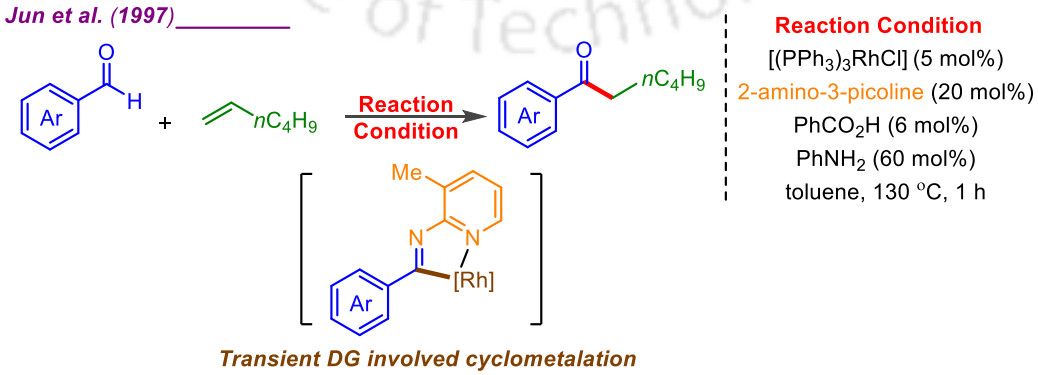

TH-3369_166122017

Scheme IA.1.1.6. *Rh(I)-catalyzed transient imine-directed hydroacylation of alkenes*

Takai and co-workers described a Re(I)-catalyzed transient imine-directed annulation reaction of aryl ketones and acrylates (Scheme IA.1.1.7).[11] Here in catalytic *p*-anisidine *in situ* generates the corresponding transient imine DG.

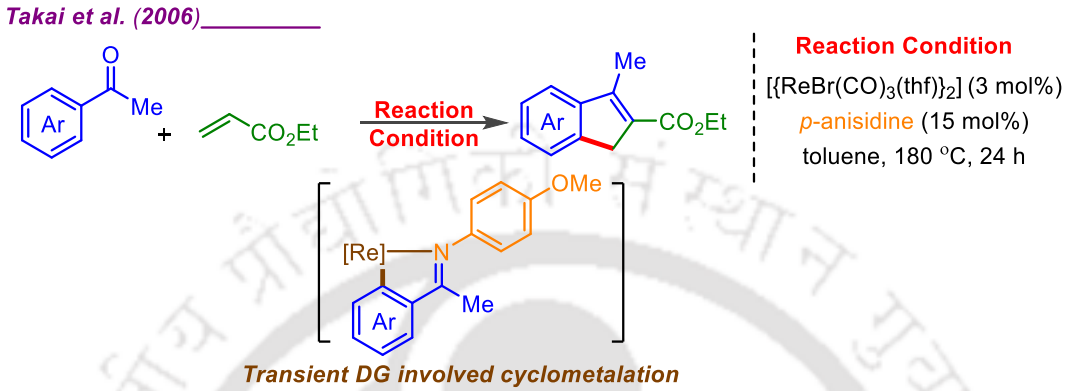

Scheme IA.1.1.7. *Re(I)-catalyzed transient imine-directed annulation of ketone with acrylate*

❖ Traceless DG Strategy

In traceless DG strategy, a pre-existing coordinating group serves as a directing group during the C–H functionalization reaction and subsequently it is removed from the product without the requisite of an additional step. Among the other functionalities, carboxylic acids are mostly utilized as traceless directing groups. For example, In the year 2016, Gooßen *et al.* described a Ru(II)-catalyzed hydroalkenylation of benzoic acid with internal alkynes (Scheme IA.1.1.8).[12] In this reaction carboxyl acid group serves as a traceless DG, eliminated from the reaction medium via the decarboxylation path.

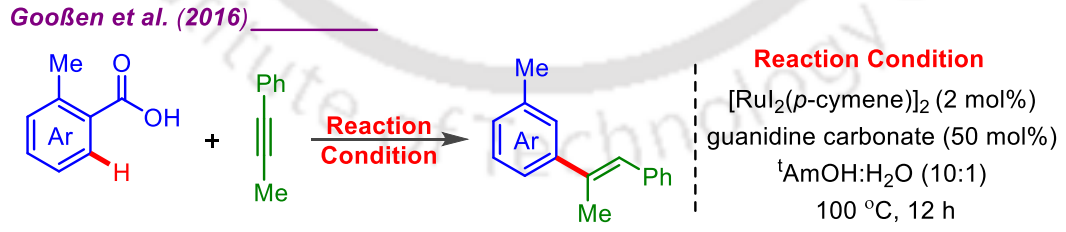

Scheme IA.1.1.8. *Ru(II)-catalyzed regioselective C–H hydroalkenylation involving carboxylic acid as a traceless DG*

Similarly, sulfoxonium ylides are also utilized in traceless DG strategy. Prabhu and co-workers established a Rh(III)-catalyzed oxidative annulation of sulfoxonium ylides with unsymmetrical alkyne,

TH-3369_166122017

4-hydroxy-2-alkynoate (Scheme IA.1.1.9).[13] In this reaction, sulfoxonium ylide acts as a traceless DG to enable the synthesis of substituted 1-naphthols.

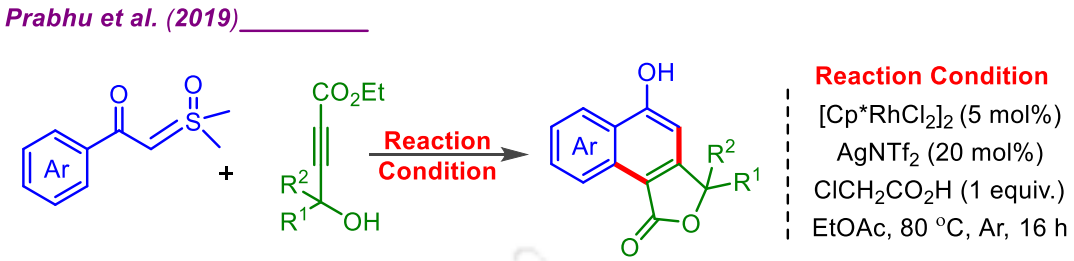

Scheme IA.1.1.9. *Rh(III)-catalyzed oxidative annulation involving sulfoxonium ylide as a traceless DG*

Amides functionalities are also involved in traceless-directed strategy. In 2020, Wang group disclosed a Rh(III)-catalyzed cascade cyclization reactions of 3-amide substituted indoles with diynes (Scheme IA.1.1.10).[14] This reaction is associated with the simultaneous C–H activation and C–C cleavage *via* Friedel–Crafts-retro reaction to synthesize cyclopenta[*b*]carbazoles.

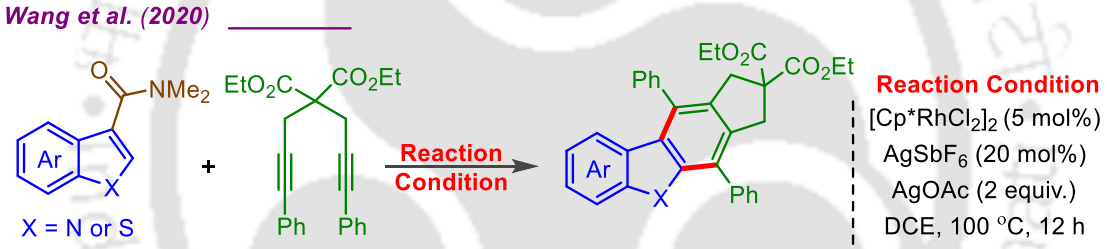

Scheme IA.1.1.10. *Rh(III)-catalyzed synthesis of cyclopenta[b]carbazoles via cascade C–H/C–C activation*

IA.1.2. Transition-metal Catalyzed Oxidative Annulation/Cyclization

Transition-metal-catalyzed C–H activation followed by oxidative annulation has emerged as a straightforward and versatile tool for constructing various π-conjugated poly-heterocyclic and carbocyclic luminogens.[15] This method provides an efficient and atom-economic route for the elaboration of simple arenes, resulting in diversely substituted poly-heterocyclic compounds. Overall, this approach enhances the efficiency of the desired transformation.

Annulation is a term that comes from the Latin word "annulatus," meaning "ringed." In organic chemistry, this term refers to the process of building a ring onto an existing system, whether cyclic or non-cyclic. The added ring can be of any size, but typically five and six-membered rings are formed. Annulation reactions are particularly useful in constructing products with complex cyclic scaffolds from

TH-3369_166122017

simpler, acyclic starting materials. This type of reaction usually involves metal-catalyzed C–H activation, migratory insertion, and reductive elimination, as shown in Scheme IA.1.2.1. Such reactions occur through an oxidative coupling pathway in which two reactants are coupled with each other, resulting in the elimination of two electrons captured by the oxidant from the reaction.

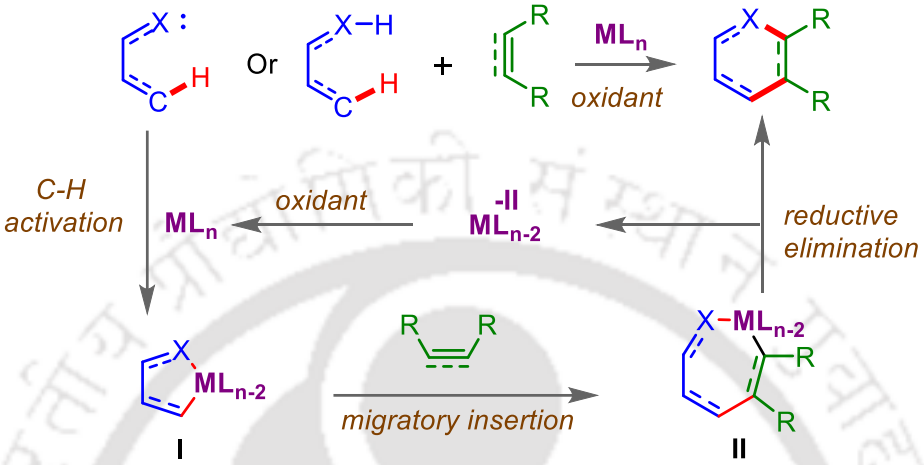

Scheme IA.1.2.1. *Site-selective oxidative annulation via C–H activation*

IA.1.2.1. Classification of Annulation Reaction (*based on no. of reacting atoms*)

Based on the numbers of participating atoms, annulation reactions are classified as follows

❖ [2+1] Annulation:

Cyclopropanes are surfaced as a valuable subunit of many biologically active scaffolds and natural products. Thus several reports have described to synthesize this important scaffold among them, [2+1] annulation reaction came out an interesting strategy. In the year 2014, Nacci *et al.* proposed a Pd(II)-catalyzed formal [2+1] annulation reaction among aryl methyl ketones and styrenes to afford a substituted cyclopropane scaffolds. This reaction is associated with the Pd(II)-catalyzed cleavage of two α-hydrogens of ketones in presence of $Cu(OAc)_2$ oxidant and molten tetrabutylammonium acetate (TBAA) solvent (Scheme IA.1.2.2).[16]

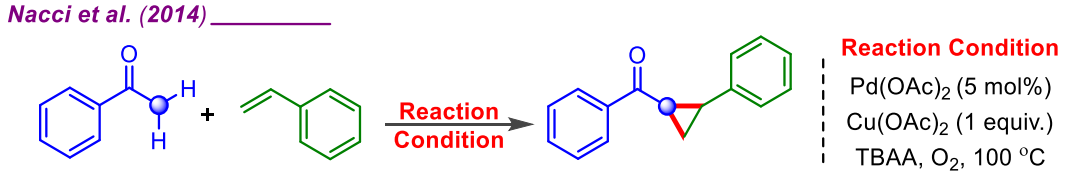

Scheme IA.1.2.2. *Pd(II)-catalyzed synthesis of cyclopropane via [2+1] annulation*

TH-3369_166122017

❖ **[3+1] Annulation:**

In the year of 2014, Gaunt group demonstrated a Pd(II)-catalyzed C(sp^3)–H carbonylation of hindered cyclic aliphatic amines *via* [3+1] annulation (Scheme IA.1.2.3).[17] The reaction proceeds through a four-membered cyclopalladation pathway to synthesize β-lactames.

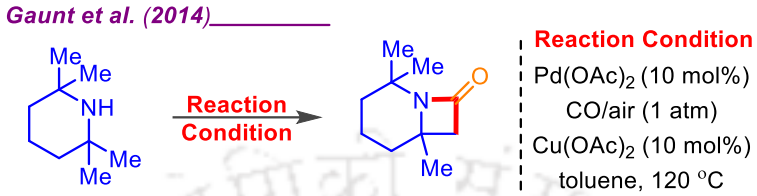

Scheme IA.1.2.3. *Pd(II)-catalyzed [3+1] annulation*

❖ **[3+2] Annulation:**

Indole has emerged as a privileged structural motif due to their esteemed presence in many of natural products, commercial drugs, and other functional molecules. Thus, in past years several synthetic methods have documented, among them metal catalyzed [3+2] annulation represent a unique one-step synthetic strategy. In 2013, Glorius and co-workers developed an oxidant-free indole synthesis *via* a redox-neutral C–H functionalization strategy. In this reaction, the reacting substrate contained functional group serves both as a directing group and an internal oxidant (Scheme IA.1.2.4).[18]

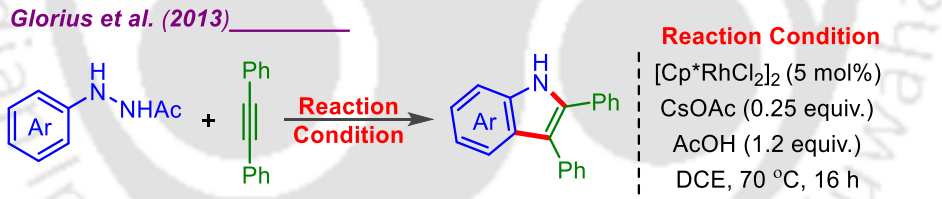

Scheme IA.1.2.4. *Rh(III)-catalyzed redox-neutral synthesis of indole*

Gulias and co-workers described a Rh(III)-catalyzed dearomatized [3+2] annulation reaction between 2-alkenylphenol and alkynes in the presence of copper oxidant (Scheme IA.1.2.5).[19] This reaction is associated with the selective cleavage of terminal C–H bond of alkenyl substrate, followed by a dearomatization of phenol ring to deliver spirocyclic scaffolds.

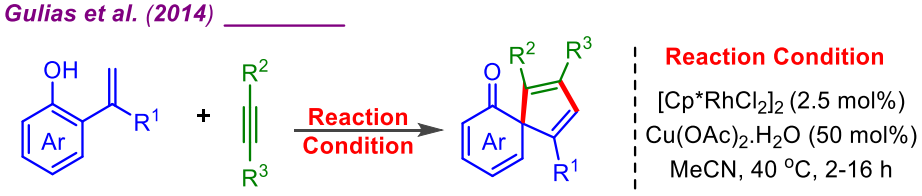

TH-3369_166122017

Scheme IA.1.2.5. *Rh(III)-catalyzed dearomatized [3+2] annulation*

❖ **[4+1] Annulation:**

You and co-workers disclosed a Pd(II)-catalyzed C(sp^3)-H carbonylation of a-substituted amides *via* [4+1] annulation (Scheme IA.1.2.6).[20] In this reaction TEMPO serves as a co-oxidant for the re-oxidation of Pd(0) to Pd(II).

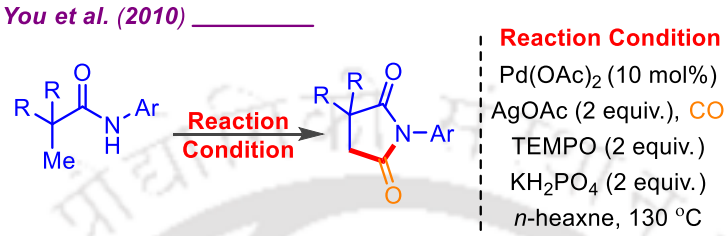

Scheme IA.1.2.6. *Pd(II)-catalyzed C(sp^3)–H carbonylation via [4+1] annulation*

❖ **[4+2] Annulation:**

Six membered cyclic structures are the important structural motifs for many of organic compounds. This annulation manner affords the substituted six membered ring. A Rh(III)-catalyzed [4+2] annulation of benzoic acids with internal alkynes was reported by Ueura *et al.* in 2007 (Scheme IA.1.2.7).[21] This reaction proceeds through the activation of O–H/C(sp^2)–H bond to synthesize isocoumarins.

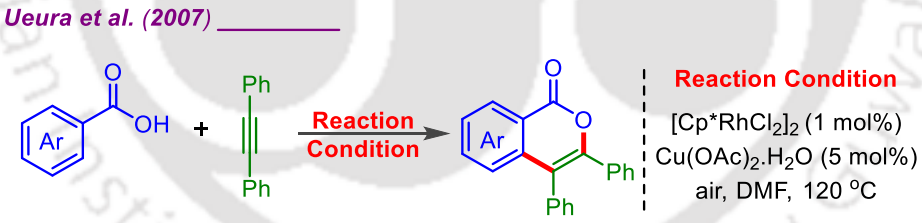

Scheme IA.1.2.7. *Rh(III)-catalyzed [3+2] annulation between benzoic acid and alkyne*

Whereas Guimond *et al.* reported a redox-neutral [4+2] annulation between amides and alkynes (Scheme IA.1.2.8).[22] This reaction proceeds without the involvement of external oxidant, as the reacting amides substrate acts as an internal oxidant through cleavage of its N–O bond.

TH-3369_166122017

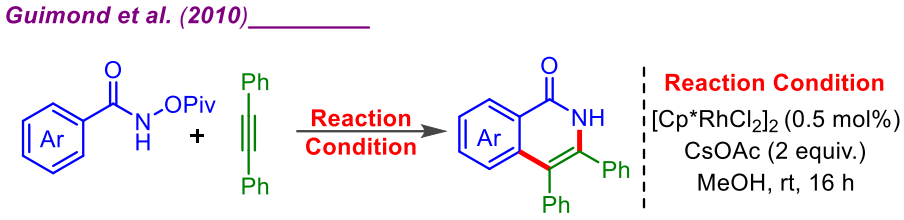

Scheme IA.1.2.8. *Rh(III)-catalyzed redox-neutral synthesis of isoqionolones*

In the year of 2013, Huang group disclosed a Rh(III)-catalyzed synthesis of aza-fused heterocyclic through [4+2] annulation between *N*-vinyl benzimidazole and alkynes (Scheme IA.1.2.9).[23] This reaction associated with the dual C(sp^2)–H activations *via* a non-directed C–H metalation strategy.

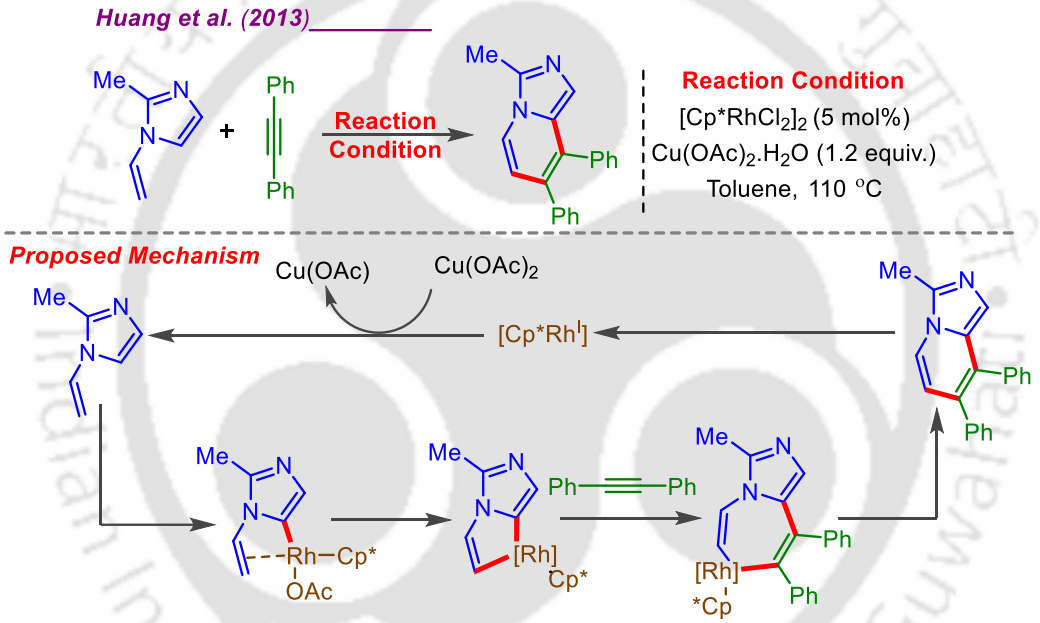

Scheme IA.1.2.9. *Rh(III)-catalyzed synthesis of aza-fused heterocycles*

Similarly, maleimides are also familiar for oxidative [4+2] annulation reactions. In the year 2016, Abbasnia group reported a [4+2] annulation between styrenes and maleimides to construct Benzo[*e*]isoindole-1,3-diones *via* dual C(sp^2)–H activation (Scheme IA.1.2.10).[24]

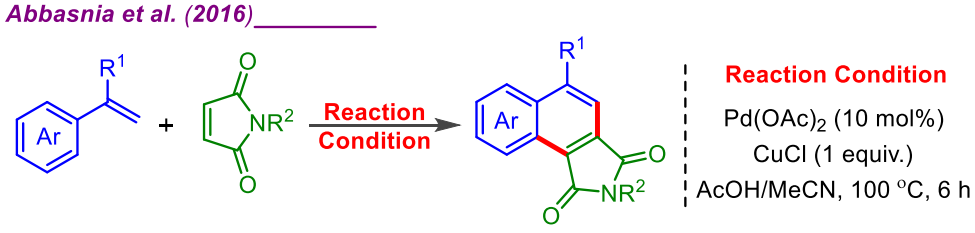

TH-3369_166122017

Scheme IA.1.2.10. *Pd(II)-catalyzed [4+2] annulation of styrenes and maleimides*

❖ **[2+2+2] Annulation:**

A pioneering [2+2+2] annulation was introduced by Umeda and co-workers. They have reacted 1-phenylpyrazole with two equivalents of alkynes under Rh(III)-catalysis to construct substituted naphthalene (Scheme IA.1.2.11).[25]

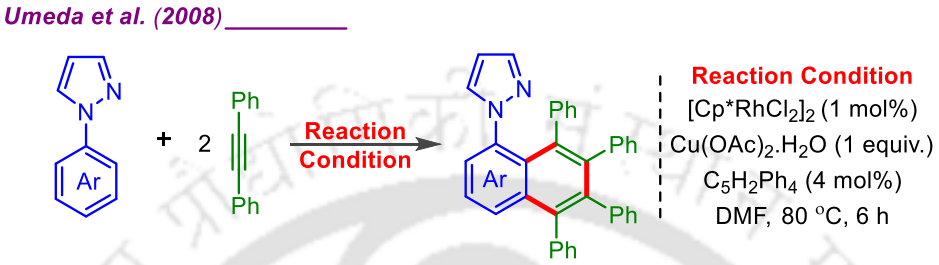

Scheme IA.1.2.11. *Rh(III)-catalyzed [2+2+2] annulation of arylpyrazole with alkyne*

❖ **[5+2] Annulation:**

In 2014, Gulias *et al.* described a Rh(III)-catalyzed (5 + 2) heteroannulation of *o*-vinyl phenols with alkynes to construct valuable benzoxepine skeletons in presence of copper oxidant (Scheme IA.1.2.12).[26]

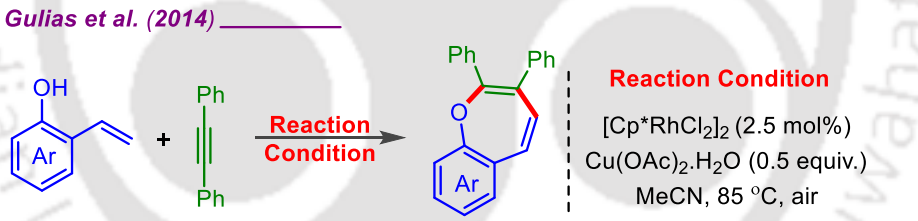

Scheme IA.1.2.12. *Rh(III)-catalyzed [5+2] hetero-annulation*

IA.1.2.2. Annulation Strategies Involving Various Bond Activations:

Transition-metal catalyzed oxidative annulation strategies leads to the activation of various carbon-hydrogen and heteroatom-hydrogen bonds. Based on this the annulation reactions can be further classified- (1) *annulation via C–H/C–H activation*

(2) *via C–H/N–H activation*

(3) *via C–H/O–H activation*

(4) *via C–H/S–H activation*

(5) *via C–H/P–H activation*

(6) *via C–H/N activation (quaternization of nitrogen centers)*

TH-3369_166122017

For each section some representative examples are depicted below.

(1) *Annulation via C–H/C–H Activation*

The oxidative annulation involving dual C–H/C–H activation turns out to be a challenging task, due to the simultaneous activation of two inert C–H bonds. In the year of 2018, Li group disclosed a Rh(III)-catalyzed regioselective oxidative annulation of β-enaminonitriles with alkynes in presence of copper oxidant (Scheme IA.1.2.13).[27] The simultaneous dual C(sp^2)–H activation leads to the synthesis of substituted 1-naphthylamines.

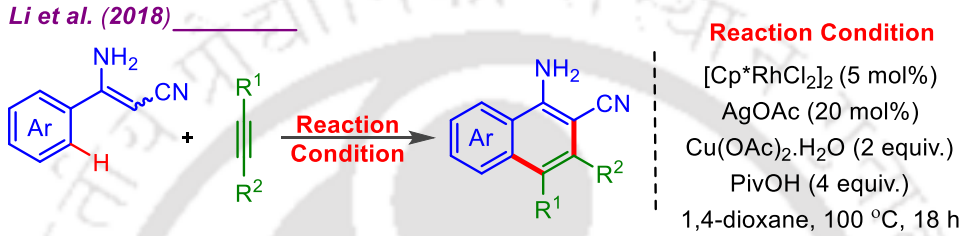

Scheme IA.1.2.13. *Rh(III)-catalyzed oxidative annulation of β-enaminonitriles with alkyne*

In the year of 2021, our group demonstrated a Cu(I)-mediated cascade annulation of *o*-alkynylanilines with maleimides (Scheme IA.1.2.14).[28] This reaction proceeds through the *in situ* formation of 2-aryl indole and followed by an oxidative C–H/C–H annulation with maleimides leads to the access of fused NH-free benzo[*a*]carbazoles. Furthermore, the synthesized annulated adducts showed strong fluorescence emission at 485–502 nm with a large Stokes shift and possess a fluorescence lifetime of ~17 ns. Moreover, such compounds exhibit Aggregation enhanced emission (AEE) in ethanol/hexane and in the aggregated state they possess a marigold-flower-like morphology. Due to having very good fluorescence properties such compounds are also utilized as cellular imaging biocompatible fluorescence probe.

TH-3369_166122017

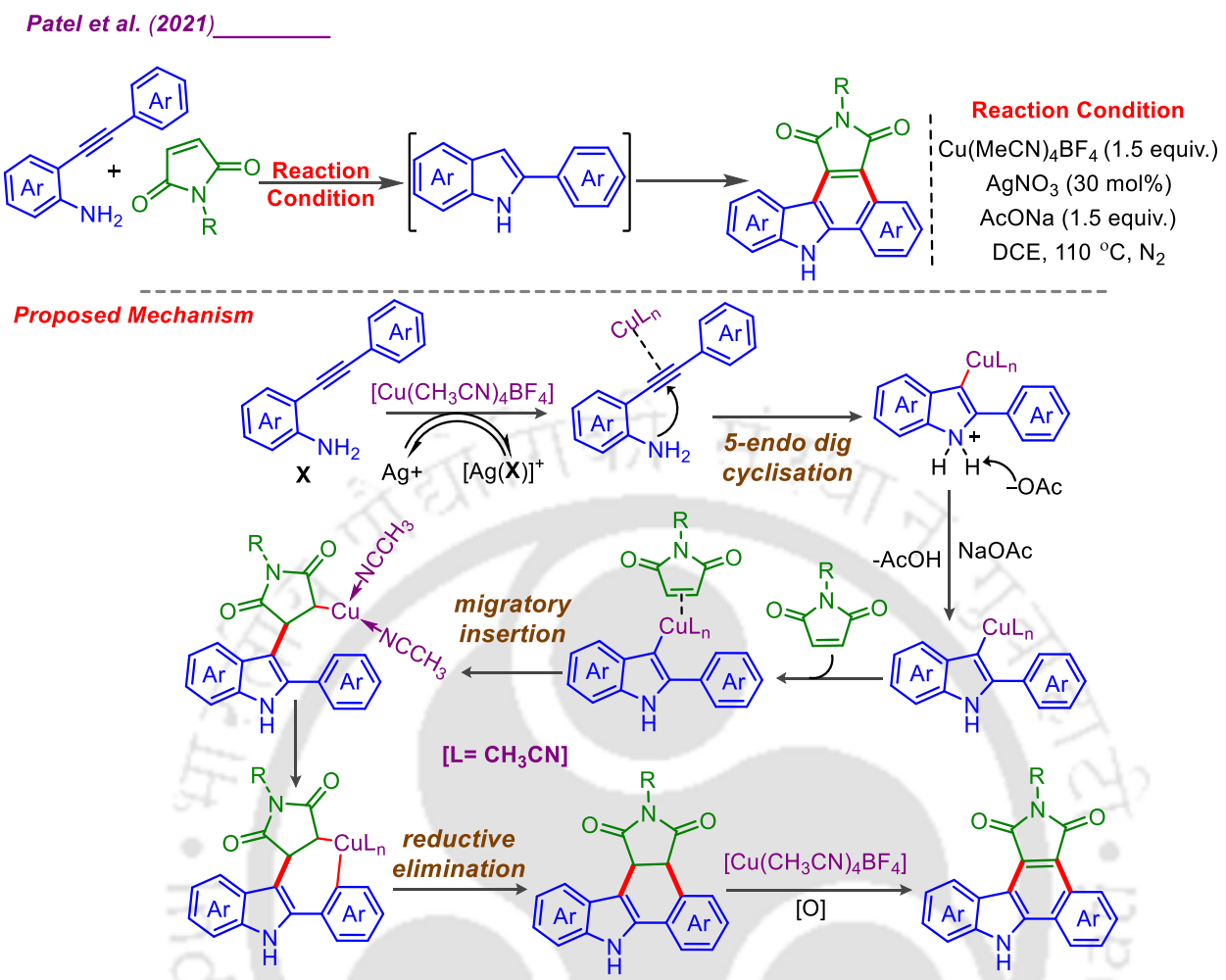

Scheme IA.1.2.14. *Cu(II)-mediated regioselective cascade annulation of o-*alkynylanilines *with maleimides*

(2) *Annulation via C–H/N–H Activation*

A Rh(III)-catalyzed oxidative C–H/N–H annulation of *N*-azoloimines with sulfoxonium ylides, diazoketones and alkynes leads to the access of substituted Azolopyrimidines (Scheme IA.1.2.15).[29] The annulation of sulfoxonium ylides and diazoketones take place under redox-neutral condition whereas, the annulation of alkynes proceeds in the presence of copper oxidant.

TH-3369_166122017

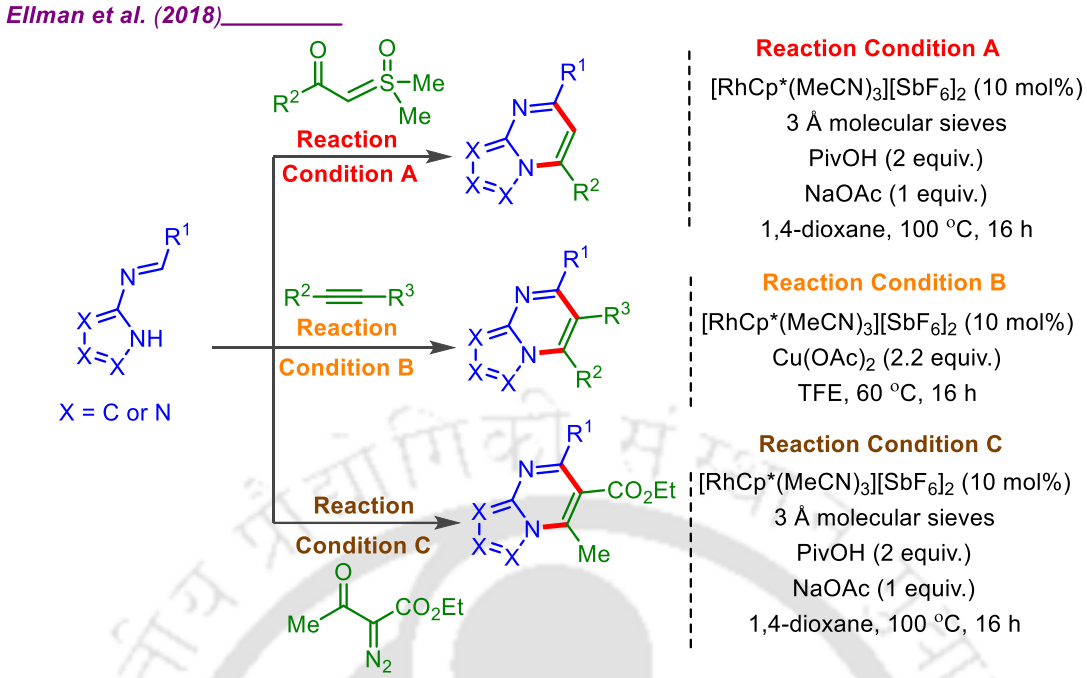

Scheme IA.1.2.15. *Rh(III)-catalyzed synthesis of azolopyrimidines via oxidative C–H/N–H annulation*

Recently, Liu and co-workers developed a Rh(III)-catalyzed oxidative C–H/N–H annulation of aromatic amides with allenes (Scheme IA.1.2.16).[30] This report depicts that *N*-(pivaloyloxy)benzamide couples with allenes via Rh–σ–alkenyl intermediates, whereas *N*-(pivaloyloxy)indol undergoes through Rh–π–allyl intermediate formation.

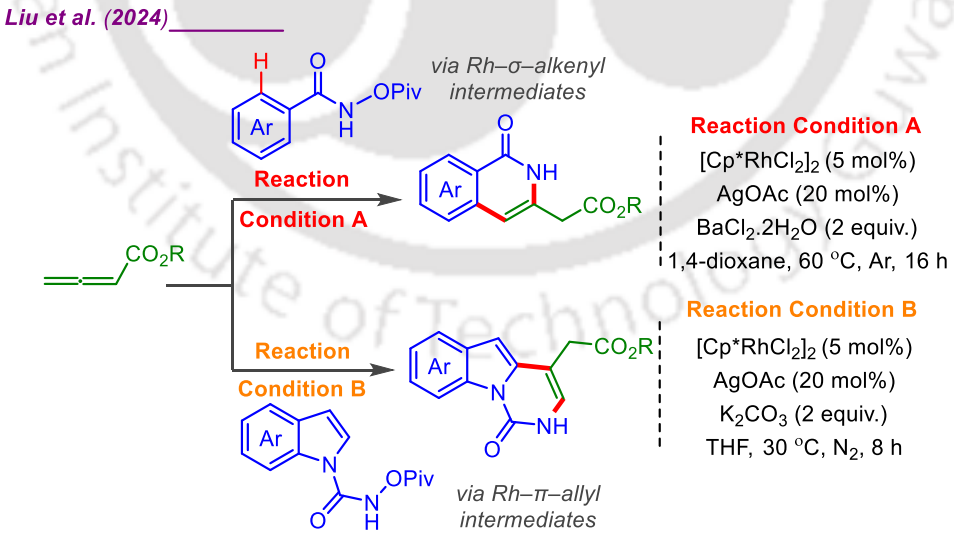

Scheme IA.1.2.16. *Rh(III)-catalyzed C−H/N−H annulation of amide with allene*

TH-3369_166122017

(3) *Annulation via C–H/O–H Activation*

An oxidative C–H/O–H annulation of salicylaldehydes with alkynes and alkenes leads to the access of substituted chromones under Ru(II)-catalysis (Scheme IA.1.2.17).[31]

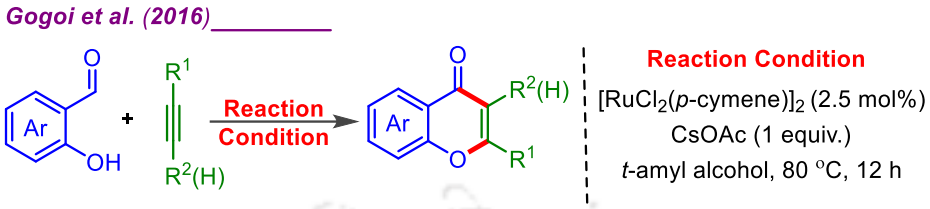

Scheme IA.1.2.17. *Ru(II)-catalyzed oxidative annulation of salicylaldehydes with alkyne*

In 2017, Perumal *et al.* described a Ru(II)-catalyzed regiospecific *C−H/O−H* oxidative annulation of benzo[*a*]phenazin-5-ol with alkyne to synthesize isochromeno[8,1-*ab*]phenazines scaffolds (Scheme IA.1.2.18).[32] Furthermore, the synthesized annulated compound exhibits a strong red-fluorescence emission and serves as a biocompatible live cancer cellular imaging probes.

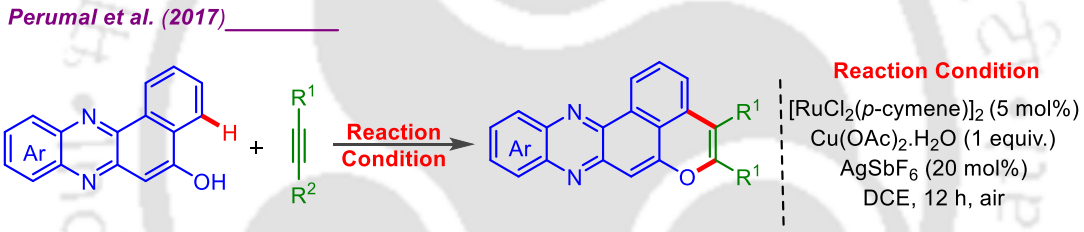

Scheme IA.1.2.18. *Ru(II)-catalyzed regiospecific C−H/O−H oxidative annulation of benzo[a]phenazin-5-ol with alkyne*

(4) *Annulation via C–H/S–H Activation*

In 2019, our group demonstrated a Ru(II)-catalyzed regioselective annulation of quinoline-4(1*H*)-thiones with alkynes (Scheme IA.1.2.19).[33] This reaction is associated with the thiocarbonyl-directed selective peri C(sp^2)–H/S–H activation.

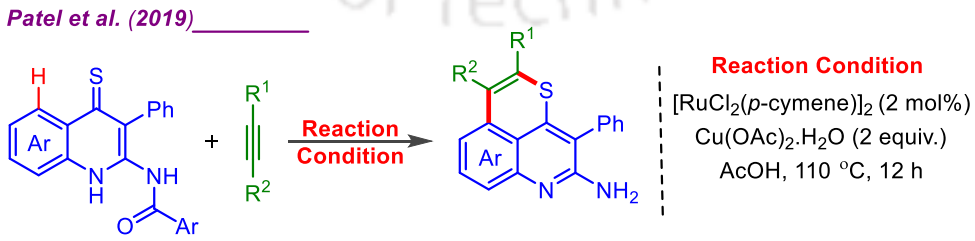

Scheme IA.1.2.19. *Ru(II)-catalyzed regiospecific C−H/S−H annulation of quinoline-4(1H)-thione with alkyne*

TH-3369_166122017

In the year of 2020, Wang *et al.* described a sulfhydryl-directed Rh(III)-catalyzed oxidative annulation of naphthalene-1-thiols and alkynes in presence of copper oxidant (Scheme IA.1.2.20).[34] This reaction is associated through the dual activation of S–H and peri-C(sp^2)–H of naphthalene-1-thiols derivatives to construct a library of naphthothiopyrans.

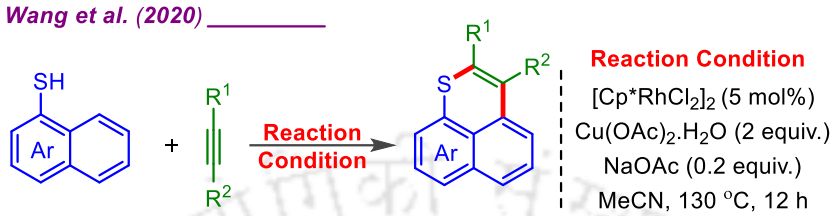

Scheme IA.1.2.20. *Rh(III)-catalyzed synthesis of naphthothiopyrans via C–H/S–H activation*

(5) *Annulation via C–H/P–H Activation*

Phosphorus compounds have found important contributions in organic synthesis, medicinal chemistry, and also in material industries. Several methods have described towards their synthesis. In 2013, Duan group disclosed a silver mediated benzo[*b*]phosphole oxides synthesis from arylphosphine oxides and internal alkynes (Scheme IA.1.2.21).[35] This annulation reaction is associated with the dual activation of C(sp^2)–H/P–H.

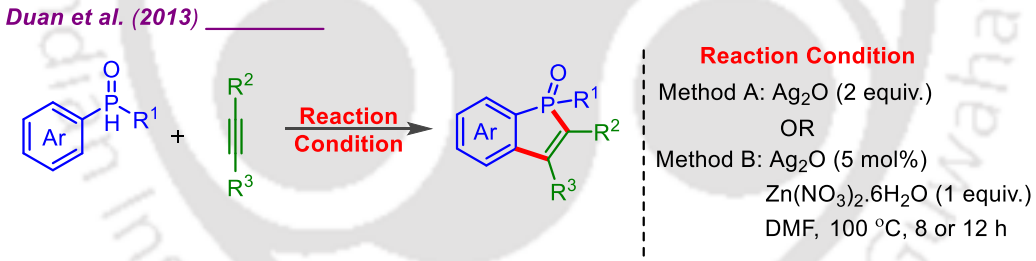

Scheme IA.1.2.21. *Ag-mediated or catalyzed oxidative annulation via C–H/P–H activation*

(6) *Annulation via C–H/N Activation*

An oxidative annulation involving C–H/N activation leads to the access of cyclized quaternary ammonium salts. In the year of 2016, Li *et al.* developed a Co(III)-catalyzed oxidative annulation strategy of *N*-substituted indoles with alkynes to develop quaternary ammonium salt pyrido[2′,1′:2,3]pyrimido[1,6-*a*]indol-5-iums in good to moderate yields (Scheme IA.1.2.22).[36]

TH-3369_166122017

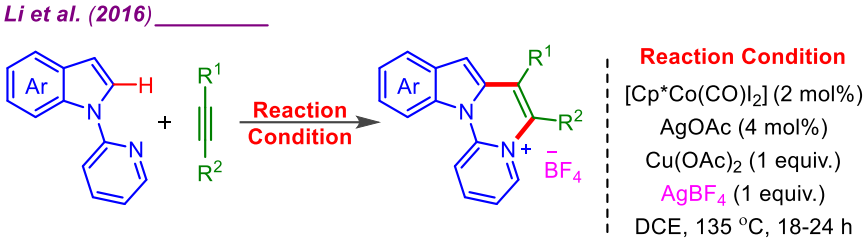

Scheme IA.1.2.22. *Co(III)-catalyzed synthesis of quaternary ammonium salts via C–H/N activation*

IA.2. References

1. (a) Wencel-Delord, J.; Glorius, F. C–H Bond Activation Enables the Rapid Construction and Late-stage Diversification of Functional Molecules. *Nat. Chem*. **2013**, *5*, 369. (b) Yamaguchi, J.; Yamaguchi, A. D.; Itami, K. C–H Bond Functionalization: Emerging Synthetic Tools for Natural Products and Pharmaceuticals. *Angew. Chem., Int. Ed*. **2012**, *51*, 8960. (c) Schipper, D. J.; Fagnou, K. Direct Arylation as a Synthetic Tool for the Synthesis of Thiophene-Based Organic Electronic Materials. Chem. Mater. **2011**, *23*, 1594.
2. (a) Trost, B. M. The Atom Economy—A Search for Synthetic Efficiency. *Science* **1991**, *254*, 1471. (b) Trost, B. M. On Inventing Reactions for Atom Economy. *Acc. Chem. Res*. **2002**, *35*, 695. (c) Wender, P. A. Toward the Ideal Synthesis and Transformative Therapies: The Roles of Step Economy and Function Oriented Synthesis. *Tetrahedron* **2013**, *69*, 7529. (d) Wender, P. A.; Verma, V. A.; Paxton, T. J.; Pillow, T. H. Function-Oriented Synthesis, Step Economy, and Drug Design. *Acc. Chem. Res*. **2008**, *41*, 40.
3. Qin, Y.; Zhu, L.; Luo, S. Organocatalysis in Inert C–H Bond Functionalization. *Chem. Rev*. **2017**, *117*, 9433.
4. Mandal, R.; Garai, B.; Sundararaju, B. Weak-Coordination in C–H Bond Functionalizations Catalyzed by 3d Metals. *ACS Catal*. **2022**, *12*, 3452.
5. Lim, Y.-G.; Lee, K.-H.; Koo, B. T.; Kang, J.-B. Rhodium(I)-Catalyzed ortho-Alkenylation of 2-Phenylpyridines with Alkynes. *Tetrahedron Lett*. **2001**, *42*, 7609.
6. Boele, M. D. K.; van Strijdonck, G. P. F.; de Vries, A. H. M.; Kamer, P. C. J.; de Vries, J. G.; van Leeuwen, P. W. N. M. Selective Pd-catalyzed oxidative coupling of anilides with olefins through C-H bond activation at room temperature. *J. Am. Chem. Soc*. **2002**, *124*, 1586.

TH-3369_166122017

7. Rej, S.; Ano, Y.; Chatani, N. Bidentate Directing Groups: An Efficient Tool in C–H Bond Functionalization Chemistry for the Expedient Construction of C–C Bonds. *Chem. Rev*. **2020**, *120*, 1788.
8. Zaitsev, V. G.; Shabashov, D.; Daugulis, O. Highly Regioselective Arylation of sp3C-H Bonds Catalyzed by Palladium Acetate. *J. Am. Chem. Soc*. **2005**, *127*, 13154.
9. Sharma, N.; Bahadur, V.; Sharma, U. K.; Saha, D.; Li, Z.; Kumar, Y.; Colaers, J.; Singh, B. K.; Van der Eycken, E. V. MicrowaveAssisted Ruthenium-Catalysed Ortho-C−H Functionalization of NBenzoyl α-Amino Ester Derivatives. *Adv. Synth. Catal*. **2018**, *360*, 3083.
10. Jun, C.-H.; Lee, H.; Hong, J.-B. Chelation-Assisted Intermolecular hydroacylation: Direct Synthesis of Ketone from Aldehyde and 1-alkene. *J. Org. Chem*. **1997**, *62*, 1200.
11. Kuninobu, Y.; Nishina, Y.; Shouho, M.; Takai, K. Rhenium- and Aniline-Catalyzed One-Pot Annulation of Aromatic Ketones and α, β-Unsaturated Esters Initiated by C–H Bond Activation. *Angew. Chem., Int. Ed*. **2006**, *45*, 2766.
12. Huang, L.; Biafora, A.; Zhang, G.; Bragoni, V.; Gooßen, L. J. Regioselective C−H Hydroarylation of Internal Alkynes with Arenecarboxylates: Carboxylates as Deciduous Directing Groups. *Angew. Chem., Int. Ed*. **2016**, *55*, 6933.
13. Hanchate, V.; Kumar, A.; Prabhu, K. R. Synthesis of Naphthols by Rh(III)-Catalyzed Domino C-H Activation, Annulation, and Lactonization Using Sulfoxonium Ylide as a Traceless Directing Group. *Org. Lett*. **2019**, *21*, 8424.
14. Wang, Y.; Li, B.; Wang, B. RhIII-Catalyzed Synthesis of Cyclopenta[*b*]carbazoles *via* Cascade C–H/C–C Bond Cleavage and Cyclization Reactions: Using Amide as a Traceless Directing Group. *Org. Lett*. **2020**, *22*, 83.
15. Gulías, M.; Mascareñas, J. L. Metal-Catalyzed Annulations through Activation and Cleavage of C–H Bonds. *Angew. Chem., Int. Ed*. **2016**, *55*, 11000.
16. Cotugno, P.; Monopoli, A.; Ciminale, F.; Milella, A.; Nacci, A. Palladium-Catalyzed Cross-Coupling of Styrenes with Aryl Methyl Ketones in Ionic Liquids: Direct Access to Cyclopropanes. *Angew. Chem., Int. Ed*. **2014**, *53*, 13563.
17. McNally, A.; Haffemayer, B.; Collins, B. S. L.; Gaunt, M. J. Palladium-Catalysed C-H Activation of Aliphatic Amines to Give Strained Nitrogen Heterocycles. *Nature* **2014**, *510*, 129.

TH-3369_166122017

18. Zhao, D.; Shi, Z.; Glorius, F. Indole Synthesis by Rhodium(III)-Catalyzed Hydrazine-Directed C-H Activation: Redox-Neutral and Traceless by N-N Bond Cleavage. *Angew. Chem., Int. Ed*. **2013**, *52*, 12426.
19. Seoane, A.; Casanova, N.; Quiñones, N.; Mascareñas, J. L.; Gulías, M. Rhodium(III)-Catalyzed Dearomatizing (3 + 2) Annulation of 2-Alkenylphenols and Alkynes. *J. Am. Chem. Soc*. **2014**, *136*, 7607.
20. Yoo, E. J.; Wasa, M.; Yu, J.-Q. Pd(II)-Catalyzed Carbonylation of C(sp^3)–H Bonds: A New Entry to 1,4-Dicarbonyl Compounds. *J. Am. Chem. Soc*. **2010**, *132*, 17378.
21. Ueura, K.; Satoh, T.; Miura, M. An Efficient Waste-Free Oxidative Coupling via Regioselective C–H Bond Cleavage: Rh/Cu-Catalyzed Reaction of Benzoic Acids with Alkynes and Acrylates under Air. *Org. Lett*. **2007**, *9*, 1407.
22. Guimond, N.; Gouliaras, C.; Fagnou, K. Rhodium(III)-catalyzed isoquinolone synthesis: the N-O bond as a handle for C-N bond formation and catalyst turnover. *J. Am. Chem. Soc*. **2010**, *132*, 6908.
23. Huang, J.-R.; Zhang, Q.-R.; Qu, C.-H.; Sun, X.-H.; Dong, L.; Chen, Y.-C. Rhodium(III)-Catalyzed Direct Selective C(5)–H Oxidative Annulations of 2-Substituted Imidazoles and Alkynes by Double C–H Activation. *Org. Lett*. **2013**, *15*, 1878.
24. Sheykhan, M.; Shafiee-Pour, M.; Abbasnia, M. C–H Activation under the Guise of Diels–Alder Reaction: Annulation toward the Synthesis of Benzo[e]Isoindole-1,3-Diones. *Org. Lett*. **2017**, *19*, 1270.
25. Umeda, N.; Tsurugi, H.; Satoh, T.; Miura, M. Fluorescent Naphthyl- and Anthrylazoles from the Catalytic Coupling of Phenyla-zoles with Internal Alkynes through the Cleavage of Multiple C-H Bonds. *Angew. Chem., Int. Ed*. **2008**, *47*, 4019.
26. Seoane, A.; Casanova, N.; Quiñones, N.; Mascarenas, J. L.; Gulías, M. Straightforward Assembly of Benzoxepines by Means of a Rhodium(III)-Catalyzed C–H Functionalization of o-Vinylphenols. J. Am. Chem. Soc. 2014, 136, 834.
27. Wang, H.; Xu, H.; Li, B.; Wang, B. Annulation of β-enaminonitriles with alkynes *via* RhIII-catalyzed C–H activation: Direct access to highly substituted 1-naphthylamines and naphtho[1,8-*bc*]pyridines. *Org. Lett*. **2018**, *20*, 5640.
28. Khandelia, T.; Ghosh, S.; Panigrahi, P.; Shome, R.; Ghosh, S. S.; Patel, B. K. Copper(I)-Mediated Cascade Annulation *via* Dual C–H/C–H Activation: Access to Benzo[*a*]carbazolic AEEgens. *J. Org. Chem*. **2021**, *86*, 16948.

TH-3369_166122017

29. Halskov, K. S.; Witten, M. R.; Hoang, G. L.; Mercado, B. Q.; Ellman, J. A. Rhodium(III)-Catalyzed Imidoyl C–H Activation for Annulations to Azolopyrimidines. *Org. Lett*. **2018**, *20*, 2464.
30. Liu, J.; Liu, D.-Y.; Yang, Q.; Zeng, Y.-F.; Wang, X.-L.; Wang, P.-F.; Ruan, Y.-J.; Wen, M.-M.; Zhang, S.-S.; Du, L.d.; Liu, X.-G. Cp*Rh(iii)-Catalyzed Regioselective Cyclization of Aromatic Amides with Allenes. *Chem. Commun*. **2024**, *60*, 598.
31. Baruah, S.; Kaishap, P. P.; Gogoi, S. Ru(II)-Catalyzed C-H Activation and Annulation of Salicylaldehydes with Monosubstituted and Disubstituted alkynes. *Chem. Commun*. **2016**, *52*, 13004.
32. Mayakrishnan, S.; Arun, Y.; Balachran, C.; Awale, S.; Maheswari, N. U.; Perumal, P. T. Ru(II)-Catalyzed Regiospecific C-H/O-H Oxidative Annulation to Access Isochromeno[8,1-*ab*]phenazines: Far-Red Fluorescence and Live Cancer Cell Imaging. *ACS Omega* **2017**, *2*, 2694.
33. Modi, A.; Sau, P.; Chakraborty, N.; Patel, B. K. A "Thiocarbonyl-Directed" Regiospecific C–H/S–H Annulation of Quinoline-4(1*H*)-thiones with Alkynes. *Adv. Synth. Catal*. **2019**, *361*, 1368.
34. Yan, K.; Liu, M.; Wen, J.; Wang, S.; Li, J.; Wang, H. Synthesis of Substituted Naphtho[1,8-*bc*]thiopyrans by Sulfhydryl-Directed Rhodium-Catalyzed peri-Selective C-H Bond Activation and Cyclization of Naphthalene-1-thiols. *Org. Lett*. **2020**, *22*, 7825.
35. Chen, Y.-R.; Duan, W.-L. Silver-Mediated Oxidative C–H/P–H Functionalization: An EfficientRoute for the Synthesis of Benzo[*b*]phosphole Oxides. *J. Am. Chem. Soc*. **2013**, *135*, 16754.
36. Yang, Y.; Li, B.; Liu, W.; Zhang, R.; Yu, L.; Ma, Q.-G.; Lv, R.; Du, D.; Li, T. Cp*CoIII-Catalyzed Synthesis of Pyrido[2′,1′:2,3]pyrimido[1,6-*a*]indol-5-iums via Tandem C–H Activation and Subsequent Annulation from 1-(Pyridin-2-yl)-1H-indoles and Internal Alkynes. *J. Org. Chem*. **2016**, *81*, 11335.

TH-3369_166122017

CHAPTER IB

IB.1. Introduction

In 1912, an Italian chemist Prof. Giacomo Ciamician in his article "The photochemistry of the future" discover that light has the potential to be utilized as a green energy for chemical synthesis.[1] Now his predictions have come true in the modern era with the remarkable development of various technologies that harness the power of light for different transformations. Although the journey was not so easy, on the initial days the scientists faced major obstruction as the most common organic molecules are found to be incapable of absorbing the visible-light wavelength, which is most abundant in the solar spectrum. The requisition of high-intensity UV light for the photochemical transformations was the major hurdle. To combat these issues, photo-catalysts were introduced, which absorb the photon of light and transfer its energy in the form of an electron to the reacting substrates. Based on the mechanistic aspects, the photocatalysis has mainly fragmented into four sections-

(1) *Photoredox Catalysis (via single electron transfer)*
(2) *Energy Transfer Catalysis (EnT) (via triplet energy transfer)*
(3) *Electron Donor-Acceptor Complexation (via inter or intramolecular charge-separation)*
(4) *Direct Photo-Excitation (photochromic substrates)*

IB.2. Classification of Different Modes of Photo-Catalytic Strategies

IB.2.1. Photoredox Catalysis

Over the past few decades, photoredox catalysis has gained enormous gratitude from all over the globe for its involvement in the preparation of fine chemicals, medicinal drugs, novel solar cell materials, and numerous functional group installations into organic molecules.[2] Nowadays this section of photochemistry is getting huge admiration for offering mild, environmentally benign, and operationally simple reaction protocols.[3] Mainly photoredox catalytic operations are based on transition metal-based photo-catalysts (Ru, Ir, etc.)[4] and some metal-free organic dyes[5] (eosin y, rose bengal, methylene blue, acridinium salts, etc.), which are summarized in Figure IB.2.1.

TH-3369_166122017

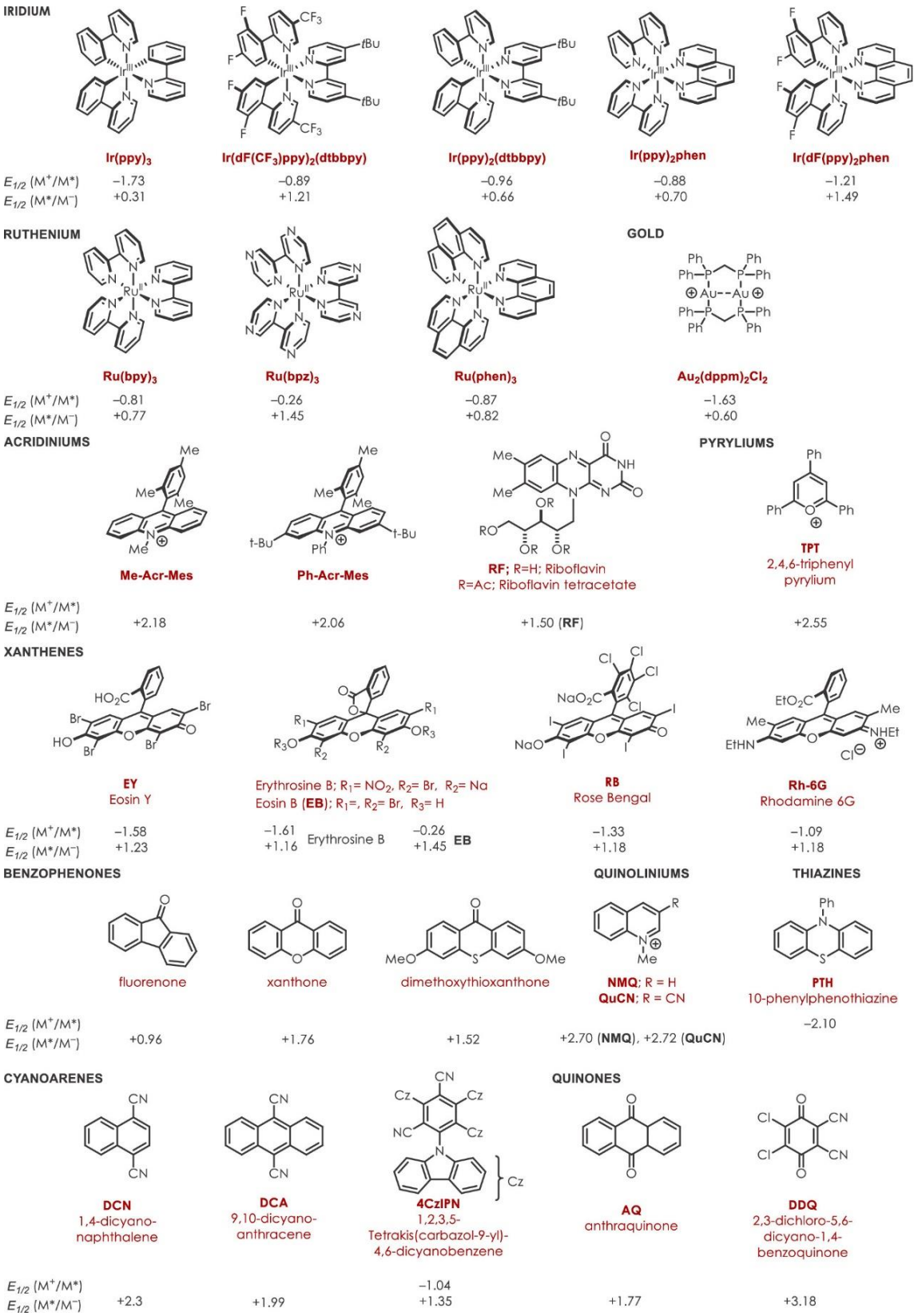

Figure IB.2.1. *Examples of photoredox catalysts and their excited-state redox values (vs SCE). Reproduced with permission from ref (4c). Copyright 2021 American Chemical Society*

TH-3369_166122017

Typically, a metal or metal-free photocatalyst (**PC**) absorbs visible light and gets excited to **PC***. Then depending on the redox properties of reacting substrates, two consecutive single electron transfers (SET) take place between donor components (**D**) and acceptor components (**A**). If these two consecutive SETs start by gaining electrons from the donor (**D**), it is termed reductive quenching; if it starts with a release of electrons, it is termed oxidative quenching (Figure IB.2.2).

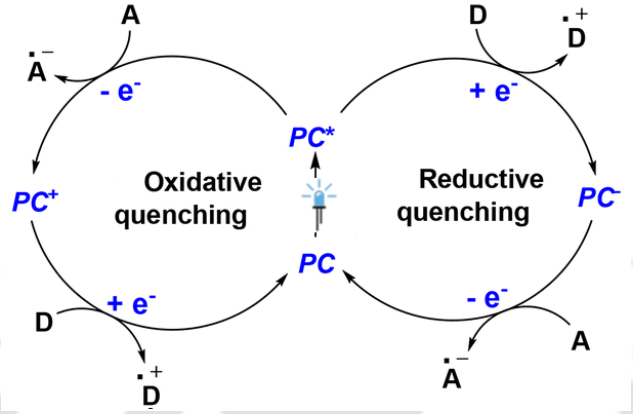

Figure IB.2.2. *Photoredox catalysis*

IB.2.1.1. Early Precedents of Photoredox Catalysis

The demonstration of photoredox catalysis to organic synthesis was commenced in 1978 by Kellogg. The first photo-induced reduction of sulfonium salt to the corresponding alkene was reported by Kellogg *et al.* (Scheme IB.2.1).[6] This photo-induced desulfuration reaction was carried out in the presence of $[Ru(bpy)_3]Cl_2$ photocatalyst and terminal reductant 1,4-dihydropyridines.

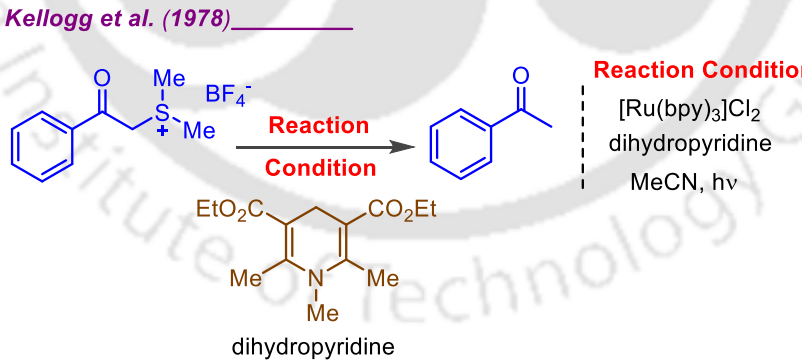

Scheme IB.2.1. *Photo-induced reduction of sulfonium salt*

Subsequently Pac and co-workers reported photo-reduction of electron-deficient alkenes by using the same catalyst $[Ru(bpy)_3]Cl_2$ and 1-benzyl-1,4-dihydronicotinamide (BNAH) reductant (Scheme IB.2.2).[7]

TH-3369_166122017

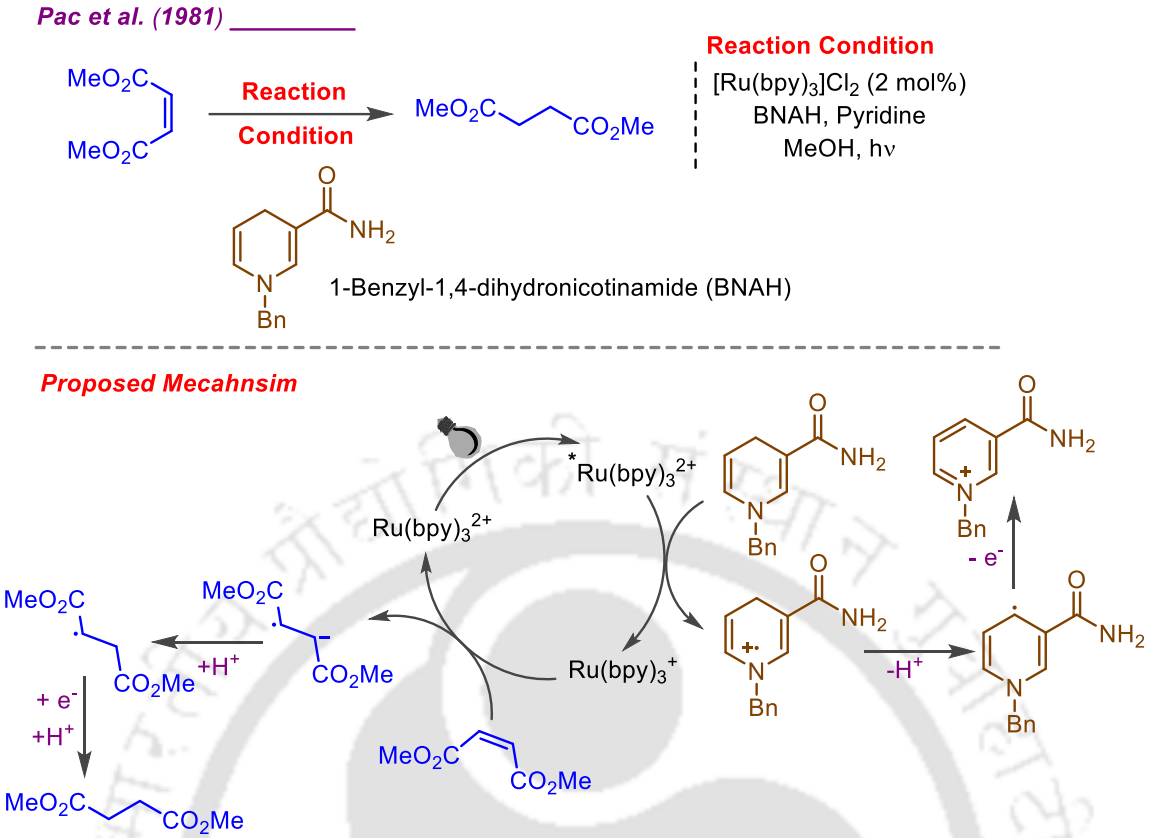

Scheme IB.2.2. *Photo-induced reduction of electron-deficient alkenes*

In the year of 1984, Deronzier described a $[Ru(bpy)_3]Cl_2$ photocatalyzed Pschorr reaction to synthesize a series of phenanthrene scaffolds (Scheme IB.2.3).[8]

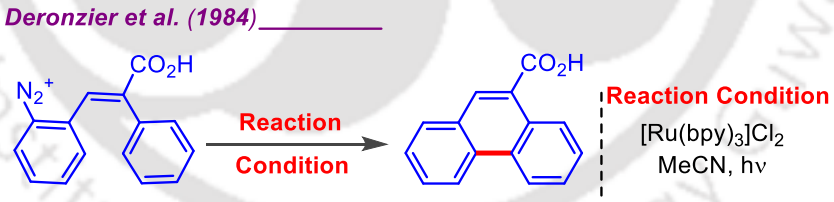

Scheme IB.2.3. *Photo-induced* Pschorr reaction

IB.2.1.2. Modern Advent of Photoredox Catalysis

Although the year of 1980s and 1990s witnessed some seminal photoredox catalysis applications towards organic synthesis, dramatically this field was amplified through the three reports, published during 2008 to 2009.

TH-3369_166122017

In the year of 2008, Yoon and co-workers reported a photo-induced intramolecular [2+2] cycloaddition reaction of bisenone (Scheme IB.2.4).[9] In this report, Lewis acid was used to modulate the reactivity of the bisenone substrate.

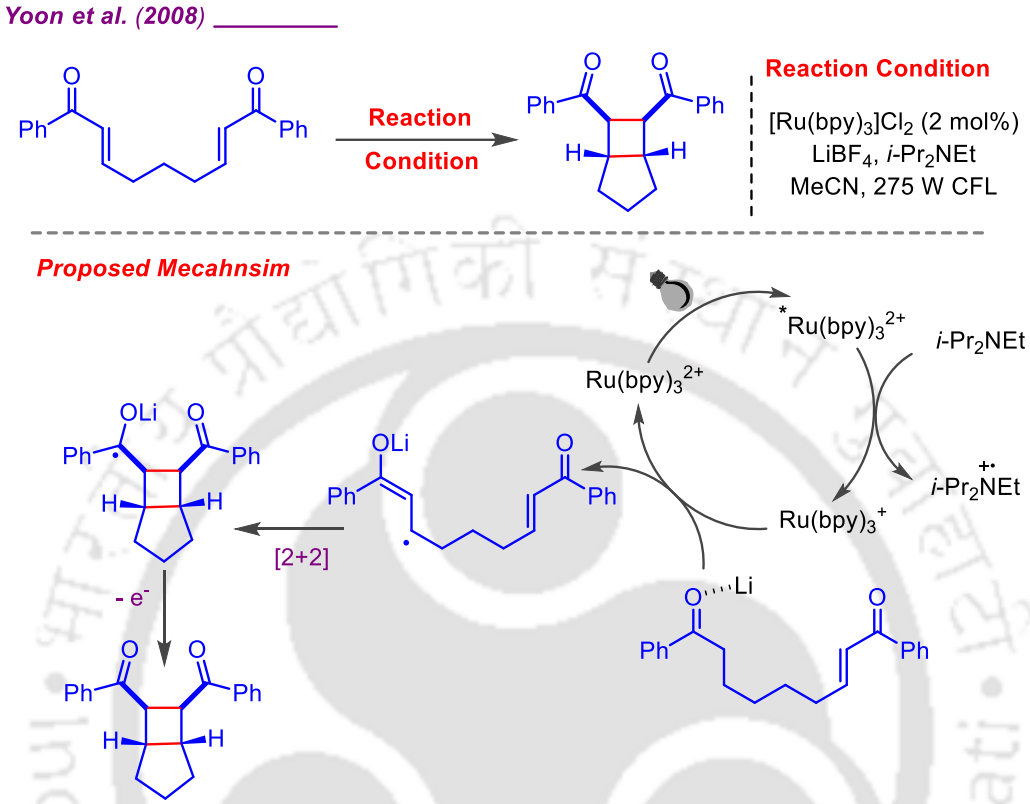

Scheme IB.2.4. *Photo-induced [2+2] cycloaddition of bisenone*

In the same year, MacMillan *et al.* disclosed a dual photoredox organocatalyzed enantioselective alkylation of aldehydes (Scheme IB.2.5).[10] This seminal report offered access to electron-deficient radical which can further enantioselectively add to the *in situ* generated enamines.

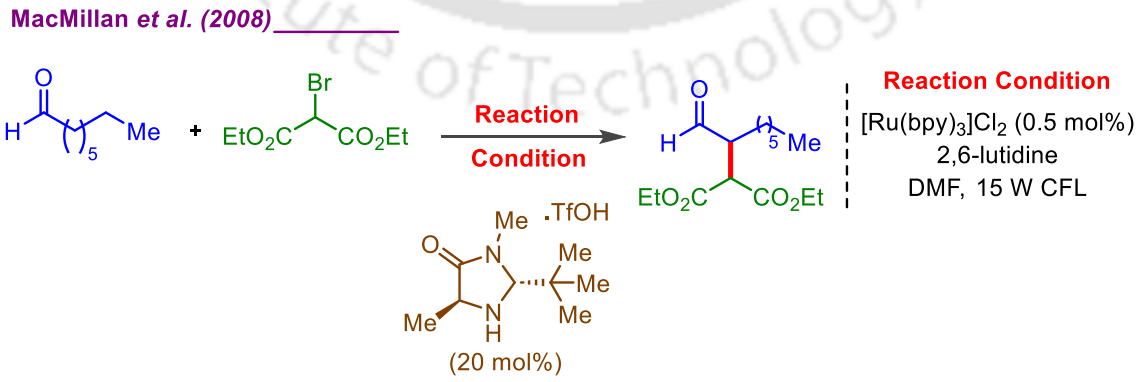

Scheme IB.2.5. *Dual photoredox organocatalyzed asymmetric alkylation of aldehyde*

TH-3369_166122017

Later Stephenson group demonstrated a photoredox catalyzed reductive cleavage of alkyl halides (Scheme IB.2.6).[11] This report includes a broad range of alkyl halides and offers an alternative to the prior toxic tin-catalyzed reductive dehalogenation.

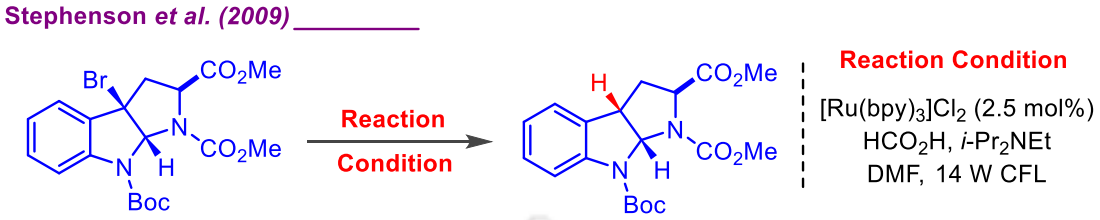

Scheme IB.2.6. *Photoredox catalyzed reductive dehalogenation*

IB.2.2. Energy Transfer (EnT) Catalysis

Organic substrates having incompatible redox potentials with the excited photo-catalysts cannot undergo SET path. To encounter these incompatibility issues, the triplet energy transfer (EnT) has emerged as an alternative to photo-redox catalysis.[12] In this process, the photo-excited triplet sensitizer transfers its triplet energy to one of the reacting substrates (Figure IB.2.3). Following this, the activated triplet species reacts with the other reacting partners to generate a complex molecular entity.

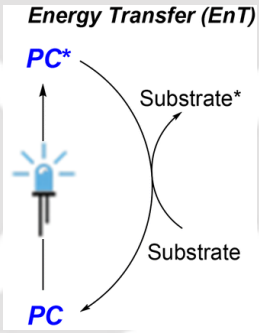

Figure IB.2.3. *Photo-induced energy transfer catalysis*

IB.2.2.1. Triplet Photosensitizer

As this energy transfer transformations are governed by the use of suitable photosensitizers. So there are some salient requirements for choosing these photosensitizers.

(a) The used photosensitizer should possess a higher triplet energy **(E_T)** than that of the reacting substrate. Furthermore, this triplet energy should be close to the substrate. Triplet energies of commonly used photosensitizers are summarized in Figure IB.2.4.

(b) The sensitizers should have high inter-system crossing efficiency.

(c) Also they should possess a long-lived triplet state.

TH-3369_166122017

(d) Throughout the reaction they should remain unreactive.

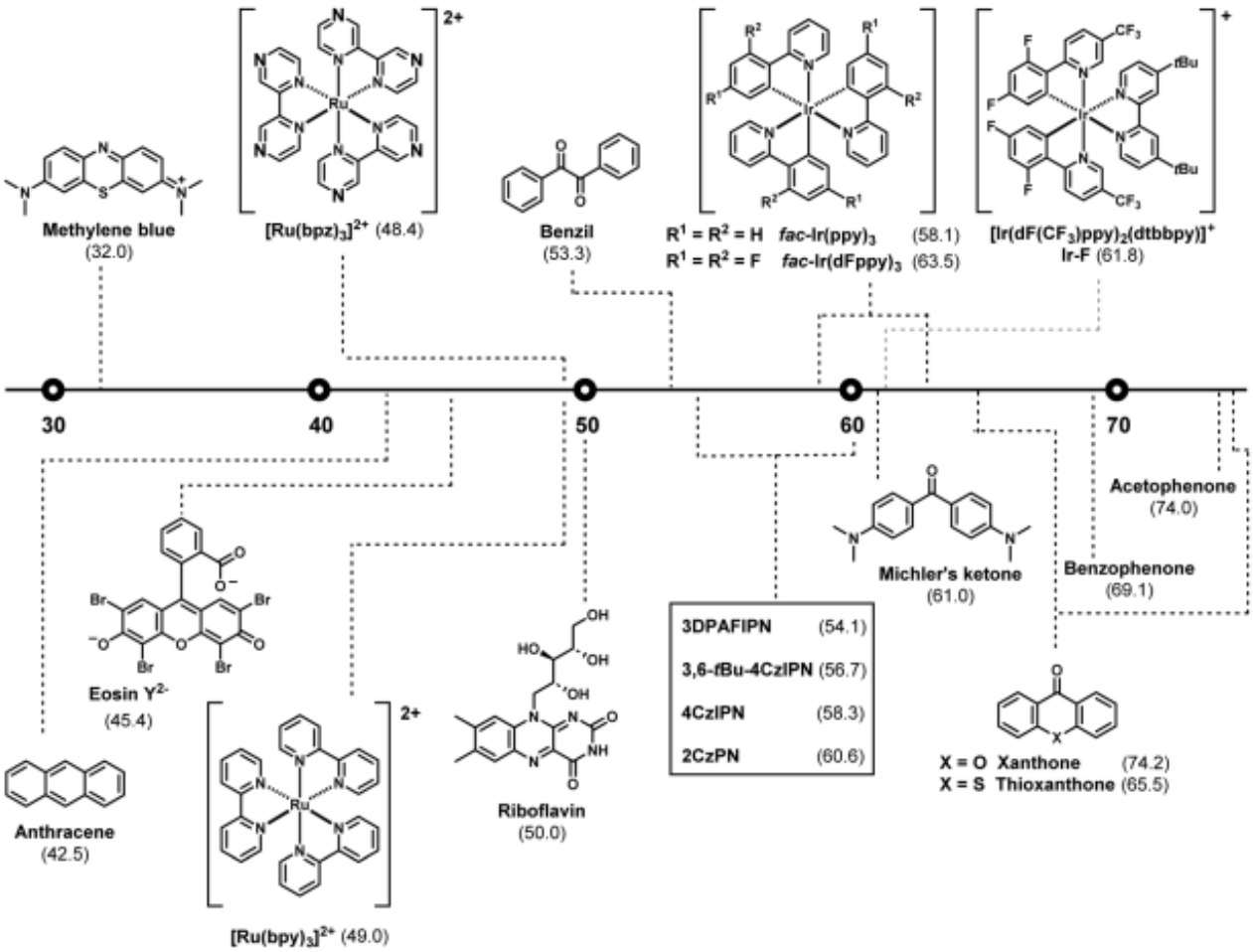

Figure IB.2.4. *Examples of triplet photosensitizers and their triplet energies in K Cal mol^{-1}. Reproduced with permission from ref (12d). Copyright The Royal Society of Chemistry 2024*

IB.2.2.2. Triplet-Triplet Energy Transfer Mechanism

In most of the triplet energy transfer reactions, the reacting substrate cannot absorb the visible light, thus the energy transfer (EnT) takes place non-radiatively. Two different mechanisms are proposed for this non-radiative EnT, Forster energy transfer (*via* dipole-dipole interaction) and Dexter energy transfer (*via* exchange or collision interaction). In the Forster energy transfer process, energy can be transferred through the transmitter-antenna mode. Where electronic oscillation in excited **D*** induces a dipole which is exchanged with the acceptor (**A**) through the Coulombic interaction (Figure IB.2.5). This mechanism violates Wigner's spin conservation rule, so EnT cannot be described by the Forster energy transfer mechanism. Whereas Dexter theory demonstrates the energy transfer *via* the simultaneous electron exchange from excited donor D* (or photosensitizer) to the

TH-3369_166122017

ground state of acceptor or reacting substrate **A** and *vice versa* (Figure IB.2.5). Thus this energy transfer is spin-allowed as the overall multiplicity remains unchanged.

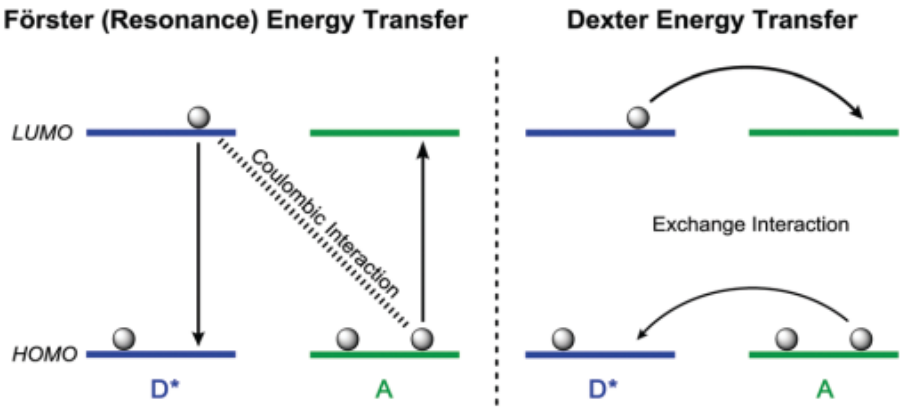

Figure IB.2.5. *Energy transfer mechanism. Reproduced with permission from ref (12a). Copyright The Royal Society of Chemistry 2018*

IB.2.2.3. Advancement of Triplet-Triplet Energy Transfer (EnT)

Excited state-involved triplet energy transfer catalysis efficiently offers various photochemical transformations including cycloaddition, homolytic σ-bond cleavage, strain-releasing cyclization, isomerization and deracemization.

❖ Cycloaddition

Photochemically-induced cycloaddition reactions mainly [2+2] cycloadditions have been extensively scrutinized using triplet energy transfer process. In [2+2] cycloaddition reaction, two olefins are combined to synthesize cyclic complex molecular entities. In this type of photo-cycloaddition, one of the olefins (**I**) gets excited to its triplet state (**II**) by absorbing the triplet energy from the photosensitizer (**PC**), following this a radical addition took place to the other olefins unit (in its ground state) to form a triplet intermediate (**III**) (Figure IB.2.6). Later it undergoes ISC and then the radical-radical combination gives the cycloadduct (**V**).

TH-3369_166122017

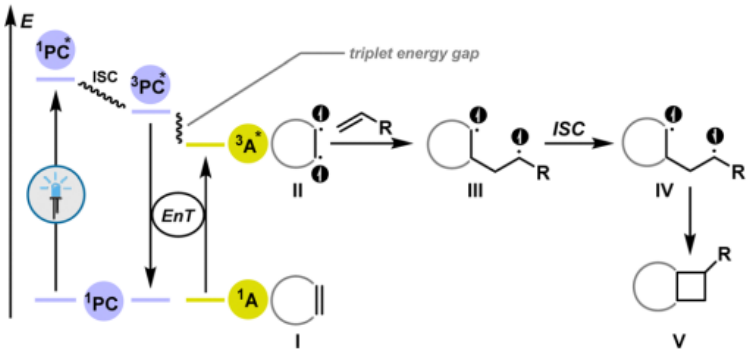

Figure IB.2.6. *General mechanism of cycloaddition reaction via EnT. Reproduced with permission from ref (12d). Copyright The Royal Society of Chemistry 2024*

In 2017, Kwon group introduced a EnT catalysed photo-induced crossed [2+2] cycloaddition of dienones (Scheme IB.2.7).[13] This intramolecular cycloaddition reaction offered access to a series of bridged cyclobutane scaffolds in a single step. Furthermore, the diversified form of this bridged cyclobutane can be utilized for the development of known therapeutic potential candidates for inflammatory disease and cancer.

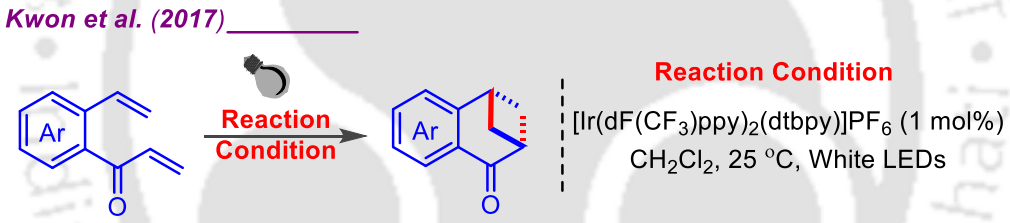

Scheme IB.2.7. *EnT-enabled crossed [2+2] cycloaddition*

In the year of 2022, Brown *et al.* reported a EnT-enabled dearomative para selective-cycloaddition of quinolones with various activated and non-activated alkenes (Scheme IB.2.8).[14] A detailed mechanistic studies suggest the involvement of photosensitization of Lewis acid-quinoline adduct to afford 3D-complex molecular scaffolds. In the same year, they introduced an interesting [2+2] cycloaddition of alkenylboronates with alkenes in the presence of triplet sensitizer *fac*-Ir(ppy)$_3$ (Scheme IB.2.9).[15]

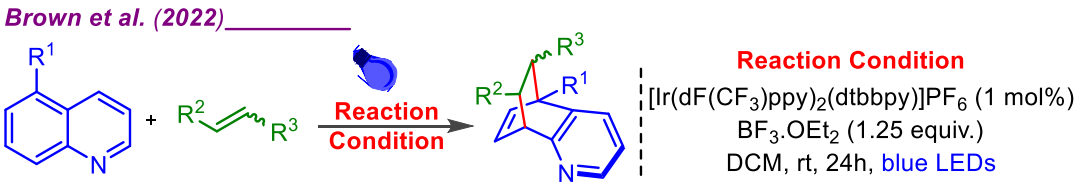

Scheme IB.2.8. *EnT-enabled dearomative cycloaddition of quinoline with alkene*

TH-3369_166122017

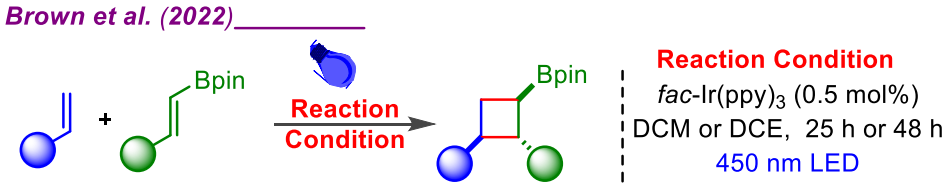

Scheme IB.2.9. *Photosensitized [2+2] cycloaddition of alkenylboronates and alkenes*

❖ Homolytic σ-bond cleavage

In 2018, the Glörius group described a triplet energy transfer enabled disulfide-ene reaction between alkyl or aryl disulfides and electron-rich alkenes (Scheme IB.2.10).[16] In this reaction, $[Ir(dF(CF_3)ppy)_2(dtbpy)]PF_6$ photosensitizer transfers its triplet energy (E_T = 61.8 kcal mol^{-1}) to disulfides to generate thiyl radicals *via* homolytic σ-bond cleavage which further add to alkenes to afford anti-Markovnikov adduct.

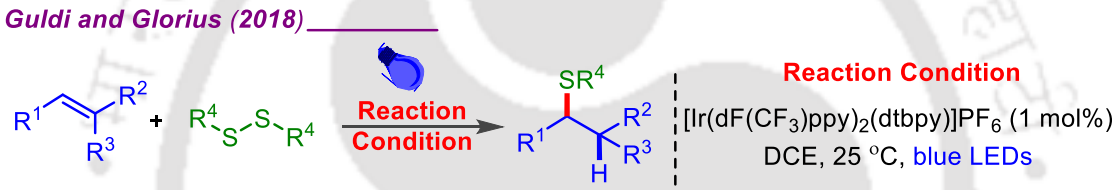

Scheme IB.2.10. *EnT-enabled disulfide-ene reaction*

❖ Strain-releasing cyclization

Brown *et al.* demonstrated a strain-release driven photo-induced synthesis of bicyclo[2.1.1]hexanes (Scheme IB.2.11).[17] This [2π+2σ] cycloaddition reaction proceeds through the 2,2'-dimethoxy thioxanthone (2,2'-OMeTX) sensitized triplet energy transfer pathway.

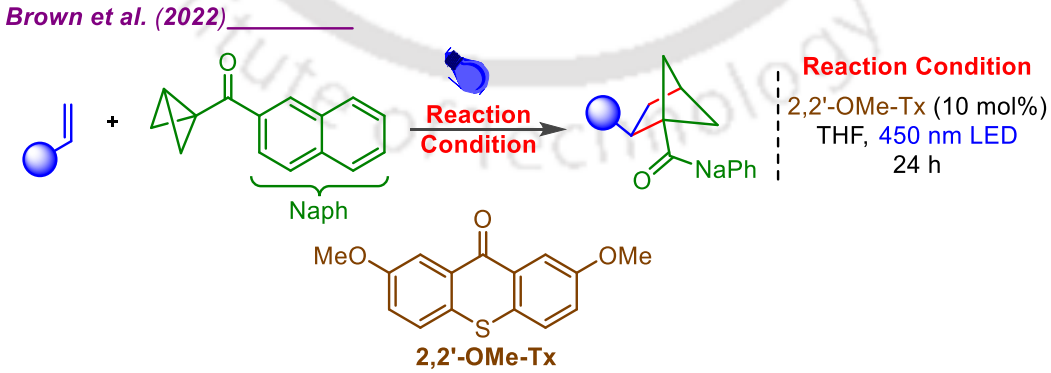

Scheme IB.2.11. *EnT-enabled photosensitized strain-releasing [2π+2σ] cycloaddition*

TH-3369_166122017

❖ **Isomerization**

Triplet-triplet energy transfer enabled photo-isomerization of substituted olefins has also been well investigated. Recently a thioxanthone sensitized EnT-enabled photo-induced geometrical isomerization (*Z* to *E*) of alkenyl fluorides has been demonstrated by Gilmour and co-workers (Scheme IB.2.12).[18]

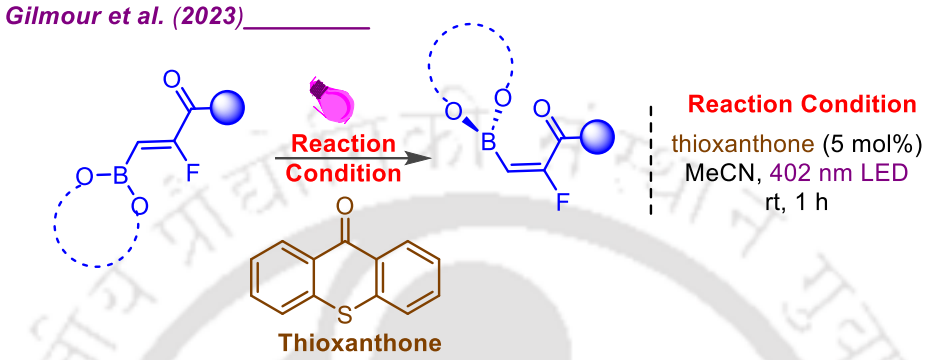

Scheme IB.2.12. *EnT-enabled photo-induced geometrical isomerization*

❖ **De-racemization**

In 2019, Bach group disclosed a chiral thioxanthone sensitized de-racemization of cyclopropane ring of cyclic amide (Scheme IB.2.13).[19] Mechanistic studies suggest the triplet-sensitizer sensitized ring-opening of cyclopropane ring attributed to the de-racemization.

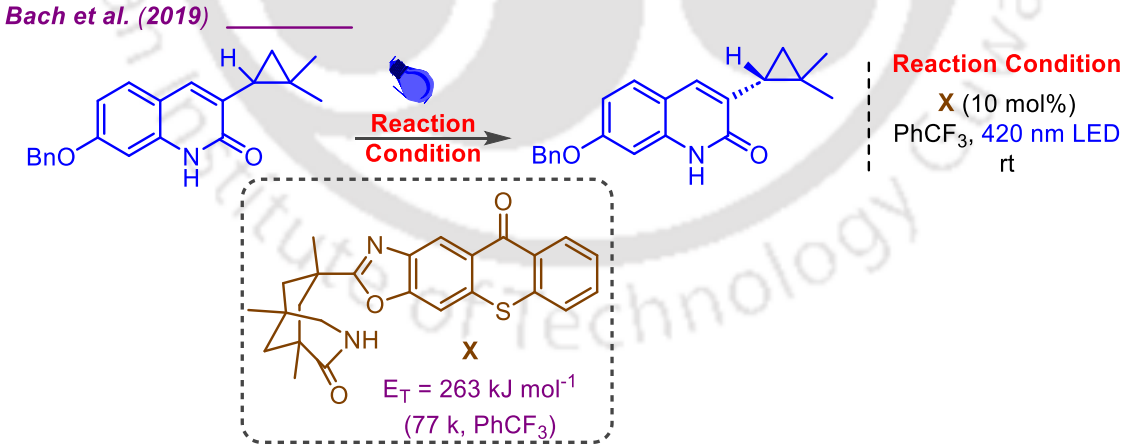

Scheme IB.2.13. *EnT-enabled photosensitized de-racemization of cyclopropyl scaffolds*

TH-3369_166122017

IB.2.3. Electron Donor-Acceptor (EDA) Complexation-enabled Catalysis

Despite having significant efficacy, such metal photo-catalysts (Ru and Ir) are too expensive and toxic, which restricts them to be utilized for the synthesis of medicinal feedstock. In the past few years, researchers are showing immense attention to photo-induced electron donor-acceptor (EDA) complexation-enabled photochemical approaches.[20] This approach is intrinsically different from redox photocatalysis, as it does not require any involvement of exogenous redox catalysts. This EDA complex was introduced by Muliken, defined as a non-covalent interaction.[21] In this strategy, a good electron donor (**D**) and a good electron acceptor (**A**) substances aggregate together to form a colored molecular aggregation in the ground state which is known as an electron donor–acceptor (EDA) complex. Surprisingly, before complexation individually both the substances may not absorb visible light but their aggregated EDA complex does. Upon visible light irradiation on EDA complex, an intramolecular electronic charge transfer occurred from donor to acceptor to deliver radical ion pair as $\mathbf{D}^{+\bullet}$ and $\mathbf{A}^{-\bullet}$. Then the coupling of these radicals gives the complex organic molecules (Figure IB.2.7).

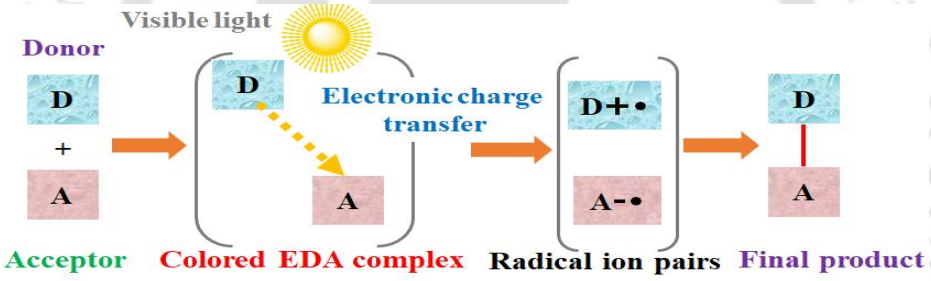

Figure IB.2.7*. General photoactivity of EDA complexes for radical generation*

IB.2.3.1. Recent Advent of EDA Complexation

IB.2.3.1.1. Photo-induced intramolecular radical cyclization

In the year of 2015, Paixão and co-workers reported a photo-catalyst free visible light irradiated reductive intramolecular cyclization for the synthesis of indoles (Scheme IB.2.14a) and oxindoles (Scheme IB.2.14b).[22]

TH-3369_166122017

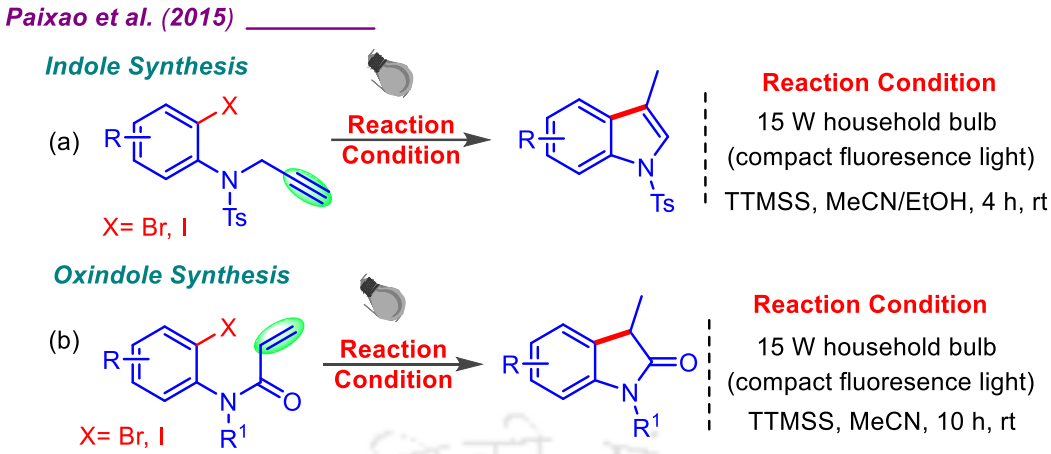

Scheme IB.2.14. *Intramolecular reductive cyclization for synthesis of indoles (**a**) and oxindoles (**b**)*

A visible light-induced photo-catalyst free synthesis of phenanthridines and quinolines from O-2,4-dinitrophenyl oximes was reported by Yu and co-workers in 2018.[23] In this report, trimethylamine acted as a donor to initiate the EDA complexation with O-aryl oximes which forms an *N*-centered iminyl radical to promote the intramolecular cyclization (Scheme IB.2.15).

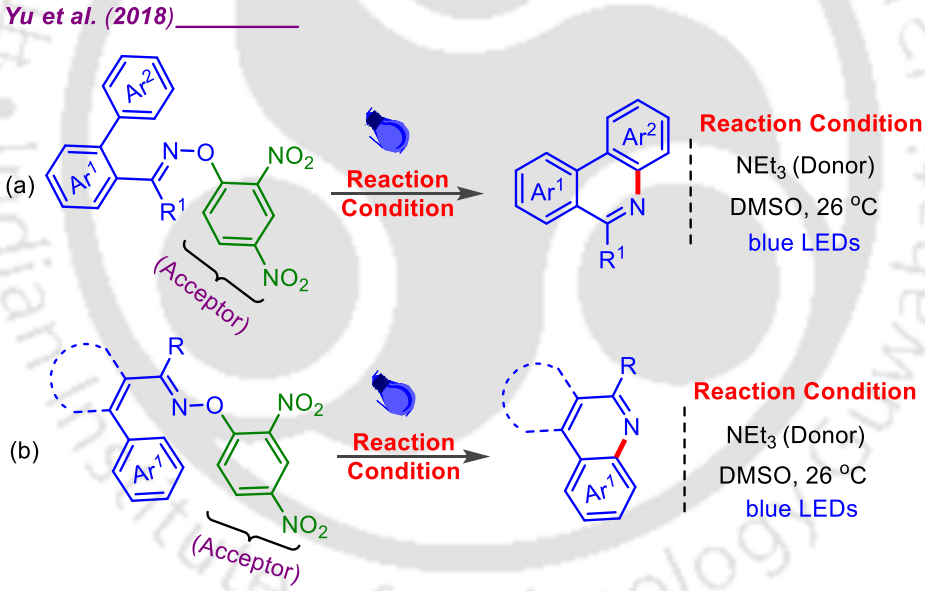

Scheme IB.2.15. *Intramolecular iminyl radical cyclization for synthesis of phenanthridines (**a**) and quinolines (**b**)*

In the same year, pioneering work by You and co-workers demonstrated visible light promoted an intramolecular dearomative cascade cyclization of indole derivatives *via* EDA complexation (Scheme IB.2.16).[24]

TH-3369_166122017

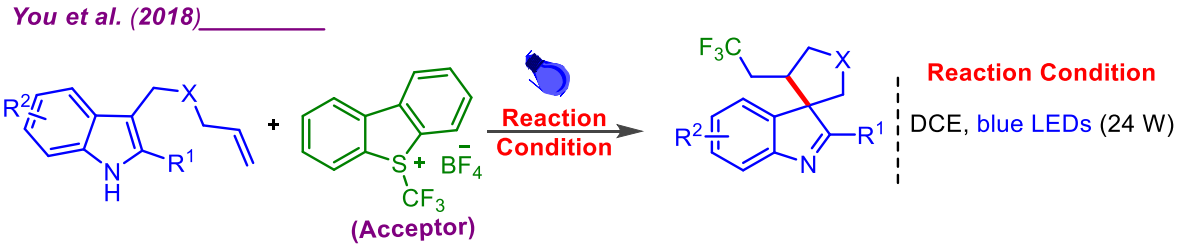

Scheme IB.2.16. *Intramolecular EDA complex involved dearomatization of indoles*

An elegant metal-free *N*-centered radical based iminohydroxylated cyclization reaction protocol was developed by Leonori and co-workers (Scheme IB.2.17).[25]

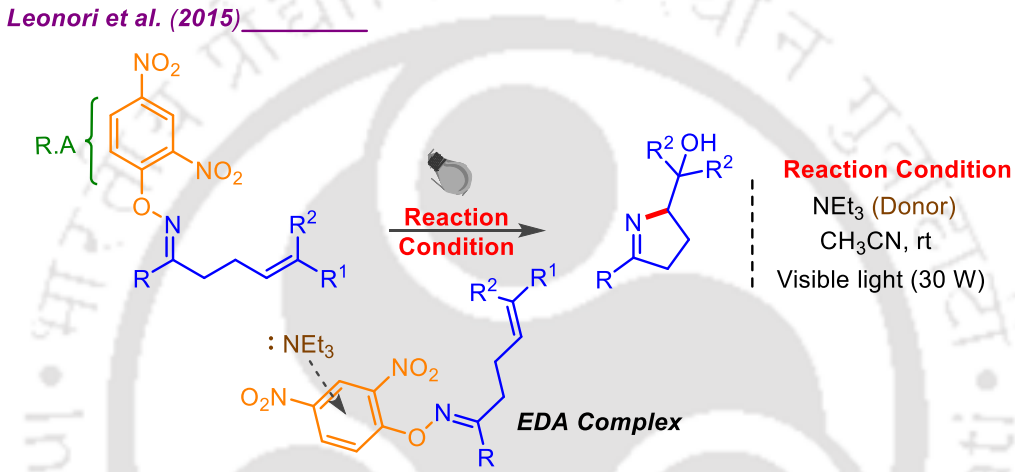

Scheme IB.2.17. *Intramolecular iminohydroxylated cyclization driven by EDA complex*

An excellent photo-catalyst free photo-induced C(sp^2)–Cl cleavage followed by a reductive intramolecular Heck-type cyclization to accesses fused indoles was introduced by Che *et al.* (Scheme IB.2.18). The mechanistic studies reveal the presence of intramolecular electron transfer between indole and DIPEA.[26]

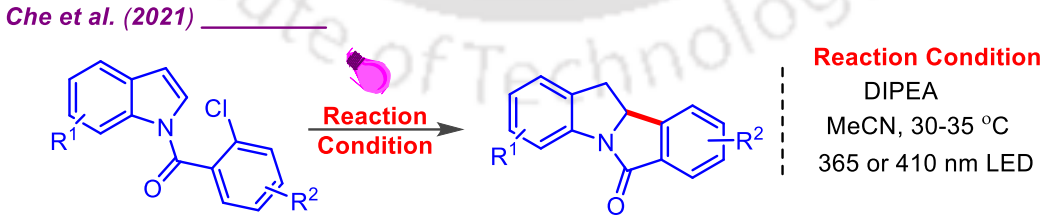

Scheme IB.2.18. *Intramolecular reductive Heck cyclization*

In a Similar fashion, Yang and co-workers reported a photo catalyst free visible light induced intramolecular cyclization of 4-phenylsulfonyl-2,3,5,6-tetrachloropyridine through the cleavage of

TH-3369_166122017

C(sp^2)–Cl to promote benzo-thiopyridines (Scheme IB.2.19). It was found that a charge transfer complex between carbonate and 4-phenylsulfonyl-2,3,5,6-tetrachloropyridine is crucial for this intramolecular cyclization.[27]

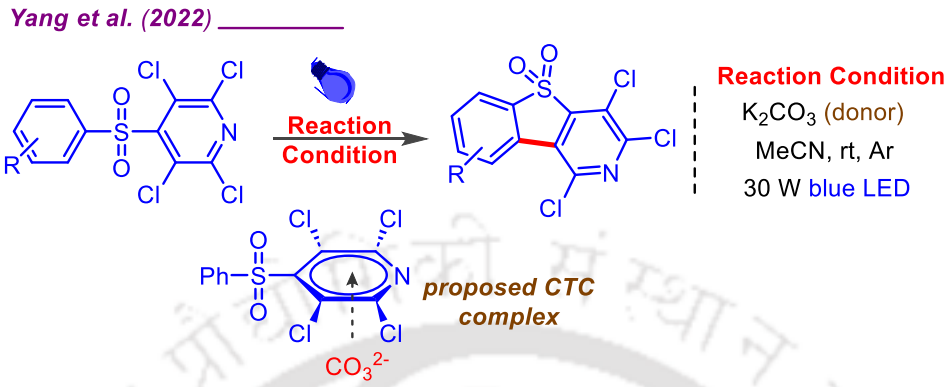

Scheme IB.2.19. *Intramolecular dechlorinated cyclization*

Last year a pioneering photo-induced intramolecular cyclization was introduced by Li group (Scheme IB.2.20). The dehalogenative cyclization to 2-aryl benzothiazoles was achieved under photo-catalyst free visible light irradiated protocol through intramolecular charge transfer from sulfur end to C–Br bond.[28]

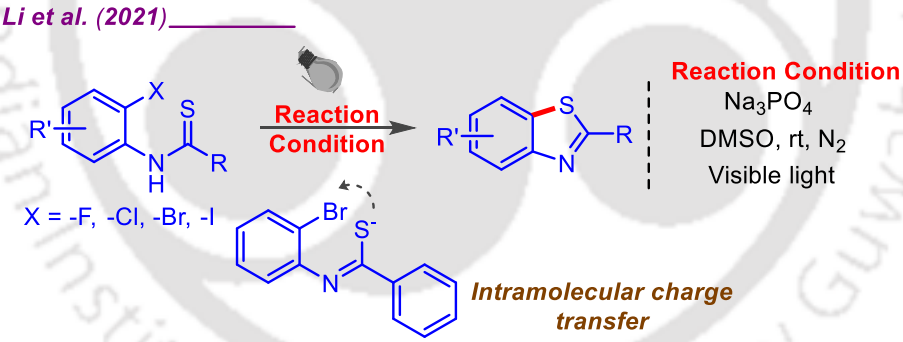

Scheme IB.2.20. *Intramolecular EDA complex enabled dehalogenative cyclization.*

In the same year, Jin group developed a photo-catalyst free visible light induced tandem radical cyclization followed by C–H arylation reaction between 2-amino-1,4-naphthoquinone and *N*-allyl-2-bromo-2,2-difluoroacetamides (Scheme IB.2.21). This reaction is found to be driven by the formation of EDA complex between amine and *N*-allyl-2-bromo-2,2-difluoroacetamides.[29]

TH-3369_166122017

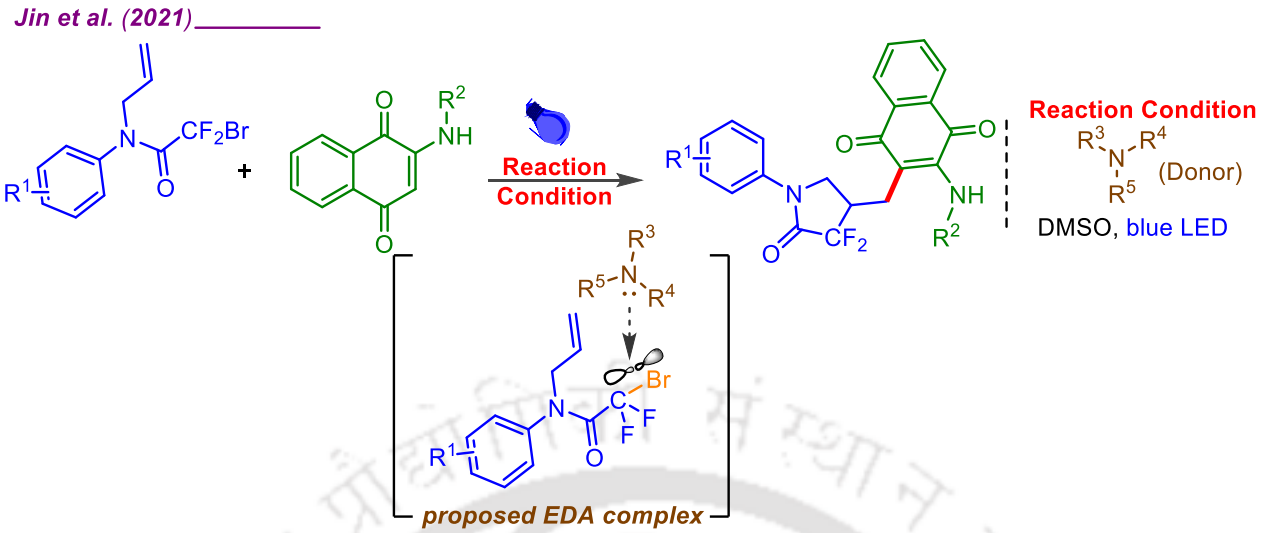

Scheme IB.2.21. *EDA complex enabled tandem cyclization*

IB.2.3.1.2. Photo-induced intermolecular radical cyclization

In the year of 2018, Sunden group described the photocatalyst free oxidative coupling of maleimides with dialkylamines to generate tetrahydroquinolines (Scheme IB.2.22).[30]

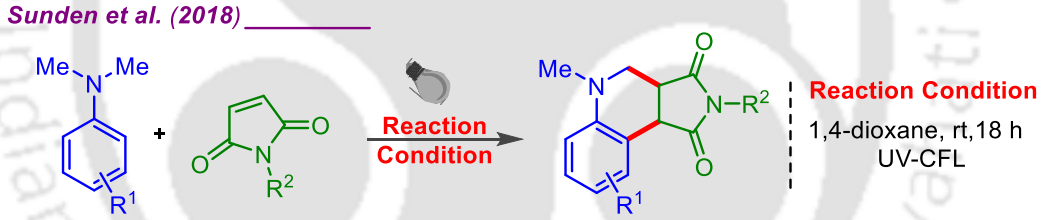

Scheme IB.2.22. *EDA complex driven intermolecular cyclization*

Similarly, in 2020 the same group demonstrated a photocatalyst-free visible light induced stereoselective annulation alkenes and *N*, *N*-substituted dialkyl anilines to access tetrahydroquinolines (Scheme IB.2.23).[31]

TH-3369_166122017

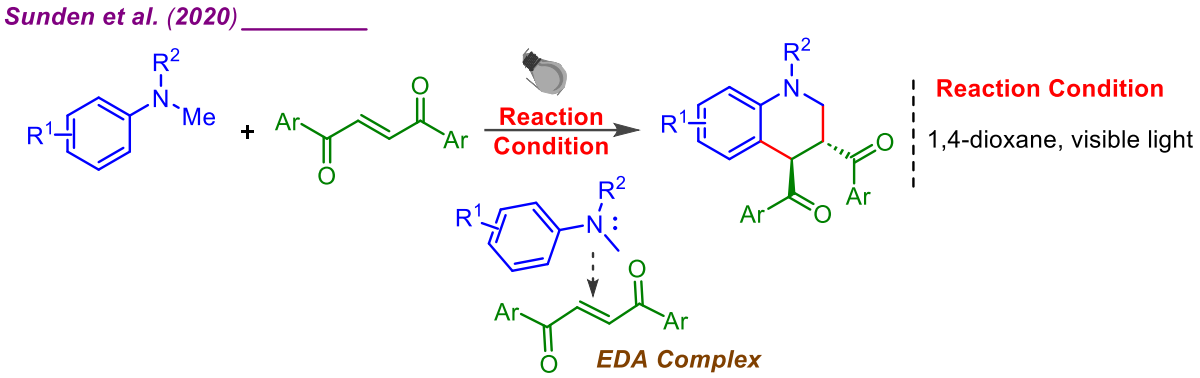

Scheme IB.2.23. *EDA complex driven stereoselective cyclization*

IB.2.3.1.3. Photo-induced C–H functionalization

In the year of 2020, Zhang group demonstrated a visible light-driven α-alkylation of *N*-aryl tetrahydroisoquinolines enabled by EDA complex between amine and *N*-aryl tetrahydroisoquinolines (Scheme IB.2.24).[32]

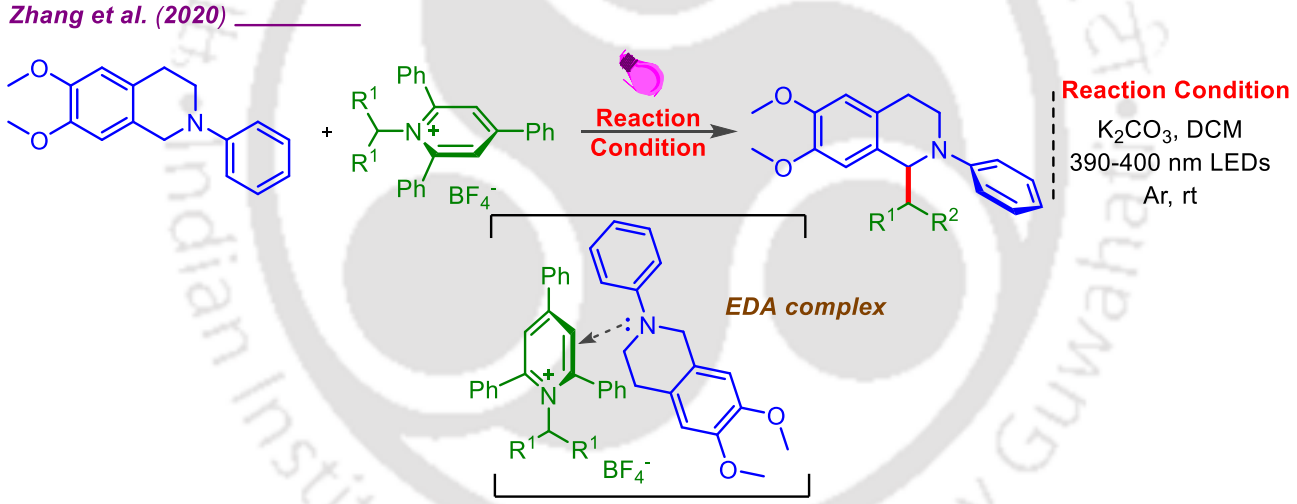

Scheme IB.2.24. *EDA complex assisted α-alkylation of N-aryl tetrahydroisoquinolines.*

A pioneering photocatalyst-free visible-light induced *α*-amino C−H bond arylation protocol was established by Jin group (Scheme IB.2.25). This reaction was found to be driven by the EDA complex formed between electron rich tertiary amines and electron deficient benzonitriles.[33]

TH-3369_166122017

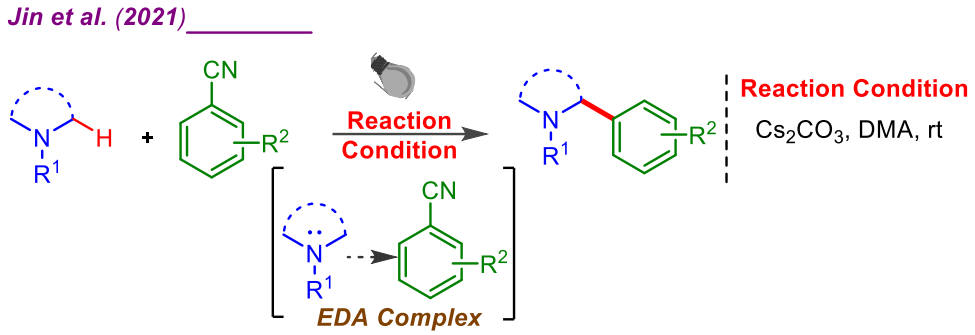

Scheme IB.2.25. *EDA complex-driven α-amino C−H bond arylation*

In the year of 2021, Barham and co-workers reported a solvent-caged EDA complex enabled photocatalyst-free visible-light mediated C(sp^3)–H arylation of amides. The EDA complex was observed between electron rich arene and electron deficient persulfate oxidant (Scheme IB.2.26).[34]

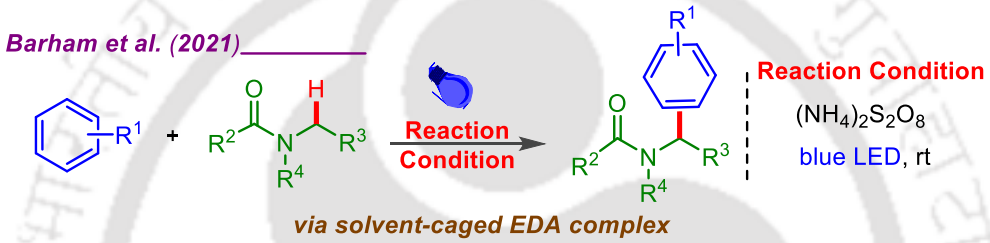

Scheme IB.2.26. *Solvent-caged EDA complex driven C(sp^3)-H arylation of amides*

Yang and coworkers reported a catalyst free visible light promoted protocol for the regioselective sulfonation of alkyl α-trifluoromethylstyrenes with sodium sulfinates enabled by charge transfer complex between sulfinate and oxygen (Scheme IB.2.27).[35]

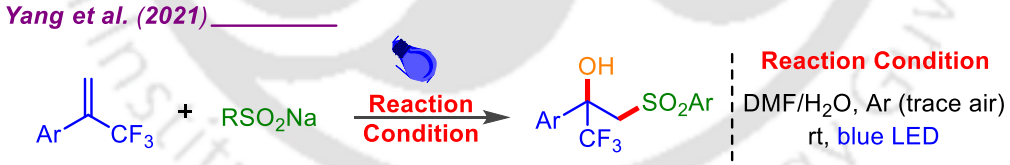

Scheme IB.2.27. *regioselective sulfonation of alkyl α-trifluoromethylstyrenes*

In the same year, the group proposed a visible light mediated regioselective hydroxydifluoroalkylation of alkenes with alkyl bromides *via* EDA complexation (Scheme IB.2.28).[36]

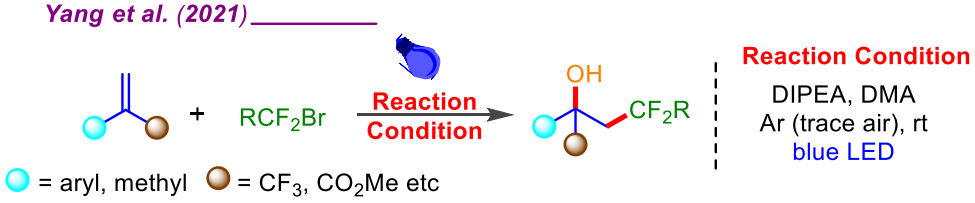

TH-3369_166122017

Scheme IB.2.28. *Regioselective sulfonation of alkyl α-trifluoromethylstyrenes*

Sun and co-workers reported a photocatalyst free visible light induced dehydrogenative sulfonylation of tertiary amines with thiosulfonates (Scheme IB.2.29). This reaction was carried out through the formation of EDA complex.[37]

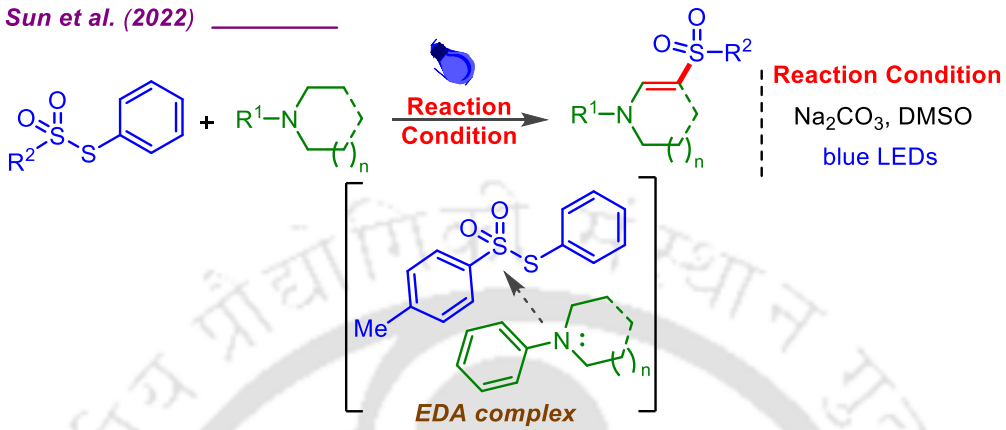

Scheme IB.2.29. *EDA complex enabled dehydrogenative sulfonylation*

Recently, Song group demonstrated a photocatalyst-free visible light driven decarboxylative alkylation of pyridinaldehydes through the EDA complexation between amine and active esters (Scheme IB.2.30).[38]

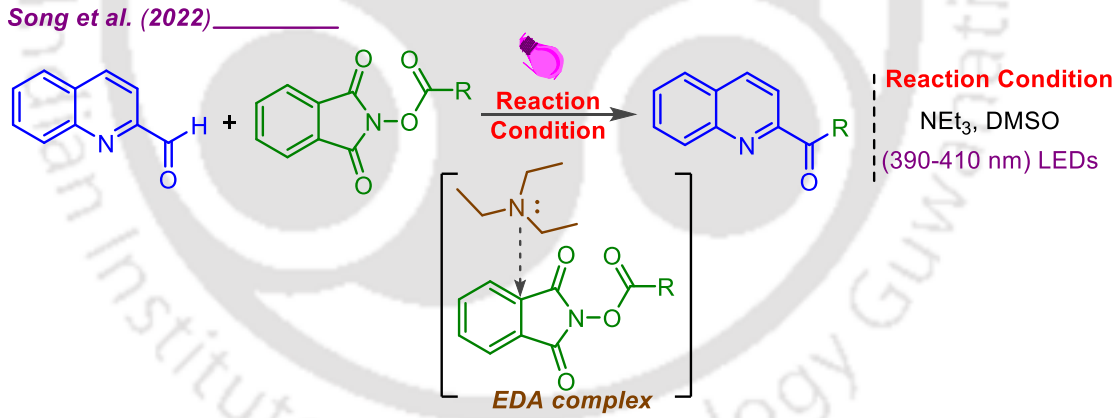

Scheme IB.2.30. *EDA complex enabled decarboxylative alkylation of pyridinaldehydes*

Similarly, He group developed a catalyst-free decarboxylative process for the synthesis of secondary trifluoromethylated alkyl bromides through the formation of an EDA complex between an activated ester and a Hantzsch ester (Scheme IB.2.31).[39]

TH-3369_166122017

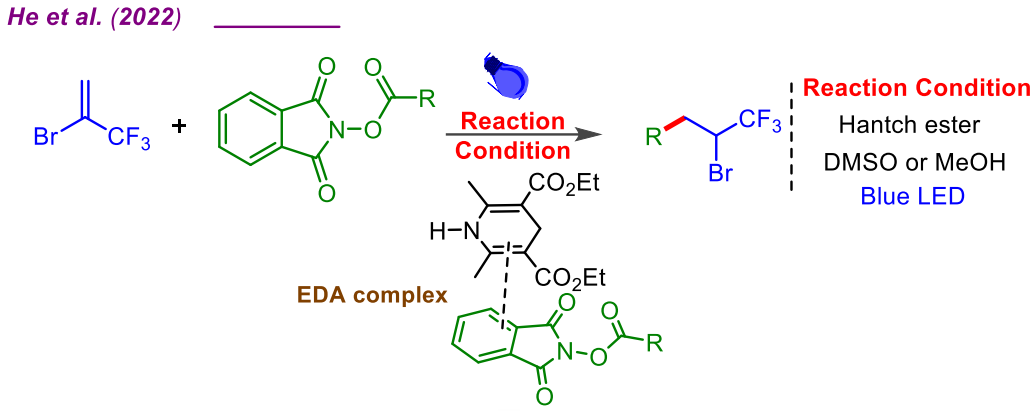

Scheme IB.2.31. *EDA complex enabled decarboxylative alkylation of alkene*

IB.2.3.1.4. Photo-induced three component reaction

Recently, Yu group demonstrated a visible light induced photocatalyst free three component radical cascade bicyclization to afford difluoroamidosulfonylated dihydrobenzofurans (Scheme IB.2.32).[40]

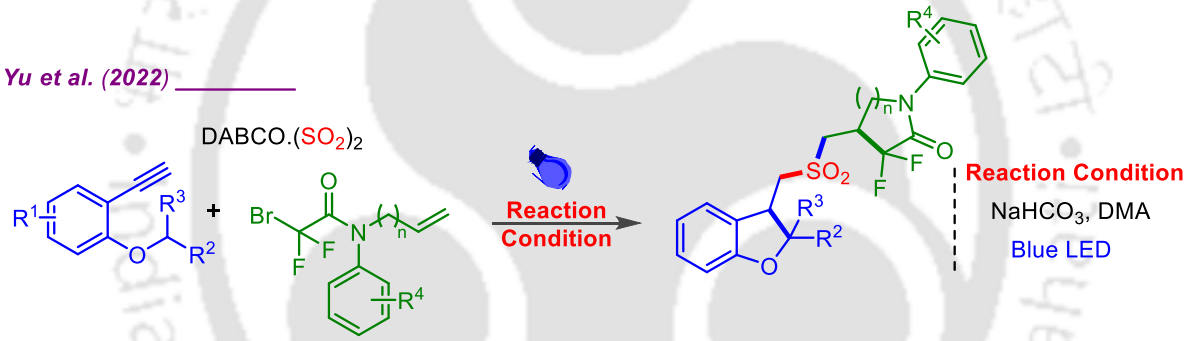

Scheme IB.2.32. *EDA complex enabled three component cascade bicyclization.*

In 2022, an excellent visible-light-induced three-component sulfonyl-heteroarylation of vinyl ethers with sulfinates and five-membered heteroaryl chlorides was introduced by Chu and co-workers. This reaction protocol was driven by electron-donor-acceptor (EDA) complexes between sulfinates and heteroaryl chlorides (Scheme IB.2.33).[41]

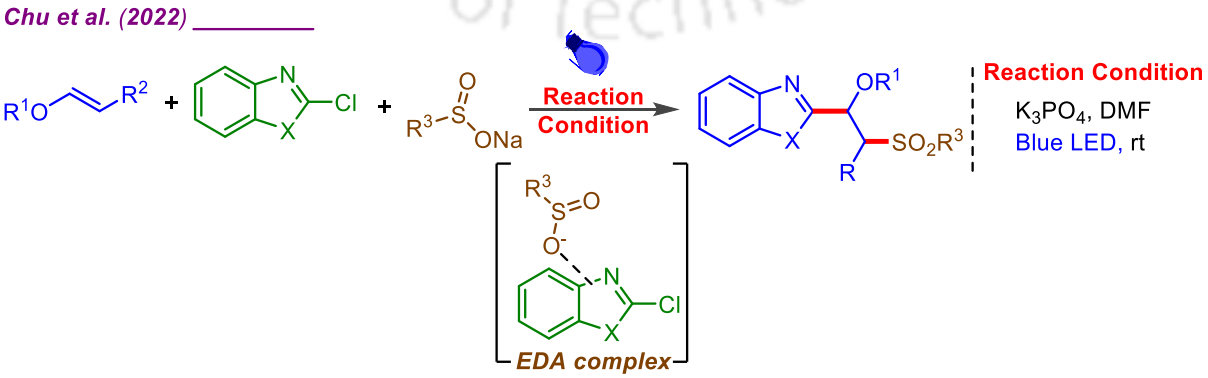

TH-3369_166122017

Scheme IB.2.33. *EDA complex enabled three component bifunctionalization of alkene*

IB.2.4. Direct Photo-Excitation of Photochromic Substrate

Generally, most of the organic substrates do not directly absorb the visible light, therefore transition metal complexes, organic dyes, photosensitizers or inorganic heterogeneous photocatalysts are utilized to carry out the photochemical transformations. However, some sensitizer-free photocatalysis are described, where the substrate itself converted to a photoactive species *via* some protonation or deprotonation process. Further, some reports revealed that sometimes a photosensitive functional group of reacting substrate triggers the photocatalysis to enable intra or intermolecular transformations.[42]

In the year of 2017, Malacarne and co-workers demonstrated a photo-induced sensitizer-free synthesis of aryl or hetero-aryl amides from arylazo sulfones and isocyanides (Scheme IB.2.34).[43] Furthermore, this protocol was utilized for the preparation of antidepressant moclobemide.

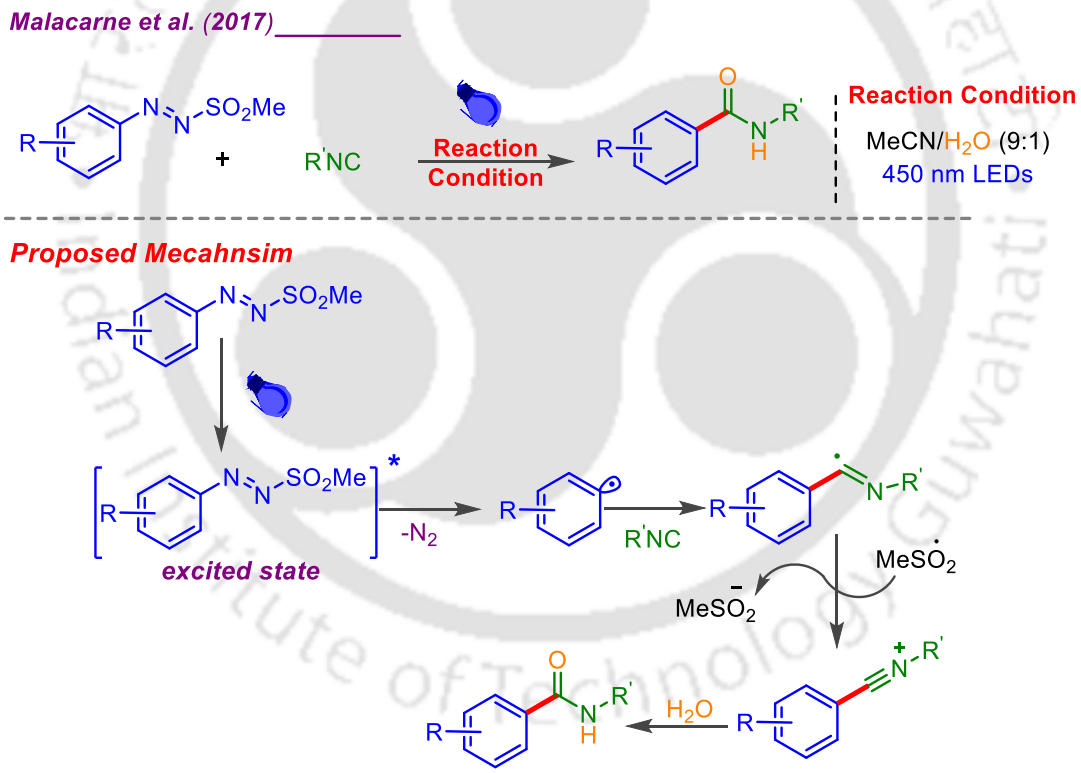

Scheme IB.2.34. *Photo-induced sensitizer-free amidation*

In 2019, Jiao group disclosed an external sensitizer-free C–H arylation of BODIPY derivatives. The reaction proceeds *via* the excited BODIPY derivatives triggered aryl radical generation from the aryl diazonium salts (Scheme IB.2.35).[44]

TH-3369_166122017

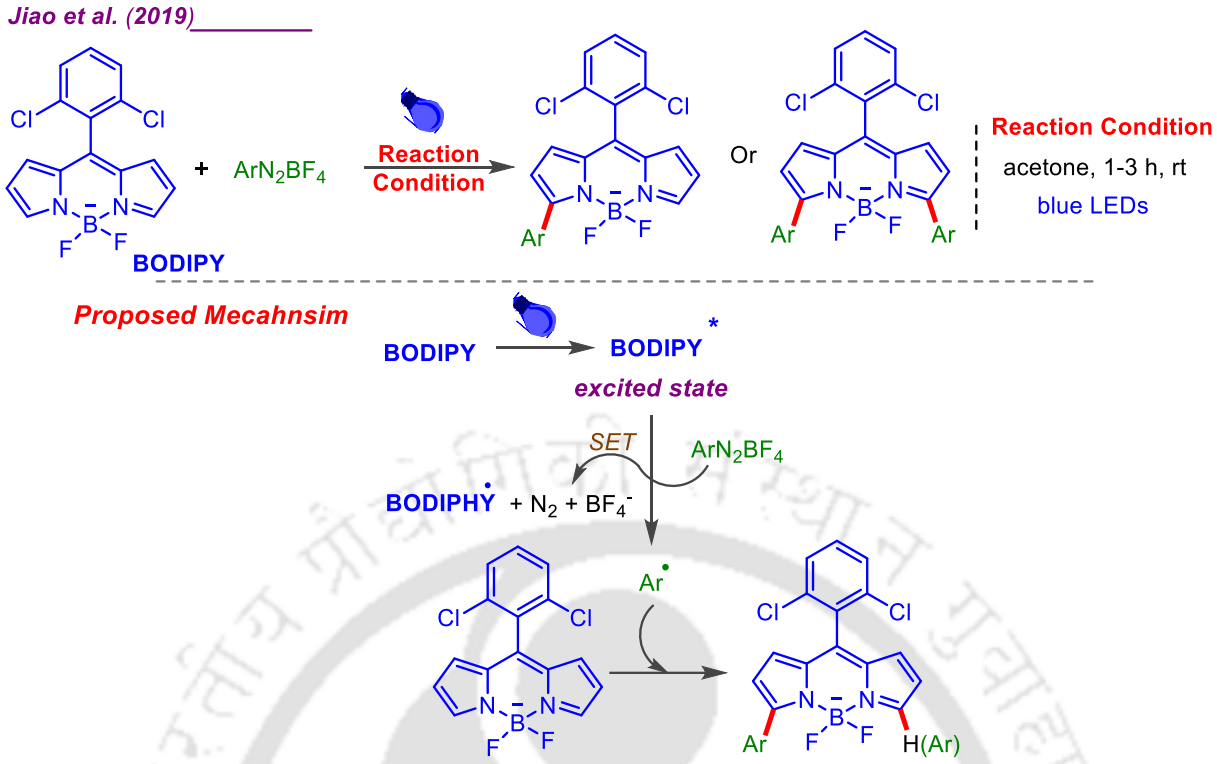

Scheme IB.2.35. *Self-photo-induced radical arylation in BODIPYs*

Li group in 2020, introduced a photosensitizer-free direct C–H arylation of quinoxaline-2(1*H*)-ones using aryl acyl peroxides (Scheme IB.2.36).[45]

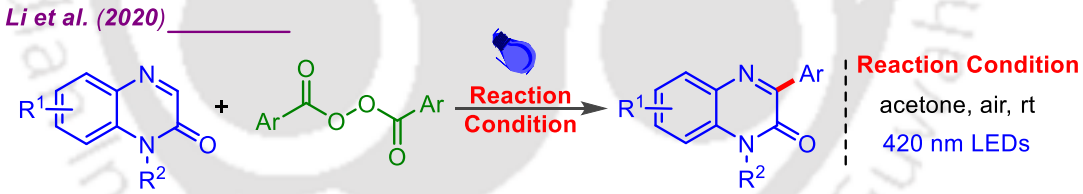

Scheme IB.2.36. *Self-photo-induced arylation of quinoxaline-2(1H)-ones with peroxide*

A photo-induced sensitizer-free multicomponent-type carbohydroxylation and carboetherification from aryl diazonium salts and styrene derivatives was described by Heinrich et *al.* (Scheme IB.2.37).[46]

TH-3369_166122017

Heinrich et al. (2021)

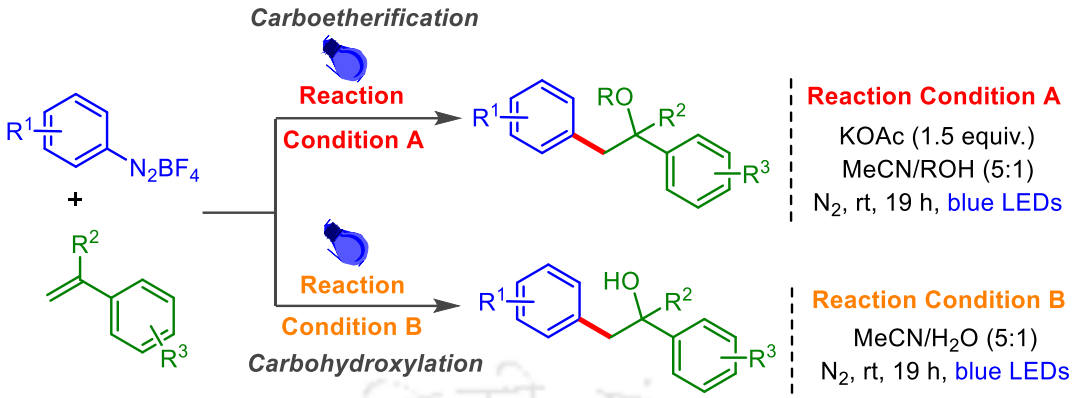

Scheme IB.2.37. *Photo-induced carboetherification and carbohydroxylation of styrene*

IB.3. References

1. Ciamician, G. The Photochemistry of the Future. *Science*. **1912**, *36*, 385.
2. (a) Ravelli, D.; Protti, S.; Fagnoni, M. Carbon–Carbon Bond Forming Reactions *via* Photogenerated Intermediates. *Chem. Rev*. **2016**, *116*, 9850. (b) Romero, N. A.; Nicewicz, D. A. Organic Photoredox Catalysis. *Chem. Rev*. **2016**, *116*, 10075. (c) Kalyanasundaram, K.; Gratzel, M. Applications of Functionalized Transition Metal Complexes in Photonic and Optoelectronic Devices. *Coord. Chem. Rev*. **1998**, *177*, 347. (d) Bellotti, P.; Huang, H.-M.; Faber, T.; Glorius, F. Photocatalytic Late-Stage C-H Functionalization. *Chem. Rev*. **2023**, *123*, 4237.
3. (a) Skubi, K. L.; Blum, T. R.; Yoon, T. P. Dual Catalysis Strategies in Photochemical Synthesis. *Chem. Rev*. **2016**, *116*, 10035. (b) Yoon, T. P. Photochemical Stereocontrol Using Tandem Photoredox–Chiral Lewis Acid Catalysis. *Acc. Chem. Res*. **2016**, *49*, 2307.
4. (a) Prier, C.K.; Rankic, D. A.; MacMillan, D.W.C. Visible Light Photoredox Catalysis with Transition Metal Complexes: Applications in Organic Synthesis. *Chem. Rev*. **2013**, *113*, 5322. (b) Shaw, M. H.; Twilton, J.; MacMillan, D. W. C. Photoredox Catalysis in Organic Chemistry. *J. Org. Chem*. **2016**, *81*, 6898. (c) Holmberg-Douglas, N.; Nicewicz, D. A. Photoredox-Catalyzed C–H Functionalization Reactions. *Chem. Rev*. **2022**, *122*, 1925.
5. (a) Romero, N. A.; Nicewicz, D. A. Organic Photoredox Catalysis. *Chem. Rev*. **2016**, *116*, 10075. (b) Uygur, M.; García-Mancheño, O. Visible Light-Mediated Organophotocatalyzed C–H Bond Functionalization Reactions. *Org. Biomol. Chem*. **2019**, *17*, 5475.

TH-3369_166122017

6. Hedstrand, D. M.; Kruizinga, W. M.; Kellogg, R. M. *Tetrahedron Lett*. **1978**, *19*, 1255.
7. Pac, C.; Ihama, M.; Yasuda, M.; Miyauchi, Y.; Sakurai, H. *J. Am. Chem. Soc*. **1981**, *103*, 6495.
8. Cano-Yelo, H.; Deronzier, A. *J. Photochem*. **1987**, *37*, 315.
9. Ischay, M. A.; Anzovino, M. E.; Du, J.; Yoon, T. P. *J. Am. Chem. Soc*. **2008**, *130*, 12886.
10. Nicewicz, D. A.; MacMillan, D. W. C. *Science* **2008**, *322*, 77.
11. Narayanam, J. M. R.; Tucker, J. W.; Stephenson, C. R. J. *J. Am. Chem. Soc*. **2009**, *131*, 8756.
12. (a) StriethKalthoff, F.; James, M. J.; Teders, M.; Pitzer, L.; Glorius, F. Energy Transfer Catalysis Mediated by Visible Light: Principles, Applications, Directions. *Chem. Soc. Rev*. **2018**, *47*, 7190. (b) Zhou, Q.-Q.; Zou, Y.-Q.; Lu, L.-Q.; Xiao, W.-J. Visible-Light-Induced Organic Photochemical Reactions through Energy-Transfer Pathways. *Angew. Chem., Int. Ed*. **2019**, *58*, 1586. (c) Großkopf, J.; Kratz, T.; Rigotti, T.; Bach, T. Enantioselective Photochemical Reactions Enabled by Triplet Energy Transfer. *Chem. Rev*. **2022**, *122*, 1626. (d) Dutta, S.; Erchinger, J. E.; Strieth-Kalthoff, F.; Kleinmans, R.; Glorius, F. Energy Transfer Photocatalysis: Exciting Modes of Reactivity. *Chem. Soc. Rev*. **2024**, DOI: 10.1039/d3cs00190c.
13. Zhao, J.; Brosmer, J. L.; Tang, Q.; Yang, Z.; Houk, K. N.; Diaconescu, P. L.; Kwon, O. Intramolecular Crossed [2 + 2] Photocycloaddition through Visible Light-Induced Energy Transfer. *J. Am. Chem. Soc*. **2017**, *139*, 9807.
14. Guo, R.; Adak, S.; Bellotti, P.; Gao, X.; Smith, W. W.; Le, S. N.; Ma, J.; Houk, K. N.; Glorius, F.; Chen, S.; Brown, M. K. Photochemical Dearomative Cycloadditions of Quinolines and Alkenes: Scope and Mechanism Studies. *J. Am. Chem. Soc*. **2022**, *144*, 17680.
15. Liu, Y.; Ni, D.; Stevenson, B. G.; Tripathy, V.; Braley, S. E.; Raghavachari, K.; Swierk, J. R.; Brown, M. K. Photosensitized [2+2]-Cycloadditions of Alkenylboronates and Alkenes. *Angew. Chem., Int. Ed*. **2022**, *61*, e202200725.
16. Teders, M., Henkel, C., Anhäuser, L. Strieth-Kalthoff, F.; Gomez-Suarez, A.; Kleinmans, R.; Kahnt, A.; Rentmeister, A.; Guldi, D. M.; Glorius, F. The Energy-Transfer-Enabled Biocompatible Disulfide–Ene Reaction. *Nat. Chem*. **2018**, *10*, 981.
17. Guo, R. Y.; Chang, Y. C.; Herter, L.; Salome, C.; Braley, S. E.; Fessard, T. C.; Brown, M. K. Strain-Release [2π+2σ] Cycloadditions for the Synthesis of Bicyclo[2.1.1]Hexanes Initiated by Energy Transfer. *J. Am. Chem. Soc*. **2022**, *144*, 7988.
18. Wienhold, M.; Kweon, B.; McLaughlin, C.; Schmitz, M.; Zähringer, T.; Daniliuc, C. G.; Kerzig, C.; Gilmour, R. Geometric Isomerisation of Bifunctional Alkenyl Fluoride Linchpins:

TH-3369_166122017

Stereodivergence in Amide and Polyene Bioisostere Synthesis. *Angew. Chem. Int. Ed*. **2023**, *62*, e202304150.

19. Tröster, A.; Bauer, A.; Jandl, C.; Bach, T. Enantioselective Visible-Light-Mediated Formation of 3-Cyclopropylquinolones by Triplet-Sensitized Deracemization. *Angew. Chem., Int. Ed*. **2019**, *58*, 3538.
20. (a) Foster, R. Electron Donor-Acceptor Complexes. *J. Phys. Chem.* **1980**, *84*, 2135. (b) Crisenza, G. E. M.; Mazzarella, D.; Melchiorre, P. Synthetic Methods Driven by the Photoactivity of Electron Donor–Acceptor Complexes. *J. Am. Chem. Soc*. **2020**, *142*, 5461.
21. Mulliken, R.S. Molecular Compounds and their Spectra. III. The Interaction of Electron Donors and Acceptors. *J. Phys. Chem.* **1952**, *56*, 801.
22. Silva, G. P. da; Ali, A.; Silva, R. C. da, Jianga, H.; Paixão, M. W. Tris(trimethylsilyl)silane and Visible-Light Irradiation: A New Metal- and Additive-Free Photochemical Process for the Synthesis of Indoles and Oxindoles. *Chem. Commun*. **2015**, *51*, 15110.
23. Sun, J.; He, Y.; An, X.-D.; Zhang, X.; Yu, L.; Yu, S. Visible-Light-Induced Iminyl Radical Formation via Electron-Donor–Acceptor Complexes: A Photocatalyst-Free Approach to Phenanthridines and Quinolines. *Org. Chem. Front*. **2018**, *5*, 977.
24. Zhu, M.; Zhou, K.; Zhang, X.; You, S.-L. isible-Light-Promoted Cascade Alkene Trifluoromethylation and Dearomatization of Indole Derivatives via Intermolecular Charge Transfer. *Org. Lett*. **2018**, *20*, 4379.
25. Davies, J.; Booth, S. G.; Essafi, S.; Dryfe, R. A.; Leonori, D. Visible-Light-Mediated Generation of Nitrogen-Centered Radicals: Metal-Free Hydroimination and Iminohydroxylation Cyclization Reactions. *Angew. Chem., Int. Ed.* **2015**, *54*, 14017.
26. Yu, D.; To, W.-P.; Liu, Y.; Wu, L.-L.; You, T.; Linge, J.; Che, C.-M. Direct Photo-Induced Reductive Heck Cyclization of Indoles for the Efficient Preparation of Polycyclic Indolinyl Compounds. *Chem. Sci*. **2021**, *12*, 14050.
27. Wang, Z.-J.; Zheng, Y.; Tang, K.; Guan, J.-P.; Ye, Z.-P.; He, J.-T.; Xiao, J.-A.; Chen, K.; Xiang, H.-Y.; Yang, H. Photoinduced Construction of a Benzothienopyridine-S,S-dioxide Framework Enabled by Polychloropyridyl Multifunctional Motifs. *J. Org. Chem.* **2022**, *87*, 4732.
28. Wang, H.; Wu, Q.; Zhang, J.-D.; Li, H.-Y.; Li, H.-X. Photocatalyst- and Transition-Metal-Free Visible-Light-Promoted Intramolecular C(sp^2)–S Formation. *Org. Lett.* **2021**, *23*, 2078.

TH-3369_166122017

29. Sun, B.; Shi, X.; Zhuang, X.; Huang, P.; Shi, R.; Zhu, R.; Jin, C. Photoinduced EDA Complexes Enabled Radical Tandem Cyclization/Arylation of Unactivated Alkene with 2-Amino-1,4-Naphthoquinones. *Org. Lett*. **2021**, *23*, 1862.
30. Hsu, C.-W.; Sundén, H. α-Aminoalkyl Radical Addition to Maleimides *via* Electron Donor–Acceptor Complexes. *Org. Lett.* **2018**, *20*, 2051.
31. Runemark, A.; Zacharias, S. C.; Sundén, H. Visible-Light-Driven Stereoselective Annulation of Alkyl Anilines and Dibenzoylethylenes *via* Electron Donor–Acceptor Complexes. *J. Org. Chem*. **2021**, *86*, 1901.
32. Xia, Q.; Li, Y.; Wang, X.; Dai, P.; Deng, H.; Zhang, W.-H. Visible Light-Driven α-Alkylation of N-Aryl tetrahydroisoquinolines Initiated by Electron Donor-Acceptor Complexes. *Org. Lett*. **2020**, *22*, 7290.
33. Xu, C.; Shen, F.-Q.; Feng, G.; Jin, J. Visible-Light-Induced α-Amino C–H Bond Arylation Enabled by Electron Donor-Acceptor Complexes. *Org. Lett.* **2021**, *23*, 3913.
34. Kaur, J.; Shahin, A.; Barham, J. P. Photocatalyst-Free, Visible-Light-Mediated C(sp^3)–H Arylation of Amides *via* a Solvent-Caged EDA Complex. *Org. Lett.* **2021**, *23*, 2002.
35. Chen, Y.-X.; Wang, Z.-J.; Xiao, J.-A.; Chen, K.; Xiang, H.-Y.; Yang, H. Visible-light-driven sulfonation of α-trifluoromethylstyrenes: access to densely functionalized CF3-substituted tertiary alcohol. *Org. Lett*. **2021**, *23*, 6558.
36. Xie, Z.-Z.; Zheng, Y.; Tang, K.; Guan, J.-P.; Yuan, C.-P.; Xiao, J.-A.; Xiang, H.-Y.; Chen, K.; Chen, X.-Q.; Yang, H. Visible-Light-Promoted Hydroxydifluoroalkylation of Alkenes Enabled by Electron Donor-Acceptor Complex. *Org. Lett*. **2021**, *23*, 9474.
37. Tong, J.; Li, H.; Zhu, Y.; Liu, P.; Sun, P. Visible-Light-Induced Dehydrogenative Sulfonylation of Tertiary Amines under Transition-Metal- and Photocatalyst-Free Conditions. *Green Chem*. **2022**, *24*, 1995.
38. Nie, F.-Y.; Cai, Y.-P. Song, Q.-H. Visible Light-Driven Decarboxylative Alkylation of Aldehydes via Electron Donor–Acceptor Complexes of Active Esters. *J. Org. Chem.* **2022**, *87*, 1262.
39. Guo, P.; Tao, M.; Xu, W.-W.; Wang, A.-J.; Li, W.; Yao, Q.; Tong, J.; He, C.-Y. *Org. Lett.* **2022**, *24*, 2143.
40. Shen, Q.; Zheng, X.; Li, L.; Zhong, T.; Yin, C.; Yu, C. Photoinduced Three-Component Difluoroamidosulfonylation/Bicyclization: A Route to Dihydrobenzofuran Derivatives. *Org. Lett*. **2022**, *24*, 2556.

TH-3369_166122017

41. Long, T.; Pan, S.; Zhu, S.; Chu, L. Catalyst-Free Intermolecular Sulfonyl/Fluoromethyl Heteroarylation of Vinyl Ethers *via* Visible-Light-Induced Charge Transfer. *Chem. Eur. J.* **2022**, *28*, e202104080.
42. Braga, F. C.; Martins, G. M.; Franco, M. S.; Belli, L. P. A.; Oliveira, K. T. de; Assis, F. F. de. Catalyst-free Photoarylation Reactions Promoted by Visible Light. *Org. Chem. Front*, **2024**, DOI: 10.1039/d3qo01738a.
43. Malacarne, M.; Protti, S.; Fagnoni, M. A Visible-Light-Driven, Metal-free Route to Aromatic Amides via Radical Arylation of Isonitriles. *Adv. Synth. Catal*. **2017**, *359*, 3826.
44. Wang, D.; Cheng, C.; Wu, Q.; Wang, J.; Kang, Z.; Guo, X.; Wu, H.; Hao, E.; Jiao, L. Visible-light excitation of BODIPYs enables self-promoted radical arylation at their 3,5-positions with diazonium salts. *Org. Lett*. **2019**, *21*, 5121.
45. Xu, J.; Zhang, H.; Zhao, J.; Ni, Z.; Zhang, P.; Shi, B.-F.; Li, W. Photocatalyst-, Metal- and Additive-Free, Direct C–H Arylation of Quinoxalin-2(1*H*)-ones with Aryl Acyl Peroxides Induced by Visible Light. *Org. Chem. Front*. **2020**, *7*, 4031.
46. Altmann, L.-M.; Zantop, V.; Wenisch, P.; Diesendorf, N.; Heinrich, M. R. Visible Light Promoted, Catalyst-Free Radical Carbohydroxylation and Carboetherification under Mild Biomimetic Conditions. *Chem. - Eur. J*. **2021**, *27*, 2452.

TH-3369_166122017

CHAPTER II

Access to Multifunctional AEEgens via Ru(II)-Catalyzed Quinoxaline-Directed Oxidative Annulation

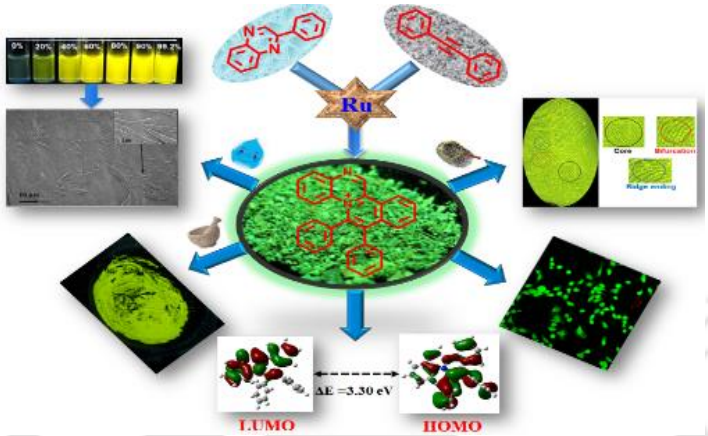

Abstract: *The multifaceted application potential of AEEgens in bio-imaging, theranostic, chemo/biosensors, and organic photo-electronic opens up a new research paradigm to develop such luminogens. Herein, N-directed Ru(II)-catalyzed oxidative annulation of 2-aryl quinoxalines with internal alkynes leads to the formation of luminogenic annulated quaternary salts with the aid of copper oxidant. The synthesized compounds possess a twisted donor–π–acceptor configuration and exhibit strong emission in the yellow-to-green region. Single crystal analysis depicts the presence of multiple intermolecular non-covalent and weak π–π interactions that are possibly responsible for the luminescent behavior in crystalline as well as solid states. The advent of AEE in quinoxalinium salt in DMF/water is due to the restriction of intramolecular motion (RIM) and suppression of intermolecular charge transfer in the aggregated state. Such AEEgens display reversible mechanochromism on changing from crystalline to amorphous state upon grinding and returning back to the crystalline state upon DCM fuming, where a few of such compounds are utilized for the development of latent fingerprints on an adhesive tape. Furthermore, a representative group of synthesized luminescent quinoxalinium salts portray dose-dependent cell growth inhibition of HeLa cells with concomitant cell arrest in G1 phases. Hence, these AEE luminogens are not only attractive as luminescent "light-up" probes for cell imaging but also important as anticancer agents.*

Keywords:

quinoxaline, oxidative-annulation, multifunctional-AEEgens, reversible mechanochromism, latent fingerprint, light-up probes.

ACS OMEGA

Cite this: *ACS Omega* 2019, 4, 3, 5565−5577
Publication Date: March 20, 2019
https://doi.org/10.1021/acsomega.9b00274
Copyright © 2019 American Chemical Society. This publication is licensed under these Terms of Use.
Request reuse permissions Open Access

ACS AuthorChoice

Article Views 2331 | Altmetric 1 | Citations 25
LEARN ABOUT THESE METRICS

CHAPTER II

II.1. Introduction

Heteroarenes-directed transition metal-catalyzed C–H bond functionalization has emerged as a versatile method for forging carbon-carbon (C–C) and carbon-heteroatom (C–X) bonds. This strategy appeared as step-atom economical over the traditional cross couplings, as they do not require any prefunctionalization.[1] The last decades have witnessed numerous advances in this arena, among which chelation-assisted oxidative *N*-annulation with alkynes *via* C–H activation for constructing *N*-heterocyclic salts has gained significant attention.[2]

The *N*-fused cationic poly-heterocyclic materials are recognized as a privileged class of functional molecules with widespread application in material science, particularly as a potential OLED device fabricator.[3] They have found crucial prevalence in many natural[4] and bio-active pharmaceutical[5] molecules. Besides, such compounds are also utilized for biological studies as cellular imaging probes, or due to having charged skeletons they can intercalate with DNA.[6] Owing to their pervasive real-world applications, over the years several transition-metal-catalyzed oxidative annulation protocols have been developed by various research groups (*viz.* Cheng, Choudhury, Wang, Huang, Macgregor, Saa, and Li, etc.) to construct such π–conjugated materials.[7-10]

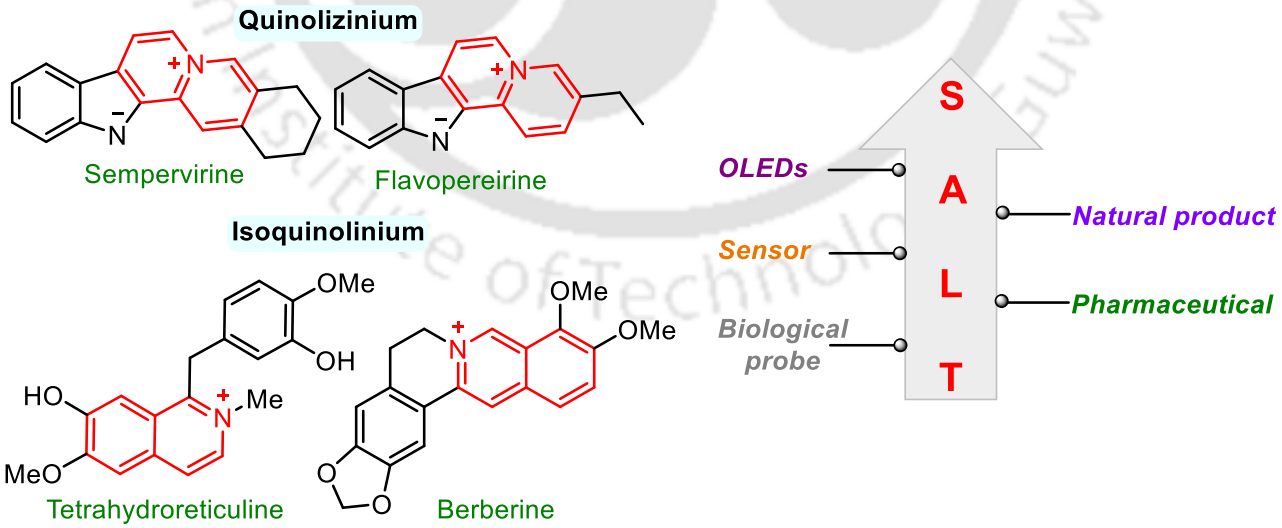

Figure II.1.1. *Importance of cationic N-heterocycles*

TH-3369_166122017

II.2. Prior Strategies for Forging Various *N*-Heterocyclic Quaternary Salts

➢ **Isoquinolinium Salt:**

In the year of 2012, Cheng and co-workers developed a rhodium(III)-catalyzed synthesis of isoquinolinium salts *via* oxidative C–H/N annulation (Scheme II.2.1).[11a] This reaction proceeds through the *in situ* formation of imine involving benzaldehyde and amine, followed by oxidative coupling with alkynes to afford a library of π-conjugated isoquinolinium salts.

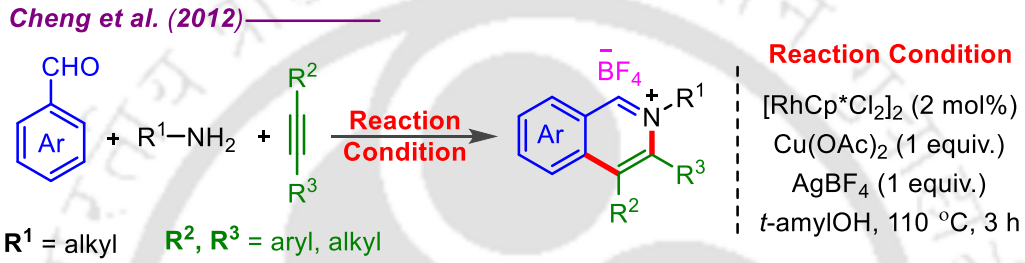

Scheme II.2.1. *Rh(III)-catalyzed synthesis of isoquinolinium salts*

Meanwhile, Huang and co-workers proposed a Rh(III)-catalyzed oxidative C–H/N annulation for forging substituted pyrido-isoquinolinium salts with high turnover numbers (up to 740) (Scheme II.2.2).[11b] Further the mechanistic studies conclude the participation of molecular oxygen in Rh(I) to Rh(III) oxidation.

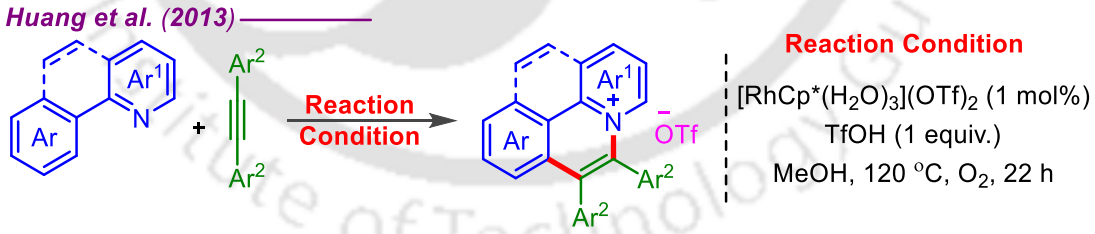

Scheme II.2.2. *Rh(III)-catalyzed synthesis of pyrido-isoquinolinium salts*

➢ **Indolizidinium Salt:**

Cheng group reported a one-pot Rh(III)-catalyzed synthesis of bi-, tri-, and hetero-cyclic fused quaternary indolizidinium salts, starting from substituted benzaldehydes or α,β-unsaturated aldehydes and amine tethered internal alkynes under Cu(II)/O_2 oxidant (Scheme II.2.3).[11c]

TH-3369_166122017

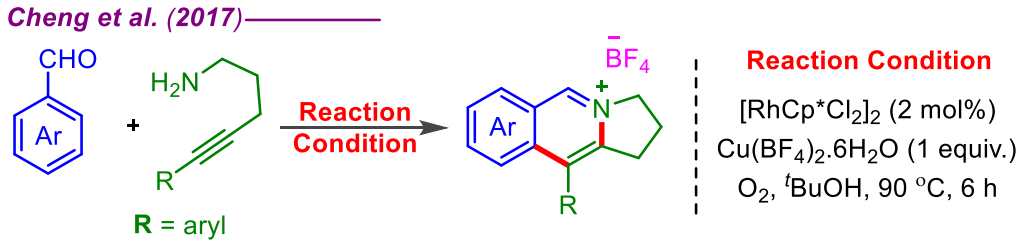

Scheme II.2.3. *Rh(III)-catalyzed synthesis of indolizidinium salts*

➢ **Benz[a]acridizinium Salt:**

You *et al.* reported an elegant Rh(III)-catalyzed two-fold cascade oxidative annulation of aldoxime with internal alkynes to synthesize diversely substituted benz[*a*]acridizinium salts in presence of sole oxidant O_2 (Scheme II.2.4).[11d]

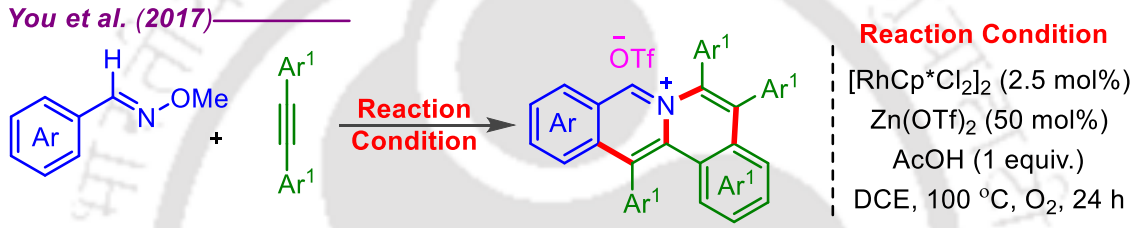

Scheme II.2.4. *Rh(III)-catalyzed synthesis of benz[a]acridizinium salts*

➢ **Benzoquinolizinium Salt:**

A Rh(III)-catalyzed newer cascade annulation for synthesizing benzoquinolizinium salts was described by Jun et al. (Scheme II.2.5).[11e] In this report, with the assistance of HBF_4, the coupling of allyl amines with internal alkynes delivered a series of substituted π-conjugated benzoquinolizinium salts with a broad scope and good yields. Furthermore, such compounds displayed good fluorescent properties with functional group-altered fluorescence emission.

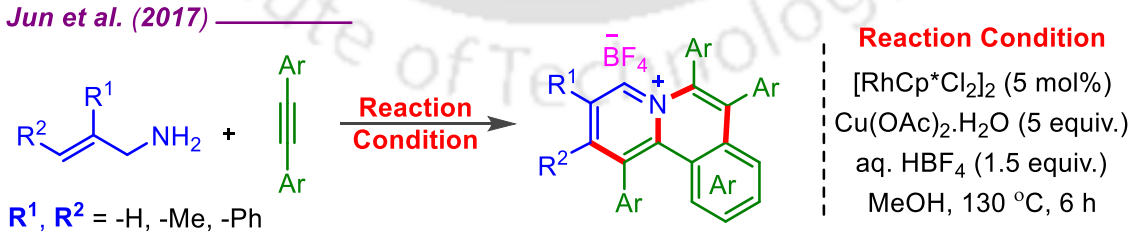

Scheme II.2.5. *Rh(III)-catalyzed synthesis of benzoquinolizinium salt*

➢ **Cinnolinium Salt:**

You and co-workers divulged a Rh(III)-catalyzed oxidative C–H activation/cyclization of azo compounds with internal alkynes to access dual *N*-doped cationic cinnolinium-based poly-aromatic

TH-3369_166122017

heterocycles (Scheme II.2.6).[11f] This methodology enabled the broad installation of various functional groups on the cinnoline rings with good yields. In light of mechanistic studies, this reaction proceeded through C–H metalation *via* concerted metalation–deprotonation (CMD) mechanism, which underwent a subsequent alkyne insertion to provide C–H/N annulation.

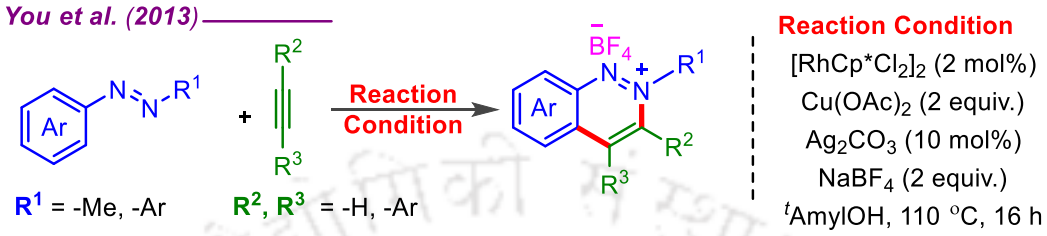

Scheme II.2.6. *Rh(III)-catalyzed synthesis of polycyclic cinnolinium salts*

Whereas in 2018, Wang et al. introduced Boc-hydrazine template to afford the new class of cinnolinium salts under Rh(III) catalysis (Scheme II.2.7).[12a] This reaction required an excess of Ag(I)/Cu(II) to convert the Boc-arylhydrazines into the corresponding diazo species. These diazo compounds underwent cyclometalation to couple with alkynes.

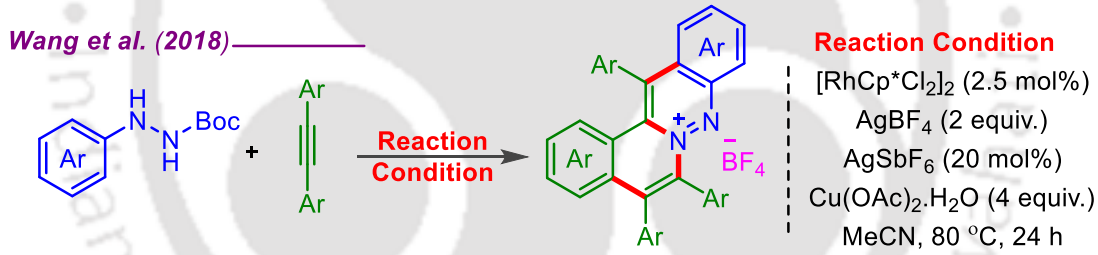

Scheme II.2.7. *Rh(III)-catalyzed synthesis of cinnolinium salts from Boc-arylhydrazines*

➢ **Acridinium Salt:**

A new series of tetracyclic acridinium salts were accomplished by You *et al. via* Rh(III) catalyzed oxidative [4+2] cyclization (Scheme II.2.8).[11b] The annulation reaction took place between the C=N imine segment of acridine derivatives with the alkynes to afford an array of diversely substituted *N*-doped acridinium salts. Such annulated salts displayed fluorescence emission at 563–577 nm with quantum yield of up to 0.79. Furthermore, such cationic compounds were also exploited for living cell imaging, their low cytotoxicity makes them a potential candidate for organelle tracking.

TH-3369_166122017

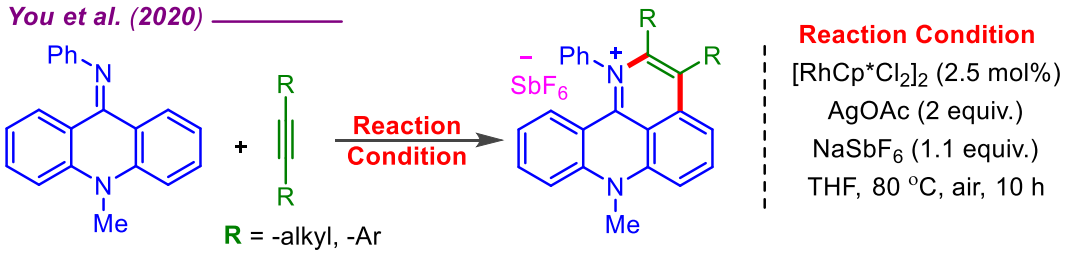

Scheme II.2.8. *Rh(III)-catalyzed synthesis of tetracyclic acridinium salts*

➢ **Imidazolinium Salt:**

A Rh(III)-catalyzed [2+2+2] oxidative cyclization of pyridyl imidazoles with internal alkynes was demonstrated by Choudhury and co-workers to deliver a library of imidazolinium salts (Scheme II.2.9).[11c] In light of mechanistic studies, the non-coordinating BF_4 anion dictates the pathway towards selective dual alkyne annulated C–N annulation.

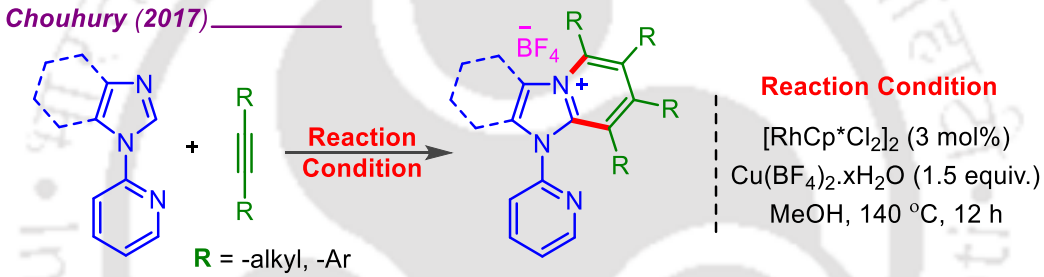

Scheme II.2.9. *Rh(III)-catalyzed synthesis of pyridyl imidazolinium salts*

Ruthenium has gained significant importance among various transition-metal catalysts due to its ready availability, stability, selectivity, and low cost compared to Pd or Rh.[1e,13] However, despite the emergent interests for cationic annulated adducts, only a few Ru(II)-catalyzed C–H bond activation methods are delineated towards annulation. In this context, Cheng and co-workers described Ru-catalyzed synthesis of quinolizinium and isoqinolinium salts from their corresponding reaction partners (Scheme II.2.10 and Scheme II.2.11).[14a,14b]

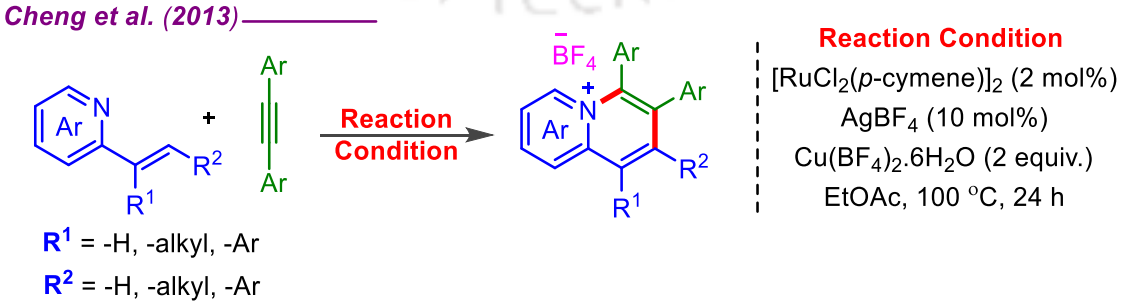

Scheme II.2.10. *Ru(II)-catalyzed synthesis of quinolizinium salts*

TH-3369_166122017

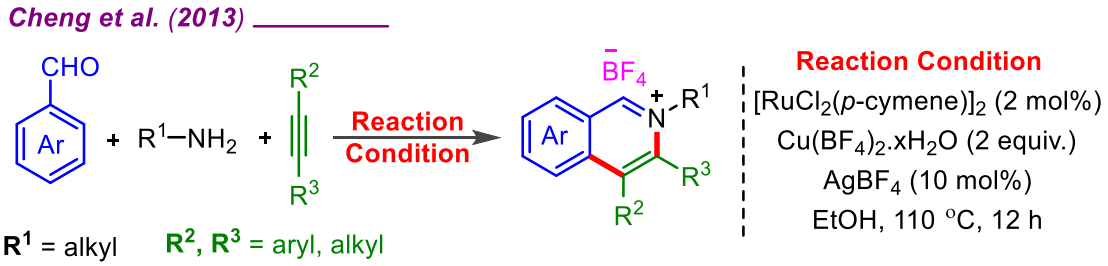

Scheme II.2.11. *Ru(II)-catalyzed synthesis of isoquinolinium salts*

Intrigued by these aforementioned findings and emergent application potential of *N*-doped annulated scaffolds, herein we are interested to couple di-nitrogen capped heteroarene 2-aryl (hetero)aryl quinoxalines with internal alkynes under Ru(II)-catalysis. But this directing group-aided C–H activation proposal faces two possible critical site-selectivity issues (i) participation of one nitrogen atom and *ortho*-C–H of 2-aryl quinoxalines with internal alkynes and (ii) oxidative annulation through the dual activation of C3–H and *ortho*-H of 2-aryl quinoxalines.

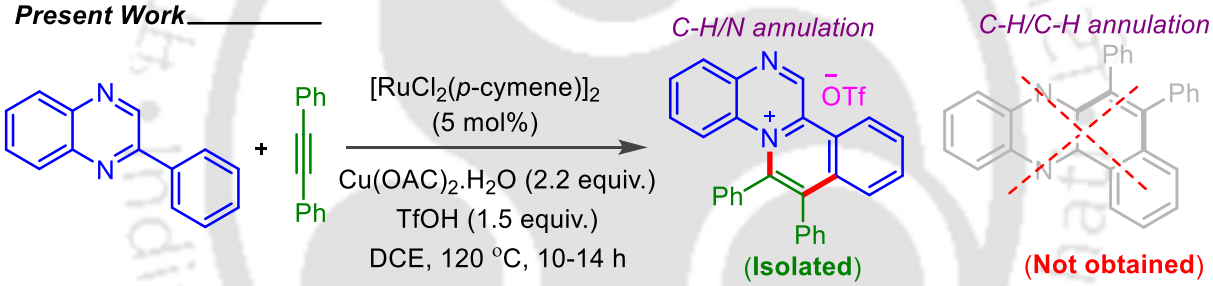

Scheme II.2.12. *Ru(II)-catalyzed synthesis of N-doped quinoxalinium salts*

II.3. Present Strategy

To realize this, a reaction was carried out with 2-phenyl quinoxaline (**1a**) and diphenylacetylene (**2a**) by taking as model substrate with the aid of [$RuCl_2$(*p*-cymene)]$_2$ (5 mol%), $Cu(OAc)_2.H_2O$ (1.2 equiv) and triflic acid (TfOH) (1.5 equiv) in 1,2-dichloroethane (DCE) at 85 °C (Scheme II.2.12). Pleasingly after 20 h, a fluorescent annulated *N*-containing quaternary salt **3aa** was isolated in 56% yield. Further, the structure was confirmed by NMR and X-ray crystallographic analysis (Figure II.3.1). After a series of optimizations (Table II.3.1) in terms of catalyst, oxidants, additives, solvents and reaction temperature, the use of 2-phenyl quinoxaline (**1a**, 0.3 mmol), diphenylacetylene (**2a**, 0.36 mmol), [$RuCl_2$(*p*-cymene)]$_2$ (5.0 mol %), $Cu(OAc)_2.H_2O$ (0.66 mmol), triflic acid (TfOH) (0.45 mmol) in 1,2-DCE at 120 °C was obtained as the optimized reaction protocol (with 85% isolated yield).

TH-3369_166122017

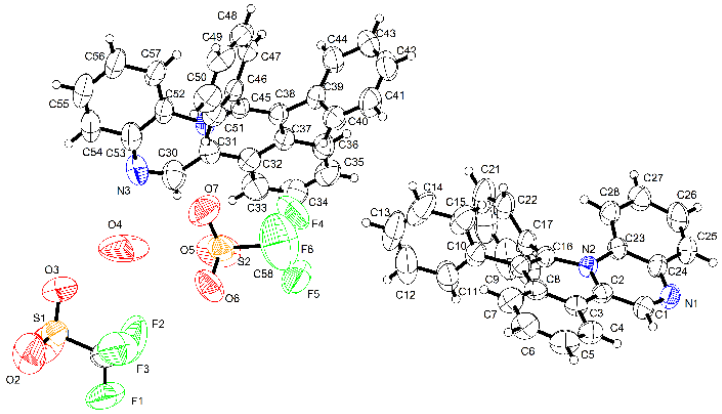

Figure II.3.1. *ORTEP diagram of* ***3aa*** *(40% probability)*

Table II.3.1. Optimization of reaction conditions[a, b]

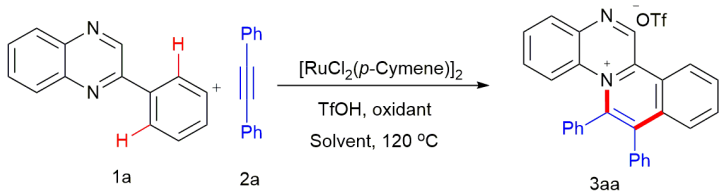

Entry	**Oxidant (equiv.)**	**Solvent**	**Temp (°C)**	**Yield[b] of 3aa**
1	$Cu(OAc)_2.H_2O$ (1.2)	DCE	85	56
2	$Cu(OAc)_2.H_2O$ (1.2)	DCE	100	64
3	$Cu(OAc)_2.H_2O$ (1.2)	DCE	120	71
4	---	DCE	120	14
5[c]	$Cu(OAc)_2.H_2O$ (1.2)	DCE	120	nr
6	AgOAc (1.2)	DCE	120	51
7	**$Cu(OAc)_2.H_2O$ (2.2)**	**DCE**	**120**	**85**
8	$Cu(OAc)_2.H_2O$ (2.2)	CH3CN	120	42
9	$Cu(OAc)_2.H_2O$ (2.2)	DMF	120	nr
10	$Cu(OAc)_2.H_2O$ (2.2)	*t*-amylOH	120	nr
11	$Cu(OAc)_2.H_2O$ (2.2)	MeOH	120	46
12	$Cu(OAc)_2.H_2O$ (2.2)	1,4-dioxane	120	36
13[d]	$Cu(OAc)_2.H_2O$ (2.2)	DCE	120	59

[a]*Reaction conditions: unless otherwise noted, all reactions were carried out with 1a (0.3 mmol), 2a (0.36 mmol), [$RuCl_2$(p-Cymene)]$_2$ (5 mol%), oxidant (0.66 mmol), TfOH (0.45 mmol), solvent (2.0 mL) under air atmosphere for 12 h.* [b]*Isolated yield.* [c]*Without [$RuCl_2$(p-Cymene)]$_2$.* [d]*[$RuCl_2$(p-Cymene)]$_2$ (2.5 mol%) was used. nr = no reaction.*

Scope of Oxidative Annulation:

After establishing the optimized protocol, the scope of the reaction was examined with various 2-arylquinoxalines **1**(**a**–**o**) and diphenylacetylenes **2**(**a**–**h**) (Scheme II.3.1). The reaction of

TH-3369_166122017

diphenylacetylene (**2a**) with 2-arylquinoxaline bearing electron-donating groups like *p*-Me (**1b**), *o*-OMe (**1c**), *p*- OMe (**1d**), *m*-OMe (**1e**), in the phenyl ring, resulted in the formation of their respective annulated products (**3ba**, 76%), (**3ca**, 65%), (**3da**, 73%). (**3ea+3´ea**, 82%). It was observed that the phenyl ring substituted with ortho and para substituents gave single isomeric products (**3ba**, **3ca,** and **3da**). In contrast, the presence of a meta substituent gave an inseparable mixture of regioisomers **3ea** and **3´ea**.

Scheme II.3.1. *Substrate scope of quinoxalines with diphenylacetylene*[a-c]

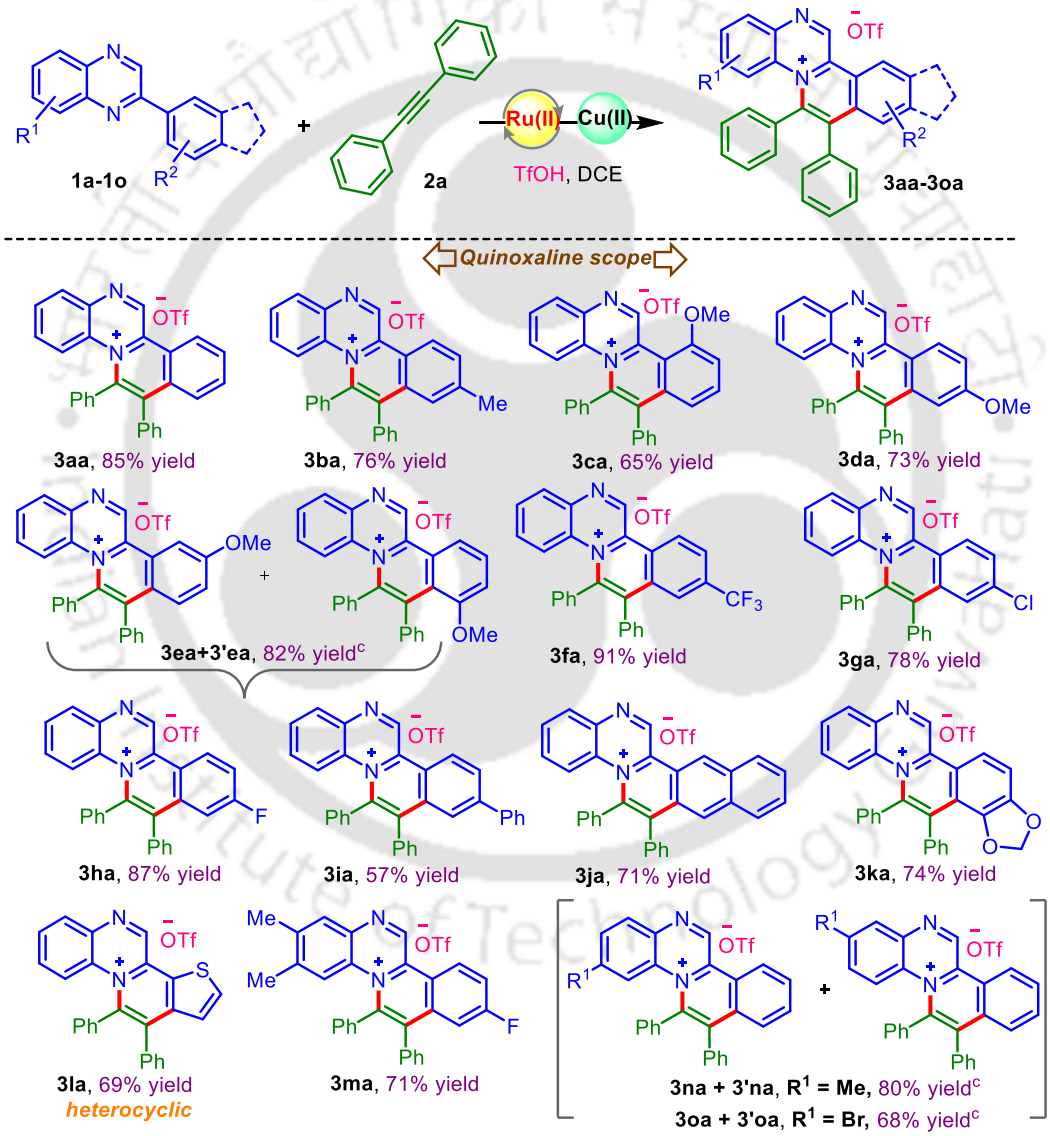

[a]Reaction Condition: **1a-1o** (0.3 mmol), **2a** (0.36 mmol), [Ru(*p*-cymene)Cl_2] (5 mol%), Cu(OAC)$_2$. 2H_2O (0.66 mmol) and TfOH (0.45 mmol) in DCE at 120 ^oC for 10-14 h under an air atmosphere. [b]Isolated yield after column chromatography. [c]Isomers were confirmed by ^1H NMR.

TH-3369_166122017

The attachment of strongly and moderately electron-withdrawing substituents *viz.* *p*-CF_3 (**1f**), *p*-Cl (**1g**), and *p*-F (**1h**) in the phenyl ring of 2-aryl quinoxaline, all underwent efficient annulations with diphenylacetylene (**2a**) providing their corresponding products (**3fa**, 91%), (**3ga**, 78%) and (**3ha**, 87%).

Scheme II.3.2. *Substrate scope of diphenyl acetylene with quinoxaline* [a,b]

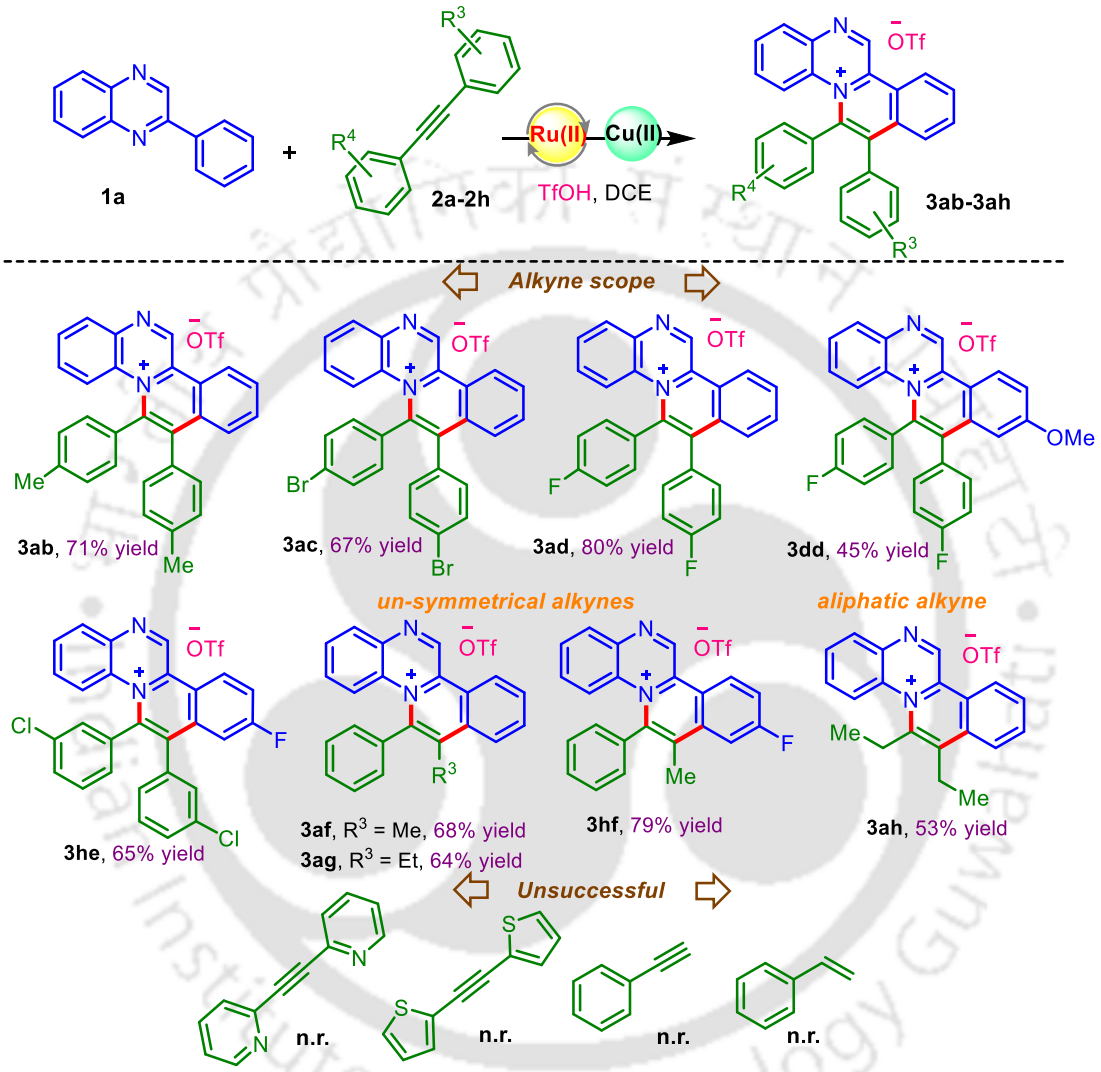

[a]Reaction Condition: **1a** (0.3 mmol), **2a-2h** (0.36 mmol), [Ru(*p*-cymene)Cl_2] (5 mol%), Cu(OAC)$_2$. $2H_2O$ (0.66 mmol) and TfOH (0.45 mmol) in DCE at 120 °C for 10-14 h under an air atmosphere. [b]Isolated yield after column chromatography.

Similarly, other aryl or heteroaryl such as *p*-phenyl (**1i**), 2-naphthalene (**1j**), 2-benzo[*d*]-dioxolyl (**1k**) and 2-thiophenyl (**1l**) all afforded annulated products with diphenylacetylene (**2a**) providing respective quinoxalinium salts (**3ia**, 57%), (**3ja**, 71%), **(3ka**, 74%) and (**3la**, 69%) in modest yields. An electron-donating substituent (–Me) in the quinoxaline moiety and an electron-withdrawing (–F) group in the 2-aryl ring, as in 2-(4-fluorophenyl)-6,7-dimethylquinoxaline (**1m**) afforded it annulated product (**3ma**)

TH-3369_166122017

in 71% yield when reacted with diphenylacetylene (**2a**). The substrate (**1m**) is symmetrical in nature, so there is no regio-selectivity issue. However, any substitution [either electron-donating–Me (**1n**) or electron-withdrawing –Br (**1o**)] at the unsymmetrical C–7 position gave a mixture of regio-isomeric products (**3na + 3´na**) and (**3oa + 3´oa**) in a combined yield of 80% and 68%, respectively. Besides diphenylacetylene, other substituted symmetrical 1,2-diarylalkynes having an electron-donating, *p*-Me (**2b**) and an electron-withdrawing, *p*-Br (**2c**) and *p*-F (**2d**) all efficiently provided their respective annulated products (**3ab**, 71%), (**3ac**, 67%), and (**3ad**, 80%) (Scheme II.3.2). Further, 1,2-diarylalkynes having electron-withdrawing *p*-F (**2d**) and the 2-phenyl ring having electron-donating substituents *p*-OMe (**1d**) provided inferior yield (45%) of the π–conjugated heterocycle (**3dd**). A *m*-chloro diphenyl acetylene (**2e**) also annulated successfully with 2-(4-fluorophenyl)quinoxaline (**1h**) giving quinoxalinium salt (**3he**) in 65% yield. To check the regioselectivity of the reaction, unsymmetrical alkynes, 1-phenyl-1-propyne (**2f**) and 1-phenyl-1-butyne (**2g**) were examined. Interestingly, both yielded single regioisomeric product (**3af**, 68%) and (**3ag**, 64%) respectively. Substrate (**1h**) reacted with an unsymmetrical alkyne, phenyl-1-propyne (**2f**) under the standardized condition, giving a single regioisomeric product (**3hf**) in 79% yield. The structure of the regioisomer (**3hf**) has been unambiguously confirmed by X-ray crystallography. In addition to symmetrical and unsymmetrical aryl alkynes, aliphatic alkyne such as 3-hexyne (**2h**) when treated with 2-phenylquinoxalines (**1a**) afforded its annulated product (**3ah**) in a modest yield of 53%. Unfortunately, the heteroaryl (*viz*. pyridyl and thiophenyl) bearing internal alkynes are unsuccessful in this present protocol. Furthermore, terminal alkyne and alkenes also failed to offer the desired oxidative annulation (Scheme II.3.2).

A possible mechanism for this annulation reaction is proposed in Scheme II.3.3 based on literature precedence on Ru(II) catalyzed oxidative annulations.[14b] Initially, an active ruthenium catalyst (**B**) is generated through anion exchange with copper acetate monohydrate. Then coordination of the nitrogen atom of quinoxaline (**1a**) to the ruthenium acetate species (**B**) and subsequent ortho-metalation afforded a five-membered ruthenacycle intermediate (**C**). Then the regioselective coordination and migratory insertion of alkyne **2a** into the Ru-carbon bond of intermediate (**C**) generates the seven membered intermediate (**E**). Reductive elimination of intermediate (**E**) in the presence of TfOH delivers the product **3aa**.

TH-3369_166122017

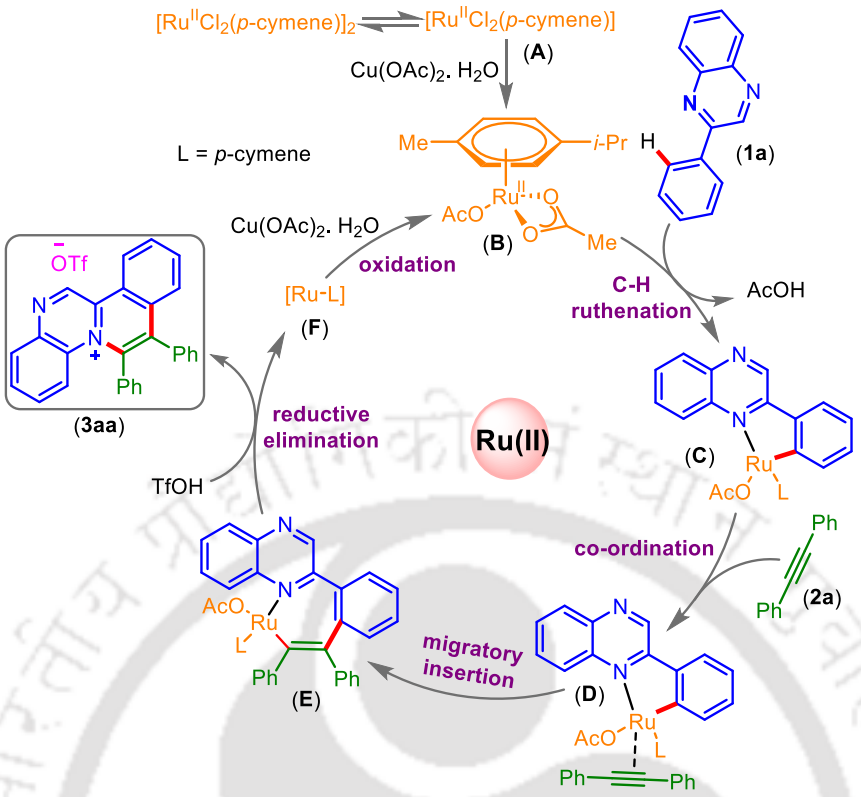

Scheme II.3.3. *Ru(II)-Catalyzed oxidative annulation of 2-phenylquinoxaline with diphenylacetylene*

II.4. Multifaceted Application

One of the synthetic chemist's major focuses is to design and develop new luminescent materials with diverse functionality.[15-18] The development of extended π–conjugated polycyclic and heterocyclic fluorescent materials is quite noteworthy owing to their versatile real-world applications.[19,20] However, several such materials developed in the past have inherent aggregation-caused quenching (ACQ) problems because of strong π–π stacking interactions.[21] To overcome this impediment in 2001 and 2002, Tang and Park group first presented aggregation-induced emission (AIE)[22] and aggregation-induced emission enhancement (AIEE)[23] phenomenon, which is contrary to ACQ. Particularly, the donor-π-acceptor (D–π–A) configuration-based solid-state luminescent AIEgens or AEEgens are either non-emissive or weak emissive in solution but deliver strong emission in the aggregated or solid states.[19b,24] To date, restriction in intramolecular motion (RIM) including both rotation and vibration and the twisted conformations, which impede the strong intermolecular π–π stacking interactions, is reported as the most acceptable mechanism for AIE/AEEgen systems.[19a,19b,22,24,25] In solution, because of the dynamic intramolecular motions these luminescence materials undergo non-radiative decay on

TH-3369_166122017

excitation. Whereas, in the aggregated and solid state, due to locked conformation through the formation of nano or micro aggregates and various intermolecular interactions, the intramolecular motions are restricted by making them highly emissive.[19a,19b]

The development of solid-state luminescent AIEgens or AEEgens has become an emergent ongoing research area due to their wide application in "turn-on" or "light-up" bio-sensors or chemo-sensors,[26,27] optoelectronics,[28] bio-imaging,[29,30] DNA visualization[30] and many more.[31] In the past few years, AIE/AEEgens have also served as mechanochromic luminogens, which are a special class of materials that undergo morphological transformations from crystalline to amorphous state. This is associated with a noticeable change in their photo-physical properties, thereby exhibiting new luminescent behavior under the influence of external mechanical stimuli including crushing, grinding, and hydrostatic pressure.[19b,32-37] This phenomenon is termed as mechanochromic luminescence or piezochromic luminescence. Currently, the progress of AIE/AEE-based mechanochromic luminescent materials is quite remarkable due to their use in mechanical sensors,[38] optical data storage devices,[39] security links[40], and various biological applications.[33a] Besides these, the optical bio-imaging techniques have gained prominence owing to their easy visualization of the biological structural and functional process along with targeting cancerous cells and tissues.[41-45] Among all the imaging techniques, fluorescence imaging is preferred due to its non-invasive character, fast response, huge temporal resolution, good sensitivity and high biocompatibility.[46] The AIE or AEE based fluorophores with large Stoke shift (> 80 nm) and non-interference character between excitation and fluorescence emission wavelengths, offers high signal-to-noise ratio without self-quenching and scattering light of fluorophores.[47-49] Lately, various research groups have introduced plenty of such multifunctional AIE/AEEgens.[50-52] The current approach of synthetic chemists is to design highly efficient solid-state luminescent organic materials by controlling molecular orientations and π– π stacking in an aggregated state. Here in, we unveil a new methodology for synthesizing quinoxalinium salts with a donor–π–acceptor systems. Further, we explored some synthesized quinoxalinium salts for their various photophysical and biological evaluations. The synthesized annulated quinoxalinium salts having a donor-acceptor (D–A) character is confirmed through theoretical HOMO–LUMO calculations and also experimentally supported by measuring their redox potential using cyclic voltammetry (CV). In solution, selected quaternary ammonium salts display strong fluorescence emission in green to yellow to red region (488–645 nm) with moderate quantum yields and large Stokes shifts. Their fluorescence lifetime using time-resolved photoluminescence (TRPL) has been measured. Besides these, we extensively investigated the AEE behavior of one the annulated salt (**3aa**) through

TH-3369_166122017

photoluminescence titration in DMF/water solvent system and confirmed by field-emission scanning electron microscope (FESEM) and transmission electron microscope (TEM) measurements. The mechanism of aggregation was confirmed by single crystal XRD investigation and viscosity-dependent fluorescence experiment. In addition, the AEEgen (**3aa**) exhibits reversible mechanochromism by changing its morphology under grinding and DCM solvent fuming. Its potential as a latent fingerprint has been explored using adhesive tape. Furthermore, a few of those luminescent compounds showed dose-dependent anti-cell proliferative effects on cervical cancer cells in vitro involving cell cycle arrest in G1 phases. The uptake of those compounds inside the cells was monitored by confocal imaging followed by Z-stack analysis. In brief, such AEEgens with multifunctional properties have great potential for their practical applications in various fields of biomedical research. The advantage of this class of molecule is their solubility both in the aqueous as well as in the organic medium. Moreover, due to their cationic nature, they can interact with negatively charged biomaterials such as heparin, DNA, and protein.

Theoretical Investigation:

To have an insight into the geometry and electronic structure of the annulated quaternary ammonium salts, density functional theory (DFT) calculations were performed with B3LYP/6-31G (d, p) basis set level in acetonitrile solvent modeled by the PCM approach (the Gaussian 09 program).[53] The density functional theory (DFT) calculation of **3aa** reveals that the electron density in the highest occupied molecular orbital (HOMO) is localized at the two phenyl rings derived from diphenylacetylenes, whereas the lowest unoccupied molecular orbital (LUMO) is localized at the extended quinoxalium core (Figure II.4.1).

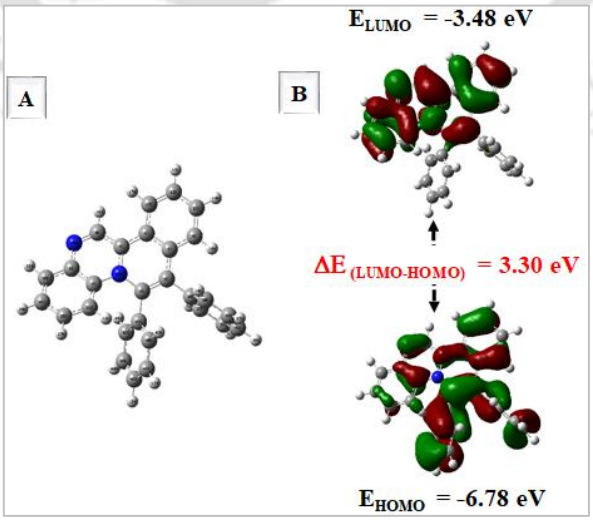

TH-3369_166122017

Figure II.4.1. *(A) Optimized structure of **3aa**. (B) Molecular orbitals amplitude plots of HOMO and LUMO of **3aa** using density functional theory calculation at the B3LYP/6-31G (d, p) basis set level in acetonitrile solvent modeled by the PCM approach*

The optimized ground state structure of **3aa** indicates the existence of a positively charged quinoxaline core as an acceptor (A) and two phenyl rings as the donors (D) flanked by a π–bridge, thus forming a D–A type configuration with a HOMO–LUMO energy gap of 3.30 eV (Figure II.4.1B). The computed HOMO (-6.78 eV) and LUMO (-3.48 eV) energy level and the energy gap (3.30 eV) of **3aa** is nearly in agreement with the experimentally determined HOMO (-6.16 eV) and LUMO (-3.51 eV) energy level having an energy gap of 2.65 eV obtained from cyclic voltammetry (Figure II.4.2).

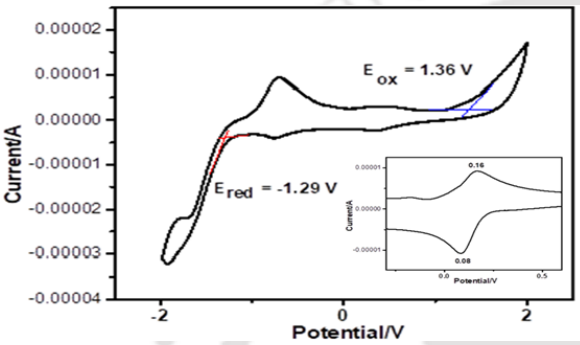

CV calculations for HOMO-LUMO:

From CV calculation,

$\mathbf{E_{LUMO}} = -[E_{red} - E_{1/2}(\text{ferrocene}) + 4.8]$ eV $\quad \mathbf{E_{red}} = -1.29$ V

$\mathbf{E_{HOMO}} = -[E_{ox} - E_{1/2}(\text{ferrocene}) + 4.8]$ eV $\quad \mathbf{E_{ox}} = 1.36$ V

$\mathbf{E_{LUMO}} = -[-1.29 + 4.8]$ eV $= -3.51$ eV.

$\mathbf{E_{HOMO}} = -[1.36 + 4.8]$ eV $= -6.16$ eV.

$\mathbf{E_{LUMO\text{ - }HOMO}} = [-3.51 + 6.16]$ eV $= 2.65$ eV

Figure II.4.2. *CV spectra of synthesized **3aa** in acetonitrile. Inset: CV spectra of Ferrocene*

Since the HOMO is located at the diphenylacetylene moiety, the presence of an electron-donating group such as –Me (**3ab**) in the para position *via* +I effect or less electron-donating group such as *p*-F (**3ad**) through +R and –I effect would lower the HOMO–LUMO energy gap compared to the unsubstituted analog (**3aa**) (Figure II.4.3).

TH-3369_166122017

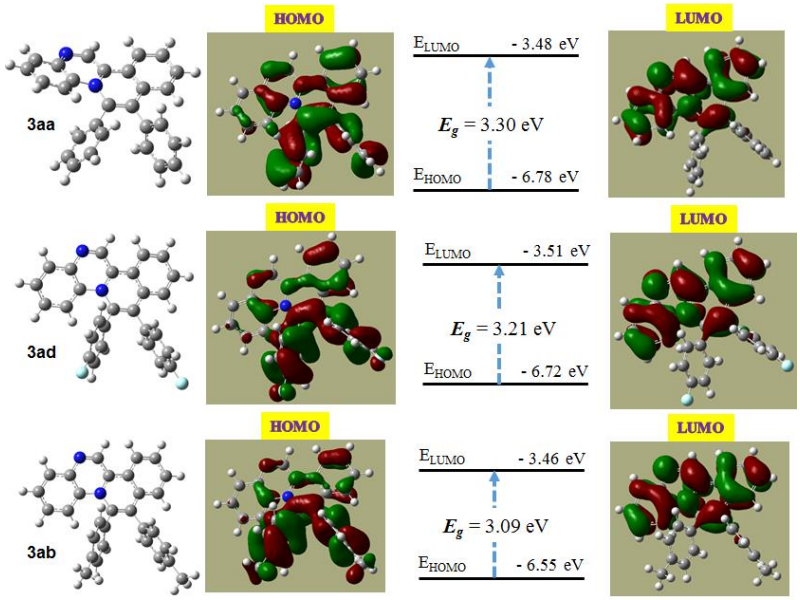

Figure II.4.3. *DFT optimized structures and HOMO-LUMO energy level diagrams of synthesized compounds* ***3aa***, ***3ad***, *and* ***3ab*** *respectively using the B3LYP/6-31G (d, p) basis set level in acetonitrile solvent modeled by PCM approach*

The observed energy gap for unsubstituted (**3aa**), *p*-F substituted (**3ad**) and *p*-Me substituted (**3ab**) quinoxalium salts respectively are 3.30, 3.21 and 3.09 eV, thus supporting our postulation (Figure II.4.3). Similarly, in the LUMO, the presence of an electron-withdrawing *p*-CF_3 (**3fa**) should lower the energy gap and an electron-donating *p*-CH_3 (**3ba**) should enhance the energy gap between the two frontier orbitals with respect to the parent analog **3aa**. The calculated energy gap of 3.30 eV, 3.36 eV, and 3.22 eV for **3aa**, **3ba**, and **3fa** is in agreement with our previous assumption (Figure II.4.4). Further, the acceptor (LUMO) part remains unchanged irrespective of the substitutions (either phenyl or ethyl) derived from the internal alkynes. However, the phenyl ring being a better electron-donating than the ethyl group, in a substitution pattern (-Ph, -Ph) (**3aa**), (-Ph, -Et) (**3ag**), (-Et, -Et) (**3ah**) the HOMO-LUMO energy gap should increase sequentially. The computed energy gap of 3.30, 3.43, and 3.48 eV, respectively for (**3aa**), (**3ag**), (**3ah**) is in strong agreement (Figure II.4.5).

TH-3369_166122017

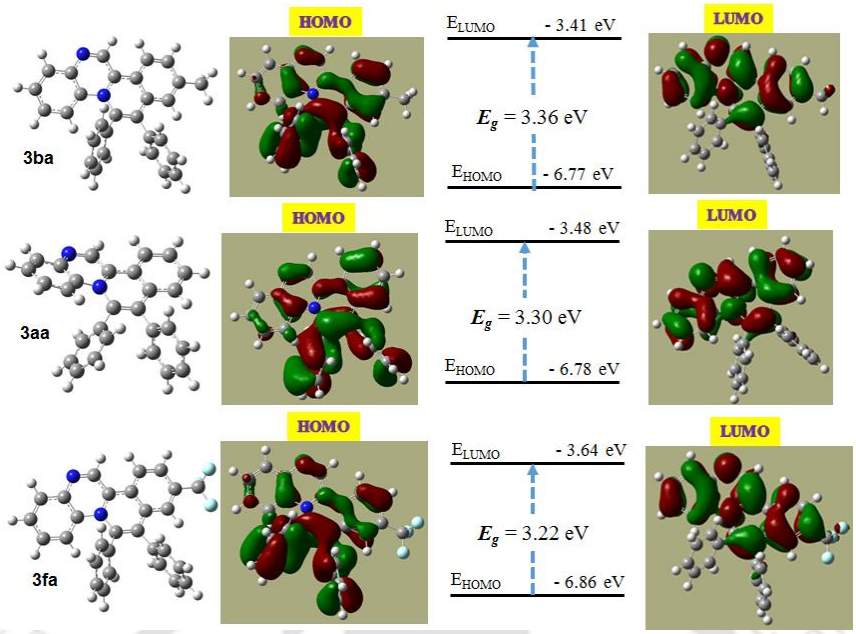

Figure II.4.4. *DFT optimized structures and HOMO-LUMO energy level diagrams of synthesized compounds* ***3ba****,* ***3aa****, and* ***3fa*** *respectively using the B3LYP/6-31G (d, p) basis set level in acetonitrile solvent modeled by PCM approach*

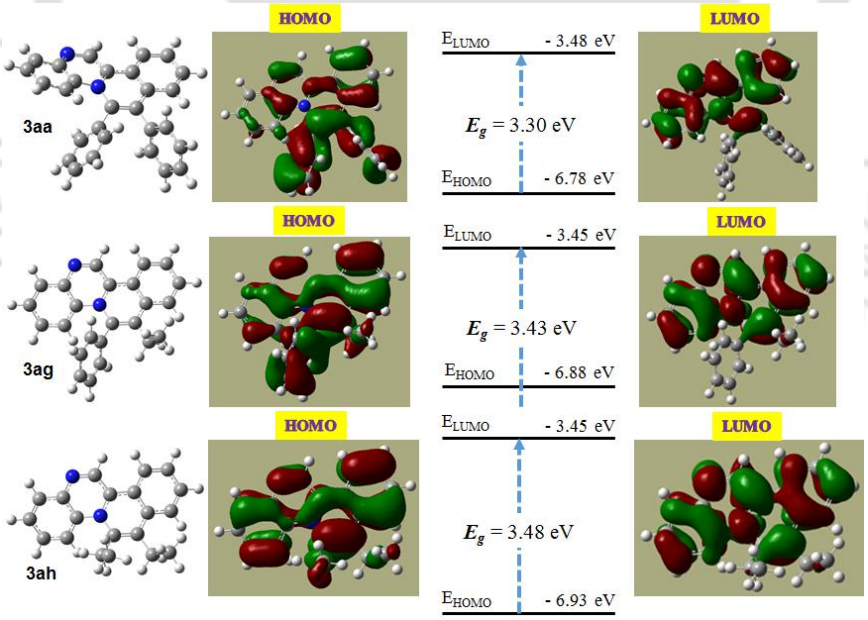

Figure II.4.5. *DFT optimized structures and HOMO-LUMO energy level diagrams of synthesized compounds* ***3aa****,* ***3ag****, and* ***3ah*** *respectively using the B3LYP/6-31G (d, p) basis set level in acetonitrile solvent modeled by PCM approach*

TH-3369_166122017

Photo-physical Properties:

Having synthesized a series of quinoxalinium salts, the photo-physical behavior of the compounds was explored. The donor-acceptor type annulated quinoxalinium salts exhibited two absorption bands in the UV–visible region (Table II.4.1). One is attributed to π–π* transitions in the molecular backbone at 369–410 nm and the other appearing at 403–430 nm is for the charge transfer transitions between electron-donating diphenyl units and the electron-accepting quinoxaline core. In acetonitrile solution, the quinoxalinium salt **3aa** showed absorption peaks at 378 nm and 422 nm with high extinction coefficients (ε) 9800 and 10900 M^{-1} cm^{-1}, respectively (Table II.4.1).

Table II.4.1. *Optical Properties of Representative Quinoxalinium Salts*

Entry	$\lambda_{max,abs}$ *(nm)*[a]	*ε (1 x* 10^4*)* M^{-1} cm^{-1}	$\lambda_{max,em}$ *(nm)*[b] $\lambda_{max,ex}$ *(nm)*	*Stokes shift*[c] *(nm)*	*Quantum yield*[d] *(*Φ_F*)*	*Life time (ns)*[e] *(τ)*
3aa	378, 422	0.98, 1.09	535 (378)	158	0.20	10.9
3ba	385, 413	1.32, 1.29	529 (385)	144	0.13	10.2
3da[f]	411	1.61	529 (411)	118	0.10	4.6
3ea+3e´a	380, 455	0.75, 0.89	562 (380)	182	0.14	14.8
3fa	369, 429	0.86, 1.06	554 (369)	185	0.15	12.8
3ga	380, 421	1.19, 1.20	539 (380)	159	0.10	7.0
3ha	380, 414	0.96, 1.06	535 (380)	155	0.17	10.1
3ja	410, 430, 493	1.21, 1.60, 0.37	645 (430)	215	---	1.1
3la	382	0.75	512 (382)	130	0.03	2.3
3ma	382, 428	1.01, 1.59	518 (382)	136	0.19	6.4
3na+3n´a	382, 430	0.98, 1.28	528 (382)	146	0.18	8.2

[a]Recorded in 15 μM HPLC grade acetonitrile solvent at 25 °C. [b]Measured in 3 μM HPLC grade acetonitrile solvent at 25 °C excited at their corresponding π-π absorption wavelengths. [c]Stokes shift =* $\lambda_{max,abs}$ *-* $\lambda_{max,em}$ *(nm),* $\lambda_{max,ab}$ *are their π-π* absorption wavelengths. [d]Determined by quinine sulfate (*Φ_F *= 0.577), as standard in 0.1 M* H_2SO_4 *solution on excitation at 370 nm. [e]Excited at 375 nm. [f]merged π-π* and CT band both are together.*

The localization of HOMO and LUMO along with the presence of prominent charge transfer bands in the UV–vis spectrum suggest charge transfer in the ground as well as excited states, which is confirmed by TD–DFT calculation. The positively charged site in quinoxalinium salt is a strong electron acceptor, thereby it should be possible to tune their absorptions and more so the emissions by altering the donor (HOMO) and acceptor (LUMO) part of the molecules. However, the absorption spectra of these compounds barely changed, suggesting a stable ground state of these compounds. The UV–vis absorption data of selected compounds are summarized in Table II.4.1 and Figure II.4.6. The fluorescence emission of some selected quinoxalinium salts was also recorded which is summarized in

TH-3369_166122017

Table II.4.1 and Figure II.4.6. In acetonitrile solution (**3aa**–**3ah**) salts exhibited strong fluorescence emission in the range of 488–645 nm with large Stokes shifts (108–215 nm). The fluorescence lifetime of the selected compounds is summarized in Table II.4.1.

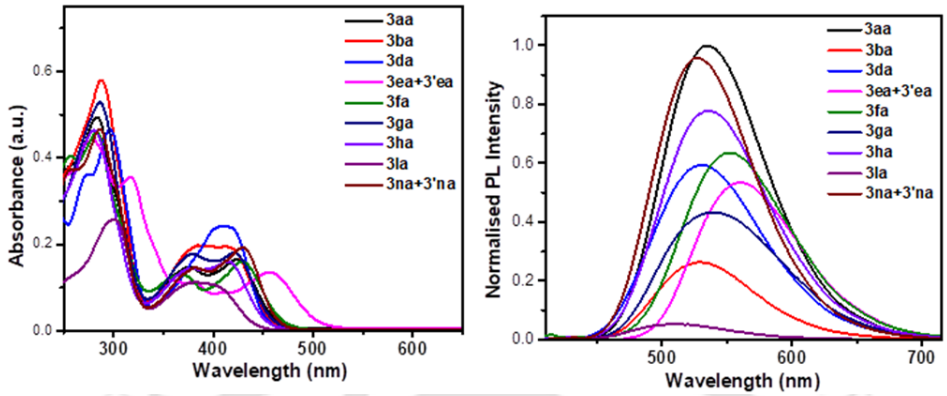

Figure II.4.6. *UV-vis and photoluminescence spectra of some representative quinoxalinium salts*

The quantum yields of these compounds were assessed with respect to quinine sulphate in 0.1 M H_2SO_4 reference in acetonitrile solution (Table II.4.1). Unlike their UV-vis absorption spectra which barely changed either in the presence of electron-donating or electron-withdrawing groups in their donor (HOMO) or acceptor (LUMO), their emission spectra are quite sensitive. Emission spectra of a few sets of quinoxalinium salts can be correlated well with the energy gap of the HOMO–LUMO obtained from the theoretical calculation (Figures II.4.7, II.4.8, and II.4.9).

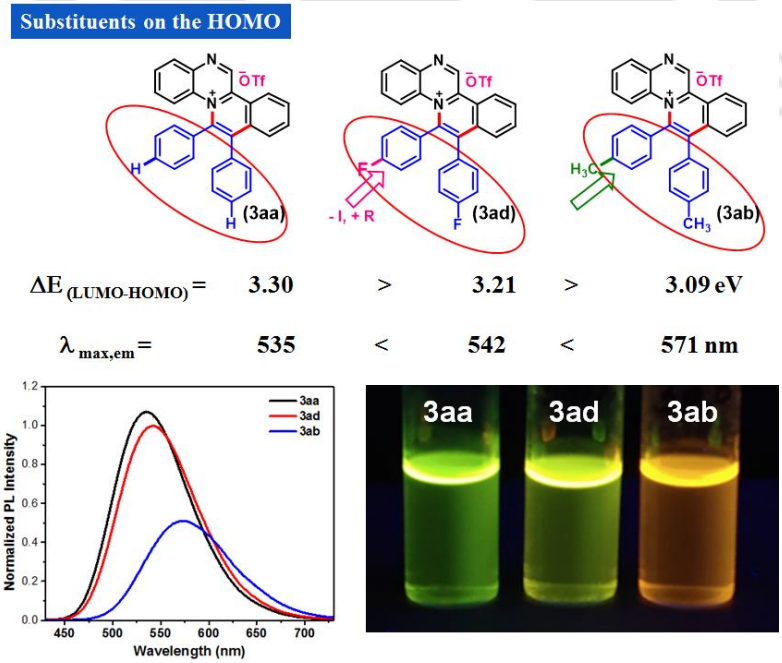

TH-3369_166122017

Figure II.4.7. *Effect of the substituents of HOMO to fluorescence emissions of* ***3aa***, ***3ad***, *and* ***3ab***

The unsubstituted quinoxalinium salt **3aa** gives strong fluorescence emission at 535 nm with a large Stoke shift of 158 nm (Table II.4.1). As ascertained from the theoretical calculation that the presence of an electron-donating group at the HOMO and an electron-withdrawing group in the LUMO should decrease the energy gap. Thus, the introduction of a *p*-F (**3ad**) or a *p*-Me (**3ab**) group at the two phenyl rings i.e the HOMO part cause a drop in energy gap of 3.21 eV and 3.09 eV compared to **3aa** (3.30 eV). This reduction in the energy gap results in red-shifted emissions at 542 and 571 nm, respectively (Table II.4.1 and Figure II.4.7). Further, the presence of an electron-donating *p*-Me (**3ba**) at the quinoxaline (LUMO) causes an increase in energy gap thereby giving a blue-shifted emission at 529 nm compared to **3aa** (535 nm).

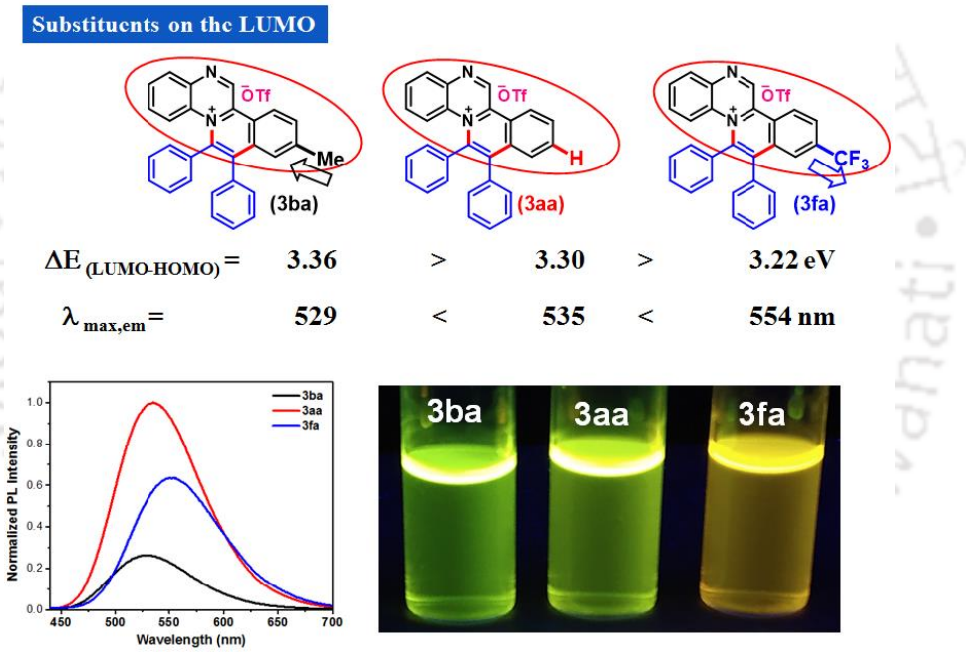

Figure II.4.8. *Effect of the substituents of LUMO to fluorescence emissions of* ***3ba***, ***3aa***, *and* ***3fa***

An exactly opposite effect was observed in the presence of an electron-withdrawing *p*-CF_3 (**3fa**) group in the LUMO, which reduced the energy gap to 3.22 eV giving a red-shifted emission peak at 554 nm (Table II.4.1 and Figure II.4.8). The phenyl group is a better electron donor than the alkyl (ethyl) group. Thus, the replacement of one or both phenyl groups in the donor (HOMO) part with ethyl groups should increase their energy gaps causing hypsochromic shifts. An observed blue-shifted emission peaks at 515 and 488 nm (Table II.4.1 and Figure II.4.9) respectively for (-Ph, -Et) (**3ag**), (-Et, -Et) (**3ah**) donor-acceptor systems confirms our proposition.

TH-3369_166122017

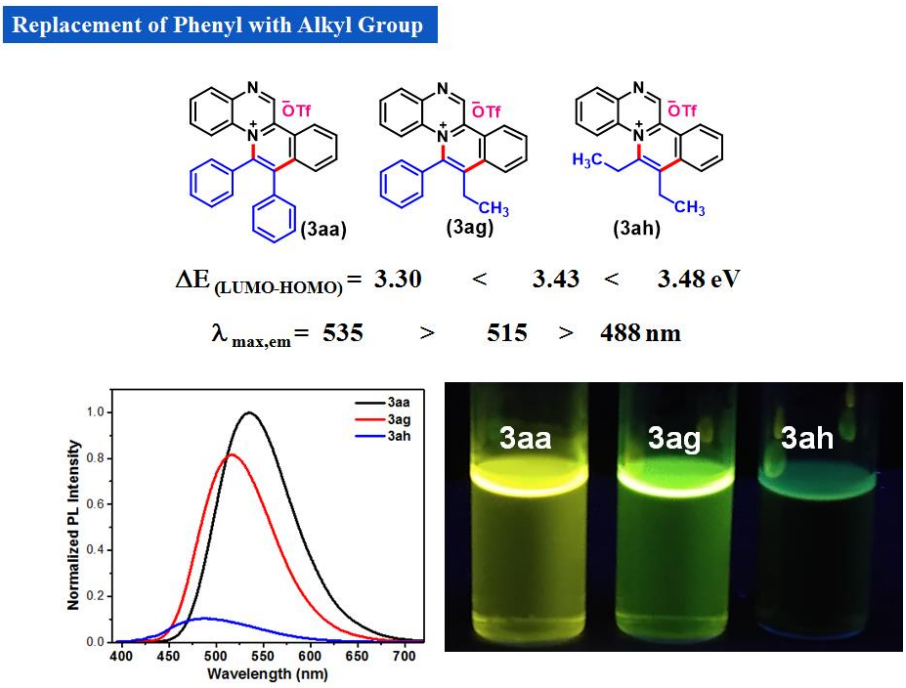

Figure II.4.9. *Effect of the substituents of HOMO to fluorescence emissions of* ***3aa***, ***3ag***, *and* ***3ah***

Aggregation-Enhanced Emission (AEE):

Usually, organic molecules possessing propeller-shaped structures or rotatory groups are weakly emissive in polar solvents due to the ultrafast motions of the rotors consuming the excitation energy of the excited state molecules. However, they are amenable to aggregation-induced emission (AIE) or aggregation-enhanced emission (AEE) because of their restricted intramolecular motion caused by mechanistic restriction, constraints of neighboring molecules, or deleterious π–π stackings.[19a,19b,22,24,25] The synthesized quinoxalinium salt (**3aa**) having a D-π-A configuration exhibited aggregation in DMF/water solvent system. With increase in the water fraction (f_w) in pure DMF reveals that **3aa** has AEE active luminogenic character (Figure II.4.10A). Initially, **3aa** is moderately emissive when dissolved in pure DMF due to the two phenyl rotors' rapid dynamic rotation and vibration. A progressive increase in the water fraction in pure DMF (10% to 90%) displayed a gradual enhancement in the fluorescence intensity with the red-shifted emissions from 535 to 557 nm (Figure II.4.10A). At 99.2% f_w, **3aa** reached an extreme level and formed a nano-aggregation which gained a maximum intensity of 6.36 fold compared to pure DMF (Figure II.4.10B). In an aggregated state, the enhancement in fluorescence intensity is responsible for the restricted intramolecular motion (RIM) which modulates the deactivation in a radiative manner. The difference in emissions of the solid and the solution state of (**3aa**) may be due to the change in packing mode and intermolecular interactions. In the solid state, the two phenyl rings are twisted out of the quinoxaline core thereby diminishing the extended

TH-3369_166122017

π–conjugation and emitting in the green region. Whereas, in solution, due to the aggregation they acquire planarity hence extending the π–conjugation and causing a bathochromic shift to the yellow region.

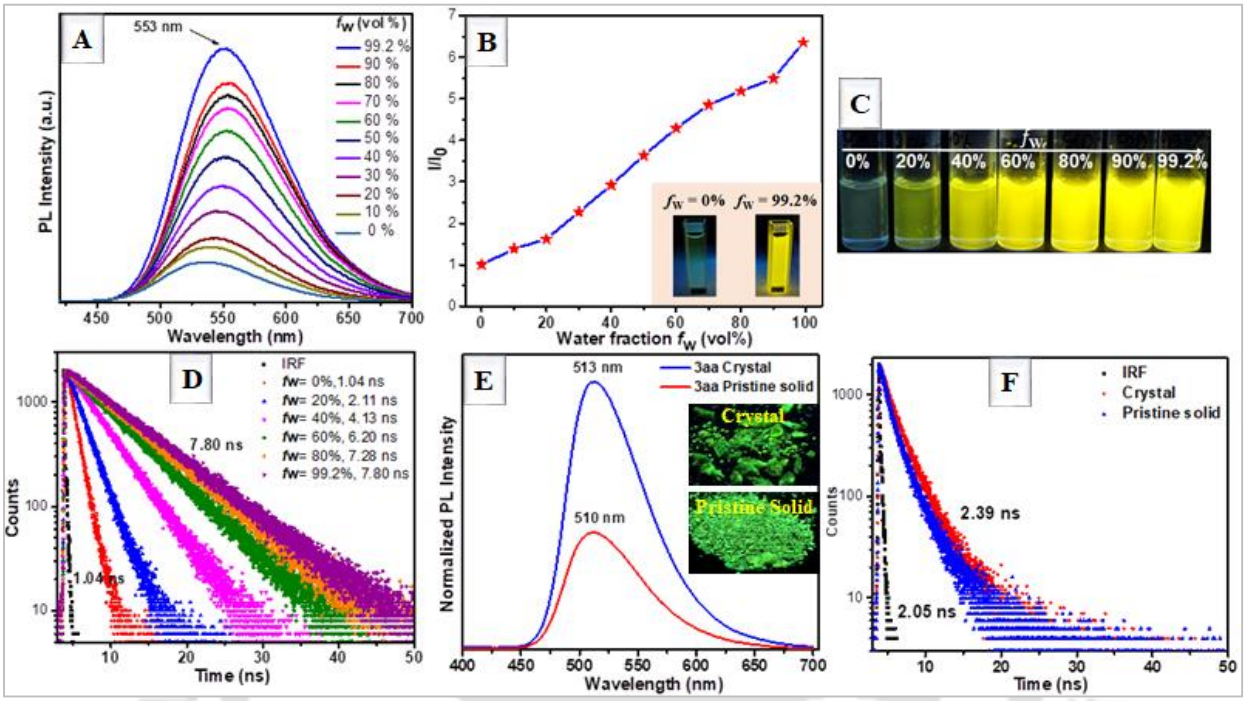

Figure II.4.10. *(A) PL spectra of* ***3aa*** *in DMF/water mixtures with different water fraction (f_w), concentration = 60 μM, λ_{ex} = 375 nm and slit = 2. (B) The plot of emission maximum and the relative intensity (I/I_0) versus the composition of DMF/water mixture of* ***3aa****, where I_0 is the intensity at 0% f_w. Inset: fluorescence photograph of* ***3aa*** *in DMF and in DMF/water mixture with 99.2% f_w under 365 nm UV lamp. (C) Fluorescence photographs of* ***3aa*** *in DMF/water mixture with 0, 20, 40, 60, 80, 90 and 99.2% water content taken under 365 nm UV lamp. (D) Fluorescence decay curves of* ***3aa*** *in DMF/water mixture with 0, 20, 40, 60, 80 and 99.2% water content at excitation at their corresponding fluorescence λ_{max}. (E) The normalized solid state PL spectra of crystalline* ***3aa*** *and pristine solid* ***3aa*** *at, λ_{ex} = 375 nm and slit = 5. Inset: fluorescence photographs of crystalline and pristine solid state of* ***3aa*** *under 365 nm UV lamp. (F) Fluorescence decay curves of* ***3aa*** *in crystalline and pristine solid state*

The AEEgen-concentration dependent morphological investigation confirmed the formation of a nano-crystalline at 60 μM (Figure II.4.11A) and distorted nano-spherical aggregates at 30 μM (Figure II.4.11C) concentration in 99.2% and 99.6% f_w in DMF, respectively. Time-resolved photoluminescence study also reveals that with increasing water fraction in DMF at a probe concentration of 60 μM (from f_w 0 to 99.2 vol%), the life time of quinoxalinium salt **3aa** boosted from 1.043 ns to 7.798 ns, thus confirming their substantial stability in the excited state (Figure II.4.10D). This result further endorses the formation of aggregation in higher water fractions. Transmission

TH-3369_166122017

electron microscopic (TEM) analysis also suggests the formation of crystalline aggregates at 60 µM (99.2% f_w) (Figure II.4.11B) and distorted spherical aggregates (~40 to ~80 nm) at 30 µM (99.6% f_w) concentration of AEEgen **3aa** (Figure II.4.11D and Figure II.4.12B). The formation of crystalline aggregates for 60 µM concentration was further confirmed by selected area electron diffraction (SAED) pattern from TEM (Figure II.4.12A).

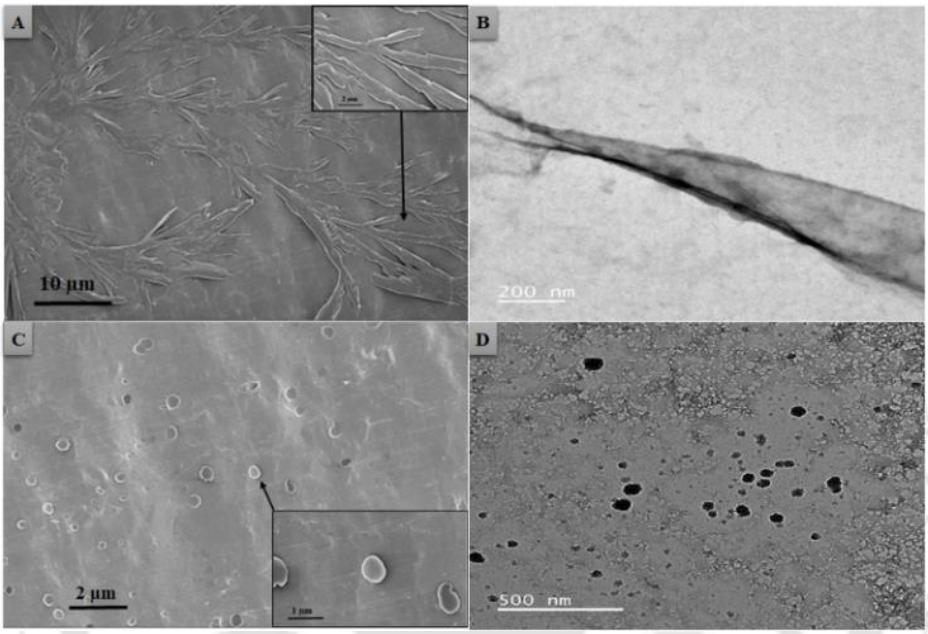

Figure II.4.11. *FESEM images of the morphology of the luminogen* ***3aa*** *formed in 99.2% f_w at conc. 60 µM (A) and in 99.6% f_w at conc. 30 µM (C) by drop casting technique applied on aluminum foil at room temperature. The insets are the magnified images of the corresponding morphology. (B) TEM image of crystalline* ***3aa*** *aggregates formed in DMF/water mixture with a 99.2% water fraction. Concentration: 60 µM. (D) TEM image of distorted spherical* ***3aa*** *aggregates formed in DMF/water mixture with a 99.6% water fraction. Concentration: 30 µM*

Dynamic light scattering (DLS) measurement divulges the average hydrodynamic diameter of the aggregates are 375.7 nm for 60 µM concentration and for 30 µM concentration it is 164.9 nm (Figure II.4.13). In pristine solid and crystalline states, **3aa** exhibits strong fluorescence emissions at 510 nm and 513 nm with a tri-exponential decay having an average lifetime of 2.05 and 2.39 ns (Figure II.4.10E and Figure II.4.10F).

TH-3369_166122017

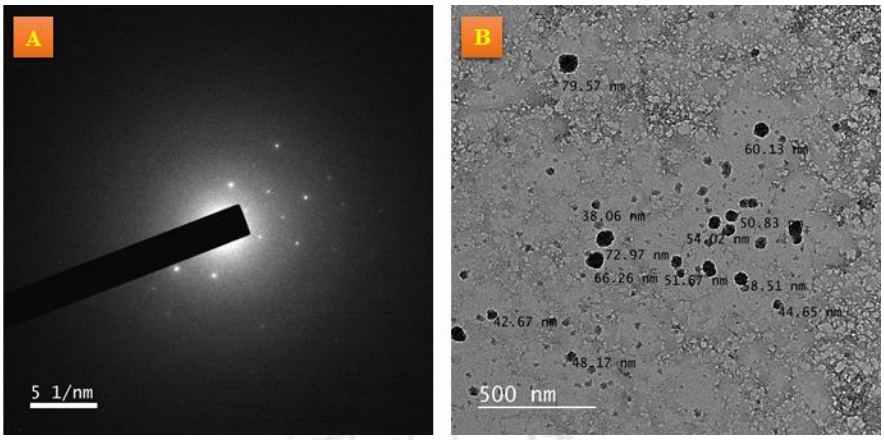

Figure II.4.12. *(A) SAED pattern of the crystalline aggregates at 60 µM conc. of* ***3aa****. (B) Sizes of the distorted spherical aggregates at 30 µM conc. of* ***3aa***

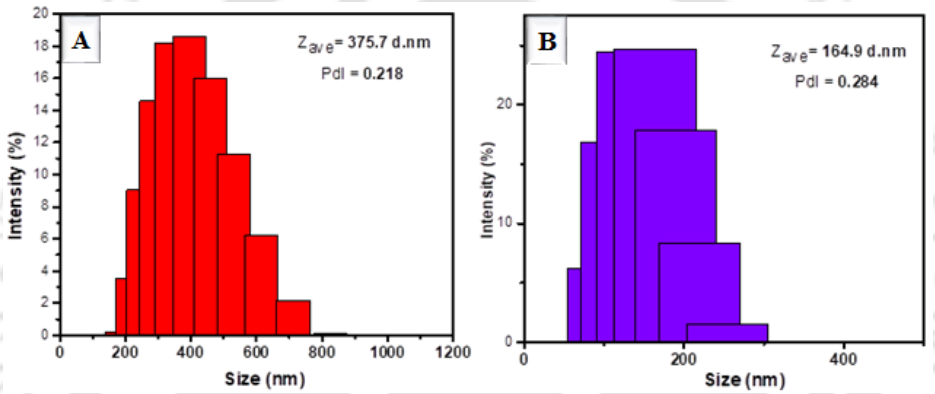

Figure II.4.13. *Size distribution plot of* ***3aa****. (**A**) crystalline aggregates in 99.2 % water – 0.8 % DMF solution at 25 °C. Concentration = 60 µM. (**B**) distorted spherical aggregates in 99.6 % water – 0.4 % DMF solution at 25 °C. Concentration = 30 µM*

AEE Mechanism:

The restriction in intramolecular motions including rotation and vibration is the main reason behind the turn-on fluorescence emission in any aggregated state. Single crystal X-ray and DFT-optimized structure of AEEgen **3aa** reveals that the two rotatable phenyl rings and the slightly bent propeller-shaped vibrate-able quinoxaline core are available for non-radiative deactivation. To ascertain the existence of RIM in the aggregated state two control experiments viz. viscochromism and thermo-chromism were carried out. In the viscochromism experiment, the photoluminescence (PL) measurement of **3aa** was carried out at varying compositions of three-fold more viscus glycerol solvent (f_G = 0, 30, 60, and 90%) in MeOH (Figure II.4.14A). With varying percentages of glycerol, a progressive increase in the PL intensity was observed and at f_G = 90%, it gained an enhancement of

TH-3369_166122017

1.77 fold compared to **3aa** in pure MeOH. This enhancement in the PL intensity is due to the freezing of intramolecular rotations and vibrations in the more viscous medium (Figure II.4.14A).

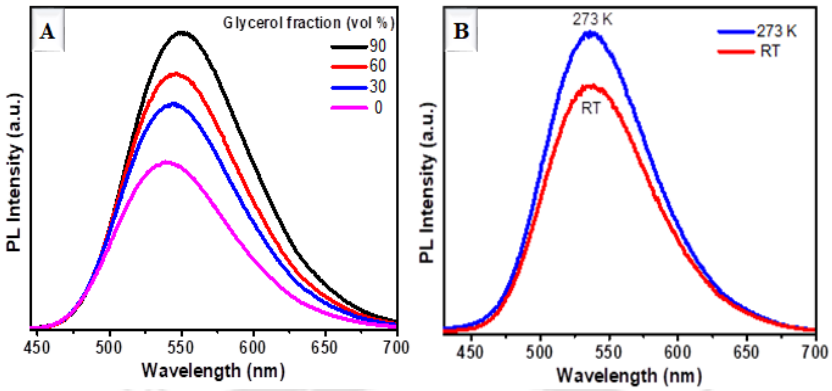

Figure II.4.14. *(A) PL spectra of **3aa** in MeOH/Glycerol mixtures with different glycerol fraction (f_G), concentration = 15 μM. (B) PL spectra of **3aa** in DMF, concentration = 60 μM. λ_{ex} = 375 nm and slit = 2*

A 1.21-fold enhancement in PL intensity was observed on freezing the DMF solution of **3aa** from room temp to 273 K (Figure II.4.14B), which is due to the thermochromic behavior of the molecule. These observations suggest that a drop in temperature or an increase in the viscosity of the medium diminishes the molecular dynamic motions, thereby restricting the non-radiative deactivation processes reminiscent of the RIM mechanism of the present system. Furthermore, due to a donor-acceptor type configuration, the AEEgen (**3aa**) showed weak solvent-dependent photophysical behaviors. The two UV absorptions maxima observed were in the range of 372-378 nm for π–π* and 422-428 nm for the CT band measured in a range of solvents such as DCM, acetone, DMF, acetonitrile, methanol, DMSO (Figure II.4.15). Thus, the absorption maxima barely changed from a less polar solvent such as DCM (378 and 430 nm) to a more polar DMSO (375 and 428 nm). With an increase in the solvent polarity, slight red-shifted emissions from 527 to 537 nm were observed, associated with reduced fluorescence intensity on increasing the solvent polarity from DCM to MeOH. In a more polar aprotic solvent, DMSO, there was no emission at all (Figure II.4.15). Interestingly, in acetonitrile, **3aa** showed fluorescence emission, which may be because of the interaction intense of quaternary ammonium salt and coordinating acetonitrile solvent. This quenching in fluorescence emission suggests the presence of an intramolecular charge transfer (ICT) in (**3aa**) in the solution state. Whereas, in the aggregated state the suppression of ICT effect is responsible for delivering strong fluorescence emission to AEEgen (**3aa**).

TH-3369_166122017

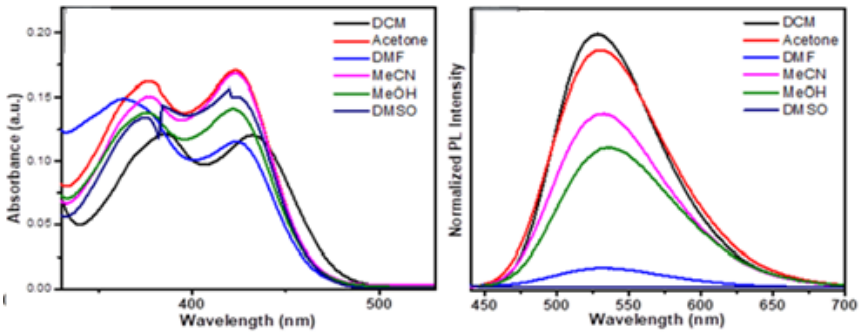

Figure II.4.15. *AEE mechanism: UV absorption (conc= 15 µM) and PL spectra (conc= 3 µM) of* ***3aa*** *in different polarity*

Single Crystal Structural Interpretation:

To elucidate the fluorescence character in the solid state as well as the AEE phenomenon of quinoxalinium salt **3aa**, it was crystallized from acetonitrile. Interestingly, **3aa** crystallized with one molecule of water having a triflate counter anion (Figure II.4.16A). Single crystal X-ray crystallographic investigation of **3aa** reveals the existence of several non-covalent interactions such as C–H...N, C–H...π, C–H...O, C–H...F which play crucial roles in restricting intramolecular motions toward non-radiative decays thus giving highly fluorescent appearance. The oxygen atom of the adopted water molecule in the molecular core of **3aa** delivers strong short-contact intermolecular H-bonding interaction (2.519 Å) with the adjacent aromatic C–H of the quinoxaline core (Figure II.4.16B). Multiple intermolecular C–H...N, C–H...π interactions (2.617–3.042 Å) between molecules form a two-dimensional supramolecular chain which offers rigidity in the aggregated state towards non-radiative deactivations (Figure II.4.16C and Figure II.4.16D). The crystal packing of **3aa** shows the presence of parallel displaced weak intermolecular π–π interactions in the range of (8.074–4.177 Å, centroid to centroid) which rules out possibilities of any π–π stacking interactions causing quenching in luminescence character in the solid state. Similar to theoretical calculations, the crystal structure also revealed the existence of twisted propeller-shaped donor–acceptor conformation of **3aa** (Figure II.4.17). This propeller-shaped confirmation eliminates the possibilities of specific *J* or *H*-aggregates.[54] The measured dihedral angles between the mean plane of the acceptor quinoxaline core and the donor phenyl rings are 55.74° and 85.53° (Figure II.4.16A). Thus, the two phenyl rings are twisted out of the quinoxaline core. Further, the phenyl rings are in different planes having a dihedral angle of 61° (with respect to their mean planes).

TH-3369_166122017

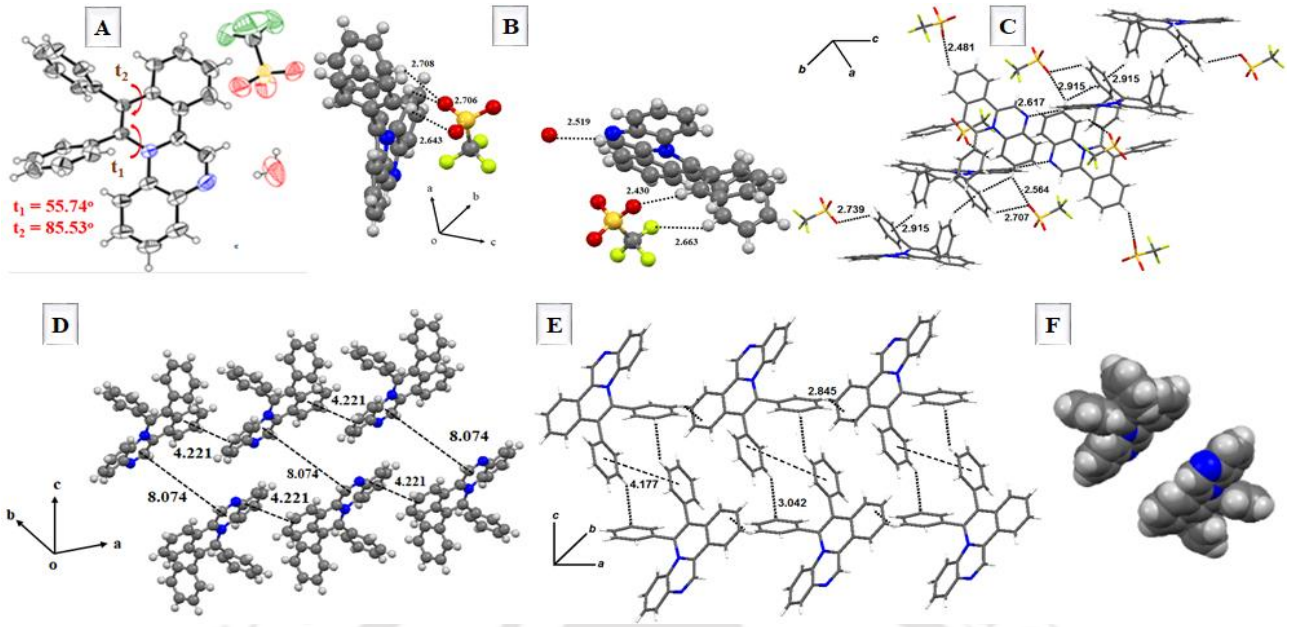

Figure II.4.16 *(A) ORTEP diagram of* ***3aa*** *along with the dihedral angles of the two phenyl rings to the quinoxaline plane are mentioned. Crystal packing of* ***3aa****. (B) showing various intramolecular H-bonding interactions in the ball-stick model, where distances are mentioned in Å. (C) C−H···O and C−H···F hydrogen bonds with triflate ions, C−H···N interaction are also shown. (D) and (E) Multiple C−H···π and weak π···π interactions between the molecules. (F) Space fill model of* ***3aa*** *showing weak π···π interactions*

This twisted conformation of **3aa** and the presence of multiple intermolecular interactions are responsible for the restriction of π–π stacking interactions, making them highly fluorescent in the solid and aggregated states.[19a,19b,22,24,25] From the crystal structure of **3aa**, it is evident the AEEgen possesses a stator-rotor structure having twisted 3D conformation held by multiple weak interactions. Thus, they are expected to be more sensitive towards mechanical forces, which may perturb the structure leading to chromic response.[19b,32-37]

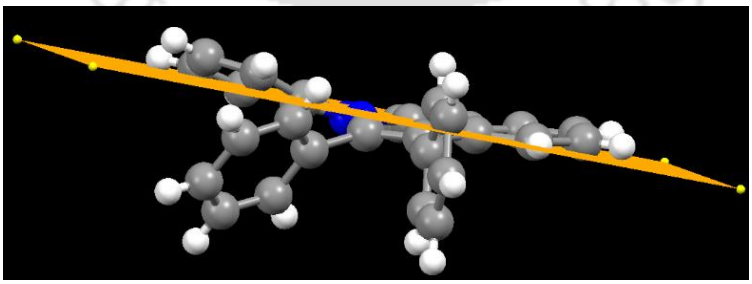

Figure II.4.17. *Molecular plane of quinoxaline core in* ***3aa****, showing propeller conformation*

TH-3369_166122017

Mechanochromic Luminescence Character:

The mechanochromic behavior was investigated by grinding the pristine sample of **3aa** in a mortar and pestle. Upon grinding, a change in the color from green to yellowish green was observed in the naked eyes as well as under a 365 nm UV lamp (Figure II.4.18A). In photoluminescence, the pristine sample showed an emission peak at 510 nm, whereas the ground sample exhibited an intense bathochromic shifted ($\Delta\lambda$ = 22 nm) emission peak at 532 nm (Figure II.4.18B). The red-shifted and intense fluorescence emission of the grounded sample conveys that upon grinding the twisted conformation of **3aa** is transformed to a planar form, which offers an extended molecular conjugation and thereby enhances D-π-A interaction.[37] To have further insight into the mechanism of mechanochromic behavior, powder X-ray diffraction (PXRD) and field emission scanning electron microscope (FESEM) of both the pristine and ground samples were recorded for analyzing their phase morphology. The PXRD pattern of the pristine **3aa** sample showed sharp and intense reflection peaks, which confirmed its crystallinity in correlation with the simulated PXRD pattern obtained from the **3aa** single crystal data (Figure II.4.18C). Interestingly, after grinding it displayed a board but very less intense diffused reflection peaks, which suggests its transformation from crystalline to an amorphous state (Figure II.4.18C). A change in size and morphology of the ground sample compared to the pristine sample has been confirmed from their FESEM images (Figure II.4.18D and Figure II.4.18E).

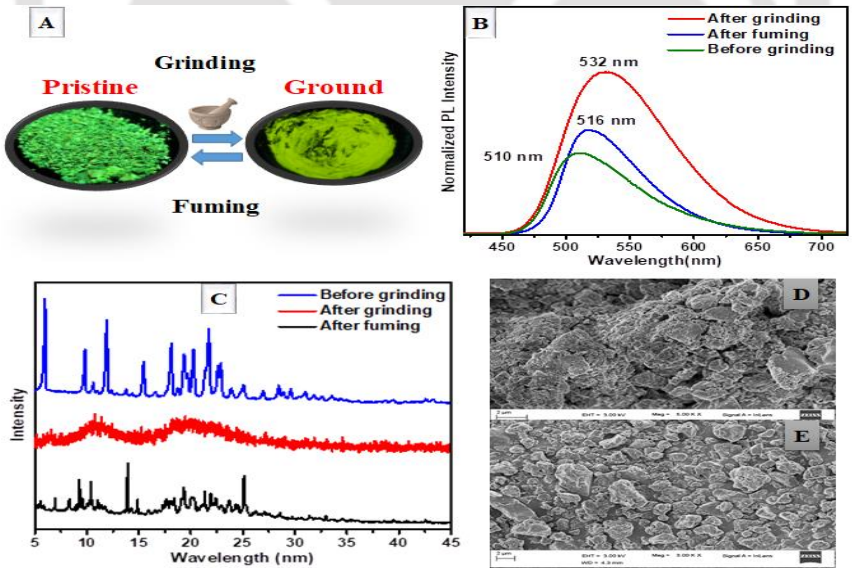

Figure II.4.18. *(A) Change in fluorescence images of **3aa** upon grinding and fuming on DCM at 365 nm UV irradiation. (B) The normalized PL spectra of **3aa** were recorded before grinding, and after grinding after fuming the sample in mortar-pestle at room temperature (λ_{ex} = 375 nm). (C) XRD diffractograms of pristine, ground and fumed **3aa** sample. (D and E) FESEM images of luminogen **3aa**, taken before grinding (D) and after grinding (E) the solid sample*

TH-3369_166122017

The fluorescence mean lifetime of the grounded sample is reduced to 1.78 ns compared to the pristine (2.05 ns) (Figure II.4.19). Further, fuming the ground sample (λ_{max} 532 nm) of **3aa** in DCM vapor for 20 minutes a near crystalline state (λ_{max} 516 nm) is restored, which is associated with the change in color from yellow to green (Figure II.4.18B). The regeneration of the pristine state from the powdered form upon exposure to solvent vapor has been confirmed from the PXRD measurement of the sample after DCM fuming (Figure II.4.18C). Thus, the outcome of all the experiments reveals that the AEEgen **3aa** endures reversible mechanochromic behavior by changing its phase from crystalline to amorphous and again returned back to a crystalline pristine solid state upon mechanical stimulation followed by DCM solvent fuming (Figure II.4.18).

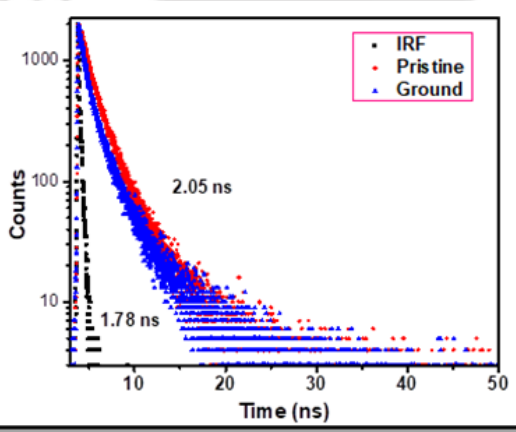

State	Emission (nm)	τ_1 ns / (a_1)	t_2 ns / (a_2)	t_3 ns / (a_3)	χ^2	< t > ns
Pristine	510	0.812 / (34.394)	2.117 / (56.616)	6.485 / (8.990)	1.003	2.05
Ground	532	0.264 / (20.065)	1.235 / (53.779)	4.087 / (26.156)	1.000	1.78

Figure II.4.19. *Fluorescence decay curves of pristine and ground* ***3aa*** *sample*

Development of Latent Fingerprint:

Fingerprint impressions are left on various surfaces from friction ridges of human fingers, which cannot be viewed efficiently in naked eyes. Because of its unique ridge pattern and unchanged nature, throughout the life of a person, detection of fingerprints is one of the key forensic investigations tool in crime cases as well as in our daily life such as in biometric identification, access control and security links.[55-57] The most common form of the fingerprints is the latent fingerprints (LFPs), developed by various means on a surface left behind by the depositions of sebum from human fingers. Generally, LFPs are invisible to the naked eye hence, several techniques such as chemical staining,[58] powder dusting[59] and fluorescent dye staining[60] have been developed for their enhanced visualization. Among

TH-3369_166122017

them fluorescent dye staining techniques offers highly intense and more selective imagining of fingerprints with low back-ground interferences.[61] Various groups have developed several fluorescent based compounds for the LFPs investi-gations.[62,63] In past few years AIEgenic fluorescence com-pounds were also introduced for the enhanced visualizations of LFPs.[64] In general, LFPs contain various inorganic salts, amino acids and lipid molecules secreted from sebaceous glands. Due to the amphiphilic nature of AEEgens, they can interact with both hydrophobic and hydrophilic components of the sebum much more efficiently than the traditional neutral luminescent materials.[64c] Proficiencies of the synthesized compounds were explored for the LFPs visualization. For this investigation one adult male volunteer rubbed his fingers near nose and forehead to accumulate sebaceous, and the fingerprints were stamped on an adhesive tape. The imprint of the latent fingerprint were then developed by staining it in an H_2O:MeOH (90:10) solution of **3ab** and **3ba** at a concentration of 70 μM for 2 minutes. The developed surfaces were washed with distilled water and dried in the open air. Subsequently, the fingerprints containing substrates were viewed under UV light (365 nm) for first-level (pattern information) and second-level (displaying core, bifurcation, and ridge ending) investigations. Compound **3ab** gave a greenish-yellow appearance to the LFPs over the adhesive tape (Figure II.4.20A) whereas **3ba** furnished deep green LFPs (Figure II.4.20B).

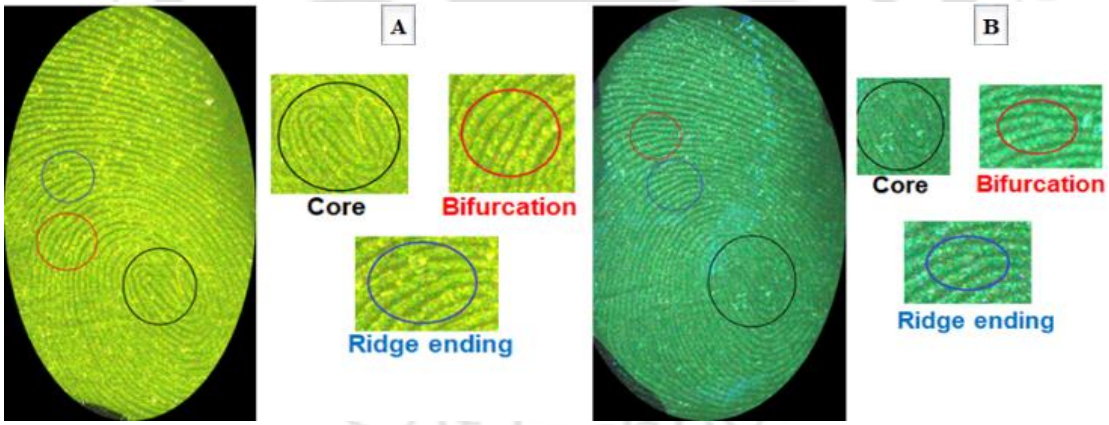

Figure II.4.20. *High-resolution fluorescence images of latent fingerprints on adhesive tape developed with* ***3ab*** *(A) and* ***3ba*** *(B) showing second-level investigation*

Evaluation of Cell Viability:

AlamarBlue-based cell viability assay was performed on HeLa cells treated with the synthesized quinoxalinium compounds for the incubation duration of 24 h. Through this assay, the anti-cell proliferative effects of the compounds were evaluated, to assess their potential for cancer therapeutic application. As depicted in Figure II.4.21, a sharp decrease in cell viability is observed in a dose-

TH-3369_166122017

dependent manner of all the compounds; however, their IC_{50} values are different. The IC_{50} evaluation of Cell Viability. AlamarBlue-based cell viability assay was performed on HeLa cells treated with the synthesized quinoxalinium compounds for the incubation duration of 24 h. Through this assay, the anti-cell proliferative effects of the compounds were evaluated, to assess their potential for cancer therapeutic application. As depicted in Figure II.4.21, a sharp decrease in cell viability is observed in a dose-dependent manner of all the compounds; however, their IC_{50} values are different. The IC_{50} values are 15.25, 3.43, 5.17, 3.54, 5.18, and 5.44 µM for the compounds **3ha**, **3aa**, **3ea+3´ea**, **3ja**, **3ad**, and **3fa** respectively. Significant anti-proliferative activity of the compounds attributed to therapeutic potential to annihilate cancer. The toxicity of the synthesized AEEgens towards noncancerous cells was not evaluated since it was a non-targeted drug delivery approach. However, from the viability assay data as performed, it is apparent that the AEEgens will have anti-proliferative effects on noncancerous cells too in the non-targeted applications.

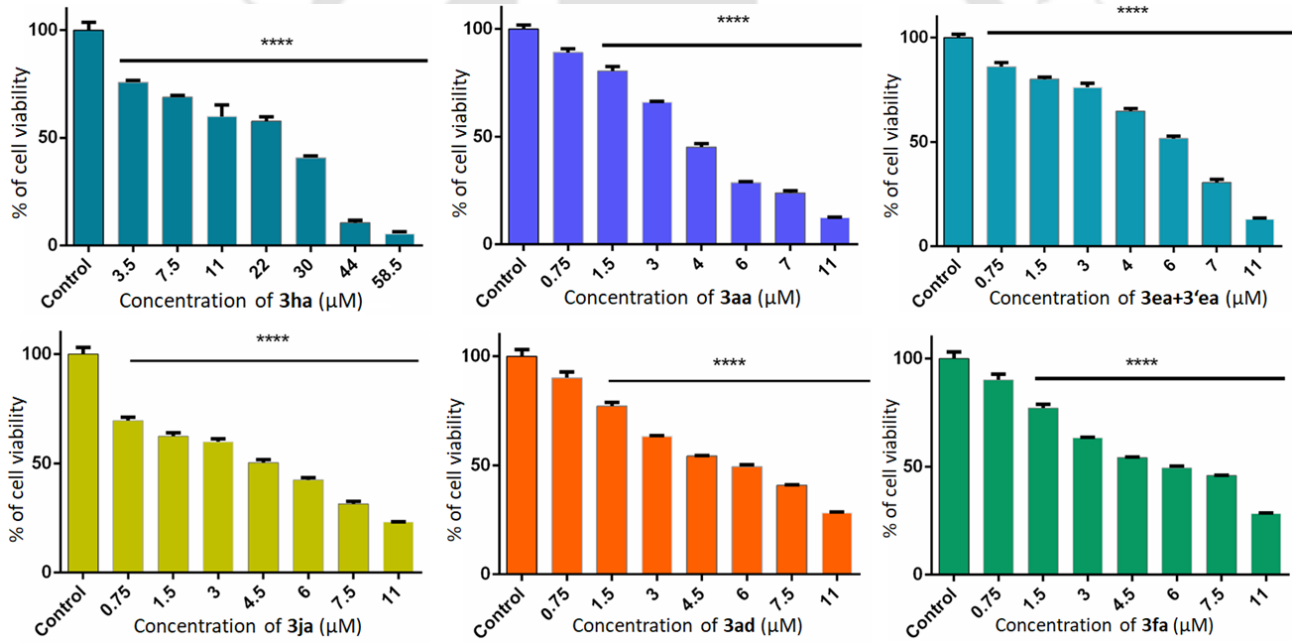

Figure II.4.21. *Effect of compound **3ha**, **3aa**, **3ea+3´ea**, **3ja**, **3ad**, and **3fa** in terms of reduction in the percentage of viable cells as demonstrated by alamerBlue assay. Statistical significance has been determined by one-way ANOVA, where *p<0.05; **p<0.01; ***p<0.001; ****p<0.0001*

Effect on Cell Cycle:

Flow cytometry-based analysis was performed to delineate the impact of compounds on the cell cycle of HeLa cells, rendering growth inhibition. Treatment of HeLa cells with compounds (**3ha**, **3aa**, **3ea+3ẻa**) substantially increased the number of cells in the G1/S phase, and decreased the cell

TH-3369_166122017

population in the G2 phase, as compared to the untreated control cells (Figure II.4.22). Thus, the results indicate that the compounds (at IC_{50}) could induce cell growth inhibition via cell cycle arrest. These findings also correlate with the results observed in the alamarBlue-based cell viability assay and the morphology studies.

Bio-imaging for Uptake Studies:

For clinical diagnostic and biological analysis in vitro cellular imaging using fluorescent bio-imaging techniques are elegant and non-invasive analytical tools.[41,46d,50b] Unfortunately, many organic fluorophores aggregate in biological media owing to the hydrophobic character of their emitting centers, therefore unsuitable for bio-imaging and theranostic application. Most of the synthesized compounds exhibited large Stoke shifts in the range of 108 to 215 nm in acetonitrile solution, which is desirable for in vitro cell imaging to negate UV damage of bio-samples, elimination of inner filtering effect, and reduction in auto-fluorescence.

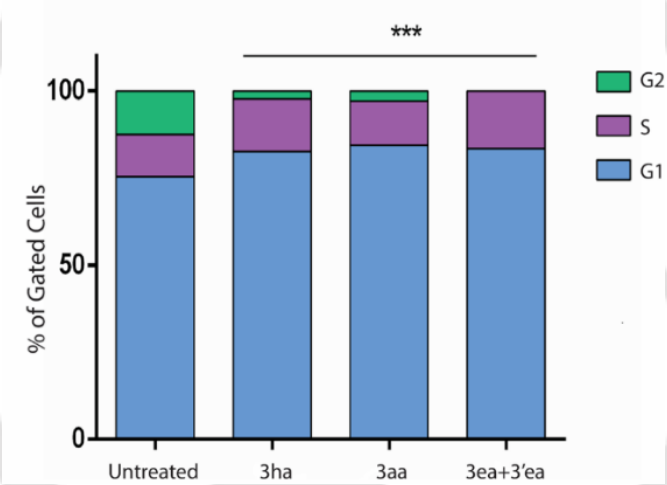

Figure II.4.22. *Flow cytometry-based analysis of the cell cycle of HeLa cells treated with compounds* ***3ha****,* ***3aa****, and* ***3ea+3'ea*** *which shows a reduction of the G2 phase. Statistical significance has been determined by one-way ANOVA, where *p<0.05; **p<0.01; ***p<0.001;****p<0.0001*

In our studies, uptake of the AEEgens into HeLa cells was performed by confocal microscopy after treatment. Figure II.4.23 depicts the clear luminescence of HeLa cells after treatment of the quaternary salts **3ha**, **3aa**, **3ea+3´ea** for a short incubation time (< 10 min).

TH-3369_166122017

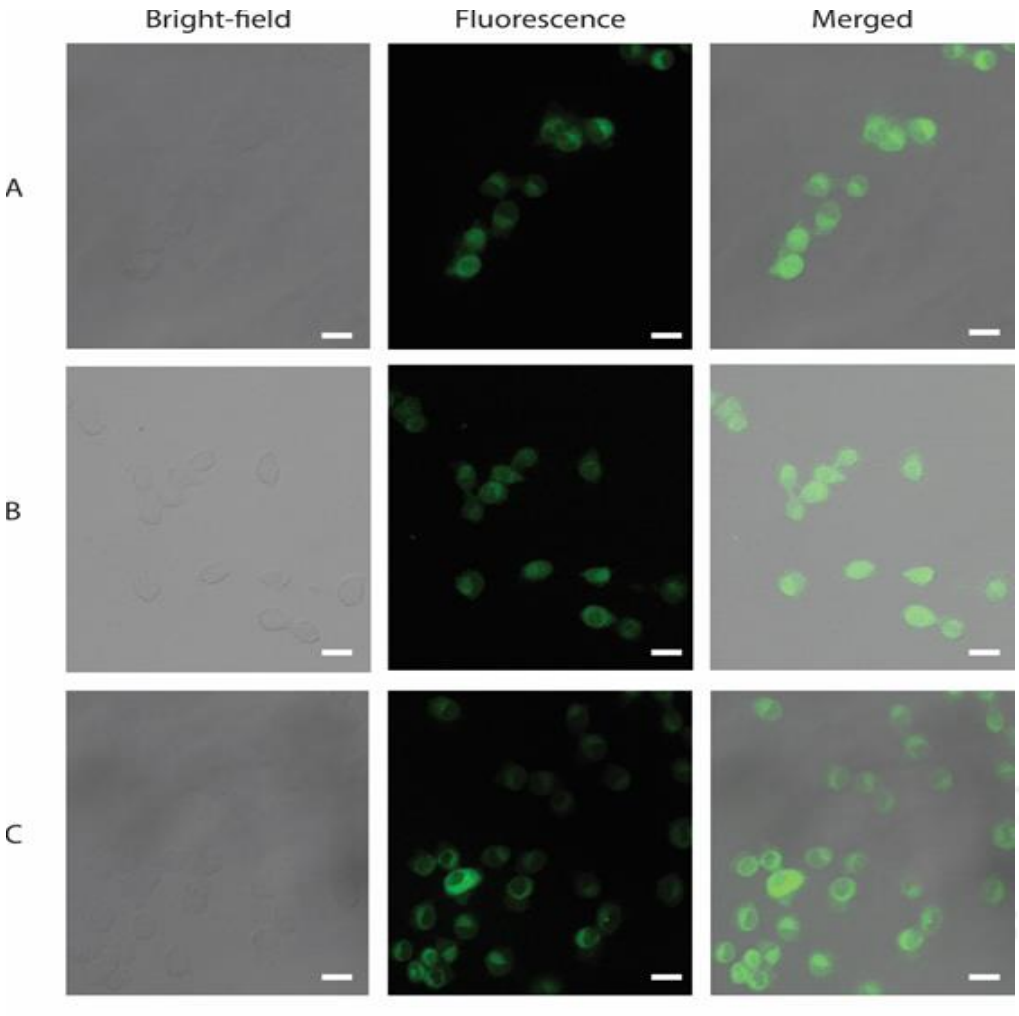

Figure II.4.23. *Confocal laser scanning microscopy images of HeLa cells stained with (**A**) **3ha**, (**B**) **3aa**, (C) **3ea+3′ea**, respectively. Cells were incubated with 145 μM of the AEEgens for 10 min. Excitation: 458 nm. Emission range: 480–605 nm. Scale bar: 20 μm*

The Z stack analysis of the treated cells clearly indicates the uptake of these compounds into HeLa cells (Figure II.4.24). Similarly, Figure II.4.25, shows the bright luminescent of HeLa cells after treatment with **3ja**, **3ad**, and **3fa**, respectively. A shorter incubation time suggests their superior penetrability to cell membranes. From CLSM images (Figure II.4.23), it is apparent that the fluorescence signals are abundant in the cell cytoplasm and to a lower extent even in the nucleus. Thus, it is evident that these compounds could be used as excellent luminescent probes for rapid staining of cell cytoplasm. The staining ability of these compounds is mainly attributed to their positive charged as well as amphiphilic character. While the positively charged species facilitate binding to the negatively charged cancer cells through electrostatic interactions.[65] The concentration of AEEgens for HeLa cell imaging was 145 uM. However, the incubation time was <10 min, whereas for the viability assay, the incubation time was 24

TH-3369_166122017

h. It is apparent that AEEgens could be used for bio-imaging of various cell types including cells of noncancerous origin, since the compounds are highly fluorescent.

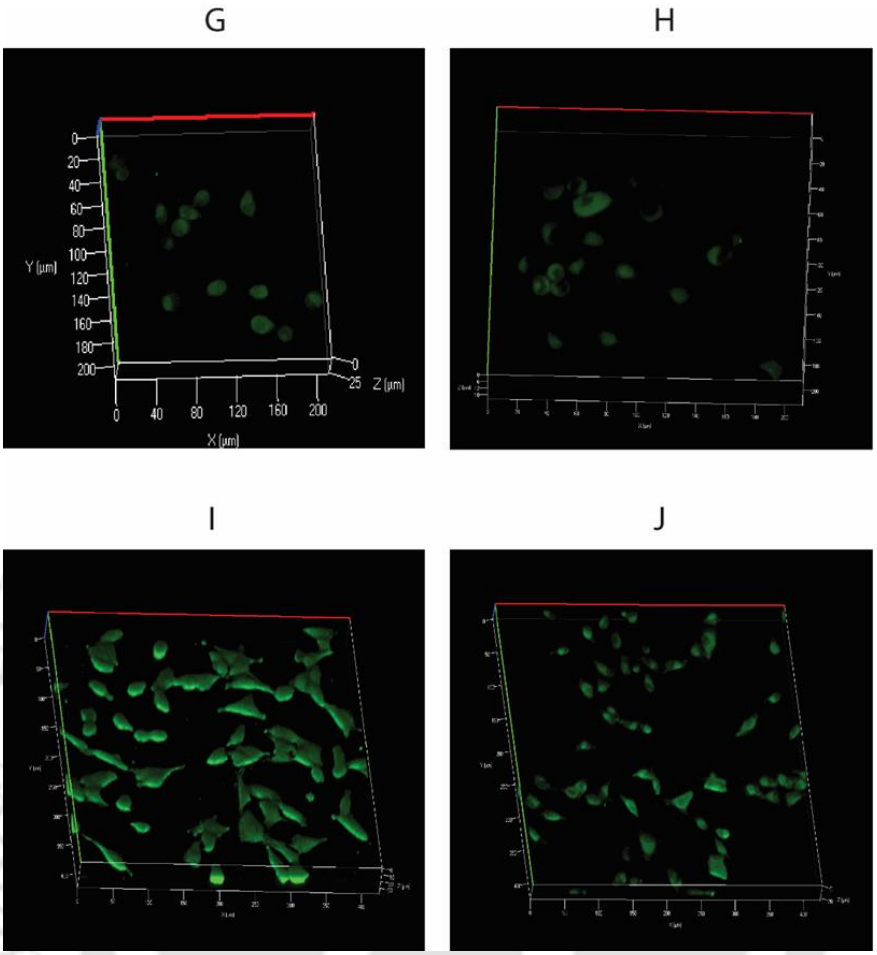

Figure II.4.24. *3D image of HeLa cells stained with* ***3aa****(G),* ***3ea+3'ea****(H),* ***3ja****(I), and* ***3fa****(J) obtained after Z-stacking in confocal laser scanning microscopy*

However, the advantage is that the compounds can bio-image cancer cells, such findings would be explored in the future for targeted delivery and bio-imaging of cancer cells after appropriate conjugations.

In conclusion, a series of multifunctional AEEgens are developed *via* quinoxaline *N*-directed Ru(II)-catalyzed oxidative annulation of 2-aryl quinoxalines with internal alkynes resulting in the formation of annulated quaternary ammonium salts in the presence of $Cu(OAc)_2.H_2O$ as the oxidant. Restriction of intramolecular motion (RIM) shows AEE behavior of the AEEgens having donor–π–acceptor (D–π–A), where two phenyl moieties could act as donors while the extended quinoxaline core is the acceptor.

TH-3369_166122017

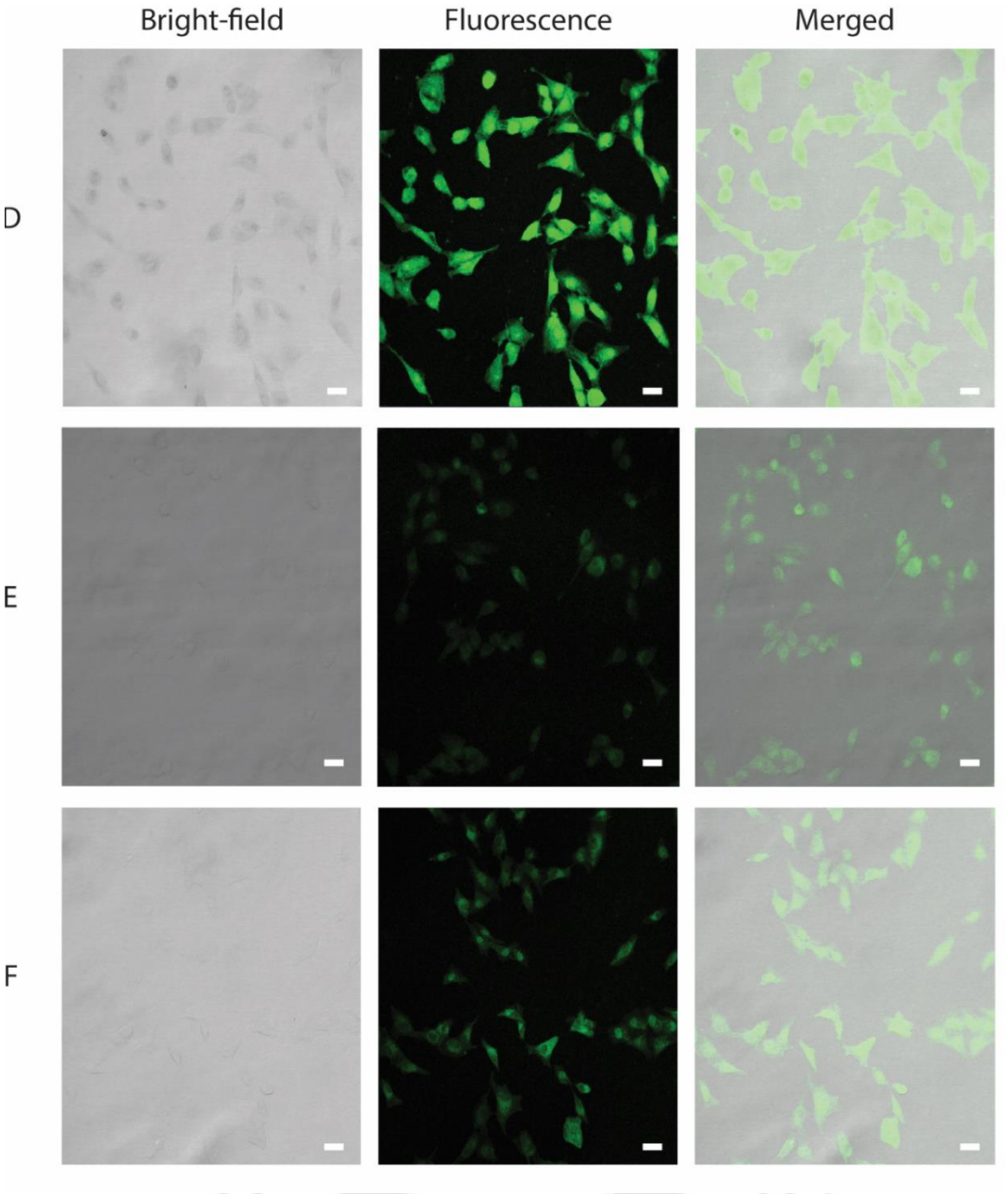

Figure II.4.25. *Confocal laser scanning microscopy images of HeLa cells stained with (D)* ***3ja****, (E)* ***3ad****, (F)* ***3fa*** *respectively. Cells were incubated with 145 µM of the AEEgens for 10 min. Excitation: 458 nm Emission range: 480-605 nm. Scale bar: 20 µm*

The compounds are easy to prepare, possessing stable structures, and tunable emission, and display strong luminescent with large Stokes shift and aggregation-enhanced emission (AEE) with moderate quantum yields. They also exhibit viscochroism and thermochroism behaviors. Such AEEgens having mechanochromic properties can be utilized for latent fingerprints for possible forensic investigation. The compounds have anti-cancer effects, where cellular uptake can be monitored by luminescent

TH-3369_166122017

imaging. Thus, the synthesized AEEgens have multifaceted application potential for forensics and biomedical research.

II.5. Experimental Section

II.5.1. General Information: All the reagents and solvents used were purchased from commercially available sources and used without further purification. HPLC-grade solvents were purchased from commercial sources. For column chromatography 60-120 mesh-sized silica gel was used. DCM-Methanol mixture was used for the purification of compounds. Reactions are monitored by TLC on silica gel 60 F_{254} (0.25 mm). Dulbecco's Modified Eagle's medium (DMEM), Phosphate Buffered Saline (PBS), Paraformaldehyde, Dimethyl sulfoxide (DMSO), Propidium Iodide (PI), RNase A were purchased from Sigma Aldrich (USA). Antibiotic-Antimycotic, Trypsin, Fetal Bovine Serum (FBS), alamarBlue™ were purchased from Thermo Fisher Scientific (USA). All the cell culture plastic wares were purchased from Eppendorf (Hamburg, Germany). All NMR spectra were recorded in acetonitile-d_3 and few were taken in $CDCl_3$ in 600 and 400 MHz NMR. The ^1H spectra were referenced to the residual CD_3CN (1.94 ppm) whereas for $CDCl_3$ it is 7.26 ppm. The ^{13}C spectra were referenced to the residual CD_3CN (118.69 ppm) and for $CDCl_3$ it is 77.16 ppm. All ^{19}F NMR spectra were recorded in 400 MHz, for a few of them hexafluorobenzene was taken as a reference. HRMS spectra were recorded using ESI mode (Q-TOF MS Analyzer spectrometer). IR spectra were recorded in KBr or neat in Perkin Elmer FT-IR spectrometer.

II.5.2. Experimental Procedure and Instrumentation:

(a) Synthesis of starting materials: 2-aryl quinoxalines (**1a–1o**) and internal alkynes (**2a–2h**) were synthesized according to the earlier reported procedures.[66]

(b) Synthesis of quinoxalinium salt (**3aa**)**:** A 25 mL oven-dried round-bottom flask fitted with a reflux condenser, magnetic pellet and stirrer was charged with 2-phenyl quinoxaline (**1a**, 0.062 g, 0.3 mmol), diphenylacetylene (**2a**, 0.074 g, 0.36 mmol), $[RuCl_2(p\text{-Cymene})]_2$ (0.0092 g, 0.015 mmol), $Cu(OAc)_2.H_2O$ (0.131 g, 0.66 mmol) and TfOH (0.067 g, 0.45 mmol) in DCE (2 mL). The combined reaction mixture was heated at 120 ^oC for 10 h by continuously stirring. The progress of the reaction was monitored by TLC. After completion of the reaction DCE was removed under vacuo. The crude reaction mixture was purified over a column of silica gel using a mixture of CH_2Cl_2: MeOH (97:3) as the eluent. The product obtained after column chromatographic purification was evaporated and after

TH-3369_166122017

drying the residual solid was washed with a little cold ethyl acetate to provide 135 mg (85%) of a green fluorescence quinoxalinium salt (**3aa**).

(c) UV, PL and Quantum Yield Measurement

All UV experiments were performed at a probe concentration of 15 µM in 1 mL quartz cuvettes of path length 1 cm at 25 ^{o}C in PerkinElmer Lambda 35 UV/VIS Spectrometer. Photoluminescence of quaternary salts was carried out at a concentration of 3 µM on exciting at their corresponding UV-absorption in 1 mL quartz cuvettes at 25 ^{o}C in Horiba Fluoromax-4 Spectrofluorometer.

Fluorescence quantum yields of the synthesized compounds were investigated by standard methods using Quinine sulphate as the reference (Φ_F = 0.577 in 0.1 M H_2SO_4, λ_{ex} = 370 nm) in HPLC grade acetonitrile solution.

Quantum yield of a probe:

$$QY = QY_{ref} (\eta^2 / \eta_{ref}^2)(I/A)(A_{ref}/I_{ref})$$

Here, QY_{ref} is the quantum yield of the reference compound, η denotes the refractive index of the solvent, η_{ref} is the refractive index of the solvent of the dissolved reference compound, and I and I_{ref} denote the integrated fluorescence intensity of the probe and reference respectively. Whereas A and A_{ref} are the absorbance of the probe and reference at the excitation wavelength.

(d) Cyclic Voltammetry (CV)

Electrochemical measurements were carried out in a three-electrode cell with platinum wire as a counter electrode, glassy carbon as the working electrode, and saturated $Ag/AgNO_3$ electrode as the reference electrode. The Fc^+/Fc (where Fc = ferrocene) couple was used as an internal reference and tetrabutylammonium hexafluorophosphate (0.1 M) in acetonitrile was taken as the supporting electrolyte. All the measurements were carried out at room temperature under an inert atmosphere.

(e) Time-Resolved Photoluminescence

Fluorescence lifetime of the quinoxalinium salts was measured in HPLC grade acetonitrile solvent at a probe concentration of 3 µM by using 375 and 445 nm laser sources in Eddinburg Instruments (Model: Lifespec II).

(f) Field Emission Scanning Electron Microscopy (FESEM)

Morphologies of the aggregates were obtained at room temperature from dried drop casted samples on aluminum foil at different probe concentrations and different DMF-water composition using Sigma Carl ZEISS field emission scanning electron microscope.

TH-3369_166122017

(g) Transmission Electron Microscopy (TEM)

TEM images were collected from room temperature dried drop casted samples on Gride at different probe concentrations and different DMF-water compositions in JEOL 2100 UHR-TEM instrument, operating at 200 KV.

(h) Dynamic Light Scattering (DLS)

For the determination of hydrodynamic diameters of the aggregates of **3aa**, DLS was performed in the Malvern Zetasizer instrument. For crystalline aggregates, DLS measurement was carried out in a concentration of 60 μM in 0.8:99.2 DMF-water mixture whereas for distorted spherical aggregates it was carried out a concentration of 30 μM in 0.4:99.6 DMF-water mixed solution at 25 ^{o}C.

(i) Mechanochromism

Mechanochromism of the **3aa** sample was carried out by grinding it in a mortar and pestle and the grounded sample showed different photophysical behavior as compared to pristine **3aa**.

(j) Powder X-ray Diffraction (PXRD)

PXRD of pristine and grounded **3aa** samples was performed in Bruker D2 Phaser X-ray diffractometer (10 mA, 30 kV) equipped with Ni-filtered Cu Kα radiation, at a wavelength of 0.154 nm. The diffraction pattern was recorded in the 2θ range of 5–45^{o} at a scan rate of 1.2^{o} min^{-1}.

(k) Latent Fingerprints Development

One adult male volunteer rubbed his fingers near his nose and forehead to accumulate sebaceous, and the fingerprints were stamped on an adhesive tape. The imprint of the latent fingerprint was then developed by staining it in a H_2O:MeOH (90:10) solution of **3ab** and **3ba** at a concentration of 70 μM for 2 minutes. The developed surfaces were washed with distilled water and dried it in open air. Subsequently, the fingerprints containing substrates were visualized under UV light (365 nm) for first-level (pattern information) and second-level (displaying core, bifurcation, and ridge ending) investigations.

(l) Cell Culture

Human cervical cancer cell line (HeLa) was obtained from National Centre for Cell Sciences, Pune, India. Cells were maintained in Dulbecco's Modified Eagle's medium (DMEM) supplemented with 10% Fetal Bovine Serum (FBS) and 1% antibiotic-antimycotic solution. The culture was kept in a

TH-3369_166122017

humidified atmosphere at 37 °C in a 5% carbon dioxide incubator. The media was changed at an interval of 3 days and the cells were subcultured upon reaching confluence.

(m) Cell Viability Assay

Cell Viability assay was performed using alamarBlue™. Resazurin, the active ingredient of alamarBlue reagent is being reduced to resorufin by the live cells. Hela cells were seeded in a 96-well plate at a density of 7000 cells/ well. After allowing the cells to attach to the surface of the plate for 12 h, they were treated with varying concentrations of synthesized compounds for 24 h. After the treatment time, 10 µL of alamarBlue was added to each well of 96 well plates and incubated at 37 ̊C for 4 h. Absorbance was measured at 570 nm with a reference wavelength of 600 nm (normalized to the 600 nm value). The treatments were done in triplicate and the experiments were done thrice. Cell viability was calculated using the following formula

% of cell viability = {(A570-A600) sample / (A570-A600) Control} X 100

The statistical tests were performed using GraphPad Prism software.

(n) Confocal Laser Scanning Microscopy

Sterilized glass coverslips were placed inside 6 well plates and Hela cells were seeded at a density of 0.5 X 10^6 cells. Following 24 h incubation, cells were treated with the compounds at a concentration of 145 µM for 10 minutes in complete media. After incubation, media was removed and cells were washed 3 times with PBS. To fix the cells PBS was removed and the cells were incubated with 4% paraformaldehyde for 15 min. Following incubation, cells were washed 3 times with PBS. Next glass coverslips were inverted and placed on a glass slide by inverting and glycerol was added in between for preservation. Untreated cells were used as control. Images were taken using ZEISS LSM 880 Confocal Laser Scanning Microscope and processed using Zen Blue software. with 458 nm excitation laser and emission filter of 480-605 nm.

(o) Cell Cycle Analysis

Cell cycle analysis was performed using Fluorescence Activated Cells Sorter (FACSCalibur, BD Biosciences, NJ, USA) to measure the DNA content of cells upon treatment with the compounds. Cells were seeded at a concentration of 0.5 X 10^6 cells/ well in a 6 well plate. After allowing the cells to attach for 12 h, they were treated with different compounds with their respective IC50 concentration. The IC_{50} concentration was determined based on cell viability assay using alamarBlue. Treatment was done for 24 h after which, cells were collected by trypsinization. Floating cells in media were collected by

TH-3369_166122017

centrifugation at 650×g for 6 min at 4 °C, whereas trypsinized cells were centrifuged at 450×g for 6 min at 4 °C. Obtained cells were fixed using drop-wise addition of 70% chilled ethanol and stored at −20 °C. Subsequently, cells were centrifuged, washed with chilled PBS, and incubated with 0.2 mg/ml RNase A (Sigma Aldrich) at 37 °C for 1 h. Thereafter, propidium iodide (PI) (Sigma Aldrich) was added at a final concentration of 10 µg/mL and incubated for 20 min in dark, at 4 °C. Cells were analyzed in FACSCalibur (BD Biosciences) using the software CellQuest Pro; where 10,000 cells were acquired and analyzed for each sample.

II.5.3. Crystallographic Description:

Crystal data were collected with Bruker Smart Apex-II CCD diffractometer using graphite monochromated MoKα radiation (λ = 0.71073 Å) at 298 K. Cell parameters were retrieved using SMART[6a] software and refined with SAINT[a] on all observed reflections. Data reduction was performed with the SAINT software and corrected for Lorentz and polarization effects. Absorption corrections were applied with the program SADABS.[b] The structure was solved by direct methods implemented in SHELX-2014[c] program and refined by full-matrix least-squares methods on F2. All non-hydrogen atomic positions were located in difference Fourier maps and refined anisotropically. The hydrogen atoms were placed in their geometrically generated positions. For **3aa** Golden yellow crystals were isolated in plate shape from acetonitrile and for **3hf** dark green crystal blocks were obtained from DCM-MeOH solvent at room temperature.

a. SMART V 4.043 Software for the CCD Detector System; Siemens Analytical Instruments Division: Madison, WI, 2008.

b. SAINT Plus (v 6.14) Bruker AXS Inc., Madison, WI, 2008.

c. Sheldrick, G. M. SHELXL-2014, Program for the Refinement of Crystal Structures; University of Göttingen: Göttingen (Germany), 1997.

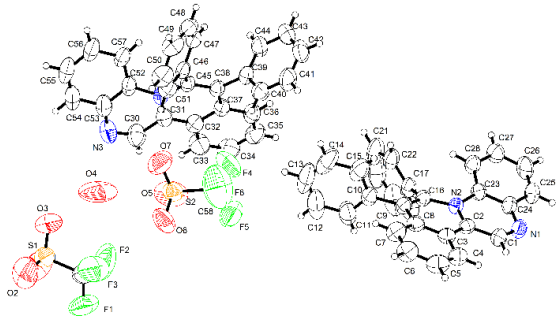

TH-3369_166122017

Figure II.5.3.1. *ORTEP Molecular Diagram of* ***3aa*** *with the thermal ellipsoids set at 40% probability*

Crystal Data Table for 3aa:

Empirical formula	$C_{29}H_{19}F_3N_2O_{3.5}S$
CCDC number	1884114
Formula weight	540.52
Temperature	273(2) K
Wavelength	0.71073 Å
Crystal system	Triclinic
Space group	P -1
Unit cell dimensions	a= 9.2376(8) Å, b= 15.8089(13) Å, c= 18.6787(15) Å α= 72.187(2)°, β= 85.340(2)°, γ= 87.364(2)°
Volume	2587.8(4) $Å^3$
Z	4
Density (calculated)	1.387 Mg/m^3
Absorption coefficient	0.183 mm^{-1}
F(000)	1112
Crystal size	0.38 x 0.28 x 0.22 mm^3
Theta range for data collection	1.353 to 24.999°
Index ranges	-10<=h<=10, -18<=k<=18, -22<=l<=22
Reflections collected	9100
Independent reflections	5912
Completeness to theta = 25.242°	100.0 %
Refinement method	Full-matrix least-squares on F^2
Data / restraints / parameters	9100 /0 /694
Goodness-of-fit on F2	1.029
Final R indices [I>2sigma(I)]	R1 = 0.0833, wR2 = 0.2299
R indices (all data)	R1 = 0.1222, wR2 = 0.2709

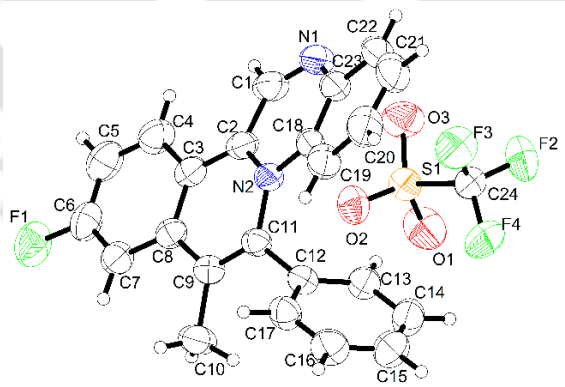

Figure II.5.3.2. *ORTEP Molecular Diagram of* ***3hf*** *with the thermal ellipsoids set at 40% probability*

TH-3369_166122017

Crystal Data Table for 3hf:

Empirical formula	$C_{24}H_{16}F_4N_2O_3S$
CCDC number	1884113
Formula weight	488.45
Temperature	273(2)
Wavelength	0.71073 Å
Crystal system	Monoclinic
Space group	P 21/n
Unit cell dimensions	a= 8.247(2) Å, b= 13.756(4) Å, c= 18.732(5) Å α= 90°, β= 95.787(5)°, γ= 90°
Volume	2114.2(9) $Å^3$
Z	4
Density (calculated)	1.535 Mg/m^3
Absorption coefficient	0.220 mm^{-1}
F(000)	1000
Crystal size	0.28 x 0.23 x 0.19 mm^3
Theta range for data collection	1.840 to 24.998°
Index ranges	-9<=h<=9, -16<=k<=16, -22<=l<=22
Reflections collected	3723
Independent reflections	2981
Completeness to theta = 25.242°	100.0 %
Refinement method	Full-matrix least-squares on F^2
Data / restraints / parameters	3723 / 0 / 308
Goodness-of-fit on F2	0.861
Final R indices [I>2sigma(I)]	R1 = 0.0398, wR2 = 0.1181
R indices (all data)	R1 = 0.0519, wR2 = 0.1355

II.6. References

1. (a) Colby, D. A.; Bergman, R. G.; Ellman, J. A. Rhodium-Catalyzed C−C Bond Formation via Heteroatom-Directed C−H Bond Activation. *Chem. Rev.* **2010**, *110*, 624. (b) Mkhalid, I. A. I.; Barnard, J. H.; Marder, T. B.; Murphy, J. M.; Hartwig, J. F. C−H Activation for the Construction of C−B Bonds. *Chem. Rev.* **2010**, *110*, 890. (c) Lyons, T. W.; Sanford, M. S. Palladium-Catalyzed Ligand-Directed C−H Functionalization Reactions. *Chem. Rev.* **2010**, *110*, 1147. (d) Wencel-Delord, J.; Dröge, T.; Liu, F.; Glorius, F. Towards mild metal-catalyzed C–H bond activation. *Chem. Soc. Rev.* **2011**, *40*, 4740. (e) Kuhl, N.; Hopkinson, M. N.; Wencel-Delord, J.; Glorius, F. Beyond Directing Groups: Transition-Metal-Catalyzed CH

TH-3369_166122017

Activation of Simple Arenes. *Angew. Chem., Int. Ed*. **2012**, *51*, 10236. (f) Yamaguchi, J.; Yamaguchi, A. D.; Itami, K. *Angew. Chem., Int. Ed*. **2012**, *51*, 8960. (g) Arockiam, P. B.; Bruneau, C.; Dixneuf, P. H. Ruthenium(II)-Catalyzed C–H Bond Activation and Functionalization. *Chem. Rev*. **2012**, *112*, 5879.

2. (a) Gandeepan, P.; Cheng C.-H. Advancements in the Synthesis and Applications of Cationic N-Heterocycles through Transition Metal-Catalyzed C−H Activation. *Chem.-Asian J*. **2016**, *11*, 448. (b) Sucunza, D.; Cuadro, A. M.; Alvarez-Builla, J.; Vaquero, J. J. Recent Advances in the Synthesis of Azonia Aromatic Heterocycles. *J. Org. Chem*. **2016**, *81*, 10126. (c) Karak, P.; Rana, S. S.; Choudhury, J. Cationic π-extended heteroaromatics via a catalytic C–H activation annulative alkyne-insertion sequence. *Chem. Commun*. **2021**, *58*, 133.

3. (a) Song, L.; Van der Eycken, E. V. Transition Metal-Catalyzed Intermolecular Cascade C−H Activation/Annulation Processes for the Synthesis of Polycycles. *Chem. –Eur. J*. **2021**, *27*, 121. (b) Stepek, I. A.; Itami, K. Recent Advances in C-H Activation for the Synthesis of π-Extended Materials. *ACS Mater. Lett*. **2020**, *2*, 951. (c) Allard, S.; Forster, M.; Souharce, B.; Thiem, H.; Scherf, U. Organic Semiconductors for Solution-Processable Field-Effect Transistors (OFETs). *Angew. Chem., Int. Ed*. **2008**, *47*, 4070.

4. (a) Noisier, A. F.; Brimble, M. A. C–H functionalization in the synthesis of amino acids and peptides. *Chem. Rev*. **2014**, *114*, 8775. (b) Krane, B. D.; Fagbule, M. O.; Shamma, M.; Gozler, B. The Benzophenanthridine Alkaloids. *J. Nat. Prod*. **1984**, *47*, 1. (c) Lipińska, T. General route to the total synthesis of sempervirine analogues containing modified E ring, potential cytostatics. Tetrahedron Lett. 2002, 43, 9565. (d) Schmidt, A. Heterocyclic mesomeric betaines and analogs in natural product chemistry. Betainic alkaloids and nucleobases. *Adv. Heterocycl. Chem*. **2003**, *85*, 67.

5. (a) Yu, Y.; Singh, S. K.; Liu, A.; Li, T.-K.; Liu, L. F.; LaVoie, E. J. Substituted dibenzo[c,h]cinnolines: topoisomerase I-targeting anticancer agents. *Bioorg. Med. Chem*. **2003**, *11*, 1475. (b) Mancini, I.; Sicurelli, A.; Guella, G.; Turk, T.; Maček, P.; Sepči, K. Synthesis and Bioactivity of Linear Oligomers Related to Polymeric Alkylpyridinium Metabolites from the Mediterranean Aponge Reniera Sarai. *Org. Biomol. Chem*. **2004**, *2*, 1368. (c) Laville, R.; Genta-Jouve, G.; Urda, C.; Fernández, R.; Thomas, O. P.; Reyes, F.; Amade, P. Njaoaminiums A, B, and C: Cyclic 3-Alkylpyridinium Salts from the Marine Sponge Reniera sp. *Molecules* **2009**, *14*, 4716.

TH-3369_166122017

6. (a) Bortolozzi, R.; Ihmels, H.; Thomas, L.; Tian, M.; Viola, G. 9-(4-Dimethylaminophenyl)benzo[b]quinolizinium: A NearInfrared Fluorophore for the Multicolor Analysis of Proteins and Nucleic Acids in Living Cells. *Chem. −Eur. J.* **2013**, *19*, 8736. (b) Bortolozzi, R.; von Gradowski, S.; Ihmels, H.; Schäfer, K.; Viola, G. Selective Ratiometric Detection of H_2O_2 in Water and in Living Cells with Boronobenzo[b]quinolizinium Derivatives. *Chem. Commun*. **2014**, *50*, 8242.

7. (a) Luo, C.-Z.; Gandeepan, P.; Wu, Y.-C.; Tsai, C.-H.; Cheng, C.-H. Cooperative C(sp3)–H and C(sp2)–H Activation of 2-Ethylpyridines by Copper and Rhodium: A Route toward Quinolizinium Salts. *ACS Catal*. **2015**, *5*, 4837. (b) Prakash S.; Muralirajan, K.; Cheng, C.-H. Cobalt-Catalyzed Oxidative Annulation of Nitrogen-Containing Arenes with Alkynes: An Atom-Economical Route to Heterocyclic Quaternary Ammonium Salts. *Angew. Chem., Int. Ed*. **2016**, *55*, 1844.

8. (a) Ghorai, D.; Choudhury, J. Exploring a Unique Reactivity of N-Heterocyclic Carbenes (NHC) in Rhodium(III)-catalyzed Intermolecular C–H Activation/Annulation. *Chem. Commun*. **2014**, *50*, 15159. (b) Ghorai, D.; Choudhury, J. Rhodium(III)–N-Heterocyclic Carbene-Driven Cascade C–H Activation Catalysis. *ACS Catal*. **2015**, *5*, 2692. (c) Thenarukandiyil, R.; Choudhury, J. Rhodium(III)-Catalyzed Activation and Functionalization of Pyridine C–H Bond by Exploring a Unique Double Role of "N-Heterocyclic Carbene–Pyridyl" Ligand Platform. *Organometallics*. **2015**, *34*, 1890. (d) Ghorai, D.; Dutta, C.; Choudhury, J. Switching of "Rollover Pathway" in Rhodium(III)-Catalyzed C–H Activation of Chelating Molecules. *ACS Catal*. **2016**, *6*, 709.

9. (a) Ge, Q.; Li, B.; Song, H.; Wang, B. Rhodium(III)-Catalyzed Cascade Oxidative Annulation Reactions of Aryl Imidazolium Salts with Alkynes Involving Multiple C–H Bond Activation. *Org. Biomol. Chem*. **2015**, *13*, 7695. (b) Li, R.; Hu, Y.; Liu, R.; Hu, R.; Li, B.; Wang, B. Ruthenium(II)-Catalyzed Oxidative Annulation Reactions of Arylimidazolium Salts via N-Heterocyclic Carbene-Directed C□H Activation. *Adv. Synth. Catal*. **2015**, *357*, 3885. (c) Ge. Q.; Hu, Y.; Li, B.; Wang, B. Synthesis of Conjugated Polycyclic Quinoliniums by Rhodium(III)-Catalyzed Multiple C–H Activation and Annulation of Arylpyridiniums with Alkynes. *Org. Lett*. **2016**, *18*, 2483.

10. (a) Davies, D. L.; Ellul, C. E.; Macgregor, S. A.; McMullin, C. L.; Singh, K. Experimental and DFT Studies Explain Solvent Control of C–H Activation and Product Selectivity in the

TH-3369_166122017

Rh(III)-Catalyzed Formation of Neutral and Cationic Heterocycles. *J. Am. Chem. Soc*. **2015**, *137*, 9659. (b) Villar, J. M.; Suarez, J.; Varela, J. A.; Saa, C. *N*-Doped Cationic PAHs by Rh(III)-Catalyzed Double C–H Activation and Annulation of 2-Arylbenzimidazoles with Alkynes. *Org. Lett*. **2017**, *19*, 1702. (c) Qi, Z.; Yu, S.; Li, X. Rh(III)-Catalyzed Oxidative Annulation of 2-Phenylimidazo[1,2-*a*]pyridines with Alkynes: Mono versus Double C–H Activation. *J. Org. Chem*. **2015**, *80*, 3471.

11. (a) Jayakumar, J.; Parthasarathy, K.; Cheng, C.-H. One-Pot Synthesis of Isoquinolinium Salts by Rhodium-Catalyzed C–H Bond Activation: Application to the Total Synthesis of Oxychelerythrine. *Angew. Chem., Int. Ed*. **2012**, *51*, 197. (b) Zhang, G.; Yang, L.; Wang, Y.; Xie, Y.; Huang, H. An Efficient Rh/O2 Catalytic System for Oxidative C–H Activation/Annulation: Evidence for Rh(I) to Rh(III) Oxidation by Molecular Oxygen. *J. Am. Chem. Soc*. **2013**, *135*, 8850. (c) Upadhyay, N. S.; Jayakumar, J.; Cheng, C. H. Facile One-pot Synthesis of 2,3-Dihydro-1H-indolizinium Derivatives by Rhodium(III)-catalyzed Intramolecular Oxidative Annulation via C-H Activation: Application to Ficuseptine Synthesis. *Chem. Commun*. **2017**, *53*, 2491. (d) Tang, S.-B.; Li, S.-Q.; Liu, Z.; Zhao, Y.-S.; She, Z.-J.; Kadam, V. D.; Gao, G.; Lan, J.-B.; You, J.-S. Cascade C–H Annulation of Aldoximes with Alkynes using O_2 as the Sole Oxidant: One-pot Access to Multisubstituted Protoberberine Skeletons. *Org. Lett*. **2017**, *19*, 604. (e) Han, Y. R.; Shim, S.-H.; Kim, D.-S.; Jun, C.-H. Synthesis of Benzoquinolizinium Salts by Rh (III)-Catalyzed Cascade Double *N*-Annulation Reactions of Allylamines, Diarylacetylenes, and HBF_4. *Org. Lett*. **2017**, *19*, 2941. (f) Zhao, D.; Wu, Q.; Huang, X.; Song, F.; Lv, T.; You, J. A General Method to Diverse Cinnolines and Cinnolinium Salts. *Chem.─Eur. J*. **2013**, *19*, 6239.

12. (a) Wang, Y.; Li, B.; Wang, B. Synthesis of Cinnolines and Cinnolinium Salt Derivatives by Rh (III)-Catalyzed Cascade Oxidative Coupling/Cyclization Reactions. *J. Org. Chem*. **2018**, *83*, 10845. (b) Ma, W.; Zhang, L.; Shi, Y.; Ran, Y.; Liu, Y.; You, J. Molecular Engineering to Access Fluorescent Trackers of Organelles by Cyclization: Chemical Environment of Nitrogen Atom-Modulated Targets. *Adv. Funct. Mater*. **2020**, *30*, 2004511. (c) Dutta, C.; Rana, S. S.; Choudhury, J. Leveraging Metallotropism-Enabled Substrate Activation in Cobalt-catalyzed Annulation Chemistry: Protic NHC Template is the Key. *ACS. Catal*. **2019**, *9*, 10674.

TH-3369_166122017

13. (a) Kozhushkov, S. I.; Ackermann, L. Ruthenium-Catalyzed Direct Oxidative Akenylation of Arenes Through Twofold C–H Bond Functionalization. *Chem. Sci*. **2013**, *4*, 886. (b) Ackermann, L. Carboxylate-Assisted Ruthenium-Catalyzed Alkyne Annulations by C–H/Het–H Bond Functionalizations. *Acc. Chem. Res*. **2014**, *47*, 281. (c) Sarkar, S. De.; Liu, W.; Kozhushkov, S. I.; Ackermann, L. Weakly Coordinating Directing Groups for Ruthenium(II)-Catalyzed C□H Activation. *Adv. Synth. Catal*. **2014**, *356*, 1461. (d) Manikandan, R.; Jeganmohan, M. Recent Advances in the Ruthenium-Catalyzed Hydroarylation of Alkynes with Aromatics: Synthesis of Trisubstituted Alkenes. *Org. Biomol. Chem*. **2015**, *13*, 10420. (e) Arockiam, P. B., Fischmeister, C., Bruneau, C.; Dixneuf, P. H. Ruthenium diacetate-catalysed oxidative alkenylation of C–H bonds in air: synthesis of alkenyl N-arylpyrazoles. *Green Chem*. **2011**, *13*, 3075.

14. (a) Luo, C.-Z.; Gandeepan, P.; Cheng, C.-H. A Convenient Synthesis of Quinolizinium Salts Through Rh(III) or Ru(II)-Catalyzed C–H Bond Activation of 2-Alkenylpyridines. *Chem. Commun*. **2013**, *49*, 8528. (b) Parthasarathy, K.; Senthilkumar, N.; Jayakumar, J.; Cheng, C. –H. Ru(II)-Catalyzed C–H Bond Activation for the Synthesis of Substituted Isoquinolinium Salts from Benzaldehydes, Amines, and Alkynes. *Org. Lett*. **2012**, *14*, 3478.

15. (a) Baldo, M. A.; O'Brien, D. F.; You, Y.; Shoustikov, A.; Sibley, S.; Thompson, M. E.; Forrest, S. R. Highly Efficient Phosphorescent Emission from Organic Electroluminescent Devices. *Nature*. **1998**, *395*, 151. (b) Friend, R. H.; Gymer, R. W.; Holmes, A. B.; Burroughes, J. H.; Marks, R. N.; Taliani, C.; Bradley, D. D. C.; Dos. Santos, D. A.; Bredas, J. L.; Logdlund, M.; Salaneck, W. R. Electroluminescence in Conjugated Polymers. *Nature*. **1999**, *397*, 121. (c) Saragi, T. P. I.; Spehr, T.; Siebert, A.; Fuhrmann-Lieker, T.; Salbeck, J. Spiro Compounds for Organic Optoelectronics. *Chem. Rev*. **2007**, *107*, 1011.

16. Lin, G.; Peng, H.; Chen, L.; Nie, H.; Luo, W.; Li, Y.; Chen, S.; Hu, R.; Qin, A.; Zhao, Z.; Tang, B. Z. Improving Electron Mobility of Tetraphenylethene-Based AIEgens to Fabricate Nondoped Organic Light-Emitting Diodes with Remarkably High Luminance and Efficiency. *ACS Appl. Mater. Interfaces*. **2016**, *8*, 16799.

17. Sun, S.-K.; Wang, H.-F.; Yan, X.-P. Engineering Persistent Luminescence Nanoparticles for Biological Applications: From Biosensing/Bioimaging to Theranostics. *Acc. Chem. Res*. **2018**, *51*, 1131.

TH-3369_166122017

18. Lochenie, C.; Schötz, K.; Panzer, F.; Kurz, H.; Maier, B.; Puchtler, F.; Agarwal, S.; Köhler, A.; Weber, B. Spin-Crossover Iron(II) Coordination Polymer with Fluorescent Properties: Correlation between Emission Properties and Spin State. *J. Am. Chem. Soc*. **2018**, *140*, 700.

19. (a) Hong, Y.; Lam, J. W. Y.; Tang, B. Z.; Aggregation-induced emission. *Chem. Soc. Rev*. **2011**, *40*, 5361. (b) Mei, J.; Leung, N. L. C.; Kwok, R. T. K.; Lam, J. W. Y.; Tang, B. Z. Aggregation-Induced Emission: Together We Shine, United We Soar!. *Chem. Rev*. **2015**, *115*, 11718.

20. (a) Stępień, M.; Gońka, E.; Żyła, M.; Sprutta, N. Heterocyclic Nanographenes and Other Polycyclic Heteroaromatic Compounds: Synthetic Routes, Properties, and Applications. *Chem. Rev*. **2017**, *117*, 3479. (b) Kulkarni, A. P.; Tonzola, C. J.; Babel, A.; Jenekhe, S. A. Electron Transport Materials for Organic Light-Emitting Diodes. *Chem. Mater*. ***2004***, *16*, 4556. (c) McMillan, N.; Smith, L. V.; de la Fuente, J. M.; Parenty, A. D. C.; Gadegaard, N.; Pitt, A. R.; Thomson, K.; MacKenzie, C.; Kelly, S. M.; Cronin, L. InCorporation of N-heterocyclic Cations into Proteins with a Highlydirected Chemical Modification. *Chem. Commun*. **2007**, 2581. (d) Wang, C.; Dong, H.; Hu, W.; Liu, Y.; Zhu, D. Semiconducting π-Conjugated Systems in Field-Effect Transistors: A Material Odyssey of Organic Electronics. *Chem. Rev*. **2012**, *112*, 2208.

21. (a) Dreuw, A.; Plöner, J.; Lorenz, L.; Wachtveitl, J.; Djanhan, J. E.; Brüning, J.; Metz, T.; Bolte, M.; Schmidt, M. U. Molecular Mechanism of the Solid-State Fluorescence Behavior of the Organic Pigment Yellow 101 and Its Derivatives. *Angew. Chem. Int. Ed*. **2005**, *44*, 7783. (b) *Photophysics of Aromatic Molecules*; Birks, J. B., Ed.;Wiley: New York, **1970**.

22. Luo, J. D.; Xie, Z. L.; Lam, J. W. Y.; Cheng, L.; Chen, H. Y.; Qiu, C. F.; Kwok, H. S.; Zhan, X. W.; Liu, Y. Q.; Zhu, D. B.; Tang, B. Z. Aggregation-induced Emission of 1-Methyl-1,2,3,4,5-Pentaphenylsilole. *Chem. Commun*. **2001**, 1740.

23. An, B. -K.; Kwon, S. -K.; Jung, S. -D.; Park, S. Y. Enhanced Emission and Its Switching in Fluorescent Organic Nanoparticles. *J. Am. Chem. Soc*. **2002**, *124*, 14410.

24. Mei, J.; Hong, Y.; Lam, J. W. Y.; Qin, A.; Tang, Y.; Tang, B. Z. Aggregation-Induced Emission: The Whole Is More Brilliant than the Parts. *Adv. Mater*. **2014**, *26*, 5429.

25. (a) Chen, J.; Xu, B.; Ouyang, X.; Tang, B. Z.; Cao, Y. Aggregation-Induced Emission of cis,cis-1,2,3,4-Tetraphenylbutadiene from Restricted Intramolecular Rotation. *J. Phys. Chem.*

TH-3369_166122017

A, **2004**, *108*, 7522. (b) Yang, Y.; Su, X.; Carroll, C. N.; Aprahamian, I. Aggregation-induced Emission in BF2–Hydrazone (BODIHY) Complexes. Chem. Sci. 2012, 3, 610. (c) Tanaka, K.; Chujo, Y. Recent Progress of Optical Functional Nanomaterials Based on Organoboron Complexes with β-Diketonate, Ketoiminate and Diiminate. *NPG Asia Mater*. **2015**, *7*, e223.

26. Wang, M.; Zhang, G.; Zhang, D.; Zhu, D.; Tang, B. Z. Fluorescent Bio/Chemosensors Based on Silole and Tetraphenylethene Luminogens with Aggregation-Induced Emission Feature. *J. Mater. Chem.* **2010**, *20*, 1858.

27. Kwok, R. T. K.; Leung, C. W. T.; Lam, J. W. Y.; Tang, B. Z. Biosensing by Luminogens with Aggregation-induced Emission Characteristics. *Chem. Soc. Rev*. **2015**, *44*, 4228.

28. Hong, Y.; Lam, J. W. Y.; Tang, B. Z. Aggregation-Induced Emission: Phenomenon, Mechanism and Applications. *Chem. Commun*. **2009**, 4332.

29. Zhao, E.; Hong, Y.; Chen, S.; Leung, C. W. T.; Chan, C. Y. K.; Kwok, R. T. K.; Lam, J. W. Y.; Tang, B. Z.; Highly Fluorescent and Photostable Probe for Long-Term Bacterial Viability Assay Based on Aggregation-Induced Emission. *Adv. Healthcare Mater*. **2014**, *3*, 88.

30. Hong, Y.; Chen, S.; Leung, C. W. T.; Lam, J. W. Y.; Tang, B. Z. Water-Soluble Tetraphenylethene Derivatives as Fluorescent “Light-Up” Probes for Nucleic Acid Detection and Their Applications in Cell Imaging. *Chem.-Asian J*. **2013**, *8*, 1806.

31. (a) Hong, Y.; Meng, L.; Chen, S.; Leung, C. W. T.; Da, L.-T.; Faisal, M.; Silva, D.-A.; Liu, J.; Lam, J. W. Y.; Huang, X. Monitoring and Inhibition of Insulin Fibrillation by a Small Organic Fluorogen with Aggregation-Induced Emission Characteristics. *J. Am. Chem. Soc*. **2012**, *134*, 1680. (b) Guo, Y.; Feng, X.; Han, T.; Wang, S.; Lin, Z.; Dong, Y.; Wang, B. Tuning the Luminescence of Metal–Organic Frameworks for Detection of Energetic Heterocyclic Compounds. *J. Am. Chem. Soc*. **2014**, *136*, 15485.

32. Santhiya, K.; Sen, S. K.; Natarajan, R.; Shankar, R.; Murugesapandian, B. D–A–D Structured Bis-acylhydrazone Exhibiting Aggregation-Induced Emission, Mechanochromic Luminescence, and Al(III) Detection. *J. Org. Chem*. **2018**, *83*, 10770.

33. (a) Dong, Y. Q.; Lam, W. Y. J.; Tang, B. Z. Mechanochromic Luminescence of Aggregation-Induced Emission Luminogens. *J. Phys. Chem. Lett*. **2015**, *6*, 3429. (b) Han, T.; Zhang, Y.; Feng, X.; Lin, Z.; Tong, B.; Shi, J.; Zhi, J.; Dong, Y. Reversible and Hydrogen Bonding-assisted Piezochromic Luminescence for Solid-state Tetraaryl-buta-1,3-diene. *Chem.*

TH-3369_166122017

Commun. **2013**, *49*, 7049. (c) Sudhakar, P.; Neena, K. K.; Thilagar, P. H-Bond assisted mechanoluminescenceof borylated aryl amines: tunable emissionand polymorphism. *J. Mater. Chem. C*. **2017**, *5*, 6537.

34. (a) Li, Y.; Ma, Z.; Li, A.; Xu, W.; Wang, Y.; Jiang, H.; Wang, K.; Zhao, Y.; Jia, X. A Single Crystal with Multiple Functions of Optical Waveguide, Aggregation-Induced Emission, and Mechanochromism. *ACS Appl. Mater. Interfaces*, **2017**, *9*, 8910. (b) Mukherjee, S.; Thilagar, P. Stimuli and Shape Responsive 'Boron-Containing' Luminescent Organic Materials. *J. Mater. Chem. C*. **2016**, *4*, 2647.

35. (a) Qi, Y.; Liu, W.; Wang, Y.; Ma, L.; Yu, Y.; Zhang, Y.; Ren, L.; The Inherent Mechanism of Mechanochromism Under Different Stress: Electron Cloud Density Distribution, J-type Stacking, Pore Structure and Collapse of J-type Stacking. *New J. Chem*. **2018**, *42*, 11373. (b) (c) Jadhav, T.; Dhokale, B.; Mobin, S. M.; Misra, R. Mechanochromism and Aggregation Induced Emission in Benzothiazole Substituted Tetraphenylethylenes: A Structure Function Correlation. *RSC Adv*. **2015**, *5*, 29878.

36. (a) Shi, P.; Duan, Y.; Wei, W.; Xu, Z.; Li, Z.; Han, T. A turn-on Type Mechanochromic Fluorescent Material Based on Defect-Induced Emission: Implication for Pressure Sensing and Mechanical Printing. *J. Mater. Chem. C*, **2018**, *6*, 2476. (b) Qi, Q.; Qian, J.; Tan, X.; Zhang, J.; Wang, L.; Xu, B.; Zou, B.; Tian, W. Remarkable Turn-On and Color-Tuned Piezochromic Luminescence: Mechanically Switching Intramolecular Charge Transfer in Molecular Crystals. *Adv. Funct. Mater*. **2015**, *25*, 4005. (c) Imoto, H.; Kizaki, K.; Naka, K. A Mechanochromic Luminescent Dye Exhibiting On/Off Switching by Crystalline–Amorphous Transitions. *Chem.-Asian J*. **2015**, *10*, 1698.

37. (a) Yang, Z.; Chi, Z.; Mao, Z.; Zhang, Y.; Liu, S.; Zhao, J.; Aldred, M. P.; Chi, Z. Recent Advances in Mechano-Responsive Luminescence of Tetraphenylethylene Derivatives with Aggregation-Induced Emission Properties. *Mater. Chem. Front*. **2018**, *2*, 861. (b) Yu, C-Y.; Hsu, C-C.; Weng, H-C. Synthesis, Characterization, Aggregation-Induced Emission, Solvatochromism and Mechanochromism of Fluorinated Benzothiadiazole Bonded to Tetraphenylethenes. *RSC Adv*. **2018**, *8*, 12619.

38. Zeng, S.; Zhang, D.; Huang, W.; Wang, Z.; Freire, S. G.; Yu, X.; Smith, A. T.; Huang, E. Y.; Nguon, H.; Sun, L. Bio-Inspired Sensitive and Reversible Mechanochromisms via Strain-Dependent Cracks and Folds. *Nat. Commun*. **2016**, *7*, 11802.

TH-3369_166122017

39. Hirata, S.; Watanabe, T. Reversible Thermoresponsive Recording of Fluorescent Images (TRF). *Adv. Mater*. **2006**, *18*, 2725.

40. Hou, X.; Ke, C.; Bruns, C. J.; Mcgonigal, P. R.; Pettman, R. B.; Stoddart, J. F.; Tunable solid-state fluorescent materials for supramolecular encryption. *Nat. Commun*. **2015**, *6*, 6884.

41. Weissleder, R.; Pittet, M. J. Imaging in the Era of Molecular Oncology. *Nature.* **2008**, *452*, 580.

42. Kunjachan, S.; Ehling, J.; Storm, G.; Kiessling, F.; Lammers, T. Noninvasive Imaging of Nanomedicines and Nanotheranostics: Principles, Progress, and Prospects. *Chem. Rev*. **2015**, *115*, 10907.

43. Hsiao, W. W.; Hui, Y. Y.; Tsai, P. C.; Chang, H. C. Fluorescent Nanodiamond: A Versatile Tool for Long-Term Cell Tracking, Super-Resolution Imaging, and Nanoscale Temperature Sensing. *Acc. Chem. Res*. **2016**, *49*, 400.

44. Schaferling, M. The Art of Fluorescence Imaging with Chemical Sensors. *Angew. Chem., Int. Ed*. **2012**, *51*, 3532.

45. Shou, K.; Qu, C.; Sun, Y.; Chen, H.; Chen, S.; Zhang, L.; Xu, H.; Hong, X.; Yu, A.; Cheng, Z. Multifunctional Biomedical Imaging in Physiological and Pathological Conditions Using a NIR-II Probe. *Adv. Funct. Mater*. **2017**, *27*, 1700995.

46. (a) Wang, H.; Liu, J.; Han, A.; Xiao, N.; Xue, Z.; Wang, G.; Long, J.; Kong, D.; Liu, B.; Yang, Z.; Ding, D. Self-Assembly-Induced Far-Red/Near-Infrared Fluorescence Light-Up for Detecting and Visualizing Specific Protein–Peptide Interactions. *ACS Nano*, **2014**, *8*, 1475. (b) Kircher, M. F.; Gambhir, S. S.; Grimm, J. Noninvasive Cell-Tracking Methods. *Nat. Rev. Clin. Oncol*. **2011**, *8*, 677. (c) Gao, X.; Cui, Y.; Levenson, R. M.; Chung, L. W. K.; Nie, S. In Vivo Cancer Targeting and Imaging with Semiconductor Quantum Dots. *Nat. Biotechnol*. **2004**, *22*, 969. (d) Nuriya, M.; Fukushima, S.; Momotake, A.; Shinotsuka, T.; Yasui, M.; Arai, T. Multimodal Two-Photon Imaging Using a Second Harmonic Generation-Specific Dye. *Nat. Commun*. **2016**, *7*, 11557.

47. Wu, X.; Sun, X.; Guo, Z.; Tang, J.; Shen, Y.; James, T. D.; Tian, H.; Zhu, W. In Vivo and in Situ Tracking Cancer Chemotherapy by Highly Photostable NIR Fluorescent Theranostic Prodrug. *J. Am. Chem. Soc*. **2014**, *136*, 3579.

TH-3369_166122017

48. Araneda, J. F.; Piers, W. E.; Heyne, B.; Parvez, M.; McDonald, R. High Stokes Shift Anilido-Pyridine Boron Difluoride Dyes. *Angew. Chem., Int. Ed*. **2011**, *50*, 12214.

49. (a) Bochkov, A. Y.; Akchurin, I. O.; Dyachenkob, O. A.; Travena, V. F. NIR-Fluorescent Coumarin-Fused BODIPY Dyes with Large Stokes Shifts. *Chem. Commun*. **2013**, *49*, 11653. (b) Guo, T.; Cui, L.; Shen, J.; Wang, R.; Zhu, W.; Xu, Y.; Qian, X. A Dual-Emission and Large Stokes Shift Fluorescence Probe for Real-time Discrimination of ROS/RNS and Imaging in Live Cells. *Chem. Commun*. **2013**, *49*, 1862.

50. (a) Jiang, M.; Gu, X.; Kwok, R. T. K.; Li, Y.; Sung, H. H. Y.; Zheng, X.; Zhang, Y.; Lam, J. W. Y.; Williams, I. D.; Huang, X.; Wong, K. S.; Tang, B. Z. Multifunctional AIEgens: Ready Synthesis, Tunable Emission, Mechanochromism, Mitochondrial, and Bacterial Imaging. *Adv. Funct. Mater*. **2018**, *28*, 1704589. (b) Wang, D.; Su, H.; Kwok, R. T.K.; Hu, X.; Zou, H.; Luo, Q.; Lee, M. M. S.; Xu, W.; Lam, J. W. Y.; Tang, B. Z. Rational Design of a Water-Soluble NIR AIEgen, and Its Application in Ultrafast Wash-free Cellular Imaging and Photodynamic Cancer Cell Ablation. *Chem. Sci*. **2018**, *9*, 3685. (c) Jiang, M.; Kwok, R. T. K.; Li, X.; Gui, C.; Lam, J. W. Y.; Qu, J.; Tang, B. Z. A Simple Mitochondrial Targeting AIEgen for Image-Guided Two-Photon Excited Photodynamic Therapy. *J. Mater. Chem. B*. **2018**, *6*, 2557. (d) Gu, Y.; Zhao, Z.; Su, H.; Zhang, P.; Liu, J.; Niu, G.; Li, S.; Wang, Z.; Kwok, R. T. K.; Ni, X-L.; Sun, J.; Qin, A.; Lam, J. W. Y.; Tang, B. Z. Exploration of Biocompatible AIEgens from Natural Resources. *Chem. Sci.* **2018**, *9*, 6497. (e) Zhao, N.; Lam, J. W. Y.; Sung, H. H. Y.; Su, H. M.; Williams, I. D.; Wong, K. S.; Tang, B. Z. Effect of the Counterion on Light Emission: A Displacement Strategy to Change the Emission Behaviour from Aggregation-Caused Quenching to Aggregation-Induced Emission and to Construct Sensitive Fluorescent Sensors for Hg^{2+} Detection. *Chem. - Eur. J.* **2014**, *20*, 133. (f) Wei, P.; Zhang, J-X.; Zhao, Z.; Chen, Y.; He, X.; Chen, M.; Gong, J.; Sung, H. H.-Y.; Williams, I. D.; Lam, J. W. Y.; Tang, B. Z. Multiple yet Controllable Photoswitching in a Single AIEgen System. *J. Am. Chem. Soc*. **2018**, *140*, 1966. (g) Hu, F.; Cai, X.; Manghnani, P. N.; Kenry.; Wu, W.; Liu, B. Multicolor Monitoring of Cellular Organelles by Single Wavelength Excitation to Visualize the Mitophagy Process. *Chem. Sci*. **2018**, *9*, 2756. (h) Chiang, Y-C.; Lai, Z-L.; Chen, C-M.; Chang, C-C.; Liu, B. Construction of Emission-Tunable Nanoparticles based on a TICT-AIEgen: Impact of Aggregationinduced Emission versus Twisted Intramolecular Charge Transfer. *J. Mater. Chem. B.* **2018**, *6*, 2869. (i) Kamino, S.; Horio, Y.; Komeda, S.; Minoura, K.; Ichikawa, H.; Horigome, J.; Tatsumi, A.; Kaji, S.; Yamaguchi, T.; Usami, Y.; et al. A New

TH-3369_166122017

Class of Rhodamine Luminophores: Design, Syntheses and Aggregation-Induced Emission Enhancement. *Chem. Commun*. **2010**, *46*, 9013. (j) Tanabe, K.; Kodama, D.; Hasegawa, M.; Kato, T. Aggregation- Induced Emission of a Liquid-Crystalline Quinolinium Salt Molecule in Aqueous Solution. *Chem. Lett*. **2014**, *43*, 184.

51. (a) Cai, M.; Gao, Z.; Zhou, X.; Wang, X.; Chen, S.; Zhao, Y.; Qian, Y.; Shi, N.; Mi, B.; Xie, L.; Huang, W. A Small Change in Molecular Structure, a Big Difference in the AIEE Mechanism. *Phys. Chem. Chem. Phys.* **2012**, *14*, 5289. (b) Mukherjee, S.; Thilagar, P. Molecular flexibility tuned emission in ‘‘V’’ shapednaphthalimides: Hg(II) detection and aggregation-induced emission enhancement (AIEE). *Chem. Commun*. **2013**, *49*, 7292. (c) Chang, Z.; Jiang, Y.; He, B.; Chen, J.; Yang, Z.; Lu, P.; Kwok, H. S.; Zhao, Z.; Qiua, H.; Tang, B. Z. Aggregation-Enhanced Emission and Efficient Electroluminescence of Tetraphenylethene-cored Luminogens. *Chem. Commun*. **2013**, *49*, 594.

52. (a) Meher, N.; Panda, S.; Kumar, S.; Iyer, P. K. Aldehyde Group Driven Aggregation-Induced Enhanced Emission in Naphthalimides and Its Application for Ultradetection of Hydrazine on Multiple Platforms. *Chem. Sci*. **2018**, *9*, 3978. (b) Meher, N.; Iyer, P. K. Spontaneously Self-Assembled Naphthalimide Nanosheets: Aggregation-Induced Emission and Unveiling a-PET for Sensitive Detection of Organic Volatile Contaminants in Water. *Angew. Chem., Int. Ed*. **2018**, *57*, 8488. (c) Kalluvettukuzhy, N. K.; Thillagar, P. Bistable Polyaromatic Aminoboranes: Bright Solid State Emissionand Mechanochromism. *Organometallics*, **2017**, *36*, 2692.

53. Frisch, M. J.; Trucks, G. W.; Schlegel, H. B.; Scuseria, G. E.; Robb, M. A.; Cheeseman, J. R.; Scalmani, G.; Barone, V.; Mennucci, B.; Petersson, G. A.; Nakatsuji, H.; Caricato, M.; Li, X.; Hratchian, H. P.; Izmaylov, A. F.; Bloino, J.; Zheng, G.; Sonnenberg, J. L.; Hada, M.; Ehara, M.; Toyota, K.; Fukuda, R.; Hasegawa, J.; Ishida, M.; Nakajima, T.; Honda, Y.; Kitao, O.; Nakai, H.; Vreven, T.; Montgomery, J. A., Jr.; Peralta, J. E.; Ogliaro, F.; Bearpark, M.; Heyd, J. J.; Brothers, E.; Kudin, K. N.; Staroverov, V. N.; Kobayashi, R.; Normand, J.; Raghavachari, K.; Rendell, A.; Burant, J. C.; Iyengar, S. S.; Tomasi, J.; Cossi, M.; Rega, N.; Millam, J. M.; Klene, M.; Knox, J. E.; Cross, J. B.; Bakken, V.; Adamo, C.; Jaramillo, J.; Gomperts, R.; Stratmann, R. E.; Yazyev, O.; Austin, A. J.; Cammi, R.; Pomelli, C.; Ochterski, J. W.; Martin, R. L.; Morokuma, K.; Zakrzewski, V. G.; Voth, G. A.; Salvador, P.; Dannenberg, J. J.;

TH-3369_166122017

Dapprich, S.; Daniels, A. D.; Farkas, Ö.; Foresman, J. B.; Ortiz, J. V.; Cioslowski, J.; Fox, D. J. *Gaussian 09*; Gaussian, Inc., Wallingford CT, 2009.

54. Luo, X.; Li, J.; Li, C.; Heng, L.; Dong, Y. Q.; Liu, Z.; Bo, Z.; Tang, B. Z. Reversible Switching of the Emission of Diphenyldibenzofulvenes by Thermal and Mechanical Stimuli. *Adv. Mater*. **2011**, *23*, 3261.

55. Faulds, H. On the Skin-Furrows of the Hand. *Nature*, **1880**, *22*, 605.

56. Hazarika, P.; Russell, D. A. Advances in Fingerprint Analysis. *Angew. Chem., Int. Ed*. **2012**, *51*, 3524.

57. Xu, L.; Li, Y.; Wu, S.; Liu, X.; Su, B. Imaging Latent Fingerprints by Electrochemiluminescence. *Angew. Chem., Int. Ed*. **2012**, *51*, 8068.

58. Hansen, D. B.; Joullie, M. M. The Development of Novel Ninhydrin Analogues. *Chem. Soc. Rev*. **2005**, *34*, 408.

59. He, Y.; Xu, L.; Zhu, Y.; Wei, Q.; Zhang, M.; Su, B. Immunological Multimetal Deposition for Rapid Visualization of Sweat Fingerprints. *Angew. Chem., Int. Ed*. **2014**, *22*, 12609.

60. Frick, A. A.; Busetti, F.; Cross, A.; Lewis, S. W. Aqueous Nile Blue: A Simple, Versatile and Safe Reagent for the Detection of Latent Fingermarks. *Chem. Commun*. **2014**, *50*, 3341.

61. Almog, J.; Levinton-Shamuilov, G.; Cohen, Y.; Azoury, M. Fingerprint Reagents with Dual Action: Colour and Fluorescence. *J. Forensic Sci*. **2007**, *52*, 330.

62. Yang, S.; Wang, C. F.; Chen, S. A Release-Induced Response for the Rapid Recognition of Latent Fingerprints and Formation of Inkjet-Printed Patterns. *Angew. Chem., Int. Ed*. **2011**, *123*, 3790.

63. Wang, J.; Wei, T.; Li, X.; Zhang, B.; Wang, J.; Huang, C.; Yuan, Q. Near-Infrared-Light-Mediated Imaging of Latent Fingerprints based on Molecular Recognition. *Angew. Chem., Int. Ed*. **2014**, *53*, 1616.

64. (a) Li, Y.; Xu, L.; Su, B. Aggregation Induced Emission for the Recognition of Latent Fingerprints. *Chem. Commun*. **2012**, *48*, 4109. (b) Singh, P.; Singh, H.; Sharma, R.; Bhargava, G.; Kumar, S. Diphenylpyrimidinone–Salicylideneamine – New ESIPTB AIEgens with Applications in Latent Fingerprinting. *J. Mater. Chem. C*. **2016**, *4*, 11180. (c) Malik, A. H.; Kalita, A.; Iyer, P. K. Development of Well-Preserved, Substrate-Versatile Latent Fingerprints

TH-3369_166122017

by Aggregation-Induced Enhanced Emission-Active Conjugated Polyelectrolyte. *ACS Appl. Mater. Interfaces*. **2017**, *9*, 37501.

65. Chen, B.; Le, W.; Wang, Y.; Li, Z.; Wang, D.; Ren, L.; Lin, L.; Cui, S.; Hu, J. J.; Hu, Y.; Yang, P.; Ewing, R. C.; Shi, D.; Cui, Z.; Targeting Negative Surface Charges of Cancer Cells by Multifunctional Nanoprobes. *Theranostics*. **2016**, *6*, 1887.

66. (a) Kumar, K.; Mudshinge, S. R.; Goyal, S.; Gangar, M.; Nair, V. A. A Catalyst Free, One Pot Approach for the Synthesis of Quinoxaline Derivatives via Oxidative Cyclization of 1,2-Diamines and Phenacyl Bromides. Tetrahedron Lett. **2015**, *56*, 1266. (b) Sonogashira, K.; Tohda, Y.; Hagihara, N. A Convenient Synthesis of Acetylenes: Catalytic Substitutions of Acetylenic Hydrogen with Bromoalkenes, Iodoarenes, and Bromopyridines. Tetrahedron Lett. **1975**, *50*, 4467.

II.7. Spectral Data

6,7-diphenylisoquinolino[2,1-*a*]quinoxalin-5-ium trifluoromethanesulfonate (3aa)

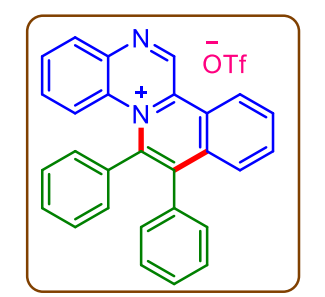

Greenish solid (135 mg, 85% yield); ^{1}H NMR (CD_3CN, 600 MHz): δ 10.69 (s, 1H), 9.41 (d, J = 8.6 Hz, 1H), 8.42 (d, J = 8.2 Hz, 1H), 8.28 (t, J = 7.3 Hz, 1H), 8.21 (t, J = 7.3 Hz, 1H), 7.90 (t, J = 7.5 Hz, 1H), 7.82 (t, J = 9.9 Hz, 2H), 7.47–7.42 (m, 4H), 7.36–7.33 (m, 1H), 7.27–7.23 (m, 6H); ^{13}C NMR (CD_3CN, 151 MHz): δ 147.4, 143.58, 143.56, 142.3, 138.3, 138.2, 137.9, 136.6, 135.2, 133.8, 132.8, 132.0, 131.8, 131.5, 131.4, 131.1, 130.15, 130.11, 129.8, 129.2, 129.0, 127.7, 126.3, 125.6; IR (KBr, cm^{-1}): 3062, 2924, 2853, 1731, 1582, 1440, 1341, 1267, 1152, 1030, 762, 634; HRMS (ESI) calcd for $C_{28}H_{19}N_2^+$ 383.1548, found 383.1548.

TH-3369_166122017

9-Methyl-6,7-diphenylisoquinolino[2,1-*a*]quinoxalin-5-ium trifluoromethanesulfonate (3ba)

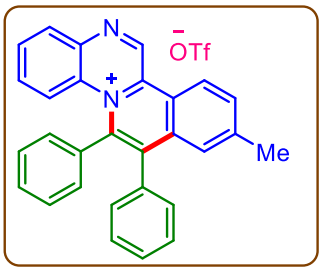

Green solid (124 mg, 76% yield); ^{1}H NMR (CD_3CN, 400 MHz): δ 10.62 (s, 1H), 9.30 (d, J = 8.8 Hz, 1H), 8.39 (d, J = 8.4 Hz, 1H), 8.13 (d, J = 8.8 Hz, 1H), 7.86 (t, J = 7.6 Hz, 1H), 7.78 (d, J = 8.9 Hz, 1H), 7.61 (s, 1H), 7.47–7.39 (m, 4H), 7.36–7.32 (m, 1H), 7.27–7.22 (m, 6H), 2.61 (s, 3H); ^{13}C NMR (CD_3CN, 101 MHz): δ 151.0, 147.5, 143.3, 143.1, 142.5, 138.3, 136.7, 135.9, 135.3, 132.6, 132.1, 131.9, 131.6, 131.4, 131.1, 130.2, 129.9, 129.3, 128.2, 128.1, 127.6, 125.6, 125.5, 124.6, 23.2; IR (KBr, cm^{-1}): 3060, 1612, 1520, 1436, 1339, 1267, 1148, 1030, 764, 701, 635; HRMS (ESI) calcd for $C_{29}H_{21}N_2^+$ 397.1705, found 397.1707.

11-Methoxy-6,7-diphenylisoquinolino[2,1-*a*]quinoxalin-5-ium trifluoromethanesulfonate (3ca)

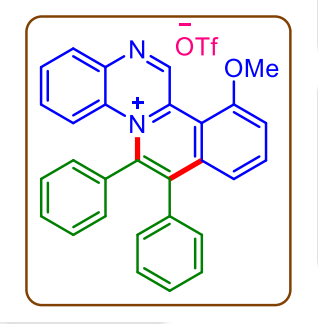

Light yellow solid (109 mg, 65% yield); ^{1}H NMR (CD_3CN, 600 MHz): δ 11.09 (s, 1H), 8.34 (d, J = 8.4 Hz, 1H), 8.15 (t, J = 8.2 Hz, 1H), 7.83 (t, J = 7.6 Hz, 1H), 7.77 (d, J = 8.9 Hz, 1H), 7.74 (d, J = 7.8 Hz, 1H), 7.44–7.41 (m, 3H), 7.40–7.35 (m, 3H), 7.31–7.28 (m, 1H), 7.23 (d, J = 7.2 Hz, 2H), 7.21–7.19 (m, 3H), 4.34 (s, 3H); ^{13}C NMR (CD_3CN, 151 MHz): δ 160.8, 150.3, 142.8, 142.7, 142.5, 140.1, 139.7, 139.4, 136.7, 135.7, 132.3, 132.2, 131.4, 130.9, 130.8, 130.7, 130.0, 129.9, 129.8, 129.5, 125.7, 120.9, 117.2, 114.5, 58.8; IR (KBr, cm^{-1}): 3061, 2930, 2849, 1602, 1491, 1342, 1267, 1154, 1031, 761, 702, 635; HRMS (ESI) calcd for $C_{29}H_{21}N_2O^+$ 413.1654, found 413.1659.

TH-3369_166122017

9-Methoxy-6,7-diphenylisoquinolino[2,1-*a*]quinoxalin-5-ium trifluoromethanesulfonate (3da)

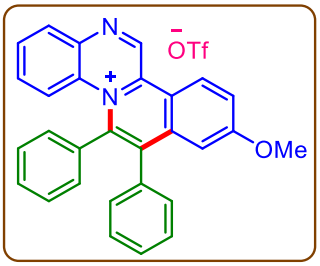

Green solid (122 mg, 73% yield); ^{1}H NMR (CD_3CN, 600 MHz): δ 10.49 (s, 1H), 9.29 (d, J = 9.5 Hz, 1H), 8.33 (d, J = 8.4 Hz, 1H), 7.85 (dd, J = 9.4, 2.5 Hz, 1H), 7.81 (t, J = 8.1 Hz, 1H), 7.68 (d, J = 8.8 Hz, 1H), 7.46–7.43 (m, 3H), 7.39–7.32 (m, 2H), 7.26–7.22 (m, 6H), 7.02 (d, J = 2.5 Hz, 1H), 3.87 (s, 3H); ^{13}C NMR (CD_3CN, 151 MHz): δ 167.5, 147.6, 142.5, 141.9, 141.1, 137.8, 136.5, 135.2, 132.0, 131.7, 131.3, 131.1, 131.0, 130.2, 130.09, 130.08, 129.9, 129.2, 125.4, 125.3, 121.1, 108.5, 57.6; IR (KBr, cm^{-1}): 2917, 2849, 1727, 1602, 1441, 1399, 1254, 1023, 732, 698, 631; HRMS (ESI) calcd for $C_{29}H_{21}N_2O^+$ 413.1654, found 413.1652.

10-Methoxy-6,7-diphenylisoquinolino[2,1-*a*]quinoxalin-5-ium trifluoromethanesulfonate (3ea) and 8-methoxy-6,7-diphenylisoquinolino[2,1-*a*]quinoxalin-5-ium trifluoromethanesulfonate (3'ea):

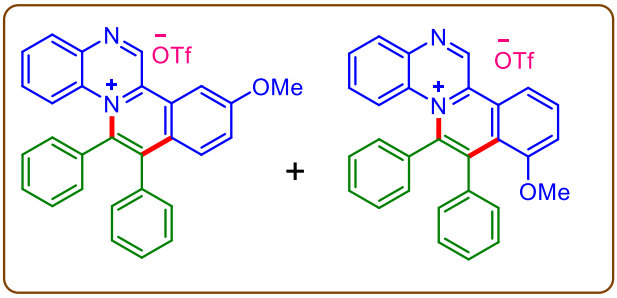

Inseparable regioisomer (1:0.55); Orange solid (138 mg, 82% yield); ^{1}H NMR (CD_3CN, 600 MHz): δ 10.65 (s, 1H), 10.63 (s, 0.55H), 8.96 (d, J = 8.4 Hz, 0.77H), 8.59 (d, J = 2.4 Hz, 1.21H), 8.38 (t, J = 8.1 Hz, 1.21H), 8.21 (t, J = 8.1 Hz, 0.59H), 7.90–7.85 (m, 2.14H), 7.81–7.78 (m, 1.81H), 7.74 (d, J = 9.6 Hz, 0.85H), 7.67 (d, J = 7.8Hz, 0.56H), 7.47–7.39 (m, 4.60H), 7.35–7.32 (m, 0.98H), 7.28–7.24 (m, 4.95H), 7.23–7.20 (m, 5.18H), 7.18–7.15 (m, 1.17H), 4.21 (s, 3.16H), 3.48 (s, 1.69H); ^{13}C NMR (CD_3CN, 151 MHz): δ 163.7, 158.5, 147.8, 147.5, 143.55, 143.50, 143.47, 142.3, 142.2, 140.8, 138.8, 136.8, 136.67, 135.4, 135.0, 133.4, 132.75, 132.68, 132.6, 132.1, 131.7, 131.62, 131.60, 131.4, 131.1, 130.9, 130.8, 130.7, 130.12, 130.10, 130.06, 129.8, 129.7, 129.2, 128.75, 128.73, 128.5, 128.2, 128.1,

TH-3369_166122017

125.72, 125.69, 119.2, 119.0, 106.0, 58.0, 57.4; IR (KBr, cm^{-1}): 3061, 2935, 1613, 1511, 1423, 1267, 1154, 1078, 1031, 763, 701, 636; HRMS (ESI) calcd for $C_{29}H_{21}N_2O^+$ 413.1654, found 413.1664.

6,7-Diphenyl-9-(trifluoromethyl)isoquinolino[2,1-*a*]quinoxalin-5-ium trifluoromethanesulfonate (3fa)

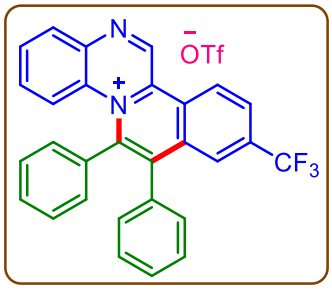

Light green solid (163 mg, 91% yield); ^{1}H NMR (CD_3CN, 600 MHz): δ 10.75 (s, 1H), 9.59 (d, J = 8.9 Hz, 1H), 8.49–8.46 (m, 2H), 8.03 (s, 1H), 7.95 (t, J = 8.1 Hz, 1H), 7.86 (d, J = 9.0 Hz, 1H), 7.51–7.45 (m, 4H), 7.38–7.35 (m, 1H), 7.28–7.25 (m, 6H); ^{13}C NMR (CD_3CN, 151 MHz): δ 147.3, 144.3, 143.8, 137.9, 137.4, 137.3, 137.1, 136.3, 134.3, 133.5, 131.99, 131.96, 131.5, 131.4, 130.5, 130.3, 120.0, 129.7, 129.2, 129.1(d, J = 2.9 Hz), 128.2, 126.1 (q, J = 4.4 Hz), 125.6, 123.4 (d, J = 2.9 Hz); ^{19}F NMR (CD_3CN+ Hexafluorobenzene, 377 MHz): δ -64.73 (s), -79.85 (s);. IR (KBr, cm^{-1}): 3061, 2924, 2851, 1694, 1589, 1318, 1264, 1219, 1030, 759, 701, 635; HRMS (ESI) calcd for $C_{29}H_{18}F_3N_2^+$ 451.1422, found 451.1423.

9-Chloro-6,7-diphenylisoquinolino[2,1-*a*]quinoxalin-5-ium trifluoromethanesulfonate (3ga)

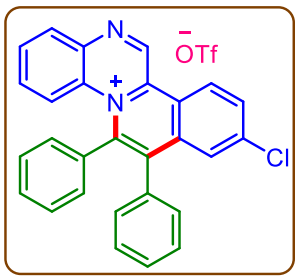

Green solid (132 mg, 78% yield); ^{1}H NMR (CD_3CN, 600 MHz): δ 10.63 (s, 1H), 9.37 (d, J = 9.2 Hz, 1H), 8.42 (d, J = 8.1 Hz, 1H), 8.24 (d, J = 9.0 Hz, 1H), 7.90 (t, J = 7.3 Hz, 1H), 7.79 (d, J = 9.0 Hz, 1H), 7.73 (s, 1H), 7.49–7.43 (m, 4H), 7.37–7.33 (m, 1H), 7.25–7.23 (m, 6H); ^{13}C NMR (CD_3CN, 151 MHz): δ 147.3, 144.7, 143.6, 143.5, 142.4, 138.8, 138.2, 136.4, 134.6, 134.4, 133.0, 131.96, 131.90, 131.7, 131.4, 131.3, 130.4, 130.2, 130.0, 129.8, 129.2, 128.0, 125.5, 124.9; IR (KBr, cm^{-1}): 3061, 2922, 1659, 1594, 1512, 1256, 1155, 1028, 969, 768, 700, 634; HRMS (ESI) calcd for $C_{28}H_{18}ClN_2^+$ 417.1159, found 417.1160.

TH-3369_166122017

9-Fluoro-6,7-diphenylisoquinolino[2,1-*a*]quinoxalin-5-ium trifluoromethanesulfonate (3ha)

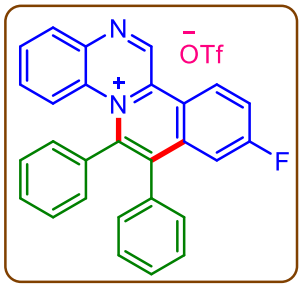

Green solid (143 mg, 87% yield); ^{1}H NMR (CD_3CN, 600 MHz): δ 10.62 (s, 1H), 9.49 (dd, J = 9.4, 5.1 Hz, 1H), 8.41 (d, J = 8.4 Hz, 1H), 8.08–8.05 (m, 1H), 7.89 (t, J = 7.2 Hz, 1H), 7.78 (d, J = 8.9 Hz, 1H), 7.48–7.41 (m, 5H), 7.37–7.34 (m, 1H), 7.27–7.23 (m, 6H); ^{13}C NMR (CD_3CN, 151 MHz): δ 168.1 (d, J = 262.7 Hz), 147.4, 143.3, 143.1, 142.8 (d, J = 4.9 Hz), 140.7 (d, J = 11.5 Hz), 138.1, 136.3, 134.8, 132.8, 132.05, 131.99, 131.9, 131.6, 131.3, 131.2, 130.3, 130.2, 130.0, 129.1, 125.5, 123.9 (d, J = 25.5 Hz), 123.5, 113.7 (d, J = 23.9 Hz); ^{19}F NMR (CD_3CN, 377 MHz) δ -79.35 (s), -95.93(s); IR (KBr, cm^{-1}): 3108, 3066, 1615, 1521, 1429, 1262, 1219, 1155, 1029, 734, 700, 635; HRMS (ESI) calcd for $C_{28}H_{18}FN_2^+$ 401.1454, found 401.1455.

6,7,9-Triphenylisoquinolino[2,1-*a*]quinoxalin-5-ium trifluoromethanesulfonate (3ia)

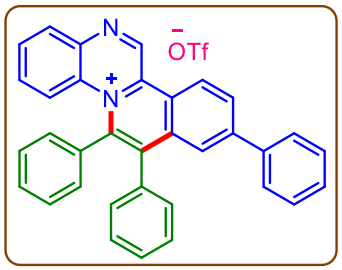

Green solid (103 mg, 57% yield); ^{1}H NMR (CD_3CN, 600 MHz): δ 10.68 (s, 1H), 9.46 (d, J = 9.0 Hz, 1H), 8.58 (dd, J = 8.9, 1.7 Hz, 1H), 8.41 (dd, J = 8.1, 1.3 Hz, 1H), 7.94 (s, 1H), 7.89 (t, J = 7.2 Hz, 1H), 7.79 (d, J = 8.7 Hz, 1H), 7.72 (dd, J = 8.0, 1.5 Hz, 2H), 7.55–7.51 (m, 3H), 7.48–7.42 (m, 4H), 7.37–7.34 (m, 1H), 7.30–7.24 (m, 6H); ^{13}C NMR (CD_3CN, 151 MHz): δ 149.9, 147.5, 143.4, 143.3, 142.6, 139.1, 138.3, 138.1, 136.5, 135.0, 132.9, 132.6, 132.0, 131.8, 131.5, 131.4, 131.3, 131.1, 130.8, 130.14, 130.11, 129.8, 129.2, 129.1, 128.5, 125.9, 125.4, 125.3; IR (KBr, cm^{-1}): 3059, 2925, 2856, 1738, 1609, 1443, 1267, 1151, 1078, 1030, 761, 700, 635; HRMS (ESI) calcd for $C_{34}H_{23}N_2^+$ 459.1861, found 459.1856.

TH-3369_166122017

6,7-Diphenylbenzo[6,7]isoquinolino[2,1-*a*]quinoxalin-5-ium trifluoromethanesulfonate (**3ja**)

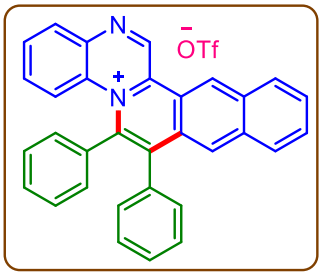

Red solid (123 mg, 71% yield); ^{1}H NMR (CD_3CN, 600 MHz): δ 10.88 (s, 1H), 10.16 (s, 1H), 8.50 (d, J = 8.0 Hz, 1H), 8.45 (d, J = 7.8 Hz, 1H), 8.34 (s, 1H), 8.13 (d, J = 7.8 Hz, 1H), 7.92–7.87 (m, 3H), 7.85 (d, J = 9.0 Hz, 1H), 7.53–7.46 (m, 4H), 7.34–7.30 (m, 3H), 7.27–7.22 (m, 4H).; ^{13}C NMR (CD_3CN, 151 MHz): δ 147.3, 144.1, 143.4, 140.2, 139.1, 137.9, 136.8, 135.6, 135.1, 132.9, 132.7, 132.1, 132.1, 132.0, 131.9, 131.5, 131.0, 130.91, 130.87, 130.8, 130.1, 130.05, 130.00, 129.9, 129.6, 129.0, 125.3, 123.0; ^{19}F NMR (CD_3CN+Hexafluorobenzene, 377 MHz): δ -79.77(s); IR (KBr, cm^{-1}): 3058, 2955, 2925, 1727, 1592, 1445, 1264, 1152, 1029, 759, 701, 636; HRMS (ESI) calcd for $C_{32}H_{21}N_2^+$ 433.1705, found 433.1703.

13,14-Diphenyl-[1,3]dioxolo[4',5':5,6]isoquinolino[2,1-*a*]quinoxalin-12-ium trifluoromethanesulfonate (**3ka**)

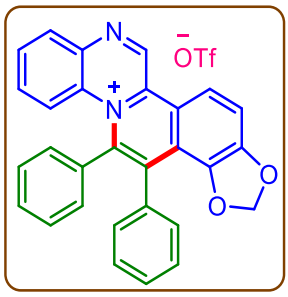

Red solid (127 mg, 74% yield); ^{1}H NMR (CD_3CN, 600 MHz): δ 10.46 (s, 1H), 9.07 (d, J = 9.6 Hz, 1H), 8.30 (d, J = 7.8 Hz, 1H), 7.88 (d, J = 9.0 Hz, 1H), 7.79 (t, J = 7.4 Hz, 1H), 7.72 (d, J = 8.4 Hz, 1H), 7.39–7.34 (m, 2H), 7.31 (t, J = 7.6 Hz, 2H), 7.27 (t, J = 7.4 Hz, 3H), 7.22 (d, J = 7.1 Hz, 2H), 7.18 (t, J = 7.7 Hz, 2H), 6.04 (s, 2H); ^{13}C NMR (CD_3CN, 151 MHz): δ 156.3, 147.6, 145.3, 142.7, 141.4, 139.5, 138.6, 136.2, 136.1, 132.2, 132.1, 131.55, 131.46, 131.4, 130.7, 129.8, 129.7, 129.2, 128.7, 125.8, 125.3, 121.7, 121.4, 116.8, 105.8; IR (KBr, cm^{-1}): 3061, 2921, 2853, 1611, 1575, 1428, 1394, 1259, 1148, 1092, 1028, 699, 634; HRMS (ESI) calcd for $C_{29}H_{19}N_2O_2^+$ 427.1447, found 427.1445.

TH-3369_166122017

11,12-Diphenylthieno[2',3':3,4]pyrido[1,2-*a*]quinoxalin-10-ium trifluoromethanesulfonate (**3la**)

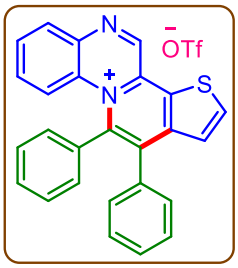

Brown solid (111 mg, 69% yield); ^{1}H NMR (CD_3CN, 600 MHz): δ 9.98 (s, 1H), 8.68 (d, J = 5.3 Hz, 1H), 8.33 (d, J = 7.2 Hz, 1H), 7.83 (t, J = 7.5 Hz, 1H), 7.62 (d, J = 8.9 Hz, 1H), 7.46–7.36 (m, 6H), 7.33–7.29 (m, 4H), 7.21 (d, J = 6.9 Hz, 2H); ^{13}C NMR (CD_3CN, 151 MHz): δ 150.7, 148.7, 145.6, 144.5, 142.8, 140.0, 137.4, 135.6, 134.0, 132.29, 132.26, 132.0, 131.5, 131.1, 130.8, 130.5, 130.2, 129.9, 129.2, 126.6, 125.3; IR (KBr, cm^{-1}): 3067, 2924, 2854, 1575, 1508, 1452, 1410, 1265, 1151, 1029, 762, 727, 700, 635; HRMS (ESI) calcd for $C_{26}H_{17}N_2S^+$ 389.1112, found 389.1119.

9-Fluoro-2,3-dimethyl-6,7-diphenylisoquinolino[2,1-*a*]quinoxalin-5-ium trifluoromethanesulfonate (**3ma**)

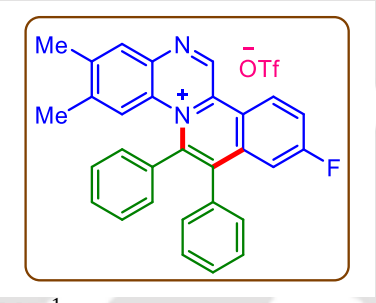

Light green solid (123 mg, 71% yield); ^{1}H NMR (CD_3CN, 600 MHz) δ 10.55 (s, 1H), 9.46 (dd, J = 9.4, 5.0 Hz, 1H), 8.17 (s, 1H), 8.05–8.02 (m, 1H), 7.46–7.42 (m, 4H), 7.40–7.36 (m, 2H), 7.29–7.26(m, 4H), 7.25 (dd, J = 7.5, 1.5 Hz, 2H), 2.45 (s, 3H), 2.04 (s, 3H); ^{13}C NMR (CD_3CN, 151 MHz): δ 167.8 (d, J = 261.5 Hz), 146.1, 143.9, 143.3, 142.7, 142.4, 142.3 (d, J = 4.8 Hz), 140.0 (d, J = 11.2 Hz), 137.4, 136.5, 134.9, 132.0, 131.7 (d, J = 10.7 Hz), 131.4, 131.2, 131.1, 130.3, 130.1, 130.0, 127.2, 125.2, 123.7, 123.5, 113.6 (d, J = 23.7 Hz), 21.1, 20.1; ^{19}F NMR (CD_3CN + Hexafluorobenzene, 377 MHz): δ -79.80 (s), -97.66 (s); IR (KBr, cm^{-1}): 3061, 2924, 2853, 1616, 1517, 1443, 1266, 1219, 1029, 872, 635; HRMS (ESI) calcd for $C_{30}H_{22}FN_2^+$ 429.1767, found 429.1775.

TH-3369_166122017

2-Methyl-6,7-diphenylisoquinolino[2,1-*a*]quinoxalin-5-ium trifluoromethanesulfonate (3na) and 3-Methyl-6,7-diphenylisoquinolino[2,1-*a*]quinoxalin-5-ium trifluoromethanesulfonate (3'na)

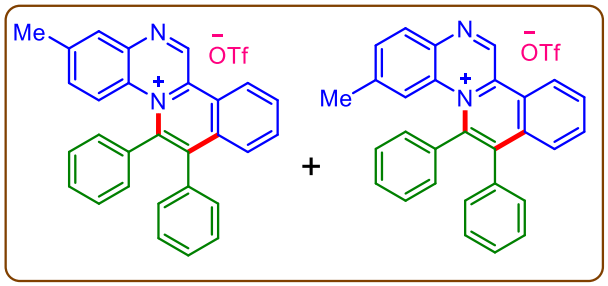

Inseparable regioisomer (1:0.6); Green solid (131 mg, 80% yield); ^{1}H NMR ($CDCl_3$, 600 MHz): δ 10.58 (s, 0.6H), 10.55 (s, 1H), 9.27 (dd, J = 8.4, 4.7 Hz, 1.78H), 8.25 (d, J = 8.4 Hz, 1.04H), 8.15–8.12 (m, 2.13H), 8.05 (dd, J = 14.4, 7.2 Hz, 1.84H), 7.82 (t, J = 7.8 Hz, 1.73H), 7.73 (d, J = 9.0 Hz, 0.69H), 7.61 (d, J = 8.4 Hz, 0.87H), 7.59 (s, 1H), 7.40–7.36 (m, 5.01H), 7.32–7.17 (m, 14.03H), 2.54 (s, 3.08H), 2.15 (s, 2H); ^{13}C NMR ($CDCl_3$, 151 MHz): δ 13C NMR (151 MHz, CDCl3) δ 145.3, 144.2, 142.6, 142.5, 142.4, 142.4, 142.2, 140.9, 140.8, 136.50, 136.46, 136.4, 136.3, 136.2, 135.3, 135.2, 133.72, 133.69, 132.9, 132.5, 131.9, 130.8, 130.7, 130.6, 130.4, 130.3, 130.2, 129.8, 129.7, 129.1, 129.0, 128.9, 128.8, 128.6, 128.0, 127.8, 126.3, 126.2, 126.1, 125.2, 125.1, 124.6, 124.0, 22.2, 21.3; IR (KBr, cm^{-1}): 3061, 2924, 2853, 1609, 1518, 1444, 1342, 1266, 1152, 1030, 700, 635; HRMS (ESI) calcd for $C_{29}H_{21}N_2^+$ 397.1705, found 397.1713.

2-Bromo-6,7-diphenylisoquinolino[2,1-*a*]quinoxalin-5-ium trifluoromethanesulfonate (3oa) and 3-Bromo-6,7-diphenylisoquinolino[2,1-*a*]quinoxalin-5-ium trifluoromethanesulfonate (3'oa)

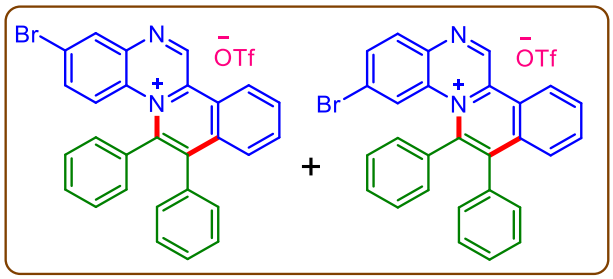

Inseparable regioisomer (1:0.3); Light green solid (124 mg, 68% yield); ^{1}H NMR (CD_3CN, 600 MHz): δ 10.70 (s, 1H), 10.68 (s, 0.3H), 9.42 (d, J = 8.4 Hz, 1.30H), 8.29 (t, J = 9.0 Hz, 2.08H), 8.23 (t, J = 7.5 Hz, 1.24H), 8.01 (d, J = 8.4 Hz, 0.83H), 7.89 (s, 0.78H), 7.84 (t, J = 7.8 Hz, 1.17H), 7.67 (d, J = 9.6 Hz, 0.35H), 7.52 (d, J = 9.6 Hz, 0.32H), 7.47–7.43 (m, 3.51H), 7.41 (dd, J = 9, 4.4 Hz, 1H), 7.31 (d, J = 4.2 Hz, 4H), 7.28–7.23 (m, 3.48H); ^{13}C NMR (CD_3CN, 151 MHz): δ 148.9, 147.9, 143.7, 142.5, 142.2, 138.6, 138.48, 138.46, 138.1, 137.0, 136.0, 135.0, 134.0, 133.8, 133.1, 132.1, 132.0, 131.5,

TH-3369_166122017

131.4, 131.35, 131.26, 130.34, 130.29, 130.2, 129.82, 129.80, 129.6, 129.0, 128.6, 127.9, 127.8, 126.9, 126.3, 125.1; IR (KBr, cm^{-1}): 3063, 2927, 2858, 2261, 1605, 1505, 1439, 1397, 1340, 1267, 1156, 1076, 1031, 835, 743, 703, 634; HRMS (ESI) calcd for $C_{28}H_{18}BrN_2^+$ 461.0653, found 461.0659.

6,7-Di-*p*-tolylisoquinolino[2,1-*a*]quinoxalin-5-ium trifluoromethanesulfonate (3ab)

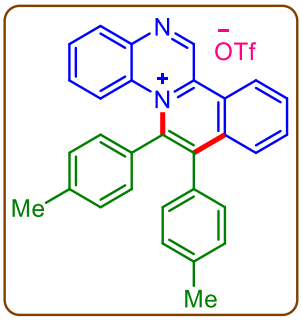

Yellow solid (119 mg, 71% yield); ^{1}H NMR ($CDCl_3$, 600 MHz): δ 10.61 (s, 1H), 9.28 (d, J = 8.4 Hz, 1H), 8.35 (d, J = 7.2 Hz, 1H), 8.14 (t, J = 7.5 Hz, 1H), 8.05 (t, J = 7.5 Hz, 1H), 7.86 (d, J = 8.4 Hz, 1H), 7.83 (d, J = 8.4 Hz, 1H), 7.77 (t, J = 7.2 Hz, 1H), 7.36 (t, J = 7.2 Hz, 1H), 7.19 (d, J = 7.8 Hz, 2H), 7.11 (dd, J = 11.7, 8.1 Hz, 4H), 7.01 (d, J = 7.8 Hz, 2H), 2.40 (s, 3H), 2.30 (s, 3H); ^{13}C NMR ($CDCl_3$, 151 MHz): δ 145.5, 142.9, 142.3, 141.3, 140.2, 138.8, 137.1, 136.4, 132.5, 132.4, 131.2, 131.0, 130.6, 130.5, 130.2, 130.1, 129.9, 129.4, 128.20, 128.16, 126.3, 125.1, 124.5, 21.6, 21.5; IR (KBr, cm^{-1}): 3053, 2924, 2855, 1608, 1516, 1437, 1341, 1266, 1153, 1030, 775, 635; HRMS (ESI) calcd for $C_{30}H_{23}N_2^+$ 411.1861, found 411.1864.

6,7-Bis(4-bromophenyl)isoquinolino[2,1-*a*]quinoxalin-5-ium trifluoromethanesulfonate (3ac)

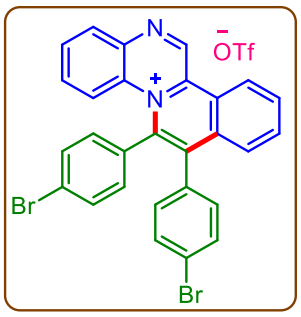

Light green solid (138 mg, 67% yield); ^{1}H NMR (CD_3CN, 600 MHz): δ 10.69 (s, 1H), 9.42 (d, J = 8.6 Hz, 1H), 8.44 (d, J = 7.8 Hz, 1H), 8.29 (t, J = 7.7 Hz, 1H), 8.22 (t, J = 7.7 Hz, 1H), 7.93 (t, J = 7.6 Hz, 1H), 7.84 (d, J = 8.3 Hz, 1H), 7.79 (d, J = 8.9 Hz, 1H), 7.64 (d, J = 8.4 Hz, 2H), 7.53 (t, J = 7.8 Hz, 1H), 7.46 (d, J = 8.5 Hz, 2H), 7.17 (dd, J = 8.7, 2.4 Hz, 4H).^{13}C NMR (CD_3CN, 151 MHz): δ 147.4, 143.7, 142.5, 141.1, 138.5, 138.4, 137.4, 135.4, 134.1, 134.1, 133.9, 133.4, 133.3, 133.1, 133.0, 131.95,

TH-3369_166122017

131.86, 129.0, 128.9, 127.9, 126.3, 125.6, 125.3, 124.2; IR (KBr, cm^{-1}): 2922, 2853, 1589, 1487, 1391, 1258, 1146, 1025, 763, 631; HRMS (ESI) calcd for $C_{28}H_{17}Br_2N_2^+$ 538.9758, found 538.9755.

6,7-Bis(4-fluorophenyl)isoquinolino[2,1-*a*]quinoxalin-5-ium trifluoromethanesulfonate (**3ad**)

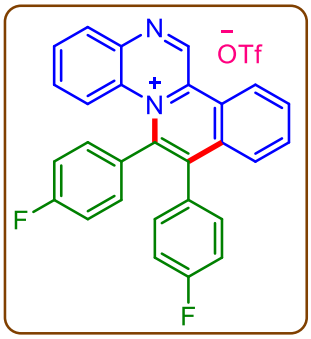

Green solid (136 mg, 80% yield); ^{1}H NMR (CD_3CN, 600 MHz): δ 10.69 (s, 1H), 9.41 (d, J = 8.5 Hz, 1H), 8.43 (dd, J = 8.2, 1.4 Hz, 1H), 8.29 (ddd, J = 8.4, 7.0, 1.1 Hz, 1H), 8.23 (t, J = 7.2 Hz, 1H), 7.92 (td, J = 7.7, 0.8 Hz, 1H), 7.86 (d, J = 8.2 Hz, 1H), 7.79 (d, J = 8.8 Hz, 1H), 7.53–7.50 (m, 1H), 7.29–7.24 (m, 4H), 7.23–7.19 (m, 2H), 7.03 (t, J = 8.7 Hz, 2H); ^{13}C NMR (CD_3CN, 151 MHz): δ 164.2 (d, J = 250.3 Hz), 164.0 (d, J = 247.2), 147.4, 143.6, 142.9, 141.6, 138.5, 138.3, 137.8, 134.5 (d, J = 8.7 Hz), 133.9, 133.6 (d, J = 8.6 Hz), 132.9, 132.8 (d, J = 3.6 Hz), 131.9, 131.7, 131.2 (d, J = 3.6 Hz), 129.1, 128.9, 127.8, 126.3, 125.6, 117.4 (d, J = 22.3 Hz), 117.0 (d, J = 22.2 Hz); ^{19}F NMR (CD_3CN+Hexafluorobenzene, 377 MHz) δ -79.82 (s), -111.56(s), -114.27(s); IR (KBr, cm^{-1}): 3071, 2924, 2849, 1735, 1604, 1510, 1263, 1159, 1030, 833, 757, 636; HRMS (ESI) calcd for $C_{28}H_{17}F_2N_2^+$ 419.1360, found 419.1361.

6,7-Bis(4-fluorophenyl)-9-methoxyisoquinolino[2,1-*a*]quinoxalin-5-ium trifluoromethanesulfonate (**3dd**)

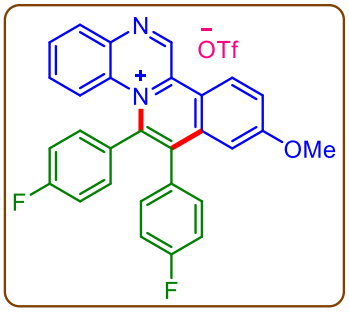

Green solid (80 mg, 45% yield); ^{1}H NMR (CD_3CN, 400 MHz): δ 10.49 (s, 1H), 9.30 (d, J = 9.5 Hz, 1H), 8.34 (d, J = 8.1 Hz, 1H), 7.87–7.82 (m, 2H), 7.66 (d, J = 8.9 Hz, 1H), 7.47–7.42 (m, 1H), 7.28–7.19 (m, 6H), 7.05–6.99 (m, 3H), 3.91 (s, 3H); ^{13}C NMR (CD_3CN, 151 MHz): δ 167.7, 164.2 (d, J = 250.2 Hz), 164.0 (d, J = 247 Hz), 147.6, 142.6, 141.8, 141.1, 141.0, 137.9, 134.4 (d, J = 8.7 Hz), 133.6

TH-3369_166122017

(d, *J* = 8.6 Hz), 132.7 (d, *J* = 3.7 Hz), 132.1, 131.8, 131.31, 131.27 (d, *J* = 3.5 Hz), 130.3, 129.0, 125.5, 125.3, 121.1, 117.3 (d, *J* = 22.3 Hz), 117.1 (d, *J* = 22.2 Hz), 108.4, 57.7; ^{19}F NMR (CD_3CN, 377 MHz) δ -79.33 (s), -111.20 (s), -113.78 (s); IR (KBr, cm^{-1}): 3069, 2947, 1605, 1513, 1446, 1401, 1262, 1156, 1028, 843, 769, 636; HRMS (ESI) calcd for $C_{29}H_{19}F_2N_2O^+$ 449.1465, found 449.1459.

6,7-Bis(3-chlorophenyl)-9-fluoroisoquinolino[2,1-*a*]quinoxalin-5-ium trifluoromethanesulfonate (3he)

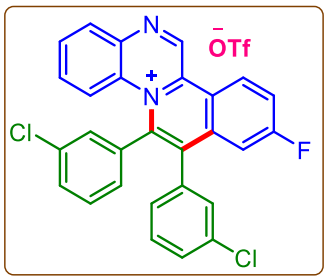

Green solid (120 mg, 65% yield); ^{1}H NMR (CD_3CN, 600 MHz) δ 10.64 (s, 1H), 9.51 (dd, *J* = 9.6, 4.8 Hz, 1H), 8.45 (d, *J* = 7.8 Hz, 1H), 8.12–8.08 (m, 1H), 7.94 (t, *J* = 7.8 Hz, 1H), 7.81 (d, *J* = 9.0 Hz, 1H), 7.54 (t, *J* = 8.7 Hz, 1H), 7.51–7.43 (m, 3H), 7.40 (d, *J* = 7.8 Hz, 1H), 7.35–7.30 (m, 1H), 7.29–7.22 (m, 3H), 7.16 (dd, *J* = 22.2, 7.7 Hz, 1H); ^{13}C NMR (CD_3CN, 151 MHz): δ 168.3 (d, *J* = 263.2 Hz), 147.3, 143.5, 141.5 (t, *J* = 4.3 Hz), 141.4, 140.1 (d, *J* = 11.5 Hz), 138.2, 137.7, 136.4, 135.8, 135.6 (d, *J* = 6.5 Hz), 133.1, 132.24, 132.16, 132.13, 132.07, 132.0, 131.92, 131.88, 131.81, 131.77, 131.7, 131.4 (d, *J* = 4.7 Hz), 131.2, 131.0, 130.6 (d, *J* = 4.4 Hz), 130.5, 130.4, 130.1, 129.9, 128.8, 125.5, 124.3, 124.2, 123.5, 114.0 (d, *J* = 23.8 Hz); ^{19}F NMR (CD_3CN, 377 MHz) δ -79.35 (s), -95.31 (s); IR (KBr, cm^{-1}): 3063, 1732, 1616, 1524, 1430, 1263, 1219, 1155, 1030, 763, 732, 635; HRMS (ESI) calcd for $C_{28}H_{16}Cl_2FN_2^+$ 469.0675, found 469.0679.

7-Methyl-6-phenylisoquinolino[2,1-*a*]quinoxalin-5-ium trifluoromethanesulfonate (3af)

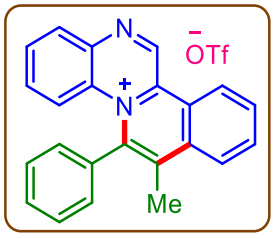

Green solid (95 mg, 68% yield); ^{1}H NMR (CD_3CN, 600 MHz): δ 10.58 (s, 1H), 9.34 (d, *J* = 8.4 Hz, 1H), 8.60 (d, *J* = 8.4 Hz, 1H), 8.38 (t, *J* = 7.5 Hz, 1H), 8.35 (d, *J* = 7.8 Hz, 1H), 8.28 (t, *J* = 7.8 Hz, 1H), 7.85 (t, *J* = 7.6 Hz, 1H), 7.77 (d, *J* = 8.9 Hz, 1H), 7.64 (t, *J* = 7.3 Hz, 1H), 7.59 (t, *J* = 7.2 Hz, 2H), 7.56–7.54 (m, 2H), 7.42 (t, *J* = 7.8 Hz, 1H), 2.80 (s, 3H); ^{13}C NMR (CD_3CN, 151 MHz): δ 147.3, 143.5,

TH-3369_166122017

141.7, 139.0, 138.1, 137.6, 136.6, 133.6, 132.5, 132.1, 131.8, 131.6, 131.4, 131.2, 130.9, 129.2, 127.9, 127.4, 125.8, 125.5, 18.7; IR (KBr, cm^{-1}): 3061, 2928, 2855, 1608, 1519, 1446, 1265, 1155, 1030, 762, 705, 636; HRMS (ESI) calcd for $C_{23}H_{17}N_2^+$ 321.1392, found 321.1393.

7-Ethyl-6-phenylisoquinolino[2,1-*a*]quinoxalin-5-ium trifluoromethanesulfonate (3ag)

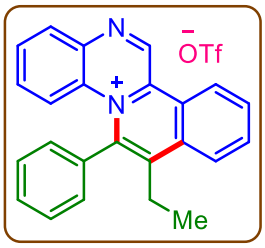

Green solid (93 mg, 64% yield); ^{1}H NMR (CD_3CN, 600 MHz): δ 10.58 (s, 1H), 9.37 (d, J = 8.5 Hz, 1H), 8.65 (d, J = 8.4 Hz, 1H), 8.39 (t, J = 7.6 Hz, 1H), 8.35 (d, J = 7.8 Hz, 1H), 8.28 (t, J = 7.6 Hz, 1H), 7.85 (dd, J = 8.0, 4.0 Hz, 2H), 7.63–7.58 (m, 5H), 7.43 (t, J = 7.2 Hz, 1H), 3.26 (q, J = 7.5 Hz, 2H), 1.24 (t, J = 7.6 Hz, 3H); ^{13}C NMR (CD_3CN, 151 MHz): δ 147.4, 144.4, 143.4, 141.9, 138.2, 137.7, 136.6, 136.5, 133.6, 132.5, 131.8, 131.8, 131.6, 131.3, 131.0, 129.2, 128.2, 127.2, 126.3, 125.6, 24.6, 15.5; IR (KBr, cm^{-1}): 3065, 2975, 1578, 1517, 1439, 1335, 1261, 1151, 1028, 758, 701, 635; HRMS (ESI) calcd for $C_{24}H_{19}N_2^+$ 335.1548, found 335.1554.

9-Fluoro-7-methyl-6-phenylisoquinolino[2,1-*a*]quinoxalin-5-ium trifluoromethanesulfonate (3hf)

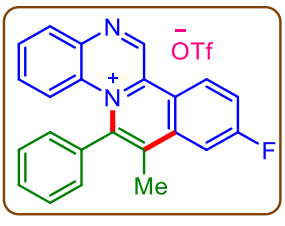

Green solid (115 mg, 79% yield); ^{1}H NMR (CD_3CN, 600 MHz): δ 10.52 (s, 1H), 9.42 (dd, J = 9.6, 5.4 Hz, 1H), 8.36 (d, J = 8.4 Hz, 1H), 8.27 (d, J = 9.8 Hz, 1H), 8.09 (t, J = 8.1 Hz, 1H), 7.86 (t, J = 7.6 Hz, 1H), 7.74 (d, J = 8.4 Hz, 1H), 7.64 (t, J = 7.4 Hz, 1H), 7.60 (t, J = 7.5 Hz, 2H), 7.56–7.53 (m, 2H), 7.42 (t, J = 7.8 Hz, 1H), 2.76 (s, 3H); ^{13}C NMR (CD_3CN, 151 MHz): δ 168.3 (d, J = 261.9 Hz), 147.3, 143.3, 142.4, 140.5 (d, J = 11.5 Hz), 138.3 (d, J = 4.8 Hz), 137.4, 136.4, 132.6, 132.2, 132.1, 132.02, 131.96, 131.6, 131.3, 131.0, 129.1, 125.4, 123.6 (d, J = 25.4 Hz), 123.0, 112.6 (d, J = 23.4 Hz), 18.9; ^{19}F NMR (CD_3CN+Hexafluorobenzene, 377 MHz) δ -80.05 (s), -97.22(s); IR (KBr, cm^{-1}): 3106, 3068, 1619, 1524, 1430, 1265, 1219, 1153, 1030, 767, 706, 636; HRMS (ESI) calcd for $C_{23}H_{16}FN_2^+$ 339.1298, found 339.1297.

TH-3369_166122017

6,7-Diethylisoquinolino[2,1-*a*]quinoxalin-5-ium trifluoromethanesulfonate (3ah)

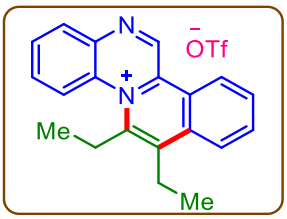

Brown solid (69 mg, 53% yield); ^{1}H NMR (CD_3CN, 600 MHz): δ 10.46 (s, 1H), 9.23 (d, J = 8.5 Hz, 1H), 8.56 (d, J = 8.5 Hz, 1H), 8.46–8.44 (m, 2H), 8.32 (t, J = 7.8 Hz, 1H), 8.19 (t, J = 7.7 Hz, 1H), 8.09 (t, J = 7.8 Hz, 1H), 8.02 (t, J = 7.2 Hz, 1H), 3.68 (q, J = 7.3 Hz, 2H), 3.51 (q, J = 7.6 Hz, 2H), 1.47 (t, J = 7.6 Hz, 3H), 1.23 (t, J = 7.3 Hz, 3H); ^{13}C NMR (CD_3CN, 151 MHz): δ 147.2, 145.6, 144.7, 142.9, 138.0, 137.7, 136.6, 133.2, 133.0, 132.2, 131.4, 128.9, 127.7, 126.5, 125.7, 125.2, 28.4, 24.1, 15.6, 15.0; IR (KBr, cm^{-1}): 3092, 2975, 2930, 2871, 1592, 1516, 1441, 1389, 1264, 1153, 1029, 775, 692, 634; HRMS (ESI) calcd for $C_{20}H_{19}N_2^+$ 287.1548, found 287.1559.

TH-3369_166122017

II.8. NMR Spectra

6,7-Diphenylisoquinolino[2,1-*a*]quinoxalin-5-ium trifluoromethanesulfonate (3aa): ^{1}H NMR (CD_3CN, 600 MHz)

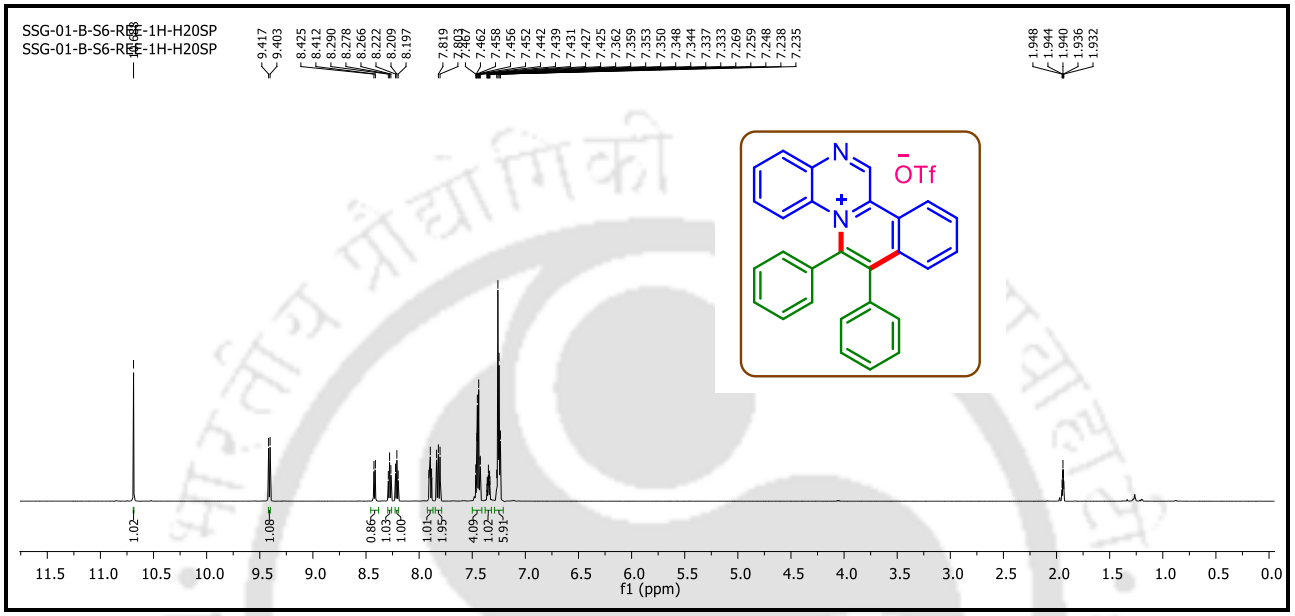

6,7-Diphenylisoquinolino[2,1-*a*]quinoxalin-5-ium trifluoromethanesulfonate (3aa): ^{13}C NMR (CD_3CN, 151 MHz)

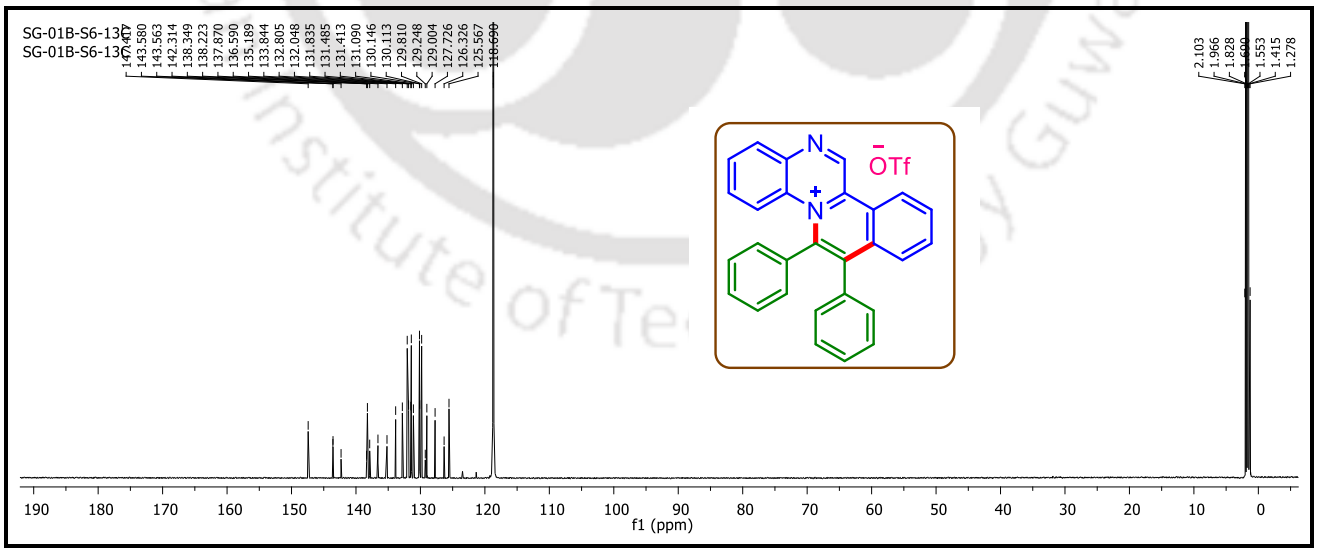

TH-3369_166122017

The remaining NMR spectra are available on

https://pubs.acs.org/doi/suppl/10.1021/acsomega.9b00274/suppl_file/ao9b00274_si_001.pdf

TH-3369_166122017

CHAPTER III

Solvent Switched Manganese(I) Catalyzed Regiodivergent Distal vs Proximal C-H Alkylation of Imidazopyridine with Maleimide

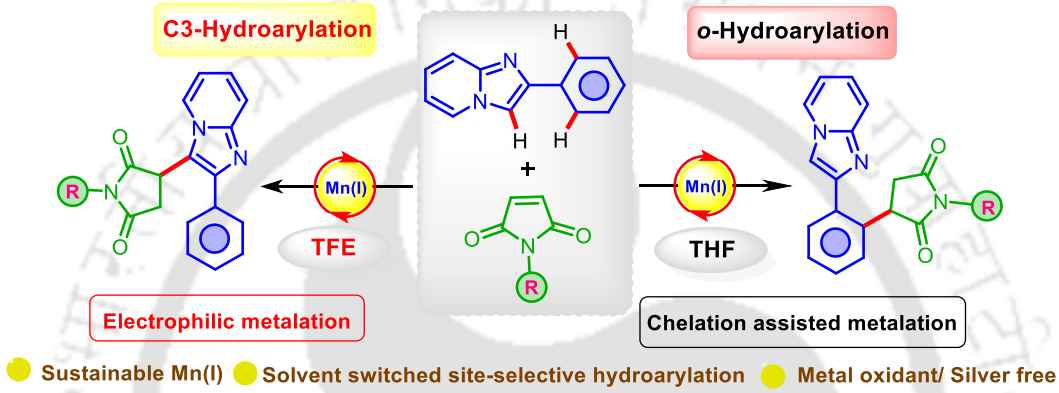

Abstract: *A sustainable Mn(I)-catalyzed exclusive solvent-dependent functionalization of imidazopyridine with maleimide via an electrophilic metalation at the distal (in 2,2,2-trifluoroethanol (TFE)) and chelation assisted at the proximal (in tetrahydrofuran (THF)) has been developed. The strategy was successfully applied to the drug Zolimidine and a broad range of substrates, thereby reflecting the method's versatility.*

Keywords:
Mn(I)-catalysis, regio-divergent alkylation, solvent-switching, imidazopyridine, maleimide

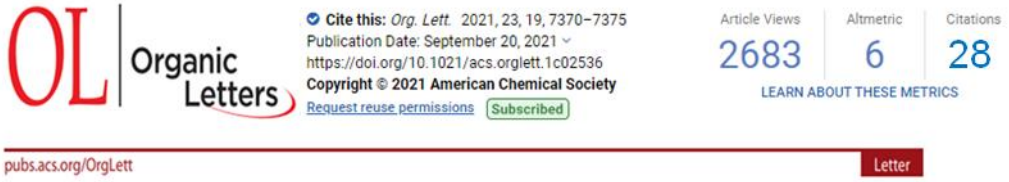

CHAPTER III

III.1. Introduction

Achieving predictable site-selective C–H functionalization in organic scaffolds having multiple reactive C–H bonds is thrilling and challenging.[1] In this context, the transition metal-catalyzed regio and site-selective C–H bond activation open a new paradigm for developing various functional molecules and their late-stage diversification.[2] Accomplishing the target without pre-functionalization is associated with step and atom economy, so it is widely accepted over the traditional approach.[3] Various research groups have made remarkable contributions towards selective C–H bond functionalization, through the controlled choice of solvents,[4] catalyst,[5] ligands,[6] and temperature[7] etc. to achieve the regioselectivity over the indiscriminate possibilities (Scheme III.1.1).

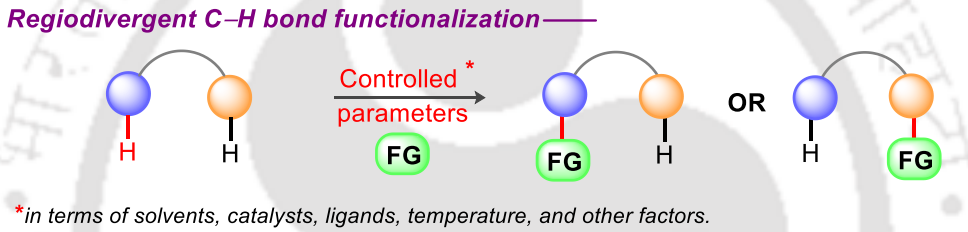

Scheme III.1.1. *Pictorial representation of regiodivergent C–H functionalization*

III.2. Prior Strategies of Metal-Catalyzed Controlled Regiodivergent C–H Functionalization

➢ **Solvent-Controlled:**

A solvent-controlled divergent C–H alkenylation of 3,4-disubstituted pyrroles has been demonstrated by Yao group (Scheme III.2.1).[4a] This reaction proceeds *via* a heck coupling of the pyrroles and activated olefins to afford the regioselective alkenylated pyrroles with good to moderate yields. Apolar toluene solvent offered C2-alkenylaed product whereas, polar DMSO provided selective C5-alkenylated adduct. Furthermore, C5-alkenylation protocol can be extended towards the total synthesis of (±)-rhazinilam.

TH-3369_166122017

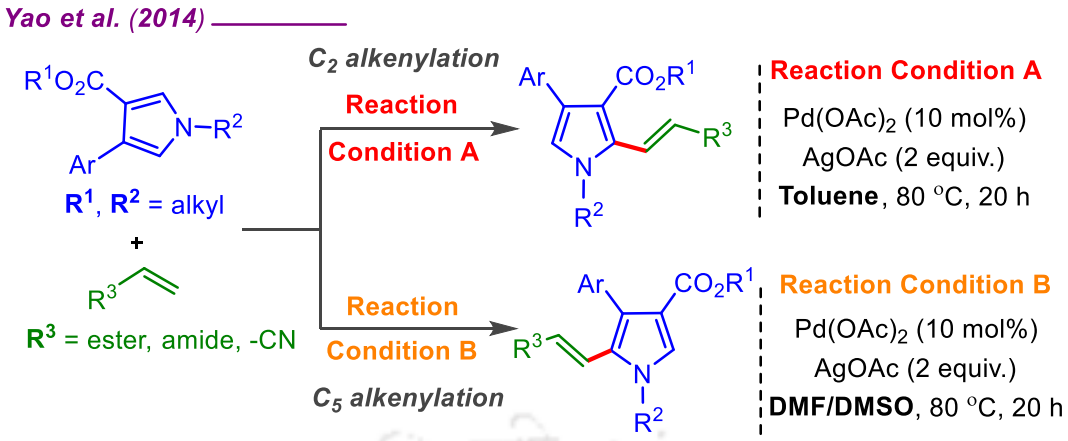

Scheme III.2.1. *Pd(II)-catalyzed solvent-switched divergent C–H alkenylation of pyrrole*

Lu *et al*. realized a Rh(III) catalyzed solvent-controlled *β*-elimination dictated C–H cross-coupling of arenes and allyl acetate (Scheme III.2.2).[4b] Herein, THF solvent offered *β*-H elimination to deliver cinnamyl derivatives, meanwhile, MeOH afforded allyl adducts *via β*-OAc elimination.

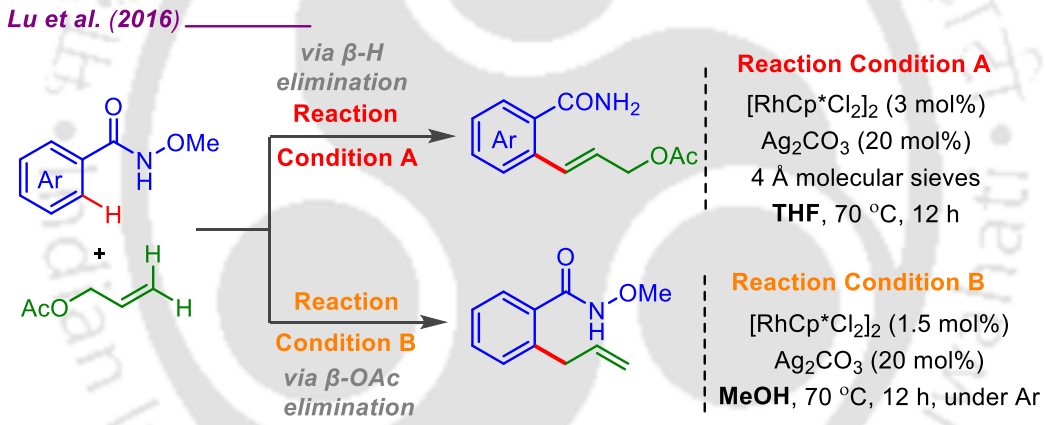

Scheme III.2.2. *Rh(III)-catalyzed divergent β-H and β-OAc elimination*

Chusov and his co-workers reported an excellent Rh-catalyzed solvent-altered reductive amidation and tertiary amine synthesis, starting from aldehydes and amides (Scheme III.2.3).[4c] This protocol described a non-requirement of external hydrogen sources along with the exploitation of carbon monoxide as a deoxygenative agent.

TH-3369_166122017

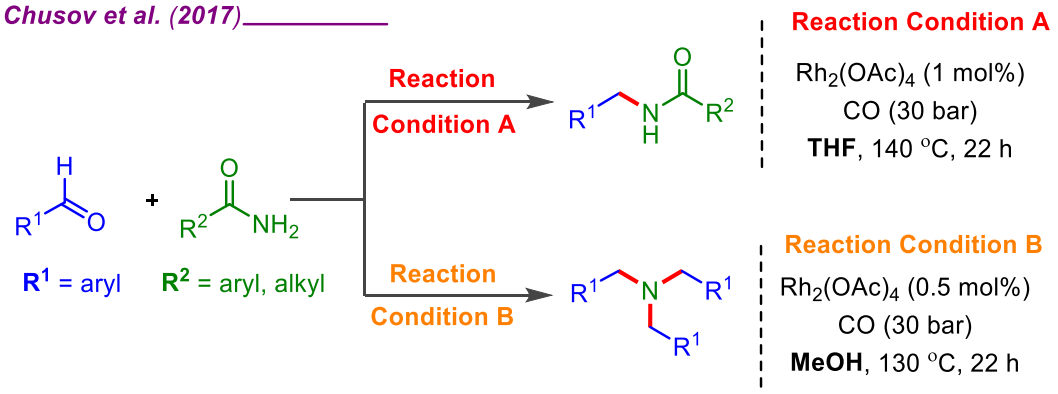

Scheme III.2.3. *Rh(II)-catalyzed solvent-switched divergent reductive amidation and amination*

In the year of 2018, Gao and co-workers described a solvent-controlled Rh(III)-catalyzed redox-neutral C–H functionalization reaction of *N*-phenoxyacetamides with propargyl alcohols to construct chalcone derivatives and benzofuran frameworks in an excellent regioselectivity (Scheme III.2.4).[4d] In this report, the more polar MeCN solvent offered *ortho*-alkenylated chalcone adducts whereas, the less polar DCM afforded the formation of benzofuran *via* a [3+2] cycloaddition product.A detailed experimental studies and DFT calculations firmly rationalized the divergent reaction pathway of propargyl alcohols towards *N*-phenoxyacetamides.

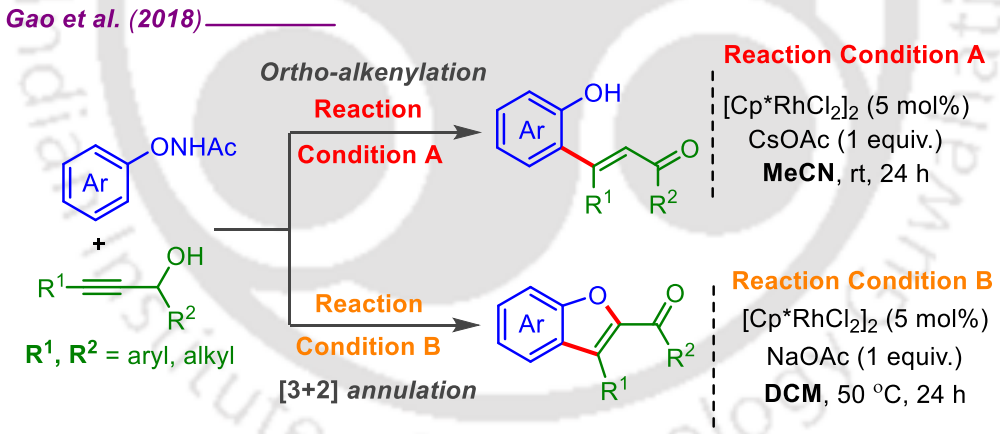

Scheme III.2.4. *Solvent-controlled divergent synthesis of chalcone and benzofuran*

A Pd(II)-catalyzed solvent polarity-guided divergent synthesis of fused and spiro-cyclopropanated indolines was introduced by Lee and co-workers (Scheme III.2.5).[4e] This present protocol proceeds *via* a Heck/regioselective C(sp^3)–H activation of *N*-methallylated 2-bromoarylamides. DFT calculations showed that the formation of fused-cyclopropanated indolines are more favorable in a low dielectric solvent such as *p*-xylene, whereas the spiro-cyclopropanated indolines are more likely to form in high dielectric media like DMSO.

TH-3369_166122017

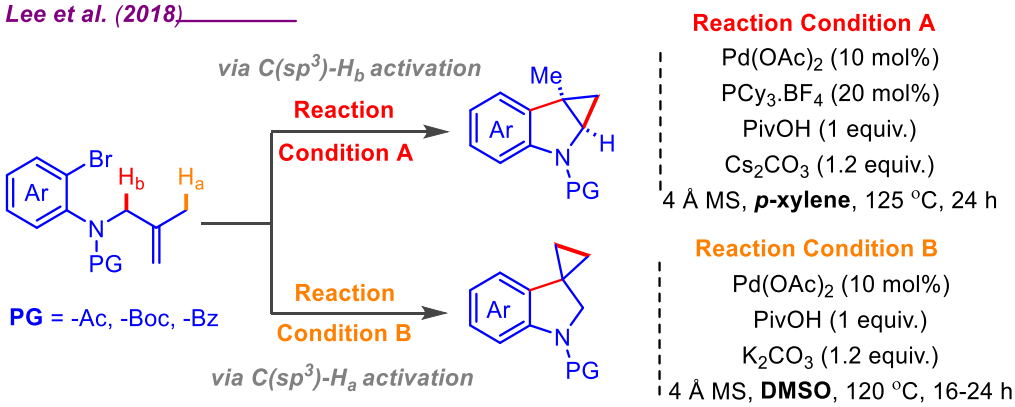

Scheme III.2.5. *Pd(II)-catalyzed solvent-driven divergent fused and spiro-cyclopropanation*

A solvent-controlled Rh(III)-catalyzed divergent coupling of benzamides and methyleneoxetanones leads to the access of alkylated benzamides and seven-membered 1*H*-benzo[*c*]azepine-1,3(2*H*)-diones *via* a highly chemo-selective dual C–H functionalization (Scheme III.2.6).[4f] A series of control experiments and theoretical calculations envisaged that in TFE solvent, alkyl C–O cleavage (*β*–O elimination) of methyleneoxetanones delivered the alkylated benzamide, whereas in DCE solvent acyl C–O cleavage (*β*–H elimination) offered cyclic 1*H*-benzo[*c*]azepine-1,3(2*H*)-diones.

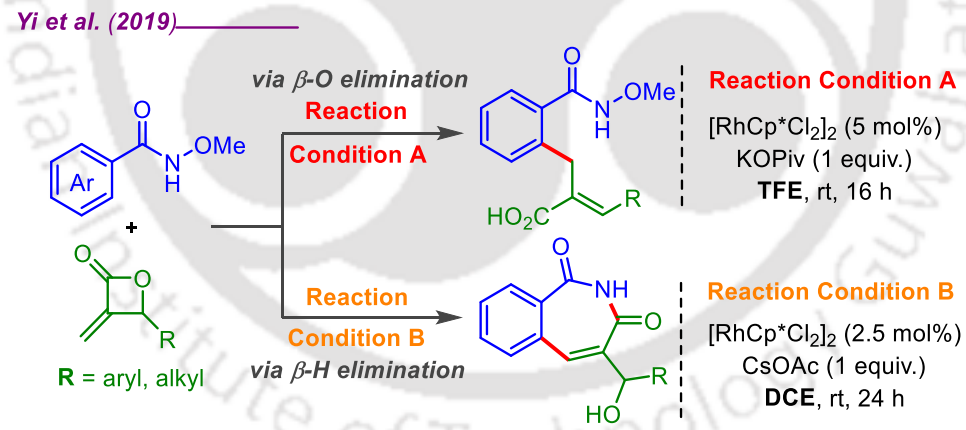

Scheme III.2.6. *Rh(III)-catalyzed divergent coupling of benzamides with methyleneoxetanones*

Loh *et al.* realized a Cp*Co(III)-catalyzed solvent dictated divergent addition of 1,2-oxazetidines with heteroarenes to deliver regioselective C–H aminomethylation and C–H hydroxymethylation (Scheme III.2.7).[4g] This protocol proceeds through the regioselective C–H functionalization followed by a concomitant N–O/C–C bond cleavage of 1, 2-oxazetidines.

TH-3369_166122017

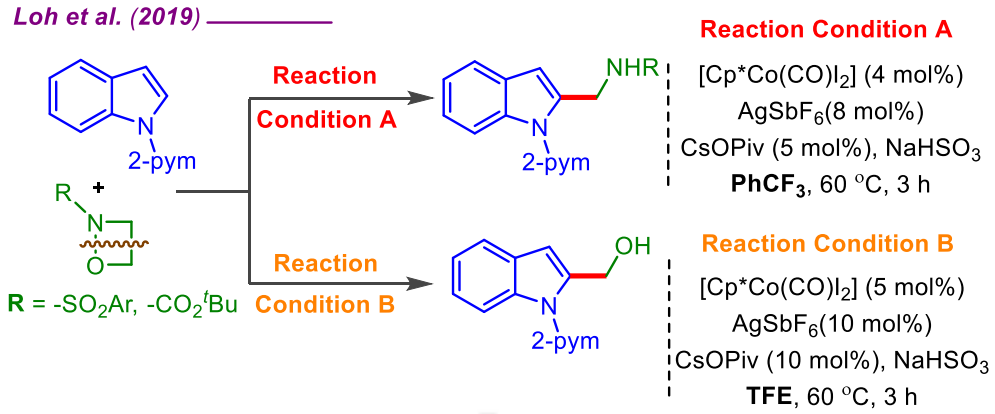

Scheme III.2.7. *Co(III)-catalyzed divergent ring-opening coupling of 1,2-oxazetidines*

A Rh(III) catalyzed solvent-switched C–H amidation of anilines with dioxazolones was developed by Chatani and co-workers using pyrimidine as a directing template (Scheme III.2.8).[4h] These findings revealed that 1,1,1,3,3,3-hexafluoro-2-propanol (HFIP) solvent afforded 1,2-diaminobenzene derivatives whereas 2,2,2-trifluoroethanol (TFE) offered the synthesis of benzimidazoles.

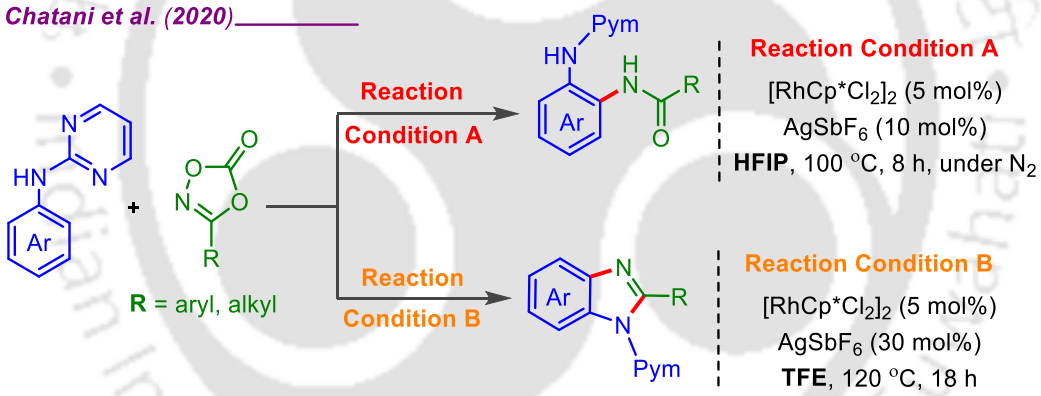

Scheme III.2.8. *Rh(III)-catalyzed solvent-controlled C–H amidation*

Fan *et al.* developed an elegant Pd(II)-catalyzed divergent cascade reaction of 2-alkynylbenzaldehydes with saturated cyclic amines to synthesize 1,2,3,4-tetrahydrobenzo[*g*]quinoline and naphthyl chain amine derivatives (Scheme III.2.9).[4i] This reaction outcome has been controlled by simply choosing the appropriate solvent. Non-polar toluene solvent offered a dehydrogenation [4+2] cycloaddition of saturated cyclic amines with 2-alkynylbenzaldehydes to provide cyclized 1,2,3,4-tetrahydrobenzo[*g*]quinolones. Whereas, polar DMSO/H_2O solvent system delivered naphthyl chain amines *via* a dehydrogenation/intermolecular condensation/C–N bond cleavage/intramolecular condensation pathway.

TH-3369_166122017

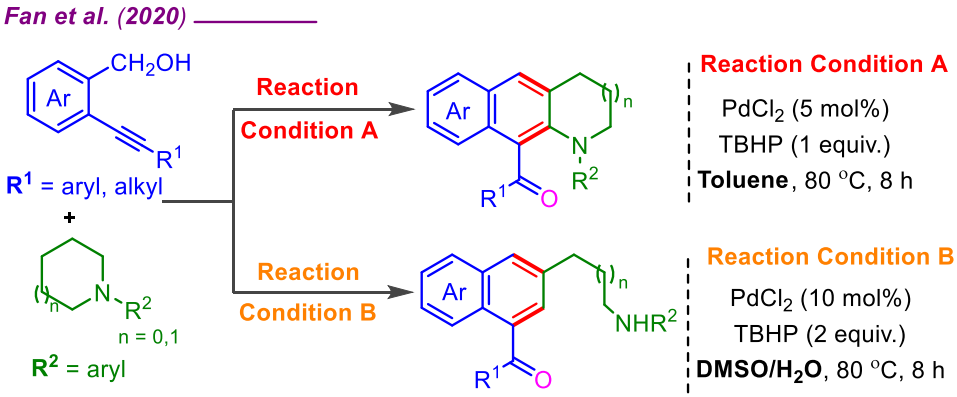

Scheme III.2.9. *Pd(II)-catalyzed solvent-tuned divergent cascade reaction*

Recently, Kanchupalli group reported a Rh(III)-catalyzed regeiodivergent [4+2] annulation reaction of 2-aryl indoles with idodnium ylides (Scheme III.2.10).[4j] In DCM solvent, the coupling of 2-arylindoles with idonium salts offered indolo[2,1-*a*]isoquinoline derivatives through N–H/C–H activation whereas, polar protic HFIP solvent facilitated the synthesis of benzo[*a*]carbazoles *via* C–H/C–H bond activations.

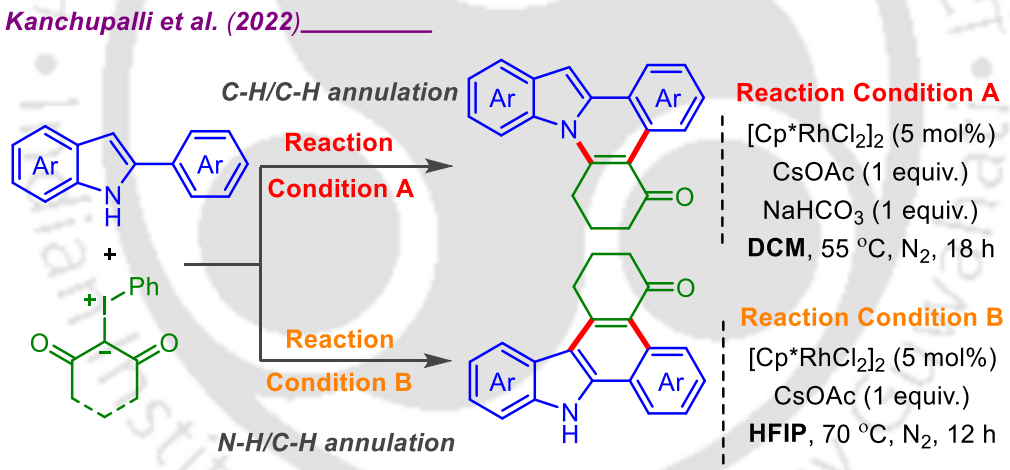

Scheme III.2.10. *Solvent-switched [4+2] annulation of 2-arylindole with idonium ylide*

➢ **Catalyst-Controlled:**

In 2020, Kapur *et al.* introduced a catalyst-controlled regioselective C–H olefination of 1,2-dihydroquinolines with terminal olefins (Scheme III.2.11).[5a] This protocol revealed that Pd-catalyst offered C3-olefination *via* distal electrophilic metalation, whereas, Ru-catalysis delivered C8-olefinated quinolones through proximal directed metalation.

TH-3369_166122017

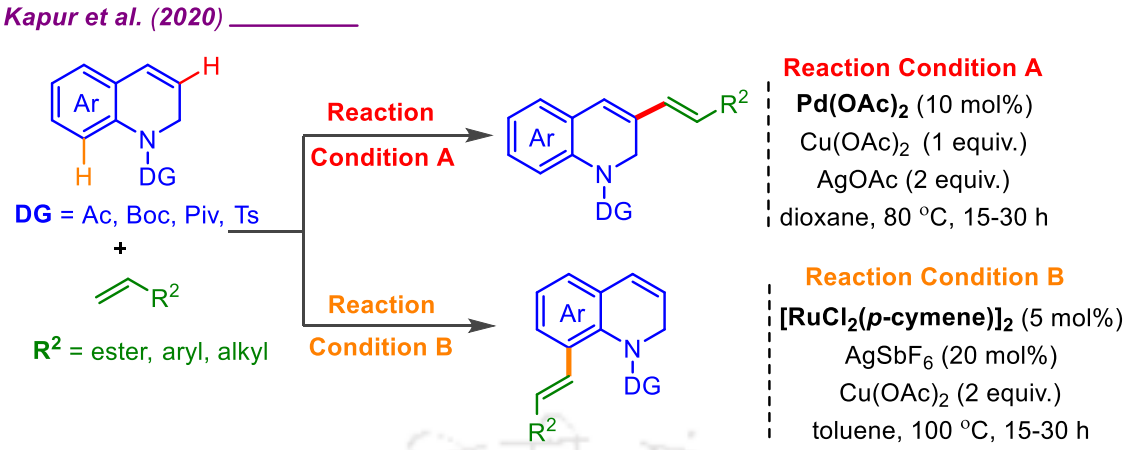

Scheme III.2.11. *Catalyst-controlled site-selective C–H olefination of 1,2-dihydroquinolines*

Recently, a catalyst-switched regiodivergent Heck coupling of 2-pyridylthiophene with activated olefins has been documented by Zhang research group (Scheme III.2.12).[5b] This protocol provided a C5-alkenylation through electrophilic palladation whereas Rh-catalysis offered chelation directed C3-alkenylation. Furthermore, this regiodivergent alkylation strategy may extended towards the development of π-conjugated di-functionalized 2-pyridylthophenes.

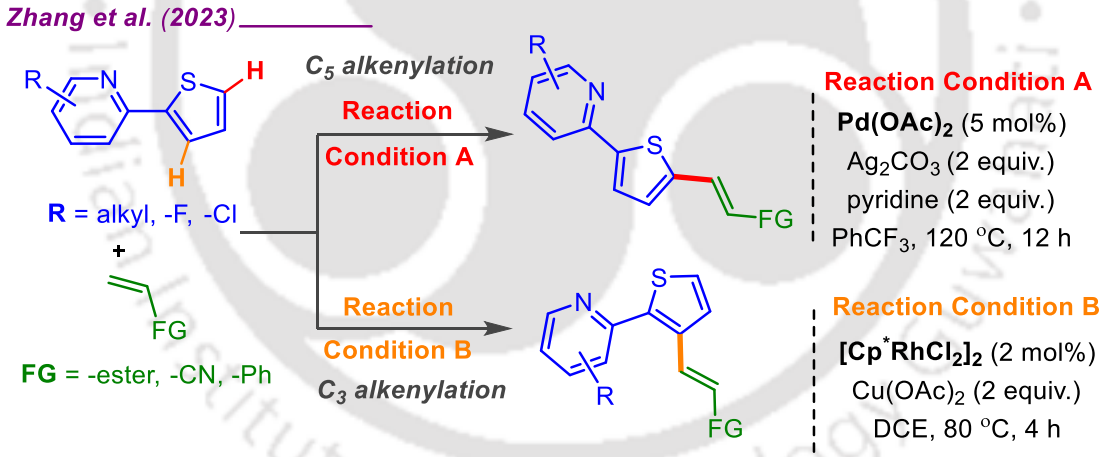

Scheme III.2.12. *Catalyst-controlled regiodivergent C-H alkenylation of 2-pyridylthiophenes*

In the same year, Kumar and co-workers introduced a catalyst-dependent regiodivergent oxidative annulation of imidazopyridines with cinnamaldehydes to synthesize two sets of annulated *N*-heterocyclic scaffolds (Scheme III.2.13).[5c] This annulation reaction revealed that in the presence of Rh(III)-catalyst a six-membered annulated adduct 5-arylnaphtho-[1′,2′:4,5]imidazo[1,2-*a*]pyridine-6-carbaldehydes through C3–H/*ortho* C–H activation. In contrast, Pd(II) catalyst offered annulation reaction *via* C3–H/C5–H activation to synthesis five membered 1,7-diarylimidazo[5,1,2-*cd*]indolizine-

TH-3369_166122017

6-carbaldehydes. This protocol presented good yield of annulated adducts with broad substrate scope and well tolerated functional groups.

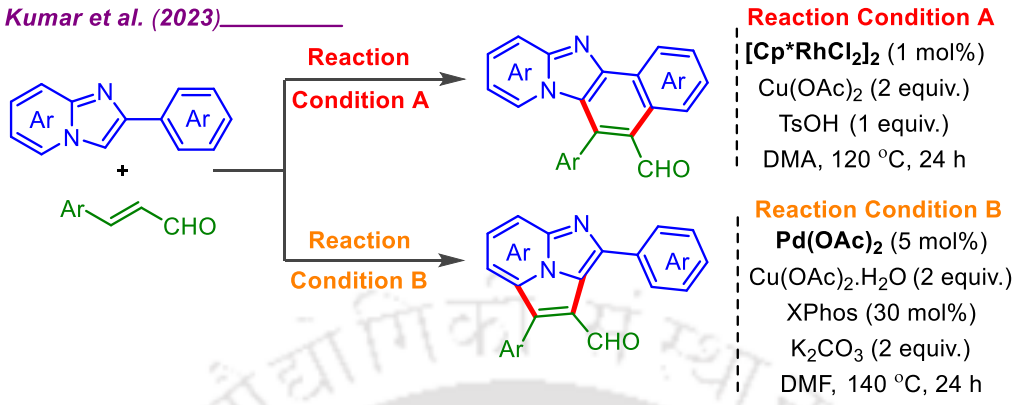

Scheme III.2.13. *Catalyst-controlled regiodivergent oxidative annulation of imidazopyridine*

➢ **Ligand-Controlled:**

Fu and co-workers developed a copper-catalyzed regiodivergent alkylboration of alkenes using bis(pinacolato)diboron and alkyl halides (Scheme III.2.14).[6a] The regioselectivity was dictated by the presence of suitable ligand. Cu-salts to afford two different alkyl boronic esters with molecular complexities. In light of the mechanistic aspects, the heteroatom on the alkenes may facilitated the addition of Cu-Bpin to the alkenes which was found to be decisive for this transformation. Moreover, this protocol can be extended toward copper-catalyzed divergent deuterboration and aminoboration reactions.

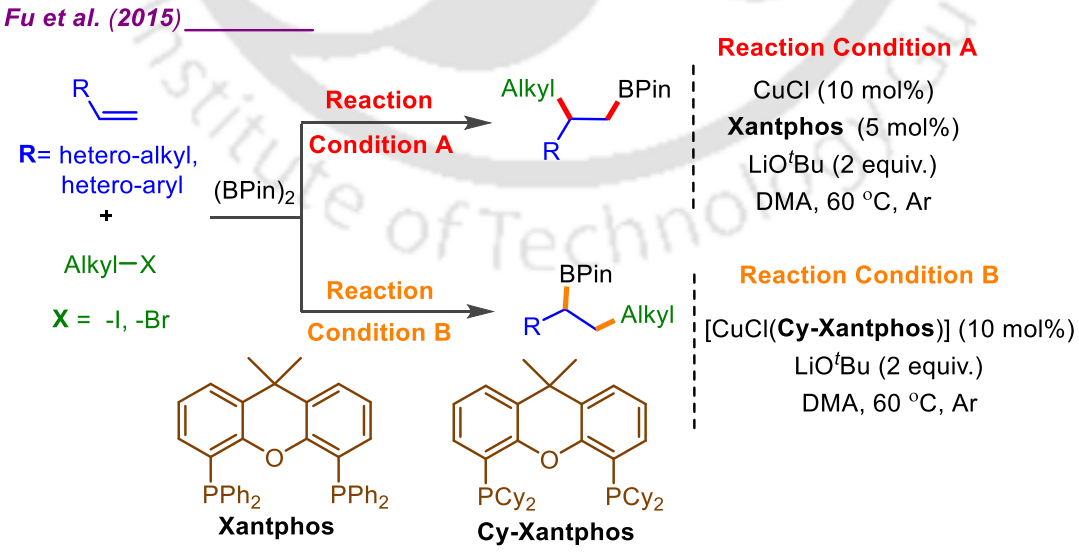

Scheme III.2.14. *Ligand-controlled regiodivergent alkylboration of alkene*

TH-3369_166122017

In 2016, the same group reported a Cu-catalyzed alkylboration of unactivated terminal alkynes in regiodivergent and stereospecific manner (Scheme III.2.15).[6b] This di-functionalization reaction was controlled by the use of two different ligands 1,2-bis(diphenylphosphino)benzene (dpppbz) and 4-dimethylaminopyridine (DMAP). In this reaction, Anti-Markovnikov alkylboration was observed in the presence of dppbz ligand, in contrast, a Markovnikov alkylboration was obtained using DMAP ligand.

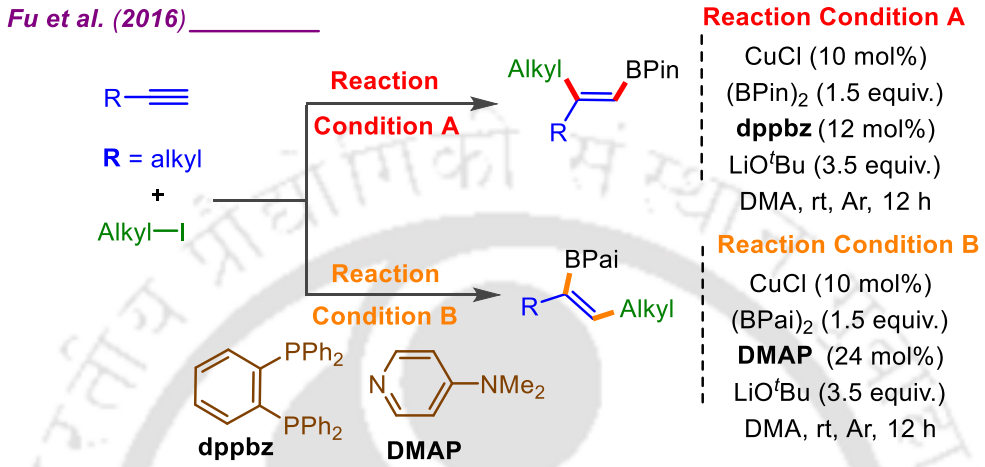

Scheme III.2.15. *Ligand-controlled Cu-catalyzed regiodivergent alkylboration of terminal alkynes*

A ligand-controlled palladium-catalyzed regiodivergent [3+2] and [3+3] cycloaddition reactions between naphthols and vinylethylene carbonates has been realized by Liang group (Scheme III.2.16).[6c] For this transformation in the presence of 2-dicyclohexylphosphino-3,6-dimethoxy-2',4',6'-triisopropyl-1,1'-biphenyl (brettphos) ligand, a regioselective [3+2] cycloaddition was observed. Meanwhile, 1,3-bis(diphenylphosphino)propane (dppp) ligand afforded [3+2] cycloaddition product from naphthols and vinylethylene carbonates. Both 1-naphthols and 2-naphthols are found to be equally efficient there by enriching economic efficiency of this protocol.

TH-3369_166122017

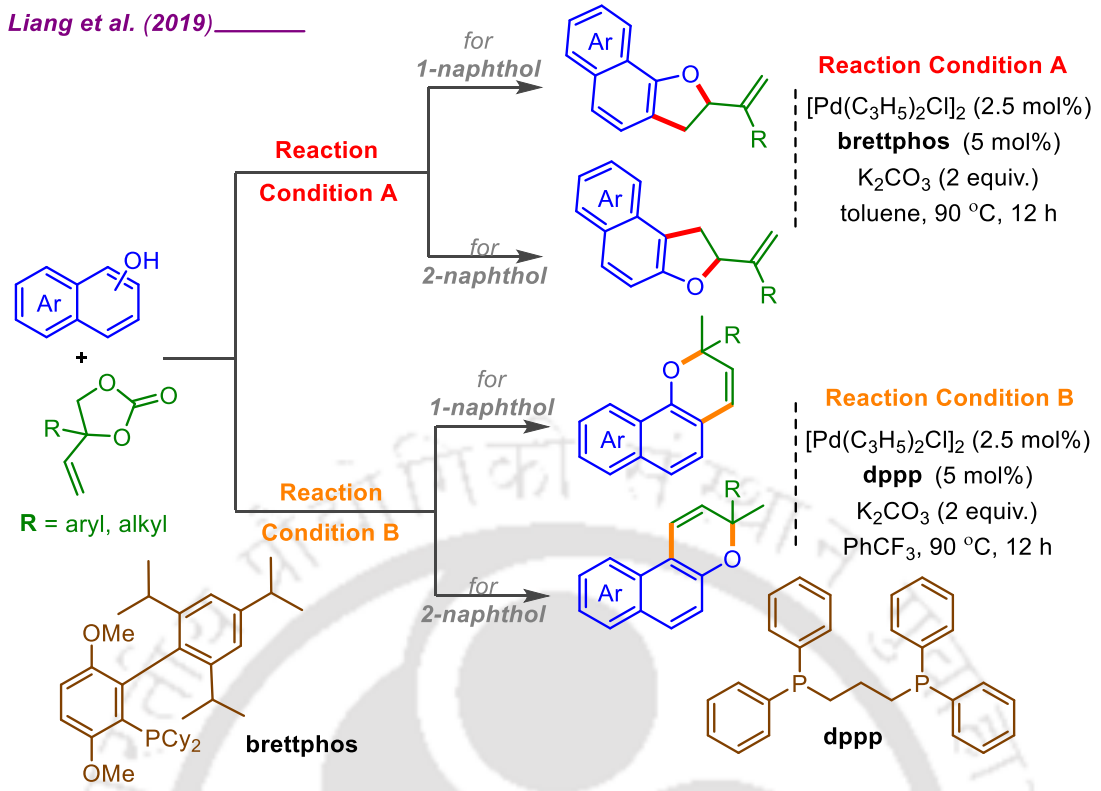

Scheme III.2.16. *Ligand-controlled regiodivergent [3+2] and [3+3] cycloaddition reactions*

A robust Pd-catalyzed ligand-controlled regiodivergent thiocarbonylation of alkynes have offered to access linear and branched α,β-unsaturated thioesters in straightforward manner (Scheme III.2.17).[6d] Here in, boronic acid and 5-chlorosalicyclic acid was used to *in situ* synthesize 5-chloroborosalicylic acid, which along with the ligands, plays a crucial role in regiodivergent thiocarbonylation reaction. In the presence of bis(2-diphenylphosphinophenyl)ether (DPEphos, **L1**) ligand, the catalytic protocol delivered selectively the linear α,β-unsaturated thioesters. Whereas, simply switching the ligand to tri(2-furyl)phosphine (**L2**) gave branched α,β-unsaturated thioesters. The developed protocol is the first such thiocarbonylation of internal alkyne.

TH-3369_166122017

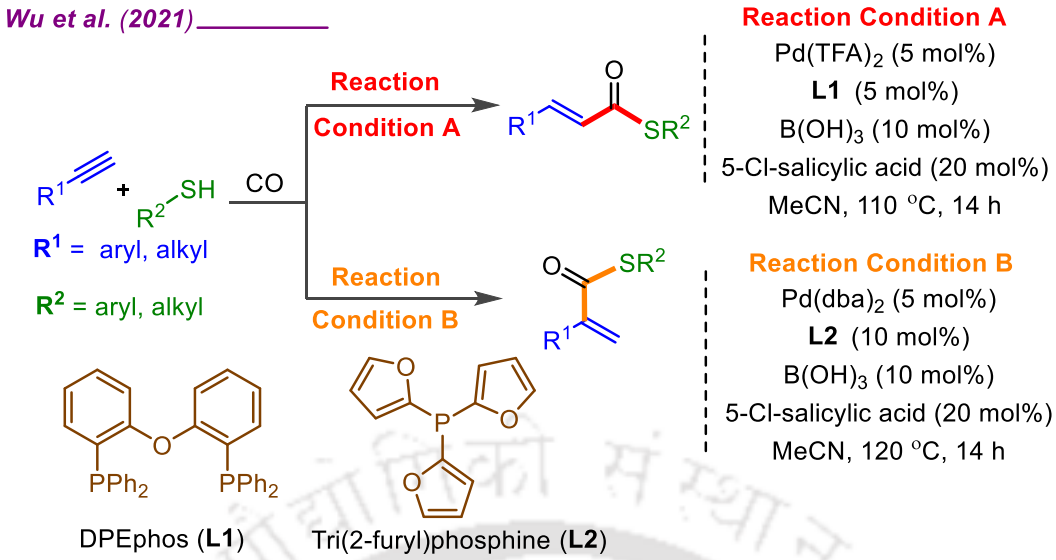

Scheme III.2.17. *Ligand-controlled regiodivergent thiocarbonylation of alkyne*

In the same year, Zi group established a Lewis-acid promoted palladium-catalyzed regiodivergent [3+2] and [4+3] cycloaddition of methylene ethylidene carbonate with 1,3-diene (Scheme III.2.18).[6e] This cycloaddition proceeds through the *in situ* formation of palladium-oxyallyl intermediate and the regioselectivity is truly guided by steric properties of indenephos ligands. The course of the reaction revealed that indenephos ligand **L3** gave five-membered carbocyclic adduct *via* a [3+2] cycloaddition reaction. In contrast, indenephos ligand **L4** preferred a [4+3] cycloaddition reaction to construct a seven-membered carbocyclic addition product. Moreover, DFT studies suggested a dispersion interaction between the reacting substrate and **L3** ligand offered the selective [3+2] cycloaddition. Meanwhile, the through-bond interaction between Pd-center and reacting substrate as well as the steric repulsion of **L4** ligand with Pd-center preferred the [4+3] pathway.

TH-3369_166122017

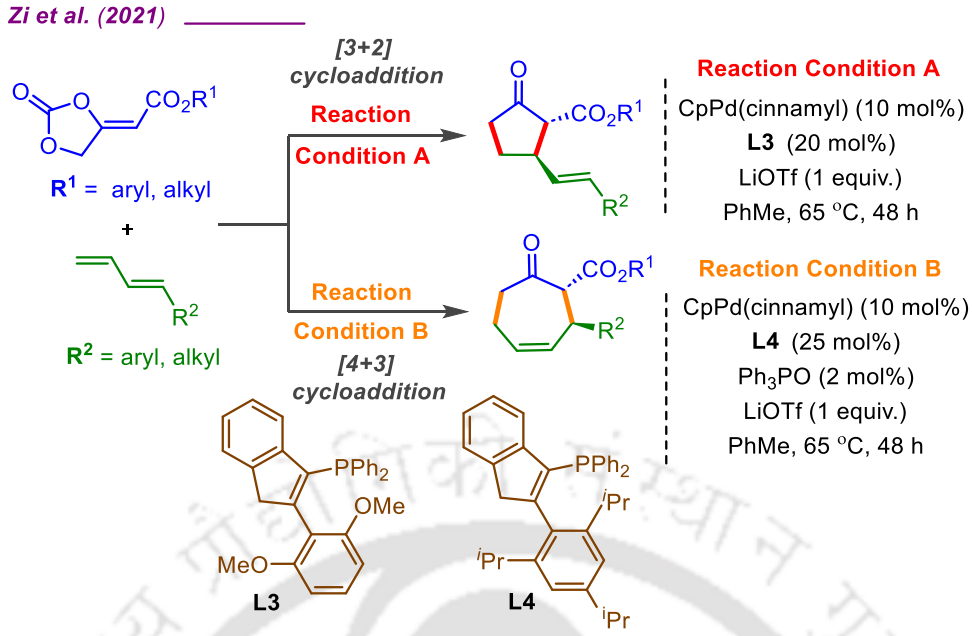

Scheme III.2.18. *Ligand-controlled regiodivergent [3+2] and [4+3] cycloaddition reactions*

➢ **Temperature-Controlled:**

In 2019, Rao *et al.* demonstrated Ga-catalyzed elegant synthetic approach for trifluoromethylated unsymmetrical 3,3′-and 3,6′-bis(indolyl)methanes *via* temperature-controlled regiodivergent Friedel-Crafts C–H alkylation of 2-substituted indoles with trifluoro-methylated 3-indolylmethanols (Scheme III.2.19).[7a] This protocol could be extended towards the synthesis of difluoromethylated3,3′- and 3,6′-bis(indolyl)methanes.

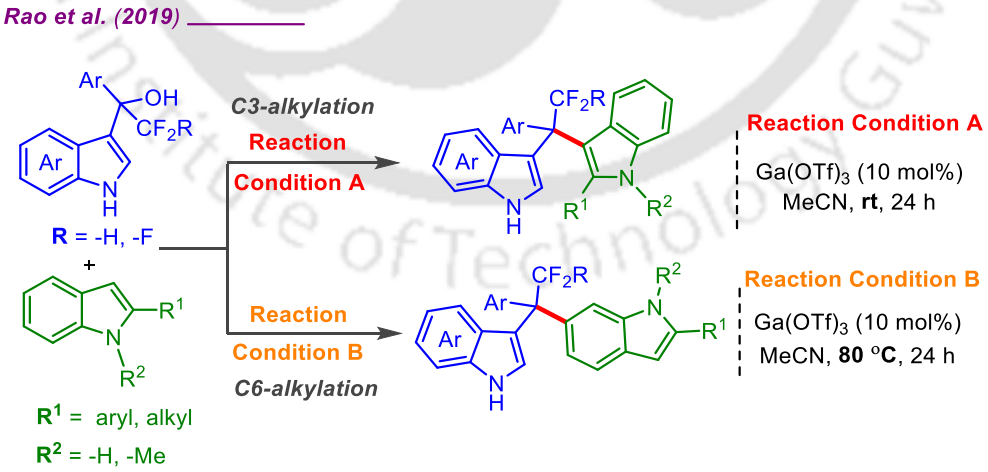

Scheme III.2.19. *Ga(OTf)$_3$-catalyzed regiodivergent synthesis of trifluoromethylated unsymmetrical 3,3′-and 3,6′-bis(indolyl)methanes*

TH-3369_166122017

In the same year, Li and co-workers disclosed an interesting temperature-controlled hydroaminated cascade-cyclization of homopropargylic amines with the electron-deficient 2-butynedioates (Scheme III.2.20).[7b] This reports revealed that at 120 °C reaction temperature the cascade reaction selectively delivered pyrrolo-*b*-cyclobutenes *via* the formation of active dihydropyrroles intermediates and followed by a [2+2]-cycloaddition with 2-butynedioates. Whereas at 150 °C reaction temperature, dihydro-1*H*-azepines were isolated through the direct coupling of homopropargylic amines and alkynes.

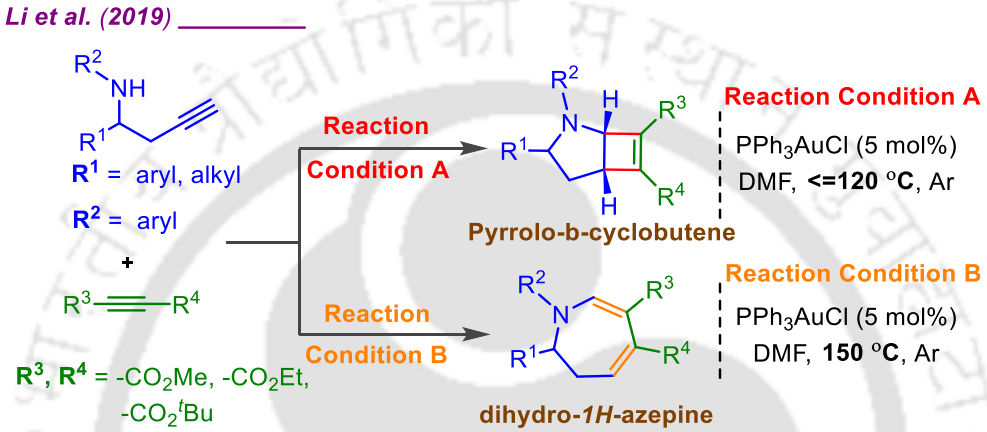

Scheme III.2.20. *Temperature-controlled hydroaminated cascade-cyclization*

The past decades have witnessed notable contributions using precious 4d and 5d-metals. However, the high cost, toxicity, and low abundance are some of the major impediments to their usage.[8] Successfully many of these are replaced with more Earth-abundant, cost-effective, sustainable, and environmentally benign 3d-metal catalysts such as Mn, Fe, Co, Ni, and Cu.[9] Further, among these, Mn the third most abundant metal in Earth's crust, has gained greater acceptability due to its low cost, lesser toxicity, and biocompatibility in the realm of homogeneous catalysis.[10] Despite the significant advances in C–H bond activation, the utilization of Mn as a catalyst for controlled regio and site-selective manner is highly desired.[11]

Among various *N*-containing heterocyclic scaffolds, imidazo[1,2-*a*]pyridine is unique due to its presence in a plethora of natural products and pharmaceutical feedstocks (Figure III.2.1).[12] Many commercial drugs are embedded with this privileged core,[13] and they have valuable existence in the field of material sciences (Figure III.2.2).[14]

TH-3369_166122017

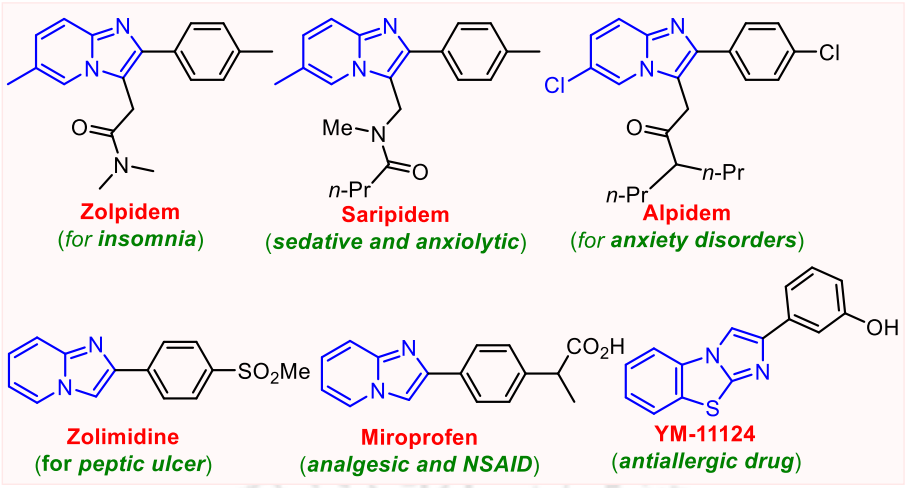

Figure III.2.1. *Pharmaceutical importance of imidazopyridine-based compounds*

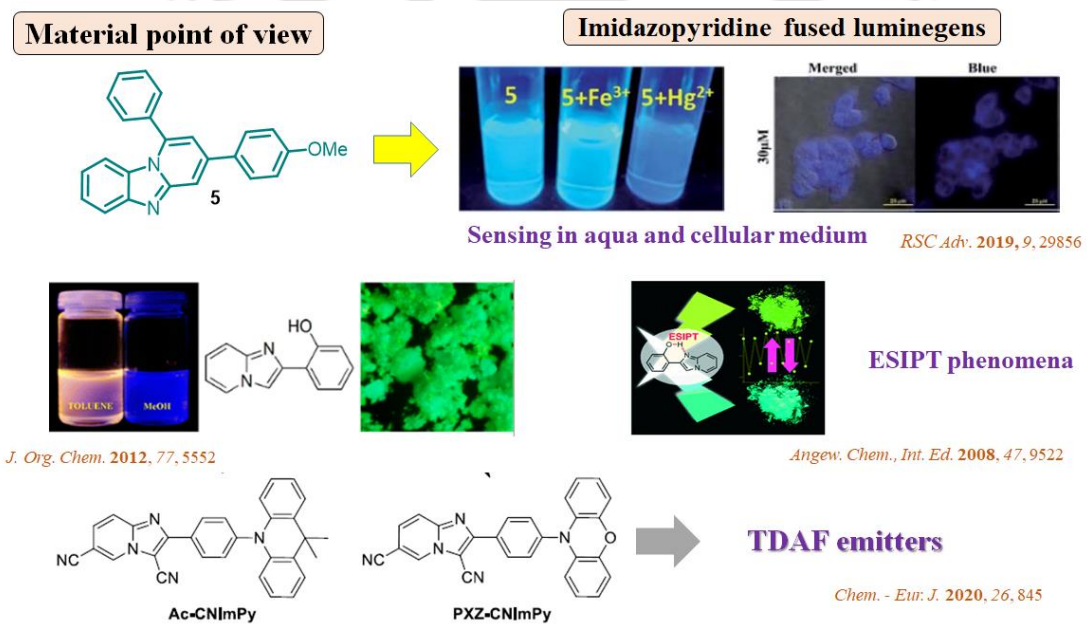

Figure III.2.2. *Application of imidazopyridine-based scaffolds in material sciences*

III.3. Prior Strategies of Metal-Catalyzed C–H Functionalization of Imidazopyridne

Various research groups have devoted themselves towards C–H bond functionalization on imidazopyridine,[15] most of which revolve around the active nucleophilic C-3 site.[16] Selective *o*-functionalization without protecting the active C-3 site is quite challenging,[17] and as such there is no

TH-3369_166122017

report on site-selective alkylation at the ortho and C-3 position of imidazo[1,2-*a*]pyridine using a single catalytic system (Scheme III.3.1).

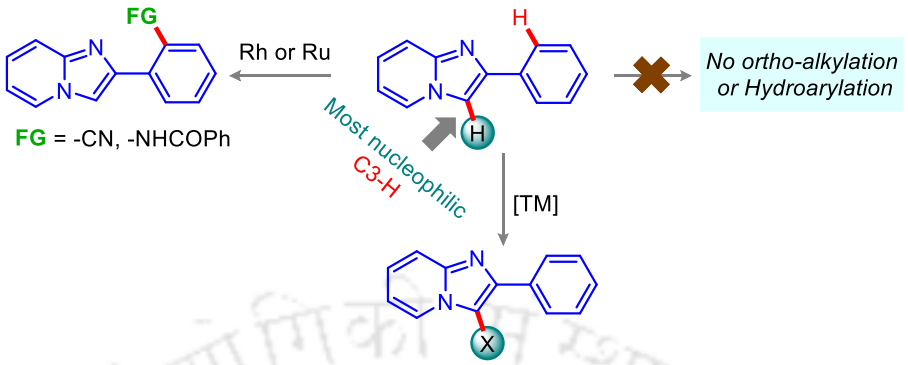

Scheme III.3.1. *C-H functionalization reactions of imidazopyridine*

➢ **C3–H Functionalization:**

In the year of 2018, Zhao group reported a Pd-catalyzed oxidative C–H/C–H cross-couplings of 2-arylimidazopyridnes with azole in using air as sole oxidant (Scheme III.3.2).[16c] This reaction presented a simple-straightforward strategy to develop a library of 3-azolyl-imidazopyridines with good to moderate yields and good functional group tolerance. Furthermore, biological study of the synthesized compounds revealed the anti-proliferative activity against the human lung cancer cell lines.

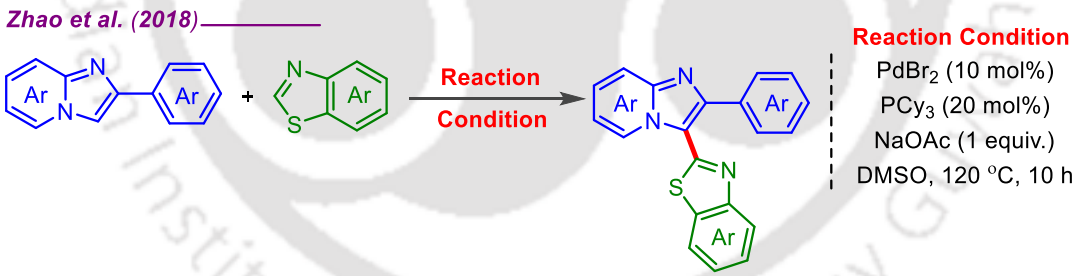

Scheme III.3.2. *Pd-catalyzed oxidative C–H/C–H cross-coupling*

In the same year, a copper-mediated regioselective C3-amidation of 2-aryl imidazopyridines with NFSI has been demonstrated by Song group under mild and additive free conditions with shorter reaction time (Scheme III.3.3).[16d] The control experiments suggested a radical mechanism for this transformation.

TH-3369_166122017

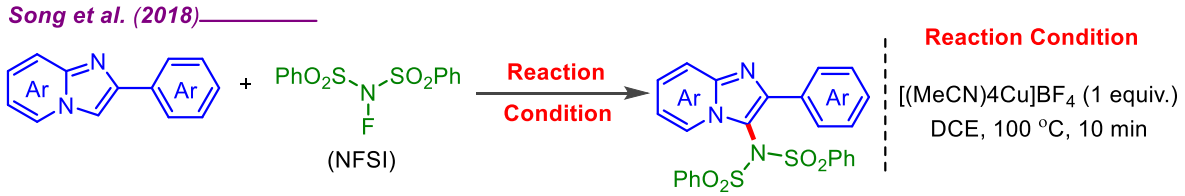

Scheme III.3.3. *Cu-mediated C3-H amination of imidazopyridine*

A palladium-catalyzed C3-selective carbonylation of imidazopyridines with CO and alcohol a series of imidazopyridne-tethered carboxylate esters have been synthesized with good yields and excellent functional group tolerance (Scheme III.3.4).[16e] This reaction portrayed the successful utilization of leaf alcohol, phytol, nerol and tetrahydrogeraniol for the synthesis of C3-carboxylate esters.

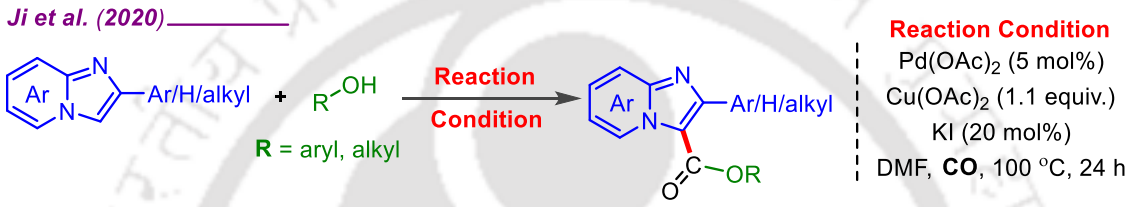

Scheme III.3.4. *Pd-catalyzed oxidative C3-carbonylation of imidazopyridine*

Lee *et al*. introduced a C3-selctive alkoxycarbonylmethylation of 2-arylimidazopyridnes with diazo esters under additive-free Rh-catalysis (Scheme III.3.5).[16f] This protocol can lead to the access of benzoimidazoquinolizinone and cycloheptaimidazopyridinone heterocyclic scaffolds.

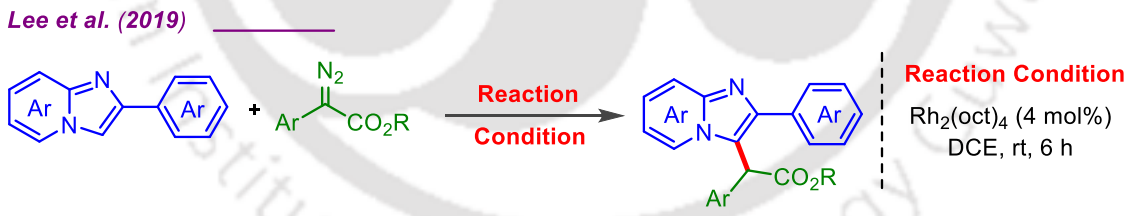

Scheme III.3.5. *Rh-catalyzed C3-alkoxycarbonylmethylation of imidazopyridine*

Recently, kaliyamoorthy and co-workers introduce a site-selective Pd-catalyzed C3-allylic alkylation of 2-arylimidazopyridnes with MBH carbonates (Scheme III.3.6).[16g] This protocol offered access of a broad spectrum of C3-allylic alkylated imidazopyridine scaffolds with good yields and very good functional group tolerance.

TH-3369_166122017

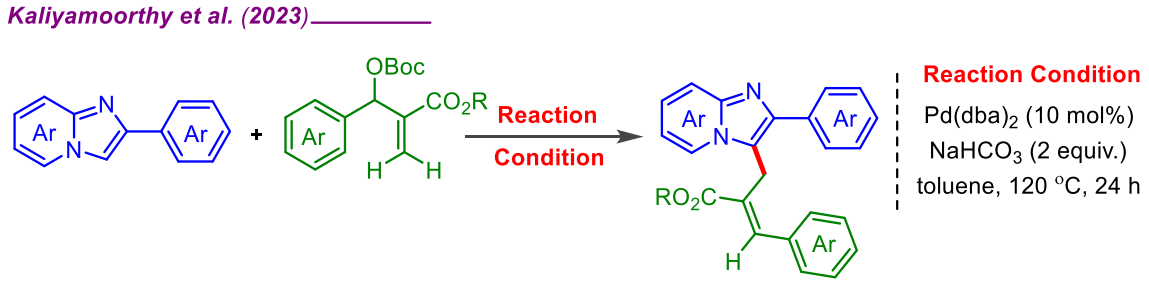

Scheme III.3.6. *Pd-catalyzed C3-allylic alkylation of imidazopyridine*

➢ **Ortho C–H Functionalization:**

A Rh-catalyzed *ortho* bis-cyanation of 2-arylimidazopyridine using cyanating agent *N*-cyano-*N*-phenyl *p*-methylbenzenesulfonamide (NCTS) has been established by Hao group (Scheme III.3.7).[17a] This reaction proceeds through regioselctive *N*-directed *ortho* double C–H activation.

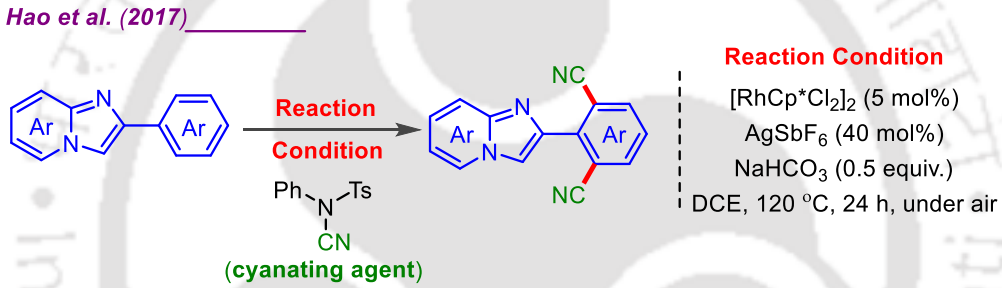

Scheme III.3.7. *Rhodium-catalyzed ortho bis-cyanation of imidazopyridine*

In 2019, Hajra *et al.* reported a Rh-catalyzed *ortho* C–H amidation of 2-arylimidazopyridnes using dioxazolone as the amidating agent (Scheme III.3.8).[17c] This reaction presented a straightforward development strategy of a library of *ortho*-amidated imidazopyridines with good yields and broad scope.

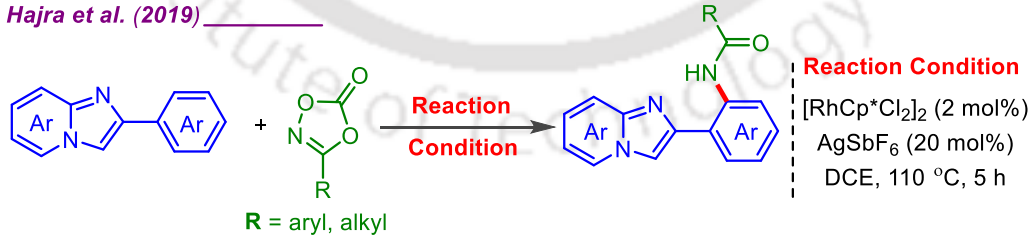

Scheme III.3.8. *Rhodium-catalyzed ortho-amidation of imidazopyridine*

An oxidative Ru(II)-catalyzed *ortho*-alkenylation of 2-arylimidazopyridne-3-carboxylate with acrylate ester has been demonstrated by Bharatam and co-workers (Scheme III.3.9).[17e] This alkenylation reaction can be extended for the functionalization of 2-arylbenzoxazole and 2-arylbenzothiazole derivatives.

TH-3369_166122017

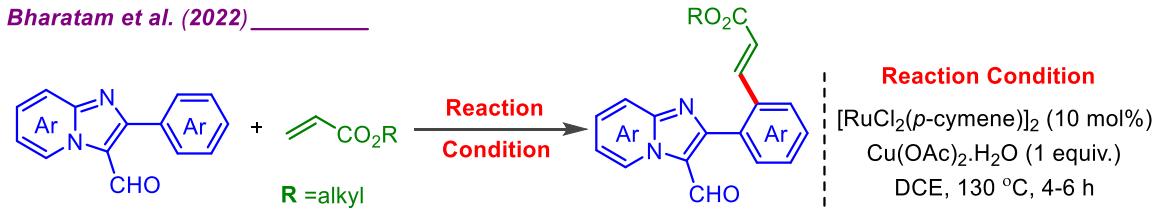

Scheme III.3.9. *Ruthenium-catalyzed ortho-alkenylation of imidazopyridine*

➢ **Cyclization involving C3–H/Ortho–H:**

Over the last few years many groups have reported a series of cyclization reactions of imidazopyridines with several electrophiles *viz.* (a) diphenyl acetylene,[18a,18b] (b) diazo compound,[18c] (c) α,β-unsaturated system,[18d] (d) diarylidonium salts,[18e] and (e) vinylene carbonates[18f] (Scheme III.3.10). All, these reactions proceed through the dual activation of C3–H and *ortho* C–H to provide the annulated carbocyclic scaffolds.

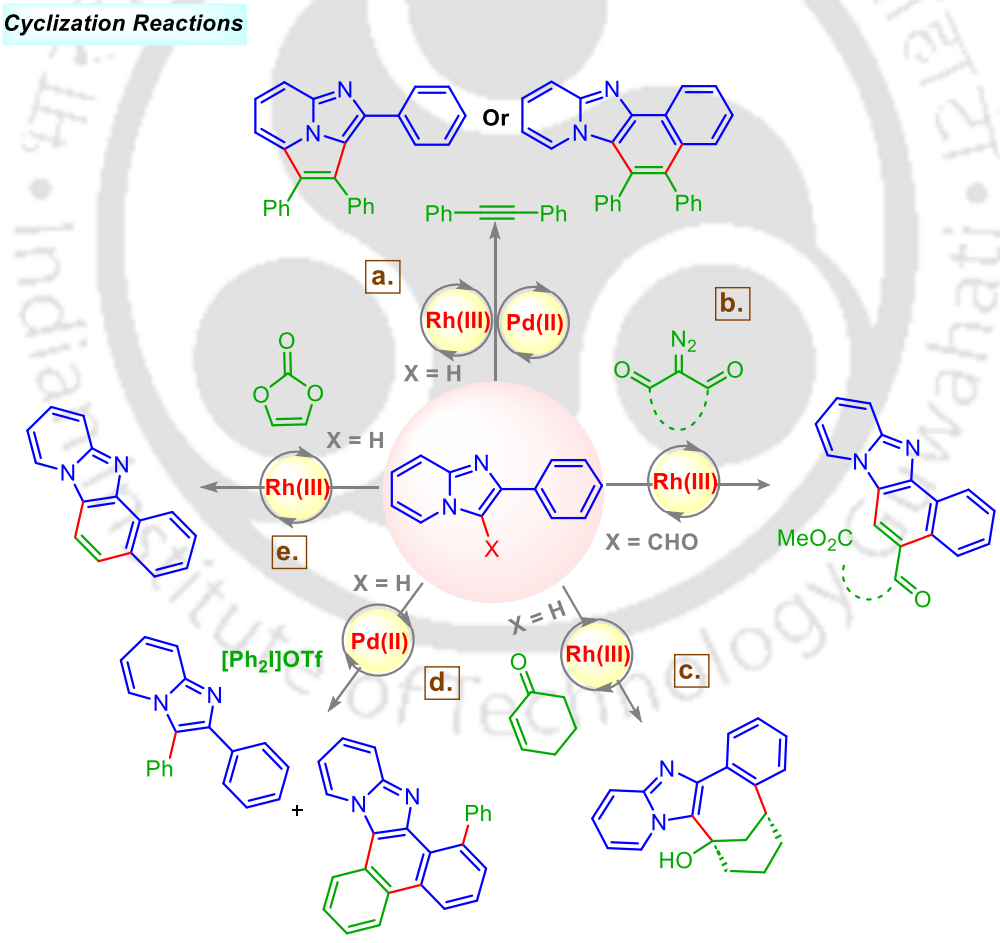

Scheme III.3.10. *Transition-metal catalyzed cyclization reactions of imidazopyridines*

TH-3369_166122017

Maleimide plays a pivotal role in pharmaceuticals and material sciences is a well-investigated coupling partner.[19] As a consequence, a growing repertoire of C–H bond activation involving maleimides have been reported lately, including 1,4-conjugate addition, [1,1] spiro-annulation, [3+2], [4+2] cyclization and Heck-type reactions with various substituted hetero-aromatics.[20] The reported metal-catalyzed alkylation of maleimides in various other scaffolds, uses 4d and 5d transition metals in the presence of other metal co-oxidants including expensive Ag salt.[21] Thus a sustainable regioselective (*ortho* C–H *vs* C3–H) alkylation in 2-arylimidazopyridine using 3d-metal without silver and oxidant is highly appreciable. Manganese catalyzed C–H functionalization of acrylates with heteroarenes is well documented by Wang *et al.*,[22] but the functionalization of maleimides is confined to a single report of $Mn_2(CO)_{10}$ catalyzed *N*-directed alkylation of 1-(pyridin-2-yl)-1*H*-indole. Where the appended pyridine moiety plays the crucial directing role in assisting the chelation (Scheme III.3.11).[23]

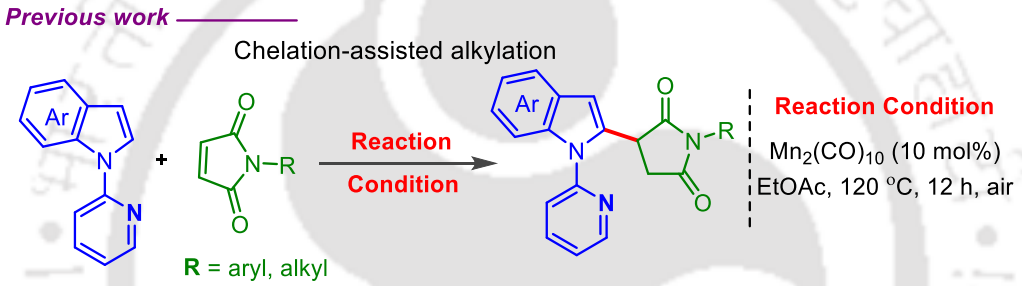

Scheme III.3.11. *Mn(0)-catalyzed chelation-aided C–H malemidation*

III.4. Present Strategy

Herein, we unveiled a solvent-switched selective *ortho* and C–3 alkylation of 2-arylimidazopyidines under Mn(I) catalysis to access 1-phenyl-3-(2-phenylimidazo[1,2-*a*]pyridin-3-yl)pyrrolidine-2,5-dione (**3aa**) and 3-(2-(imidazo[1,2-*a*]pyridin-2-yl)phenyl)-1-phenylpyrrolidine-2,5-dione (**4aa**).

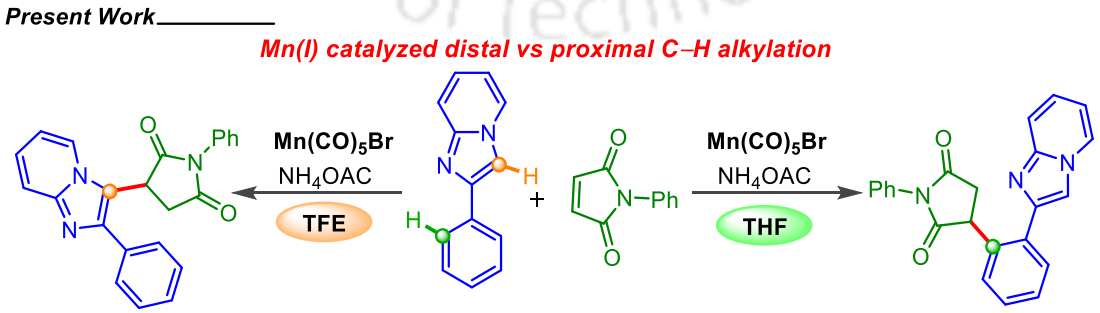

Scheme II.4.1. *Mn(I)-catalyzed regiodivergent C–H alkylation of imidazopyridine*

TH-3369_166122017

The optimization study was initiated using 2-phenylimidazo[1,2-*a*]pyridine (**1a**) (0.3 mmol) and *N*-phenyl maleimide (**2a**) (0.45 mmol). Initially, (**1a**) was reacted with (**2a**) in the presence of 15 mol% of $Mn(CO)_5Br$ and a stoichiometric amount of NaOAc as an additive in 2,2,2-trifluoroethanol (TFE) at 100 °C for 18 h. The reaction ended up giving a mixture of C3-alkylated (**3aa**) and *o*-alkylated (**4aa**) products in 41% and 20% isolated yields (Table III.4.1, entry1). Now When the loading of the additive (NaOAc) was reduced to 30 mol%, the yield of (**3aa**) enhanced to 49% and (**4aa**) reduced to 15% (Table III.4.1, entry 2). Further lowering of the NaOAc loading to 15 mol% was not found beneficial as yields of both the products (**3aa**, 37%) and (**4aa**, 12%) decreased (Table III.4.1, entry 3). We examined the efficacy of various other additives such as NaOPiv, NaOTf, K^{t}OBu, Na_2CO_3, Cs_2CO_3, NH_4OAc, $(Bu)_4NOAc$, AgOAc and CsOAc under the identical reaction conditions (Table III.4.1, entries 4–12). Only NH_4OAc (30 mol%) was found to be superior to other additives providing the product (**3aa**) exclusively in 68% isolated yield (Table III.4.1, entry 9). The absence of NH_4OAc was found to be completely ineffective in giving any of the products (Table III.4.1, entry 13). Similarly, the reaction without the catalyst $Mn(CO)_5Br$ gave no traces of C3-hydroarylation (Table III.4.1, entry 14). Then a series of polar-protic, aprotic, and nonpolar solvents were screened to examine the effect of solvents on this reaction (Table III.4.1, entries 15–27). The use of polar-protic solvents such as EtOH and 1,1,1,3,3,3-hexafluoro-2-propanol (HFIP) gave exclusively C3-hydroarylated product (**3aa**) but in inferior yields of 34% and 21% respectively giving no trace of (**4aa**) (Table III.4.1, entries 17 and 19). Interestingly, by switching the polar-protic solvent TFE to 1,2-DCE, the selectivity was altered giving ortho-hydroarylated adduct (**4aa**, 31%) as the major product along with a trace of (**3aa**) (Table III.4.1, entry 20). Similarly, other nonpolar-aprotic ethereal solvents such as tetrahydrofuran (THF), 1,2-dimethoxyethane (DME), methyl tert-butyl ether (MTBE), tetrahydropyran (THP), 1,4-dioxane were screened (Table III.4.1, entries 21–25). It was found that THF furnished exclusive ortho-hydroarylated product (**4aa**, 73%) while 1,2-DME gave only 42% of the same product giving only a trace of (**3aa**). The other ethereal solvents were not found suitable in terms of selectivity or improving the yield. Further, other non-polar solvents α,α,α-trifluorotoluene ($PhCF_3$), and toluene were found to be inefficient (Table III.4.1, entries 26 and 27). Here, the additive NH_4OAc and catalyst $Mn(CO)_5Br$ both are essential for the ortho-hydroarylation (Table III.4.1, entries 28 and 29). The use of bis-manganese salt $Mn_2(CO)_{10}$ also showed similar selectivity in THF and TFE solvents but was found to be inferior to $Mn(CO)_5Br$ in terms of conversion (Table III.4.1, entries 30 and 31). After screening of several reaction parameters the optimal condition for the C3-maleimidation was the use of (**1a**, 0.3 mmol), (**2a**, 0.45 mmol), $Mn(CO)_5Br$ (15 mol%) and NH_4OAc (30 mol%) in TFE (1.5 mL) at 100 °C for 18 h (Table III.4.1, entry 9, SI). Similarly, for the *o*-maleimidation the best condition was: (**1a**, 0.3 mmol), (**2a**, 0.45

TH-3369_166122017

mmol), $Mn(CO)_5Br$ (15 mol%) and NH_4OAc (30 mol%) in THF (1.5 mL) at 100 °C for 18 h (Table III.4.1, entry 21, SI).

Table III.4.1. *Optimization of Reaction Conditions.*[a,b]

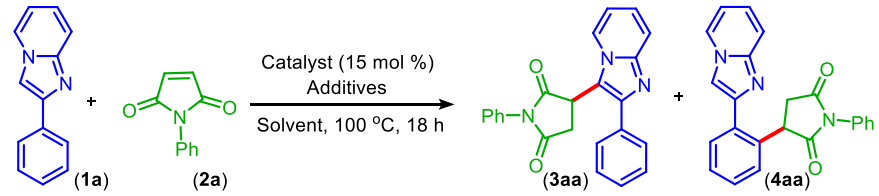

Entry	Catalyst (15 mol%)	Additive	Solvent	Yield%[b] (3aa/4aa)
1.	$Mn(CO)_5Br$	NaOAc (1.0 equiv.)	TFE	41 / 20
2.	$Mn(CO)_5Br$	NaOAc (30 mol%)	TFE	49 / 15
3.	$Mn(CO)_5Br$	NaOAc (15 mol%)	TFE	37 / 12
4.	$Mn(CO)_5Br$	NaOPiv (30 mol%)	TFE	28/ n.d
5.	$Mn(CO)_5Br$	NaOTf (30 mol%)	TFE	n.d / n.d
6.	$Mn(CO)_5Br$	KO^tBu (30 mol%)	TFE	n.d / n.d
7.	$Mn(CO)_5Br$	Na_2CO_3 (30 mol%)	TFE	n.d. / n.d
8.	$Mn(CO)_5Br$	Cs_2CO_3 (30 mol%)	TFE	n.d. / n.d
9.	**$Mn(CO)_5Br$**	**NH_4OAc (30 mol%)**	**TFE**	**68 / n.d.**
10.	$Mn(CO)_5Br$	$(Bu)_4NOAc$ (30 mol%)	TFE	n.d./ n.d
11.	$Mn(CO)_5Br$	AgOAc (30 mol%)	TFE	n.d./ n.d
12.	$Mn(CO)_5Br$	CsOAc (30 mol%)	TFE	n.d./ n.d
13.	$Mn(CO)_5Br$	---	TFE	12 / n.d
14.	---	NH_4OAc (30 mol%)	TFE	n.d / n.d
15.	$Mn(CO)_5Br$	NH_4OAc (30 mol%)	MeCN	n.d./ n.d
16.	$Mn(CO)_5Br$	NH_4OAc (30 mol%)	DMF	n.d./ n.d
17.	$Mn(CO)_5Br$	NH_4OAc (30 mol%)	EtOH	34 / n.d.
18.	$Mn(CO)_5Br$	NH_4OAc (30 mol%)	MeOH	n.d./ n.d
19.	$Mn(CO)_5Br$	NH_4OAc (30 mol%)	HFIP	21 / n.d.
20.	$Mn(CO)_5Br$	NH_4OAc (30 mol%)	1,2-DCE	traces / 31
21.	**$Mn(CO)_5Br$**	**NH_4OAc (30 mol%)**	**THF**	**13 / 73**
22.	$Mn(CO)_5Br$	NH_4OAc (30 mol%)	1,2-DME	traces / 42
23	$Mn(CO)_5Br$	NH_4OAc (30 mol%)	MTBE	n.d./ traces
24	$Mn(CO)_5Br$	NH_4OAc (30 mol%)	THP	traces / 15
25.	$Mn(CO)_5Br$	NH_4OAc (30 mol%)	1,4-dioxane	n.d./ n.d
26.	$Mn(CO)_5Br$	NH_4OAc (30 mol%)	$PhCF_3$	n.d./ 15
27.	$Mn(CO)_5Br$	NH_4OAc (30 mol%)	Toluene	n.d./ n.d
28.	$Mn(CO)_5Br$	---	THF	n.d. / 18
29.	---	NH_4OAc (30 mol%)	THF	n.d./ n.d
30.	$Mn_2(CO)_{10}$	NH_4OAc (30 mol%)	THF	12 / 66
31.	$Mn_2(CO)_{10}$	NH_4OAc (30 mol%)	TFE	35 / n.d.

[a]Reaction Conditions unless specified otherwise: **1a** (0.3 mmol), **2a** (0.45 mmol), $Mn(CO)_5Br$ (15 mol%), additives, solvent (1.5 mL) under an open air at 100 °C for 18 h. [b]Isolated yield. n.d. = not detected.

TH-3369_166122017

Scope of Distal and Proximal C-H Maleimidation:

By executing the optimized condition for the selective distal C3-alkylation, the versatility and scope of various 2-arylimidazopyridines and *N*-substituted maleimides were examined and the results are summarized in Scheme III.4.2. An array of electronically varied substituents *p*–OMe (**1b**), *p*–F (**1c**), *p*–Cl (**1d**), *p*-phenyl (**1e**), *m*–Me (**1f**), *m*–Cl (**1g**), *o*–OMe (**1h**), *o*–F (**1i**) on the phenyl ring and C7-Me on the pyridine ring (**1j**) of 2-arylimidazopyridines, all reacted well with *N*-phenyl maleimide (**2a**) to furnish **3ba**–**3ja** in good to moderate yields (55–73%). Notably, an imidazopyridine containing 3′,4′-methylenedioxyl (**1k**) group also responded to this protocol giving the adduct (**3ka**) in decent yield of 63%. A 2-thiophene containing imidazopyridines (**1l**), delivered its corresponding C-3 maleimidated product (**3la**, 54%) without affecting the thiophene ring. Further, similar *N*-containing cores such as imidazothiazo (**1m**) and benzothiazo (**1n**) moieties also provided their corresponding distal C-3 maleimidated products (**3ma**, 68%) and (**3na**, 56%) in acceptable yields. Interestingly, the well-known peptic ulcer drug Zolimidine having a *p*-SO_2Me (**1o**) group successfully underwent C-3 alkylation, giving the product (**3oa)** in 55% yield.

As shown in Scheme III.4.3, several *N*-alkylated maleimides such as benzyl (**2b**), methyl (**2c**), ethyl (**2d**), propyl (**2e**), isobutyl (**2f**) and cyclohexyl (**2g**) underwent C-3 maleimidation to furnish **3ab**–**3ag** in yields ranging from 65–75%. Further, the structure of **3ac** was confirmed by single-crystal X-ray analysis. The *N*-phenyl maleimides having *p*–Me (**2h**) and *p*–F (**2i**) substitutions reacted smoothly with (**1a**) to give (**3ah**) and (**3ai**) in decent yields (Scheme III.4.3). Also, phenethyl (**2j**) and cyclohexylmethyl (**2k**) functionalized maleimides reacted efficiently to give C-3 alkylated products (**3aj**, 64%) and (**3ak**, 70%) respectively. Interestingly, long alkyl chain bearing maleimides (**2l**–**2o**) also responded well to this protocol giving **3al**–**3ao** in good yields 64–69%. A chiral (*R*)-(+)-1-phenylethyl substituted maleimide (**2p**) was easily converted to its diastereomeric (dr 1:1) product (**3ap**, 65%). The free NH bearing maleimide (**2q**) also well responded to provide C3 alkylated adduct **3aq** (61%).

During the optimization, we found a complete change in the regioselective alkylation from a distal (C-3) to a proximal (-ortho) in imidazopyridine by switching the solvent from 2,2,2-trifluroethanol (TFE) to THF (Table III.4.1). To extend the scope and generality of this o-alkylation we examined various 2-arylimidazopyridines and maleimides under the established reaction condition.

TH-3369_166122017

Scheme III.4.2. *Scope of imidazopyridines of distal C3-H maleimidation* [a,b]

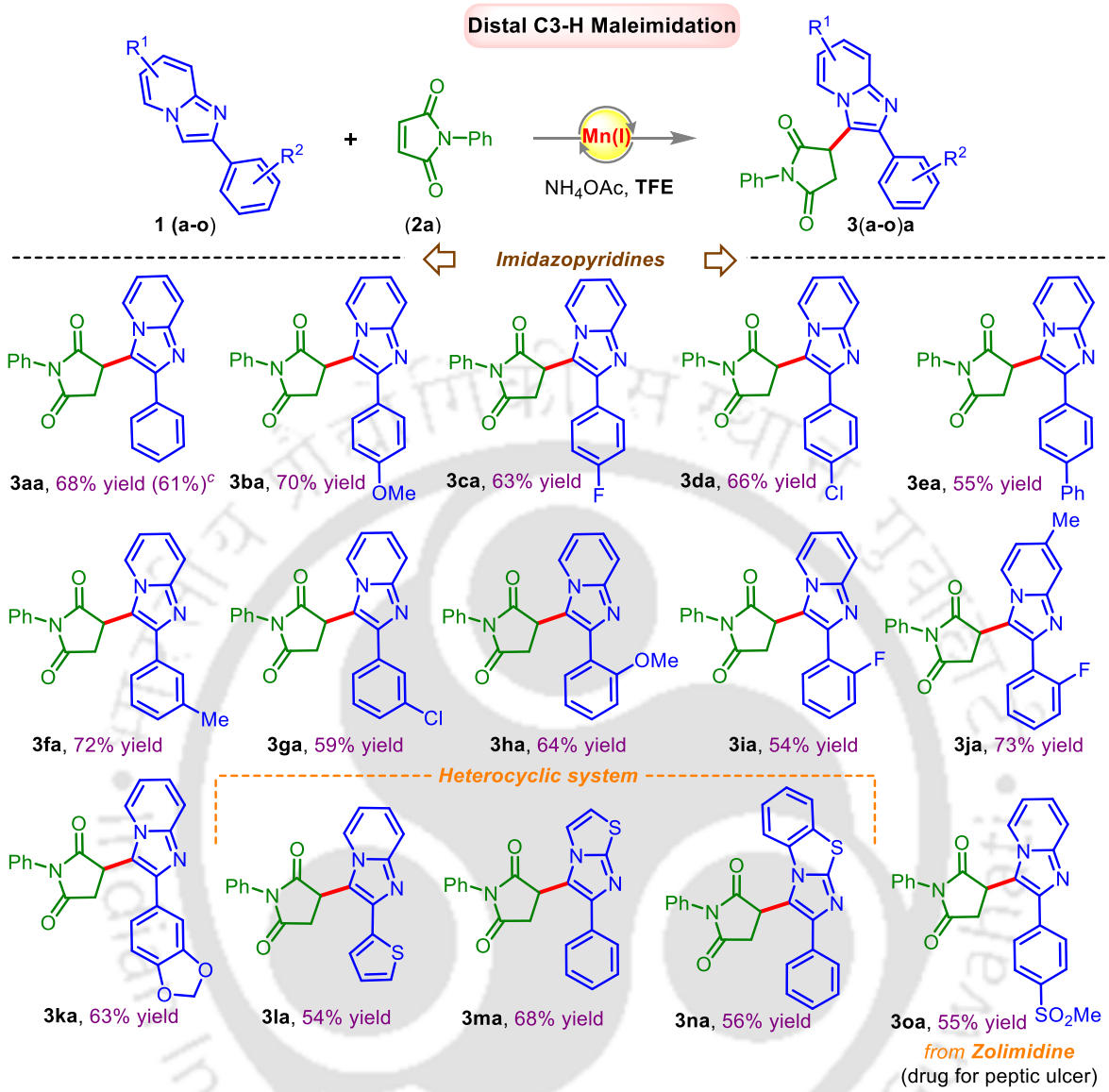

[a,b]Reaction Condition: **1**(**a-o**) (0.3 mmol), **2a** (0.45 mmol), $Mn(CO)_5Br$ (15 mol%), and NH_4OAc (30 mol%) in TFE (1.5 mL) at 100 °C for 18 h under an air atmosphere. [b]Isolated yield after column chromatography. [c]Reaction performed at 1 mmole scale.

As summarized in Scheme III.4.4, numerous electronically varied substituents *p*–Me (**1p**), *p*–OMe (**1b**), *p*–F (**1c**), *p*–CF_3 (**1q**), *p*-phenyl (**1e**), *m*-Me (**1f**), *m*-CF_3 (**1r**), *o*-OMe (**1h**) and *o*-F (**1i**) on the phenyl ring and C7-methyl on the pyridine ring (**1j**) of 2-arylimidazopyridines reacted efficiently with *N*-phenyl maleimide (**2a**) to give *o*-alkylated products **4pa-4ja** in good yields (63–79%). For substrates (**1f**) and (**1r**), out of the two available *o*-sites, the reaction took place at the less sterically hindered position. Besides the attached phenyl moiety, a 2-thiophenyl containing imidazopyridine (**1l**) provided maleimidated adduct (**4la**, 58%) at the C3-position of thiophenyl ring which is directed by the N^1 nitrogen of imidazopyridine. Similarly, other *N*-containing skeletons such as imidazothiazo (**1m**)

TH-3369_166122017

and benzothiazo (**1n)** also provided their *o*-maleimidated products (**4ma**, 71%) and (**4na**, 59%). Similar to C3-alkylation, here also the Zolimidine drug (**1o**) efficiently provided *o*-adduct **4oa** (64%) in THF.

Further, this site-selective alkylation was extended to a wide range of *N*-substituted maleimides (Scheme 3). It was observed that various *N*-alkylated maleimides such as benzyl (**2b**), methyl (**2c**), ethyl (**2d**), propyl (**2e**), isobutyl (**2f**), cyclohexyl (**2g**) reacted smoothly with imidazopyridine (**1a**), to deliver *o*-alkylated products **4ab**–**4ag** in the range of 65–73% yields. Besides this, long alkyl chain bearing maleimides such as *N*-heptyl (**2m**) and *N*-decyl (**2o**) were well compatible giving their desired products (**4am**, 66%) and (**4ao**, 63%) in decent yields. The *N*-phenyl maleimides having *p*–Me (**2h**), *p*–OMe (**2r**), *p*–F (**2i**), *p*–CF_3 (**2s**), *m*–Me (**2t**), and *m*–CF_3 (**2u**) groups were successfully converted to their corresponding *o*-alkylated products **4ah-4au** in decent yields (59-79%). The *ortho*-Me substituted *N*-phenyl maleimides (**2v**) successfully combined with (**1a**) to furnish a racemic product (**4av**) in 68% yield. The racemization is due to the existence of two rotamers of the attached *o*-Me phenyl ring. A *bis*-maleimide (**2w**) as the coupling partner provided a cross-linked *o*-alkylated product (**4aw**, 42%) utilizing two units of (**1a**). Similar to C-3 alkylation here also, the chiral maleimide (**2p**) display good reactivity with (**1a**) giving a diastereomeric mixture (dr 1:1) of product **4ap** in 67% yield. Furthermore, *N*-methyl maleimide (**2c**) successfully coupled with *p*–Me (**1p**) bearing imidazopyridine to provide the corresponding alkylated product (**4pc**) in 71% isolated yield. The structure of this regioisomer was further confirmed by single-crystal X-ray analysis (Scheme 3). Notably, the free NH bearing maleimide (**2q**) afforded the *o*-alkylated product (**4aq**, 63%).

TH-3369_166122017

Scheme III.4.3. *Scope of maleimides of distal C3-H maleimidation* [a,b]

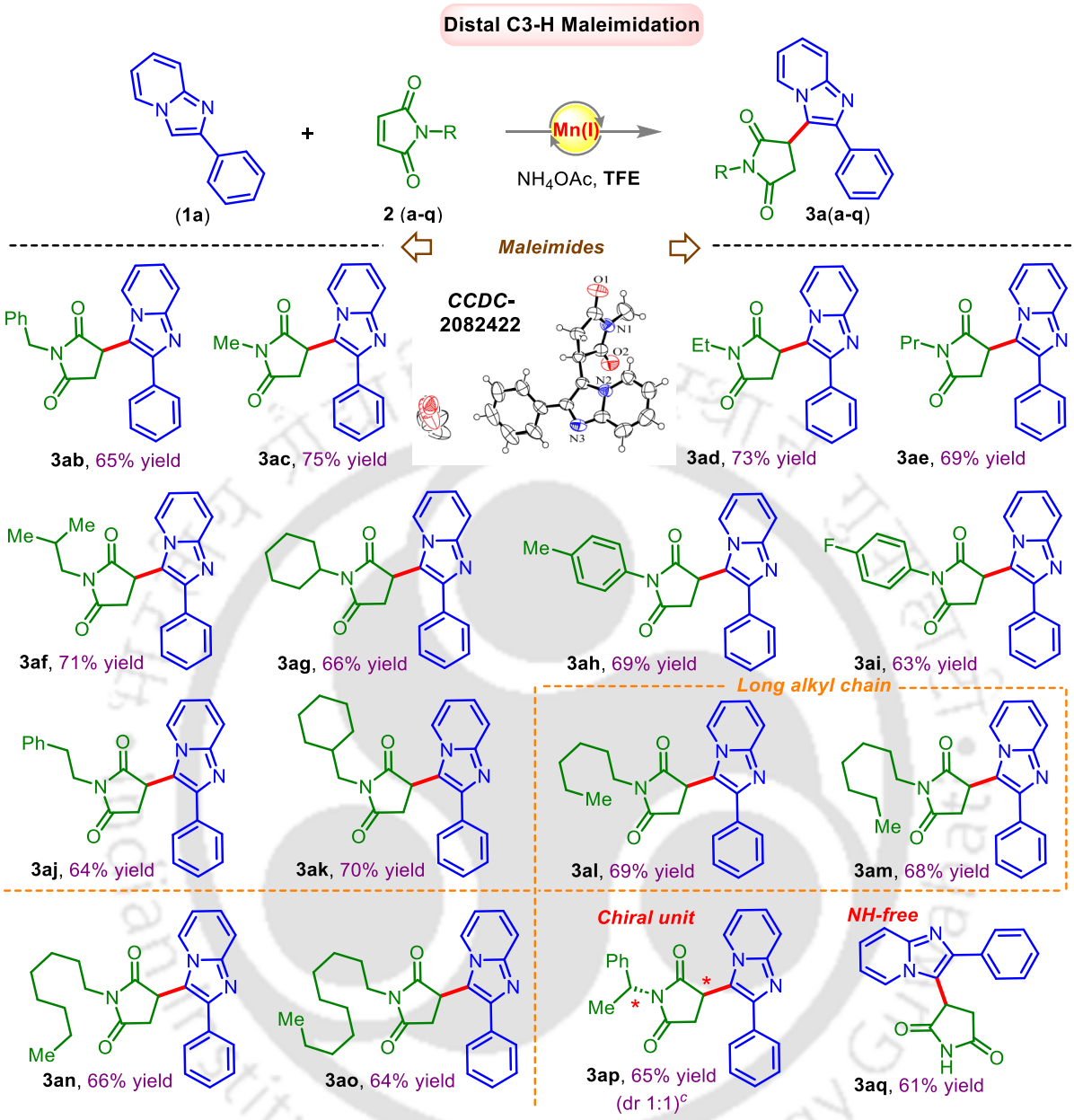

[a,b]Reaction Condition: **1a** (0.3 mmol), **2** (**a-q**) (0.45 mmol), $Mn(CO)_5Br$ (15 mol%), and NH_4OAc (30 mol%) in TFE (1.5 mL) at 100 °C for 18 h under an air atmosphere. [b]Isolated yield after column chromatography. [c]Based on ^1H NMR analysis.

TH-3369_166122017

Scheme III.4.4. *Scope of imidazopyridines of proximal ortho-maleimidation* [a,b]

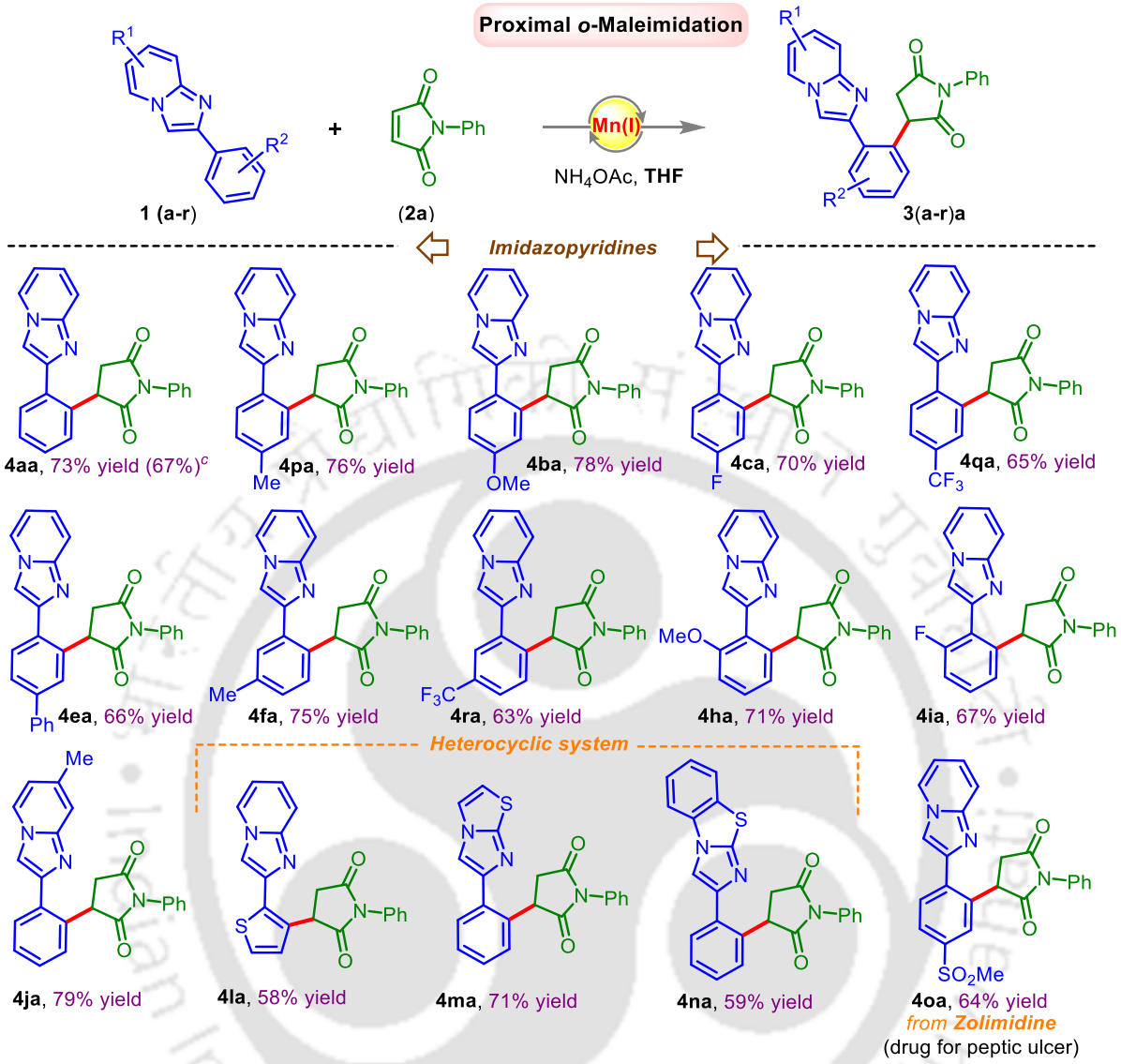

[a,b]Reaction Condition: **1(a-r)** (0.3 mmol), **2a** (0.45 mmol), $Mn(CO)_5Br$ (15 mol%), and NH_4OAc (30 mol%) in THF (1.5 mL) at 100 °C for 18 h under an air atmosphere. [b]Isolated yield after column chromatography. [c]Reaction performed at 1 mmole scale.

TH-3369_166122017

Scheme III.4.5. *Scope of maleimides of proximal ortho-maleimidation* [a,b]

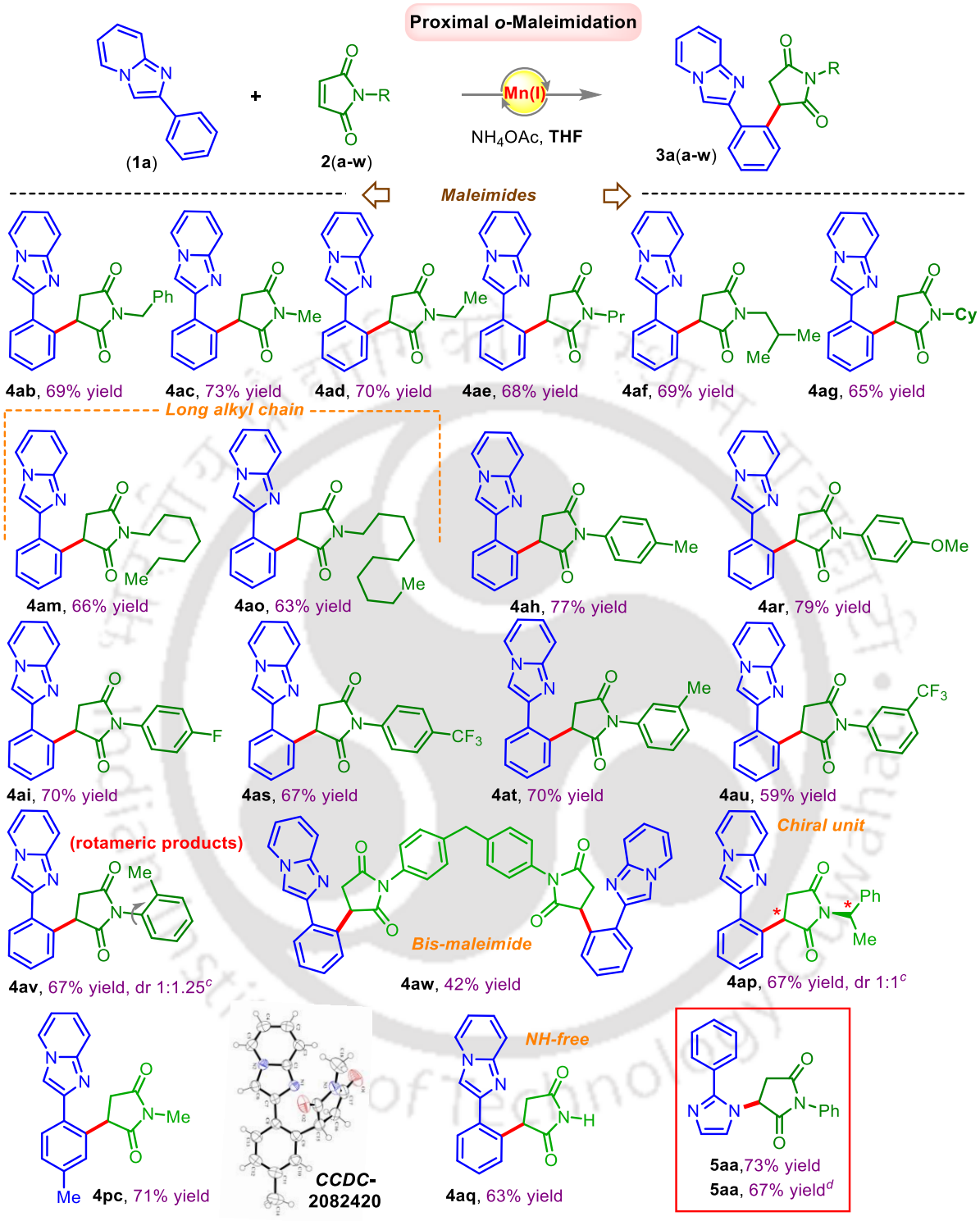

[a,b]Reaction Condition: **1a** (0.3 mmol), **2(a-w)** (0.45 mmol), $Mn(CO)_5Br$ (15 mol%), and NH_4OAc (30 mol%) in THF (1.5 mL) at 100 °C for 18 h under an air atmosphere. [b]Isolated yield after column chromatography. [c]Based on ^1H NMR analysis. [d]TFE was used as solvent.

Unfortunately, besides maleimides other alkenes such as methyl acrylate, styrene, diethyl malonate, maleic anhydride, cumarine, 1,4-napthoquinone and *p*-benzoquinone all failed to provide the

TH-3369_166122017

desired regiodivergent C-H alkylation with imidazopyridine scaffolds. Perhaps, the lone pair of nitrogen in maleimide is polarizing one of the carbonyl groups, thereby making the other end of the alkene more electrophilic. Such a type of polarization is not favorable for other alkenes, thus, they are reluctant to participate in electrophilic metalation. The reaction of 2-phenylimidazole (**5**) with (**2a**) under the standard condition in both the solvents (TFF and THF) provided identical *N*-malemidated product (**5aa**) in 73% and 67% yields respectively (Scheme III.4.5). Subsequently, this protocol was applied for the di-alkylation of *bis*-imidazopyridine scaffolds (Scheme III.4.6). Bis(2-phenylimidazo[1,2-*a*]pyridin-3-yl)methane (**1s**) and bis(2-phenylimidazo[1,2-*a*]pyridin-3-yl)sulfane (**1t**) on reaction with two equivalents of *N*-phenyl maleimide (**2a**) under similar conditions. provide *bis*-adducts (**4sa**) and (**4ta**) in 56% and 51% yields, demonstrating the utility of this protocol even in complex and sterically hindered substrates.

Scheme III.4.6. *Scope of di-alkylation of bis-imidazopyridines* [a,b]

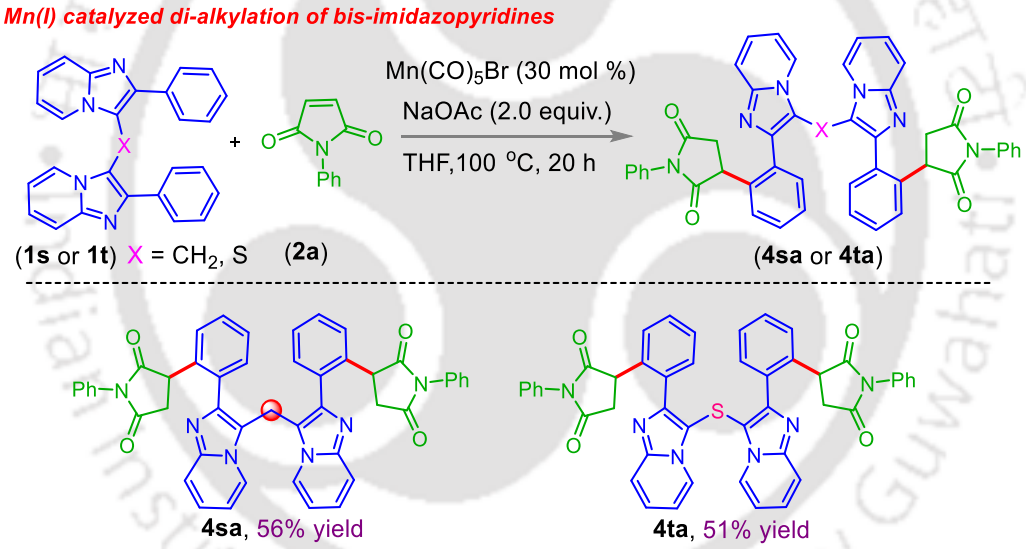

[a,b]Reaction Condition: **1s or 1t** (0.3 mmol), **2a** (0.75 mmol), $Mn(CO)_5Br$ (30 mol%), and NaOAc (60 mol%) in THF (1.5 mL) at 100 °C for 20 h under an air atmosphere. [b]Isolated yield after column chromatography.

Control experiments:

To shed light on the mechanism, a series of control experiments were performed (Scheme III.4.7). Both C3-alkylation and *o*-alkylation reactions were unperturbed in the presence of a radical scavenger BHT, suggesting the non-involvement of radical pathways [Scheme III.4.7(A)]. When 2-phenylimidazopyridine (**1a**) was treated with D_2O (5 equiv.) under the C3-alkylation condition in the absence of (**2a**), it provided exclusive deuterium incorporation (82% D) at the C3 position of (**1a**). On the other hand, under the *o*-alkylation condition in the presence of D_2O (5 equiv.), the C3 position was

TH-3369_166122017

deuterated (31% D) and *ortho* positions (89% D i.e. ~ 45% each). However, using an equiv. of D_2O, deuterium incorporation occurred at C3 (2% D) and both *ortho* positions (64% D i.e. 32% each) [Scheme III.4.7(B)]. These deuterium labelings not only suggest a reversible C–H metalation but also support the solvent-dependent selectivity. To ascertain the rate-determining step, k_H/k_D for C3 alkylation in TFE and *o*-alkylation in THF were estimated and found to be 2.57 and 2.70 respectively. These results suggest the cleavage of their respective C–H bond in the rate-determining step. The extreme solvent reliance of the reaction has been further confirmed with a C-3-protected 2-phenylimidazopyridine, where it is reluctant to undergo *o*-alkylation in TFE despite the availability of four *ortho* C–H sites [Scheme III.4.7(C)].

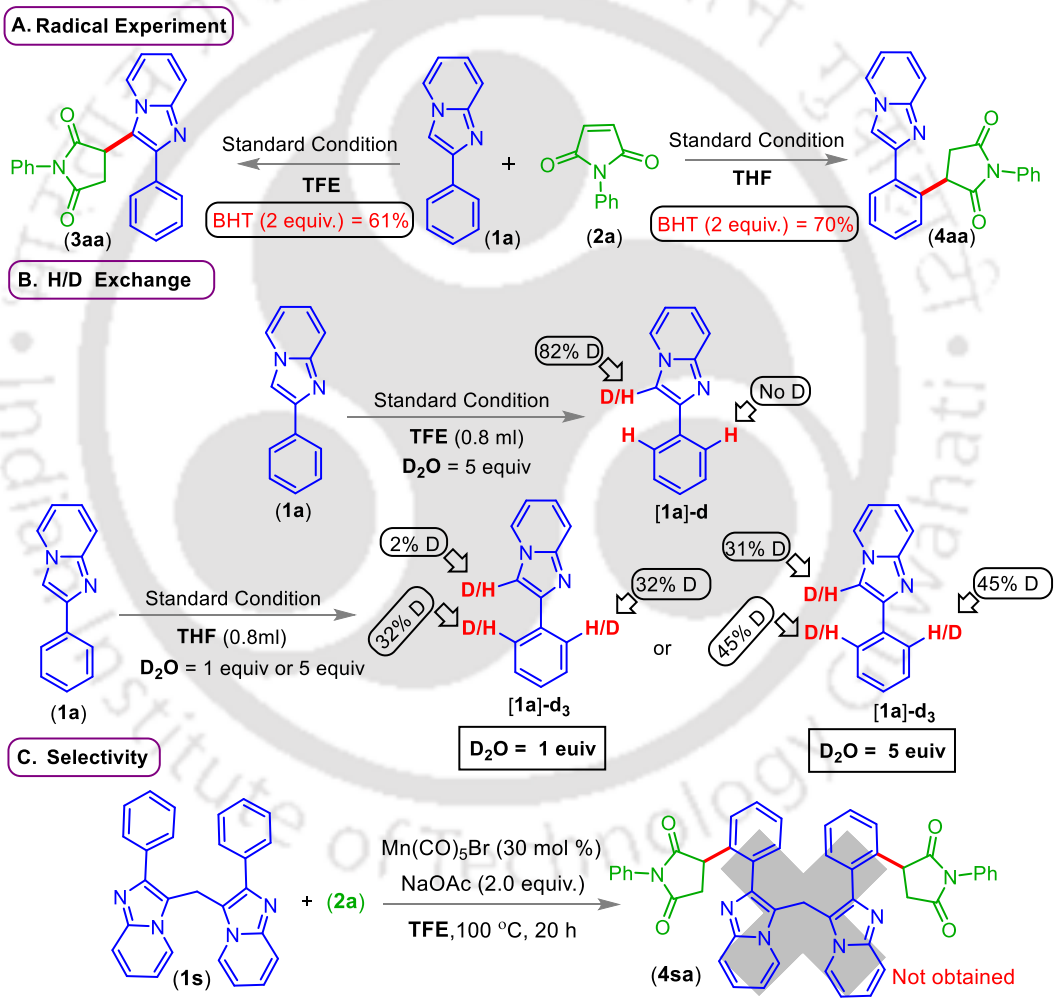

Scheme III.4.7. *Control experiments*

Based on the experimental results obtained from control reactions and previous reports on Mn-catalyzed C–H alkylation[23] and transition-metal catalyzed C-3 functionalization of imidazopyridines,[16] a plausible catalytic cycle for this regiodivergent alkylations in TFE and THF is depicted in (Scheme

TH-3369_166122017

III.4.8). Initially, $Mn(CO)_5Br$ reacts with NH_4OAc, to provide the active $Mn(CO)_5OAc$ species (**I**). In polar protic TFE solvent, the substrate (**1a**) undergo electrophilic metalation with the Mn complex to give a metalated species (**A**), detected in ESI-MS (Figure III.5.11). The C3-alkylation is most favorable in strongly hydrogen bonding acidic solvents such as TFE (pKa 12.46). The additive NH_4OAc (pKa 9.9) help protonating TFE thereby enhancing its hydrogen bonding capability and also serve as a buffering agent for the C3-alkylation. This is then followed by the coordination of *N*-phenyl maleimide (**2a**) and subsequent insertion to Mn-C bond to generate intermediate (**C**). Then a proto-demetalation in the presence of AcOH delivered the C3-alkylated product (**3aa**) along with the regeneration of the active catalyst by recombination of CO. Substrates possessing strongly electron-withdrawing substituents such as *p*-CF_3 (**1q**), *p*-CN (**1u**), 6-CN (**1v**) failed to provide any C3-alkylated products (Scheme III.5.2), which further supports the electrophilic metalation path. On the other hand, in THF, (**1a**) undergoes *N*-directed chelation assisted cyclometalation of Mn at the *ortho* C–H to give a five-membered cyclometalated complex **A'**, detected in ESI-MS (Figure III.5.13). This is then followed by coordination of *N*-phenyl maleimide (**2a**) and subsequent insertion to Mn–C bond. Finally, the proto-demetalation in presence of AcOH and CO leads to *o*-alkylated product (**4aa**) with the regeneration of the active catalyst (Scheme III.4.8).

TH-3369_166122017

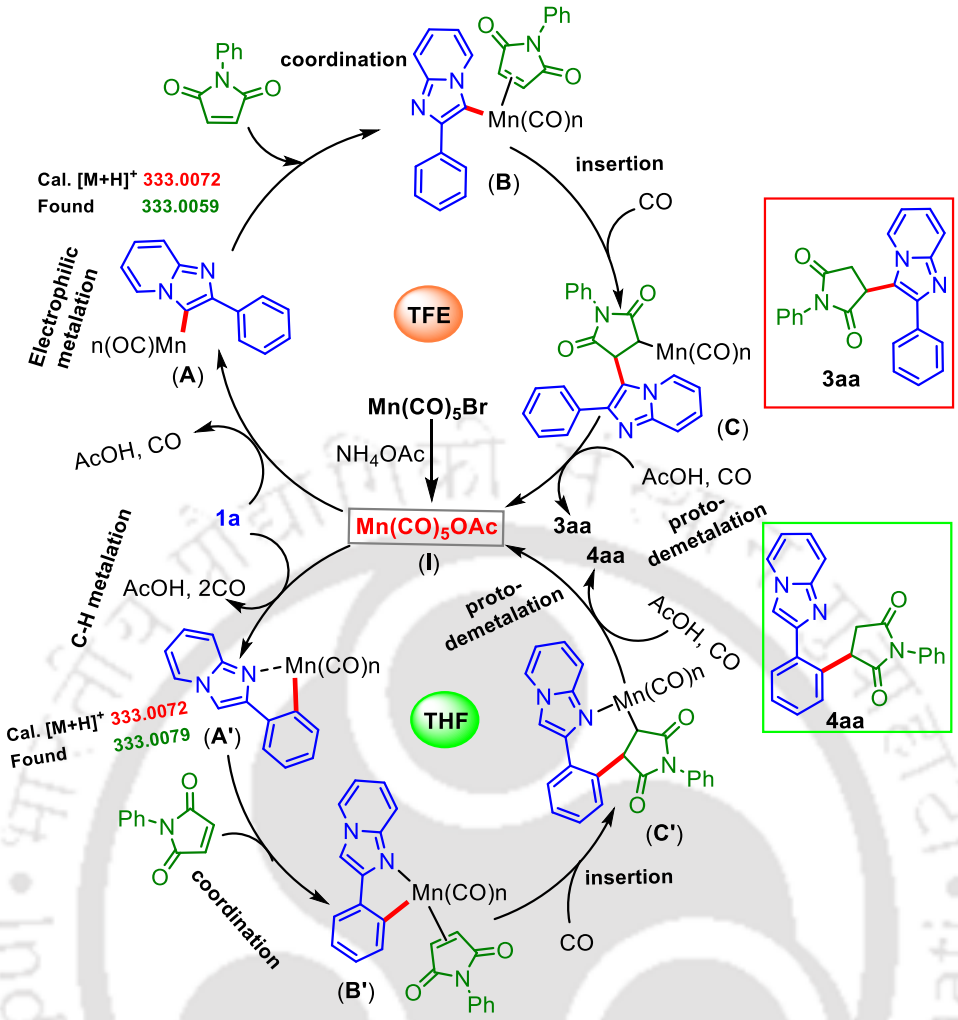

Scheme III.4.8. *Mechanism for regiodivergent alkylation*

In summary, we have developed a sustainable Mn(I) catalyzed solvent switched C3 (in TFE) and *o*-alkylation (in THF) of various imidazopyridines and imidazopyridine fused scaffolds towards a broad range of *N*-substituted maleimides. The protocol was successfully explored for the alkylation of Zolimidine drug. Here, the polar protic solvent TFE preferred electrophilic metalation whereas polar aprotic solvent THF went for *N*-chelation assisted metalation under the same catalytic scenario; thereby preparing the imidazopyridine unit for superior utilities. The protocol offers a metal oxidant and silver salt-free regiodivergent alkylation with good to moderate yields. A solvent-controlled selective deuteration was also observed**.**

III.5. Experimental Section

III.5.1. General Information: All the reagents were commercial grade and purified according to the established procedures. All the reactions were carried out in oven-dried glassware. The highest commercial quality reagents were purchased and were used without further purification unless

TH-3369_166122017

otherwise stated. Reactions were monitored by thin-layer chromatography (TLC) on a 0.25 mm silica gel plates ($60F_{254}$) visualized under UV illumination at 254 nm. Organic extracts were dried over anhydrous sodium sulfate (Na_2SO_4). Solvents were removed using a rotary evaporator under reduced pressure. Column chromatography was performed to purify the crude product on silica gel 60–120 mesh using a mixture of hexane and ethyl acetate as eluent. All the isolated compounds were characterized by ^1H, $^{13}C\{^1H\}$ NMR and IR spectroscopic (HRMS-spectrometric) techniques. NMR spectra for all the samples were recorded in deuterochloroform ($CDCl_3$) or deuterated dimethyl sulfoxide (DMSO-d_6). ^1H, $^{13}C\{^1H\}$ were recorded in 600 (151), 500 (126) or 400 (101) MHz spectrometer and were calibrated using tetramethylsilane or residual undeuterated solvent for ^1H NMR, deuterochloroform for ^{13}C NMR as an internal reference {$Si(CH_3)_4$: 0.00 ppm or $CHCl_3$: 7.26 ppm for ^1H NMR, 77.16 ppm for ^{13}C NMR or $(CH_3)_2SO$: 2.50 ppm for ^1H NMR, 39.52 ppm for ^{13}C NMR}. The chemical shifts are quoted in δ units, parts per million (ppm). ^1H NMR data is represented as follows: Chemical shift, multiplicity (s = singlet, d = doublet, t = triplet, q = quartet, m = multiplet, br = broad, dd = doublet of doublet, integration and coupling constant(s) *J* in hertz (Hz). High-resolution mass spectra (HRMS) were recorded on a mass spectrometer using electrospray ionization-time of flight (ESI-TOF) reflection experiments. FT-IR spectra were recorded as neat and reported in the frequency of absorption (cm^{-1}).

III.5.2. Experimental Procedure

(a) Procedure for the synthesis of starting materials

All 2-aryl imidazopyridines (**1a-1r**) were synthesized following the reported procedure.[16f] The *N*-alkylated maleimides (**2a-2w)** were also prepared according to the literature reported procedure.[24] The bis-imidazopyridines **1s**[25] and **1t**[26] were synthesized according to the reported procedures.

(b) General procedure for the synthesis of C3-alkylation 3(a-o)(a-q)

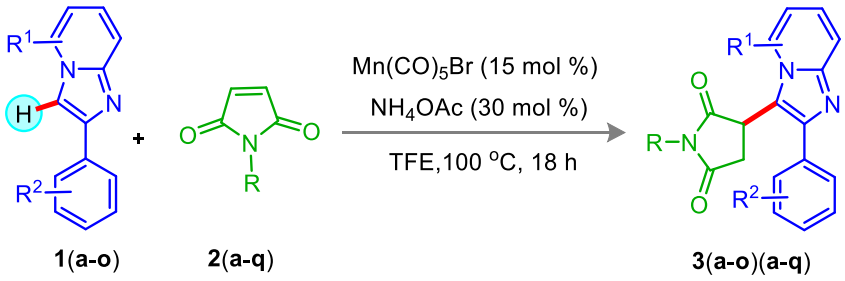

An oven-dried 25 mL round-bottom flask was charged with 2-arylimidazopyridine (**1a-1o**, 0.3 mmol, 1 equiv), maleimide (**2a-2q**, 0.45 mmol, 1.5 equiv), $Mn(CO)_5Br$ (15 mol%, 0.15 equiv),

TH-3369_166122017

NH_4OAc (30 mol%, 0.3 equiv) and a magnetic bead in TFE (1.5 mL) under an open atmosphere and was refluxed in an oil bath at 100 °C for 18 h. The progress of the reaction was monitored by TLC. After completion of the reaction, the solvent was removed in vacuo. The reaction mixture was then mixed with water (5 mL) and extracted with ethyl acetate (2 x 15 mL). The organic layer was dried over anhydrous sodium sulfate and was evaporated under reduced pressure. Then the crude mixture was purified over column chromatography (60-120 mesh silica) by eluting it with hexane/EtOAc (55:45) mixture to afford the desired products **3**(**a-o**)(**a-q**).

(c) General procedure for the synthesis of *o*-alkylation 4(a-r)(a-w)

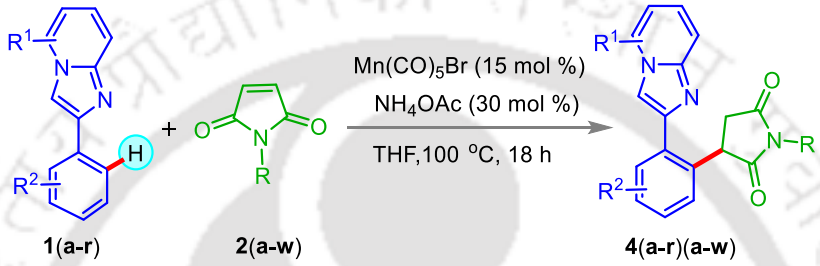

An oven-dried 25 mL round-bottom flask was charged with 2-arylimidazopyridine (**1a-1r**, 0.3 mmol, 1 equiv), maleimide (**2a-2w**, 0.45 mmol, 1.5 equiv), $Mn(CO)_5Br$ (15 mol%, 0.15 equiv), NH_4OAc (30 mol%, 0.3 equiv) and a magnetic bead in distilled THF (1.5 mL) under an open atmosphere and was refluxed in an oil bath at 100 °C for 18 h. The progress of the reaction was monitored by TLC. After completion of the reaction, the solvent was removed in vacuo. The reaction mixture was then mixed with water (5 mL) and extracted with ethyl acetate (2 x 15 mL). The organic layer was dried over anhydrous sodium sulfate and was evaporated under reduced pressure. Then the crude mixture was purified over column chromatography (60-120 mesh silica) by eluting it with hexane/EtOAc (65:35) mixture to afford the desired product **4** (**a-r**)(**a-w**).

(d) Procedure for Di-alkylation of bis-imidazopyridines

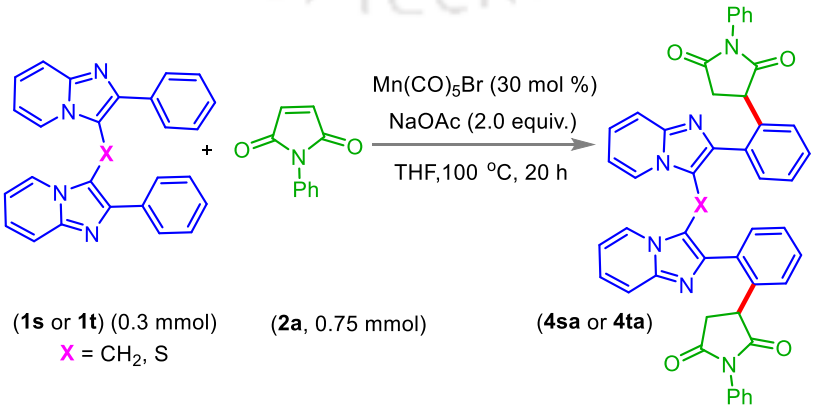

TH-3369_166122017

An oven-dried 25 mL round-bottom flask was charged with **1s** or **1t** (0.3 mmol, 120.1 or 125.5 mg), *N*-phenyl maleimide) (**2a**, 0.75 mmol, 129.8 mg), $Mn(CO)_5Br$ (30 mol%, 24.7 mg), NaOAc (0.6 mmol, 49.2 mg) and a magnetic bead in distilled THF (1.5 mL) under an open atmosphere and was refluxed in an oil bath at 100 ^oC for 20 h. The progress of the reaction was monitored by TLC. After completion of the reaction, the solvent was removed in vacuo. The reaction mixture was then mixed with water (5 mL) and extracted with ethyl acetate (2 x 15 mL). The organic layer was dried over anhydrous sodium sulfate and was evaporated under reduced pressure. Then the obtained residue was purified over column chromatography (60-120 mesh silica) by eluting it with hexane/EtOAc mixture to afford the desired products **4sa** (56%, 125 mg) or **4ta** (51%, 117 mg).

(e) Procedure for 1mmole scale synthesis of C3-alkylated 3aa

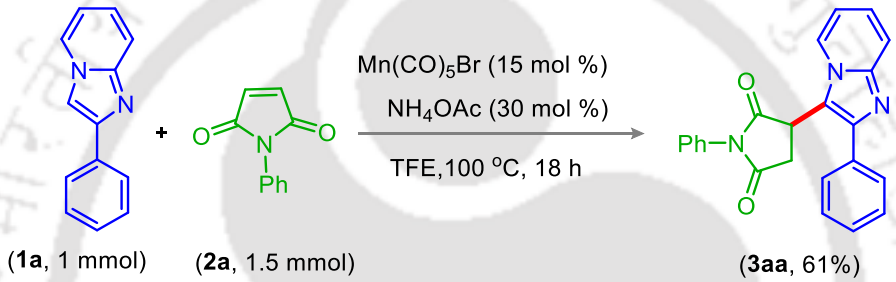

(**1a**, 1 mmol) (**2a**, 1.5 mmol) (**3aa**, 61%)

An oven-dried 25 mL round-bottom flask was charged with 2-arylimidazopyridine (**1a**, 1 mmol, 194 mg), maleimide (**2a**, 1.5 mmol, 260 mg), $Mn(CO)_5Br$ (15 mol%, 41 mg), NH_4OAc (30 mol%, 23 mg) and a magnetic bead in TFE (1.5 mL) under an open atmosphere and was refluxed in an oil bath at 100 ^oC for 18 h. The progress of the reaction was monitored by TLC. After completion of the reaction, the solvent was removed in vacuo. The reaction mixture was then mixed with water (5 mL) and extracted with ethyl acetate (2 x 15 mL). The organic layer was dried over anhydrous sodium sulfate and was evaporated under reduced pressure. Then the crude mixture was purified over column chromatography (60-120 mesh silica) by eluting it with hexane/EtOAc (55:45) mixture to afford the desired product **3aa** in 61% yield (224 mg).

(f) Procedure for 1mmole scale synthesis of *o*-alkylated 4aa

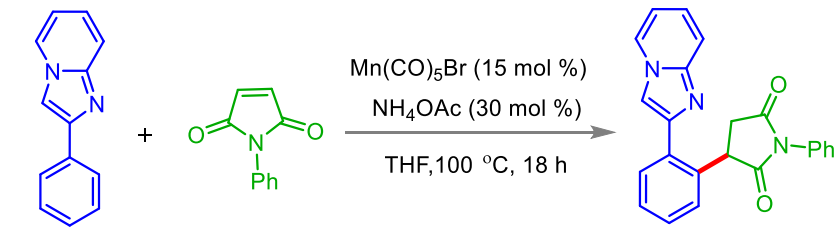

(**1a**, 1 mmol) (**2a**, 1.5 mmol) (**4aa**, 67%)

TH-3369_166122017

An oven-dried 25 mL round-bottom flask was charged with 2-arylimidazopyridine (**1a**, 1 mmol, 194 mg), maleimide (**2a**, 1.5 mmol, 260 mg), $Mn(CO)_5Br$ (15 mol%, 41 mg), NH_4OAc (30 mol%, 23 mg) and a magnetic bead in distilled THF (1.5 mL) under an open atmosphere and was refluxed in an oil bath at 100 ^oC for 18 h. The progress of the reaction was monitored by TLC. After completion of the reaction, the solvent was removed in vacuo. The reaction mixture was then mixed with water (5 mL) and extracted with ethyl acetate (2 x 15 mL). The organic layer was dried over anhydrous sodium sulfate and was evaporated under reduced pressure. Then the crude mixture was purified over column chromatography (60-120 mesh silica) by eluting it with hexane/EtOAc (65:35) mixture to afford the desired product **4aa** in 67% yield (246 mg).

III.5.3. Crystallographic Description

Crystal data were collected with Bruker Smart Apex-II CCD diffractometer using graphite monochromated MoKα radiation (λ = 0.71073 Å) at 296 K. Cell parameters were retrieved using SMART[a] software and refined with SAINT[a] on all observed reflections. Data reduction was performed with the SAINT software and corrected for Lorentz and polarization effects. Absorption corrections were applied with the program SADABS.[b] The structure was solved by direct methods implemented in SHELX-2014[c] program and refined by full-matrix least-squares methods on F2. All non-hydrogen atomic positions were located in difference Fourier maps and refined anisotropically. The hydrogen atoms were placed in their geometrically generated positions. colorless crystals of **3ac** were isolated from ethanol/DCM mixed solvent at room temperature. Yellow crystals of **4pc** were isolated from acetonitrile at room temperature.

a. SMART V 4.043 Software for the CCD Detector System; Siemens Analytical Instruments Division: Madison, WI, 2008.

b. SAINT Plus (v 6.14) Bruker AXS Inc., Madison, WI, 2008.

c. Sheldrick, G. M. SHELXL-2014, Program for the Refinement of Crystal Structures; University of Göttingen: Göttingen (Germany), 1997

TH-3369_166122017

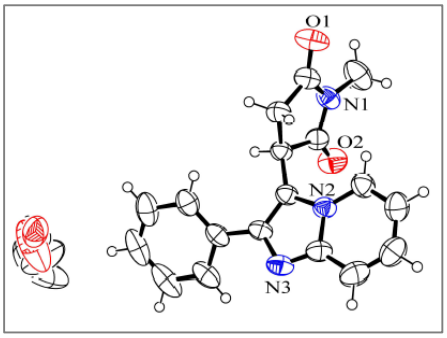

Figure III.5.1. *ORTEP diagram of* ***3ac*** *with the thermal ellipsoids set at 50% probability*

A disordered ethanol molecules found in the crystal lattice. The disordered ethanol molecule was modeled accordingly (without adding H-atoms). Hence the exact molecular formula may differ.

Crystal Data table for 3ac

Empirical formula	$C_{20}H_{15}N_3O_3$
CCDC number	2082422
Formula weight	345.36
Temperature	296(2)
Wavelength	0.71073 Å
Crystal system	monoclinic
Space group	C 2/c
Unit cell dimensions	A = 21.7602(16) Å, b = 10.7264(7) Å, c = 14.9919(10) Å α = 90°, β = 99.451(2)°, γ= 90°
Volume	3451.7(4) $Å^3$
Z	8
Absorption coefficient	0.092 mm^{-1}
F(000)	1440.709
Theta range for data collection	3.80 to 25°
Index ranges	-30<=h<=30, -14<=k<=15, -18<=l<=21
Reflections collected	24857
Independent reflections	3016
Data completeness	0.992
Refinement method	Full-matrix least-squares on F^2
Data / restraints / parameters	3016 / 0/ 264
Goodness-of-fit on F2	1.0646
Final R indices [I>2sigma(I)]	R1 = 0.0592, wR2 = 0.1596
R indices (all data)	R1= 0.0705, wR2 = 0.1834

TH-3369_166122017

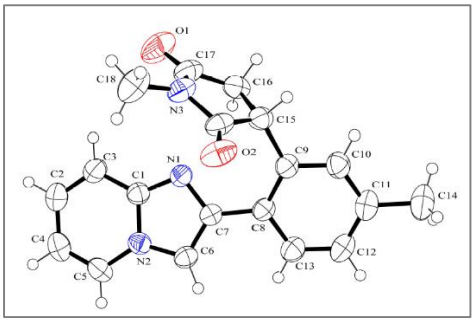

Figure III.5.2. *ORTEP diagram of* ***4pc*** *with the thermal ellipsoids set at 50% probability*

Crystal Data table for 4pc

Empirical formula	$C_{19}H_{17}N_3O_2$
CCDC number	2082420
Formula weight	319.36
Temperature	296(2)
Wavelength	0.71073 Å
Crystal system	Monoclinic
Space group	P 21/c
Unit cell dimensions	a= 11.4006(16) Å, b= 12.8149(19) Å, c= 11.1006(15) Å $\alpha = 90^o$, $\beta = 96.273(8)^o$, $\gamma = 90^o$
Volume	1612.1(4)Å^3
Z	4
Absorption coefficient	0.088 mm^{-1}
F(000)	672
Theta range for data collection	2.40 to 25.81°
Index ranges	-15<=h<=15, -17<=k<=17, -14<=l<=14
Reflections collected	18821
Independent reflections	5626
Data completeness	1.000
Refinement method	Full-matrix least-squares on F^2
Data / restraints / parameters	4066 / 0 / 219
Goodness-of-fit on F2	1.052
Final R indices [I>2sigma(I)]	R1 = 0.0452, wR2 = 0.1434
R indices (all data)	R1 = 0.0673, wR2 = 0.1593

III.5.4. Control Experiments

III.5.4.1. Procedure to confirm the nature of the reaction path way for C3-alkylation

An oven-dried 25 mL round-bottom flask was charged with 2-phenylimidazopyridine (**1a**, 0.3 mmol, 58.2 mg), *N*-phenyl maleimide (**2a**, 0.45 mmol, 77.8 mg), $Mn(CO)_5Br$ (15 mol%, 12 mg),

TH-3369_166122017

NH_4OAc (30 mol%, 6.93 mg), BHT (0.6 mmol, 132.2 mg) and a magnetic bead in TFE (1.5 mL) under an open atmosphere and was refluxed in an oil bath at 100 ^oC for 18 h. The progress of the reaction was monitored by TLC. After the completion of the reaction, the solvent was removed in vacuo. The reaction mixture was then mixed with water (5 mL) and extracted with ethyl acetate (2 x 15 mL). The organic layer was dried over anhydrous sodium sulfate and was evaporated under reduced pressure. The crude mixture was purified over column chromatography by eluting it with hexane/EtOAc mixture to afford the desired products **3aa** (61%, 67 mg). This observation suggests the non-involvement of any radical pathway.

III.5.4.2. Procedure to confirm the nature of the reaction path way for *o*-alkylation

An oven-dried 25 mL round-bottom flask was charged with 2-phenylimidazopyridine (**1a**, 0.3 mmol, 58.2 mg), *N*-phenyl maleimide (**2a**, 0.45 mmol, 77.8 mg), $Mn(CO)_5Br$ (15 mol%, 12 mg), NH_4OAc (30 mol%, 6.93 mg), BHT (0.6 mmol, 132.2 mg) and a magnetic bead in distilled THF (1.5 mL) under an open atmosphere and was refluxed in an oil bath at 100 ^oC for 18 h. The progress of the reaction was monitored by TLC. After the completion of the reaction, the solvent was removed in vacuo. The reaction mixture was then mixed with water (5 mL) and extracted with ethyl acetate (2 x 15 mL). The organic layer was dried over anhydrous sodium sulfate and was evaporated under reduced pressure. The crude mixture was purified over column chromatography by eluting it with hexane/EtOAc mixture (65:35) to afford the desired products **4aa** (70%, 77 mg). This observation also confirms the non-involvement of any radical pathway.

III.5.4.3. Procedure for H/D exchange for C3-alkylation

An oven-dried 25 mL round-bottom flask was charged with 2-phenylimidazopyridine (**1a**, 0.3 mmol, 58.2 mg), $Mn(CO)_5Br$ (15 mol%, 12 mg), NH_4OAc (30 mol%, 6.93 mg), D_2O (5 equiv) and a magnetic bead in TFE (0.8 mL) under an open atmosphere and was refluxed in an oil bath at 100 ^oC for 18 h. After the completion of the reaction, the solvent was removed in vacuo. The reaction mixture was then mixed with water (5 mL) and extracted with ethyl acetate (2 x 15 mL). The organic layer was dried over anhydrous sodium sulfate and was evaporated under reduced pressure. The crude mixture was purified over column chromatography by eluting it with hexane/EtOAc (70:30) mixture to afford the deuterated products [**1a**]-**d**. The extent of H/D exchange was determined by comparing the ^1H NMR of deuterated [**1a**]-**d** to that of undeuterated **1a.** The peak at δ 8.03 ppm (d) which has an integral value of 1.00 was considered as the reference in both the spectra. Integrating accordingly in both of them, it was found that upon deuteration the characteristic peak for C3-H which appears at 7.78 ppm was reduced

TH-3369_166122017

to an integral value 0.18 from 1.00. Thus, there was 82% deuteration (1.00-0.18= 0.82 i.e. 82% D) observed at C3-H without affecting other C–H sites (Figure III.5.3 and III.5.4).

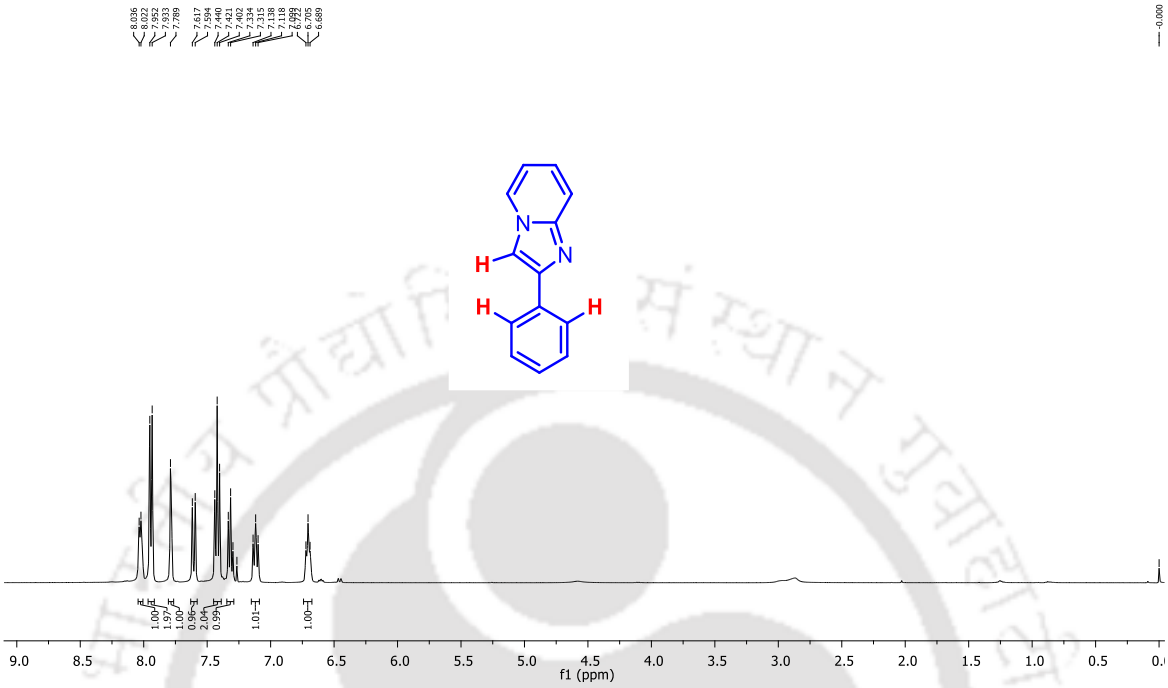

Figure III.5.3. *^{1}H NMR spectrum of undeuterated [**1a**]*

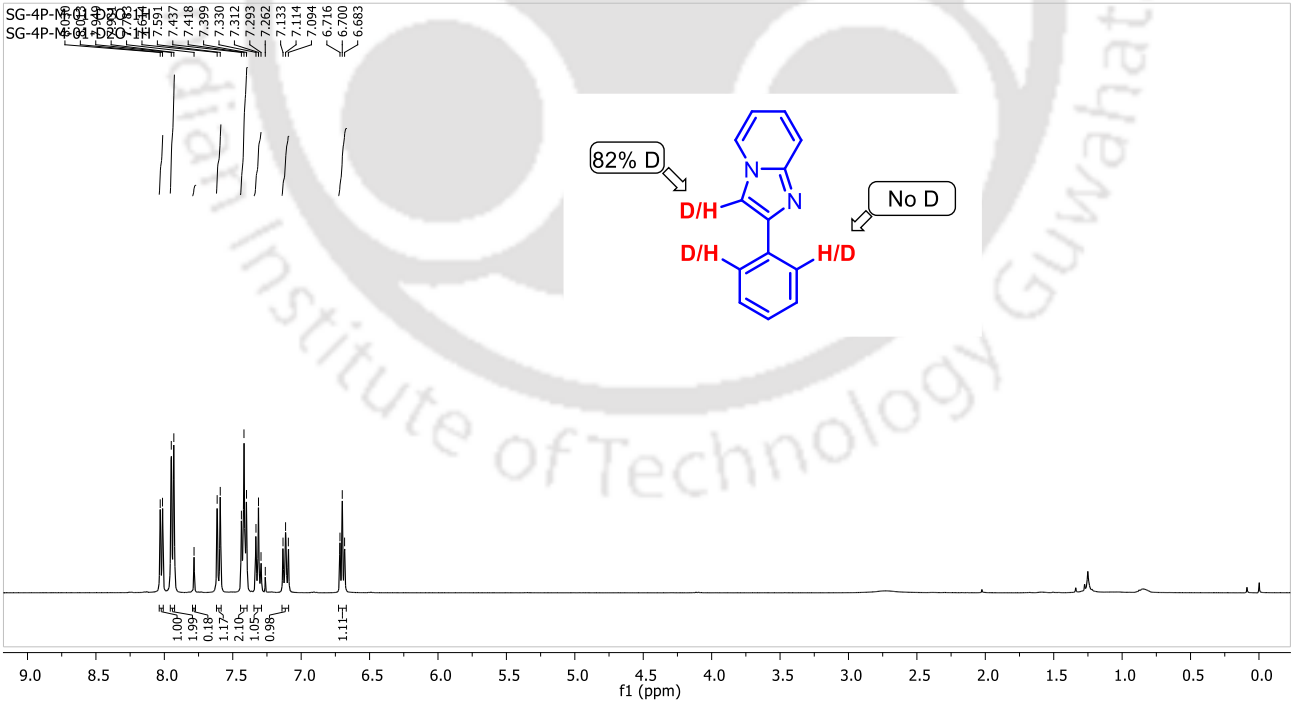

Figure III.5.4. *^{1}H NMR of deuterated [**1a**]-**d** in 5 equiv D_2O*

TH-3369_166122017

III.5.4.4. Procedure for H/D exchange for *o*-alkylation

An oven-dried 25 mL round-bottom flask was charged with 2-phenylimidazopyridine (**1a**, 0.3 mmol, 58.2 mg), $Mn(CO)_5Br$ (15 mol%, 12 mg), NH_4OAc (30 mol%, 6.93 mg), D_2O (5 equiv or 1 equiv) and a magnetic bead in distilled THF (0.8 mL) under an open atmosphere and was refluxed in an oil bath at 100 °C for 18 h. After the completion of the reaction, the solvent was removed in vacuo. The reaction mixture was then mixed with water (5 mL) and extracted with ethyl acetate (2 x 15 mL). The organic layer was dried over anhydrous sodium sulfate and was evaporated under reduced pressure. The crude mixture was purified over column chromatography by eluting it with hexane/EtOAc (70:30) mixture to afford the deuterated products [**1a**]**d**$_3$. Similar to the study of H/D exchange for C3-alkylation here, upon treatment with 5 equiv D_2O we have observed a 31% D at C3-H and 45% D at *ortho* C-Hs. Whereas in presence of 1 equiv D_2O, the C3-H was deuterated by 2% D and the *ortho* C-Hs were deuterated by 32% D (Figure III.5.5 and III.5.6).

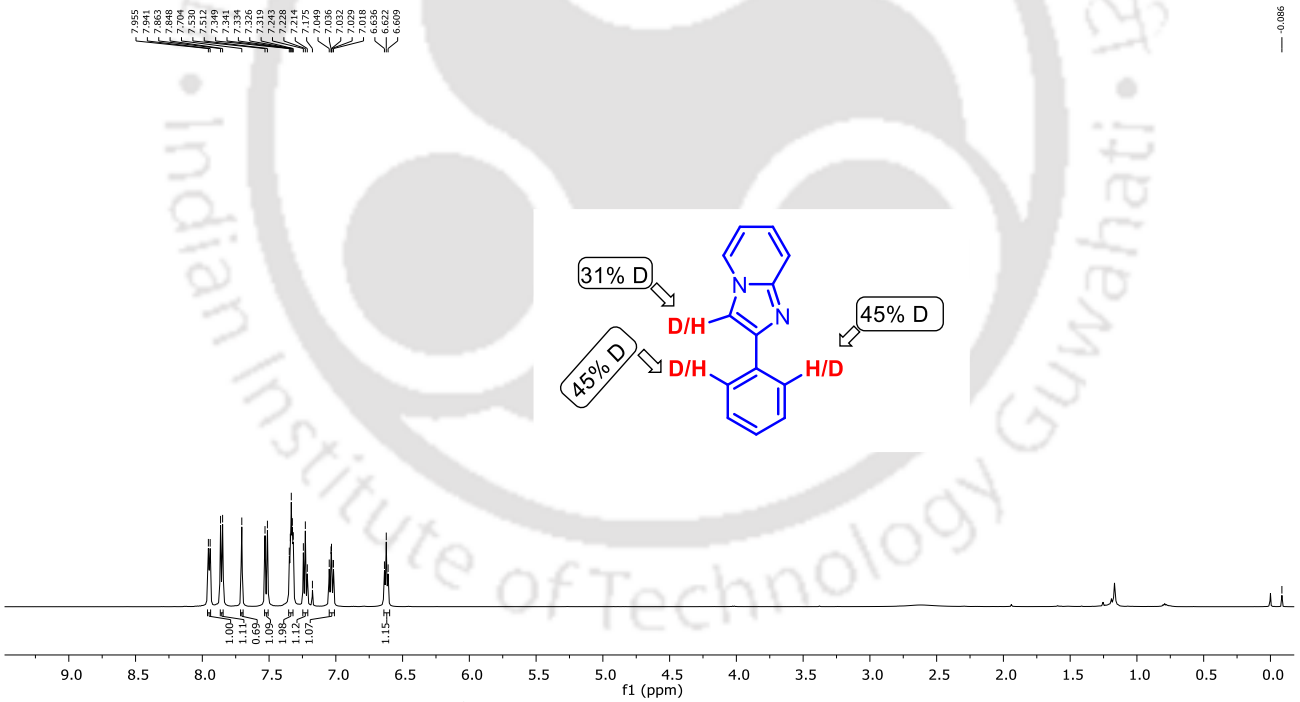

Figure III.5.5. *^{1}H NMR of deuterated [**1a**]-**d**$_3$ in 5 equiv D_2O*

TH-3369_166122017

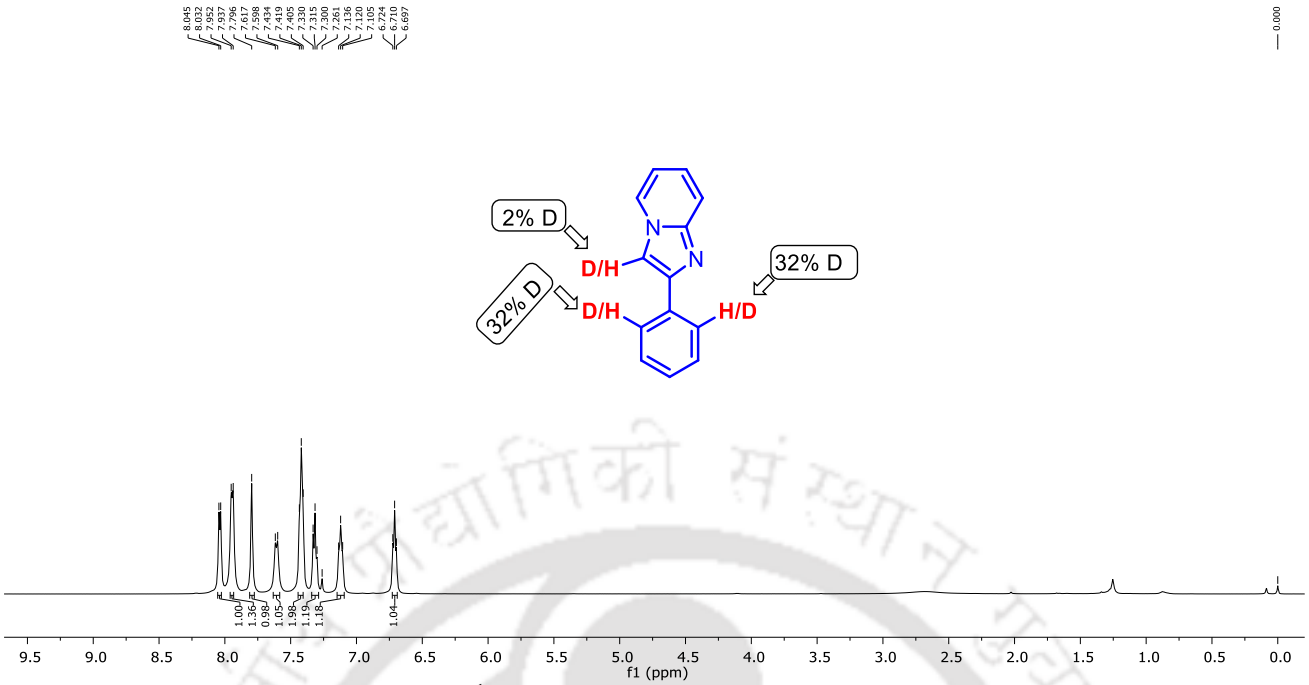

Figure III.5.6. *^{1}H NMR of deuterated **[1a]-d$_3$** in 1 equiv D_2O*

III.5.4.5. Procedure for the synthesis of [1a]-d$_3$

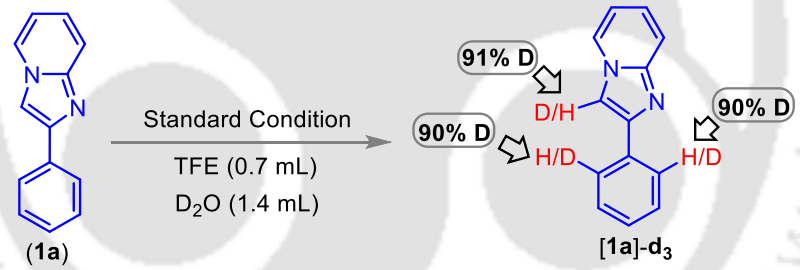

An oven-dried 10 mL round-bottom flask was charged with 2-phenylimidazopyridine (**1a**, 0.3 mmol, 58.2 mg), $Mn(CO)_5Br$ (15 mol%, 12 mg), NH_4OAc (30 mol%, 6.93 mg), D_2O (1.4 mL) and charged with a magnetic bead in TFE (0.7 mL) under an open atmosphere and was refluxed in an oil bath at 100 ^oC for 15 h. The reaction mixture was then admixed with water (5 mL) and extracted with ethyl acetate (2 x 15 mL). The organic layer was dried over anhydrous Na_2SO_4, filtered and was evaporated under reduced pressure. The crude mixture was purified over column chromatography by eluting it with hexane/EtOAc (70:30) mixture to afford the deuterated product [**1a**]-**d$_3$** as a light yellowish solid in 86% isolated yield. The percentage of deuterium labelling/incorporation was determined from the 500 MHz ^{1}HNMR integration similar to the one described for H/D exchange for C3-alkylation and the estimated deuterium incorporation in ortho position was found to be 90% and for C3 it was 91% (Figure III.5.7).

TH-3369_166122017

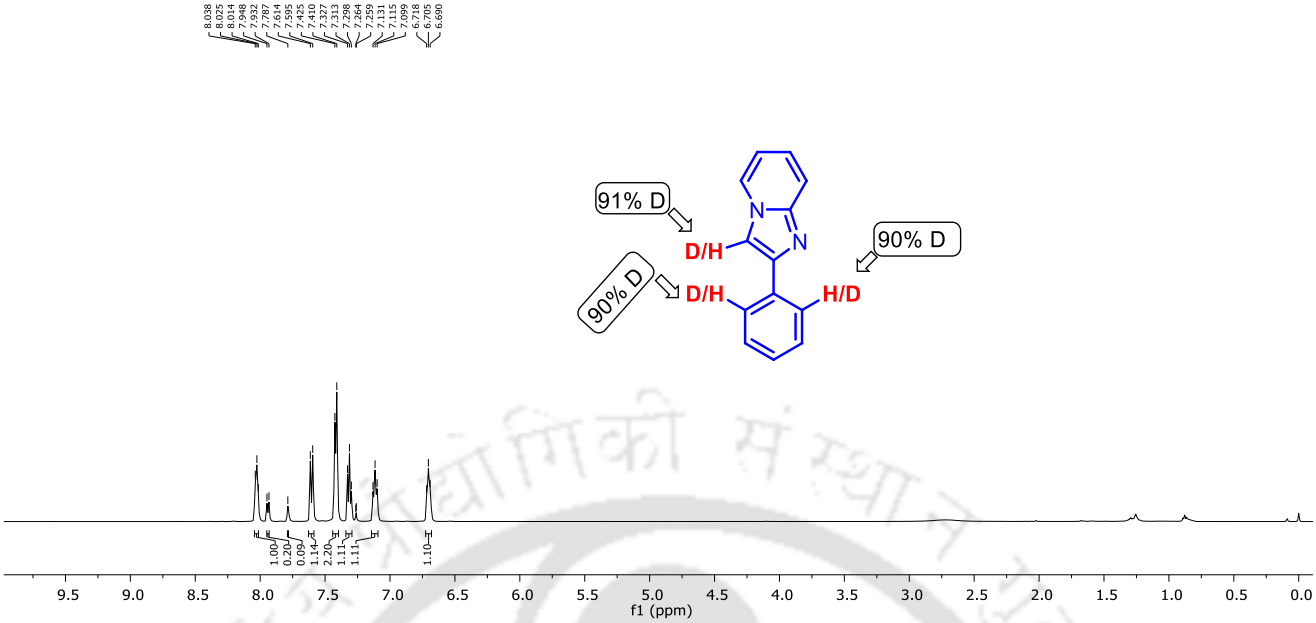

Figure III.5.7. *^{1}H NMR of deuterated [**1a**]-**d$_3$***

III.5.4.6. Modified procedure for synthesis of [1a]-d$_2$ of 2-phenyl imidazopyridine[27]

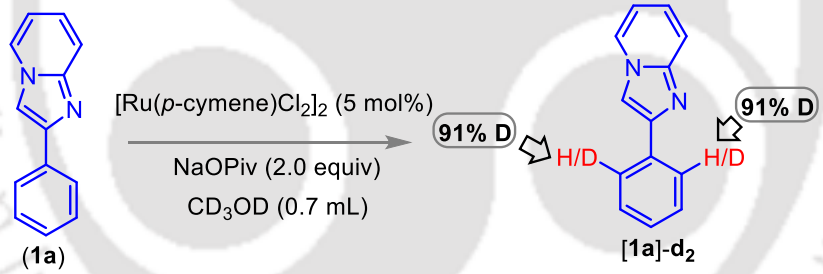

An oven-dried 10 mL sealed tube was charged with 2-phenylimidazopyridine (**1a**, 0.3 mmol, 58.2 mg), [Ru(*p*-cymene)Cl_2]$_2$ (5 mol%, 9.2 mg), PivONa (0.6 mmol, 74.4 mg) and a magnetic bead in CD_3OD (0.7 mL) was refluxed in an oil bath at 70 ^oC for 10 h. After completion of the reaction, the solvent was removed in vacuo. The reaction mixture was then mixed with water (5 mL) and extracted with ethyl acetate (2 x 15 mL). The organic layer was dried over anhydrous Na_2SO_4, filtered and was evaporated under reduced pressure. The crude mixture was purified over a column of silica gel by eluting it with hexane/EtOAc (70:30) mixture to afford the deuterated product [**1a**]-**d$_2$** as a grey solid in 88% isolated yield. From 500 MHz ^{1}HNMR integration the estimated deuterium incorporation in *ortho* position was found to be 91% (Figure III.5.8).

TH-3369_166122017

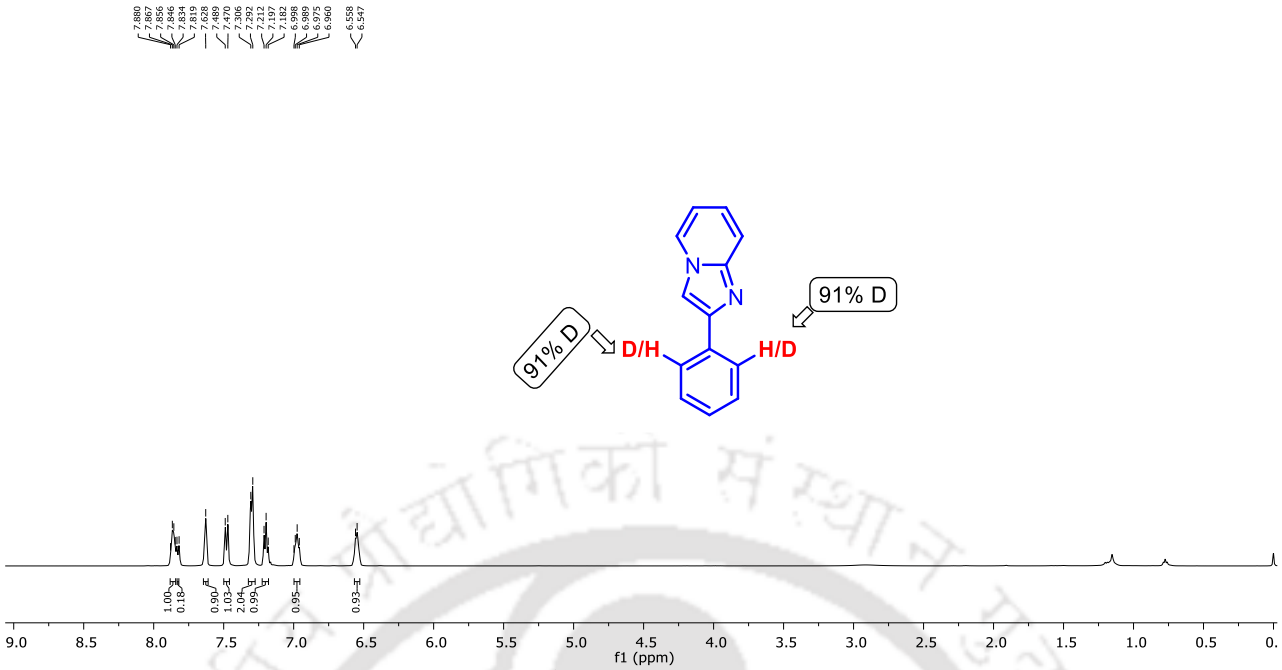

Figure III.5.8. *^{1}H NMR of deuterated [**1a**]-d_2*

III.5.4.7. Procedure of intramolecular KIE for C-3 Alkylation in TFE

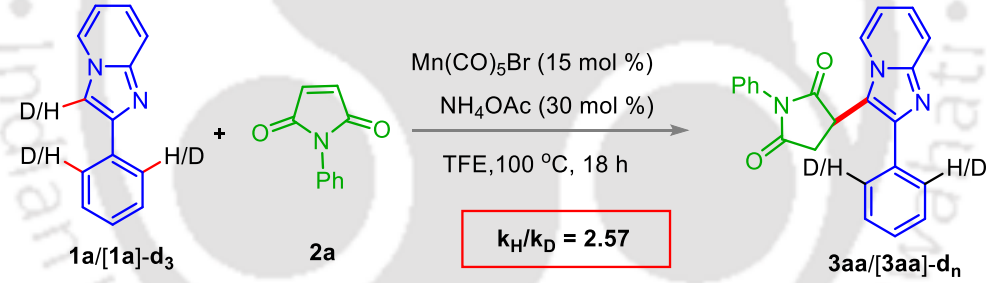

An oven-dried 10 mL round-bottom flask was charged with 2-phenylimidazopyridine **1a** (0.15 mmol, 29.1 mg), **[1a]-d_3** (0.15 mmol, 29.6 mg), *N*-phenyl maleimide **2a** (0.225 mmol, 38.9 mg), $Mn(CO)_5Br$ (15 mol%, 6.2 mg), NH_4OAc (30 mol%, 3.5 mg) and a magnetic bead in TFE (1.0 mL) under an open atmosphere and was refluxed in an oil bath at 100 °C for 18 h. After completion of the reaction, the solvent was removed in vacuo. The reaction mixture was then mixed with water (5 mL) and extracted with ethyl acetate (2 x 15 mL). The organic layer was dried over anhydrous sodium sulfate and was evaporated under reduced pressure. The crude mixture was purified over a column of silica gel by eluting it with hexane/EtOAc (55:45) mixture to afford the mixture of alkylated products **3aa** and [**3aa**]-**d_n** as brownish solid. By analyzing the ^{1}H NMR of the mixture **3aa** and [**3aa**]-**d_n** as shown in Figure III.5.9, the ratio of **3aa** to [**3aa**]-**d_n** was determined to be 1.44:0.56. Accordingly, the intermolecular KIE (k_H/k_D)= 1.44/2.00-1.44 = 2.57.

TH-3369_166122017

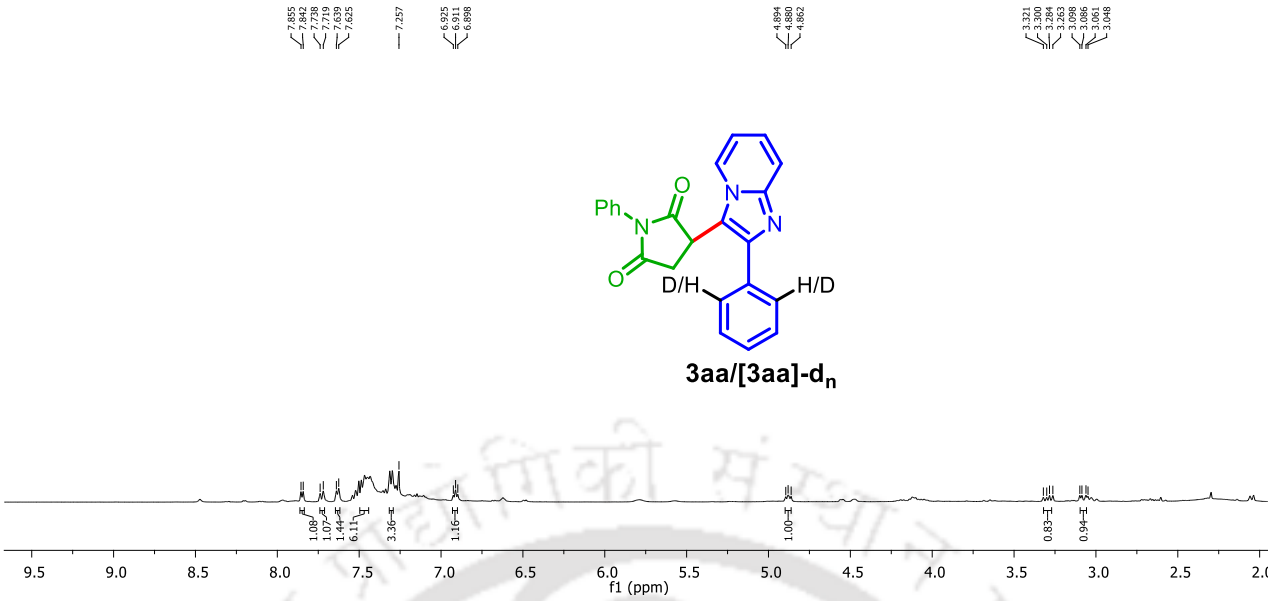

Figure III.5.9. *^{1}H NMR of mixture* ***3aa*** *and* ***[3aa]-d_n***

III.5.4.8. Procedure of intramolecular KIE for *o*-Alkylation in THF

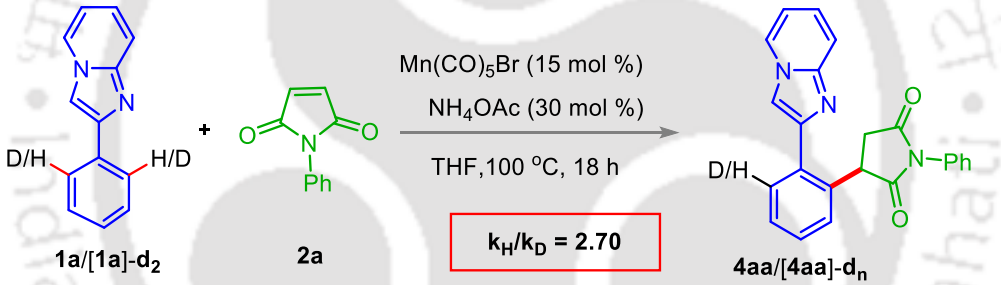

An oven-dried 10 mL round-bottom flask was charged with 2-phenylimidazopyridine **1a** (0.15 mmol, 29.1 mg), **[1a]-d_2** (0.15 mmol, 29.6 mg), *N*-phenyl maleimide **2a** (0.225 mmol, 38.9 mg), $Mn(CO)_5Br$ (15 mol%, 6.2 mg), NH_4OAc (30 mol%, 3.5 mg) and a magnetic bead in distilled THF (1.0 mL) under an open atmosphere and was refluxed in an oil bath at 100 °C for 18 h. After the completion of the reaction, the solvent was removed in vacuo. The reaction mixture was then mixed with water (5 mL) and extracted with ethyl acetate (2 x 15 mL). The organic layer was dried over anhydrous sodium sulfate, filtered and was evaporated under reduced pressure. The crude mixture was purified over a column of silica gel by eluting it with hexane/EtOAc (65:35) mixture to afford the mixture of *o*-alkylated products **4aa** and [**4aa**]-$\mathbf{d_n}$ as a pale yellow solid. Similarly, by analyzing the ^{1}H NMR of the mixture **4aa** and [**4aa**]-$\mathbf{d_n}$ as shown in Figure III.5.10, the ratio of **3aa** to [**3aa**]-$\mathbf{d_n}$ was determined to be 0.73:0.27. Accordingly, the intermolecular KIE (k_H/k_D)= 0.73/1.00-0.73 = 2.70.

TH-3369_166122017

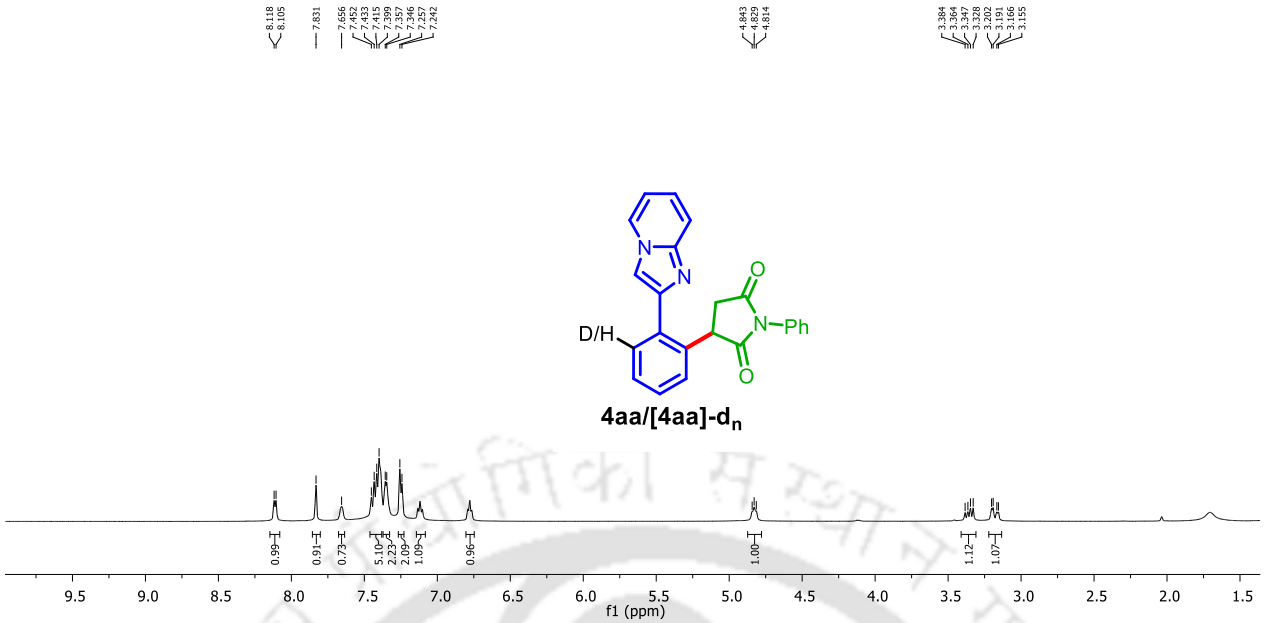

Figure III.5.10. *^{1}H NMR of mixture* ***4aa*** *and* ***[4aa]-d$_n$***

III.5.4.9. HRMS Analysis of Crude Reaction Mixture in ESI-MS

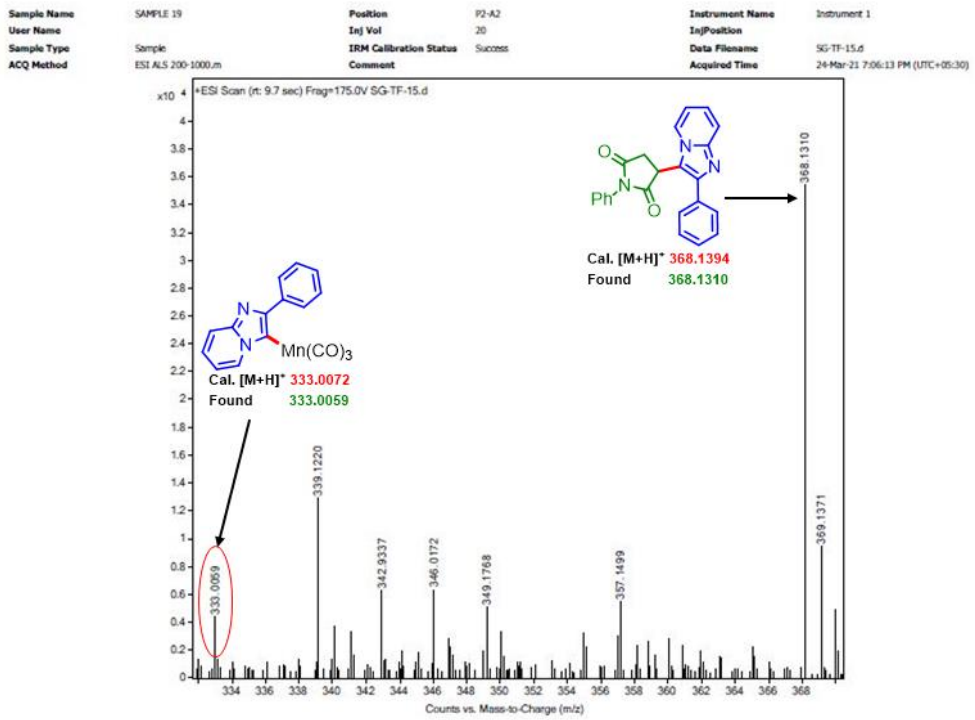

Figure III.5.11. *HRMS spectra of crude reaction mixture in* ***TFE***

TH-3369_166122017

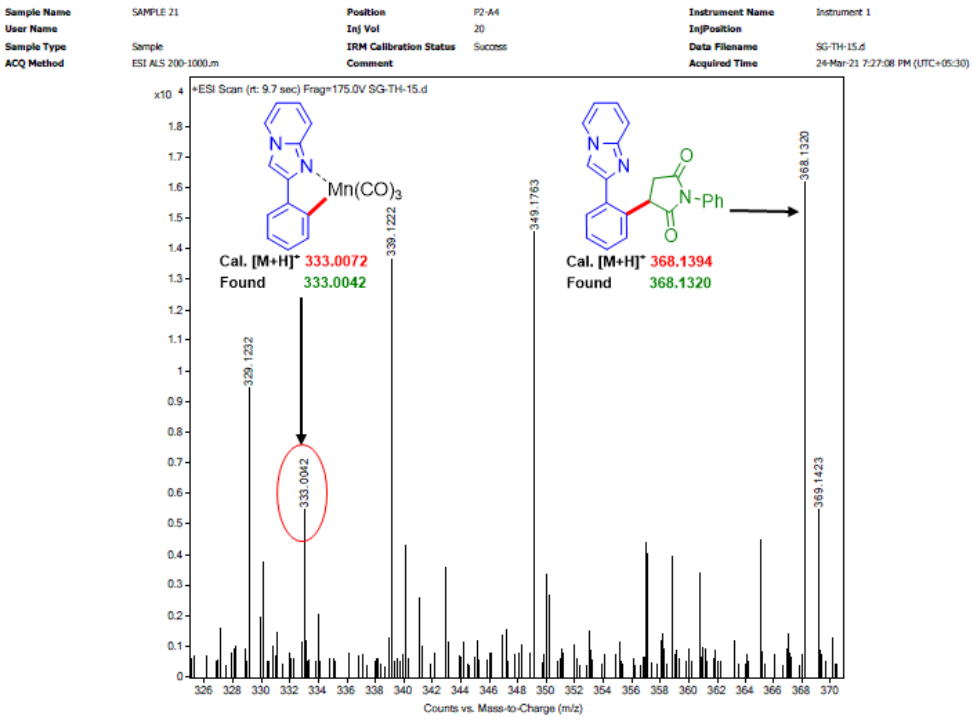

Figure III.5.12. HRMS spectra of crude reaction mixture in **THF**.

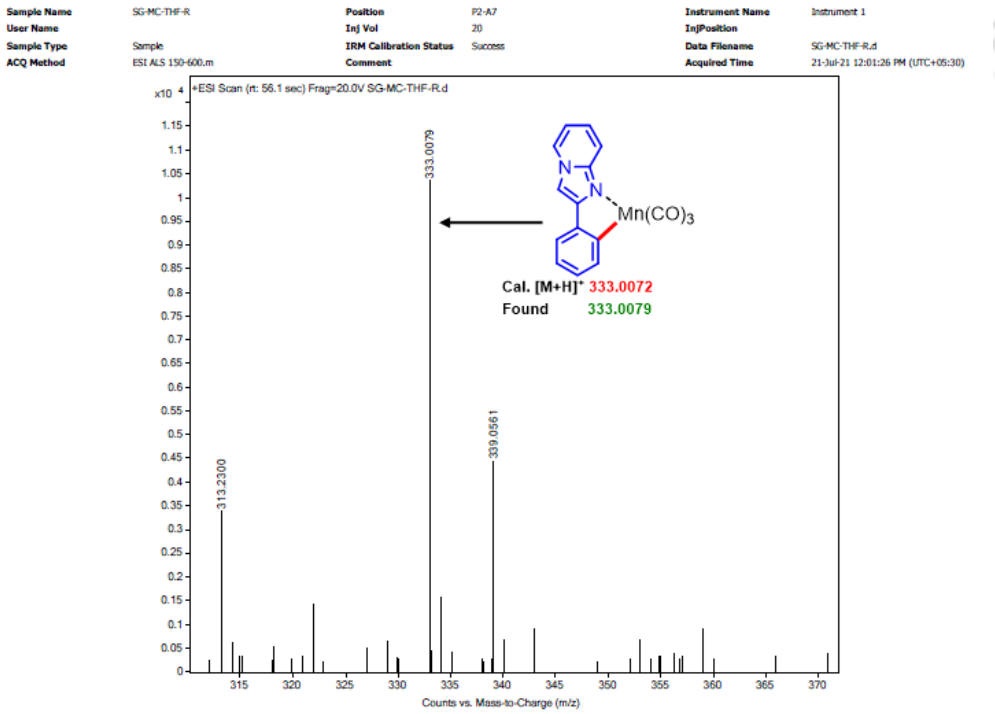

Figure III.5.13. *HRMS spectra of crude metal complex reaction mixture in* ***THF***

TH-3369_166122017

III.5.4.10. Electronic Effect on Electrophilic Metalation

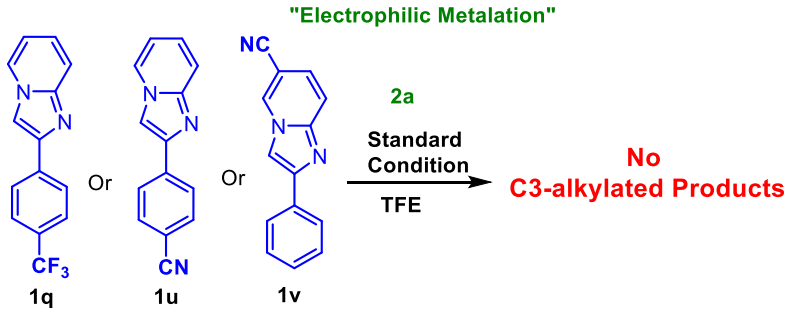

Scheme III.5.2. *Electronic effect*

III.6. References

1. (a) Noyori, R. Synthesizing our future. *Nat. Chem*. **2009**, *1*, 5. (b) Ping, L.; Chung, D. S.; Bouffard, J.; Lee, S.-g. Transition Metal-Catalyzed Site- and Regio-divergent C–H Bond Functionalization. *Chem. Soc. Rev*. **2017**, *46*, 4299. (c) Zhang, Z.; Tanaka, K.; Yu, J.-Q. Remote Site-Selective C–H Activation Directed by A Catalytic Bifunctional Template. *Nature*, **2017**, *543*, 538. (d) Gramage-Doria, R. Steering Site-Selectivity in Transition Metal-Catalyzed C−H Bond Functionalization: the Challenge of Benzanilides. *Chem. Eur. J*. **2020**, 26, 9688. (e) Zhang, Q.; Shi, B-F. Site-Selective Functionalization of Remote Aliphatic C–H Bonds via C–H Metalation. *Chem. Sci*. **2021**, *12*, 841.
2. (a) Yuan, Z.; Hu, X.; Zhang, H.; Liu, L.; Chen, P.; He, M.; Xie, X.; Wang. X.; She, X. Total Synthesis of Conosilane A via A Site-Selective C–H Functionalization Strategy. *Chem. Commun*. **2018**, *54*, 912. (b) Wang, W.; Lorion, M. M.; Shah, J.; Kapdi, A. R.; Ackermann, L. Late-Stage Peptide Diversification by Position-Selective C-H Activation. *Angew. Chem. Int. Ed*. **2018**, 57, 14700. (c) Lorion, M. M.; Kaplaneris, N.; Son, J.; Kuniyi, R.; Ackermann, L. Late-Stage Peptide Diversification through Cobalt-Catalyzed C−H Activation: Sequential Multicatalysis for Stapled Peptides. *Angew. Chem. Int. Ed*. **2019**, *58*, 1684. (d) Robles, O.; Romo, D. Chemo- and Site-Selective Derivatizations of Natural Products Enabling Biological Studies. *Nat. Prod. Rep*. **2014**, *31*, 318. (e) Shang, W.; He, B.; Niu, D. Ligand-Controlled, Transition-Metal Catalyzed Site-Selective Modification of Glycosides. *Carbohydr. Res.* **2019**, *474*, 16. (f) Chu, L.; Shang, M.; Tanaka, K.; Chen, Q.; Pissarnitski, N.; Streckfuss, E.; Yu, J.-Q. Remote Meta-C–H Activation Using a Pyridine-Based Template: Achieving Site-Selectivity via the Recognition of Distance and Geometry. *ACS Cent. Sci*. **2015**, *1*, 394. (g) Liao, G.; Yao, Q-J.; Zhang, Z-Z.; Wu, Y-J.; Huang, D-Y.; Shi, B-F. Scalable, Stereocontrolled Formal Syntheses of (+)-Isoschizandrin and (+)-Steganone:

TH-3369_166122017

Development and Applications of Palladium(II)-Catalyzed Atroposelective C-H Alkynylation. *Angew.Chem. Int. Ed.* **2018**, *57*, 3661.

3. (a) McMurray, L.; O'Hara, F.; Gaunt, M. J. Recent Developments in Natural Product Synthesis using Metal-Catalysed C–H Bond Functionalization. *Chem. Soc. Rev*. **2011**, *40*, 1885. (b) Yamaguchi, J.; Yamaguchi, A. D.; Itami, K. C–H Bond Functionalization: Emerging Synthetic Tools for Natural Products and Pharmaceuticals. *Angew. Chem. Int. Ed*. **2012**, *51*, 8960.
4. (a) Su, Y.; Zhou, H.; Chen, J.; Xu, J.; Wu, X.; Lin, A.; Yao, H. Solvent-Controlled Switchable C–H Alkenylation of 4-Aryl-1H-pyrrole-3-carboxylates: Application to the Total Synthesis of (±)-Rhazinilam. *Org. Lett.* **2014**, *16*, 4884. (b) Dai, H.-M.; Yu, C.; Wang, Z.-H; Yan, H.; Lu, C.-S. Solvent- Controlled, Tunable β-OAc and β-H Elimination in Rh(III)-Catalyzed Allyl Acetate and Aryl Amide Coupling via C-H Activation. *Org. Lett*. **2016**, *18*, 3410. (c) Kolesnikov, P. N.; Usanov, D. L.; Muratov, K. M.; Chusov, D. Dichotomy of Atom-Economical Hydrogen-Free Reductive Amidation vs Exhaustive Reductive Amination. *Org. Lett*. **2017**, *19*, 5657. (d) Yi, W.; Chen, W.; Liu, F.; Zhong, Y.; Wu, D.; Zhou, Z.; Gao, H. Rh(III)-Catalyzed and Solvent-Controlled Chemoselective Synthesis of Chalcone and Benzofuran Frameworks via Synergistic Dual Directing Groups Enabled Regioselective C-H Functionalization: A Combined Experimental and Computational Study. *ACS Catal.* **2018**, *8*, 9508. (e) D. S. Chung, J. S. Lee, H. Ryu, J. Park, H. Kim, J. H. Lee, U. B. Kim, W. K. Lee, M. -H. Baik and S. -g. Lee, *Angew. Chem., Int. Ed*., 2018, **57**, 15460. (f) Bian, M.; Ma, K.; Mawjuda, H.; Yu, X.; Li, X.; Gao, H.; Zhou, Z.; Yi, W. Rhodium(III)-Catalyzed Chemoselective C-H Functionalization of Benzamides with Methyleneoxetanones Controlled by the Solvent. *Org. Biomol. Chem.* **2019**, *17*, 6114. (g) Li, S.; Shi, P.; Liu, R.-H.; Hu, X.-H.; Loh, T.-P. Cobalt-Catalyzed N–O and C–C Bond Cleavage in 1,2-Oxazetidines: Solvent-Controlled C–H Aminomethylation and Hydroxymethylation of Heteroarenes. *Org. Lett.* **2019**, *21*, 1602. (h) Khake, S. M.; Chatani, N. The Direct Rh(III)-Catalyzed C–H Amidation of Aniline Derivatives Using a Pyrimidine Directing Group: The Selective Solvent Controlled Synthesis of 1,2-Diaminobenzenes and Benzimidazoles. *Org. Lett*. **2020**, *22*, 3655. (i) He, Y.; Zheng, Z.; Liu, Q.; Zhang, X.; Fan, X. Solvent-Regulated Coupling of 2-Alkynylbenzaldehydes with Cyclic Amines: Selective Synthesis of Fused N-Heterocycles and Functionalized Naphthalene Derivatives. *Org. Lett.* **2020**, *22*, 9053. (j) Nunewar, S.; Kumar, S.; Priyanka, P.; Girase, P.; Kanchupalli, V. The Solvent-controlled Rh(iii)-Catalyzed Switchable [4+2]-Annulation of 2-arylIndoles with Iodonium Ylides. *Chem. Commun.* **2022**, *58*, 6140.
5. (a) Das, R.; Khot, N. P.; Deshpande, A. S.; Kapur, M. Catalyst control in switching the site selectivity of C−H olefinations of 1,2-dihydroquinolines: An approach to positional-selective

TH-3369_166122017

functionalization of quinolines. *Chem. − Eur. J.* **2020**, *26*, 927. (b) Zhang, Q.; Zhou, P.; Zhao, Y.; Liu, Y.; Liang, T.; Jiang, J.; Zhang, Z. Catalyst-Controlled Regiodivergent C–H Bond Alkenylation of 2-Pyridylthiophenes. *Chem. Commun.* **2023**, *59*, 8842. (c) Meena, N.; Shinde, V. N.; Sonam, Swami, P. N.; Rangan, K.; Kumar, A. *J. Org. Chem.* **2023**, *88*, 12902.

6. (a) Su, W.; Gong, T. J.; Lu, X.; Xu, M.-Y.; Yu, C.-G.; Xu, Z.-Y.; Yu, H.-Z.; Xiao, B.; Fu, Y. Ligand-Controlled Regiodivergent Copper-Catalyzed Alkylboration of Alkenes. *Angew. Chem., Int. Ed.* **2015**, *54*, 12957. (b) Su, W.; Gong, T.-J.; Zhang, Q.; Zhang, Q.; Xiao, B.; Fu, Y. Ligand-Controlled Regiodivergent Copper-Catalyzed Alkylboration of Unactivated Terminal Alkynes. *ACS Catal.* **2016**, *6*, 6417. (c) Xia, Y.; Bao, Q.-F.; Li, Y.; Wang, L.-J.; Zhang, B.-S.; Liu, H.-C.; Liang, Y.-M. Ligand-controlled regiodivergent π-allyl palladium catalysis enables a switch between [3+2] and [3+3] cycloadditions. *Chem. Commun.* **2019**, *55*, 4675. (d) Ai, H.-J.; Lu, W.; Wu, X.-F. Ligand-Controlled Regiodivergent Thiocarbonylation of Alkynes toward Linear and Branched *α,β*-Unsaturated Thioesters. *Angew. Chem., Int. Ed.* **2021**, *60*, 17178. (e) Chai, W.; Zhou, Q.; Ai, W.; Zheng, Y.; Qin, T.; Xu, Xiu; Zi, W. Lewis-Acid-Promoted Ligand-Controlled Regiodivergent Cycloaddition of Pd-Oxyallyl with 1,3-Dienes: Reaction Development and Origins of Selectivities. *J. Am. Chem. Soc.* **2021**, *143*, 3595.
7. (a) Ling, Y.; An, D.; Zhou, Y.; Rao, W. Ga(OTf) 3-catalyzed temperature-controlled regioselective Friedel–Crafts alkylation of trifluoromethylated 3-indolylmethanols with 2-substituted indoles: divergent synthesis of trifluoromethylated unsymmetrical 3, 3′-and 3, 6′-bis (indolyl) methanes. *Org. Lett*. **2019**, *21*, 3396. (b) Li, X. H.; Wang, S. M.; Li, S. L.; Li, K. M.; Mo, X.; Liu, L. Y.; Chang, W. X.; Li, J. Temperature-Controlled Divergent Hydroamination Cyclization [2+2]-Cycloaddition Cascade Reactions of Homopropargylic Amines with 2-Butynedioates: Direct Access To Pyrrolo-b-cyclobutene and Dihydro-1H-azepines. *J. Org. Chem*. **2019**, *84*, 1288.
8. (a) Ritleng, V.; Sirlin, C.; Pfeffer, M. Ru-, Rh-, and Pd-Catalyzed C−C Bond Formation Involving C−H Activation and Addition on Unsaturated Substrates: Reactions and Mechanistic Aspects. *Chem. Rev*. **2002**, *102*, 1731. (b) Li, H.; Li, B. J.; Shi, Z. J. Challenge and Progress: Palladium-Catalyzed sp3 C–H Activation. *Catal. Sci. Technol*. **2011**, *1*, 191. (c) Kong, W.-J.; Liu, Y.-J.; Xu, H.; Chen, Y.-Q.; Dai, H.-X.; Yu, J.-Q. Pd-Catalyzed α-Selective C–H Functionalization of Olefins: En Route to 4-Imino-β-Lactams. *J. Am. Chem. Soc*. **2016**, *138*, 2146.
9. (a) Gandeepan, P.; Müller, T.; Zell, D.; Cera, G.; Warratz, S.; Ackermann, L. 3d Transition Metals for C–H Activation. *Chem. Rev*. **2019**, *119*, 2192. (b) Rao, W-H.; Shi, B-F. Recent Advances in Copper-Mediated Chelation-Assisted Functionalization of Unactivated C–H Bonds. *Org. Chem.*

TH-3369_166122017

Front. **2016**, *3*, 1028. (c) Liu, Y-H.; Xia, Y-N.; Shi, B-F. Ni-Catalyzed Chelation-Assisted Direct Functionalization of Inert C–H Bonds. *Chin. J. Chem.* **2020**, *38*, 635.

10. (a) Liu, W.; Ackermann, L. Manganese-Catalyzed C–H Activation. *ACS Catal*. **2016**, *6*, 3743. (b) Cano, R.; Mackey, K.; McGlacken, G. P. Recent Advances in Manganese-Catalysed C–H Activation: Scope and Mechanism. *Catal. Sci. Technol*. **2018**, *8*, 1251. (c) Hu, Y.; Zhou, B.; Wang, C. Inert C–H Bond Transformations Enabled by Organometallic Manganese Catalysis. *Acc. Chem. Res.* **2018**, *51*, 816. (d) Aneeja, T.; Neetha, M.; Afsinaa. C. M. A.; Anilkumar, G. Recent Advances and Perspectives in Manganese-Catalyzed C–H Activation. *Catal. Sci. Technol*. **2021**, *11*, 444.
11. (a) Borghs, J. C.; Zubar, V.; Azofra, L. M.; Sklyaruk, J.; Rueping, M. Manganese-Catalyzed Regioselective Dehydrogenative C- versus N-Alkylation Enabled by a Solvent Switch: Experiment and Computation. *Org. Lett*. **2020**, *22*, 4222. (b) Burg, M. Sc. F.; Gicquel, M.; Breitenlechner, S.; Pöthig, A.; Bach, T. Site- and Enantioselective C−H Oxygenation Catalyzed by a Chiral Manganese Porphyrin Complex with a Remote Binding Site. *Angew.Chem. Int. Ed*. **2018**, *57*, 2953.
12. (a) Shukla, N. M.; Salunke, D. B.; Yoo, E.; Mutz, C. A.; Balakrishna, R.; David, S. A. Antibacterial Activities of Groebke–Blackburn–Bienaymé-derived Imidazo[1,2-*a*]pyridin-3-amines. *Bioorg. Med. Chem*. **2012**, *20*, 5850. (b) Enguehard-Gueiffier, C.; Gueiffier, A. Recent Progress in the Pharmacology of Imidazo[1,2-*a*]pyridines. *Mini-Rev. Med. Chem*. **2007**, *7*, 888.
13. Rupert, K. C.; Henry, J. R.; Dodd, J. H.; Wadsworth, S. A.; Cavender, D. E.; Olini, G. C.; Fahmy, B.; Siekierka, J. Imidazopyrimidines, Potent Inhibitors of p38 MAP Kinase. *Bioorg. Med. Chem. Lett*. **2003**, *13*, 347.
14. Mutai, T.; Tomoda, H.; Ohkawa, T.; Yabe, Y.; Araki, K. Switching of Polymorph-Dependent ESIPT Luminescence of an Imidazo[1,2-*a*]pyridine Derivative. *Angew. Chem. Int. Ed*. **2008**, *47*, 9522.
15. (a) Ghosh, K.; Nishii, Y.; Miura, M. Oxidative C–H/C–H Annulation of Imidazopyridines and Indazoles through Rhodium-Catalyzed Vinylene Transfer. *Org. Lett*. **2020**, *22*, 3547. (b) Li, B.; Shen, N.; Yang, Y.; Zhang, X.; Fan, X. Synthesis of Naphtho[1′,2′:4,5]imidazo[1,2-*a*]pyridines via Rh(iii)-Catalyzed C–H Functionalization of 2-Arylimidazo[1,2-*a*]pyridines with Cyclic 2-Diazo-1,3-diketones Featuring with a Ring Opening and Reannulation. *Org. Chem. Front*. **2020**, *7*, 919. (c) Bagdi, A. K.; Hajra, A. Design, Synthesis, and Functionalization of Imidazoheterocycles. *Chem. Rec*. **2016**, *16*, 1868. (d) Shinde, V. N.; Roy, T. K.; Jaspal, S.; Nipate, D. S.; Meena, N.; Rangan, K.; Kumar, D.; Kumar, A. Rhodium(III)-Catalyzed Annulation of 2-Arylimidazo[1,2-*a*]pyridines with Maleimides: Synthesis of 1H-Benzo[*e*]pyrido[1′,2′:1,2]imidazo[4,5-*g*]isoindole-1,3(2*H*)-Diones and their Photophysical Studies. *Adv. Synth. Catal*. **2020**, *362*, 5751. (e) Chary, D. Y.;

TH-3369_166122017

Reddy, K. N.; Sridhar, B.; Reddy, B. V. S. Ru(II) Catalyzed Dehydrogenative Annulation of 2-Arylimidazo[1,2-*a*]pyridines with maleimides. *Tetrahedron Lett.* **2021**, *66*, 152830. (f) Li, B.; Guo, C.; Shen, N.; Zhang, X.; Fan, X. Synthesis of Maleimide Fused Benzocarbazoles and Imidazo[1,2-*a*]pyridines via Rhodium(III)-Catalyzed [4 + 2] Oxidative Cycloaddition. *Org. Chem. Front.* **2020**, *7*, 3698.

16. (a) Tashrifi, Z.; Mohammadi-Khanaposhtani, M.; Larijani, B.; Mahdavi, M. C3-Functionalization of Imidazo[1,2-a]pyridines. *Eur. J. Org. Chem*. **2020**, 269. (b) Konwar, D.; Bora, U. Recent Developments in Transition-Metal-Catalyzed Regioselective Functionalization of Imidazo[1, 2-a]pyridine. *ChemistrySelect*. **2021**, *6*, 2716. (c) Guo, T.; Liang, J. -J.; Yang, S.; Chen, H.; Fu, Y. -N.; Han, S. -L.; Zhao, Y. -H. Palladium-Catalyzed Oxidative C-H/C-H Cross-Coupling of Imidazopyridines with Azoles. *Org. Biomol. Chem*. **2018**, *16*, 6039. (d) Lu, S.; Tian, L.-L.; Cui, T.-W.; Zhu, Y.-S.; Zhu, X.; Hao, X.-Q.; Song, M.-P. Copper-Mediated C–H Amination of Imidazopyridines with N-Fluorobenzenesulfonimide. *J. Org. Chem*. **2018**, *83*, 13991. (e) Wang, S.; Zhang, S.; Liu, M.; Zang, J.; Jiang, G.; Ji, F. Palladium-Catalyzed C3-selective C-H Oxidative Carbonylation of Imidazo[1,2-a]Pyridines with CO and Alcohols: A Way to Access Esters. *Org. Chem. Front*. **2020**, *7*, 697. (f) Kim, H.; Byeon, M.; Jeong, E.; Baek, Y.; Jeong, S. J.; Um, K.; Han, S. H.; Han, G. U.; Ko, G. H.; Maeng, C.; Son, J. Y.; Kim, D.; Kim, S. H.; Lee, K.; Lee, P. H. Rhodium (II)-Catalyzed Regioselective C3-Alkylation of 2-Arylimidazo [1,2-a] Pyridines with Aryl Diazoesters. *Adv. Synth. Catal*. **2019**, *361*, 2094. (g) Murugesan, T.; Elikkottil, A.; Kaliyamoorthy, A. Palladium-Catalyzed Regioselective C3-Allylic Alkylation of 2-Aryl Imidazopyridines with MBH Carbonates. *J. Org. Chem*. **2023**, *88*, 2655.
17. (a) Zhu, X.; Shen, X.-J.; Tian, Z.-Y.; Lu, S.; Tian, L.-L.; Liu, W.-B.; Song, B.; Hao, X.-Q. Rhodium-Catalyzed Direct Bis-cyanation of Arylimidazo[1,2-*a*]pyridine *via* Double C–H Activation. *J. Org. Chem*. **2017**, *82*, 6022. (b) Shakoor, S. M.; Kumari, A. S.; Khullar, S.; Mandal, S. K.; Kumar, A.; Sakhuja, R. Ruthenium(II)-Catalyzed Regioselective Ortho Amidation of Imidazo Heterocycles with Isocyanates. *J. Org. Chem*. **2016**, *81*, 12340. (c) Samanta, S.; Mondal, S.; Ghosh, D.; Hajra, A. Rhodium-Catalyzed Directed C–H Amidation of Imidazoheterocycles with Dioxazolones. *Org. Lett*. **2019**, *21*, 4905. (d) Liu, S.; Jiang, H.; Liu, W.; Zhu, X.; Hao, X.-Q.; Song, M.-P. Ruthenium-Catalyzed C(sp^2)–H Bond Bisallylation with Imidazopyridines as Directing Groups. *J. Org. Chem*. **2020**, *85*, 15167. (e) Jahan, K.; Salim, S. A.; Bharatam, P. V. Ruthenium(II) Catalysed Regioselective C-2′-Alkenylation of 2-Phenylimidazo[1,2-a]pyridine-3-carbaldehydes. *Tetrahedron*. **2022**, *122*, 132956.

TH-3369_166122017

18. (a) Li, P.; Zhang, X.; Fan, X. Synthesis of naphtho[1′,2′:4,5]imidazo[1,2-a]pyridines and imidazo[5,1,2-cd]indolizines through Pd-catalyzed cycloaromatization of 2-phenylimidazo[1,2-a]pyridines with alkynes. *J. Org. Chem*. **2015**, *80*, 7508. (b) Qi, Z.; Yu, S.; Li, X. Rh(III)-catalyzed oxidative annulation of 2-phenylimidazo[1,2-a]pyridines with alkynes: Mono versus double C–H activation. *J. Org. Chem*. **2015**, *80*, 3471. (c) Li, B.; Shen, N.; Yang, Y.; Zhang, X.; Fan, X. Synthesis of naphtho[1′,2′:4,5]imidazo[1,2-a]pyridines via Rh(III)-catalyzed C-H functionalization of 2-arylimidazo[1,2-a]pyridines with cyclic 2-diazo-1,3-diketones featuring with a ring opening and reannulation. *Org. Chem. Front*. **2020**, *7*, 919. (d) Reddy, K. N.; Chary, D. Y.; Sridhar, B.; Reddy, B. V. S. Rh(III)-catalyzed tandem bicyclization of 2-arylimidazo[1,2-a]pyridines with cyclic enones for the construction of bridged scaffolds. *Org. Lett*. **2019**, *21*, 8548. (e) Xue, C.; Han, J.; Zhao, M.; Wang, L. Rapid construction of fused heteropolycyclic aromatics via palladium-catalyzed domino arylations of imidazopyridine derivatives. *Org. Lett*. **2019**, *21*, 4402. (f) Ghosh, K.; Nishii, Y.; Miura, M. Oxidative C-H/C-H annulation of imidazopyridines and indazoles through rhodium-catalyzed vinylene transfer. *Org. Lett*. **2020**, *22*, 3547.

19. (a) Kavitha, K.; Praveena, K. S. S.; Ramarao, E. V. V. S.; Murthy, N. Y. S.; Pal, S. Chemistry of Cyclic Imides: An Overview on the Past, Present and Future. *Curr. Org. Chem*. **2016**, *20*, 1955. (b) Xie, Y.-J.; Husband, J. T.; Sucarrat, M. T.; Yang, H.; Liu, W.-S.; O'Reilly, R. K. Rational Design of Substituted Maleimide Dyes with Tunable Fluorescence and Solvafluorochromism. *Chem. Commun*. **2018**, *54*, 3339.

20. Manoharan, R.; Jeganmohan, M. Alkylation, Annulation, and Alkenylation of Organic Molecules with Maleimides by Transition-Metal-Catalyzed C-H Bond Activation. *Asian J. Org. Chem*. **2019**, *8*, 1949.

21. (a) Bettadapur, K. R.; Lanke. V.; Prabhu, K. R. Ru (II)-Catalyzed C–H Activation: Ketone-Directed Novel 1,4-Addition of Ortho C–H Bond to Maleimides. *Org. Lett*. **2015**, *17*, 4658. (b) Han, S.; Park, J.; Kim, S.; Lee, S. H.; Sharma, S.; Mishra, N. K. Y.; Jung, H.; Kim, I. Rhodium(III)-Catalyzed C(sp3)–H Alkylation of 8-Methylquinolines with Maleimides. *Org. Lett*. **2016**, *18*, 4666. (c) Ghosh, A. K.; Samanta, S.; Ghosh, P.; Neogia, S.; Hajra, A. Regioselective Hydroarylation and Arylation of Maleimides with Indazoles via a Rh(III)-Catalyzed C–H Activation. *Org. Biomol. Chem*. **2020**, *18*, 3093.

22. (a) Zhou, B.; Ma, P.; Chen, H.; Wang, C. Amine-Accelerated Manganese-Catalyzed Aromatic C–H Conjugate Addition to α,β-Unsaturated Carbonyls. *Chem. Commun.* **2014**, *50*, 14558. (b) Liu, W.; Zell, D.; John, M.; Ackermann, L. Manganese-Catalyzed Synthesis of cis-β-Amino Acid Esters through Organometallic C–H Activation of Ketimines. *Angew. Chem. Int. Ed.* **2015**, *54*, 4092. (c)

TH-3369_166122017

Hu, Y.; Wang, C. Manganese-Catalyzed Bicyclic Annulations of Imines and α,β-Unsaturated Esters via C−H Activation. *Sci China Chem.* **2016**, *59*: 1301. (d) Wang, Z.; Wang, C. Manganese/NaOPh Co-Catalyzed C2-Selective C–H Conjugate Addition of Indoles to α,β-Unsaturated Carbonyls. *Green Synth.Catal*. **2021**, *2*, 66.

23. Liu, S.-L.; Li, Y.; Guo, J.-R.; Yang, G.-C.; Li, X.-H.; Gong, J.-F.; Song, M.-P. An Approach to 3-(Indol-2-yl)succinimide Derivatives by Manganese-Catalyzed C–H Activation. *Org. Lett*. **2017**, *19*, 4042.
24. Mandal, R.; Emayavaramban, B.; Sundararaju, B. Cp*Co(III)-Catalyzed C–H Alkylation with Maleimides Using Weakly Coordinating Carbonyl Directing Groups. *Org. Lett.* **2018**, *20*, 2835.
25. Liu, P.; Shen, Z.; Yuan, Y.; Sun, P. Synthesis of Symmetrical Methylene-Bridged Imidazoheterocycles using DMSO as Methylene Source under Metal-free Conditions. *Org. Biomol. Chem*. **2016**, *14*, 6523.
26. Shakoor, S. M. A.; Agarwal, D. S.; Khullar, S.; Mandal, S. K.; Sakhuja, R. Solvent-Driven Iodine-Mediated Oxidative Strategies for the Synthesis of Bis(imidazo[1,2-a]pyridin-3-yl)sulfanes and Disulfanes. *Chem. Asian J*. **2017**, *12*, 3061.
27. Liu, S.; Jiang, H.; Liu, W.; Zhu, X.; Hao, X.-Q.; Song, M.-P. Ruthenium-Catalyzed C(sp^2)–H Bond Bisallylation with Imidazopyridines as Directing Groups. *J. Org. Chem*. **2020**, *85*, 15167.

III.7. Spectral Data

1-Phenyl-3-(2-phenylimidazo[1,2-*a*]pyridin-3-yl)pyrrolidine-2,5-dione (**3aa**)

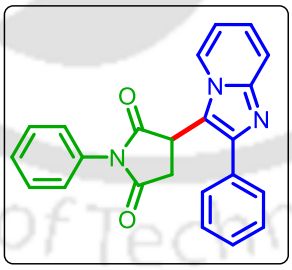

Light brown solid (75 mg, 68% yield); mp 238–240 °C; purified over a column of silica gel (45% EtOAc in hexane); ^{1}H NMR (DMSO-d_6, 600 MHz): δ 8.29 (d, J = 7.2 Hz, 1H), 7.69 (d, J = 9.6 Hz, 1H), 7.67 (d, J = 7.8 Hz, 2H), 7.54 – 7.50 (m, 4H), 7.46 – 7.43 (m, 2H), 7.38 – 7.35 (m, 3H), 7.03 (t, J = 6.6 Hz, 1H), 5.28 (dd, J = 9.6, 7.2 Hz, 1H), 3.44 (dd, J = 18.0, 10.2 Hz, 1H), 3.21 (dd, J = 18.0, 7.2 Hz, 1H); ^{13}C{^{1}H} NMR (DMSO-d_6, 151 MHz): δ 175.1, 174.4, 144.8, 144.4, 134.2, 132.4, 128.9, 128.6, 128.5, 128.0, 127.2, 125.0, 124.7, 117.2, 114.8, 112.9, 36.9, 33.5; IR (KBr, cm^{-1}): 2922, 2853, 1589,

TH-3369_166122017

1487, 1391, 1258, 1146, 1025, 763, 631; HRMS (ESI-TOF) calcd for $C_{23}H_{18}N_3O_2$ $[M + H]^+$ 368.1394, found 368.1400.

3-(2-(4-Methoxyphenyl)imidazo[1,2-*a*]pyridin-3-yl)-1-phenylpyrrolidine-2,5-dione (**3ba**)

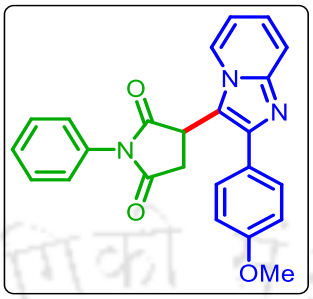

Brown solid (83 mg, 70% yield); mp 190–193 °C; purified over a column of silica gel (50% EtOAc in hexane); ^{1}H NMR ($CDCl_3$, 400 MHz): δ 7.82 (d, J = 6.8 Hz, 1H), 7.70 (d, J = 9.2 Hz, 1H), 7.55 (d, J = 8.8 Hz, 2H), 7.50 (t, J = 7.6 Hz, 2H), 7.43 (t, J = 7.4 Hz, 1H), 7.31 – 7.23 (m, 3H), 6.99 (d, J = 8.8 Hz, 2H), 6.88 (t, J = 6.8 Hz, 1H), 4.85 (dd, J = 10.0, 6.4 Hz, 1H), 3.84 (s, 3H), 3.27 (dd, J = 18.8, 10.4 Hz, 1H), 3.07 (dd, J = 18.8, 6.4 Hz, 1H). ^{13}C{^{1}H} NMR ($CDCl_3$, 101 MHz): δ 174.8, 174.0, 160.1, 146.0, 145.3, 131.7, 130.3, 129.4, 129.1, 126.5, 126.3, 124.9, 122.6, 118.4, 114.5, 113.9, 113.3, 55.5, 37.0, 33.5; IR (neat, cm^{-1}): 2922, 1779, 1700, 1596, 1385, 1184, 1084, 795, 746, 692; HRMS (ESI-TOF) calcd for $C_{24}H_{20}N_3O_3$ $[M + H]^+$ 398.1499, found 398.1503.

3-(2-(4-Fluorophenyl)imidazo[1,2-*a*]pyridin-3-yl)-1-phenylpyrrolidine-2,5-dione (**3ca**)

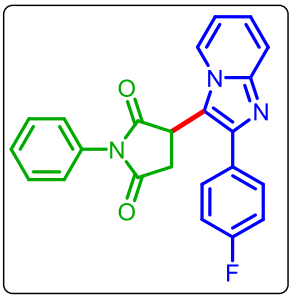

A light brown solid (73 mg, 63% yield); mp 200–202 °C; purified over a column of silica gel (45% EtOAc in hexane); ^{1}H NMR ($CDCl_3$, 500 MHz): δ 7.82 (d, J = 7.0 Hz, 1H), 7.72 (d, J = 9.0 Hz, 1H), 7.63 (t, J = 6.3 Hz, 2H), 7.52 (t, J = 7.5 Hz, 2H), 7.44 (t, J = 7.3 Hz, 1H), 7.32 – 7.26 (m, 3H), 7.17 (t, J = 8.0 Hz, 2H), 6.92 (t, J = 6.5 Hz, 1H), 4.85 (dd, J = 9.8, 6.8 Hz, 1H), 3.31 (dd, J = 18.8, 10.3 Hz, 1H), 3.08 (dd, J = 18.8, 6.3 Hz, 1H); ^{13}C {^{1}H} NMR ($CDCl_3$, 126 MHz): δ 174.6, 173.8, 164.2 (d, J = 249.3 Hz), 145.5 (d, J = 3.3 Hz), 131.8, 130.9 (d, J = 8.2 Hz), 130.3 (d, J = 3.5 Hz), 129.5, 129.20, 126.3, 125.2, 122.7, 118.7, 116.2, 115.9, 114.3, 113.6, 37.0, 33.5; ^{19}F NMR ($CDCl_3$) δ -112.8 (s); IR

TH-3369_166122017

(neat, cm^{-1}): 3540, 2923, 1776, 1702, 1499, 1390, 1188, 847, 729, 693; HRMS (ESI-TOF) calcd for $C_{23}H_{17}FN_3O_2$ $[M + H]^+$ 386.1299, found 386.1304.

3-(2-(4-Chlorophenyl)imidazo[1,2-*a*]pyridin-3-yl)-1-phenylpyrrolidine-2,5-dione (3da)

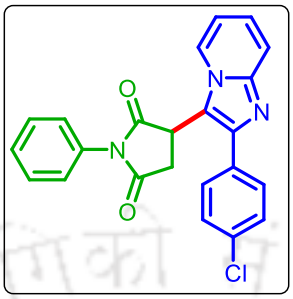

Brown solid (79 mg, 66% yield); mp 170–172 °C; purified over a column of silica gel (45% EtOAc in hexane); ^{1}H NMR ($CDCl_3$, 400 MHz): δ 7.80 (d, J = 7.2 Hz, 1H), 7.73 (d, J = 9.2 Hz, 1H), 7.58 (d, J = 8.4 Hz, 2H), 7.51 (t, J = 7.6 Hz, 2H), 7.45 (d, J = 7.6 Hz, 3H), 7.30 (d, J = 7.6 Hz, 3H), 6.91 (t, J = 6.8 Hz, 1H), 4.85 (dd, J = 10.0, 6.4 Hz, 1H), 3.30 (dd, J = 18.6, 10.2 Hz, 1H), 3.07 (dd, J = 18.8, 6.4 Hz, 1H).^{13}C {^{1}H} NMR ($CDCl_3$, 101 MHz): δ 174.5, 173.8, 145.5, 145.1, 134.9, 132.6, 131.6, 130.4, 129.5, 129.4, 129.2, 129.2, 126.4, 126.2, 125.3, 122.7, 118.7, 114.5, 113.7, 36.9, 33.4; IR (neat, cm^{-1}): 2962, 2922, 1778, 1702, 1595, 1497, 1389, 1260, 1183, 1093, 692; HRMS (ESI-TOF) calcd for $C_{23}H_{17}ClN_3O_2$ $[M + H]^+$ 402.1004, found 402.1008.

3-(2-([1,1'-Biphenyl]-4-yl)imidazo[1,2-a]pyridin-3-yl)-1-phenylpyrrolidine-2,5-dione (3ea)

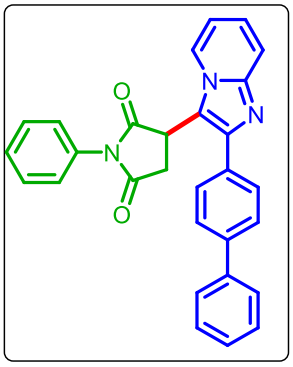

A brown solid (73 mg, 55% yield); mp 110–112 °C; purified over a column of silica gel (45% EtOAc in hexane); ^{1}H NMR ($CDCl_3$, 500 MHz): δ 7.85 (d, J = 7.0 Hz, 1H), 7.76 (d, J = 9.0 Hz, 1H), 7.71 (brs, 3H), 7.64 (d, J = 7.5 Hz, 2H), 7.51 – 7.36 (m, 8H), 7.31 (d, J = 7.5 Hz, 2H), 6.94 (t, J = 7.0 Hz, 1H), 4.94 (dd, J = 10.3, 6.8 Hz, 1H), 3.36 (dd, J = 18.8, 10.3 Hz, 1H), 3.15 (dd, J = 18.5, 6.5 Hz, 1H); ^{13}C {^{1}H} NMR ($CDCl_3$, 126 MHz): δ 174.6, 173.9, 145.9, 145.5, 141.6, 140.6, 132.9, 131.8, 129.53, 129.51, 129.2, 129.0, 127.7, 127.3, 126.6, 126.3, 125.2, 122.7, 118.7, 114.5, 113.6, 37.1, 33.7; IR (neat,

TH-3369_166122017

cm^{-1}): 2924, 2196, 1779, 1705, 1597, 1496, 1383, 1172, 933, 694; HRMS (ESI-TOF) calcd for $C_{29}H_{22}N_3O_2$ $[M + H]^+$ 444.1707, found 444.1720.

1-Phenyl-3-(2-(*m*-tolyl)imidazo[1,2-*a*]pyridin-3-yl)pyrrolidine-2,5-dione (**3fa**)

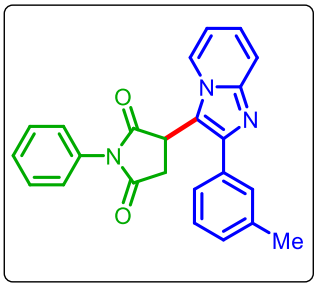

Light brown solid (82 mg, 72% yield); mp 210–212 °C; purified over a column of silica gel (45% EtOAc in hexane); ^{1}H NMR (DMSO-d_6, 400 MHz): δ 8.30 (d, J = 7.2 Hz, 1H), 7.68 (d, J = 9.2 Hz, 1H), 7.53 (t, J = 7.4 Hz, 2H), 7.49 (s, 1H), 7.45 (d, J = 7.2 Hz, 2H), 7.42 – 7.34 (m, 4H), 7.25 (d, J = 7.6 Hz, 1H), 7.03 (t, J = 6.6 Hz, 1H), 5.29 (dd, J = 9.8, 7.0 Hz, 1H), 3.44 (dd, J = 18.0, 10.0 Hz, 1H), 3.19 (dd, J = 18.0, 7.2 Hz, 1H), 2.38 (s, 3H).^{13}C {^{1}H} NMR (DMSO-d_6, 101 MHz): δ 175.1, 174.4, 144.8, 144.3, 137.9, 134.2, 132.4, 129.1, 128.9, 128.7, 128.53, 128.50, 127.1, 125.6, 125.0, 124.6, 117.1, 114.8, 112.9, 36.8, 33.5, 21.1; IR (neat, cm^{-1}): 2923, 2854, 1781, 1702, 1498, 1389, 1181, 1015, 794, 740, 694; HRMS (ESI-TOF) calcd for $C_{24}H_{20}N_3O_2$ $[M + H]^+$ 382.1550, found 382.1561.

3-(2-(3-Chlorophenyl)imidazo[1,2-*a*]pyridin-3-yl)-1-phenylpyrrolidine-2,5-dione (**3ga**)

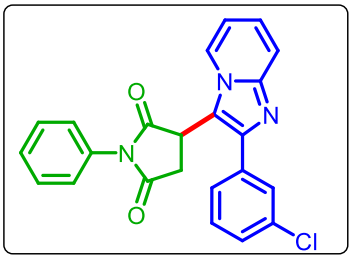

A light yellow solid (71 mg, 59% yield); mp 175–177 °C; purified over a column of silica gel (40% EtOAc in hexane); ^{1}H NMR ($CDCl_3$, 500 MHz): δ 7.83 (d, J = 7.0 Hz, 1H), 7.72 (d, J = 9.0 Hz, 1H), 7.66 (s, 1H), 7.52 – 7.47 (m, 3H), 7.44 (d, J = 7.5 Hz, 1H), 7.40 (d, J = 4.5 Hz, 2H), 7.34 (d, J = 8.0 Hz, 2H), 7.30 – 7.27 (m, 1H), 6.92 (t, J = 6.8 Hz, 1H), 4.87 (dd, J = 10.0, 6.5 Hz, 1H), 3.31 (dd, J = 18.7, 10.2 Hz, 1H), 3.07 (dd, J = 18.7, 6.2 Hz, 1H); ^{13}C {^{1}H} NMR ($CDCl_3$, 126 MHz): δ 174.5, 173.7, 145.5, 144.9, 136.0, 135.0, 131.7, 130.2, 129.5, 129.19, 129.18, 128.9, 127.2, 126.3, 125.29, 122.8,

TH-3369_166122017

118.8, 114.6, 113.7, 37.0, 33.4; IR (neat, cm^{-1}): 2957, 2918, 1782, 1707, 1582, 1488, 1387, 1252, 1179, 1076, 686; HRMS (ESI-TOF) calcd for $C_{23}H_{17}ClN_3O_2$ $[M + H]^+$ 402.1004, found 402.1008.

3-(2-(2-Methoxyphenyl)imidazo[1,2-*a*]pyridin-3-yl)-1-phenylpyrrolidine-2,5-dione (3ha)

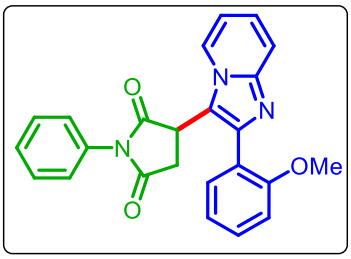

A brown solid (76 mg, 64% yield); mp 185–187 °C; purified over a column of silica gel (50% EtOAc in hexane); ^1H NMR ($CDCl_3$, 500 MHz): δ 8.01 (d, J = 6.5 Hz, 1H), 7.70 (d, J = 9.0 Hz, 1H), 7.60 (d, J = 7.5 Hz, 1H), 7.44 (t, J = 7.5 Hz, 2H), 7.41 – 7.35 (m, 2H), 7.22 (d, J = 7.5 Hz, 3H), 7.10 (t, J = 7.5 Hz, 1H), 6.96 (d, J = 8.5 Hz, 1H), 6.89 (t, J = 6.8 Hz, 1H), 4.66 – 4.63 (m, 1H), 3.65 (s, 3H), 3.22 – 3.09 (m, 2H); ^{13}C {^1H} NMR ($CDCl_3$, 126 MHz): δ 174.6, 174.5, 156.9, 145.1, 140.8, 132.3, 131.9, 130.4, 129.2, 128.7, 126.1, 124.7, 123.6, 122.7, 121.7, 118.2, 115.9, 113.1, 111.8, 56.3, 37.4, 32.9; IR (neat, cm^{-1}): 3540, 2923, 1776, 1702, 1499, 1390, 1188, 847, 729, 693; HRMS (ESI-TOF) calcd for $C_{24}H_{20}N_3O_3$ $[M + H]^+$ 398.1499, found 398.1503.

3-(2-(2-Fluorophenyl)imidazo[1,2-*a*]pyridin-3-yl)-1-phenylpyrrolidine-2,5-dione (3ia)

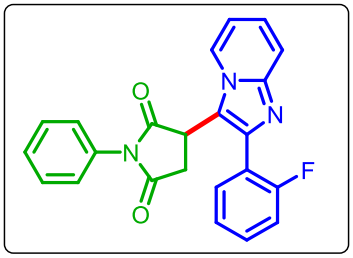

A light yellow solid (62 mg, 54% yield); mp 195–197 °C; purified over a column of silica gel (40% EtOAc in hexane); ^1H NMR ($CDCl_3$+DMSO-d_6, 500 MHz): δ 8.56 (d, J = 7.0 Hz, 1H), 8.20 (t, J = 6.8 Hz, 1H), 8.16 (d, J = 9.0 Hz, 1H), 7.95 (t, J = 7.5 Hz, 2H), 7.89 (d, J = 6.5 Hz, 2H), 7.79 – 7.73 (m, 4H), 7.64 – 7.60 (m, 1H), 7.43 (t, J = 6.7 Hz, 1H), 5.30 (dd, J = 10.0, 6.0 Hz, 1H), 3.83 (dd, J = 18.5, 10.0 Hz, 1H), 3.56 (dd, J = 18.5, 6.0 Hz, 1H); ^{13}C {^1H} NMR ($CDCl_3$+DMSO-d_6, 126 MHz): δ 174.1, 174.0, 159.5 (d, J = 245.3 Hz), 145.1, 138.3, 132.0, 131.9, 131.7, 130.3 (d, J = 8.3 Hz), 128.9, 128.5, 126.2, 124.8, 124.7, 124.6, 122.9, 122.0 (d, J = 14.6 Hz), 117.9, 115.9, 115.4 (d, J = 22.1 Hz), 113.0, 36.9, 32.8; ^{19}F NMR ($CDCl_3$+DMSO-d_6) δ -115.9 (s); IR (neat, cm^{-1}): 2962, 2921, 1782, 1705, 1520, 1385, 1192, 855, 685; HRMS (ESI-TOF) calcd for $C_{23}H_{17}FN_3O_2$ $[M + H]^+$ 386.1299, found 386.1304.

TH-3369_166122017

3-(7-Methyl-2-phenylimidazo[1,2-*a*]pyridin-3-yl)-1-phenylpyrrolidine-2,5-dione (**3ja**)

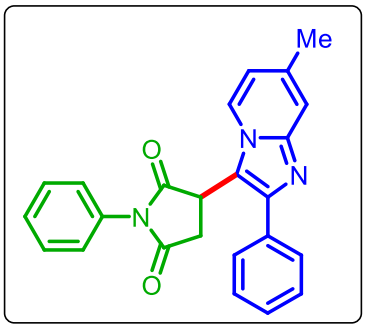

Brown solid (83 mg, 73% yield); mp 196–198 °C; purified over a column of silica gel (45% EtOAc in hexane); ^{1}H NMR (DMSO-d_6, 400 MHz): δ 8.16 (d, J = 7.2 Hz, 1H), 7.65 (d, J = 7.2 Hz, 2H), 7.50 (q, J = 7.6 Hz, 4H), 7.43 (t, J = 8.0 Hz, 3H), 7.36 (d, J = 7.2 Hz, 2H), 6.85 (d, J = 7.2 Hz, 1H), 5.23 (dd, J = 10.0, 7.2 Hz, 1H), 3.44 – 3. 39 (m, 1H), 3.14 (dd, J = 18.2, 7.0 Hz, 1H), 2.40 (s, 3H).^{13}C {^{1}H} NMR (DMSO-d_6 + $CDCl_3$, 151 MHz): δ 175.1, 174.3, 144.8, 144.4, 135.5, 134.3, 132.4, 128.8, 128.5, 128.4, 127.8, 127.1, 123.9, 119.2, 115.4, 115.3, 114.1, 36.8, 33.5, 20.7; IR (neat, cm^{-1}): 3059, 2918, 1702, 1646, 1499, 1385, 1174, 766, 737, 694, 620; HRMS (ESI-TOF) calcd for $C_{24}H_{20}N_3O_2$ [M + H]$^{+}$ 382.1550, found 382.1559.

3-(2-(Benzo[*d*][1,3]dioxol-5-yl)imidazo[1,2-*a*]pyridin-3-yl)-1-phenylpyrrolidine-2,5-dione (**3ka**)

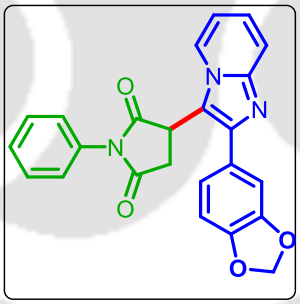

A black solid (77 mg, 63% yield); mp 101–103 °C; purified over a column of silica gel (50% EtOAc in hexane); ^{1}H NMR ($CDCl_3$, 400 MHz): δ 7.84 (d, J = 6.4 Hz, 1H), 7.70 (d, J = 6.8 Hz, 1H), 7.51 (t, J = 7.4 Hz, 2H), 7.43 (t, J = 7.4 Hz, 2H), 7.33 (d, J = 8.0 Hz, 2H), 7.13 (s, 1H), 7.06 (d, J = 6.8 Hz, 1H), 6.90 (t, J = 6.6 Hz, 2H), 6.01 (s, 2H), 4.87 (dd, J = 9.2, 6.8 Hz, 1H), 3.28 (dd, J = 18.4, 10.0 Hz, 1H), 3.07 (dd, J = 18.6, 6.2 Hz, 1H); ^{13}C {^{1}H} NMR ($CDCl_3$, 126 MHz): δ 174.8, 173.9, 148.3, 148.2, 145.9, 145.2, 131.8, 129.45, 129.1, 128.0, 126.4, 125.0, 122.8, 122.7, 118.5, 114.0, 113.4, 109.5, 108.8, 101.5, 37.0, 33.4; IR (neat, cm^{-1}): 2921, 1776, 1703, 1498, 1383, 1172, 1035, 908, 731, 693; HRMS (ESI-TOF) calcd for $C_{24}H_{18}N_3O_4$ [M + H]$^{+}$ 412.1292, found 412.1301.

TH-3369_166122017

1-Phenyl-3-(2-(thiophen-2-yl)imidazo[1,2-*a*]pyridin-3-yl)pyrrolidine-2,5-dione (3la)

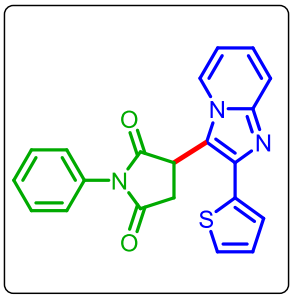

Black solid (60 mg, 54% yield); mp 155–157 °C; purified over a column of silica gel (45% EtOAc in hexane); ^{1}H NMR ($CDCl_3$, 500 MHz): δ 7.80 (d, J = 6.5 Hz, 1H), 7.70 (d, J = 9.0 Hz, 1H), 7.51 (t, J = 7.5 Hz, 2H), 7.45 – 7.43 (m, 2H), 7.33 (t, J = 7.5 Hz, 3H), 7.27 – 7.24 (m, 2H), 7.14 – 7.12 (m, 1H), 6.89 (t, J = 6.5 Hz, 1H), 5.00 – 4.97 (m, 1H), 3.35 (dd, J = 18.5, 10.0 Hz, 1H), 3.11 (dd, J = 18.5, 6.5 Hz, 1H); ^{13}C {^{1}H} NMR ($CDCl_3$, 126 MHz): δ 174.2, 173.9, 145.5, 139.8, 136.0, 131.8, 129.5, 129.2, 127.9, 127.2, 126.8, 126.4, 125.4, 122.7, 118.6, 114.4, 113.6, 37.0, 33.6; IR (neat, cm^{-1}): 3375, 2964, 1702, 1496, 1384, 1259, 1181, 1023, 1001, 749, 696; HRMS (ESI-TOF) calcd for $C_{21}H_{16}N_3O_2S$ [M + H]$^{+}$ 374.0958, found 374.0961.

1-Phenyl-3-(6-phenylimidazo[2,1-*b*]thiazol-5-yl)pyrrolidine-2,5-dione (3ma)

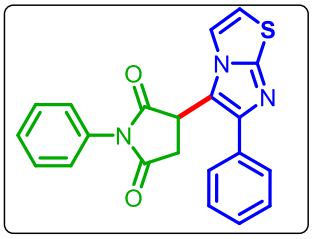

Off-white solid (76 mg, 68% yield); mp 230–232 °C; purified over a column of silica gel (45% EtOAc in hexane); ^{1}H NMR ($CDCl_3$, 400 MHz): δ 7.62 (d, J = 7.2 Hz, 2H), 7.52 (t, J = 7.6 Hz, 2H), 7.47 – 7.37 (m, 4H), 7.32 (d, J = 7.6 Hz, 2H), 7.22 (d, J = 4.4 Hz, 1H), 6.94 (t, J = 4.8 Hz, 1H), 4.75 (dd, J = 10.4, 6.0 Hz, 1H), 3.32 (dd, J = 18.8, 10.4 Hz, 1H), 3.01 (dd, J = 18.8, 6.0 Hz, 1H).^{13}C {^{1}H} NMR ($CDCl_3$, 101 MHz): δ 174.7, 173.9, 149.9, 147.4, 134.1, 131.7, 129.5, 129.2, 128.9, 128.6, 128.4, 126.3, 116.6, 116.3, 114.1, 37.8, 34.5; IR (neat, cm^{-1}): 3108, 1700, 1497, 1464, 1385, 1173, 1129, 774, 753, 698, 663. HRMS (ESI-TOF) calcd for $C_{21}H_{16}N_3O_2S$ [M + H]$^{+}$ 374.0958, found 374.0958.

TH-3369_166122017

1-Phenyl-3-(2-phenylbenzo[*d*]imidazo[2,1-*b*]thiazol-3-yl)pyrrolidine-2,5-dione (**3na**)

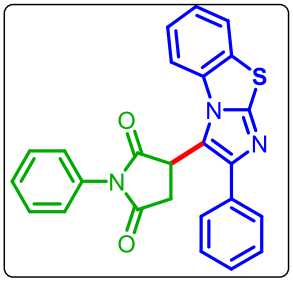

A pale yellow solid (71 mg, 56% yield); mp 141–143 °C; purified over a column of silica gel (45% EtOAc in hexane); ^{1}H NMR ($CDCl_3$, 600 MHz): δ 7.75 (d, J = 7.8 Hz, 1H), 7.67 – 7.40 (m, 10H), 7.36 (t, J = 7.5 Hz, 2H), 7.27 – 7.25 (m, 1H), 5.06 – 5.03 (m, 1H), 3.34 (dd, J = 18.6, 10.2 Hz, 1H), 3.11 (br s, 1H); ^{13}C {^{1}H} NMR ($CDCl_3$, 126 MHz): δ 174.7, 173.6, 132.8, 131.8, 130.7, 129.5, 129.3, 129.1, 129.0, 128.9, 128.7, 128.6, 126.6, 126.4, 126.2, 125.1, 125.0, 112.3, 37.9, 35.3; IR (neat, cm^{-1}): 2923, 1784, 1705, 1496, 1376, 1167, 738, 694, 494; HRMS (ESI-TOF) calcd for $C_{25}H_{18}N_3O_2S$ $[M + H]^+$ 424.1114, found 424.1130.

3-(2-(4-(Methylsulfonyl)phenyl)imidazo[1,2-*a*]pyridin-3-yl)-1-phenylpyrrolidine-2,5-dione (**3oa**)

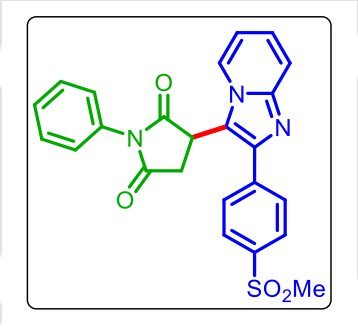

Light brown solid (73 mg, 55% yield); mp 230–232 °C; purified over a column of silica gel (50% EtOAc in hexane); ^{1}H NMR ($CDCl_3$, 400 MHz): δ 8.04 (d, J = 8.0 Hz, 2H), 7.89 (d, J = 8.4 Hz, 2H), 7.80 (d, J = 6.8 Hz, 1H), 7.75 (d, J = 9.2 Hz, 1H), 7.52 (t, J = 7.6 Hz, 2H), 7.46 (d, J = 6.8 Hz, 1H), 7.34 – 7.31 (m, 3H), 6.96 (t, J = 6.8 Hz, 1H), 4.93 (dd, J = 10.2, 6.6 Hz, 1H), 3.36 (dd, J = 18.8, 10.4 Hz, 1H), 3.14 – 3.06 (m, 4H).^{13}C {^{1}H} NMR ($CDCl_3$, 101 MHz): δ 174.3, 173.5, 145.7, 144.4, 140.4, 139.7, 131.6, 129.9, 129.6, 129.3, 128.0, 126.2, 125.7, 122.9, 118.9, 115.3, 114.1, 44.7, 37.1, 33.3; IR (neat, cm^{-1}): 2921, 1704, 1597, 1498, 1384, 1311, 1184, 1145, 958, 843, 736; HRMS (ESI-TOF) calcd for $C_{24}H_{20}N_3O_4S$ $[M + H]^+$ 446.1169, found 446.1168.

TH-3369_166122017

1-Benzyl-3-(2-phenylimidazo[1,2-*a*]pyridin-3-yl)pyrrolidine-2,5-dione (**3ab**)

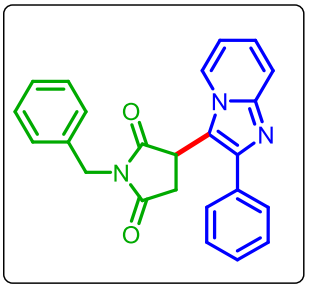

Gray solid (74 mg, 65% yield); mp 161–163 °C; purified over a column of silica gel (45% EtOAc in hexane); ^{1}H NMR ($CDCl_3$, 500 MHz): δ 7.64 (d, J = 9.0 Hz, 1H), 7.52 – 7.47 (m, 4H), 7.35 (br s, 7H), 7.17 (t, J = 7.8 Hz, 1H), 6.60 (t, J = 6.8 Hz, 1H), 4.77 (s, 2H), 4.71 (dd, J = 10.0, 6.0 Hz, 1H), 3.08 (dd, J = 19.0, 10.0 Hz, 1H), 2.82 (dd, J = 18.5, 6.0 Hz, 1H); ^{13}C {^{1}H} NMR ($CDCl_3$, 151 MHz): δ 175.4, 174.6, 145.9, 145.2, 135.4, 133.7, 129.4, 128.9, 128.9, 128.8, 128.5, 128.5, 124.9, 122.7, 118.3, 114.1, 113.1, 43.1, 36.7, 33.0; IR (neat, cm^{-1}): 2933, 1692, 1634, 1497, 1394, 1345, 1163, 1080, 910, 730, 635; HRMS (ESI-TOF) calcd for $C_{24}H_{20}N_3O_2$ $[M + H]^+$ 382.1550, found 382.1557.

1-Methyl-3-(2-phenylimidazo[1,2-*a*]pyridin-3-yl)pyrrolidine-2,5-dione (**3ac**)

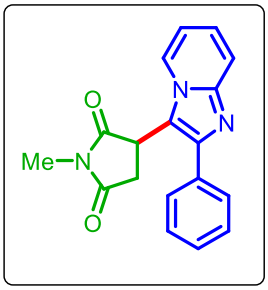

Off-white solid (69 mg, 75% yield); mp 112–114 °C; purified over a column of silica gel (40% EtOAc in hexane); ^{1}H NMR ($CDCl_3$, 500 MHz): δ 7.70 (d, J = 9.5 Hz, 1H), 7.63 (d, J = 7.0 Hz, 1H), 7.58 (d, J = 8.5 Hz, 2H), 7.45 (t, J = 7.5 Hz, 2H), 7.41 (t, J = 7.0 Hz, 1H), 7.27 – 7.23 (m, 1H), 6.86 (t, J = 6.8 Hz, 1H), 4.73 (dd, J = 10.0, 6.0 Hz, 1H), 3.17 – 3.10 (m, 4H), 2.92 (dd, J = 18.8, 6.3 Hz, 1H); ^{13}C {^{1}H} NMR ($CDCl_3$, 126 MHz): δ 175.7, 174.9, 146.3, 145.4, 134.1, 129.0, 128.8, 128.6, 124.8, 122.7, 118.6, 114.2, 113.3, 36.9, 33.4, 25.5; IR (neat, cm^{-1}): 3315, 2928, 1777, 1691, 1434, 1383, 1281, 1116, 959, 698, 625; HRMS (ESI-TOF) calcd for $C_{18}H_{16}N_3O_2$ $[M + H]^+$ 306.1237, found 306.1237.

TH-3369_166122017

1-Ethyl-3-(2-phenylimidazo[1,2-*a*]pyridin-3-yl)pyrrolidine-2,5-dione (**3ad**)

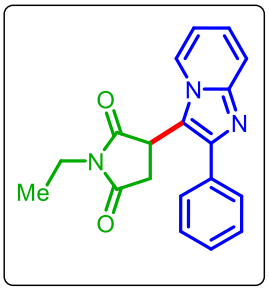

Brown solid (70 mg, 73% yield); mp 140–142 °C; purified over a column of silica gel (40% EtOAc in hexane); ^{1}H NMR ($CDCl_3$, 400 MHz): δ 7.69 (d, J = 9.2 Hz, 1H), 7.65 (d, J = 6.8 Hz, 1H), 7.58 (d, J = 6.8 Hz, 2H), 7.46 – 7.37 (m, 3H), 7.24 (t, J = 7.8 Hz, 1H), 6.85 (t, J = 6.8 Hz, 1H), 4.71 (dd, J = 10.0, 6.4 Hz, 1H), 3.70 – 7.64 (m, 2H), 3.10 (dd, J = 18.6, 10.2 Hz, 1H), 2.88 (dd, J = 18.6, 6.2 Hz, 1H), 1.27 – 1.24 (m, 3H).^{13}C {^{1}H} NMR ($CDCl_3$, 151 MHz): δ 175.5, 174.7, 146.0, 145.2, 133.9, 128.9, 128.8, 128.5, 124.8, 122.6, 118.4, 114.2, 113.2, 36.8, 34.4, 33.2, 13.0; IR (neat, cm^{-1}) 2939, 1771, 1687, 1502, 1442, 1401, 1347, 1222, 1124, 753, 678; HRMS (ESI-TOF) calcd for $C_{19}H_{18}N_3O_2$ $[M + H]^+$ 320.1394, found 320.1394.

3-(2-Phenylimidazo[1,2-*a*]pyridin-3-yl)-1-propylpyrrolidine-2,5-dione (**3ae**)

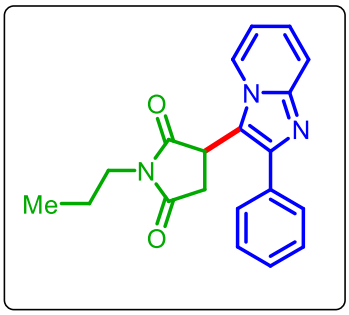

Gray solid (69 mg, 69% yield); mp 142–145 °C; purified over a column of silica gel (40% EtOAc in hexane); ^{1}H NMR ($CDCl_3$, 400 MHz): δ 7.69 (d, J = 9.2 Hz, 1H), 7.64 (d, J = 7.2 Hz, 1H), 7.59 (d, J = 6.8 Hz, 2H), 7.46 – 7.37 (m, 3H), 7.24 (t, J = 8.0 Hz, 1H), 6.84 (t, J = 6.8 Hz, 1H), 4.72 (dd, J = 10.0, 6.4 Hz, 1H), 3.58 (t, J = 7.6 Hz, 2H), 3.10 (dd, J = 18.8, 10.0 Hz, 1H), 2.90 (dd, J = 18.6, 6.2 Hz, 1H), 1.72 – 1.63 (m, 2H), 0.97 (t, J = 7.4 Hz, 3H); ^{13}C {^{1}H} NMR ($CDCl_3$, 101 MHz): δ 175.7, 174.9, 146.1, 145.2, 134.0, 128.9, 128.8, 128.5, 124.8, 122.6, 118.5, 114.1, 113.2, 41.1, 36.8, 33.0, 21.1, 11.5; IR (neat, cm^{-1}): 2933, 1692, 1502, 1401, 1358, 1201, 1123, 776, 733, 698; HRMS (ESI-TOF) calcd for $C_{20}H_{20}N_3O_2$ $[M + H]^+$ 334.1550, found 334.1572.

TH-3369_166122017

1-Isobutyl-3-(2-phenylimidazo[1,2-*a*]pyridin-3-yl)pyrrolidine-2,5-dione (**3af**)

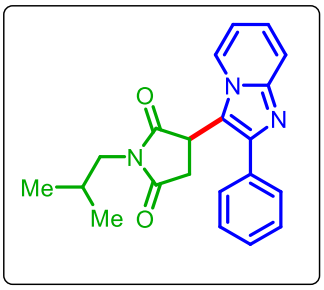

Pale yellow solid (74 mg, 71% yield); mp 163–165 °C; purified over a column of silica gel (40% EtOAc in hexane); ^{1}H NMR ($CDCl_3$, 400 MHz): δ 7.71 (d, J = 8.8 Hz, 1H), 7.66 (d, J = 6.8 Hz, 1H), 7.62 (d, J = 6.8 Hz, 2H), 7.48 – 7.39 (m, 3H), 7.26 – 7.23 (m, 1H), 6.86 (t, J = 6.8 Hz, 1H), 4.74 (dd, J = 10.0, 6.4 Hz, 1H), 3.46 (d, J = 7.2 Hz, 2H), 3.13 (dd, J = 18.4, 10.0 Hz, 1H), 2.96 (dd, J = 18.6, 6.6 Hz, 1H), 2.16 – 2.08 (m, 1H), 0.96 (dd, J = 6.8, 4.8 Hz, 6H).^{13}C {^{1}H} NMR ($CDCl_3$, 101 MHz): δ 175.9, 175.2, 146.4, 145.3, 134.1, 129.1, 128.9, 128.6, 124.9, 122.7, 118.6, 114.1, 113.3, 46.9, 36.9, 32.9, 27.4, 20.4, 20.4; IR (neat, cm^{-1}): 3523, 2931, 1689, 1502, 1400, 1358, 1203, 1130, 778, 732, 701, 624; HRMS (ESI-TOF) calcd for $C_{21}H_{22}N_3O_2$ $[M + H]^+$ 348.1707, found 348.1715.

1-Cyclohexyl-3-(2-phenylimidazo[1,2-*a*]pyridin-3-yl)pyrrolidine-2,5-dione (**3ag**)

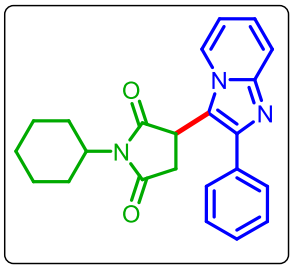

A brown solid (74 mg, 66% yield); mp 205–207 °C; purified over a column of silica gel (40% EtOAc in hexane); ^{1}H NMR ($CDCl_3$, 500 MHz): δ 7.71 (d, J = 9.0 Hz, 1H), 7.67 (d, J = 7.0 Hz, 1H), 7.61 (d, J = 7.5 Hz, 2H), 7.46 (t, J = 7.5 Hz, 2H), 7.41 (t, J = 7.5 Hz, 1H), 7.24 (d, J = 8.5 Hz, 1H), 6.86 (t, J = 6.8 Hz, 1H), 4.66 (dd, J = 10.0, 6.5 Hz, 1H), 4.15 – 4.10 (m, 1H), 3.06 (dd, J = 18.5, 10.0 Hz, 1H), 2.86 (dd, J = 18.5, 6.5 Hz, 1H), 2.26 – 2.20 (m, 2H), 1.89 – 1.86 (m, 1H), 1.70 – 1.67 (m, 3H) 1.38 – 1.23 (m, 4H); ^{13}C {^{1}H} NMR ($CDCl_3$, 101 MHz): δ 175.8, 175.1, 146.2, 145.3, 134.1, 129.1, 128.9, 128.6, 124.8, 122.7, 118.6, 114.5, 113.3, 52.7, 36.6, 32.9, 28.95, 28.90, 25.95, 25.94, 25.1; IR (neat, cm^{-1}): 2962, 2926, 1688, 1504, 1448, 1370, 1259, 1019, 796, 729, 698; HRMS (ESI-TOF) calcd for $C_{23}H_{24}N_3O_2$ $[M + H]^+$ 374.1863, found 374.1877.

TH-3369_166122017

3-(2-Phenylimidazo[1,2-*a*]pyridin-3-yl)-1-(*p*-tolyl)pyrrolidine-2,5-dione (3ah)

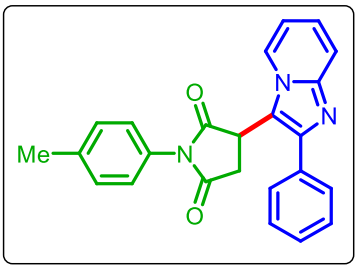

A light brown solid (79 mg, 69% yield); mp 143–145 ºC; purified over a column of silica gel (45% EtOAc in hexane); ^{1}H NMR ($CDCl_3$, 600 MHz): δ 7.82 (d, J = 7.2 Hz, 1H), 7.71 (d, J = 9.0 Hz, 1H), 7.63 (d, J = 7.8 Hz, 2H), 7.47 (t, J = 7.2 Hz, 2H), 7.42 (t, J = 7.2 Hz, 1H), 7.29 (d, J = 7.8 Hz, 2H), 7.26 (t, J = 7.5 Hz, 1H), 7.17 (d, J = 7.8 Hz, 2H), 6.89 (t, J = 6.6 Hz, 1H), 4.86 (dd, J = 10.2, 6.6 Hz, 1H), 3.26 (dd, J = 18.6, 10.2 Hz, 1H), 3.04 (dd, J = 18.6, 6.0 Hz, 1H), 2.39 (s, 3H); ^{13}C {^{1}H} NMR ($CDCl_3$, 151 MHz): δ 174.8, 174.1, 146.2, 145.3, 139.2, 134.1, 130.1, 129.0, 128.9, 128.7, 126.3, 126.1, 124.9, 122.7, 118.6, 114.4, 113.4, 36.9, 33.5, 21.3; IR (neat, cm^{-1}): 2922, 1779, 1703, 1513, 1386, 1270, 1173, 928, 728, 638; HRMS (ESI-TOF) calcd for $C_{24}H_{20}N_3O_2$ $[M + H]^+$ 382.1550, found 382.1560.

1-(4-Fluorophenyl)-3-(2-phenylimidazo[1,2-*a*]pyridin-3-yl)pyrrolidine-2,5-dione (3ai)

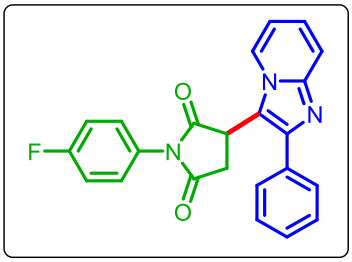

Brown solid (73 mg, 63% yield); mp 167–169 ºC; purified over a column of silica gel (45% EtOAc in hexane); ^{1}H NMR ($CDCl_3$, 500 MHz): δ 7.84 (d, J = 7.0 Hz, 1H), 7.73 (d, J = 9.0 Hz, 1H), 7.61 (d, J = 7.5 Hz, 2H), 7.48 – 7.41 (m, 3H), 7.28 (d, J = 8.5 Hz, 3H), 7.18 (t, J = 8.5 Hz, 2H), 6.92 (t, J = 6.8 Hz, 1H), 4.86 (dd, J = 9.8, 6.8 Hz, 1H), 3.30 (dd, J = 18.5, 10.5 Hz, 1H), 3.07 (dd, J = 19.0, 6.5 Hz, 1H); ^{13}C {^{1}H} NMR ($CDCl_3$, 126 MHz): δ 174.6, 173.8, 162.5 (d, J = 249.7 Hz), 146.2, 145.4, 134.1, 129.1 (d, J = 12.8 Hz), 128.9, 128.2, 128.1, 127.7 (d, J = 3.0 Hz), 125.1, 122.6, 118.7, 116.6, 116.4, 114.4, 113.6, 36.9, 33.7; ^{19}F NMR ($CDCl_3$) δ -111.5 (s); IR (neat, cm^{-1}): 3552, 1703, 1508, 1394, 1179, 834, 779, 723, 586, 515; HRMS (ESI-TOF) calcd for $C_{23}H_{17}FN_3O_2$ $[M + H]^+$ 386.1299, found 386.1320.

TH-3369_166122017

1-Phenethyl-3-(2-phenylimidazo[1,2-*a*]pyridin-3-yl)pyrrolidine-2,5-dione (3aj)

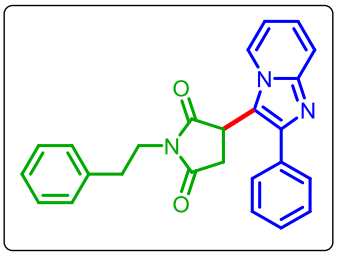

Gray solid (76 mg, 64% yield); mp 227–230 °C; purified over a column of silica gel (45% EtOAc in hexane); ^{1}H NMR ($CDCl_3$, 500 MHz): δ 7.68 (d, J = 9.5 Hz, 1H), 7.59 (d, J = 7.5 Hz, 2H), 7.45 (t, J = 7.3 Hz, 2H), 7.41 (d, J = 7.5 Hz, 1H), 7.36 – 7.31 (m, 3H), 7.27 (d, J = 7.0 Hz, 2H), 7.22 (t, J = 8.0 Hz, 2H), 6.76 (t, J = 6.8 Hz, 1H), 4.68 – 4.65 (m, 1H), 3.97 – 3.87 (m, 2H), 3.06 – 3.01 (m, 3H), 2.87 (dd, J = 18.5, 6.5 Hz, 1H); ^{13}C {^{1}H} NMR ($CDCl_3$, 126 MHz): δ 175.5, 174.8, 146.6, 145.4, 137.5, 134.1, 129.1, 128.9, 128.89, 128.85, 128.6, 127.1, 124.8, 122.8, 118.6, 113.9, 113.4, 40.4, 37.0, 33.4, 32.9; IR (neat, cm^{-1}): 2931, 1779, 1691, 1431, 1401, 1257, 1025, 779, 734, 697; HRMS (ESI-TOF) calcd for $C_{25}H_{22}N_3O_2$ $[M + H]^+$ 396.1707, found 396.1722.

1-(Cyclohexylmethyl)-3-(2-phenylimidazo[1,2-*a*]pyridin-3-yl)pyrrolidine-2,5-dione (3ak)

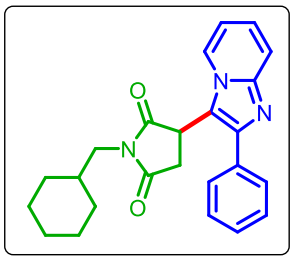

Light brown solid (81 mg, 70% yield); mp 211–213 °C; purified over a column of silica gel (40% EtOAc in hexane); ^{1}H NMR ($CDCl_3$, 400 MHz): δ 7.71 (d, J = 9.2 Hz, 1H), 7.66 (d, J = 6.8 Hz, 1H), 7.61 (d, J = 7.2 Hz, 2H), 7.48 – 7.39 (m, 3H), 7.24 (d, J = 8.4 Hz, 1H), 6.85 (t, J = 6.8 Hz, 1H), 4.73 (dd, J = 10.0, 6.4 Hz, 1H), 3.48 (d, J = 7.2 Hz, 2H), 3.12 (dd, J = 18.4, 10.0 Hz, 1H), 2.94 (dd, J = 18.4, 6.2 Hz, 1H), 1.77 – 1.66 (m, 6H), 1.28 – 1.16 (m, 4H), 1.08 – 1.00 (m, 1H); ^{13}C {^{1}H} NMR ($CDCl_3$, 101 MHz): δ 175.9, 175.2, 146.4, 145.4, 134.1, 129.1, 128.9, 128.6, 124.9, 122.8, 118.6, 114.1, 113.2, 45.7, 36.9, 36.6, 32.9, 31.1, 31.1, 26.2, 25.7, 25.7; IR (neat, cm^{-1}) 2924, 2847, 1776, 1694, 1395, 1358, 1131, 912, 732, 700; HRMS (ESI-TOF) calcd for $C_{24}H_{26}N_3O_2$ $[M + H]^+$ 388.2020, found 388.2041.

TH-3369_166122017

1-Hexyl-3-(2-phenylimidazo[1,2-*a*]pyridin-3-yl)pyrrolidine-2,5-dione (3al)

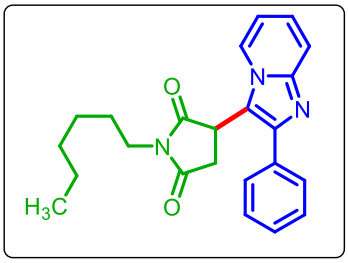

Gray solid (78 mg, 69% yield); mp 146–148 °C; purified over a column of silica gel (40% EtOAc in hexane); ^{1}H NMR ($CDCl_3$, 400 MHz): δ 7.69 (d, J = 9.2 Hz, 1H), 7.64 (d, J = 6.8 Hz, 1H), 7.60 (d, J = 6.4 Hz, 2H), 7.47 – 7.38 (m, 3H), 7.24 (t, J = 8.0 Hz, 1H), 6.84 (t, J = 6.8 Hz, 1H), 4.72 (dd, J = 10.0, 6.4 Hz, 1H), 3.61 (t, J = 7.4 Hz, 2H), 3.10 (dd, J = 18.6, 10.2 Hz, 1H), 2.90 (dd, J = 18.8, 6.4 Hz, 1H), 1.66 – 1.60 (m, 2H), 1.39 – 1.33 (m, 6H), 0.90 (t, J = 6.8 Hz, 3H).^{13}C {^{1}H} NMR ($CDCl_3$, 101 MHz): δ 175.7, 174.9, 146.2, 145.3, 134.0, 128.9, 128.8, 128.5, 124.8, 122.7, 118.5, 114.2, 113.2, 39.6, 36.8, 33.1, 31.4, 27.8, 26.7, 22.6, 14.1; IR (neat, cm^{-1}): 3049, 2938, 1694, 1400, 1358, 1231, 1179, 1131, 917, 749, 731; HRMS (ESI-TOF) calcd for $C_{23}H_{26}N_3O_2$ $[M + H]^+$ 376.2020, found 376.2020.

1-Heptyl-3-(2-phenylimidazo[1,2-*a*]pyridin-3-yl)pyrrolidine-2,5-dione (3am)

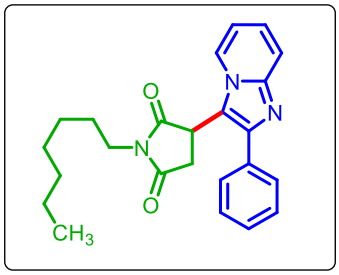

Light brown solid (79 mg, 68% yield); mp 91–94 °C; purified over a column of silica gel (45% EtOAc in hexane); ^{1}H NMR ($CDCl_3$, 400 MHz): δ 7.69 (d, J = 9.2 Hz, 1H), 7.64 (d, J = 6.8 Hz, 1H), 7.59 (d, J = 6.8 Hz, 2H), 7.46 – 7.37 (m, 3H), 7.23 (t, J = 7.8 Hz, 1H), 6.83 (t, J = 6.8 Hz, 1H), 4.72 (dd, J = 10.0, 6.4 Hz, 1H), 3.60 (t, J = 7.4 Hz, 2H), 3.09 (dd, J = 18.4, 9.8 Hz, 1H), 2.89 (dd, J = 18.4, 6.4 Hz, 1H), 1.66 – 1.62 (m, 2H), 1.34 – 1.26 (m, 8H), 0.89 (t, J = 6.8 Hz, 3H); ^{13}C {^{1}H} NMR ($CDCl_3$, 101 MHz): δ 175.6, 174.9, 146.1, 145.2, 134.0, 128.9, 128.8, 128.5, 124.8, 122.7, 118.5, 114.2, 113.1, 39.6, 36.8, 33.0, 31.7, 28.8, 27.8, 26.9, 22.6, 14.1; IR (neat, cm^{-1}): 2920, 2851, 1699, 1596, 1496, 1384, 1182, 910, 750, 692, 623; HRMS (ESI-TOF) calcd for $C_{24}H_{28}N_3O_2$ $[M + H]^+$ 390.2176, found 390.2188.

TH-3369_166122017

1-Octyl-3-(2-phenylimidazo[1,2-*a*]pyridin-3-yl)pyrrolidine-2,5-dione (**3an**)

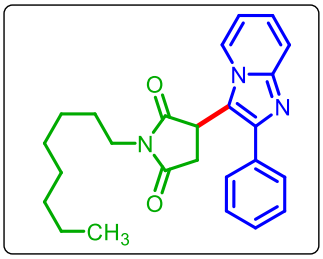

Light brown solid (80 mg, 66% yield); mp 118–120 °C; purified over a column of silica gel (40% EtOAc in hexane); ^{1}H NMR ($CDCl_3$, 400 MHz): δ 7.69 (d, J = 9.2 Hz, 1H), 7.64 (d, J = 6.8 Hz, 1H), 7.60 (d, J = 6.4 Hz, 2H), 7.47 – 7.38 (m, 3H), 7.24 (t, J = 7.8 Hz, 1H), 6.84 (t, J = 6.8 Hz, 1H), 4.72 (dd, J = 10.0, 6.4 Hz, 1H), 3.60 (t, J = 7.4 Hz, 2H), 3.10 (dd, J = 18.8, 10.0 Hz, 1H), 2.90 (dd, J = 18.6, 6.2 Hz, 1H), 1.66 – 1.62 (m, 2H), 1.34 – 1.27 (m, 10H), 0.88 (t, J = 6.8 Hz, 3H); ^{13}C {^{1}H} NMR ($CDCl_3$, 101 MHz): δ 175.7, 174.9, 146.2, 145.3, 134.0, 128.9, 128.8, 128.5, 124.8, 122.7, 118.5, 114.2, 113.2, 39.6, 36.8, 33.0, 31.8, 29.2, 29.2, 27.8, 27.0, 22.7, 14.1; IR (neat, cm^{-1}): 2918, 2849, 1779, 1693, 1435, 1400, 1358, 1229, 1129, 776, 730, 698; HRMS (ESI-TOF) calcd for $C_{225}H_{30}N_3O_2$ $[M + H]^+$ 404.2333, found 404.2338.

1-Decyl-3-(2-phenylimidazo[1,2-*a*]pyridin-3-yl)pyrrolidine-2,5-dione (**3ao**)

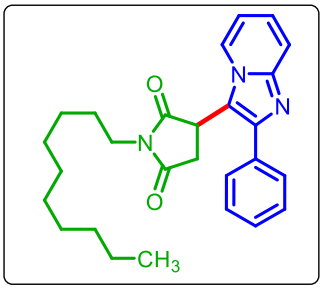

Light brown solid (83 mg, 64% yield); mp 108–111 °C; purified over a column of silica gel (40% EtOAc in hexane); ^{1}H NMR ($CDCl_3$, 600 MHz): δ 7.69 (d, J = 9.6 Hz, 1H), 7.64 (d, J = 6.6 Hz, 1H), 7.60 (d, J = 7.2 Hz, 2H), 7.44 (t, J = 7.2 Hz, 2H), 7.40 (t, J = 7.2 Hz, 1H), 7.24 (t, J = 7.8 Hz, 1H), 6.84 (t, J = 6.6 Hz, 1H), 4.72 (dd, J = 10.2, 6.6 Hz, 1H), 3.63 – 3.58 (m, 2H), 3.10 (dd, J = 18.6, 10.2 Hz, 1H), 2.90 (dd, J = 18.6, 6.0 Hz, 1H), 1.65 – 1.62 (m, 2H), 1.34 – 1.27 (m, 14H), 0.88 (t, J = 6.9 Hz, 3H); ^{13}C {^{1}H} NMR ($CDCl_3$, 151 MHz): δ 175.7, 174.9, 146.1, 145.2, 133.9, 128.9, 128.8, 128.5, 124.8, 122.7, 118.5, 114.1, 113.2, 39.6, 36.8, 33.0, 31.9, 29.6, 29.5, 29.3, 29.2, 27.8, 27.0, 22.7, 14.2; IR (neat, cm^{-1}): 2916, 2849, 1696, 1634, 1396, 1360, 1175, 1127, 1072, 783, 733, 703; HRMS (ESI-TOF) calcd for $C_{27}H_{34}N_3O_2$ $[M + H]^+$ 432.2646, found 432.2648.

TH-3369_166122017

1-((*R*)-1-Phenylethyl)-3-(2-phenylimidazo[1,2-*a*]pyridin-3-yl)pyrrolidine-2,5-dione (3ap)

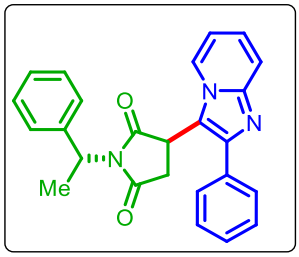

Light brown solid (77 mg, 65% yield, dr 1:1); mp 140–142 °C; purified over a column of silica gel (45% EtOAc in hexane); ^{1}H NMR ($CDCl_3$, 400 MHz): δ 7.64 (dd, J = 11.8, 9.4 Hz, 2H), 7.57 – 7.50 (m, 8H), 7.42 – 7.30 (m, 13H), 7.24 – 7.12 (m, 3H), 6.65 (t, J = 6.6 Hz, 1H), 6.55 (t, J = 6.6 Hz, 1H), 5.59 – 5.53 (m, 2H), 4.68 – 4.62 (m, 2H), 3.08 – 2.98 (m, 2H), 2.81 – 2.72 (m, 2H), 1.90 (dd, J = 7.2, 4.4 Hz, 6H); ^{13}C {^{1}H} NMR ($CDCl_3$, 101 MHz): δ 175.6, 175.6, 174.8, 174.7, 146.1, 146.1, 145.2, 145.2, 139.2, 139.1, 133.9, 128.95, 128.92, 128.8, 128.7, 128.50, 128.49, 128.4, 128.38, 128.0, 127.9, 124.8, 124.7, 122.8, 122.7, 118.4, 118.4, 114.3, 113.0, 112.9, 51.4, 51.4, 36.5, 32.9, 32.8, 16.3, 16.2; IR (neat, cm^{-1}): 2931, 1774, 1692, 1499, 1448, 1389, 1357, 1184, 732, 697; HRMS (ESI-TOF) calcd for $C_{25}H_{22}N_3O_2$ $[M + H]^+$ 396.1707, found 396.1706.

3-(2-Phenylimidazo[1,2-*a*]pyridin-3-yl)pyrrolidine-2,5-dione (3aq)

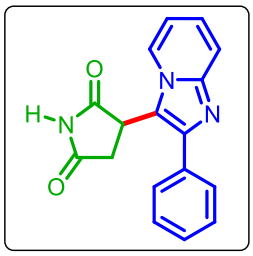

A white solid (53 mg, 61% yield); mp 252–255 °C; purified over a column of silica gel (50% EtOAc in hexane); ^{1}H NMR (DMSO-d_6, 500 MHz) δ 11.63 (s, 1H), 8.07 (d, J = 6.5 Hz, 1H), 7.66 (d, J = 9.0 Hz, 1H), 7.62 (d, J = 6.5 Hz, 2H), 7.48 (t, J = 7.5 Hz, 2H), 7.41 (t, J = 7.3 Hz, 1H), 7.34 (t, J = 8.0 Hz, 1H), 7.00 (t, J = 6.8 Hz, 1H), 5.04 (dd, J = 10.0, 7.0 Hz, 1H), 3.17 (dd, J = 18.0, 10.0 Hz, 1H), 2.92 (dd, J = 18.0, 7.0 Hz, 1H); ^{13}C {^{1}H} NMR (DMSO-d_6, 126 MHz): δ 177.6, 176.8, 144.5, 144.3, 134.2, 128.6, 128.5, 128.0, 125.0, 124.4, 117.2, 115.1, 112.9, 37.9, 34.3; IR (neat, cm^{-1}): 3542, 3299, 3057, 1774, 1703, 1499, 1340, 1183, 933, 738, 699; HRMS (ESI-TOF) calcd for $C_{17}H_{14}N_3O_2$ $[M + H]^+$ 292.1080, found 292.1081.

TH-3369_166122017

3-(2-(Imidazo[1,2-*a*]pyridin-2-yl)phenyl)-1-phenylpyrrolidine-2,5-dione (4aa)

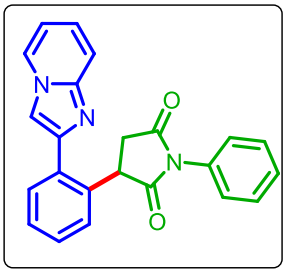

Brown solid (80 mg, 73% yield); mp 181–183 °C; purified over a column of silica gel (35% EtOAc in hexane); ^{1}H NMR ($CDCl_3$, 600 MHz): δ 8.13 (d, J = 6.6 Hz, 1H), 7.85 (s, 1H), 7.67 (dd, J = 6.0, 3.0 Hz, 1H), 7.48 – 7.39 (m, 5H), 7.37 – 7.34 (m, 2H), 7.25 (d, J = 8.4 Hz, 2H), 7.13 (t, J = 8.4 Hz, 1H), 6.79 (t, J = 6.3 Hz, 1H), 4.82 (dd, J = 9.6, 6.0 Hz, 1H), 3.36 (dd, J = 18.3, 9.9 Hz, 1H), 3.19 (dd, J = 18.6, 6.0 Hz, 1H); ^{13}C {^{1}H} NMR ($CDCl_3$, 101 MHz): δ 177.7, 176.1, 145.6, 145.3, 135.3, 133.7, 132.5, 130.7, 130.3, 129.4, 129.1, 128.8, 128.4, 128.2, 126.5, 125.7, 124.9, 117.9, 112.8, 110.8, 45.7, 38.3; IR (neat, cm^{-1}): 2925, 1772, 1698, 1496, 1379, 1273, 1161, 752, 695, 624; HRMS (ESI-TOF) calcd for $C_{23}H_{18}N_3O_2$ [M + H]$^+$ 368.1394, found 368.1392.

3-(2-(Imidazo[1,2-*a*]pyridin-2-yl)-5-methylphenyl)-1-phenylpyrrolidine-2,5-dione (4pa)

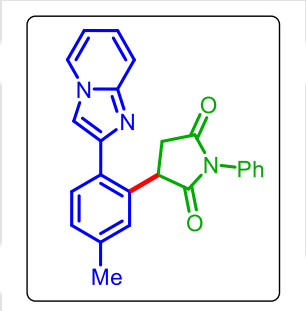

Brown solid (87 mg, 76% yield); mp 183–185 °C; purified over a column of silica gel (35% EtOAc in hexane); ^{1}H NMR ($CDCl_3$, 400 MHz): δ 8.09 (d, J = 6.8 Hz, 1H), 7.79 (s, 1H), 7.54 (d, J = 8 Hz, 1H), 7.44 – 7.39 (m, 3H), 7.37 – 7.32 (m, 1H), 7.27 – 7.24 (m, 2H), 7.19 (d, J = 8 Hz, 1H), 7.14 (s, 1H), 7.12 – 7.07 (m, 1H), 6.76 (t, J = 6.8 Hz, 1H), 4.78 (dd, J = 9.6, 6.0 Hz, 1H), 3.34 (dd, J = 18.3, 9.7 Hz, 1H), 3.16 (dd, J = 18.3, 6.0 Hz, 1H), 2.40 (s, 3H); ^{13}C {^{1}H} NMR ($CDCl_3$, 101 MHz): δ 177.8, 176.2, 145.6, 145.2, 138.7, 135.0, 132.6, 131.0, 130.8, 130.6, 129.0, 129.0, 128.3, 126.5, 125.6, 124.7, 117.8, 112.7, 110.5, 45.7, 38.3, 21.3; IR (neat, cm^{-1}): 2958, 1699, 1496, 1379, 1274, 1160, 967, 880, 747, 692, 649; HRMS (ESI-TOF) calcd for $C_{24}H_{20}N_3O_2$ [M + H]$^+$ 382.1550, found 382.1550.

TH-3369_166122017

3-(2-(Imidazo[1,2-*a*]pyridin-2-yl)-5-methoxyphenyl)-1-phenylpyrrolidine-2,5-dione (4ba)

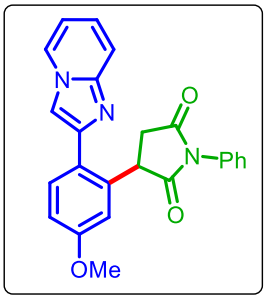

Brown solid (93 mg, 78% yield); mp 195–197 °C; purified over a column of silica gel (40% EtOAc in hexane); ^{1}H NMR ($CDCl_3$, 600 MHz): δ 8.09 (d, J = 6.6 Hz, 1H), 7.77 (s, 1H), 7.59 (d, J = 9.0 Hz, 1H), 7.43 – 7.40 (m, 3H), 7.35 (t, J = 7.5 Hz, 1H), 7.24 (d, J = 6.9 Hz, 2H), 7.10 (t, J = 7.5 Hz, 1H), 6.93 (dd, J = 8.4, 2.4 Hz, 1H), 6.88 (d, J = 2.4 Hz, 1H), 6.76 (t, J = 6.6 Hz, 1H), 4.78 (dd, J = 9.6, 6.0 Hz, 1H), 3.85 (s, 3H), 3.34 (dd, J = 18.3, 9.9 Hz, 1H), 3.18 (dd, J = 18.0, 6.0 Hz, 1H); ^{13}C {^{1}H} NMR ($CDCl_3$, 151 MHz): δ 177.6, 176.1, 159.7, 145.3, 145.1, 136.5, 132.4, 131.9, 129.1, 128.4, 126.4, 126.2, 125.6, 124.7, 117.7, 116.2, 113.2, 112.6, 110.2, 55.5, 45.8, 38.1; IR (neat, cm^{-1}): 2924, 1776, 1699, 1607, 1497, 1380, 1256, 1164, 1074, 752, 693; HRMS (ESI-TOF) calcd for $C_{24}H_{20}N_3O_3$ $[M + H]^+$ 398.1499, found 398.1507.

3-(5-Fluoro-2-(imidazo[1,2-*a*]pyridin-2-yl)phenyl)-1-phenylpyrrolidine-2,5-dione (4ca)

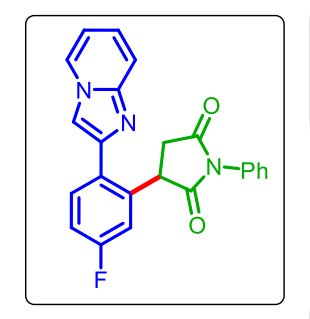

Black solid (81 mg, 70% yield); mp 201–203 °C; purified over a column of silica gel (35% EtOAc in hexane); ^{1}H NMR ($CDCl_3$, 600 MHz): δ 8.12 (d, J = 7.2 Hz, 1H), 7.80 (s, 1H), 7.63 (dd, J = 8.4, 6.0 Hz, 1H), 7.45 – 7.41 (m, 3H), 7.36 (t, J = 7.5 Hz, 1H), 7.23 (d, J = 7.2 Hz, 2H), 7.16 – 7.07 (m, 3H), 6.81 (t, J = 6.6 Hz, 1H), 4.81 (dd, J = 9.6, 6.0 Hz, 1H), 3.37 (dd, J = 18.3, 9.8 Hz, 1H), 3.17 (dd, J = 18.0, 6.0 Hz, 1H); ^{13}C {^{1}H} NMR ($CDCl_3$, 151 MHz): δ 177.1, 175.7, 162.6 (d, J = 248.7 Hz), 145.3, 144.6, 137.4 (d, J = 7.2 Hz), 132.5 (d, J = 8.3 Hz), 132.3, 129.9 (d, J = 3.3 Hz), 129.1, 128.5, 126.4, 125.7, 125.1, 117.8, 117.1 (d, J = 22.2 Hz), 115.3 (d, J = 21.0 Hz), 112.9, 110.7, 45.6, 38.1; ^{19}F NMR ($CDCl_3$) δ -112.9 (s); IR (neat, cm^{-1}): 2923, 1783, 1701, 1495, 1379, 1167, 874, 826, 751, 691, 621; HRMS (ESI-TOF) calcd for $C_{27}H_{17}FN_3O_2$ $[M + H]^+$ 386.1299, found 386.1307.

TH-3369_166122017

3-(2-(Imidazo[1,2-*a*]pyridin-2-yl)-5-(trifluoromethyl)phenyl)-1-phenylpyrrolidine-2,5-dione (4qa)

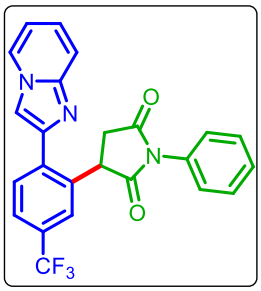

Black solid (85 mg, 65% yield); mp 152–155 °C; purified over a column of silica gel (35% EtOAc in hexane); ^{1}H NMR ($CDCl_3$, 600 MHz): δ 8.09 (d, J = 6.8 Hz, 1H), 7.86 (s, 1H), 7.76 (d, J = 7.8 Hz, 1H), 7.61 (d, J = 8.0 Hz, 2H), 7.43 – 7.37 (m, 3H), 7.35 (t, J = 7.4 Hz, 1H), 7.23 (d, J = 7.4 Hz, 2H), 7.13 – 7.10 (m, 1H), 6.78 (t, J = 6.8 Hz, 1H), 4.80 (dd, J = 9.0, 6.8 Hz, 1H), 3.36 (dd, J = 18.2, 9.8 Hz, 1H), 3.24 (dd, J = 18.2, 6.4 Hz, 1H); ^{13}C {^{1}H} NMR ($CDCl_3$, 151 MHz): δ 176.9, 175.7, 145.3, 144.1, 137.0, 135.4, 132.3, 130.8, 130.5, 130.3, 129.3, 129.1, 128.4, 126.3, 125.8, 125.3, 125.1 (dd, J = 6.8, 3.8 Hz), 117.9, 113.2, 111.3, 46.4, 37.9; ^{19}F NMR ($CDCl_3$) δ -62.5 (s); IR (neat, cm^{-1}): 2931, 1779, 1700, 1496, 1384, 1323, 1157, 1120, 1027, 751, 692, 646; HRMS (ESI-TOF) calcd for $C_{24}H_{17}F_3N_3O_2$ $[M + H]^+$ 436.1267, found 436.1267.

3-(4-(Imidazo[1,2-*a*]pyridin-2-yl)-[1,1'-biphenyl]-3-yl)-1-phenylpyrrolidine-2,5-dione (4ea)

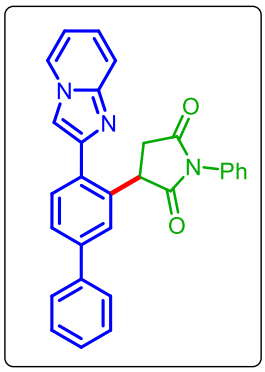

Brown solid (88 mg, 66% yield); mp 180–182 °C; purified over a column of silica gel (35% EtOAc in hexane); ^{1}H NMR ($CDCl_3$, 600 MHz): δ 8.13 (d, J = 6.6 Hz, 1H), 7.88 (s, 1H), 7.75 (d, J = 7.8 Hz, 1H), 7.63 (t, J = 6.6 Hz, 3H), 7.56 (s, 1H), 7.47 (t, J = 7.8 Hz, 2H), 7.43 (t, J = 7.5 Hz, 3H), 7.40 – 7.34 (m, 2H), 7.26 (d, J = 8.4 Hz, 2H), 7.12 (t, J = 7.8 Hz, 1H), 6.79 (t, J = 6.6 Hz, 1H), 4.88 (dd, J = 8.7, 6.3 Hz, 1H), 3.39 (dd, J = 18.6, 9.6 Hz, 1H), 3.27 (dd, J = 18.3, 6.3 Hz, 1H); ^{13}C {^{1}H} NMR ($CDCl_3$, 151 MHz): δ 177.6, 176.1, 145.3, 141.6, 140.3, 135.5, 132.6, 132.5, 131.1, 129.6, 129.1, 129.0, 128.3, 127.8, 127.3, 126.9, 126.5, 125.7, 124.9, 117.9, 112.9, 110.7, 46.3, 38.3;. IR (neat, cm^{-1}): 3064, 1775, 1702,

TH-3369_166122017

1597, 1495, 1378, 1279, 1167, 840, 694; HRMS (ESI-TOF) calcd for $C_{29}H_{22}N_3O_2$ $[M + H]^+$ 444.1707, found 444.1706.

3-(2-(Imidazo[1,2-*a*]pyridin-2-yl)-4-methylphenyl)-1-phenylpyrrolidine-2,5-dione (4fa)

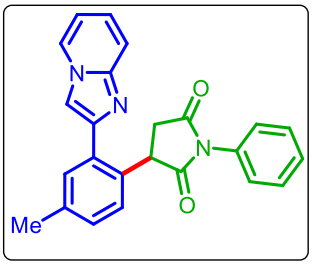

Light brown solid (86 mg, 75% yield); mp 144–147 °C; purified over a column of silica gel (35% EtOAc in hexane); ^{1}H NMR ($CDCl_3$, 400 MHz): δ 8.04 (d, J = 6.8 Hz, 1H), 7.80 (s, 1H), 7.47 (s, 1H), 7.40 (t, J = 8.2 Hz, 3H), 7.32 (t, J = 7.2 Hz, 1H), 7.25 – 7.16 (m, 4H), 7.07 (t, J = 8 Hz, 1H), 6.71 (t, J = 6.8 Hz, 1H), 4.74 (dd, J = 9.6, 6 Hz, 1H), 3.30 (dd, J = 18, 9.6 Hz, 1H), 3.13 (dd, J = 18.2, 5.8 Hz, 1H), 2.37 (s, 3H); ^{13}C {^{1}H} NMR ($CDCl_3$, 151 MHz): δ 177.9, 176.2, 145.3, 145.0, 137.8, 133.3, 132.4, 132.0, 131.2, 130.2, 129.4, 128.9, 128.2, 126.4, 125.6, 124.7, 117.6, 112.6, 110.7, 45.3, 38.2, 21.1; IR (neat, cm^{-1}): 2919, 1775, 1698, 1496, 1368, 1282, 1153, 826, 738, 690, 623; HRMS (ESI-TOF) calcd for $C_{24}H_{20}N_3O_2$ $[M + H]^+$ 382.1550, found 382.1556.

3-(2-(Imidazo[1,2-*a*]pyridin-2-yl)-4-(trifluoromethyl)phenyl)-1-phenylpyrrolidine-2,5-dione (4ra)

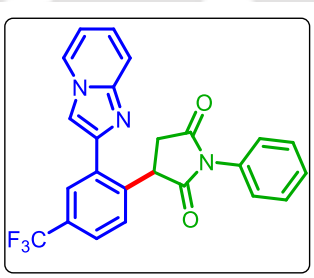

Black solid (82 mg, 63% yield); mp 144–146 °C; purified over a column of silica gel (35% EtOAc in hexane); ^{1}H NMR ($CDCl_3$, 400 MHz): δ 7.98 (d, J = 6.8 Hz, 1H), 7.80 (s, 1H), 7.77 (s, 1H), 7.50 (d, J = 8.0 Hz, 1H), 7.36 (d, J = 8.0 Hz, 1H), 7.30 (t, J = 7.6 Hz, 3H), 7.24 (t, J = 7.2 Hz, 1H), 7.13 (d, J = 7.6 Hz, 2H), 7.01 (t, J = 7.8 Hz, 1H), 6.65 (t, J = 6.6 Hz, 1H), 4.77 (dd, J = 9.6, 6.4 Hz, 1H), 3.26 (dd, J = 18.4, 9.6 Hz, 1H), 3.06 (dd, J = 18.0, 6.0 Hz, 1H); ^{13}C {^{1}H} NMR ($CDCl_3$, 151 MHz): δ 176.9, 175.5, 145.3, 144.1, 138.9, 134.5, 132.4, 131.3, 130.4 (q, J = 32.8 Hz), 128.9, 128.3, 127.2 (t, J = 3.2 Hz), 126.3, 125.8, 125.2, 125.0 (t, J = 3.2 Hz), 124.8, 123.0, 117.8 (d, J = 3.3 Hz), 113.0, 112.9, 111.1,

TH-3369_166122017

45.8, 37.9; ^{19}F NMR ($CDCl_3$) δ -62.7 (s); IR (neat, cm^{-1}): 3050, 1775, 1696, 1495, 1375, 1313, 1156, 1111, 961, 838, 737, 689; HRMS (ESI-TOF) calcd for $C_{24}H_{17}F_3N_3O_2$ $[M + H]^+$ 436.1267, found 436.1273.

3-(2-(Imidazo[1,2-*a*]pyridin-2-yl)-3-methoxyphenyl)-1-phenylpyrrolidine-2,5-dione (**4ha**)

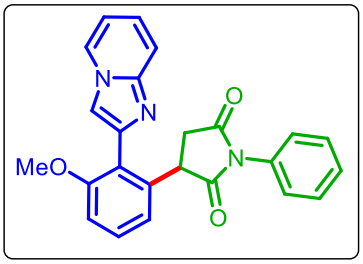

Brown solid (84 mg, 71% yield); mp 125–128 ºC; purified over a column of silica gel (40% EtOAc in hexane); ^{1}H NMR ($CDCl_3$, 400 MHz): δ 8.07 (d, J = 6.8 Hz, 1H), 7.82 (s, 1H), 7.50 (d, J = 9.1 Hz, 1H), 7.40 – 7.29 (m, 4H), 7.16 – 7.07 (m, 3H), 6.96 (dd, J = 9.9, 8 Hz, 2H), 6.75 (t, J = 6.8 Hz, 1H), 4.51 (dd, J = 9.6, 6.0 Hz, 1H), 3.79 (s, 3H), 3.28 (dd, J = 18.6, 9.8 Hz, 1H), 3.16 (dd, J = 18.4, 6.0 Hz, 1H); ^{13}C {^{1}H} NMR ($CDCl_3$, 151 MHz): δ 177.5, 175.9, 158.2, 144.5, 139.6, 138.2, 132.2, 129.7, 129.0, 128.3, 126.3, 125.6, 124.4, 123.2, 121.5, 117.7, 113.9, 112.5, 110.6, 55.9, 45.6, 38.3; IR (neat, cm^{-1}): 2926, 1776, 1703,1591, 1496, 1378, 1260, 1176, 1081, 837, 743,693; HRMS (ESI-TOF) calcd for $C_{24}H_{20}N_3O_3$ $[M + H]^+$ 398.1499, found 398.1504.

3-(3-Fluoro-2-(imidazo[1,2-*a*]pyridin-2-yl)phenyl)-1-phenylpyrrolidine-2,5-dione (**4ia**)

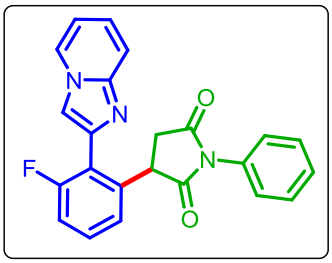

Brown solid (77 mg, 67% yield); mp 186–188 ºC; purified over a column of silica gel (35% EtOAc in hexane); ^{1}H NMR ($CDCl_3$, 600 MHz): δ 8.11 (d, J = 6.8 Hz, 1H), 7.92 (d, J = 3.6 Hz, 1H), 7.42 (d, J = 3.6 Hz, 1H), 7.40 (d, J = 8.4 Hz, 2H), 7.37 – 7.32 (m, 2H), 7.20 – 7.15 (m, 4H), 7.11 (t, J = 7.8 Hz, 1H), 6.78 (t, J = 6.7 Hz, 1H), 4.75 (dd, J = 9.6, 6.3 Hz, 1H), 3.35 (dd, J = 18.3, 9.8 Hz, 1H), 3.21 (dd, J = 18.3, 6.2 Hz, 1H); ^{13}C {^{1}H} NMR ($CDCl_3$, 101 MHz): δ 177.2, 175.9, 161.1 (d, J = 248.5 Hz), 144.7, 138.2, 138.1, 137.6, 132.4, 129.6 (d, J = 9.1 Hz), 129.0, 128.3, 126.5, 126.4, 125.7, 124.9, 121.9 (d, J = 14.1 Hz), 117.9, 115.6 (d, J = 24.2 Hz), 113.9 (d, J = 11.1 Hz), 112.9, 46.2, 38.2; ^{19}F NMR

TH-3369_166122017

($CDCl_3$) δ -111.6 (s); IR (neat, cm^{-1}): 3154, 2946, 1776, 1701, 1496, 1456, 1383, 1167, 974, 745, 697, 665, 622; HRMS (ESI-TOF) calcd for $C_{23}H_{17}FN_3O_2$ $[M + H]^+$ 386.1299, found 386.1307.

3-(2-(6-Methylimidazo[1,2-*a*]pyridin-2-yl)phenyl)-1-phenylpyrrolidine-2,5-dione (**4ja**)

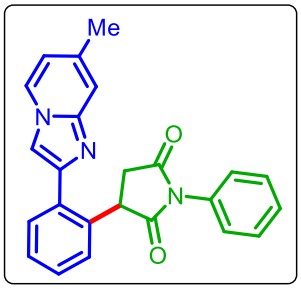

Gray solid (90 mg, 79% yield); mp 191–194 ^oC; purified over a column of silica gel (35% EtOAc in hexane); ^1H NMR ($CDCl_3$, 600 MHz): δ 7.99 (d, J = 6.6 Hz, 1H), 7.75 (s, 1H), 7.66 – 7.63 (m, 1H), 7.42 (t, J = 7.5 Hz, 2H), 7.39 – 7.33 (m, 4H), 7.25 (d, J = 9 Hz, 2H), 7.21 (s, 1H), 6.62 (d, J = 6.6 Hz, 1H), 4.83 (dd, J = 9.5, 5.9 Hz, 1H), 3.35 (dd, J = 18.4, 9.8 Hz, 1H), 3.18 (dd, J = 18.4, 5.9 Hz, 1H), 2.34 (s, 3H); ^{13}C {^1H} NMR ($CDCl_3$, 151 MHz): δ 177.8, 176.2, 145.7, 145.1, 135.9, 135.2, 133.9, 132.4, 130.7, 130.1, 129.0, 128.7, 128.4, 128.2, 126.5, 124.9, 116.1, 115.4, 110.2, 45.6, 38.4, 21.4; IR (neat, cm^{-1}): 3155, 1778, 1495, 1375, 1163, 792, 754, 692, 636, 493; HRMS (ESI-TOF) calcd for $C_{24}H_{20}N_3O_2$ $[M + H]^+$ 382.1550, found 382.1558.

3-(2-(Imidazo[1,2-*a*]pyridin-2-yl)thiophen-3-yl)-1-phenylpyrrolidine-2,5-dione (**4la**)

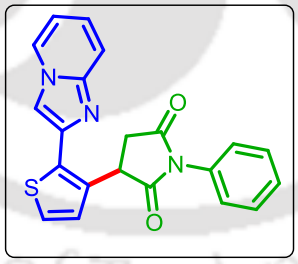

Black solid (65 mg, 58% yield); mp 185–188 ^oC; purified over a column of silica gel (35% EtOAc in hexane); ^1H NMR ($CDCl_3$, 600 MHz): δ 8.07 (d, J = 7.2 Hz, 1H), 7.85 (s, 1H), 7.45 (t, J = 7.5 Hz, 2H), 7.40 – 7.37 (m, 2H), 7.34 (d, J = 7.8 Hz, 2H), 7.30 (d, J = 5.4 Hz, 1H), 7.11 (t, J = 7.5 Hz, 1H), 7.02 (d, J = 4.8 Hz, 1H), 6.76 (t, J = 6.9 Hz, 1H), 4.85 (dd, J = 9.6, 5.4 Hz, 1H), 3.36 (dd, J = 18.6, 9.6 Hz, 1H), 3.15 (dd, J = 18.3, 5.7 Hz, 1H); ^{13}C {^1H} NMR ($CDCl_3$, 151 MHz): δ 177.2, 176.0, 145.5, 139.6, 133.7, 133.4, 132.6, 129.3, 129.1, 128.5, 126.6, 125.6, 125.1, 124.8, 117.7, 112.9, 109.6, 41.5, 37.3; IR (neat, cm^{-1}): 2965, 1774, 1702, 1492, 1380, 1274, 1186, 1094, 794, 745; HRMS (ESI-TOF) calcd for $C_{21}H_{16}N_3O_2S$ $[M + H]^+$ 374.0958, found 374.0955.

TH-3369_166122017

3-(2-(Imidazo[2,1-*b*]thiazol-6-yl)phenyl)-1-phenylpyrrolidine-2,5-dione (**4ma**)

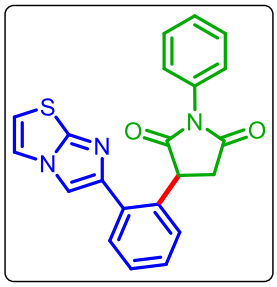

Pale yellow solid (79 mg, 71% yield); mp 175–178 ºC; purified over a column of silica gel (35% EtOAc in hexane); ^{1}H NMR ($CDCl_3$, 400 MHz): δ 7.70 (s, 1H), 7.56 (dd, J = 5.6, 3.5 Hz, 1H), 7.46 (t, J = 7.6 Hz, 2H), 7.41 (d, J = 4.4 Hz, 1H), 7.39 – 7.30 (m, 6H), 6.81 (d, J = 4.4 Hz, 1H), 4.84 (dd, J = 9.8, 5.8 Hz, 1H), 3.34 (dd, J = 18.4, 10.0 Hz, 1H), 3.07 (dd, J = 18.4, 6.0 Hz, 1H); ^{13}C {^{1}H} NMR ($CDCl_3$, 151 MHz): δ 177.9, 176.0, 149.8, 147.2, 134.9, 133.9, 132.5, 130.2, 130.0, 129.2, 128.5, 128.5, 128.2, 126.5, 118.6, 112.9, 110.7, 45.5, 38.2; IR (neat, cm^{-1}): 3100, 1772, 1698, 1535, 1497, 1380, 1161, 945, 812, 755, 697, 652; HRMS (ESI-TOF) calcd for $C_{21}H_{16}N_3O_2S$ $[M + H]^+$ 374.0958, found 374.0968.

3-(2-(Benzo[*d*]imidazo[2,1-*b*]thiazol-2-yl)phenyl)-1-phenylpyrrolidine-2,5-dione (**4na**)

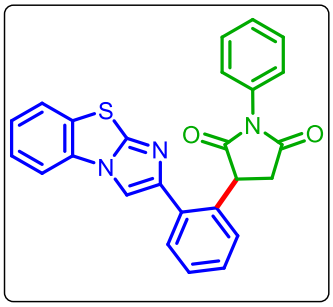

Gray solid (75 mg, 59% yield); mp 195–198 ºC; purified over a column of silica gel (35% EtOAc in hexane); ^{1}H NMR ($CDCl_3$, 500 MHz) δ 7.96 (s, 1H), 7.69 (d, J = 7.5 Hz, 1H), 7.63 – 7.60 (m, 2H), 7.43 (d, J = 7.0 Hz, 3H), 7.39 – 7.34 (m, 7H), 4.89 – 4.85 (m, 1H), 3.37 (dd, J = 18.5, 10.0 Hz, 1H), 3.08 (dd, J = 18.4, 5.8 Hz, 1H); ^{13}C {^{1}H} NMR ($CDCl_3$, 126 MHz): δ 177.8, 175.9, 147.8, 147.1, 135.1, 133.7, 132.6, 132.2, 130.4, 130.2, 129.9, 129.3, 129.2, 129.1, 128.7, 128.5, 128.2, 126.6, 126.4, 125.3, 124.6, 113.0, 109.8, 45.5, 38.2; IR (neat, cm^{-1}): 2957, 1773, 1697, 1492, 1381, 1260, 1174, 1021, 748, 697, 627; HRMS (ESI-TOF) calcd for $C_{25}H_{18}N_3O_2S$ $[M + H]^+$ 424.1114, found 424.1116.

TH-3369_166122017

3-(2-(Imidazo[1,2-*a*]pyridin-2-yl)-5-(methylsulfonyl)phenyl)-1-phenylpyrrolidine-2,5-dione (4oa)

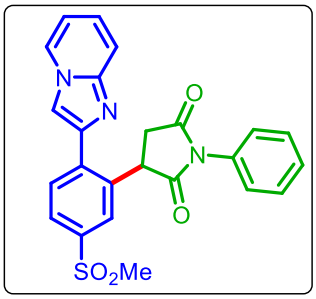

Off-white solid (85 mg, 64% yield); mp 184–187 °C; purified over a column of silica gel (40% EtOAc in hexane); ^{1}H NMR ($CDCl_3$, 400 MHz): δ 8.15 (d, J = 6.8 Hz, 1H), 7.95 (d, J = 9.2 Hz, 3H), 7.87 (d, J = 8.0 Hz, 1H), 7.44 – 7.34 (m, 4H), 7.24 (d, J = 7.2 Hz, 2H), 7.15 (t, J = 7.8 Hz, 1H), 6.84 (t, J = 6.6 Hz, 1H), 4.85 (dd, J = 9.2, 6.8 Hz, 1H), 3.38 (dd, J = 18.2, 9.8 Hz, 1H), 3.24 (dd, J = 18.0, 6.4 Hz, 1H), 3.12 (s, 3H); ^{13}C {^{1}H} NMR ($CDCl_3$, 101 MHz): δ 176.8, 175.5, 145.5, 143.6, 139.9, 139.0, 136.1, 132.3, 131.2, 130.7, 129.1, 128.4, 127.1, 126.4, 125.9, 125.6, 118.1, 113.5, 111.7, 46.6, 44.7, 37.8; IR (neat, cm^{-1}): 2912, 1770, 1694, 1594, 1492, 1376, 1306, 1129, 953, 800, 754, 697; HRMS (ESI-TOF) calcd for $C_{24}H_{20}N_3O_4S$ $[M + H]^+$ 446.1169, found 446.1171.

1-Benzyl-3-(2-(imidazo[1,2-*a*]pyridin-2-yl)phenyl)pyrrolidine-2,5-dione (4ab)

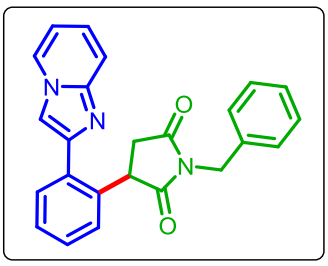

Brown solid (79 mg, 69% yield); mp 122–124 °C; purified over a column of silica gel (35% EtOAc in hexane); ^{1}H NMR ($CDCl_3$, 400 MHz): δ 8.12 (d, J = 6.8 Hz, 1H), 7.82 (s, 1H), 7.61 (dd, J = 7.2, 1.6 Hz, 1H), 7.49 (d, J = 9.2 Hz, 1H), 7.40 (d, J = 6.4 Hz, 2H), 7.36 – 7.26 (m, 5H), 7.19 – 7.11 (m, 2H), 6.80 (t, J = 6.8 Hz, 1H), 4.81 (dd, J = 9.6, 5.2 Hz, 1H), 4.73 (d, J = 14.0 Hz, 1H), 4.61 (d, J = 14.0 Hz, 1H), 3.25 (dd, J = 18.4, 9.6 Hz, 1H), 2.91 (dd, J = 18.4, 5.2 Hz, 1H); ^{13}C {^{1}H} NMR ($CDCl_3$, 101 MHz): δ 178.7, 176.7, 145.3, 145.2, 136.2, 135.9, 133.9, 130.6, 128.9, 128.9, 128.8, 128.8, 128.7, 128.0, 127.9, 125.8, 125.0, 117.7, 112.8, 110.9, 44.5, 42.7, 38.6; IR (neat, cm^{-1}): 3135, 1767, 1693, 1498, 1352, 1395, 1165, 953, 750, 700, 638, 474; HRMS (ESI-TOF) calcd for $C_{24}H_{20}N_3O_2$ $[M + H]^+$ 382.1550, found 382.1553.

TH-3369_166122017

3-(2-(Imidazo[1,2-*a*]pyridin-2-yl)phenyl)-1-methylpyrrolidine-2,5-dione (4ac)

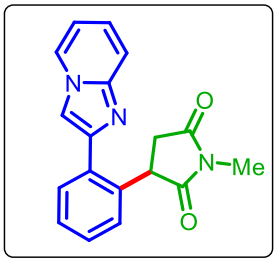

Off-white solid (67 mg, 73% yield); mp 131–134 °C; purified over a column of silica gel (30% EtOAc in hexane); ^{1}H NMR ($CDCl_3$, 400 MHz): δ 8.12 (d, J = 6.8 Hz, 1H), 7.81 (s, 1H), 7.61 (dd, J = 5.6, 3.6 Hz, 1H), 7.51 (d, J = 9.2 Hz, 1H), 7.35 (dd, J = 5.6, 3.2 Hz, 2H), 7.23 – 7.15 (m, 2H), 6.79 (t, J = 6.8 Hz, 1H), 4.73 (dd, J = 9.4, 5.4 Hz, 1H), 3.23 (dd, J = 18.4, 9.6 Hz, 1H), 2.99 – 2.93 (m, 4H); ^{13}C {^{1}H} NMR ($CDCl_3$, 151 MHz): δ 179.1, 177.1, 145.1, 144.9, 135.6, 133.6, 130.6, 129.4, 128.8, 127.9, 125.8, 125.1, 117.4, 112.8, 110.8, 44.9, 38.5, 25.1; IR (neat, cm^{-1}): 2920, 1766, 1688, 1503, 1403, 1374, 1277, 1117, 952, 836, 750; HRMS (ESI-TOF) calcd for $C_{18}H_{16}N_3O_2$ $[M + H]^+$ 306.1237, found 306.1245.

1-Ethyl-3-(2-(imidazo[1,2-*a*]pyridin-2-yl)phenyl)pyrrolidine-2,5-dione (4ad)

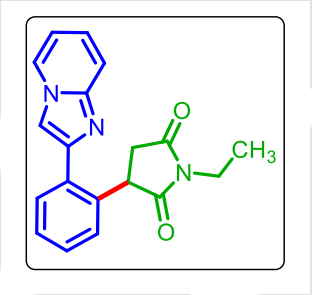

Brown gummy solid (67 mg, 70% yield); purified over a column of silica gel (30% EtOAc in hexane); ^{1}H NMR ($CDCl_3$, 400 MHz): δ 8.14 (d, J = 6.8 Hz, 1H), 7.83 (s, 1H), 7.63 – 7.59 (m, 1H), 7.55 (d, J = 9.2 Hz, 1H), 7.39 – 7.34 (m, 2H), 7.20 – 7.15 (m, 2H), 6.80 (t, J = 6.8 Hz, 1H), 4.80 (dd, J = 9.5, 5.3 Hz, 1H), 3.62 – 3.51 (m, 2H), 3.24 (dd, J = 18.4, 9.5 Hz, 1H), 2.94 (dd, J = 18.4, 5.3 Hz, 1H), 1.16 (t, J = 7.2 Hz, 3H); ^{13}C {^{1}H} NMR ($CDCl_3$, 101 MHz): δ 178.8, 176.9, 145.5, 145.2, 136.1, 134.0, 130.8, 128.9, 128.6, 127.9, 125.7, 124.9, 117.8, 112.7, 110.9, 44.4, 38.7, 33.9, 13.2; IR (neat, cm^{-1}): 2922, 2853, 1589, 1487, 1391, 1258, 1146, 1025, 763, 631; HRMS (ESI-TOF) calcd for $C_{19}H_{18}N_3O_2$ $[M + H]^+$ 320.1394, found 320.1399.

3-(2-(Imidazo[1,2-*a*]pyridin-2-yl)phenyl)-1-propylpyrrolidine-2,5-dione (4ae)

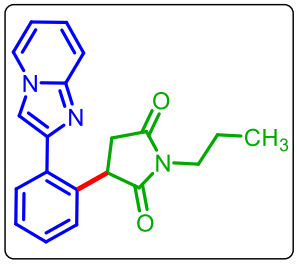

Brown gummy solid (68 mg, 68% yield); purified over a column of silica gel (30% EtOAc in hexane); ^{1}H NMR ($CDCl_3$, 400 MHz): δ 8.14 (d, J = 6.8 Hz, 1H), 7.83 (s, 1H), 7.64 – 7.59 (m, 1H), 7.55 (d, J = 9.2 Hz, 1H), 7.38 – 7.34 (m, 2H), 7.21 – 7.15 (m, 2H), 6.80 (t, J = 6.8 Hz, 1H), 4.82 (dd, J = 9.6, 5.3 Hz, 1H), 3.54 – 3.40 (m, 2H), 3.24 (dd, J = 18.4, 9.6 Hz, 1H), 2.92 (dd, J = 18.4, 5.3 Hz, 1H), 1.65 – 1.54 (m, 2H), 0.90 (t, J = 7.4 Hz, 3H); ^{13}C {^{1}H} NMR ($CDCl_3$, 101 MHz): δ 179.0, 177.2, 145.5, 145.2, 136.1, 134.1, 130.7, 128.9, 128.4, 127.9, 125.7, 124.9, 117.8, 112.7, 110.9, 44.3, 40.7, 38.7, 21.2, 11.4; IR (neat, cm^{-1}): 2932, 2872, 1770, 1688, 1634, 1501, 1399, 1348, 1278, 1200; HRMS (ESI-TOF) calcd for $C_{20}H_{20}N_3O_2$ $[M + H]^+$ 334.1550, found 334.1552.

3-(2-(Imidazo[1,2-*a*]pyridin-2-yl)phenyl)-1-isobutylpyrrolidine-2,5-dione (4af)

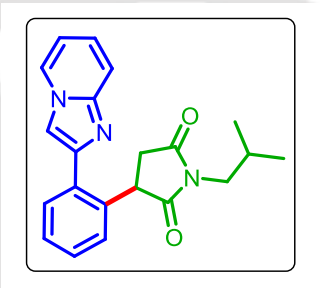

Brown gummy solid (72 mg, 69% yield); purified over a column of silica gel (30% EtOAc in hexane); ^{1}H NMR ($CDCl_3$, 600 MHz): δ 8.13 (d, J = 6.6 Hz, 1H), 7.85 (s, 1H), 7.64 – 7.61 (m, 1H), 7.55 (d, J = 9.0 Hz, 1H), 7.38 – 7.35 (m, 2H), 7.21 – 7.16 (m, 2H), 6.80 (t, J = 6.9 Hz, 1H), 4.84 (dd, J = 9.6, 4.8 Hz, 1H), 3.38 (dd, J = 12.9, 7.5 Hz, 1H), 3.29 (ddd, J = 28.1, 15.7, 8.4 Hz, 2H), 2.91 (dd, J = 18.6, 4.8 Hz, 1H), 2.10 – 2.03 (m, 1H), 0.90 (dd, J = 8.4, 6.6 Hz, 6H); ^{13}C {^{1}H} NMR ($CDCl_3$, 151 MHz): δ 179.3, 177.3, 145.3, 145.1, 136.0, 134.1, 130.7, 128.8, 128.3, 127.9, 125.7, 124.8, 117.7, 112.7, 110.9, 46.2, 44.0, 38.6, 27.2, 20.24, 20.22; IR (neat, cm^{-1}): 2958, 1776, 1691, 1465, 1396, 1319, 1201, 872, 748; HRMS (ESI-TOF) calcd for $C_{21}H_{22}N_3O_2$ $[M + H]^+$ 348.1707, found 348.1722.

1-Cyclohexyl-3-(2-(imidazo[1,2-*a*]pyridin-2-yl)phenyl)pyrrolidine-2,5-dione (4ag)

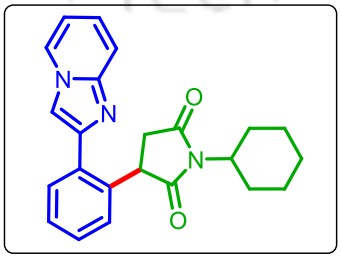

Brown solid (73 mg, 65% yield); mp 122–125 ^{o}C; purified over a column of silica gel (30% EtOAc in hexane); ^{1}H NMR ($CDCl_3$, 400 MHz): δ 8.14 (d, J = 6.8 Hz, 1H), 7.85 (s, 1H), 7.62 – 7.57 (m, 2H),

TH-3369_166122017

7.38 – 7.33 (m, 2H), 7.21 – 7.13 (m, 2H), 6.80 (t, *J* = 6.8 Hz, 1H), 4.80 (dd, *J* = 9.6, 5.2 Hz, 1H), 4.01 (m, 1H), 3.19 (dd, *J* = 18.4, 9.6 Hz, 1H), 2.86 (dd, *J* = 18.4, 5.2 Hz, 1H), 2.19 – 2.09 (m, 2H), 1.81 (d, *J* = 10.4 Hz, 2H), 1.66 – 1.56 (m, 2H), 1.36 – 1.15 (m, 4H); ^{13}C {^{1}H} NMR ($CDCl_3$, 101 MHz): *δ* 179.1, 177.2, 145.5, 145.3, 136.7, 134.3, 130.9, 128.9, 127.8, 127.6, 125.7, 124.8, 117.8, 112.7, 111.1, 51.9, 43.5, 38.7, 29.0, 28.8, 25.9, 25.2; IR (neat, cm^{-1}): 2965, 2932, 1685, 1502, 1455, 1375, 1265, 1025, 792, 725, 693; HRMS (ESI-TOF) calcd for $C_{23}H_{24}N_3O_2$ $[M + H]^+$ 374.1863, found 374.1867.

1-Heptyl-3-(2-(imidazo[1,2-*a*]pyridin-2-yl)phenyl)pyrrolidine-2,5-dione (**4am**)

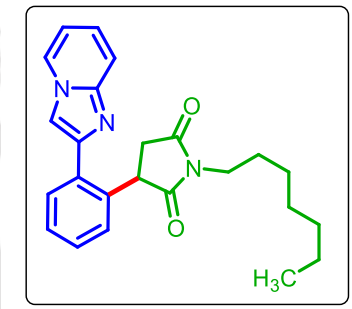

Brown gummy solid (77 mg, 66% yield); purified over a column of silica gel (30% EtOAc in hexane); ^{1}H NMR ($CDCl_3$, 600 MHz) *δ* 8.14 (d, *J* = 6.6 Hz, 1H), 7.84 (s, 1H), 7.64 – 7.61 (m, 1H), 7.56 (d, *J* = 9.0 Hz, 1H), 7.38 – 7.35 (m, 2H), 7.20 – 7.17 (m, 2H), 6.81 (t, *J* = 6.6 Hz, 1H), 4.80 (dd, *J* = 9.3, 5.1 Hz, 1H), 3.54 – 3.44 (m, 2H), 3.24 (dd, *J* = 18.6, 9.6 Hz, 1H), 2.94 (dd, *J* = 18.6, 5.4 Hz, 1H), 1.54 (dd, *J* = 12.6, 7.2 Hz, 2H), 1.29 – 1.24 (m, 8H), 0.87 (t, *J* = 6.9 Hz, 3H); ^{13}C {^{1}H} NMR ($CDCl_3$, 151 MHz): *δ* 179.0, 177.2, 145.4, 145.2, 136.1, 134.1, 130.8, 128.9, 128.4, 127.9, 125.7, 124.9, 117.8, 112.7, 110.9, 44.2, 39.1, 38.7, 31.8, 28.9, 27.9, 26.9, 22.7, 14.2; IR (neat, cm^{-1}): 2925, 2855, 1771, 1692, 1634, 1502, 1437, 1398, 1367, 1277, 1128; HRMS (ESI-TOF) calcd for $C_{24}H_{28}N_3O_2$ $[M + H]^+$ 390.2176, found 390.2184.

1-Decyl-3-(2-(imidazo[1,2-*a*]pyridin-2-yl)phenyl)pyrrolidine-2,5-dione (**4ao**)

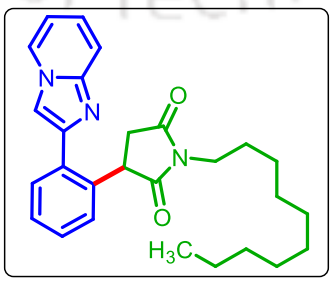

Brown gummy solid (81 mg, 63% yield); purified over a column of silica gel (30% EtOAc in hexane); ^{1}H NMR ($CDCl_3$, 600 MHz): *δ* 8.13 (d, *J* = 7.2 Hz, 1H), 7.83 (s, 1H), 7.63 – 7.60 (m, 1H), 7.55 (d, *J* =

TH-3369_166122017

9.0 Hz, 1H), 7.36 (dd, *J* = 5.4, 3.6 Hz, 2H), 7.20 – 7.16 (m, 2H), 6.80 (t, *J* = 6.9 Hz, 1H), 4.80 (dd, *J* = 9.6, 5.4 Hz, 1H), 3.54 – 3.44 (m, 2H), 3.24 (dd, *J* = 18.0, 9.6 Hz, 1H), 2.94 (dd, *J* = 18.3, 5.1 Hz, 1H), 1.54 (d, *J* = 6.0 Hz, 2H), 1.28 – 1.25 (m, 14H), 0.88 (t, *J* = 6.9 Hz, 3H); ^{13}C {^{1}H} NMR ($CDCl_3$, 151 MHz): *δ* 179.0, 177.1, 145.4, 145.2, 136.1, 134.1, 130.7, 128.8, 128.5, 127.9, 125.7, 124.8, 117.7, 112.7, 110.9, 44.3, 39.1, 38.7, 31.9, 29.6, 29.6, 29.4, 29.3, 27.9, 26.9, 22.8, 14.2; IR (neat, cm^{-1}): 2932, 2859, 1775, 1695, 1638, 1505, 1442, 1395, 1362, 1282, 1115, 885; HRMS (ESI-TOF) calcd for $C_{27}H_{34}N_3O_2$ $[M + H]^+$ 432.2646, found 432.2657.

3-(2-(Imidazo[1,2-*a*]pyridin-2-yl)phenyl)-1-(p-tolyl)pyrrolidine-2,5-dione (4ah)

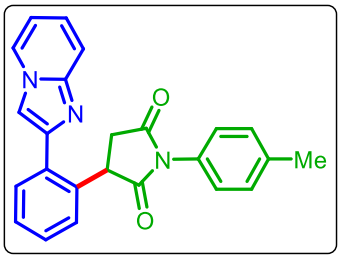

Brown solid (88 mg, 77% yield); mp 178–180 ºC; purified over a column of silica gel (35% EtOAc in hexane); ^{1}H NMR ($CDCl_3$, 400 MHz): *δ* 8.10 (d, *J* = 6.8 Hz, 1H), 7.83 (s, 1H), 7.66 – 7.63 (m, 1H), 7.45 (d, *J* = 9.2 Hz, 1H), 7.41 – 7.33 (m, 3H), 7.22 (d, *J* = 8.4 Hz, 2H), 7.14 – 7.10 (m, 3H), 6.77 (t, *J* = 6.6 Hz, 1H), 4.81 (dd, *J* = 9.6, 6.0 Hz, 1H), 3.34 (dd, *J* = 18.2, 9.8 Hz, 1H), 3.15 (dd, *J* = 18.4, 6.0 Hz, 1H), 2.36 (s, 3H); ^{13}C {^{1}H} NMR ($CDCl_3$, 151 MHz): *δ* 177.9, 176.3, 145.4, 145.2, 138.4, 135.3, 133.7, 130.7, 130.2, 129.8, 129.7, 128.8, 128.1, 126.3, 125.7, 124.8, 117.8, 112.8, 110.8, 45.6, 38.3, 21.3; IR (neat, cm^{-1}): 2922, 1775, 1700, 1511, 1380, 1275, 1161, 811, 751, 670; HRMS (ESI-TOF) calcd for $C_{24}H_{20}N_3O_2$ $[M + H]^+$ 382.1550, found 382.1549.

3-(2-(Imidazo[1,2-*a*]pyridin-2-yl)phenyl)-1-(4-methoxyphenyl)pyrrolidine-2,5-dione (4ar):

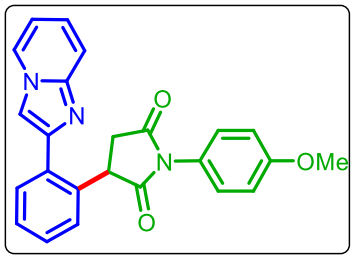

Light brown solid (94 mg, 79% yield); mp 165–168 ºC; purified over a column of silica gel (40% EtOAc in hexane); ^{1}H NMR (DMSO-d_6, 600 MHz): *δ* 8.56 (d, *J* = 6.6 Hz, 1H), 8.25 (s, 1H), 7.72 (d, *J* = 7.2 Hz, 1H), 7.48 (d, *J* = 7.2 Hz, 1H), 7.44 – 7.38 (m, 3H), 7.24 (t, *J* = 8.1 Hz, 1H), 7.15 (d, *J* = 8.4

TH-3369_166122017

Hz, 2H), 7.00 (d, *J* = 9.0 Hz, 2H), 6.92 (t, *J* = 6.6 Hz, 1H), 4.90 (br s, 1H), 3.77 (s, 3H), 3.29 (dd, *J* = 17.4, 9.6 Hz, 1H), 2.96 (dd, *J* = 17.7, 6.3 Hz, 1H); ^{13}C {^{1}H} NMR (DMSO-d_6, 151 MHz): *δ* 177.9, 175.9, 158.8, 144.5, 144.3, 135.6, 133.5, 131.4, 130.1, 128.3, 128.2, 127.9, 126.9, 125.5, 125.1, 116.7, 114.0, 112.6, 111.4, 55.4, 45.3, 37.8; IR (neat, cm^{-1}): 2930, 1774, 1699, 1513, 1388, 1245, 1165, 1023, 840, 753, 674, 552; HRMS (ESI-TOF) calcd for $C_{24}H_{20}N_3O_3$ $[M + H]^+$ 398.1499, found 398.1515.

1-(4-Fluorophenyl)-3-(2-(imidazo[1,2-*a*]pyridin-2-yl)phenyl)pyrrolidine-2,5-dione (**4ai**)

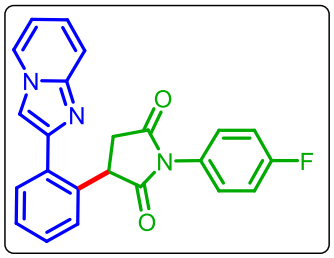

Brown solid (81 mg, 70% yield); mp 141–143 ºC; purified over a column of silica gel (35% EtOAc in hexane); ^{1}H NMR ($CDCl_3$, 600 MHz): *δ* 8.09 (d, *J* = 6.6 Hz, 1H), 7.81 (s, 1H), 7.66 – 7.64 (m, 1H), 7.40 – 7.32 (m, 4H), 7.23 (dd, *J* = 8.4, 4.8 Hz, 2H), 7.11 – 7.07 (m, 3H), 6.76 (t, *J* = 6.9 Hz, 1H), 4.76 (dd, *J* = 8.7, 6.3 Hz, 1H), 3.32 (dd, *J* = 18.6, 9.6 Hz, 1H), 3.18 (dd, *J* = 18.0, 6.0 Hz, 1H); ^{13}C {^{1}H} NMR ($CDCl_3$, 101 MHz): *δ* 177.6, 176.1, 161.9 (d, *J* = 248.5 Hz), 145.4, 145.1, 134.8, 133.4, 130.9, 130.6, 128.7, 128.4 (d, *J* = 3.0 Hz), 128.2 (d, *J* = 2.0 Hz), 128.1, 125.7, 124.8, 117.7, 115.9 (d, *J* = 23.2 Hz), 112.8, 110.7, 46.7, 38.0; ^{19}F NMR ($CDCl_3$) *δ* -112.9 (s); IR (neat, cm^{-1}): 2921, 1778, 1702, 1602, 1505, 1382, 1259, 1162, 1017, 795, 664; HRMS (ESI-TOF) calcd for $C_{23}H_{17}FN_3O_2$ $[M + H]^+$ 386.1299, found 386.1302.

3-(2-(Imidazo[1,2-*a*]pyridin-2-yl)phenyl)-1-(4-(trifluoromethyl)phenyl)pyrrolidine-2,5-dione (**4as**)

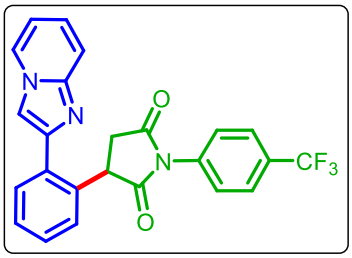

Black solid (87 mg, 67% yield); mp 165–168 ºC; purified over a column of silica gel (35% EtOAc in hexane); ^{1}H NMR ($CDCl_3$, 500 MHz): *δ* 8.12 (d, *J* = 6.5 Hz, 1H), 7.82 (s, 1H), 7.67 (d, *J* = 8.0 Hz, 3H), 7.43 – 7.35 (m, 5H), 7.32 (d, *J* = 9.0 Hz, 1H), 7.09 (t, *J* = 8.0 Hz, 1H), 6.78 (t, *J* = 6.5 Hz, 1H), 4.76 –

TH-3369_166122017

4.72 (m, 1H), 3.35 (dd, J = 18.3, 9.8 Hz, 1H), 3.24 (dd, J = 18.3, 6.3 Hz, 1H); ^{13}C {^{1}H} NMR ($CDCl_3$, 126 MHz): δ 177.2, 175.7, 145.7, 145.3, 135.8, 134.6, 133.4, 131.5, 130.6, 130.1 (q, J = 32.8 Hz), 128.8, 128.5, 126.6, 126.1 (q, J = 3.6 Hz), 125.7, 124.9, 117.8, 112.9, 110.6, 46.6, 38.1; ^{19}F NMR ($CDCl_3$) δ -62.6 (s); IR (neat, cm^{-1}): 2935, 1775, 1696, 1502, 1378, 1318, 1153, 1125, 1032, 755, 695, 642; HRMS (ESI-TOF) calcd for $C_{24}H_{17}F_3N_3O_2$ [M + H]$^+$ 436.1267, found 436.1268.

3-(2-(Imidazo[1,2-*a*]pyridin-2-yl)phenyl)-1-(*m*-tolyl)pyrrolidine-2,5-dione (**4at**)

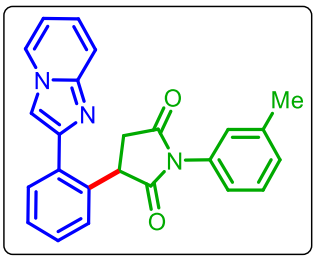

Pale yellow solid (80 mg, 70% yield); mp 155–157 °C; purified over a column of silica gel (35% EtOAc in hexane); ^{1}H NMR ($CDCl_3$, 400 MHz): δ 8.09 (d, J = 6.8 Hz, 1H), 7.82 (s, 1H), 7.64 (dd, J = 5.6, 3.0 Hz, 1H), 7.45 (d, J = 8.8 Hz, 1H), 7.39 – 7.32 (m, 3H), 7.29 (t, J = 7.8 Hz, 1H), 7.16 – 7.09 (m, 2H), 7.02 (d, J = 8.0 Hz, 1H), 6.99 (s, 1H), 6.76 (t, J = 6.8 Hz, 1H), 4.79 (dd, J = 9.6, 6.0 Hz, 1H), 3.34 (dd, J = 18.4, 9.6 Hz, 1H), 3.19 (dd, J = 18.2, 5.8 Hz, 1H), 2.31 (s, 3H); ^{13}C {^{1}H} NMR ($CDCl_3$, 151 MHz): δ 177.8, 176.2, 145.4, 145.1, 139.0, 135.2, 133.7, 132.3, 130.1, 130.3, 129.2, 128.9, 128.7, 128.1, 127.1, 125.7, 124.8, 123.6, 117.8, 112.7, 110.8, 45.7, 38.3, 21.4; IR (neat, cm^{-1}): 2925, 1781, 1705, 1514, 1385, 1262, 1169, 821, 762; HRMS (ESI-TOF) calcd for $C_{24}H_{20}N_3O_2$ [M + H]$^+$ 382.1550, found 382.1584.

3-(2-(Imidazo[1,2-*a*]pyridin-2-yl)phenyl)-1-(3-(trifluoromethyl)phenyl)pyrrolidine-2,5-dione (**4au**)

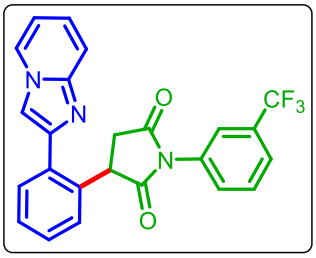

Brown solid (77 mg, 59% yield); mp 157–159 °C; purified over a column of silica gel (35% EtOAc in hexane); ^{1}H NMR ($CDCl_3$, 600 MHz): δ 8.13 (d, J = 6.6 Hz, 1H), 7.84 (s, 1H), 7.68 (d, J = 7.2, 1H), 7.60 (d, J = 7.8 Hz, 1H), 7.55 (t, J = 7.8 Hz, 1H), 7.51 (s, 1H), 7.49 (d, J = 7.8 Hz, 1H), 7.44 – 7.36 (m, 3H), 7.33 (d, J = 9.0 Hz, 1H), 7.10 (t, J = 8.1 Hz, 1H), 6.79 (t, J = 6.3 Hz, 1H), 4.72 (t, J = 7.8 Hz, 1H),

TH-3369_166122017

3.39 – 3.29 (m, 2H); ^{13}C {^{1}H} NMR ($CDCl_3$, 101 MHz): δ 177.3, 175.8, 145.5, 145.2, 134.5, 133.2 (d, J = 14.5 Hz), 131.7, 131.5, 131.3, 130.7, 129.8, 129.5, 128.8, 128.5, 125.7, 125.1, 124.9 (q, J = 3.7 Hz), 123.5 (q, J = 3.8 Hz), 122.3, 117.7, 113.0, 110.6, 46.5, 38.1; ^{19}F NMR ($CDCl_3$) δ -62.5 (s) IR (neat, cm^{-1}): 3042, 1772, 1691, 1502, 1381, 1318, 1162, 1120, 965, 835, 739, 683; HRMS (ESI-TOF) calcd for $C_{24}H_{17}F_3N_3O_2$ $[M + H]^+$ 436.1267, found 436.1265.

3-(2-(Imidazo[1,2-*a*]pyridin-2-yl)phenyl)-1-(*o*-tolyl)pyrrolidine-2,5-dione (**4av**)

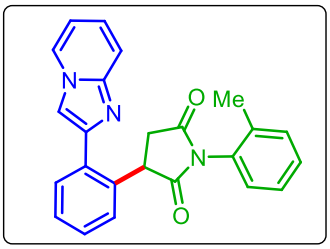

Brown gummy solid (78 mg, 68% yield, 1:1.25 rotameric diastereomer); purified over a column of silica gel (35% EtOAc in hexane); ^{1}H NMR ($CDCl_3$, 600 MHz): δ 8.12 (t, J = 6.9 Hz, 2H), 7.92 (s, 1H), 7.83 (s, 1H), 7.67 – 7.64 (m, 3H), 7.51 (d, J = 9.6 Hz, 2H), 7.44 – 7.27 (m, 10H), 7.22 – 7.19 (m, 2H), 7.15 (t, J = 7.8 Hz, 1H), 7.10 (d, J = 7.2 Hz, 1H), 6.98 (d, J = 7.8 Hz, 1H), 6.81 – 6.77 (m, 2H), 5.27 (dd, J = 9.6, 5.4 Hz, 1H), 4.86 (dd, J = 9.6, 6.0 Hz, 1H), 3.52 (dd, J = 18.9, 9.9 Hz, 1H), 3.40 (dd, J = 18.3, 9.9 Hz, 1H), 3.21 (dd, J = 18.3, 5.7 Hz, 1H), 3.04 (dd, J = 18.9, 5.1 Hz, 1H), 2.24 (s, 2.4H), 2.18 (s, 3H); ^{13}C {^{1}H} NMR ($CDCl_3$, 151 MHz): δ 177.9, 177.8, 176.0, 175.9, 145.5, 145.3, 145.2, 145.0, 136.1, 135.8, 135.7, 135.3, 134.6, 133.7, 131.6, 131.4, 131.3, 131.2, 130.9, 130.8, 130.0, 129.6, 129.3, 129.1, 128.8, 128.2, 128.1, 127.9, 127.1, 126.8, 125.8, 125.7, 125.1, 124.9, 117.9, 117.8, 112.83, 112.79, 111.4, 110.9, 45.8, 43.6, 39.1, 38.5, 18.1, 18.0; IR (neat, cm^{-1}): 2922, 1776, 1703, 1494, 1373, 1168, 912, 747, 676, 626, 487; HRMS (ESI-TOF) calcd for $C_{24}H_{20}N_3O_2$ $[M + H]^+$ 382.1550, found 382.1561.

1,1'-(Methylenebis(4,1-phenylene))bis(3-(2-(imidazo[1,2-*a*]pyridin-2-yl)phenyl)pyrrolidine-2,5-dione) (**4aw**)

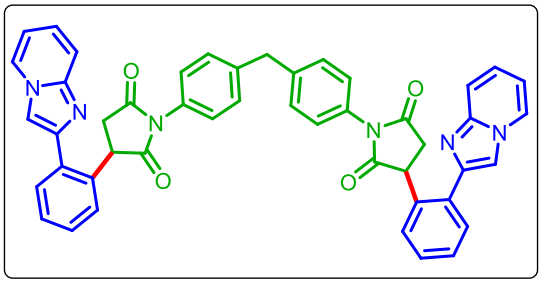

A brown solid (94 mg, 42% yield); mp 196–198 °C; purified over a column of silica gel (55% EtOAc in hexane); ^{1}H NMR ($CDCl_3$, 500 MHz): δ 8.11 (d, J = 6.5 Hz, 2H), 7.83 (s, 2H), 7.65 (dd, J = 5.5, 3.0

TH-3369_166122017

Hz, 2H), 7.44 (d, *J* = 9.5 Hz, 2H), 7.40 – 7.37 (m, 4H), 7.35 – 7.33 (m, 2H), 7.22 (d, *J* = 8.0 Hz, 4H), 7.16 (d, *J* = 8.0 Hz, 4H), 7.12 (t, *J* = 7.8 Hz, 2H), 6.78 (t, *J* = 6.8 Hz, 2H), 4.80 (dd, *J* = 9.8, 5.8 Hz, 2H), 4.00 (s, 2H), 3.35 (dd, *J* = 18.5, 10.0 Hz, 2H), 3.19 (dd, *J* = 18.5, 6.0 Hz, 2H); ^{13}C {^{1}H} NMR ($CDCl_3$, 101 MHz): *δ* 177.8, 176.2, 145.5, 145.2, 140.7, 135.3, 133.7, 130.7, 130.7, 130.3, 129.7, 128.8, 128.2, 126.5, 125.7, 124.9, 117.9, 112.9, 110.8, 45.7, 41.3, 38.4; IR (neat, cm^{-1}): 2920, 1775, 1702, 1508, 1377, 1278, 1169, 915, 841, 748, 674; HRMS (ESI-TOF) calcd for $C_{47}H_{35}N_6O_4$ [M + H]$^+$ 747.2714, found 747.2716.

3-(2-(Imidazo[1,2-*a*]pyridin-2-yl)phenyl)-1-((S)-1-phenylethyl)pyrrolidine-2,5-dione (**4ap**)

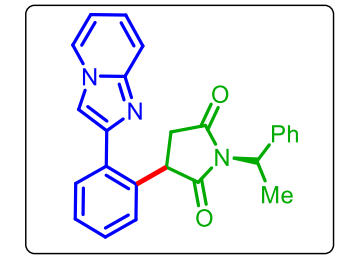

Brown solid (79 mg, 67% yield, dr 1:1), mp 115–118 ºC; purified over a column of silica gel (35% EtOAc in hexane); ^{1}H NMR ($CDCl_3$, 400 MHz): *δ* 8.09 (d, *J* = 6.8 Hz, 2H), 7.81 (d, *J* = 4.4 Hz, 2H), 7.62 – 7.58 (m, 2H), 7.52– 7.47 (m, 6H), 7.35 – 7.26 (m, 10H), 7.18 – 7.13 (m, 2H), 7.11 – 7.08 (m, 1H), 7.05 – 7.03(m, 1H), 6.77 (t, *J* = 6.8 Hz, 2H), 5.52 – 5.42 (m, 2H), 4.85 (dd, *J* = 9.6, 5.2 Hz, 1H), 4.80 (dd, *J* = 9.6, 5.2 Hz, 1H), 3.24 – 3.15 (m, 2H), 2.86 (t, *J* = 5.4 Hz, 1H), 2.81 (t, *J* = 5.4 Hz, 1H), 1.83 (d, *J* = 7.2 Hz, 3H), 1.78 (d, *J* = 7.6 Hz, 3H); ^{13}C {^{1}H} NMR ($CDCl_3$, 151 MHz): *δ* 178.8, 178.8, 176.7, 145.2, 145.2, 145.1, 139.9, 139.8, 136.25, 136.22, 134.14, 134.12, 130.7, 128.87, 128.86, 128.5, 127.82, 127.80, 127.77, 127.69, 127.6, 125.7, 124.9, 124.8, 117.7, 117.6, 112.6, 111.04, 111.03, 50.6, 50.4, 43.6, 43.5, 38.6, 38.5, 16.9, 16.4.; IR (neat, cm^{-1}): 2926, 1769, 1692, 1495, 1355, 1277, 1220, 1183, 1102, 952, 749; HRMS (ESI-TOF) calcd for $C_{25}H_{21}N_3O_2$ [M + H]$^+$ 396.1707, found 396.1720.

3-(2-(Imidazo[1,2-*a*]pyridin-2-yl)-5-methylphenyl)-1-methylpyrrolidine-2,5-dione (**4pc**)

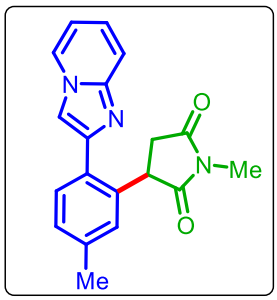

White solid (68 mg, 71% yield); mp 107–1 olumn of silica gel (35% EtOAc in hexane); ^{1}H NMR ($CDCl_3$, 400 MHz): *δ* 8 7.78 (s, 1H), 7.53 – 7.49 (m, 2H),

TH-3369_166122017

7.18 – 7.13 (m, 2H), 7.02 (s, 1H), 6.78 (t, *J* = 6.8 Hz, 1H), 4.72 (dd, *J* = 9.4, 5.4 Hz, 1H), 3.22 (dd, *J* = 18.2, 9.4 Hz, 1H), 3.00 – 2.94 (m, 4H), 2.37 (s, 3H); ^{13}C {^{1}H} NMR ($CDCl_3$, 101 MHz): *δ* 179.3, 177.4, 145.6, 145.1, 138.7, 135.4, 130.9, 130.5, 130.2, 128.9, 125.7, 124.7, 117.6, 112.7, 110.5, 45.0, 38.6, 25.1, 21.3; IR (neat, cm^{-1}): 3123, 1763, 1684, 1471, 1433, 1373, 1277, 1116, 974, 824, 785, 757; HRMS (ESI-TOF) calcd for $C_{19}H_{18}N_3O_2$ $[M + H]^+$ 320.1394, found 320.1398.

3-(2-(Imidazo[1,2-*a*]pyridin-2-yl)phenyl)pyrrolidine-2,5-dione (**4aq**)

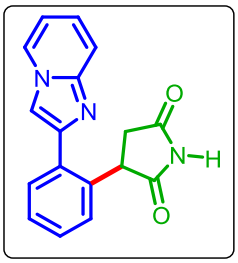

A brown gummy solid (55 mg, 63% yield); purified over a column of silica gel (40% EtOAc in hexane); ^{1}H NMR ($CDCl_3$, 400 MHz): *δ* 8.91 (s, 1H), 8.13 (d, *J* = 6.8 Hz, 1H), 7.81 (s, 1H), 7.64 – 7.61 (m, 1H), 7.57 (d, *J* = 9.2 Hz, 1H), 7.38 – 7.35 (m, 2H), 7.26 (br s, 1H), 7.17 (t, *J* = 7.8 Hz, 1H), 6.79 (t, *J* = 6.6 Hz, 1H), 4.85 (dd, *J* = 9.0, 5.8 Hz, 1H), 3.24 (dd, *J* = 18.4, 9.6 Hz, 1H), 2.97 (dd, *J* = 18.4, 5.6 Hz, 1H); ^{13}C {^{1}H} NMR ($CDCl_3$, 126 MHz): *δ* 179.6, 177.4, 145.4, 145.2, 135.4, 133.9, 130.6, 129.0, 128.9, 128.1, 125.8, 124.9, 117.7, 112.8, 110.9, 46.1, 39.8; IR (neat, cm^{-1}): 3138, 2929, 2746, 1774, 1702, 1500, 1347, 1280, 1175, 908, 725; HRMS (ESI-TOF) calcd for $C_{17}H_{14}N_3O_2$ $[M + H]^+$ 292.1080, found 292.1082.

3,3'-((Methylenebis(imidazo[1,2-*a*]pyridine-3,2-diyl))bis(2,1-phenylene))bis(1-phenylpyrrolidine-2,5-dione) (**4sa**)

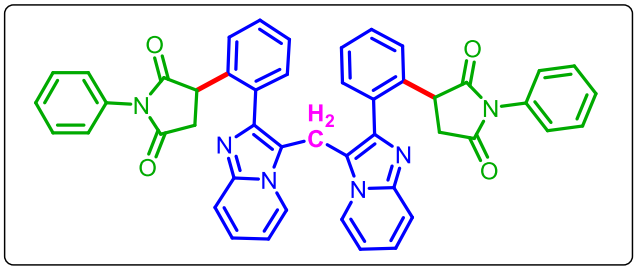

A brown solid (125 mg, 56% yield); mp 178–181 °C; purified over a column of silica gel (40% EtOAc in hexane); ^{1}H NMR ($CDCl_3$, 500 MHz): *δ* 7.60 (d, *J* = 7.0 Hz, 2H), 7.47 (d, *J* = 9.0 Hz, 2H), 7.41 – 7.32 (m, 10H), 7.22 – 7.17 (m, 4H), 7.07 – 7.02 (m, 6H), 6.56 (t, *J* = 6.8 Hz, 2H), 4.79 (d, *J* = 17.0 Hz, 1H), 4.63 (d, *J* = 17.0 Hz, 1H), 4.57 – 4.53 (m, 2H), 3.44 – 3.31 (m, 4H); ^{13}C {^{1}H} NMR ($CDCl_3$, 126 MHz): *δ* 177.8, 175.7, 144.6, 142.9, 137.9, 133.9, 132.2, 131.6, 129.4, 129.39, 129.1, 128.6, 127.9,

TH-3369_166122017

126.4, 124.7, 124.0, 117.5, 117.2, 113.1, 45.3, 39.2, 19.0; IR (neat, cm^{-1}): 2923, 1779, 1705, 1496, 1376, 1170, 956, 749, 692, 627; HRMS (ESI-TOF) calcd for $C_{47}H_{35}N_6O_4$ $[M + H]^+$ 747.2714, found 747.2727.

3,3'-((Thiobis(imidazo[1,2-*a*]pyridine-3,2-diyl))bis(2,1-phenylene))bis(1-phenylpyrrolidine-2,5-dione) (**4ta**)

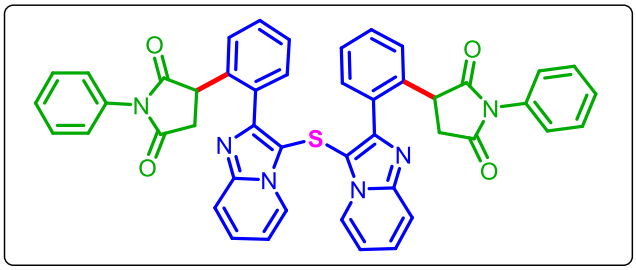

A pale yellow solid (117 mg, 51% yield); mp 218–220 ºC; purified over a column of silica gel (45% EtOAc in hexane); ^{1}H NMR ($CDCl_3$, 400 MHz): δ 7.68 (d, J = 7.6 Hz, 2H), 7.60 (t, J = 7.6 Hz, 2H), 7.54 (d, J = 6.8 Hz, 4H), 7.45 – 7.41 (m, 6H), 7.39 – 7.37 (m, 4H), 7.26 (d, J = 7.2 Hz, 4H), 7.12 (t, J = 7.6 Hz, 2H), 6.68 (t, J = 6.6 Hz, 2H), 4.42 (dd, J = 9.8, 6.2 Hz, 2H), 3.33 (dd, J = 18.6, 9.8 Hz, 2H), 2.72 (dd, J = 18.8, 6.0 Hz, 2H); ^{13}C {^{1}H} NMR ($CDCl_3$, 151 MHz): δ 177.3, 175.5, 150.3, 146.2, 137.6, 133.1, 133.1, 132.2, 129.9, 129.2, 129.2, 128.5, 127.7, 126.9, 126.5, 124.9, 117.4, 113.9, 109.1, 45.2, 38.8; IR (neat, cm^{-1}): 2930, 1776, 1703, 1494, 1446, 1371, 1234, 1159, 837, 745, 692; HRMS (ESI-TOF) calcd for $C_{46}H_{33}N_6O_4S$ $[M + H]^+$ 765.2279 found 765.2297.

1-Phenyl-3-(2-phenyl-1*H*-imidazol-1-yl)pyrrolidine-2,5-dione (**5aa**)

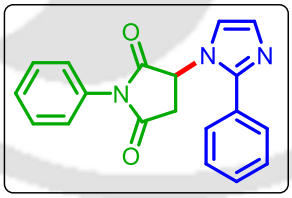

Brown solid (69 mg, 73% yield); mp 175–178 ºC; purified over a column of silica gel (30% EtOAc in hexane); ^{1}H NMR ($CDCl_3$, 500 MHz): δ 7.68 – 7.66 (m, 2H), 7.52 – 7.49 (m, 5H), 7.44 (t, J = 7.5 Hz, 1H), 7.32 (d, J = 7.5 Hz, 1H), 7.27 (d, J = 1.0 Hz, 1H), 7.02 (d, J = 1.0 Hz, 1H), 5.52 (dd, J = 9.8, 5.8 Hz, 1H), 3.42 (dd, J = 18.5, 9.5 Hz, 1H), 3.09 (dd, J = 18.5, 6.0 Hz, 1H); ^{13}C{^{1}H} NMR ($CDCl_3$, 126 MHz): δ 172.4, 171.8, 149.5, 131.2, 130.6, 129.8, 129.6, 129.5, 129.3, 129.1, 126.3, 120.2, 116.6, 54.1, 37.2; IR (KBr, cm^{-1}): 3130, 3063, 1717, 1598, 1499, 1394, 1183, 1126, 747, 696; HRMS (ESI-TOF) calcd for $C_{19}H_{16}N_3O_2$ $[M + H]^+$ 318.1237, found 318.1238.

TH-3369_166122017

III.8. NMR Spectra

^{1}H NMR of **1-Phenyl-3-(2-phenylimidazo[1,2-*a*]pyridin-3-yl)pyrrolidine-2,5-dione** (**3aa**) (DMSO-d_6, 600 MHz)

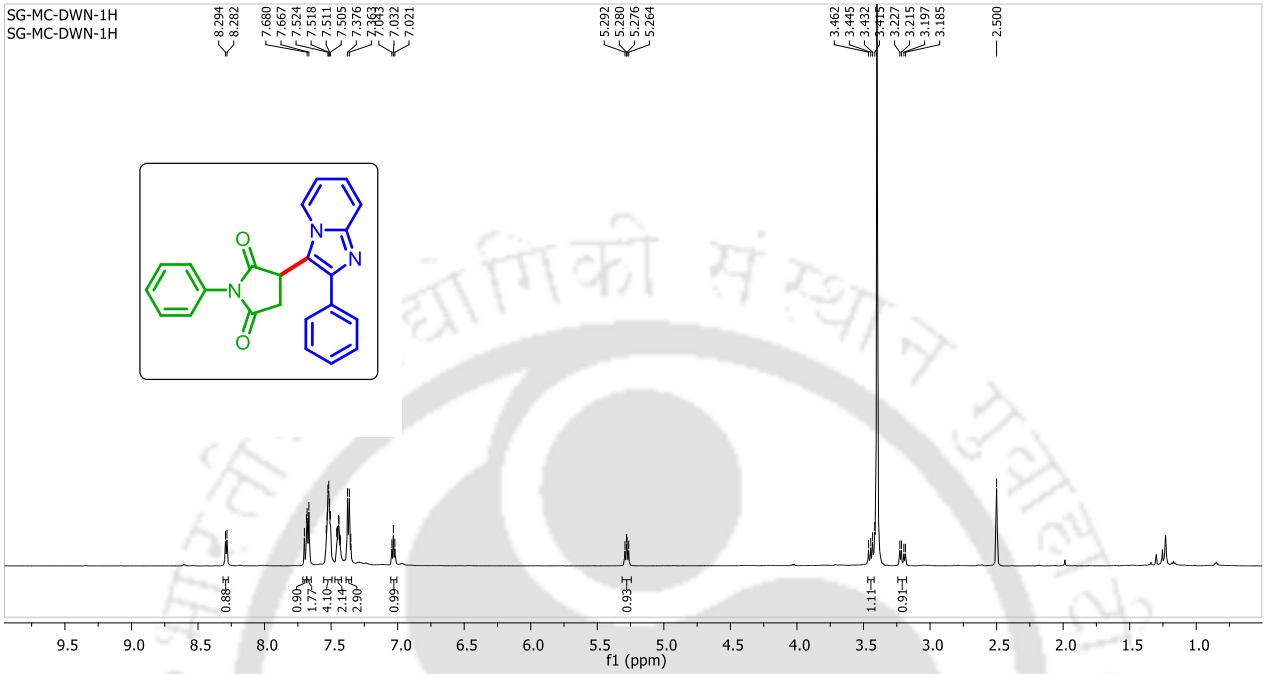

^{13}C NMR of **1-Phenyl-3-(2-phenylimidazo[1,2-*a*]pyridin-3-yl)pyrrolidine-2,5-dione** (**3aa**) (DMSO-d_6, 151 MHz)

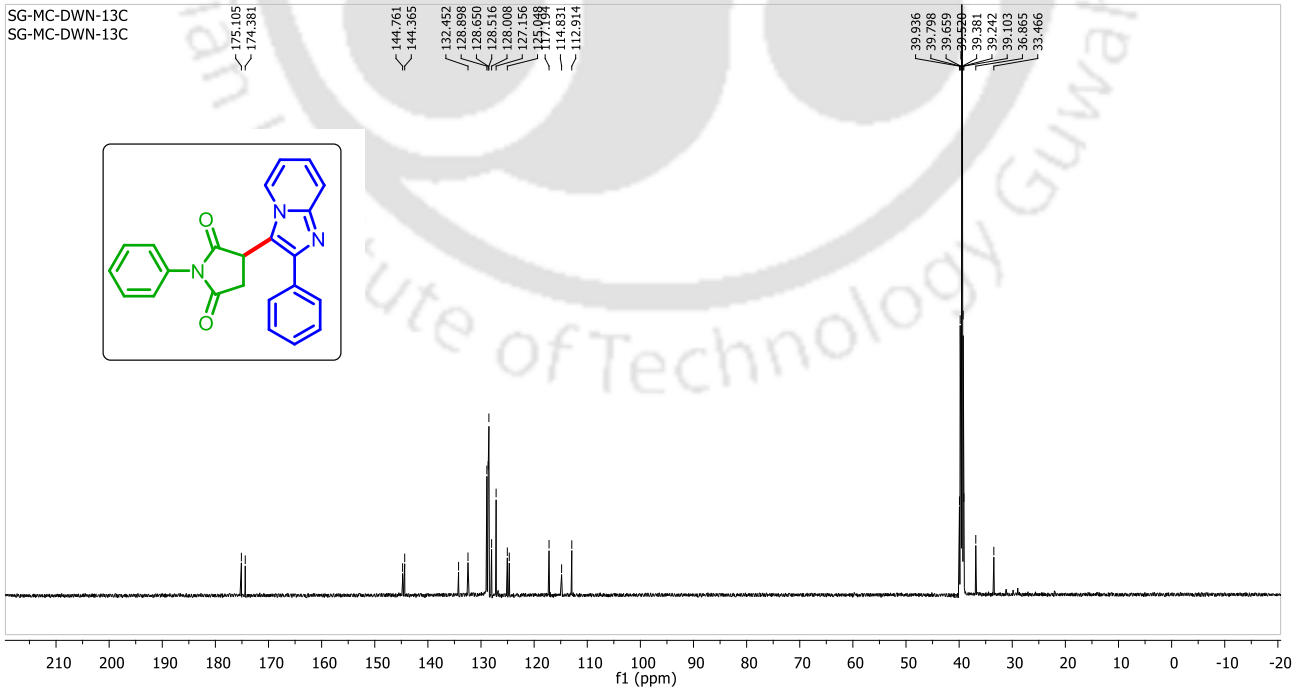

TH-3369_166122017

^{1}H NMR of **3-(2-(Imidazo[1,2-*a*]pyridin-2-yl)phenyl)-1-phenylpyrrolidine-2,5-dione** (**4aa**) ($CDCl_3$, 600 MHz)

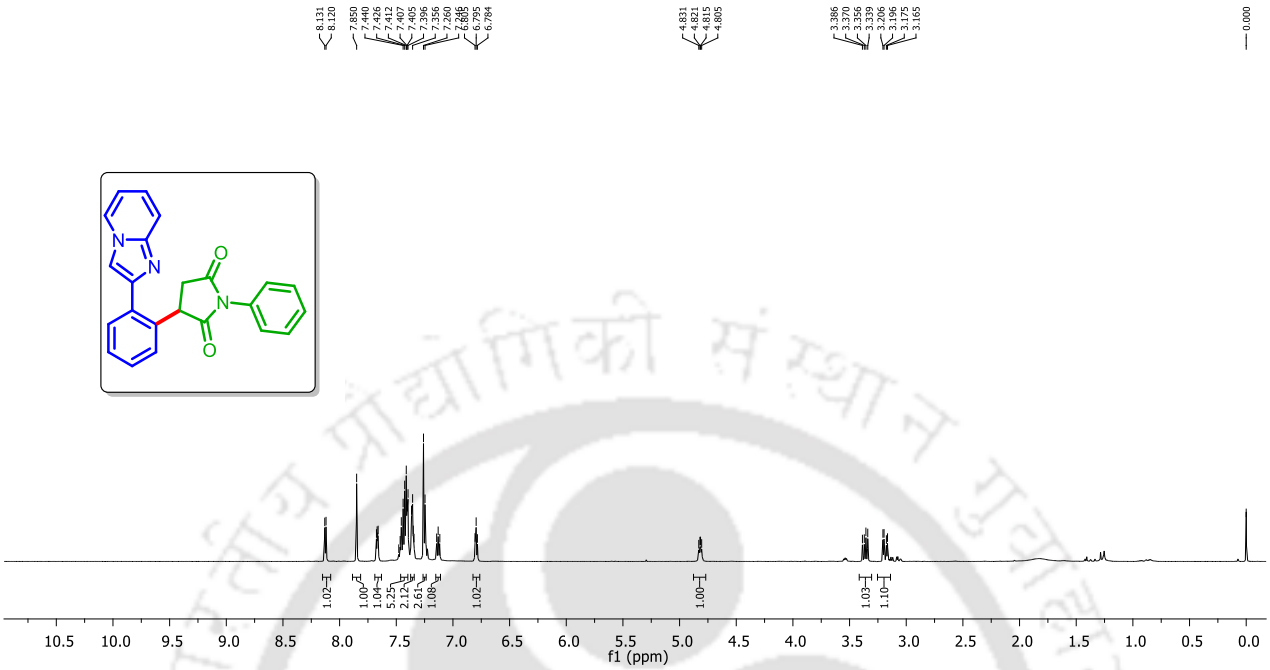

^{13}C NMR of **3-(2-(Imidazo[1,2-*a*]pyridin-2-yl)phenyl)-1-phenylpyrrolidine-2,5-dione** (**4aa**) ($CDCl_3$, 101 MHz)

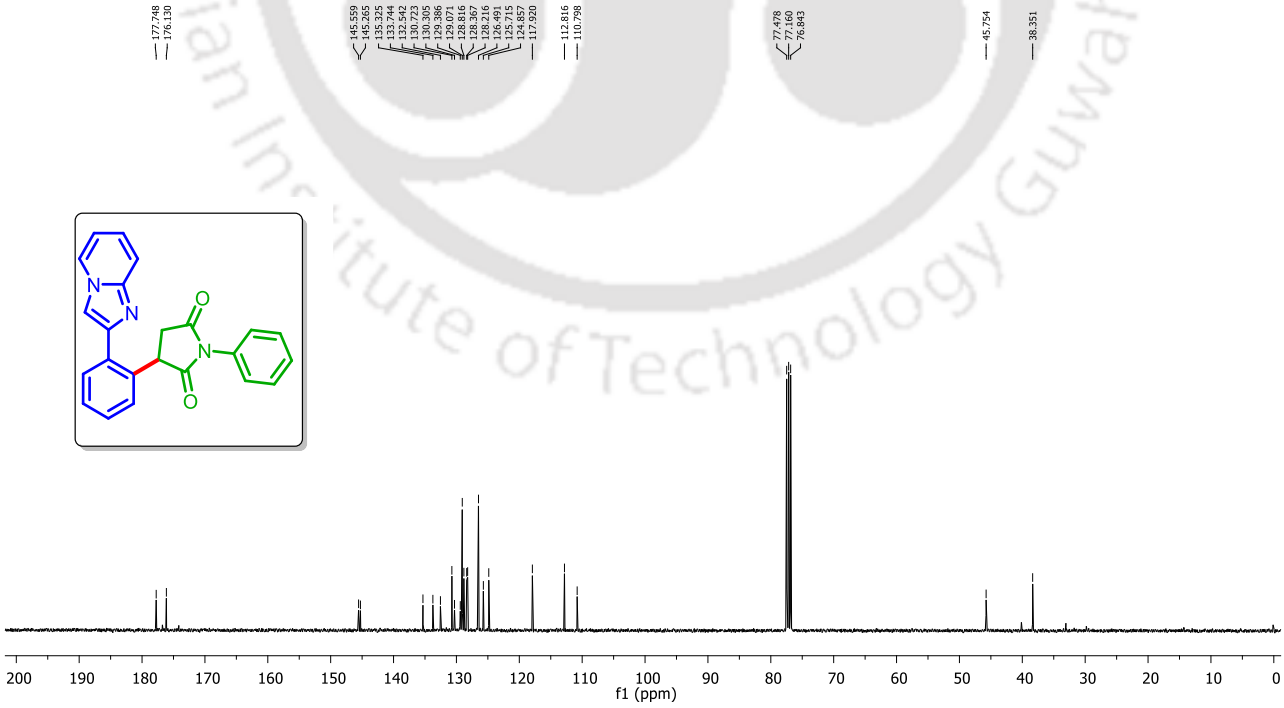

TH-3369_166122017

The remaining NMR spectra are available on

https://pubs.acs.org/doi/suppl/10.1021/acs.orglett.1c02536/suppl_file/ol1c02536_si_001.pdf

TH-3369_166122017

CHAPTER IV

Mn(I)-Catalyzed Preferential Electrophilic C3-Maleimidation in Quinoxaline Leading to Spirocyclization and Dehydrogenation of Succinimides

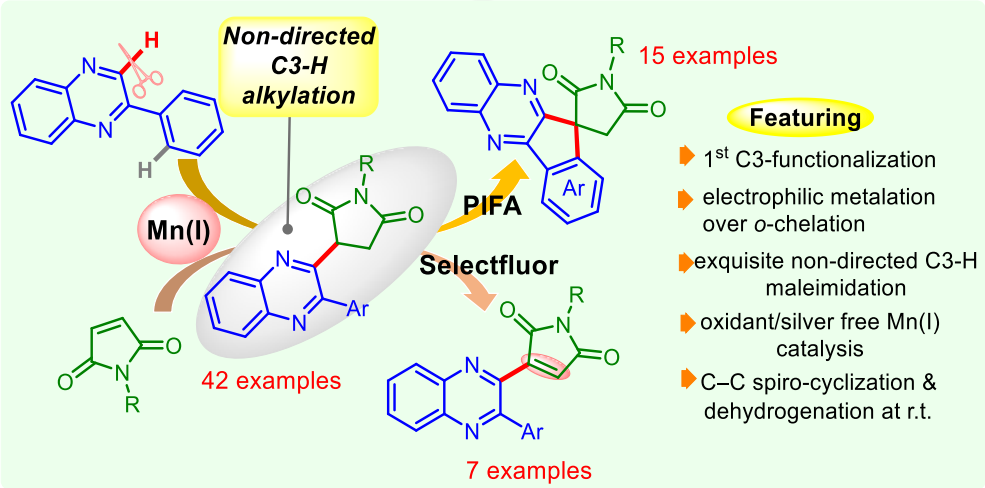

Abstract: *A Mn(I)-catalyzed site-selective nondirected C3-maleimidation of quinoxaline is established. Herein, the electrophilic C3-metalation precedes over the o-directed strategy to access diversely substituted quinoxaline-appended succinimides. The products undergo PIFA-promoted C(sp2)–C(sp3) spirocyclization via π-electrons drifting from aryls and Selectfluor-mediated dehydrogenation of succinimide at room temperature.*

Keywords:

Mn(I) catalysis, regio-divergent alkylation, solvent-switching, imidazopyridine, maleimide

OL | Organic Letters

Cite this: *Org. Lett.* 2023, 25, 20, 3806−3811
Publication Date: May 17, 2023
https://doi.org/10.1021/acs.orglett.3c01350
Copyright © 2023 American Chemical Society
Request reuse permissions Subscribed

Article Views 1580 | Altmetric 7 | Citations 7
LEARN ABOUT THESE METRICS

CHAPTER IV

IV.1. Introduction

Succinimide is a well-known structural motif found in natural products and value-added clinical drugs, which can be fragmented into pyrrolidines and γ-lactams to construct promising natural products (Figure IV.1.1).[1] In this context, transition metal-catalyzed C–H bond activation has emerged as a powerful tool to construct substituted succinimides by coupling maleimides with heteroarenes.[2]

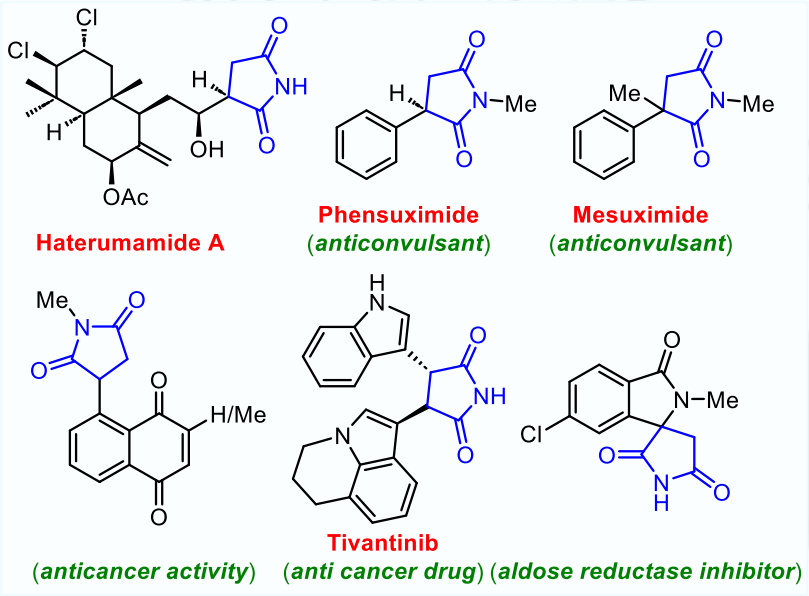

Figure IV.1.1. *Succinimide-containing bioactive scaffolds*

IV.2. Prior Strategies of Metal-Catalyzed Synthesis of Succinimide Scaffolds

➢ **Directed C-H Maleimidation:**

In last decade various groups have introduced transition-metal catalyzed C–H maleimidation of several arenes and heterarenes. To accomplish such strategies various heteroatom-contained directing groups have utilized. Such directing groups dictated the C–H maleimidation towards ortho, peri C–H of arenes along with proximal C(sp^3)-H sites. Further, in some reports traces-less directed strategy has also been developed to access C-H maleimidation. These reactions are briefly summarized in Scheme IV.2.1.

TH-3369_166122017

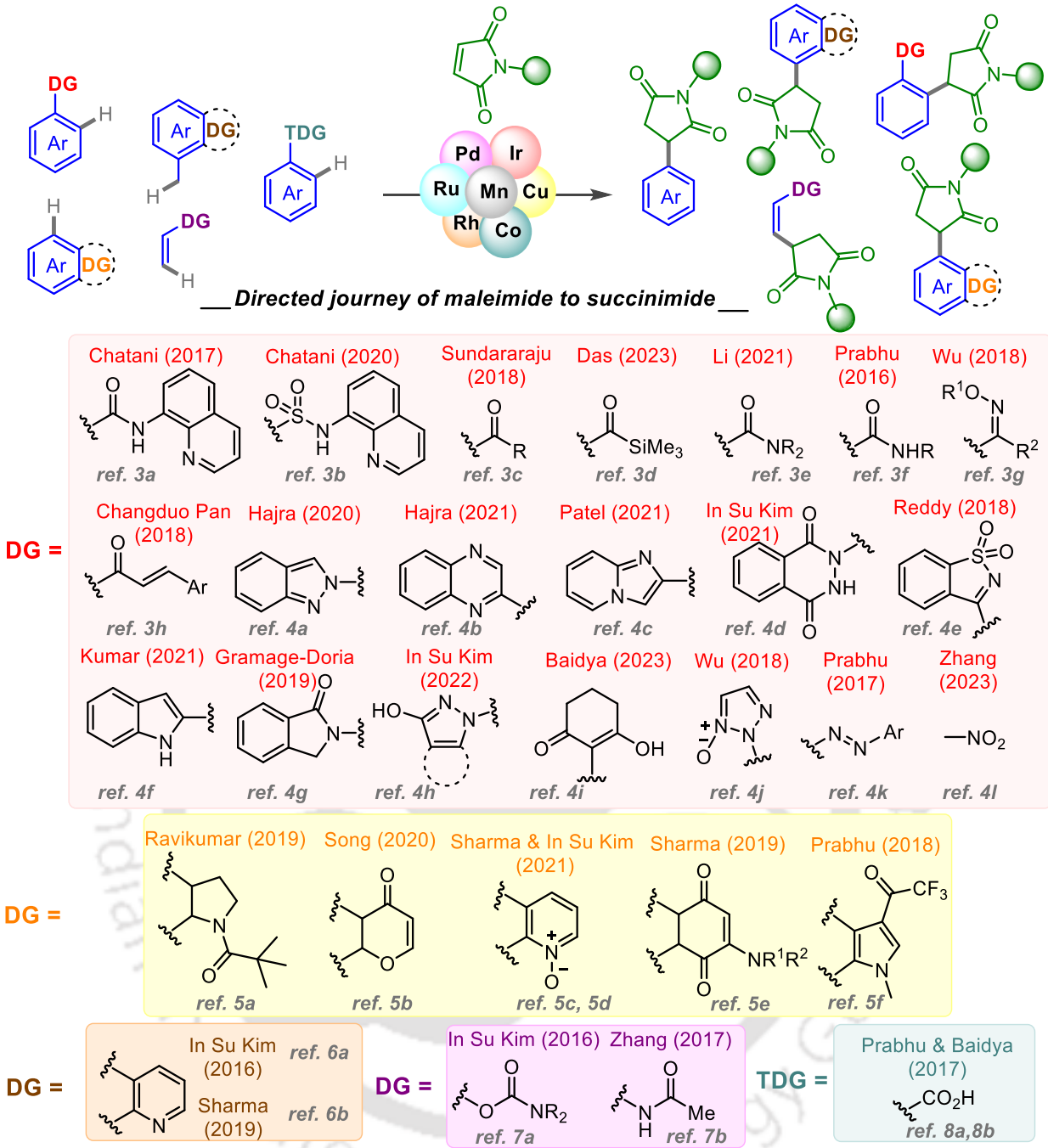

Scheme IV.2.1. *Transition-metal catalyzed directed synthesis of succinimides from maleimides [DG= Directing group, TDG= Traceless directing group]*

However, these protocols rely on directing groups (DGs) to functionalize adjacent proximal C–H bonds.[3-8] Thus, an unbiased electrophilic-metalation over DG-assisted strategy at the non-directed C–H bond is desirable.[9] Quinoxaline is a privileged *N*-containing fused heterocycle, found in natural products, pharmaceuticals, and material sciences (Figure IV.2.1).[10] In 2-aryl substituted quinoxaline

TH-3369_166122017

core as well, the directing group strategy invariably leads to *o*-C–H functionalizations (Scheme IV.2.2).[11]

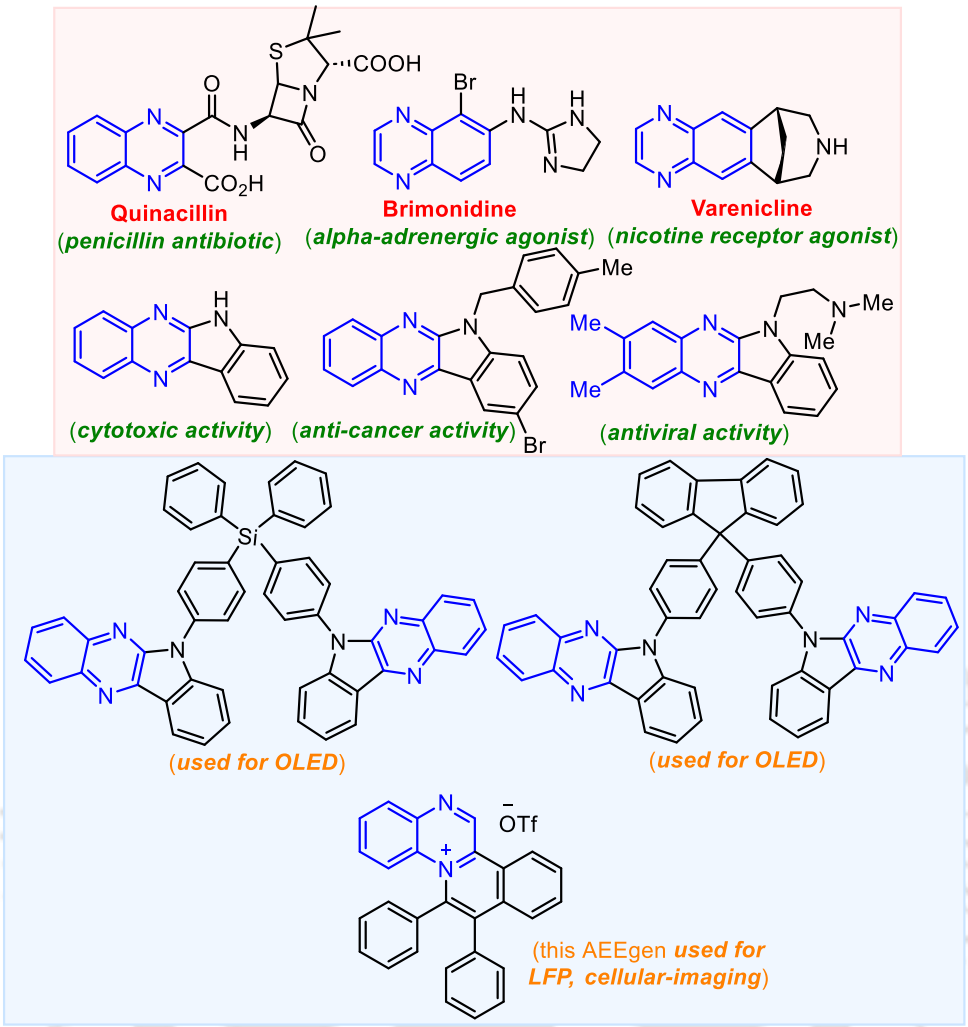

Figure IV.2.1. *Quinoxaline-containing pharmaceutical and material compounds*

IV.3. Prior *ortho*-Directed C–H Functionalization Strategies of Quinoxaline

Over the past years, many groups have dedicated significant efforts to developing various transition-metal catalyzed strategies such as acetoxylation, nitration, halogenation, Heck-type alkenylation, arylation and aroylation *via* directed *ortho* C–H functionalization of 2-aryl quinoxalines. These reactions are briefly summarized in Scheme IV.3.1.

TH-3369_166122017

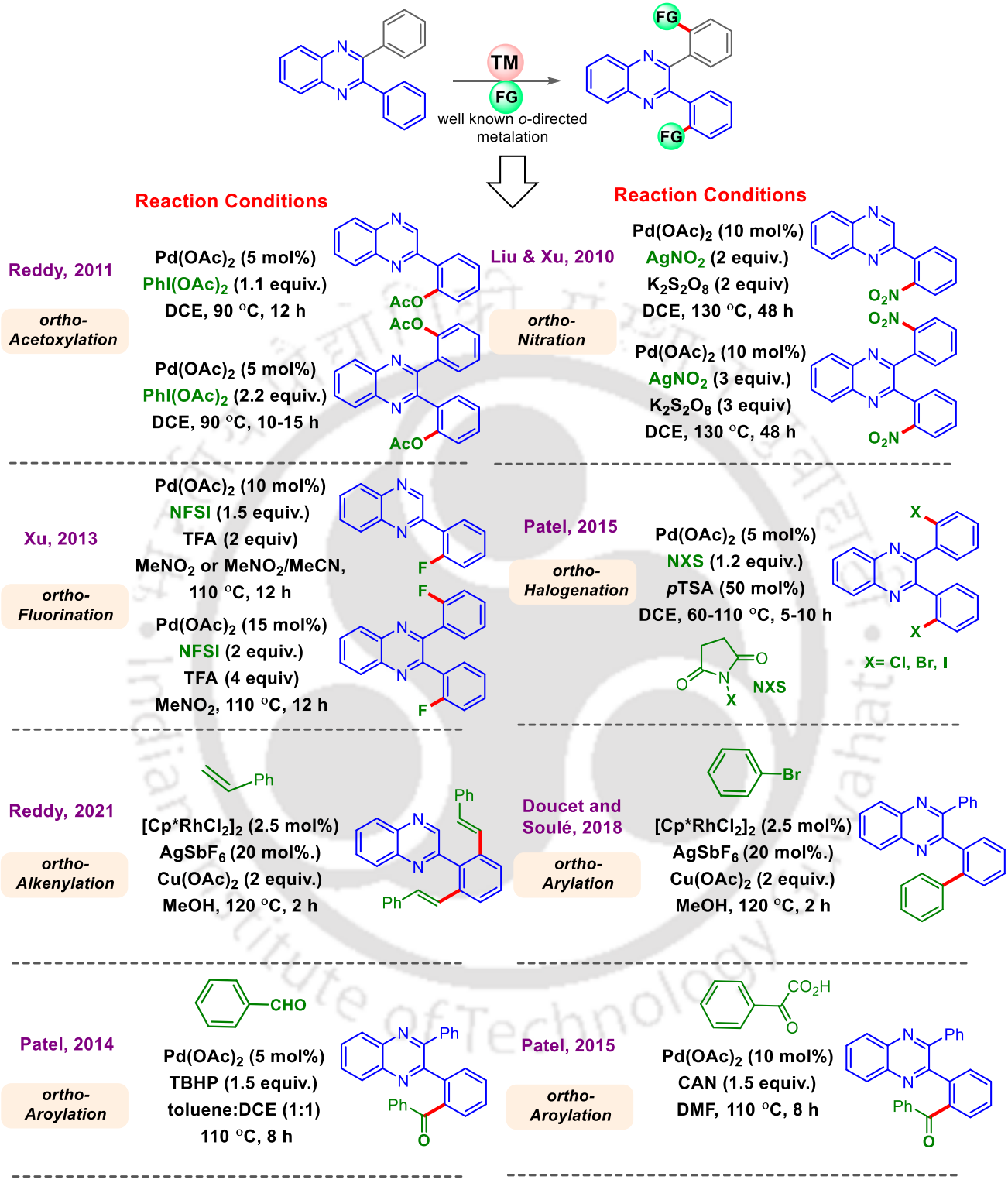

Scheme IV.3.1. *Transition-metal catalyzed directed ortho-C-H functionalization of quinoxaline*

In continuation to this recently, Hajra *et. al*. has obtained *o*-maleimidation and spiro-cyclization of 2-aryl quinoxalines under Ru(II) catalysis using Cu/Ag additives (Scheme IV.3.2).[12] The spiro-

TH-3369_166122017

cyclization proceeds *via* nucleophilic attack of the diffused quinoxaline π-electrons to the *o*-functionalized C–C bond of maleimide (Scheme IV.3.2).

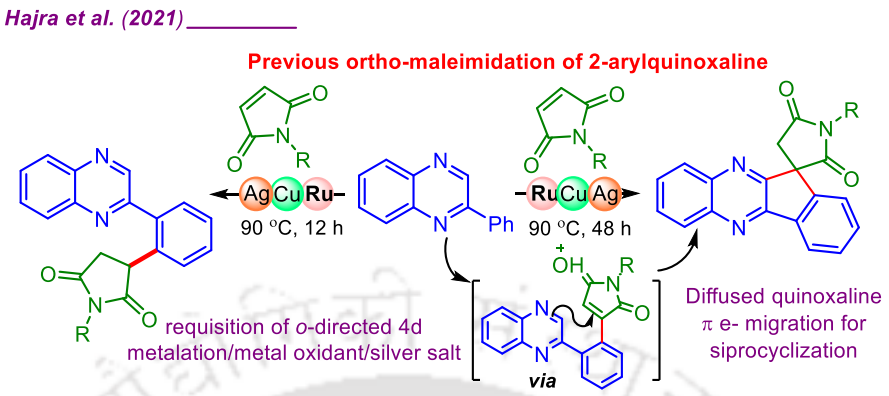

Scheme IV.3.2. *Ru-catalyzed directed ortho-C-H maleimidation of quinoxaline*

The aforementioned detailed literature survey on quinoxaline C-H functionalization indicates that regioselective functionalization at the non-directed C3-position on quinoxaline is unexplored, as it requires challenging electrophilic metalation over favorable *N*-directed *o*-chelation (Scheme IV.3.3). The use of 3d-metal catalysts to achieve such metalation is advantageous, among which Mn is the most promising one, which offers selective electrophilic metalation over directing group-enabled strategies.[13]

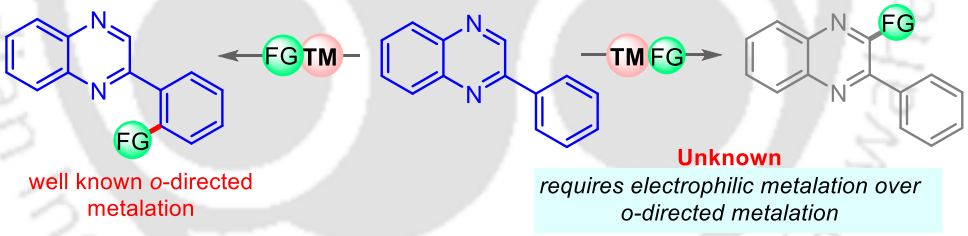

Scheme IV.3.3. *Pictorial representation of C-H functionalization reactions of quinoxalines*

IV.4. Present Strategy

Intrigued by the detailed literature assessment, here in we envisioned a C3–H maleimidation of quinoxaline over the DG-assisted *o*-functionalization under Mn(I) catalysis (Scheme IV.4.1).

TH-3369_166122017

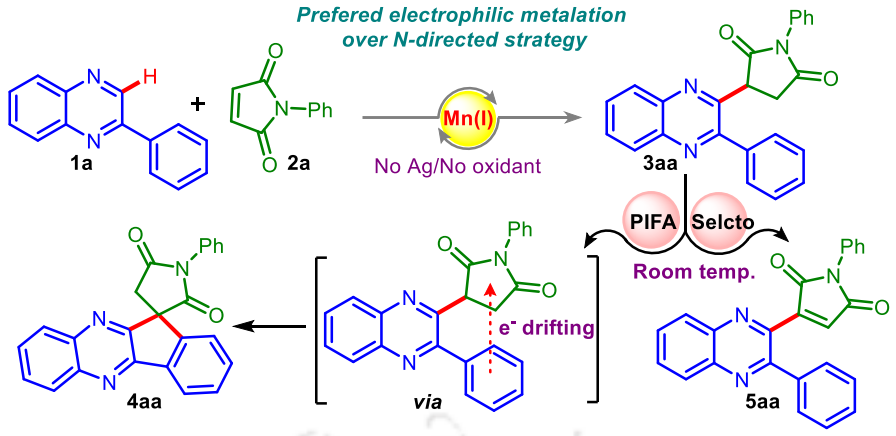

Scheme IV.4.1. *Present C–H maleimidation of quinoxalines*

Optimization of Reaction Condition:

To validate our proposition, a reaction was conducted between 2-phenyl quinoxaline (**1a**) and *N*-phenyl maleimide (**2a**) in the presence of $Mn(CO)_5Br$ (10 mol %) and NH_4OAc (20 mol %) in DCE at 100 °C. Delightfully, an exclusive C3–H maleimidated quinoxaline (**3aa**) was isolated in 52% yield (Table IV.4.1, entry 1). Now, to further improve the yield, various solvents (TFE, $CHCl_3$, EtOAc, MeCN) were examined keeping all other parameters unaltered, among which ethyl acetate was found to be the best for C3-maleimidation (Table IV.4.1, entry 4). Further, it was observed that NH_4OAc is crucial for this reaction (Table IV.4.1, entry 6). The variation in additives such as NaOAc, Na_2CO_3, Cs_2CO_3 were found unproductive (Table IV.4.1, entries 7–9). Interestingly, an increase in the loading of NH_4OAc to 30 mol %, enhanced the yield up to 88% (Table IV.4.1, entry 10). But, a further increase (50 mol %) in NH_4OAc loading was counterproductive (Table IV.4.1, entry 11). The catalyst $Mn(CO)_5Br$ is crucial for this reaction as other Mn-salt $Mn_2(CO)_{10}$ was not so effective (Table IV.4.1, entries 12 and 13). An increase or decrease in the reaction temperature was detrimental to the protocol (Table IV.4.1, entries 14 and 15). The product yield was unaffected under an argon atmosphere suggesting the non-interference of atmospheric oxygen (Table IV.4.1, entry 16).

TH-3369_166122017

Table IV.4.1. Optimization of Reaction Conditions.[a,b]

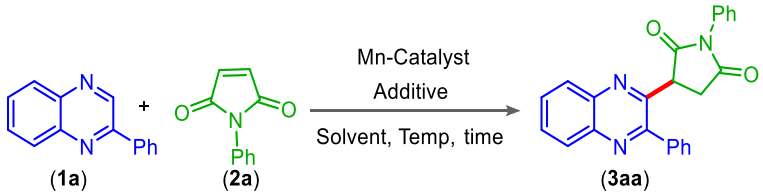

Entry	Catalyst	Additive	Solvent	Yield (%)[b]
1.	$Mn(CO)_5Br$	NH_4OAc (20 mol%)	1,2-DCE	52
2.	$Mn(CO)_5Br$	NH_4OAc (20 mol%)	TFE	n.d.
3.	$Mn(CO)_5Br$	NH_4OAc (20 mol%)	$CHCl_3$	64
4.	$Mn(CO)_5Br$	NH_4OAc (20 mol%)	ethylacetate	77
5.	$Mn(CO)_5Br$	NH_4OAc (20 mol%)	MeCN	n.d.
6.	$Mn(CO)_5Br$	---	ethylacetate	traces
7.	$Mn(CO)_5Br$	NaOAc (20 mol%)	ethylacetate	62
8.	$Mn(CO)_5Br$	Na_2CO_3 (20 mol%)	ethylacetate	n.d.
9.	$Mn(CO)_5Br$	Cs_2CO_3 (20 mol%)	ethylacetate	n.d.
10.	**$Mn(CO)_5Br$**	**NH_4OAc (30 mol%)**	**ethylacetate**	**88**
11.	$Mn(CO)_5Br$	NH_4OAc (50 mol%)	ethylacetate	82
12.	---	NH_4OAc (30 mol%)	ethylacetate	n.d.
13.	$Mn_2(CO)_{10}$	NH_4OAc (30 mol%)	ethylacetate	74
14.[c]	$Mn(CO)_5Br$	NH_4OAc (30 mol%)	ethylacetate	66
15.[d]	$Mn(CO)_5Br$	NH_4OAc (30 mol%)	ethylacetate	80
16.[e]	$Mn(CO)_5Br$	NH_4OAc (30 mol%)	ethylacetate	82

[a]Reaction Conditions unless specified otherwise: **1a** (0.2 mmol), **2a** (0.28 mmol), $Mn(CO)_5Br$ (10 mol%), additives, solvent (0.1 M) under open air at 100 °C for 9 h. [b]Isolated yield. [c]Reaction carried out at 80 °C. [d]Reaction carried out at 120 °C. [e]Reaction carried out under Ar. n.d. = not detected.

Scope of Non-directed C3-Maleimidation:

The optimized protocol was then explored towards various 2-arylquinoxalines (**1a**–**1r**) and *N*-substituted maleimides (**2a**–**2w**) and results are summarized in Scheme IV.4.2 and IV.4.3. A series of substituents *p*–Me (**1b**), *p*–OMe (**1c**), *p*–F (**1d**), *p*–Cl (**1e**), *p*–CF_3 (**1f**), *p*–Ph (**1g**), *m*–Me (**1h**), *m*-CF_3 (**1i**), *o*-OMe (**1j**), 2,6–difluoro (**1k**) groups on the phenyl ring and 6,7-di-chloro (**1l**), 2-naphthyl (**1m**), 2-thiophenyl (**1n**) and 2-benzo[1,3]dioxole (**1o**) groups on quinoxaline, all reacted smoothly with *N*-phenyl maleimide **2a** to furnish C3-maleimidated products **3ba**–**3oa** in good yields (68–94%) (Scheme IV.4.1). Various *N*-alkyl substituted maleimides such as –Me (**2b**), –Et (**2c**), –Pr (**2d**), –^{i}Bu (**2e**), –Cy (**2f**), ethylbenzene (**2g**), *n*-butylbenzene (**2h**), *n*-hexyl (**2i**) and *n*-decyl (**2j**) all reacted smoothly with 2-phenyl quinoxaline (**1a**) to provide their corresponding C3-maleimidated products (**3ab**–**3aj**) in good yields (79–88%) (Scheme IV.4.2). Similarly, substituted *N*-aryl maleimides *p*–OMe (**2k**), *p*–F (**2l**), *p*–CF_3 (**2m**), *p*–NMe_2 (**2n**) and *N*-benzyl maleimide (**2o**) having *p*–OMe (**2p**) substituents were well reacted to this protocol to deliver C3-maleimidated products **3ak**–**3ap** in excellent yields (80–91%).

TH-3369_166122017

Further, maleimides derived from cyclohexyl methyl amine (**2q**), thio-phenethyl amine (**2r**), chiral amine (**2s**), unsubstituted NH unit (**2t**), tryptamine alkaloids (**2u**) and aminopyrene probe (**2v**), all successfully gave their C3-malemidated products **3aq**–**3av** (in 76–85% yields). Natural products, *L*-menthol and (-)-borneol linked 2-aryl quinoxalines (**1p** and **1q**) smoothly reacted, delivering their corresponding maleimidated products **3pa** (85%) and **3qa** (83%). Interestingly, a di-maleimide (**2w**) provided *bis*-C3-maleimidated products **3aw** (78%) and **3rw** (81%) when reacted with two equivalents of **1a** and **1r** respectively. To validate the feasibility of the strategy in a large-scale synthesis, the reaction was performed on a 2 mmol scale under the standard protocol, which provided **3aa** in 80% isolated yield.

Scheme IV.4.2. *Scope of quinoxalines of non-directed C3-maleimidation* [a,b]

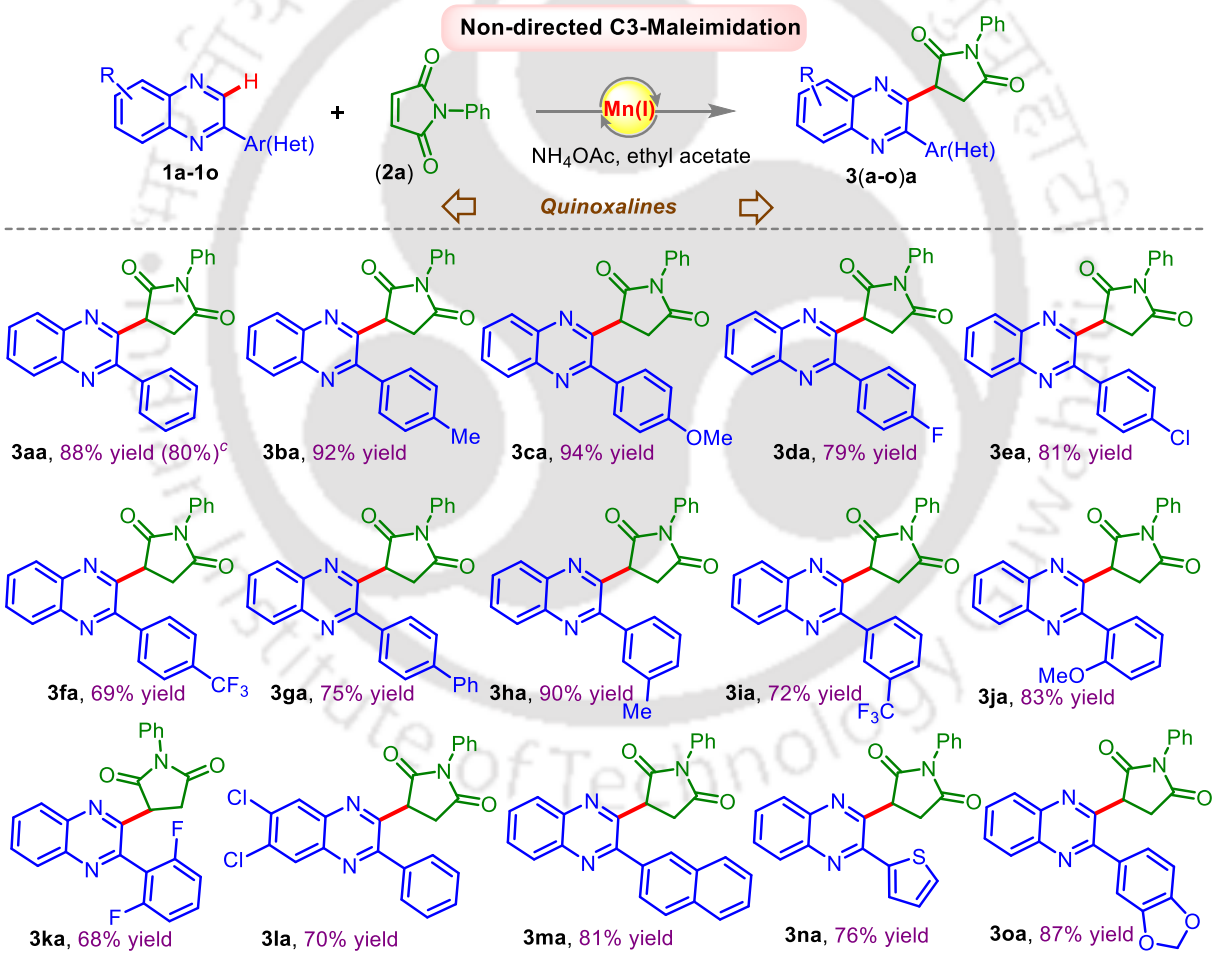

[a]Reaction Condition: **1**(**a-o**) (0.2 mmol), **2a** (0.28 mmol), $Mn(CO)_5Br$ (10 mol%), and NH_4OAc (30 mol%) in ethyl acetate (0.1 M) at 100 °C for 9 h under an air atmosphere. [b]Isolated yield after column chromatography. [c]Reaction performed at 2 mmole scale.

TH-3369_166122017

Scheme IV.4.3. *Scope of maleimides of non-directed C3-maleimidation* [a,b]

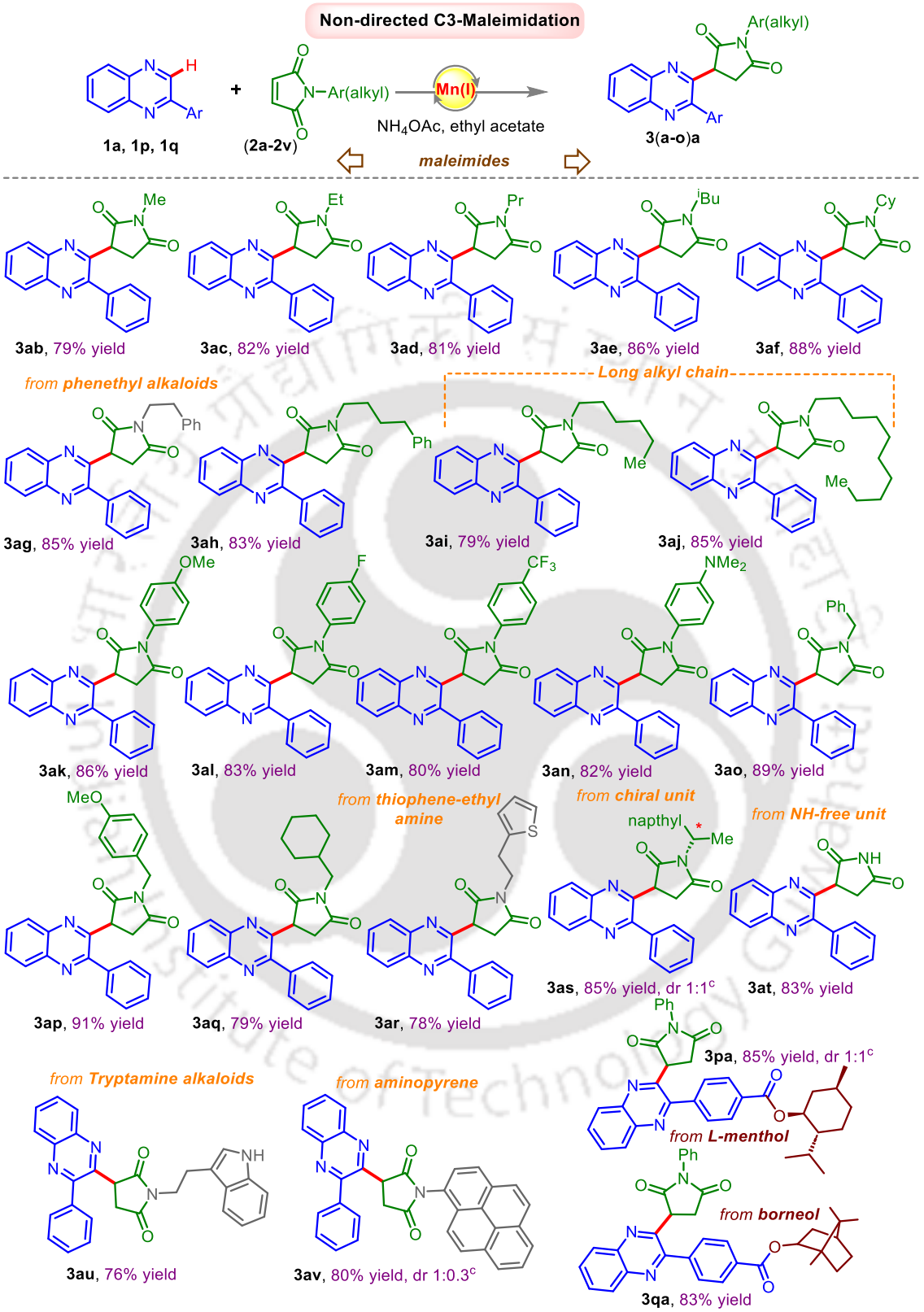

[a]Reaction Condition: **1a**, **1p**, **1q** (0.2 mmol), **2a-2v** (0.28 mmol), $Mn(CO)_5Br$ (10 mol%), and NH_4OAc (30 mol%) in ethyl acetate (0.1 M) at 100 °C for 9 h under an air atmosphere. [b]Isolated yield after column chromatography. [c]Based on ^1H NMR analysis.

TH-3369_166122017

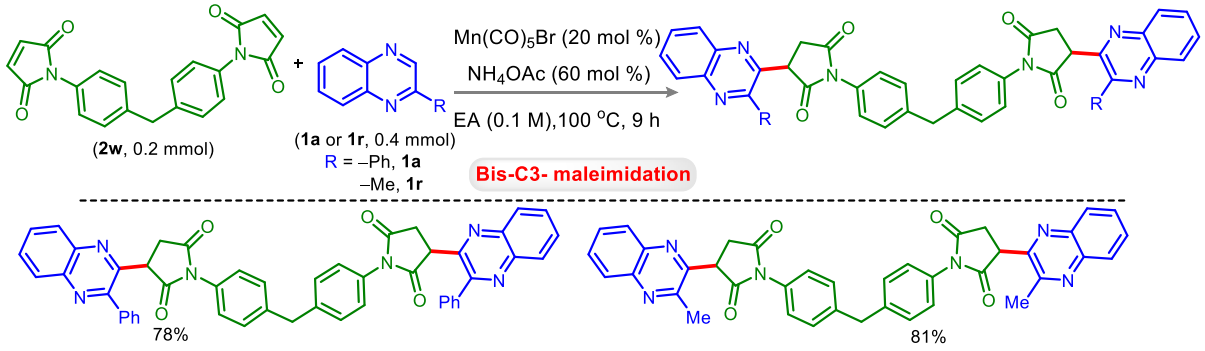

Scheme IV.4.4. *Bis-C3-maleimidation*

Spiro-cyclization and De-hydrogenation of C3-Maleimidated Quinoxaline:

The product **3aa** possesses a 2-aryl ring and a succinimide in proximity, can there be an π-electron drifted spiro-cyclization from the aryl ring to an electron-deficient succinimide in the presence of hypervalent-iodine?[14] To execute the envisioned strategy, the C3-maleimidated product (**3aa**) was reacted with *bis*(trifluoroacetoxy)iodobenzene (PIFA) in DCM at room temperature. As anticipated, an intramolecular spiro-cyclized product **4aa** was isolated in 85%. Pleasingly, this is the first report where unperturbed phenyl π-electrons offer C(sp^2)–C(sp^3) spiro-cyclization at room temperature *via* dearomatization-rearomatization pathway (Scheme IV.4.1).

Now the scope of this spiro-cyclization was explored and results are summarized in Scheme IV.4.5. An array of substituents such as *p*–Me (**3ba**), *p*–Cl (**3ea**), *m*–Me (**3ha**) and *o*–OMe (**3ja**) on 2-phenyl ring and 6,7-di-chloro (**3la**), 2-naphthyl (**3ma**) and 2-thiophenyl (**3na**) substituents on the quinoxaline system all successfully delivered intramolecular C(sp^2)–C(sp^3) spiro-cyclized products **4ba**–**4na** in good yields (71–87%). *N*-substituted maleimides such as –Me (**3ab**), –^{i}Bu (**3ae**), –Cy (**3af**), benzyl (**3ao**) of C3-maleimidated adduct, all underwent spiro-cyclization to provide their corresponding products **4ab**–**4ao** in good yields (76–81%). A *N*-substituted chiral (**3as**) and an unsubstituted (**3at**) maleimides successfully provided the desired products **4as** (78%) and **4at** (73%) respectively. While attempting fluorination at the quaternary C–H site on the succinimide (**3aa**) using fluorinating agent selectfluor®,[15] it underwent de-hydrogenation providing C3-alkenylated quinoxaline (**5aa**) in MeCN at room temperature possibly *via* a quaternary fluorinated intermediate (Scheme IV.4.5). This is a unique illustration of selectfluor® serving as a dehydrogenating agent in succinimide system. This protocol may serve as an alternative to de-hydrogenation in succinimides, where *β*-hydride elimination is unfavorable under metal-catalysis. Thus, to explore this scope, various substituted C3-appended succinimides were examined in Scheme IV.4.4. The C3-maleimidated products having *p*–F (**3da**), *p*–CF_3 (**3fa**) and *p*–Ph (**3ga**) groups on 2-aryl ring and 2-naphthyl (**3ma**) substitution on the quinoxaline, all efficiently provided their corresponding C3-alkenylated quinoxalines **5da**–**5ma** in good yields (81–

TH-3369_166122017

86%). Similarly, C3-maleimidated products having *N*-methyl (**3ab**) and *p*-methoxy *N*-phenyl (**3ak**) substitutions on maleimide, all afforded the desired de-hydrogenated products **5ab** (84%) and **5ak** (89%) respectively.

Scheme IV.4.5. *Scope of spiro-cyclization and dehydrogenation*[a,b]

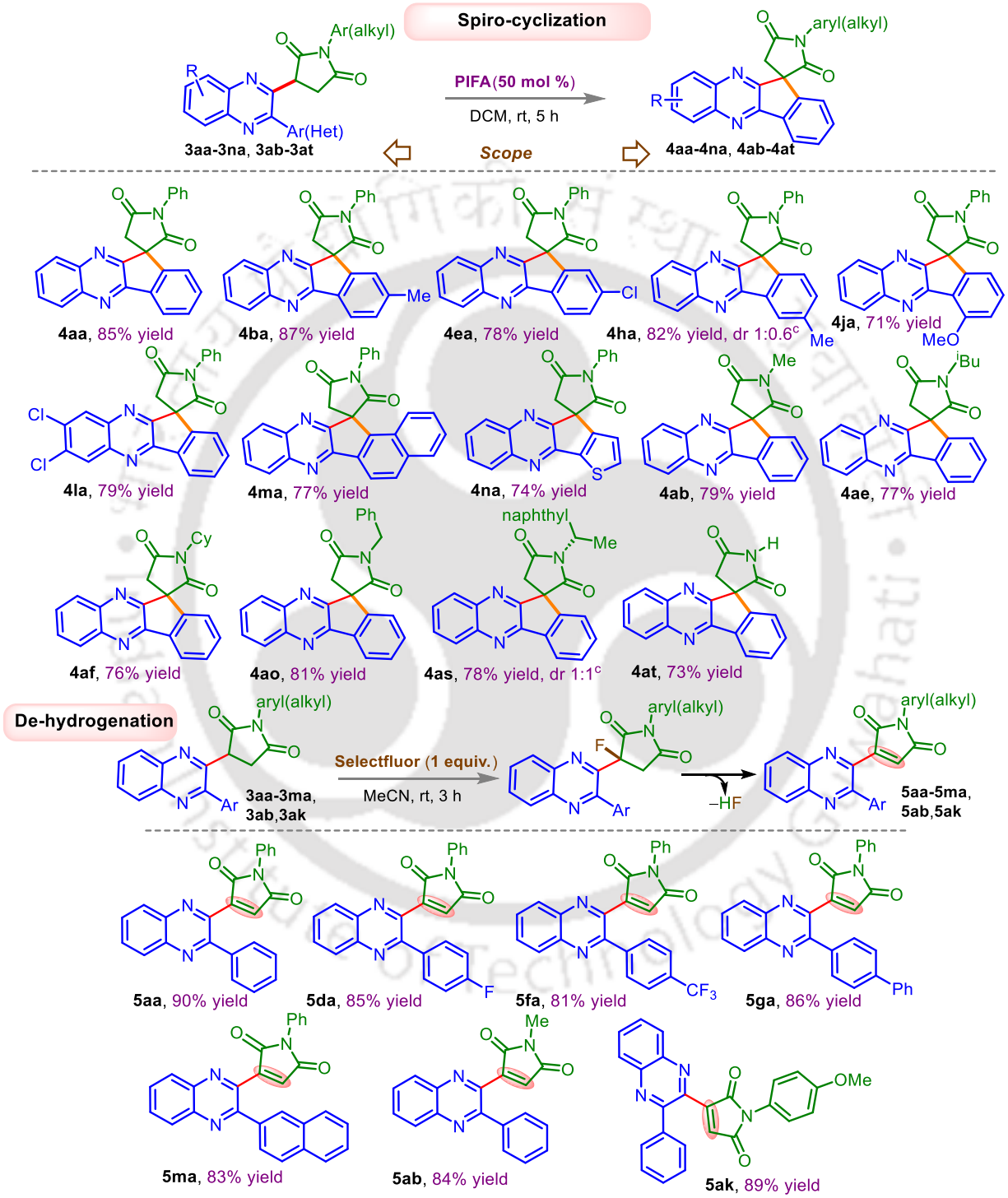

[a]Reaction conditions: *Spiro-cylization*: **3aa-3na**, **3ab-3at** (0.1 mmol), PIFA (50 mol %), DCM (0.1 M) at rt for 5 h under open-air. *De-hydrogenation:* **3aa-3ma, 3ab**, **3ak** (0.1 mmol), selectfluor® (0.1 mmol), MeCN (0.1 M) at rt for 3 h under open-air. [b]Isolated yield after column chromatography. [c]Based on ^{1}H NMR analysis.

TH-3369_166122017

Control Experiments:

In order to elucidate the underlying reaction mechanism, a series of control experiments were carried out in Scheme IV.4.6. The formation of C3-maleimidated product **3aa** was unperturbed in the presence of radical scavengers (BHT and DPE), thereby ruling out the involvement of any radical intermediate (Scheme IV.4.6a). However, the spiro-cyclization process was quenched in the presence of BHT and DPE, suggesting the radical pathway which was supported by HRMS analysis of the BHT adduct (**6**) (Scheme IV.4.6a and Figure IV.5.4). Further, the de-hydrogenation process was found unaltered in the presence of radical scavengers (Scheme IV.4.6a). Next, to check the reversibility of C–H metalation, two separate reactions (with and without maleimide) were carried out in the presence of D_2O (Scheme IV.4.6b). Without maleimide the standard reaction delivered 55% D incorporation at the C3–H of **1a** and no deuteration at the *o*-C–H (Figure IV.5.6). Whereas, in presence of maleimide the reaction provided 43% D at H_a and 30% D at each H_b protons in **3aa**-d_3 (Fig. S8, see SI). These experiments suggest reversible metalation and proto-dematalation during the process. The ability of Mn(I) towards *o*-directed metalation was tested by blocking the available electrophilic C3–H site in quinoxaline which gave no *o*-directed product (Scheme IV.4.6c). However, similar *o*-directed metalation using Mn(I) was feasible in pyridine system (Scheme IV.4.6c). Thus, this Mn(I) catalyzed maleimidation is mostly applicable to quinoxaline. To confirm the proposed electrophilic C3–H metalation, quinoxaline having electron-withdrawing 2-CO_2Me (**1t**), 2-Cl (**1u**) and electron-donating 2-Me (**1r**), 2-cyclopropyl (**1v**) group were subjected to the standard condition (Scheme IV.4.6d). While the formers failed to give any product, the latter gave the C3-maleimadated product **3ra** (85%) and **3va** (74%). This observation suggests that quinoxaline C3-site should be sufficiently electron-rich for electrophilic metalation. To ascertain the proposed electron drifting path for spiro-cyclization, two independent reactions were performed. One having an electron-withdrawing *p*-CF_3 on 2-aryl quinoxaline of **3fa** and the other a *p*-CF_3 substituents on maleimide site of **3am** were subjected to the standardized protocol (Scheme IV.4.6e). The former **3fa** failed to provide spiro-cyclization while the latter **3am** gave a spiro-cyclized product **4am** (71%). This observation supports the electron-drifting mechanism.

TH-3369_166122017

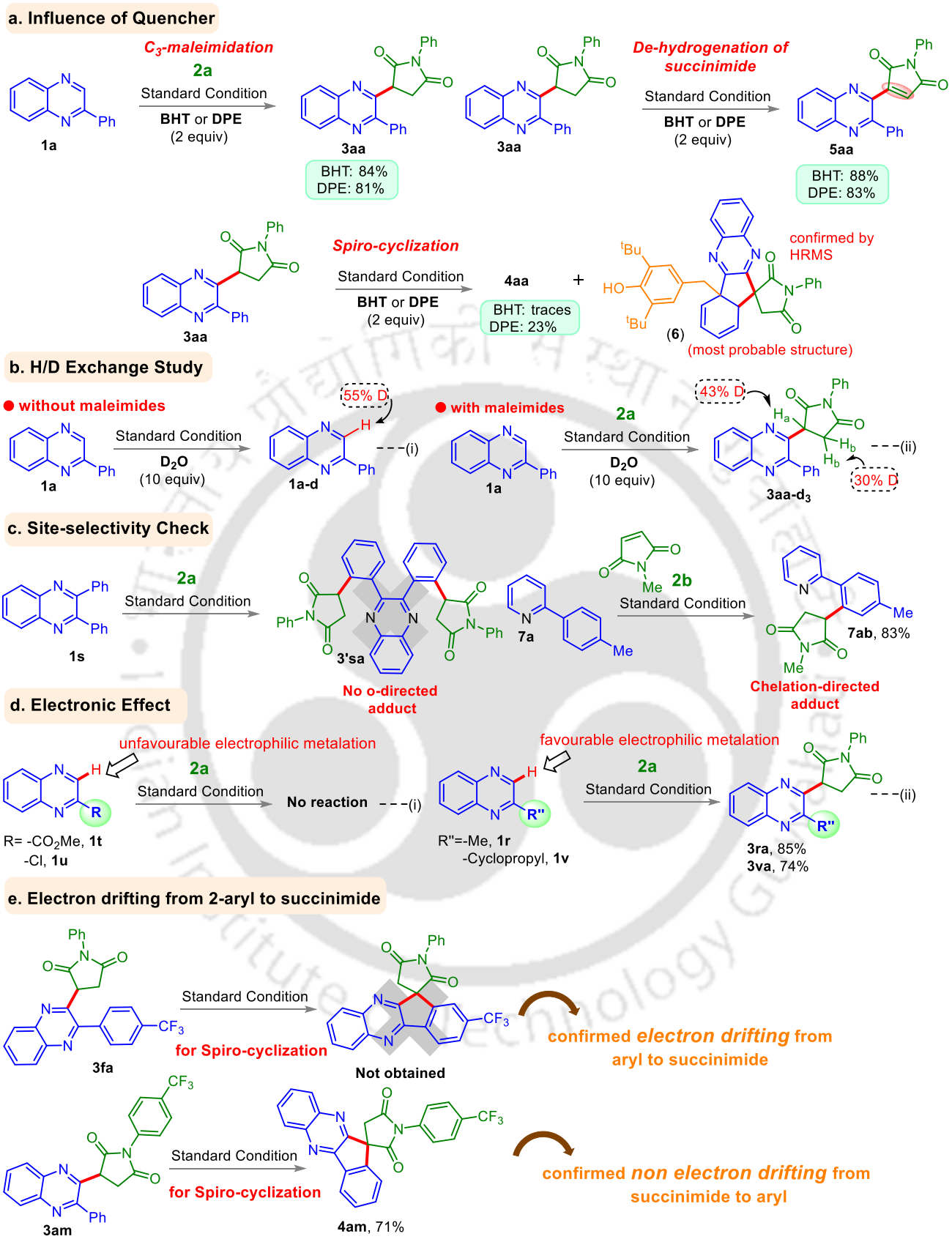

Scheme IV.4.6. *Control experiments*

TH-3369_166122017

Proposed Reaction Mechanism:

On the basis of literature precedents and control experiments, a plausible mechanism for C3-maleimidation, spiro-cyclization and de-hydrogenation has been proposed in Scheme IV.4.7 and Scheme IV.4.8.[13c,14-16] Initially, $Mn(CO)_5Br$ reacts with NH_4OAc, to provide the active $Mn(CO)_5OAc$ (**I**). Then 2-phenyl quinoxaline (**1a**) undergoes electrophilic metalation with the Mn-complex **I** to give C3-metalated species (**A**) (confirmed by HRMS, Figure IV.5.9) along with the elimination of AcOH. This is then followed by coordination of *N*-phenyl maleimide (**2a**) which undergo subsequent insertion to Mn–C bond to generate intermediate (**C**). Then a proto-demetalation in the presence of AcOH, provided the C3-maleimidated product **3aa** and the regeneration of active catalyst **I** by recombination of CO. Further in DCM **3aa** undergoes keto-enol tautomerization at room temperature and in the presence of PIFA it provides the iodo-complex **B'**. Then an electron-drifting from 2-aryl ring towards C3-appended succinimide provides a radical intermediate **C'**, which has been trapped by BHT and the adduct was confirmed by HRMS (Figure IV.5.4). Then this radical intermediate **C'** undergoes re-aromatization to afford the spiro-cyclized product **4aa**. On the other hand, in acetonitrile **3aa** undergoes electrophilic fluorination at the α-position of C3-appended succinimide to give a quaternary fluorinated species **B''**, which has been confirmed by NMR and HRMS analysis of the reaction aliquot (Figure IV.5.11- IV.5.13). The intermediate **B''** provides the de-hydrogenated succinimides **5aa** *via* the elimination of HF (Scheme IV.4.8).

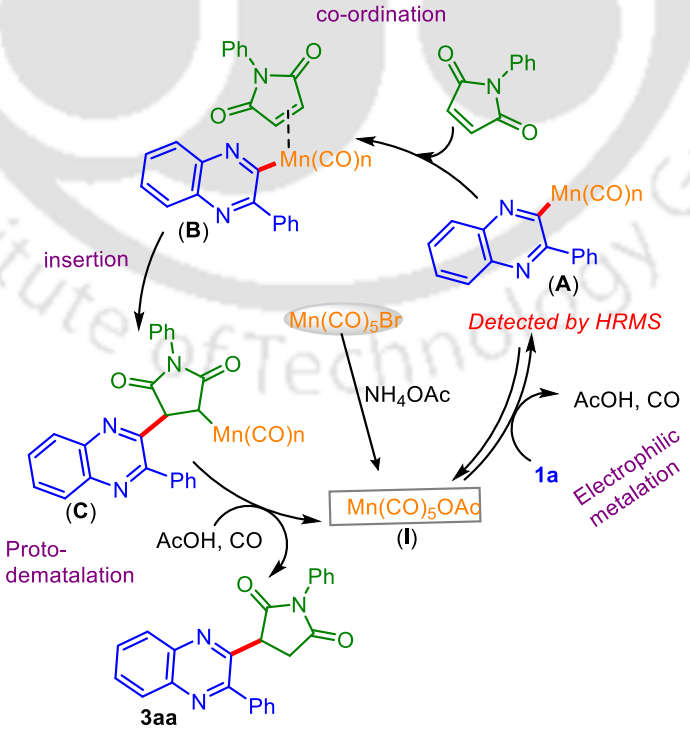

Scheme IV.4.7. *Plausible mechanism for non-directed C3-maleimidation*

TH-3369_166122017

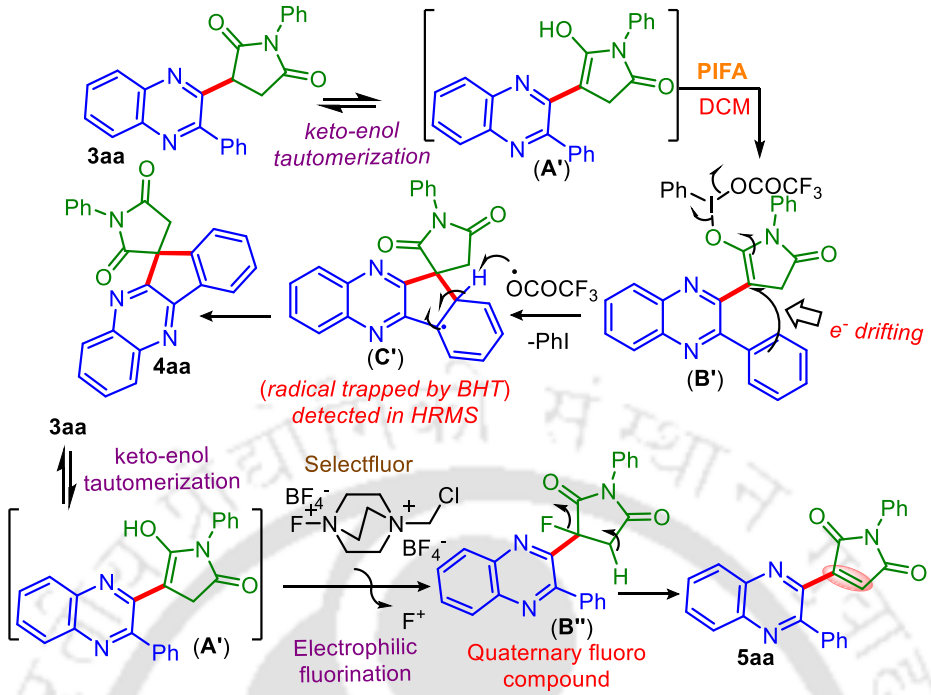

Scheme IV.4.8. *Plausible mechanism for spiro-cyclization and dehydrogenation of succinimides*

In summary, a Mn(I)-catalyzed site-selective non-directed C3-H maleimidation of quinoxaline has been introduced under oxidant/silver free protocol. This methodology offers a preference for electrophilic C3-metalation over the easily accessed *o*-directed metalation in ethyl acetate. Interestingly C3-maleimidated product undergoes PIFA promoted C(sp^2)–C(sp^3) spiro-cyclization and selectfluor® mediated dehydrogenation of succinimides at room temperature. In the spiro-cyclization, the unperturbed 2-phenyl π–electrons are utilized to construct the spiro-cyclized product. A broad range of substrates including natural products *L*-menthol and borneol, good functional group tolerance, and simple protocol are the salient features of this report.

TH-3369_166122017

IV.5. Experimental Section

IV.5.1. General Information: All the reagents were commercial grade and purified according to the established procedures. All the reactions were carried out in oven-dried glassware. The highest commercial quality reagents were purchased and were used without further purification unless otherwise stated. Reactions were monitored by thin-layer chromatography (TLC) on a 0.25 mm silica gel plates (60 F_{254}) visualized under UV illumination at 254 nm. Organic extracts were dried over anhydrous sodium sulfate (Na_2SO_4). Solvents were removed using a rotary evaporator under reduced pressure. Column chromatography was performed to purify the crude product on silica gel 60–120 mesh using a mixture of hexane and ethyl acetate as eluents. All the isolated compounds were characterized by ^1H, $^{13}C\{^1H\}$ NMR and IR spectroscopic (HRMS-spectrometric) techniques. NMR spectra for all the samples were recorded in deuterochloroform ($CDCl_3$) or deuterated dimethyl sulfoxide (DMSO-d_6). ^1H, $^{13}C\{^1H\}$ were recorded in 600 (151), 500 (126) or 400 (101) MHz spectrometer and were calibrated using tetramethylsilane or residual undeuterated solvent for ^1H NMR, deuterochloroform for ^{13}C NMR as an internal reference {$Si(CH_3)_4$: 0.00 ppm or $CHCl_3$: 7.26 ppm for ^1H NMR, 77.16 ppm for ^{13}C NMR or $(CH_3)_2SO$: 2.50 ppm for ^1H NMR, 39.52 ppm for ^{13}C NMR}. The chemical shifts are quoted in δ units, parts per million (ppm). ^1H NMR data is represented as follows: Chemical shift, multiplicity (s = singlet, d = doublet, t = triplet, q = quartet, m = multiplet, dd = doublet of doublet, integration and coupling constant(s) *J* in hertz (Hz). High-resolution mass spectra (HRMS) were recorded on a mass spectrometer using electrospray ionization-time of flight (ESI-TOF) reflection experiments. FT-IR spectra were recorded as neat and reported in the frequency of absorption (cm^{-1}).

IV.5.2. Experimental Procedure:

(a) Procedure for the synthesis of starting materials:

All 2-aryl quinoxalines (**1a-1q**) and 2-cylopropyl quinoxaline (**1v**) were synthesized following the reported procedure.[17] The *N*-alkylated maleimides (**2a-2v)** were also prepared according to the literature reported procedure.[18] 2,3-diphenylquinoxaline (**1s**) was synthesized according to the reported procedure.[19]

TH-3369_166122017

(b) General procedure for the synthesis of C3-maleimidation 3(a-q)(a-v):

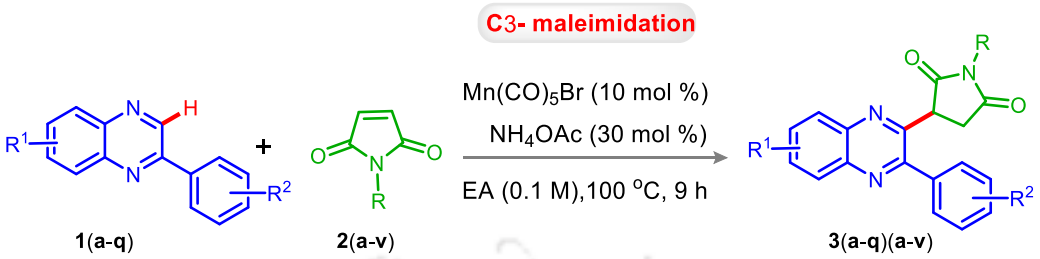

An oven-dried 10 mL round-bottom flask was charged with 2-arylquinoxaline (**1a-1q**, 0.2 mmol, 1 equiv), maleimide (**2a-2v**, 0.28 mmol, 1.4 equiv), $Mn(CO)_5Br$ (10 mol%, 0.1 equiv), NH_4OAc (30 mol%, 0.3 equiv) and a magnetic bead in ethyl acetate (0.1 M) under an open atmosphere and was refluxed in an oil bath at 100 °C for 9 h. The progress of the reaction was monitored by TLC. After completion of the reaction, the reaction mixture was then mixed with water (5 mL) and extracted with ethyl acetate (2 x 10 mL). The organic layer was dried over anhydrous sodium sulfate and was evaporated under reduced pressure. Then the crude mixture was purified over column chromatography (60-120 mesh silica) by eluting it with hexane/EtOAc mixtures to afford the desired products **3(a-q)** (**a-v**).

(c) General procedure for spiro-cyclization 4aa-4na, 4ab-4at:

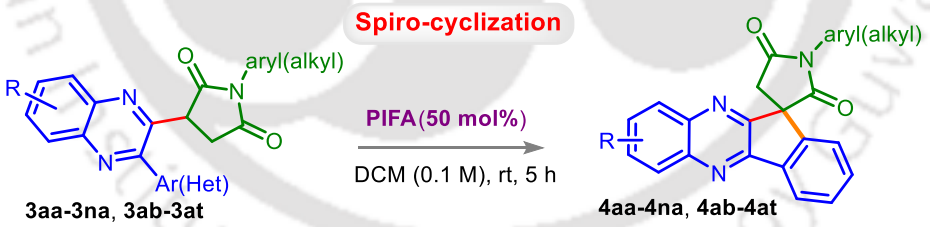

An oven-dried 10 mL round-bottom flask was charged with C3-maleimidated products (**3aa-3na** and **3ab-3at**, 0.1 mmol, 1 equiv), PIFA (50 mol%, 0.5 equiv) and a magnetic bead in dichloromethane (0.1 M) under an open atmosphere at rt for 5 h. The progress of the reaction was monitored by TLC. After completion of the reaction, the reaction mixture was then mixed with water (5 mL) and extracted with dichloromethane (2 x 10 mL). The organic layer was dried over anhydrous sodium sulfate and was evaporated under reduced pressure. Then the crude mixture was purified over column chromatography (60-120 mesh silica) by eluting it with hexane/EtOAc mixtures to afford the desired products **4aa-4na**, **4ab-4at**.

TH-3369_166122017

(d) General procedure for de-hydrogenation 5aa-5ma, 5ab-5ak:

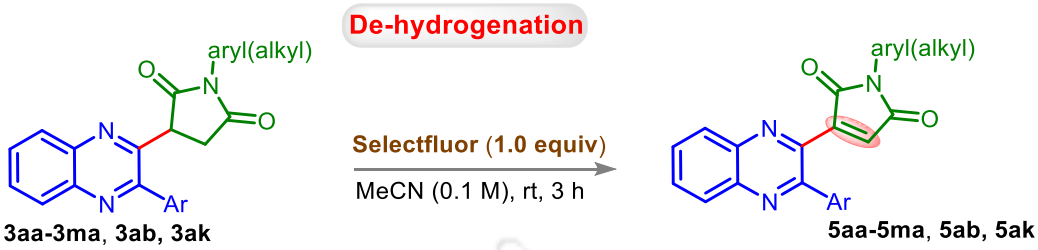

An oven-dried 10 mL round-bottom flask was charged with C3-maleimidated products (**3aa-3ma**, **3ab** and **3ak**, 0.1 mmol, 1 equiv), selectfluor (1 equiv) and a magnetic bead in MeCN (0.1 M) under an open atmosphere at rt for 3 h. The progress of the reaction was monitored by TLC. After completion of the reaction, the solvent was removed in vacuo. Then the reaction mixture was mixed with water (5 mL) and extracted with ethylacetate (2 x 10 mL). The organic layer was dried over anhydrous sodium sulfate and was evaporated under reduced pressure. Then the crude mixture was purified over column chromatography (60-120 mesh silica) by eluting it with hexane/EtOAc mixtures to afford the desired products **5aa-5ma**, **5ab** and **5ak**.

(e) Procedure for bis-C3-maleimidation:

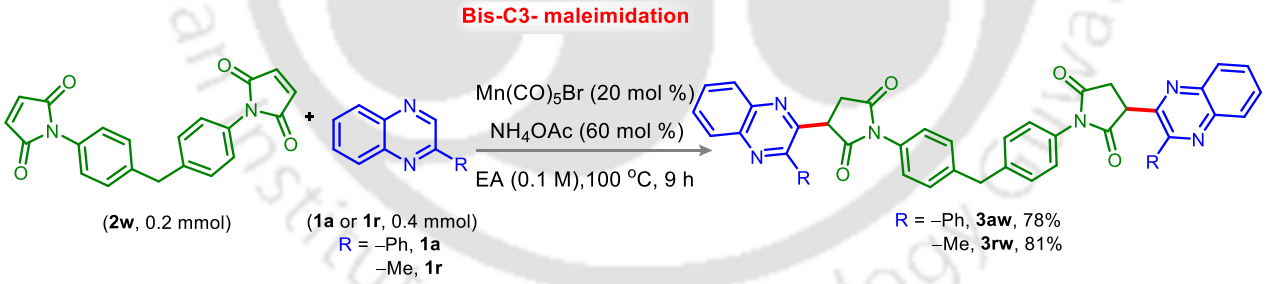

An oven-dried 10 mL round-bottom flask was charged with di-maleimide (**2w**, 0.2 mmol, 1 equiv), 2-substituted quinoxaline (**1a** or **1r**, 0.4 mmol, 2 equiv), $Mn(CO)_5Br$ (20 mol%, 0.2 equiv), NH_4OAc (60 mol%, 0.6 equiv) and a magnetic bead in ethyl acetate (0.1 M) under an open atmosphere and was refluxed in an oil bath at 100 ^oC for 9 h. The progress of the reaction was monitored by TLC. After completion of the reaction, the reaction mixture was then mixed with water (5 mL) and extracted with ethyl acetate (2 x 10 mL). The organic layer was dried over anhydrous sodium sulfate and was evaporated under reduced pressure. Then the crude mixture was purified over column chromatography (60-120 mesh silica) by eluting it with hexane/EtOAc mixture to afford the desired products **3aw** or **3rw**.

TH-3369_166122017

(f) Procedure for 2 mmol-scale synthesis of C3-maleimidated 3aa:

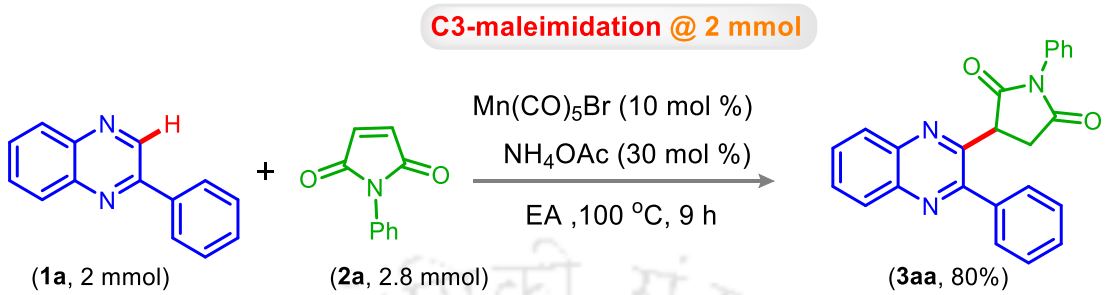

An oven-dried 25 mL round-bottom flask was charged with 2-phenylquinoxaline (**1a**, 2 mmol, 412 mg), *N*-phenyl maleimide (**2a**, 2.8 mmol, 484 mg), $Mn(CO)_5Br$ (10 mol%, 54 mg), NH_4OAc (30 mol%, 0.3 equiv) and a magnetic bead in ethyl acetate (4 mL) under an open atmosphere and was refluxed in an oil bath at 100 ^oC for 9 h. The progress of the reaction was monitored by TLC. After completion of the reaction, the reaction mixture was then mixed with water (5 mL) and extracted with ethyl acetate (2 x 15 mL). The organic layer was dried over anhydrous sodium sulfate and was evaporated under reduced pressure. Then the crude mixture was purified over column chromatography (60-120 mesh silica) by eluting it with hexane/EtOAc (80:20) mixture to afford the desired product **3aa** in 80% yield (607 mg).

IV.5.3. Crystallographic Description:

Crystal data were collected with Bruker Smart Apex-II CCD diffractometer using graphite monochromated MoKα radiation (λ = 0.71073 Å) at 296 K. Cell parameters were retrieved using SMART[a] software and refined with SAINT[a] on all observed reflections. Data reduction was performed with the SAINT software and corrected for Lorentz and polarization effects. Absorption corrections were applied with the program SADABS[b]. The structure was solved by direct methods implemented in SHELX-2014[c] program and refined by full-matrix least-squares methods on F2. All non-hydrogen atomic positions were located in difference Fourier maps and refined anisotropically. The hydrogen atoms were placed in their geometrically generated positions. yellow crystals of **3aa** were isolated from ethyl acetate solvent at room temperature. Colourless crystals of **4ba** were isolated from acetonitrile/chloroform mixed solvent at room temperature. Light yellow crystals of **5aa** were isolated from acetonitrile solvent at room temperature.

TH-3369_166122017

a. SMART V 4.043 Software for the CCD Detector System; Siemens Analytical Instruments Division: Madison, WI, 2008.

b. SAINT Plus (v 6.14) Bruker AXS Inc., Madison, WI, 2008.

c. Sheldrick, G. M. SHELXL-2014, Program for the Refinement of Crystal Structures; University of Göttingen: Göttingen (Germany), 1997

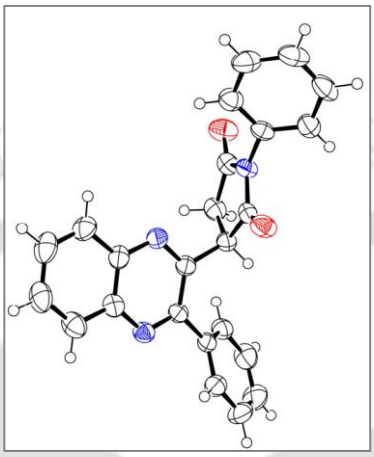

Figure IV.5.1. *ORTEP diagram of* ***3aa*** *with the thermal ellipsoids set at 50% probability*

Crystal Data table for 3aa

Empirical formula	$C_{24}H_{17}N_3O_2$
CCDC number	2249622
Formula weight	379.41
Temperature	298(2)
Wavelength	0.71073 Å
Crystal system	monoclinic
Space group	P21/c
Unit cell dimensions	a = 14.6509(10) Å, b = 5.3418(4) Å, c = 24.8144(17) Å α= 90°, β= 103.440°, γ= 90°
Volume	1888.8 (2) $Å^3$
Z	4
Density (calculated)	1.334 g/cm^{-3}
Absorption coefficient	0.129
F(000)	792
Theta range for data collection	1.429 to 24.999°
Index ranges	-17 < = h < = 17, -6 < = k < = 6, -29< = l < = 29
Reflections collected	46104
Refinement method	Full-matrix least-squares on F2
Data / restraints / parameters	3323/ 0/ 262
Goodness-of-fit on F2	1.145

TH-3369_166122017

Final R indices [I>2sigma(I)]	0.0641, wR2 = 0.1549
R indices (all data)	0.0996, wR2 = 0.1913

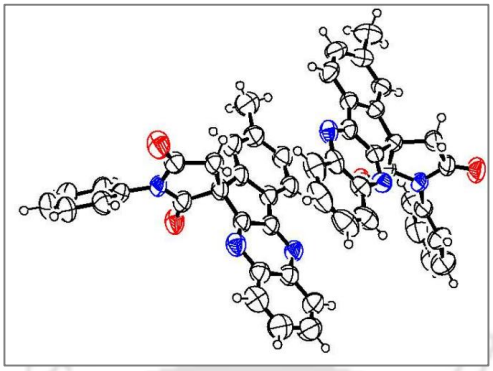

Figure IV.5.2. *ORTEP diagram of* ***4ba*** *with the thermal ellipsoids set at 50% probability*

Crystal Data table for 4ba:

Empirical formula	$C_{25}H_{17}N_3O_2$
CCDC number	2249629
Formula weight	391.42
Temperature	297(2)
Wavelength	0.71073 Å
Crystal system	orthorhombic
Space group	P 2ac 2ab
Unit cell dimensions	a = 10.3282(7) Å, b = 17.0295(11) Å, c = 24.2798(16) Å α= 90°, β= 90°, γ= 90°
Volume	4270.4 (5) $Å^3$
Z	8
Density (calculated)	1.218 g/cm^{-3}
Absorption coefficient	0.079
F(000)	1632
Theta range for data collection	1.461 to 24.000°
Index ranges	-11 < = h < = 11, -19 < = k < = 19, -27< = l < = 27
Reflections collected	113969
Refinement method	Full-matrix least-squares on F2
Data / restraints / parameters	6696/ 0/ 544
Goodness-of-fit on F2	1.164
Final R indices [I>2sigma(I)]	0.0828, wR2 = 0.2381
R indices (all data)	0.1002, wR2 = 0.2713

TH-3369_166122017

Empirical formula	$C_{24}H_{15}N_3O_2$
CCDC number	2249625
Formula weight	377.39
Temperature	297(2)
Wavelength	0.71073 Å
Crystal system	monoclinic
Space group	P21/c
Unit cell dimensions	a = 11.3273(14) Å, b = 5.4688(7) Å, c = 29.644(4) Å α= 90°, β= 92.999°, γ= 90°
Volume	1833.8 (4) $Å^3$
Z	4
Density (calculated)	1.367 g/cm^{-3}
Absorption coefficient	0.094
F(000)	784
Theta range for data collection	1.376 to 26.672°
Index ranges	-14 < = h < = 14, -6 < = k < = 6, -37< = l < = 37
Reflections collected	11732
Refinement method	Full-matrix least-squares on F2
Data / restraints / parameters	3847/ 0/ 262
Goodness-of-fit on F2	1.777
Final R indices [I>2sigma(I)]	0.0957, wR2 = 0.2879
R indices (all data)	0.1144, wR2 = 0.2943

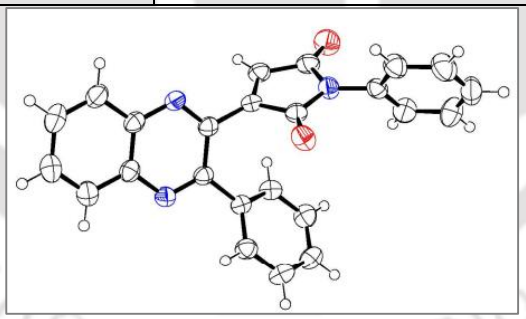

Figure IV.5.3. *ORTEP diagram of* ***5aa*** *with the thermal ellipsoids set at 50% probability*

Crystal Data table for 5aa

TH-3369_166122017

IV.5.4. Control Experiments:

IV.5.4.1. Procedure of quenching experiment for C3-maleimidation:

An oven-dried 10 mL round-bottom flask was charged with 2-phenylquinoxaline (**1a**, 0.2 mmol, 41 mg), *N*-phenyl maleimide (**2a**, 0.28 mmol, 48 mg), $Mn(CO)_5Br$ (10 mol%, 5 mg), NH_4OAc (30 mol%, 5 mg), BHT (0.4 mmol, 88 mg) or 1,1-DPE (0.4 mmol, 72 mg) and a magnetic bead in ethyl acetate (0.1 M) under an open atmosphere and was refluxed in an oil bath at 100 ^oC for 9 h. The progress of the reaction was monitored by TLC. After completion of the reaction, the reaction mixture was then mixed with water (5 mL) and extracted with ethyl acetate (2 x 10 mL). The organic layer was dried over anhydrous sodium sulfate and was evaporated under reduced pressure. Then the crude mixture was purified over column chromatography (60-120 mesh silica) by eluting it with hexane/EtOAc (80:20) mixture to afford the desired products **3aa** in 84% (for BHT) and 81% (for 1,1-DPE). This observation suggests the non-involvement of any radical pathway.

IV.5.4.2. Procedure of quenching experiment for spiro-cyclization reaction:

An oven-dried 10 mL round-bottom flask was charged with C3-maleimidated product (**3aa**, 0.1 mmol, 38 mg), PIFA (50 mol%, 22 mg), BHT (0.2 mmol, 44 mg) or 1,1-DPE (0.2 mmol, 36 mg) and a magnetic bead in dichloromethane (0.1 M) under an open atmosphere at rt for 5 h. The progress of the reaction was monitored by TLC. After completion of the reaction, the reaction mixture was then mixed with water (5 mL) and extracted with dichloromethane (2 x 10 mL). The organic layer was dried over anhydrous sodium sulfate and was evaporated under reduced pressure. Then the crude mixture was

TH-3369_166122017

purified over column chromatography (60-120 mesh silica) by eluting it with hexane/EtOAc (80:20) mixture to afford the desired products **4aa** in 23% (for 1,1-DPE**)**. Whereas, in case of BHT, traces of **4aa** detected and a plausible BHT-adduct (**6**) was detected by HRMS analysis of crude reaction aliquot (Figure IV.5.4). This observation suggests the involvement of radical pathway.

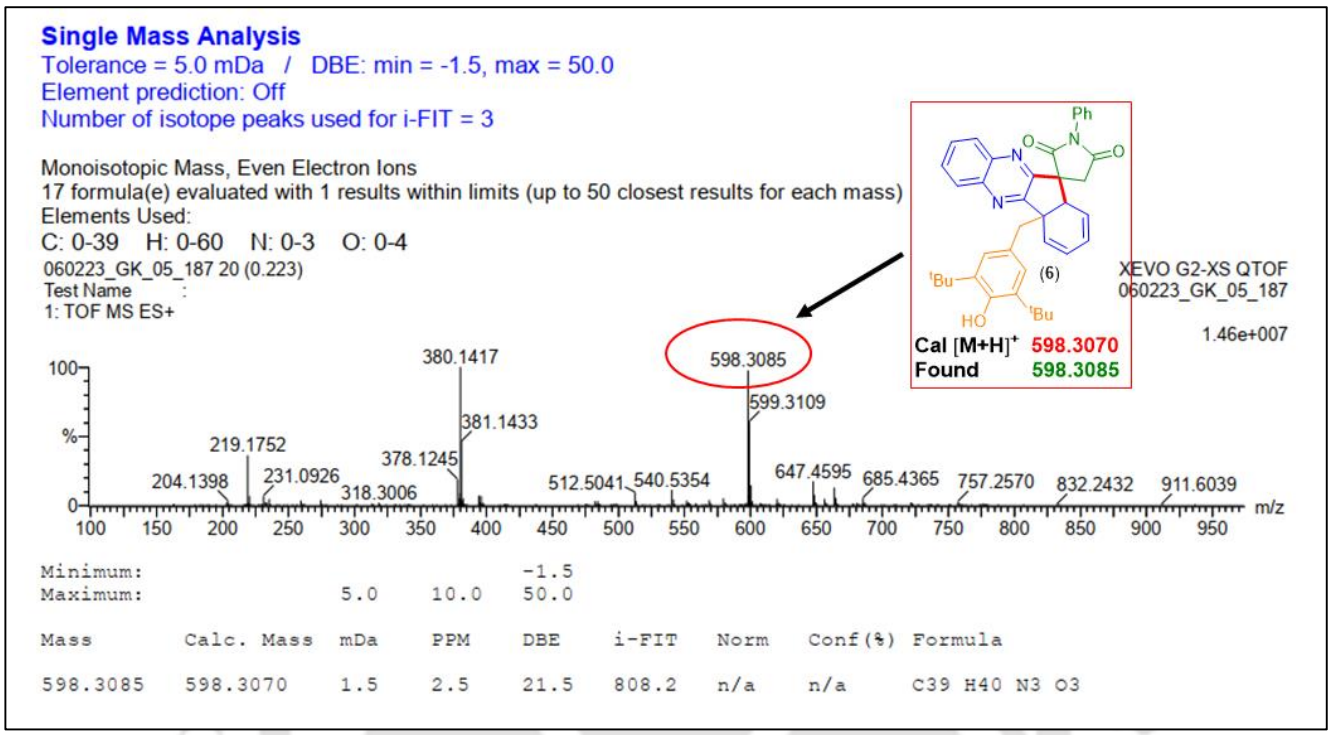

Figure IV.5.4. *HRMS spectra of the crude spiro-cyclization reaction mixture*

IV.5.4.2. Procedure of quenching experiment for de-hydrogenation of succinimide:

An oven-dried 10 mL round-bottom flask was charged with C3-maleimidated product (**3aa**, 0.1 mmol, 38 mg), selectfluor (0.1 mmol, 35 mg), BHT (0.2 mmol, 44 mg) or 1,1-DPE (0.2 mmol, 36 mg) and a magnetic bead in MeCN (0.1 M) under an open atmosphere at rt for 3 h. The progress of the reaction was monitored by TLC. After completion of the reaction, the solvent was removed in vacuo. Then the reaction mixture was mixed with water (5 mL) and extracted with ethylacetate (2 x 10 mL). The organic layer was dried over anhydrous sodium sulfate and was evaporated under reduced pressure. Then the crude mixture was purified over column chromatography (60-120 mesh silica) by eluting it with hexane/EtOAc (85:15) mixture to afford the desired products **5aa** in 88% (for BHT) and 83% (for 1,1-DPE) isolated yield. This observation suggests the non-involvement of any radical pathway.

IV.5.4.3. Procedure of H/D exchange (without maleimide):

TH-3369_166122017

An oven-dried 10 mL round-bottom flask was charged with 2-phenylquinoxaline (**1a**, 0.2 mmol, 41 mg), $Mn(CO)_5Br$ (10 mol%, 5 mg), NH_4OAc (30 mol%, 5 mg), D_2O (10 equiv) and a magnetic bead in EA (0.1 M) under an open atmosphere and was refluxed in an oil bath at 100 ^oC for 9 h. After completion of the reaction, the reaction mixture was then mixed with water (5 mL) and extracted with ethyl acetate (2 x 10 mL). The organic layer was dried over anhydrous sodium sulfate and was evaporated under reduced pressure. Then the crude mixture was purified over column chromatography (60-120 mesh silica) by eluting it with hexane/EtOAc (90:10) mixture to afford the deuterated products **1a-d**. The extent of H/D exchange was determined by comparing the ^1H NMR of deuterated **1a-d** to that of undeuterated **1a.** The multiplet peak at δ 7.8-7.73 ppm which has an integral value of 2.00 was considered as the reference in both the spectra. Integrating accordingly in both of them, it was found that upon deuteration the characteristic peak for C3-H which appears at 9.33 ppm was reduced to an integral value 0.45 from 1.00. Thus, there was 55% deuteration (1.00-0.45= 0.55 i.e. 55% D) observed at C3-H without affecting *o*-C-Hs (Figure IV.5.5 and Figure IV.5.6).

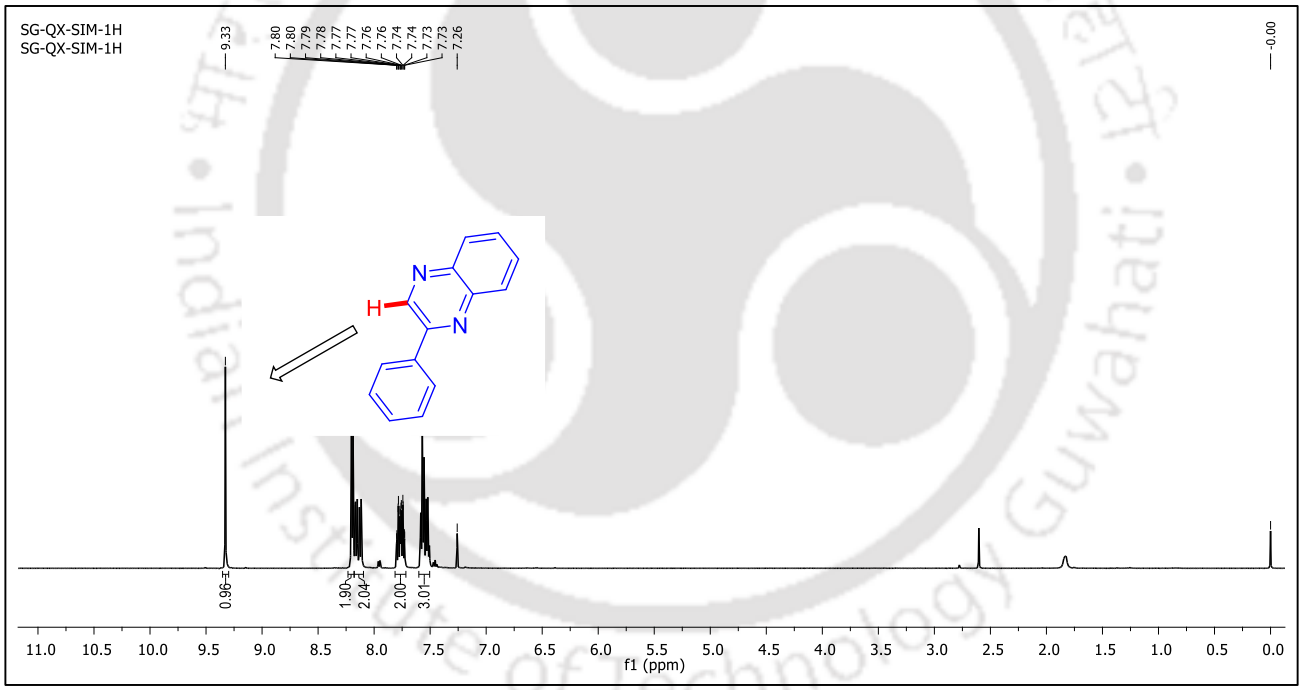

Figure IV.5.5. *^1H spectra of undeuterated **1a***

TH-3369_166122017

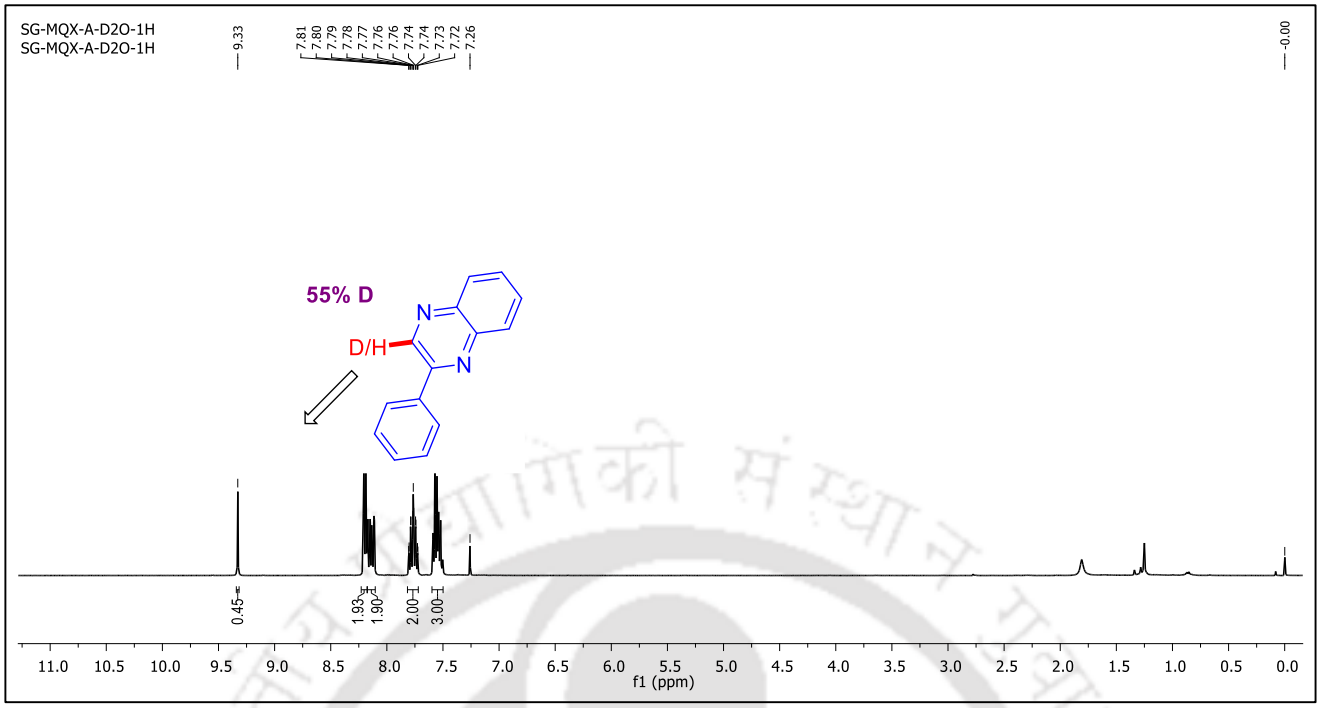

Figure IV.5.6. *^{1}H spectra of deuterated* ***1a-d***

IV.5.4.4. Procedure of H/D exchange (with maleimide):

An oven-dried 10 mL round-bottom flask was charged with 2-phenylquinoxaline (**1a**, 0.2 mmol, 41 mg), *N*-phenyl maleimide (**2a**, 0.28 mmol, 48 mg), $Mn(CO)_5Br$ (10 mol%, 5 mg), NH_4OAc (30 mol%, 5 mg), D_2O (10 equiv) and a magnetic bead in EA (0.1 M) under an open atmosphere and was refluxed in an oil bath at 100 ^oC for 9 h. After completion of the reaction, the reaction mixture was then mixed with water (5 mL) and extracted with ethyl acetate (2 x 10 mL). The organic layer was dried over anhydrous sodium sulfate and was evaporated under reduced pressure. Then the crude mixture was purified over column chromatography (60-120 mesh silica) by eluting it with hexane/EtOAc (80:20) mixture to afford the deuterated C3-maleimidated product **3aa-d$_3$**. The extent of H/D exchange was determined by comparing the ^{1}H NMR of deuterated **3aa-d$_3$** to that of undeuterated **3aa.** The muliplet peak at δ 8.18-8.15 ppm which has an integral value of 1.00 was considered as the reference in both the spectra. Integrating accordingly in both of them, it was found that upon deuteration the characteristic peak for Ha- which appears at 4.88-4.84 ppm and for H_b protons at 3.47-3.41 ppm, 3.22-3.15 ppm were reduced to an integral value 0.57 and 0.70 respectively from 1.00. Thus, there was 43% deuteration (1.00-0.57= 0.43 i.e. 43% D) at H_a and 30% deuteration (1.00-0.70= 0.30 i.e. 30% D) at H_b were observed (Figure IV.5.7 and Figure IV.5.8).

TH-3369_166122017

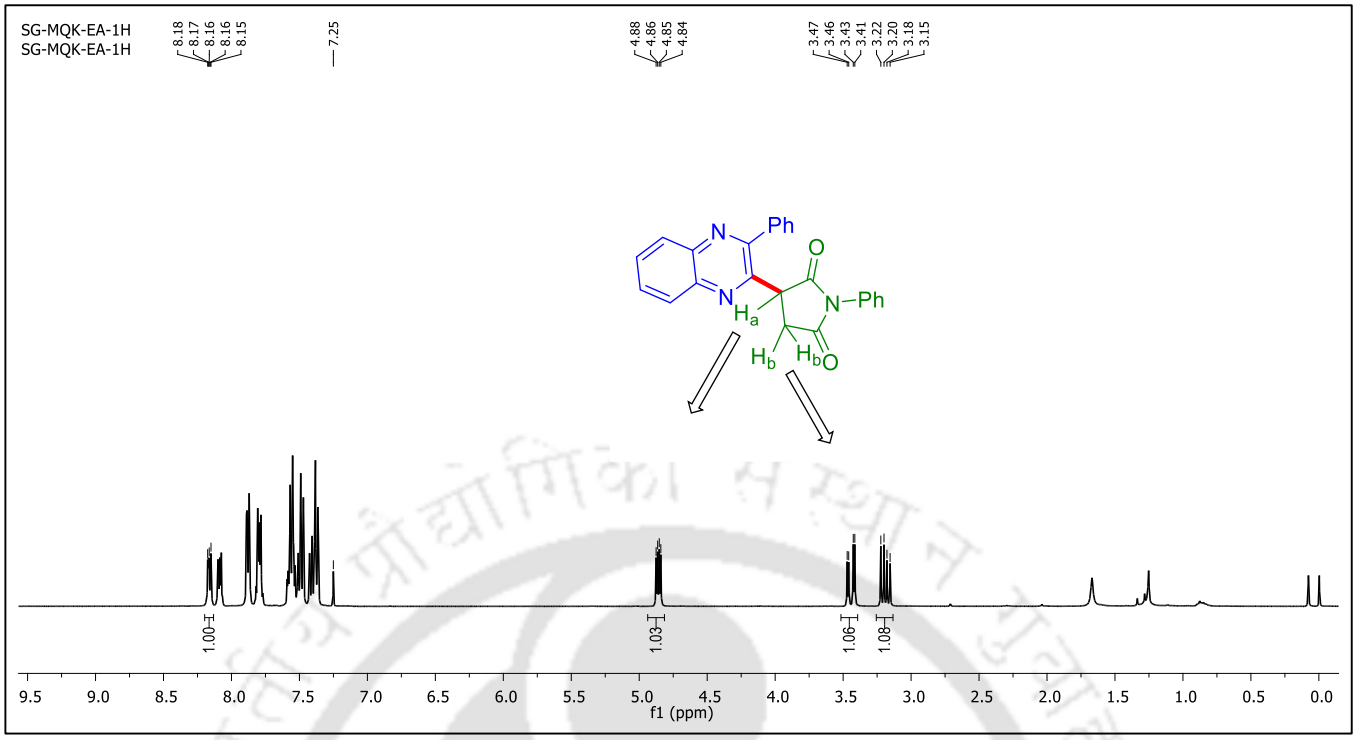

Figure IV.5.7. *^{1}H spectra of undeuterated* ***3aa***

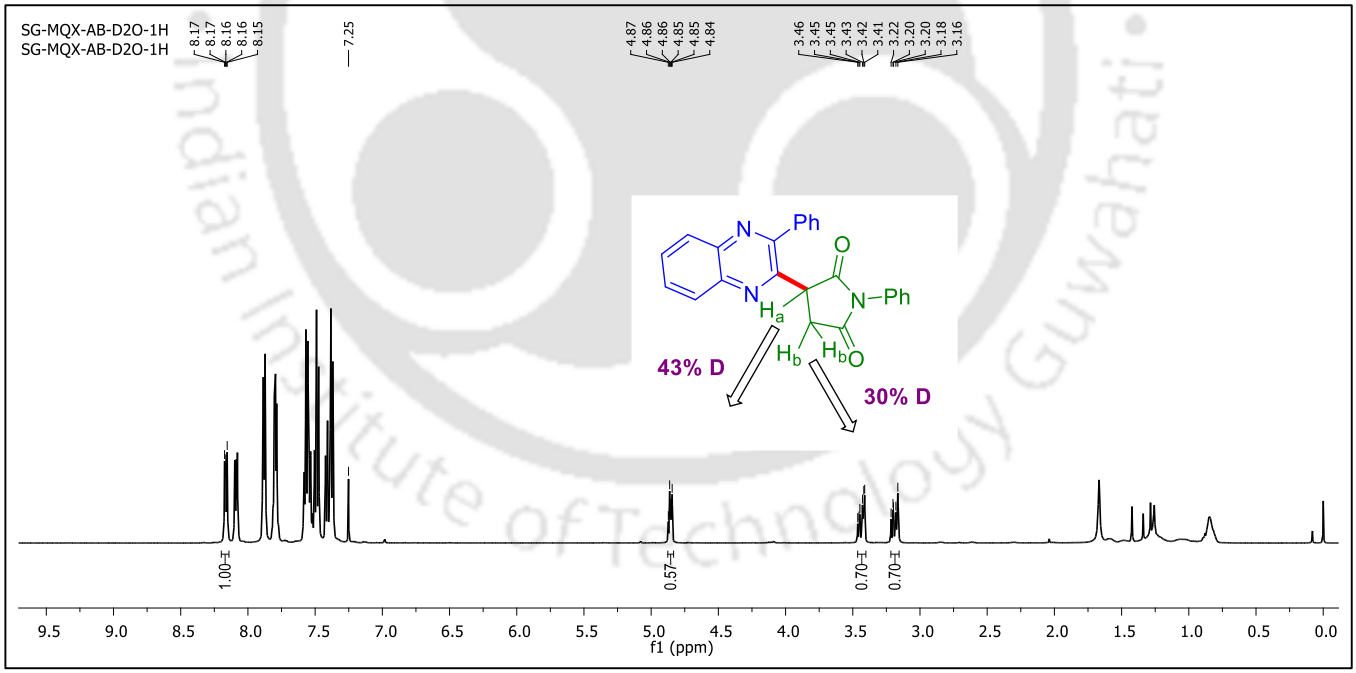

Figure IV.5.8. *^{1}H spectra of deuterated* ***3aa-d$_3$***

TH-3369_166122017

IV.5.4.5. Procedure for *o*-maleimidation of 2-phenyl pyridine:

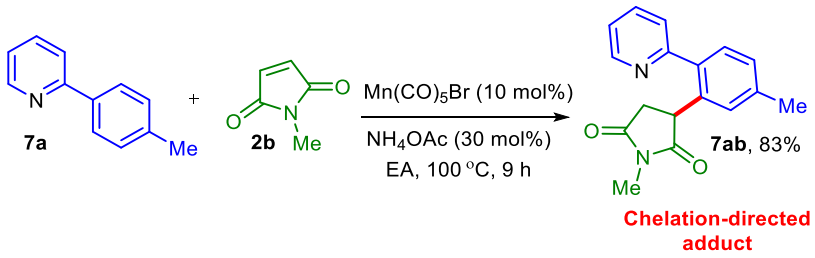

An oven-dried 10 mL round-bottom flask was charged with 2-(*p*-tolyl)pyridine (**7a**, 0.2 mmol, 34 mg), *N*-methyl maleimide (**2b**, 0.28 mmol, 48 mg), $Mn(CO)_5Br$ (10 mol%, 5 mg), NH_4OAc (30 mol%, 5 mg), and a magnetic bead in EA (0.1 M) under an open atmosphere and was refluxed in an oil bath at 100 °C for 9 h. The progress of the reaction was monitored by TLC. After completion of the reaction, the reaction mixture was then mixed with water (5 mL) and extracted with ethyl acetate (2 x 10 mL). The organic layer was dried over anhydrous sodium sulfate and was evaporated under reduced pressure. Then the crude mixture was purified over column chromatography (60-120 mesh silica) by eluting it with hexane/EtOAc (65:35) mixture to afford the *o*-maleimidated product **7ab** (83%, 46 mg).

IV.5.5. HRMS analysis of crude reaction mixture (C3-maleimidation):

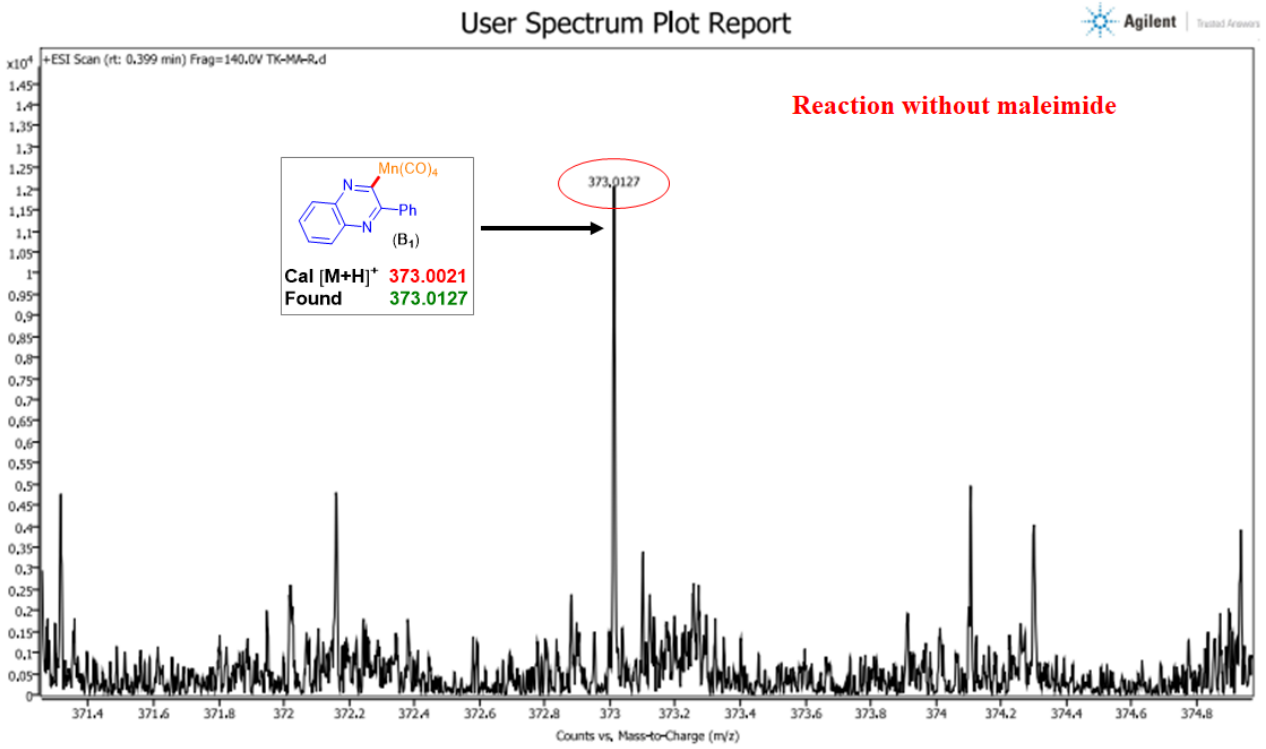

Figure IV.5.9. *HRMS spectra of the crude reaction mixture for C3-maleimidation*

TH-3369_166122017

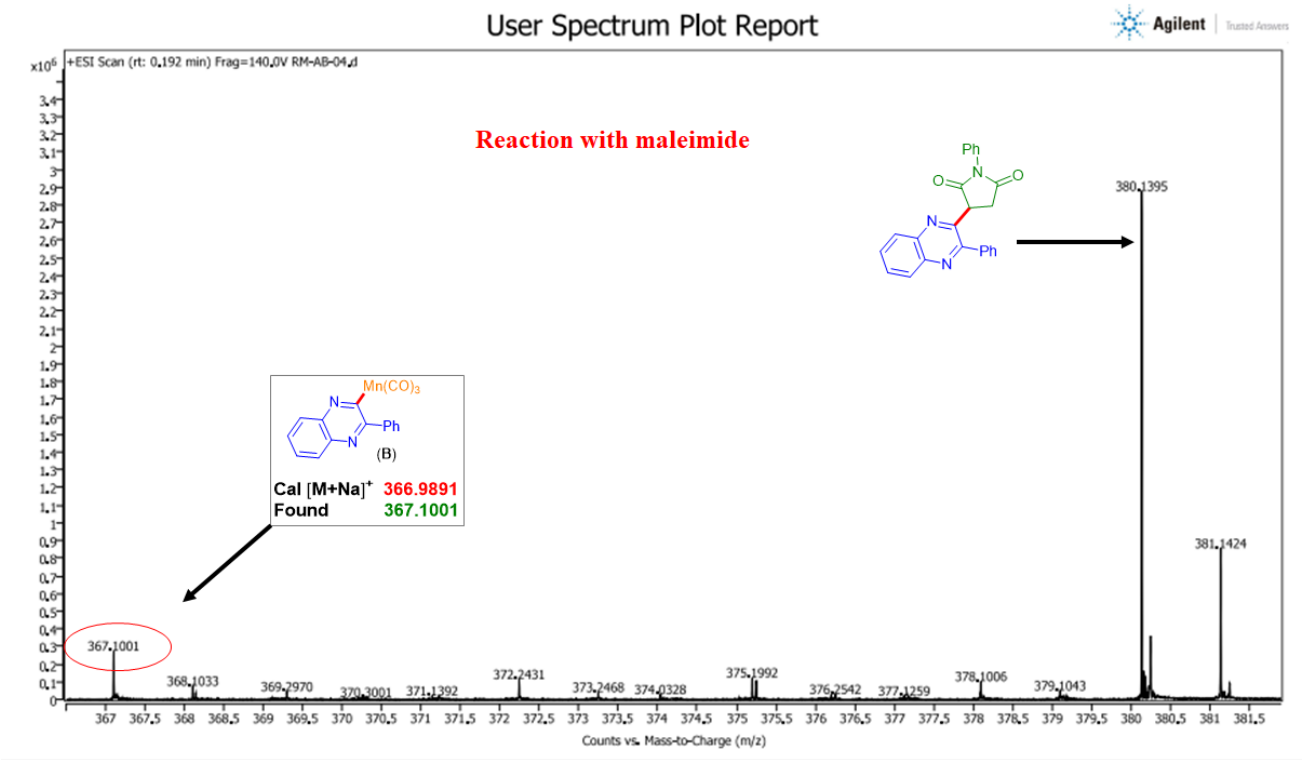

Figure IV.5.10. *HRMS spectra of crude reaction mixture for C3-maleimidation*

IV.5.6. Detection of *in situ* generated quaternary fluorinated compound:

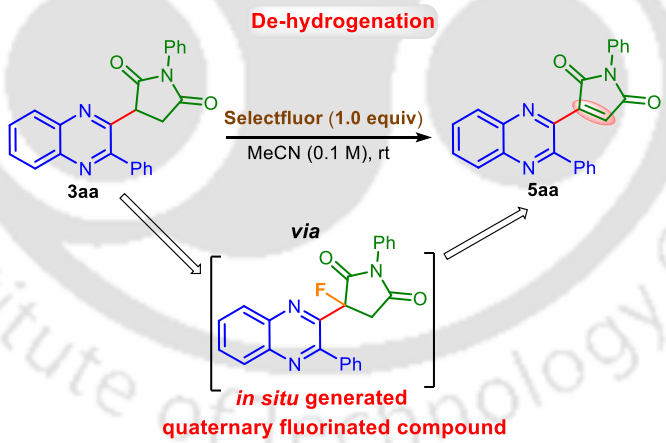

A reaction was carried out under above-mentioned condition, during the process of reaction one portion of the reaction aliquot had taken out for HRMS and NMR (^{1}H, ^{19}F) analysis to detect the *in situ* generated fluorinated species in the selectofluor mediated dehydrogenation of succinimides. The HRMS and NMR spctras are attached below.

TH-3369_166122017

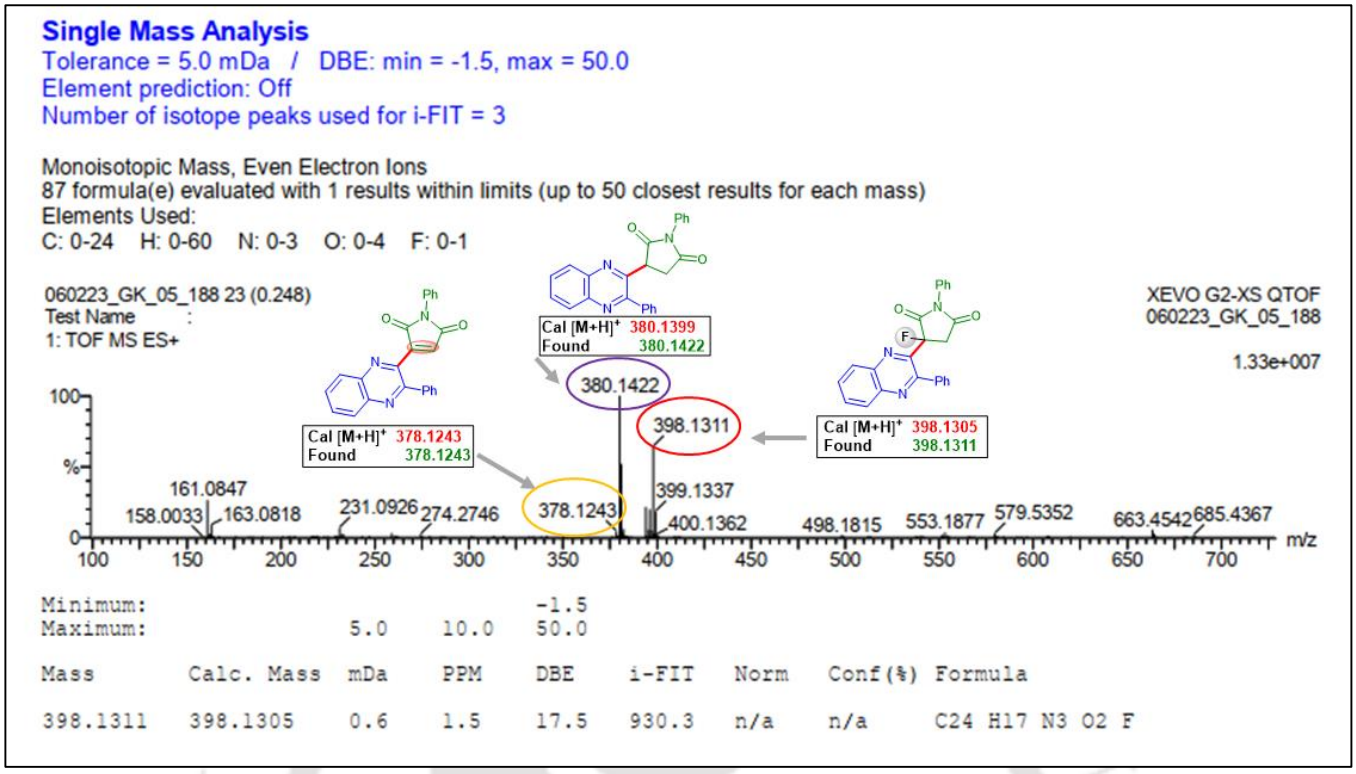

Figure IV.5.11. *HRMS spectra of crude reaction mixture for dehydrogenation*

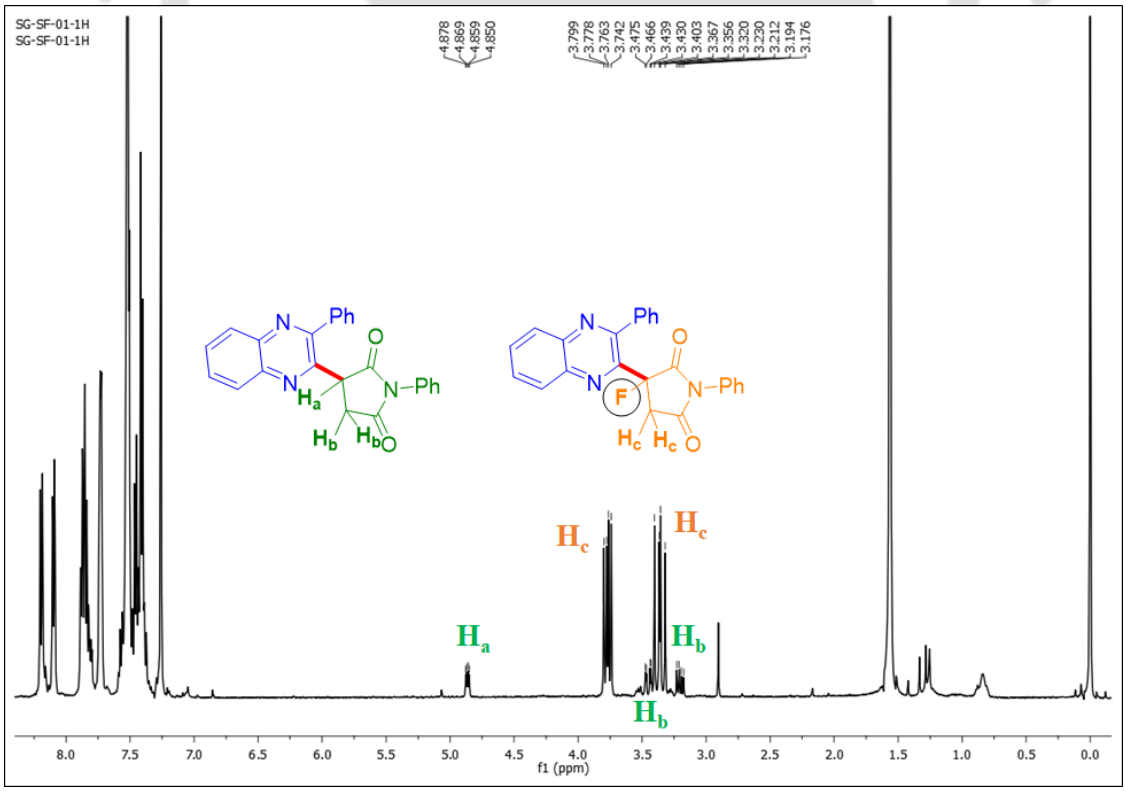

Figure IV.5.12. *^{1}H spectra of crude reaction mixture for dehydrogenation*

TH-3369_166122017

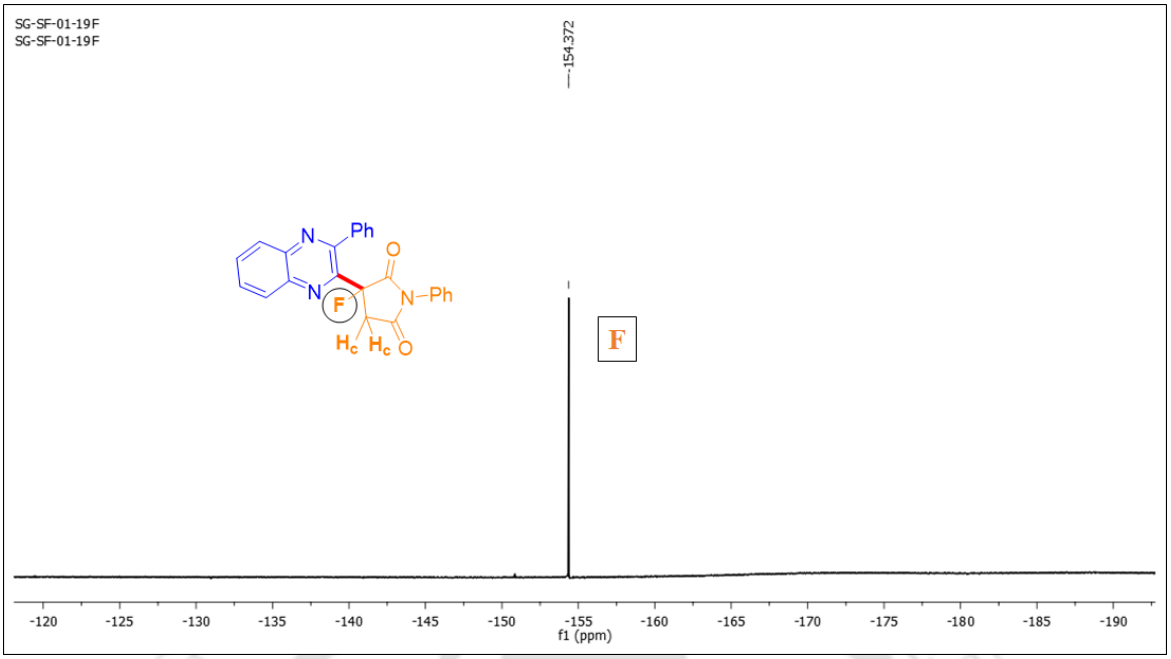

Figure IV.5.13. *^{19}F spectra of crude reaction mixture for dehydrogenation*

IV.6. References

1. (a) Isaka, M.; Rugseree, N.; Maithip, P.; Kongsaeree, P.; Prabpai, S.; Thebtaranonth, Y. Hirsutellones A−E, antimycobacterial alkaloids from the insect pathogenic fungus Hirsutella nivea BCC 2594. *Tetrahedron* **2005**, *61*, 5577. (b) Zhang, L.; Tan, Y.; Wang, N.-X.; Wu, Q.-Y.; Xi, Z.; Yang, G.-F. Design, Syntheses and 3D-QSAR Studies of Novel *N*-Phenyl Pyrrolidin-2-ones and *N*-Phenyl-1*H*-pyrrol-2-ones as Protoporphyrinogen Oxidase Inhibitors. *Bioorg. Med. Chem.* **2010**, *18*, 7948.
2. (a) Manoharan, R.; Jeganmohan, M. Alkylation, Annulation, and Alkenylation of Organic Molecules with Maleimides by Transition-Metal-Catalyzed C-H Bond Activation. *Asian J. Org. Chem.* **2019**, *8*, 1949. (b) Liu, S.-L.; Shi, Y.; Xue, C.; Zhang, L.; Zhou, L.; Song, M.-P. Maleimides in Directing Group-Controlled Transition-Metal-Catalyzed Selective C−H Alkylation. *Eur. J. Org. Chem.* **2021**, *2021*, 5862.
3. (a) He, Q.; Yamaguchi, T.; Chatani, N. Rh(I)-catalyzed alkylation of ortho-C-H bonds in aromatic amides with maleimides. *Org. Lett.* **2017**, *19*, 4544. (b) Ohara, N.; Rej, S.; Chatani, N. Rh(I)-catalyzed Addition of the ortho C-H Bond in Aryl Sulfonamides to Maleimides. *Chem. Lett.* **2020**, *49*, 1053. (c) Mandal, R.; Emayavaramban, B.; Sundararaju, B. Cp*Co(III)-Catalyzed C–H Alkylation with Maleimides Using Weakly Coordinating Carbonyl Directing Groups. *Org. Lett.* **2018**, *20*, 2835. (d) Vaggu, R.; Thadem, N.; Rajesh, M.; Grée, R.; Das, S. Acylsilane Directed Rh-Catalyzed Arene C–H Alkylation with Maleimides and Visible-Light-Induced Siloxycarbene-Amide

TH-3369_166122017

Cyclization: [3 + 2] Carbo-Annulation in Ru Catalysis. *Org. Lett*. **2023**, *25*, 2594. (e) Wang, J.; Chen, H.; Kong, L.; Wang, F.; Lan, Y.; Li, X. Enantioselective and Diastereoselective C-H Alkylation of Benzamides: Synergized Axial and Central Chirality via a Single Stereodetermining Step. *ACS Catal*. **2021**, *11*, 9151. (f) Keshri, P.; Bettadapur, K. R.; Lanke, V.; Prabhu, K. R. Ru(II)-Catalyzed C–H Activation: Amide-Directed 1,4-Addition of the Ortho C–H Bond to Maleimides. *J. Org. Chem*. **2016**, *81*, 6056. (g) Chen, X.; Ren, J.; Xie, H.; Sun, W.; Sun, M.; Wu, B. Cobalt(III)-catalyzed 1,4-addition of C–H bonds of oximes to maleimides. *Org. Chem. Front*. **2018**, *5*, 184. (h) Yu, J. T.; Chen, R.; Jia, H.; Pan, C. Rhodium-Catalyzed Site-Selective Ortho-C–H Activation: Enone Carbonyl Directed Hydroarylation of Maleimides. *J. Org. Chem*. **2018**, *83*, 12086.

4. (a) Ghosh, A. K.; Samanta, S.; Ghosh, P.; Neogi, S.; Hajra, A. Regioselective hydroarylation and arylation of maleimides with indazoles via a Rh (III)-catalyzed C-H activation. *Org. Biomol. Chem.* **2020**, *18*, 3093. (b) Laru, S.; Bhattacharjee, S.; Singsardar, M.; Samanta, S.; Hajra, A. Ru(II)-Catalyzed Switchable C-H Alkylation and Spirocyclization of 2-Arylquinoxalines with Maleimides via Ortho-C-H Activation. *J. Org. Chem.* **2021**, *86*, 2784. (c) Ghosh, S.; Khandelia, T.; Patel, B. K. Solvent-Switched Manganese(I) Catalyzed Regiodivergent Distal vs Proximal C–H Alkylation of Imidazopyridine with Maleimide. *Org. Lett*. **2021**, *23*, 7370. (d) Cho, Y. S.; Kim, H. D.; Kim, E.; Han, S. H.; Han, S. B.; Mishra, N. K.; Jung, Y. H.; Jeong, T.; Kim, I. S. Direct Integration of Phthalazinone and Succinimide Scaffolds via Rh(III)-Catalyzed C-H Functionalization. *Asian J. Org. Chem*. **2021**, *10*, 202. (e) Reddy, K. N.; Krishna Rao, M. V.; Sridhar, B.; Reddy, B. V. S. Ru(II)-Catalyzed Hydroarylation of Maleimides with Cyclic N-Sulfonyl Ketimines through Ortho-C-H Bond Activation. *ChemistrySelect* **2018**, *3*, 5062. (f) Nipate, D. S.; Shinde, V. N.; Rangan, K.; Kumar, A. Switchable regioselective hydroalkylation of 2-arylindoles with maleimides. *Org. Biomol. Chem*. **2021**, *19*, 4910. (g) Yuan, Y.-C.; Goujon, M.; Bruneau, C.; Roisnel, T.; Gramage-Doria, R. C–H Bond Alkylation of Cyclic Amides with Maleimides via a SiteSelective-Determining Six-Membered Ruthenacycle. *J. Org. Chem*. **2019**, *84*, 16183. (h) Kang, J. Y.; Kim, S.; Moon, J.; Chung, E.; Kim, J.; Kyung, S. Y.; Kim, H. S.; Mishra, N. K.; Kim, I. S. Synthesis of Succinimide-Linked Indazol-3-ols Derived from Maleimides under Rh(III) Catalysis. *ACS Omega* **2022**, *7*, 14712. (i) Mondal, S.; Bera, R.; Chowdhury, D.; Dana, S.; Baidya, M. Redox-Neutral Ruthenium(II)-Catalyzed Enol-Directed Arene C–H Alkylation with Maleimides. *Org. Lett*. **2023**, *25*, 70. (j) Zhao, J. L.; Pi, C.; You, C.; Wang, Y.; Cui, X. L.; Wu, Y. Rhodium(III)-Catalyzed Direct C–H Alkylation of 2-Aryl-1,2,3-triazole N-Oxides with Maleimides. *Eur. J. Org. Chem*. **2018**, *2018*, 6919. (k) Muniraj, N.; Prabhu, K. R. Cobalt(III)-Catalyzed C–H Activation: Azo Directed Selective 1,4-Addition of Ortho C–H Bond to Maleimides. *J. Org. Chem*. **2017**, *82*, 6913.

TH-3369_166122017

(l) Xiao, L.; Liu, X.-G.; Bao, M. -Z.; Song, J.-L.; Chen, S.-Y.; Zheng, Y.-C.; Liu, Y.-Z.; Zhang, S.-S. Cp*Rh(III)-Catalyzed ortho-Alkylation/Alkenylation of Nitroarenes. *Org. Lett*. **2023**, *25*, 5185.

5. (a) Banjare, S. K.; Chebolu, R.; Ravikumar, P. C. Cobalt Catalyzed Hydroarylation of Michael Acceptors with Indolines Directed by a Weakly Coordinating Functional Group. *Org. Lett.* **2019**, *21*, 4049. (b) Zhou, Y.; Liang, H.; Sheng, Y.; Wang, S.; Gao, Y.; Zhan, L.; Zheng, Z.; Yang, M.; Liang, G.; Zhou, J.; Deng, J.; Song, Z. Ruthenium(II)-Catalyzed C-H Activation of Chromones with Maleimides to Synthesize Succinimide/Maleimide-Containing Chromones. *J. Org. Chem*. **2020**, *85*, 9230. (c) Thakur, A.; Dhiman, A. K.; Sumit; Kumar, R.; Sharma, U. Rh(III)-Catalyzed Regioselective C8-Alkylation of Quinoline N-Oxides with Maleimides and Acrylates. *J. Org. Chem*. **2021**, *86*, 6612. (d) An, W.; Lee, S. H.; Kim, D.; Oh, H.; Kim, S.; Byun, Y.; Kim, H. J.; Mishra, N. K.; Kim, I. S. Site-Selective C8-Alkylation of Quinoline N-Oxides with Maleimides under Rh(III) Catalysis. *J. Org. Chem*. *2021*, **86**, 7579. (e) Yakkala, P. A.; Giri, D.; Chaudhary, B.; Auti, P.; Sharma, S. Regioselective C-H Alkylation and Alkenylation at the C5 Position of 2-Amino-1,4-naphthoquinones with Maleimides under Rh(III) Catalysis. *Org. Chem. Front*. **2019**, *6*, 2441. (f) Sherikar, M. S.; Kapanaiah, R.; Lanke, V.; Prabhu, K. R. Rhodium(III)-catalyzed C-H activation at the C4-position of indole: switchable hydroarylation and oxidative Heck-type reactions of maleimides. *Chem. Commun*. **2018**, *54*, 11200.
6. (a) Han, S.; Park, J.; Kim, S.; Lee, S. H.; Sharma, S.; Mishra, N. K.; Jung, Y. H.; Kim, I. S. Rhodium(III) Catalyzed C(sp^3)-H Alkylation of 8-Methylquinolines with Maleimides. *Org. Lett.* **2016**, *18*, 4666. (b) Kumar, R.; Kumar, R.; Chandra, D.; Sharma, U. Cp*CoIII-catalyzed alkylation of primary and secondary C(sp^3)-H bonds of 8-alkylquinolines with maleimides. *J. Org. Chem*. **2019**, *84*, 1542.
7. (a) Sharma, S.; Han, S. H.; Jo, H.; Han, S.; Mishra, N. K.; Choi, M.; Jeong, T.; Park, J.; Kim, I. S. Rhodium-Catalyzed Vinylic C-H Functionalization of Enol Carbamates with Maleimides. *Eur. J. Org. Chem*. **2016**, *2016*, 3611. (b) Yu, W.; Zhang, W.; Liu, Y.; Liu, Z.; Zhang, Y. Cobalt(III)-Catalyzed Cross-Coupling of Enamides with Allyl Acetates/Maleimides. *Org. Chem. Front*. **2017**, *4*, 77.
8. (a) Bettadapur, K. R.; Lanke, V.; Prabhu, K. R. A deciduous directing group approach for the addition of aryl and vinyl nucleophiles to maleimides. *Chem. Commun*. **2017**, *53*, 6251. (b) Mandal, A.; Sahoo, H.; Dana, S.; Baidya, M. Ruthenium(II)-Catalyzed Hydroarylation of Maleimides Using Carboxylic Acids as a Traceless Directing Group. *Org. Lett*. **2017**, *19*, 4138.
9. (a) Ye, M. C.; Gao, G.-L.; Yu, J.-Q. Ligand-promoted C–3 selective C–H olefination of pyridines with Pd catalysts. *J. Am. Chem. Soc*. **2011**, *133*, 6964. (b) Cao, H.; Cheng, Q.; Studer, A. Radical

TH-3369_166122017

and Ionic Meta-C-H Functionalization of Pyridines, Quinolines, and Isoquinolines. *Science*. **2022**, *378*, 779. (c) Dutta, U.; Maiti, S.; Bhattacharya, T.; Maiti, D. Arene Diversification Through Distal C(sp^2)−H Functionalization. *Science*. **2021**, *372*, 701. (d) Meng, G.; Wang, Z.; Chan, H. S. S.; Chekshin, N.; Li, Z.; Wang, P.; Yu, J.-Q. Dual-Ligand Catalyst for the Nondirected C–H Olefination of Heteroarenes. *J. Am. Chem. Soc*. **2023**, *145*, 8198.

10. (a) Yashwantrao, G.; Saha, S. Recent advances in the synthesis and reactivity of quinoxaline. *Org. Chem. Front*. **2021**, *8*, 2820. (b) Ghosh, S.; Pal, S.; Rajamanickam, S.; Shome, R.; Mohanta, P. R.; Ghosh, S. S.; Patel, B. K. Access to Multifunctional AEEgens via Ru(II)-Catalyzed Quinoxaline-Directed Oxidative Annulation. *ACS Omega*. **2019**, *4*, 5565. (c) Khandelia, T.; Ghosh, S.; Patel, B. K.; Dearomative Bis-functionalization of Quinoxalines and Bis-*N*-arylation of (Benz)Imidazoles via Cu(II)-mediated Addition of Boronic Acids. *Chem. Commun*. **2023**, *59*, 2118.
11. Mondal, K.; Ghosh, S.; Hajra, A. Transition-metal-catalyzed Ortho C-H Functionalization of 2-Arylquinoxalines. *Org. Biomol. Chem*. **2022**, *20*, 7361.
12. Laru, S.; Bhattacharjee, S.; Singsardar, M.; Samanta, S.; Hajra, A. Ru(II)-Catalyzed Switchable C-H Alkylation and Spirocyclization of 2-Arylquinoxalines with Maleimides via Ortho-C-H Activation. *J. Org. Chem*. **2021**, *86*, 2784.
13. (a) Wang, L.; Carrow, B. P. Oligothiophene Synthesis by a General C–H Activation Mechanism: Electrophilic Concerted Metalation–Deprotonation (eCMD). *ACS Catal*. **2019**, *9*, 6821. (b) Wedi, P.; Farizyan, M.; Bergander, K.; Mück-Lichtenfeld, C.; Gemmeren, M. V. Mechanism of the Arene-Limited Nondirected C−H Activation of Arenes with Palladium. *Angew. Chem., Int. Ed*. **2021**, *60*, 15641. (c) Ghosh, S.; Khandelia, T.; Patel, B. K. Solvent-Switched Manganese(I) Catalyzed Regiodivergent Distal vs Proximal C–H Alkylation of Imidazopyridine with Maleimide. *Org. Lett*. **2021**, *23*, 7370. (d) Liu, W.; Ackermann, L. Manganese-Catalyzed C–H Activation. *ACS Catal*. **2016**, *6*, 3743. (e) Hu, Y.; Zhou, B.; Wang, C. Inert C-H Bond Transformations Enabled by Organometallic Manganese Catalysis. *Acc. Chem. Res*. **2018**, *51*, 816.
14. Paul, S.; Khanal, H. D.; Clinton, C. D.; Kim, S. H.; Lee, Y. R. $Pd(TFA)_2$-Catalyzed Direct Arylation of Quinoxalinones with Arenes. *Org. Chem. Front*. **2019**, *6*, 231.
15. (a) Reddy, C. R.; Prajapti, S. K.; Warudikar, K.; Ranjan, R.; Rao, B. B. ipso-Cyclization: An Emerging Tool for Multifunctional Spirocyclohexadienones. *Org. Biomol. Chem*. **2017**, *15*, 3130. (b) Deguchi, H.; Hanaya, K.; Sugai, T.; Higashibayashi, S. Intramolecular Cyclization of *m*-Homoprenylphenols Through Oxidative Nucleophilic Aromatic Substitution. *Chem. Commun*. **2023**, *59*, 748.

TH-3369_166122017

16. (a) Xia, X. -F.; Huang, Q.; Sun, T. -Y.; Jiang, Y.; Ran, G. Catalytic Desaturation and β-Fluorination of Aliphatic Amides Enabled by an Oxidative-Promoted Bond Destabilization. *ACS Catal*. **2022**, *12*, 12964. (b) Yang, K.; Song, M.; Ali, A. I. M.; Mudassir, S. M.; Ge, H. Recent Advances in the Application of Selectfluor as a "Fluorine-free" Functional Reagent in Organic Synthesis. *Chem. - Asian J*. **2020**, *15*, 729.
17. Kumar, K.; Mudshinge, S. R.; Goyal, S.; Gangar, M.; Nair, V. A. *Tetrahedron Letters*. **2015**, *56*, 1266.
18. Mandal, R.; Emayavaramban, B.; Sundararaju, B. *Org. Lett.* **2018**, *20*, 2835.
19. Lassagne, F.; Chevallier, F.; Roisnel, T.; Dorcet, V.; Mongin, F.; Domingo, L. R. *Synthesis* **2015**, *47*, 2680.

IV.7. Spectral Data

1-Phenyl-3-(3-phenylquinoxalin-2-yl)pyrrolidine-2,5-dione (3aa):

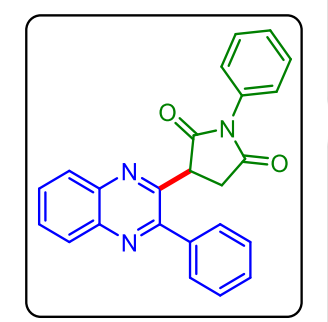

A off-white solid (67 mg, 88% yield); mp 184–186 ^{o}C; purified over a column of silica gel (20% EtOAc in hexane); ^{1}H NMR ($CDCl_3$, 400 MHz): δ 8.18 – 8.15 (m, 1H), 8.10 – 8.07 (m, 1H), 7.88 (d, J = 7.6 Hz, 2H), 7.83 – 7.77 (m, 2H), 7.59 – 7.53 (m, 3H), 7.49 (t, J = 7.6 Hz, 2H), 7.42 (d, J = 7.2 Hz, 1H), 7.39 – 7.36 (m, 2H), 4.86 (dd, J = 9.2, 4.8 Hz, 1H), 3.45 (dd, J = 18.0, 4.4 Hz, 1H), 3.19 (dd, J = 18.0, 9.6 Hz, 1H); ^{13}C {^{1}H} NMR ($CDCl_3$, 101 MHz): δ 176.2, 175.6, 154.7, 151.5, 141.5, 137.9, 132.1, 130.8, 130.5, 129.8, 129.5, 129.4, 129.3, 129.0, 128.9, 126.7, 45.0, 36.9; IR (neat, cm^{-1}): 3055, 1698, 1481, 1188, 1008, 727, 695, 608, 473; HRMS (ESI-TOF) calcd for $C_{24}H_{18}N_3O_2$ $[M + H]^+$ 380.1399, found 380.1394.

TH-3369_166122017

1-Phenyl-3-(3-(*p*-tolyl)quinoxalin-2-yl)pyrrolidine-2,5-dione (3ba):

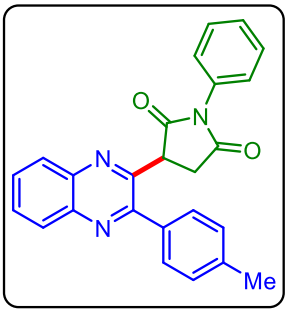

A light brown solid (72 mg, 92% yield); mp 189–191 ºC; purified over a column of silica gel (20% EtOAc in hexane); ^{1}H NMR ($CDCl_3$, 400 MHz): δ 8.17 – 8.14 (m, 1H), 8.09 – 8.06 (m, 1H), 7.81 – 7.76 (m, 4H), 7.50 (t, *J* = 7.6 Hz, 2H), 7.42 (d, *J* = 7.2 Hz, 1H), 7.38 (d, *J* = 7.6 Hz, 4H), 4.89 (dd, *J* = 9.2, 4.4 Hz, 1H), 3.43 (dd, *J* = 18.0, 4.8 Hz, 1H), 3.19 (dd, *J* = 18.0, 9.6 Hz, 1H), 2.46 (s, 3H); ^{13}C {^{1}H} NMR ($CDCl_3$, 126 MHz): δ 176.2, 175.6, 154.9, 151.7, 141.7, 141.5, 139.7, 135.1, 132.2, 130.7, 130.3, 129.8, 129.7, 129.5, 129.3, 129.0, 128.9, 126.8, 45.1, 37.0, 21.5; IR (neat, cm^{-1}): 2978, 1711, 1522, 1358, 1187, 1025, 858, 728, 508, 509; HRMS (ESI-TOF) calcd for $C_{25}H_{20}N_3O_2$ $[M + H]^+$ 394.1556, found 394.1548.

3-(3-(4-Methoxyphenyl)quinoxalin-2-yl)-1-phenylpyrrolidine-2,5-dione (3ca):

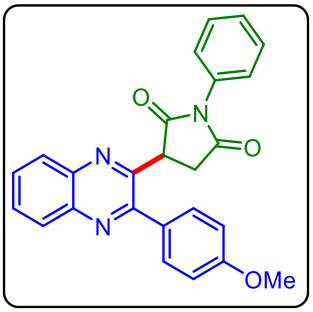

A light brown solid (77mg, 94% yield); mp 175–178 ºC; purified over a column of silica gel (25% EtOAc in hexane); ^{1}H NMR ($CDCl_3$, 500 MHz): δ 8.15 – 8.13 (m, 1H), 8.07 – 8.05 (m, 1H), 7.85 (d, *J* = 8.5 Hz, 2H), 7.80 – 7.74 (m, 2H), 7.49 (t, *J* = 7.7 Hz, 2H), 7.42 (d, *J* = 7.0 Hz, 1H), 7.38 (d, *J* = 8.0 Hz, 2H), 7.09 (d, *J* = 8.5 Hz, 2H), 4.91 (dd, *J* = 9.5, 4.5 Hz, 1H), 3.89 (s, 3H), 3.43 (dd, *J* = 18.0, 4.5 Hz, 1H), 3.19 (dd, *J* = 18.0, 9.5 Hz, 1H); ^{13}C {^{1}H} NMR ($CDCl_3$, 126 MHz): δ 176.3, 175.6, 160.8, 154.5, 151.7, 141.6, 141.3, 132.1, 131.3, 130.7, 130.3, 130.2, 129.4, 129.3, 128.9, 128.8, 126.7, 114.5, 55.6, 45.0, 37.1; IR (neat, cm^{-1}): 3011, 1723, 1508, 1327, 1101, 1025, 851, 719, 578, 556; HRMS (ESI-TOF) calcd for $C_{25}H_{20}N_3O_3$ $[M + H]^+$ 410.1505, found 410.1501.

TH-3369_166122017

3-(3-(4-Fluorophenyl)quinoxalin-2-yl)-1-phenylpyrrolidine-2,5-dione (3da):

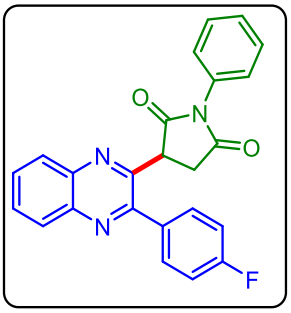

A off-white solid (63 mg, 79% yield); mp 189–191 °C; purified over a column of silica gel (23% EtOAc in hexane); ^{1}H NMR ($CDCl_3$, 400 MHz): δ 8.17 – 8.12 (m, 1H), 8.11 – 8.07 (m, 1H), 7.95 – 7.90 (m, 2H), 7.83 – 7.77 (m, 2H), 7.49 (t, *J* = 7.6 Hz, 2H), 7.42 (d, *J* = 7.2 Hz, 1H), 7.37 (d, *J* = 7.2 Hz, 2H), 7.26 (t, *J* = 8.6 Hz, 2H), 4.83 (dd, *J* = 9.2, 4.4 Hz, 1H), 3.48 (dd, *J* = 18.0, 4.4 Hz, 1H), 3.19 (dd, *J* = 18.0, 9.2 Hz, 1H); ^{13}C {^{1}H} NMR ($CDCl_3$, 101 MHz): δ 176.2, 175.5, 163.7 (d, *J* = 250.7 Hz) , 153.8, 151.3, 141.5 (d, *J* = 4.8 Hz), 134.3, 133.9 (d, *J* = 3.5 Hz), 132.0, 131.9, 130.9, 130.6, 129.4, 129.3, 128.9 (d, *J* = 2.1 Hz), 126.7, 116.1, 115.9, 44.9, 36.9; ^{19}F NMR ($CDCl_3$) δ -111.4 (s); IR (neat, cm^{-1}): 3009, 1722, 1504, 1326, 1108, 1036, 868, 701, 588, 569; HRMS (ESI-TOF) calcd for $C_{24}H_{17}FN_3O_2$ [M + H]$^{+}$ 398.1305, found 398.1306.

3-(3-(4-Chlorophenyl)quinoxalin-2-yl)-1-phenylpyrrolidine-2,5-dione (3ea):

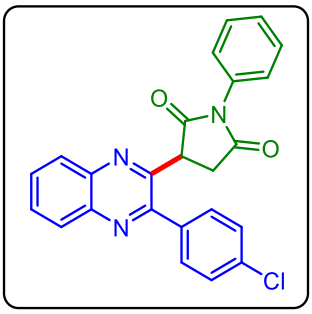

A brown solid (67 mg, 81% yield); mp 187–190 °C; purified over a column of silica gel (20% EtOAc in hexane); ^{1}H NMR ($CDCl_3$, 500 MHz): δ 8.16 – 8.14 (m, 1H), 8.10 – 8.08 (m, 1H), 7.87 (d, *J* = 8.0 Hz, 2H), 7.82 – 7.80 (m, 2H), 7.54 (d, *J* = 8.5 Hz, 2H), 7.49 (t, *J* = 7.7 Hz, 2H), 7.41 (t, *J* = 7.5 Hz, 1H), 7.37 (d, *J* = 8.0 Hz, 2H), 4.81 (dd, *J* = 9.2, 4.2 Hz, 1H), 3.48 (dd, *J* = 18.0, 4.5 Hz, 1H), 3.19 (dd, *J* = 18.0, 9.0 Hz, 1H); ^{13}C {^{1}H} NMR ($CDCl_3$, 126 MHz): δ 176.1, 175.5, 153.6, 151.1, 141.6, 141.5, 136.3, 136.0, 132.0, 131.3, 130.9, 130.7, 129.4, 129.3, 129.2, 129.0, 128.9, 126.7, 44.9, 36.8; IR (neat, cm^{-1}): 3039, 1623, 1450, 1269, 1109, 1027, 788, 623, 591, 589; HRMS (ESI-TOF) calcd for $C_{24}H_{17}ClN_3O_2$ [M + H]$^{+}$ 414.1009, found 414.1002.

TH-3369_166122017

1-Phenyl-3-(3-(4-(trifluoromethyl)phenyl)quinoxalin-2-yl)pyrrolidine-2,5-dione (3fa):

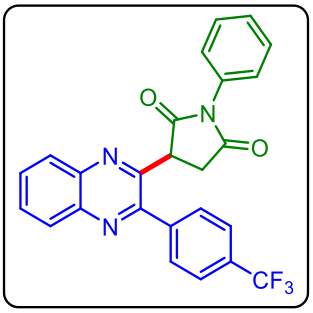

A plae yellow solid (62 mg, 69% yield); mp 168–171 ºC; purified over a column of silica gel (22% EtOAc in hexane); ^{1}H NMR ($CDCl_3$, 400 MHz): δ 8.18 – 8.14 (m, 1H), 8.13 – 8.09 (m, 1H), 8.06 (d, *J* = 8.0 Hz, 2H), 7.85 – 7.81 (m, 4H), 7.49 (t, *J* = 7.2 Hz, 2H), 7.41 (t, *J* = 7.4 Hz, 1H), 7.38 – 7.35 (m, 2H), 4.77 (dd, *J* = 9.2, 4.4 Hz, 1H), 3.52 (dd, *J* = 18.0, 4.8 Hz, 1H), 3.20 (dd, *J* = 18.0, 9.6 Hz, 1H); ^{13}C {^{1}H} NMR ($CDCl_3$, 126 MHz): δ 176.0, 175.4, 153.4, 150.9, 141.8, 141.5, 141.4, 131.9, 131.7, 131.5, 131.1, 131.0, 130.4, 129.5, 129.4, 129.05, 129.00, 126.7, 125.9 (q, *J* = 3.6 Hz), 44.9, 36.6; ^{19}F NMR ($CDCl_3$) δ -62.7 (s); IR (neat, cm^{-1}): 3059, 1622, 1405, 1369, 1120, 1052, 768, 651, 599, 509; HRMS (ESI-TOF) calcd for $C_{25}H_{17}F_3N_3O_2$ $[M + H]^+$ 448.1273, found 448.1264.

3-(3-([1,1'-Biphenyl]-4-yl)quinoxalin-2-yl)-1-phenylpyrrolidine-2,5-dione (3ga):

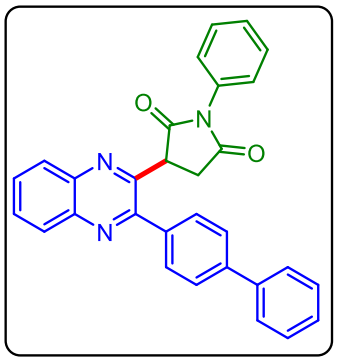

A orange solid (68 mg, 75% yield); mp 178–180 ºC; purified over a column of silica gel (20% EtOAc in hexane); ^{1}H NMR ($CDCl_3$, 500 MHz): δ 8.18 – 8.16 (m, 1H), 8.10 – 8.08 (m, 1H), 7.97 (d, *J* = 8.0 Hz, 2H), 7.79 (d, *J* = 7.0 Hz, 4H), 7.66 (d, *J* = 7.5 Hz, 2H), 7.48 (t, *J* = 7.2 Hz, 4H), 7.42 – 7.37 (m, 4H), 4.94 (dd, *J* = 9.0, 4.5 Hz, 1H), 3.47 (dd, *J* = 18.0, 4.0 Hz, 1H), 3.21 (dd, *J* = 18.0, 9.5 Hz, 1H); ^{13}C {^{1}H} NMR ($CDCl_3$, 101 MHz): δ 176.2, 175.6, 154.5, 151.5, 142.5, 141.6, 141.5, 140.4, 136.7, 134.3, 132.1, 130.8, 130.5, 130.3, 129.5, 129.3, 129.1, 129.0, 128.9, 127.9, 127.7, 127.3, 126.7, 45.0, 37.0; IR (neat, cm^{-1}): 2932, 1769, 1723, 1503, 1376, 1270, 1163, 928, 728, 628; HRMS (ESI-TOF) calcd for $C_{30}H_{22}N_3O_2$ $[M + H]^+$ 456.1712, found 456.1712.

TH-3369_166122017

1-Phenyl-3-(3-(*m*-tolyl)quinoxalin-2-yl)pyrrolidine-2,5-dione (3ha):

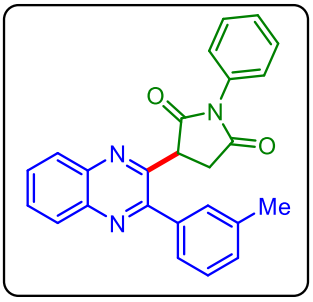

A off-white solid (71 mg, 90% yield); mp 172–175 °C; purified over a column of silica gel (20% EtOAc in hexane); ^{1}H NMR ($CDCl_3$, 400 MHz): δ 8.17 – 8.15 (m, 1H), 8.10 – 8.06 (m, 1H), 7.81 – 7.75 (m, 2H), 7.67 – 7.62 (d, J = 1.4 Hz, 2H), 7.49 (t, J = 7.6 Hz, 2H), 7.45 – 7.33 (m, 5H), 4.87 (dd, J = 9.2, 4.4 Hz, 1H), 3.42 (dd, J = 18.0, 4.4 Hz, 1H), 3.19 (dd, J = 18.0, 9.2 Hz, 1H), 2.46 (s, 3H); ^{13}C {^{1}H} NMR ($CDCl_3$, 101 MHz): δ 176.1, 175.6, 154.9, 151.7, 141.5, 141.4, 138.9, 137.8, 132.1, 130.7, 130.3, 130.2, 129.4, 129.3, 128.9, 128.8, 128.7, 126.73, 126.70, 45.0, 37.0, 21.6; IR (neat, cm^{-1}): 2912, 1789, 1723, 1513, 1386, 1270, 1173, 928, 728, 638; HRMS (ESI-TOF) calcd for $C_{25}H_{20}N_3O_2$ $[M + H]^+$ 394.1556, found 394.1556.

1-Phenyl-3-(3-(3-(trifluoromethyl)phenyl)quinoxalin-2-yl)pyrrolidine-2,5-dione (3ia):

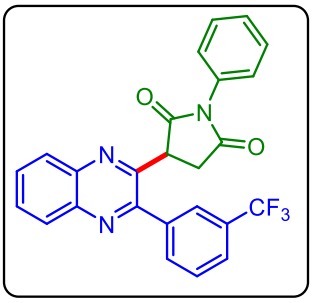

A off-white solid (64 mg, 72% yield); mp 179–181 °C; purified over a column of silica gel (22% EtOAc in hexane); ^{1}H NMR ($CDCl_3$, 400 MHz): δ 8.20 – 8.16 (m, 3H), 8.13 – 8.09 (m, 1H), 7.86 – 7.82 (m, 2H), 7.80 (s, 1H), 7.71 (t, J = 8.0 Hz, 1H), 7.50 (t, J = 7.6 Hz, 2H), 7.42 (t, J = 7.4 Hz, 1H), 7.37 (d, J = 7.6 Hz, 2H), 4.76 (dd, J = 9.2, 4.4 Hz, 1H), 3.51 (dd, J = 18.0, 4.4 Hz, 1H), 3.21 (dd, J = 18.0, 9.4 Hz, 1H); ^{13}C {^{1}H} NMR ($CDCl_3$, 101 MHz): δ 176.0, 175.4, 153.2, 151.0, 141.7, 141.5, 138.6, 133.3, 132.0, 131.7, 131.3, 131.1, 131.0, 129.5 (d, J = 3.3 Hz), 129.4, 129.0 (d, J = 4.6 Hz), 126.9 (q, J = 3.8 Hz), 126.7, 126.3 (q, J = 3.6 Hz), 125.3, 122.6, 44.9, 36.8; ^{19}F NMR ($CDCl_3$) δ -62.5 (s); IR (neat, cm^{-1}): 2922, 1789, 1700, 1513, 1306, 1290, 1123, 908, 728, 607; HRMS (ESI-TOF) calcd for $C_{25}H_{17}F_3N_3O_2$ $[M + H]^+$ 448.1273, found 448.1278.

TH-3369_166122017

3-(3-(2-Methoxyphenyl)quinoxalin-2-yl)-1-phenylpyrrolidine-2,5-dione (3ja):

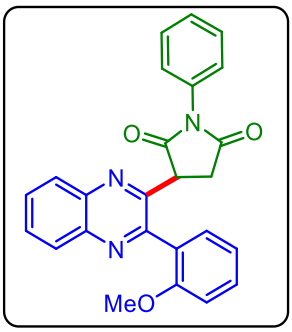

Reddish gummy (68 mg, 83% yield); purified over a column of silica gel (35% EtOAc in hexane); ^{1}H NMR ($CDCl_3$, 400 MHz): δ 8.16 – 8.12 (m, 1H), 8.09 – 8.06 (m, 1H), 7.78 – 7.73 (m, 2H), 7.67 (d, J = 7.2 Hz, 1H), 7.51 – 7.42 (m, 3H), 7.38 – 7.31 (m, 3H), 7.18 (t, J = 7.4 Hz, 1H), 7.02 (d, J = 8.0 Hz, 1H), 4.51 (dd, J = 9.0, 4.2 Hz, 1H), 3.77 (s, 3H), 3.54 (dd, J = 18.0, 4.0 Hz, 1H), 3.25 (dd, J = 18.0, 9.2 Hz, 1H); ^{13}C{^{1}H} NMR ($CDCl_3$, 126 MHz): δ 176.0, 175.9, 156.3, 153.5, 152.9, 141.8, 141.5, 132.1, 132.0, 131.2, 130.3, 130.2, 129.4, 129.2, 128.9, 128.7, 127.0, 126.6, 121.9, 110.7, 55.5, 45.5, 36.6; IR (neat, cm^{-1}): 3004, 1725, 1501, 1324, 1106, 1022, 856, 715, 572, 554; HRMS (ESI-TOF) calcd for $C_{25}H_{20}N_3O_3$ $[M + H]^+$ 410.1505, found 410.1504.

3-(2,6-Difluorophenyl)quinoxalin-2-yl)-1-phenylpyrrolidine-2,5-dione (3ka):

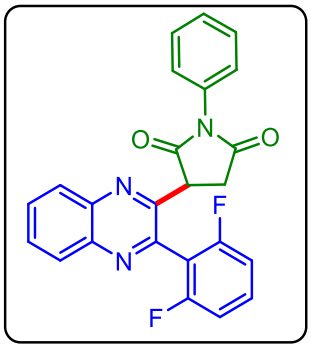

A light brown gummy (57 mg, 68% yield); purified over a column of silica gel (25% EtOAc in hexane); ^{1}H NMR ($CDCl_3$, 500 MHz): δ 8.18 – 8.15 (m, 1H), 8.13 – 8.10 (m, 1H), 7.85 – 7.79 (m, 2H), 7.5 – 7.42 (m, 3H), 7.37 (t, J = 7.5 Hz, 1H), 7.32 (d, J = 8.0 Hz, 2H), 7.14 (t, J = 8.5 Hz, 1H), 7.07 (t, J = 8.5 Hz, 1H), 4.52 (dd, J = 9.5, 4.5 Hz, 1H), 3.61 (dd, J = 18.2, 4.7 Hz, 1H), 3.28 (dd, J = 18.5, 9.5 Hz, 1H); ^{13}C {^{1}H} NMR ($CDCl_3$, 126 MHz): δ 175.4, 174.9, 162.4, 162.3, 160.97, 160.92, 160.3, 160.2, 159.0, 158.9, 152.2, 145.1, 141.8, 141.7, 132.0, 131.9, 131.8, 131.7, 131.3, 130.9, 129.5, 129.2, 129.1, 128.8, 126.6, 115.4, 115.3, 115.1, 113.1, 113.0, 112.89, 112.86, 111.56, 111.54, 111.4, 111.3, 45.3, 35.5; ^{19}F NMR ($CDCl_3$) δ -109.9 (s), -113.2 (s); IR (neat, cm^{-1}): 2902, 1789, 1723, 1523, 1376, 1260, 1174, 918, 733, 608; HRMS (ESI-TOF) calcd for $C_{24}H_{16}F_2N_3O_2$ $[M + H]^+$ 416.1211, found 416.1205.

TH-3369_166122017

3-(6,7-Dichloro-3-phenylquinoxalin-2-yl)-1-phenylpyrrolidine-2,5-dione (3la):

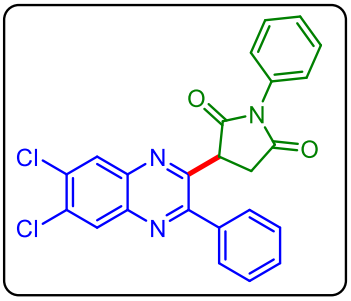

A light brown solid (63 mg, 70% yield); mp 186–189 °C; purified over a column of silica gel (22% EtOAc in hexane); ^{1}H NMR ($CDCl_3$, 500 MHz): δ 8.27 (s, 1H), 8.22 (s, 1H), 7.86 (d, J = 5.5 Hz, 2H), 7.57 – 7.53 (m, 3H), 7.48 (t, J = 7.5 Hz, 2H), 7.41 (t, J = 7.5 Hz, 1H), 7.35 (d, J = 8.0 Hz, 2H), 4.85 (dd, J = 9.0, 4.5 Hz, 1H), 3.37 (dd, J = 18.0, 4.5 Hz, 1H), 3.17 (dd, J = 18.0, 9.5 Hz, 1H); ^{13}C {^{1}H} NMR ($CDCl_3$, 126 MHz): δ 175.7, 175.1, 155.8, 152.9, 140.3, 140.1, 137.2, 135.5, 135.2, 131.9, 130.0, 129.9, 129.7, 129.5, 129.3, 129.0, 128.9, 126.6, 45.0, 36.9 IR (neat, cm^{-1}): 3074, 2922, 1703, 1442, 1390, 1136, 1011, 693, 525; HRMS (ESI-TOF) calcd for $C_{24}H_{16}Cl_2N_3O_2$ $[M + H]^+$ 448.0620, found 448.0610.

3-(3-(Naphthalen-2-yl)quinoxalin-2-yl)-1-phenylpyrrolidine-2,5-dione (3ma):

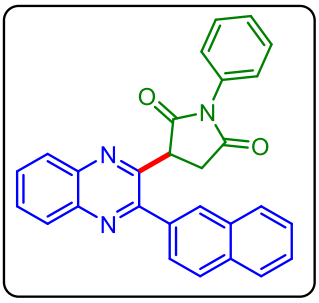

A pale yellow solid (69 mg, 81% yield); mp 177–180 °C; purified over a column of silica gel (20% EtOAc in hexane); ^{1}H NMR ($CDCl_3$, 500 MHz): δ 8.41 (s, 1H), 8.20 – 8.18 (m, 1H), 8.12 – 8.10 (m, 1H), 8.04 (d, J = 8.5 Hz, 1H), 7.98 – 7.91 (m, 3H), 7.84 – 7.79 (m, 2H), 7.60 – 7.55 (m, 2H), 7.49 (t, J = 7.5 Hz, 2H), 7.41 (t, J = 7.5 Hz, 1H), 7.37 (d, J = 7.5 Hz, 2H), 4.93 (dd, J = 9.5, 4.5 Hz, 1H), 3.48 (dd, J = 18.0, 4.5 Hz, 1H), 3.18 (dd, J = 18.0, 9.5 Hz, 1H); ^{13}C {^{1}H} NMR ($CDCl_3$, 126 MHz): δ 176.1, 175.4, 154.7, 151.7, 141.55, 141.50, 135.1, 133.5, 133.1, 132.1, 130.7, 130.4, 129.7, 129.4, 129.2, 128.9, 128.8, 128.75, 128.71, 127.9, 127.2, 126.9, 126.8, 126.7, 45.1, 36.9; IR (neat, cm^{-1}): 2922, 1799, 1703, 1513, 1286, 1260, 1173, 928, 738, 630; HRMS (ESI-TOF) calcd for $C_{28}H_{20}N_3O_2$ $[M + H]^+$ 430.1556, found 430.1549.

TH-3369_166122017

1-Phenyl-3-(3-(thiophen-2-yl)quinoxalin-2-yl)pyrrolidine-2,5-dione (3na):

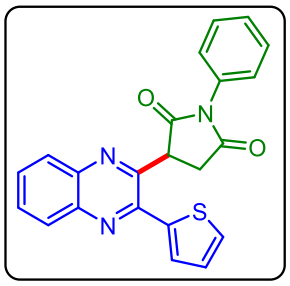

A off-white solid (59 mg, 76% yield); mp 165–167 °C; purified over a column of silica gel (20% EtOAc in hexane); ^{1}H NMR ($CDCl_3$, 400 MHz): δ 8.15 – 8.11 (m, 1H), 8.06 – 8.02 (m, 1H), 7.93 (d, *J* = 3.6 Hz, 1H), 7.81 – 7.74 (m, 2H), 7.61 (d, *J* = 4.8 Hz, 1H), 7.51 (t, *J* = 7.6 Hz, 2H), 7.44 – 7.39 (m, 3H), 7.22 (t, *J* = 7.4 Hz, 1H), 5.19 (dd, *J* = 9.2, 4.4 Hz, 1H), 3.53 (dd, *J* = 18.0, 4.0 Hz, 1H), 3.28 (dd, *J* = 18.0, 9.2 Hz, 1H); ^{13}C {^{1}H} NMR ($CDCl_3$, 101 MHz): δ 176.1, 175.6, 150.3, 148.2, 141.4, 140.9, 140.7, 132.1, 130.9, 130.5, 130.1, 129.9, 129.4, 129.2, 128.94, 128.90, 128.3, 126.7, 45.0, 36.9 IR (neat, cm^{-1}): 3108, 1704, 1499, 1389, 1183, 981, 697, 659, 544; HRMS (ESI-TOF) calcd for $C_{22}H_{16}N_3O_2S$ [M + H]$^+$ 386.0963, found 386.0960.

3-(3-(Benzo[*d*][1,3]dioxol-5-yl)quinoxalin-2-yl)-1-phenylpyrrolidine-2,5-dione (3oa):

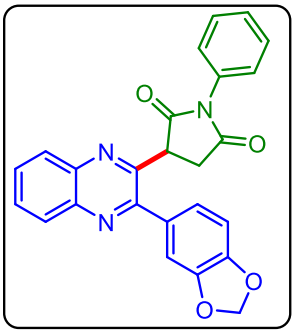

A light orange solid (74 mg, 87% yield); mp 174–177 °C; purified over a column of silica gel (30% EtOAc in hexane); ^{1}H NMR ($CDCl_3$, 500 MHz): δ 8.14 – 8.12 (m, 1H), 8.07 – 8.04(m, 1H), 7.80 – 7.75 (m, 2H), 7.49 (t, *J* = 7.5 Hz, 2H), 7.42 – 7.38 (m, 4H), 7.37 (s, 1H), 6.98 (d, *J* = 8.5 Hz, 1H), 6.05 (s, 2H), 4.93 (dd, *J* = 9.5, 4.5 Hz, 1H), 3.43 (dd, *J* = 18.0, 4.5 Hz, 1H), 3.20 (dd, *J* = 18.0, 9.5 Hz, 1H); ^{13}C {^{1}H} NMR ($CDCl_3$, 126 MHz): δ 176.2, 175.6, 154.3, 151.6, 149.0, 148.3, 141.5, 141.4, 132.2, 131.8, 130.8, 130.3, 129.4, 129.3, 129.0, 128.9, 126.8, 124.2, 110.4, 108.8, 101.7, 45.0, 37.0; IR (neat, cm^{-1}): 2910, 1705, 1497, 1440, 1359, 1237, 1172, 1034, 908, 691, 537; HRMS (ESI-TOF) calcd for $C_{25}H_{18}N_3O_4$ [M + H]$^+$ 424.1297, found 424.1313.

TH-3369_166122017

1-Methyl-3-(3-phenylquinoxalin-2-yl)pyrrolidine-2,5-dione (3ab):

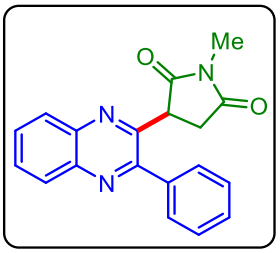

A off-white solid (50 mg, 79% yield); mp 162–165 ºC; purified over a column of silica gel (20% EtOAc in hexane); ^{1}H NMR ($CDCl_3$, 600 MHz): δ 8.14 – 8.12 (m, 1H), 8.04 – 8.01 (m, 1H), 7.85 (d, J = 7.2 Hz, 2H), 7.78 – 7.74 (m, 2H), 7.56 – 7.50 (m, 3H), 4.70 (dd, J = 9.0, 4.8 Hz, 1H), 3.29 (dd, J = 17.7, 4.5 Hz, 1H), 3.09 (s, 3H), 3.02 (dd, J = 18.0, 9.0 Hz, 1H); ^{13}C {^{1}H} NMR ($CDCl_3$, 151 MHz): δ 177.1, 176.5, 154.7, 151.3, 141.43, 141.40, 137.9, 130.6, 130.3, 129.7, 129.4, 129.3, 128.8, 44.9, 36.7, 25.3; IR (neat, cm^{-1}): 2961, 1696, 1380, 1259, 1106, 1011, 776, 694, 592, 515; HRMS (ESI-TOF) calcd for $C_{19}H_{16}N_3O_2$ $[M + H]^+$ 318.1243, found 318.1239.

1-Ethyl-3-(3-phenylquinoxalin-2-yl)pyrrolidine-2,5-dione (3ac):

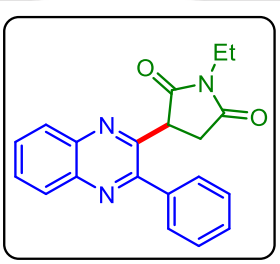

A light brown solid (54 mg, 82% yield); mp 167–170 ºC; purified over a column of silica gel (20% EtOAc in hexane); ^{1}H NMR ($CDCl_3$, 500 MHz): δ 8.15 – 8.13 (m, 1H), 8.03 – 8.01 (m, 1H), 7.86 (d, J = 6.5 Hz, 2H), 7.79 – 7.74 (m, 2H), 7.58 – 7.50 (m, 3H), 4.67 (dd, J = 9.5, 4.5 Hz, 1H), 3.66 (q, J = 7.2 Hz, 2H), 3.24 (dd, J = 17.5, 4.5 Hz, 1H), 3.00 (dd, J = 18.0, 9.0 Hz, 1H), 1.24 (t, J = 7.2 Hz, 3H); ^{13}C {^{1}H} NMR ($CDCl_3$, 126 MHz): δ 176.9, 176.4, 154.8, 151.7, 141.6, 141.5, 138.0, 130.6, 130.3, 129.8, 129.5, 129.0, 128.9, 44.9, 36.9, 34.4, 13.1; IR (neat, cm^{-1}): 3069, 1632, 1404, 1369, 1100, 1025, 758, 601, 589, 559; HRMS (ESI-TOF) calcd for $C_{20}H_{18}N_3O_2$ $[M + H]^+$ 332.1399, found 332.1394.

3-(3-Phenylquinoxalin-2-yl)-1-propylpyrrolidine-2,5-dione (3ad):

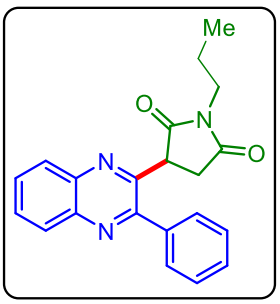

A off-white solid (56 mg, 81% yield); mp 158–160 ºC; purified over a column of silica gel (20% EtOAc in hexane); ^{1}H NMR ($CDCl_3$, 600 MHz): δ 8.15 – 8.11 (m, 1H), 8.02 – 7.99 (m, 1H), 7.87 (d, *J* = 6.6 Hz, 2H), 7.78 – 7.73 (m, 2H), 7.56 (t, *J* = 7.2 Hz, 2H), 7.52 (t, *J* = 7.2 Hz, 1H), 4.68 (dd, *J* = 9.3, 4.5 Hz, 1H), 3.58 (t, *J* = 7.2 Hz, 2H), 3.22 (dd, *J* = 18.0, 4.2 Hz, 1H), 3.00 (dd, *J* = 17.7, 9.3 Hz, 1H), 1.72 – 1.65 (m, 2H), 0.97 (t, *J* = 7.5 Hz, 3H); ^{13}C {^{1}H} NMR ($CDCl_3$, 151 MHz): δ 177.1, 176.6, 154.5, 151.7, 141.4, 141.3, 137.8, 130.5, 130.2, 129.7, 129.4, 129.3, 128.83, 128.80, 44.7, 40.9, 36.9, 21.0, 11.2 IR (neat, cm^{-1}): 3096, 1629, 1514, 1423, 1269, 1128, 758, 601, 599, 514; HRMS (ESI-TOF) calcd for $C_{21}H_{20}N_3O_2$ $[M + H]^+$ 346.1556, found 346.1555.

1-Isobutyl-3-(3-phenylquinoxalin-2-yl)pyrrolidine-2,5-dione (3ae):

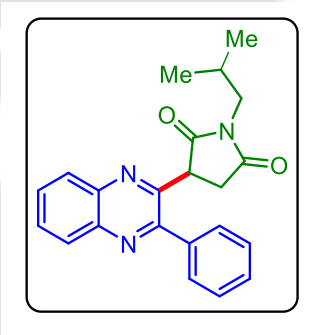

A pale yellow solid (62 mg, 86% yield); mp 152–155 ºC; purified over a column of silica gel (20% EtOAc in hexane); ^{1}H NMR ($CDCl_3$, 400 MHz): δ 8.17 – 8.10 (m, 1H), 8.02 – 7.98 (m, 1H), 7.88 (d, *J* = 8.0 Hz, 2H), 7.79 – 7.723 (m, 2H), 7.58 – 7.50 (m, 3H), 4.68 (dd, *J* = 9.0, 4.2 Hz, 1H), 3.48 – 3.39 (m, 2H), 3.21 (dd, *J* = 18.0, 4.0 Hz, 1H), 3.01 (dd, *J* = 17.8, 9.0 Hz, 1H), 2.19 – 2.08 (m, 1H), 0.97 (dd, *J* = 16.8, 6.8 Hz, 6H); ^{13}C {^{1}H} NMR ($CDCl_3$, 101 MHz): δ 177.3, 176.9, 154.5, 152.0, 141.5, 141.4, 137.8, 130.6, 130.3, 129.8, 129.43, 129.40, 128.9, 128.8, 46.5, 44.6, 36.9, 27.1, 20.1, 20.0; IR (neat, cm^{-1}): 3048, 1627, 1414, 1447, 1169, 1038, 858, 621, 599, 576; HRMS (ESI-TOF) calcd for $C_{22}H_{22}N_3O_2$ $[M + H]^+$ 360.1712, found 360.1708.

1-Cyclohexyl-3-(3-phenylquinoxalin-2-yl)pyrrolidine-2,5-dione (3af):

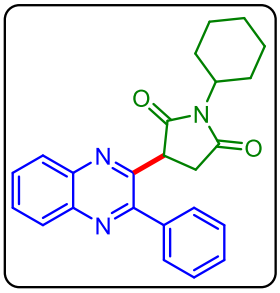

TH-3369_166122017

A light green solid (68 mg, 88% yield); mp 155–157 ºC; purified over a column of silica gel (20% EtOAc in hexane); ^{1}H NMR ($CDCl_3$, 500 MHz): δ 8.15 – 8.13 (m, 1H), 8.02 – 8.00 (m, 1H), 7.86 (d, *J* = 7.0 Hz, 2H), 7.79 – 7.74 (m, 2H), 7.57 – 7.50 (m, 3H), 4.61 (dd, *J* = 9.2, 4.2 Hz, 1H), 4.09 – 4.03 (m, 1H), 3.17 (dd, *J* = 17.7, 4.2 Hz, 1H), 2.95 (dd, *J* = 17.7, 9.2 Hz, 1H), 2.26 – 2.12 (m, 2H), 1.91 – 1.83 (m, 2H), 1.76 – 1.6 (m, 2H), 1.37 – 1.18 (m, 4H); ^{13}C {^{1}H} NMR ($CDCl_3$, 126 MHz): δ 177.3, 176.8, 154.7, 152.0, 141.6, 141.4, 138.0, 130.6, 130.3, 129.8, 129.4, 129.0, 128.9, 52.4, 44.5, 36.8, 29.0, 28.8, 26.02, 26.00, 25.2; IR (neat, cm^{-1}): 3098, 1667, 1596, 1509, 1168, 1055, 809, 727, 626, 504; HRMS (ESI-TOF) calcd for $C_{24}H_{24}N_3O_2$ $[M + H]^+$ 386.1869, found 386.1861.

1-Phenethyl-3-(3-phenylquinoxalin-2-yl)pyrrolidine-2,5-dione (3ag):

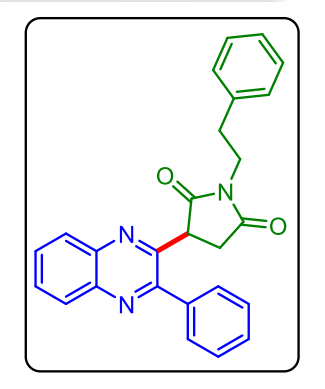

A light brown solid (69 mg, 85% yield); mp 172–174 ºC; purified over a column of silica gel (20% EtOAc in hexane); ^{1}H NMR ($CDCl_3$, 600 MHz): δ 8.17 – 8.14 (m, 1H), 8.05 – 8.02 (m, 1H), 7.85 (d, *J* = 6.6 Hz, 2H), 7.80 – 7.76 (m, 2H), 7.58 – 7.52 (m, 3H), 7.29 – 7.26 (m, 4H), 7.23 – 7.20 (m, 1H), 4.64 (dd, *J* = 9.3, 4.5 Hz, 1H), 3.84 (t, *J* = 7.5 Hz, 2H), 3.26 (dd, *J* = 18.0, 4.8 Hz, 1H), 2.99 – 2.91 (m, 3H); ^{13}C {^{1}H} NMR ($CDCl_3$, 151 MHz): δ 176.9, 176.3, 154.8, 151.5, 141.53, 141.50, 137.9, 130.7, 130.4, 129.8, 129.5, 129.4, 129.0, 128.96, 128.93, 128.6, 126.8, 44.8, 40.6, 36.8, 33.8; IR (neat, cm^{-1}): 2936, 1698, 1396, 1358, 1150, 1014, 696, 577, 500; HRMS (ESI-TOF) calcd for $C_{26}H_{22}N_3O_2$ $[M + H]^+$ 408.1712, found 408.1711.

1-(4-Phenylbutyl)-3-(3-phenylquinoxalin-2-yl)pyrrolidine-2,5-dione (3ah):

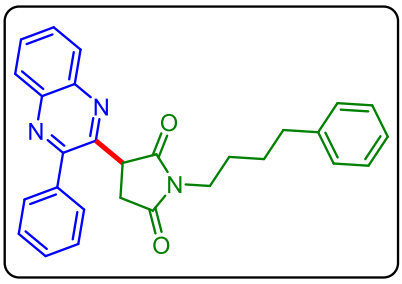

TH-3369_166122017

A light brown gummy (72 mg, 83% yield); purified over a column of silica gel (20% EtOAc in hexane); ^{1}H NMR ($CDCl_3$, 600 MHz): δ 8.13 (d, J = 7.8 Hz, 1H), 7.90 (d, J = 8.4 Hz, 1H), 7.85 (d, J = 6.6 Hz, 2H), 7.75 (t, J = 6.9 Hz, 1H), 7.70 (t, J = 7.2 Hz, 1H), 7.55 (t, J = 7.2 Hz, 2H), 7.51 (t, J = 7.2 Hz, 1H), 7.23 (t, J = 7.5 Hz, 2H), 7.15 (t, J = 6.6 Hz, 3H), 4.65 (dd, J = 9.6, 4.2 Hz, 1H), 3.64 (t, J = 6.3 Hz, 2H), 3.19 (dd, J = 18.0, 4.2 Hz, 1H), 2.97 (dd, J = 18.0, 9.0 Hz, 1H), 2.64 (t, J = 6.9 Hz, 2H), 1.74 – 1.66 (m, 4H); ^{13}C {^{1}H} NMR ($CDCl_3$, 151 MHz): δ 177.1, 176.6, 154.5, 151.7, 142.0, 141.4, 141.3, 137.8, 130.5, 130.3, 129.7, 129.4, 129.3, 128.9, 128.82, 128.4, 128.3, 125.8, 44.7, 39.0, 36.9, 35.4, 28.4, 27.2; IR (neat, cm^{-1}): 3028, 1527, 1496, 1404, 1123, 1041, 849, 627, 536, 526; HRMS (ESI-TOF) calcd for $C_{28}H_{26}N_3O_2$ $[M + H]^+$ 436.2025, found 436.2018.

1-Hexyl-3-(3-phenylquinoxalin-2-yl)pyrrolidine-2,5-dione (3ai):

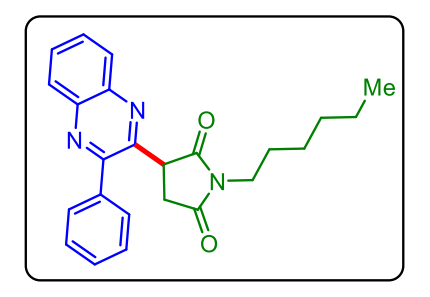

A orange gummy (61 mg, 79% yield); mp 143–145 ^{o}C; purified over a column of silica gel (20% EtOAc in hexane); ^{1}H NMR ($CDCl_3$, 400 MHz): δ 8.16 – 8.12 (m, 1H), 8.03 – 7.98 (m, 1H), 7.87 (d, J = 6.8 Hz, 2H), 7.80 – 7.73 (m, 2H), 7.58 – 7.49 (m, 3H), 4.68 (dd, J = 9.2, 4.4 Hz, 1H), 3.60 (t, J = 7.2 Hz, 2H), 3.23 (dd, J = 17.8, 4.2 Hz, 1H), 3.00 (dd, J = 17.8, 9.0 Hz, 1H), 1.68 – 1.61 (m, 2H), 1.37 – 1.25 (m, 6H), 0.88 (t, J = 6.8 Hz, 3H); ^{13}C {^{1}H} NMR ($CDCl_3$, 101 MHz): δ 177.2, 176.7, 154.6, 151.7, 141.5, 141.4, 137.9, 130.6, 130.3, 129.8, 129.41, 129.40, 128.9, 128.8, 44.7, 39.4, 36.9, 31.4, 27.6, 26.4, 22.6, 14.1; IR (neat, cm^{-1}): 3027, 1637, 1537, 1344, 1129, 1057, 963, 652, 557, 515; HRMS (ESI-TOF) calcd for $C_{24}H_{26}N_3O_2$ $[M + H]^+$ 388.2025, found 388.2021.

1-Decyl-3-(3-phenylquinoxalin-2-yl)pyrrolidine-2,5-dione (3aj):

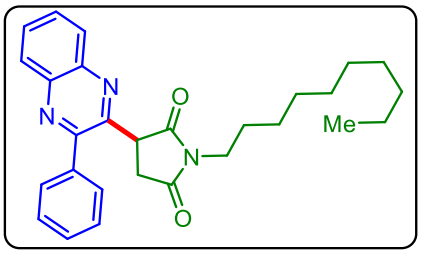

A orange gummy (75 mg, 85% yield); purified over a column of silica gel (20% EtOAc in hexane); ^{1}H NMR ($CDCl_3$, 400 MHz): δ 8.17 – 8.12 (m, 1H), 8.02 – 7.99 (m, 1H), 7.87 (d, J = 6.4 Hz, 2H), 7.80 –

TH-3369_166122017

7.74 (m, 2H), 7.59 – 7.50 (m, 3H), 4.68 (dd, *J* = 9.0, 4.2 Hz, 1H), 3.60 (t, *J* = 7.2 Hz, 2H), 3.23 (dd, *J* = 17.8, 4.2 Hz, 1H), 3.00 (dd, *J* = 17.6, 9.2 Hz, 1H), 1.68 – 1.61 (m, 2H), 1.40 – 1.24 (m, 14H), 0.87 (t, *J* = 6.8 Hz, 3H); ^{13}C {^{1}H} NMR ($CDCl_3$, 101 MHz): *δ* 177.2, 176.7, 154.7, 151.8, 141.5, 141.4, 137.9, 130.6, 130.3, 129.8, 129.4, 128.9, 128.8, 44.7, 39.5, 36.9, 31.9, 29.6, 29.4, 29.3, 27.7, 26.8, 22.8, 14.2; IR (neat, cm^{-1}): 3039, 1687, 1535, 1354, 1193, 1004, 957, 654, 537, 551; HRMS (ESI-TOF) calcd for $C_{28}H_{34}N_3O_2$ $[M + H]^+$ 444.2651, found 444.2642.

1-(4-Methoxyphenyl)-3-(3-phenylquinoxalin-2-yl)pyrrolidine-2,5-dione (3ak):

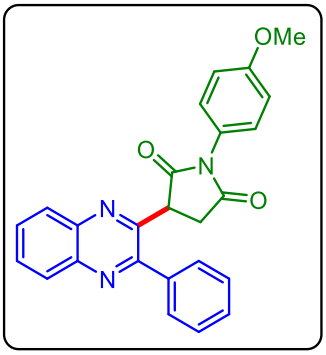

A pale yellow solid (70 mg, 86% yield); mp 189–191°C; purified over a column of silica gel (25% EtOAc in hexane); ^{1}H NMR ($CDCl_3$, 500 MHz): *δ* 8.17 – 8.14 (m, 1H), 8.09 – 8.07 (m, 1H), 7.87 (d, *J* = 6.5 Hz, 2H), 7.80 – 7.76 (m, 2H), 7.58 – 7.51 (m, 3H), 7.28 (d, *J* = 8.5 Hz, 2H), 6.98 (d, *J* = 9.5 Hz, 2H), 4.83 (dd, *J* = 9.0, 4.5 Hz, 1H), 3.82 (s, 3H), 3.42 (dd, *J* = 18.0, 4.5 Hz, 1H), 3.16 (dd, *J* = 18.0, 9.5 Hz, 1H); ^{13}C {^{1}H} NMR ($CDCl_3$, 126 MHz): *δ* 176.4, 175.8, 169.9, 159.7, 154.8, 151.6, 141.54, 141.53, 137.9, 134.2, 130.7, 130.4, 129.8, 129.5, 129.4, 128.9, 127.9, 127.7, 124.7, 114.6, 55.6, 44.9, 36.9; IR (neat, cm^{-1}): 3018, 1696, 1521, 1378, 1147, 1054, 967, 671, 527, 509; HRMS (ESI-TOF) calcd for $C_{25}H_{20}N_3O_3$ $[M + H]^+$ 410.1505, found 410.1501.

1-(4-Fluorophenyl)-3-(3-phenylquinoxalin-2-yl)pyrrolidine-2,5-dione (3al):

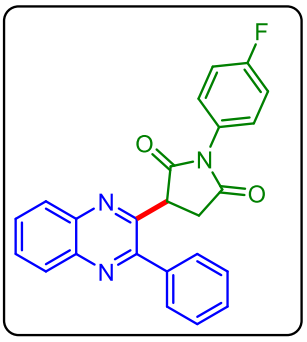

TH-3369_166122017

A off-white solid (66 mg, 83% yield); mp 196–198 °C; purified over a column of silica gel (25% EtOAc in hexane); ^{1}H NMR ($CDCl_3$, 400 MHz): δ 8.19 – 8.15 (m, 1H), 8.10 – 8.05 (m, 1H), 7.88 – 7.85 (m, 2H), 7.83 – 7.77 (m, 2H), 7.59 – 7.53 (m, 3H), 7.39 – 7.35 (m, 2H), 7.18 (t, J = 8.6 Hz, 2H), 4.86 (dd, J = 9.2, 4.8 Hz, 1H), 3.44 (dd, J = 18.0, 4.8 Hz, 1H), 3.19 (dd, J = 18.0, 9.2 Hz, 1H); ^{13}C {^{1}H} NMR ($CDCl_3$, 126 MHz): δ 176.1, 175.4, 162.5 (d, J = 248.9 Hz), 154.8, 151.5, 141.6, 141.5, 137.9, 130.8, 130.5, 129.8, 129.5 (d, J = 2.8 Hz), 129.0, 128.9, 128.6, 128.5, 128.0 (d, J = 3.0 Hz), 116.4, 116.3, 45.0, 36.9; ^{19}F NMR ($CDCl_3$) δ -112.1 (s); IR (neat, cm^{-1}): 3015, 1648, 1511, 1387, 1151, 1013, 987, 651, 557, 518; HRMS (ESI-TOF) calcd for $C_{24}H_{17}FN_3O_2$ $[M + H]^+$ 398.1305, found 398.1302.

3-(3-Phenylquinoxalin-2-yl)-1-(4-(trifluoromethyl)phenyl)pyrrolidine-2,5-dione (3am):

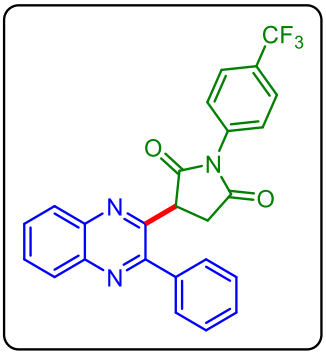

A light brown solid (71 mg, 80% yield); mp 187–189 °C; purified over a column of silica gel (22% EtOAc in hexane); ^{1}H NMR ($CDCl_3$, 600 MHz): δ 8.17 – 8.15 (m, 1H), 8.08 – 8.06 (m, 1H), 7.86 (d, J = 7.2 Hz, 2H), 7.80 – 7.77 (m, 2H), 7.74 (d, J = 8.4 Hz, 2H), 7.57 – 7.51 (m, 5H), 4.88 (dd, J = 9.3, 4.5 Hz, 1H), 3.44 (dd, J = 18.0, 4.2 Hz, 1H), 3.19 (dd, J = 18.0, 9.6 Hz, 1H); ^{13}C {^{1}H} NMR ($CDCl_3$, 151 MHz): δ 175.6, 174.9, 154.6, 151.2, 141.5, 141.4, 137.7, 135.1, 134.4, 130.8, 130.5, 129.7, 129.6, 129.5, 128.9, 128.8, 126.9, 126.3 (q, J = 3.6 Hz), 125.8, 45.0, 36.9; ^{19}F NMR ($CDCl_3$) δ -62.6 (s); IR (neat, cm^{-1}): 3058, 1658, 1627, 1329, 1109, 1025, 877, 623, 577, 588; HRMS (ESI-TOF) calcd for $C_{25}H_{17}F_3N_3O_2$ $[M + H]^+$ 448.1273, found 448.1270.

1-(4-(Dimethylamino)phenyl)-3-(3-phenylquinoxalin-2-yl)pyrrolidine-2,5-dione (3an):

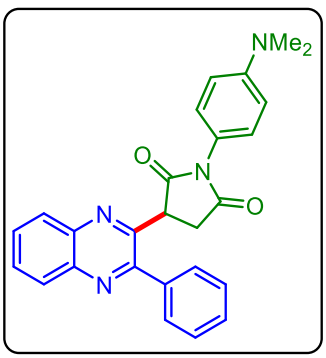

A light orange solid (69 mg, 82% yield); mp 179–181°C; purified over a column of silica gel (25% EtOAc in hexane); ^{1}H NMR ($CDCl_3$, 500 MHz): δ 8.16 – 8.13 (m, 1H), 8.08 – 8.06 (m, 1H), 7.88 (d, *J* = 6.5 Hz, 2H), 7.79 – 7.75 (m, 2H), 7.57– 7.50 (m, 3H), 7.18 (d, *J* = 9.0 Hz, 2H), 6.75 (d, *J* = 9.0 Hz, 2H), 4.81 (dd, *J* = 9.0, 4.5 Hz, 1H), 3.40 (dd, *J* = 18.0, 4.5 Hz, 1H), 3.13 (dd, *J* = 18.0, 9.5 Hz, 1H), 2.96 (s, 6H); ^{13}C {^{1}H} NMR ($CDCl_3$, 126 MHz): δ 176.6, 176.1, 154.8, 151.8, 150.7, 141.6, 141.5, 138.0, 130.6, 130.3, 129.8, 129.5, 129.4, 129.0, 128.9, 127.3, 120.6, 112.5, 45.0, 40.5, 36.9; IR (neat, cm^{-1}): 2920, 2852, 1703, 1522, 1356, 1180, 968, 765, 700, 527; HRMS (ESI-TOF) calcd for $C_{26}H_{23}N_4O_2$ $[M + H]^+$ 423.1821, found 423.1826.

1-Benzyl-3-(3-phenylquinoxalin-2-yl)pyrrolidine-2,5-dione (3ao):

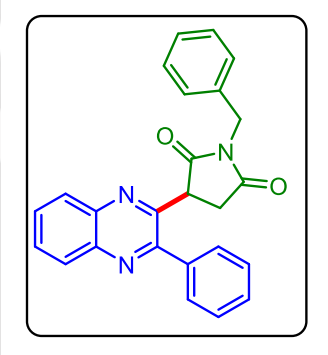

A light brown solid (70 mg, 89% yield); mp 180–182 °C; purified over a column of silica gel (20% EtOAc in hexane); ^{1}H NMR ($CDCl_3$, 600 MHz): δ 8.16 – 8.12 (m, 1H), 7.98 – 7.96 (m, 1H), 7.87 – 7.82 (d, *J* = 7.2, 2H), 7.79 – 7.74 (m, 2H), 7.56 – 7.49 (m, 3H), 7.43 (d, *J* = 7.2 Hz, 2H), 7.32 (t, *J* = 7.5 Hz, 2H), 7.29 – 7.26 (m, 1H), 4.78 (dd, *J* = 27.0, 12.0 Hz, 2H), 4.70 (dd, *J* = 9.3, 3.9 Hz, 1H), 3.23 (dd, *J* = 18.0, 4.2 Hz, 1H), 3.03 (dd, *J* = 18.0, 9.0 Hz, 1H); ^{13}C {^{1}H} NMR ($CDCl_3$, 151 MHz): δ 176.8, 176.3, 154.6, 151.7, 141.5, 141.4, 137.8, 135.6, 130.7, 130.4, 129.8, 129.5, 129.4, 128.9, 128.8, 128.7, 128.5, 127.9, 44.9, 42.9, 37.0; IR (neat, cm^{-1}): 3042, 1703, 1481, 1396, 1334, 1170, 880, 700, 502; HRMS (ESI-TOF) calcd for $C_{25}H_{20}N_3O_2$ $[M + H]^+$ 394.1556, found 394.1550.

1-(4-Methoxybenzyl)-3-(3-phenylquinoxalin-2-yl)pyrrolidine-2,5-dione (3ap):

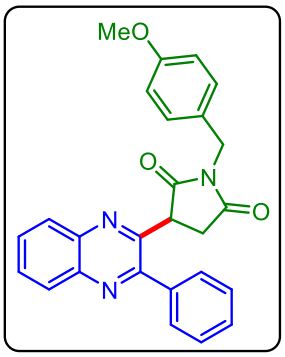

A pale yellow solid (77 mg, 91% yield); mp 189–191 °C; purified over a column of silica gel 25% EtOAc in hexane); ^{1}H NMR ($CDCl_3$, 500 MHz): δ 8.15 – 8.12 (m, 1H), 7.97 – 7.95 (m, 1H), 7.84 (d, *J* = 6.5, 2H), 7.79 – 7.74 (m, 2H), 7.56 – 7.51 (m, 3H), 7.37 (d, *J* = 8.5 Hz, 2H), 6.84 (d, *J* = 8.5 Hz, 2H), 4.75 – 4.66 (m, 3H), 3.78 (s, 3H), 3.22 (dd, *J* = 18.0, 4.0 Hz, 1H), 3.00 (dd, *J* = 18.0, 9.0 Hz, 1H); ^{13}C {^{1}H} NMR ($CDCl_3$, 126 MHz): δ 176.8, 176.3, 159.5, 154.7, 151.8, 141.6, 141.5, 137.9, 130.7, 130.3, 130.1, 129.8, 129.5, 129.0, 128.9, 128.0, 114.1, 55.4, 44.9, 42.4, 37.1; IR (neat, cm^{-1}): 3017, 1658, 1527, 1389, 1104, 1015, 887, 601, 587, 548; HRMS (ESI-TOF) calcd for $C_{26}H_{22}N_3O_3$ $[M + H]^+$ 424.1661, found 424.1667.

1-(Cyclohexylmethyl)-3-(3-phenylquinoxalin-2-yl)pyrrolidine-2,5-dione (3aq):

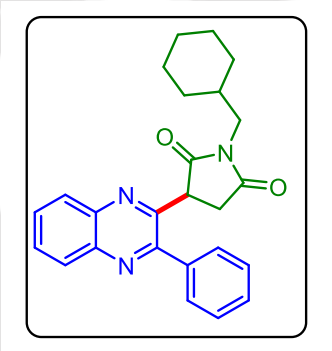

A off-white solid (63 mg, 79% yield); mp 165–168 °C; purified over a column of silica gel (20% EtOAc in hexane); ^{1}H NMR ($CDCl_3$, 600 MHz): δ 8.15 – 8.13 (m, 1H), 7.99 – 7.96 (m, 1H), 7.87 (d, *J* = 7.2 Hz, 2H), 7.79 – 7.74 (m, 2H), 7.56 (t, *J* = 7.2 Hz, 2H), 7.52 (t, *J* = 7.2 Hz, 1H), 4.68 (dd, *J* = 9.3, 3.9 Hz, 1H), 3.48 – 3.42 (m, 2H), 3.18 (dd, *J* = 17.7, 3.9 Hz, 1H), 3.00 (dd, *J* = 18.0, 9.0 Hz, 1H), 1.82 – 1.64 (m, 6H), 1.26 – 1.14 (m, 3H), 1.04 – 0.96 (m, 2H); ^{13}C {^{1}H} NMR ($CDCl_3$, 151 MHz): δ 177.4, 176.9, 154.5, 152.0, 141.5, 141.4, 137.8, 130.6, 130.3, 129.8, 129.4, 128.9, 128.7, 45.3, 44.7, 37.0, 36.3, 30.6, 26.3, 25.8, 25.7; IR (neat, cm^{-1}): 2920, 2852, 1739, 1692, 1479, 1372, 1190, 1644, 760, 697, 573; HRMS (ESI-TOF) calcd for $C_{25}H_{26}N_3O_2$ $[M + H]^+$ 400.2025, found 400.2024.

3-(3-Phenylquinoxalin-2-yl)-1-(2-(thiophen-2-yl)ethyl)pyrrolidine-2,5-dione (3ar):

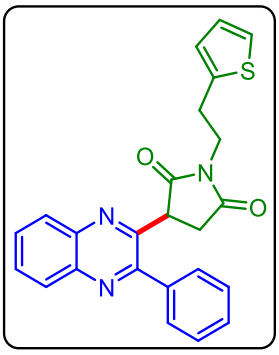

A light green solid (64 mg, 78% yield); mp 155–157°C; purified over a column of silica gel (20% EtOAc in hexane); ^{1}H NMR ($CDCl_3$, 500 MHz): δ 8.16 – 8.13 (m, 1H), 8.04 – 8.02 (m, 1H), 7.85 (d, *J* = 6.5 Hz, 2H), 7.80 – 7.75 (m, 2H), 7.57 – 7.51 (m, 3H), 7.13 (d, *J* = 4.5 Hz, 1H), 6.91 – 6.89 (m, 2H), 4.66 (dd, *J* = 9.0, 4.5 Hz, 1H), 3.87 (t, *J* = 7.2 Hz, 2H), 3.27 (dd, *J* = 17.5, 4.5 Hz, 1H), 3.22 – 3.15 (m, 2H), 2.98 (dd, *J* = 17.7, 9.2 Hz, 1H); ^{13}C {^{1}H} NMR ($CDCl_3$, 126 MHz): δ 176.8, 176.2, 154.8, 151.4, 141.5, 139.9, 138.0, 130.7, 130.4, 129.8, 129.53, 129.51, 128.9, 127.1, 125.9, 124.3, 44.8, 40.6, 36.8, 27.7; IR (neat, cm^{-1}): 2940, 1695, 1479, 1401, 1346, 1174, 1008, 735, 698, 552; HRMS (ESI-TOF) calcd for $C_{24}H_{20}N_3O_2S$ $[M + H]^+$ 414.1276, found 414.1276.

1-((S)-1-(Naphthalen-1-yl)ethyl)-3-(3-phenylquinoxalin-2-yl)pyrrolidine-2,5-dione (3as):

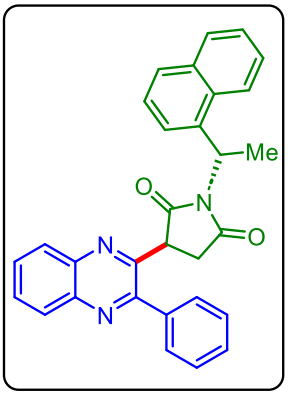

A light brown gummy (77 mg, 85% yield); dr 1:1; purified over a column of silica gel (22% EtOAc in hexane); ^{1}H NMR ($CDCl_3$, 400 MHz): δ 8.17 – 8.11 (m, 2H), 8.07 (d, *J* = 7.2 Hz, 1H), 8.01 (d, *J* = 8.4 Hz, 1H), 7.92 (t, *J* = 6.4 Hz, 2H), 7.89 – 7.83 (m, 3H), 7.81 – 7.73 (m, 8H), 7.72 – 7.58 (m, 4H), 7.55 – 7.43 (m, 10H), 7.38 (t, *J* = 7.0 Hz, 1H), 6.26 – 6.20 (m, 2H), 4.60 – 4.55 (m, 2H), 3.10 – 3.02 (m, 2H), 2.95 – 2.86 (m, 2H), 2.01 (d, *J* = 7.2 Hz, 3H), 1.96 (d, *J* = 7.2 Hz, 3H); ^{13}C {^{1}H} NMR ($CDCl_3$, 101 MHz): δ 177.0, 176.9, 176.5, 176.4, 154.5, 154.4, 152.1, 152.0, 141.5, 141.47, 141.42, 141.3, 137.8, 133.9, 133.8, 133.7, 131.6, 131.4, 130.6, 130.5, 130.2, 130.1, 129.8, 129.45, 129.40, 129.3, 129.1, 129.04, 129.00, 128.96, 128.95, 128.9, 128.87, 128.86, 126.8, 126.70, 126.7, 126.4, 125.6, 125.5, 125.1, 125.0, 123.2, 47.1, 46.9, 44.6, 44.5, 37.1, 37.0, 17.4, 17.0 IR (neat, cm^{-1}): 3085, 1768, 1574, 1390, 1124, 1015, 797, 628, 586, 528; HRMS (ESI-TOF) calcd for $C_{30}H_{24}N_3O_2$ $[M + H]^+$ 458.1869, found 458.1862.

TH-3369_166122017

3-(3-Phenylquinoxalin-2-yl)pyrrolidine-2,5-dione (3at):

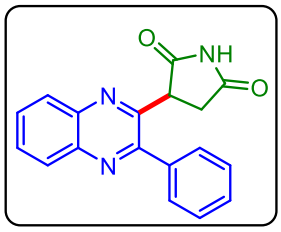

A light brown solid (50 mg, 83% yield); mp 169–171 °C; purified over a column of silica gel (30% EtOAc in hexane); ^{1}H NMR ($CDCl_3$, 500 MHz): δ 8.96 (s, 1H), 8.16 – 8.13 (m, 1H), 8.07 – 8.04 (m, 1H), 7.83 (d, J = 6.5 Hz, 2H), 7.80 – 7.75 (m, 2H), 7.57 – 7.50 (m, 3H), 4.74 (dd, J = 9.2, 4.7 Hz, 1H), 3.32 (dd, J = 18.2, 4.7 Hz, 1H), 3.05 (dd, J = 18.0, 9.0 Hz, 1H); ^{13}C {^{1}H} NMR ($CDCl_3$, 126 MHz): δ 177.4, 176.9, 154.7, 151.0, 141.5, 137.8, 130.8, 130.4, 129.7, 129.5, 129.4, 129.0, 128.9, 46.3, 38.0; IR (neat, cm^{-1}): 3192, 2922, 1784, 1687, 1482, 1352, 1178, 757, 700, 685, 584; HRMS (ESI-TOF) calcd for $C_{18}H_{14}N_3O_2$ $[M + H]^+$ 304.1086, found 304.1097.

1-(2-(1*H*-indol-3-yl)ethyl)-3-(3-phenylquinoxalin-2-yl)pyrrolidine-2,5-dione (3au):

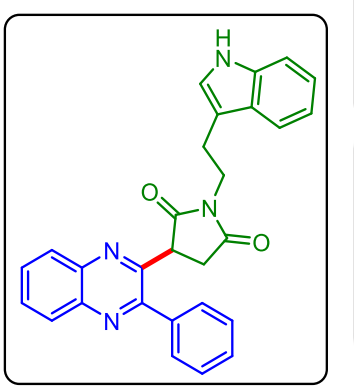

A brown solid (68 mg, 76% yield); mp 206–208 °C; purified over a column of silica gel (30% EtOAc in hexane); ^{1}H NMR ($CDCl_3$, 500 MHz): δ 8.14 (d, J = 7.9 Hz, 1H), 8.03 (s, 1H), 7.97 (d, J = 8.0 Hz, 1H), 7.85 (d, J = 7.0 Hz, 2H), 7.79 – 73 (m, 2H), 7.70 (d, J = 7.5 Hz, 1H), 7.58 – 7.53 (m, 3H), 7.32 (d, J = 8.0 Hz, 1H), 7.17 (t, J = 6.6 Hz, 1H), 7.11 – 7.09 (m, 2H), 4.62 (dd, J = 9.0, 4.0 Hz, 1H), 3.91 (t, J = 6.7 Hz, 2H), 3.23 (dd, J = 17.7, 4.2 Hz, 1H), 3.13 – 3.07 (m, 2H), 2.93 (dd, J = 18.0, 9.0 Hz, 1H); ^{13}C {^{1}H} NMR ($CDCl_3$, 126 MHz): δ 177.1, 176.5, 154.8, 151.6, 141.6, 141.5, 137.9, 136.3, 130.7, 130.4, 129.8, 129.5, 129.5, 128.9, 128.9, 127.6, 122.3, 122.2, 119.7, 118.9, 112.3, 111.2, 44.9, 40.0, 36.9, 23.5; IR (neat, cm^{-1}): 3307, 1692, 1433, 1274, 1043, 1011, 1099, 824, 769, 696, 602, 576; HRMS (ESI-TOF) calcd for $C_{28}H_{23}N_4O_2$ $[M + H]^+$ 447.1821, found 447.1815.

TH-3369_166122017

3-(3-Phenylquinoxalin-2-yl)-1-(pyren-1-yl)pyrrolidine-2,5-dione (3av):

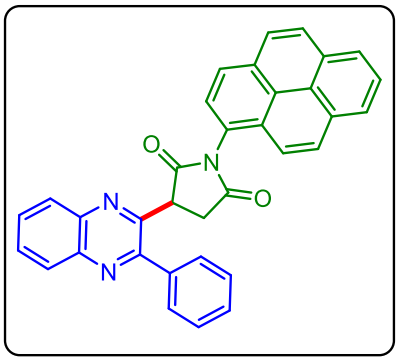

A light brown gummy (80 mg, 80% yield); dr 1:0.3; purified over a column of silica gel (22% EtOAc in hexane); ^{1}H NMR ($CDCl_3$, 500 MHz): δ 8.48 (d, J = 9.0 Hz, 1H), 8.33 (d, J = 8.0 Hz, 1H), 8.27 – 8.14 (m, 7H), 8.11 – 8.04 (m, 3H), 8.02 – 7.96 (m, 2H), 7.94 – 7.89 (m, 4H), 7.85 (d, J = 8.0 Hz, 2H), 7.81 – 7.77 (m, 1H), 7.59 – 7.52 (m, 4H), 5.11 (dd, J = 9.5, 4.0 Hz, 0.3H), 5.05 (dd, J = 9.5, 3.5 Hz, 1H), 3.60 – 3.30 (m, 3H); ^{13}C {^{1}H} NMR ($CDCl_3$, 126 MHz): δ 176.9, 176.7, 176.4, 176.2, 154.7, 154.6, 152.5, 151.9, 141.8, 141.7, 141.6, 137.9, 137.8, 132.4, 132.3, 131.0, 130.9, 130.87, 130.84, 130.81, 130.5, 129.9, 129.8, 129.7, 129.6, 129.59, 129.54, 129.2, 129.1, 129.0, 128.7, 128.6, 128.0, 127.2, 126.5, 126.2, 126.1, 126.0, 125.9, 125.74, 125.70, 125.6, 125.5, 125.3, 125.2, 124.5, 121.9, 121.2, 45.6, 45.5, 37.9, 37.5; IR (neat, cm^{-1}): 3077, 1758, 1567, 1389, 1154, 1025, 787, 608, 597, 508; HRMS (ESI-TOF) calcd for $C_{34}H_{22}N_3O_2$ $[M + H]^+$ 504.1712, found 504.1702.

(1S,2R,5S)-2-Isopropyl-5-methylcyclohexyl 4-(3-(2,5-dioxo-1-phenylpyrrolidin-3-yl)quinoxalin-2-yl)benzoate (3pa):

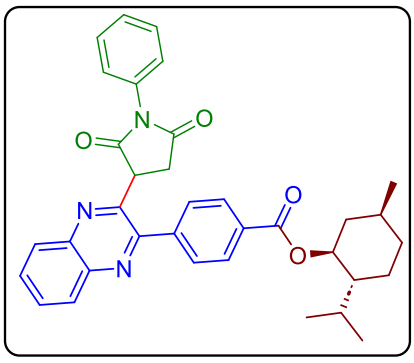

A reddish brown gummy (95 mg, 85% yield); dr 1:1; purified over a column of silica gel (30% EtOAc in hexane); ^{1}H NMR ($CDCl_3$, 500 MHz): δ 8.25 (d, J = 8.2 Hz, 4H), 8.18 – 8.15 (m, 2H), 8.11 – 8.09 (m, 2H), 7.98 (t, J = 8.2 Hz, 4H), 7.82 – 7.79 (m, 4H), 7.48 (t, J = 7.0 Hz, 4H), 7.41 (d, J = 7.0 Hz, 2H), 7.37 – 7.35 (m, 4H), 5.01 – 4.96 (m, 2H), 4.82 – 4.78 (m, 2H), 3.51 – 3.46 (m, 2H), 3.21 – 3.15 (m, 2H), 2.18 – 2.16 (m, 2H), 2.00 – 1.96 (m, 2H), 1.76 – 1.73 (m, 4H), 1.61 – 1.57 (m, 5H), 1.19 – 1.11

TH-3369_166122017

(m, 5H), 0.96 – 0.93 (m, 12H), 0.83 (d, J = 7.0 Hz, 6H); ^{13}C {^{1}H} NMR ($CDCl_3$, 126 MHz): δ 176.0, 175.9, 175.4, 175.3, 165.6, 153.8, 151.1, 142.0, 141.6, 141.4, 132.0, 131.72, 131.70, 130.9, 130.8, 130.0, 129.9, 129.8, 129.5, 129.3, 128.9, 128.8, 126.6, 75.4, 47.4, 44.9, 44.8, 41.0, 36.73, 36.70, 34.4, 31.5, 26.9, 26.7, 26.6, 23.8, 23.7, 22.1, 20.85, 20.83, 16.7, 16.6; IR (neat, cm^{-1}): 2954, 2925, 1709, 1499, 1378, 1269, 1179, 960, 615, 467; HRMS (ESI-TOF) calcd for $C_{35}H_{36}N_3O_4$ $[M + H]^+$ 562.2706, found 562.2701.

(1R,2S,4S)-1,7,7-Trimethylbicyclo[2.2.1]heptan-2-yl-4-(3-(2,5-dioxo-1-phenylpyrrolidin-3-yl)quinoxalin-2-yl)benzoate (3qa):

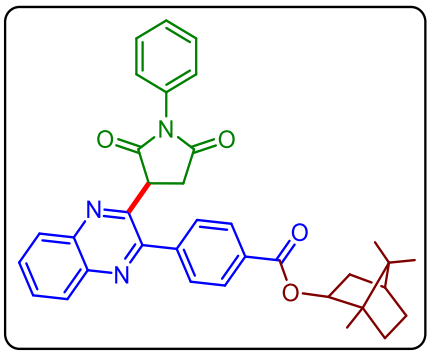

A reddish brown gummy (93 mg, 83% yield); purified over a column of silica gel (30% EtOAc in hexane); ^{1}H NMR ($CDCl_3$, 500 MHz): δ 8.25 (d, J = 7.5 Hz, 2H), 8.16 – 8.14 (m, 1H), 8.10 – 8.08 (m, 1H), 8.00 (d, J = 6.0 Hz, 2H), 7.80 – 7.77 (m, 2H), 7.46 (t, J = 7.7 Hz, 2H), 7.39 – 7.35 (m, 3H), 5.17 (d, J = 9.5 Hz, 1H), 4.81 (dd, J = 9.5, 4.5 Hz, 1H), 3.49 – 3.44 (m, 1H), 3.17 (dd, J = 17.7, 9.2 Hz, 1H),), 2.52 – 2.47 (m, 1H), 2.18 – 2.13 (m, 1H), 1.85 – 1.79 (m, 1H),), 1.78 – 1.72 (m, 1H), 1.45 – 1.40(m, 1H), 1.36 – 1.29 (m, 1H), 1.17 – 1.13 (m, 1H), 0.97 (s, 3H), 0.93 (d, J = 9.0 Hz, 6H); ^{13}C {^{1}H} NMR ($CDCl_3$, 126 MHz): δ 175.9, 175.8, 175.3, 166.2, 153.7, 151.0, 141.9, 141.5, 141.3, 131.9, 131.6, 130.8, 130.6, 129.9, 129.4, 129.1, 128.8, 128.7, 126.5, 80.8, 49.1, 47.9, 44.9, 44.8, 36.9, 36.6, 28.1, 27.4, 19.7, 18.9, 13.6; IR (neat, cm^{-1}): 2987, 2939, 1769, 1487, 1332, 1252, 1106, 860, 515, 487; HRMS (ESI-TOF) calcd for $C_{35}H_{34}N_3O_4$ $[M + H]^+$ 560.2549, found 560.2541.

1,1'-(methylenebis(4,1-phenylene))bis(3-(3-phenylquinoxalin-2-yl)pyrrolidine-2,5-dione) (3aw):

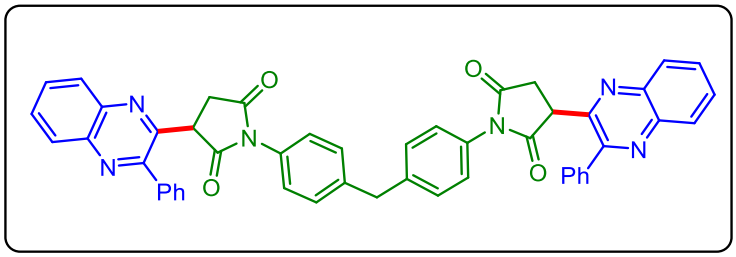

TH-3369_166122017

A orange solid (120 mg, 78% yield); mp 151–154 °C; purified over a column of silica gel (40% EtOAc in hexane); ^{1}H NMR ($CDCl_3$, 500 MHz): δ 8.16 – 8.14 (m, 2H), 8.08 – 8.06 (m, 2H), 7.87 (d, J = 7.0 Hz, 4H), 7.80 – 7.76 (m, 4H), 7.57 – 7.50 (m, 6H), 7.30 (sharp singlet, 6H), 7.26 (t, J = 7.0 Hz, 2H), 4.84 (dd, J = 9.0, 4.5 Hz, 2H), 4.05 (s, 2H), 3.41 (dd, J = 18.0, 4.5 Hz, 2H), 3.18 (dd, J = 18.0, 9.0 Hz, 2H); ^{13}C {^{1}H} NMR ($CDCl_3$, 126 MHz): δ 176.1, 175.5, 154.7, 151.6, 141.5, 141.1, 137.9, 130.7, 130.4, 130.3, 129.8, 129.7, 129.5, 129.4, 128.95, 128.92, 128.1, 126.7, 45.0, 41.2, 36.9; IR (neat, cm^{-1}): 3058, 1707, 1511, 1384, 1184, 1008, 766, 698, 607, 578; HRMS (ESI-TOF) calcd for $C_{49}H_{35}N_6O_4$ $[M + H]^+$ 771.2720, found 771.2739.

1,1'-(methylenebis(4,1-phenylene))bis(3-(3-methylquinoxalin-2-yl)pyrrolidine-2,5-dione) (3rw):

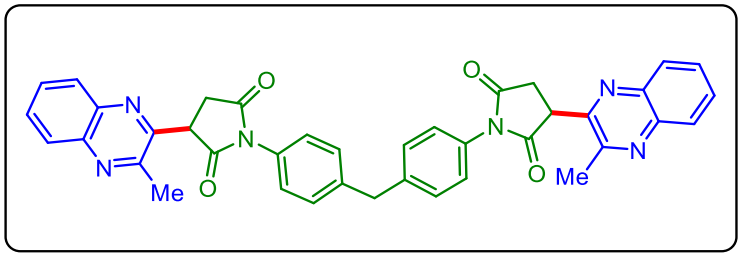

A orange solid (104 mg, 81% yield); mp 143–145 °C; purified over a column of silica gel (70% EtOAc in hexane); ^{1}H NMR ($CDCl_3$, 500 MHz): δ 8.01 (d, J = 7.7 Hz, 4H), 7.75 – 7.68 (m, 4H), 7.26 (sharp singlet, 8H), 4.79 (dd, J = 9.0, 4.5 Hz, 2H), 4.03 (s, 2H), 3.78 (dd, J = 18.0, 4.5 Hz, 2H), 3.26 (dd, J = 18.0, 9.0 Hz, 2H), 2.99 (s, 6H); ^{13}C {^{1}H} NMR ($CDCl_3$, 126 MHz): δ 175.6, 175.3, 153.4, 151.0, 141.7, 141.2, 140.8, 130.4, 130.2, 129.9, 129.5, 129.0, 128.6, 126.7, 45.0, 41.2, 34.4, 23.1; IR (neat, cm^{-1}): 3098, 1607, 1541, 1399, 1125, 1014, 866, 608, 604, 518; HRMS (ESI-TOF) calcd for $C_{39}H_{31}N_6O_4$ $[M + H]^+$ 647.2407, found 647.2399.

3-(3-Methylquinoxalin-2-yl)-1-phenylpyrrolidine-2,5-dione (3ra):

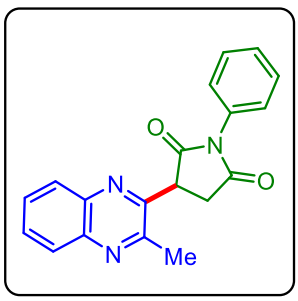

A off-white solid (54 mg, 85% yield); mp 175–177 °C; purified over a column of silica gel (20% EtOAc in hexane); ^{1}H NMR ($CDCl_3$, 500 MHz): δ 8.02 (t, J = 7.0 Hz, 2H), 7.76 – 7.69 (m, 2H), 7.49 – 7.42

TH-3369_166122017

(m, 2H), 7.39 (t, *J* = 7.2 Hz, 1H), 7.33 (d, *J* = 8.0 Hz, 2H), 4.80 (dd, *J* = 9.0, 4.5 Hz, 1H), 3.78 (dd, *J* = 18.0, 4.5 Hz, 1H), 3.27 (dd, *J* = 18.0, 9.0 Hz, 1H), 2.99 (s, 3H); ^{13}C {^{1}H} NMR ($CDCl_3$, 126 MHz): *δ* 175.5, 175.3, 153.4, 150.9, 141.7, 140.8, 132.0, 130.3, 129.5, 129.3, 129.0, 128.9, 128.6, 126.7, 45.0, 34.5, 23.2; IR (neat, cm^{-1}): 3087, 1796, 1557, 1382, 1194, 1015, 796, 688, 617, 558; HRMS (ESI-TOF) calcd for $C_{19}H_{16}N_3O_2$ $[M + H]^+$ 318.1243, found 318.1249.

3-(3-Cyclopropylquinoxalin-2-yl)-1-phenylpyrrolidine-2,5-dione (3va):

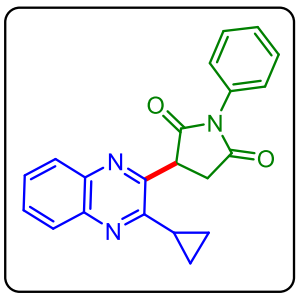

Gummy liquid (51 mg, 74% yield); purified over a column of silica gel (25% EtOAc in hexane); ^{1}H NMR ($CDCl_3$, 500 MHz): *δ* 7.99 – 7.94 (m, 2H), 7.73 – 7.64 (m, 2H), 7.48 (t, *J* = 7.7 Hz, 2H), 7.40 (t, *J* = 7.5 Hz, 1H), 7.36 (d, *J* = 7.5 Hz, 2H), 5.12 (dd, *J* = 9.0, 4.0 Hz, 1H), 3.77 (dd, *J* = 18.0, 4.5 Hz, 1H), 3.32 (dd, J = 18.0, 9.5 Hz, 1H), 2.63 – 2.58 (m, 1H), 1.58 – 1.53 (m, 2H), 1.20 – 1.14 (m, 2H); ^{13}C {^{1}H} NMR ($CDCl_3$, 126 MHz): *δ* 175.7, 175.5, 156.9, 150.9, 141.8, 140.2, 132.1, 130.1, 129.3, 129.0, 128.9, 128.8, 128.7, 126.7, 44.5, 34.8, 14.5, 10.9, 9.6; IR (neat, cm^{-1}): 3075, 1785, 1562, 1376, 1188, 1010, 792, 684, 614, 552; HRMS (ESI-TOF) calcd for $C_{21}H_{18}N_3O_2$ $[M + H]^+$ 344.1394, found 344.1393.

1-Methyl-3-(5-methyl-2-(pyridin-2-yl)phenyl)pyrrolidine-2,5-dione (7ab):

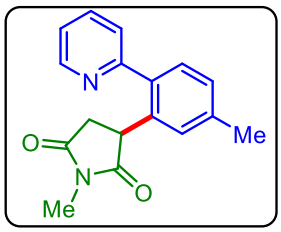

A brown solid (46 mg, 83% yield); mp 168–170 °C; purified over a column of silica gel (35% EtOAc in hexane); ^{1}H NMR ($CDCl_3$, 500 MHz): *δ* 8.53 (d, *J* = 4.0 Hz, 1H), 7.76 (t, *J* = 7.5 Hz, 1H), 7.55 (d, *J* = 8.0 Hz, 1H), 7.37 (d, *J* = 7.5 Hz, 1H), 7.24 – 7.20 (m, 2H), 7.02 (s, 1H), 4.35 (dd, *J* = 9.5, 5.5 Hz, 1H), 3.16 (dd, *J* = 18.0, 9.5 Hz, 1H), 2.95 (s, 3H), 2.91 (dd, *J* = 18.5, 5.5 Hz, 1H), 2.39 (s, 3H); ^{13}C {^{1}H} NMR ($CDCl_3$, 126 MHz): *δ* 178.9, 177.0, 159.2, 148.6, 139.3, 137.4, 137.0, 135.5, 130.7, 130.2,

TH-3369_166122017

128.9, 124.3, 122.1, 44.9, 38.8, 25.1, 21.3; IR (neat, cm^{-1}): 3036, 1784, 1569, 1314, 1125, 1029, 725, 658, 697, 588; HRMS (ESI-TOF) calcd for $C_{17}H_{17}N_2O_2$ $[M + H]^+$ 281.1290, found 281.1294.

1'-Phenylspiro[indeno[1,2-*b*]quinoxaline-11,3'-pyrrolidine]-2',5'-dione (4aa):

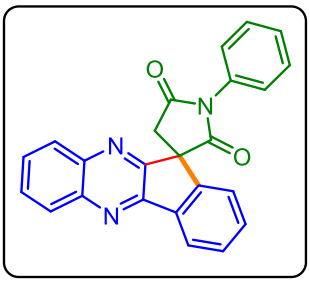

A light brown solid (32 mg, 85% yield); mp 252–254 °C; purified over a column of silica gel (25% EtOAc in hexane); ^1H NMR ($CDCl_3$, 500 MHz): δ 8.30 – 8.28 (m, 2H), 8.20 (d, J = 8.0 Hz, 1H), 8.11 (d, J = 8.0 Hz, 1H), 7.80 (t, J = 6.7 Hz, 1H), 7.75 (t, J = 6.7 Hz, 1H), 7.66 – 7.60 (m, 3H), 7.51 (t, J = 7.7 Hz, 2H), 7.46 – 7.41 (m, 2H), 3.78 (d, J = 18.0 Hz, 1H), 3.40 (d, J = 18.5 Hz, 1H); ^{13}C {^1H} NMR ($CDCl_3$, 126 MHz): δ 174.9, 174.4, 159.8, 154.1, 145.6, 143.1, 141.6, 138.3, 132.5, 132.1, 130.5, 130.4, 129.7, 129.6, 129.5, 129.4, 129.1, 126.7, 123.5, 123.3, 56.7, 39.7; IR (neat, cm^{-1}): 2924, 1710, 1498, 1377, 1196, 1102, 1046, 914, 754, 585; HRMS (ESI-TOF) calcd for $C_{24}H_{16}N_3O_2$ $[M + H]^+$ 378.1243, found 378.1238.

2-Methyl-1'-phenylspiro[indeno[1,2-*b*]quinoxaline-11,3'-pyrrolidine]-2',5'-dione (4ba):

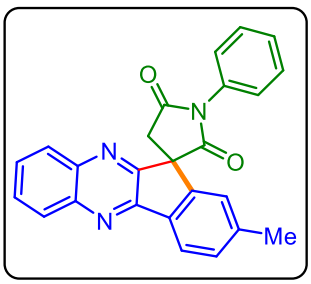

A brown solid (34 mg, 87% yield); mp 246–248 °C; purified over a column of silica gel (25% EtOAc in hexane); ^1H NMR ($CDCl_3$ 500 MHz): δ 8.17 (d, J = 8.0 Hz, 2H), 8.09 (d, J = 8.5 Hz, 1H), 7.79 (t, J = 6.7 Hz, 1H), 7.74 (t, J = 7.0 Hz, 1H), 7.52 (t, J = 7.7 Hz, 2H), 7.47 – 7.43 (m, 4H), 7.40 (s, 1H), 3.76 (d, J = 18.5 Hz, 1H), 3.39 (d, J = 18.5 Hz, 1H), 2.53 (s, 3H); ^{13}C {^1H} NMR ($CDCl_3$, 126 MHz): δ 175.1, 174.5, 160.1, 154.3, 145.9, 143.6, 143.1, 141.4, 135.7, 132.1, 131.5, 130.4, 130.1, 129.6, 129.4, 129.1, 128.9, 126.7, 123.8, 123.3, 56.5, 39.8, 22.3; IR (neat, cm^{-1}): 2933, 1674, 1328, 1278, 1258, 1187, 1112, 1011, 798, 587; HRMS (ESI-TOF) calcd for $C_{25}H_{18}N_3O_2$ $[M + H]^+$ 392.1399, found 392.1391.

TH-3369_166122017

2-Chloro-1'-phenylspiro[indeno[1,2-*b*]quinoxaline-11,3'-pyrrolidine]-2',5'-dione (4ea):

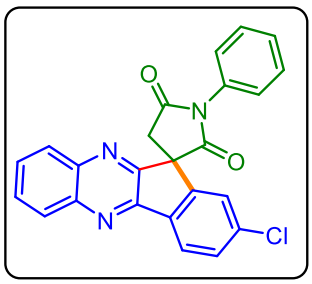

A plae yellow solid (32 mg, 78% yield); mp 214–216 °C; purified over a column of silica gel (25% EtOAc in hexane); ^{1}H NMR ($CDCl_3$, 500 MHz): δ 8.22 (d, J = 8.0 Hz, 1H), 8.18 (d, J = 7.0 Hz, 1H), 8.11 (d, J = 8.0 Hz, 1H), 7.82 (t, J = 7.0 Hz, 1H), 7.77 (t, J = 7.0 Hz, 1H), 7.63 (d, J = 8.0 Hz, 1H), 7.61 (s, 1H), 7.52 (t, J = 7.7 Hz, 2H), 7.46 – 7.43 (m, 3H), 3.75 (d, J = 18.0 Hz, 1H), 3.41 (d, J = 18.5 Hz, 1H); ^{13}C {^{1}H} NMR ($CDCl_3$, 126 MHz): δ 174.3, 173.9, 159.5, 152.9, 146.8, 143.1, 141.6, 138.5, 136.9, 131.9, 131.0, 130.7, 129.9, 129.64, 129.60, 129.5, 129.2, 126.7, 124.5, 124.0, 56.6, 39.5; IR (neat, cm^{-1}): 3054, 1711, 1602, 1500, 1380, 1198, 1078, 839, 733, 620; HRMS (ESI-TOF) calcd for $C_{24}H_{15}ClN_3O_2$ $[M + H]^+$ 412.0853, found 412.0868.

3-(2-(Benzo[*d*][1,3]dioxol-5-yl)imidazo[1,2-*a*]pyridin-3-yl)-1-phenylpyrrolidine-2,5-dione (4ha):

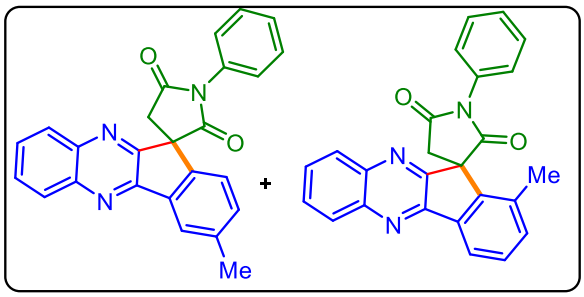

A light yellow solid (32 mg, 82% yield); dr 1:0.6; mp 208–210 °C; purified over a column of silica gel (25% EtOAc in hexane); ^{1}H NMR ($CDCl_3$, 500 MHz): δ 8.19 – 8.11 (m, 5H), 7.81 – 7.73 (m, 3H), 7.57 – 7.49 (m, 6H), 7.46 – 7.41 (m, 7H), 3.76 (d, J = 18.5 Hz, 1H), 3.60 (d, J = 18.5 Hz, 0.64 H), 3.53 (d, J = 18.5 Hz, 0.65 H), 3.37 (d, J = 18.5 Hz, 1H), 2.56 (s, 3H), 2.50 (s, 1.8 H); ^{13}C {^{1}H} NMR ($CDCl_3$, 126 MHz): δ 175.1, 175.0, 174.5, 174.4, 160.8, 160.3, 154.3, 153.9, 143.2, 143.1, 142.9, 141.8, 141.6, 140.8, 139.0, 138.3, 134.6, 134.4, 134.3, 133.6, 132.2, 132.1, 131.6, 130.45, 130.42, 129.63, 129.60, 129.57, 129.52, 129.49, 129.4, 129.3, 129.2, 129.0, 126.7, 126.6, 126.2, 126.1, 123.8, 123.0, 121.0, 56.4, 39.8,

TH-3369_166122017

38.5, 21.7, 18.8; IR (neat, cm^{-1}): 2945, 1665, 1322, 1296, 1208, 1177, 1112, 1009, 732, 623; HRMS (ESI-TOF) calcd for $C_{25}H_{18}N_3O_2$ $[M + H]^+$ 392.1399, found 392.1395.

4-Methoxy-1'-phenylspiro[indeno[1,2-*b*]quinoxaline-11,3'-pyrrolidine]-2',5'-dione (4ja):

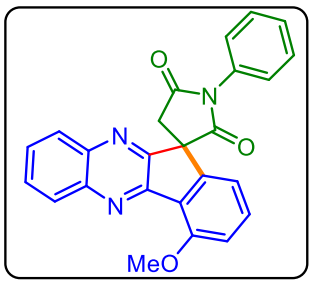

Reddish solid (30 mg, 71% yield); mp 204–206 °C; purified over a column of silica gel (45% EtOAc in hexane); ^{1}H NMR ($CDCl_3$, 500 MHz): δ 8.27 (d, J = 8.0 Hz, 1H), 8.07 (d, J = 8.0 Hz, 1H), 7.77 (t, J = 8.2 Hz, 1H), 7.72 (t, J = 8.2 Hz, 1H), 7.60 (t, J = 8.0 Hz, 1H), 7.51 (t, J = 7.5 Hz, 2H), 7.45 – 7.40 (m, 3H), 7.19 (d, J = 7.5 Hz, 1H), 7.13 (d, J = 8.0 Hz, 1H), 4.16 (s, 3H), 3.77 (d, J = 18.5 Hz, 1H), 3.39 (d, J = 18.5 Hz, 1H).; ^{13}C {^{1}H} NMR ($CDCl_3$, 126 MHz): δ 174.7, 174.4, 159.3, 157.9, 154.2, 147.4, 143.1, 140.5, 134.1, 132.1, 130.1, 130.0, 129.44, 129.40, 129.3, 129.0, 126.7, 126.2, 115.1, 112.4, 56.6, 56.5, 39.9; IR (neat, cm^{-1}): 3056, 2926, 1715, 1499, 1385, 1195, 1171, 1106, 748; HRMS (ESI-TOF) calcd for $C_{25}H_{18}N_3O_3$ $[M + H]^+$ 408.1343, found 408.1350.

7,8-Dichloro-1'-phenylspiro[indeno[1,2-*b*]quinoxaline-11,3'-pyrrolidine]-2',5'-dione (4la):

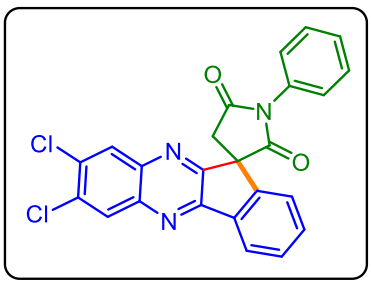

A pale yellow solid (35 mg, 79% yield); mp 225–228 °C; purified over a column of silica gel (27% EtOAc in hexane); ^{1}H NMR ($CDCl_3$, 500 MHz): δ 8.29 (s, 1H), 8.26 – 8.24 (m, 1H), 8.22 (s, 1H), 7.69 – 7.65 (m, 2H), 7.62 – 7.60 (m, 1H), 7.51 (t, J = 7.7Hz, 2H), 7.45 – 7.42 (m, 3H), 3.73 (d, J = 18.0 Hz, 1H), 3.40 (d, J = 18.5 Hz, 1H); ^{13}C {^{1}H} NMR ($CDCl_3$, 126 MHz): δ 174.5, 174.0, 161.0, 155.1, 145.7, 141.9, 140.2, 137.7, 135.0, 134.1, 133.2, 131.9, 130.6, 130.14, 130.11, 129.4, 129.2, 126.6, 123.8, 123.4, 56.7, 39.6; IR (neat, cm^{-1}): 2987, 1653, 1305, 1285, 1208, 1127, 1100, 910, 618, 519; HRMS (ESI-TOF) calcd for $C_{24}H_{14}Cl_2N_3O_2$ $[M + H]^+$ 446.0463, found 446.0458.

TH-3369_166122017

1'-Phenylspiro[benzo[5,6]indeno[1,2-*b*]quinoxaline-12,3'-pyrrolidine]-2',5'-dione (4ma):

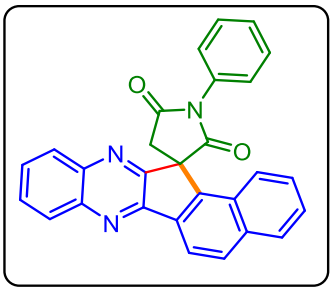

A light brown solid (33 mg, 77% yield); mp 217–220 °C; purified over a column of silica gel (25% EtOAc in hexane); ^{1}H NMR ($CDCl_3$, 500 MHz): δ 8.33 (d, J = 8.5 Hz, 1H), 8.20 (d, J = 8.0 Hz, 1H), 8.12 (t, J = 9.0 Hz, 2H), 8.05 (d, J = 8.0 Hz, 1H), 7.79 (t, J = 7.0 Hz, 1H), 7.74 (t, J = 8.0 Hz, 2H), 7.68 (t, J = 7.0 Hz, 1H), 7.64 (d, J = 7.5 Hz, 1H), 7.55 – 7.53 (m, 4H), 7.48 – 7.44 (m, 1H), 3.74 – 3.64 (m, 2H); ^{13}C {^{1}H} NMR ($CDCl_3$, 126 MHz): δ 175.0, 174.5, 161.5, 154.2, 143.1, 141.7, 141.5, 137.5, 136.1, 132.3, 131.8, 130.6, 130.4, 129.6, 129.5, 129.4, 129.2, 128.9, 128.6, 127.9, 126.75, 126.70, 122.6, 119.6, 56.6, 39.2; IR (neat, cm^{-1}): 3062, 2922, 1710, 1497, 1380, 1199, 1175, 1100, 752; HRMS (ESI-TOF) calcd for $C_{28}H_{18}N_3O_2$ $[M + H]^+$ 428.1399, found 428.1413.

1-Phenylspiro[pyrrolidine-3,4'-thieno[2',3':3,4]cyclopenta[1,2-*b*]quinoxaline]-2,5-dione (4na):

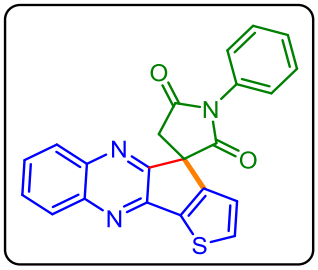

A orange solid (28 mg, 74% yield); mp 204–207 °C; purified over a column of silica gel (25% EtOAc in hexane); ^{1}H NMR ($CDCl_3$, 500 MHz): δ 8.10 (d, J = 8.5 Hz, 1H), 8.05 (d, J = 8.5 Hz, 1H), 7.82 (d, J = 5.0 Hz, 1H), 7.77 (t, J = 7.0 Hz, 1H), 7.71 (t, J = 6.7 Hz, 1H), 7.52 (t, J = 7.7 Hz, 2H), 7.44 (t, J = 7.7 Hz, 3H), 7.27 (d, J = 5.0 Hz, 1H), 3.68 (d, J = 18.0 Hz, 1H), 3.37 (d, J = 18.0 Hz, 1H); ^{13}C {^{1}H} NMR ($CDCl_3$, 126 MHz): δ 174.0, 173.9, 162.5, 152.3, 151.7, 142.8, 142.3, 139.7, 135.9, 132.0, 130.5, 129.5, 129.4, 129.15, 129.10, 126.7, 121.1, 55.3, 38.1; IR (neat, cm^{-1}): 2925, 1656, 1315, 1291, 1218, 1117, 1108, 1010, 688, 579; HRMS (ESI-TOF) calcd for $C_{22}H_{14}N_3O_2S$ $[M + H]^+$ 384.0807, found 384.0806.

TH-3369_166122017

1'-Methylspiro[indeno[1,2-*b*]quinoxaline-11,3'-pyrrolidine]-2',5'-dione (4ab):

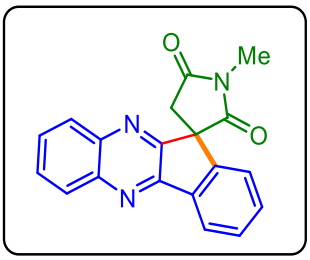

A light brown solid (25 mg, 79% yield); mp 238–240 °C; purified over a column of silica gel (25% EtOAc in hexane); ^{1}H NMR ($CDCl_3$, 500 MHz): δ 8.27 (d, J = 6.5 Hz, 1H), 8.19 (d, J = 8.5 Hz, 1H), 8.07 (d, J = 8.0 Hz, 1H), 7.79 (t, J = 7.0 Hz, 1H), 7.74 (t, J = 7.2 Hz, 1H), 7.64 – 7.59 (m, 2H), 7.47 (d, J = 7.0 Hz, 1H), 3.63 (d, J = 18.0 Hz, 1H), 3.24 (d, J = 20.0 Hz, 4H); ^{13}C {^{1}H} NMR ($CDCl_3$, 126 MHz): δ 176.0, 175.6, 159.9, 154.2, 145.7, 143.0, 141.6, 138.3, 132.5, 130.4, 130.3, 129.64, 129.60, 129.5, 123.4, 123.3, 56.6, 39.7, 26.2; IR (neat, cm^{-1}): 2996, 1681, 1351, 1321, 1278, 1197, 1148, 1017, 628, 529; HRMS (ESI-TOF) calcd for $C_{19}H_{14}N_3O_2$ $[M + H]^+$ 316.1086, found 316.1084.

1'-Isobutylspiro[indeno[1,2-*b*]quinoxaline-11,3'-pyrrolidine]-2',5'-dione (4ae):

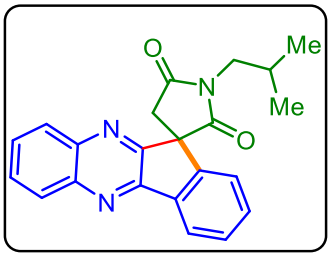

A light brown solid (28 mg, 77% yield); mp 225–227 °C; purified over a column of silica gel (25% EtOAc in hexane); ^{1}H NMR ($CDCl_3$, 500 MHz): δ 8.27 – 8.25 (m, 1H), 8.18 (d, J = 7.5 Hz, 1H), 8.05 (d, J = 7.0 Hz, 1H), 7.78 (t, J = 7.0 Hz, 1H), 7.72 (t, J = 7.0 Hz, 1H), 7.63 – 7.58 (m, 2H), 7.50 – 7.47 (m, 1H), 3.59 (d, J = 18.0 Hz, 1H), 3.53 (dd, J = 7.5, 2.5 Hz, 2H), 3.25 (d, J = 18.5 Hz, 1H), 2.21 – 2.15 (m, 1H), 1.00 (dd, J = 8.5, 6.5 Hz, 6H); ^{13}C {^{1}H} NMR ($CDCl_3$, 126 MHz): δ 176.1, 175.7, 160.2, 154.0, 145.7, 142.9, 141.6, 138.3, 132.4, 130.3, 130.2, 129.6, 129.5, 129.4, 123.4, 123.3, 56.5, 47.2, 39.6, 27.2, 20.15, 20.14; IR (neat, cm^{-1}): 2958, 1697, 1386, 1337, 1204, 1139, 1103, 1048, 767,688; HRMS (ESI-TOF) calcd for $C_{22}H_{20}N_3O_2$ $[M + H]^+$ 358.1556, found 358.1548.

TH-3369_166122017

1'-Cyclohexylspiro[indeno[1,2-*b*]quinoxaline-11,3'-pyrrolidine]-2',5'-dione (4af):

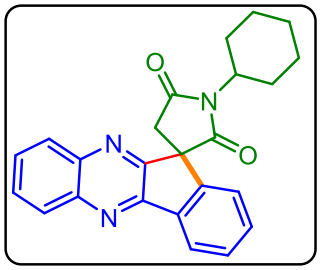

A brown solid (29 mg, 76% yield); mp 218–220 ºC; purified over a column of silica gel (25% EtOAc in hexane); ^{1}H NMR ($CDCl_3$, 500 MHz): δ 8.26 (d, J = 6.5, 1H), 8.17 (d, J = 7.0 Hz, 1H), 8.07 (d, J = 7.0 Hz, 1H), 7.78 (t, J = 7.0 Hz, 1H), 7.73 (t, J = 6.7 Hz, 1H), 7.63 – 7.57 (m, 2H), 7.44 (d, J = 6.5 Hz, 1H), 4.17 – 4.10 (m, 1H), 3.57 (d, J = 18.0 Hz, 1H), 3.16 (d, J = 18.0 Hz, 1H), 2.25 – 2.17 (m, 2H), 1.86 (d, J = 13.0 Hz, 2H), 1.79 (d, J = 12.0 Hz, 2H), 1.67 (d, J = 13.0 Hz, 1H), 1.39 – 1.31 (m, 2H), 1.27 – 1.17 (m, 1H); ^{13}C {^{1}H} NMR ($CDCl_3$, 126 MHz): δ 175.9, 175.6, 160.0, 154.2, 146.1, 142.9, 141.6, 138.2, 132.4, 130.3, 130.1, 129.6, 129.5, 129.4, 123.3, 123.0, 56.2, 53.1, 39.5, 29.1, 29.0, 25.9, 25.1; IR (neat, cm^{-1}): 2922, 1687, 1328, 1307, 1198, 1126, 1155, 1041, 787,611; HRMS (ESI-TOF) calcd for $C_{24}H_{22}N_3O_2$ $[M + H]^+$ 384.1712, found 384.1714.

1'-Benzylspiro[indeno[1,2-*b*]quinoxaline-11,3'-pyrrolidine]-2',5'-dione (4ao):

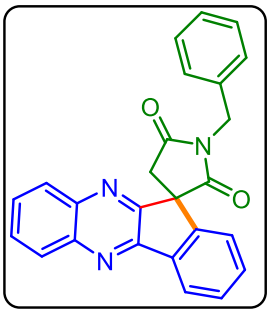

A brown solid (32 mg, 81% yield); mp 221–224ºC; purified over a column of silica gel (25% EtOAc in hexane); ^{1}H NMR ($CDCl_3$, 500 MHz): δ 8.25 (d, J = 7.5 Hz, 1H), 8.18 (d, J = 8.5 Hz, 1H), 8.04 (d, J = 7.5 Hz, 1H), 7.79 (t, J = 6.7 Hz, 1H), 7.74 (t, J = 6.7 Hz, 1H), 7.60 (t, J = 7.2 Hz, 1H), 7.54 (t, J = 7.5 Hz, 1H), 7.45 (d, J = 7.0 Hz, 2H), 7.36 (t, J = 7.2 Hz, 2H), 7.33 – 7.30 (m, 2H), 4.86 (s, 2H), 3.62 (d, J = 18.0 Hz, 1H), 3.23 (d, J = 18.5 Hz, 1H); ^{13}C {^{1}H} NMR ($CDCl_3$, 126 MHz): δ 175.7, 175.0, 159.8, 154.1, 145.6, 143.0, 141.6, 138.3, 135.6, 132.5, 130.4, 130.2, 129.6, 129.5, 128.9, 128.5, 128.2, 123.4, 123.3, 56.6, 43.6, 39.7; IR (neat, cm^{-1}) 2998, 1657, 1311, 1381, 1298, 1124, 1105, 1039, 778, 511; HRMS (ESI-TOF) calcd for $C_{25}H_{18}N_3O_2$ $[M + H]^+$ 392.1399, found 392.1387.

TH-3369_166122017

1'-((S)-1-(Naphthalen-1-yl)ethyl)spiro[indeno[1,2-*b*]quinoxaline-11,3'-pyrrolidine]-2',5'-dione (4as):

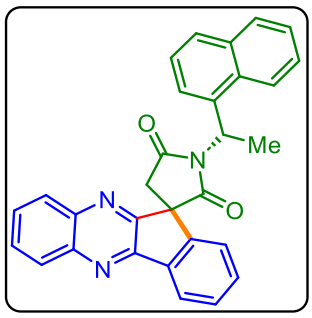

A off-white solid (35 mg, 78% yield); dr 1:1; mp 215–217 °C; purified over a column of silica gel (25% EtOAc in hexane); ^{1}H NMR ($CDCl_3$, 500 MHz): δ 8.24 (d, J = 7.5 Hz, 1H), 8.16 (t, J = 9.0 Hz, 2H), 8.11 – 8.09 (m, 1H), 8.02 (d, J = 8.0 Hz, 1H), 7.95 (d, J = 8.0 Hz, 2H), 7.90 – 7.81 (m, 6H), 7.77 – 7.68 (m, 4H), 7.58 (t, J = 7.5 Hz, 2H), 7.54 – 7.44 (m, 8H), 7.32 (t, J = 7.5 Hz, 1H), 7.17 (d, J = 7.5 Hz, 1H), 7.01 (d, J = 8.0 Hz, 1H), 6.33 – 6.29 (m, 1H), 6.27 – 6.23 (m, 1H), 3.54 (d, J = 18.0 Hz, 1H), 3.48 (d, J = 18.5 Hz, 1H), 3.13 (d, J = 18.5 Hz, 1H), 3.03 (d, J = 18.5 Hz, 1H), 2.07 (d, J = 7.0 Hz, 3H), 2.04 (d, J = 7.0 Hz, 3H); ^{13}C {^{1}H} NMR ($CDCl_3$, 126 MHz): δ 175.8, 175.6, 175.1, 174.9, 159.9, 159.8, 154.1, 154.0, 145.7, 145.6, 142.9, 141.63, 141.60, 138.3, 138.1, 134.0, 133.9, 133.5, 133.4, 132.3, 131.4, 131.3, 130.3, 130.2, 130.0, 129.6, 129.5, 129.3, 129.2, 129.0, 126.9, 126.8, 126.7, 126.6, 125.72, 125.71, 125.2, 125.1, 123.4, 123.27, 123.2, 123.1, 122.9, 56.3, 56.2, 47.8, 47.7, 39.5, 39.4, 17.2; IR (neat, cm^{-1}) 2934, 1699, 1509, 1347, 1197, 1101, 801, 771, 691, 582; HRMS (ESI-TOF) calcd for $C_{30}H_{22}N_3O_2$ $[M + H]^+$ 456.1712, found 456.1727.

Spiro[indeno[1,2-*b*]quinoxaline-11,3'-pyrrolidine]-2',5'-dione (4at):

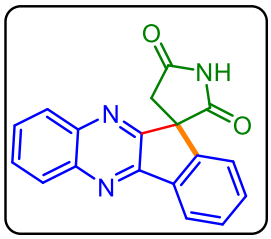

A brown solid (22 mg, 73% yield); mp 221–224 °C; purified over a column of silica gel (30% EtOAc in hexane); ^{1}H NMR ($CDCl_3$+DMSO-d_6, 500 MHz): δ 11.27 (s, 1H), 8.28 – 8.26 (m, 1H), 8.18 (t, J = 6.5 Hz, 1H), 8.10 (t, J = 6.5 Hz, 1H), 7.82 – 7.73 (m, 2H), 7.64 – 7.59 (m, 3H), 3.61 (d, J = 18.5, 1H), 3.23 (d, J = 18.5 Hz, 1H); ^{13}C {^{1}H} NMR ($CDCl_3$+DMSO-d_6, 126 MHz): δ 176.8, 176.3, 159.8, 153.8, 145.6, 142.6, 141.2, 137.7, 132.2, 130.0, 129.8, 129.2, 129.16, 129.11, 123.2, 122.8, 57.7, 40.3; IR (neat, cm^{-1}): 2938, 1622, 1301, 1396, 1288, 1127, 1158, 1057, 698, 526; HRMS (ESI-TOF) calcd for $C_{18}H_{12}N_3O_2$ $[M + H]^+$ 302.0930, found 302.0928.

TH-3369_166122017

1'-(4-(Trifluoromethyl)phenyl)spiro[indeno[1,2-*b*]quinoxaline-11,3'-pyrrolidine]-2',5'-dione (4am):

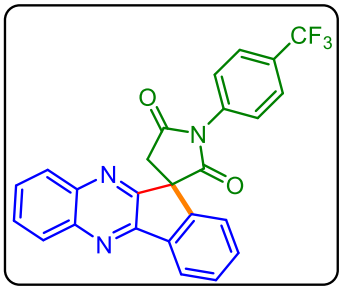

A light brown solid (32 mg, 71% yield); mp 212–214 ºC; purified over a column of silica gel (28% EtOAc in hexane); ^{1}H NMR ($CDCl_3$, 500 MHz): δ 8.32 – 8.30 (m, 1H), 8.21 (d, J = 8.0 Hz, 1H), 8.11 (d, J = 8.5 Hz, 1H), 7.83 – 7.74 (m, 4H), 7.69 – 7.60 (m, 5H), 3.79 (d, J = 18.5 Hz, 1H), 3.44 (d, J = 18.5 Hz, 1H); ^{13}C {^{1}H} NMR ($CDCl_3$, 126 MHz): δ 174.6, 173.9, 159.6, 154.0, 145.2, 143.2, 141.6, 138.4, 135.1, 132.6, 130.6 (d, J = 6.7 Hz), 129.8, 129.6 (d, J = 6.9 Hz), 129.0, 126.9, 126.5 (q, J = 7.3 Hz), 126.4, 123.6, 123.3, 56.7, 39.7; ^{19}F NMR ($CDCl_3$) δ -62.7 (s); IR (neat, cm^{-1}): 2969, 1601, 1324, 1309, 1298, 1155, 1166, 1088, 598, 586; HRMS (ESI-TOF) calcd for $C_{25}H_{15}F_3N_3O_2$ $[M + H]^+$ 446.1116, found 446.1100.

1-Phenyl-3-(3-phenylquinoxalin-2-yl)-1*H*-pyrrole-2,5-dione (5aa):

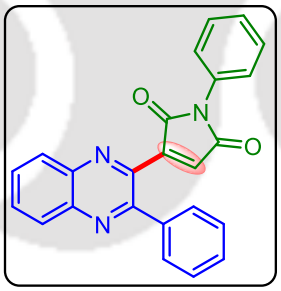

A plae yellow solid (34 mg, 90% yield); mp 202–204 ºC; purified over a column of silica gel (15% EtOAc in hexane); ^{1}H NMR ($CDCl_3$, 500 MHz): δ 8.22 (dd, J = 14.2, 8.2 Hz, 2H), 7.90 – 7.83 (m, 2H), 7.73 – 7.71 (m, 2H), 7.52 – 7.50 (m, 3H), 7.41 (t, J = 7.5 Hz, 2H), 7.33 (t, J = 7.2 Hz, 1H), 7.19 (d, J = 8.0 Hz, 2H), 7.09 (s, 1H); ^{13}C{^{1}H} NMR ($CDCl_3$, 126 MHz): δ 168.4, 167.4, 153.6, 145.7, 143.0, 142.3, 141.0, 138.5, 131.9, 131.7, 131.3, 130.8, 129.8, 129.6, 129.5, 129.2, 129.1, 129.0, 128.1, 126.1; IR (neat, cm^{-1}): 2918, 2850, 1708, 1596, 1500, 1395, 1337, 1206, 870, 759; HRMS (ESI-TOF) calcd for $C_{24}H_{16}N_3O_2$ $[M + H]^+$ 378.1243, found 378.1242.

TH-3369_166122017

3-(3-(4-Fluorophenyl)quinoxalin-2-yl)-1-phenyl-1*H*-pyrrole-2,5-dione (5da):

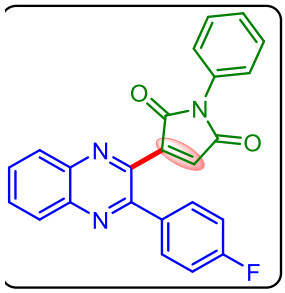

A pale yellow solid (34 mg, 85% yield); mp 215–218 °C; purified over a column of silica gel (15% EtOAc in hexane); ^{1}H NMR ($CDCl_3$, 500 MHz): δ 8.21 (t, J = 8.0 Hz, 2H), 7.91 – 7.84 (m, 2H), 7.73 (dd, J = 8.5, 5.0 Hz, 2H), 7.43 (t, J = 7.7 Hz, 2H), 7.35 (t, J = 7.5 Hz, 1H), 7.21 (dd, J = 10, 7.5 Hz, 4H), 7.15 (s, 1H); ^{13}C{^{1}H} NMR ($CDCl_3$, 156 MHz): δ 168.4, 167.4, 163.8 (d, J = 251.2 Hz), 152.5, 145.8, 142.8, 142.3, 141.1, 134.8 (d, J = 3.4 Hz), 132.1, 131.9, 131.2 (d, J = 8.8 Hz), 130.9, 129.6 (d, J = 1.9 Hz), 129.3, 128.2, 126.1, 116.3, 116.1; ^{19}F NMR ($CDCl_3$) δ -110.5 (s); IR (neat, cm^{-1}): 2933, 1703, 1599, 1431, 1355, 1127, 912, 718, 522; HRMS (ESI-TOF) calcd for $C_{24}H_{15}FN_3O_2$ $[M + H]^+$ 396.1148, found 396.1142.

1-Phenyl-3-(3-(4-(trifluoromethyl)phenyl)quinoxalin-2-yl)-1*H*-pyrrole-2,5-dione (5fa):

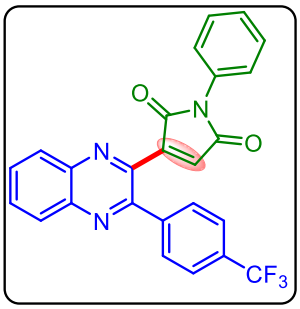

A light yellow solid (36 mg, 81% yield); mp 220–222 °C; purified over a column of silica gel (15% EtOAc in hexane); ^{1}H NMR ($CDCl_3$, 500 MHz): δ 8.23 (t, J = 8.2 Hz, 2H), 7.93 – 7.88 (m, 2H), 7.86 (d, J = 8.0 Hz, 2H), 7.79 (d, J = 8.0 Hz, 2H), 7.41 (t, J = 7.7 Hz, 2H), 7.33 (t, J = 7. Hz, 1H), 7.18 (s, 1H), 7.14 (d, J = 7.5 Hz, 2H); ^{13}C {^{1}H} NMR ($CDCl_3$, 126 MHz): δ 168.2, 167.4, 152.1, 145.4, 142.6, 142.3, 142.2, 141.3, 132.2, 132.1, 131.8, 131.6, 131.4, 131.1, 129.7, 129.6, 129.3, 128.3, 126.0, 125.9 (q, J = 3.6 Hz); ^{19}F NMR ($CDCl_3$) δ -62.7 (s); IR (neat, cm^{-1}): 3110, 1704, 1502, 1396, 1323, 887, 1110, 857, 692; HRMS (ESI-TOF) calcd for $C_{25}H_{15}F_3N_3O_2$ $[M + H]^+$ 446.1116, found 446.1112.

TH-3369_166122017

3-(3-([1,1'-Biphenyl]-4-yl)quinoxalin-2-yl)-1-phenyl-1*H*-pyrrole-2,5-dione (5ga):

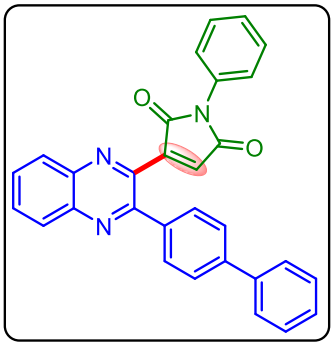

A light yellow solid (39 mg, 86% yield); mp 215–217 °C; purified over a column of silica gel (15% EtOAc in hexane); ^{1}H NMR ($CDCl_3$, 500 MHz): δ 8.25 – 8.20 (m, 2H), 7.91 – 7.84 (m, 2H), 7.82 (d, J = 8.5 Hz, 2H), 7.75 (d, J = 8.5 Hz, 2H), 7.66 (d, J = 7.0 Hz, 2H), 7.49 (t, J = 7.5 Hz, 2H), 7.41 – 7.37 (m, 3H), 7.31 (t, J = 7.5 Hz, 1H), 7.19 (d, J = 7.5 Hz, 2H), 7.15 (s, 1H); ^{13}C {^{1}H} NMR ($CDCl_3$, 126 MHz): δ 168.5, 167.5, 153.3, 145.9, 143.0, 142.7, 142.4, 141.1, 140.3, 137.5, 131.9, 131.8, 131.4, 130.8, 129.7, 129.68, 129.62, 129.3, 129.1, 128.1, 128.0, 127.8, 127.4, 126.1; IR (neat, cm^{-1}): 2982, 1720, 1533, 1453, 1356, 1131, 968, 761, 511; HRMS (ESI-TOF) calcd for $C_{30}H_{20}N_3O_2$ $[M + H]^+$ 454.1556, found 454.1550.

3-(3-(Naphthalen-2-yl)quinoxalin-2-yl)-1-phenyl-1*H*-pyrrole-2,5-dione (5ma):

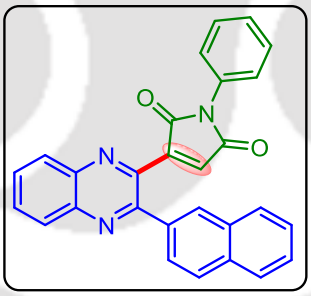

A pale yellow solid (35 mg, 83% yield); mp 210–212 °C; purified over a column of silica gel (15% EtOAc in hexane); ^{1}H NMR ($CDCl_3$, 500 MHz): δ 8.26 (d, J = 8.5 Hz, 1H), 8.23 (d, J = 8.0 Hz, 1H), 8.18 (s, 1H), 7.99 (d, J = 8.5 Hz, 1H), 7.92 – 7.84 (m, 5H), 7.59 – 7.52 (m, 2H), 7.32 (t, J = 7.5 Hz, 2H), 7.28 (d, J = 7.0 Hz, 1H), 7.12 (s, 1H), 7.02 (d, J = 7.5 Hz, 2H); ^{13}C {^{1}H} NMR ($CDCl_3$, 126 MHz): δ 168.5, 167.5, 153.5, 145.9, 143.2, 142.4, 141.1, 135.9, 133.7, 133.2, 132.0, 131.7, 131.2, 130.8, 129.7, 129.6, 129.2, 129.1, 128.6, 128.1, 128.0, 127.5, 127.0, 126.2, 126.1; IR (neat, cm^{-1}): 2921, 1710, 1598, 1500, 1386, 1187, 1120, 1081, 872, 748, 476; HRMS (ESI-TOF) calcd for $C_{28}H_{18}N_3O_2$ $[M + H]^+$ 428.1399, found 428.1392.

TH-3369_166122017

1-Methyl-3-(3-phenylquinoxalin-2-yl)-1*H*-pyrrole-2,5-dione (5ab):

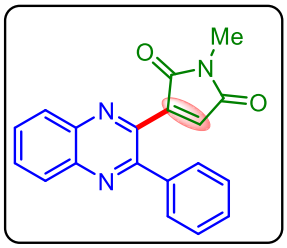

A pale yellow solid (26 mg, 84% yield); mp 195–198 °C; purified over a column of silica gel (15% EtOAc in hexane); ^{1}H NMR ($CDCl_3$, 500 MHz): δ 8.19 (t, J = 10.5 Hz, 2H), 7.88 – 7.81 (m, 2H), 7.67 – 7.64 (m, 2H), 7.50 – 7.47 (m, 3H), 6.83 (s, 1H), 2.98 (s, 3H); ^{13}C {^{1}H} NMR ($CDCl_3$, 126 MHz): δ 169.8, 168.8, 153.6, 145.4, 143.1, 142.1, 141.0, 138.4, 131.8, 130.7, 129.8, 129.6, 129.5, 129.1, 128.9, 128.1, 24.2; IR (neat, cm^{-1}): 2992, 1710, 1530, 1433, 1346, 1134, 959, 768, 553; HRMS (ESI-TOF) calcd for $C_{19}H_{14}N_3O_2$ $[M + H]^+$ 316.1086, found 316.1084.

1-(4-Methoxyphenyl)-3-(3-phenylquinoxalin-2-yl)-1*H*-pyrrole-2,5-dione (5ak):

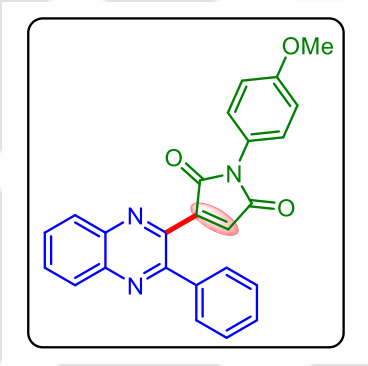

A light yellow solid (36 mg, 89% yield); mp 215–217 °C; purified over a column of silica gel (18% EtOAc in hexane); ^{1}H NMR ($CDCl_3$, 500 MHz): δ 8.21 (dd, J = 13.0, 8.0 Hz, 2H), 7.90 – 7.83 (m, 2H), 7.73 – 7.70 (m, 2H), 7.54 – 7.50 (m, 3H), 7.09 (s, 1H), 7.07 (d, J = 5.0 Hz, 2H), 6.93 (d, J = 8.5 Hz, 2H), 3.80 (s, 3H); ^{13}C {^{1}H} NMR ($CDCl_3$, 126 MHz): δ 168.8, 167.7, 159.3, 153.6, 145.7, 143.1, 142.3, 141.1, 138.6, 131.9, 131.7, 130.8, 129.8, 129.65, 129.60, 129.2, 129.0, 127.6, 123.9, 114.6, 55.6; IR (neat, cm^{-1}): 2988, 1763, 1523, 1430, 1396, 1130, 952, 788, 503; HRMS (ESI-TOF) calcd for $C_{25}H_{18}N_3O_3$ $[M + H]^+$ 408.1348, found 408.1352.

TH-3369_166122017

IV.8. NMR Spectra

^{1}H NMR of **1-Phenyl-3-(3-phenylquinoxalin-2-yl)pyrrolidine-2,5-dione** (**3aa**) ($CDCl_3$, 400 MHz)

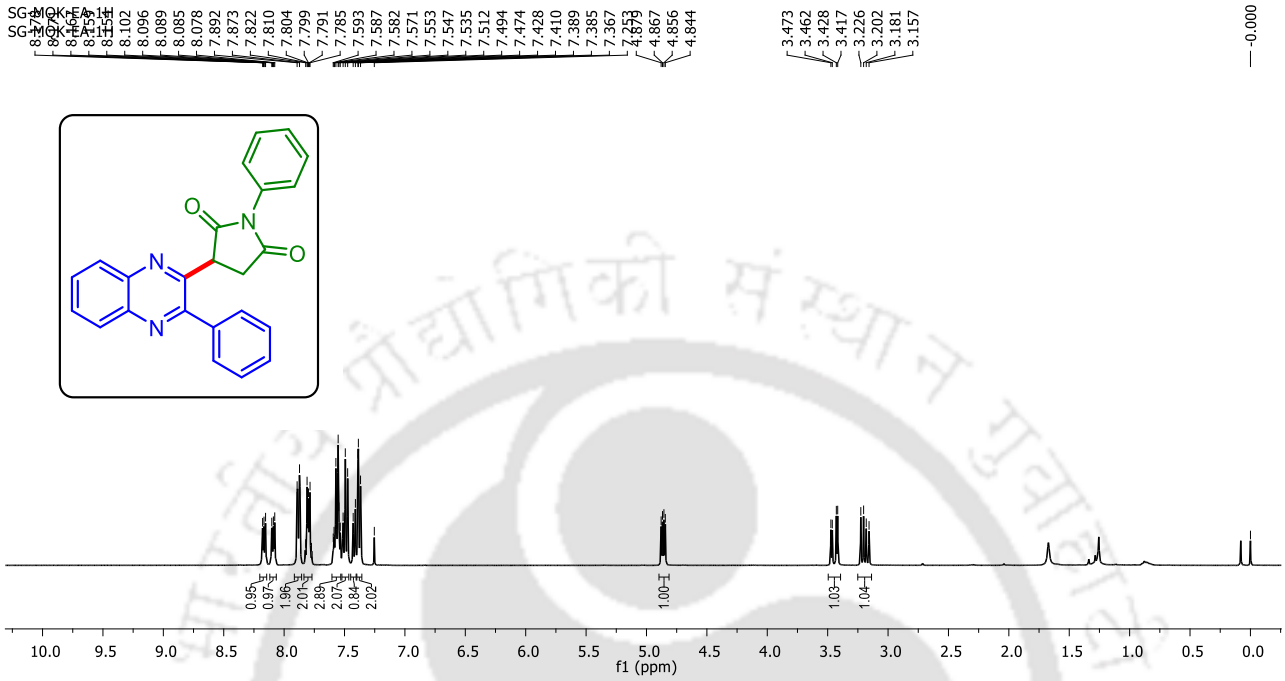

^{13}C{^{1}H} NMR of **1-Phenyl-3-(3-phenylquinoxalin-2-yl)pyrrolidine-2,5-dione** (**3aa**) ($CDCl_3$, 101 MHz)

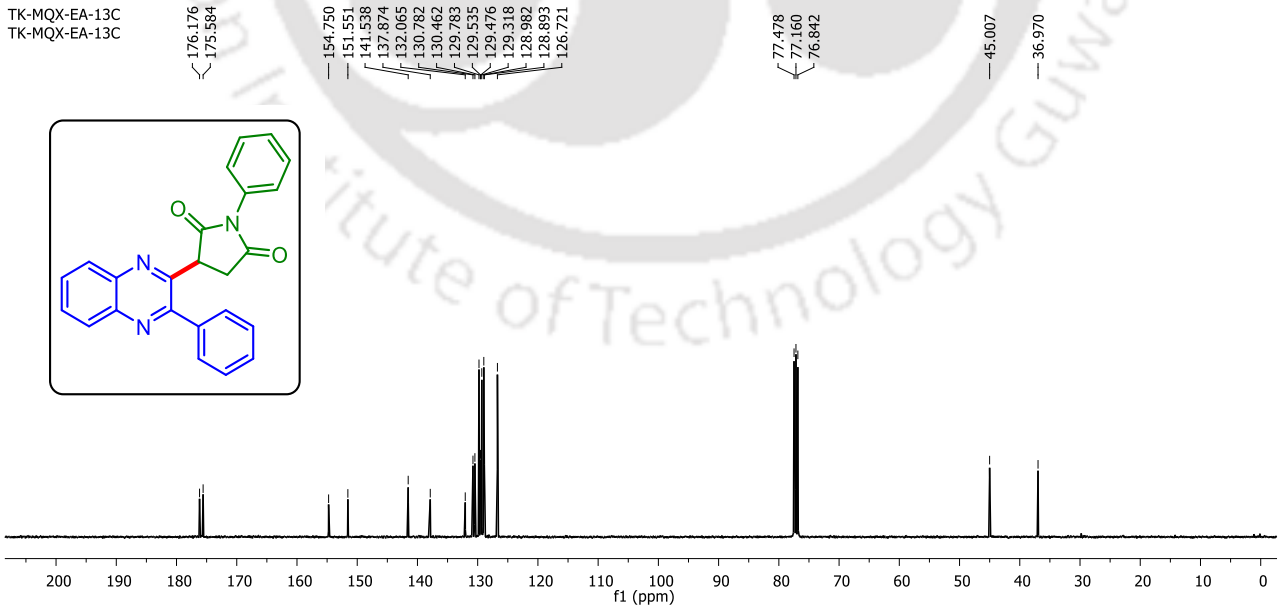

TH-3369_166122017

The remaining NMR spectra are available on

https://pubs.acs.org/doi/suppl/10.1021/acs.orglett.3c01350/suppl_file/ol3c01350_si_001.pdf

TH-3369_166122017

CHAPTER V

Photo-Induced Generation of Oxygenated Quaternary Centers via EnT Enabled Singlet O_2 Addition to C3-Maleimidated Quinoxaline: A Reagent-Less Approach

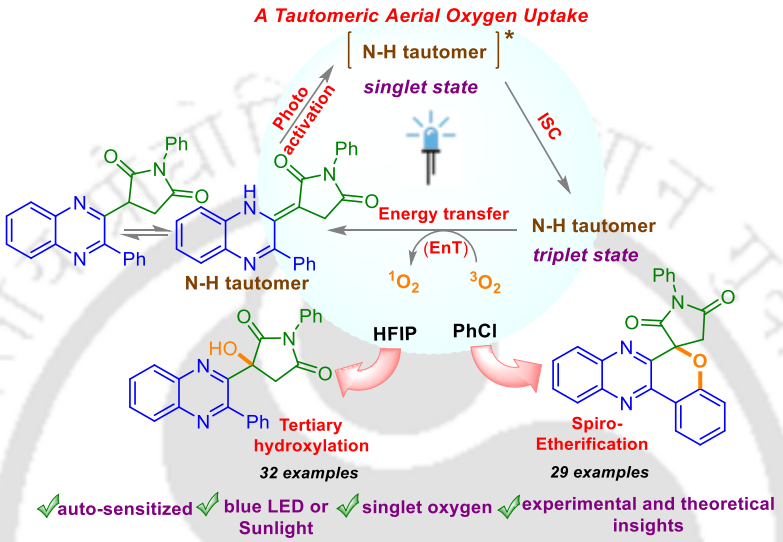

Abstract: *Demonstrated here is an external photo-sensitizer-free (auto-sensitized) singlet oxygen-enabled solvent-dependent tertiary hydroxylation and aryl-alkyl spiro-etherification of C3-maleimidated quinoxalines. Such "reagent-less" photo-oxygenation at Csp^3–H and etherification involving Csp^3–H/Csp^2–H are unparalleled. Possibly, the highly π-conjugated N–H tautomer allows the substrate to get excited by irradiation, and subsequently, it attains the triplet state via ISC. This excited triplet-state sensitized molecule then transfers its energy to a triplet-state oxygen ($^3O_2$) generating reactive singlet oxygen ($^1O_2$) for hydroxylation and spirocyclization depending on the solvent used. In a protic solvent HFIP, the generated alkoxy radical accepts a proton via HAT giving hydroxylated product. In contrast, in an aprotic PhCl it underwent a radical addition at the ortho-position of the C2 aryl to provide spiro-ether. An unprecedented orthogonal spiro-etherification was observed via the displacement of o-substitutents for ortho (–OEt, –OMe, –F, –Cl, –Br) substituted substrates. The order of ipso substitution follows the trend –OEt ~ –OMe > –F > –H > –Cl > Br. Both these oxygenation reactions can be carried out with nearly equal ease using direct sunlight without the requirement of any elaborate reaction-setup. Demonstration of large-scale synthesis and a few interesting transformations have also been realized. Furthermore, several insightful control experiments and quantum chemical computations were performed to unravel the mechanism.*

Keywords: *auto-sensitized, photo-oxygenation, singlet-oxygen, oxygenated quaternary centers, experimental and theoretical insights*

'Under Revision in Chemistry: A European Journal'

CHAPTER V

V.1. Introduction

Carbon-carbon bonds are the primary structural backbone of myriads of functional organic compounds; however, their biological activities and functional properties are mostly steered due to the installed C–heteroatom linkages.[1] Particularly, the C–O bonds containing scaffolds are found in numerous drugs, natural products, and functional molecules.[2] Consequently, selective C–H oxygenation (C–O bond formation) becomes a burgeoning research to construct new oxygenated scaffolds.[3] Among oxygenated systems, cyclic and acyclic tertiary alcohols are important structural motifs due to their occurrence in bioactive molecules, agrochemicals, and natural products (Figure V.1.1).[4] But, installation of hydroxyl functionality at the sterically hindered Csp^3–H site is challenging. Over the years, attempts have been made to synthesize such tertiary alcohols. Traditionally, Barbier-type nucleophilic addition to carbonyl groups provides tertiary alcohols, but the employment of stoichiometric organometallic reagents encounters several side reactions along with poor functional group tolerance (Scheme V.1.1).[5]

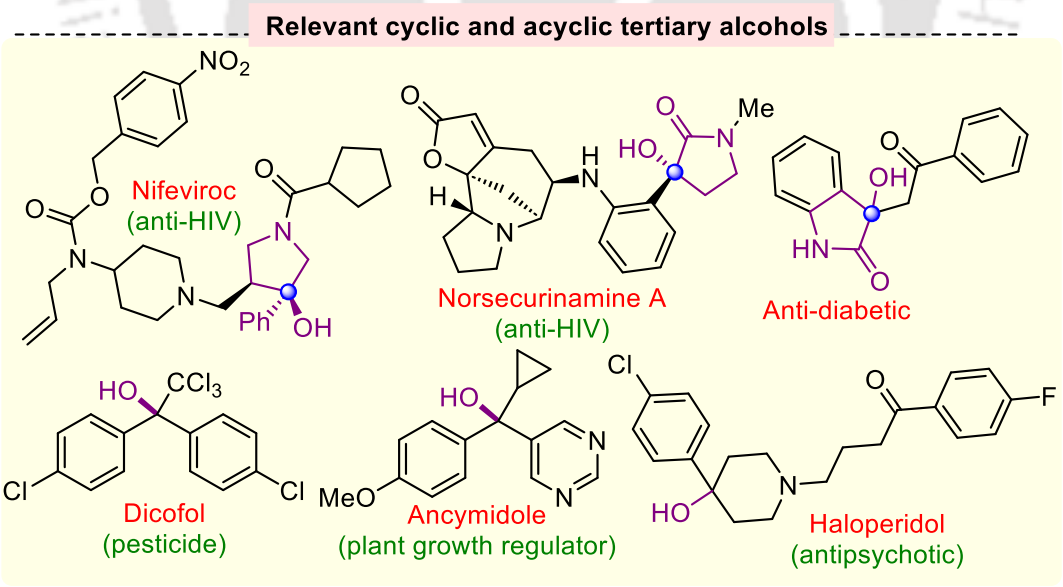

Figure V.1.1. *Representative example of relevant cyclic and acyclic tertiary alcohols*

TH-3369_166122017

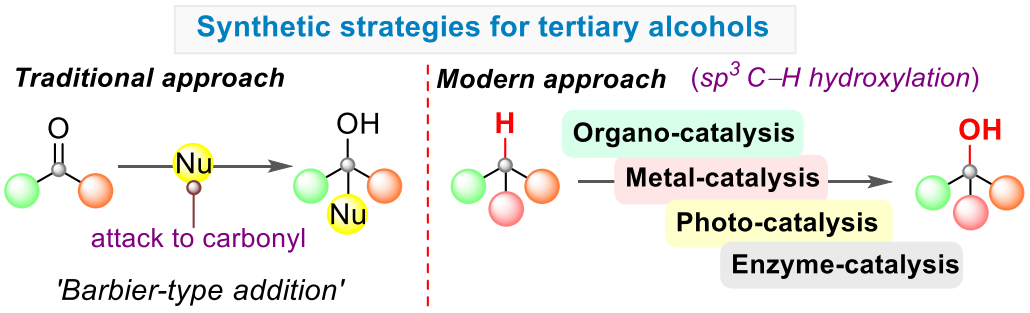

Scheme V.1.1. *General outline of the prior strategies of tertiary alcohol synthesis*

V.2. Modern Tertiary Hydroxylation Strategies

In the modern approach, the tertiary hydroxyl groups are introduced *via* organo-catalysis,[6] directed or non-directed metal catalysis,[7] photo-induced C–H oxidation[8] and enzymatic oxidation[9] of appropriately placed C–H bonds (Scheme V.1.1).

➢ **Organo-Catalysis:**

Hilinski and co-worker introduced an aryl trifluoromethyl ketone-catalyzed C(sp^3)–H hydroxylation of aliphatic system using hydrogen peroxide as terminal oxidant (Scheme V.2.1).[6a] This organo-catalytic oxidation reaction proceeds through the *in situ* generation of dioxirane, which serves as the active oxidant for this transformation.

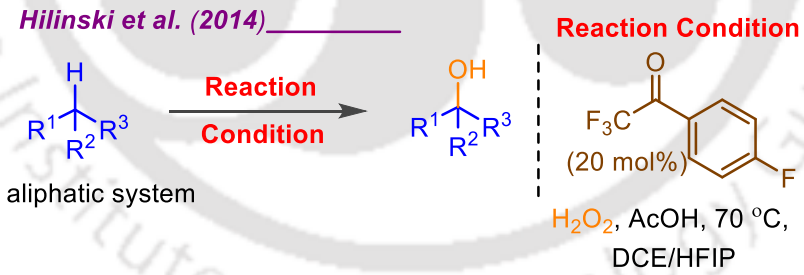

Scheme V.2.1. *Ketone-catalyzed C(sp^3)–H Hydroxylation*

A metal-free iodic-acid mediated tertiary C–H hydroxylation was described by Minakata group (Scheme V.2.2).[6b] In this reaction, HIO_3 serves as an oxidant along with the participation of *N*-hydroxyphthalimide (NHPI).

TH-3369_166122017

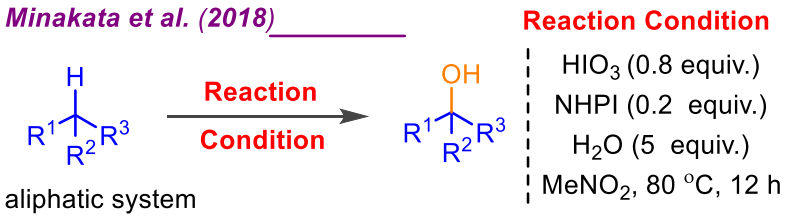

Scheme V.2.2. *Iodic-acid mediated C(sp^3)–H Hydroxylation*

➢ **Metal-Catalysis:**

Over the last decade, various research groups have made significant advances on transition metal-catalyzed C-H hydroxylation using molecular oxygen and stoichiometric oxidants $NaIO_4$, $KBrO_3$, HIO_3, *tert*-butyl hydroperoxide (TBHP) and H_2O_2 (Scheme V.2.3).

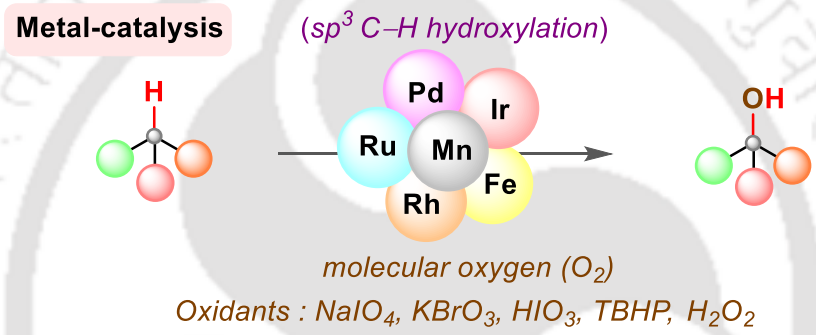

Scheme V.2.3. *Metal-catalyzed C(sp^3)–H Hydroxylation*

➢ **Photo-Catalysis:**

The tertiary C(sp^3)–H hydroxylation has also been realized by using several metal or metal-free photo-catalytic strategies (Scheme V.2.4). In 2017, Chen group reported a photo-redox catalytic selective C(sp^3)–H hydroxylation using $Ru(bpy)_3Cl_2$ as photocatalyst and hydroxyl perfluorobenziodoxole (PFBI-OH) as an oxidant.[8a] Later Das *et al.* demonstrated a metal-free heterogeneous photocatalytic tertiary benzylic C(sp^3)–H hydroxylation.[8b] This reaction was carried out under polymeric carbon nitride (PCN) catalysis along with the involvement of molecular oxygen as an oxidant. Recently, an anaerobic photo-induced C(sp^3)–H hydroxylation has also been described by Parasaram and co-workers.[8c] In this reaction, a photo-excited nitroarene played a bi-functional character to serve as the C−H bond activator as well as an oxygen atom supplier.

TH-3369_166122017

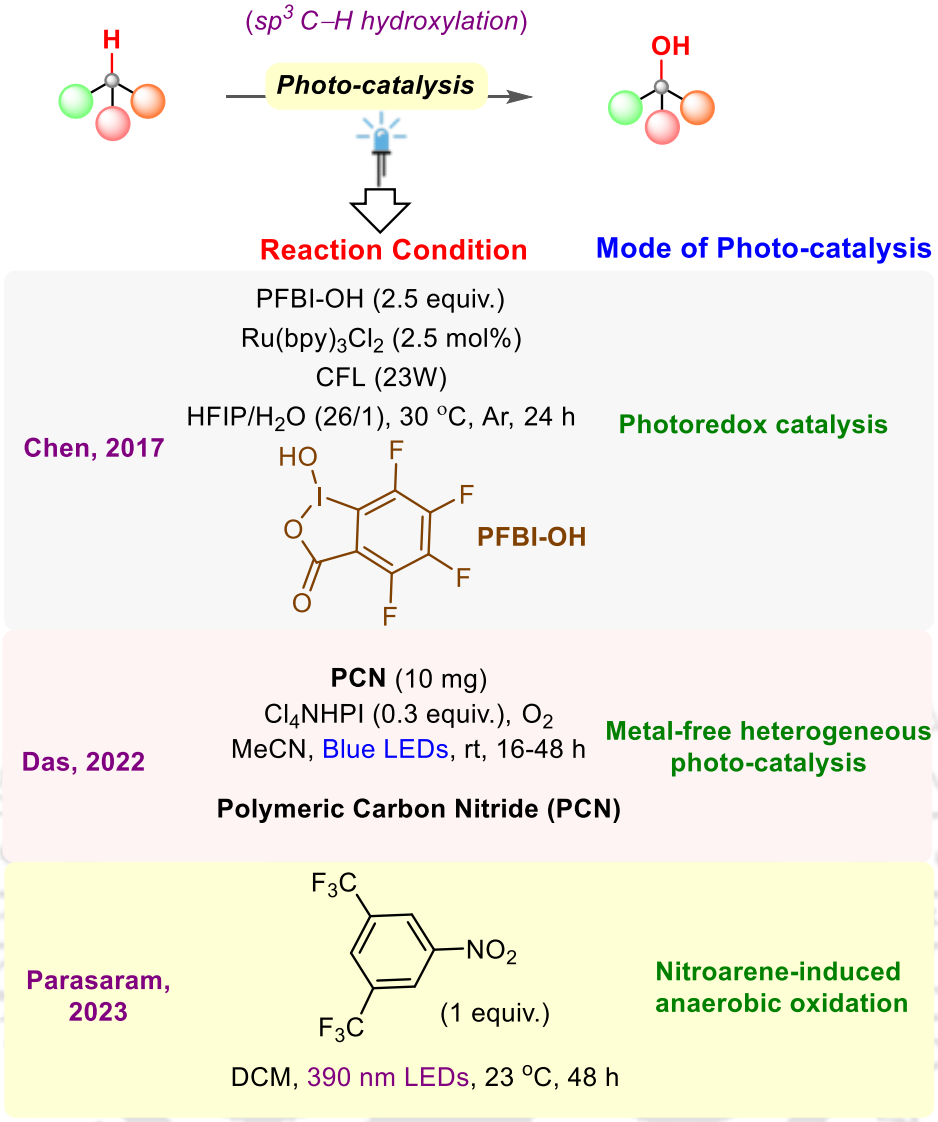

Scheme V.2.4. *Photo-induced tertiary C(sp^3)-H hydroxylation*

➢ **Enzyme-Catalysis:**

Similarly, C(sp^3)–H hydroxylation was also achieved using various metal or metal-free enzymes. These reactions are carried out in aerobic and anaerobic conditions. For aerobic hydroxylation reaction, hydroxylating enzyme utilizes molecular oxygen (O_2) and H_2O_2 whereas for anaerobic condition H_2O serves as the oxygen source.

TH-3369_166122017

Further, aryl-alkyl ethers are also important oxygenated motifs, spread across myriads of pharmaceuticals and medicinally pertinent natural products.[10] In particular, hindered α-tertiary ethers have valuable contributions to pharmaceuticals, agrochemicals, functional materials, and fuel additives (Figure V.1.2).[11]

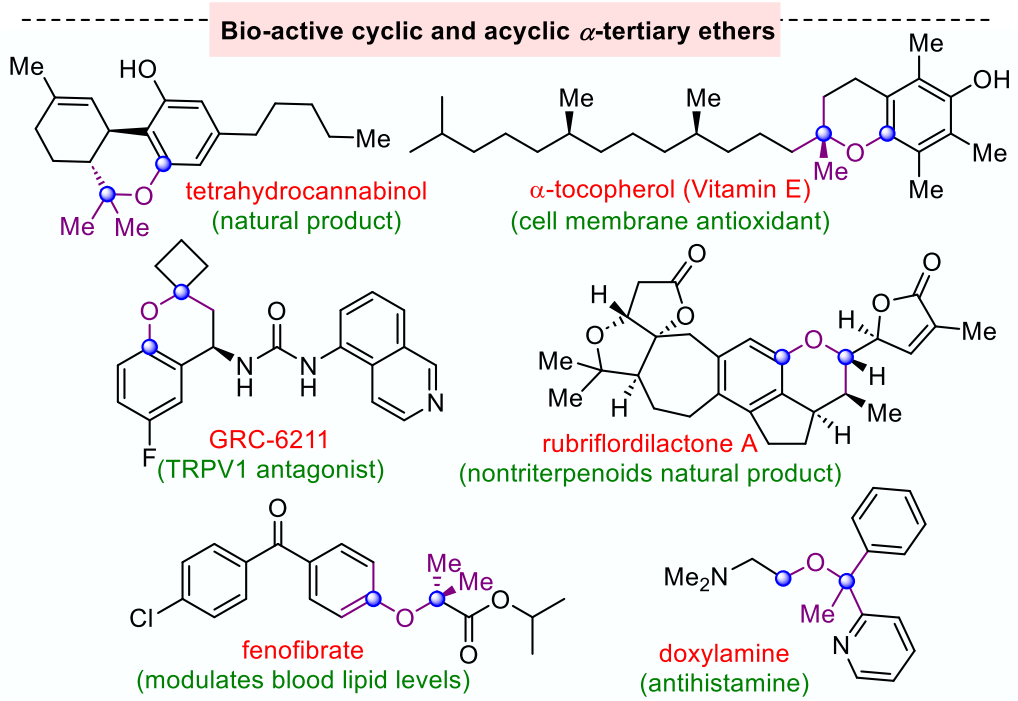

Figure V.1.2. *Representative example of relevant cyclic and acyclic tertiary ethers*

V.3. Modern Etherification Strategies

Traditionally, such ethers are synthesized by Williamson-ether synthesis, but the protocol is limited to primary and secondary ethers.[12] whereas in a modern way,[13,14] these ethers are accessed through (i) alkene-difucntionalizations, (ii) decarboxylative addition reactions under photo- and electro-catalysis, (iii) regioselctive C–H activation reactions and (iv) various thermal (Buchwald-Hartwig, Ullman, etc.) and photo-catalyzed couplings reactions using the pre-functionalized substrates (Scheme V.3.1). Despite the notable advancements, a synthetic access to hindered tertiary alcohols and cyclic aryl-alkyl ethers under mild conditions involving sp^3–sp^2 C–H bonds without metal or additives remains an arduous but desirable task.

TH-3369_166122017

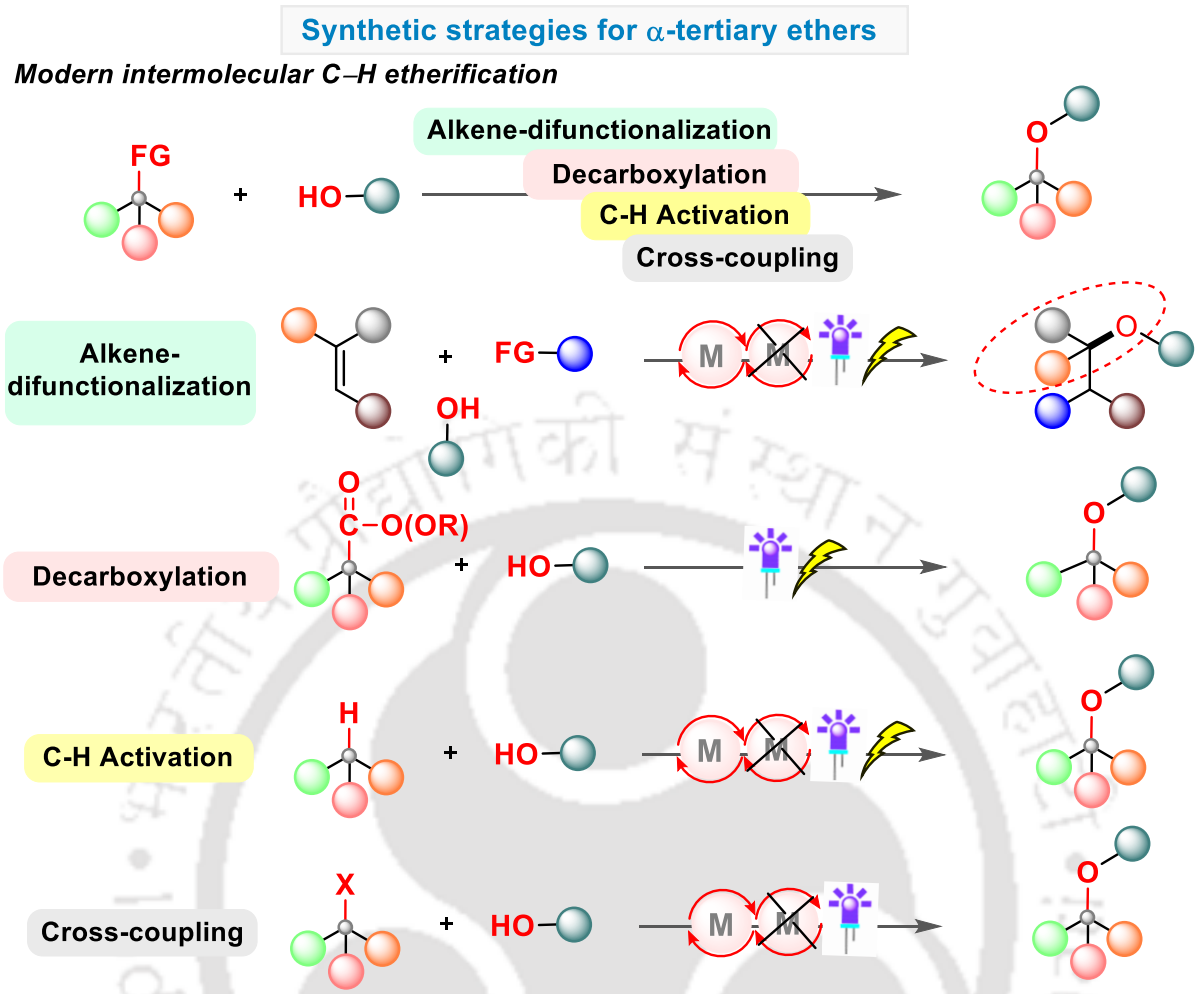

Scheme V.3.1. *Outline of the prior strategies of tertiary ether synthesis*

In recent years, visible light-driven photochemical reactions have made significant progress and are well-elaborated towards the development of fine chemicals, drugs, and natural products.[15] Most of these transformations rely on metal or metal-free photo redox catalyzed single electron transfer (SET) processes. Here, the photo-excited catalyst exchanges an electron with the organic substrate either *via* an oxidative or a reductive quenching path to generate a radical species. Therefore, such transformations are dictated by the redox property of the photo-catalyst as well as the reacting systems. Organic substrates having incompatible redox potentials with the excited photo-catalysts cannot undergo such a SET path and fail to undergo any reaction. To encounter these incompatibility issues, the triplet energy transfer (EnT) process has emerged as an alternative to photoredox catalysis.[16] In this process, the photo-excited triplet sensitizer transfers its triplet energy to one of the reacting substrates. Following this, the activated triplet species reacts with the other reacting partners to generate a reactive radical, leading to photo isomerization, cycloaddition, and ring-closing reactions. Most triplet energy transfer

TH-3369_166122017

(EnT) reactions require the assistance of an external triplet sensitizer and to date, there is no "auto-sensitized" process known to carry out intramolecular functionalization. Thus, it would be interesting if the substrate itself acts as a triplet sensitizer, transfers its energy to a triplet oxygen ($^3O_2$), and generates a reactive singlet oxygen ($^1O_2$). The process would produce a reactive oxygen species (ROS) which may facilitate oxygenation/hydroxylation at the other C–H sites within the molecule making it an auto-sensitized process.

In C3-maleimidated quinoxalines, the electron-deficient succinimide scaffold is linked to a dinitrogen-containing quinoxaline heterocycle. So, there is a possibility of electron drifting from the quinoxaline core to the succinimide inducing a partial dipole, which may be attributed to photo-responsive behavior under irradiation conditions.

V.4. Present Strategy

This aforementioned conundrum encouraged us to envisage a photo-induced oxygenation of C3-maleimidated quinoxaline. Herein, we demonstrate an external photo-sensitizer-free singlet oxygen-enabled tertiary hydroxylation and aryl-alkyl spiro-etherification of C3-maleimidated quinoxaline (Scheme V.4.1). These photo-oxygenation reactions presumably proceed *via* the generation of a hindered tertiary alkoxy radical, in HFIP solvent which abstracts a hydrogen atom to yield a *tert*-hydroxylated product. Alternatively, the *tert*-alkoxy radical may undergo electrophilic addition at the electron-rich C2-aryl ring of C3-maleimidated quinoxaline to provide spiro-ethers.

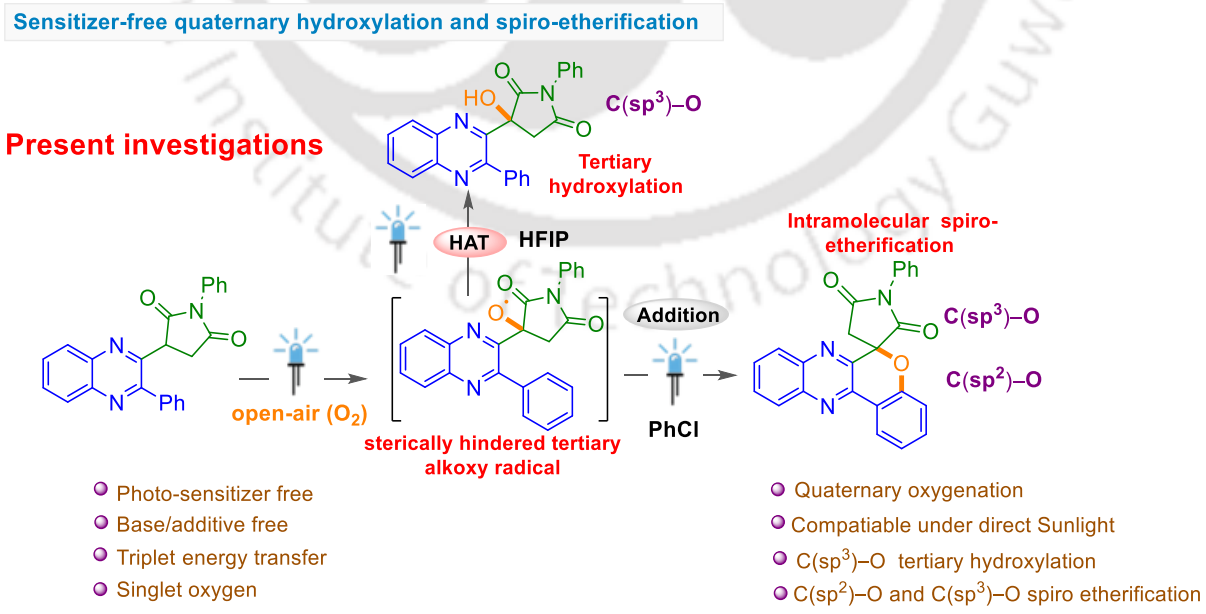

Scheme V.4.1. *Present strategy for forging tertiary alcohols and ethers*

TH-3369_166122017

Optimization of Reaction Condition:

At the outset, 1-phenyl-3-(3-phenylquinoxalin-2-yl)pyrrolidine-2,5-dione (**1**) as the starting material was subjected to blue LEDs irradiation (4 x 3W, 480 nm) in ethyl acetate under an open air. After 12 h of irradiation, two new spots were detected by TLC, both of which were separated and characterized (^{1}H, ^{13}C NMR, and mass spectroscopy). To our delight, two oxygenated quaternary adducts *viz.* 3-hydroxy-1-phenyl-3-(3-phenylquinoxalin-2-yl)pyrrolidine-2,5-dione (**1a**, 17%) and 1'-phenylspiro[chromeno[3,4-*b*]quinoxaline-6,3'-pyrrolidine]-2',5'-dione (**1b**, 39%) were isolated (Table V.4.1, entry 1). Intrigued by this outcome, and to see if there is any solvent-dependency on the product selectivity, various organic solvents such as tetrahydrofuran (THF), dichloromethane (DCM), 2,2,2-trifluoroethanol (TFE), 1,1,1,3,3,3-hexafluoro-2-propanol (HFIP), methanol, ethanol, acetonitrile (MeCN), 1,2-dichloroethane (DCE), chlorobenzene (PhCl), 1,2-dichlorobenzene (DCB) and dimethyl formamide (DMF) were examined (Table V.4.1, entries 2-11). It was observed that the use of solvent HFIP exclusively provided the hydroxylated adduct (**1a**, 79%) and a trace of (**1b**, 5%) (Table V.4.1, entry 5), whereas, in chlorobenzene, the spiro-ether (**1b**) was obtained as the major (82%) and (**1a**) as the minor (14%) product (Table V.4.1, entry 9). It was observed that enhancement in the reaction time from 12 h to 15 h was not found beneficial as some other products started to form for both these reactions (Table V.4.1, entries 12 and 13). White and green LEDs were less effective as compared to blue LED-mediated excitation (Table V.4.1, entries 14-17). Thus, the optimized conditions for the formation of the hydroxylated adduct (**1a**) is the use of HFIP solvent, and for the spiro-ether (**1b**) chlorobenzene was the best under the irradiation of blue LEDs (4 x 3W, 480 nm).

Table V.4.1. *Optimization of Reaction Conditions*[a,b]

TH-3369_166122017

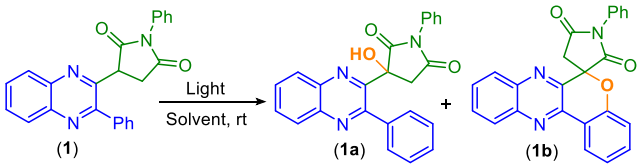

Entry	Solvent	Light Source	Yield (%)[b] **1a**/**1b**
1.	Ethyl acetate	Blue LEDs	17/39
2.	THF	Blue LEDs	n.d./n.d.
3.	DCM	Blue LEDs	16/43
4.	TFE	Blue LEDs	41/14
5.	**HFIP**	**Blue LEDs**	**79/traces**
6.	MeOH or EtOH	Blue LEDs	traces/traces
7.	MeCN	Blue LEDs	traces/61
8.	1,2-DCE	Blue LEDs	26/58
9.	**PhCl**	Blue LEDs	**14/82**
10.	DCB	Blue LEDs	n.d./31
11.	DMF	Blue LEDs	n.d./n.d.
12.[c]	HFIP	Blue LEDs	73/traces
13.[d]	PhCl	Blue LEDs	13/77
14.	HFIP	Green LEDs	42/n.d.
15.	PhCl	Green LEDs	traces/n.d.
16.[c]	HFIP	White LEDs	64/traces
17.	PhCl	White LEDs	traces/67

[a]Reaction conditions unless specified otherwise: **1** (0.15 mmol) in solvent (0.15 M) under open air at 25-30 °C for 12 h. [b]Isolated yield. [c,d]irradiated for 15 h. n.d. = not detected. Blue LEDs (λ = 480 nm), Green LEDs (λ = 530).

Scope of *tert*-Hydroxylation:

The optimized photo-induced selective *tert*-hydroxylation protocol was then explored to rationalize its scope and generality. For this, various *N*-alkyl and aryl substitutions on *N*-maleimide and electronically variable substituents on C3-maleimidated quinoxaline were investigated and the results are summarized in Scheme V.4.2. An array of diversely substituted C3-maleimiated quinoxalines having electron-donating and electron-withdrawing groups such as *p*–Me (**2**), *p*–F (**3**), *p*–Cl (**4**), *p*–Br (**5**), *p*–CF_3 (**6**), *p*–Ph (**7**), *m*–Me (**8**), *m*–CF_3 (**9**), *o*–OMe (**10**), *o*–Br (**11**), 2,6–di-F (**12**) on the C2-aryl ring on quinoxaline unit, all reacted smoothly to deliver their corresponding *tert*-hydroxylated adducts **1a–12a** in moderate to good yields (61–82%). 2-Naphthyl (**13**) and 2-thiophenyl (**14**) derived C3-maleimiated quinoxalines, both reacted competently giving hydroxylated products (**13a**, 76%) and (**14a**, 74%) respectively. Similarly, the C3-maleimidated quinoxalines having various *N*-substitutions on maleimide such as –Me (**15**), –Et (**16**), –^{i}Bu (**17**), benzyl (**18**), methylcyclohexyl (**19**), all successfully

TH-3369_166122017

responded to this protocol, affording the desired hydroxylated adducts **15a–19a** in good to moderate yields (76–82%). Further, various *N*-aryl substituted C3-maleimidated quinoxalines **20–22** all provided their anticipated hydroxylated products **20a–22a** in good yields (72–84%). *N*-Substituted maleimides having long alkyl chain such as *n*-butylbenzene (**23**), *n*-heptyl (**24**), and *n*-decyl (**25**) all afforded their expected alcohols **23a** (81%), **24a** (76%), and **25a** (80%) in good yields (76–81%). Notably, substrates having free *N*-H (**26**) and *N*-chiral units bearing maleimides (**27** and **28**) were found compatible giving their awaited hydroxylated products **26a** (71%), **27a** (70%) and **28a** (77%) in modest yields. Interestingly, functional maleimides such as phenethyl amine (**29**), and thiophenethyl amine (**30**) all reacted smoothly to deliver their hydroxylated products **29a** (78%) and **30a** (74%) in moderate yields. Further, natural products *L*-menthol (**31**) and borneol (**32**) linked C3-maleimidated substrates having multiple tertiary C–H sites, the selective hydroxylation took place at the maleimide center only, providing their respective products **31a** (63%) and **32a** (74%). Such functionalized molecules possessing quaternary hydroxyl groups might show interesting biological activity. To showcase the feasibility of this protocol towards large-scale synthesis, the reaction was performed on a 1 mmol scale under the standard condition, which gave **1a** with 72% isolated yield (Scheme V.4.2 and Scheme V.5.4).

TH-3369_166122017

Scheme V.4.2. *Scope of tertiary C–H hydroxylation* [a,b]

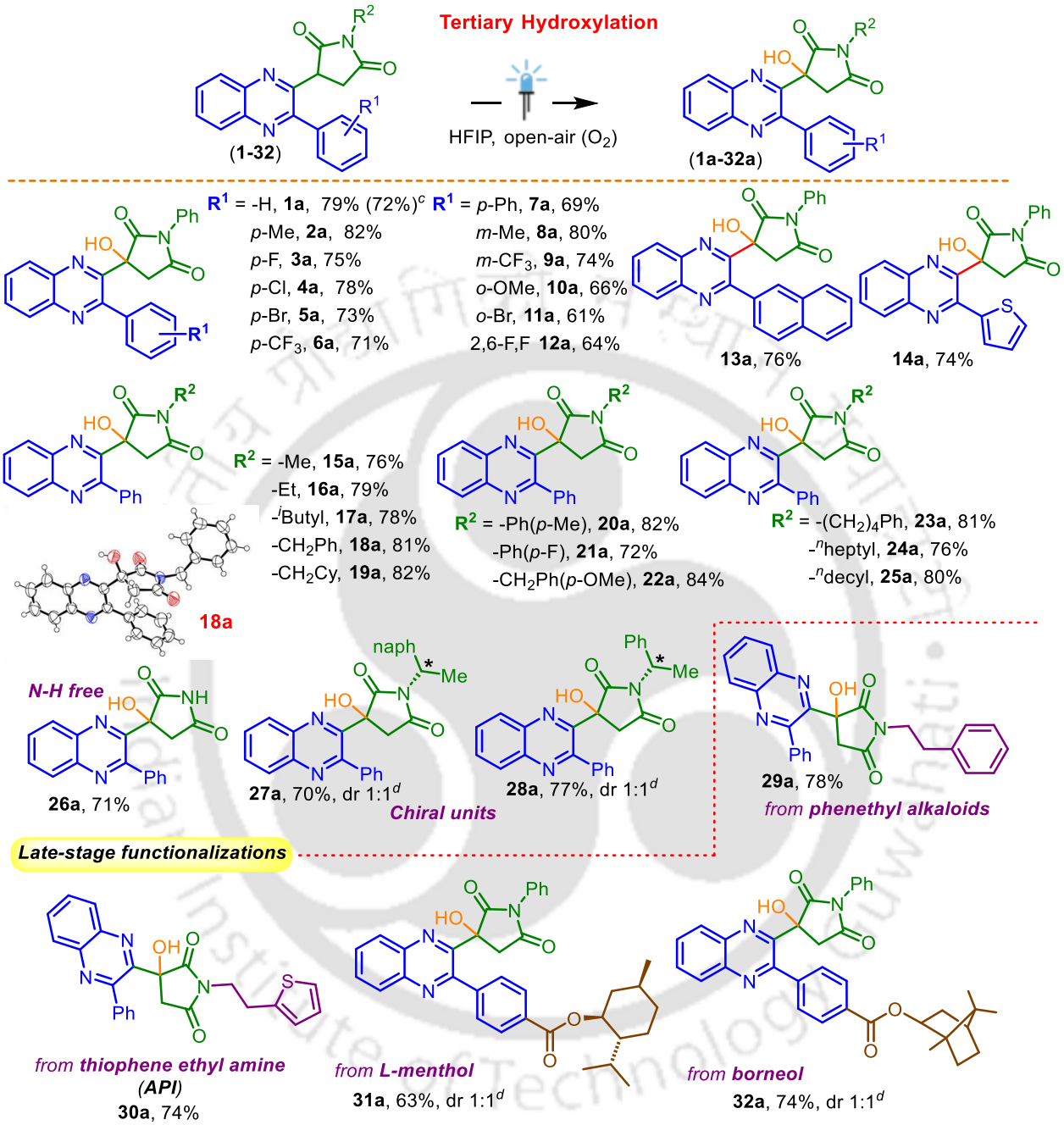

[a]*Reaction conditions:* ***1-32*** *(0.15 mmol) were dissolved in HFIP (0.15 M) and subjected to blue LEDs irradiation at 25-30 °C for 12 h under an open atmosphere.* [b]*Isolated yield after column chromatography.* [c]*Reaction at 1 mmol scale.* [d]*Based on* ^{1}*H NMR.*

TH-3369_166122017

Scope of *Spiro-Etherification*:

In the initial trial reaction (Table V.4.1, entry 1) and subsequently during solvent-dependent optimization using chlorobenzene, a spiro-ether (**1b**) was obtained as the major product (Table V.4.1, entry 9). Such photochemical "reagent less" etherification involving Csp^3–H and Csp^2–H is unparalleled. Thus, the scope and generality of spiro-etherification were also investigated by varying substituents on quinoxaline and maleimide units, and the results are summarized in Scheme V.4.3. A series of electronically varied substituents such as *p*–Me (**2**), *p*–F (**3**), *p*–Br (**5**), *m*–Me (**8**), and *m*–CF_3 (**9**) groups on the C2-aryl ring responded to this protocol providing their respective spirocyclic products (**2b**–**9b**) in 72-85% yields. Besides C-2 substituted aryl rings, 2-naphthyl (**13**) undergoes spiro cyclization at the C1 site of the naphthyl ring giving the product (**13b**) in 76% yield. However, a thiophenyl-bearing substrate (**14**) failed to provide its spiro-ether (**14b**), unlike its phenyl or naphthyl analogues. The C3 position of thiophene ring where the etherification is supposed to take place is electronically unfavorable or the generated radical is quenched by the sulfur atom of the substrate. Further, various *N*-substituted maleimides such as –Me (**15**), –Et (**16**), –^{i}Bu (**17**), and benzyl (**18**) all smoothly underwent spiro cyclization providing ethers **15b–18b** in good yields (75–80%). *N*-Arylated substrates having substituents such as *p*–Me (**20**), *p*–F (**21**), and *p*–OMe benzyl (**22**) all provided their desired spiro-ethers **20b** (84%), **21b** (73%), and **22b** (81%) respectively. Further, C3-maleimidated quinoxalines having long alkyl chains such as *n*-butylbenzene (**23**), *n*-heptyl (**24**), and *n*-decyl (**25**) all yielded their respective spiro-ethers **23b** (73%), **24b** (76%), and **25b** (77%). The free N-H substrate (**26**) provided spiro-ether **26b** in 70% yield. Interestingly, *N*-chiral tertiary scaffolds (**27**) and (**28**) both delivered their spiro-ethers **27b** (75%) and **28b** (78%) in good yields without affecting the chiral tertiary C–H site. Further, maleimides possessing functional *N*-substituents like phenethyl (**29**), and thiophenethyl (**30**) all afforded spiro-ethers (**29b**, 76%), and (**30b**, 72%). The natural products L-menthol (**31**) and borneol-linked (**32**) C3-maleimidated quinoxalines both reacted well to deliver the desired spiro products **31b** (66%) and **32b** (78%) respectively. Notably a tryptamine derived C3-maleimidated substrate (**33**) provided its spirocyclic ether **33b** in 70% isolated yield. The bis-maleimidated substrate **34** yielded the corresponding *bis*-spiro-ether (**34b**, 67%) thereby demonstrating the robustness of the developed protocol. Further, to showcase the feasibility of this protocol towards large-scale synthesis, the reaction was performed on a 1 mmol scale under the standard condition, which gave **1b** with 76% isolated yield (Scheme V.4.3 and Scheme V.5.5).

TH-3369_166122017

Scheme V.4.3. *Scope of Spiro-Etherification* [a,b]

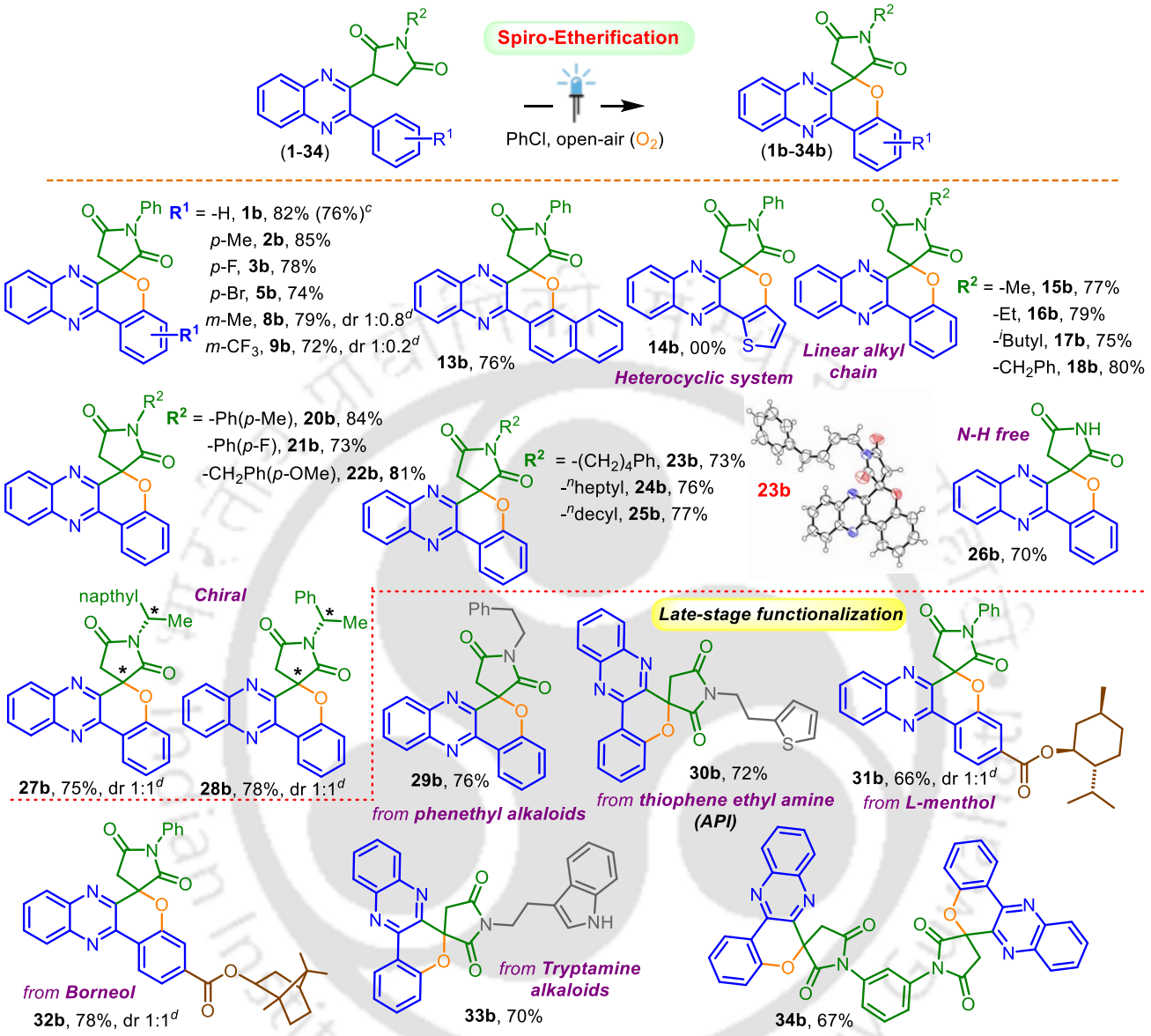

[a]Reaction conditions: ***1-34*** *(0.15 mmol) were dissolved in PhCl (0.15 M) and subjected to blue LEDs irradiation at 25-30 °C for 12 h under an open atmosphere. [b]Isolated yield after column chromatography. [c]Reaction at 1 mmol scale. [d]Based on ^{1}H NMR.*

Unusual Orthogonal Spiro-Etherification:

Recently, an intermolecular orthogonal C−O bond formation involving aryl-germanes and alkyl alcohols has been reported (Scheme V.4.4). Herein a Pd-catalyzed selective C–O cross-coupling took place at the C–Ge site even in the presence of other C–X sites (X = I, Br, Cl, F, OTf, Bpin).[17]

TH-3369_166122017

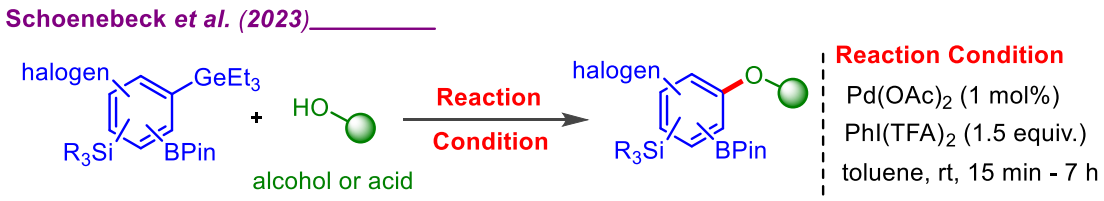

Scheme V.4.4. *Pd-catalyzed orthogonal C-O formation with organogermanes*

Now herein when the spiro-etherification strategy was extended to *ortho*-substituted C2-aryl ring of C3-maleimidated quinoxalines, an unusual "orthogonal spiro-etherification" was realized (Scheme V.4.5). For example, the C3-maleimidated quinoxaline (**10**) possessing an *o*-OMe on the C2-aryl ring, provided spiro-ether (**1b**, 72%) *via* the elimination of *o*-OMe group. Such an unusual *ipso* "oxy-demethoxylation" (spiro-cyclization) is unprecedented in the literature. Not only the –OMe group but also –OEt group as in **35** underwent similar "oxy-deethoxylation", giving the product **1b** in 78% yield. When a 2,6-difluoro-substituted C2-aryl (**12**) substrate was subjected to the present spiro-etherification condition it delivered mono-defluorinated spiro-ether **36b** in 68% with the loss of one of the *o*-fluoro group *via* "oxy-defluorination". Now the query arises in a mono *o*-fluoro substituted substrate (**36**) whether the spiro-etherification would take place at the *o*-C–H or the *o*-C–F site. Upon photo-irradiation, the mono-*o*-fluoro substrate (**36**) delivered de-fluorinated spiro-ether (**1b**, 65%) as the major product along with *o*-fluoro spiro-ether (**36b**, 22%) as the minor product suggesting a preferential *ipso* "oxy-defluorination" (Scheme V.4.5). On the contrary, an analogous mono-*o*-chloro substrate (**37**) having *o*-C–H and *o*-C–Cl sites provided non-dechlorinated spiro-ether (**37b**, 68%) as a major and oxy-dechlorinated spiro-ether (**1b**, 24%) as the minor product. Extending the scope to corresponding mono-*o*-bromo substrate (**11**) having *o*-C–H and *o*-C–Br sites yielded non-debrominated spiro-ether (**11b**, 60%) as the major and oxy-debrominated spiro-ether (**1b**, 15%) as the minor product (Scheme V.4.5). These observations suggest a preferential non-dechlorinative and non-debrominative spiro-cyclization over orthogonal spiro etherification involving the *o*-C–H site. Thus, the observed leaving tendency of halo substituents (–F > –Cl > –Br) in this radical-induced intramolecular spiro cyclization is similar to the aromatic nucleophilic substitution reaction (S_NAr). From these observations, the order of leaving group in this intramolecular spiroetherification *via* *ipso*-substitution follows the trend: –OEt ~ –OMe > –F > –H > –Cl > –Br.

TH-3369_166122017

Scheme V.4.5. *Scope of Orthogonal Spiro-Etherification* [a,b]

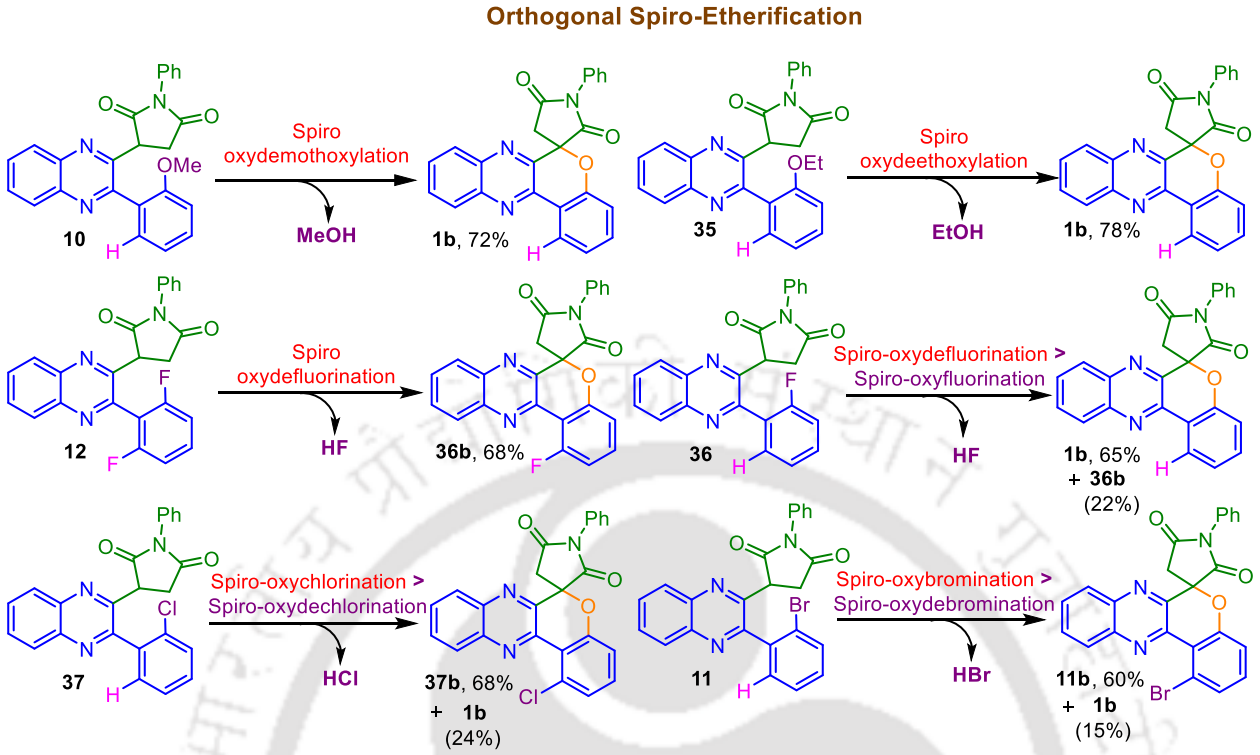

[a]*Reaction Conditions.* ***10***, ***11***, ***12***, ***35***, ***36*** *and* ***37*** *(0.15 mmol) were dissolved in PhCl (0.15 M) and subjected to blue LEDs irradiation at 25-30 °C for 12 h under an open atmosphere.* [b]*Isolated yield after column chromatography.*

Sunlight-Driven Oxygenation:

Any LED-mediated reactions require a specialized and expensive reaction setup. On the other hand, sunlight is the source of several wavelengths, in which the blue wavelength contributes up to 25%.[18] Thus, instead of a blue LED source some of the representative reactions were carried out under the irradiation of direct sunlight without stirring in a test tube (Scheme V.4.6A and Scheme V.5.6). C3-Maleimidated quinoxalines **1**, **5**, and **18** were irradiated under direct sunlight for 24 hours (over three days) in HFIP solvent in an open test tube as shown in Scheme 5A. Their corresponding *tert*-hydroxylated products (**1a**, 74%), (**5a**, 69%), and (**18a**, 77%) were obtained in comparable yields to that of blue LED mediated reactions (Scheme 2). Whereas for spiro-etherification in chlorobenzene, the substrates **1**, **5**, and **18** all provide their corresponding spiro-ethers **1b** (77%), **5b** (67%), and **18b** (74%) when irradiated under direct sunlight for 24 hours (8 h each for three days). The sunlight-driven oxygenation reactions efficiently delivered hydroxylated adduct **1a** (67%) and spiro-ether **1b** (70%) even at 1 mmol scale (Scheme V.4.6A).

TH-3369_166122017

Scheme V.4.6. *Sunlight-driven Oxygenation[a,b] and UV-vis Analysis of C3-maleimidated Quinoxaline*

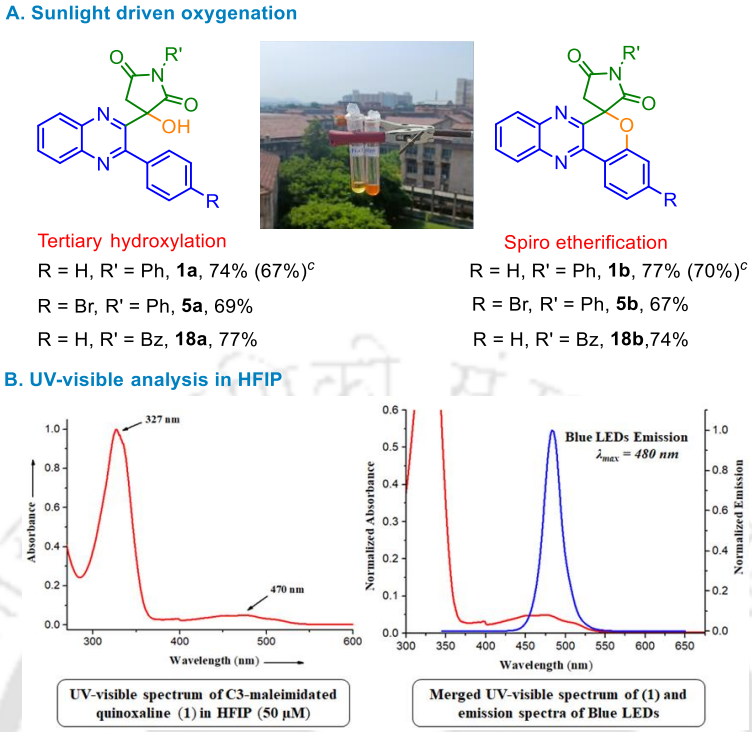

A. *Sunlight-driven oxygenation.* [a]*Reaction Conditions for hydroxylation,* ***1****,* ***5****, and* ***18*** *(0.15 mmol) were dissolved in HFIP (0.15 M) and for etherification,* ***1****,* ***5****, and* ***18*** *(0.15 mmol) were dissolved in PhCl (0.15 M) then subjected to Sunlight irradiation for 24 h (over 3 days) under an open atmosphere.* [b]*Isolated yield after column chromatography.* [c]*Reaction performed at 1 mmol scale. Isolated yields are reported.* ***B.*** *UV-visible analysis of (****1****) in HFIP and emission spectrum of blue LEDs.*

Mechanistic Studies:

To elucidate a plausible reaction mechanism, various control experiments were performed (Scheme V.4.7). At first, subjecting both the standard tertiary hydroxylation and spiro-etherification in the absence of light failed to provide any products suggesting the essential role of light and the photochemical nature of these reactions (Scheme V.4.7A). This suggests the self-photo-sensitization of the reacting substrate. To ascertain the light-absorbing species in this sensitizer-free transformation, UV-Vis absorption of C3-maleimidated quinoxaline (**1**) in HFIP and PhCl was recorded (Scheme V.4.6B; Figures V.5.4 and V.5.5). In HFIP, the absorption spectra of (**1**) showed a sharp peak at 327 nm and a broad-weak absorption around 470 nm. The emission spectrum of the used blue LEDs light was observed at 480 nm, which overlaps with the weak absorption band region (~470 nm) of C3-maleimidated quinoxaline (**1**) (Scheme V.4.6B). This suggests that the light-absorbing species is not the C3-maleimidated quinoxaline (**1**). The observed broad absorption at a higher wavelength is due to its O–H or N–H tautomer, which may be the possible photo-absorbing species.

TH-3369_166122017

Further, the involvement of reactive radical intermediate has been confirmed by TEMPO and BHT-mediated radical quenching and trapping experiments (Scheme V.4.7B). Both these photochemical reactions were completely retarded in the presence of radical scavengers TEMPO or BHT (Scheme V.4.7B). The corresponding TEMPO (**I**) and BHT (**II**) trapped adducts were also detected by ESI-MS analysis (Figures V.5.6, V.5.7, V.5.8 and V.5.9), confirming the radical nature of both these processes. Further, to reconfirm the radical nature of the reaction a spin-trapping experiment was conducted using 5,5-dimethyl-pyrroline *N*-oxide (DMPO). After the addition of DMPO and continuing the reaction for a further period of 30 min, a small amount of the reaction aliquot was subjected to EPR analysis at room temperature. The appearance of a strong EPR signal (Scheme V.4.7C and Scheme V.5.13) confirmed the radical nature of the reaction. Subsequently, the formation of DMPO-trapped adduct (**III**) was also detected by ESI-MS (Figure V.5.10). The atmospheric oxygen or moisture are two possible sources of hydroxyl/ethereal oxygen in this photo oxygenation reaction. However, when the standard hydroxylation reaction was carried out in the presence of $H_2{}^{18}O$ under otherwise identical conditions no ^{18}O-labeled oxygenated product (**1a**) could be detected by HRMS analysis. This rules out moisture (water) as the possible source of hydroxyl oxygen in product (**1a**), and atmospheric oxygen to be the possible source of oxygen. Further, when the standard hydroxylation reaction was carried out in an inert nitrogen atmosphere using degassed HFIP solvent, the yield of the product (**1a**) dropped significantly (<5%) which is due to the lack of oxygen (Scheme V.4.7D).

Now the question arises whether the oxygen that is participating in the hydroxylation and etherification is singlet ($^1O_2$) or triplet ($^3O_2$) in nature. When the standard hydroxylation and etherification reactions were carried out in the presence of singlet oxygen scavenger DABCO (2.5 equiv.) no product formation was observed (Scheme V.4.7E). This result confirms the involvement of singlet oxygen in these oxygenation reactions. Next, the *in situ*-generated singlet oxygen was trapped using a stoichiometric quantity of 1,4-dimethyl naphthalene (**iv**) or 1,3-diphenylisobenzofuran (**v**). Their respective singlet oxygen-trapped adducts (**IV**) and (**V**) were detected by ESI-MS analysis of the reaction aliquots (Figures V.5.11, V.5.12, V.5.13 and V.5.14), thereby confirming the active involvement of singlet oxygen ($^1O_2$) (Scheme V.4.7E). Now another pertinent query arises is without the involvement of any photo sensitizers how such reactive singlet oxygen is generated? There is a possibility of triplet energy transfer (EnT) from the triplet state of the tautomer of (**1**) to the triplet oxygen ($^3O_2$) to generate reactive singlet oxygen ($^1O_2$). To verify our above assumption, these reactions in the presence of triplet quenchers such as 2,5-dimethylhexa-2,4-diene or perylene failed to yield any product. These results support the involvement of an energy transfer (EnT) path in this external

TH-3369_166122017

sensitizer-free oxygenation reaction (Scheme V.4.7F). A further query arises as to whether the spiro-ether (**1b**) obtained is from the hydroxylated product (**1a**) or *via* an independent path. To verify this, irradiation of blue LED light to the isolated hydroxylated product (**1a**) gave no spiro-ether (**1b**), thus ruling out its intermediacy (Scheme V.4.7G). If not the hydroxyl (**1a**), its radical (–O•) generated in the reaction medium during the photoactivation may be serving as the reactive species leading to spiro-ether (**1b**). To support our proposition, phenyliodine(III) *bis*(trifluoracetate) (PIFA), which is known to generate alkoxy radical from the corresponding alcohol was employed.[19] Thus, the treatment of (**1a**) with hypervalent PIFA (1.5 equiv.) under the irradiation of blue light provided the expected spiro-ether (**1b**) in 74% isolated yield, thus supporting the generation of an alkoxy radical intermediate (**D**) (Scheme V.4.7G).

Theoretical Calculations and Plausible Mechanism for Photo-Oxygenation:

Now, to understand the above photo-physical observation, the C3-maleimidated quinoxaline **1** and its possible tautomers were optimized in the gas phase and solvent medium (HFIP and PhCl using SMD model) and their energies {gas phase: normal font; in a solvent medium, HFIP: italics font, PhCl: bold font} were computed and compared. As expected, the ground state O-H (**A_0**) and N-H (**A_0'**) tautomers were found to be higher in energy by 10.8/*13.3*/**11.5** and 3.4/*12.5*/**2.6** kcal/mol, respectively (Scheme V.4.8 and Figure V.4.1). On probing the vertical excitation of C3-maleimidated quinoxaline (**1**), the Franck-Condon state (**S_1**) was found to be 88.5/*116.1*/**89.2** kcal/mol higher as compared to the ground state (**S_0**). The corresponding triplet excited state of (**1**) was found to lie at 29.3/*57.6*/**31.2** kcal/mol, below the Franck-Condon state; interestingly, such states were also optimized for their tautomers, **A_0** and **A_0'**. However, the tautomer's corresponding excited states (singlet and triplet states) were found to be low-lying relative to that of (**1**). Using the optimized geometries of (**1**) and its tautomers (**A_0** and **A_0'**) at ωB97X-D/6-31G(d,p) level of theory, the electronic spectral data were computed in the gas phase and solvent medium (HFIP and PhCl). According to TD-DFT calculations, the C3-maleimidated quinoxaline (**1**) is expected to show no transition in the region above 350 nm. As the photocatalysis occurs at longer wavelengths, there is a possibility of solvent-dependent tautomeric equilibrium and the absorption of the light by the resulting tautomer (Table V.5.3 and Figure V.5.15). Indeed, the computed spectral data revealed that both **A_0'** (N-H tautomer) and its triplet state **$^3A_0$'**, exhibit absorption features at longer wavelengths than 375 nm. This indicates the possibility of a photochemical reaction originating from the tautomeric structures. Also, the solvent-dependent variation in the intensities supports the influence of solvent on the tautomeric equilibrium.

TH-3369_166122017

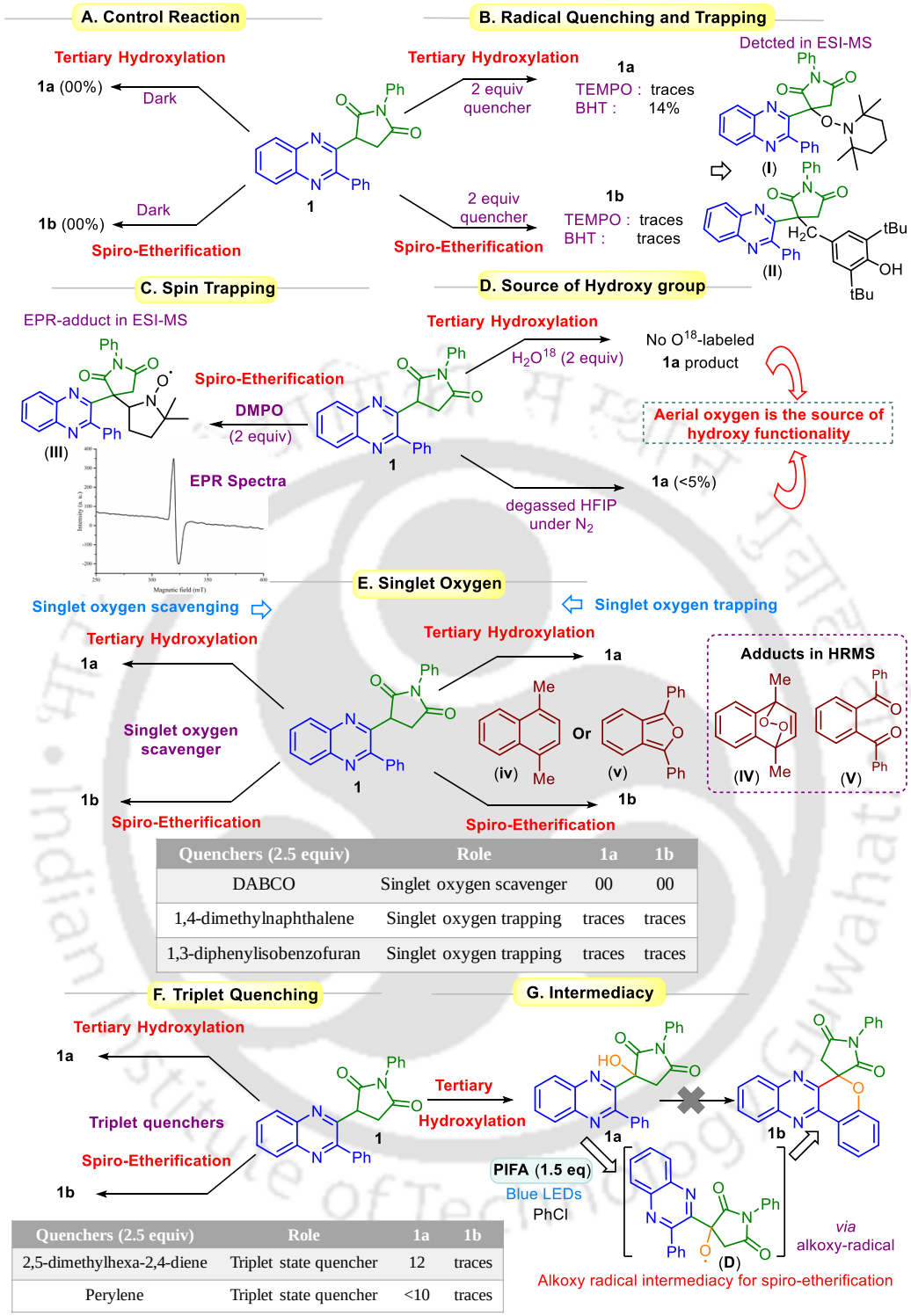

Quenchers (2.5 equiv)	Role	1a	1b
DABCO	Singlet oxygen scavenger	00	00
1,4-dimethylnaphthalene	Singlet oxygen trapping	traces	traces
1,3-diphenylisobenzofuran	Singlet oxygen trapping	traces	traces

Quenchers (2.5 equiv)	Role	1a	1b
2,5-dimethylhexa-2,4-diene	Triplet state quencher	12	traces
Perylene	Triplet state quencher	<10	traces

Scheme V.4.7. *Mechanistic studies*

Based on mechanistic studies, plausible mechanisms for both these oxygenation reactions are depicted in Scheme V.4.8. Due to the fact that the longer wavelength absorption is computationally predicted only for the N-H tautomer, possibly the tautomer **A₀'** of C3-maleimidated quinoxaline (**1**) upon photo-irradiation gets excited to its singlet state (^{1}**A₀'**), followed by an ISC to triplet state (^{3}**A₀'**).

TH-3369_166122017

This triplet species (^{3}**A$_0$'**) then transfers its energy to a triplet oxygen ($^3O_2$) generating singlet oxygen ($^1O_2$) and returns to the ground state (**A$_0$**) (Scheme V.4.8, path-I). This auto-sensitized photocatalytic cycle generates sufficient reactive singlet oxygen ($^1O_2$) for further reaction. The singlet oxygen produces a *tert*-radical species (**B**) and HOO$^\bullet$ *via* an ene-type reaction with (**A$_0$**). The formation of *tert*-radical species (**B**) has been confirmed by ESI-MS analysis of its radical trapped adduct with scavenger TEMPO and BHT (Scheme V.4.7B and Figures V.5.6, V.5.7, V.5.8 and V.5.9). Subsequently, the *tert*-radical (**B**) combines with HOO$^\bullet$ to provide a hydroperoxylated (**C**) intermediate, the formation of which has been confirmed by ESI-MS (Figure V.5.21). The photochemical homolytic cleavage of the peroxy bond in intermediate (**C**) produces a hindered *tert*-alkoxy radical (**D**) and a hydroxyl radical HO$^\bullet$. Recombination of two such hydroxyl radicals generates H_2O_2. The formation of H_2O_2 has been confirmed by $KMnO_4$ and iodometric tests (Figures V.5.19 and V.5.20). In HFIP solvent, a hydrogen atom transfer (HAT) lead to produce the hydroxylated product (**1a**). On the other hand, in an aprotic solvent PhCl, this alkoxy radical **D** underwent electrophilic radical addition at the *ortho*-position of the C2-phenyl ring to generate a spirocyclic de-aromatized radical intermediate (**E**). Now, abstraction of the adjacent *tert*-hydrogen from the intermediate (**E**) by HOO$^\bullet$ radical provides the spiro-ether (**1b**) with the release of H_2O_2. This is an excellent illustration of solvent-dependent selectivity. Despite this, the possible involvement of an O–H tautomer (**A$_0$**) in the above process, cannot be completely ruled out.

TH-3369_166122017

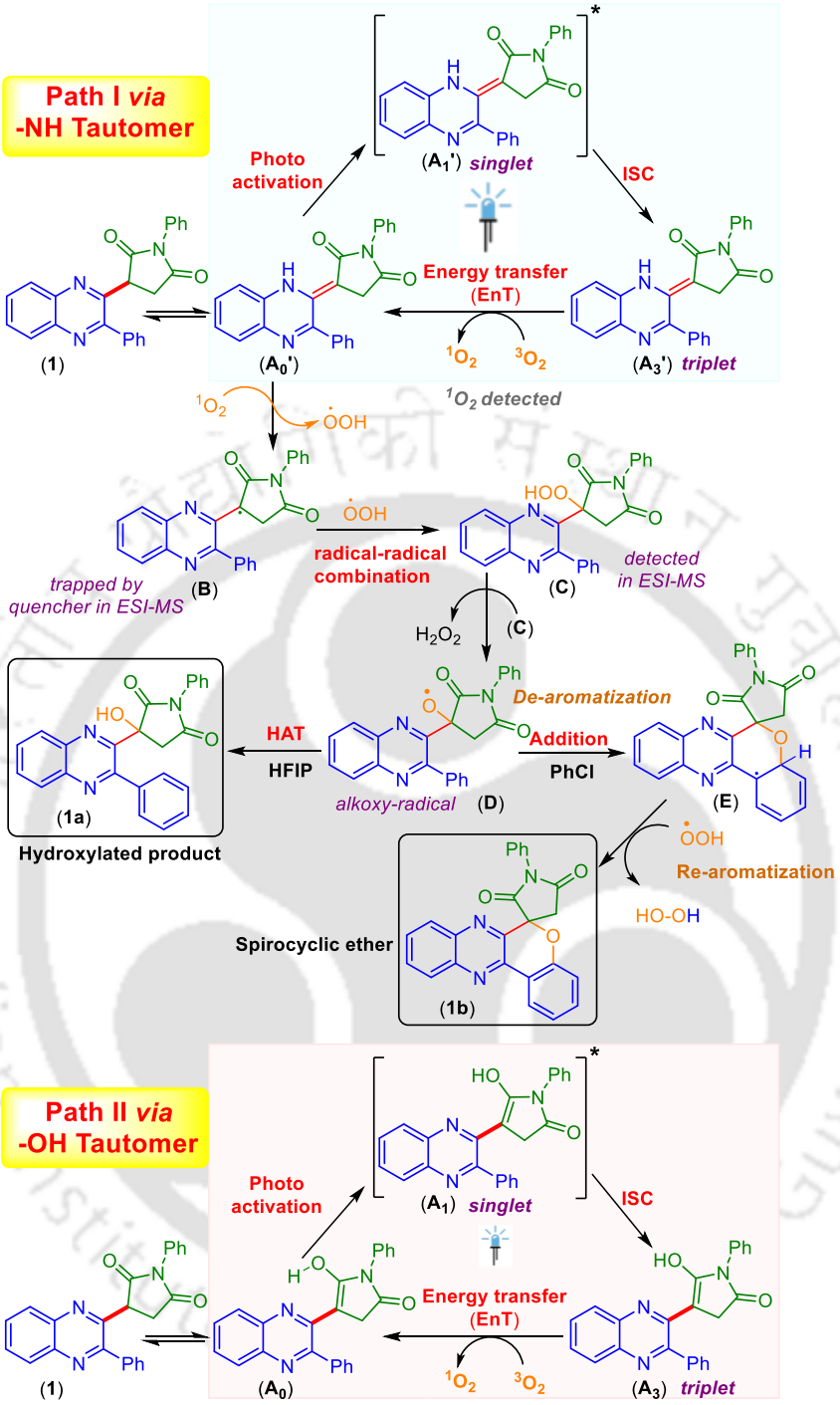

Scheme V.4.8. *Plausible mechanism of quaternary oxygenation reactions*

To gain further insights into solvent-dependent selectivity, the reaction pathways have been investigated in the gas phase and solvents (HFIP and PhCl) (Figure V.4.1, and Figure V.5.16). The thermal tautomerism channel between **1** and **A₀'** exhibited a high activation barrier ($\Delta G^{\#}$) of 53.9/*53.2*/**53.4** kcal/mol, which supports the importance of solvent-assisted tautomerism. Through

TH-3369_166122017

photochemical excitation of the tautomer of **1**, followed by ISC, the so-formed triplet species possibly transfer its energy in the generation of $^1O_2$ and self-relaxing to **A_0'**. Subsequently, the $^1O_2$ abstracts a proton from **A_0'** to create a radical species **B•** and HOO•. The radical species **B•** lies in a downhill potential (2.4/*17.8*/**4.4** kcal/mol) as to **A_0'**; the radical **B•** has a delocalized spin with larger spin accumulated on the *C*-centre and a lower spin delocalization at *N* and *O*-centers as evident from the spin density mapping (Figure V.4.1, Figure V.5.17). Furthermore, the radical species combines with HOO• to form the hydroperoxylated intermediate **C**, lying 41.0/*34.1*/**36.7** kcal/mol below **B•**. Considering the intermediates formed being lower in energy as compared to **A_0'**, the reaction until this point is exergonic. Later, the homolytic cleavage of the peroxy bond in intermediate **C** results in the formation of an alkoxy radical **D** and •OH. The **D** is found to be lying in the uphill potential above **C** (36.0/ *32.7*/**32.8** kcal/mol) indicating this step proceeds through a transition state **$TS_{C\text{-}D}$** with an energy barrier of 51.1/**52.6** kcal/mol.[20] Conversely, **D** in polar protic solvent (HFIP) leads to product **1a** lying 96.6/*98.6*/**97.3** kcal/mol in a downhill potential, whereas in the presence of aprotic solvent like PhCl, **D** gives an intermediate **E** with an estimated barrier of **3.1** kcal/mol. Eventually, the deprotonation of **E** gives the final product **1b**, which lies 61.5/*62.2*/**61.1** kcal/mol below **E**. It is noteworthy to mention that the phenyl ring (attached to quinoxaline part) in **D** exhibited a twist when PhCl is used as a solvent that allows a possible approach of the alkoxy radical to undergo radical addition-elimination channel at the *ortho* position (Figure V.5.18).

TH-3369_166122017

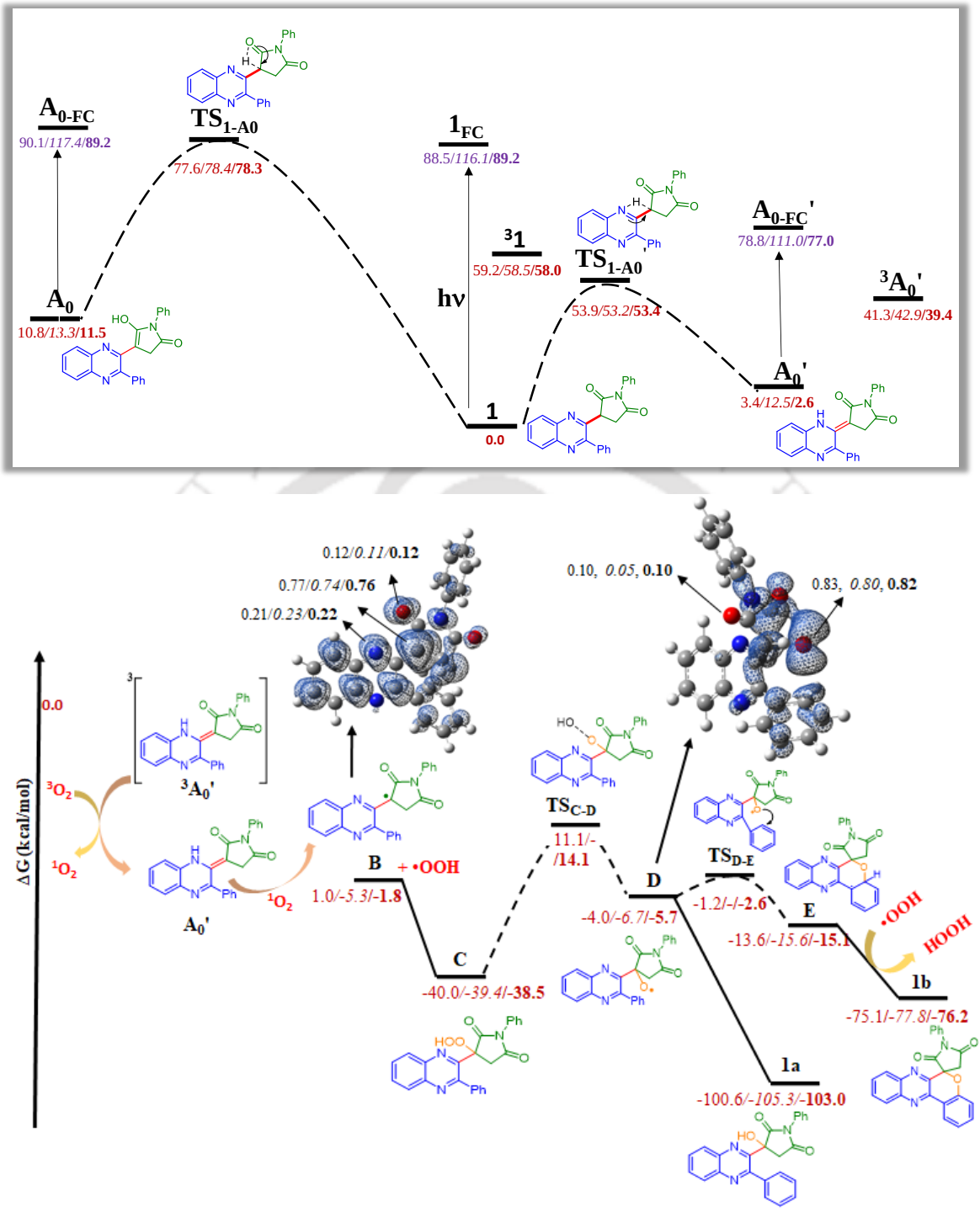

Figure V.4.1. *Energy profile diagram depicting the solvent-dependent product selectivity originating from the intermediate* ***D****. The thermal barriers corresponding to the formation of tautomers* ***A₀*** *and* ***A₀'*** *from* ***(1)****, their Franck Condon states, and their triplet states are included in the inset. The spin density plots corresponding to the radical intermediates* ***B*** *and* ***D*** *are also included. (The energy values in brown correspond to free energy changes accompanying the reactions, whereas those indicated in purple correspond to single point energies; the energy values are indicated as follows: Gas phase-normal, Solvent: HFIP-italics, Solvent: PhCl-bold).*

TH-3369_166122017

Post-Synthetic Modification:

Further, to demonstrate the practical utilities of the synthesized spiro-ethers a few post-synthetic modifications were carried out (Scheme V.4.9). The NH free spiro ether (**26b**) was efficiently propargylated (**26bb**, 77%) using propargyl bromide. The spiro-ether (**1b**) having N, C–H sites underwent efficient oxidative C–H/N annulation providing *N*-quaternized annulated product (**1bc**, 92%) in excellent yield when reacted with diphenylacetylene catalyzed by Ru(II).[21] The treatment of spiro-ether (**1b)** with *N*-bromosuccinimide (NBS) in the presence of *p*-toluene sulfonic acid (*p*-TSA) in acetonitrile afforded mono-brominated product (**1bd**, 94%) in excellent yield. This is a unique illustration of an ethereal oxygen-driven aromatic electrophilic bromination.

Scheme V.4.9. *Post-Synthetic Modifications*

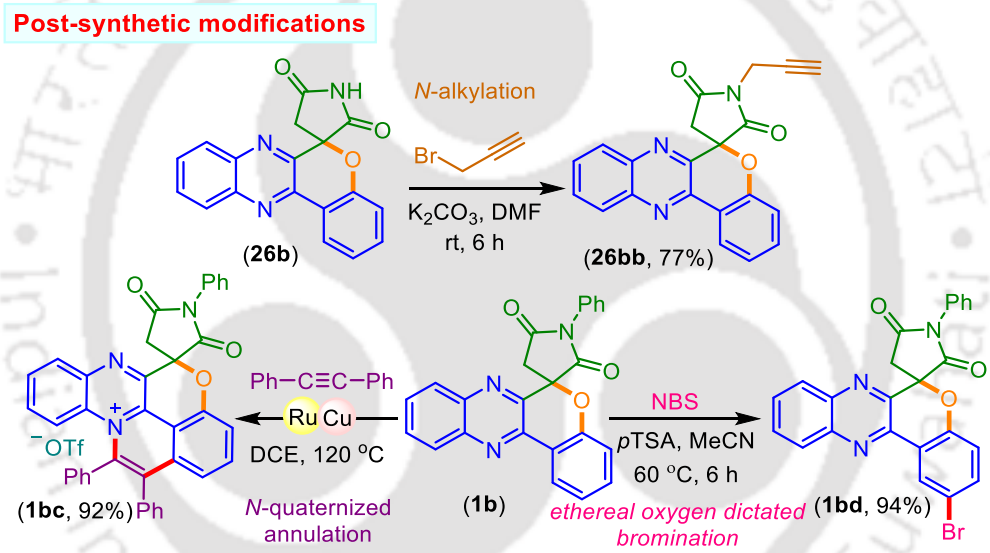

Reaction Conditions. (i) ***N-alkylation****. **26b** (0.1 mmol), K_2CO_3 (1.5 equiv), propargyl bromide (2.0 equiv) and DMF (1.5 mL) at rt for 6 h (ii)* ***N-quaternized annulation****. **1b** (0.1 mmol), diphenyl acetylene (1.5 equiv), $[Ru(p\text{-cymene})Cl_2]_2$ (5 mol%), $Cu(OAc)_2.H_2O$ (2.2 equiv), TfOH (1.5 equiv) and 1,2-DCE (1.5 mL) at 120 °C for 10 h. (iii)* ***Bromination****. **1b** (0.1 mmol), NBS (1 equiv), $pTSA.H_2O$ (1.2 equiv) and MeCN (1.5 mL) at 60 °C for 6 h.*

In conclusion, we have comprehended a photoinduced "self-sensitized" energy transfer enabled singlet O_2 driven tertiary hydroxylation at Csp^3–H and intramolecular spiro-etherification involving sp^3–sp^2 C–H bonds of C3-maleimidated quinoxalines. Most triplet energy transfer (EnT) processes require the assistance of an external triplet sensitizer. So far any "auto-sensitized" process leading to oxygenation is rare. The present process involves the exchange of triplet energy between the excited state substrate and triplet oxygen ($^3O_2$) to generate a reactive singlet oxygen ($^1O_2$) involving

TH-3369_166122017

photoactivation, ISC, and energy transfer (EnT). Remarkable solvent-dependent quaternary oxygenation has been observed. The *in situ*-generated alkoxy radical provides *tert*-hydroxylated product in HFIP, whereas in PhCl it underwent spirocyclization. Some interesting "orthogonal spiro-etherification" was noticed for *ortho*-substituted C2-aryl ring *via* the loss of *ortho* groups (*ipso* substitution). The order of leaving group ability during spiro-etherification for a set of *o*-substituents examined follows the trend –OEt ~ –OMe > –F > –H > –Cl > Br. The preferential oxy-demethoxylation and oxy-defluorination over regular radical-mediated nucleophilic substitution are noteworthy. This unique "self-sensitized" process avoids any metal catalyst/additive, external photosensitizer, or pre-functionalization and the possibility of using sunlight to showcase a divergent substrate scope involving many bioactive and functional cores.

V.5. Experimental Section

V.5.1. Experimental General Information: All the reagents were of commercial grade and purified according to the established procedures. All the reactions were carried out in oven-dried glassware. The highest commercial quality reagents were purchased and were used without further purification unless otherwise stated. Reactions were monitored by thin-layer chromatography (TLC) on a 0.25 mm silica gel plates (60 F_{254}) visualized under UV illumination at 254 nm. Organic extracts were dried over anhydrous sodium sulfate (Na_2SO_4). Solvents were removed using a rotary evaporator under reduced pressure. Column chromatography was performed to purify the crude product on silica gel 60–120 mesh using a mixture of hexane and ethyl acetate as eluents. All the isolated compounds were characterized by ^1H, $^{13}C\{^1H\}$ NMR, IR spectroscopic, and HRMS analysis. NMR spectra for all the samples were recorded in deutero-chloroform ($CDCl_3$) or deuterated dimethyl sulfoxide (DMSO-d_6). ^1H, $^{13}C\{^1H\}$ were recorded in 500 (126) or 400 (101) MHz spectrometer and were calibrated using tetramethylsilane or residual undeuterated solvent for ^1H NMR, deutero-chloroform for ^{13}C NMR as an internal reference {$Si(CH_3)_4$: 0.00 ppm or $CHCl_3$: 7.26 ppm for ^1H NMR, 77.16 ppm for ^{13}C NMR or $(CH_3)_2SO$: 2.50 ppm for ^1H NMR, 39.52 ppm for ^{13}C NMR}. The chemical shifts are quoted in δ units, parts per million (ppm). ^1H NMR data is represented as follows: Chemical shift, multiplicity (s = singlet, d = doublet, t = triplet, q = quartet, m = multiplet, dd = doublet of doublet, integration and coupling constant(s) *J* in hertz (Hz). High-resolution mass spectra (HRMS) were recorded on a mass spectrometer using electrospray ionization-time of flight (ESI-TOF) reflection experiments. FT-IR spectra were recorded as neat and reported in the frequency of absorption (cm^{-1}).

TH-3369_166122017

V.5.2. Theoretical General Information:

To elucidate the mechanism, density functional theory (DFT)[22] calculations have been performed using ωB97X-D[23] functional in conjugation with 6-31G(d,p)[24] basis set using SMD[25] solvent model for hexafluoroisopropanol (HFIP) and chlorobenzene (PhCl). For obtaining the solvent parameters for HFIP, those of isopropanol were used and the dielectric constant of it was modified for HFIP[26] (ε = 16.7) by using the keywords "scrf = (smd, solvent = 2-propanol, read)" in the Gaussian 09. The vibrational analysis was taken into account at the same level for each structure to ensure that the structure is a true minimum (with zero imaginary vibrational frequency) and first-order saddle point corresponding to the transition state (with one imaginary vibrational frequency). All the quantum chemical calculations were performed using the Gaussian 09 suite of program.[27] In order to obtain UV-Vis spectral data, TD-DFT[28] calculations have been performed using the ωB97X-D/6-31G(d,p) optimized geometries with n = 60 states. All TD-DFT calculations were performed in Gaussian16 program.[29] For non-covalent interactions (NCI) and Atoms in molecules (AIM) analysis, an open-source multiwfn program was used.[30,31]

V.5.3. Experimental Description:

(a) Photochemical Set-up for Blue LEDs and Sunlight Irradiation:

A rebel quads blue LEDs (λ_{em}^{max} = 480 nm, 4 × 3W) module was used as the light source for carrying out these photo-oxygenation reactions without using any filter. A borosilicate 10 mL oven-dried glass vial was used as the reaction vessel. The distance from the light source to the irradiation vessel was ~1-2 cm. A DC fan was used to ventilate the area to maintain the temperature 25–30 ºC. A typical reaction setup for blue LEDs and sunlight irradiations is portrayed below (Figure V.5.1).

TH-3369_166122017

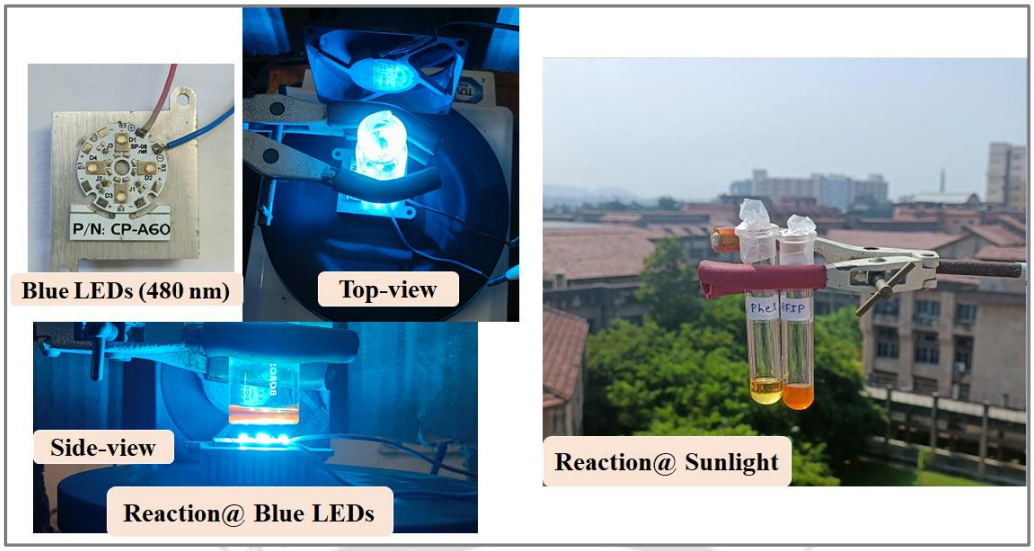

Figure V.5.1. *Typical photochemical reaction set-up under Blue LEDs* (*inside the Laboratory*) *and Sunlight* (*on the rooftop*) *irradiation*

(b) General Procedure for the Synthesis of C3-Maleimidated Quinoxalines:

All the C3-maleimidated quinoxalines (**1**–**37**) were synthesized by following the reported method.[32] In general an oven-dried 25 mL round-bottom flask was charged with 2-aryl quinoxaline (0.5 mmol, 1 equiv), maleimide (0.7 mmol, 1.4 equiv), $Mn(CO)_5Br$ (10 mol%, 0.1 equiv), NH_4OAc (30 mol%, 0.3 equiv) and a magnetic bead in ethyl acetate (2 mL) under an open atmosphere and was refluxed in an oil bath at 100 ^oC for 9 h. The progress of the reaction was monitored by TLC. After completion of the reaction, the reaction mixture was then mixed with water (5 mL) and extracted with ethyl acetate (2 x 10 mL). The organic layer was dried over anhydrous sodium sulfate and was evaporated under reduced pressure. Then the crude mixture was purified over column chromatography (60-120 mesh silica) by eluting hexane/EtOAc mixtures to afford the C3-maleimidaed quinoxalines **1**–**37**.

(c) General Procedure for Tertiary Hydroxylation Reaction:

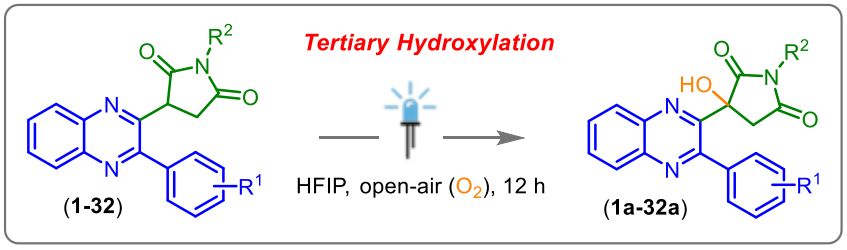

Scheme V.5.1. *Typical Tertiary Hydroxylation Reaction*

TH-3369_166122017

An oven-dried 10 mL glass vial was charged with C3-maleimidated quinoxaline (**1**–**32**, 0.15 mmol) and a magnetic stir bar in 1,1,1,3,3,3-hexafluoroisopropanol (HFIP) (1 mL, 0.15 M) and was stirred at room temperature in an open-air for 12 h under the irradiation of blue LEDs (λ_{em}^{max} = 480 nm, 4 × 3W) approximately at a distance of ~1-2 cm. The progress of the reaction was monitored *via* TLC. After completion of the reaction, the solvent was removed by rotary evaporation. The obtained residue was then directly purified over column chromatography by eluting hexane/EtOAc mixtures to afford desired tertiary hydroxylated adducts **1a**–**32a**.

(d) General Procedure for Spiro-Etherification Reaction:

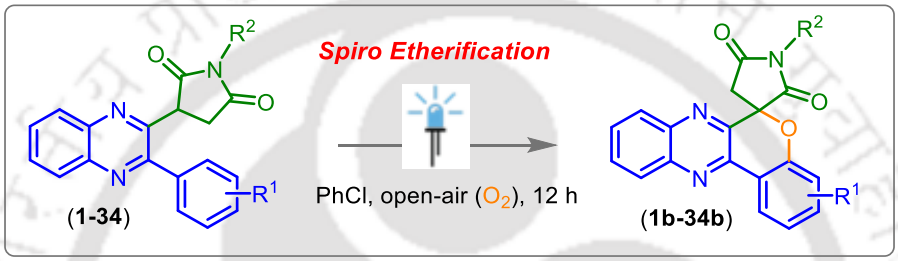

Scheme V.5.2. *Typical Spiro-Etherification Reaction*

An oven-dried 10 mL glass vial was charged with C3-maleimidated quinoxaline (0.15 mmol) and a magnetic stir bar in chlorobenzene (PhCl) (1 mL, 0.15 M) and was stirred at room temperature in open-air for 12 h under the irradiation of blue LEDs (λ_{em}^{max} = 480 nm, 4 × 3W) approximately at a distance of ~1-2 cm. The progress of the reaction was monitored *via* TLC. After completion of the reaction, the reaction mixture was then mixed with water (5 mL) and extracted with dichloromethane (2 x 10 mL). The organic layer was dried over anhydrous sodium sulfate and was evaporated under reduced pressure. Then the crude mixture was purified over column chromatography (60-120 mesh silica) by eluting hexane/EtOAc mixtures to afford desired spiro-cyclic ether adducts.

(e) General Procedure for Orthogonal Spiro-Etherification:

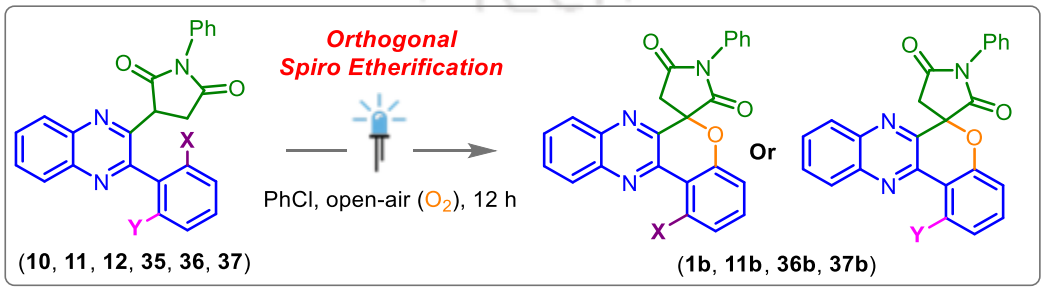

Scheme V.5.3. *Typical Orthogonal Spiro-Etherification Reaction*

TH-3369_166122017

An oven-dried 10 mL glass vial was charged with C3-maleimidated quinoxaline (**10**, **11**, **12**, **35**, **36**, **37**; 0.15 mmol) and a magnetic stir bar in chlorobenzene (PhCl) (1 mL, 0.15 M) and was stirred at room temperature in an open-air for 12 h under the irradiation of blue LEDs (λ_{em}^{max} = 480 nm, 4 × 3W) approximately at a distance of ~1-2 cm. The progress of the reaction was monitored *via* TLC. After completion of the reaction, the reaction mixture was then mixed with water (5 mL) and extracted with dichloromethane (2 x 10 mL). The organic layer was dried over anhydrous sodium sulfate and was evaporated under reduced pressure. Then the crude mixture was purified over column chromatography (60-120 mesh silica) by eluting hexane/EtOAc mixtures to afford desired orthogonal spiro-cyclic ethers.

(d) General Procedure for Oxygenation Reaction at 1 mmol Scale:

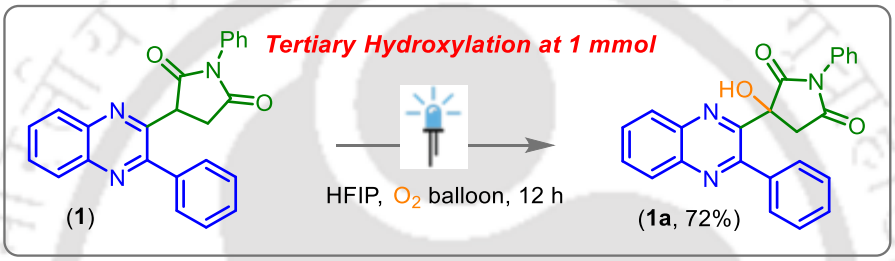

Scheme V.5.4. *Tertiary hydroxylation reaction at 1 mmol scale*

An oven-dried 10 mL glass vial was charged with C3-maleimidated quinoxaline (**1**, 1 mmol) and a magnetic stir bar in 1,1,1,3,3,3-hexafluoroisopropanol (HFIP) (4 mL, 0.25 M) and was stirred at room temperature under an O_2 atmosphere for 12 h under the irradiation of blue LEDs (λ_{em}^{max} = 480 nm, 4 × 3W) approximately at a distance of ~1-2 cm. The progress of the reaction was monitored *via* TLC. After completion of the reaction, the solvent was removed by rotary evaporation. The obtained residue was then directly purified over column chromatography by eluting hexane/EtOAc mixtures (85/15) to afford the desired tertiary hydroxylated adducts **1a** (72%).

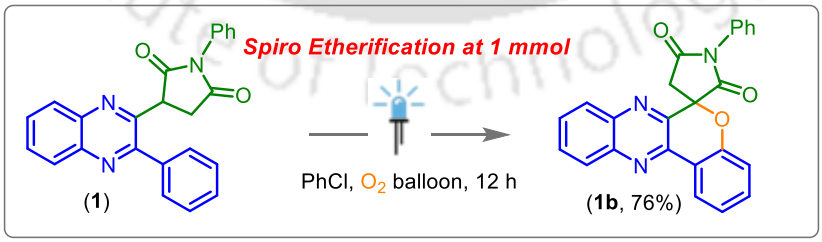

Scheme V.5.5. *Spiro-Etherification reaction at 1 mmol scale*

An oven-dried 10 mL glass vial was charged with C3-maleimidated quinoxaline (**1**, 1 mmol) and a magnetic stir bar in chlorobenzene (PhCl) (4 mL, 0.25 M) and was stirred at room temperature

TH-3369_166122017

under an O_2 atmosphere for 12 h under the irradiation of blue LEDs (λ_{em}^{max} = 480 nm, 4 × 3W) approximately at a distance of ~1-2 cm. The progress of the reaction was monitored *via* TLC. After completion of the reaction, the reaction mixture was then mixed with water (5 mL) and extracted with dichloromethane (3 x 10 mL). The organic layer was dried over anhydrous sodium sulfate and was evaporated under reduced pressure. Then the crude mixture was purified over column chromatography (60-120 mesh silica) by eluting hexane/EtOAc mixtures (93/07) to afford the desired spiro-cyclic ether adduct **1b** (76%).

(e) General Procedure for Sunlight-Driven Oxygenation Reaction:

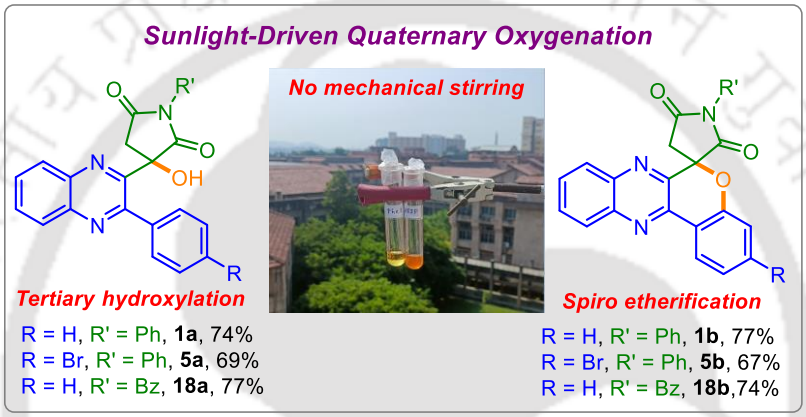

Scheme V.5.6. *Sunlight-driven oxygenation reaction*

Tertiary Hydroxylation.

An oven-dried 10 mL glass tube was charged with C3-maleimidated quinoxaline (**1**, **5**, **18**; 0.15 mmol) in 1,1,1,3,3,3-hexafluoroisopropanol (HFIP) (1 mL, 0.15 M) and was irradiated under bright Sunlight in open-air for 24 h (over a period of 3 days). The progress of the reaction was monitored *via* TLC. After completion of the reaction, the solvent was removed by rotary evaporation. The obtained residue was then directly purified over column chromatography by eluting with hexane/EtOAc mixtures to afford the desired tertiary hydroxylated adducts **1a** (74%), **5a** (69%), and **18a** (77%).

Spiro-Etherification.

An oven-dried 10 mL glass tube was charged with C3-maleimidated quinoxaline (**1**, **5**, **18**; 0.15 mmol) in chlorobenzene (PhCl) (1 mL, 0.15 M) and was irradiated under bright Sunlight in open-air for 24 h (over a period of 3 days). The progress of the reaction was monitored *via* TLC. After completion of the reaction, the reaction mixture was then mixed with water (5 mL) and extracted with

TH-3369_166122017

dichloromethane (2 x 10 mL). The organic layer was dried over anhydrous sodium sulfate and was evaporated under reduced pressure. Then the crude mixture was purified over column chromatography (60-120 mesh silica) by eluting with hexane/EtOAc mixtures to afford the desired spiro-cyclic ethers **1b** (77%), **5b** (67%), and **18b** (74%).

(f) General Procedure for Sunlight-Driven Oxygenation Reaction at 1 mmol scale:

Tertiary Hydroxylation at 1 mmol

An oven-dried 10 mL glass tube was charged with C3-maleimidated quinoxaline (**1**, 1 mmol) in 1,1,1,3,3,3-hexafluoroisopropanol (HFIP) (4 mL, 0.25 M) and was irradiated under bright Sunlight in an O_2 atmosphere for 24 h (over a period of 3 days). The progress of the reaction was monitored *via* TLC. After completion of the reaction, the solvent was removed by rotary evaporation. The obtained residue was then directly purified over column chromatography by eluting with hexane/EtOAc mixtures (85/15) to afford the desired tertiary hydroxylated adducts **1a** (67%).

Spiro-Etherification at 1 mmol

An oven-dried 10 mL glass tube was charged with C3-maleimidated quinoxaline (**1**, 1 mmol) in chlorobenzene (PhCl) (4 mL, 0.25 M) and was irradiated under bright Sunlight in an O_2 atmosphere for 24 h (over a period of 3 days). The progress of the reaction was monitored *via* TLC. After completion of the reaction, the reaction mixture was then mixed with water (5 mL) and extracted with dichloromethane (3 x 10 mL). The organic layer was dried over anhydrous sodium sulfate and was evaporated under reduced pressure. Then, the crude mixture was purified over column chromatography (60-120 mesh silica) by eluting with hexane/EtOAc mixtures (93/07) to afford the desired spiro-cyclic ethers **1b** (70%).

(g) General Procedure for Post-Synthetic Manipulations:

N-Alkylation:

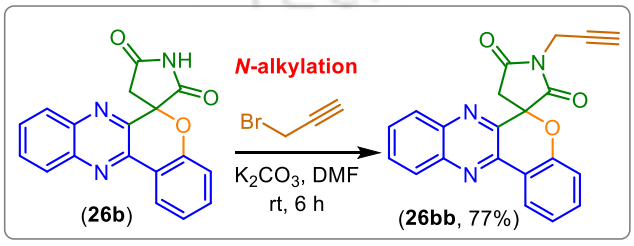

Scheme V.5.7. *N-Alkylation of* ***26b***

TH-3369_166122017

An oven-dried 10 mL round-bottom flask was charged with spiro[chromeno[3,4-*b*]quinoxaline-6,3'-pyrrolidine]-2',5'-dione (**26b**, 0.1 mmol, 32 mg), propergyl bromide (0.2 mmol, 24 mg), K_2CO_3 (0.15 mmol, 21 mg), and a magnetic bead in DMF (1.5 mL) under an open atmosphere and was stirred at room temperature for 6 h. The progress of the reaction was monitored by TLC. After completion of the reaction, the reaction mixture was then mixed with chilled water (5 mL) and extracted with ethyl acetate (2 x 10 mL). The organic layer was dried over anhydrous sodium sulfate and was evaporated under reduced pressure. Then the crude mixture was purified over column chromatography (60-120 mesh silica) by eluting it with hexane/EtOAc (95:05) mixture to afford the desired product **26bb** in 77% yield.

C-H/N-Oxidative Annulation:

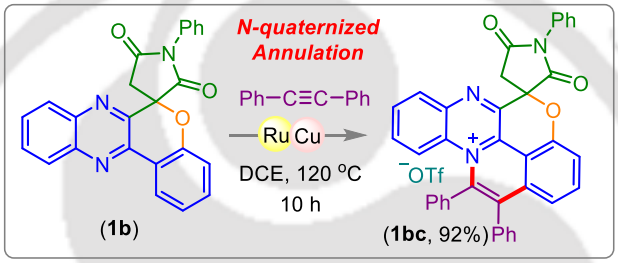

Scheme V.5.8. *C-H/N Annulation of* ***1b***

An oven-dried 10 mL round-bottom flask was charged with 1'-phenylspiro[chromeno[3,4-*b*]quinoxaline-6,3'-pyrrolidine]-2',5'-dione (**1b**, 0.1 mmol, 39 mg), diphenyl acetylene (0.15 mmol, 27 mg), [Ru(*p*-cymene)Cl_2]$_2$ (0.005 mmol, 3 mg), Cu(OAc)$_2$.H_2O (0.22 mmol, 44 mg) and a magnetic bead in 1,2-DCE (1.5 mL) under an open atmosphere and was refluxed in an oil bath at 120 °C for 10 h. The progress of the reaction was monitored by TLC. After completion of the reaction, the solvent was removed by rotary evaporation. Then the crude reaction mixture was directly purified over column chromatography (60-120 mesh silica) by eluting it with DCM/MeOH (97:03) mixture to afford the desired product **1bc** in 92% yield.

Ethereal Oxygen-dictated Bromination:

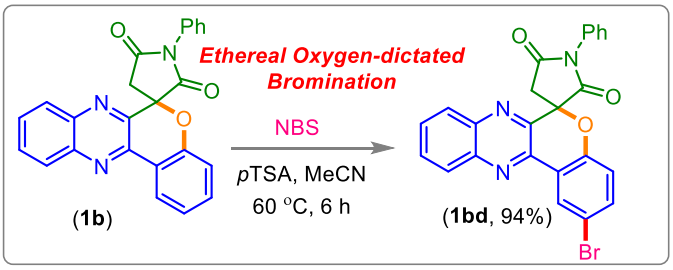

Scheme V.5.9. *Bromination of* ***1b***

TH-3369_166122017

An oven-dried 10 mL round-bottom flask was charged with 1'-phenylspiro[chromeno[3,4-*b*]quinoxaline-6,3'-pyrrolidine]-2',5'-dione (**1b**, 0.1 mmol, 39 mg), *N*-bromo succinimide (0.1 mmol, 18 mg), *p*-TSA.H_2O (0.12 mmol, 23 mg), and a magnetic bead in acetonitrile (1.5 mL) under an open atmosphere and was stirred in an oil bath at 60 ^oC for 6 h. The progress of the reaction was monitored by TLC. After completion of the reaction, the solvent was removed by rotary evaporation. Then, the reaction mixture was then mixed with water (5 mL) and extracted with ethyl acetate (2 x 10 mL). The organic layer was dried over anhydrous sodium sulfate and was evaporated under reduced pressure. Then the crude mixture was purified over column chromatography (60-120 mesh silica) by eluting it with hexane/EtOAc (92:08) mixture to afford the desired product **1bd** in 94% yield.

V.5.4. Crystallographic Description:

Crystal data were collected with Bruker Smart Apex-II CCD diffractometer using graphite monochromated MoKα radiation (λ = 0.71073 Å). Cell parameters were retrieved using SMART[a] software and refined with SAINT[a] on all observed reflections. Data reduction was performed with the SAINT software and corrected for Lorentz and polarization effects. Absorption corrections were applied with the program SADABS[b]. The structure was solved by direct methods implemented in SHELX-2014[c] program and refined by full-matrix least-squares methods on F2. All non-hydrogen atomic positions were located in difference Fourier maps and refined anisotropically. The hydrogen atoms were placed in their geometrically generated positions. Pale yellow crystals of **18a** were isolated from ethyl acetate solvent at room temperature. yellow crystals of **23b** were isolated from ethyl acetate solvent at room temperature.

a. SMART V 4.043 Software for the CCD Detector System; Siemens Analytical Instruments Division: Madison, WI, 2008.

b. SAINT Plus (v 6.14) Bruker AXS Inc., Madison, WI, 2008.

c. Sheldrick, G. M. SHELXL-2014, Program for the Refinement of Crystal Structures; University of Göttingen: Göttingen (Germany), 1997

TH-3369_166122017

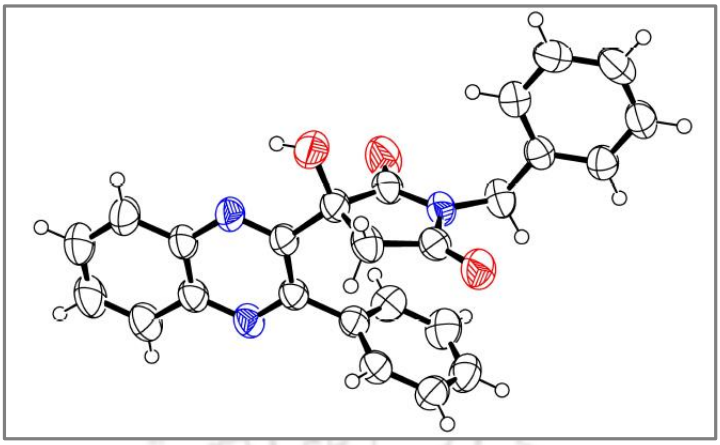

Figure V.5.2. *ORTEP diagram of* ***18a*** *with the thermal ellipsoids set at 50% probability*

Table V.5.1. Crystal Data Table for 18a

Empirical formula	$C_{25}H_{19}N_3O_3$
CCDC number	2308071
Formula weight	409.43
Temperature	293(2)
Wavelength	0.71073 Å
Crystal system	monoclinic
Space group	P21/c
Unit cell dimensions	a = 17.7801(14)) Å, b = 15.4535(12)Å, c = 7.6821(6) Å α= 90°, β= 101.114(2)°, γ= 90°
Volume	2071.2(3) $Å^3$
Z	4
Density (calculated)	1.313 g/cm^{-3}
Absorption coefficient	0.088
F(000)	856
Theta range for data collection	1.760 to 24.993°
Index ranges	-21 <= h <= 21, -18 <= k <= 18, -9<= l <= 9
Reflections collected	72869
Refinement method	Full-matrix least-squares on F2
Data / restraints / parameters	3618/ 0/ 281
Goodness-of-fit on F2	1.122
Final R indices [I>2sigma(I)]	0.0581, wR2 = 0.1684
R indices (all data)	0.0671, wR2 = 0.1883

TH-3369_166122017

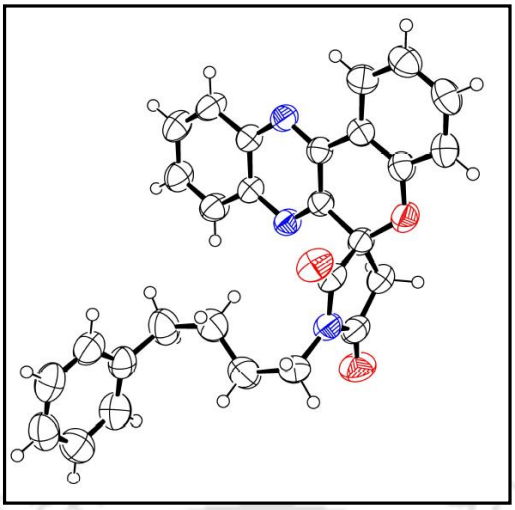

Figure V.5.3. *ORTEP diagram of* ***23b*** *with the thermal ellipsoids set at 50% probability*

Table V.5.2. Crystal Data table for 23b

Empirical formula	$C_{28}H_{23}N_3O_3$
CCDC number	2308235
Formula weight	449.49
Temperature	273(2)
Wavelength	0.71073 Å
Crystal system	monoclinic
Space group	P 21/c
Unit cell dimensions	a = 11.2065(19) Å, b = 21.982(4) Å, c = 9.0640(15) Å α= 90°, β= 95.383(5)°, γ= 90°
Volume	2223.0(6) $Å^3$
Z	4
Density (calculated)	1.343 g/cm^{-3}
Absorption coefficient	0.089
F(000)	944
Theta range for data collection	1.825 to 24.998°
Index ranges	-13 < = h < = 13, -24 < = k < = 24, -9< = l < = 10
Reflections collected	49624
Refinement method	Full-matrix least-squares on F2
Data / restraints / parameters	3680/ 0/ 307
Goodness-of-fit on F2	0.995
Final R indices [I>2sigma(I)]	0.0535, wR2 = 0.1486
R indices (all data)	0.0699, wR2 = 0.1747

TH-3369_166122017

V.5.5. Mechanistic Studies:

V.5.5.1. Dark (Absence of Light) Reaction:

Tertiary Hydroxylation under Dark

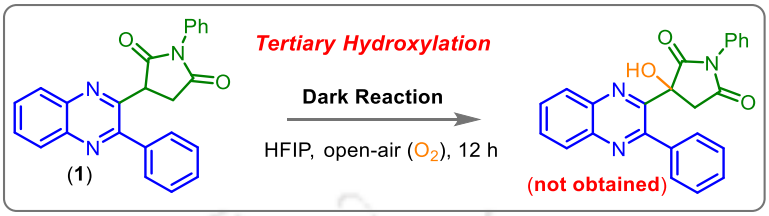

Scheme V.5.10. *Tertiary-hydroxylation reaction under dark*

An oven-dried 10 mL glass vial was charged with C3-maleimidated quinoxaline (**1**, 0.15 mmol) and a magnetic stir bar in 1,1,1,3,3,3-hexafluoroisopropanol (HFIP) (1 mL, 0.15 M) and was stirred at room temperature in open-air for 12 h under dark condition. The progress of the reaction was monitored *via* TLC, even after 12 h, the expected tertiary hydroxylated adduct was not observed. This observation suggests the essential role of photo-irradiation.

Spiro-Etherification under Dark

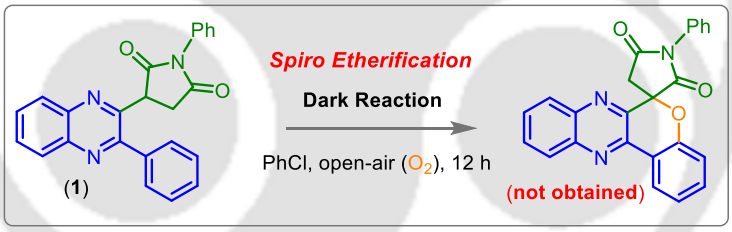

Scheme V.5.11. *Spiro-Etherification reaction under dark*

An oven-dried 10 mL glass vial was charged with C3-maleimidated quinoxaline (**1**, 0.15 mmol) and a magnetic stir bar in chlorobenzene (PhCl) (1 mL, 0.15 M) and was stirred at room temperature in open-air for 12 h under dark condition. The progress of the reaction was monitored *via* TLC, even after 12 h, the expected spiro-etherification adduct was not observed. This observation suggests the essential role of photo irradiation.

V.5.5.2. UV-visible analysis:

TH-3369_166122017

The UV-vis spectrum of (**1**) was recorded in HFIP at a conc. of 50 µM. The observed spectrum is portrayed below. Further to ascertain the light-absorbing species, this absorption spectrum was merged with the recorded emission spectra of used blue LEDs (Figure V.5.4).

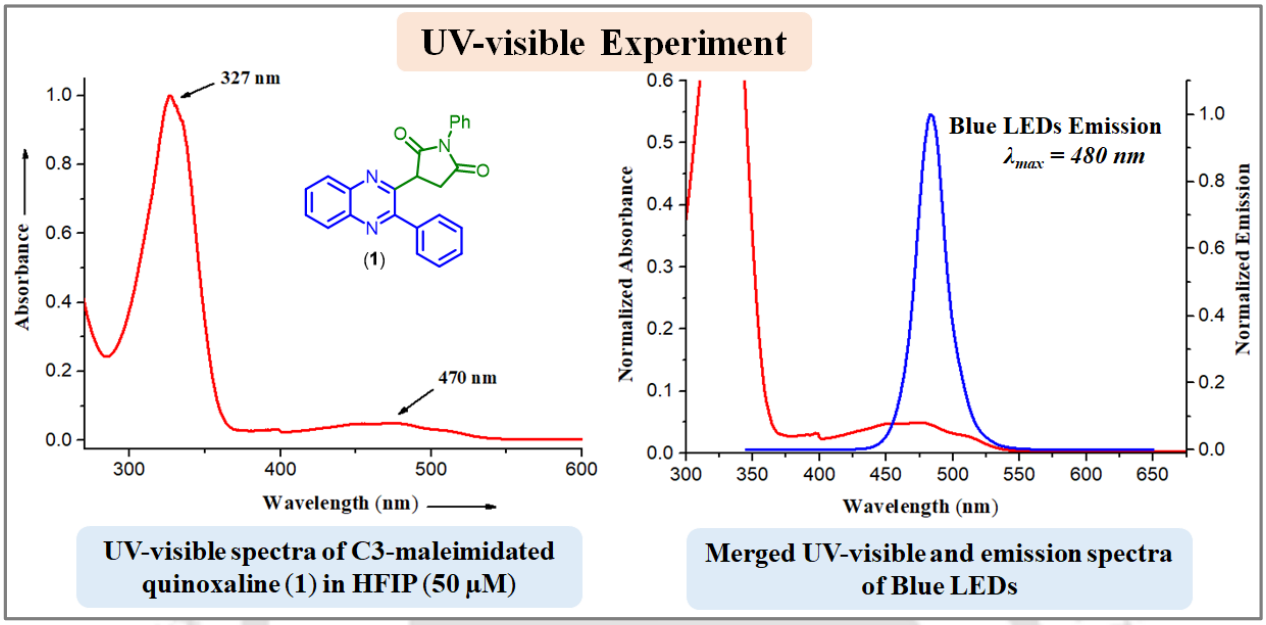

Figure V.5.4. *UV-visible spectrum of* ***1*** *and merged spectrum with the emission spectrum of blue LEDs*

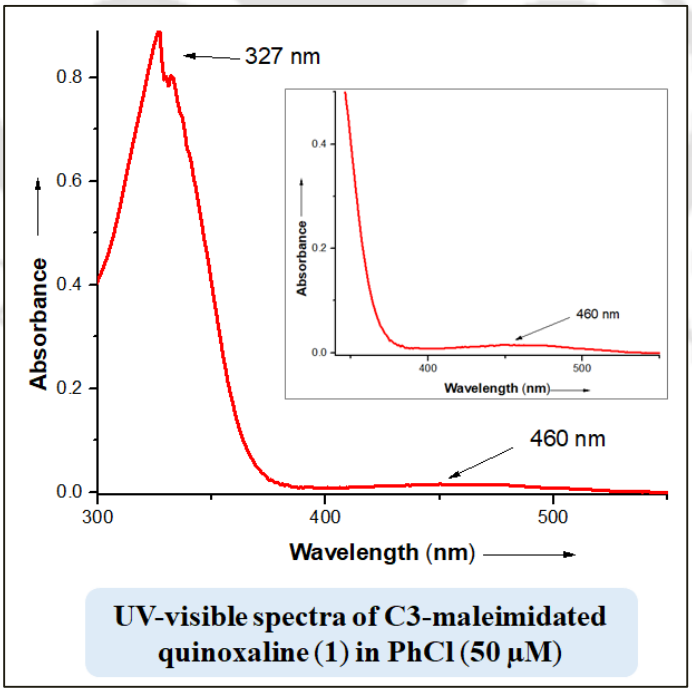

FigureV.5.5. *UV-visible spectrum of* ***1*** *in PhCl solvent. Inset: the zoomed version of 400-500 nm region*

V.5.5.3. Radical Quenching and Trapping:

TH-3369_166122017

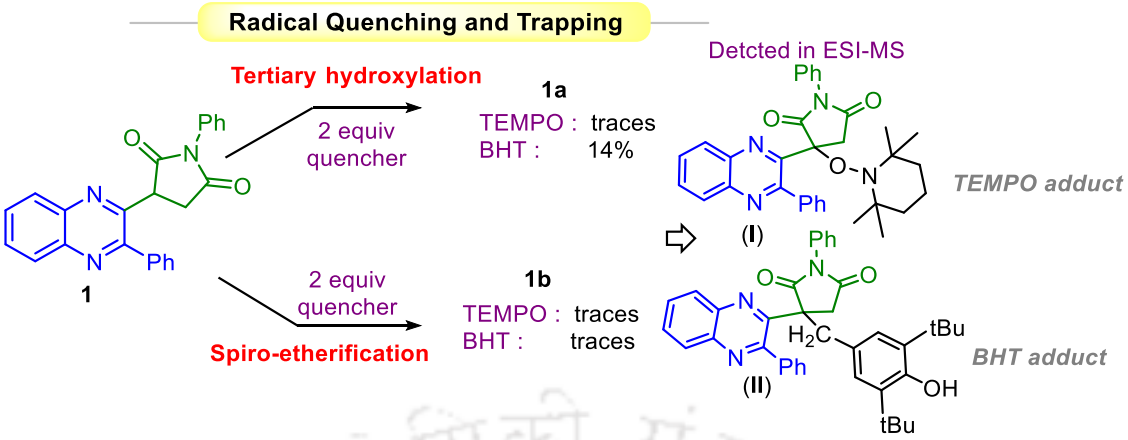

Scheme V.5.12. *Radical quenching and trapping by quenchers*

Tertiary Hydroxylation in Presence of Radical Quenchers

An oven-dried 10 mL glass vial was charged with C3-maleimidated quinoxaline (**1**, 0.15 mmol), 2,2,6,6-tetramethylpiperidine 1-oxyl (TEMPO) (0.30 mmol, 2 equiv.) or butylated hydroxytoluene (BHT) (0.30 mmol, 2 equiv.) and a magnetic stir bar in 1,1,1,3,3,3-hexafluoroisopropanol (HFIP) (1 mL, 0.15 M) and was stirred at room temperature in open-air for 12 h under the irradiation of blue LEDs (λ_{em}^{max} = 480 nm, 4 × 3W) approximately at a distance of ~1-2 cm. The progress of the reaction was monitored *via* TLC. After completion of the reaction, the solvent was removed by rotary evaporation. The obtained residue was then directly purified over column chromatography by eluting hexane/EtOAc mixtures to afford the desired tertiary hydroxylated adducts **1a**. In case of TEMPO, traces of **1a** was observed, whereas for BHT 14% of **1a** was isolated. This suggests the involvement of radical intermediate (Scheme V.5.12). Further, the plausible TEMPO and BHT trapped adducts (**I** and **II**) were detected by ESI-MS analysis of the reaction aliquot (Figure V.5.6 and V.5.7).

TH-3369_166122017

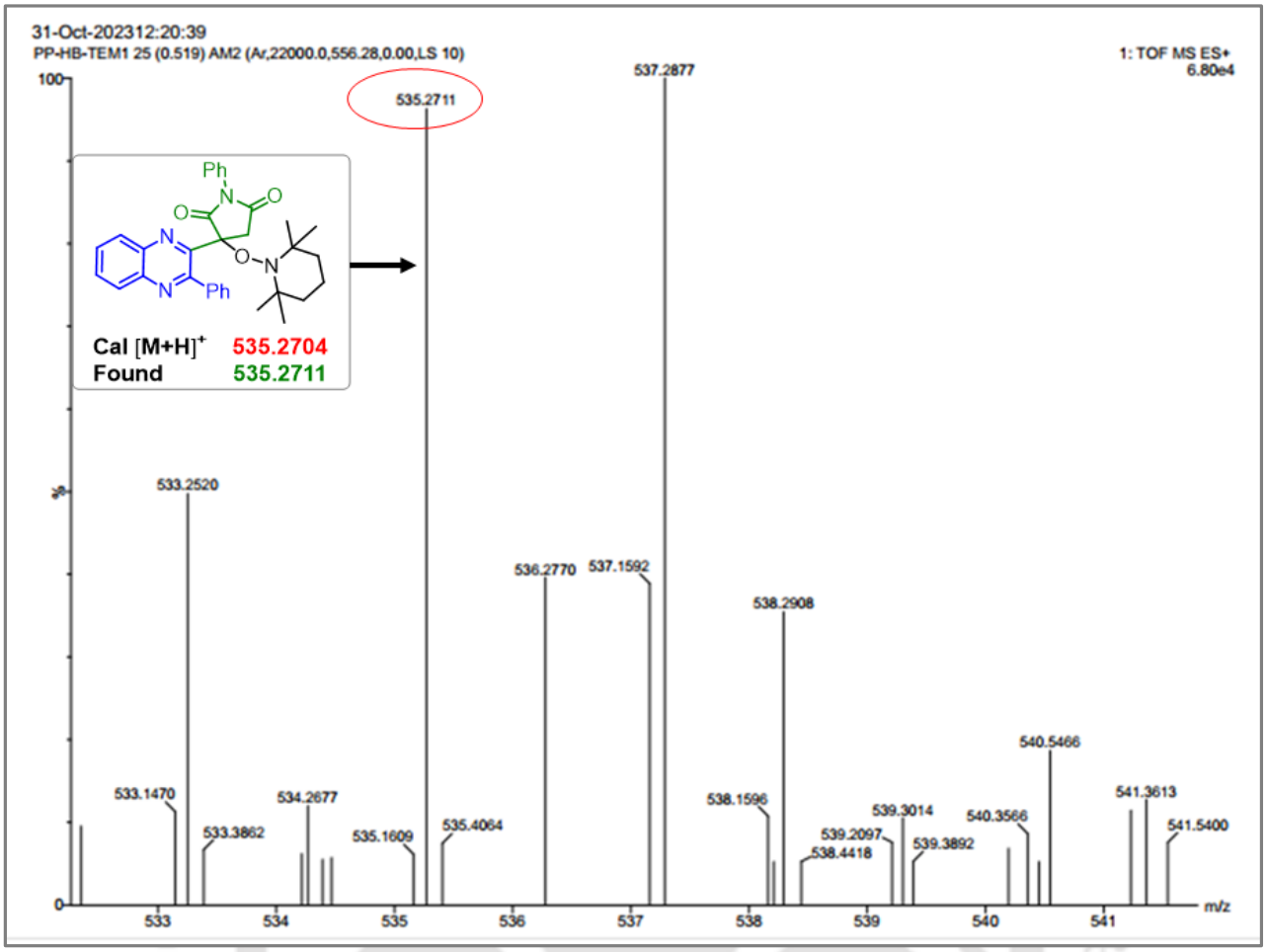

Figure V.5.6. *ESI-MS spectrum for TEMPO adduct* ***I*** *of tertiary hydroxylation reaction in HFIP*

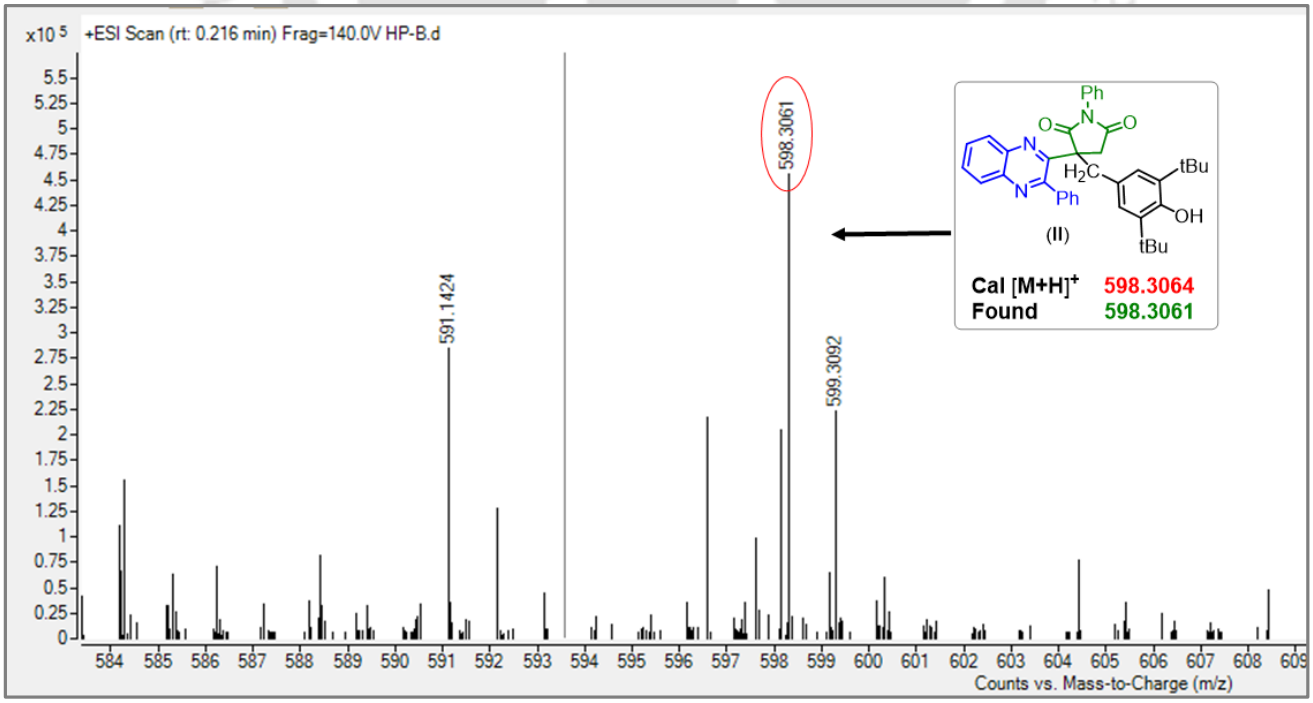

TH-3369_166122017

Figure V.5.7. *ESI-MS spectrum for BHT adduct* ***II*** *of tertiary hydroxylation reaction in HFIP*

Spiro-Etherification in the Presence of Radical Quenchers

An oven-dried 10 mL glass vial was charged with C3-maleimidated quinoxaline (**1**, 0.15 mmol), 2,2,6,6-tetramethylpiperidine 1-oxyl (TEMPO) (0.30 mmol, 2 equiv.) or butylated hydroxytoluene (BHT) (0.30 mmol, 2 equiv.) and a magnetic stir bar in chlorobenzene (PhCl) (1 mL, 0.15 M) and was stirred at room temperature in open-air for 12 h under the irradiation of blue LEDs (λ_{em}^{max} = 480 nm, 4 × 3W) approximately at a distance of ~1-2 cm. The progress of the reaction was monitored *via* TLC. After 12 h of the reaction, for both TEMPO and BHT case, very traces of the spiro-cyclized ether **1b** was observed. This observation supports the involvement of radical intermediate. Further, the plausible TEMPO and BHT trapped adducts (**I** and **II**) were detected by ESI-MS analysis of the reaction aliquot (Figure V.5.8 and V.5.9).

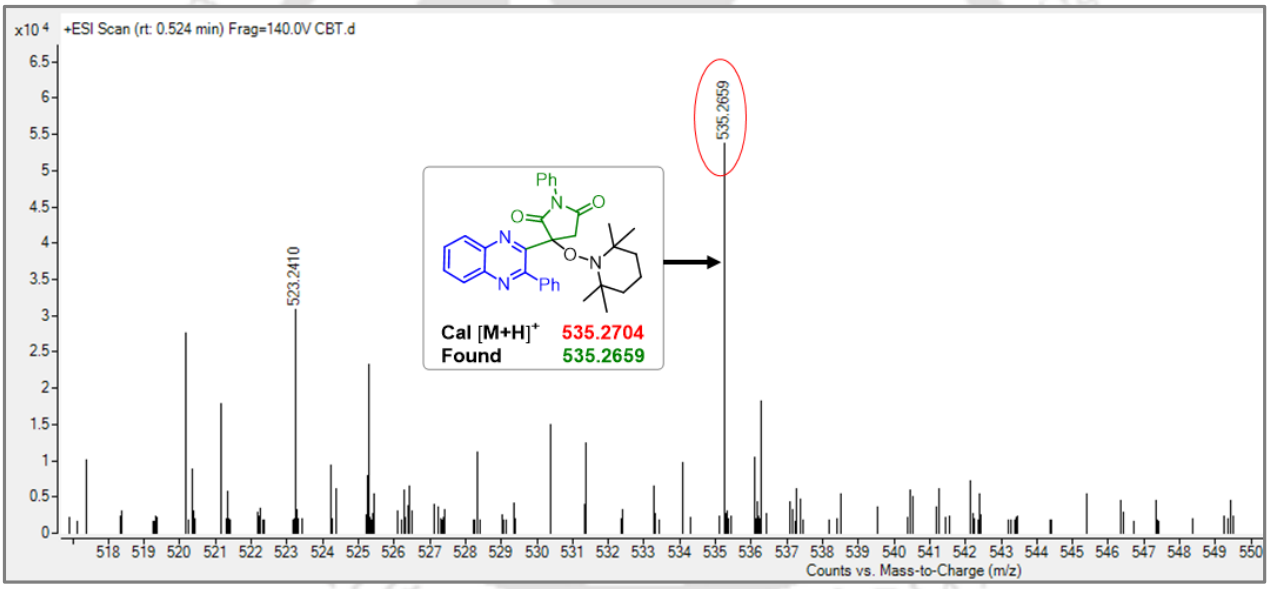

Figure V.5.8. *ESI-MS spectrum for TEMPO adduct* ***I*** *of Spiro-Etherification reaction*

TH-3369_166122017

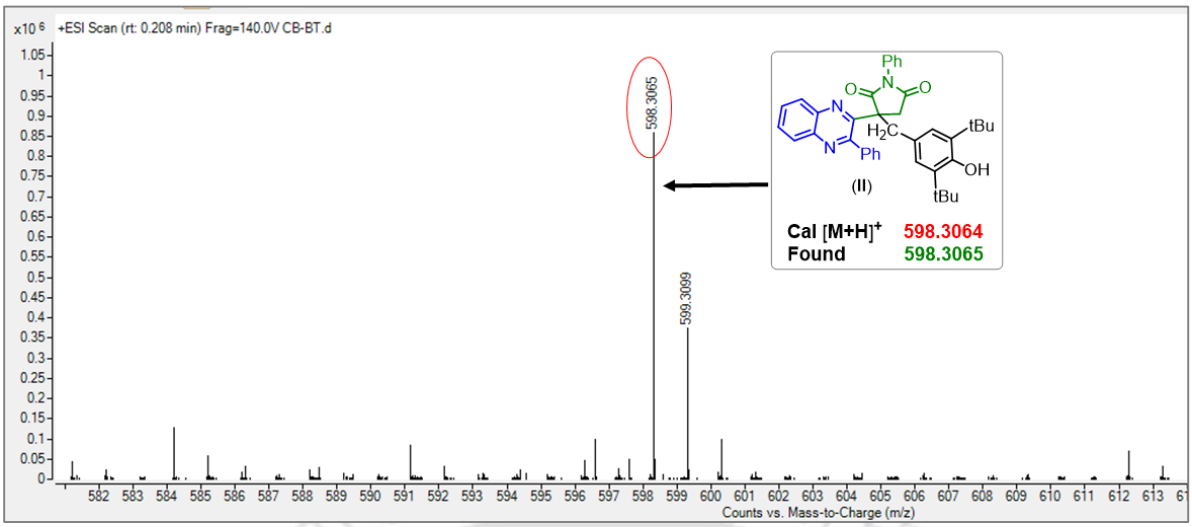

Figure V.5.9. *ESI-MS spectrum for BHT adduct* ***II*** *of Spiro-Etherification reaction*

V.5.5.4. Spin-Trapping EPR Experiment:

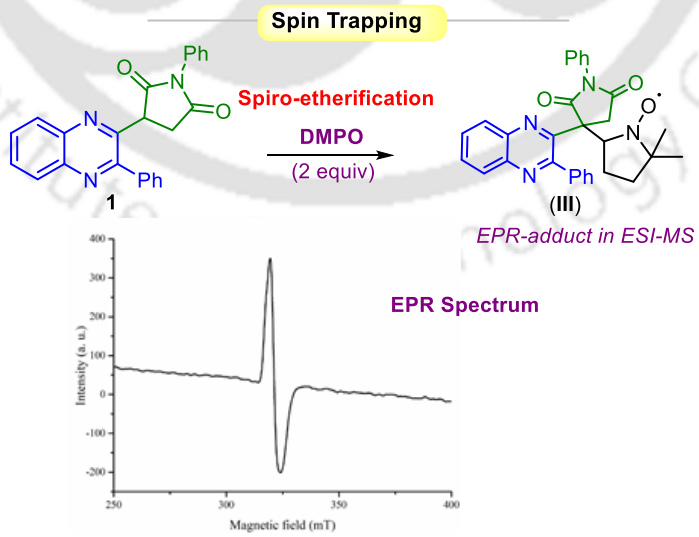

SchemeV.5.13. *EPR experiment for Spiro-Etherification reaction*

TH-3369_166122017

An oven-dried 10 mL glass vial was charged with C3-maleimidated quinoxaline (**1**, 0.15 mmol), 5,5-dimethyl-1-pyrroline *N*-oxide (DMPO) (0.30 mmol, 2 equiv.) and a magnetic stir bar in chlorobenzene (PhCl) (1 mL, 0.15 M) and was stirred at room temperature in open-air under the irradiation of blue LEDs (λ_{em}^{max} = 480 nm, 4 × 3W) approximately at a distance of ~1-2 cm. Now, after 30 min a small portion of the reaction aliquots was collected and electron paramagnetic resonance (EPR) was recorded at room temperature. The observed EPR signal supports the formation of radical intermediate in this photochemical reaction (Scheme V.5.13). Furthermore, the EPR adduct also detected by ESI-MS analysis of the reaction aliquot (Figure V.5.10).

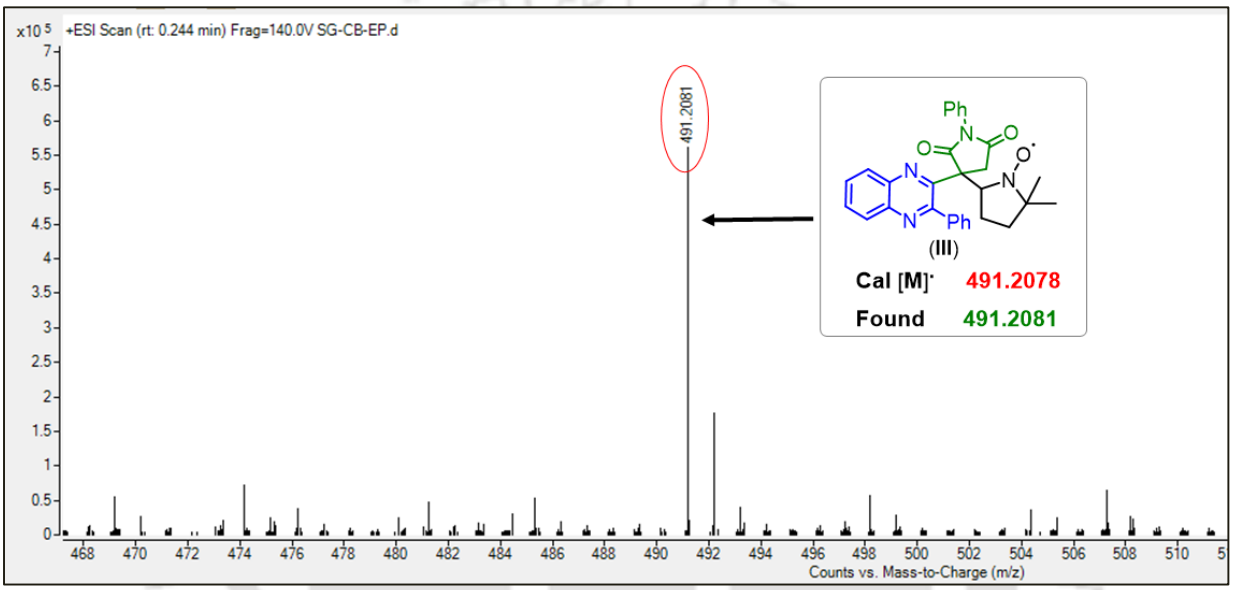

Figure V.5.10. *ESI-MS spectrum for EPR adduct* ***III*** *of Spiro-Etherification in PhCl*

V.5.5.5. Elucidation for the Source of Hydroxyl Group:

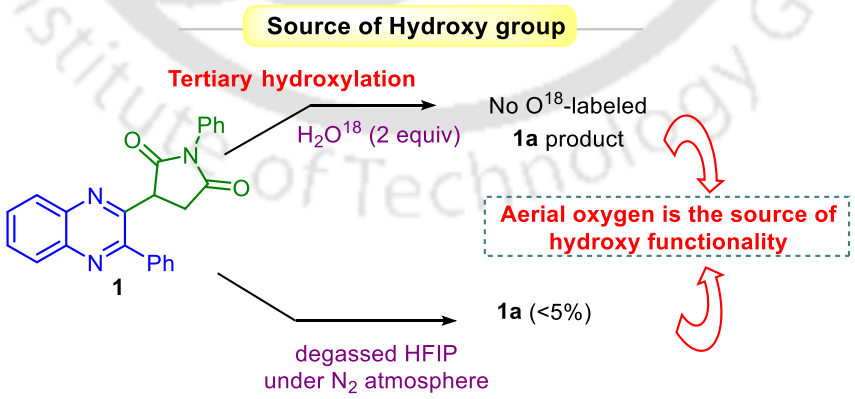

Scheme V.5.14. *Elucidation of the basis of hydroxyl group in tertiary hydroxylation reaction*

An oven-dried 10 mL glass vial was charged with C3-maleimidated quinoxaline (**1**, 0.15 mmol), H_2O^{18} (0.30 mmol, 2 equiv.), and a magnetic stir bar in 1,1,1,3,3,3-hexafluoroisopropanol (HFIP) (1

TH-3369_166122017

mL, 0.15 M) and was stirred at room temperature in open-air for 6 h under the irradiation of blue LEDs (λ_{em}^{max} = 480 nm, 4 × 3W) approximately at a distance of ~1-2 cm. The progress of the reaction was monitored *via* TLC. After completion of the reaction, a small portion of reaction aliquot was collected and subjected to ESI-MS analysis to detect any ^{18}O labeled hydroxylated adduct of **1a**. However, no ^{18}O-labeled hydroxylated adduct could be detected and only usual **1a** product was observed. This suggests aerial oxygen to be the source of hydroxyl groups in the product (Scheme V.5.14). Further, under standard tertiary hydroxylation conditions, one reaction was conducted using degassed HFIP in the presence of N_2 atmosphere. After 12 h reaction time, we observed very traces (<5%) of **1a**. Which supports the aerial oxygen involvement (Scheme V.5.14).

V.5.5.6. Singlet Oxygen Quenching and Trapping:

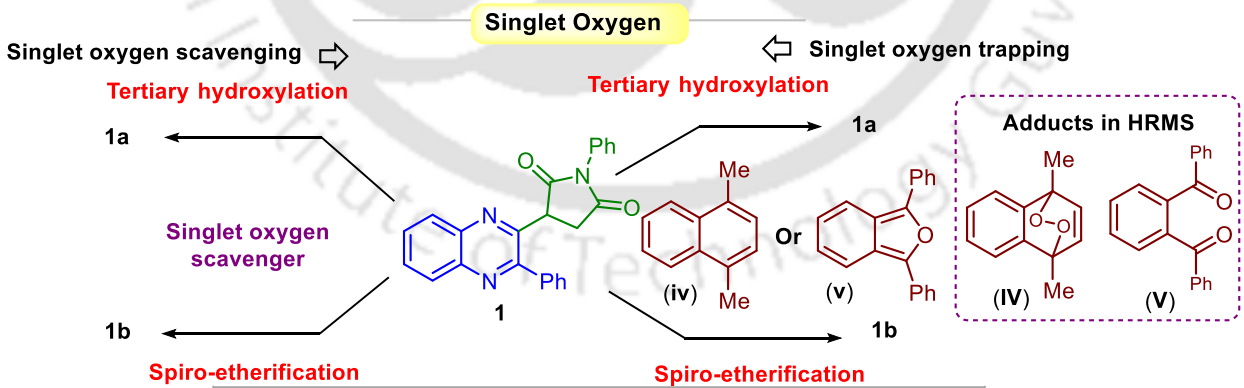

Quenchers (2.5 equiv)	Role	1a	1b
DABCO	Singlet oxygen scavenger	00	00
1,4-dimethylnaphthalene	Singlet oxygen trapping	traces	traces
1,3-diphenylisobenzofuran	Singlet oxygen trapping	traces	traces

Scheme V.5.15. *Singlet oxygen quenching and trapping*

TH-3369_166122017

Tertiary Hydroxylation in the Presence of Singlet Oxygen Quenchers

An oven-dried 10 mL glass vial was charged with C3-maleimidated quinoxaline (**1**, 0.15 mmol), 1,4-diazabicyclo[2.2.2]octane (DABCO) (0.375 mmol, 2.5 equiv.) or 1,4-dimethylnaphthalene (0.375 mmol, 2.5 equiv.) or 1,3-diphenylisobenzofuran (0.375 mmol, 2.5 equiv.) and a magnetic stir bar in 1,1,1,3,3,3-hexafluoroisopropanol (HFIP) (1 mL, 0.15 M) and was stirred at room temperature in an open-air for 12 h under the irradiation of blue LEDs (λ_{em}^{max} = 480 nm, 4 × 3W) approximately at a distance of ~1-2 cm. After 12 h for DABCO, the reaction was found to be fully quenched. Whereas in the presence of other two singlet oxygen trapping reagents such as 1,4-dimethylnaphthalene and 1,3-diphenylisobenzofuran, trace of the expected hydroxylated adduct **1a** was observed. Furthermore, the trapped singlet oxygen adducts (**IV**) and (**V**) were detected by ESI-MS analysis of the reaction aliquot (Figures V.5.11 and V.5.12). These observations strongly support the formation and involvement of singlet oxygen for this hydroxylation reaction.

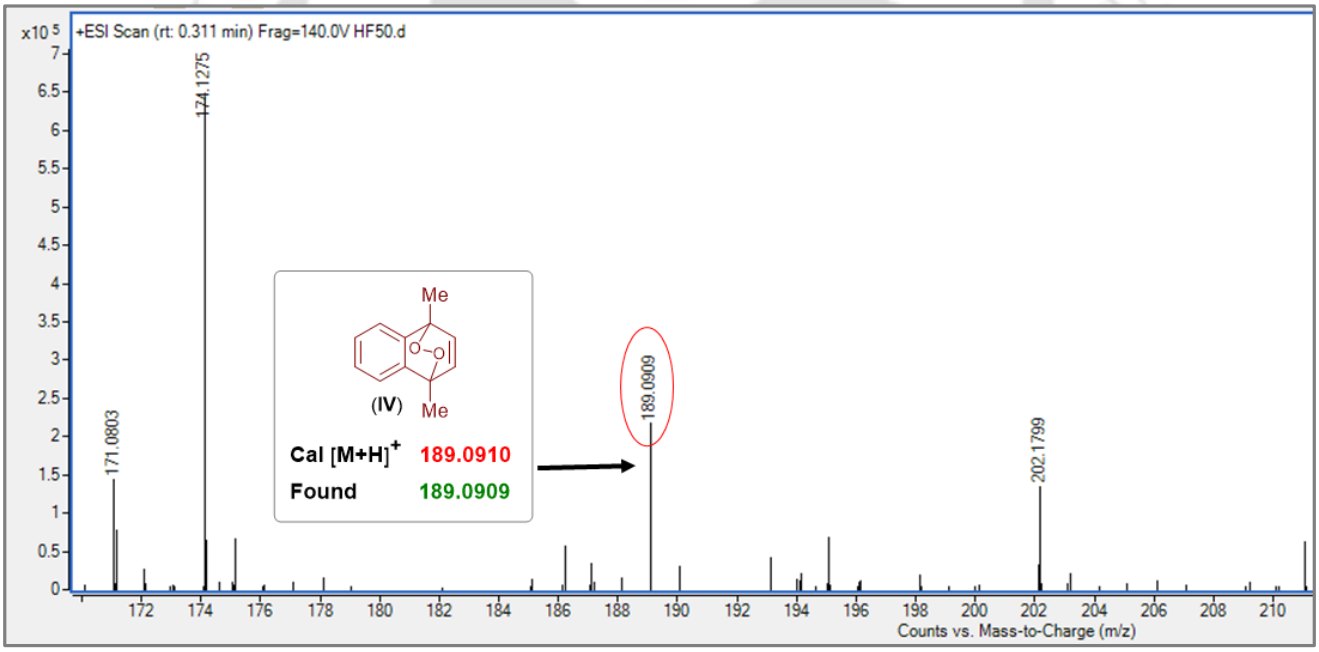

Figure V.5.11. *ESI-MS spectrum of singlet oxygen adduct* ***IV*** *for tertiary hydroxylation*

TH-3369_166122017

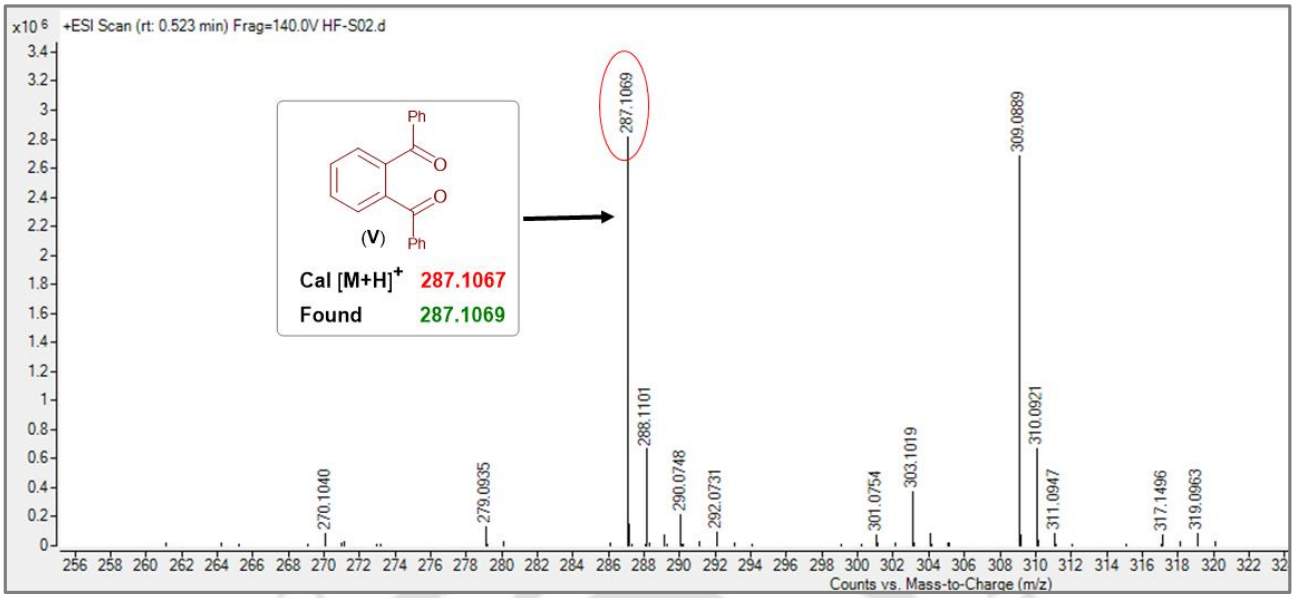

Figure V.5.12. *ESI-MS spectrum of singlet oxygen adduct* ***V*** *for tertiary hydroxylation*

Spiro-Etherification in the Presence of Singlet Oxygen Quenchers

An oven-dried 10 mL glass vial was charged with C3-maleimidated quinoxaline (**1**, 0.15 mmol), 1,4-diazabicyclo[2.2.2]octane (DABCO) (0.375 mmol, 2.5 equiv.) or 1,4-dimethylnaphthalene (0.375 mmol, 2.5 equiv.) or 1,3-diphenylisobenzofuran (0.375 mmol, 2.5 equiv.) and a magnetic stir bar in chlorobenzene (PhCl) (1 mL, 0.15 M) and was stirred at room temperature in an open-air for 12 h under the irradiation of blue LEDs (λ_{em}^{max} = 480 nm, 4 × 3W) approximately at a distance of ~1-2 cm. After 12 h for DABCO reaction, the reaction was found to be fully quenched. Whereas in the presence of other two singlet oxygen trapping reagents such as 1,4-dimethylnaphthalene and 1,3-diphenylisobenzofuran, a trace of the expected hydroxylated adduct **1b** was observed. Furthermore, the trapped singlet oxygen adducts (**IV**) and (**V**) were detected by ESI-MS analysis of the reaction aliquot (Figures V.5.13 and V.5.14). These observations strongly support the formation and involvement of singlet oxygen in this spiro-etherification reaction.

TH-3369_166122017

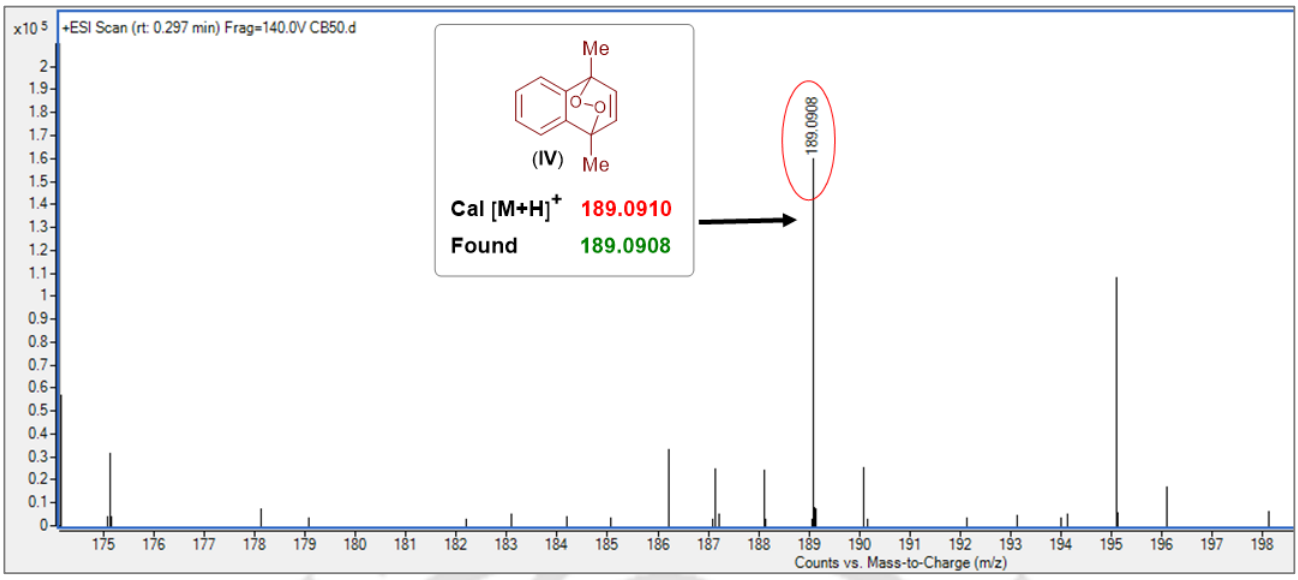

Figure V.5.13. *ESI-MS spectrum of singlet oxygen adduct* ***IV*** *for Spiro-Etherification*

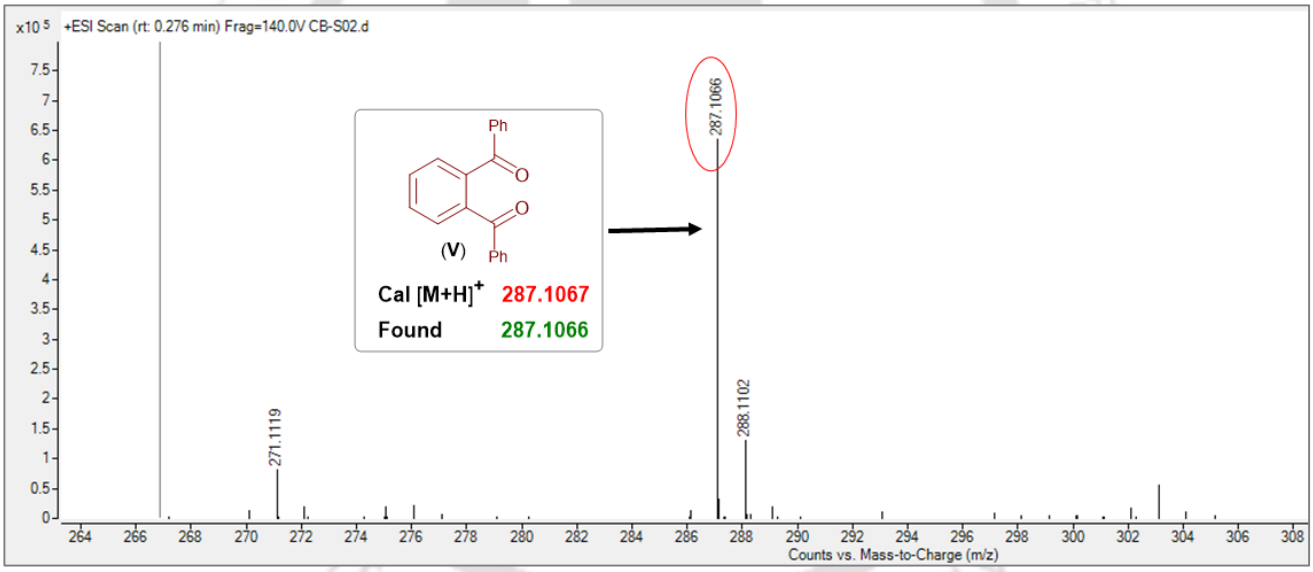

Figure V.5.14. *ESI-MS spectrum of singlet oxygen adduct* ***V*** *for Spiro-Etherification*

V.5.5.7. Triplet-State Quenching:

TH-3369_166122017

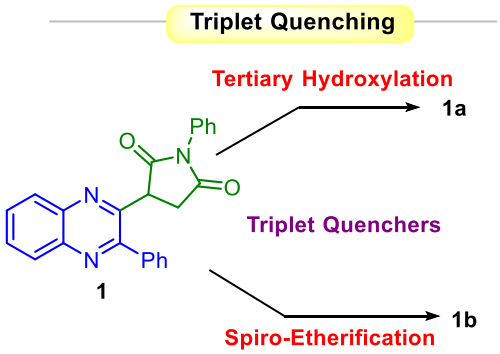

Quenchers (2.5 equiv)	Role	1a	1b
2,5-dimethylhexa-2,4-diene	Triplet state quencher	12	traces
Perylene	Triplet state quencher	<10	traces

Scheme V.5.16. *Triplet-state quenching*

Tertiary Hydroxylation in the Presence of Triplet State Quenchers

An oven-dried 10 mL glass vial was charged with C3-maleimidated quinoxaline (**1**, 0.15 mmol), 2,5-dimethylhexa-2,4-diene (0.375 mmol, 2.5 equiv.) or perylene (0.375 mmol, 2.5 equiv.) and a magnetic stir bar in 1,1,1,3,3,3-hexafluoroisopropanol (HFIP) (1 mL, 0.15 M) and was stirred at room temperature in open-air for 12 h under the irradiation of blue LEDs (λ_{em}^{max} = 480 nm, 4 × 3W) approximately at a distance of ~1-2 cm. After 12 h, the solvent was removed by rotary evaporation. The obtained residue was then directly purified over column chromatography by eluting hexane/EtOAc mixtures to afford the desired tertiary hydroxylated adducts **1a**. In the case of 2,5-dimethylhexa-2,4-diene, 12% of desired hydroxylated adduct **1a** was isolated, whereas for perylene very small amount (<10%) of **1a** was observed. Thus these observations suggest the triplet energy transfer during the hydroxylation reaction.

Spiro-Etherification in the Presence of Triplet State Quenchers.

An oven-dried 10 mL glass vial was charged with C3-maleimidated quinoxaline (**1**, 0.15 mmol), 2,5-dimethylhexa-2,4-diene (0.375 mmol, 2.5 equiv.) or perylene (0.375 mmol, 2.5 equiv.) and a magnetic stir bar in chlorobenzene (PhCl) (1 mL, 0.15 M) and was stirred at room temperature in open-air for 12 h under the irradiation of blue LEDs (λ_{em}^{max} = 480 nm, 4 × 3W) approximately at a distance of ~1-2 cm. After 12 h, in presence of both quencher, traces of **1b** was observed. This result suggest the involvement of triplet energy transfer pathway.

V.5.5.8. Intermediacy of Alkoxy Radical:

TH-3369_166122017

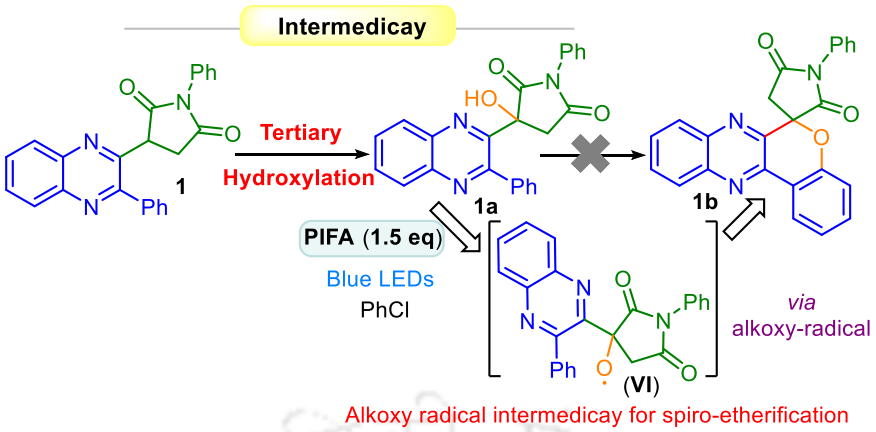

Scheme V.5.17. *Intermediacy of alkoxy radical*

Spiro-Etherification from hydroxylated product (1a)

An oven-dried 10 mL glass vial was charged with hydroxylated product (**1a**, 0.15 mmol), and a magnetic stir bar in chlorobenzene (PhCl) (1 mL, 0.15 M) and was stirred at room temperature in open-air for 12 h under the irradiation of blue LEDs (λ_{em}^{max} = 480 nm, 4 × 3W) approximately at a distance of ~1-2 cm. After 12 h, no spiro-cyclic ether **1b** was observed. This result completely rules out the intermediacy of hydroxylated product (**1a**) for spiro-etherification.

Spiro-Etherification from hydroxylated product (1a) in the presence of PIFA

An oven-dried 10 mL glass vial was charged with hydroxylated product (**1a**, 0.15 mmol), PIFA (1.5 equiv.) and a magnetic stir bar in chlorobenzene (PhCl) (1 mL, 0.15 M) and was stirred at room temperature in open-air for 8 h under the irradiation of blue LEDs (λ_{em}^{max} = 480 nm, 4 × 3W) approximately at a distance of ~1-2 cm. After 8 h, the reaction mixture was mixed with water (5 mL) and extracted with dichloromethane (2 x 10 mL). The organic layer was dried over anhydrous sodium sulfate and was evaporated under reduced pressure. Then the crude mixture was purified over column chromatography (60-120 mesh silica) by eluting hexane/EtOAc mixtures to afford desired spiro-cyclic ether adducts in 74% isolated yield. This result supports the generation of an alkoxy radical and its intermediacy for spiro-etherification.

V.5.6. Theoretical Calculations:

TH-3369_166122017

Table V.5.3. *Computed electronic spectroscopic parameters corresponding to precursor and its triplet state (**1** and **^{3}1**), tautomers in singlet and triplet states (**A_0**, **A_0'**, **$^3A_0$'**) intermediates (**B**, **C**, **D**, **E**) and products (**1a** and **1b**) using TD-DFT calculations at ωB97X-D/6-31G(d,p) level of theory. (f- oscillator strength)*

Structure	Gas phase			Solvent: HFIP			Solvent: PhCl		
	Wavelength (nm)	Transition	f	Wavelength (nm)	Transition	f	Wavelength (nm)	Transition	f
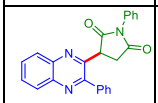 **1**	283.9	H→L π→ π*	0.2276	282.9	H→L π→ π*	0.3017	H→L 289.0	π→ π*	0.3801
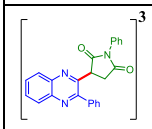 **^{3}1**	377.5	H-1→L π→ π*	0.0624	366.4	H-5→L π→ π*	0.1974	372.2	H→L+1 π→ π*	0.2230
	284.5	H→L+1 π→ π*	0.2472	283.2	H→L+6 π→ π*	0.1597	286.8	H→L+1 π→ π*	0.2188
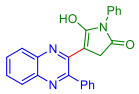 **A_0**	364.7	H→L π→ π*	0.4082	H→L 364.9	π→ π*	0.5107	H→L 374.7	π→ π*	0.5544
	288.3	H→L+1 π→ π*	0.2702	H→L+1 280.8	π→ π*	0.1668	H→L+1 285.3	π→ π*	0.2724
	261.2	H-1→L π→ π	0.3260	H-1→L 261.8	π→ π*	0.4363	H-1→L 263.1	π→ π*	0.4438
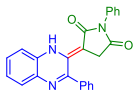 **A_0'**	377.1	H→L π→ π*	0.3790	379.2	H→L π→ π*	0.6016	388.2	H→L π→ π*	0.5404
	284.2	H→L+1 π→ π*	0.3601	293.0	H→L+1 π→ π*	0.1140	H→L+1 284.4	π→ π*	0.3439
	260.4	H-2→L π→ π*	0.2096	H-2→L 284.3	π→ π*	0.2690	261.8	H-2→L π→ π*	0.3222
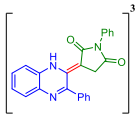 **$^3A_0$'**	458.7	H-1→L π→ π*	0.0282	462.5	H→L π→ π*	0.0260	478.3	H-5→L n+π→ π*	0.0135
	441.7	H-1→L π→ π*	0.0705	439.6	H→L π→ π*	0.0145	444.8	H-3→L n→ π*	0.1573
	388.3	H-10→L π→ π*	0.0622	401.4	H-1→L π→ π*	0.0565	397.2	H-1→L π→ π*	0.0688

TH-3369_166122017

				339.1	H-5→L n+π → π*	0.1502	357.3	H-6→L n+π→ π*	0.1178
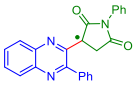 **B**	458.6	H-4→L π→ π*	0.0008	461.7	π→ π*	0.0035	457.0	π→ π*	0.0014
	430.9	H-6→L n→ π*	0.0022	410.0	π→ π*	0.0248	417.2	n→ π*	0.0051
	399.5	H→L π→ π*	0.0588	387.1	π→ π*	0.0985	396.2	π→ π*	0.079
	335.1	H→L π→ π*	0.1486	340.6	π→ π*	0.2949	339.9	π→ π*	0.2827
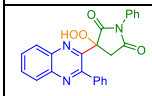 **C**	276.8	H→L π→ π*	0.1635	274.8	H→L π→ π*	0.1854	280.1	H→L π→ π*	0.2587
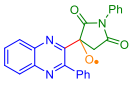 **D**	441.2	H→L π→ π*	0.0352	501.0	H→L π→ π*	0.1252	440.0	H→L π→ π*	0.0588
	436.6	H-8→L n+π→ π*	0.0190	447.4	H-3→L π→ π*	0.0210	434.8	H-4→L n→ π*	0.0362
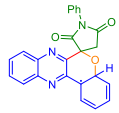 **E**	406.6	H→L π→ π*	0.0988	416.6	H-1→L π→ π*	0.0237	419.1	H→L π→ π*	0.2846
	394.9	H→L π→ π*	0.1027	415.5	H→L π→ π*	0.2091	390.4	H-4→L n→ π*	0.0278
				384.6	H-4→L n→ π*	0.0214			
	357.3	H→L+1 π→ π*	0.1281	361.6	H→L+1 π→ π*	0.1447	363.9	H→L+1 π→ π*	0.1376
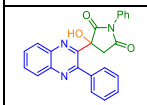 **1a**	281.3	H→L π→ π*	0.1981	274.7	H→L π→ π*	0.2114	284.6	H→L π→ π*	0.3229
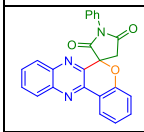	283.9	H→L π→ π*	0.2276	282.9	H→L π→ π*	0.3017	289.0	H→L π→ π*	0.3801

TH-3369_166122017

1b									

TH-3369_166122017

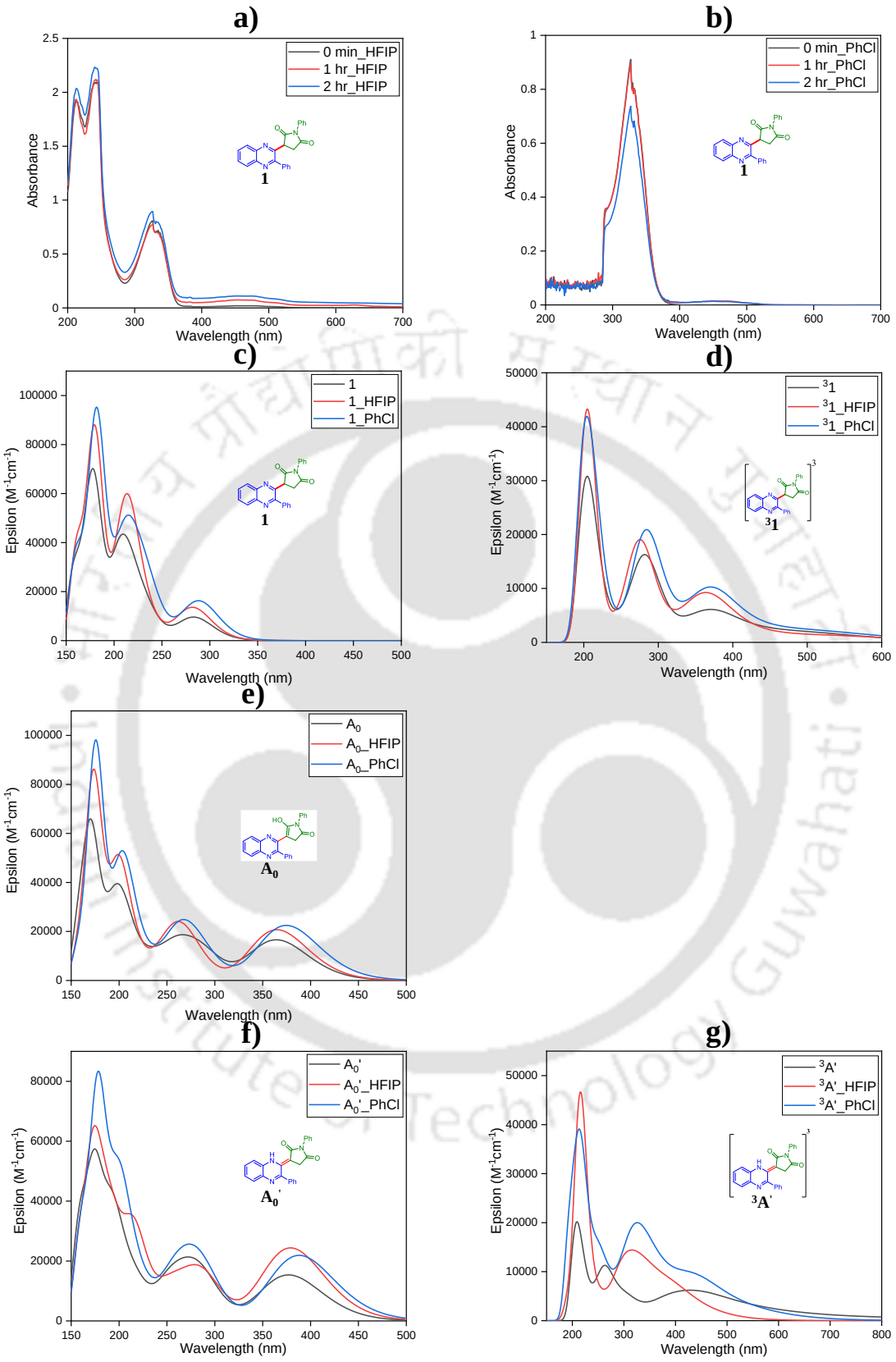

TH-3369_166122017

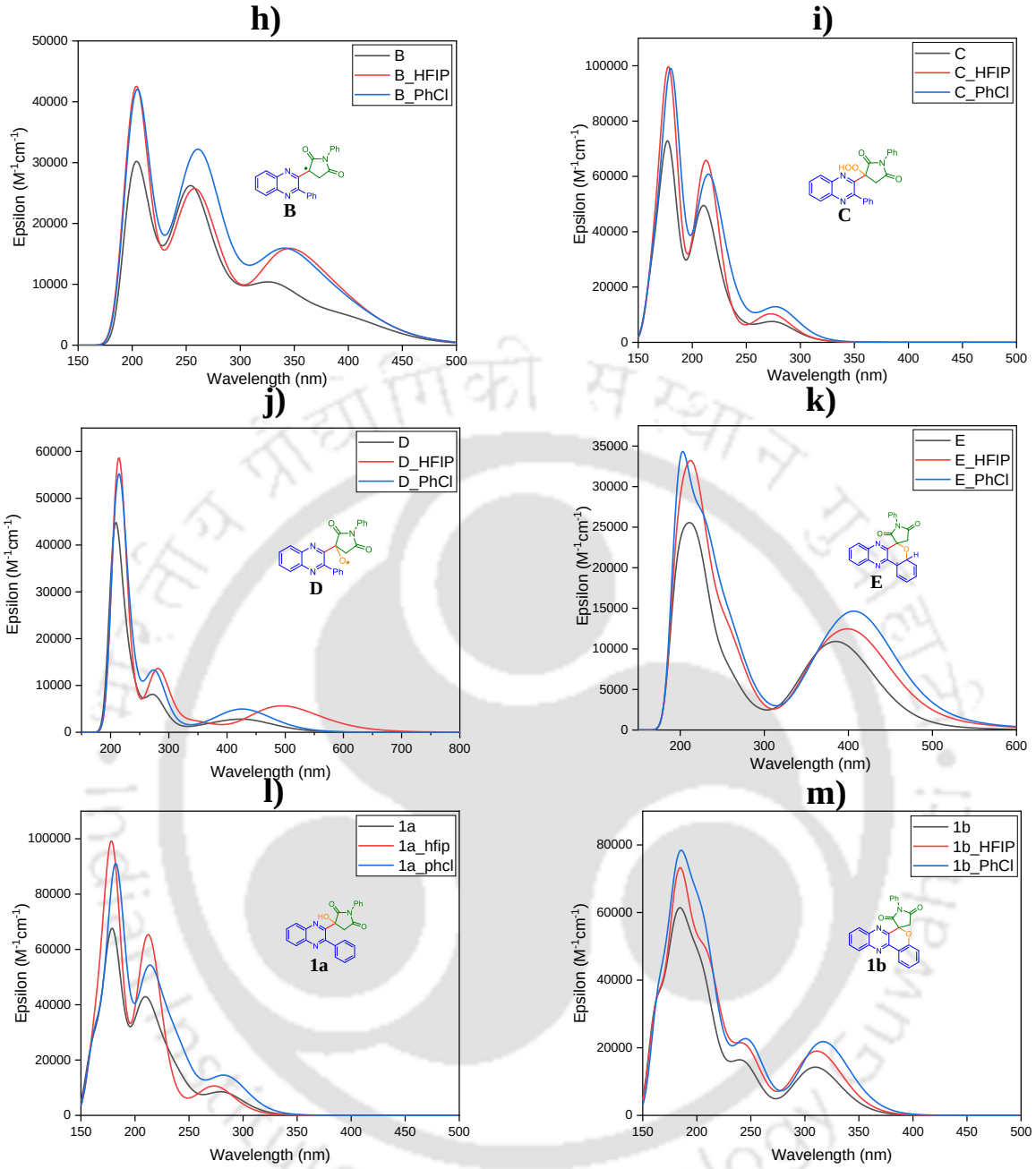

Figure V.5.15. *Experimental UV-data of* ***1****: a) in HFIP (before and after irradiation using blue light); b) in PhCl (before and after irradiation using blue light); TD-DFT computed electronic absorption data of : c)* ***1*** *in singlet state; d)* ***1*** *in triplet state (*^{3}***1****); e) O-H tautomer* $\mathbf{A_0}$ *in singlet state; f) N-H tautomer* $\mathbf{A_0}$*' in singlet state; g) N-H tautomer* $\mathbf{A_0}$*' in triplet state (*$^3\mathbf{A_0}$*'); h) the radical intermediate* ***B****; i) the hydroperoxide intermediate* ***C****; j) the oxy radical* ***D****; k) the intermediate E; l) the hydroxy product* ***1a****; m) the spiro-product* ***1b*** *(All the TD-DFT calculations were performed at ωB97X-D/6-31G(d,p) level of theory; the data obtained in gas phase (black), in solvent HFIP (red) and PhCl (blue) are included).*

TH-3369_166122017

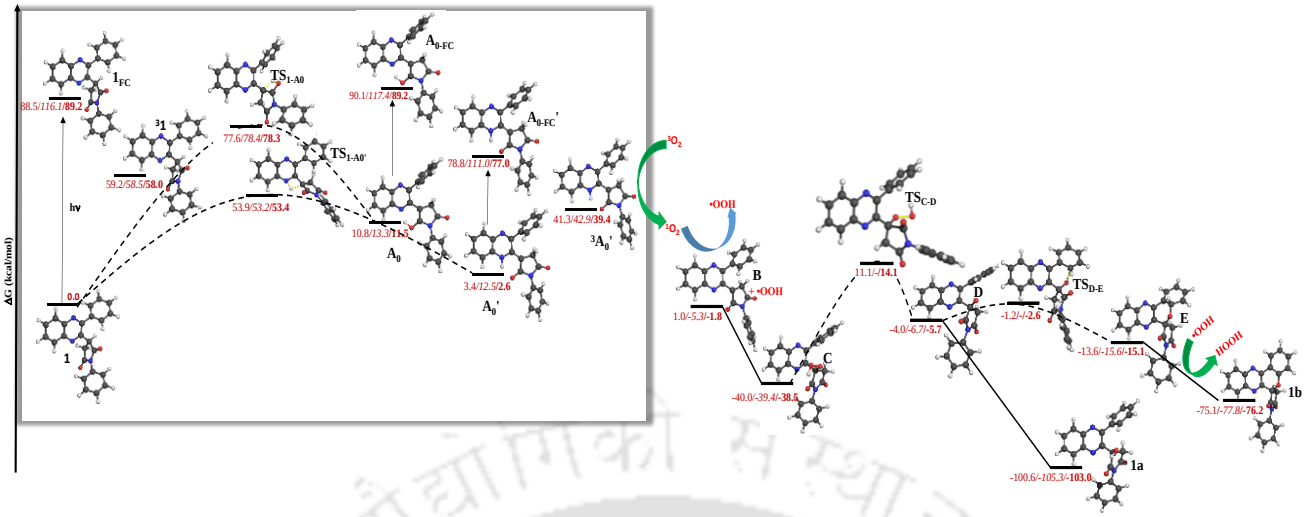

Figure V.5.16*. Energy profile diagram depicting the solvent-dependent product selectivity; all the optimized geometries at ωB97X-D/6-31G(d,p) level of theory are included. (The energy values are indicated as follows: Gas phase-normal, Solvent: HFIP-italics, Solvent: PhCl-bold)*

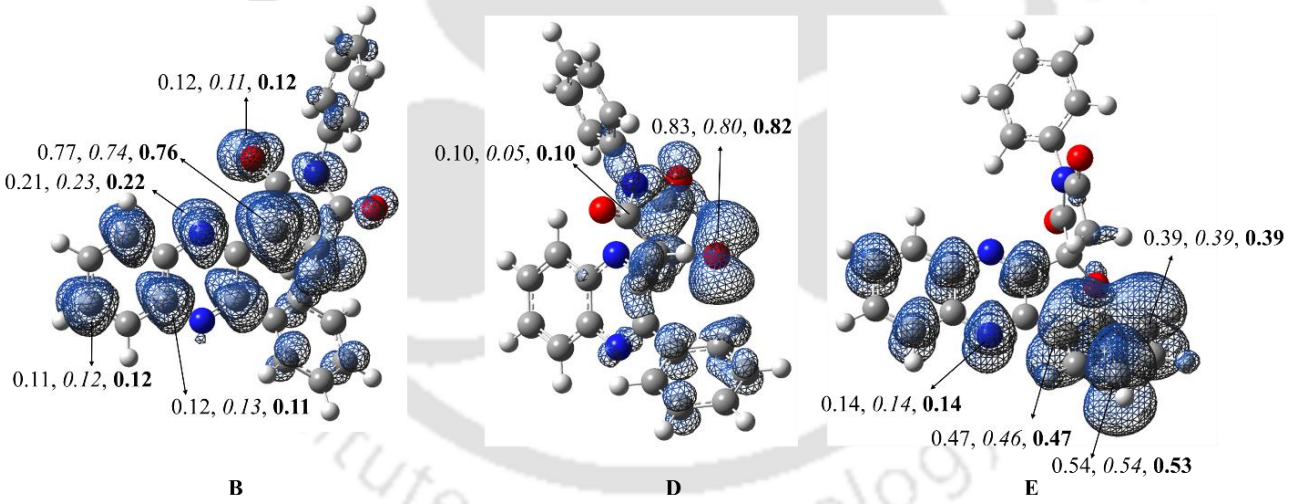

Figure V.5.17. *The spin density mapping for the radical intermediates* ***B****,* ***D*** *and* ***E*** *is depicted (isovalue=0.0004) at ωB97X-D/6-31G(d,p) level of theory. (The spin density values at selected sites are indicated as follows: Gas phase-normal, Solvent: HFIP-italics, Solvent: PhCl-bold)*

TH-3369_166122017

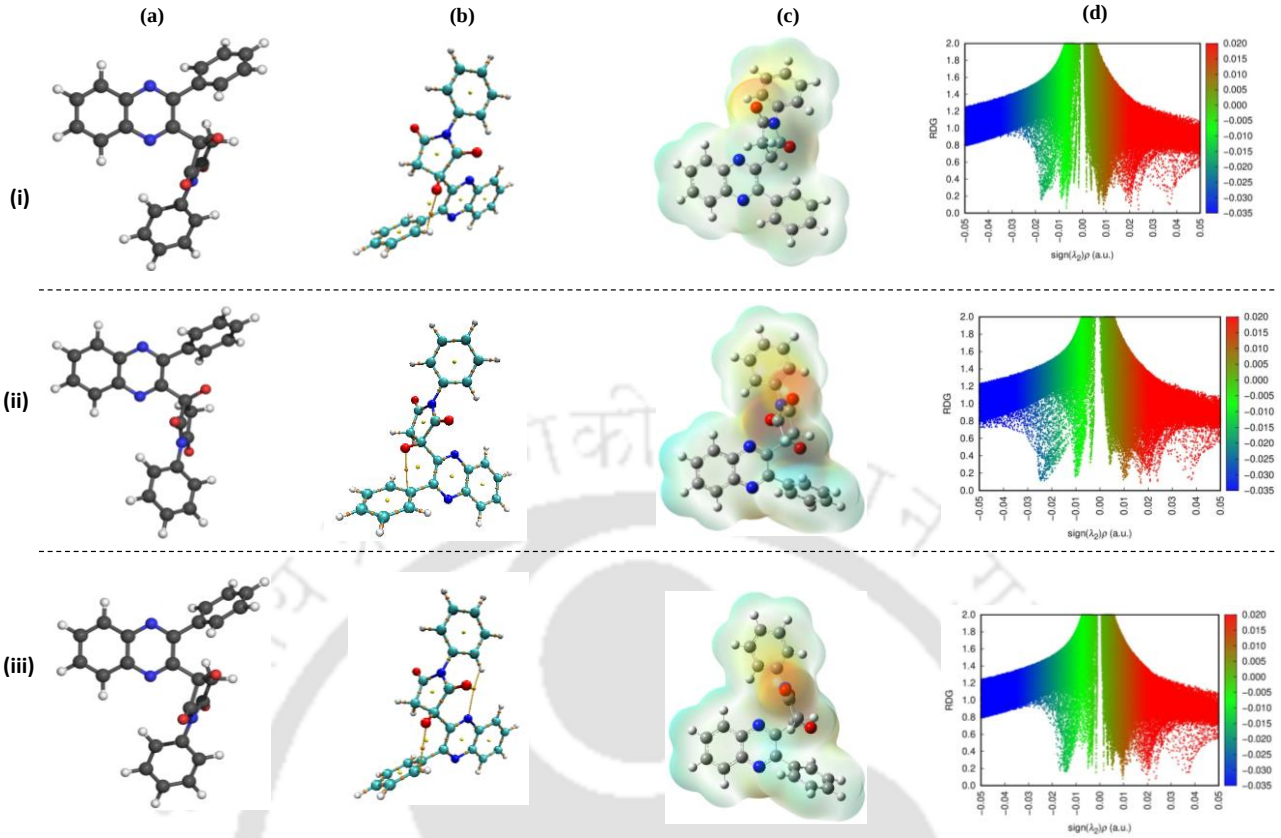

Figure V.5.18. *Computational evidences for the solvent-dependent product selectivity from the intermediate* ***D****: (**a**) Optimized structures of* ***D;*** *(**b**) AIM analysis; (**c**) Electrostatic potential (ESP) mapping; (**d**) Non-covalent interactions (NCI) plots in gas phase (**i**), HFIP (**ii**) and PhCl (**iii**), respectively. {To understand the solvent-dependent product selectivity originated from the intermediate* ***D*** *in HFIP and PhCl, we have inspected the geometrical parameters and Atoms in Molecule (AIM) analysis of* ***D*** *in gas phase, HFIP and PhCl. The optimized structure of* ***D*** *showed different orientation preferences in PhCl and HFIP. The dihedral angle $OC_{suc}C_{qui}C_{qui}$ showed significant deviation in PhCl (**56.8°**) relative to HFIP (20.7°); also, in PhCl the O is more oriented towards the phenyl group favouring the spiro cycle ring formation. A similar but rather smaller deviation were observed for the $C_{qui}C_{qui}C_{ph}C_{ph}$ dihedral angle (**66.9°** in PhCl vs 59.9° in HFIP). The AIM analysis also showed an interaction between the O and C(6) phenyl of* ***D*** *in PhCl; on the other hand, in HFIP, the O is strongly interacting with C(5) of phenyl ring restricting the formation of intermediate* ***E****, and thus abstracts a proton from solvent to form the product* ***1a****. In addition, the NCI plots support the hydrogen bonding like interaction between O and C(5) of phenyl ring when HFIP is used as a solvent*

TH-3369_166122017

Table V.5.4. *Computational data (electronic and thermodynamic parameters) of various species at ωB97X-D/6-31G(d,p) level of theory. (Gas phase-normal, Solvent: HFIP-italics, Solvent: PhCl-bold)*

Species	Thermal corrected Electronic energy (E)	ZPVE (Hartree)	Lowest frequency (cm^{-1})	Spin Contamination		Point group	Electronic state	Free Energy (G) (Hartree)	Enthalpy (H) (Hartree)	Entropy (S) (Cal/Mol-Kelvin)
				Before annihilation	After annihilation					
1	-1238.780014	0.362867	16.47	0.0000	0.0000	C_1	^1A	-1238.855276	-1238.779070	160.388
	-1238.811522	*0.362291*	*7.41*	*0.0000*	*0.0000*	*C_1*	*^1A*	*-1238.888020*	*-1238.810578*	*162.990*
	-1238.816347	**0.362758**	**15.95**	**0.0000**	**0.0000**	**C_1**	**^1A**	**-1238.891095**	**-1238.815403**	**159.307**
^{3}1	-1238.683864	0.358159	16.21	2.0390	2.0007	C_1	^3A	-1238.760885	-1238.682920	164.090
	-1238.717298	*0.357735*	*15.67*	*2.0360*	*2.0005*	*C_1*	*^3A*	*-1238.794747*	*-1238.716354*	*164.993*
	-1238.721797	**0.358205**	**17.16**	**2.0369**	**2.0006**	**C_1**	**^3A**	**-1238.798721**	**-1238.720853**	**163.887**
$TS_{1\text{-}A0}$	-1238.656307	0.356261	2117.58i	0.0000	0.0000	C_1	^1A	-1238.731680	-1238.655362	160.624
	-1238.686611	*0.355205*	*2180.27i*	*0.0000*	*0.0000*	*C_1*	*^1A*	*-1238.763065*	*-1238.685667*	*162.899*
	-1238.691283	**0.356136**	**2128.71i**	**0.0000**	**0.0000**	**C_1**	**^1A**	**-1238.766230**	**-1238.690339**	**159.727**
A_0	-1238.762763	0.361518	11.78	0.0000	0.0000	C_1	^1A	-1238.838022	-1238.761819	160.384
	-1238.791607	*0.361046*	*12.00*	*0.0000*	*0.0000*	*C_1*	*^1A*	*-1238.866758*	*-1238.790663*	*160.156*
	-1238.797513	**0.360854**	**19.39**	**0.0000**	**0.0000**	**C_1**	**^1A**	**-1238.872784**	**-1238.796569**	**160.408**
$TS_{1\text{-}A0'}$	-1238.693840	0.357012	1732.81i	0.0000	0.0000	C_1	^1A	-1238.769442	-1238.692896	161.106
	-1238.730714	*0.356561*	*1845.81i*	*0.0000*	*0.0000*	*C_1*	*^1A*	*-1238.803235*	*-1238.729770*	*154.620*
	-1238.731882	**0.357180**	**1888.86i**	**0.0000**	**0.0000**	**C_1**	**^1A**	**-1238.805960**	**-1238.730938**	**157.896**
A_0'	-1238.775238	0.362837	20.19	0.0000	0.0000	C_1	^1A	-1238.849835	-1238.774294	158.989
	-1238.794075	*0.362336*	*24.08*	*0.0000*	*0.0000*	*C_1*	*^1A*	*-1238.868142*	*-1238.793131*	*157.875*
	-1238.811640	**0.361961**	**20.40**	**0.0000**	**0.0000**	**C_1**	**^1A**	**-1238.886954**	**-1238.810696**	**160.497**
$^3A'$	-1238.712786	0.359816	21.35	2.0205	2.0002	C_1	^3A	-1238.789432	-1238.711842	163.302
	-1238.742905	*0.359689*	*11.27*	*2.0218*	*2.0003*	*C_1*	*^3A*	*-1238.819730*	*-1238.741961*	*163.678*
	-1238.695079	**0.357801**	**24.55**	**2.0400**	**2.0008**	**C_1**	**^3A**	**-1238.772089**	**-1238.694135**	**164.068**
	-1238.731882	0.357180	1888.86i	**0.0000**	**0.0000**	**C_1**	**^1A**	-1238.805960	-1238.730938	157.896
B	-1238.137422	0.348400	5.52	0.7878	0.7510	C_1	^2A	-1238.214930	-1238.136478	165.115
	-1238.172637	*0.348249*	*20.38*	*0.7909*	*0.7512*	*C_1*	*^2A*	*-1238.248591*	*-1238.171693*	*161.845*
	-1238.175433	**0.348461**	**22.63**	**0.7890**	**0.7511**	**C_1**	**^2A**	**-1238.251210**	**-1238.174488**	**161.474**
C	-1389.063985	0.370332	20.24	0.0000	0.0000	C_1	^1A	-1389.143357	-1389.063041	169.038
	-1389.098494	*0.369668*	*13.20*	*0.0000*	*0.0000*	*C_1*	*^1A*	*-1389.179039*	*-1389.097550*	*171.509*
	-1389.100341	**0.370012**	**22.72**	**0.0000**	**0.0000**	**C_1**	**^1A**	**-1389.179384**	**-1389.099397**	**168.348**
D	-1313.295679	0.352362	15.69	0.7555	0.7500	C_1	^2A	-1313.374173	-1313.294735	167.192
	-1313.329077	*0.352514*	*9.57*	*0.7554*	*0.7500*	*C_1*	*^2A*	*-1313.407692*	*-1313.328133*	*167.448*
	-1313.333015	**0.352225**	**21.10**	**0.7555**	**0.7500**	**C_1**	**^2A**	**-1313.410757**	**-1313.332070**	**165.610**

TH-3369_166122017

TS_{C-D}	-1388.982973	0.366118	933.40i	0.0000	0.0000	C_1	^{1}A	-1389.061889	-1388.982029	168.080
	-1389.017277	**0.366911**	**937.14i**	**0.0000**	**0.0000**	**C_1**	**^{1}A**	**-1389.095531**	**-1389.016332**	**166.686**
1a	-1313.963206	0.366848	26.65	0.0000	0.0000	C_1	^{1}A	-1314.039301	-1313.962262	162.143
	-1313.996266	*0.365866*	*4.74*	*0.0000*	*0.0000*	*C_1*	*^{1}A*	*-1314.075806*	*-1313.995322*	*169.394*
	-1313.998998	**0.366082**	**15.32**	**0.0000**	**0.0000**	**C_1**	**^{1}A**	**-1314.076415**	**-1313.998054**	**164.925**
E	-1313.313178	0.353384	12.07	0.8202	0.7533	C_1	^{2}A	-1313.389325	-1313.312234	162.253
	-1313.346227	*0.353599*	*13.59*	*0.8174*	*0.7530*	*C_1*	*^{2}A*	*-1313.421942*	*-1313.345283*	*161.343*
	-1313.350489	**0.353277**	**19.00**	**0.8194**	**0.7532**	**C_1**	**^{2}A**	**-1313.425627**	**-1313.349545**	**160.128**
TS_{D-E}	-1313.295145	0.352825	340.88i	0.7984	0.7516	C_1	^{2}A	-1313.369738	-1313.294201	158.983
	-1313.331260	**0.352592**	**333.89i**	**0.7971**	**0.7515**	**C_1**	**^{2}A**	**-1313.405727**	**-1313.330316**	**158.718**
1b	-1312.785045	0.344635	9.25	0.0000	0.0000	C_1	^{1}A	-1312.859628	-1312.784101	158.959
	-1312.816318	*0.344543*	*13.54*	*0.0000*	*0.0000*	*C_1*	*^{1}A*	*-1312.890133*	*-1312.815374*	*157.344*
	-1312.821673	**0.344700**	**22.61**	**0.0000**	**0.0000**	**C_1**	**^{1}A**	**-1312.894629**	**-1312.820728**	**155.536**

Table V.5.5. Cartesian Coordinates

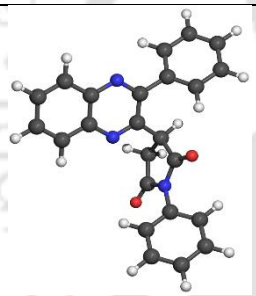

1

C	-0.93305600	0.17401500	0.47683600
C	-1.16794500	2.41254500	0.05483100
C	-2.47734900	2.18307200	-0.43113400
C	-2.24330300	-0.07187300	-0.06483400
H	0.36262800	3.87192600	0.45403700
C	-0.64266800	3.72704900	0.07369700
C	-3.25285400	3.27813700	-0.88671600
C	-2.72372800	4.54228700	-0.86121700
C	-1.41004200	4.76847200	-0.37905300
H	-4.25280500	3.07787000	-1.25543400
H	-3.31225600	5.38300100	-1.21370800
H	-1.01283400	5.77817800	-0.36889000
N	-0.42281900	1.37990600	0.52380500
N	-2.99390800	0.92832800	-0.47462300
C	-2.84782000	-1.42869600	-0.15055100
C	-2.15844000	-2.50842600	-0.71158200
C	-4.15984300	-1.60949300	0.29747400
C	-2.77316500	-3.75372000	-0.80438600
H	-1.15038200	-2.37063600	-1.09350400
C	-4.76531500	-2.85650600	0.21078800
H	-4.69669500	-0.76149700	0.70946700

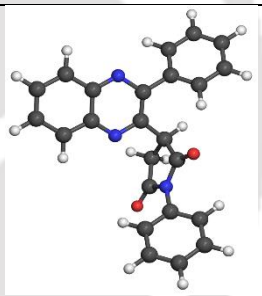

^{3}1

C	-0.95014100	0.12403900	0.45270000
C	-1.14446200	2.37749200	-0.00175500
C	-2.52231600	2.15695600	-0.36118900
C	-2.23023900	-0.10930700	-0.00157100
H	0.41584400	3.83413600	0.20432700
C	-0.61987700	3.68428400	-0.07999200
C	-3.31265500	3.28266700	-0.73867600
C	-2.74651600	4.60878300	-0.80894600
C	-1.44361700	4.80552100	-0.50141600
H	-4.35118300	3.10385400	-0.99395000
H	-3.37941700	5.43372300	-1.11620100
H	-0.99605900	5.79125500	-0.55662200
N	-0.38302300	1.37081500	0.43050500
N	-3.05895500	0.94740600	-0.35157300
C	-2.85603300	-1.44382500	-0.12759600
C	-2.16278800	-2.53737400	-0.66168300
C	-4.19475500	-1.60567200	0.25133100
C	-2.78922100	-3.77465900	-0.77607100
H	-1.14395100	-2.41039100	-1.01712600
C	-4.81283100	-2.84362300	0.14005700
H	-4.73933800	-0.74746600	0.62972400

TH-3369_166122017

C	-4.07186500	-3.93240600	-0.33869500	C	-4.11012400	-3.93372300	-0.36985800
H	-2.23526100	-4.58408900	-1.25029000	H	-2.24474000	-4.61265000	-1.19940800
H	-5.78060600	-2.98954800	0.57057000	H	-5.84767400	-2.95962500	0.44654500
H	-4.54675500	-4.90575200	-0.41043300	H	-4.59639900	-4.89969200	-0.46306100
C	-0.04970000	-0.91266400	1.06969000	C	-0.03424100	-0.92293500	1.05057000
C	0.65046100	-0.45695500	2.35316300	C	0.64859100	-0.42410600	2.32953800
C	1.10446200	-1.15933100	0.09130000	C	1.13093800	-1.16709300	0.08731300
C	2.05942800	-0.09537400	1.93071600	C	2.05692000	-0.05586300	1.91318300
H	0.71472300	-1.26428000	3.08846200	H	0.71466200	-1.21035000	3.08734300
N	2.25524400	-0.60081700	0.63379400	N	2.27405800	-0.58948200	0.63183100
O	1.03075900	-1.70614600	-0.98440600	O	1.07503000	-1.73512200	-0.97851500
O	2.89328000	0.48293300	2.57846600	O	2.87657600	0.54847200	2.55702000
H	0.18436500	0.40676400	2.82641100	H	0.16766700	0.44529900	2.77727900
H	-0.61033600	-1.83876400	1.19317100	H	-0.56845700	-1.86187300	1.19462800
C	3.48962300	-0.49649400	-0.07341500	C	3.51536500	-0.49089200	-0.06215500
C	4.12420100	0.73980100	-0.15959500	C	4.16013900	0.74104000	-0.14080000
C	4.04260800	-1.62574600	-0.67027700	C	4.06832300	-1.62267500	-0.65516100
C	5.32948700	0.84005800	-0.84423400	C	5.37343600	0.83399800	-0.81220900
H	3.67879200	1.60623000	0.31378000	H	3.71654600	1.60948200	0.33006100
C	5.24265600	-1.51112000	-1.36275000	C	5.27645200	-1.51516500	-1.33459800
H	3.53195700	-2.57849100	-0.60056800	H	3.55028100	-2.57177700	-0.59334900
C	5.88936400	-0.28190800	-1.44838400	C	5.93280300	-0.29057500	-1.41187500
H	5.82880800	1.80100700	-0.90946200	H	5.87998000	1.79175600	-0.87001900
H	5.67430300	-2.38848600	-1.83280400	H	5.70692300	-2.39508500	-1.80108500
H	6.82923200	-0.19799200	-1.98414500	H	6.87901200	-0.21231500	-1.93730200
	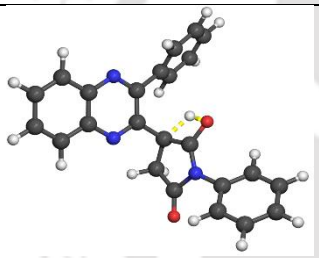				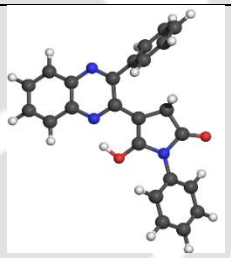		
	TS_{1-A0}				**A_0**		
C	-1.11301800	0.28293600	0.63349500	C	-1.04958400	-0.31268000	0.09290200
C	-2.47294400	2.05899600	0.09836200	C	-2.25282900	-2.30905600	0.04637100
C	-3.34203900	1.19620000	-0.60749600	C	-3.44782000	-1.58992400	-0.17397900
C	-2.06402400	-0.60879400	0.00215300	C	-2.31303200	0.40313400	-0.01268000
H	-2.07415400	4.08396000	0.70698400	H	-1.36738200	-4.25939000	0.28773600
C	-2.75503400	3.44472900	0.15541800	C	-2.29265800	-3.71998600	0.11351400
C	-4.47549500	1.73047200	-1.26619700	C	-4.66398000	-2.28492000	-0.34646700
C	-4.72559100	3.07771700	-1.20482000	C	-4.68284400	-3.65751500	-0.28807000
C	-3.86197700	3.93966100	-0.48562100	C	-3.48899300	-4.37531700	-0.05203300
H	-5.12512100	1.04683300	-1.80175300	H	-5.56388200	-1.70320700	-0.51420800
H	-5.59488700	3.49178800	-1.70513600	H	-5.61603600	-4.19505000	-0.41786400
H	-4.08046400	5.00190800	-0.44618100	H	-3.51946900	-5.45908000	-0.00267500
N	-1.34929500	1.57293200	0.68861000	N	-1.07130900	-1.64596500	0.16264200
N	-3.11896500	-0.14503400	-0.62673900	N	-3.44513300	-0.22322900	-0.18034300
C	-1.93125600	-2.09379200	0.02755300	C	-2.39070500	1.88625800	0.09239700
C	-2.08209300	-2.81524600	-1.15781500	C	-2.00020100	2.52860500	1.26932200
C	-1.72486600	-2.78596300	1.22576300	C	-2.91427300	2.63989100	-0.95840600
C	-2.00163200	-4.20279100	-1.15184100	C	-2.11621100	3.90923300	1.38767300
H	-2.26117300	-2.27733900	-2.08245100	H	-1.60782300	1.94082400	2.09459200
C	-1.65417500	-4.17487400	1.23090500	C	-3.01906300	4.02208100	-0.84388800
H	-1.62035600	-2.23472600	2.15401500	H	-3.23978000	2.13502800	-1.86209600
C	-1.78464100	-4.88573800	0.04149000	C	-2.61863100	4.65888300	0.32740000

TH-3369_166122017

H	-2.10936900	-4.75122800	-2.08206600	H	-1.81630200	4.39946300	2.30816200
H	-1.50081200	-4.70071600	2.16776700	H	-3.41810500	4.60236700	-1.66952800
H	-1.72013300	-5.96918500	0.04541300	H	-2.70508000	5.73677600	0.41775000
C	0.18194300	-0.19485600	1.23726500	C	0.24561900	0.30525600	0.07306000
C	0.78896500	0.73735900	2.28163200	C	0.68785400	1.72531300	-0.15641000
C	1.25785600	-0.38088200	0.30769700	C	1.38089000	-0.47226100	0.09781000
C	2.09249000	1.22480500	1.66139300	C	2.20193400	1.62290100	-0.26068000
H	1.04961700	0.23387000	3.21937300	H	0.45679600	2.41871700	0.65687900
N	2.31597800	0.44473700	0.47124100	N	2.54078500	0.27284000	-0.06391700
O	1.15659700	-1.43458400	-0.40484900	O	1.46073500	-1.76984800	0.21845500
O	2.87033700	2.03911600	2.07334100	O	2.98961000	2.51551300	-0.45944500
H	0.15923900	1.59796800	2.51186900	H	0.29104500	2.17942900	-1.06988300
H	0.33798800	-1.57059600	0.56513400	C	3.86900200	-0.23701000	-0.03905600
C	3.55620100	0.39583500	-0.23530900	C	4.79203600	0.20680600	-0.98472000
C	4.17297800	1.59060500	-0.59551000	C	4.24436400	-1.15917300	0.93689400
C	4.13615500	-0.83318100	-0.54390100	C	6.09421500	-0.27779500	-0.94788400
C	5.38884900	1.54999500	-1.26875200	H	4.49384700	0.93600400	-1.72692300
H	3.70970400	2.53539400	-0.34070900	C	5.54459600	-1.64957000	0.95153800
C	5.34523400	-0.85784100	-1.22855200	H	3.51996400	-1.49602700	1.66840400
H	3.63787400	-1.75417800	-0.26701200	C	6.47369300	-1.20902000	0.01372600
C	5.97576300	0.32984800	-1.58853600	H	6.81343400	0.07281300	-1.68067700
H	5.87561500	2.47907800	-1.54564600	H	5.83288800	-2.37374300	1.70626400
H	5.79829300	-1.81233900	-1.47460100	H	7.48951800	-1.58997800	0.03369600
H	6.92274400	0.30360000	-2.11737600	H	0.48294600	-2.06058800	0.23960800

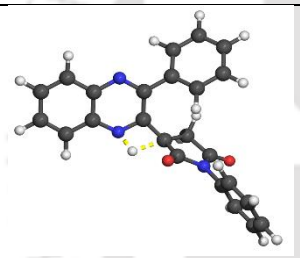

$TS_{1\text{-}A0'}$

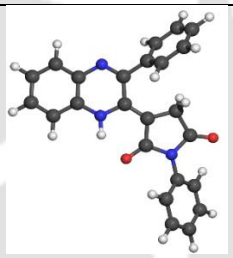

A_{0}'

C	-1.29148100	0.30491600	0.52459700	C	-1.01050700	-0.29359700	0.15604100
C	-3.14227300	1.73839600	0.21296700	C	-2.32429500	-2.32157300	0.09839100
C	-3.85289800	0.62645900	-0.30311400	C	-3.46032700	-1.56375100	-0.22607200
C	-2.03738600	-0.78523100	-0.03657400	C	-2.29012600	0.42643900	-0.01376700
H	-3.16819200	3.83784900	0.70650000	H	-1.52087700	-4.29322600	0.43942100
C	-3.73950600	3.00865300	0.30467300	C	-2.40447900	-3.71718400	0.18298200
C	-5.18672000	0.81854600	-0.73233700	C	-4.67486200	-2.21441400	-0.47969800
C	-5.76113100	2.06237300	-0.64517800	C	-4.75230600	-3.59248800	-0.40982000
C	-5.03521800	3.15978100	-0.12673800	C	-3.61342700	-4.33852800	-0.07336800
H	-5.71918900	-0.03672700	-1.13244000	H	-5.53711200	-1.60267100	-0.72180300
H	-6.78239000	2.21141900	-0.97855500	H	-5.69196100	-4.09670100	-0.60568800
H	-5.51077300	4.13281500	-0.06758500	H	-3.67818900	-5.41990000	-0.01139700
N	-1.87983700	1.48280700	0.66192800	N	-1.14668000	-1.64726200	0.31221300
N	-3.28786600	-0.61043800	-0.40147400	N	-3.40911000	-0.18053700	-0.23604700
C	-1.43132300	-2.12631400	-0.19984200	C	-2.35278900	1.90870800	0.09525900
C	-0.12203700	-2.26850600	-0.67019500	C	-1.93922100	2.54568800	1.26739000
C	-2.18440500	-3.26421100	0.10007200	C	-2.90085300	2.66448500	-0.94132500
C	0.43110100	-3.53484500	-0.81811900	C	-2.05862600	3.92480800	1.39468300
H	0.44977600	-1.39137100	-0.95402100	H	-1.52690200	1.95555600	2.08114600
C	-1.62465000	-4.52780500	-0.04158100	C	-3.00637200	4.04565300	-0.81828200
H	-3.20507900	-3.14487300	0.44810700	H	-3.24410700	2.16164800	-1.83933500
C	-0.31529200	-4.66494600	-0.49576400	C	-2.58453900	4.67768100	0.34800200
H	1.44501500	-3.63746000	-1.18999600	H	-1.74153800	4.41165400	2.31107500

TH-3369_166122017

H	-2.20969500	-5.40778500	0.20517800
H	0.12226700	-5.65206300	-0.60388500
C	0.07406500	0.51061100	1.02735700
C	0.75444000	-0.38284400	2.03555900
C	1.06650200	0.86684000	0.01814200
C	2.23288800	-0.19371300	1.74289800
H	0.52665500	-1.44904600	1.90369800
N	2.33976400	0.50732000	0.54157300
O	0.89886400	1.36784400	-1.08002400
O	3.15749500	-0.58376000	2.41859200
H	0.56019900	-0.13290100	3.08187100
H	-0.81499900	1.83588000	1.15890000
C	3.57717000	0.80463500	-0.09477000
C	4.65878100	1.24740700	0.66665000
C	3.70986100	0.63954100	-1.47359000
C	5.87287000	1.51493600	0.04502300
H	4.55027700	1.35978300	1.73760400
C	4.92552500	0.92369900	-2.08497200
H	2.86036400	0.31244500	-2.05868100
C	6.01144300	1.35710900	-1.33050700
H	6.71384600	1.85154100	0.64281400
H	5.02389200	0.79788400	-3.15843900
H	6.96076300	1.56918300	-1.81175100

H	-3.42277900	4.62869100	-1.63323100
H	-2.67166400	5.75489400	0.44498300
C	0.24746200	0.26499800	0.11849500
C	0.69281200	1.67294600	-0.15791300
C	1.42807400	-0.57268600	0.19763800
C	2.20088700	1.56011200	-0.29341400
H	0.48742500	2.38664300	0.64494000
N	2.55769000	0.23204900	-0.03797200
O	1.49419300	-1.78296700	0.41294000
O	2.96767100	2.45477700	-0.55890200
H	0.28022000	2.11014200	-1.07173700
C	3.89620500	-0.25397900	-0.04701800
C	4.77953300	0.17038900	-1.03872200
C	4.31751600	-1.14614600	0.93815100
C	6.08800400	-0.29863000	-1.03666700
H	4.44826400	0.87465600	-1.79072100
C	5.62412000	-1.61953800	0.91992500
H	3.62128600	-1.47687100	1.69813600
C	6.51389500	-1.19622100	-0.06275200
H	6.77606200	0.03902000	-1.80474400
H	5.94727300	-2.32046000	1.68264500
H	7.53447800	-1.56508900	-0.06925200
H	-0.26276300	-2.15125100	0.43706500

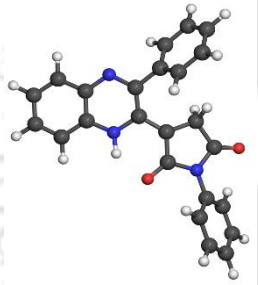

$^3A_0'$

C	-1.08594800	-0.26530200	0.09389500
C	-2.36811800	-2.30340200	0.02378500
C	-3.52795700	-1.49301500	-0.16049300
C	-2.27033900	0.45253900	0.02774500
H	-1.54955100	-4.28608700	0.20476200
C	-2.45203600	-3.70090500	0.05465200
C	-4.76143200	-2.15936600	-0.33848400
C	-4.83469800	-3.53633300	-0.31028200
C	-3.68100300	-4.31345800	-0.10710200
H	-5.64210500	-1.54389500	-0.48331900
H	-5.79386200	-4.02642900	-0.44174300
H	-3.75291200	-5.39516600	-0.07833800
N	-1.17007100	-1.65250500	0.14135900
N	-3.48934300	-0.13838600	-0.14861900
C	-2.31532000	1.92614600	0.17660500
C	-1.67458600	2.56020000	1.24592000
C	-3.07224700	2.69540000	-0.71176200
C	-1.75178700	3.94027500	1.40047400
H	-1.12588300	1.96039800	1.96701400
C	-3.14554200	4.07476500	-0.56026300
H	-3.60356400	2.19549000	-1.51457300
C	-2.48188100	4.70166700	0.49208600
H	-1.25495600	4.41861200	2.23855000

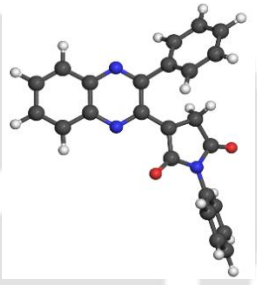

B

C	-1.11033300	-0.36476300	0.06893200
C	-2.44709300	-2.22954400	0.02422600
C	-3.59270700	-1.41321400	-0.16809100
C	-2.29878300	0.46779400	0.01636600
H	-1.70053500	-4.23636600	0.22821100
C	-2.59268300	-3.64035000	0.07134900
C	-4.85874000	-2.01645200	-0.34345100
C	-4.97152700	-3.38400800	-0.30491300
C	-3.83284500	-4.20053900	-0.08914500
H	-5.71718900	-1.37076200	-0.49250500
H	-5.94259700	-3.85041200	-0.43494700
H	-3.95067400	-5.27856600	-0.05513900
N	-1.21351700	-1.68849500	0.11568400
N	-3.48912100	-0.05614800	-0.14266600
C	-2.24259500	1.94064300	0.19659500
C	-1.53917900	2.49899300	1.26811600
C	-2.94225500	2.77861100	-0.67381900
C	-1.51671000	3.87687800	1.45122500
H	-1.01263800	1.84926900	1.96177700
C	-2.91026500	4.15682000	-0.49551500
H	-3.50709400	2.33840600	-1.48877100
C	-2.19596500	4.70873100	0.56456900
H	-0.97452600	4.30102200	2.28995500

TH-3369_166122017

H	-3.72779600	4.66404200	-1.26146400	H	-3.44734400	4.80169400	-1.18334400
H	-2.54675600	5.77820100	0.61273600	H	-2.17296700	5.78461200	0.70411800
C	0.26142300	0.24656800	-0.01741900	C	0.22149900	0.17095000	-0.03262600
C	0.69835500	1.55566200	-0.57997000	C	0.65506300	1.38733400	-0.78112400
C	1.44683600	-0.56834300	0.21712400	C	1.42432000	-0.56797300	0.39363400
C	2.20807100	1.43759700	-0.68109800	C	2.15554000	1.20845400	-0.94383000
H	0.45533700	2.41935700	0.04615000	H	0.48579400	2.32775400	-0.24553200
N	2.56849600	0.18770200	-0.16297400	N	2.53142800	0.08980400	-0.20229000
O	1.50812600	-1.71672200	0.64565300	O	1.51361000	-1.52084400	1.13257500
O	2.97074000	2.26552500	-1.11258400	O	2.89359100	1.92234800	-1.57837200
H	0.25793400	1.76172600	-1.56202400	H	0.17211300	1.49618300	-1.75716600
C	3.91055100	-0.27690700	-0.04654400	C	3.87950100	-0.34488700	-0.04904200
C	4.80489100	-0.08754700	-1.09821400	C	4.71965700	-0.39103100	-1.16045000
C	4.31851800	-0.91050000	1.12607100	C	4.34942100	-0.71695500	1.20945800
C	6.11539800	-0.53245800	-0.96694800	C	6.03716200	-0.80483400	-1.00432200
H	4.48107200	0.41534000	-2.00047100	H	4.34692500	-0.09096600	-2.13155200
C	5.62739100	-1.36233100	1.23942700	C	5.66537800	-1.14169500	1.34969700
H	3.61189600	-1.05936200	1.93301600	H	3.68412000	-0.69026100	2.06289500
C	6.52969600	-1.17258300	0.19697100	C	6.51326900	-1.18368900	0.24716000
H	6.81440700	-0.37920600	-1.78245400	H	6.69270000	-0.83348600	-1.86853500
H	5.94246900	-1.86048000	2.15023400	H	6.02858100	-1.43713200	2.32857100
H	7.55236300	-1.52248700	0.29213400	H	7.54140300	-1.51079400	0.36326500
H	-0.30200400	-2.15837000	0.30980800				

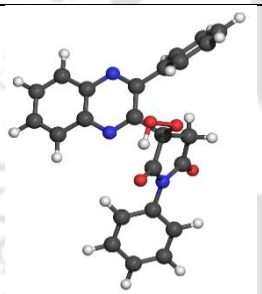

C

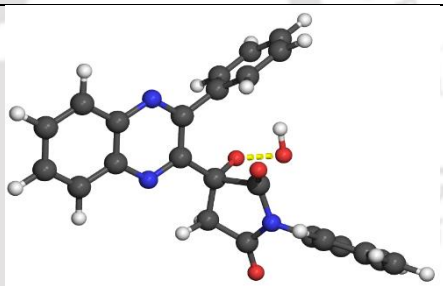

TS_{C-D}

C	1.35122000	5.06429500	-0.53513900	C	5.63599400	-2.03418400	-1.17428000
C	2.20580800	3.99670300	-0.63521300	C	5.05114900	-0.79411700	-1.18368200
C	1.75495600	2.70331100	-0.27712200	C	3.79650000	-0.60687000	-0.55544900
C	0.42644200	2.52839700	0.17357800	C	3.15734700	-1.70208300	0.06949600
C	-0.43947500	3.64321100	0.26661200	C	3.77892300	-2.97363300	0.06702600
C	0.02126100	4.88713800	-0.08036400	C	4.99638300	-3.13024900	-0.54394400
H	1.69242600	6.05834300	-0.80508400	H	6.59848700	-2.18325300	-1.65241000
H	3.22831700	4.10474400	-0.97963800	H	5.51833900	0.06288000	-1.65607400
H	-1.45306000	3.48138100	0.61681400	H	3.26772700	-3.79765400	0.55267300
H	-0.63628500	5.74735100	-0.01043700	H	5.47866200	-4.10213400	-0.54953400
C	0.80514000	0.28120700	0.41403800	C	1.40011500	-0.35205700	0.65514600
C	2.16570300	0.45636300	-0.02864000	C	2.06399200	0.77371700	0.04398400
C	3.12738000	-0.66780600	-0.21158300	C	1.50841600	2.16182300	0.01794200
C	3.67669500	-0.86405700	-1.48283200	C	0.98202500	2.66881600	-1.17253700
C	3.53074000	-1.48625600	0.84501500	C	1.55341700	2.97594800	1.15103500
C	4.59139600	-1.88660200	-1.70335500	C	0.48175900	3.96923100	-1.21886900
H	3.38204900	-0.20471000	-2.29329300	H	0.94695500	2.03253000	-2.04956300
C	4.45670800	-2.50042100	0.62263100	C	1.06240700	4.27492700	1.09996500
H	3.13114300	-1.32253700	1.83786900	H	1.96010300	2.58225500	2.07652600
C	4.98083500	-2.70888600	-0.64931200	C	0.52014100	4.77237800	-0.08289900
H	5.00567500	-2.03670800	-2.69503600	H	0.06250200	4.35164600	-2.14367000
H	4.77052300	-3.12839200	1.45007000	H	1.09561100	4.89798900	1.98762600
H	5.69891200	-3.50518200	-0.81787000	H	0.12617400	5.78281500	-0.11837600

TH-3369_166122017

C	0.17837500	-1.08640900	0.68366000
C	-1.30832900	-0.89468000	1.03258500
C	0.11642400	-1.95750300	-0.57187000
C	-1.27337900	-1.70914900	-1.13308200
H	0.19765600	-3.01293600	-0.29188900
H	0.88310800	-1.74425200	-1.31575700
N	-0.02656700	1.28816000	0.49575300
N	2.60156200	1.64465900	-0.38001700
N	-2.04866900	-1.12604600	-0.11611300
C	-3.43478800	-0.81319600	-0.23360200
C	-3.87835300	0.42828500	0.21568400
C	-4.31880000	-1.73215100	-0.79009200
C	-5.22751600	0.74400500	0.11763400
H	-3.16583800	1.12782200	0.63838600
C	-5.66457600	-1.39880700	-0.89541300
H	-3.95378900	-2.68640600	-1.14957600
C	-6.12212700	-0.16654800	-0.43852500
H	-5.58002000	1.70642400	0.47362700
H	-6.35804500	-2.10963000	-1.33216500
H	-7.17464900	0.08453200	-0.51880900
O	-1.67203400	-1.99064600	-2.23313000
O	-1.74672300	-0.65782400	2.13568900
O	0.78843400	-1.82319200	1.72129700
O	0.92154000	-0.96711600	2.85664800
H	-0.01258400	-0.85969200	3.11962500

C	0.01078100	-0.28202900	1.24627300
C	-1.15185800	-0.11311000	-0.10120100
C	-0.54836800	-1.51257000	1.94751100
C	-1.98927200	-1.66301400	1.51429100
H	-0.50160900	-1.41435600	3.03279400
H	0.01078800	-2.40289600	1.65383600
N	1.94425800	-1.54223600	0.65934600
N	3.22283800	0.62585300	-0.55336800
N	-2.20012900	-0.95252000	0.33893500
C	-3.46693900	-0.88144400	-0.32012800
C	-4.59963200	-0.53092100	0.41066800
C	-3.55162500	-1.14867800	-1.68394400
C	-5.83002400	-0.46291800	-0.23156500
H	-4.51192500	-0.32897000	1.47105000
C	-4.78473900	-1.05854900	-2.32007900
H	-2.65509400	-1.41068300	-2.23332700
C	-5.92476200	-0.72112500	-1.59624000
H	-6.71613400	-0.19804400	0.33581700
H	-4.85470500	-1.25938200	-3.38405700
H	-6.88630800	-0.65777100	-2.09517200
O	-2.82754100	-2.33244500	2.06909800
O	-0.75771500	0.00382900	-1.23917900
O	-0.35775800	0.85832200	1.79870500
O	-1.51866500	1.38934000	0.54233300
H	-0.92767100	1.99924400	0.05866400

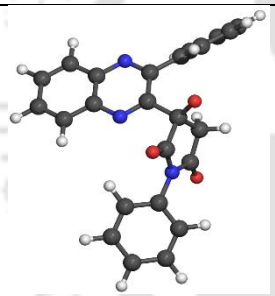

D

C	1.55697400	4.99959800	-0.47184400
C	2.39711000	3.91620900	-0.48582300
C	1.89267500	2.63422400	-0.15885700
C	0.52673700	2.48718000	0.17804000
C	-0.32348600	3.61812000	0.17987300
C	0.18824600	4.84967800	-0.13822000
H	1.93964900	5.98451300	-0.71834500
H	3.44829600	4.00324600	-0.73719800
H	-1.36723900	3.47727200	0.43827700
H	-0.45770200	5.72148100	-0.13623000
C	0.84209100	0.24151200	0.48641400
C	2.23458900	0.38526500	0.14129800
C	3.15890200	-0.77509800	0.01881700
C	3.81067500	-0.96790800	-1.20408100
C	3.41106700	-1.65337400	1.07572700
C	4.67585000	-2.04008400	-1.37738500
H	3.63226100	-0.26655100	-2.01282100
C	4.28370900	-2.72415600	0.89941500
H	2.94279300	-1.48709200	2.03892600
C	4.91032100	-2.92356700	-0.32565200
H	5.16918100	-2.18631300	-2.33275500

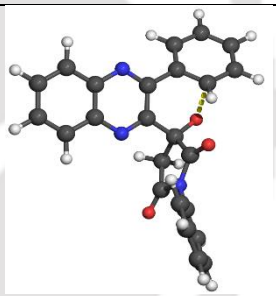

TS_{D-E}

C	2.58211900	4.75751800	0.44014400
C	3.15947400	3.52416900	0.59836700
C	2.42323900	2.35705300	0.27905500
C	1.09759600	2.48220000	-0.20827000
C	0.52315200	3.76556000	-0.36405300
C	1.25567800	4.87942600	-0.04276900
H	3.14183900	5.65364600	0.68736400
H	4.17055700	3.40306300	0.97135900
H	-0.49143200	3.82991000	-0.74183200
H	0.81947700	5.86593800	-0.15969800
C	0.94693600	0.21201700	-0.38183900
C	2.26649100	0.07976700	0.16715900
C	2.83798800	-1.26388400	0.35911000
C	4.16148800	-1.53596700	0.04107600
C	1.96349100	-2.31413200	0.75845100
C	4.63621900	-2.84306700	0.10810100
H	4.80593300	-0.72333200	-0.27616300
C	2.47495900	-3.63396900	0.83379800
H	1.05799300	-2.08269400	1.31148100
C	3.78503800	-3.89216600	0.49244900
H	5.67016400	-3.05351400	-0.14494400

TH-3369_166122017

H	4.47707000	-3.39871400	1.72689200	H	1.81891600	-4.42955300	1.16826100
H	5.58850800	-3.76020400	-0.45977600	H	4.17210700	-4.90459700	0.54433700
C	0.22932500	-1.14376800	0.74915100	C	0.13400900	-1.01511100	-0.82045600
C	-1.29898700	-0.89324100	1.14485700	C	-1.07104200	-1.10652300	0.15617000
C	0.09791200	-1.96116500	-0.55138400	C	-0.54949500	-0.75763100	-2.17529900
C	-1.31360200	-1.73328800	-1.04205500	C	-1.95962700	-0.32255400	-1.84357000
H	0.23103300	-3.02164400	-0.31946200	H	-0.59948000	-1.69837100	-2.73160000
H	0.82015000	-1.68808200	-1.32202900	H	-0.05384700	-0.00640100	-2.78837100
N	0.02359800	1.26103000	0.48200500	N	0.38067700	1.37700800	-0.54819900
N	2.72412600	1.55910100	-0.18701500	N	2.99208800	1.13529500	0.45911100
N	-2.04734000	-1.16496900	0.00972100	N	-2.19838200	-0.62140100	-0.49127300
C	-3.42793200	-0.81264500	-0.08851500	C	-3.44975600	-0.40191100	0.15694900
C	-3.81582700	0.48285300	0.24094600	C	-3.47885400	0.26601800	1.37844400
C	-4.35560400	-1.75339700	-0.52171700	C	-4.62577900	-0.84980100	-0.43781600
C	-5.15656100	0.83389400	0.14428900	C	-4.69772200	0.47517200	2.01213100
H	-3.06804000	1.19454400	0.57251600	H	-2.55448500	0.60809100	1.82819500
C	-5.69280000	-1.38670900	-0.62728100	C	-5.84073400	-0.62399100	0.19884500
H	-4.03096800	-2.75364500	-0.78234500	H	-4.58758800	-1.35574900	-1.39475300
C	-6.09526000	-0.09745100	-0.29189000	C	-5.87981600	0.03376800	1.42453700
H	-5.46696600	1.84049700	0.40417800	H	-4.72226800	0.98898100	2.96739800
H	-6.42131000	-2.11400500	-0.96931600	H	-6.75888800	-0.96804400	-0.26549500
H	-7.14077600	0.18155300	-0.37211300	H	-6.83000800	0.20259400	1.92057300
O	-1.76601400	-2.00762000	-2.12372500	O	-2.76934600	0.15378200	-2.59667500
O	-1.69991400	-0.53187500	2.20978400	O	-1.03074100	-1.49900500	1.30000000
O	0.76400600	-1.81164100	1.78942800	O	0.86884100	-2.17953100	-0.90555800
	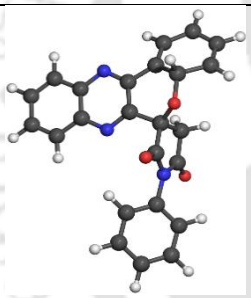				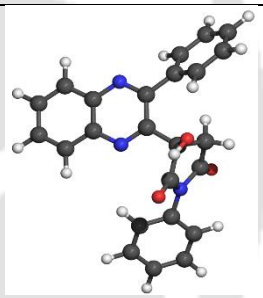		
	E				**1a**		
C	2.26074400	4.93431000	-0.35930900	C	1.36284700	5.00611600	-0.56966900
C	2.97266400	3.76351100	-0.29902700	C	2.19883800	3.92378300	-0.66794600
C	2.29888500	2.53489100	-0.09410700	C	1.74838300	2.65132000	-0.23985300
C	0.88379700	2.53523500	0.03933000	C	0.44080300	2.51240000	0.27659100
C	0.17327200	3.75383100	-0.02904900	C	-0.40610100	3.64214300	0.36859200
C	0.85207800	4.93082400	-0.22246500	C	0.05353700	4.86543000	-0.04631800
H	2.77787300	5.87572700	-0.51292200	H	1.70319300	5.98412200	-0.89395600
H	4.05214400	3.73959600	-0.40037200	H	3.20513000	4.00488100	-1.06374200
H	-0.90583400	3.72100500	0.07490300	H	-1.40221900	3.50773200	0.77614300
H	0.30904200	5.86862900	-0.27397700	H	-0.58801700	5.73770000	0.02310500
C	0.90929600	0.28113300	0.28984700	C	0.79944900	0.26467000	0.59327300
C	2.33918400	0.27467300	0.18191400	C	2.14485800	0.40609300	0.08193400
C	2.97645300	-1.02804300	0.21148500	C	3.10370900	-0.71995700	-0.10666400
C	4.13523200	-1.31633900	-0.48126900	C	3.78094300	-0.79882300	-1.32941400
C	2.31275900	-2.10564200	1.02991600	C	3.37504800	-1.66630100	0.88498200
C	4.56711400	-2.63652500	-0.64332400	C	4.69340900	-1.81867300	-1.56570800
H	4.65804000	-0.49982900	-0.96958800	H	3.58260600	-0.04998600	-2.08867700
C	2.62838200	-3.48651800	0.53357900	C	4.29754100	-2.68060900	0.64698900
C	3.74830000	-3.71763300	-0.19457600	H	2.86092600	-1.61098000	1.83599900
H	5.46946200	-2.84385000	-1.20745100	C	4.95301800	-2.76440400	-0.57685400
H	1.98124800	-4.28777200	0.87479500	H	5.20238900	-1.87552000	-2.52239400
H	4.01590700	-4.73253700	-0.47155200	H	4.50461000	-3.40750700	1.42576000

TH-3369_166122017

C	0.23088500	-1.07464500	0.38480600
C	-1.18909700	-0.87657100	0.94362200
C	-0.01235300	-1.67110500	-1.01231800
C	-1.45761500	-1.33479900	-1.32799000
H	0.09392300	-2.75964400	-0.96851000
H	0.64587100	-1.29323900	-1.79603900
N	0.19605800	1.36741300	0.21481700
N	3.02025500	1.38265200	-0.02852000
N	-2.07049200	-0.92846800	-0.13813300
C	-3.43430000	-0.52382500	-0.04725400
C	-3.73603800	0.68512300	0.57466900
C	-4.43861000	-1.32217800	-0.58514400
C	-5.06209700	1.08829700	0.66938800
H	-2.93365900	1.29183300	0.97842500
C	-5.76118600	-0.90159500	-0.49670200
H	-4.18445500	-2.25260900	-1.07814500
C	-6.07582800	0.29840100	0.13357000
H	-5.30217500	2.02609700	1.15937100
H	-6.54734500	-1.51850600	-0.91920400
H	-7.11010300	0.61859900	0.20675500
O	-2.00425400	-1.42407100	-2.39842100
O	-1.48223100	-0.68312000	2.09161300
O	0.92026400	-1.91535900	1.27273600
H	2.75754800	-2.03313500	2.04139400
H	5.66785200	-3.56049900	-0.75940600
C	0.18727800	-1.07194500	1.03939000
C	-1.31953400	-0.85328000	1.25420300
C	0.19596300	-2.11730400	-0.07988100
C	-1.13988800	-1.92697800	-0.78019100
H	0.22528400	-3.11799000	0.36197600
H	1.01202000	-2.03745400	-0.79655900
N	-0.00941000	1.29260800	0.66885500
N	2.57371800	1.57758200	-0.33480600
N	-1.97489800	-1.19424700	0.08070000
C	-3.33313600	-0.85967500	-0.18892600
C	-3.76286300	0.43729300	0.08213300
C	-4.20411600	-1.80670800	-0.71865000
C	-5.08464000	0.78216400	-0.16965600
H	-3.05982100	1.15722100	0.48650300
C	-5.52148900	-1.44522800	-0.97879300
H	-3.84971800	-2.80647600	-0.93663600
C	-5.96543200	-0.15585400	-0.70162400
H	-5.42540700	1.78981000	0.04423400
H	-6.20383400	-2.17858900	-1.39550200
H	-6.99635700	0.11754100	-0.90102700
O	-1.46156600	-2.34933700	-1.86118200
O	-1.81369600	-0.50969900	2.29968000
O	0.73067600	-1.53013800	2.25029500
H	0.20162600	-1.10625800	2.94294600

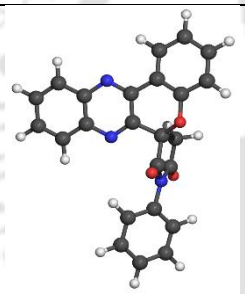

1b

C	-2.26264200	4.90602700	0.16298400
C	-2.97599600	3.73531800	0.13244900
C	-2.29544800	2.49595000	0.05850500
C	-0.87590400	2.48592500	0.02068500
C	-0.16281700	3.70617500	0.05198800
C	-0.84715500	4.89259700	0.12121700
H	-2.78362000	5.85605800	0.22004600
H	-4.05994800	3.71975400	0.16216200
H	0.92061800	3.66479300	0.02238300
H	-0.30452500	5.83171600	0.14614500
C	-0.90424100	0.21883600	-0.06254000
C	-2.33237600	0.21932300	-0.03989500
C	-3.01147700	-1.07849600	-0.09520100
C	-4.38612800	-1.21856600	0.11614600
C	-2.25430300	-2.21066100	-0.41968100
C	-4.99277900	-2.45873000	-0.00101700
H	-4.95811900	-0.33056500	0.36269900
C	-2.85874100	-3.45748500	-0.55017600
C	-4.22572700	-3.57516000	-0.34119800
H	-6.05924100	-2.56144600	0.16583300
H	-2.24544000	-4.31081900	-0.81623900

TH-3369_166122017

H	-4.69730500	-4.54744200	-0.44010000
C	-0.18997900	-1.11850800	-0.01504200
C	1.16677900	-0.98572000	-0.73168100
C	0.19175200	-1.48756400	1.42691400
C	1.65956700	-1.12093400	1.54261200
H	0.08823900	-2.56726400	1.57098700
H	-0.38517700	-0.97618600	2.19845900
N	-0.18997800	1.30883100	-0.03460900
N	-3.01276200	1.33992900	0.02255000
N	2.15088400	-0.90060000	0.25037100
C	3.50134700	-0.54046700	-0.03308500
C	3.74948100	0.55839100	-0.85172000
C	4.54769000	-1.27665000	0.51358700
C	5.06304700	0.91166500	-1.13483300
H	2.91729400	1.11846400	-1.26202500
C	5.85810600	-0.90503800	0.23458700
H	4.33557100	-2.12019400	1.15928700
C	6.11849700	0.18396600	-0.59174400
H	5.26162500	1.76200700	-1.77877700
H	6.67756600	-1.47196200	0.66357400
H	7.14325300	0.46518700	-0.81129200
O	2.30950500	-1.05750500	2.55466400
O	1.33378400	-0.93740700	-1.91995600
O	-0.91467900	-2.13638600	-0.67401900

V.5.7. Detection of in situ Generated H_2O_2:

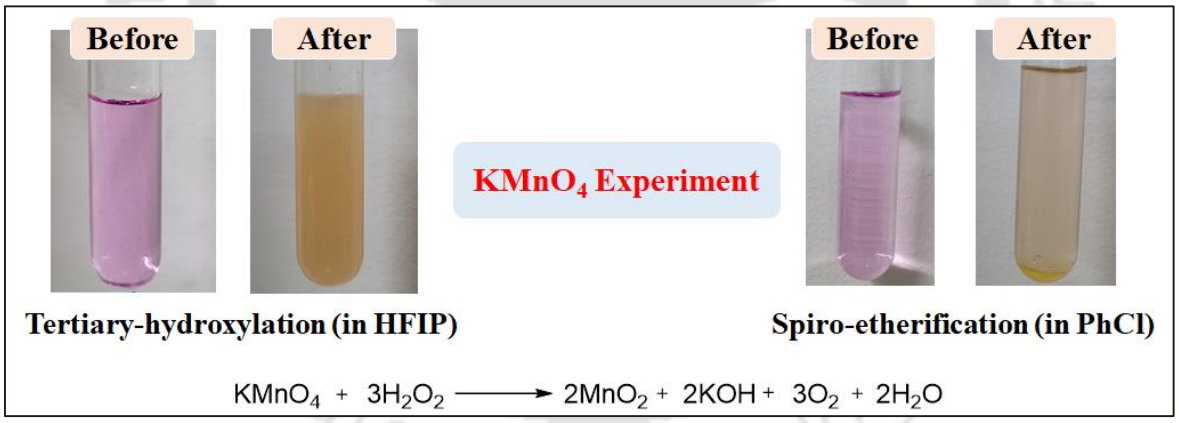

Figure V.5.19. *$KMnO_4$ experiment during the course of the reaction for H_2O_2 detection*

TH-3369_166122017

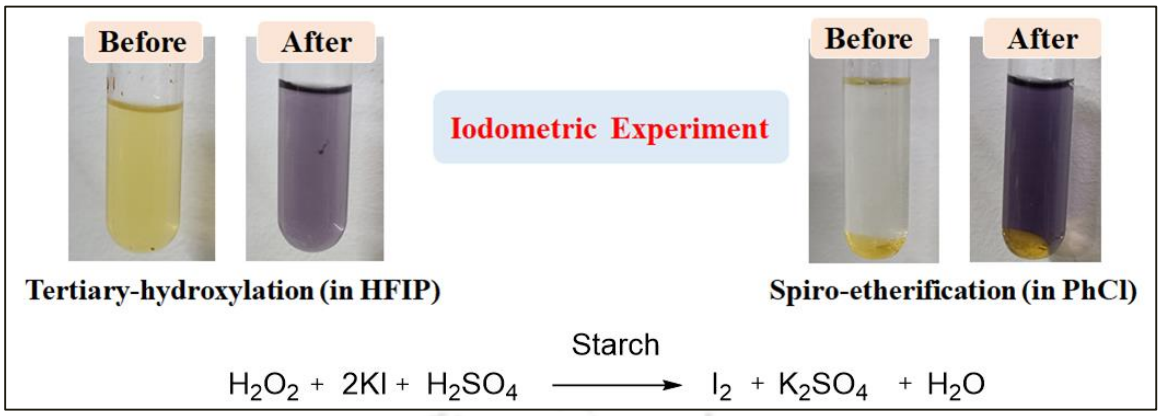

Figure V.5.20. *Iodometric experiment during the course of the reaction for H_2O_2 detection*

V.5.8. Detection of Intermediates of *tertiary*-Hydroxylation (HRMS analysis of reaction aliquot):

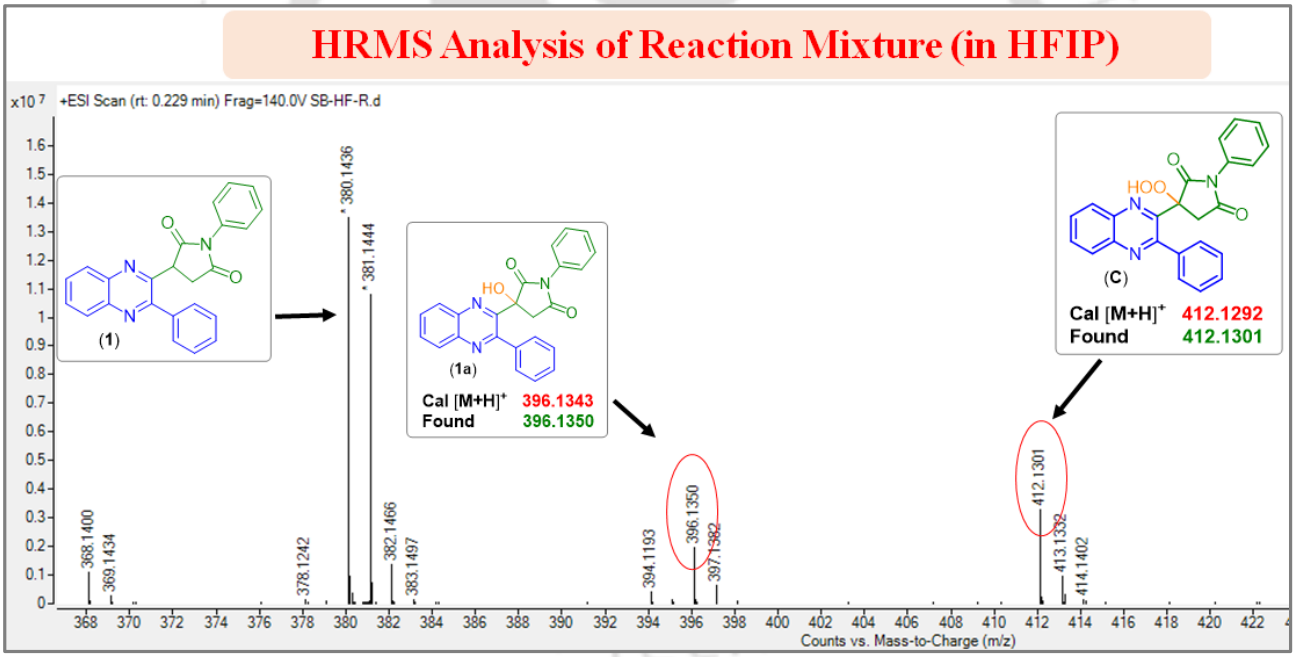

Figure V.5.21. Detection of intermediate: *HRMS analysis during the course of the tertiary-hydroxylation reaction*

TH-3369_166122017

V.6. References

1. (a) Hartwig, J. F. Carbon−Heteroatom Bond Formation Catalysed by Organometallic Complexes. *Nature* **2008**, *455*, 314. (b) Bagley, M. C.; Dale, J. W.; Merritt, E. A.; Xiong, X. Thiopeptide Antibiotics. *Chem. Rev.* **2005**, *105*, 685. (c) Kim, J.; Movassaghi, M. Biogenetically Inspired Syntheses of Alkaloid Natural Products. *Chem. Soc. Rev*. **2009**, *38*, 3035.
2. (a) Roughley, S. D.; Jordan, A. M. The Medicinal Chemist's Toolbox: An Analysis of Reactions Used in the Pursuit of Drug Candidates. *J. Med. Chem*. **2011**, *54*, 3451. (b) Delost, M. D.; Smith, D. T.; Anderson, B. J.; Njardarson, J. T. From Oxiranes to Oligomers: Architectures of U.S. FDA Approved Pharmaceuticals Containing Oxygen Heterocycles. *J. Med. Chem*. **2018**, *61*, 10996. (c) Cramer, J.; Sager, C. P.; Ernst, B. Hydroxyl Groups in Synthetic and Natural-Product-Derived Therapeutics: A Perspective on a Common Functional Group. *J. Med. Chem*. **2019**, *62*, 8915.
3. (a) Chen, K.; Baran, P. S. Total Synthesis of Eudesmane Terpenes by Site-Selective C–H Oxidations. *Nature* **2009**, *459*, 824. (b) Jørgensen, L.; McKerrall, S. J.; Kuttruff, C. A.; Ungeheuer, F.; Felding, J.; Baran, P. S. 14-Step Synthesis of (+)-Ingenol from (+)-3-Carene. *Science* **2013**, *341*, 878. (c) Howell, J. M.; Feng, K.; Clark, J. R.; Trzepkowski, L. J.; White, M. C. Remote Oxidation of Aliphatic C-H Bonds in Nitrogen-containing Molecules. *J. Am. Chem. Soc*. **2015**, *137*, 14590. (c) Chen, M. S.; White, M. C. A Predictably Selective Aliphatic C−H Oxidation Reaction for Complex Molecule Synthesis. *Science* **2007**, *318*, 783. (d) Newhouse, T.; Baran, P. S. If C−H Bonds Could Talk: Selective C−H Bond Oxidation. *Angew. Chem., Int. Ed*. **2011**, *50*, 3362. (e) White, M. C.; Zhao, J. Aliphatic C–H Oxidations for Late-Stage Functionalization. *J. Am. Chem. Soc.* **2018**, *140*, 13988. (f) Wein, L. A.; Wurst, K.; Magauer, T. Total Synthesis and Late-Stage C−H Oxidations of ent-Trachylobane Natural Products. *Angew. Chem., Int. Ed*. **2022**, *61*, e202113829. (g) Venugopal, N.; Moser, J.; Vojtíčková, M.; Císařová I.; König, B.; Jahn, U. Single Electron Transfer-Induced Selective α-Oxygenation of Glycine Derivatives. *Adv. Synth. Catal*., **2022**, *364*, 405.
4. (a) Cramer, J.; Sager, C. P.; Ernst, B. Hydroxyl Groups in Synthetic and Natural-Product-Derived Therapeutics: A Perspective on a Common Functional Group. *J. Med. Chem*. **2019**, *62*, 8915. (b) Chen, S.-T.; Fang, J.-M. Preparation of Optically Active Tertiary Alcohols by Enzymatic Methods. Application to the Synthesis of Drugs and Natural Products. *J. Org. Chem*. **1997**, *62*, 4349. (c) Müller, M. Chemoenzymatic Synthesis of Building Blocks for Statin Side Chains. *Angew. Chem., Int. Ed*. **2005**, *44*, 362.

TH-3369_166122017

5. (a) Keh, C. C. K.; Wei, C.; Li, C.-J. The Barbier−Grignard-Type Carbonyl Alkylation Using Unactivated Alkyl Halides in Water. *J. Am. Chem. Soc*. **2003**, *125*, 4062. (b) Li, J. J., Barbier Reaction. *Name Reactions: A Collection of Detailed Mechanisms and Synthetic Applications*, 5th Edition; Springer International Publishing: Cham, 2014; pp 21−22.
6. (a) Pierce, C. J.; Hilinski, M. K. Chemoselective Hydroxylation of Aliphatic sp^3 C–H Bonds Using a Ketone Catalyst and Aqueous H_2O_2. *Org. Lett.* **2014**, *16*, 6504. (b) Kiyokawa, K.; Ito, R.; Takemoto, K.; Minakata, S. C–H Oxygenation at Tertiary Carbon Centers using Iodine Oxidant. *Chem. Commun*. **2018**, *54*, 7609.
7. (a) Chen, J.; Song, W.; Yao, J.; Wu, Z.; Lee, Y.-M.; Wang, Y.; Nam, W.; Wang, B. Hydrogen Bonding-Assisted and Nonheme Manganese-Catalyzed Remote Hydroxylation of C-H Bonds in Nitrogen-Containing Molecules. *J. Am. Chem. Soc*. **2023**, *145*, 5456. (b) Burg, F.; Breitenlechner, S.; Jandl, C.; Bach, T. Enantioselective Oxygenation of Exocyclic Methylene Groups by a Manganese Porphyrin Catalyst with a Chiral Recognition Site. *Chem. Sci*. **2020**, *11*, 2121. (c) Bryliakov, K. P. Transition Metal-Catalyzed Direct Stereoselective Oxygenations of C(sp^3)–H Groups. *ACS Catalysis* **2023**, *13* (16), 10770. (d) Lu, H.; Zhang, X. P. Catalytic C−H Functionalization by Metalloporphyrins: Recent Developments and Future Directions. *Chem. Soc. Rev*. **2011**, *40*, 1899.
8. (a) Li, G. X.; Morales-Rivera, C. A.; Gao, F.; Wang, Y.; He, G.; Liu, P.; Chen, G. A Unified Photoredox-Catalysis Strategy for C(sp^3)–H Hydroxylation and Amidation Using Hypervalent Iodine. *Chem. Sci*. **2017**, *8*, 7180. (b) Zhang, Y.; Qin, S.; Claes, N.; Schilling, W.; Sahoo, P. K.; Ching, H. Y. V.; Jaworski, A.; Lemière, F.; Slabon, A.; Van Doorslaer, S.; Bals, S.; Das, S. Direct Solar Energy-Mediated Synthesis of Tertiary Benzylic Alcohols Using a Metal-Free Heterogeneous Photocatalyst. *ACS Sustain. Chem. Eng*. **2022**, *10*, 530. (c) Paolillo, J. M.; Duke, A. D.; Gogarnoiu, E. S.; Wise, D. E.; Parasram, M. Anaerobic Hydroxylation of C(Sp^3)-H Bonds Enabled by the Synergistic Nature of Photoexcited Nitroarenes. *J. Am. Chem. Soc*. **2023**, *145*, 2794. (d) Khandelia, T.; Ghosh, S.; Panigrahi, P.; Mandal, R.; Boruah, D.; Patel, B. K. Photo-induced 1, 2-Thiohydroxylation of Maleimide Involving Disulfide and Singlet Oxygen. *Chem. Commun*. **2023**, *59*, 11196.
9. (a) Roiban, G. D.; Agudo, R.; Reetz, M. T. Cytochrome P450 Catalyzed Oxidative Hydroxylation of Achiral Organic Compounds with Simultaneous Creation of Two Chirality Centers in a Single C-H Activation Step. *Angew. Chem., Int. Ed*. **2014**, *53*, 8659. (b) Münch, J.; Püllmann, P.; Zhang, W.; Weissenborn, M. J. Enzymatic Hydroxylations of sp^3-Carbons. *ACS Catal*. **2021**, *11*, 9168. (c)

TH-3369_166122017

Lu, J.; Lai, W.; Chen, H. C(sp^3)-H Hydroxylation in Diiron β-Hydroxylase CmlA Transpires by Amine-Assisted O_2 Activation Avoiding $FeIV_2O_2$ Species. *Angew. Chem., Int. Ed*. **2022**, *61*, e202211843. (d) Mao, Y.; Zhang, W.; Fu, Z.; Liu, Y.; Chen, L.; Lian, X.; Zhuo, D.; Wu, J.; Zheng, M.; Liao C. Versatile Biocatalytic C(sp^3)−H Oxyfunctionalization for the Site- Selective and Stereodivergent Synthesis of α- and β-Hydroxy Acids. *Angew. Chem., Int. Ed*. **2023**, *62*, e202305250. (e) Milan, M.; Bietti, M.; Costas, M. Enantioselective Aliphatic C-H Bond Oxidation Catalyzed by Bioinspired Complexes. *Chem. Commun*. **2018**, *54*, 9559.

10. (a) Schutyser, W.; Renders, T.; Van den Bosch, S.; Koelewijn, S. F.; Beckham, G. T.; Sels, B. F. Chemicals from Lignin: An Interplay of Lignocellulose Fractionation, Depolymerisation, and Upgrading. *Chem. Soc. Rev*. **2018**, *47*, 852. (b) Evano, G.; Wang, J.; Nitelet, A. Metal-mediated C−O bond forming reactions in natural product synthesis. *Org. Chem. Front*. **2017**, *4*, 2480. (c) Connolly, S. J.; Kates, R. E.; Lebsack, C. S.; Harrison, D. C.; Winkle, R. A. Clinical pharmacology of propafenone. *Circulation* **1983**, *68*, 589.
11. (a) María, P. D. de; van Gemert, R. W.; Straathof, A. J. J.; Hanefeld, U. Biosynthesis of ethers: Unusual or common natural events?. *Nat. Prod. Rep*. **2010**, *27*, 370. (b) Koiso, Y.; Natori, M.; Iwasaki, S.; Sato, S.; Sonoda, R.; Fujita, Y.; Yaegashi, H.; Sato, Z. Ustiloxin: A Phytotoxin and A Mycotoxin from False Smuth Balls on Rice Panicles. *Tetrahedron Lett*. **1992**, *33*, 4157. (c) Shennan, B. D. A.; Berheci, D.; Crompton, J. L.; Davidson, T. A.; Field, J. L.; Williams, B. A.; Dixon, D. J. Branching Out: Redox Strategies Towards the Synthesis of Acyclic α-Tertiary Ethers. *Chem. Soc. Rev*. **2022**, *51*, 5878.
12. (a) Williamson, A. Theory of etherification. *Philos. Mag*. **1850**, *37*, 350. (b) Fuhrmann, E.; Talbiersky, J. Synthesis of Alkyl Aryl Ethers by Catalytic Williamson Ether Synthesis with Weak Alkylation Agents. *Org. Process Res. Dev*. **2005**, *9*, 206.
13. (a) Bhunia, S.; Pawar, G. G.; Kumar, S. V.; Jiang, Y.; Ma, D. Selected Copper-Based Reactions for C–N, C–O, C–S, and C–C Bond Formation. *Angew. Chem., Int. Ed*. **2017**, *56*, 16136. (b) Enthaler, S.; Company, A. Palladium-catalysed Hydroxylation and Alkoxylation. *Chem. Soc. Rev*. **2011**, *40*, 4912. (c) Wu, X.; Fors, B. P.; Buchwald, S. L. A Single Phosphine Ligand Allows Palladium-Catalyzed Intermolecular C□O Bond Formation with Secondary and Primary Alcohols. *Angew. Chem., Int. Ed*. **2011**, *50*, 9943. (d) Chen, Z.; Jiang, Y.; Zhang, L.; Guo, Y.; Ma, D. Oxalic Diamides and tert-Butoxide: Two Types of Ligands Enabling Practical Access to Alkyl Aryl Ethers via Cu-Catalyzed Coupling Reaction. *J. Am. Chem. Soc*. **2019**, *141*, 3541. (e) Zhou, Z.; Behnke, N. E.; Kürti, L. Copper-Catalyzed Synthesis of Hindered Ethers from α-Bromo Carbonyl

TH-3369_166122017

Compounds. *Org. Lett*. **2018**, *20*, 5452. (f) Wang, P.-Z.; Chen, J.-R.; Xiao, W.-J. Emerging Trends in Copper-Promoted Radical-Involved C–O Bond Formations. *J. Am. Chem. Soc*. **2023**, *145*, 17527. (g) MacQueen, P. M.; Tassone, J. P.; Diaz, C.; Stradiotto, M. Exploiting Ancillary Ligation To Enable Nickel-Catalyzed C–O Cross-Couplings of Aryl Electrophiles with Aliphatic Alcohols. *J. Am. Chem. Soc*. **2018**, *140*, 5023.

14. (a) Terrett, J. A.; Cuthbertson, J. D.; Shurtleff, V. W.; MacMillan, D. W. C. Switching on elusive organometallic mechanisms with photoredox catalysis. *Nature* **2015**, *524*, 330. (b) Zhang, L.; Israel, E. M.; Yan, J.; Ritter, T. Copper-mediated etherification via aryl radicals generated from triplet states. *Nature Synthesis* **2022**, *1*, 376. (c) Sang, R.; Korkis, S. E.; Su, W.; Ye, F.; Engl, P. S.; Berger, F.; Ritter, T. Site-Selective C–H Oxygenation via Aryl Sulfonium Salts. *Angew. Chem., Int. Ed*. **2019**, *58*, 16161. (d) Vijeta, A.; Casadevall, C.; Roy, S.; Reisner, E. Visible-Light Promoted C-O Bond Formation with an Integrated Carbon Nitride-Nickel Heterogeneous Photocatalyst. *Angew. Chem., Int. Ed*. **2021**, *60*, 8494. (e) Ali, W.; Saha, A.; Ge, H.; Maiti, D. Photoinduced meta-Selective C-H Oxygenation of Arenes. *JACS Au*, **2023**, *3*, 1790.
15. (a) Prier, C. K.; Rankic, D. A.; MacMillan, D. W. C. Visible Light Photoredox Catalysis with Transition Metal Complexes: Applications in Organic Synthesis. *Chem. Rev*. **2013**, *113*, 5322. (b) Romero, N. A.; Nicewicz, D. A. Organic Photoredox Catalysis. *Chem. Rev*. **2016**, *116*, 10075. (c) Bell, J. D.; Murphy, J. A. Recent Advances in Visible Light-Activated Radical Coupling Reactions Triggered by (I) Ruthenium, (II) Iridium And (III) Organic Photoredox Agents. *Chem. Soc. Rev*. **2021**, *50*, 9540. (d) Cannalire, R.; Pelliccia, S.; Sancineto, L.; Novellino, E.; Tron, G. C.; Giustiniano, M. Visible Light Photocatalysis in the Late-Stage Functionalization of Pharmaceutically Relevant Compounds. *Chem. Soc. Rev*. **2021**, *50*, 766. (e) Pei, C.; Empel, C.; Koenigs, R. M. Visible-Light-Induced, Single-Metal-Catalyzed, Directed C–H Functionalization: Metal-Substrate-Bound Complexes as Light-Harvesting Agents. *Angew. Chem., Int. Ed*. **2022**, *61*, e202201743.
16. (a) StriethKalthoff, F.; James, M. J.; Teders, M.; Pitzer, L.; Glorius, F. Energy Transfer Catalysis Mediated by Visible Light: Principles, Applications, Directions. *Chem. Soc. Rev*. **2018**, *47*, 7190. (b) Zhou, Q.-Q.; Zou, Y.-Q.; Lu, L.-Q.; Xiao, W.-J. Visible-Light-Induced Organic Photochemical Reactions through Energy-Transfer Pathways. *Angew. Chem., Int. Ed*. **2019**, *58*, 1586. (c) Großkopf, J.; Kratz, T.; Rigotti, T.; Bach, T. Enantioselective Photochemical Reactions Enabled by Triplet Energy Transfer. *Chem. Rev*. **2022**, *122*, 1626.
17. Dahiya, A.; Gevondian, A. G.; Schoenebeck, F. Orthogonal C-O Bond Construction with

TH-3369_166122017

Organogermanes. *J. Am. Chem. Soc*. **2023**, *145*, 7729.

18. Liu, Y.; Wang, B.; Qiao, X.; Tung, C.-H.; Wang, Y. Iodine/Visible Light Photocatalysis for Activation of Alkynes for Electrophilic Cyclization Reactions. *ACS Catal*. **2017**, *7*, 4093.
19. Rivero, A. R.; Fodran, P.; Ondrejková, A.; Wallentin, C.-J. Alcohol Etherification via Alkoxy Radicals Generated by Visible-Light Photoredox Catalysis. *Org. Lett*. **2020**, *22*, 8436.
20. Even after several attempts, the corresponding transition state in HFIP solvent was not optimized.
21. Ghosh, S.; Pal, S.; Rajamanickam, S.; Shome, R.; Mohanta, P. R.; Ghosh, S. S.; Patel, B. K. Access to Multifunctional AEEgens via Ru(II)-Catalyzed Quinoxaline–Directed Oxidative Annulation. *ACS Omega* **2019**, *4*, 5565.
22. Stratmann, R. E.; Burant, J. C.; Scuseria, G. E; Frisch, M. J. Improving harmonic vibrational frequencies calculations in density functional theory. *J. Chem. Phys.* **1997**, *106*, 10175.
23. Chai, J.-D.; Head-Gordon, M. Long-Range Corrected Hybrid Density Functionals with Damped Atom–Atom Dispersion Corrections. *Phys. Chem. Chem. Phys.* **2008**, *10*, 6615.
24. Ditchfield, R.; Hehre, W. J.; Pople, J. A. Self-Consistent Molecular-Orbital Methods. IX. An Extended Gaussian-Type Basis for Molecular-Orbital Studies of Organic Molecules. *J. Chem. Phys.* **1971**, *54*, 724.
25. Marenich, A. V.; Cramer, C. J.; Truhlar, D. G. Universal Solvation Model Based on Solute Electron Density and on a Continuum Model of the Solvent Defined by the Bulk Dielectric Constant and Atomic Surface Tensions. *J. Phys. Chem. B* **2009**, *113*, 6378.
26. Li, G.-X.; Morales-Rivera, C. A.; Gao, F.; Wang, Y.; He, G.; Liu, P.; Chen, G. A Unified Photoredox-Catalysis Strategy for C(sp^3)–H Hydroxylation and Amidation Using Hypervalent Iodine. *Chem. Sci.* **2017**, *8*, 7180.
27. Gaussian 09, Revision D.01, M. J. Frisch, G. W. Trucks, H. B. Schlegel, G. E. Scuseria, M. A. Robb, J. R. Cheeseman, G. Scalmani, V. Barone, B. Mennucci, G. A. Petersson, H. Nakatsuji, M. Caricato, X. Li, H. P. Hratchian, A. F. Izmaylov, J. Bloino, G. Zheng, J. L. Sonnenberg, M. Hada, M. Ehara, K. Toyota, R. Fukuda, J. Hasegawa, M. Ishida, T. Nakajima, Y. Honda, O. Kitao, H. Nakai, T. Vreven, J. A. Montgomery, Jr., J. E. Peralta, F. Ogliaro, M. Bearpark, J. J. Heyd, E. Brothers, K. N. Kudin, V. N. Staroverov, R. Kobayashi, J. Normand, K. Raghavachari, A. Rendell, J. C. Burant, S. S. Iyengar, J. Tomasi, M. Cossi, N. Rega, J. M. Millam, M. Klene, J. E. Knox, J. B. Cross, V. Bakken, C. Adamo, J. Jaramillo, R. Gomperts, R. E. Stratmann, O. Yazyev, A. J. Austin, R. Cammi, C. Pomelli, J. W. Ochterski, R. L. Martin, K. Morokuma, V. G. Zakrzewski, G. A. Voth, P. Salvador, J. J. Dannenberg, S. Dapprich, A. D. Daniels, Ö. Farkas, J. B. Foresman, J.

TH-3369_166122017

V. Ortiz, J. Cioslowski, and D. J. Fox, Gaussian, Inc., Wallingford CT, 2009.

28. Adamo, C.; Jacquemin, D. The calculations of excited-state properties with Time-Dependent Density Functional Theory. *Chem. Soc. Rev.* **2013**, *42*, 845.
29. Gaussian 16, Revision B.01, M. J. Frisch, G. W. Trucks, H. B. Schlegel, G. E. Scuseria, M. A. Robb, J. R. Cheeseman, G. Scalmani, V. Barone, G. A. Petersson, H. Nakatsuji, X. Li, M. Caricato, A. V. Marenich, J. Bloino, B. G. Janesko, R. Gomperts, B. Mennucci, H. P. Hratchian, J. V. Ortiz, A. F. Izmaylov, J. L. Sonnenberg, D. Williams-Young, F. Ding, F. Lipparini, F. Egidi, J. Goings, B. Peng, A. Petrone, T. Henderson, D. Ranasinghe, V. G. Zakrzewski, J. Gao, N. Rega, G. Zheng, W. Liang, M. Hada, M. Ehara, K. Toyota, R. Fukuda, J. Hasegawa, M. Ishida, T. Nakajima, Y. Honda, O. Kitao, H. Nakai, T. Vreven, K. Throssell, J. A. Montgomery, Jr., J. E. Peralta, F. Ogliaro, M. J. Bearpark, J. J. Heyd, E. N. Brothers, K. N. Kudin, V. N. Staroverov, T. A. Keith, R. Kobayashi, J. Normand, K. Raghavachari, A. P. Rendell, J. C. Burant, S. S. Iyengar, J. Tomasi, M. Cossi, J. M. Millam, M. Klene, C. Adamo, R. Cammi, J. W. Ochterski, R. L. Martin, K. Morokuma, O. Farkas, J. B. Foresman, and D. J. Fox, Gaussian, Inc., Wallingford CT, 2016.
30. Lu, T.; Chen, F. Multiwfn: A Multifunctional Wavefunction Analyzer. *J. Comput. Chem.* **2012**, *33*, 580.
31. Bader, R. F. W.; Bader, R. F. *Atoms in Molecules: A Quantum Theory; International Series of Monographs on Chemistry*; Clarendon Press, 1990.
32. Ghosh, S.; Khandelia, T.; Panigrahi, P.; Mandal, R.; Patel, B. K. Mn(I)-Catalyzed Preferential Electrophilic C3-Maleimidation in Quinoxa-line Leading to Spirocyclization and Dehydrogenation of Succinimides. *Org. Lett.* **2023**, *25*, 3806.

V.7. Spectral Data

❖ *Tertiary Hydroxylation……..*

3-Hydroxy-1-phenyl-3-(3-phenylquinoxalin-2-yl)pyrrolidine-2,5-dione (1a)

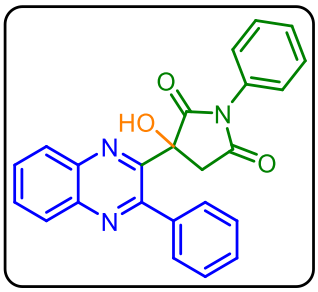

TH-3369_166122017

A pale yellow solid (47 mg, 79% yield); mp 196–198 °C; purified over a column of silica gel (15% EtOAc in hexane); ^{1}H NMR ($CDCl_3$, 500 MHz): δ 8.25 – 8.20 (m, 2H), 7.92 – 7.88 (m, 2H), 7.56 – 7.44 (m, 7H), 7.40 (t, J = 7.0 Hz, 1H), 7.20 (d, J = 8.0 Hz, 2H), 6.86 (s, 1H), 3.26 (d, J = 18.5 Hz, 1H), 2.99 (d, J = 18.5 Hz, 1H); ^{13}C {^{1}H} NMR ($CDCl_3$, 126 MHz): δ 176.1, 172.7, 153.2, 148.6, 142.1, 138.9, 137.6, 131.7, 131.6, 131.4, 130.1, 129.44, 129.41, 129.2, 128.9, 128.8, 128.7, 126.2, 75.9, 43.4; IR (neat, cm^{-1}): 3362, 2941, 1789, 1710, 1498, 1380, 1343, 1262, 1114, 1064, 1022, 816, 693, 614; HRMS (ESI-TOF) calcd for $C_{24}H_{18}N_3O_3$ $[M + H]^+$ 396.1343, found 396.1350.

3-Hydroxy-1-phenyl-3-(3-(*p*-tolyl)quinoxalin-2-yl)pyrrolidine-2,5-dione (**2a**)

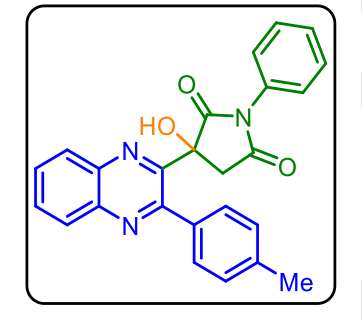

A pale yellow solid (50 mg, 82% yield); mp 155–157 °C; purified over a column of silica gel (15% EtOAc in hexane); ^{1}H NMR ($CDCl_3$, 500 MHz): δ 8.23 – 8.19 (m, 2H), 7.90 – 7.86 (m, 2H), 7.47 (t, J = 7.7 Hz, 2H), 7.40 (t, J = 7.2 Hz, 1H), 7.33 (d, J = 7.5 Hz, 2H), 7.28 (d, J = 8.0 Hz, 2H), 7.16 (d, J = 8.0 Hz, 2H), 6.86 (s, 1H), 3.29 (d, J = 18.5 Hz, 1H), 2.99 (d, J = 18.6 Hz, 1H), 2.44 (s, 3H); ^{13}C {^{1}H} NMR ($CDCl_3$, 126 MHz): δ 176.0, 172.9, 153.4, 148.8, 142.2, 140.1, 138.8, 134.6, 131.6, 131.5, 131.3, 130.0, 129.4, 129.1, 128.9, 128.8, 128.6, 126.2, 75.9, 43.6, 21.5; IR (neat, cm^{-1}): 3360, 2922, 1792, 1711, 1499, 1378, 1189, 1118, 1063, 883, 834, 758, 692; HRMS (ESI-TOF) calcd for $C_{25}H_{20}N_3O_3$ $[M + H]^+$ 410.1499, found 410.1506.

3-(3-(4-Fluorophenyl)quinoxalin-2-yl)-3-hydroxy-1-phenylpyrrolidine-2,5-dione (**3a**)

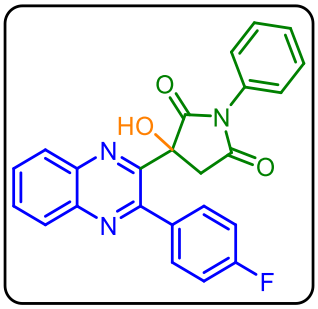

TH-3369_166122017

A light brown solid (46 mg, 75% yield); mp 162–164 ºC; purified over a column of silica gel (15% EtOAc in hexane); ^{1}H NMR ($CDCl_3$, 500 MHz): δ 8.24 – 8.18 (m, 2H), 7.93 – 7.88 (m, 2H), 7.49 (t, J = 7.7 Hz, 2H), 7.46 – 7.38 (m, 3H), 7.21 – 7.16 (m, 4H), 6.68 (s, 1H), 3.24 (d, J = 18.5 Hz, 1H), 3.03 (d, J = 18.5 Hz, 1H); ^{13}C {^{1}H} NMR ($CDCl_3$, 126 MHz): δ 176.1, 172.6, 163.5 (d, J = 251.6 Hz), 152.2, 148.9, 142.0, 138.9, 133.7 (d, J = 3.5 Hz), 131.8, 131.6, 131.5, 131.2 (d, J = 8.6 Hz), 129.4, 129.2, 128.9, 128.7, 126.0, 116.5 (d, J = 22.0 Hz), 76.1, 43.7; ^{19}F NMR ($CDCl_3$) δ -109.8 (s); IR (neat, cm^{-1}): 3322, 2920, 1788, 1716, 1600, 1496, 1378, 1201, 1109, 991, 803, 765, 692, 573; HRMS (ESI-TOF) calcd for $C_{24}H_{17}FN_3O_3$ $[M + H]^+$ 414.1248, found 414.1249.

3-(3-(4-Chlorophenyl)quinoxalin-2-yl)-3-hydroxy-1-phenylpyrrolidine-2,5-dione (**4a**)

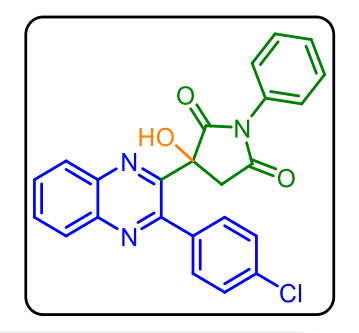

A pale yellow (50 mg, 78% yield); mp 155–157 ºC; purified over a column of silica gel (17% EtOAc in hexane); ^{1}H NMR ($CDCl_3$, 500 MHz): δ 8.24 – 8.18 (m, 2H), 7.94 – 7.89 (m, 2H), 7.50 (t, J = 7.7 Hz, 2H), 7.46 (d, J = 8.5 Hz, 2H), 7.42 (d, J = 7.5 Hz, 1H), 7.39 (d, J = 8.5 Hz, 2H), 7.16 (d, J = 7.5 Hz, 2H), 6.63 (s, 1H), 3.26 (d, J = 19.0 Hz, 1H), 3.06 (d, J = 18.5 Hz, 1H); ^{13}C {^{1}H} NMR ($CDCl_3$, 126 MHz): δ 176.0, 172.5, 152.1, 148.9, 142.0, 138.9, 136.4, 135.9, 131.8, 131.7, 131.5, 130.6, 129.6, 129.4, 129.2, 128.9, 128.7, 126.1, 76.1, 43.9; IR (neat, cm^{-1}): 3333, 2927, 1789, 1712, 1492, 1378, 1198, 1084, 990, 758, 692, 615, 593; HRMS (ESI-TOF) calcd for $C_{24}H_{17}ClN_3O_3$ $[M + H]^+$ 430.0953, found 430.0959.

3-(3-(4-Bromophenyl)quinoxalin-2-yl)-3-hydroxy-1-phenylpyrrolidine-2,5-dione (**5a**)

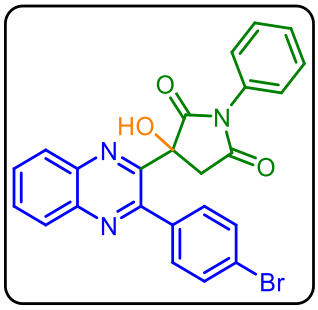

TH-3369_166122017

A brown solid (52 mg, 73% yield); mp 195–197 °C; purified over a column of silica gel (17% EtOAc in hexane); ^{1}H NMR ($CDCl_3$, 500 MHz): δ 8.23 – 8.17 (m, 2H), 7.93 – 7.88 (m, 2H), 7.61 (d, J = 8.5 Hz, 2H), 7.50 (t, J = 7.7 Hz, 2H), 7.41 (t, J = 7.5 Hz, 1H), 7.31 (d, J = 8.5 Hz, 2H), 7.15 (d, J = 7.5 Hz, 2H), 6.63 (s, 1H), 3.26 (d, J = 19.0 Hz, 1H), 3.06 (d, J = 19.0 Hz, 1H); ^{13}C {^{1}H} NMR ($CDCl_3$, 126 MHz): δ 176.0, 172.5, 152.1, 148.9, 142.0, 138.9, 136.3, 132.5, 131.8, 131.7, 131.4, 130.8, 129.4, 129.2, 128.9, 128.7, 126.1, 124.7, 76.0, 44.0; IR (neat, cm^{-1}): 3300, 1716, 1491, 1379, 1345, 1198, 1108, 1067, 988, 843, 757, 694; HRMS (ESI-TOF) calcd for $C_{24}H_{17}BrN_3O_3$ $[M + H]^+$ 474.0448, found 474.0429.

3-Hydroxy-1-phenyl-3-(3-(4-(trifluoromethyl)phenyl)quinoxalin-2-yl)pyrrolidine-2,5-dione (**6a**)

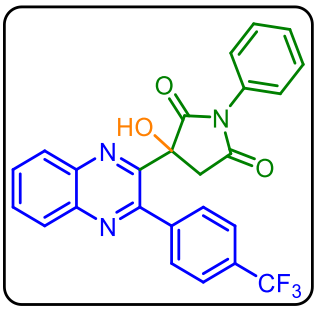

A reddish brown solid (49 mg, 71% yield); mp 151–153 °C; purified over a column of silica gel (18% EtOAc in hexane); ^{1}H NMR ($CDCl_3$, 500 MHz): δ 8.25 – 8.18 (m, 2H), 7.95 – 7.90 (m, 2H), 7.75 (d, J = 7.5 Hz, 2H), 7.60 (d, J = 8.0 Hz, 2H), 7.47 (t, J = 7.5 Hz, 2H), 7.40 (t, J = 7.5 Hz, 1H), 7.09 (d, J = 7.5 Hz, 2H), 6.45 (s, 1H), 3.27 (d, J = 18.5 Hz, 1H), 3.10 (d, J = 18.5 Hz, 1H); ^{13}C {^{1}H} NMR ($CDCl_3$, 126 MHz): δ 176.1, 172.3, 151.8, 149.0, 141.9, 141.3, 139.1, 132.0, 131.9, 131.3, 129.8, 129.4, 129.2, 129.0, 128.7, 126.2 (q, J = 3.6 Hz), 126.0, 124.9, 122.7, 76.2, 44.2; ^{19}F NMR ($CDCl_3$) δ -62.9 (s); IR (neat, cm^{-1}): 3300, 2919, 1716, 1494, 1376, 1321, 1166, 1113, 1065, 849, 752, 692, 619; HRMS (ESI-TOF) calcd for $C_{25}H_{17}F_3N_3O_3$ $[M + H]^+$ 464.1217, found 464.1225.

3-(3-([1,1'-Biphenyl]-4-yl)quinoxalin-2-yl)-3-hydroxy-1-phenylpyrrolidine-2,5-dione (**7a**)

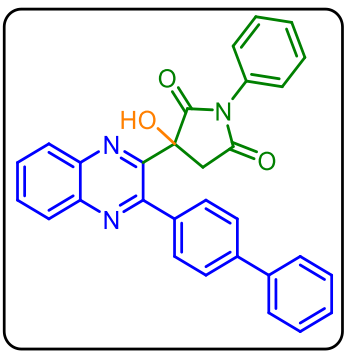

TH-3369_166122017

A light brown solid (49 mg, 69% yield); mp197–199 °C; purified over a column of silica gel (15% EtOAc in hexane); ^{1}H NMR ($CDCl_3$, 500 MHz): δ 8.23 – 8.19 (m, 2H), 7.90 – 7.86 (m, 2H), 7.69 (d, J = 8.0 Hz, 2H), 7.60 (d, J = 7.0 Hz, 2H), 7.53 – 7.45 (m, 4H), 7.41 (t, J = 7.2 Hz, 1H), 7.38 – 7.34 (m, 3H), 7.11 (d, J = 6.5 Hz, 2H), 6.81 (s, 1H), 3.37 (d, J = 18.5 Hz, 1H), 3.06 (d, J = 18.5 Hz, 1H); ^{13}C {^{1}H} NMR ($CDCl_3$, 126 MHz): δ 175.9, 172.6, 153.0, 149.0, 142.8, 142.1, 139.8, 138.8, 136.2, 131.6, 131.5, 131.4, 129.5, 129.3, 129.1, 129.0, 128.7, 128.6, 128.2, 127.9, 127.3, 126.1, 75.9, 44.0; IR (neat, cm^{-1}): 3271, 1787, 1713, 1487, 1380, 1345, 1195, 987, 843, 768, 750, 617, 568; HRMS (ESI-TOF) calcd for $C_{30}H_{22}N_3O_3$ $[M + H]^+$ 472.1656, found 472.1640.

3-Hydroxy-1-phenyl-3-(3-(*m*-tolyl)quinoxalin-2-yl)pyrrolidine-2,5-dione (8a)

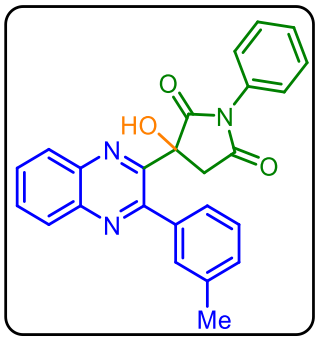

A yellow solid (49 mg, 80% yield); mp 158–160 °C; purified over a column of silica gel (15% EtOAc in hexane); ^{1}H NMR ($CDCl_3$, 500 MHz): δ 8.24 – 8.20 (m, 2H), 7.92 – 7.87 (m, 2H), 7.47 (t, J = 7.7 Hz, 2H), 7.40 – 7.36 (m, 2H), 7.33 (d, J = 7.5 Hz, 1H), 7.22 (d, J = 7.0 Hz, 1H), 7.19 (d, J = 8.0 Hz, 2H), 6.84 (s, 1H), 3.39 (d, J = 18.5 Hz, 1H), 3.00 (d, J = 18.5 Hz, 1H), 2.32 (s, 3H); ^{13}C {^{1}H} NMR ($CDCl_3$, 126 MHz): δ 176.0, 172.8, 153.4, 148.7, 142.1, 139.6, 138.8, 137.5, 131.6, 131.3, 130.9, 129.7, 129.4, 129.2, 129.1, 128.7, 128.6, 126.2, 125.9, 76.0, 43.6, 21.6; IR (neat, cm^{-1}): 3327, 1711, 1496, 1375, 1344, 1187, 1117, 1061, 855, 761, 691; HRMS (ESI-TOF) calcd for $C_{25}H_{20}N_3O_3$ $[M + H]^+$ 410.1499, found 410.1508.

3-Hydroxy-1-phenyl-3-(3-(3-(trifluoromethyl)phenyl)quinoxalin-2-yl)pyrrolidine-2,5-dione (9a)

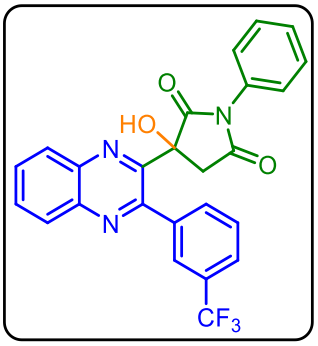

A pale yellow solid (51 mg, 74% yield); mp 138–140 °C; purified over a column of silica gel (17% EtOAc in hexane); ^{1}H NMR ($CDCl_3$, 400 MHz): δ 8.24 – 8.19 (m, 2H), 7.94 – 7.91 (m, 2H), 7.82 – 7.79 (m, 2H), 7.66 (d, J = 7.6 Hz, 1H), 7.61 (t, J = 7.6 Hz, 1H), 7.47 (t, J = 7.6 Hz, 2H), 7.40 (t, J = 7.2 Hz, 1H), 7.18 (d, J = 7.6 Hz, 2H), 6.26 (s, 1H), 3.27 (d, J = 18.4 Hz, 1H), 3.09 (d, J = 18.4 Hz, 1H); ^{13}C {^{1}H} NMR ($CDCl_3$, 126 MHz): δ 176.1, 172.3, 151.6, 149.3, 141.9, 138.8, 132.2, 132.0, 131.9, 131.8, 131.7, 131.4, 129.6, 129.4, 129.2, 128.9, 128.8, 126.7 (q, J = 3.5 Hz), 126.4 (q, J = 3.6 Hz), 126.0, 76.6, 44.0; ^{19}F NMR ($CDCl_3$) δ -62.7 (s); IR (neat, cm^{-1}): 3282, 2918, 1715, 1493, 1374, 1302, 1168, 1120, 1072, 839, 752, 694, 616; HRMS (ESI-TOF) calcd for $C_{25}H_{17}F_3N_3O_3$ [M + H]$^{+}$ 464.1217, found 464.1224.

3-Hydroxy-3-(3-(2-methoxyphenyl)quinoxalin-2-yl)-1-phenylpyrrolidine-2,5-dione (10a)

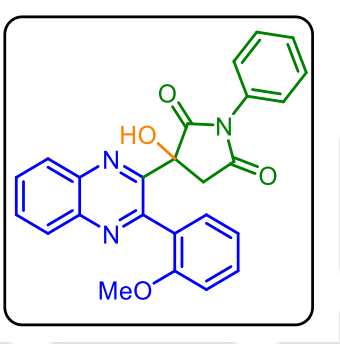

A pale yellow solid (42 mg, 66% yield); mp 162–164 °C; purified over a column of silica gel (20% EtOAc in hexane); ^{1}H NMR ($CDCl_3$, 500 MHz): δ 8.25 – 8.20 (m, 2H), 7.92 – 7.86 (m, 2H), 7.53 – 7.49 (m, 1H), 7.41 (t, J = 7.5 Hz, 2H), 7.35 (t, J = 7.2 Hz, 1H), 7.10 (t, J = 8.7 Hz, 2H), 7.06 (d, J = 7.5 Hz, 2H), 7.01 (s, 1H), 6.97 (t, J = 7.5 Hz, 1H), 3.83 (s, 3H), 3.64 (d, J = 19.0 Hz, 1H), 3.05 (d, J = 19.5 Hz, 1H); ^{13}C {^{1}H} NMR ($CDCl_3$, 126 MHz): δ 176.0, 173.4, 156.5, 151.1, 149.6, 142.4, 138.8, 131.9, 131.7, 131.4, 131.3, 131.2, 129.4, 128.9, 128.7, 126.4, 126.1, 125.6, 121.7, 111.9, 75.6, 55.7, 42.3; IR (neat, cm^{-1}): 3335, 2923, 1789, 1707, 1497, 1383, 1184, 1149, 951, 757, 693, 672, 619, 578; HRMS (ESI-TOF) calcd for $C_{25}H_{20}N_3O_4$ [M + H]$^{+}$ 426.1448, found 426.1456.

3-(3-(2-Bromophenyl)quinoxalin-2-yl)-3-hydroxy-1-phenylpyrrolidine-2,5-dione (11a)

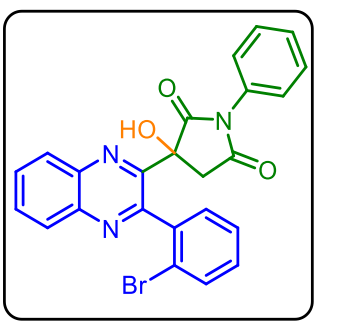

A light brown solid (43 mg, 61% yield); mp 186–188 °C; purified over a column of silica gel (17% EtOAc in hexane); ^{1}H NMR ($CDCl_3$, 500 MHz): δ 8.28 – 8.22 (m, 2H), 7.97 – 7.89 (m, 2H), 7.81 (d, J = 8.0 Hz, 1H), 7.47 (t, J = 7.5 Hz, 2H), 7.43 – 7.38 (m, 2H), 7.33 (t, J = 7.5 Hz, 1H), 7.24 (d, J = 8.0 Hz, 1H), 7.16 (d, J = 7.5 Hz, 2H), 6.97 (s, 1H), 3.53 (d, J = 19.0 Hz, 1H), 3.08 (d, J = 19.0 Hz, 1H); ^{13}C {^{1}H} NMR ($CDCl_3$, 126 MHz): δ 176.1, 172.7, 151.8, 148.2, 142.2, 139.0, 137.5, 134.1, 131.8, 131.7, 131.6, 131.5, 131.3, 129.5, 129.1, 128.80, 128.79, 128.1, 126.1, 123.5, 75.6, 42.1; IR (neat, cm^{-1}): 3322, 2920, 2852, 1782, 1712, 1494, 1375, 1192, 1064, 1023, 886, 827, 754, 570; HRMS (ESI-TOF) calcd for $C_{24}H_{17}BrN_3O_3$ $[M + H]^+$ 474.0448, found 474.0454.

3-(3-(2,6-Difluorophenyl)quinoxalin-2-yl)-3-hydroxy-1-phenylpyrrolidine-2,5-dione (12a)

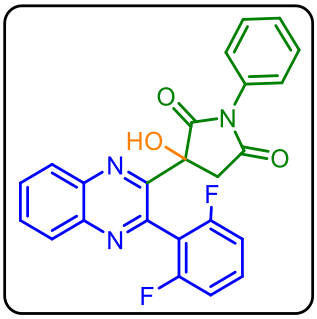

A pale yellow solid (41 mg, 64% yield); mp 206–208 °C; purified over a column of silica gel (18% EtOAc in hexane); ^{1}H NMR ($CDCl_3$, 400 MHz): δ 8.21 – 8.18 (m, 2H), 7.94 – 7.88 (m, 2H), 7.54 – 7.45 (m, 3H), 7.39 (t, J = 7.6 Hz, 1H), 7.28 (d, J = 7.2 Hz, 2H), 7.11 (t, J = 8.6 Hz, 1H), 6.97 (t, J = 8.4 Hz, 1H), 5.96 (s, 1H), 3.47 (d, J = 18.8 Hz, 1H), 3.20 (d, J = 18.8 Hz, 1H); ^{13}C {^{1}H} NMR ($CDCl_3$, 126 MHz): δ 175.3, 172.5, 161.5, 161.4, 161.3, 161.2, 159.5, 159.4, 159.35, 159.30, 151.5, 142.8, 142.1, 139.4, 132.5, 132.4, 132.3, 132.1, 131.7, 131.6, 129.5, 129.1, 128.9, 128.8, 126.0, 115.5, 115.4, 115.2, 112.5, 112.4, 112.38, 112.36, 112.30, 112.27, 112.21, 112.1, 76.8, 43.1; ^{19}F NMR ($CDCl_3$) δ -108.8 (s), -109.0 (s), -111.9 (s); IR (neat, cm^{-1}): 3446, 1703, 1630, 1461, 1397, 1209, 1123, 1074, 998, 771, 738, 694; HRMS (ESI-TOF) calcd for $C_{24}H_{16}F_2N_3O_3$ $[M + H]^+$ 432.1154, found 432.1164.

3-Hydroxy-3-(3-(naphthalen-2-yl)quinoxalin-2-yl)-1-phenylpyrrolidine-2,5-dione (13a)

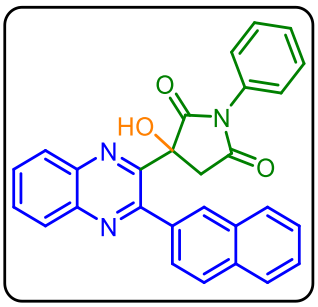

A off-white solid (51 mg, 76% yield); mp 200–202 ºC; purified over a column of silica gel (15% EtOAc in hexane); ^{1}H NMR ($CDCl_3$, 500 MHz): δ 8.24 – 8.20 (m, 2H), 7.96 (d, J = 8.0 Hz, 1H), 7.92 – 7.87 (m, 3H), 7.86 (s, 1H), 7.71 (d, J = 8.5 Hz, 1H), 7.60 (t, J = 7.5 Hz, 1H), 7.54 (d, J = 8.5 Hz, 1H), 7.51 (d, J = 7.5 Hz, 1H), 7.28 – 7.23 (m, 3H), 6.82 (s, 1H), 6.69 (d, J = 7.5 Hz, 2H), 3.34 (d, J = 18.5 Hz, 1H), 3.00 (d, J = 18.5 Hz, 1H); ^{13}C {^{1}H} NMR ($CDCl_3$, 126 MHz): δ 176.0, 172.6, 153.3, 149.0, 142.1, 138.8, 134.5, 133.5, 132.9, 131.6, 131.4, 131.2, 129.4, 129.3, 129.0, 128.8, 128.7, 128.6, 128.5, 128.0, 127.7, 127.3, 126.1, 125.8, 76.0, 43.9; IR (neat, cm^{-1}): 3348, 1712, 1495, 1379, 1345, 1187, 1125, 1065, 912, 815, 751, 729, 618; HRMS (ESI-TOF) calcd for $C_{28}H_{20}N_3O_3$ $[M + H]^+$ 446.1499, found 446.1507.

3-Hydroxy-1-phenyl-3-(3-(thiophen-2-yl)quinoxalin-2-yl)pyrrolidine-2,5-dione (**14a**)

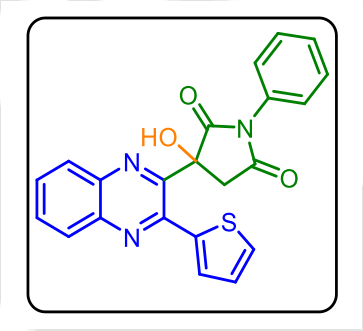

A pale yellow solid (44 mg, 74% yield); mp 208–210 ºC; purified over a column of silica gel (17% EtOAc in hexane); ^{1}H NMR ($CDCl_3$ 400 MHz): δ 8.21 – 8.18 (m, 2H), 7.91 – 7.87 (m, 2H), 7.62 (d, J = 5.2 Hz, 1H), 7.51 (t, J = 7.6 Hz, 2H), 7.43 (t, J = 7.4 Hz, 1H), 7.35 – 7.31 (m, 3H), 7.15 (t, J = 4.4 Hz, 1H), 6.58 (s, 1H), 3.36 (d, J = 18.4 Hz, 1H), 3.07 (d, J = 18.4 Hz, 1H); ^{13}C {^{1}H} NMR ($CDCl_3$, 126 MHz): δ 176.3, 172.9, 149.4, 146.8, 142.0, 138.8, 138.7, 131.8, 131.7, 131.6, 130.0, 129.9, 129.35, 129.31, 128.9, 128.6, 128.0, 126.3, 76.6, 43.4; IR (neat, cm^{-1}): 3368, 2922, 1787, 1710, 1529, 1380, 1195, 1108, 1020, 849, 755, 694, 618; HRMS (ESI-TOF) calcd for $C_{22}H_{16}N_3O_3S$ $[M + H]^+$ 402.0907, found 402.0909.

3-Hydroxy-1-methyl-3-(3-phenylquinoxalin-2-yl)pyrrolidine-2,5-dione (**15a**)

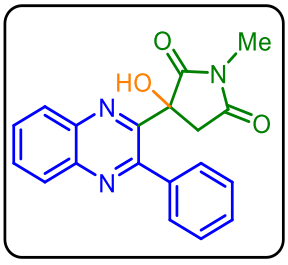

TH-3369_166122017

A light brown solid (38 mg, 76% yield); mp 171–173 °C; purified over a column of silica gel (15% EtOAc in hexane); ^{1}H NMR ($CDCl_3$, 500 MHz): δ 8.21 – 8.18 (m, 2H), 7.90 – 7.86 (m, 2H), 7.49 – 7.46 (m, 3H), 7.35 – 7.32 (m, 2H), 6.78 (s, 1H), 3.09 (d, J = 19.0 Hz, 1H), 2.88 (d, J = 19.0 Hz, 1H), 2.77 (s, 3H); ^{13}C {^{1}H} NMR ($CDCl_3$, 126 MHz): δ 177.2, 173.5, 153.2, 149.0, 142.0, 138.7, 137.0, 131.5, 131.4, 129.9, 129.3, 128.9, 128.6, 75.8, 43.8, 25.3; IR (neat, cm^{-1}): 3306, 1701, 1429, 1346, 1283, 1257, 1109, 1005, 765, 706; HRMS (ESI-TOF) calcd for $C_{19}H_{16}N_3O_3$ $[M + H]^+$ 334.1186, found 334.1186.

1-Ethyl-3-hydroxy-3-(3-phenylquinoxalin-2-yl)pyrrolidine-2,5-dione (16a)

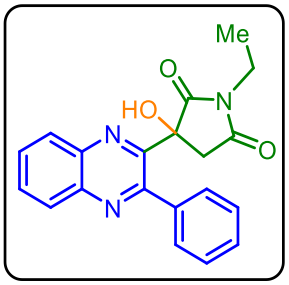

A off-white solid (41 mg, 79% yield); mp 167–169 °C; purified over a column of silica gel (15% EtOAc in hexane); ^{1}H NMR ($CDCl_3$, 500 MHz): δ 8.22 – 8.18 (m, 2H), 7.91 – 7.86 (m, 2H), 7.48 – 7.45 (m, 3H), 7.36 (d, J = 6.5 Hz, 2H), 6.75 (s, 1H), 3.39 – 3.26 (m, 2H), 3.07 (d, J = 18.5 Hz, 1H), 2.85 (d, J = 18.5 Hz, 1H), 1.13 (t, J = 7.2 Hz, 3H); ^{13}C {^{1}H} NMR ($CDCl_3$, 126 MHz): δ 177.0, 173.5, 153.2, 148.9, 142.0, 138.8, 137.2, 131.5, 131.3, 129.9, 129.3, 129.1, 128.8, 128.6, 75.8, 43.7, 34.5, 12.7; IR (neat, cm^{-1}): 3320, 2947, 1777, 1699, 1399, 1342, 1224, 1147, 1018, 897, 763, 694, 562; HRMS (ESI-TOF) calcd for $C_{20}H_{18}N_3O_3$ $[M + H]^+$ 348.1343, found 348.1350.

3-Hydroxy-1-isobutyl-3-(3-phenylquinoxalin-2-yl)pyrrolidine-2,5-dione (17a)

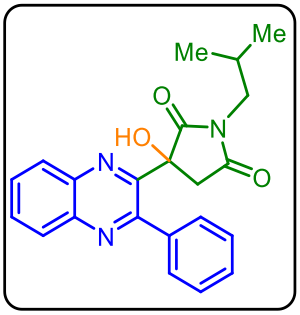

A pale yellow solid (44 mg, 78% yield); mp 142–144 °C; purified over a column of silica gel (15% EtOAc in hexane); ^{1}H NMR ($CDCl_3$, 500 MHz): δ 8.20 – 8.17 (m, 2H), 7.88 – 7.86 (m, 2H), 7.49 –

TH-3369_166122017

7.45 (m, 3H), 7.36 (d, *J* = 7.5 Hz, 2H), 6.55 (s, 1H), 3.14 – 3.04 (m, 3H), 2.88 (d, *J* = 18.5 Hz, 1H), 2.01 – 1.96 (m, 1H), 0.88 (dd, *J* = 6.5, 5.0 Hz, 6H); ^{13}C {^{1}H} NMR ($CDCl_3$, 126 MHz): *δ* 177.6, 173.8, 153.2, 149.3, 141.9, 138.8, 137.3, 131.5, 131.3, 129.9, 129.4, 128.9, 128.8, 128.6, 76.0, 46.5, 43.6, 27.2, 20.2, 20.1; IR (neat, cm^{-1}): 3312, 1708, 1465, 1349, 1324, 1279, 1254, 1118, 989, 784, 720.

1-Benzyl-3-hydroxy-3-(3-phenylquinoxalin-2-yl)pyrrolidine-2,5-dione (**18a**)

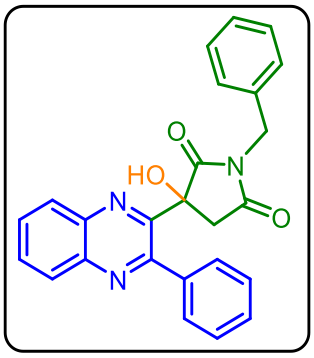

A brown solid (50 mg, 81% yield); mp 132–134 ºC; purified over a column of silica gel (15% EtOAc in hexane); ^{1}H NMR ($CDCl_3$, 500 MHz): *δ* 8.19 – 8.17 (m, 2H), 7.88 – 7.85 (m, 2H), 7.42 – 7.36 (m, 3H), 7.34 – 7.29 (m, 5H), 7.24 (t, *J* = 7.5 Hz, 2H), 6.68 (s, 1H), 4.51 (d, *J* = 14.0 Hz, 1H), 4.40 (d, *J* = 14.0 Hz, 1H), 3.03 (d, *J* = 18.5 Hz, 1H), 2.82 (d, *J* = 18.5 Hz, 1H); ^{13}C {^{1}H} NMR ($CDCl_3$, 126 MHz): *δ* 177.0, 173.3, 153.1, 148.8, 142.0, 138.8, 137.3, 134.9, 131.5, 131.3, 129.9, 129.3, 129.2, 129.0, 128.8, 128.7, 128.6, 128.2, 76.1, 43.3, 43.1; IR (neat, cm^{-1}): 3339, 2925, 1714, 1431, 1392, 1340, 1115, 1021, 948, 765, 700, 586; HRMS (ESI-TOF) calcd for $C_{25}H_{20}N_3O_3$ $[M + H]^+$ 410.1499, found 410.1501.

1-(Cyclohexylmethyl)-3-hydroxy-3-(3-phenylquinoxalin-2-yl)pyrrolidine-2,5-dione (**19a**)

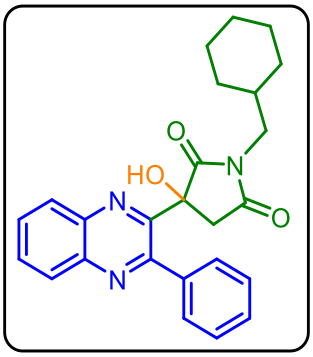

A pale yellow solid (51 mg, 82% yield); mp 195–197 ºC; purified over a column of silica gel (15% EtOAc in hexane); ^{1}H NMR ($CDCl_3$, 400 MHz): *δ* 8.22 – 8.17 (m, 2H), 7.91 – 7.86 (m, 2H), 7.50 – 7.46 (m, 3H), 7.37 – 7.34 (m, 2H), 6.63 (s, 1H), 3.18 – 3.02 (m, 3H), 2.88 (d, *J* = 18.4 Hz, 1H), 1.71 – 1.60 (m, 6H), 1.22 – 1.10 (m, 3H), 0.97 – 0.87 (m, 2H); ^{13}C {^{1}H} NMR ($CDCl_3$, 101 MHz): *δ* 177.6,

TH-3369_166122017

173.9, 153.2, 149.2, 141.9, 138.8, 137.1, 131.5, 131.3, 129.9, 129.4, 129.0, 128.8, 128.6, 75.9, 45.4, 43.6, 36.2, 30.75, 30.6, 26.3, 25.72, 25.71; IR (neat, cm^{-1}): 3333, 2927, 1789, 1712, 1492, 1378, 1198, 1084, 883, 758, 692, 615, 593.

3-Hydroxy-3-(3-phenylquinoxalin-2-yl)-1-(*p*-tolyl)pyrrolidine-2,5-dione (**20a**)

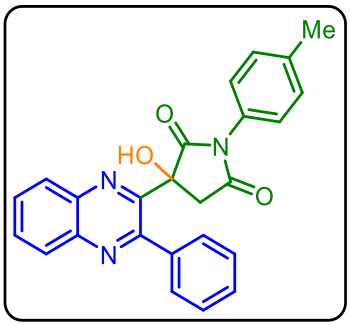

A light brown solid (50 mg, 82% yield); mp 207–209 °C; purified over a column of silica gel (15% EtOAc in hexane); ^{1}H NMR ($CDCl_3$, 500 MHz): δ 8.23 – 8.19 (m, 2H), 7.91 – 7.87 (m, 2H), 7.55 – 7.48 (m, 3H), 7.44 (d, J = 7.0 Hz, 2H), 7.27 (d, J = 8.0 Hz, 2H), 7.07 (d, J = 8.0 Hz, 2H), 6.81 (s, 1H), 3.24 (d, J = 18.5 Hz, 1H), 2.96 (d, J = 18.5 Hz, 1H), 2.39 (s, 3H); ^{13}C {^{1}H} NMR ($CDCl_3$, 126 MHz): δ 176.2, 172.8, 153.2, 148.7, 142.1, 138.89, 138.88, 137.7, 131.6, 131.4, 130.0, 129.8, 129.4, 129.0, 128.9, 128.7, 126.0, 76.0, 43.4, 21.3; IR (neat, cm^{-1}): 3361, 1712, 1513, 1374, 1343, 1181, 1111, 1073, 815, 761, 705, 650; HRMS (ESI-TOF) calcd for $C_{25}H_{20}N_3O_3$ $[M + H]^+$ 410.1499, found 410.1509.

1-(4-Fluorophenyl)-3-hydroxy-3-(3-phenylquinoxalin-2-yl)pyrrolidine-2,5-dione (**21a**)

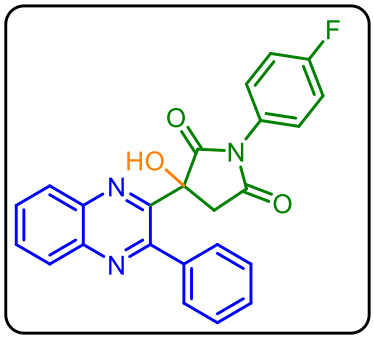

A off-white solid (45 mg, 72% yield); mp 178–180 °C; purified over a column of silica gel (15% EtOAc in hexane); ^{1}H NMR ($CDCl_3$, 400 MHz): δ 8.25 – 8.20 (m, 2H), 7.93 – 7.90 (m, 2H), 7.56 – 7.48 (m, 3H), 7.44 (d, J = 6.8 Hz, 2H), 7.17 (d, J = 5.6 Hz, 4H), 6.87 (s, 1H), 3.27 (d, J = 18.4 Hz, 1H), 3.00 (d, J = 18.8 Hz, 1H); ^{13}C {^{1}H} NMR ($CDCl_3$, 126 MHz): δ 176.0, 172.6, 162.3 (d, J = 249.6 Hz), 153.1,

TH-3369_166122017

148.4, 142.1, 138.8, 137.6, 131.7, 131.5, 130.1, 129.42, 129.40, 129.0, 128.7, 128.0 (d, J = 8.9 Hz), 127.4 (d, J = 3.1 Hz), 116.2 (d, J = 22.9 Hz), 75.9, 43.5; ^{19}F NMR ($CDCl_3$) δ -111.9 (s); IR (neat, cm^{-1}): 3380, 2931, 1708, 1509, 1389, 1229, 1195, 1127, 1073, 827, 765, 704; HRMS (ESI-TOF) calcd for $C_{24}H_{17}FN_3O_3$ $[M + H]^+$ 414.1248, found 414.1257.

3-Hydroxy-1-(4-methoxybenzyl)-3-(3-phenylquinoxalin-2-yl)pyrrolidine-2,5-dione (**22a**)

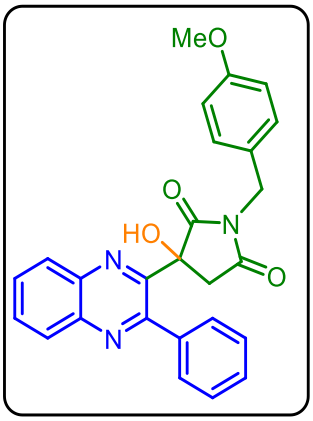

A light brown solid (55 mg, 84% yield); mp 133–135 °C; purified over a column of silica gel (20% EtOAc in hexane); ^{1}H NMR ($CDCl_3$, 400 MHz): δ 8.20 – 8.18 (m, 2H), 7.90 – 7.87 (m, 2H), 7.42 (t, J = 7.0 Hz, 1H), 7.35 – 7.24 (m, 6H), 6.85 (d, J = 8.8 Hz, 2H), 6.71 (s, 1H), 4.45 (d, J = 14.0 Hz, 1H), 4.33 (d, J = 14.0 Hz, 1H), 3.79 (s, 3H), 3.01 (d, J = 18.4 Hz, 1H), 2.80 (d, J = 18.8 Hz, 1H); ^{13}C {^{1}H} NMR ($CDCl_3$, 126 MHz): δ 177.0, 173.4, 159.6, 153.1, 148.8, 142.0, 138.8, 137.2, 131.5, 131.3, 130.7, 129.9, 129.3, 129.1, 128.7, 128.6, 127.2, 114.2, 76.0, 55.4, 43.3, 42.6; IR (neat, cm^{-1}): 3308, 2933, 1782, 1702, 1610, 1512, 1390, 1301, 1246, 1172, 991, 764, 617; HRMS (ESI-TOF) calcd for $C_{26}H_{22}N_3O_4$ $[M + H]^+$ 440.1605, found 440.1612.

3-Hydroxy-1-(4-phenylbutyl)-3-(3-phenylquinoxalin-2-yl)pyrrolidine-2,5-dione (**23a**)

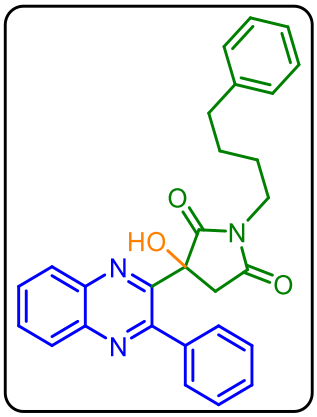

TH-3369_166122017

A pale yellow solid (55 mg, 81% yield); mp 140–142 °C; purified over a column of silica gel (15% EtOAc in hexane); ^{1}H NMR ($CDCl_3$, 500 MHz): δ 8.12 – 8.17 (m, 2H), 7.89 – 7.86 (m, 2H), 7.47 – 7.41 (m, 3H), 7.34 (d, J = 7.0 Hz, 2H), 7.27 (t, J = 7.5 Hz, 2H), 7.19 – 7.15 (m, 3H), 6.66 (s, 1H), 3.32 – 3.24 (m, 2H), 3.06 (d, J = 18.5 Hz, 1H), 2.85 (d, J = 18.5 Hz, 1H), 2.62 (t, J = 7.5 Hz, 2H), 1.63 – 1.55 (m, 4H); ^{13}C {^{1}H} NMR ($CDCl_3$, 126 MHz): δ 177.2, 173.6, 153.2, 149.0, 141.95, 141.94, 138.8, 137.2, 131.5, 131.3, 129.9, 129.3, 129.0, 128.8, 128.6, 128.5, 128.4, 126.0, 75.9, 43.6, 39.3, 35.4, 28.5, 27.0; IR (neat, cm^{-1}): 3323, 2938, 1700, 1458, 1399, 1342, 1221, 1156, 1018, 764, 745, 697, 617; HRMS (ESI-TOF) calcd for $C_{28}H_{26}N_3O_3$ $[M + H]^+$ 452.1969, found 452.2002.

1-Heptyl-3-hydroxy-3-(3-phenylquinoxalin-2-yl)pyrrolidine-2,5-dione (**24a**)

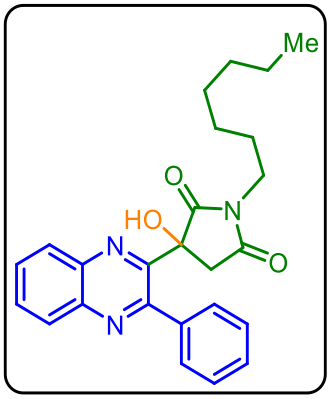

A pale yellow solid (47 mg, 76% yield); mp 98–100 °C; purified over a column of silica gel (15% EtOAc in hexane); ^{1}H NMR ($CDCl_3$, 500 MHz): δ 8.22 – 8.18 (m, 2H), 7.90 – 7.87 (m, 2H), 7.49 – 7.45 (m, 3H), 7.36 (d, J = 7.5 Hz, 2H), 6.67 (s, 1H), 3.29 – 3.17 (m, 2H), 3.07 (d, J = 18.5 Hz, 1H), 2.85 (d, J = 18.5 Hz, 1H), 1.54 – 1.49 (m, 2H), 1.29 – 1.26 (m, 8H), 0.88 (t, J = 6.7 Hz, 3H); ^{13}C {^{1}H} NMR ($CDCl_3$, 126 MHz): δ 177.2, 173.7, 153.2, 149.1, 142.0, 138.8, 137.3, 131.5, 131.3, 129.9, 129.4, 129.0, 128.9, 128.6, 75.9, 43.7, 39.6, 31.8, 28.9, 27.5, 26.8, 22.7, 14.2; IR (neat, cm^{-1}) 3408, 2927, 1782, 1706, 1439, 1398, 1369, 1220, 1175, 1070, 980, 762, 607; HRMS (ESI-TOF) calcd for $C_{25}H_{28}N_3O_3$ $[M + H]^+$ 418.2125, found 418.2195.

TH-3369_166122017

1-Decyl-3-hydroxy-3-(3-phenylquinoxalin-2-yl)pyrrolidine-2,5-dione (**25a**)

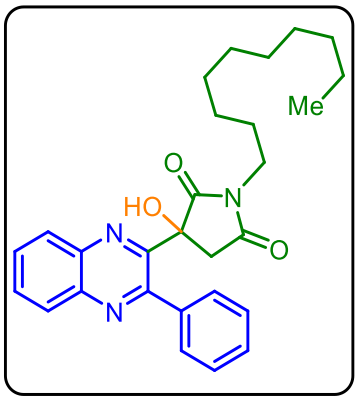

A pale yellow solid (55 mg, 80% yield); mp 97–99 °C; purified over a column of silica gel (15% EtOAc in hexane); ^{1}H NMR ($CDCl_3$, 500 MHz): δ 8.20 – 8.17 (m, 2H), 7.89 – 7.85 (m, 2H), 7.48 – 7.45 (m, 3H), 7.36 (d, J = 6.5 Hz, 2H), 6.67 (s, 1H), 3.29 – 3.19 (m, 2H), 3.06 (d, J = 18.5 Hz, 1H), 2.85 (d, J = 18.5 Hz, 1H), 1.53 – 1.49 (m, 2H), 1.28 – 1.25 (m, 14H), 0.88 (t, J = 6.7 Hz, 3H); ^{13}C {^{1}H} NMR ($CDCl_3$, 126 MHz): δ 177.2, 173.6, 153.2, 149.1, 141.9, 138.7, 137.2, 131.4, 131.3, 129.9, 129.3, 129.0, 128.8, 128.6, 75.9, 43.6, 39.5, 31.9, 29.6, 29.5, 29.3, 29.2, 27.5, 26.8, 22.7, 14.2; IR (neat, cm^{-1}) 3341, 2923, 1707, 1441, 1342, 1168, 1021, 762, 702, 564.

3-Hydroxy-3-(3-phenylquinoxalin-2-yl)pyrrolidine-2,5-dione (**26a**)

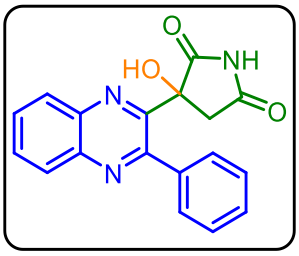

A brown solid (34 mg, 71% yield); mp 225–227 °C; purified over a column of silica gel (35% EtOAc in hexane); ^{1}H NMR ($CDCl_3$, 400 MHz): δ 8.23 – 8.20 (m, 2H), 7.92 – 7.89 (m, 2H), 7.71 (s, 1H), 7.56 – 7.49 (m, 3H), 7.43 (d, J = 7.2 Hz, 2H), 6.74 (s, 1H), 3.15 (d, J = 18.8 Hz, 1H), 2.89 (d, J = 18.8 Hz, 1H); ^{13}C {^{1}H} NMR ($CDCl_3$, 126 MHz): δ 177.1, 173.5, 153.3, 148.6, 142.0, 138.8, 137.2, 131.7, 131.4, 130.2, 129.4, 129.3, 129.1, 128.7, 77.3, 44.5; IR (neat, cm^{-1}): 3367, 2920, 1709, 1462, 1347, 1259, 1217, 1100, 967, 800, 767, 692, 578; HRMS (ESI-TOF) calcd for $C_{18}H_{14}N_3O_3$ $[M + H]^+$ 320.1030, found 320.1036.

TH-3369_166122017

3-Hydroxy-1-((*S*)-1-(naphthalen-1-yl)ethyl)-3-(3-phenylquinoxalin-2-yl)pyrrolidine-2,5-dione (27a)

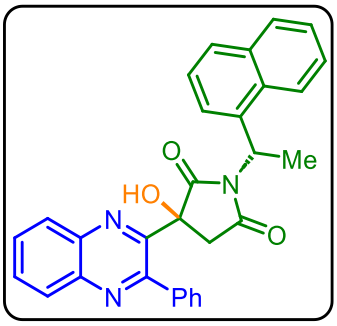

A light brown solid (49 mg mg, 70% yield); dr 1:1; mp 175–177 ^{o}C; purified over a column of silica gel (15% EtOAc in hexane); ^{1}H NMR ($CDCl_3$, 400 MHz): δ 8.24 (d, J = 8.4 Hz, 1H), 8.16 – 8.05 (m, 6H), 8.01 (d, J = 7.2 Hz, 2H), 7.94 – 7.82 (m, 10H), 7.54 – 7.44 (m, 9H), 7.27 (d, J = 8.0 Hz, 3H), 7.12 (d, J = 7.2 Hz, 2H), 7.03 (t, J = 7.4 Hz, 1H), 6.95 (t, J = 7.6 Hz, 2H), 6.78 (t, J = 7.4 Hz, 2H), 6.49 (s, 1H), 6.29 (s, 1H), 6.22 – 6.15 (m, 2H), 2.95 (dd, J = 18.0, 4.4 Hz, 2H), 2.67 (dd, J = 18.0, 13.6 Hz, 2H), 1.95 (d, J = 7.2 Hz, 3H), 1.90 (d, J = 7.2 Hz, 3H); ^{13}C {^{1}H} NMR ($CDCl_3$, 126 MHz): δ 177.3, 177.2, 174.0, 173.9, 153.1, 153.0, 148.7, 148.6, 141.8, 139.0, 138.9, 138.0, 137.7, 133.9, 133.8, 133.5, 131.9, 131.5, 131.4, 131.1, 129.7, 129.6, 129.5, 129.3, 129.2, 129.1, 129.04, 129.01, 128.9, 128.7, 128.6, 128.3, 128.2, 127.1, 126.9, 126.85, 126.82, 125.7, 125.3, 125.2, 123.4, 123.0, 76.3, 76.2, 47.1, 46.6, 42.6, 42.5, 17.5, 17.1; IR (neat, cm^{-1}): 3314, 2910, 1711, 1468, 1355, 1315, 1268, 1116, 976, 745; HRMS (ESI-TOF) calcd for $C_{30}H_{24}N_3O_3$ $[M + H]^+$ 474.1812, found 474.1815.

3-Hydroxy-1-((*S*)-1-phenylethyl)-3-(3-phenylquinoxalin-2-yl)pyrrolidine-2,5-dione (28a)

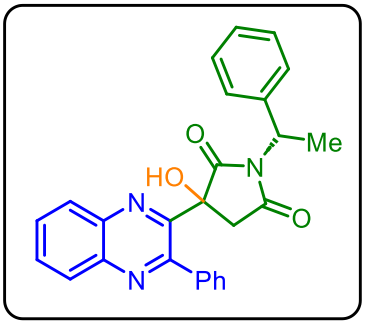

A pale yellow gummy (49 mg, 77% yield); dr 1:1; purified over a column of silica gel (15% EtOAc in hexane); ^{1}H NMR ($CDCl_3$, 400 MHz): δ 8.19 – 8.15 (m, 4H), 7.89 – 7.85 (m, 4H), 7.53 (d, J = 6.8 Hz, 2H), 7.48 (d, J = 6.8 Hz, 2H), 7.37 – 7.33 (m, 10H), 7.25 (d, J = 5.6 Hz, 2H), 7.19 (t, J = 7.8 Hz, 3H), 7.11 (t, J = 7.6 Hz, 2H), 6.60 (s, 1H), 6.44 (s, 1H), 5.40 – 5.32 (m, 2H), 2.96 (dd, J = 18.0, 12.0 Hz,

TH-3369_166122017

2H), 2.74 – 2.65 (m, 2H), 1.83 (d, *J* = 7.2 Hz, 3H), 1.77 (d, *J* = 7.2 Hz, 3H); $^{13}C\{^{1}H\}$ NMR ($CDCl_3$, 126 MHz): *δ* 177.2, 177.1, 173.8, 173.7, 153.1, 148.7, 148.6, 141.9, 141.8, 139.2, 139.1, 139.0, 139.0, 138.0, 137.8, 131.5, 131.21, 131.20, 129.83, 129.80, 129.33, 129.31, 128.7, 128.66, 128.65, 128.5, 128.4, 128.3, 128.2, 128.1, 127.9, 76.2, 76.0, 51.43, 51.40, 42.6, 42.5, 16.9, 16.7; IR (neat, cm^{-1}): 3326, 2927, 1705, 1382, 1344, 1221, 1193, 1125, 906, 763, 730, 696; HRMS (ESI-TOF) calcd for $C_{26}H_{22}N_3O_3$ $[M + H]^+$ 424.1656, found 424.1664.

3-Hydroxy-1-phenethyl-3-(3-phenylquinoxalin-2-yl)pyrrolidine-2,5-dione (**29a**)

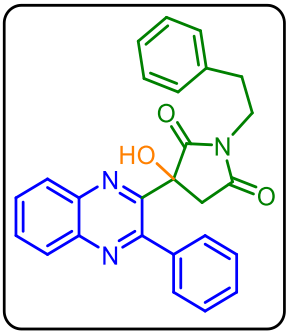

A pale yellow solid (49 mg, 78% yield); mp 167−169 °C; purified over a column of silica gel (15% EtOAc in hexane); ^{1}H NMR ($CDCl_3$, 500 MHz): *δ* 8.21 – 8.18 (m, 2H), 7.90 – 7.86 (m, 2H), 7.47 – 7.42 (m, 3H), 7.36 – 7.34 (m, 2H), 7.30 (t, *J* = 7.5 Hz, 2H), 7.25 – 7.21 (m, 3H), 6.68 (s, 1H), 3.52 – 3.40 (m, 2H), 3.08 (d, *J* = 18.5 Hz, 1H), 2.84 (d, *J* = 18.5 Hz, 1H), 2.80 (t, *J* = 8.0 Hz, 2H); $^{13}C\{^{1}H\}$ NMR ($CDCl_3$, 126 MHz): *δ* 176.9, 173.3, 153.2, 149.0, 141.9, 138.8, 137.7, 137.1, 131.5, 131.3, 129.9, 129.3, 129.0, 128.9, 128.8, 128.7, 128.6, 126.8, 75.9, 43.7, 40.6, 33.6; IR (neat, cm^{-1}): 3363, 2918, 2850, 1699, 1482, 1393, 1346, 1163, 1112, 999, 762, 693; HRMS (ESI-TOF) calcd for $C_{26}H_{22}N_3O_3$ $[M + H]^+$ 424.1656, found 424.1649.

3-Hydroxy-3-(3-phenylquinoxalin-2-yl)-1-(2-(thiophen-2-yl)ethyl)pyrrolidine-2,5-dione (**30a**)

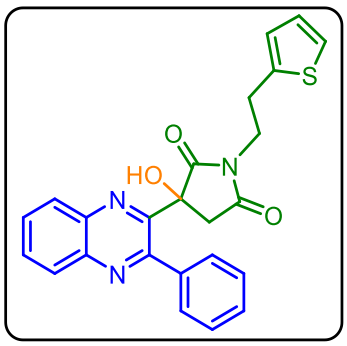

TH-3369_166122017

A light brown solid (48 mg, 74% yield); mp 164–166 ºC; purified over a column of silica gel (17% EtOAc in hexane); ^{1}H NMR ($CDCl_3$, 500 MHz): δ 8.21 – 8.18 (m, 2H), 7.90 – 7.86 (m, 2H), 7.50 – 7.44 (m, 3H), 7.35 (d, J = 7.5 Hz, 2H), 7.15 (d, J = 5.0 Hz, 1H), 6.92 (dd, J = 5.0, 3.5 Hz, 1H), 6.85 (d, J = 3.0 Hz, 1H), 6.65 (s, 1H), 3.54 – 3.46 (m, 2H), 3.09 (d, J = 18.5 Hz, 1H), 3.03 (t, J = 7.7 Hz, 2H), 2.86 (d, J = 18.5 Hz, 1H); ^{13}C {^{1}H} NMR ($CDCl_3$, 126 MHz): δ 176.9, 173.2, 153.2, 149.0, 142.0, 139.6, 138.8, 137.2, 131.5, 131.3, 129.9, 129.3, 129.0, 128.9, 128.6, 127.1, 125.8, 124.3, 75.9, 43.7, 40.6, 27.6; IR (neat, cm^{-1}): 3368, 2929, 1782, 1700, 1393, 1341, 1263, 1143, 1008, 772, 694, 611; HRMS (ESI-TOF) calcd for $C_{24}H_{20}N_3O_3S$ $[M + H]^+$ 430.1220, found 430.1228.

(1*S*,2*R*,5*S*)-2-isopropyl-5-methylcyclohexyl-4-(3-(3-hydroxy-2,5-dioxo-1-phenylpyrrolidin-3-yl)quinoxalin-2-yl)benzoate (**31a**)

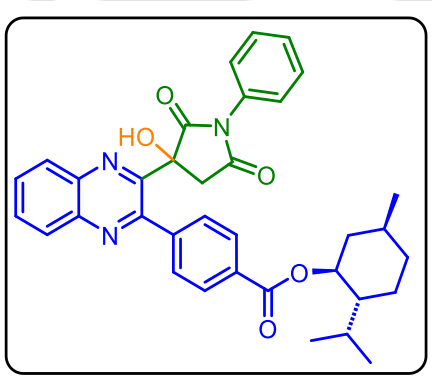

A light brown solid (54 mg, 63% yield); dr 1:1; mp 98–100 ºC; purified over a column of silica gel (25% EtOAc in hexane); ^{1}H NMR ($CDCl_3$, 500 MHz): δ 8.24 – 8.19 (m, 4H), 8.16 (dd, J = 7.5, 4.0 Hz, 4H), 7.94 – 7.89 (m, 4H), 7.55 (d, J = 8.0 Hz, 4H), 7.46 (t, J = 7.5 Hz, 4H), 7.40 (t, J = 7.2 Hz, 2H), 7.14 (t, J = 9.0 Hz, 4H), 6.57 (s, 1H), 6.53 (s, 1H), 5.03 – 4.96 (m, 2H), 3.26 (dd, J = 18.5, 7.5 Hz, 2H), 3.04 (d, J = 17.5 Hz, 2H), 2.20 – 2.16 (m, 2H), 1.98 – 1.92 (m, 2H), 1.76 (d, J = 10.5 Hz, 4H), 1.60 – 1.55 (m, 5H), 1.20 – 1.11 (m, 5H), 0.98 – 0.92 (m, 12H), 0.83 (d, J = 6.5 Hz, 6H); ^{13}C {^{1}H} NMR ($CDCl_3$, 126 MHz): δ 176.1, 172.5, 172.4, 165.24, 165.23, 152.4, 152.3, 148.9, 148.7, 142.0, 141.99, 141.93, 141.8, 139.0, 132.3, 132.2, 131.8, 131.7, 131.5, 130.43, 130.42, 129.5, 129.25, 129.21, 129.1, 128.9, 128.7, 126.1, 126.0, 76.3, 76.2, 75.7, 75.6, 47.5, 47.4, 43.9, 43.8, 41.2, 41.1, 34.46, 34.43, 31.6, 26.8, 26.7, 23.9, 23.8, 22.2, 22.1, 20.9, 20.8, 16.8, 16.7; IR (neat, cm^{-1}): 3379, 2934, 1714, 1498, 1375, 1268, 1181, 1107, 956, 762, 693; HRMS (ESI-TOF) calcd for $C_{35}H_{35}N_3O_5$ $[M + H]^+$ 578.2649, found 578.2653.

TH-3369_166122017

1,7,7-Trimethylbicyclo[2.2.1]heptan-2-yl-4-(3-(3-hydroxy-2,5-dioxo-1-phenylpyrrolidin-3-yl)quinoxalin-2-yl)benzoate (**32a**)

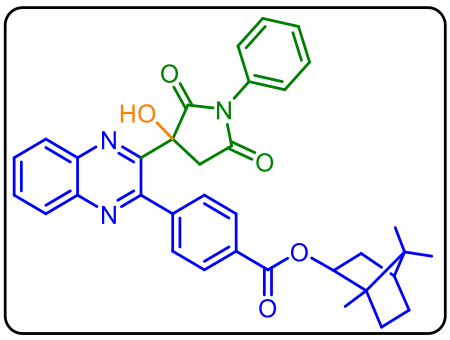

A yellow solid (64 mg, 74% yield); dr 1:1, mp 102–104 °C; purified over a column of silica gel (25% EtOAc in hexane); ^{1}H NMR ($CDCl_3$, 500 MHz): δ 8.24 – 8.17 (m, 8H), 7.93 – 7.89 (m, 4H), 7.56 (d, J = 7.5 Hz, 4H), 7.47 (t, J = 7.5 Hz, 4H), 7.40 (t, J = 7.2 Hz, 2H), 7.17 (dd, J = 6.5 Hz, 4H), 6.60 (s, 1H), 6.58 (s, 1H), 5.18 (t, J = 9.7 Hz, 2H), 3.24 (dd, J = 18.5, 5.5 Hz, 2H), 3.03 (dd, J = 18.5, 4.5 Hz, 2H), 2.56 – 2.49 (m, 2H), 2.13 – 2.08 (m, 2H), 1.85 – 1.82 (m, 2H), 1.80 – 1.77 (m, 2H), 1.47 – 1.42 (m, 2H), 1.37 – 1.32 (m, 2H), 1.19 – 1.14 (m, 2H), 1.00 (s, 6H), 0.95 (s, 12H); ^{13}C {^{1}H} NMR ($CDCl_3$, 126 MHz): δ 176.18, 176.17, 172.5, 165.9, 165.8, 152.3, 148.8, 148.7, 141.99, 141.96, 141.93, 139.0, 132.2, 131.8, 131.7, 131.5, 130.34, 130.32, 129.4, 129.3, 129.22, 129.21, 129.1, 128.9, 128.7, 126.05, 126.04, 81.3, 81.2, 76.2, 49.34, 49.31, 48.10, 48.07, 45.1, 43.8, 43.7, 37.1, 37.0, 28.3, 28.2, 27.6, 27.5, 19.9, 19.1, 13.8, 13.7; IR (neat, cm^{-1}): 3347, 2876, 1714, 1377, 1274, 1188, 1114, 1018, 990, 761, 693; HRMS (ESI-TOF) calcd for $C_{35}H_{34}N_3O_5$ $[M + H]^+$ 576.2493, found 576.2500.

❖ *Spiro-etherification……*

1'-Phenylspiro[chromeno[3,4-*b*]quinoxaline-6,3'-pyrrolidine]-2',5'-dione (**1b**)

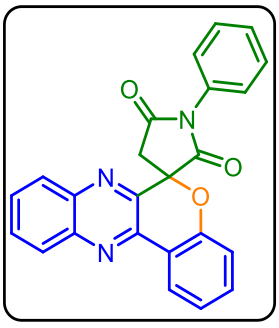

A pale yellow solid (48 mg, 82% yield); mp 209–211 °C; purified over a column of silica gel (7% EtOAc in hexane); ^{1}H NMR ($CDCl_3$, 500 MHz): δ 8.44 (d, J = 7.5 Hz, 1H), 8.14 (d, J = 8.5 Hz, 1H),

TH-3369_166122017

8.03 (d, *J* = 8.5 Hz, 1H), 7.79 (t, *J* = 7.2 Hz, 1H), 7.73 (t, *J* = 7.2 Hz, 1H), 7.45 (t, *J* = 7.5 Hz, 3H), 7.39 – 7.34 (m, 3H), 7.21 (t, *J* = 7.5 Hz, 1H), 7.09 (d, *J* = 8.0 Hz, 1H), 4.14 (d, *J* = 18.0 Hz, 1H), 3.46 (d, *J* = 17.5 Hz, 1H); ^{13}C {^{1}H} NMR ($CDCl_3$, 126 MHz): δ 172.5, 172.4, 154.8, 146.5, 143.3, 141.6, 133.3, 131.4, 131.2, 130.1, 129.5, 129.3, 129.2, 128.9, 126.5, 125.7, 123.6, 120.6, 117.6, 82.4, 42.4; IR (neat, cm^{-1}): 3063, 1788, 1716, 1612, 1493, 1378, 1197, 1176, 1128, 753, 669, 546; HRMS (ESI-TOF) calcd for $C_{24}H_{16}N_3O_3$ $[M + H]^+$ 394.1186, found 394.1188.

3-Methyl-1'-phenylspiro[chromeno[3,4-*b*]quinoxaline-6,3'-pyrrolidine]-2',5'-dione (**2b**)

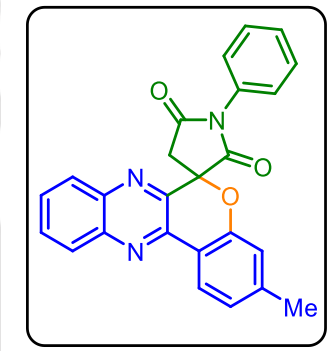

A pale yellow solid (52 mg, 85% yield); mp 228–230 °C; purified over a column of silica gel (7% EtOAc in hexane); ^{1}H NMR ($CDCl_3$, 500 MHz): δ 8.30 (d, *J* = 8.0 Hz, 1H), 8.10 (d, *J* = 8.0 Hz, 1H), 7.99 (d, *J* = 8.5 Hz, 1H), 7.76 (t, *J* = 7.5 Hz, 1H), 7.69 (t, *J* = 7.5 Hz, 1H), 7.43 (t, *J* = 7.5 Hz, 2H), 7.38 – 7.34 (m, 3H), 7.01 (d, *J* = 8.0 Hz, 1H), 6.89 (s, 1H), 4.12 (d, *J* = 18.0 Hz, 1H), 3.43 (d, *J* = 18.0 Hz, 1H), 2.39 (s, 3H); ^{13}C {^{1}H} NMR ($CDCl_3$, 126 MHz): δ 172.6, 172.5, 154.8, 146.5, 144.5, 143.5, 143.3, 141.5, 131.4, 131.1, 129.8, 129.4, 129.3, 129.2, 128.9, 126.5, 125.6, 124.8, 118.0, 117.9, 82.4, 42.4, 21.9; IR (neat, cm^{-1}): 2924, 1719, 1711, 1520, 1385, 1267, 11776, 957, 734, 615; HRMS (ESI-TOF) calcd for $C_{25}H_{18}N_3O_3$ $[M + H]^+$ 408.1343, found 408.1347.

3-Fluoro-1'-phenylspiro[chromeno[3,4-*b*]quinoxaline-6,3'-pyrrolidine]-2',5'-dione (**3b**)

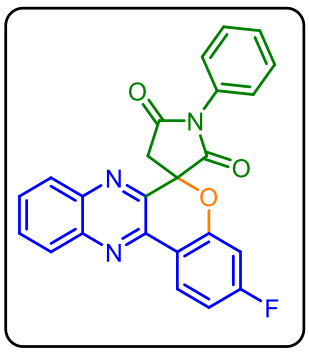

TH-3369_166122017

A off-white solid (48 mg, 78% yield); mp 233–235 °C; purified over a column of silica gel (8% EtOAc in hexane); ^{1}H NMR ($CDCl_3$, 500 MHz): δ 8.44 (t, J = 7.5 Hz, 1H), 8.12 (d, J = 8.5 Hz, 1H), 8.03 (d, J = 8.5 Hz, 1H), 7.80 (t, J = 7.5 Hz, 1H), 7.73 (t, J = 7.5 Hz, 1H), 7.45 (t, J = 7.7 Hz, 2H), 7.39 (t, J = 7.5 Hz, 1H), 7.34 (d, J = 8.0 Hz, 2H), 6.93 (t, J = 8.5 Hz, 1H), 6.85 – 6.81 (m, 1H), 4.17 (d, J = 18.0 Hz, 1H), 3.45 (d, J = 18.0 Hz, 1H); ^{13}C {^{1}H} NMR ($CDCl_3$, 126 MHz): δ 172.3, 172.2, 165.9 (d, J = 253.7 Hz), 156.2 (d, J = 12.7 Hz), 145.8, 143.3, 142.7, 141.6, 134.3, 131.4, 131.3, 130.1, 129.5, 129.4, 129.3, 129.1, 127.6 (d, J = 10.3 Hz), 126.5, 126.2, 117.2 (d, J = 3.0 Hz), 111.4 (d, J = 22.1 Hz), 105.3 (d, J = 25.3 Hz), 82.8, 42.2; ^{19}F NMR ($CDCl_3$) δ -105.2 (s); IR (neat, cm^{-1}): 2921, 1788, 1719, 1612, 1492, 1386, 1180, 1147, 1101, 984, 953, 666, 580; HRMS (ESI-TOF) calcd for $C_{24}H_{15}FN_3O_3$ $[M + H]^+$ 412.1092, found 412.1099.

3-Bromo-1'-phenylspiro[chromeno[3,4-*b*]quinoxaline-6,3'-pyrrolidine]-2',5'-dione (**5b**)

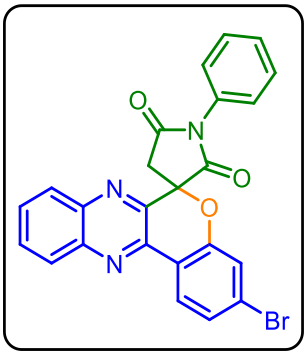

A pale yellow solid (52 mg, 74% yield); mp 258–260 °C; purified over a column of silica gel (8% EtOAc in hexane); ^{1}H NMR ($CDCl_3$, 400 MHz): δ 8.31 (d, J = 8.4 Hz, 1H), 8.13 (d, J = 8.4 Hz, 1H), 8.04 (d, J = 7.6 Hz, 1H), 7.83 – 7.74 (m, 2H), 7.45 (t, J = 7.4 Hz, 2H), 7.40 (d, J = 7.2 Hz, 1H), 7.36 – 7.33 (m, 3H), 7.29 (s, 1H), 4.18 (d, J = 18.0 Hz, 1H), 3.45 (d, J = 18.0 Hz, 1H); ^{13}C {^{1}H} NMR ($CDCl_3$, 126 MHz): δ 172.2, 172.1, 155.2, 146.0, 143.3, 142.7, 141.8, 131.5, 131.3, 130.4, 129.6, 129.4, 129.3, 129.1, 127.1, 127.0, 126.9, 126.5, 120.9, 119.8, 82.7, 42.2; IR (neat, cm^{-1}): 2920, 1789, 1720, 1596, 1490, 1384, 1199, 1066, 953, 755, 697, 578, 467.

TH-3369_166122017

2-Methyl-1'-phenylspiro[chromeno[3,4-*b*]quinoxaline-6,3'-pyrrolidine]-2',5'-dione and 4-Methyl-1'-phenylspiro[chromeno[3,4-*b*]quinoxaline-6,3'-pyrrolidine]-2',5'-dione (8b)

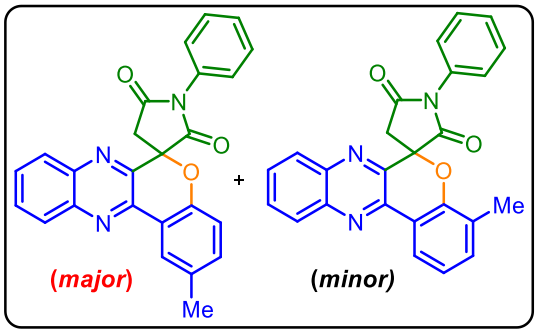

A off-white solid (48 mg, 79% yield); dr 1:0.8; mp 190–192 °C; purified over a column of silica gel (7% EtOAc in hexane); ^{1}H NMR ($CDCl_3$, 500 MHz): δ 8.27 (d, J = 7.5 Hz, 1H), 8.21 (s, 1H), 8.11 (d, J = 8.5 Hz, 2H), 7.99 (d, J = 8.0 Hz, 2H), 7.77 – 7.73 (m, 2H), 7.68 (t, J = 7.5 Hz, 2H), 7.45 – 7.41 (m, 4H), 7.38 – 7.34 (m, 5H), 7.27 (d, J = 7.5 Hz, 1H), 7.23 – 7.20 (m, 1H), 7.09 (t, J = 7.5 Hz, 1H), 6.96 (d, J = 8.0 Hz, 1H), 4.12 (dd, J = 18.0, 13.0 Hz, 2H), 3.43 (dd, J = 17.7, 15.2 Hz, 2H), 2.40 (s, 3H), 2.30 (s, 2.4H); ^{13}C {^{1}H} NMR ($CDCl_3$, 126 MHz): δ 172.5, 172.4, 152.9, 152.8, 146.8, 146.4, 143.6, 143.5, 143.3, 143.2, 141.5, 134.6, 134.2, 133.2, 131.5, 131.4, 131.1, 131.0, 129.9, 129.5, 129.4, 129.3, 129.24, 129.20, 128.9, 128.9, 126.8, 126.5, 126.4, 125.7, 123.4, 123.1, 120.3, 120.2, 117.4, 82.4, 82.3, 42.5, 42.3, 20.9, 15.9; IR (neat, cm^{-1}): 2923, 1791, 1717, 1554, 1496, 1378, 1179, 957, 765, 747, 696, 611, 477; HRMS (ESI-TOF) calcd for $C_{25}H_{18}N_3O_3$ $[M + H]^+$ 408.1343, found 408.1355.

1'-Phenyl-2-(trifluoromethyl)spiro[chromeno[3,4-*b*]quinoxaline-6,3'-pyrrolidine]-2',5'-dione and 1'-Phenyl-4-(trifluoromethyl)spiro[chromeno[3,4-*b*]quinoxaline-6,3'-pyrrolidine]-2',5'-dione (9b)

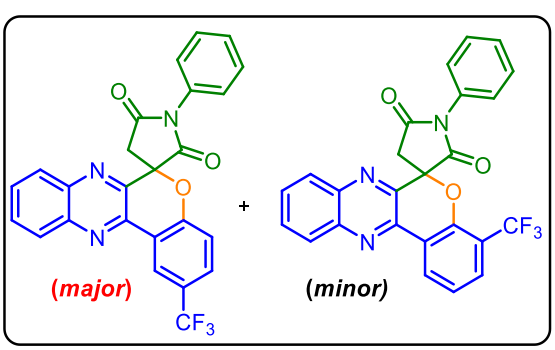

A white solid (50 mg, 72% yield); dr 1:0.2; mp 252–254 °C; purified over a column of silica gel (9% EtOAc in hexane); ^{1}H NMR ($CDCl_3$, 400 MHz): δ 8.75 (s, 1H), 8.19 (d, J = 8.0 Hz, 1H), 8.07 (d, J = 7.6 Hz, 1H), 7.86 – 7.76 (m, 2H), 7.69 (d, J = 8.4 Hz, 1H), 7.45 (t, J = 7.4 Hz, 2H), 7.40 (d, J = 6.8 Hz,

TH-3369_166122017

1H), 7.34 (d, *J* = 7.6 Hz, 2H), 7.19 (d, *J* = 8.4 Hz, 1H), 4.22 (d, *J* = 18.0 Hz, 1H), 3.49 (d, *J* = 18.0 Hz, 1H); ^{13}C {^{1}H} NMR ($CDCl_3$, 126 MHz): *δ* 172.1, 157.0, 145.7, 143.3, 142.05, 142.01, 131.7, 131.2, 130.8, 129.9 (q, *J* = 3.6 Hz), 129.7, 129.4, 129.35, 129.33, 129.2, 126.6, 126.4, 123.4 (q, *J* = 11.3 Hz), 120.9, 118.2, 82.7, 42.1; ^{19}F NMR ($CDCl_3$) *δ* -182.8 (s); IR (neat, cm^{-1}): 2920, 1795, 1723, 1623, 1499, 1352, 1318, 1110, 1064, 1005, 749, 697, 473; HRMS (ESI-TOF) calcd for $C_{25}H_{15}F_3N_3O_3$ $[M + H]^+$ 462.1060, found 462.1059.

1'-Phenylspiro[benzo[7,8]chromeno[3,4-*b*]quinoxaline-6,3'-pyrrolidine]-2',5'-dione (13b)

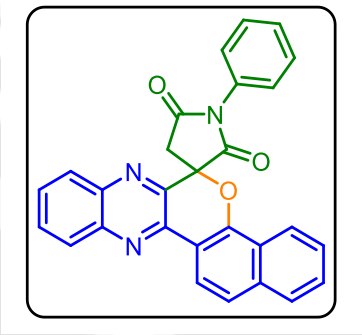

A light orange solid (50 mg, 76% yield); mp 221–223ºC; purified over a column of silica gel (7% EtOAc in hexane); ^{1}H NMR ($CDCl_3$, 500 MHz): *δ* 8.45 (d, *J* = 8.5 Hz, 1H), 8.28 (d, *J* = 8.5 Hz, 1H), 8.14 (d, *J* = 8.0 Hz, 1H), 8.02 (d, *J* = 8.5 Hz, 1H), 7.83 (d, *J* = 8.0 Hz, 1H), 7.77 (d, *J* = 8.0 Hz, 1H), 7.71 (d, *J* = 8.0 Hz, 1H), 7.64 (d, *J* = 9.0 Hz, 1H), 7.58 – 7.51 (m, 2H), 7.44 (d, *J* = 7.5 Hz, 2H), 7.37 (t, *J* = 7.2 Hz, 3H), 4.18 (d, *J* = 18.0 Hz, 1H), 3.58 (d, *J* = 18.0 Hz, 1H); ^{13}C {^{1}H} NMR ($CDCl_3$, 126 MHz): *δ* 172.4, 172.2, 151.4, 146.6, 143.6, 143.4, 141.5, 136.5, 131.4, 131.2, 129.9, 129.5, 129.3, 129.3, 129.0, 128.5, 128.2, 126.6, 126.5, 124.8, 123.4, 122.5, 121.3, 115.0, 83.0, 42.8; IR (neat, cm^{-1}): 2926, 1714, 1489, 1379, 1199, 1100, 1049, 805, 752, 693; HRMS (ESI-TOF) calcd for $C_{28}H_{18}N_3O_3$ $[M + H]^+$ 444.1343, found 444.1349.

1'-Methylspiro[chromeno[3,4-*b*]quinoxaline-6,3'-pyrrolidine]-2',5'-dione (15b)

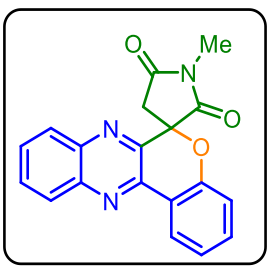

TH-3369_166122017

A light brown solid (38 mg, 77% yield); mp 207–209 °C; purified over a column of silica gel (7% EtOAc in hexane); ^{1}H NMR ($CDCl_3$, 500 MHz): δ 8.41 (d, J = 7.5 Hz, 1H), 8.09 (d, J = 8.5 Hz, 1H), 7.95 (d, J = 8.5 Hz, 1H), 7.74 (t, J = 7.5 Hz, 1H), 7.67 (t, J = 7.7 Hz, 1H), 7.40 (t, J = 7.7 Hz, 1H), 7.18 (t, J = 8.0 Hz, 1H), 7.00 (d, J = 8.5 Hz, 1H), 4.01 (d, J = 18.0 Hz, 1H), 3.25 (d, J = 18.0 Hz, 1H), 3.05 (s, 3H); ^{13}C {^{1}H} NMR ($CDCl_3$, 126 MHz): δ 173.7, 173.3, 154.8, 146.3, 143.3, 143.2, 141.6, 133.2, 131.0, 129.9, 129.5, 129.2, 125.7, 123.5, 120.7, 117.5, 82.3, 42.2, 25.2; IR (neat, cm^{-1}): 2917, 1786, 1702, 1488, 1429, 1278, 1150, 968, 766, 750, 692, 665, 566; HRMS (ESI-TOF) calcd for $C_{19}H_{14}N_3O_3$ $[M + H]^+$ 332.1030, found 332.1009.

1'-Ethylspiro[chromeno[3,4-*b*]quinoxaline-6,3'-pyrrolidine]-2',5'-dione (16b)

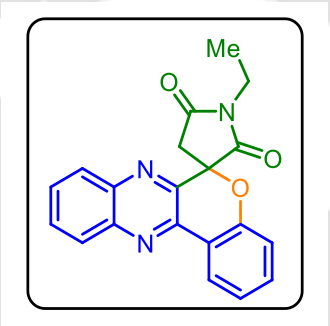

A off-white solid (41 mg, 79% yield); mp 166–168 °C; purified over a column of silica gel (7% EtOAc in hexane); ^{1}H NMR ($CDCl_3$, 500 MHz): δ 8.40 (d, J = 7.5 Hz, 1H), 8.08 (d, J = 8.5 Hz, 1H), 7.94 (d, J = 8.5 Hz, 1H), 7.73 (t, J = 7.5 Hz, 1H), 7.66 (t, J = 7.5 Hz, 1H), 7.40 (t, J = 7.7 Hz, 1H), 7.18 (t, J = 7.5 Hz, 1H), 7.01 (d, J = 8.5 Hz, 1H), 3.94 (d, J = 18.0 Hz, 1H), 3.65 – 3.57 (m, 2H), 3.23 (d, J = 18.0 Hz, 1H), 1.20 (t, J = 7.2 Hz, 3H); ^{13}C{^{1}H} NMR ($CDCl_3$, 126 MHz): δ 173.4, 173.1, 154.8, 146.5, 143.2, 143.1, 141.6, 133.2, 131.0, 129.9, 129.4, 129.2, 125.6, 123.5, 120.6, 117.5, 82.2, 42.3, 34.3, 12.9; IR (neat, cm^{-1}): 2951, 1710, 1605, 1488, 1454, 1395, 1339, 1220, 1134, 1034, 767, 750, 684; HRMS (ESI-TOF) calcd for $C_{20}H_{16}N_3O_3$ $[M + H]^+$ 346.1186, found 346.1194.

1'-Isobutylspiro[chromeno[3,4-*b*]quinoxaline-6,3'-pyrrolidine]-2',5'-dione (17b)

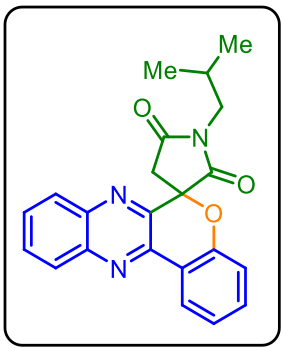

A light orange solid (42 mg, 75% yield); mp 132–134 °C; purified over a column of silica gel (6% EtOAc in hexane); ^{1}H NMR ($CDCl_3$, 500 MHz): δ 8.42 (d, J = 7.5 Hz, 1H), 8.11 (d, J = 8.0 Hz, 1H), 7.94 (d, J = 8.5 Hz, 1H), 7.75 (t, J = 7.5 Hz, 1H), 7.68 (t, J = 7.5 Hz, 1H), 7.42 (t, J = 7.7 Hz, 1H), 7.19 (t, J = 7.5 Hz, 1H), 7.02 (d, J = 8.5 Hz, 1H), 3.94 (d, J = 18.0 Hz, 1H), 3.39 (d, J = 7.5 Hz, 2H), 3.25 (d, J = 18.0 Hz, 1H), 2.10 – 2.01 (m, 1H), 0.90 (d, J = 6.5 Hz, 3H), 0.86 (d, J = 7 Hz, 3H); ^{13}C {^{1}H} NMR ($CDCl_3$, 126 MHz): δ 173.8, 173.6, 154.9, 146.9, 143.3, 143.2, 141.6, 133.3, 131.0, 130.0, 129.5, 129.2, 125.7, 123.5, 120.6, 117.5, 82.4, 46.3, 42.4, 27.0, 20.0, 19.9; IR (neat, cm^{-1}): 2956, 1786, 1712, 1611, 1457, 1397, 1211, 1153, 1037, 768, 752, 660, 581; HRMS (ESI-TOF) calcd for $C_{22}H_{20}N_3O_3$ [M + H]$^+$ 374.1499, found 374.1491.

1'-Benzylspiro[chromeno[3,4-*b*]quinoxaline-6,3'-pyrrolidine]-2',5'-dione (18b)

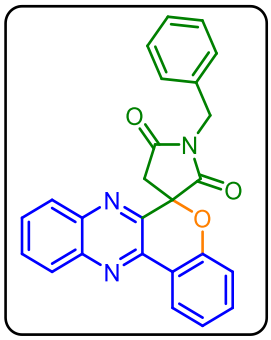

A light brown solid (49 mg, 80% yield); mp 178–180 °C; purified over a column of silica gel (7% EtOAc in hexane); ^{1}H NMR ($CDCl_3$, 500 MHz): δ 8.41 (d, J = 7.5 Hz, 1H), 8.09 (d, J = 8.5 Hz, 1H), 7.91 (d, J = 8.0 Hz, 1H), 7.74 (t, J = 7.5 Hz, 1H), 7.68 (t, J = 7.2 Hz, 1H), 7.41 (t, J = 7.0 Hz, 1H), 7.33 (d, J = 6.5 Hz, 2H), 7.27 – 7.22 (m, 3H), 7.18 (t, J = 7.5 Hz, 1H), 7.00 (d, J = 8.0 Hz, 1H), 4.71 (s, 2H), 3.96 (d, J = 18.0 Hz, 1H), 3.27 (d, J = 18.0 Hz, 1H); ^{13}C {^{1}H} NMR ($CDCl_3$, 126 MHz): δ 173.2, 173.1, 154.9, 146.5, 143.2, 143.2, 141.6, 135.1, 133.3, 131.1, 129.9, 129.5, 129.2, 128.7, 128.4, 128.1, 125.7, 123.6, 120.6, 117.5, 82.5, 42.8, 42.5; IR (neat, cm^{-1}): 2928, 1723, 1454, 1389, 1331, 1179, 1087, 1030, 769, 713, 624; HRMS (ESI-TOF) calcd for $C_{25}H_{18}N_3O_3$ [M + H]$^+$ 408.1343, found 408.1334.

1'-(*p*-Tolyl)spiro[chromeno[3,4-*b*]quinoxaline-6,3'-pyrrolidine]-2',5'-dione (20b)

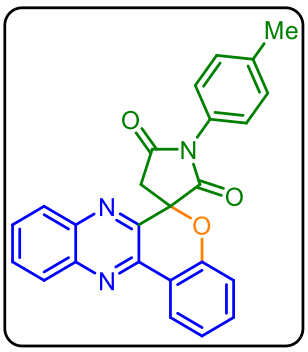

A pale yellow solid (51 mg, 84% yield); mp 228–230 °C; purified over a column of silica gel (7% EtOAc in hexane); ^{1}H NMR ($CDCl_3$, 500 MHz): δ 8.44 (d, J = 8.0 Hz, 1H), 8.14 (d, J = 8.0 Hz, 1H), 8.03 (d, J = 7.5 Hz, 1H), 7.79 (t, J = 7.0 Hz, 1H), 7.72 (t, J = 7.0 Hz, 1H), 7.44 (t, J = 7.0 Hz, 1H), 7.25 – 7.19 (m, 5H), 7.08 (d, J = 8.0 Hz, 1H), 4.12 (d, J = 18.0 Hz, 1H), 3.43 (d, J = 18.0 Hz, 1H), 2.36 (s, 3H); ^{13}C {^{1}H} NMR ($CDCl_3$, 126 MHz): δ 172.7, 172.5, 154.9, 146.7, 143.4, 141.7, 139.1, 133.3, 131.2, 130.1, 129.9, 129.6, 129.4, 128.8, 126.3, 125.8, 123.6, 120.7, 117.6, 82.5, 42.5, 21.3; IR (neat, cm^{-1}): 2919, 1720, 1611, 1459, 1384, 1199, 1179, 1079, 772, 755, 716; HRMS (ESI-TOF) calcd for $C_{25}H_{18}N_3O_3$ $[M + H]^+$ 408.1343, found 408.1350.

1'-(4-Fluorophenyl)spiro[chromeno[3,4-*b*]quinoxaline-6,3'-pyrrolidine]-2',5'-dione (21b)

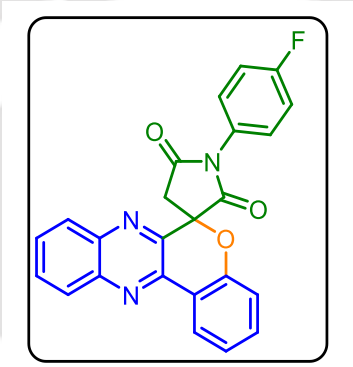

A off-white solid (45 mg, 73% yield); mp 211–213 °C; purified over a column of silica gel (7% EtOAc in hexane); ^{1}H NMR ($CDCl_3$, 500 MHz): δ 8.44 (d, J = 8.0 Hz, 1H), 8.13 (d, J = 8.5 Hz, 1H), 8.01 (d, J = 8.5 Hz, 1H), 7.78 (t, J = 8.2 Hz, 1H), 7.71 (t, J = 7.0 Hz, 1H), 7.44 (t, J = 7.0 Hz, 1H), 7.36 – 7.33 (m, 2H), 7.21 (t, J = 7.5 Hz, 1H), 7.13 (t, J = 8.5 Hz, 2H), 7.07 (d, J = 8.0 Hz, 1H), 4.12 (d, J = 18.0 Hz, 1H), 3.44 (d, J = 18.0 Hz, 1H); ^{13}C {^{1}H} NMR ($CDCl_3$, 126 MHz): δ 172.4, 172.3, 162.5 (d, J = 249.6 Hz), 154.8, 146.4, 143.3 (d, J = 9.7 Hz), 141.7, 133.4, 131.3, 130.1, 129.6, 129.3, 128.4 (d, J = 8.7 Hz), 127.3 (d, J = 3.2 Hz), 125.8, 123.7, 120.6, 117.6, 116.4, 116.2, 82.3, 42.4; ^{19}F NMR ($CDCl_3$) δ -111.6 (s); IR (neat, cm^{-1}): 2926, 1718, 1508, 1459, 1379, 1224, 1199, 1177, 1078, 840, 769, 751, 654; HRMS (ESI-TOF) calcd for $C_{24}H_{15}FN_3O_3$ $[M + H]^+$ 412.1092, found 412.1098.

TH-3369_166122017

1'-(4-Methoxybenzyl)spiro[chromeno[3,4-*b*]quinoxaline-6,3'-pyrrolidine]-2',5'-dione (22b)

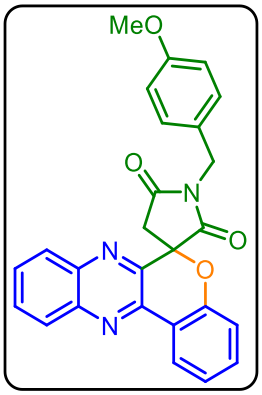

A light brown solid (53 mg, 81% yield); mp 183–185 °C; purified over a column of silica gel (10% EtOAc in hexane); ^{1}H NMR (500 MHz, $CDCl_3$) δ 8.41 (d, J = 6.5 Hz, 1H), 8.09 (d, J = 8.0 Hz, 1H), 7.90 (d, J = 8.0 Hz, 1H), 7.74 (t, J = 7.0 Hz, 1H), 7.67 (t, J = 7.7 Hz, 1H), 7.41 (t, J = 7.7 Hz, 1H), 7.27 (d, J = 8.5 Hz, 2H), 7.18 (t, J = 7.5 Hz, 1H), 7.00 (d, J = 8.0 Hz, 1H), 6.77 (d, J = 8.5 Hz, 2H), 4.64 (s, 2H), 3.94 (d, J = 18.0 Hz, 1H), 3.74 (s, 3H), 3.25 (d, J = 18.0 Hz, 1H); ^{13}C {^{1}H} NMR ($CDCl_3$, 126 MHz): δ 173.2, 173.1, 159.4, 154.9, 146.5, 143.22, 143.21, 141.6, 133.3, 131.0, 130.1, 129.9, 129.5, 129.2, 127.4, 125.7, 123.5, 120.6, 117.5, 114.1, 82.4, 55.3, 42.4, 42.3; IR (neat, cm^{-1}): 2932, 1788, 1713, 1609, 1553, 1513, 1389, 1248, 1175, 1070, 756, 694, 566; HRMS (ESI-TOF) calcd for $C_{26}H_{20}N_3O_4$ $[M + H]^+$ 438.1448, found 438.1455.

1'-(4-Phenylbutyl)spiro[chromeno[3,4-*b*]quinoxaline-6,3'-pyrrolidine]-2',5'-dione (23b)

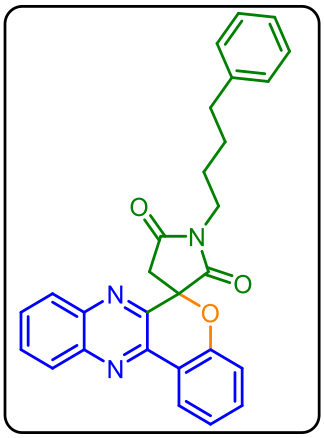

A pale yellow solid (49 mg, 73% yield); mp 138–140 °C; purified over a column of silica gel (7% EtOAc in hexane); ^{1}H NMR ($CDCl_3$, 500 MHz): δ 8.43 (d, J = 7.5 Hz, 1H), 8.12 (d, J = 8.5 Hz, 1H), 7.88 (d, J = 8.5 Hz, 1H), 7.76 (t, J = 7.2 Hz, 1H), 7.67 (t, J = 7.5 Hz, 1H), 7.42 (t, J = 7.7 Hz, 1H), 7.23

TH-3369_166122017

– 7.19 (m, 3H), 7.15 (t, *J* = 7.2 Hz, 1H), 7.08 (d, *J* = 7.5 Hz, 2H), 7.01 (d, *J* = 8.5 Hz, 1H), 3.94 (d, *J* = 17.5 Hz, 1H), 3.61 (t, *J* = 6.7 Hz, 2H), 3.25 (d, *J* = 18.0 Hz, 1H), 2.58 (t, *J* = 7.5 Hz, 2H), 1.67 – 1.63 (m, 2H), 1.62 – 1.57 (m, 2H); ^{13}C {^{1}H} NMR ($CDCl_3$, 126 MHz): δ 173.6, 173.5, 154.9, 146.7, 143.3, 143.2, 142.0, 141.7, 133.3, 131.1, 130.0, 129.5, 129.2, 128.5, 128.4, 125.9, 125.8, 123.6, 120.6, 117.6, 82.4, 42.4, 39.0, 35.4, 28.3, 27.1; IR (neat, cm^{-1}): 2920, 1778, 1705, 1550, 1491, 1391, 1358, 1213, 1074, 930, 742, 664, 564; HRMS (ESI-TOF) calcd for $C_{28}H_{24}N_3O_3$ $[M + H]^+$ 450.1812, found 450.1807.

1'-Heptylspiro[chromeno[3,4-*b*]quinoxaline-6,3'-pyrrolidine]-2',5'-dione (24b)

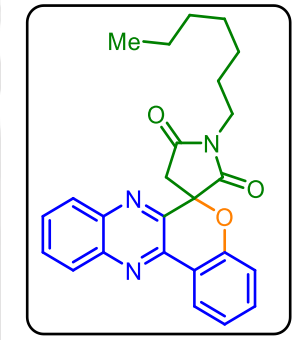

A off-white solid (47 mg, 76% yield); mp 125–127 ºC; purified over a column of silica gel (5% EtOAc in hexane); ^{1}H NMR ($CDCl_3$, 500 MHz): δ 8.41 (d, *J* = 7.5 Hz, 1H), 8.10 (d, *J* = 8.5 Hz, 1H), 7.94 (d, *J* = 8.5 Hz, 1H), 7.75 (t, *J* = 7.5 Hz, 1H), 7.67 (t, *J* = 7.5 Hz, 1H), 7.41 (t, *J* = 7.7 Hz, 1H), 7.18 (t, *J* = 7.5 Hz, 1H), 7.01 (d, *J* = 8.0 Hz, 1H), 3.95 (d, *J* = 18.0 Hz, 1H), 3.55 (t, *J* = 7.2 Hz, 2H), 3.24 (d, *J* = 18.0 Hz, 1H), 1.60 – 1.56 (m, 2H), 1.24 – 1.16 (m, 8H), 0.82 (t, *J* = 7.0 Hz, 3H); ^{13}C {^{1}H} NMR ($CDCl_3$, 126 MHz): δ 173.6, 173.4, 154.9, 146.7, 143.3, 143.2, 141.6, 133.2, 131.0, 129.9, 129.5, 129.2, 125.7, 123.5, 120.6, 117.5, 82.3, 42.3, 39.3, 31.7, 28.8, 27.4, 26.6, 22.6, 14.1; IR (neat, cm^{-1}): 2921, 1790, 1711, 1610, 1459, 1346, 1179, 1039, 875, 765, 712, 698, 566; HRMS (ESI-TOF) calcd for $C_{25}H_{26}N_3O_3$ $[M + H]^+$ 416.1969, found 416.1974.

1'-Decylspiro[chromeno[3,4-*b*]quinoxaline-6,3'-pyrrolidine]-2',5'-dione (25b)

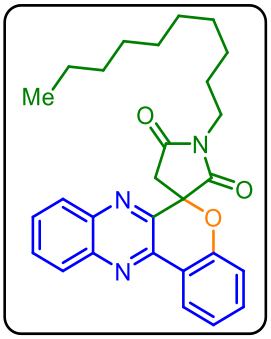

A off-white solid (53 mg, 77% yield); mp 112–114 °C; purified over a column of silica gel (5% EtOAc in hexane); ^{1}H NMR ($CDCl_3$, 500 MHz): δ 8.41 (d, J = 7.5 Hz, 1H), 8.10 (d, J = 8.5 Hz, 1H), 7.94 (d, J = 8.5 Hz, 1H), 7.75 (t, J = 7.7 Hz, 1H), 7.67 (t, J = 7.5 Hz, 1H), 7.41 (t, J = 7.7 Hz, 1H), 7.19 (t, J = 7.7 Hz, 1H), 7.01 (d, J = 8.5 Hz, 1H), 3.95 (d, J = 17.5 Hz, 1H), 3.55 (t, J = 7.2 Hz, 2H), 3.24 (d, J = 17.5 Hz, 1H), 1.60 – 1.57 (m, 2H), 1.27 – 1.18 (m, 14H), 0.86 (t, J = 7.2 Hz, 3H); ^{13}C {^{1}H} NMR ($CDCl_3$, 126 MHz): δ 173.6, 173.4, 154.9, 146.7, 143.3, 143.2, 141.6, 133.2, 131.0, 129.9, 129.5, 129.2, 125.7, 123.5, 120.6, 117.5, 82.3, 42.3, 39.3, 31.9, 29.55, 29.53, 29.3, 29.1, 27.4, 26.6, 22.8, 14.2; IR (neat, cm^{-1}): 2922, 2851, 1718, 1609, 1489, 1457, 1389, 1348, 1169, 949, 772, 750, 655, 563; HRMS (ESI-TOF) calcd for $C_{28}H_{32}N_3O_3$ $[M + H]^+$ 458.2438, found 458.2420.

Spiro[chromeno[3,4-*b*]quinoxaline-6,3'-pyrrolidine]-2',5'-dione (**26b**)

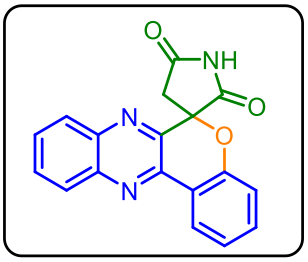

A off-white solid (33 mg, 70% yield); mp 235–237 °C; purified over a column of silica gel (20% EtOAc in hexane); ^{1}H NMR (DMSO-d_6, 500 MHz): δ 11.88 (s, 1H), 8.32 (d, J = 8.0 Hz, 1H), 8.15 (d, J = 8.0 Hz, 1H), 8.04 (d, J = 8.0 Hz, 1H), 7.90 (d, J = 6.7 Hz, 1H), 7.84 (d, J = 7.2 Hz, 1H), 7.52 (t, J = 6.7 Hz, 1H), 7.25 (t, J = 7.0 Hz, 1H), 7.13 (d, J = 8.0 Hz, 1H), 3.75 (d, J = 18.0 Hz, 1H), 3.42 (d, J = 18.0 Hz, 1H); ^{13}C {^{1}H} NMR (DMSO-d_6, 126 MHz): δ 174.5, 174.3, 154.7, 147.2, 142.4, 142.2, 140.9, 133.5, 131.5, 130.5, 129.0, 128.8, 124.9, 123.2, 119.7, 117.5, 83.5, 43.1; IR (neat, cm^{-1}): 3200, 1816, 1729, 1664, 1490, 1338, 1188, 1075, 980, 765, 718, 621, 590; HRMS (ESI-TOF) calcd for $C_{18}H_{12}N_3O_3$ $[M + H]^+$ 318.0873, found 318.0865.

1'-((*S*)-1-(Naphthalen-1-yl)ethyl)spiro[chromeno[3,4-*b*]quinoxaline-6,3'-pyrrolidine]-2',5'-dione (**27b**)

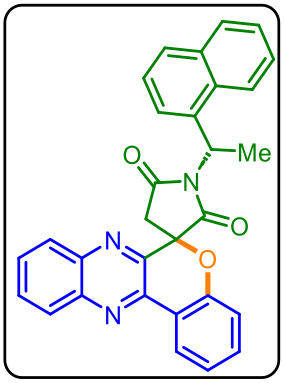

A pale yellow solid (53mg, 75% yield); dr 1:1; mp 179–181 °C; purified over a column of silica gel (7% EtOAc in hexane); ^{1}H NMR ($CDCl_3$, 500 MHz): δ 8.40 (d, J = 8.0 Hz, 1H), 8.34 (d, J = 7.5 Hz, 1H), 8.09 – 8.00 (m, 3H), 7.84 (d, J = 7.5 Hz, 1H), 7.81 – 7.76 (m, 5H), 7.73 – 7.64 (m, 4H), 7.61 – 7.58 (m, 3H), 7.54 (t, J = 7.7 Hz, 1H), 7.48 – 7.36 (m, 5H), 7.30 (t, J = 7.5 Hz, 1H), 7.18 – 7.12 (m, 3H), 6.98 (d, J = 8.5 Hz, 1H), 6.91 (d, J = 8.0 Hz, 1H), 6.18 – 6.10 (m, 2H), 3.85 (d, J = 18.0 Hz, 1H), 3.76 (d, J = 17.5 Hz, 1H), 3.20 (d, J = 6.5 Hz, 1H), 3.16 (d, J = 7.0 Hz, 1H), 1.96 (d, J = 7.0 Hz, 3H), 1.91 (d, J = 7.0 Hz, 3H); ^{13}C {^{1}H} NMR ($CDCl_3$, 126 MHz): δ 173.4, 173.2, 173.1, 173.0, 155.0, 154.9, 146.5, 146.4, 143.1, 143.09, 143.04, 141.5, 141.4, 133.7, 133.5, 133.3, 133.2, 132.9, 131.4, 131.2, 131.0, 130.9, 129.8, 129.7, 129.3, 129.3, 129.28, 129.20, 129.0, 128.9, 126.7, 126.5, 126.3, 125.6, 125.6, 125.56, 125.54, 125.1, 124.9, 123.5, 123.4, 122.9, 122.7, 120.5, 120.4, 117.5, 82.1, 82.0, 47.1, 47.0, 42.4, 42.3, 17.2, 17.0; IR (neat, cm^{-1}): 2917, 1782, 1707, 1490, 1457, 1357, 1201, 1128, 1065, 918, 769, 698, 606; HRMS (ESI-TOF) calcd for $C_{30}H_{22}N_3O_3$ $[M + H]^+$ 472.1656, found 472.1664.

1'-((*S*)-1-Phenylethyl)spiro[chromeno[3,4-*b*]quinoxaline-6,3'-pyrrolidine]-2',5'-dione (28b)

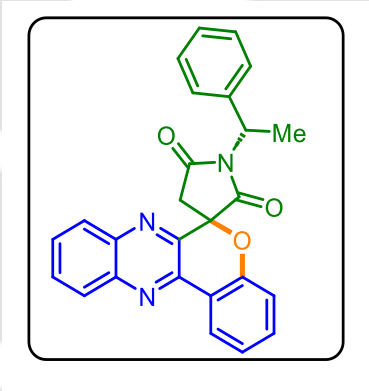

A pale yellow solid (49 mg, 78% yield); dr 1:1; mp 197–199 °C; purified over a column of silica gel (7% EtOAc in hexane); ^{1}H NMR ($CDCl_3$, 400 MHz): δ 8.42 – 8.36 (m, 2H), 8.09 (t, J = 9.0 Hz, 2H), 7.94 – 7.91 (m, 2H), 7.77 – 7.67 (m, 4H), 7.42 – 7.35 (m, 6H), 7.32 – 7.25 (m, 3H), 7.21 – 7.15 (m, 5H), 7.01 (t, J = 9.2 Hz, 2H), 5.48 – 5.43 (m, 2H), 3.86 (t, J = 17.2 Hz, 2H), 3.23 (d, J = 17.6 Hz, 2H), 1.84 (d, J = 7.2 Hz, 3H), 1.78 (d, J = 7.2 Hz, 3H); ^{13}C {^{1}H} NMR ($CDCl_3$, 126 MHz): δ 173.3, 173.1, 173.0, 154.9, 146.8, 146.6, 143.2, 143.12, 143.10, 141.6, 141.5, 139.2, 138.8, 133.26, 133.25, 131.0, 130.9, 129.93, 129.89, 129.5, 129.4, 129.15, 129.10, 128.5, 128.4, 127.9, 127.8, 127.3, 127.2, 125.6, 123.5, 123.4, 120.40, 120.38, 117.5, 117.4, 82.1, 82.0, 50.9, 50.6, 42.5, 42.4, 16.7, 16.6; IR (neat, cm^{-1}): 2923, 1782, 1709, 1608, 1490, 1454, 1355, 1222, 1069, 965, 915, 747, 696; HRMS (ESI-TOF) calcd for $C_{26}H_{20}N_3O_3$ $[M + H]^+$ 422.1499, found 422.1506.

TH-3369_166122017

1'-Phenethylspiro[chromeno[3,4-*b*]quinoxaline-6,3'-pyrrolidine]-2',5'-dione (**29b**)

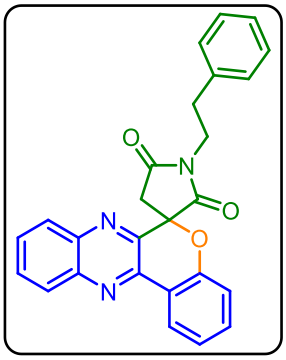

A white solid (48 mg, 76% yield); mp 164–166 °C; purified over a column of silica gel (7% EtOAc in hexane); ^{1}H NMR ($CDCl_3$, 500 MHz): δ 8.40 (d, J = 8.0 Hz, 1H), 8.09 (d, J = 8.5 Hz, 1H), 7.95 (d, J = 8.0 Hz, 1H), 7.74 (t, J = 7.5 Hz, 1H), 7.68 (t, J = 7.5 Hz, 1H), 7.40 (t, J = 7.7 Hz, 1H), 7.19 – 7.11 (m, 6H), 6.98 (d, J = 8.5 Hz, 1H), 3.96 (d, J = 17.5 Hz, 1H), 3.78 (t, J = 7.2 Hz, 2H), 3.17 (d, J = 18.0 Hz, 1H), 2.94 – 2.85 (m, 2H); ^{13}C {^{1}H} NMR ($CDCl_3$, 126 MHz): δ 173.3, 173.1, 154.8, 146.3, 143.3, 143.1, 141.5, 137.4, 133.2, 131.0, 129.9, 129.4, 129.2, 128.9, 128.5, 126.8, 125.7, 123.5, 120.7, 117.5, 82.1, 41.9, 40.3, 33.4; IR (neat, cm^{-1}): 2920, 1709, 1396, 1358, 1248, 1167, 1066, 968, 772, 748, 699, 564; HRMS (ESI-TOF) calcd for $C_{26}H_{20}N_3O_3$ $[M + H]^+$ 422.1499, found 422.1507.

1'-(2-(Thiophen-2-yl)ethyl)spiro[chromeno[3,4-*b*]quinoxaline-6,3'-pyrrolidine]-2',5'-dione (**30b**)

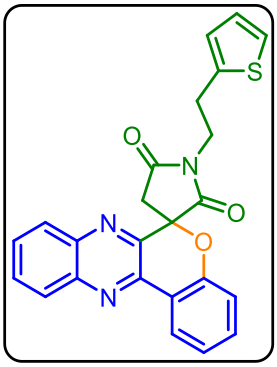

A pale yellow solid (46 mg, 72% yield); mp 149–151 °C; purified over a column of silica gel (8% EtOAc in hexane); ^{1}H NMR ($CDCl_3$, 500 MHz): δ 8.41 (d, J = 8.0 Hz, 1H), 8.11 (d, J = 8.5 Hz, 1H), 7.96 (d, J = 8.0 Hz, 1H), 7.75 (t, J = 7.0 Hz, 1H), 7.69 (t, J = 7.2 Hz, 1H), 7.41 (t, J = 7.0 Hz, 1H), 7.19 (t, J = 7.5 Hz, 1H), 7.06 – 7.04 (m, 1H), 7.00 (d, J = 8.0 Hz, 1H), 6.78 – 6.75 (m, 2H), 3.99 (d, J = 18.0 Hz, 1H), 3.83 – 3.78 (m, 2H), 3.21 (d, J = 18.0 Hz, 1H), 3.13 (t, J = 7.2 Hz, 2H); ^{13}C {^{1}H} NMR ($CDCl_3$, 126 MHz): δ 173.3, 173.1, 154.8, 146.3, 143.3, 143.2, 141.6, 139.4, 133.2, 131.0, 129.9, 129.5,

TH-3369_166122017

129.3, 126.9, 125.9, 125.7, 124.3, 123.5, 120.7, 117.5, 82.2, 42.0, 40.4, 27.4; IR (neat, cm^{-1}): 2952, 1789, 1708, 1608, 1454, 1397, 1358, 1275, 1077, 966, 770, 700, 540; HRMS (ESI-TOF) calcd for $C_{24}H_{18}N_3O_3S$ $[M + H]^+$ 428.1063, found 428.1079.

(1*S*,2*R*,5*S*)-2-isopropyl-5-methylcyclohexyl2',5'-dioxo-1'-phenylspiro[chromeno[3,4-*b*]quinoxaline-6,3'-pyrrolidine]-3-carboxylate (31b)

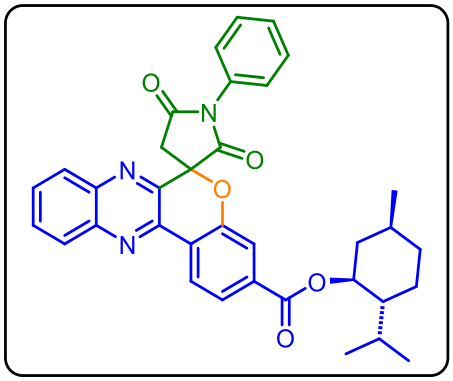

A light orange solid (57 mg, 66% yield); dr 1:1; mp 170–172 °C; purified over a column of silica gel (10% EtOAc in hexane); ^1H NMR ($CDCl_3$, 500 MHz): δ 8.51 (d, J = 8.0 Hz, 2H), 8.18 (d, J = 8.0 Hz, 2H), 8.06 (d, J = 8.0 Hz, 2H), 7.87 (d, J = 8.0 Hz, 2H), 7.83 (t, J = 7.5 Hz, 2H), 7.79 – 7.75 (m, 4H), 7.45 (t, J = 7.5 Hz, 4H), 7.39 (d, J = 6.5 Hz, 2H), 7.35 (d, J = 7.5 Hz, 4H), 4.98 – 4.94 (m, 2H), 4.21 (dd, J = 17.7, 14.2 Hz, 2H), 3.49 (dd, J = 18.0, 4.0 Hz, 2H), 2.14 (d, J = 10.0 Hz, 2H), 2.04 – 1.96 (m, 2H), 1.76 – 1.73 (m, 4H), 1.61 – 1.55 (m, 5H), 1.19 – 1.11 (m, 5H), 0.94 (d, J = 6.5 Hz, 12H), 0.82 (d, J = 6.5 Hz, 6H); ^{13}C {^1H} NMR ($CDCl_3$, 126 MHz): δ 172.4, 172.3, 172.3, 172.2, 165.2, 165.1, 154.6, 146.5, 146.5, 143.4, 142.6, 142.5, 142.0, 135.24, 135.22, 131.5, 131.31, 131.30, 130.8, 129.8, 129.4, 129.3, 129.2, 129.1, 126.5, 125.7, 124.6, 124.4, 124.3, 118.85, 118.82, 82.5, 75.6, 47.4, 42.2, 42.1, 41.1, 34.4, 31.6, 26.6, 26.5, 23.8, 23.7, 22.2, 21.0, 20.9, 16.6, 16.5; IR (neat, cm^{-1}): 2922, 1721, 1494, 1427, 1375, 1272, 1197, 1092, 978, 916, 751, 694, 597; HRMS (ESI-TOF) calcd for $C_{35}H_{34}N_3O_5$ $[M + H]^+$ 576.2493, found 576.2495.

TH-3369_166122017

1,7,7-Trimethylbicyclo[2.2.1]heptan-2-yl2',5'-dioxo-1'-phenylspiro[chromeno[3,4-*b*]quinoxaline-6,3'-pyrrolidine]-3-carboxylate (**32b**)

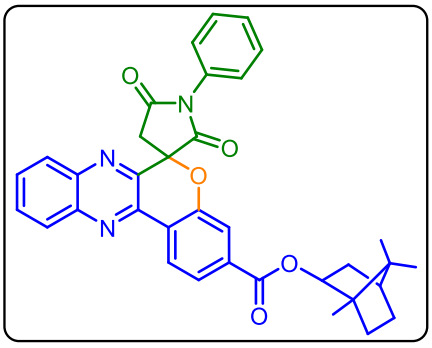

A pale yellow solid (67 mg, 78% yield); dr 1:1; mp 197–199 °C; purified over a column of silica gel (10% EtOAc in hexane); ^{1}H NMR ($CDCl_3$, 500 MHz): δ 8.52 (d, J = 8.0 Hz, 2H), 8.17 (d, J = 8.5 Hz, 2H), 8.05 (d, J = 8.5 Hz, 2H), 7.88 (d, J = 8.0 Hz, 2H), 7.82 (t, J = 7.7 Hz, 2H), 7.77 (d, J = 7.0 Hz, 2H), 7.76 (s, 2H), 7.44 (t, J = 7.7 Hz, 4H), 7.38 (d, J = 7.0 Hz, 2H), 7.35 (d, J = 7.5 Hz, 4H), 5.14 (d, J = 9.5 Hz, 2H), 4.20 (dd, J = 18.0, 3.5 Hz, 2H), 3.50 (d, J = 18.0 Hz, 2H), 2.52 – 2.47 (m, 2H), 2.19 – 2.13 (m, 2H), 1.86 – 1.80 (m, 2H), 1.76 (d, J = 3.5 Hz, 2H), 1.47 – 1.42 (m, 2H), 1.37 – 1.34 (m, 2H), 1.18 – 1.13 (m, 2H), 0.98 (s, 6H), 0.95 – 0.92 (m, 12H); ^{13}C {^{1}H} NMR ($CDCl_3$, 126 MHz): δ 172.3, 172.2, 165.84, 165.82, 154.6, 146.5, 146.4, 143.3, 142.5, 142.0, 135.2, 135.1, 131.5, 131.3, 130.8, 129.8, 129.4, 129.3, 129.1, 126.5, 125.8, 124.5, 124.4, 118.7, 82.5, 81.31, 81.30, 49.3, 48.1, 45.1, 42.1, 37.0, 36.9, 28.24, 28.23, 27.6, 19.9, 19.0, 13.8; IR (neat, cm^{-1}): 2944, 1725, 1493, 1429, 1373, 1276, 1163, 1013, 889, 762, 694, 615, 599; HRMS (ESI-TOF) calcd for $C_{35}H_{32}N_3O_5$ $[M + H]^+$ 574.2336, found 574.2342.

1'-(2-(1*H*-Indol-3-yl)ethyl)spiro[chromeno[3,4-*b*]quinoxaline-6,3'-pyrrolidine]-2',5'-dione (**33b**)

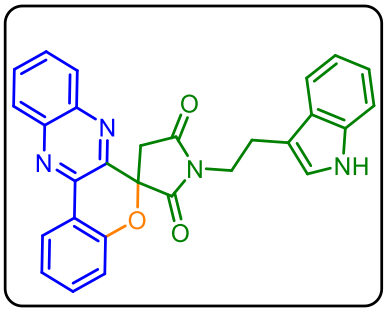

A pale yellow solid (48 mg, 70% yield); mp 122–124 °C; purified over a column of silica gel (10% EtOAc in hexane); ^{1}H NMR ($CDCl_3$, 500 MHz): δ 8.44 (d, J = 7.5 Hz, 1H), 8.12 (d, J = 8.0 Hz, 1H),

TH-3369_166122017

8.02 (br s, 1H), 7.92 (d, *J* = 8.0 Hz, 1H), 7.77 (t, *J* = 7.0 Hz, 1H), 7.69 (t, *J* = 7.5 Hz, 1H), 7.66 (d, *J* = 7.5 Hz, 1H), 7.43 (t, *J* = 7.0 Hz, 1H), 7.32 (dd, *J* = 19.7, 8.2 Hz, 1H), 7.22 – 7.15 (m, 2H), 7.13 – 7.08 (m, 1H), 7.02 (d, *J* = 7.5 Hz, 1H), 6.65 (s, 1H), 3.96 (d, *J* = 17.5 Hz, 1H), 3.89 – 3.82 (m, 2H), 3.21 (d, *J* = 18.0 Hz, 1H), 3.11 – 3.05 (m, 2H); ^{13}C {^{1}H} NMR ($CDCl_3$, 126 MHz): *δ* 173.6, 173.4, 154.9, 146.6, 143.4, 143.2, 141.7, 136.3, 134.2, 133.3, 131.1, 130.0, 129.5, 129.3, 125.7, 123.6, 122.3, 122.2, 119.7, 118.9, 117.6, 112.0, 111.3, 111.2, 82.3, 42.3, 39.9, 23.4; IR (neat, cm^{-1}): 2922, 1782, 1699, 1611, 1453, 1339, 1227, 1168, 1141, 969, 825, 744, 694; HRMS (ESI-TOF) calcd for $C_{28}H_{21}N_4O_3$ $[M + H]^+$ 461.1608, found 461.1615.

1',1'''-(1,3-Phenylene)bis(spiro[chromeno[3,4-*b*]quinoxaline-6,3'-pyrrolidine]-2',5'-dione) (34b)

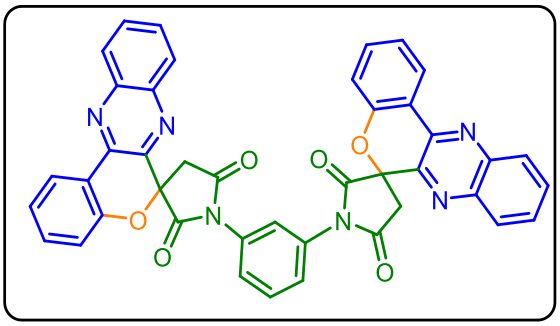

A pale yellow solid (71 mg, 67% yield); mp 207–209 °C; purified over a column of silica gel (35% EtOAc in hexane); ^{1}H NMR ($CDCl_3$, 400 MHz): *δ* 8.44 (d, *J* = 7.6 Hz, 2H), 8.13 (d, *J* = 8.4 Hz, 2H), 8.02 (d, *J* = 7.6 Hz, 2H), 7.81 – 7.76 (m, 2H), 7.73 – 7.68 (m, 2H), 7.58 (s, 1H), 7.54 – 7.50 (m, 1H), 7.46 – 7.41 (m, 4H), 7.21 (t, *J* = 7.4 Hz, 2H), 7.07 (dd, *J* = 8.0, 4.4 Hz, 2H), 4.16 (d, *J* = 18.0 Hz, 2H), 3.43 (d, *J* = 18.0 Hz, 2H); ^{13}C {^{1}H} NMR ($CDCl_3$, 126 MHz): *δ* 172.0, 171.9, 154.7, 146.3, 143.4, 143.3, 141.7, 133.4, 132.0, 131.3, 130.2, 129.6, 129.5, 129.4, 126.4, 125.7, 123.9, 123.7, 120.7, 117.7, 82.2, 42.2; IR (neat, cm^{-1}): 2921, 1724, 1604, 1490, 1457, 1354, 1175, 761, 719, 689 ; HRMS (ESI-TOF) calcd for $C_{42}H_{25}N_6O_6$ $[M + H]^+$ 709.1830, found 709.1836.

1-Fluoro-1'-phenylspiro[chromeno[3,4-*b*]quinoxaline-6,3'-pyrrolidine]-2',5'-dione (36b)

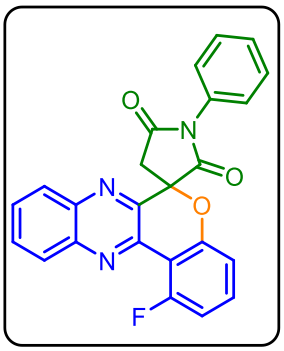

A light brown solid (42 mg, 68% yield); mp 217–219 °C; purified over a column of silica gel (8% EtOAc in hexane); ^{1}H NMR ($CDCl_3$, 500 MHz): δ 8.20 (d, J = 8.5 Hz, 1H), 8.04 (d, J = 8.0 Hz, 1H), 7.82 (t, J = 7.0 Hz, 1H), 7.77 (t, J = 7.7 Hz, 1H), 7.45 (t, J = 7.5 Hz, 2H), 7.39 (t, J = 6.2 Hz, 2H), 7.36 (t, J = 7.5 Hz, 2H), 6.97 (d, J = 9.0 Hz, 1H), 6.94 (d, J = 8.0 Hz, 1H), 4.17 (d, J = 18.0 Hz, 1H), 3.44 (d, J = 18.0 Hz, 1H); ^{13}C {^{1}H} NMR ($CDCl_3$, 126 MHz): δ 172.2, 172.1, 161.5 (d, J = 263.2 Hz) , 156.0 (d, J = 4.4 Hz), 146.1, 143.2, 142.4 (d, J = 5.5 Hz), 140.8, 133.2 (d, J = 10.7 Hz), 131.3, 130.7, 130.0, 129.3, 129.2, 129.1, 126.5, 113.7 (d, J = 3.5 Hz), 112.1, 111.9, 110.9 (d, J = 10.8 Hz), 82.5, 41.9; ^{19}F NMR ($CDCl_3$) δ -109.7 (s); IR (neat, cm^{-1}): 2921, 1794, 1722, 1620, 1585, 1492, 1376, 1181, 1050, 1015, 883, 757, 693; HRMS (ESI-TOF) calcd for $C_{24}H_{15}FN_3O_3$ $[M + H]^+$ 412.1092, found 412.1094.

1-Chloro-1'-phenylspiro[chromeno[3,4-*b*]quinoxaline-6,3'-pyrrolidine]-2',5'-dione (**37b**)

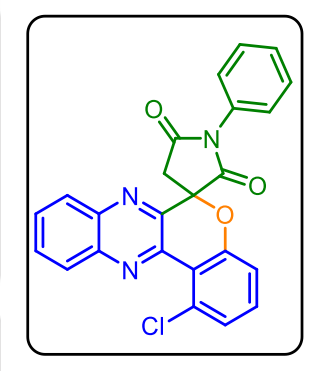

A white solid (43 mg, 68% yield); mp 212–214 °C; purified over a column of silica gel (7% EtOAc in hexane); ^{1}H NMR ($CDCl_3$, 400 MHz): δ 8.22 (d, J = 8.4 Hz, 1H), 8.05 (d, J = 8.0 Hz, 1H), 7.84 – 7.76 (m, 2H), 7.46 (t, J = 7.2 Hz, 2H), 7.40 – 7.34 (m, 3H), 7.32 – 7.27 (m, 2H), 7.07 (d, J = 8.0 Hz, 1H), 4.15 (d, J = 18.0 Hz, 1H), 3.42 (d, J = 18.0 Hz, 1H); ^{13}C {^{1}H} NMR ($CDCl_3$, 126 MHz): δ 172.2, 172.0, 156.5, 146.7, 143.1, 142.5, 140.4, 133.7, 132.2, 131.3, 131.2, 130.9, 130.0, 129.3, 129.1, 129.0, 127.6, 126.5, 119.5, 116.9, 82.3, 41.6; IR (neat, cm^{-1}): 2919, 1792, 1715, 1273, 1493, 1449, 1365, 1170, 1091, 967, 910, 755, 686, 613; HRMS (ESI-TOF) calcd for $C_{24}H_{15}ClN_3O_3$ $[M + H]^+$ 428.0796, found 428.0799.

TH-3369_166122017

1-Bromo-1'-phenylspiro[chromeno[3,4-*b*]quinoxaline-6,3'-pyrrolidine]-2',5'-dione (11b)

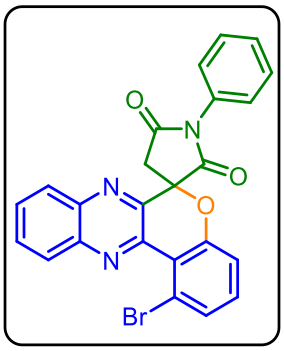

A light brown solid (42 mg, 60% yield); mp 224–226 °C; purified over a column of silica gel (7% EtOAc in hexane); ^{1}H NMR ($CDCl_3$, 400 MHz): δ 8.23 (d, J = 8.0 Hz, 1H), 8.06 (d, J = 7.6 Hz, 1H), 7.85 – 7.77 (m, 2H), 7.52 (d, J = 6.8 Hz, 1H), 7.48 – 7.43 (m, 2H), 7.41 – 7.35 (m, 3H), 7.23 (t, J = 8.2 Hz, 1H), 7.11 (d, J = 7.2 Hz, 1H), 4.15 (d, J = 18.0 Hz, 1H), 3.42 (d, J = 18.0 Hz, 1H); ^{13}C {^{1}H} NMR ($CDCl_3$, 101 MHz): δ 172.2, 171.9, 156.4, 146.6, 143.0, 142.2, 140.5, 132.6, 131.3, 131.2, 130.9, 129.9, 129.3, 129.13, 129.10, 126.5, 121.0, 120.6, 117.6, 82.2, 41.6; IR (neat, cm^{-1}): 2921, 1719, 1592, 1491, 1375, 1184, 1090, 958, 753, 692, 616, 472; HRMS (ESI-TOF) calcd for $C_{24}H_{15}BrN_3O_3$ $[M + H]^+$ 472.0291, found 472.0298.

❖ *Post-synthetic Manipulations.....*

1'-(Prop-2-yn-1-yl)spiro[chromeno[3,4-*b*]quinoxaline-6,3'-pyrrolidine]-2',5'-dione (26bb)

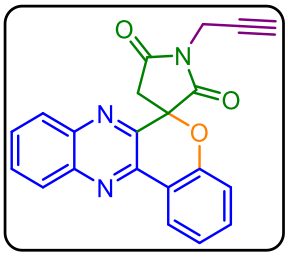

A pale yellow solid (27 mg, 77% yield); mp 165–167 °C; purified over a column of silica gel (6% EtOAc in hexane); ^{1}H NMR ($CDCl_3$, 500 MHz): δ 8.44 (d, J = 8.0 Hz, 1H), 8.13 (d, J = 8.0 Hz, 1H), 7.99 (d, J = 8.0 Hz, 1H), 7.79 (t, J = 7.0 Hz, 1H), 7.71 (t, J = 7.5 Hz, 1H), 7.44 (t, J = 7.0 Hz, 1H), 7.22 (t, J = 7.5 Hz, 1H), 7.05 (d, J = 8.5 Hz, 1H), 4.32 (dd, J = 6.0, 2.5 Hz, 2H), 4.07 (d, J = 18.0 Hz, 1H), 3.32 (d, J = 18.0 Hz, 1H), 2.21 (t, J = 2.3 Hz, 1H); ^{13}C {^{1}H} NMR ($CDCl_3$, 126 MHz): δ 172.3, 172.0, 154.7, 146.1, 143.3, 141.6, 133.4, 131.2, 130.1, 129.5, 129.3, 125.8, 123.7, 120.6, 117.6, 82.4, 76.0,

TH-3369_166122017

72.2, 42.3, 28.4; IR (neat, cm^{-1}): 2920, 1791, 1713, 1610, 1493, 1387, 1323, 1176, 1097, 957, 750, 696, 615, 562; HRMS (ESI-TOF) calcd for $C_{21}H_{14}N_3O_3$ $[M + H]^+$ 356.1030, found 356.1032.

2',5'-Dioxo-1',11,12-triphenyl-4-oxa-6,10b-diazaspiro[benzo[*pqr*]tetraphene-5,3'-pyrrolidin]-1(12a),2,3a,5a,5a^1(10b),6a,8,10,11-nonaen-10b-ium (**1bc**)

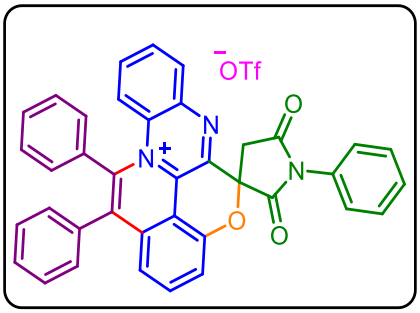

A deep orange solid (66 mg, 92% yield); mp 292–294 ºC; purified over a column of silica gel (3% MeOH in DCM); ^{1}H NMR ($CDCl_3$, 500 MHz): δ 8.29 (d, J = 8.0 Hz, 1H), 8.03 (t, J = 8.0 Hz, 1H), 7.79 (t, J = 7.5 Hz, 1H), 7.65 (d, J = 9.0 Hz, 1H), 7.60 (d, J = 7.5 Hz, 2H), 7.50 (t, J = 7.2 Hz, 2H), 7.45 – 7.40 (m, 3H), 7.37 – 7.18 (m, 10H), 7.11 (d, J = 8.0 Hz, 1H), 4.52 (d, J = 19.0 Hz, 1H), 3.83 (d, J = 18.5 Hz, 1H); ^{13}C {^{1}H} NMR ($CDCl_3$, 126 MHz): δ 172.1, 171.9, 153.7, 150.1, 143.3, 142.1, 141.1, 139.3, 136.1, 134.6, 133.5, 131.7, 131.6, 131.4, 131.2, 131.1, 131.0, 130.8, 130.2, 129.95, 129.93, 129.5, 129.4, 129.1, 128.9, 128.8, 128.4, 128.2, 126.5, 123.5, 120.9, 117.4, 113.4, 83.8, 43.8; ^{19}F NMR ($CDCl_3$) δ -78.7 (s); IR (neat, cm^{-1}): 3064, 1727, 1615, 1370, 1256, 1217, 1150, 1027, 756, 697, 631, 570; HRMS (ESI-TOF) calcd for $C_{38}H_{24}N_3O_3^+$ $[M]^+$ 570.1818, found 570.1823.

2-Bromo-1'-phenylspiro[chromeno[3,4-*b*]quinoxaline-6,3'-pyrrolidine]-2',5'-dione (**1bd**)

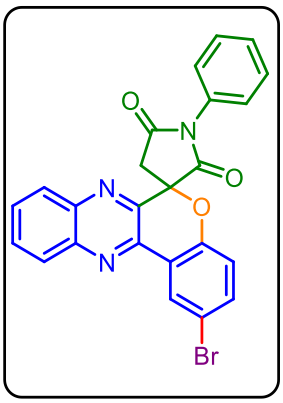

TH-3369_166122017

A pale yellow solid (44 mg, 94% yield); mp 244–246 ^{o}C; purified over a column of silica gel (6% EtOAc in hexane); ^{1}H NMR ($CDCl_3$, 500 MHz): δ 8.56 (s, 1H), 8.15 (d, J = 8.0 Hz, 1H), 8.05 (d, J = 7.5 Hz, 1H), 7.82 (t, J = 7.0 Hz, 1H), 7.76 (t, J = 7.0 Hz, 1H), 7.53 (dd, J = 8.7, 2.3 Hz, 1H), 7.45 (t, J = 7.5 Hz, 2H), 7.38 (t, J = 7.2 Hz, 1H), 7.34 (d, J = 7.5 Hz, 2H), 6.98 (d, J = 8.5 Hz, 1H), 4.17 (d, J = 18.0 Hz, 1H), 3.45 (d, J = 18.0 Hz, 1H); ^{13}C {^{1}H} NMR ($CDCl_3$, 126 MHz): δ 172.3, 172.2, 153.9, 146.1, 143.2, 142.1, 141.9, 135.9, 131.5, 131.3, 130.6, 129.7, 129.4, 129.3, 129.1, 128.3, 126.5, 122.4, 119.5, 116.4, 82.5, 42.2; IR (neat, cm^{-1}): 2920, 2851, 1720, 1492, 1432, 1378, 1187, 1051, 829, 772, 751, 695, 614; HRMS (ESI-TOF) calcd for $C_{24}H_{15}BrN_3O_3$ $[M + H]^+$ 472.0291, found 472.0293.

TH-3369_166122017

V.8. NMR Spectra

^{1}H NMR of **3-Hydroxy-1-phenyl-3-(3-phenylquinoxalin-2-yl)pyrrolidine-2,5-dione (1a)** ($CDCl_3$, 500 MHz)

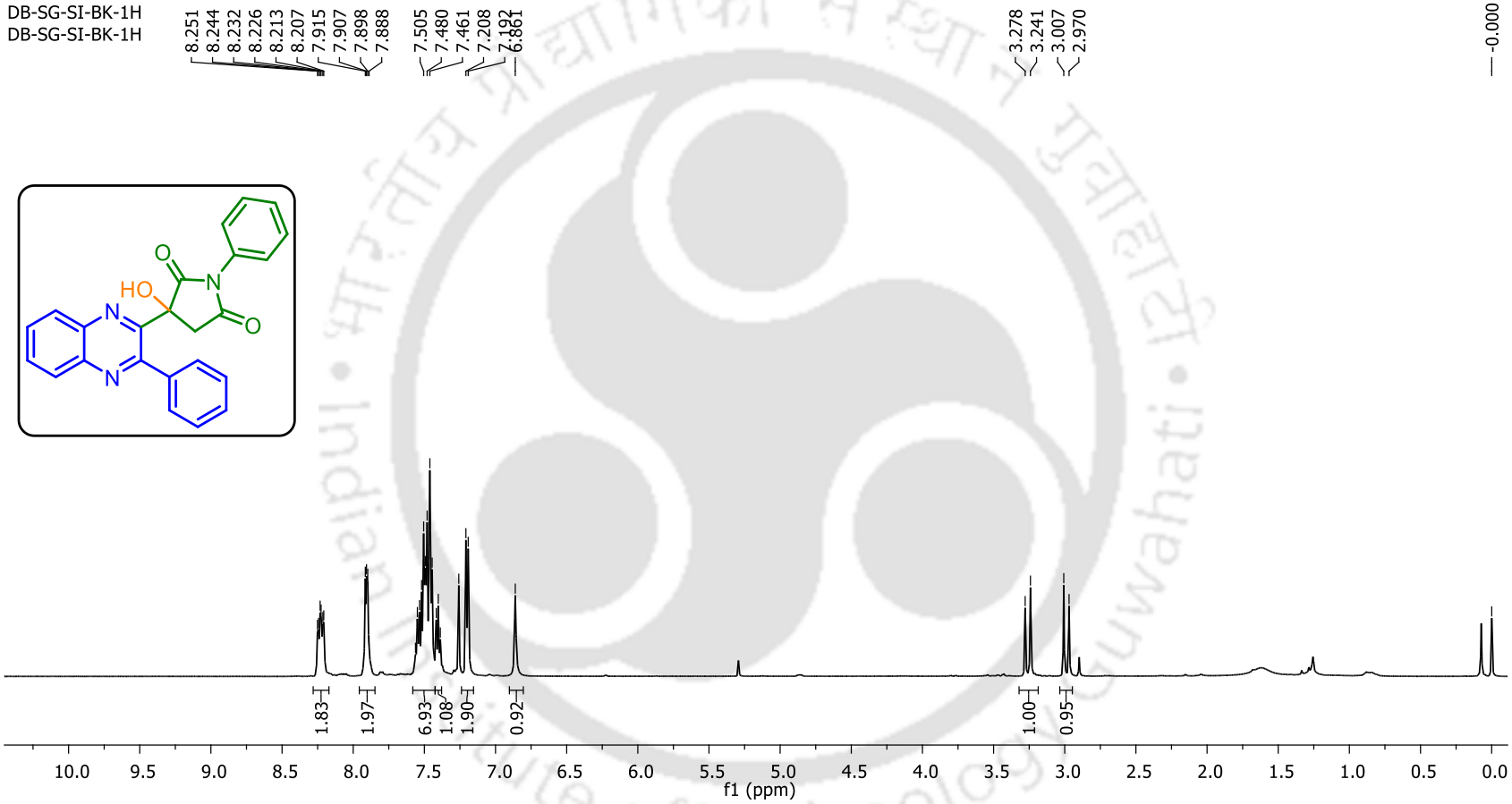

^{13}C {^{1}H} NMR of **3-Hydroxy-1-phenyl-3-(3-phenylquinoxalin-2-yl)pyrrolidine-2,5-dione** (**1a**) ($CDCl_3$, 126 MHz)

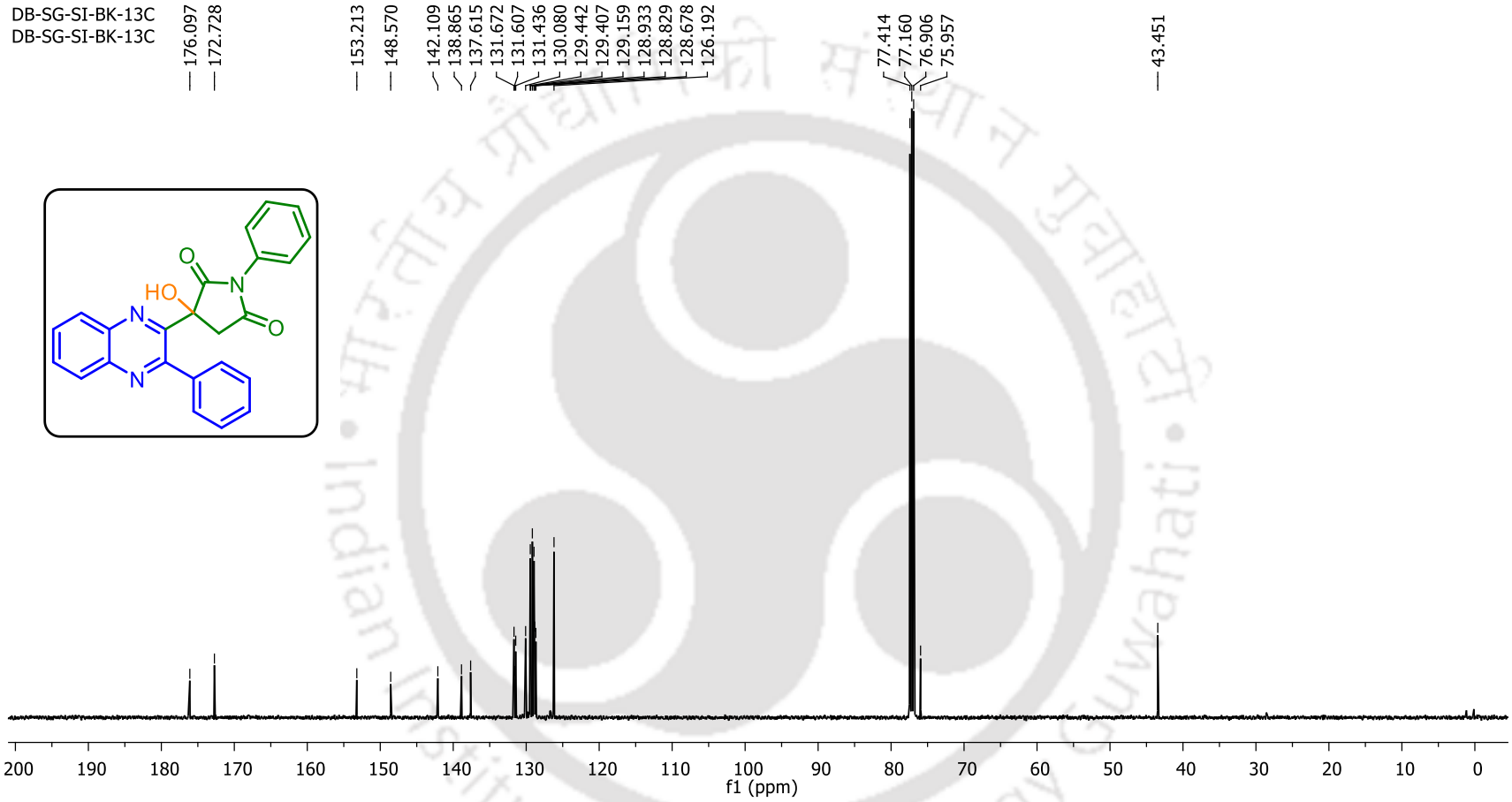

TH-3369_166122017

^{1}H NMR of **3-Hydroxy-1-phenyl-3-(3-(*p*-tolyl)quinoxalin-2-yl)pyrrolidine-2,5-dione** (**2a**) ($CDCl_3$, 500 MHz)

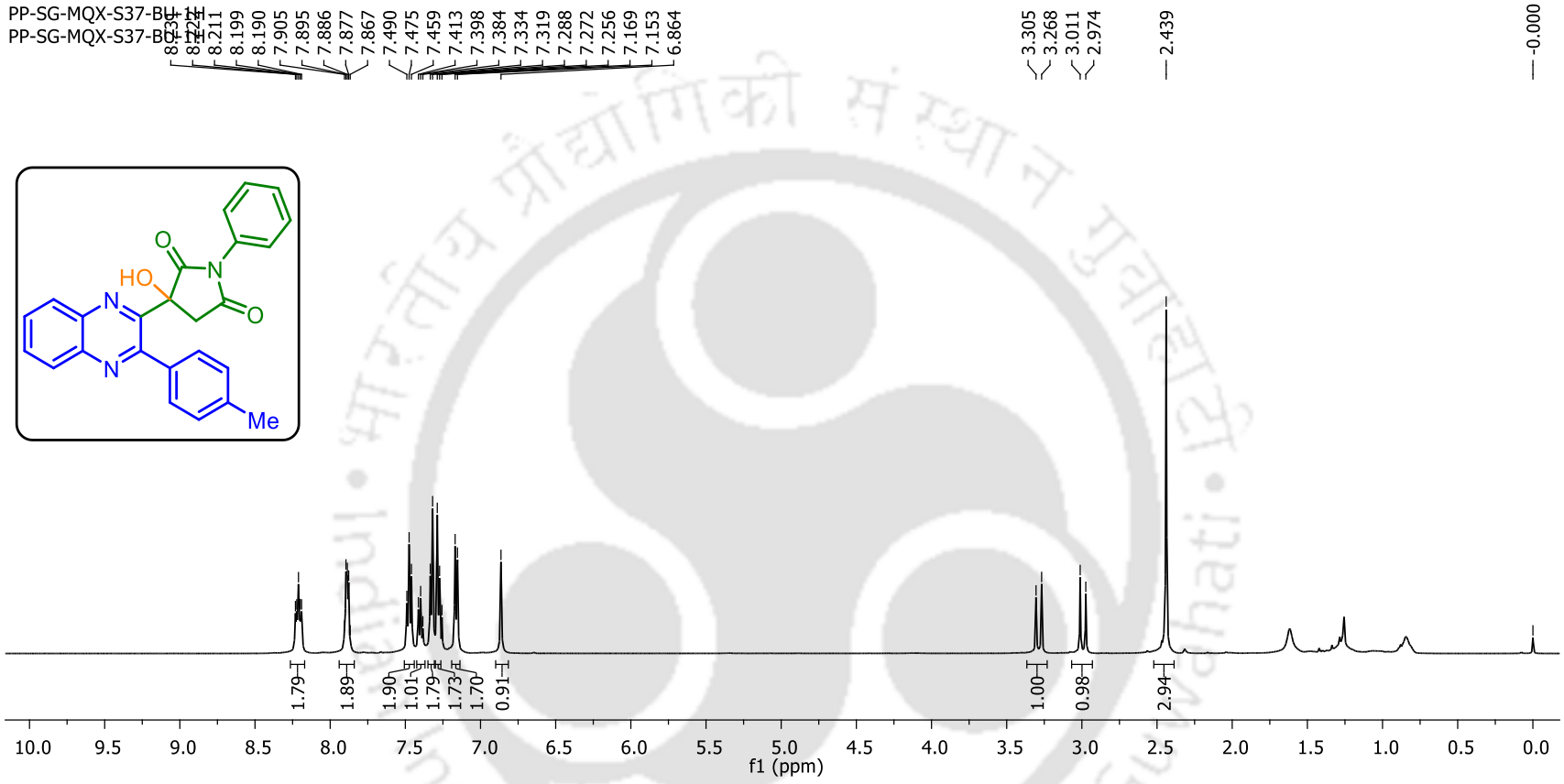

TH-3369_166122017

^{13}C {^{1}H} NMR of **3-Hydroxy-1-phenyl-3-(3-(*p*-tolyl)quinoxalin-2-yl)pyrrolidine-2,5-dione** (**2a**) ($CDCl_3$, 126 MHz)

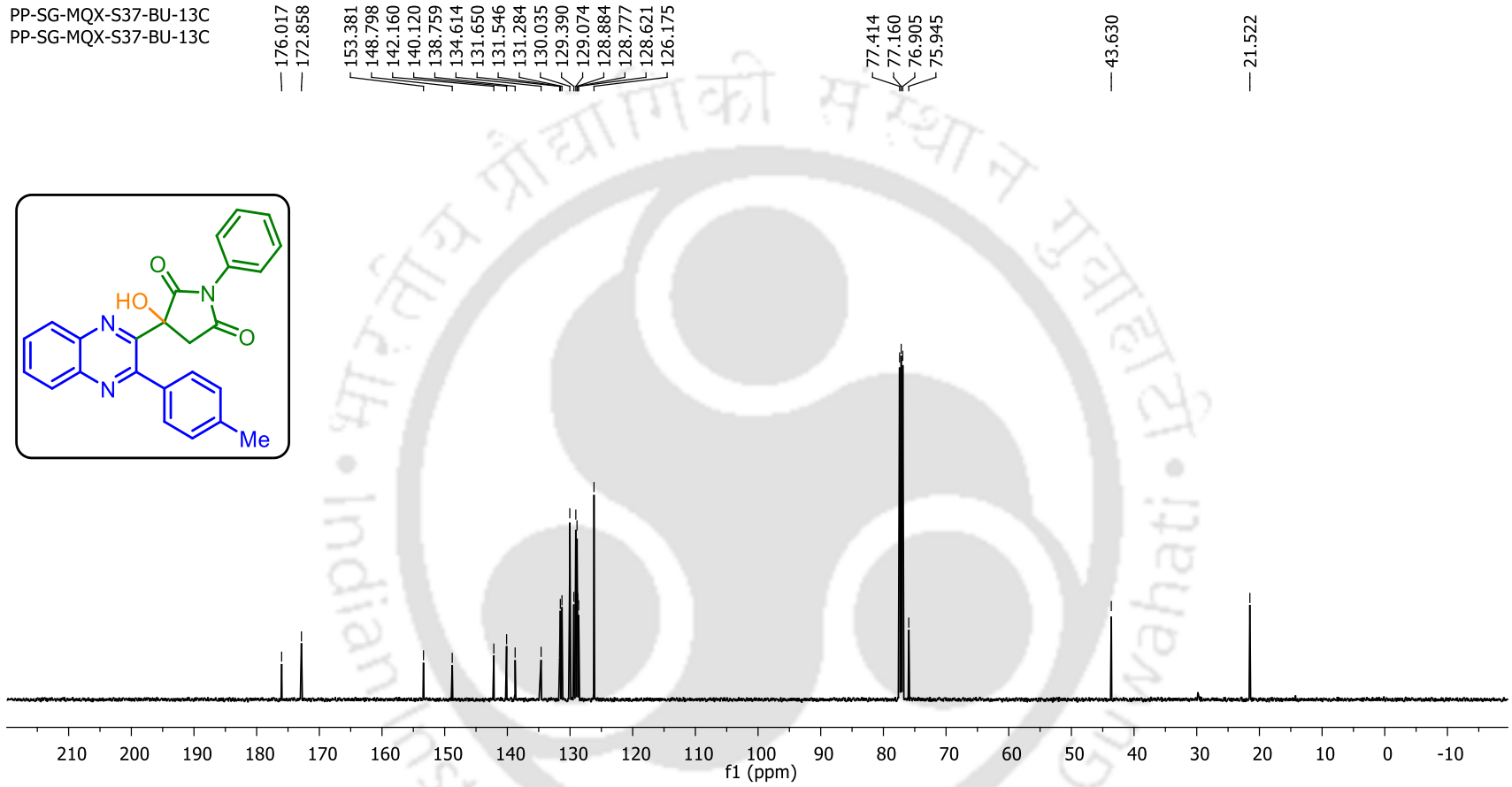

TH-3369_166122017

^{1}H NMR of **3-(3-(4-Fluorophenyl)quinoxalin-2-yl)-3-hydroxy-1-phenylpyrrolidine-2,5-dione** (**3a**) ($CDCl_3$, 500 MHz)

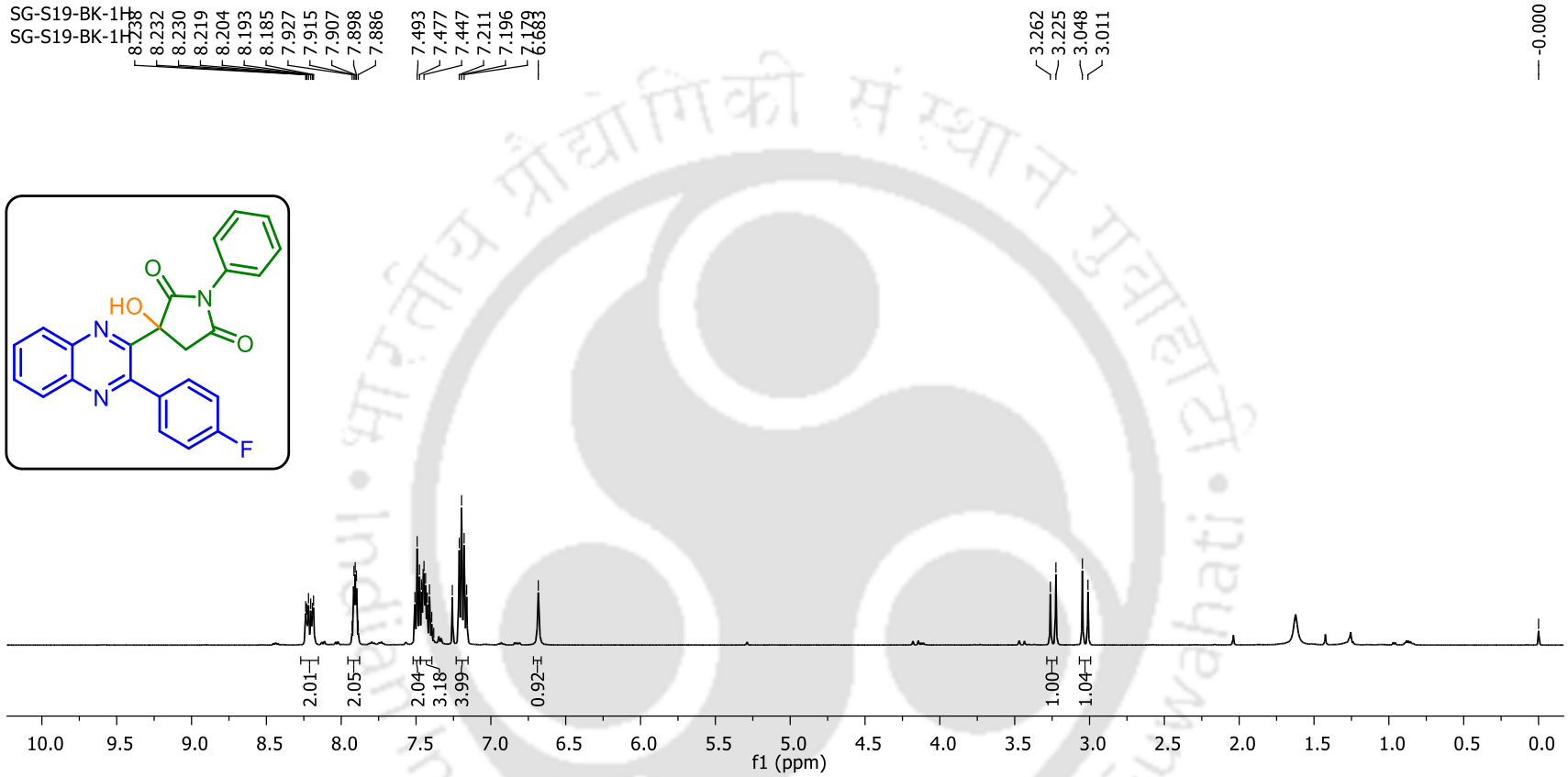

TH-3369_166122017

^{13}C {^{1}H} NMR of **3-(3-(4-Fluorophenyl)quinoxalin-2-yl)-3-hydroxy-1-phenylpyrrolidine-2,5-dione** (**3a**) ($CDCl_3$, 126 MHz)

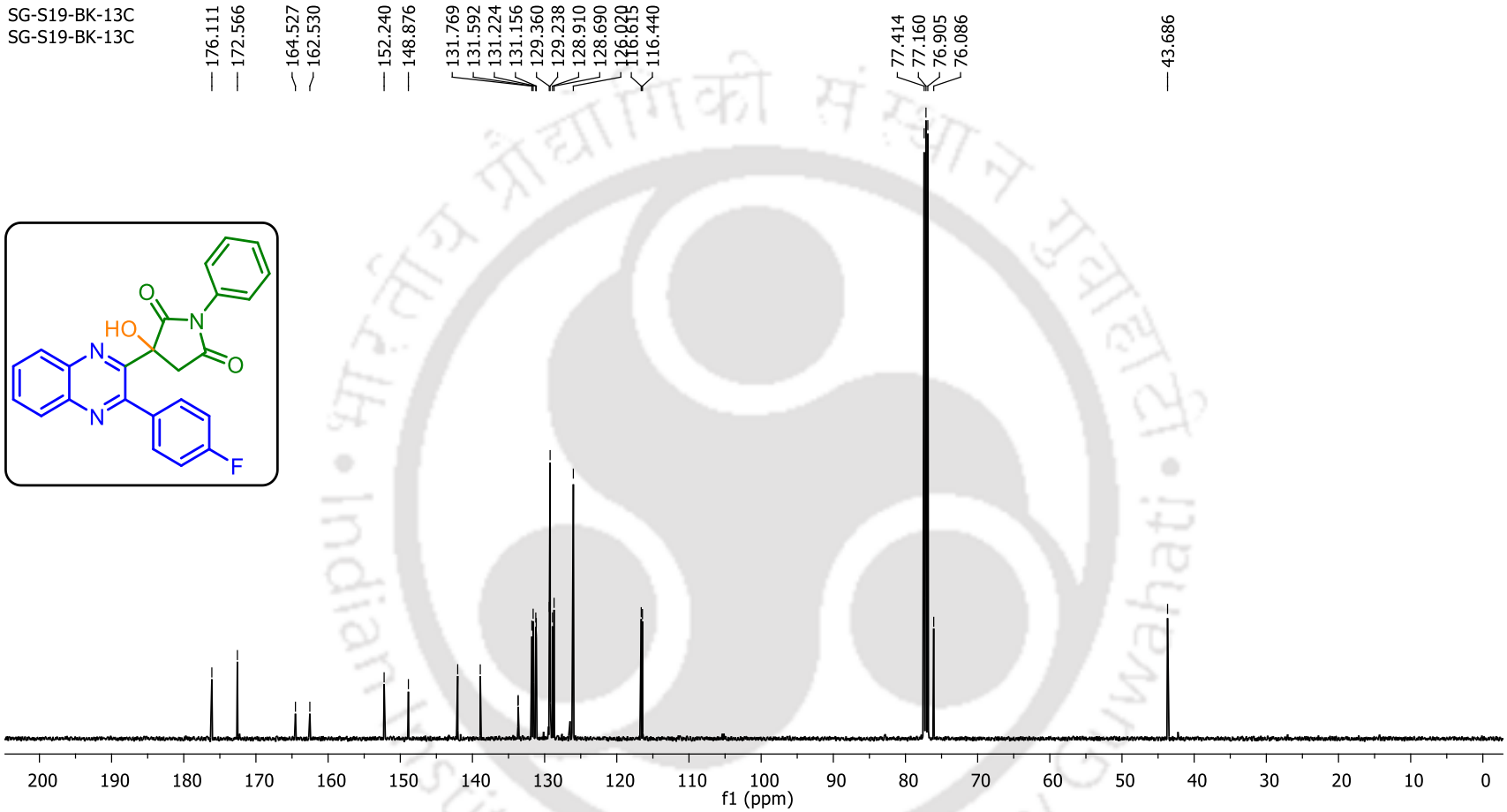

TH-3369_166122017

^{19}F NMR of **3-(3-(4-Fluorophenyl)quinoxalin-2-yl)-3-hydroxy-1-phenylpyrrolidine-2,5-dione** (**3a**) ($CDCl_3$)

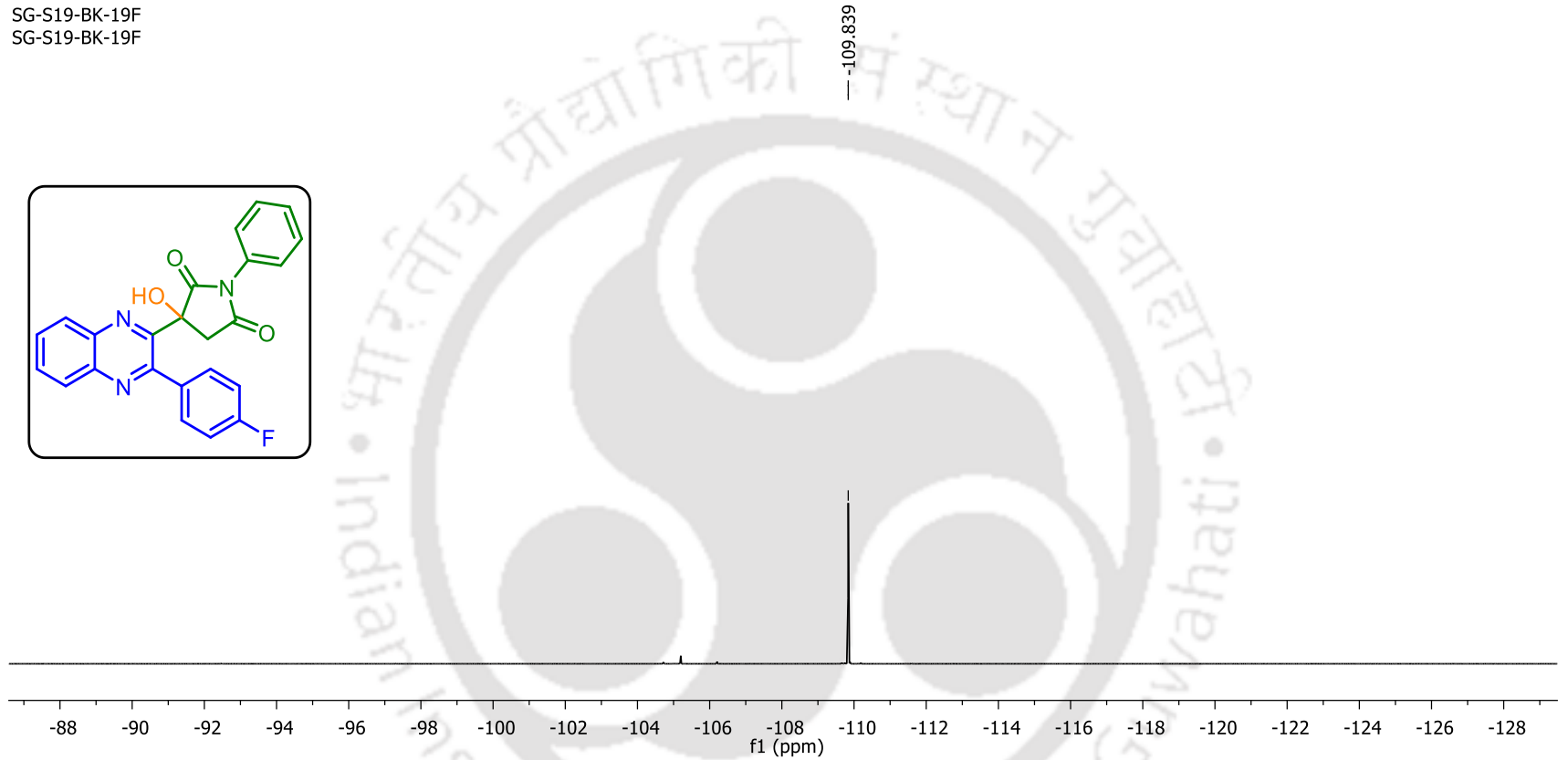

TH-3369_166122017

^{1}H NMR of **3-(3-(4-Chlorophenyl)quinoxalin-2-yl)-3-hydroxy-1-phenylpyrrolidine-2,5-dione** (**4a**) ($CDCl_3$, 500 MHz)

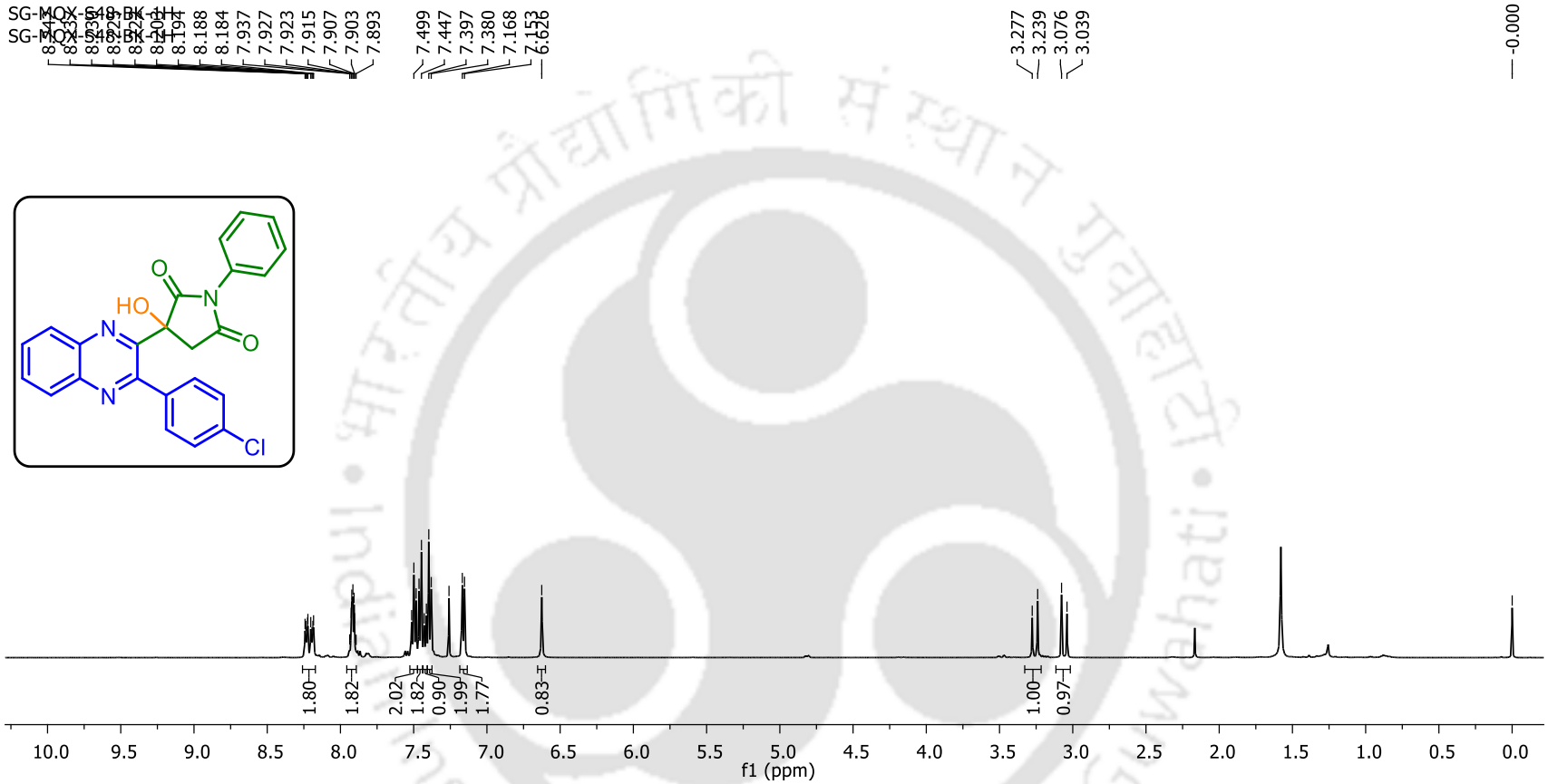

TH-3369_166122017

^{13}C {^{1}H} NMR of **3-(3-(4-Chlorophenyl)quinoxalin-2-yl)-3-hydroxy-1-phenylpyrrolidine-2,5-dione** (**4a**) ($CDCl_3$, 126 MHz)

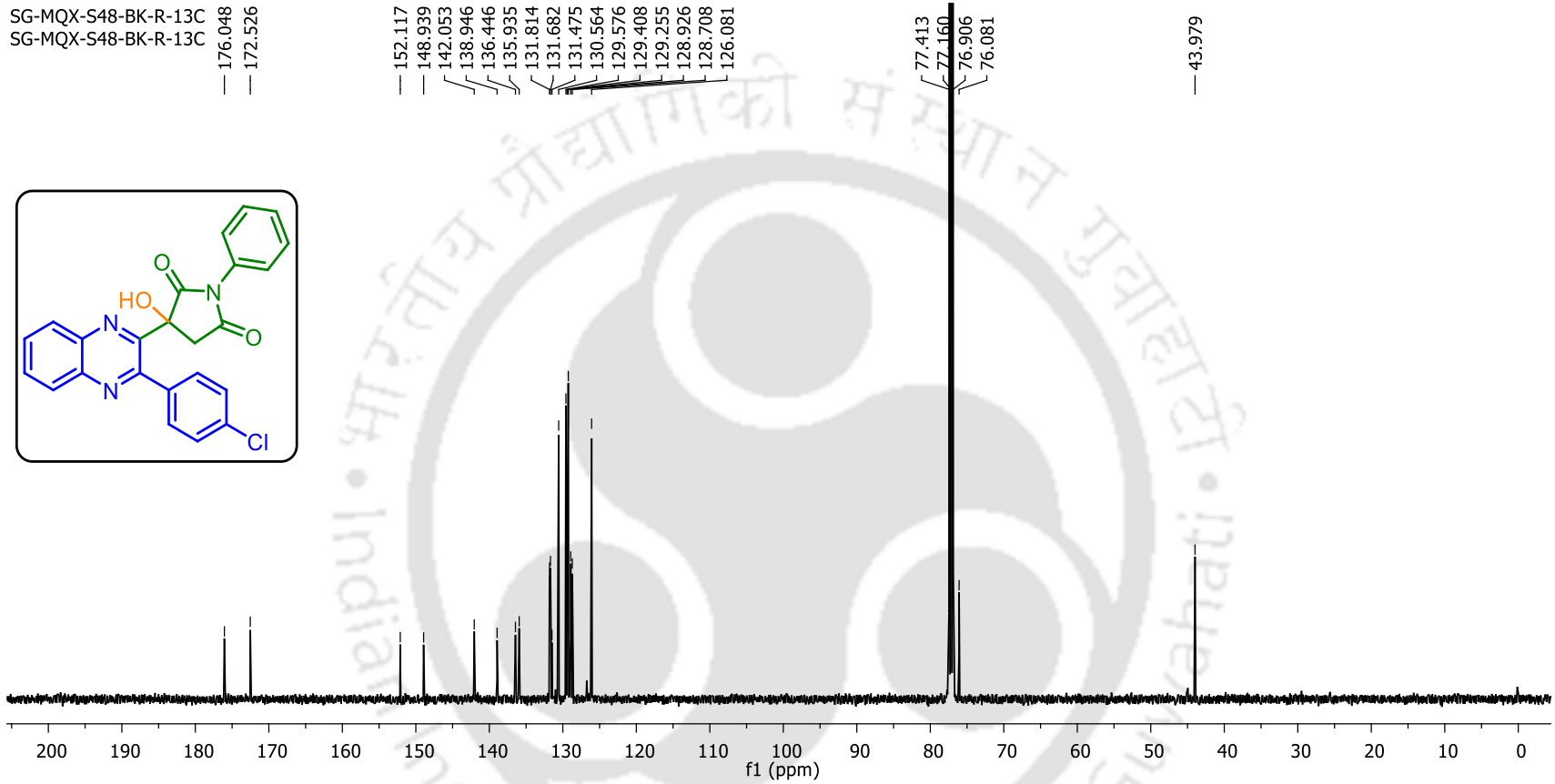

TH-3369_166122017

^{1}H NMR of **3-(3-(4-Bromophenyl)quinoxalin-2-yl)-3-hydroxy-1-phenylpyrrolidine-2,5-dione** (**5a**) ($CDCl_3$, 500 MHz)

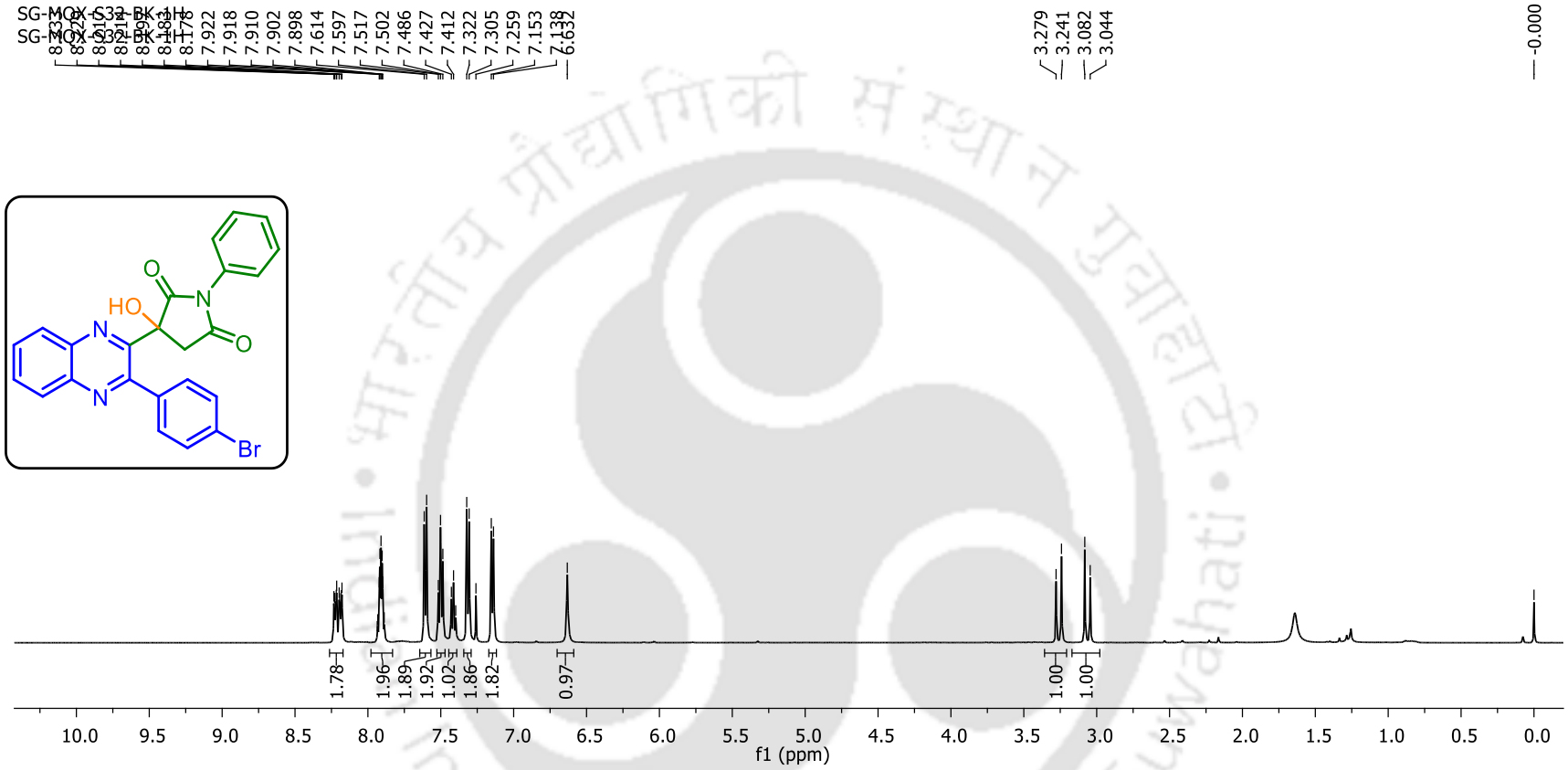

TH-3369_166122017

^{13}C {^{1}H} NMR of **3-(3-(4-Bromophenyl)quinoxalin-2-yl)-3-hydroxy-1-phenylpyrrolidine-2,5-dione** (**5a**) ($CDCl_3$, 126 MHz)

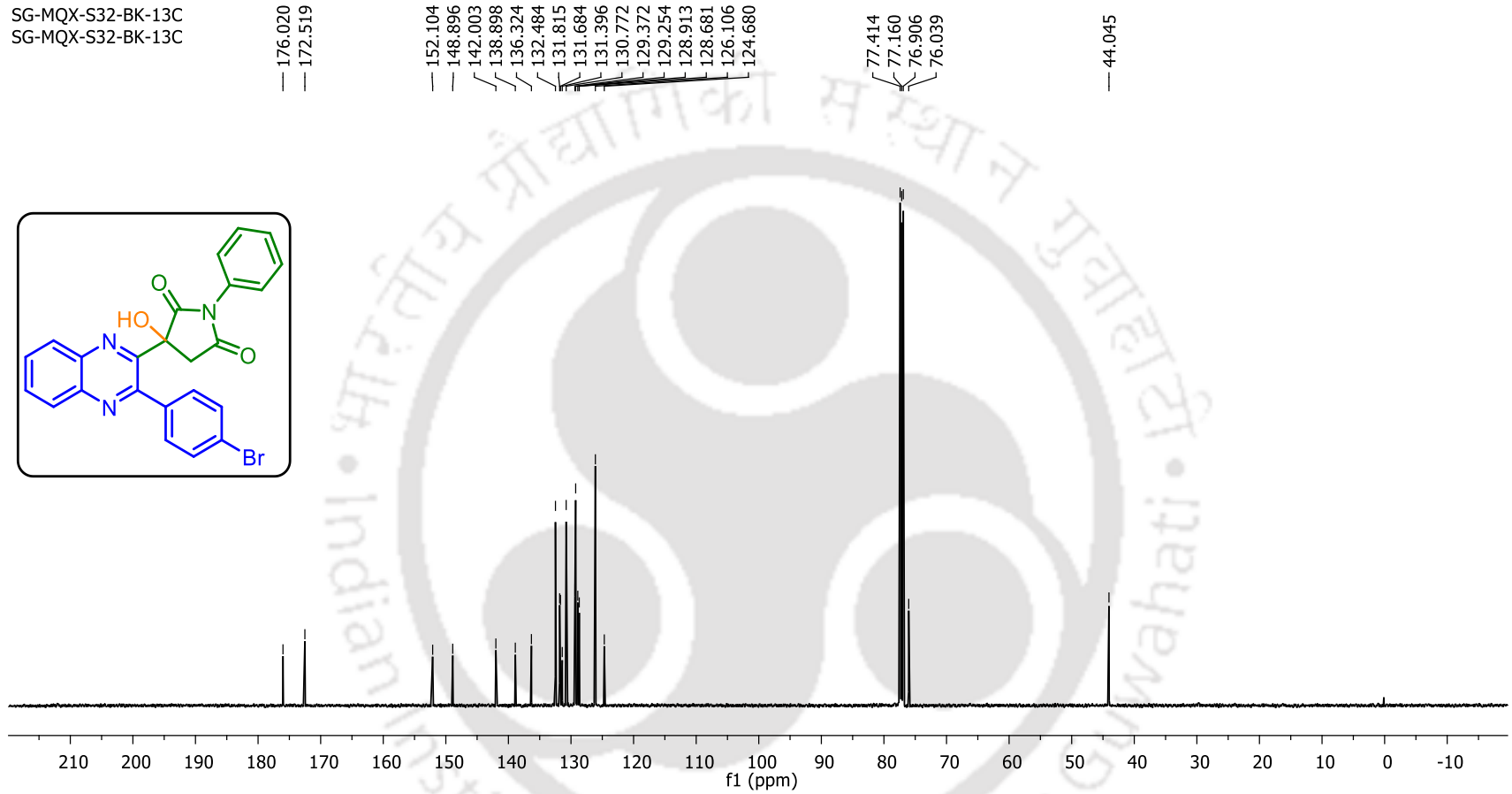

TH-3369_166122017

^{1}H NMR of **3-Hydroxy-1-phenyl-3-(3-(4-(trifluoromethyl)phenyl)quinoxalin-2-yl)pyrrolidine-2,5-dione** (**6a**) ($CDCl_3$, 500 MHz)

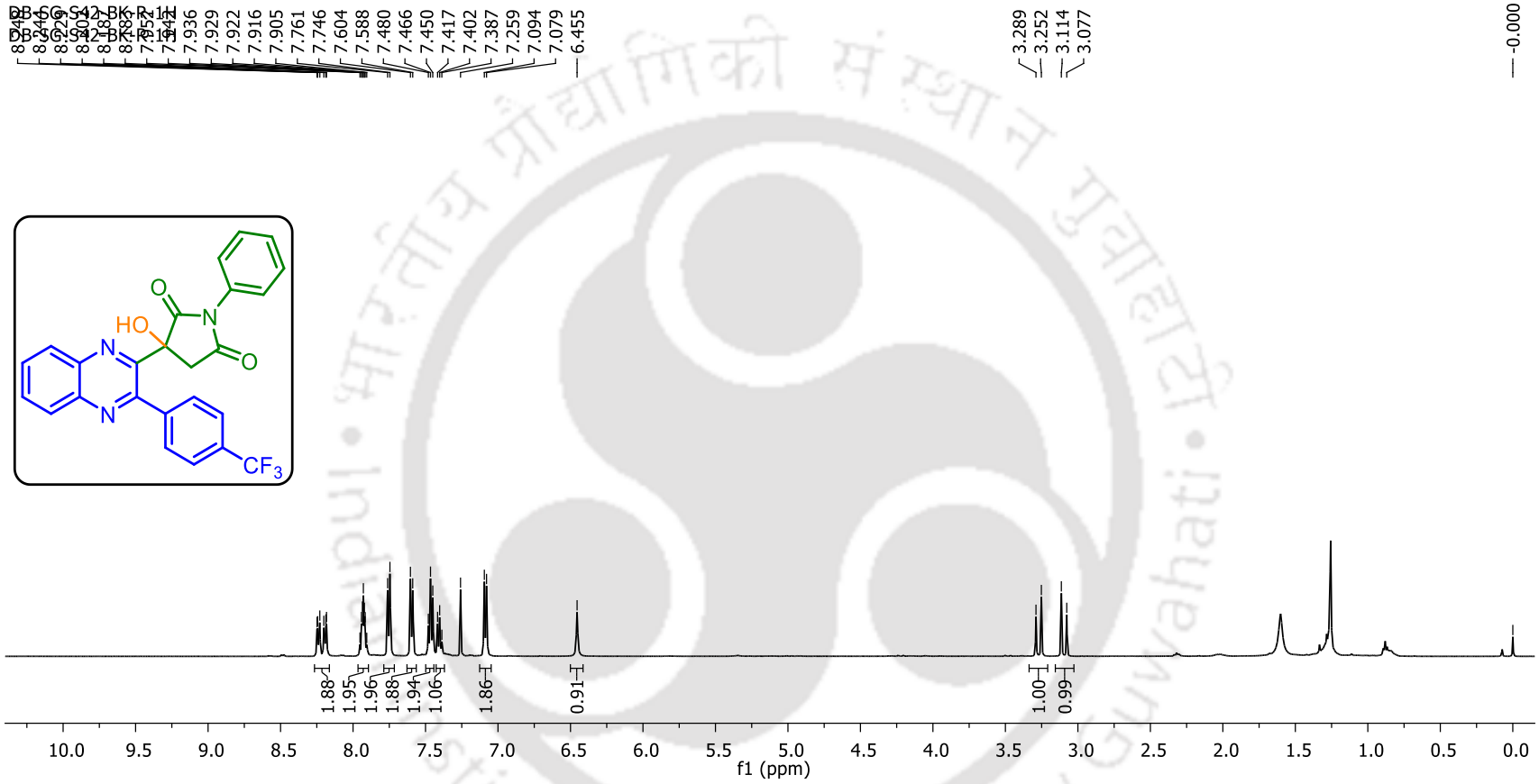

TH-3369_166122017

^{13}C {^{1}H} NMR of **3-Hydroxy-1-phenyl-3-(3-(4-(trifluoromethyl)phenyl)quinoxalin-2-yl)pyrrolidine-2,5-dione** (**6a**) ($CDCl_3$, 126 MHz)

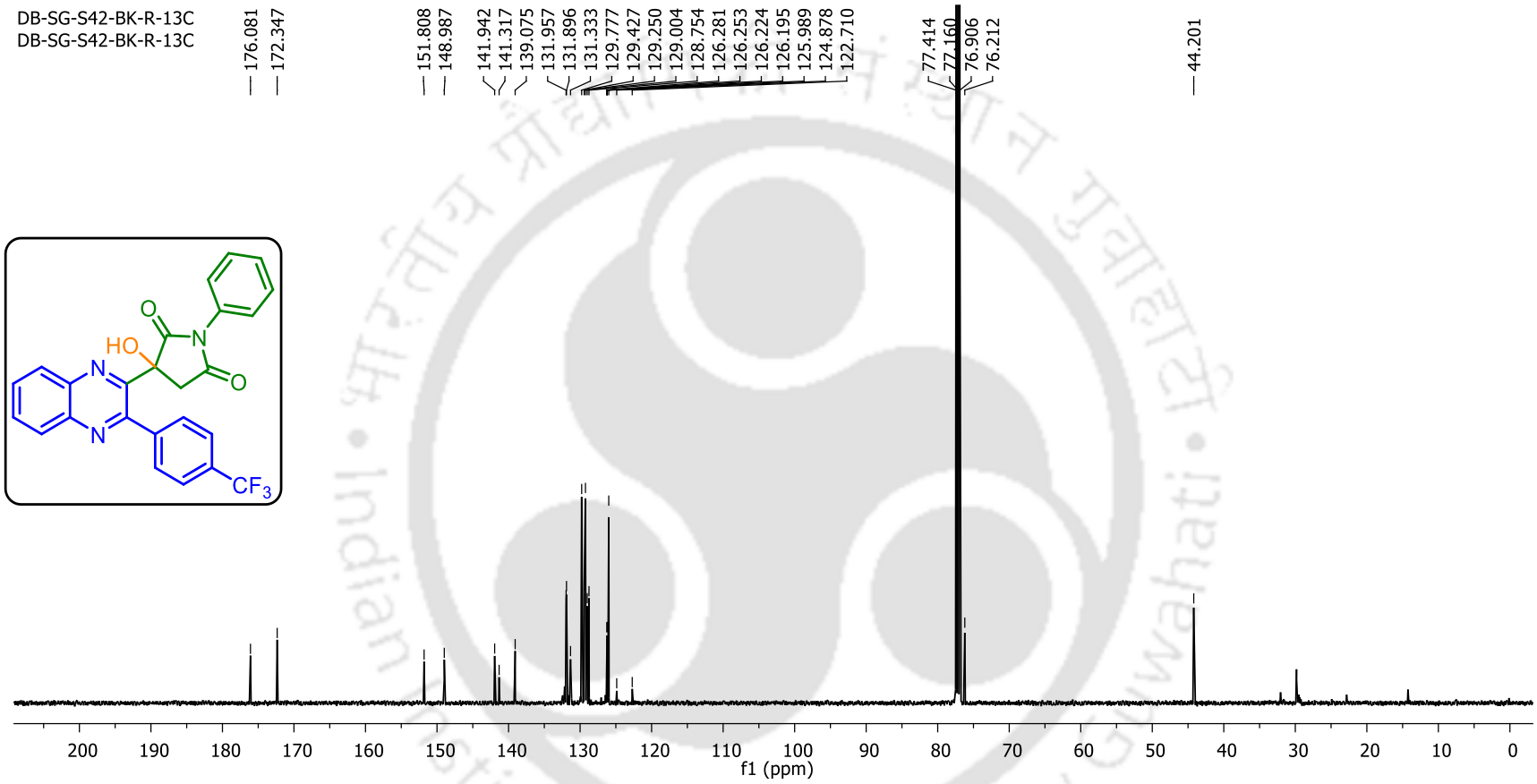

TH-3369_166122017

^{19}F NMR of **3-Hydroxy-1-phenyl-3-(3-(4-(trifluoromethyl)phenyl)quinoxalin-2-yl)pyrrolidine-2,5-dione** (**6a**) ($CDCl_3$)

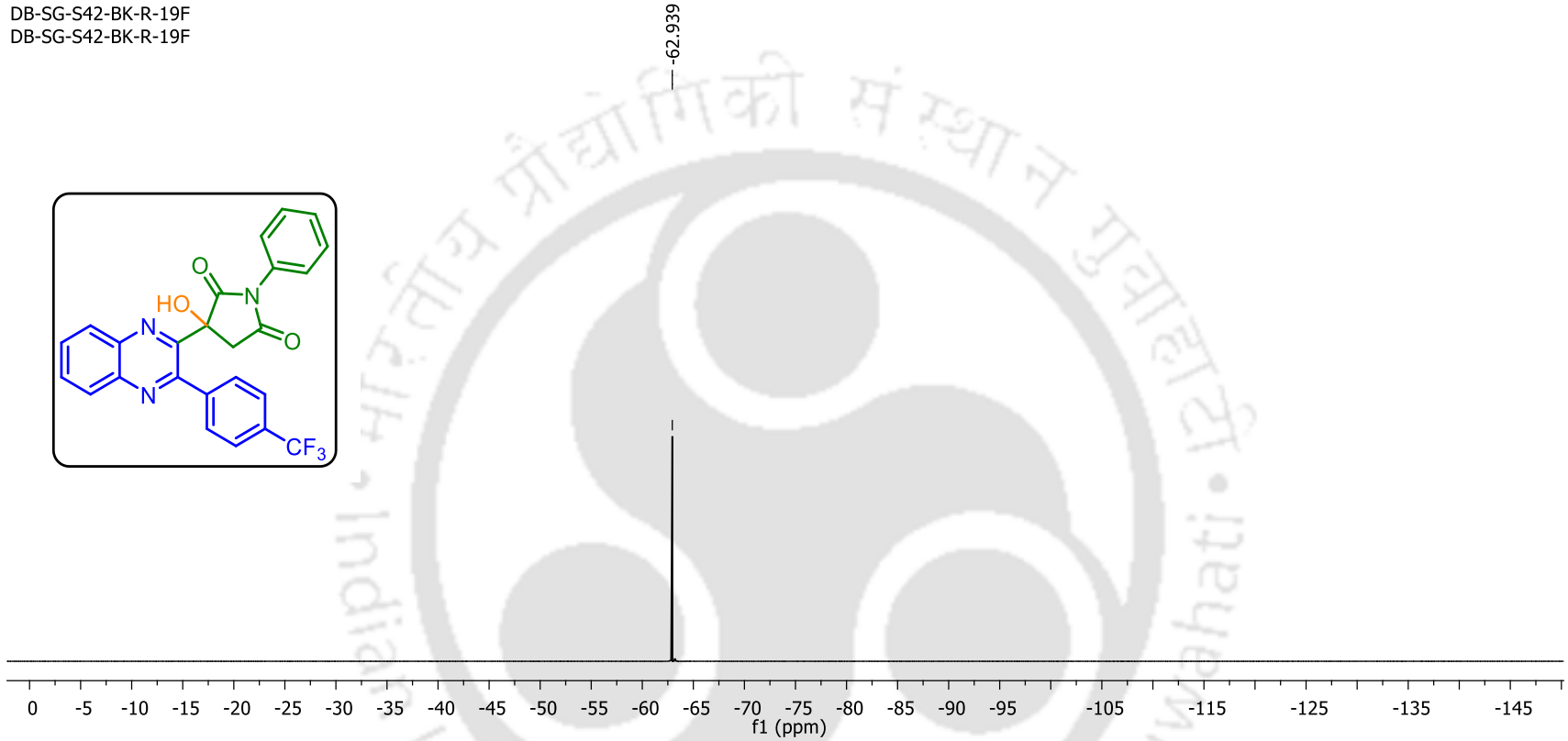

TH-3369_166122017

^{1}H NMR of **3-(3-([1,1'-Biphenyl]-4-yl)quinoxalin-2-yl)-3-hydroxy-1-phenylpyrrolidine-2,5-dione** (**7a**) ($CDCl_3$, 500 MHz)

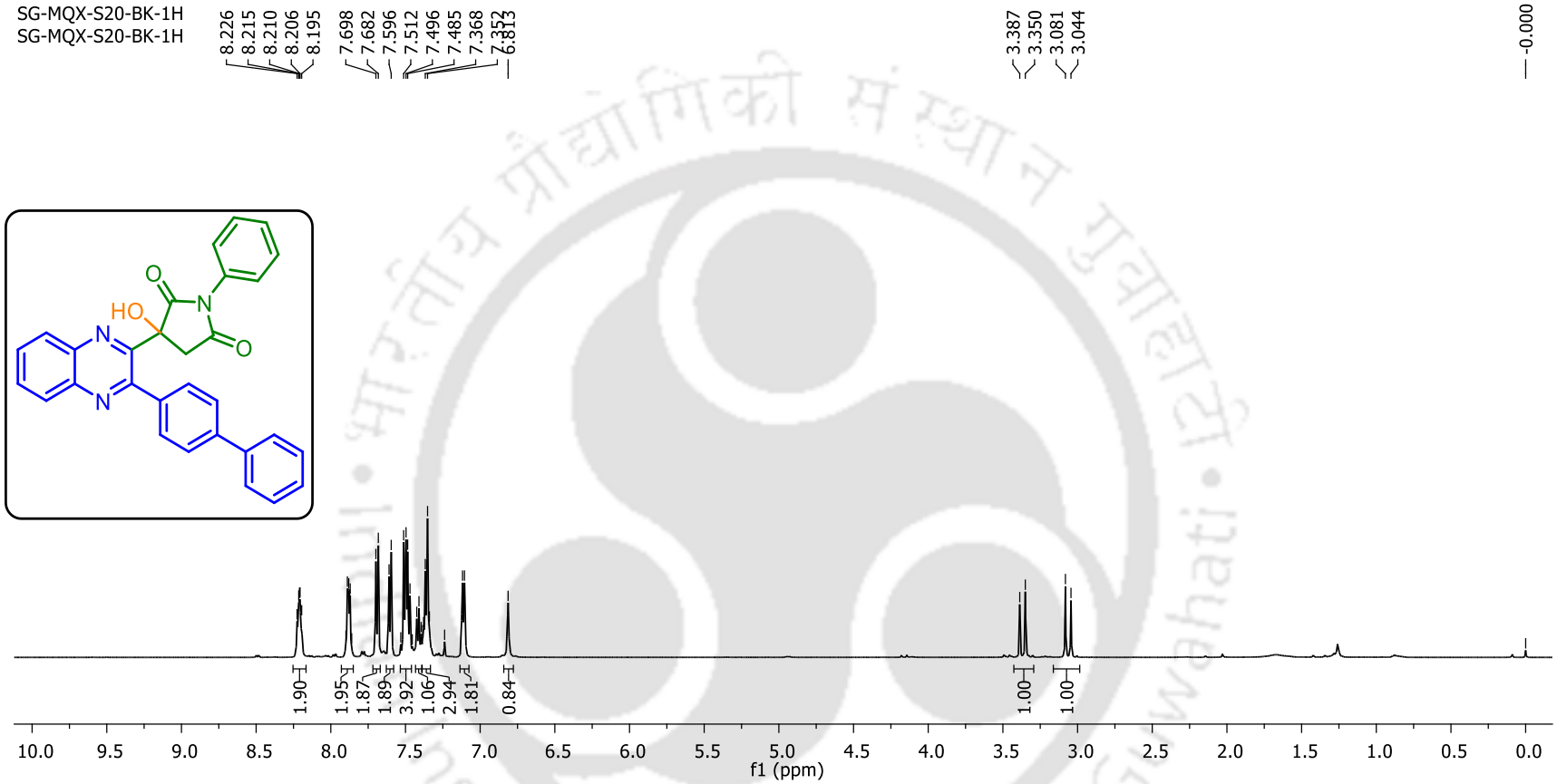

TH-3369_166122017

^{13}C {^{1}H} NMR of **3-(3-([1,1'-Biphenyl]-4-yl)quinoxalin-2-yl)-3-hydroxy-1-phenylpyrrolidine-2,5-dione** (**7a**) ($CDCl_3$, 126 MHz)

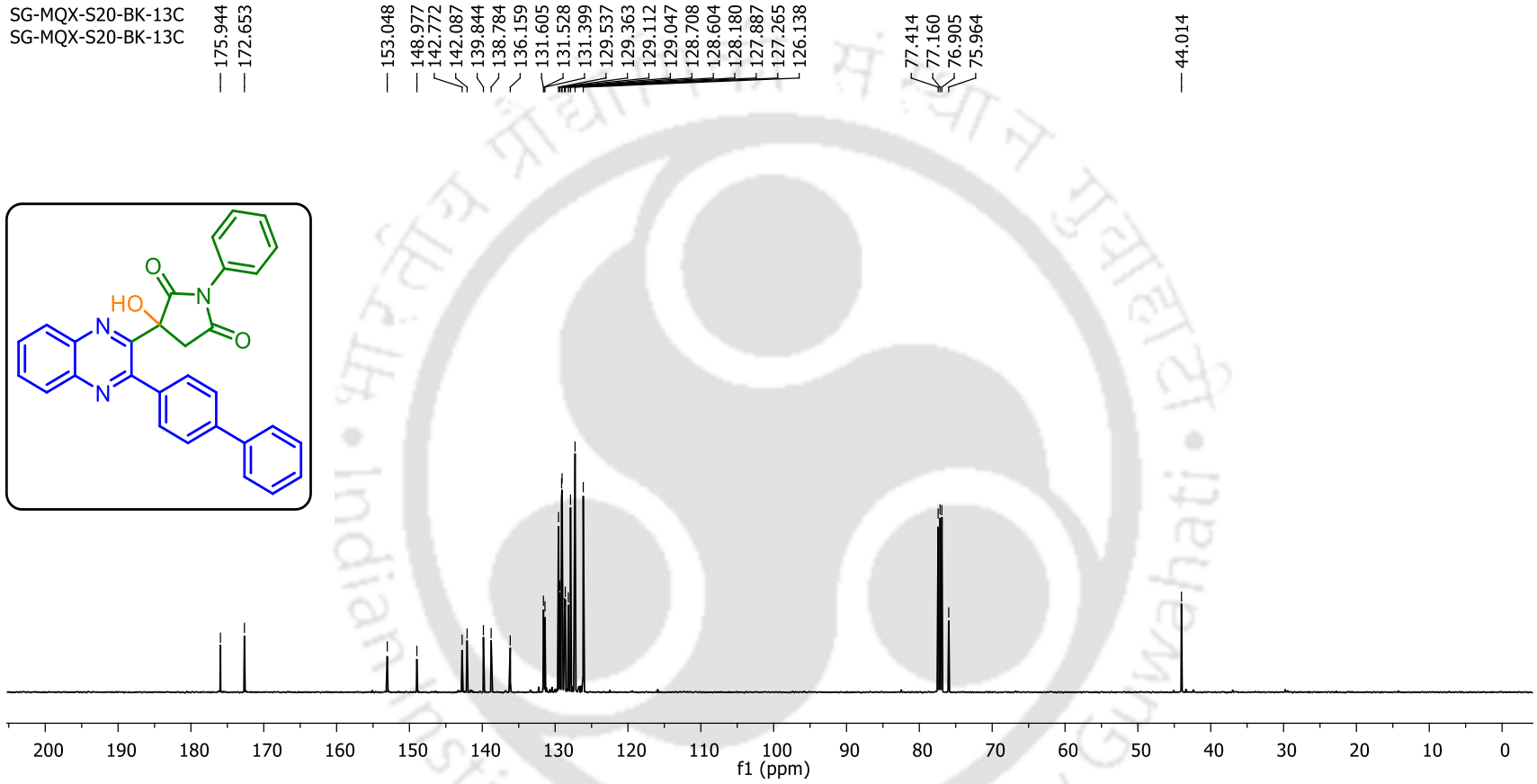

TH-3369_166122017

^{1}H NMR of **3-Hydroxy-1-phenyl-3-(3-(*m*-tolyl)quinoxalin-2-yl)pyrrolidine-2,5-dione** (**8a**) ($CDCl_3$, 500 MHz)

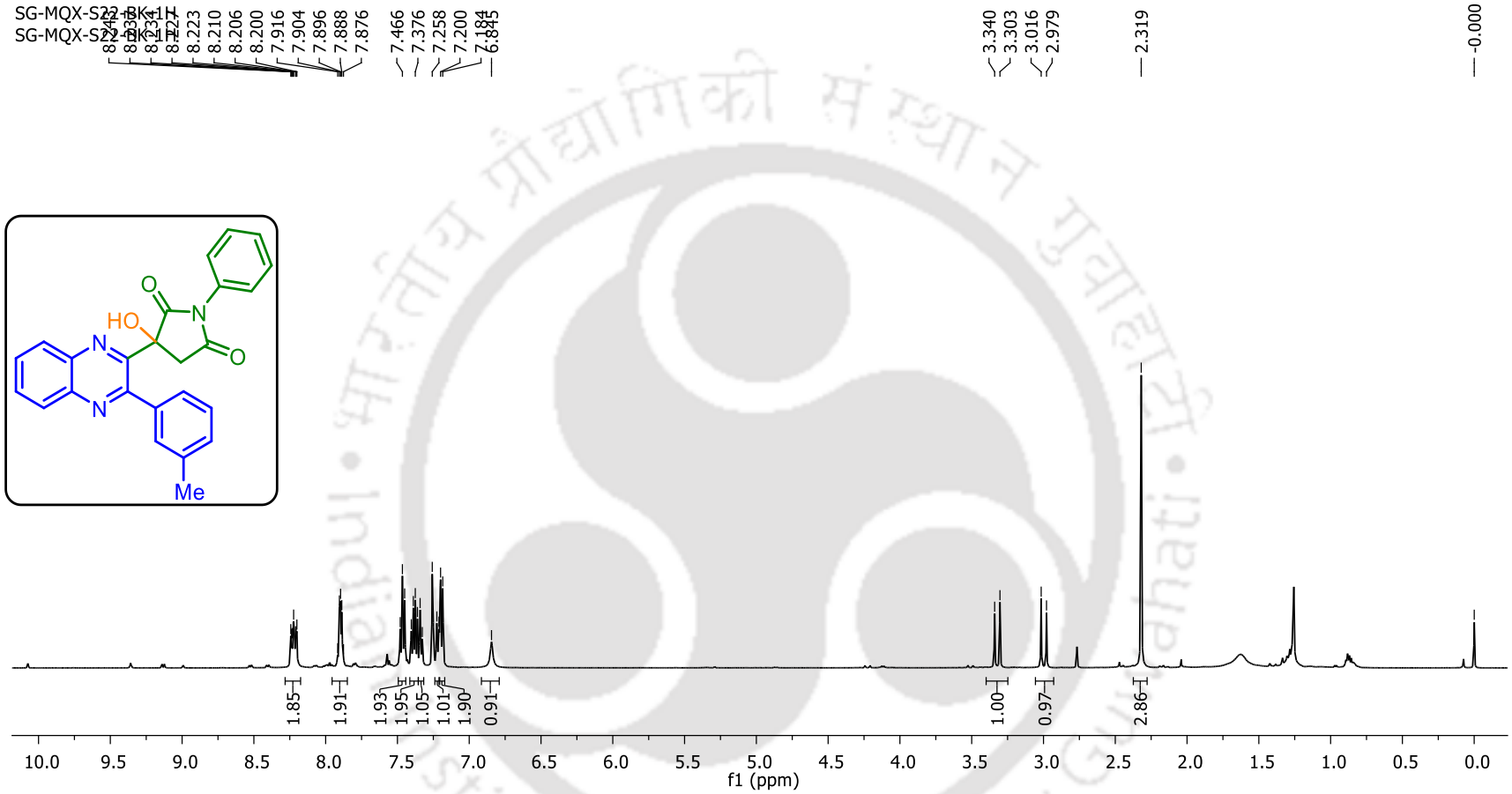

TH-3369_166122017

^{13}C {^{1}H} NMR of **3-Hydroxy-1-phenyl-3-(3-(*m*-tolyl)quinoxalin-2-yl)pyrrolidine-2,5-dione** (**8a**) ($CDCl_3$, 126 MHz)

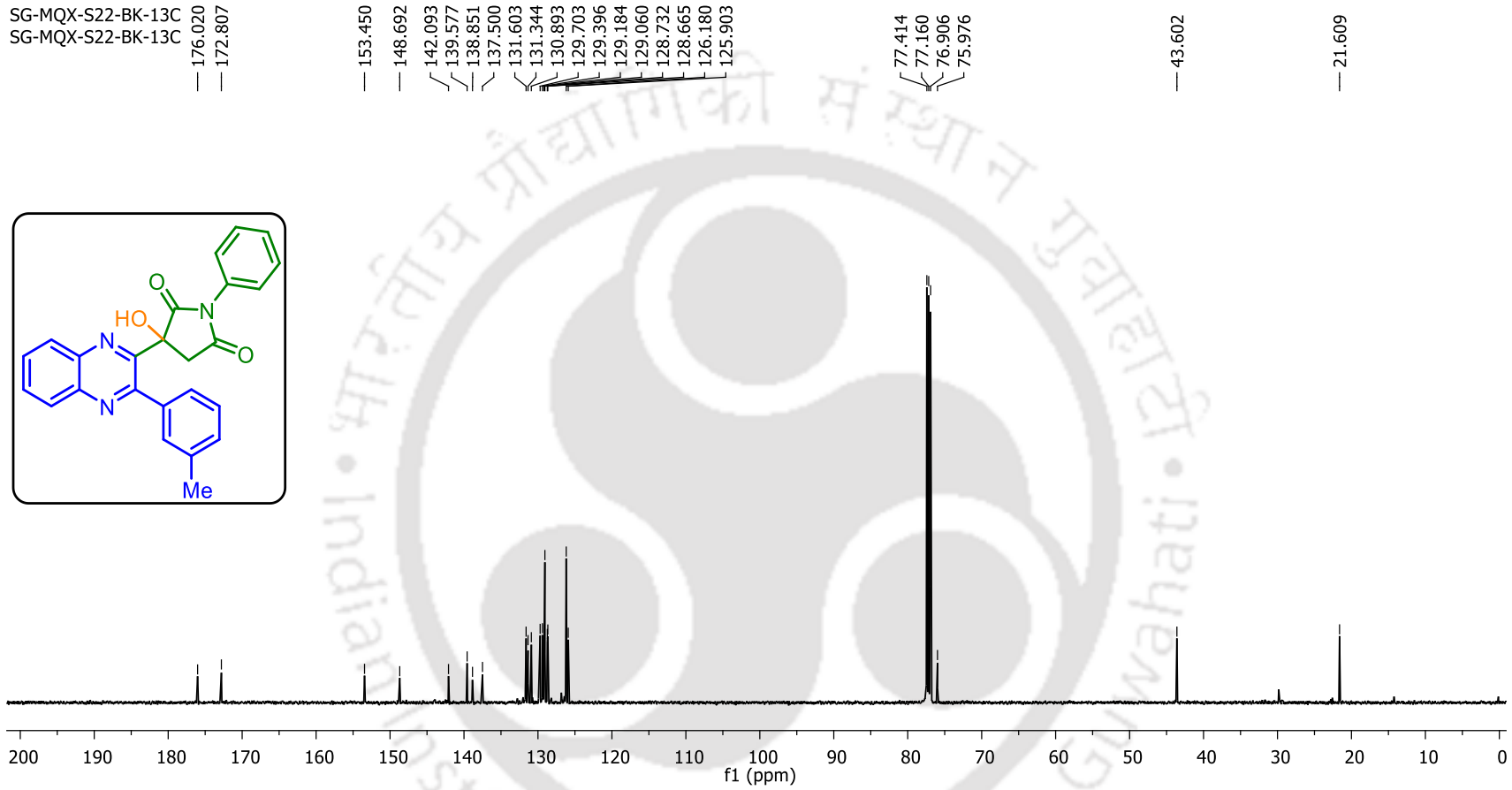

TH-3369_166122017

^{1}H NMR of **3-Hydroxy-1-phenyl-3-(3-(3-(trifluoromethyl)phenyl)quinoxalin-2-yl)pyrrolidine-2,5-dione** (**9a**) ($CDCl_3$, 400 MHz)

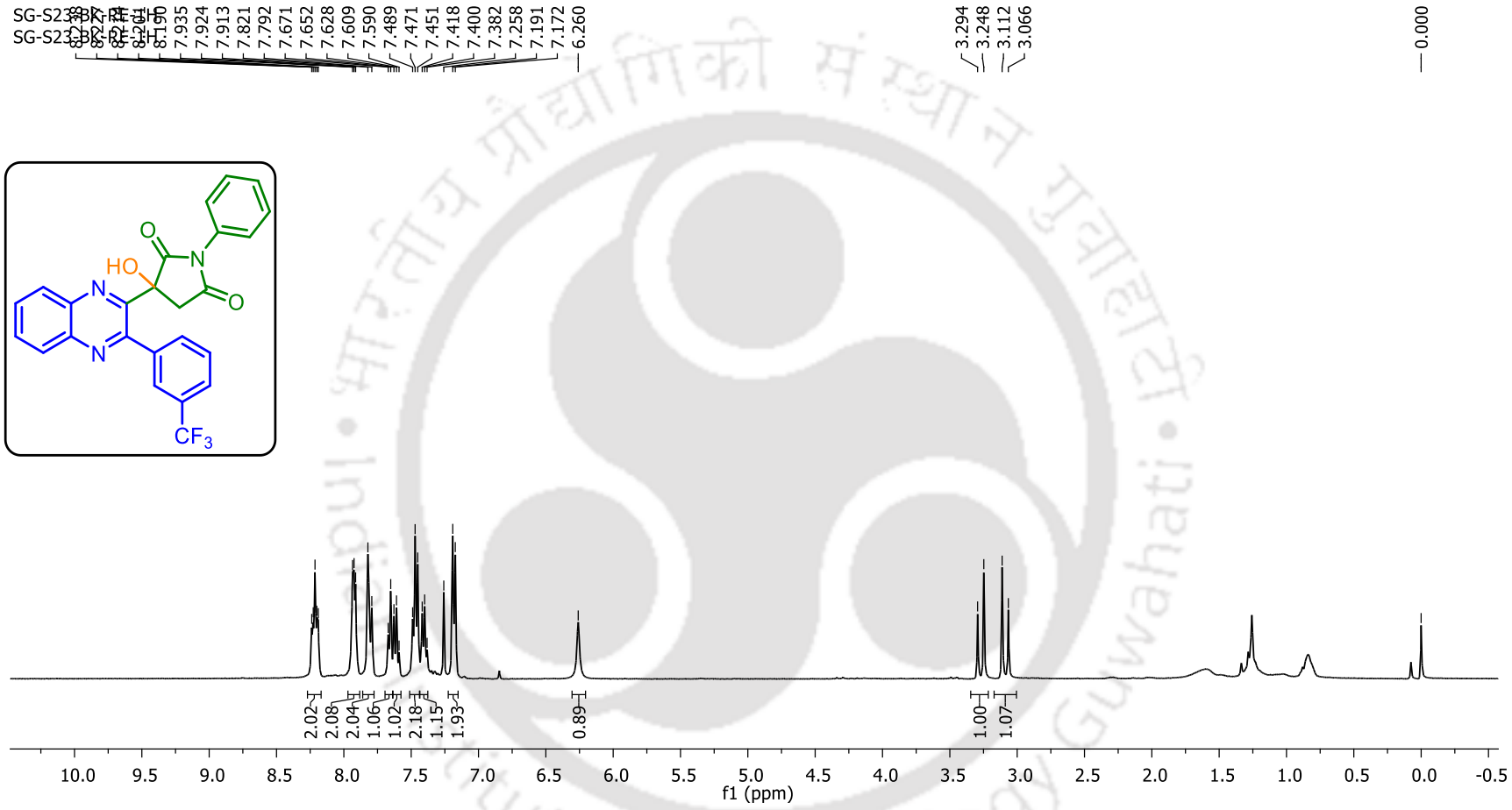

TH-3369_166122017

^{13}C {^{1}H} NMR of **3-Hydroxy-1-phenyl-3-(3-(3-(trifluoromethyl)phenyl)quinoxalin-2-yl)pyrrolidine-2,5-dione** (**9a**) ($CDCl_3$, 126 MHz)

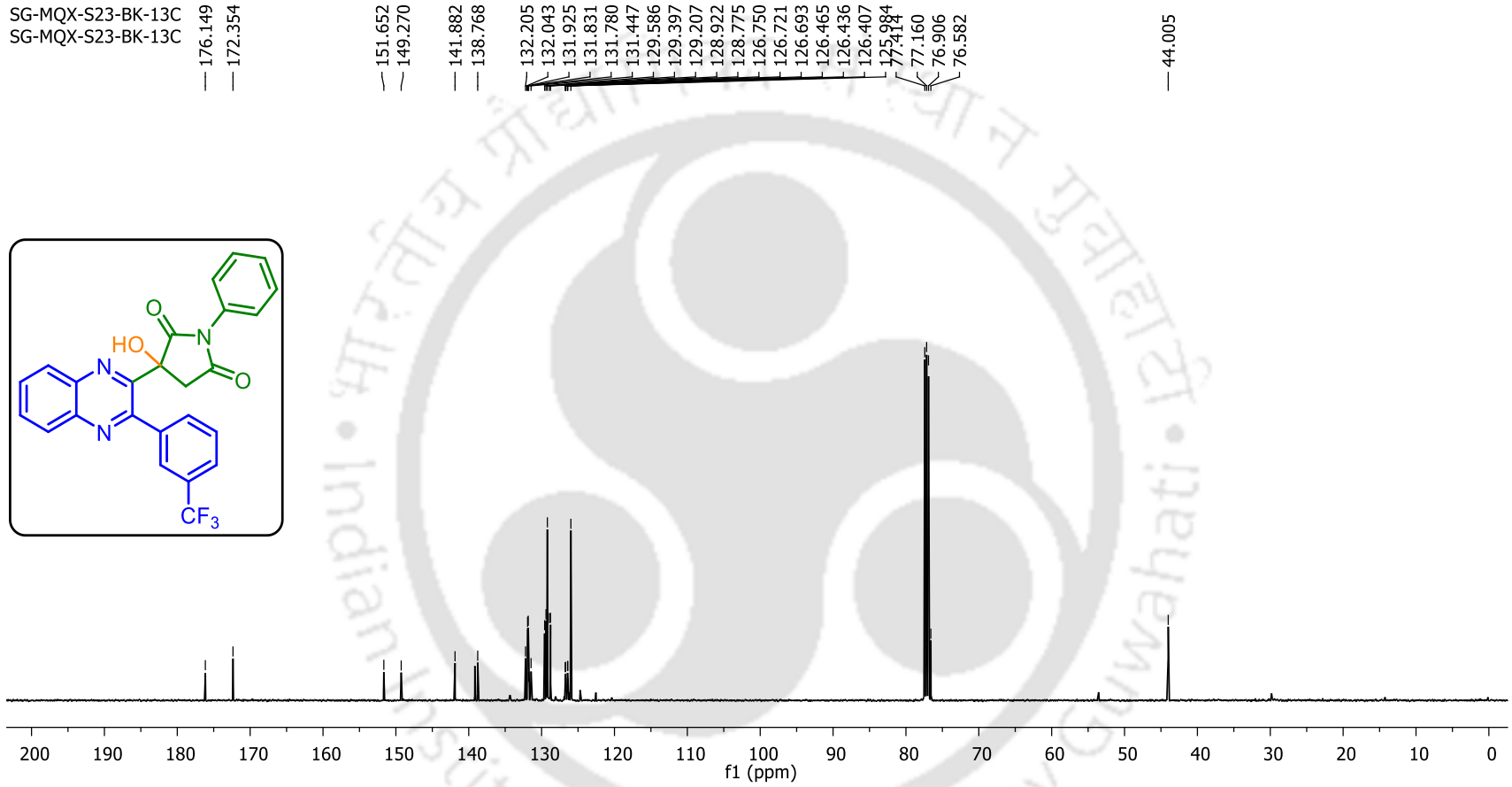

TH-3369_166122017

^{19}F NMR of **3-Hydroxy-1-phenyl-3-(3-(3-(trifluoromethyl)phenyl)quinoxalin-2-yl)pyrrolidine-2,5-dione** (**9a**) ($CDCl_3$)

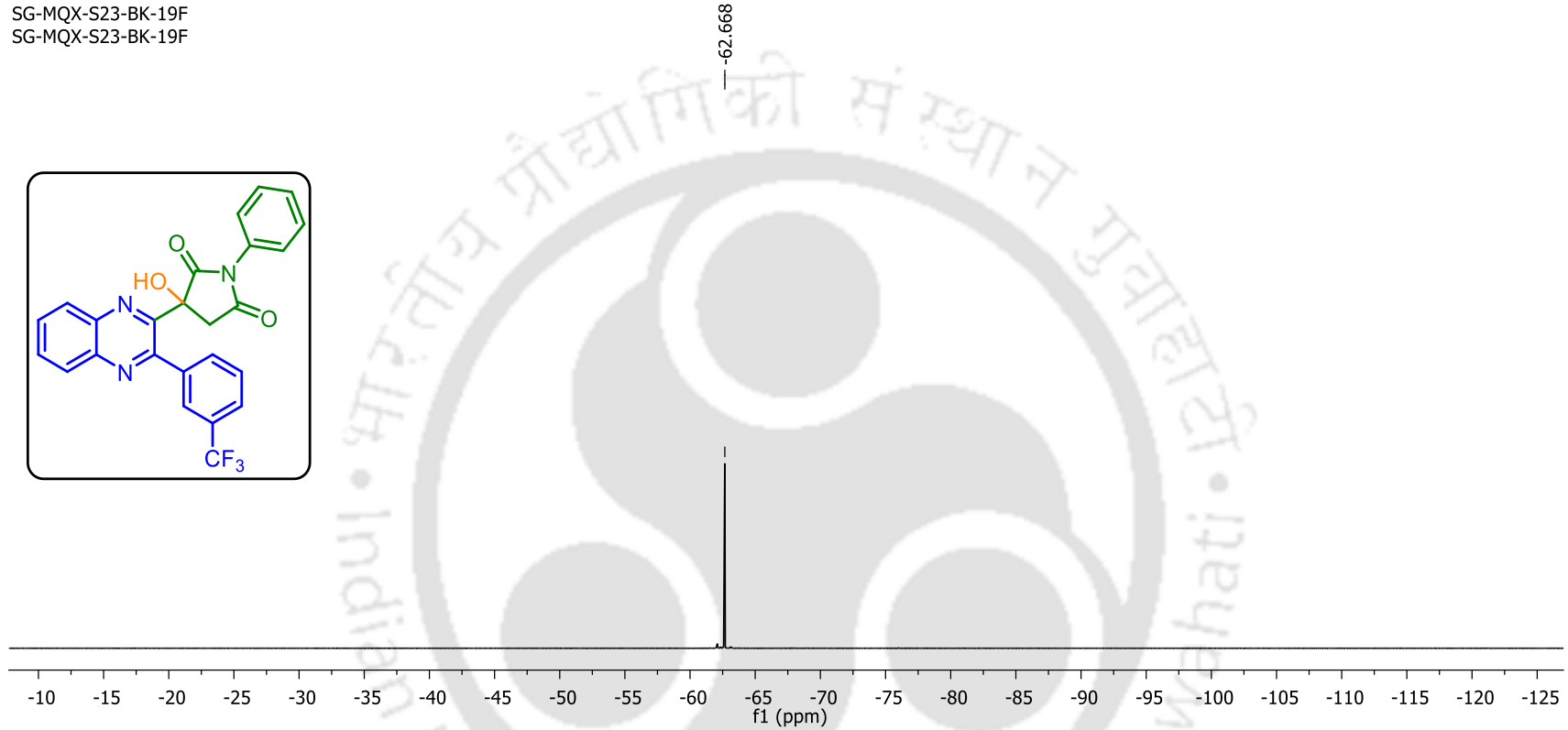

TH-3369_166122017

^{1}H NMR of **3-Hydroxy-3-(3-(2-methoxyphenyl)quinoxalin-2-yl)-1-phenylpyrrolidine-2,5-dione** (**10a**) ($CDCl_3$, 500 MHz)

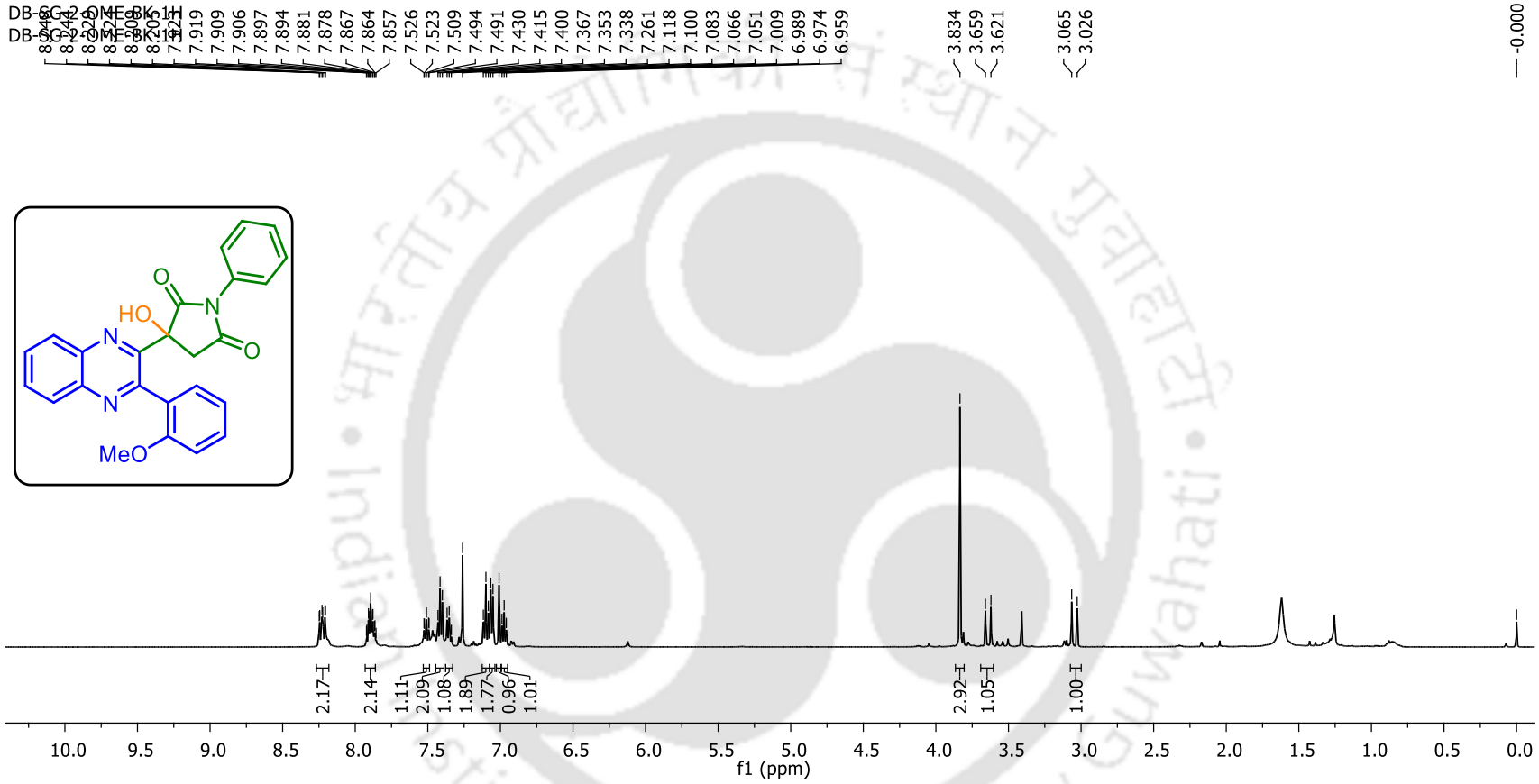

TH-3369_166122017

^{13}C {^{1}H} NMR of **3-Hydroxy-3-(3-(2-methoxyphenyl)quinoxalin-2-yl)-1-phenylpyrrolidine-2,5-dione** (**10a**) ($CDCl_3$, 126 MHz)

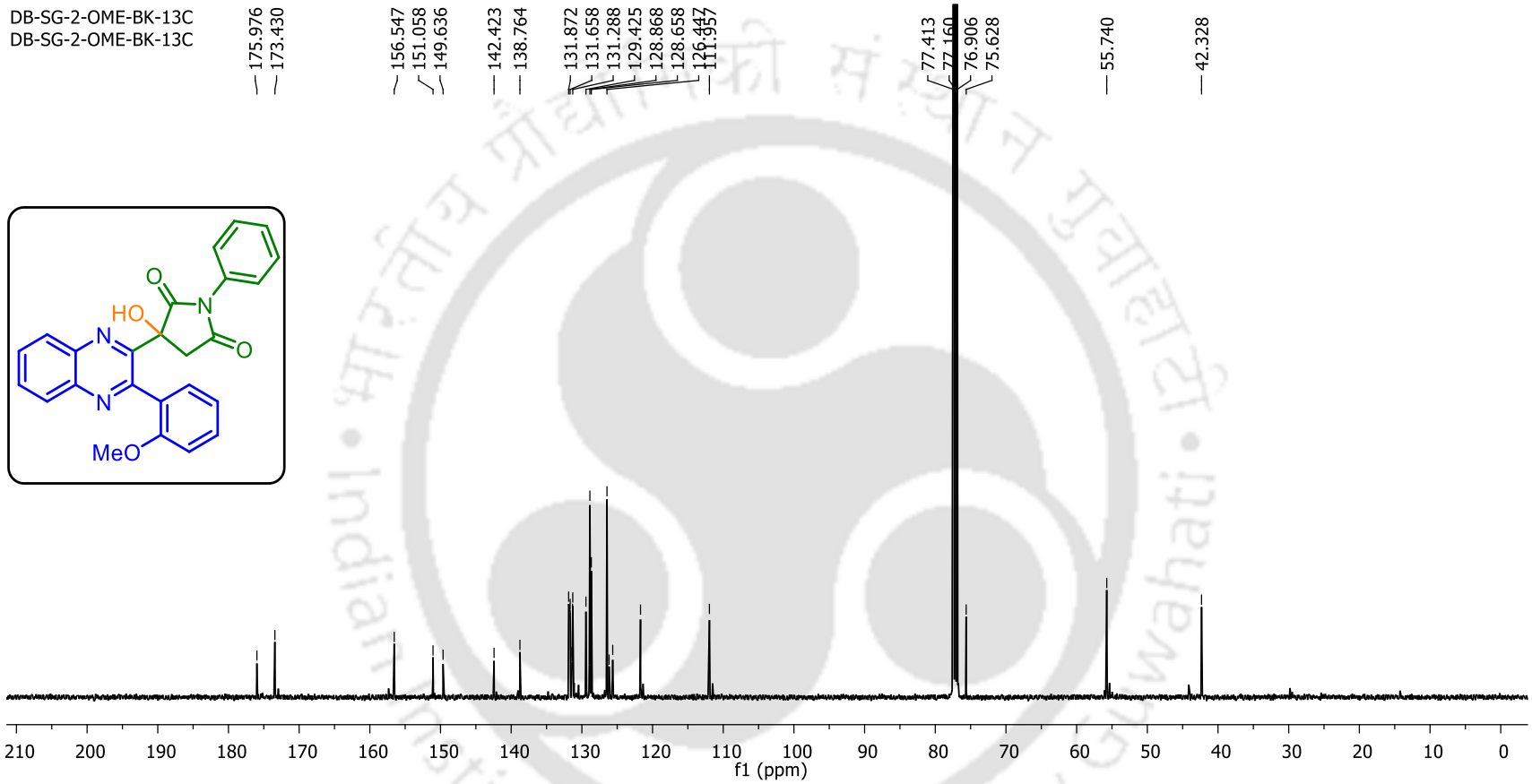

TH-3369_166122017

^{1}H NMR of **3-(3-(2-Bromophenyl)quinoxalin-2-yl)-3-hydroxy-1-phenylpyrrolidine-2,5-dione (11a)** ($CDCl_3$, 500 MHz)

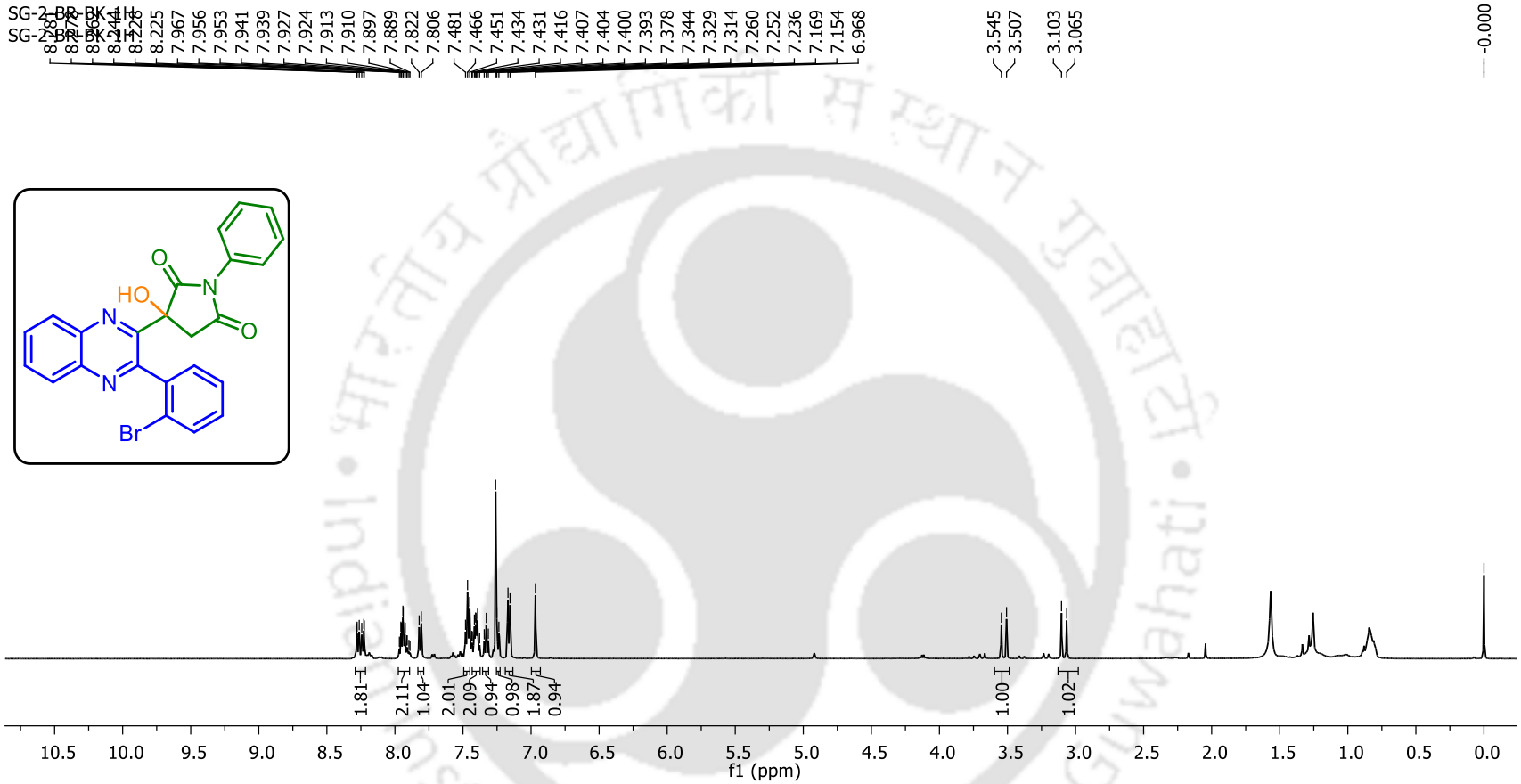

TH-3369_166122017

^{13}C {^{1}H} NMR of **3-(3-(2-Bromophenyl)quinoxalin-2-yl)-3-hydroxy-1-phenylpyrrolidine-2,5-dione** (**11a**) ($CDCl_3$, 126 MHz)

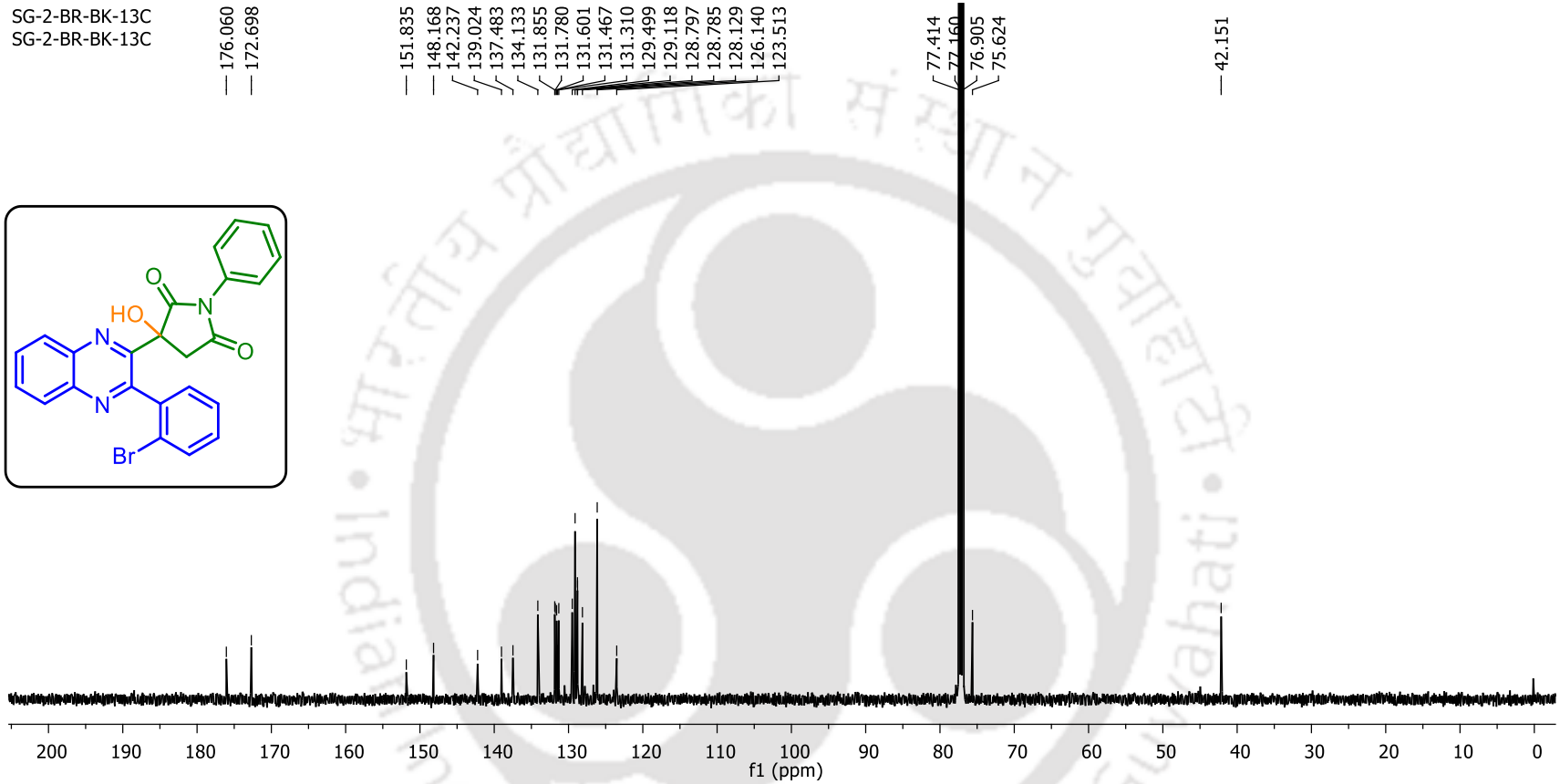

TH-3369_166122017

^{1}H NMR of **3-(3-(2,6-Difluorophenyl)quinoxalin-2-yl)-3-hydroxy-1-phenylpyrrolidine-2,5-dione** (**12a**) ($CDCl_3$, 400 MHz)

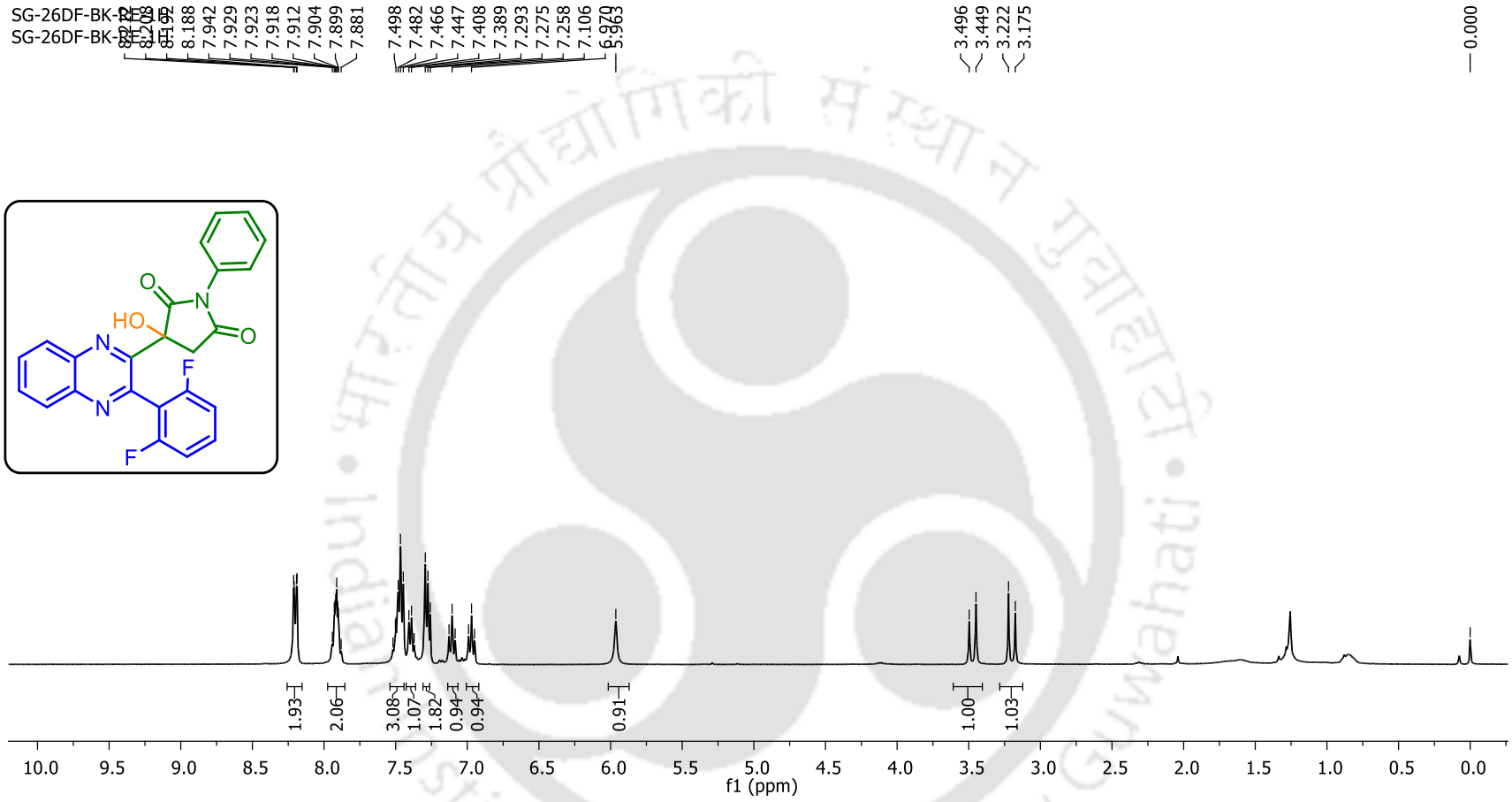

TH-3369_166122017

^{13}C {^{1}H} NMR of **3-(3-(2,6-Difluorophenyl)quinoxalin-2-yl)-3-hydroxy-1-phenylpyrrolidine-2,5-dione** (**12a**) ($CDCl_3$, 126 MHz)

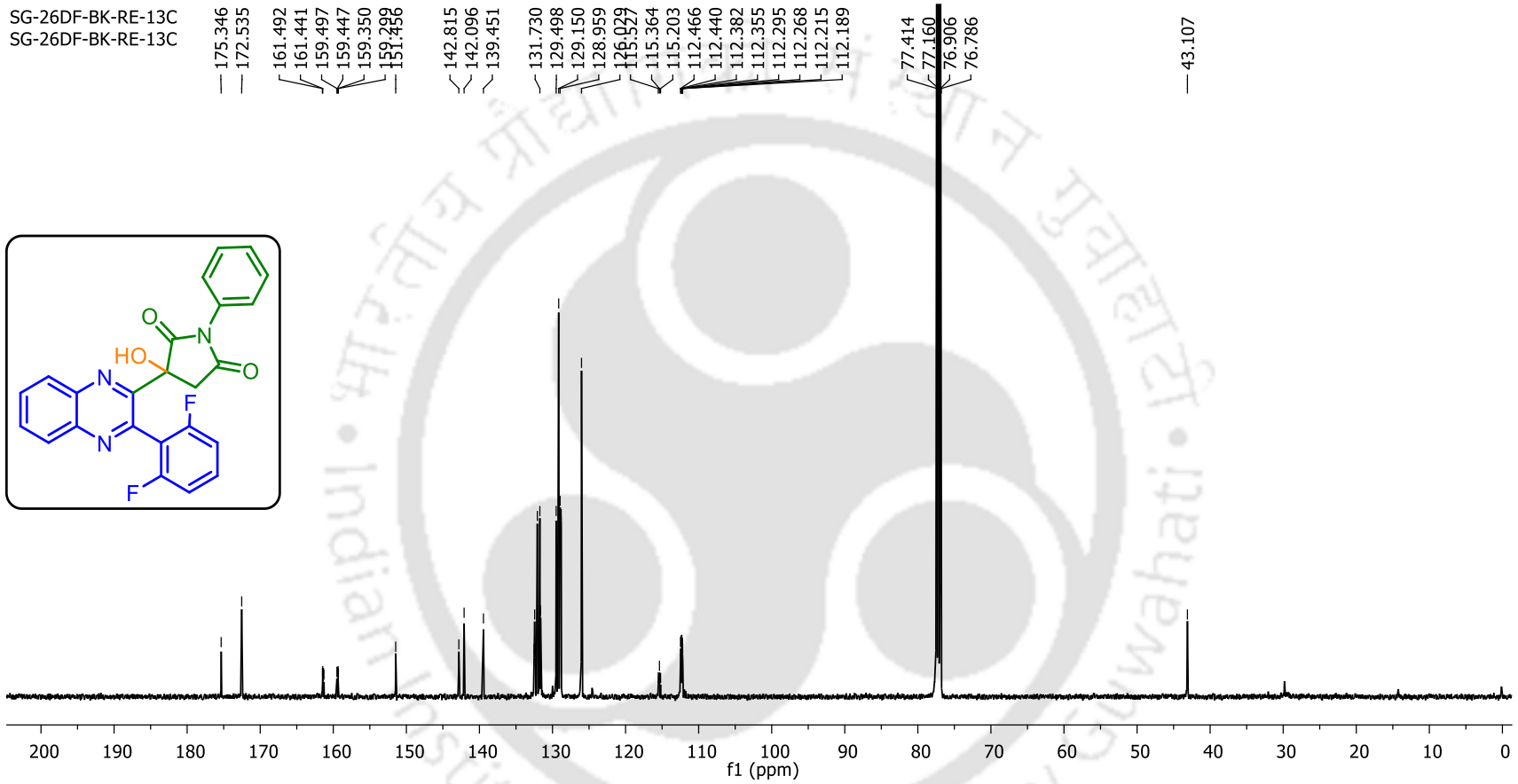

TH-3369_166122017

^{19}F NMR of **3-(3-(2,6-Difluorophenyl)quinoxalin-2-yl)-3-hydroxy-1-phenylpyrrolidine-2,5-dione** (**12a**) ($CDCl_3$)

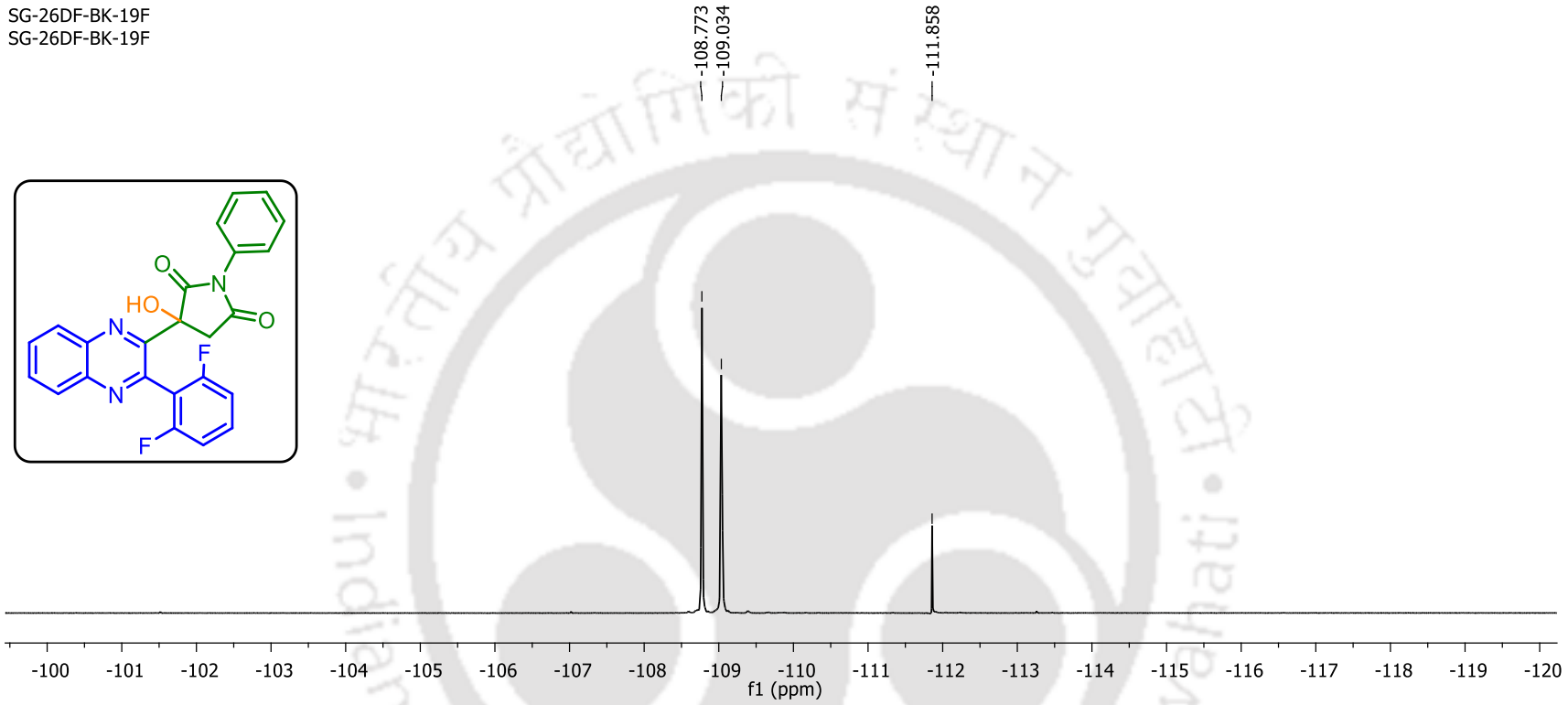

TH-3369_166122017

^{1}H NMR of **3-Hydroxy-3-(3-(naphthalen-2-yl)quinoxalin-2-yl)-1-phenylpyrrolidine-2,5-dione** (**13a**) ($CDCl_3$, 500 MHz)

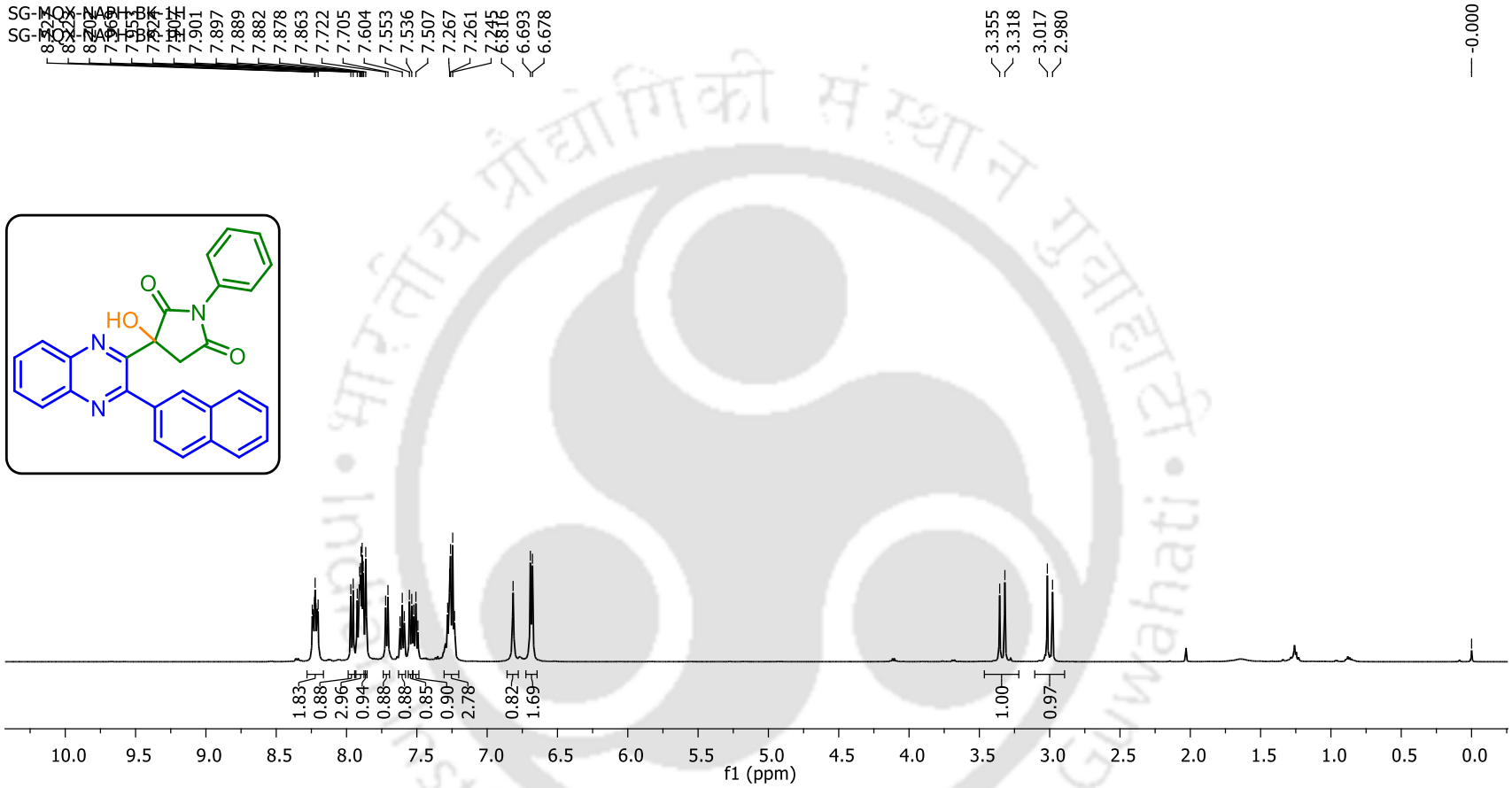

TH-3369_166122017

^{13}C {^{1}H} NMR of **3-Hydroxy-3-(3-(naphthalen-2-yl)quinoxalin-2-yl)-1-phenylpyrrolidine-2,5-dione** (**13a**) ($CDCl_3$, 126 MHz)

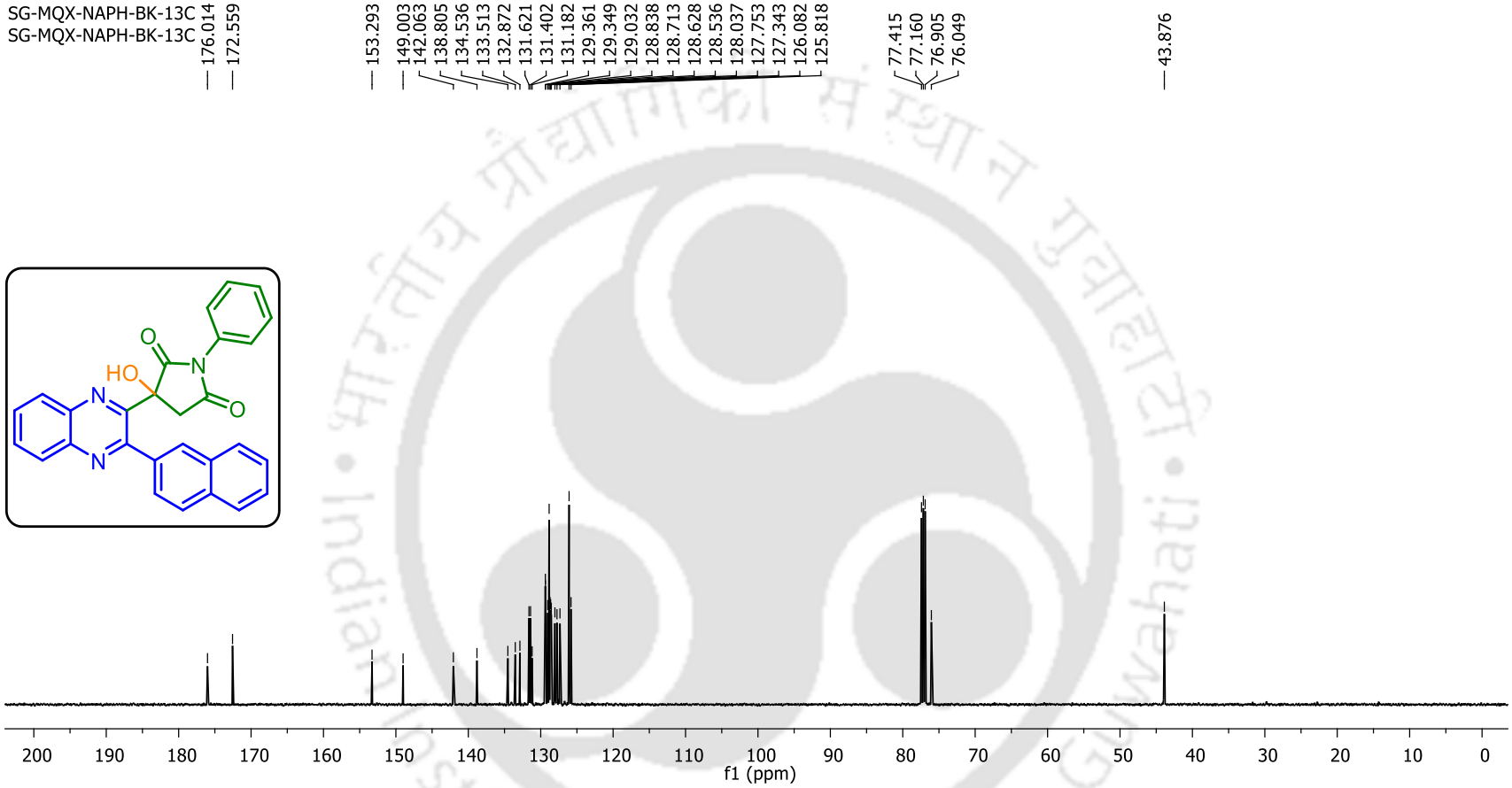

TH-3369_166122017

^{1}H NMR of **3-Hydroxy-1-phenyl-3-(3-(thiophen-2-yl)quinoxalin-2-yl)pyrrolidine-2,5-dione** (**14a**) ($CDCl_3$, 400 MHz)

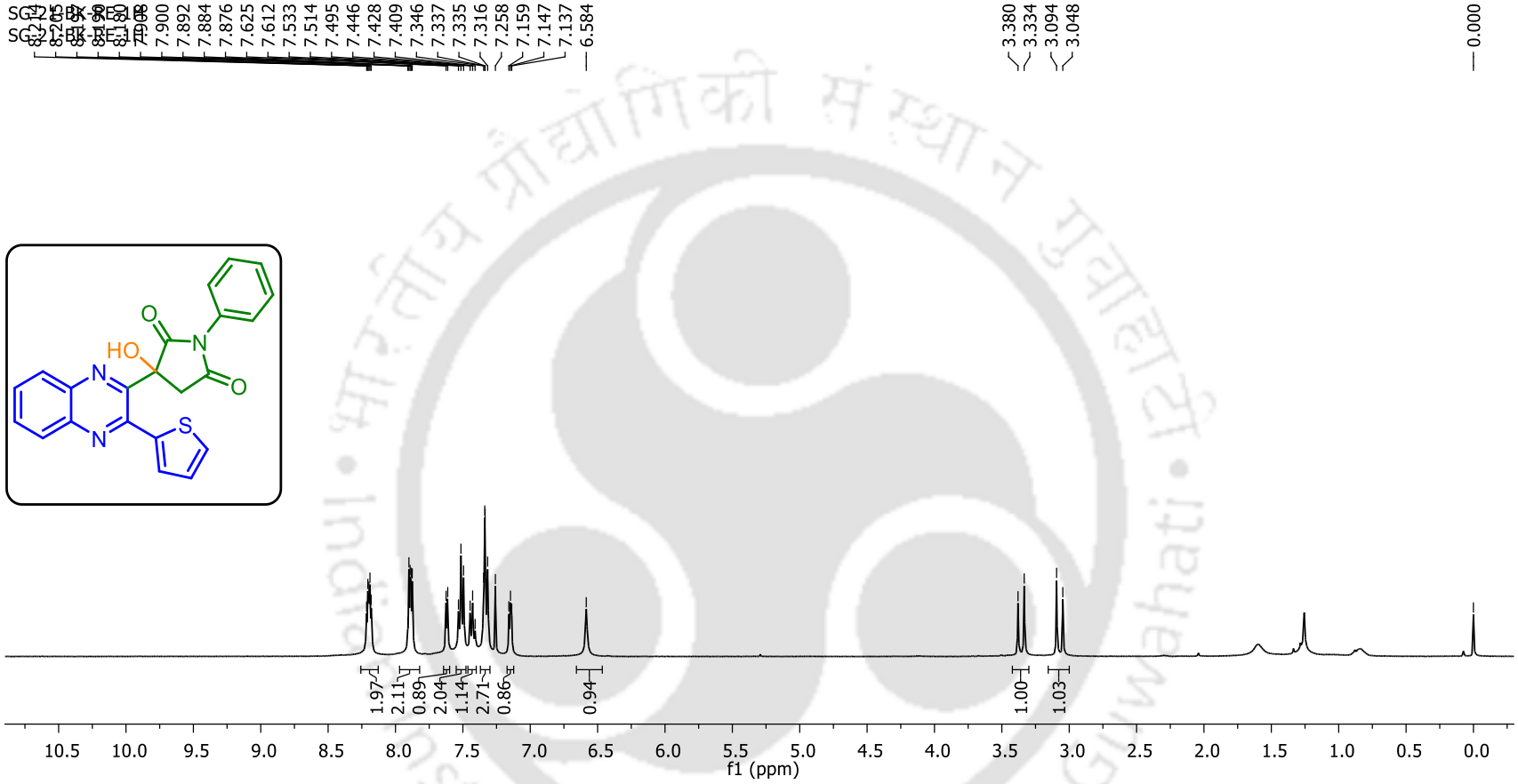

TH-3369_166122017

^{13}C {^{1}H} NMR of **3-Hydroxy-1-phenyl-3-(3-(thiophen-2-yl)quinoxalin-2-yl)pyrrolidine-2,5-dione** (**14a**) ($CDCl_3$, 126 MHz)

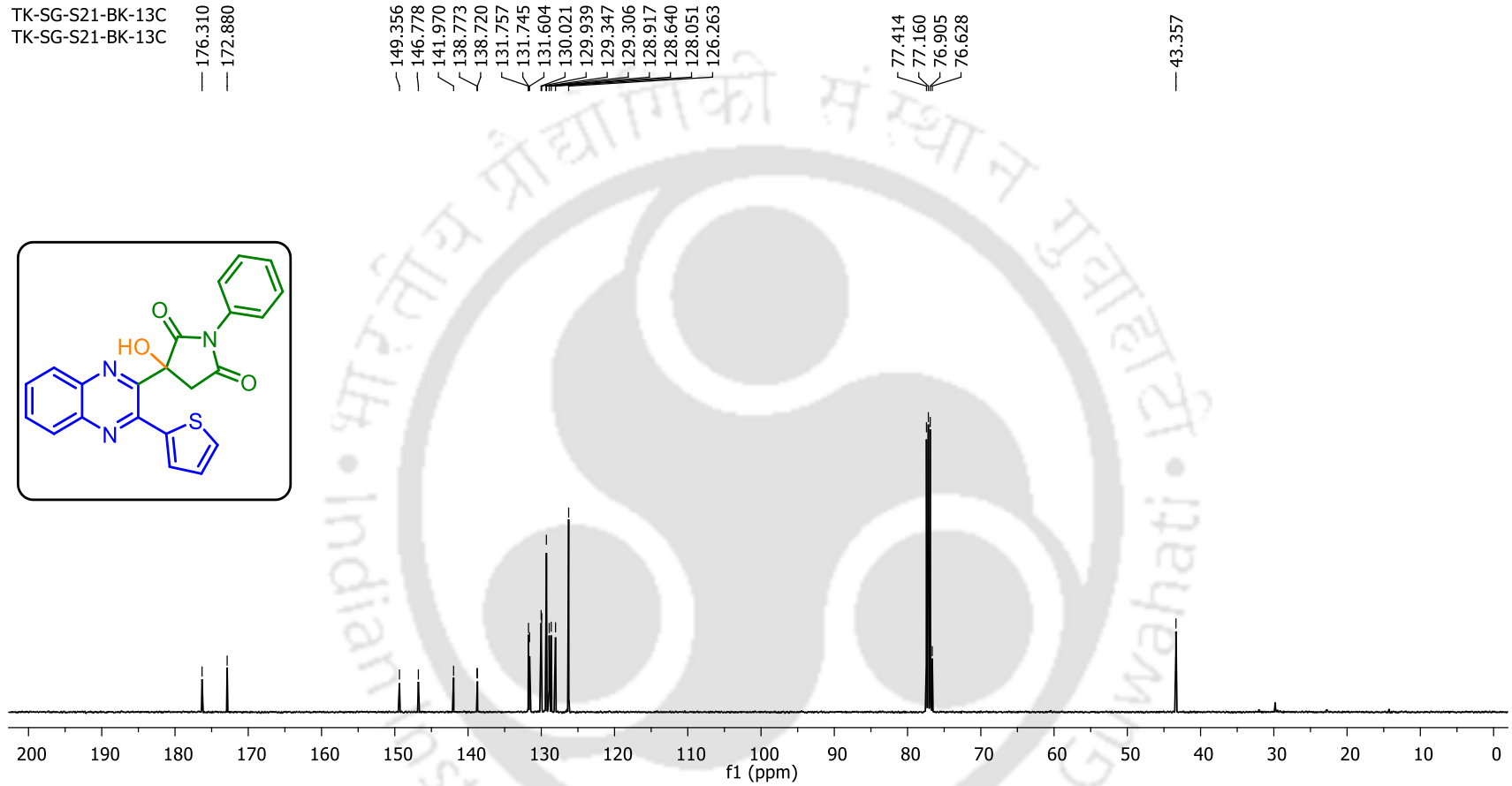

TH-3369_166122017

^{1}H NMR of **3-Hydroxy-1-methyl-3-(3-phenylquinoxalin-2-yl)pyrrolidine-2,5-dione** (**15a**) ($CDCl_3$, 500 MHz)

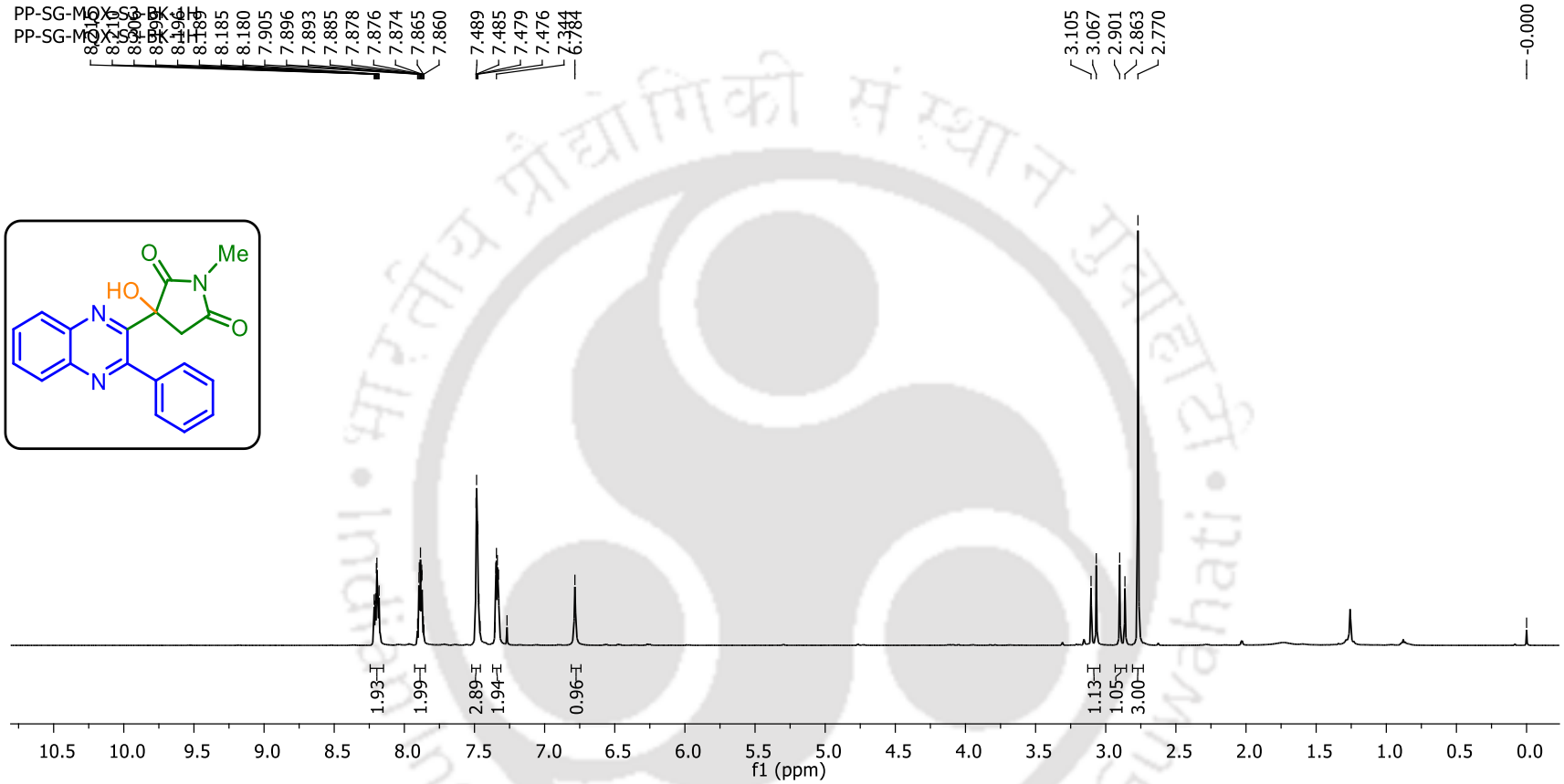

TH-3369_166122017

^{13}C {^{1}H} NMR of **3-Hydroxy-1-methyl-3-(3-phenylquinoxalin-2-yl)pyrrolidine-2,5-dione** (**15a**) ($CDCl_3$, 126 MHz)

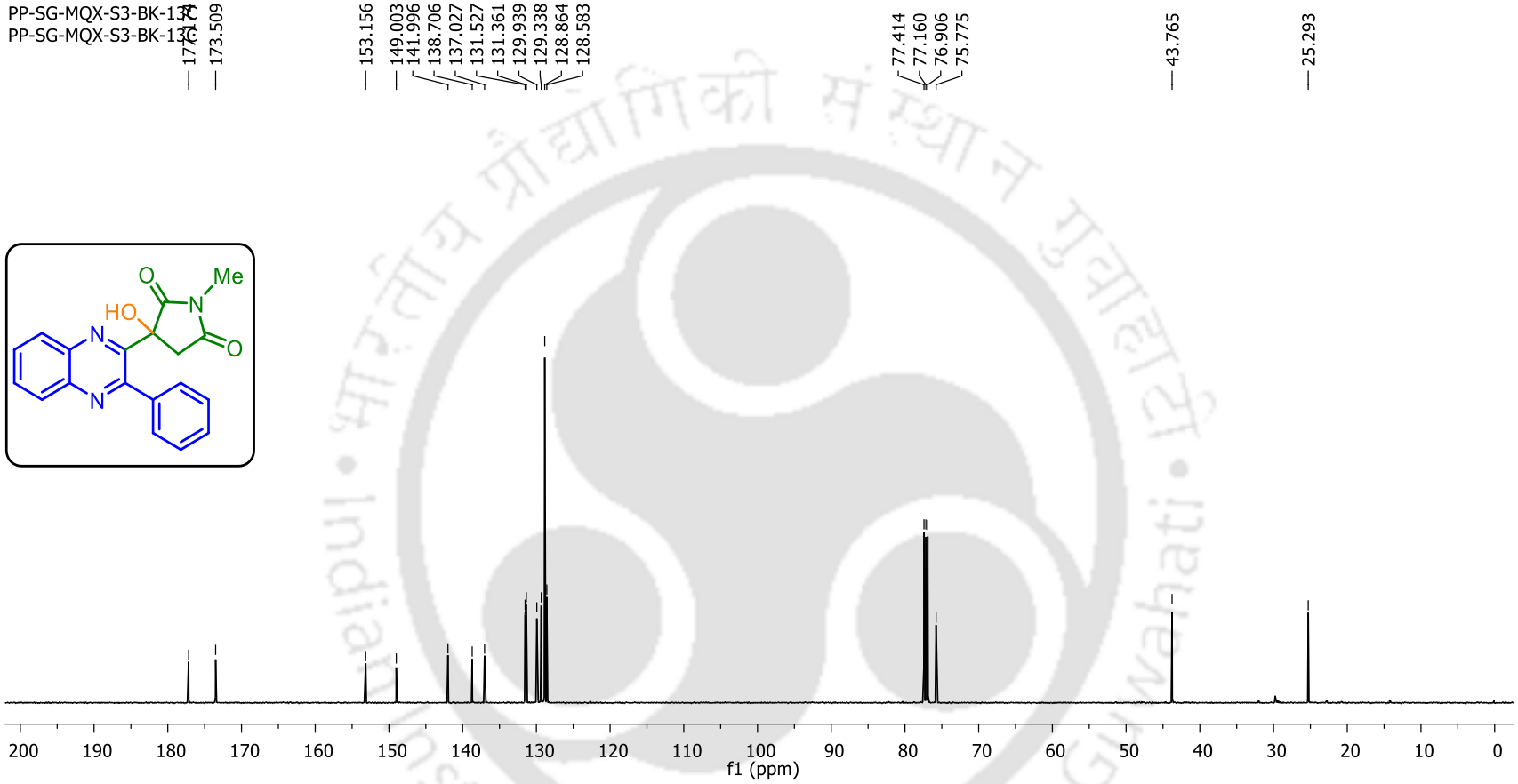

TH-3369_166122017

^{1}H NMR of **1-Ethyl-3-hydroxy-3-(3-phenylquinoxalin-2-yl)pyrrolidine-2,5-dione** (**16a**) ($CDCl_3$, 500 MHz)

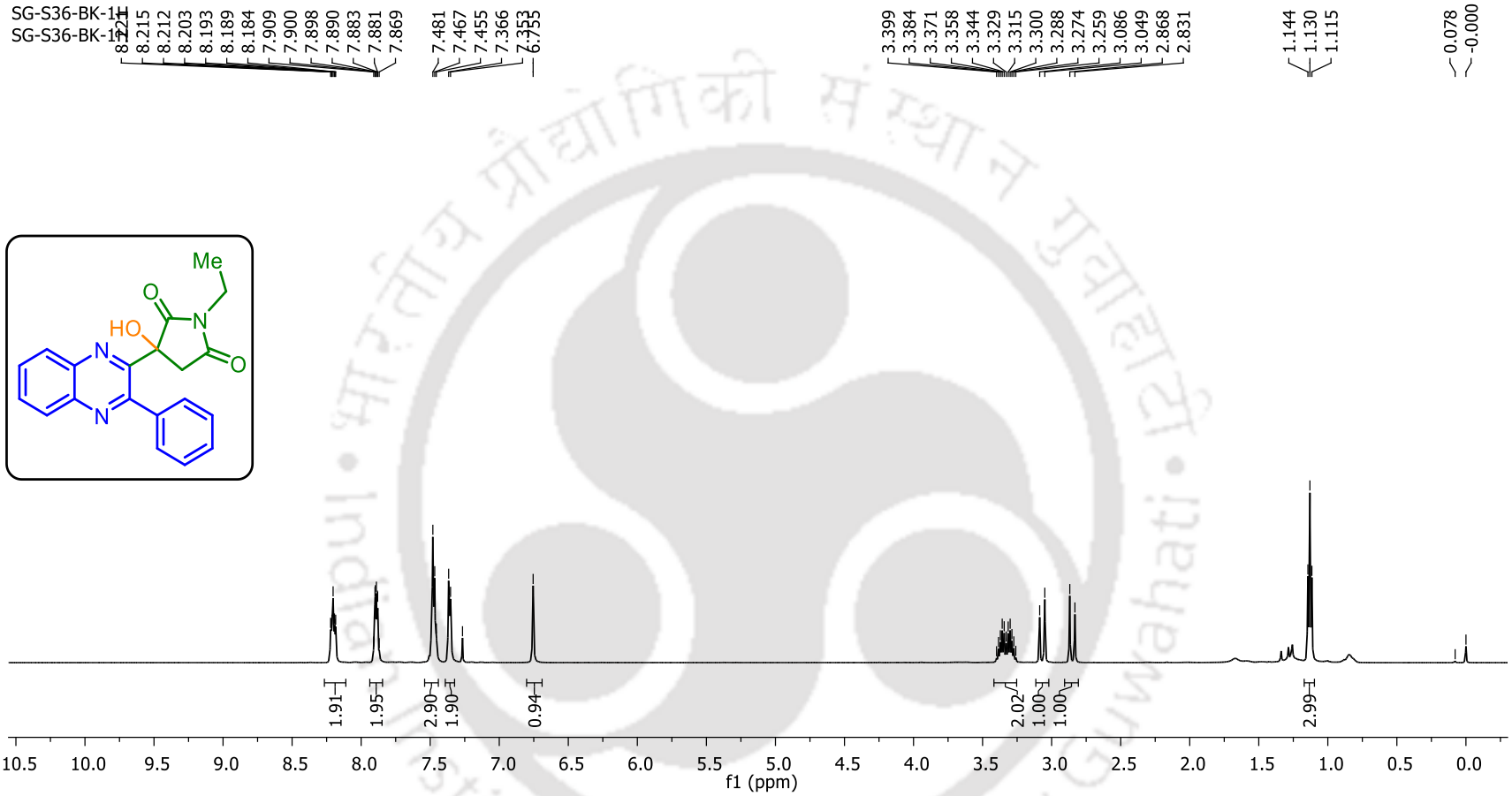

TH-3369_166122017

^{13}C {^{1}H} NMR of **1-Ethyl-3-hydroxy-3-(3-phenylquinoxalin-2-yl)pyrrolidine-2,5-dione** (**16a**) ($CDCl_3$, 126 MHz)

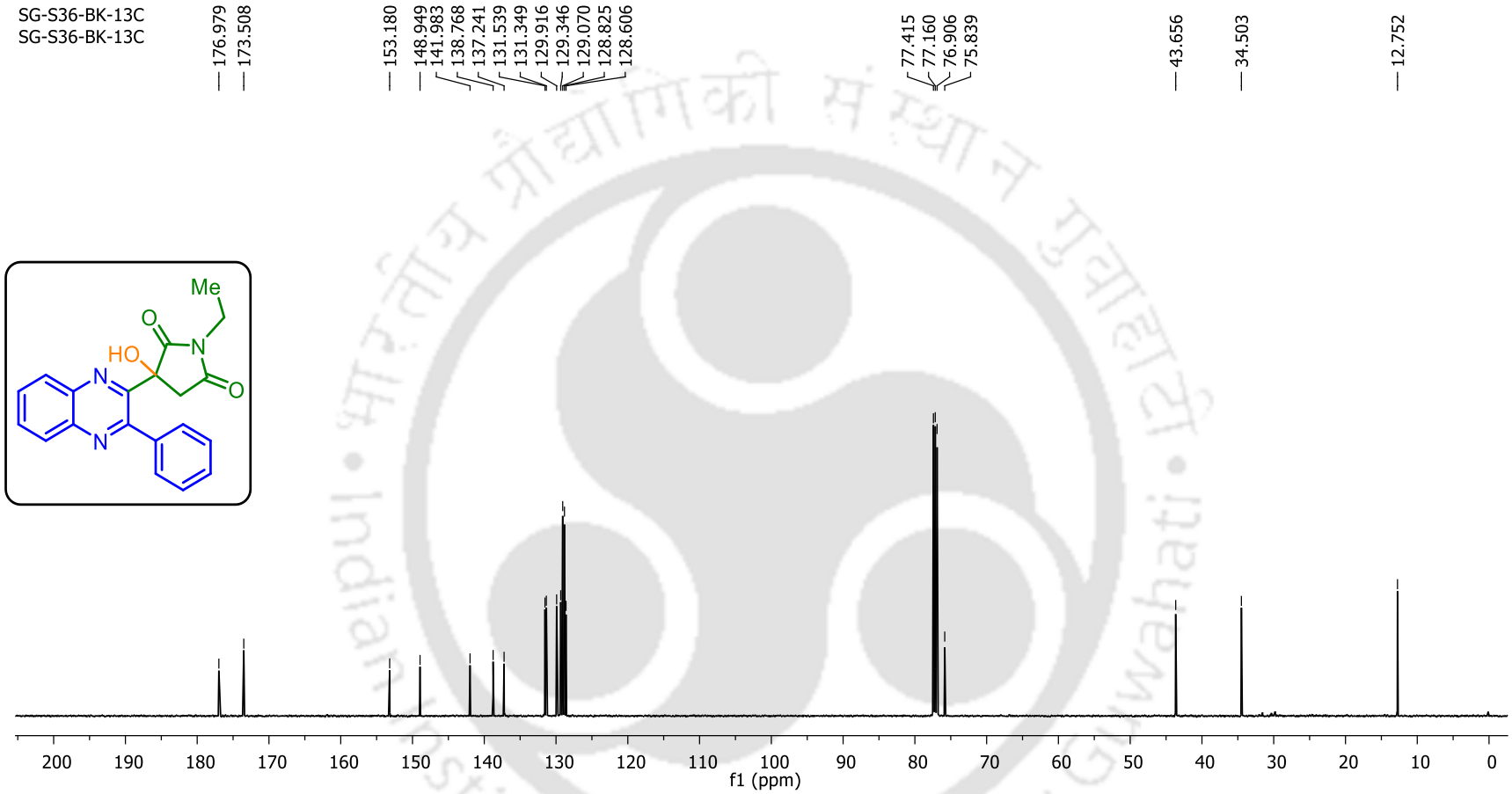

TH-3369_166122017

^{1}H NMR of **3-Hydroxy-1-isobutyl-3-(3-phenylquinoxalin-2-yl)pyrrolidine-2,5-dione** (**17a**) ($CDCl_3$, 500 MHz)

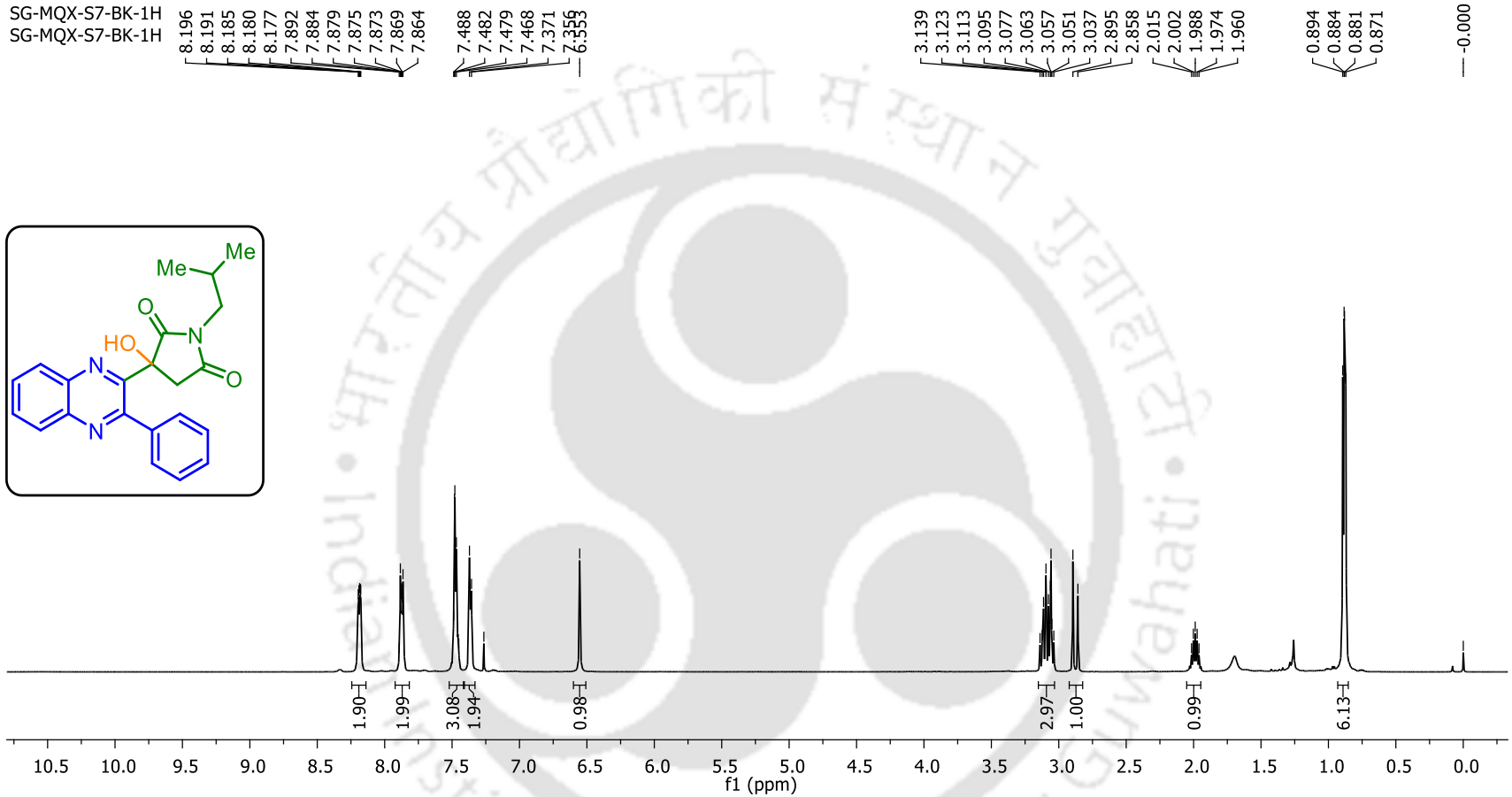

TH-3369_166122017

^{13}C {^{1}H} NMR of **3-Hydroxy-1-isobutyl-3-(3-phenylquinoxalin-2-yl)pyrrolidine-2,5-dione** (**17a**) ($CDCl_3$, 126 MHz)

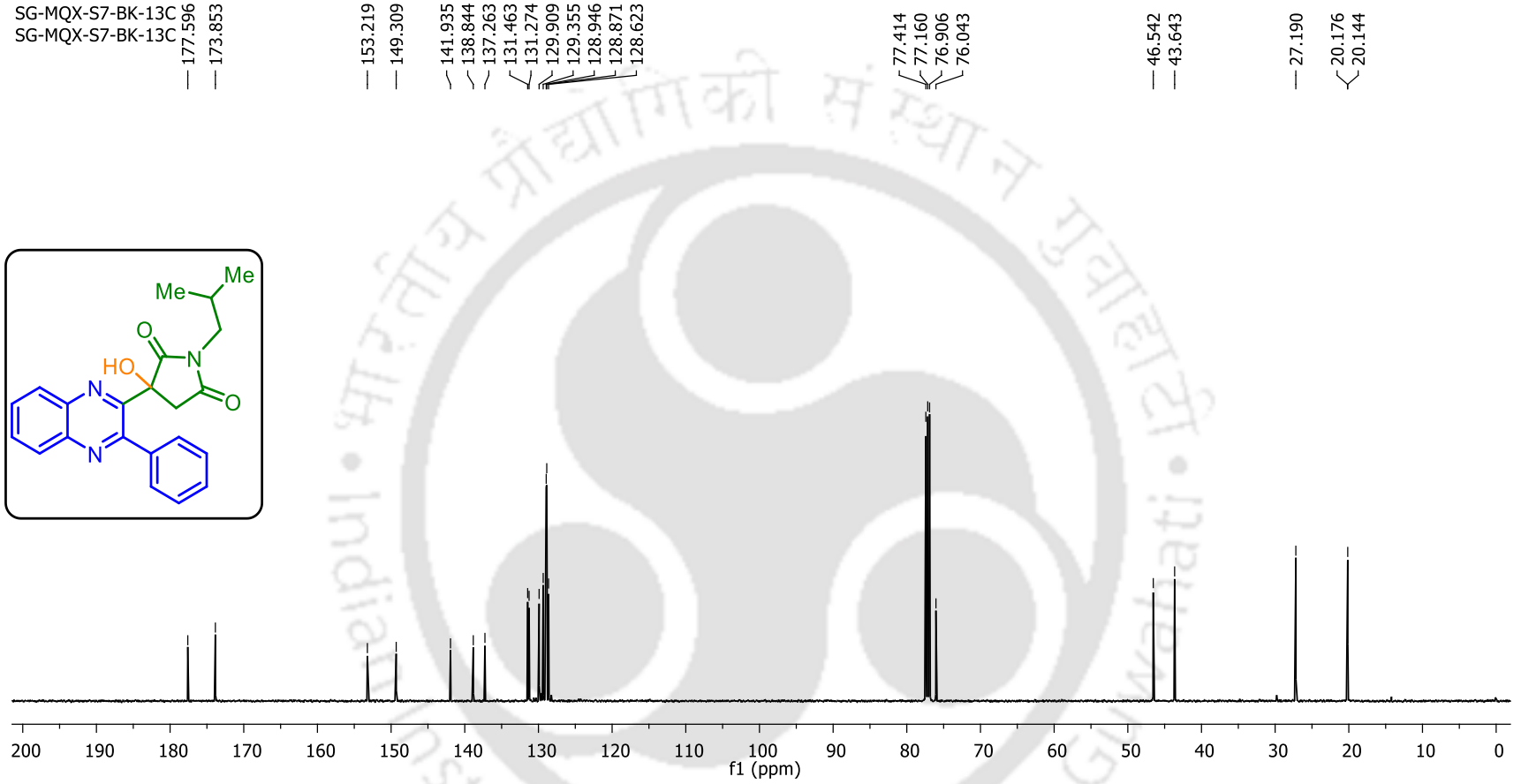

TH-3369_166122017

^{1}H NMR of **1-Benzyl-3-hydroxy-3-(3-phenylquinoxalin-2-yl)pyrrolidine-2,5-dione** (**18a**) ($CDCl_3$, 500 MHz)

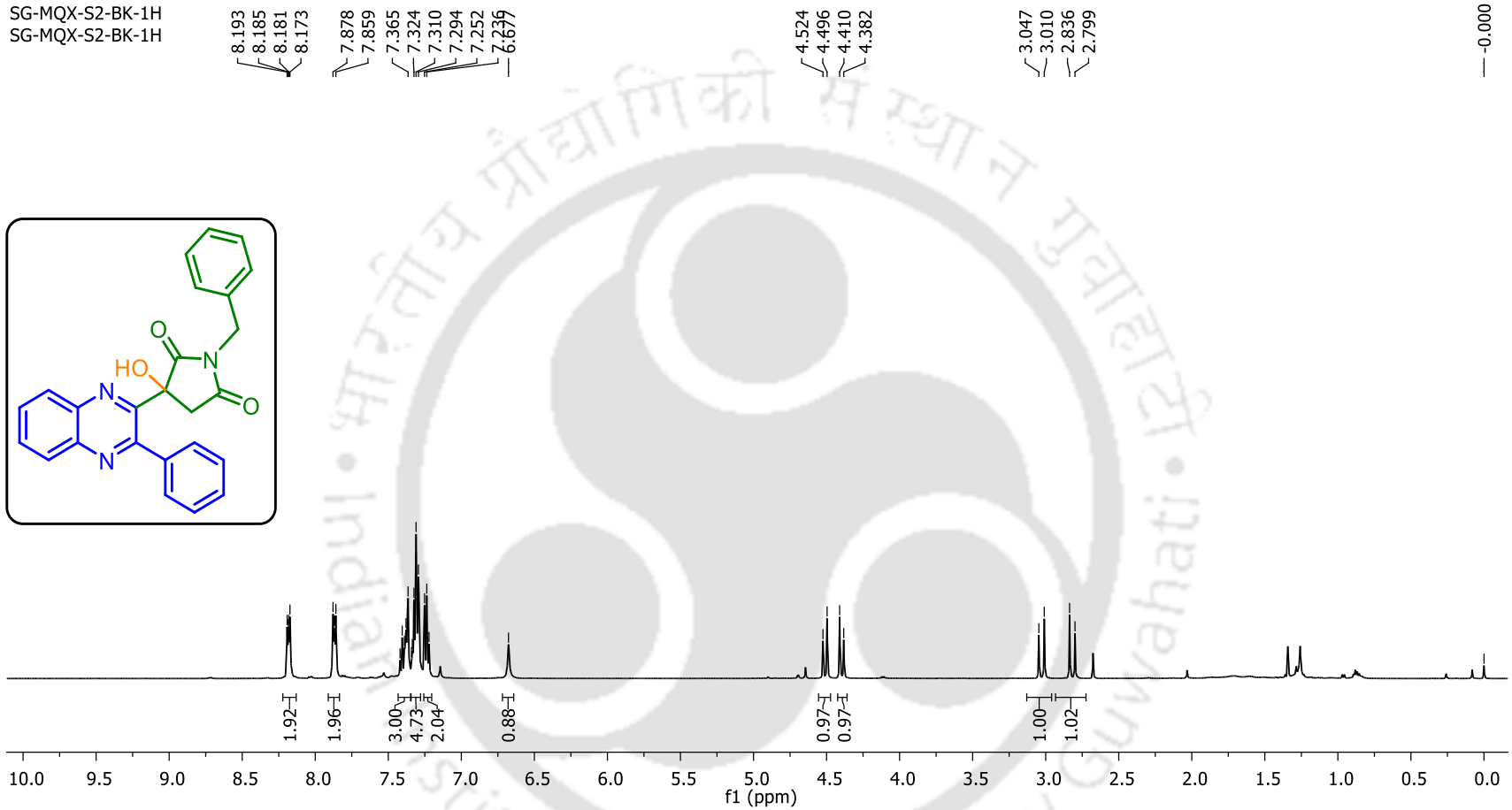

TH-3369_166122017

^{13}C {^{1}H} NMR of **1-Benzyl-3-hydroxy-3-(3-phenylquinoxalin-2-yl)pyrrolidine-2,5-dione** (**18a**) ($CDCl_3$, 126 MHz)

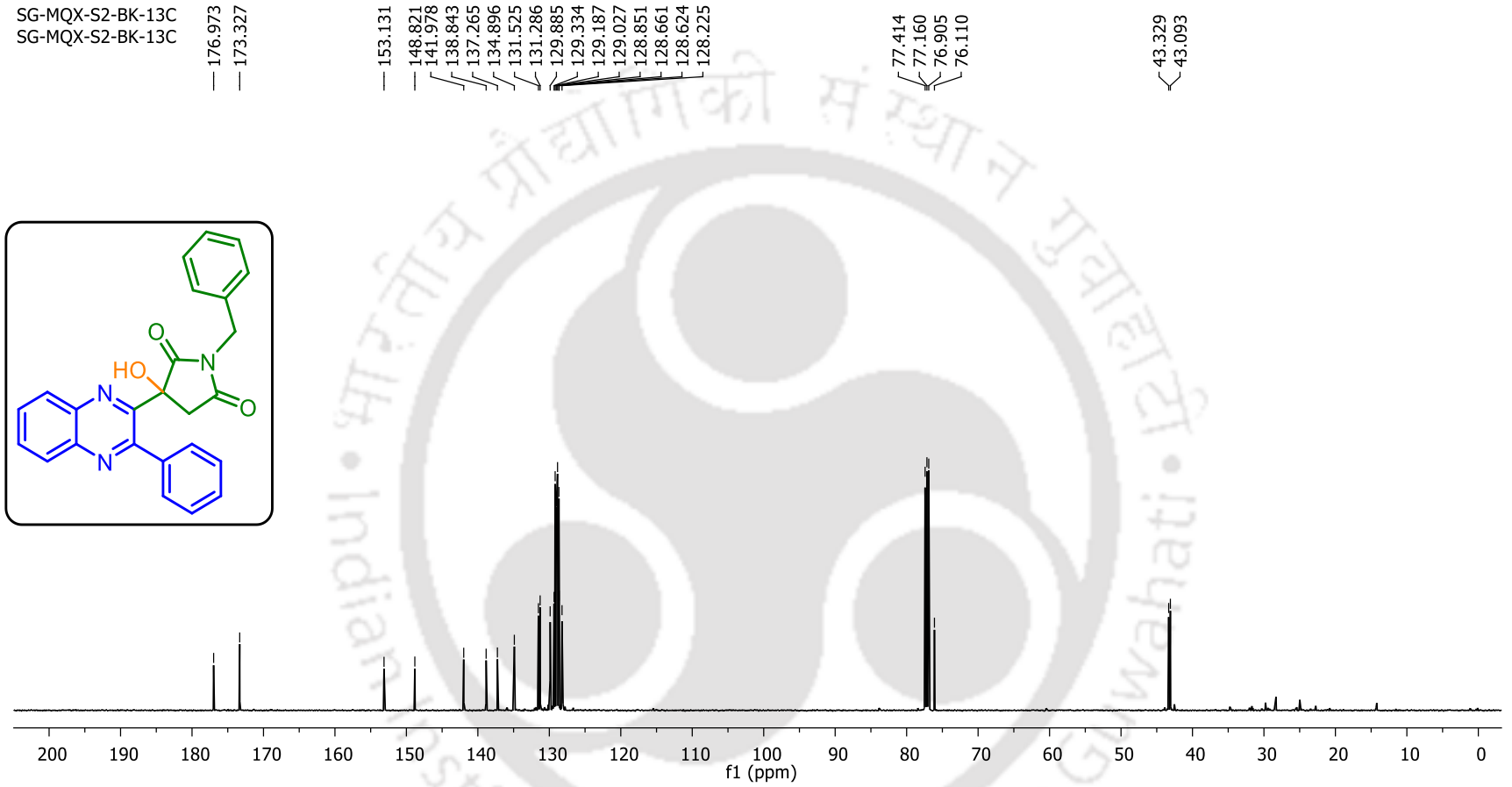

TH-3369_166122017

^{1}H NMR of **1-(Cyclohexylmethyl)-3-hydroxy-3-(3-phenylquinoxalin-2-yl)pyrrolidine-2,5-dione** (**19a**) ($CDCl_3$, 400 MHz)

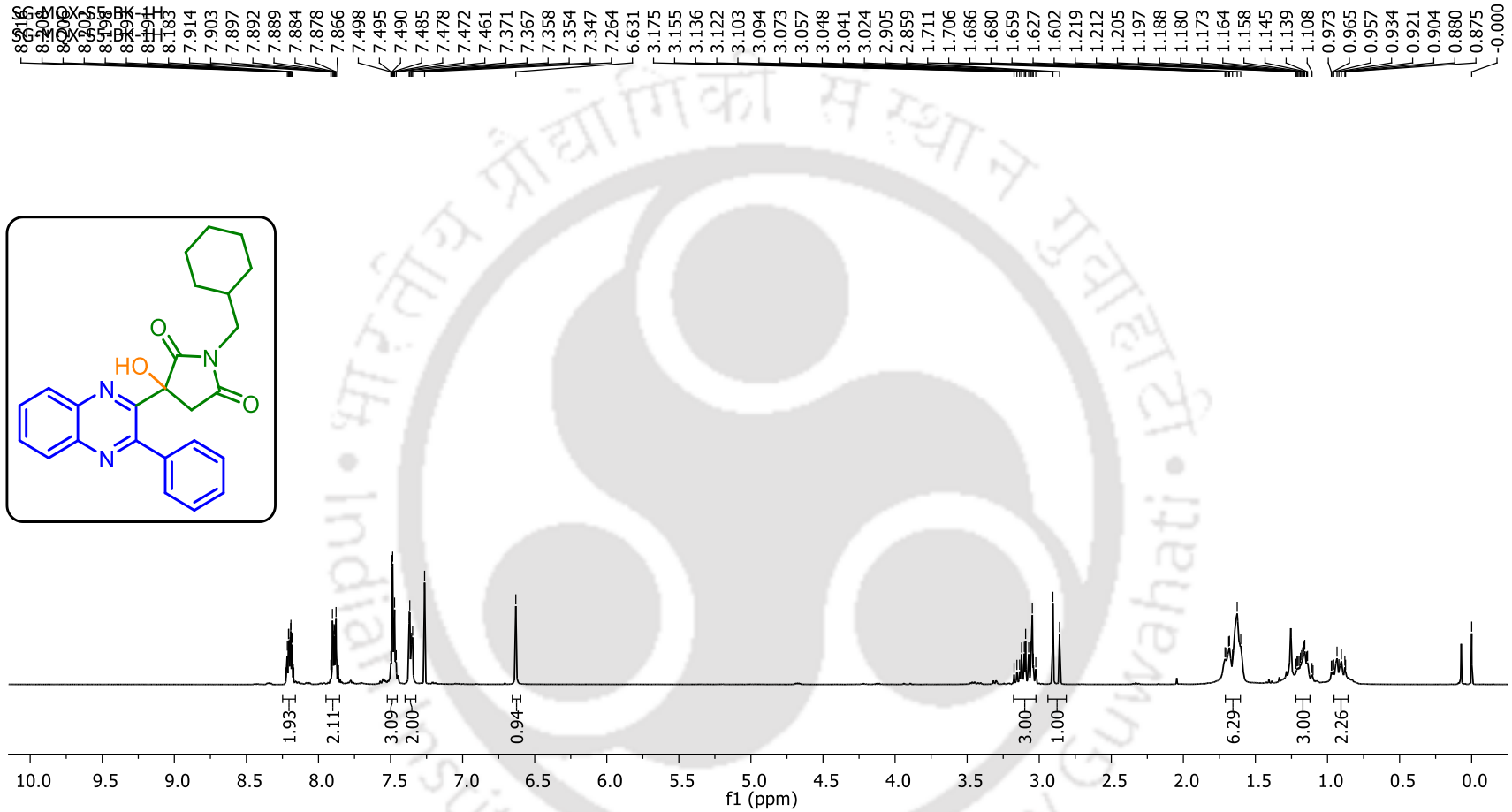

^{13}C {^{1}H} NMR of **1-(Cyclohexylmethyl)-3-hydroxy-3-(3-phenylquinoxalin-2-yl)pyrrolidine-2,5-dione** (**19a**) ($CDCl_3$, 101 MHz)

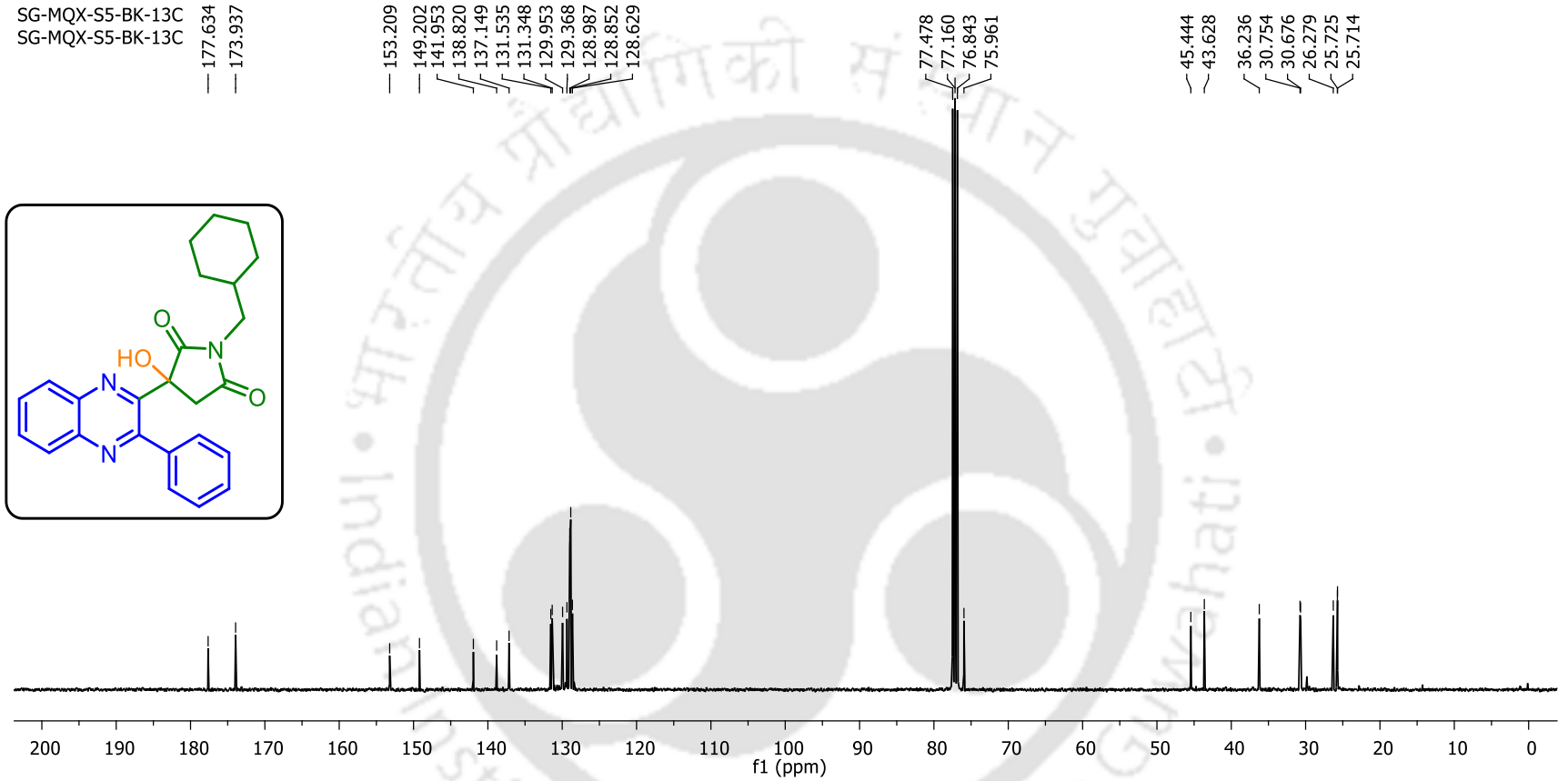

TH-3369_166122017

^{1}H NMR of **3-Hydroxy-3-(3-phenylquinoxalin-2-yl)-1-(*p*-tolyl)pyrrolidine-2,5-dione** (**20a**) ($CDCl_3$, 500 MHz)

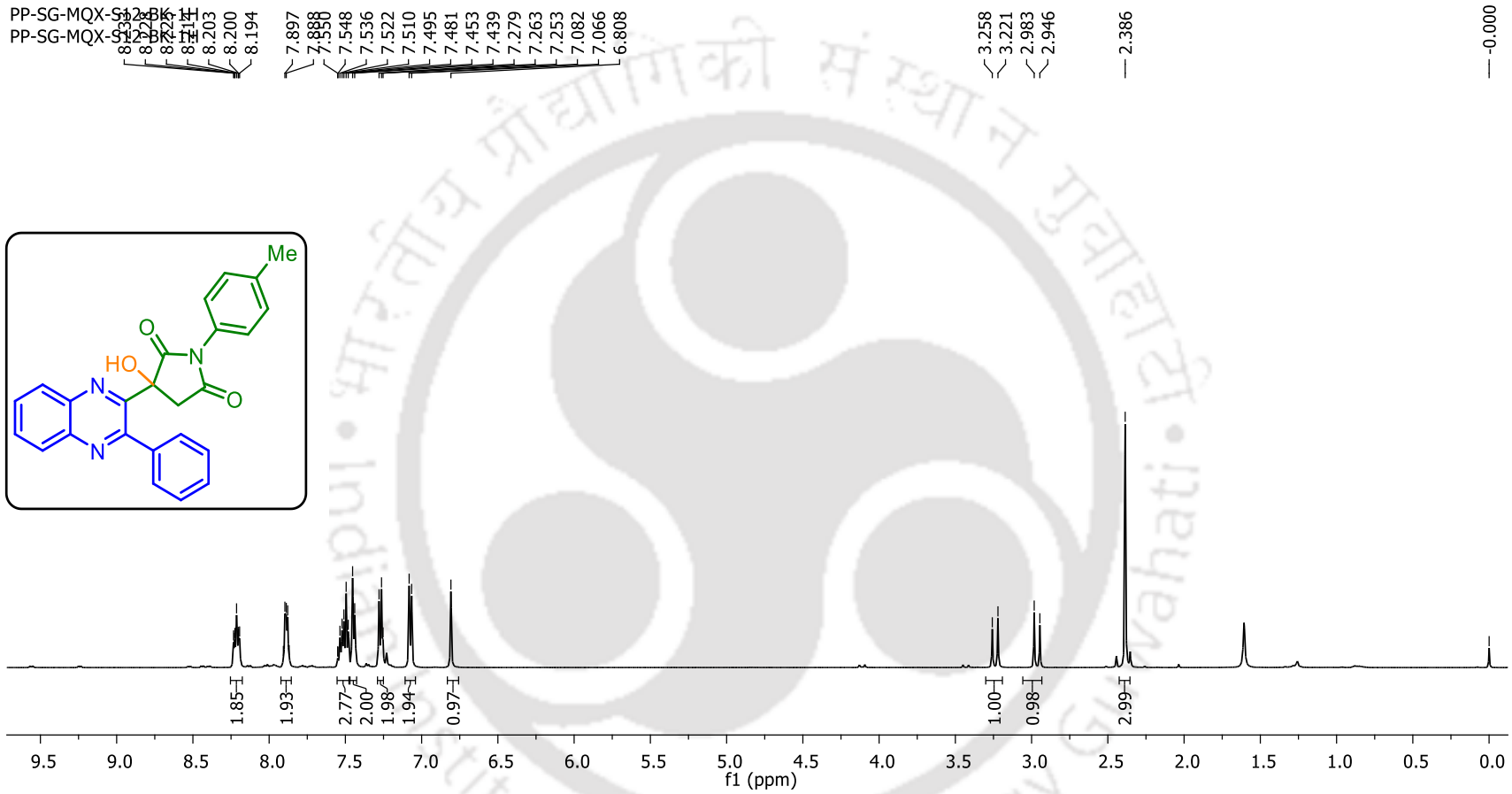

TH-3369_166122017

^{13}C {^{1}H} NMR of **3-Hydroxy-3-(3-phenylquinoxalin-2-yl)-1-(*p*-tolyl)pyrrolidine-2,5-dione** (**20a**) ($CDCl_3$, 126 MHz)

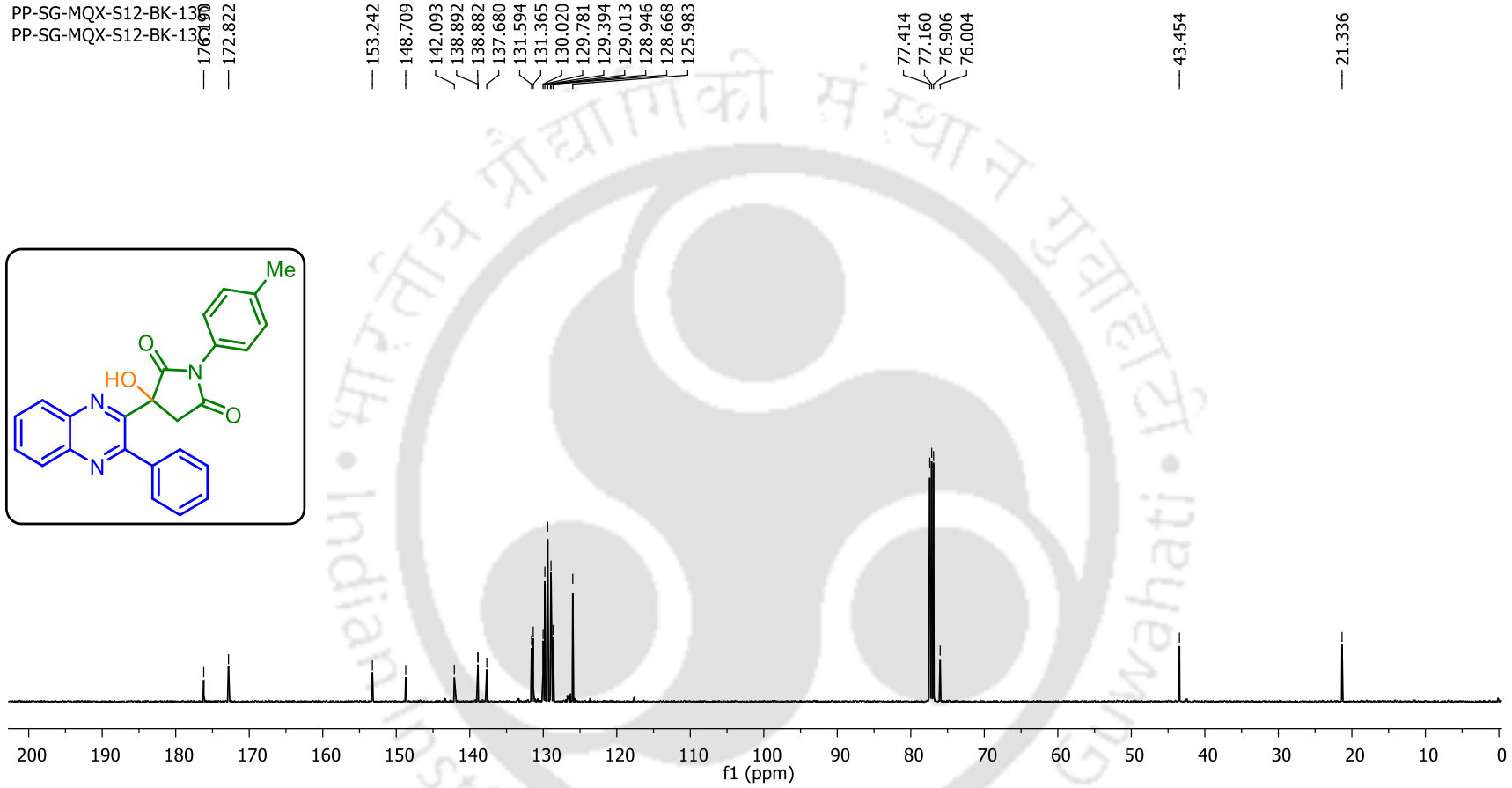

TH-3369_166122017

^{1}H NMR of **1-(4-Fluorophenyl)-3-hydroxy-3-(3-phenylquinoxalin-2-yl)pyrrolidine-2,5-dione** (**21a**) ($CDCl_3$, 400 MHz)

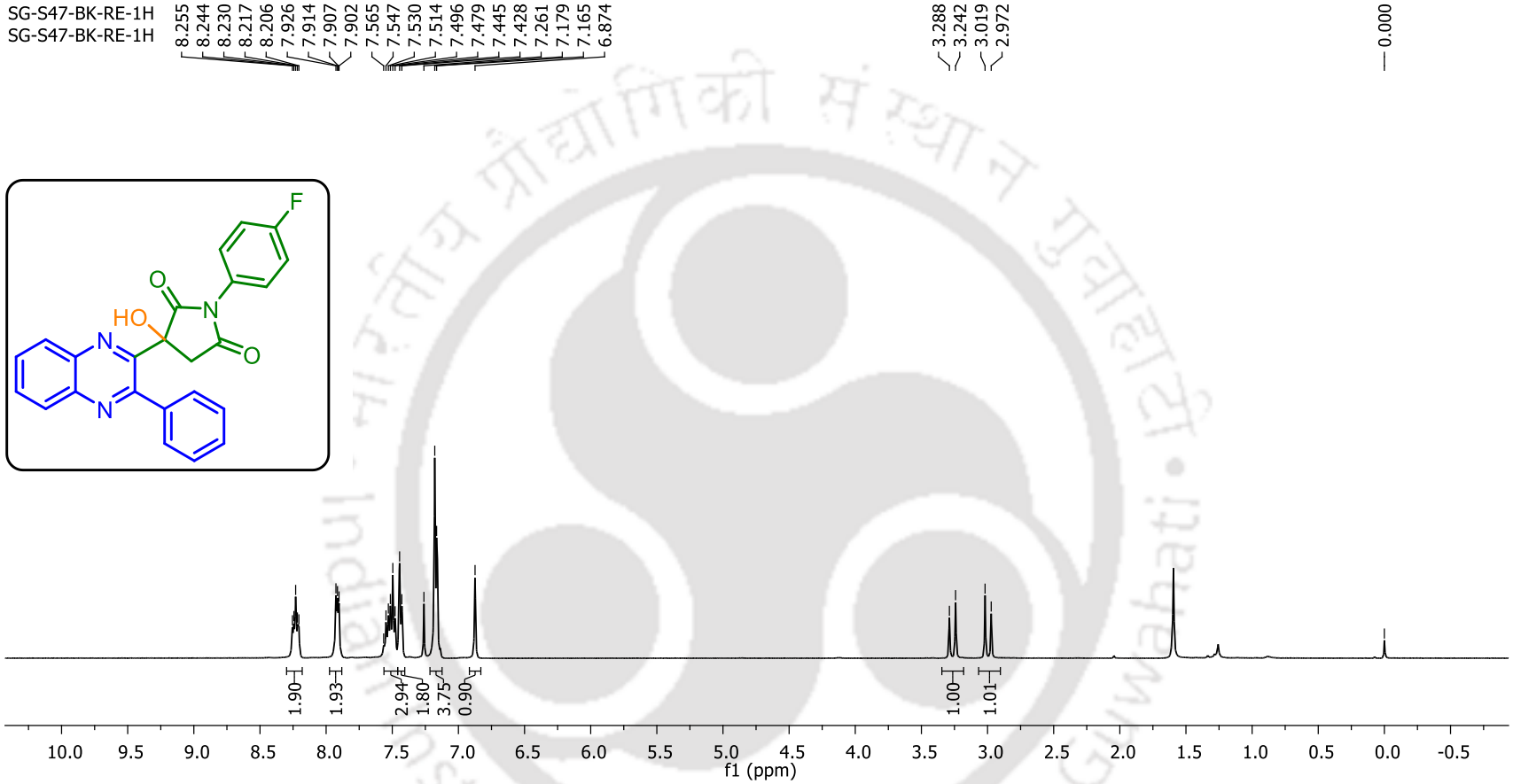

TH-3369_166122017

^{13}C {^{1}H} NMR of **1-(4-Fluorophenyl)-3-hydroxy-3-(3-phenylquinoxalin-2-yl)pyrrolidine-2,5-dione** (**21a**) ($CDCl_3$, 126 MHz)

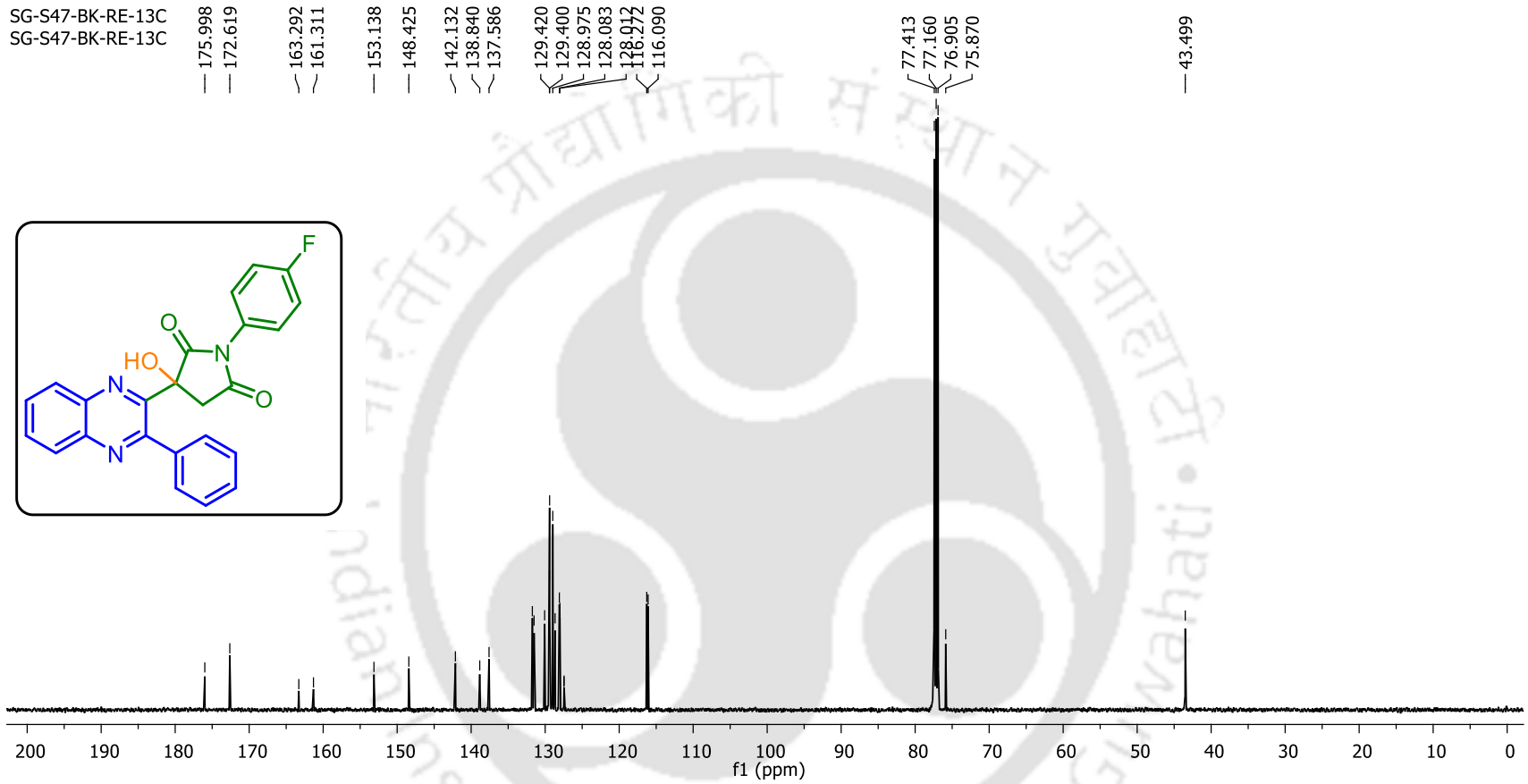

TH-3369_166122017

^{19}F NMR of **1-(4-Fluorophenyl)-3-hydroxy-3-(3-phenylquinoxalin-2-yl)pyrrolidine-2,5-dione** (**21a**) ($CDCl_3$)

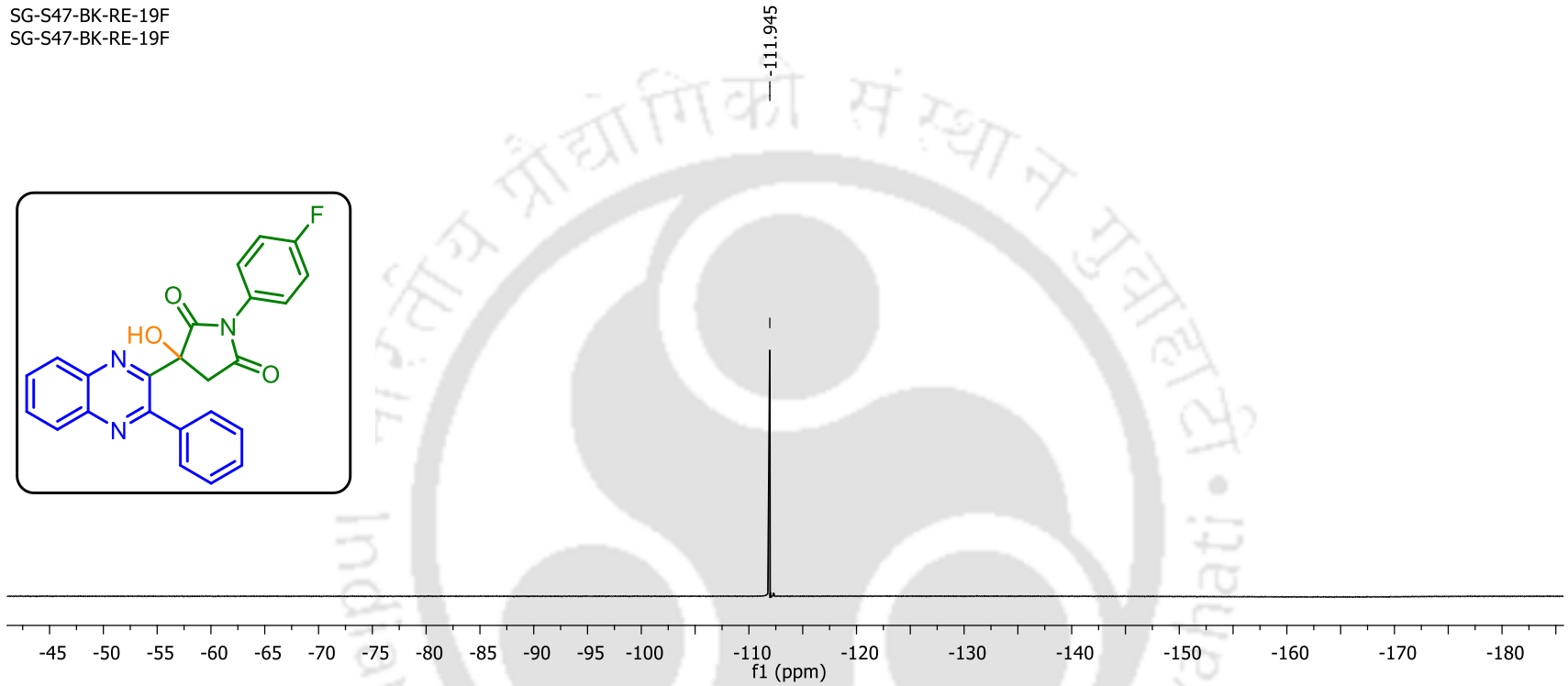

TH-3369_166122017

^{1}H NMR of **3-Hydroxy-1-(4-methoxybenzyl)-3-(3-phenylquinoxalin-2-yl)pyrrolidine-2,5-dione** (**22a**) ($CDCl_3$, 400 MHz)

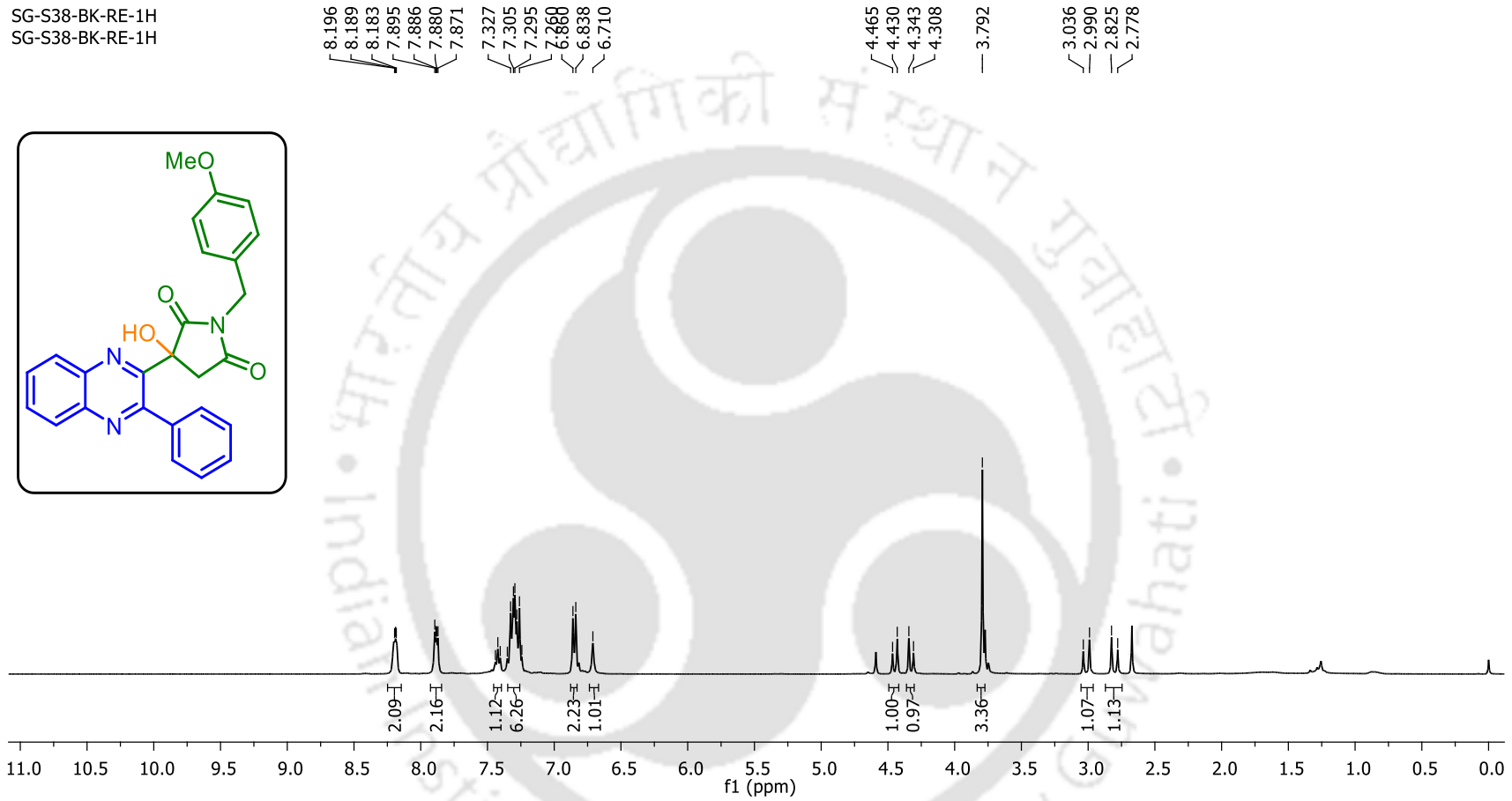

TH-3369_166122017

^{13}C {^{1}H} NMR of **3-Hydroxy-1-(4-methoxybenzyl)-3-(3-phenylquinoxalin-2-yl)pyrrolidine-2,5-dione** (**22a**) ($CDCl_3$, 126 MHz)

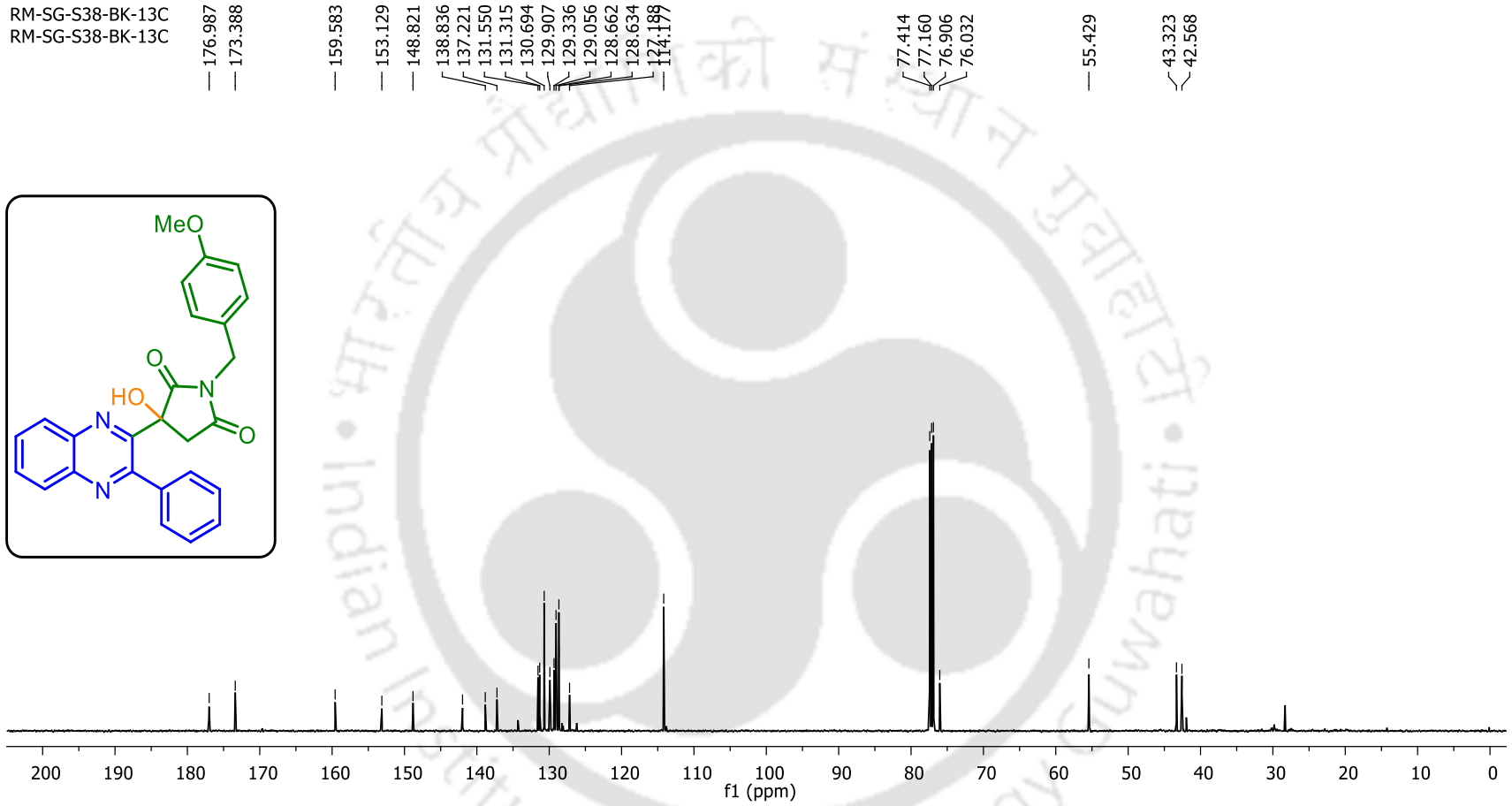

TH-3369_166122017

^{1}H NMR of **3-Hydroxy-1-(4-phenylbutyl)-3-(3-phenylquinoxalin-2-yl)pyrrolidine-2,5-dione (23a)** ($CDCl_3$, 500 MHz)

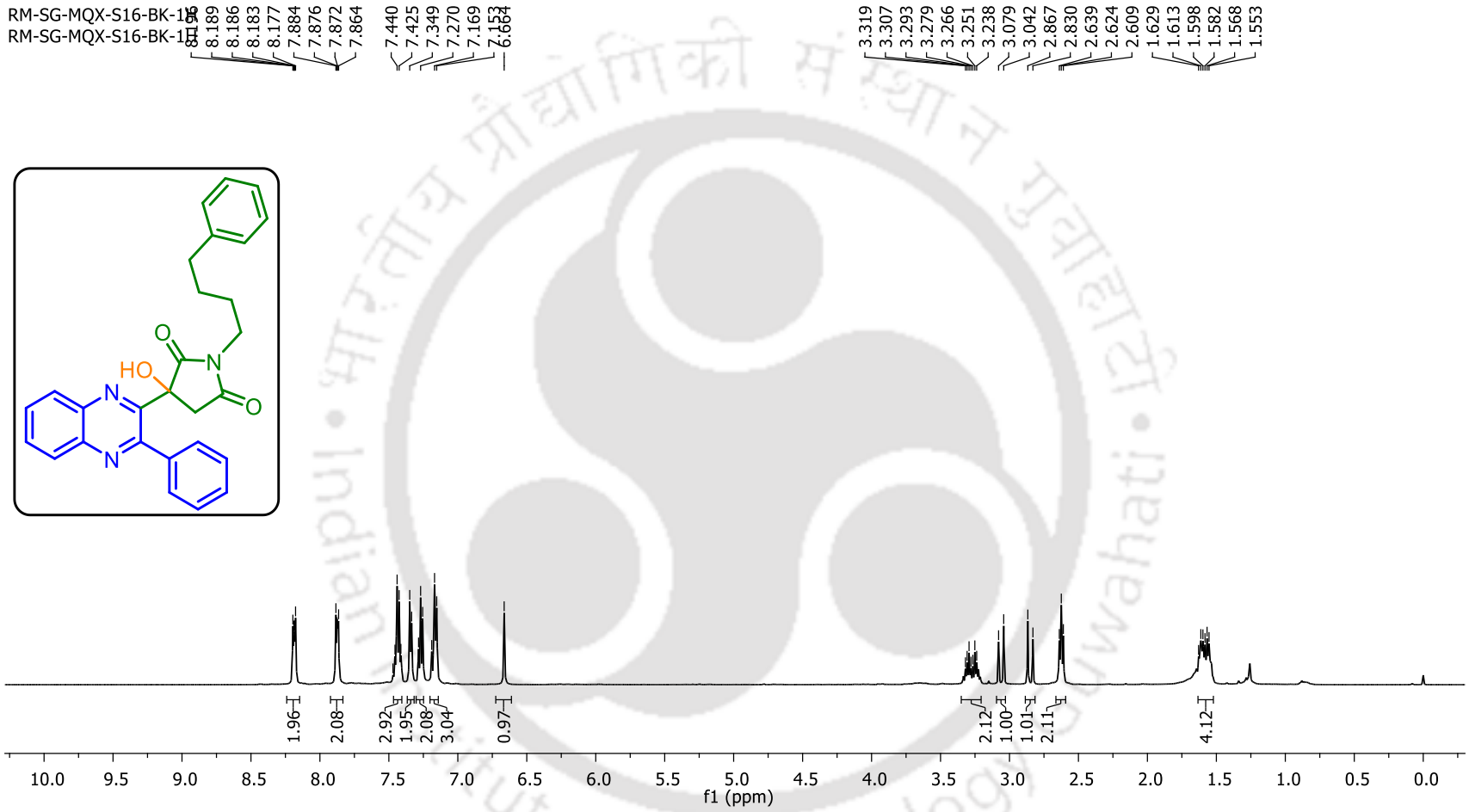

^{13}C {^{1}H} NMR of **3-Hydroxy-1-(4-phenylbutyl)-3-(3-phenylquinoxalin-2-yl)pyrrolidine-2,5-dione** (**23a**) ($CDCl_3$, 126 MHz)

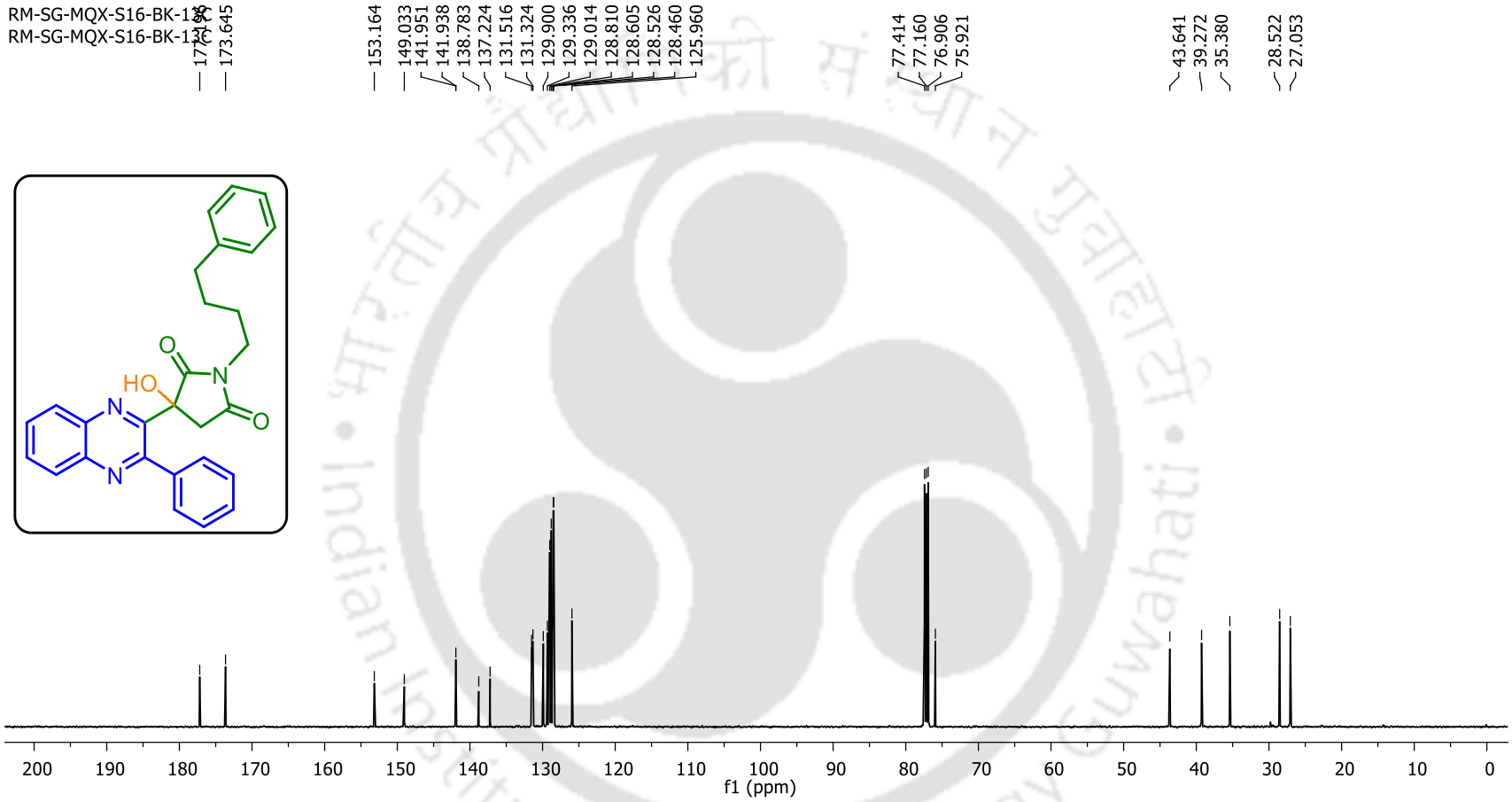

TH-3369_166122017

^{1}H NMR of **1-Heptyl-3-hydroxy-3-(3-phenylquinoxalin-2-yl)pyrrolidine-2,5-dione** (**24a**) ($CDCl_3$, 500 MHz)

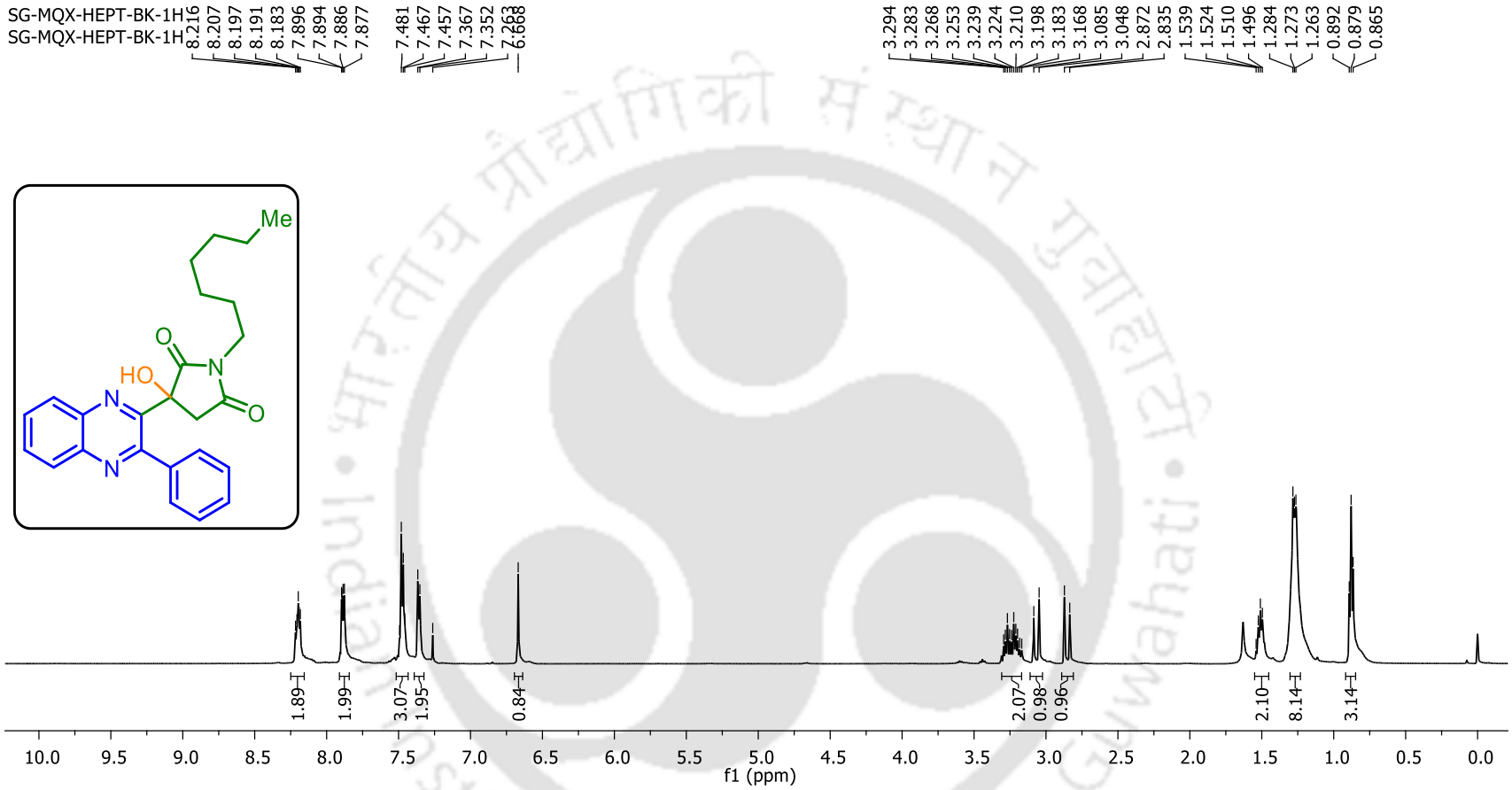

TH-3369_166122017

^{13}C {^{1}H} NMR of **1-Heptyl-3-hydroxy-3-(3-phenylquinoxalin-2-yl)pyrrolidine-2,5-dione** (**24a**) ($CDCl_3$, 126 MHz)

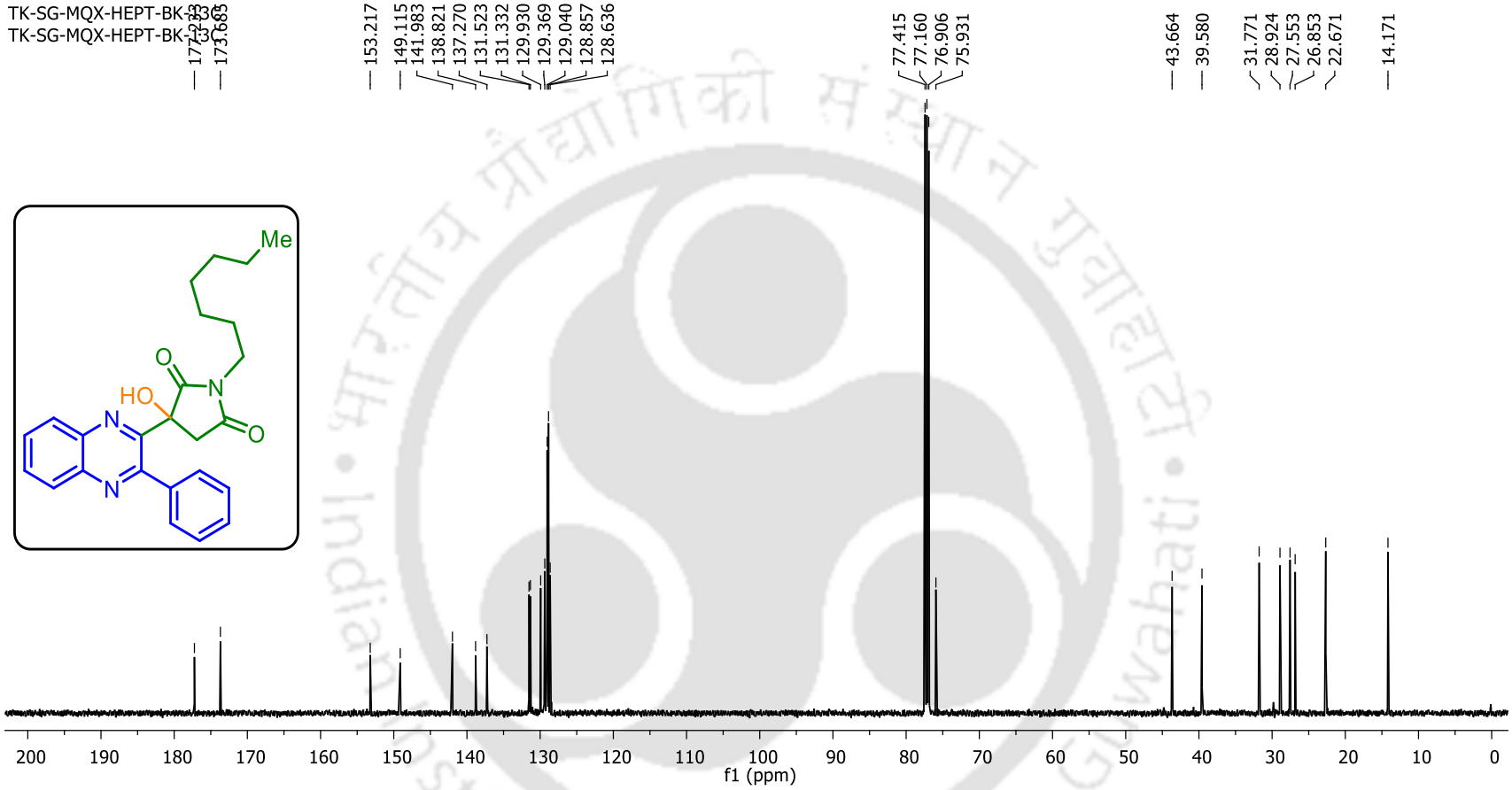

^{1}H NMR of **1-Decyl-3-hydroxy-3-(3-phenylquinoxalin-2-yl)pyrrolidine-2,5-dione** (**25a**) ($CDCl_3$, 500 MHz)

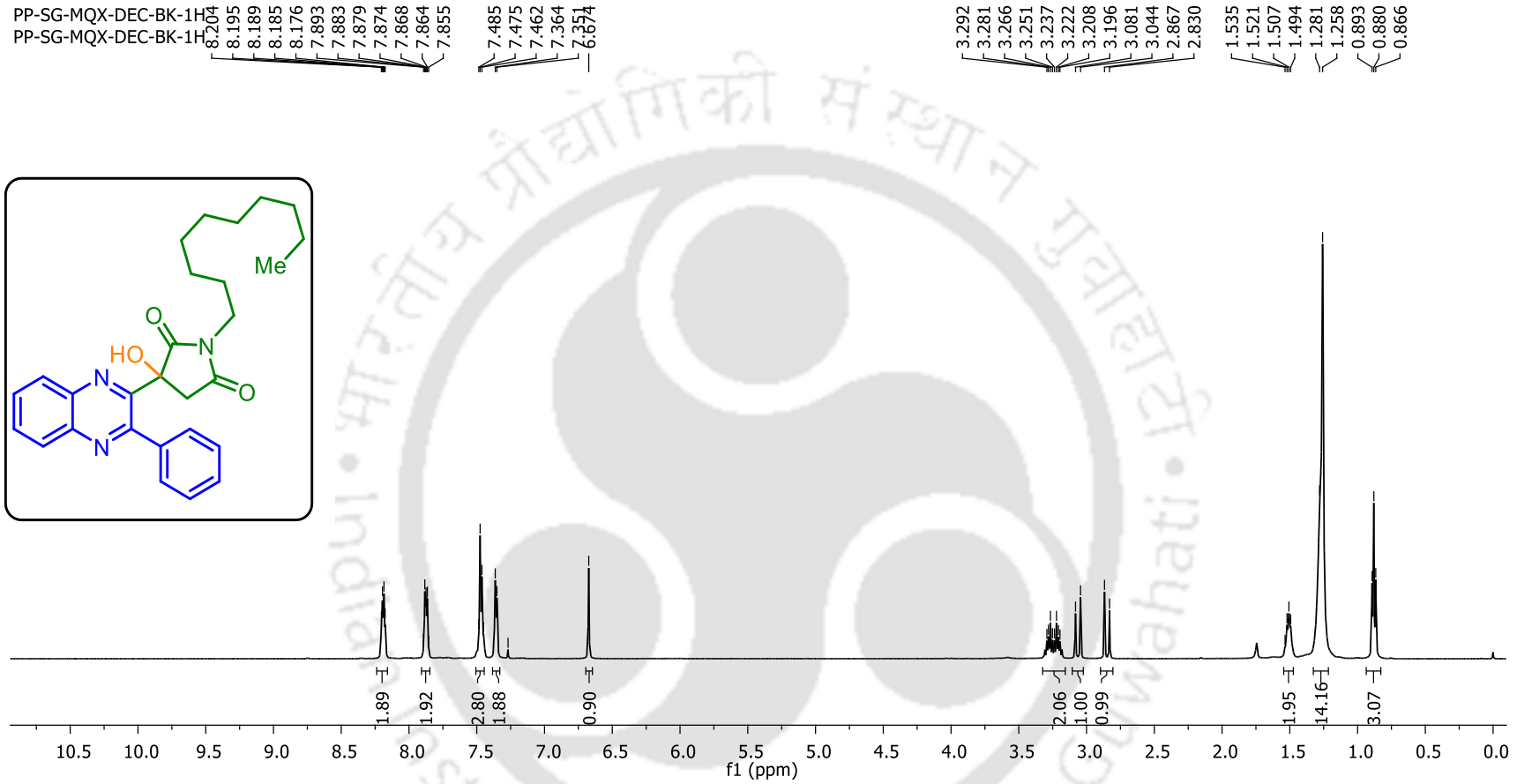

TH-3369_166122017

^{13}C {^{1}H} NMR of **1-Decyl-3-hydroxy-3-(3-phenylquinoxalin-2-yl)pyrrolidine-2,5-dione** (**25a**) ($CDCl_3$, 126 MHz)

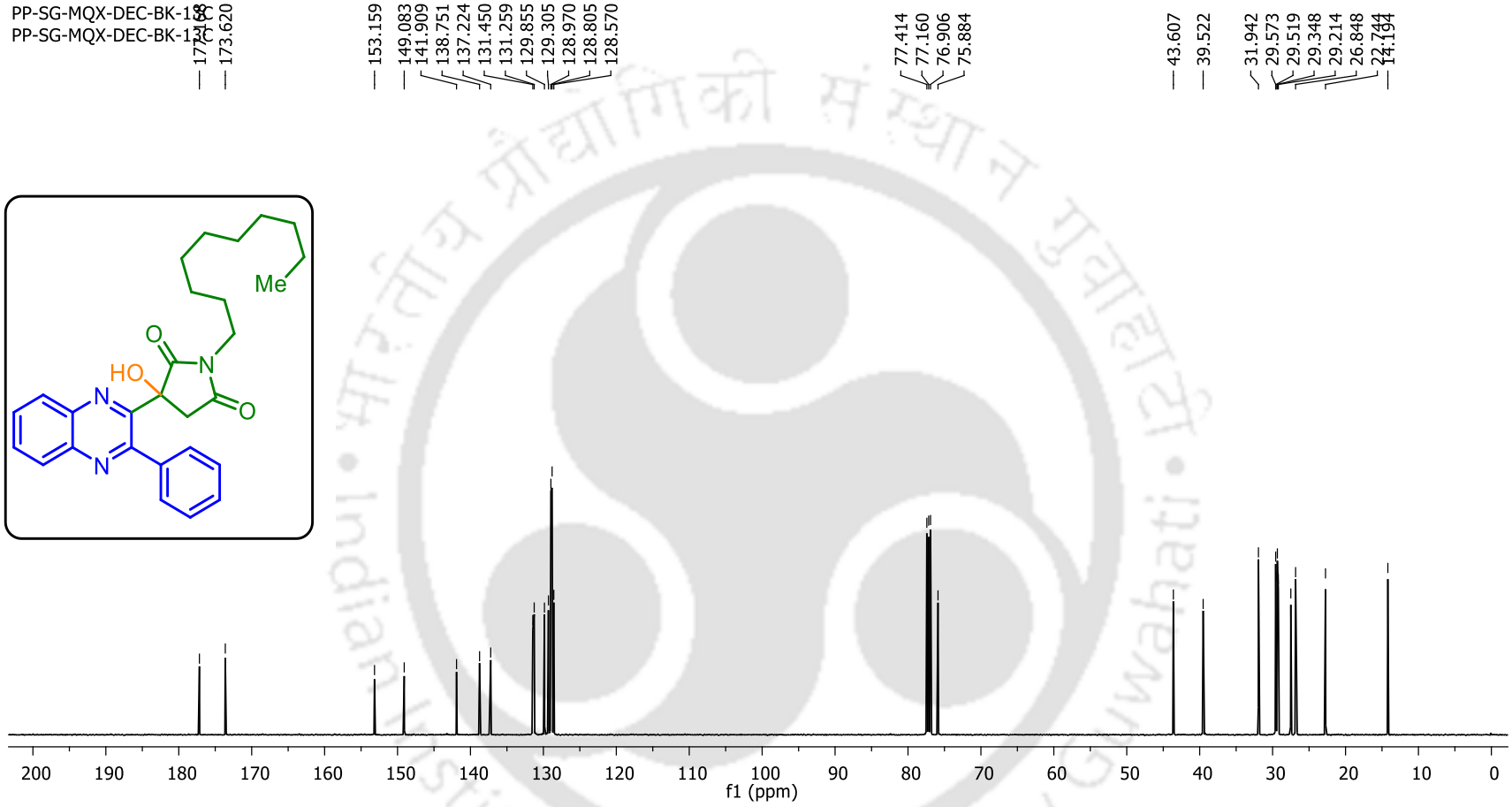

TH-3369_166122017

^{1}H NMR of **3-Hydroxy-3-(3-phenylquinoxalin-2-yl)pyrrolidine-2,5-dione** (**26a**) ($CDCl_3$, 400 MHz)

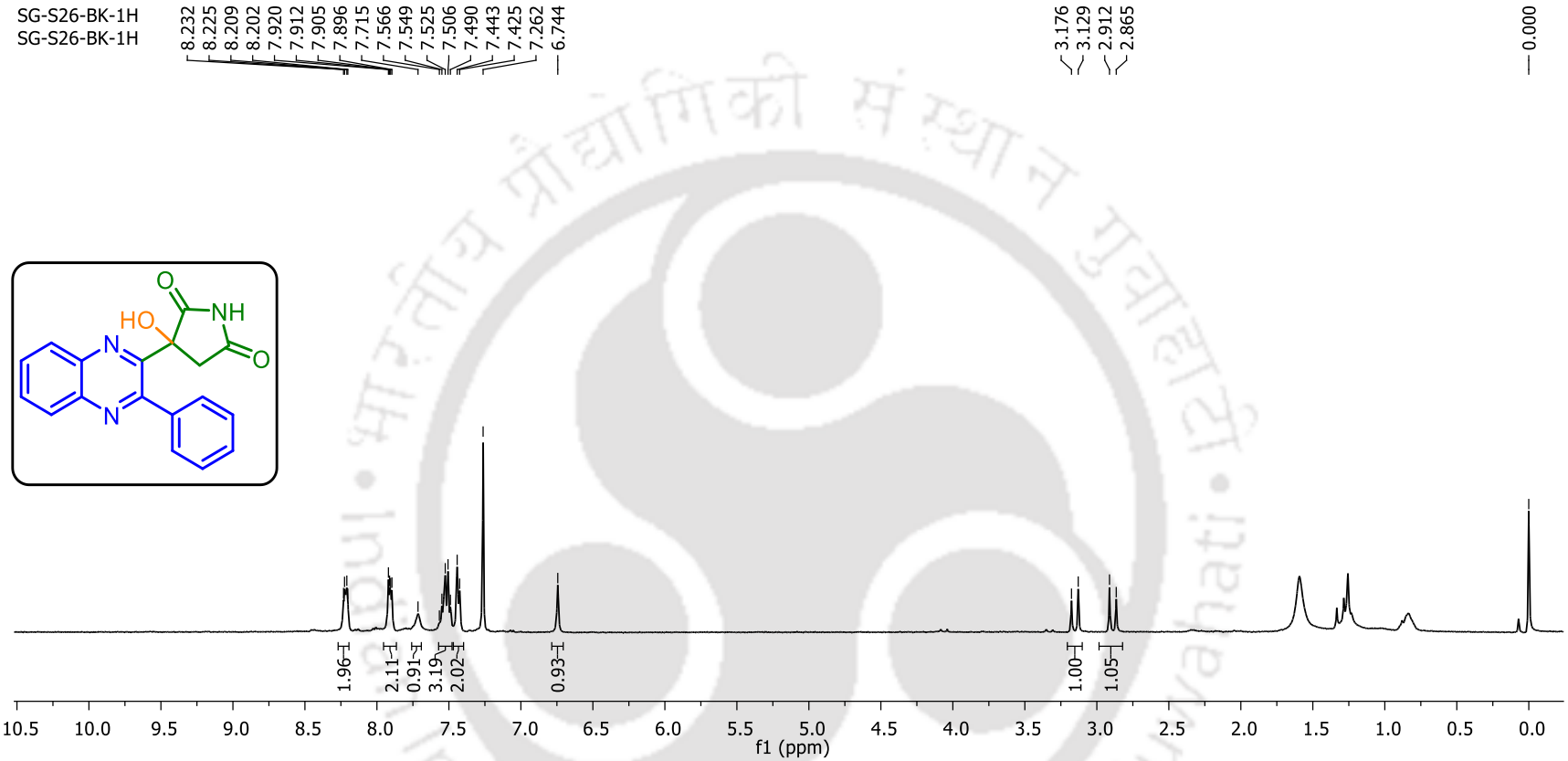

TH-3369_166122017

^{13}C {^{1}H} NMR of **3-Hydroxy-3-(3-phenylquinoxalin-2-yl)pyrrolidine-2,5-dione** (**26a**) ($CDCl_3$, 126 MHz)

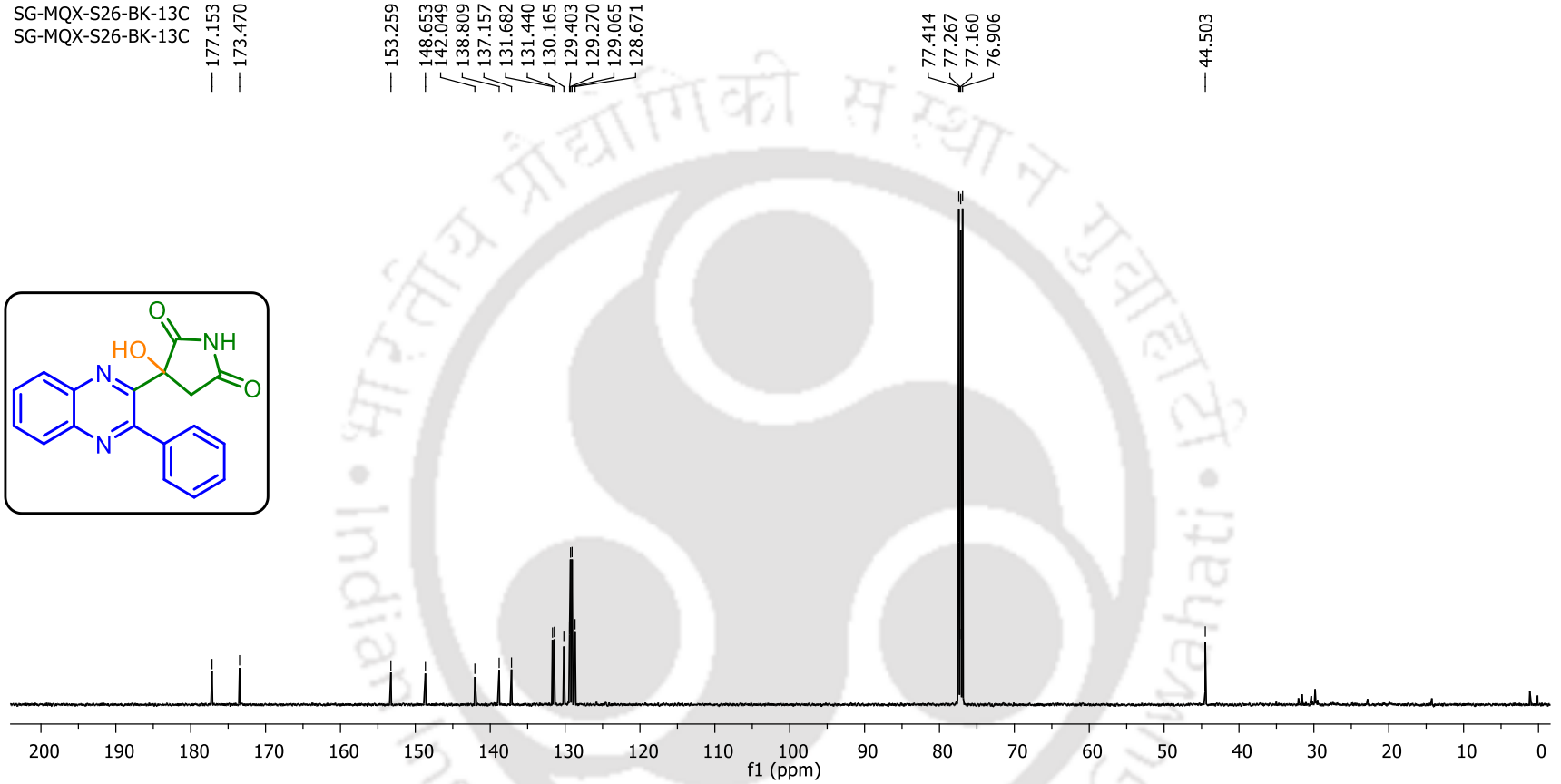

TH-3369_166122017

^{1}H NMR of **3-Hydroxy-1-((*S*)-1-(naphthalen-1-yl)ethyl)-3-(3-phenylquinoxalin-2-yl)pyrrolidine-2,5-dione** (**27a**) ($CDCl_3$, 400 MHz)

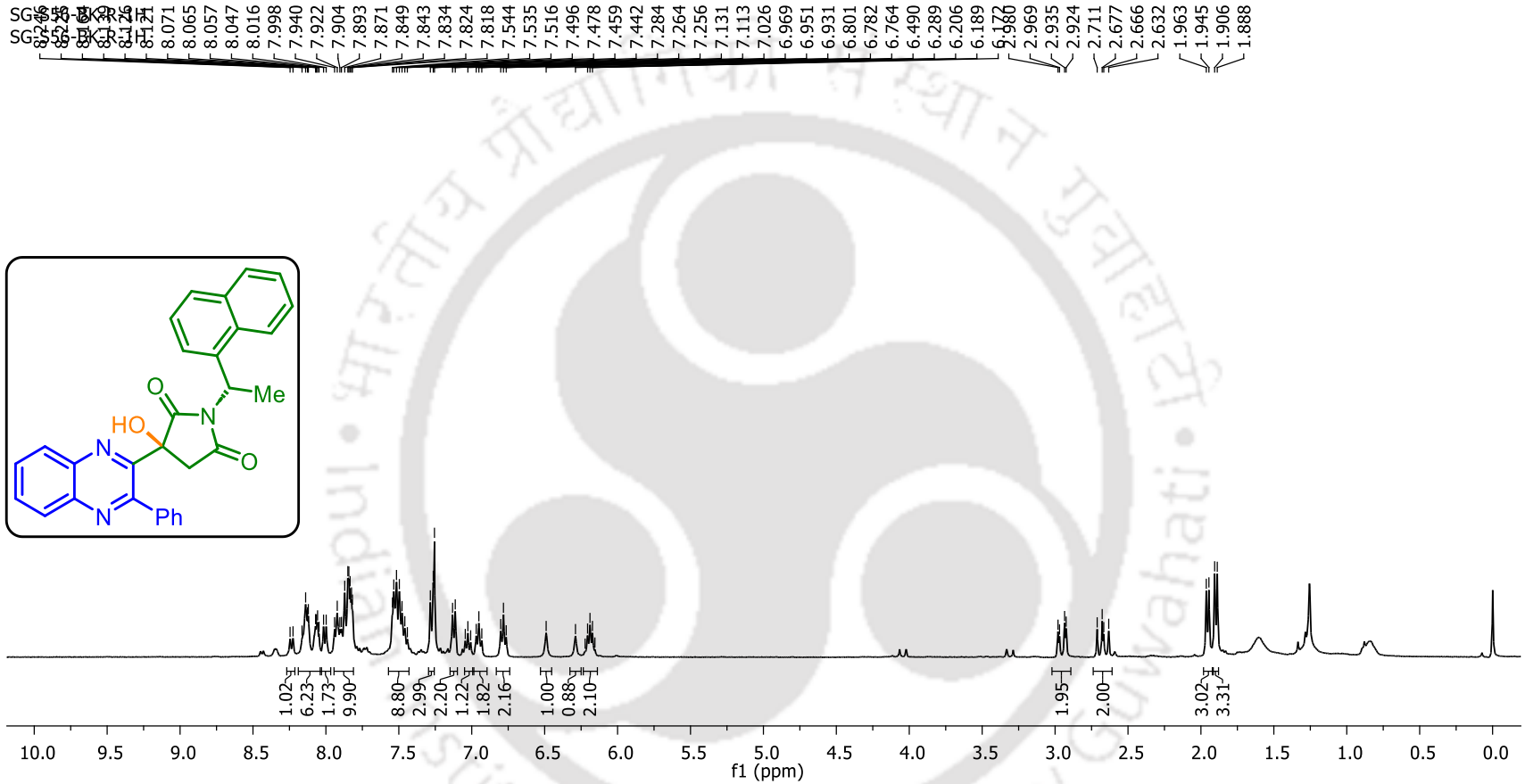

TH-3369_166122017

^{13}C {^{1}H} NMR of **3-Hydroxy-1-((*S*)-1-(naphthalen-1-yl)ethyl)-3-(3-phenylquinoxalin-2-yl)pyrrolidine-2,5-dione** (**27a**) ($CDCl_3$, 126 MHz)

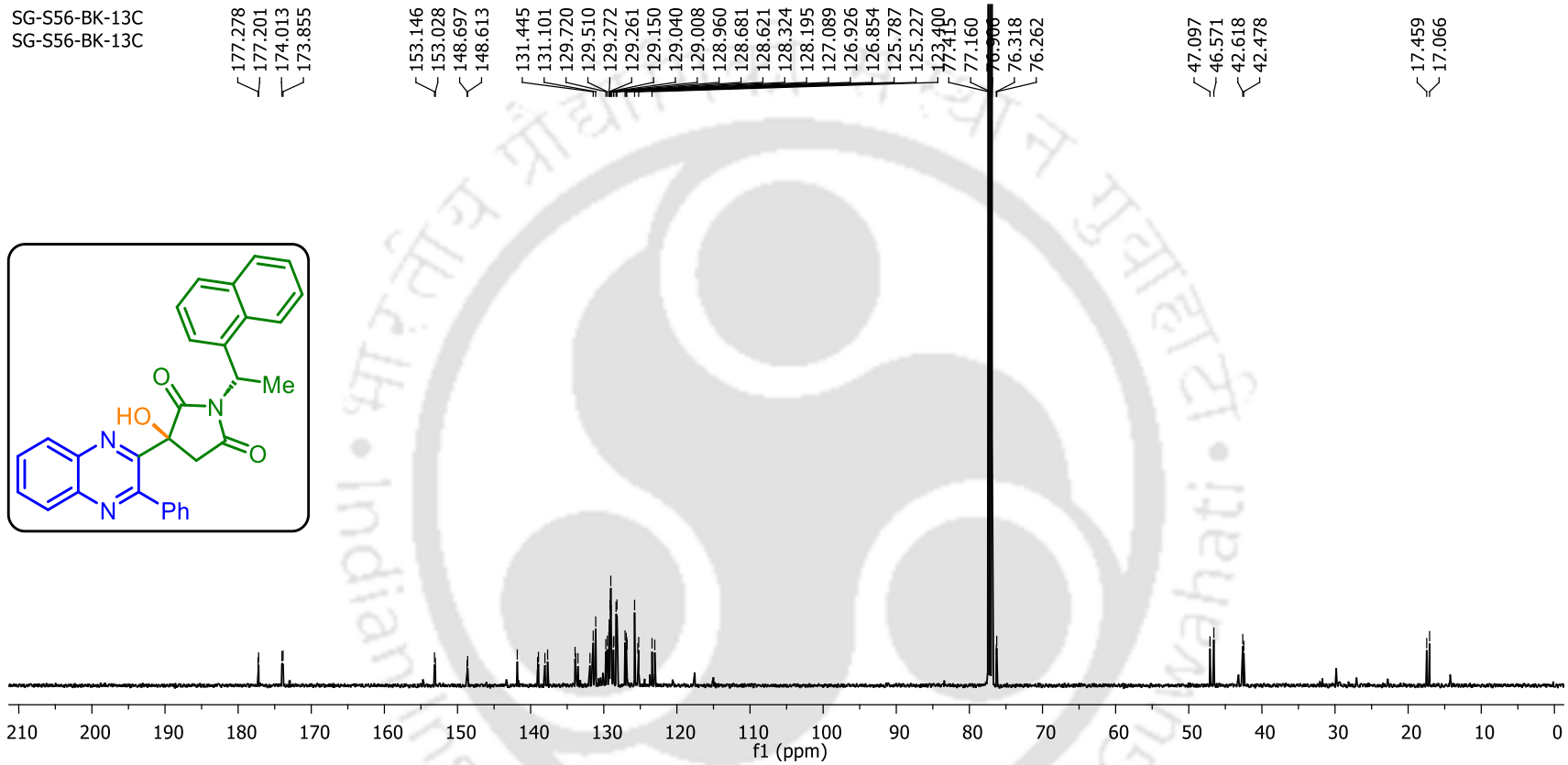

TH-3369_166122017

^{1}H NMR of **3-Hydroxy-1-((*S*)-1-phenylethyl)-3-(3-phenylquinoxalin-2-yl)pyrrolidine-2,5-dione** (**28a**) ($CDCl_3$, 400 MHz)

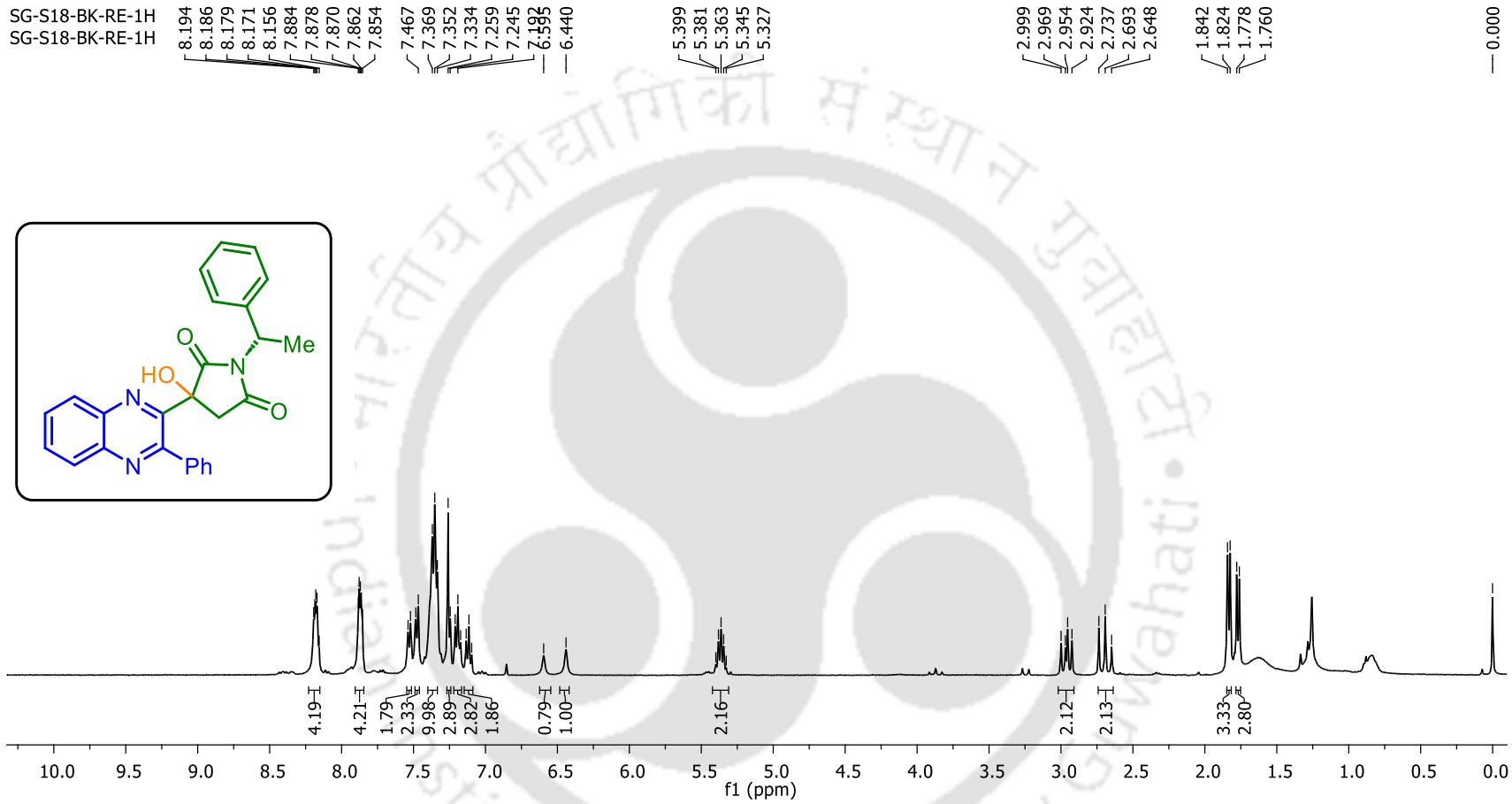

TH-3369_166122017

^{13}C {^{1}H} NMR of **3-Hydroxy-1-((*S*)-1-phenylethyl)-3-(3-phenylquinoxalin-2-yl)pyrrolidine-2,5-dione** (**28a**) ($CDCl_3$, 126 MHz)

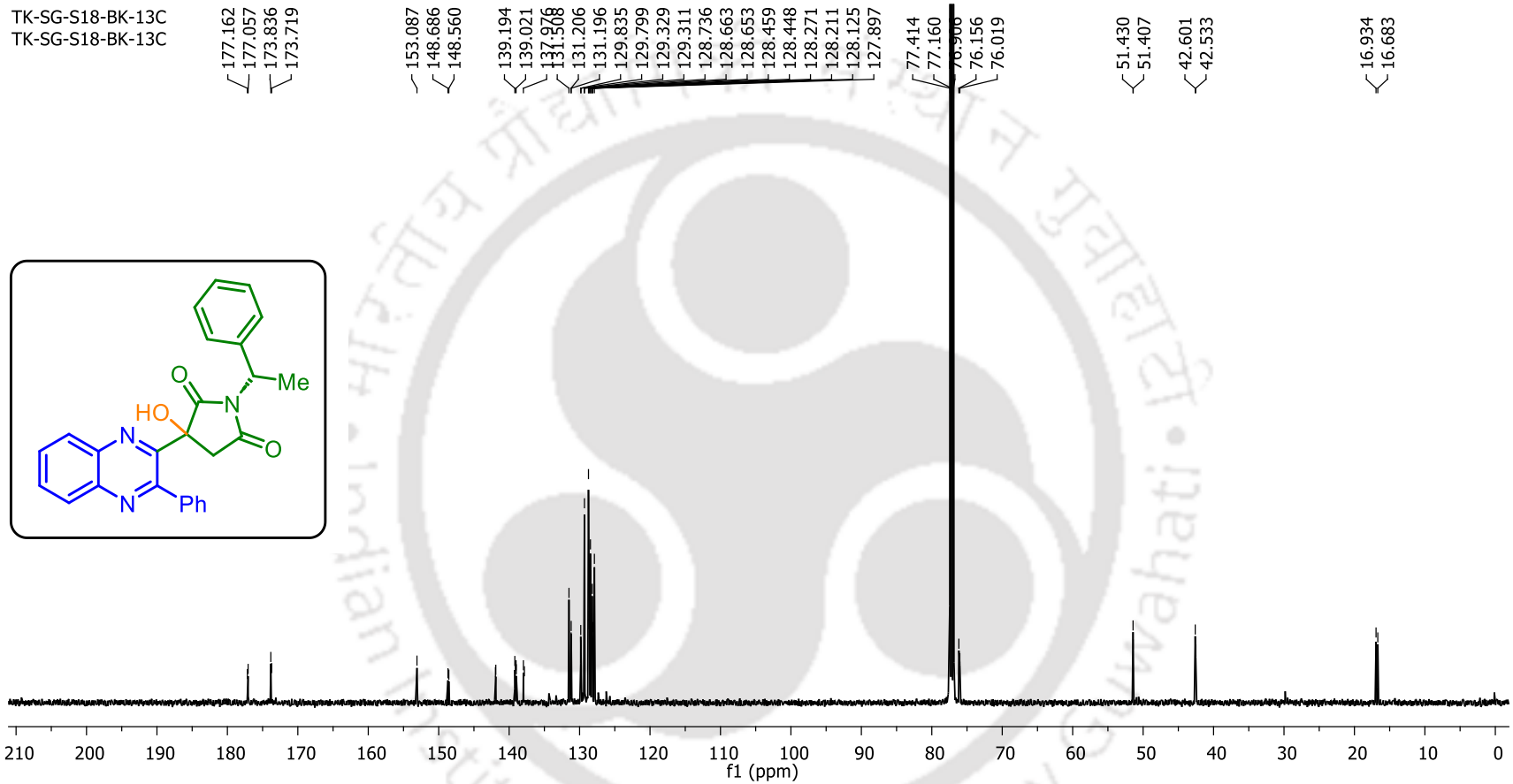

TH-3369_166122017

^{1}H NMR of **3-Hydroxy-1-phenethyl-3-(3-phenylquinoxalin-2-yl)pyrrolidine-2,5-dione** (**29a**) ($CDCl_3$, 500 MHz)

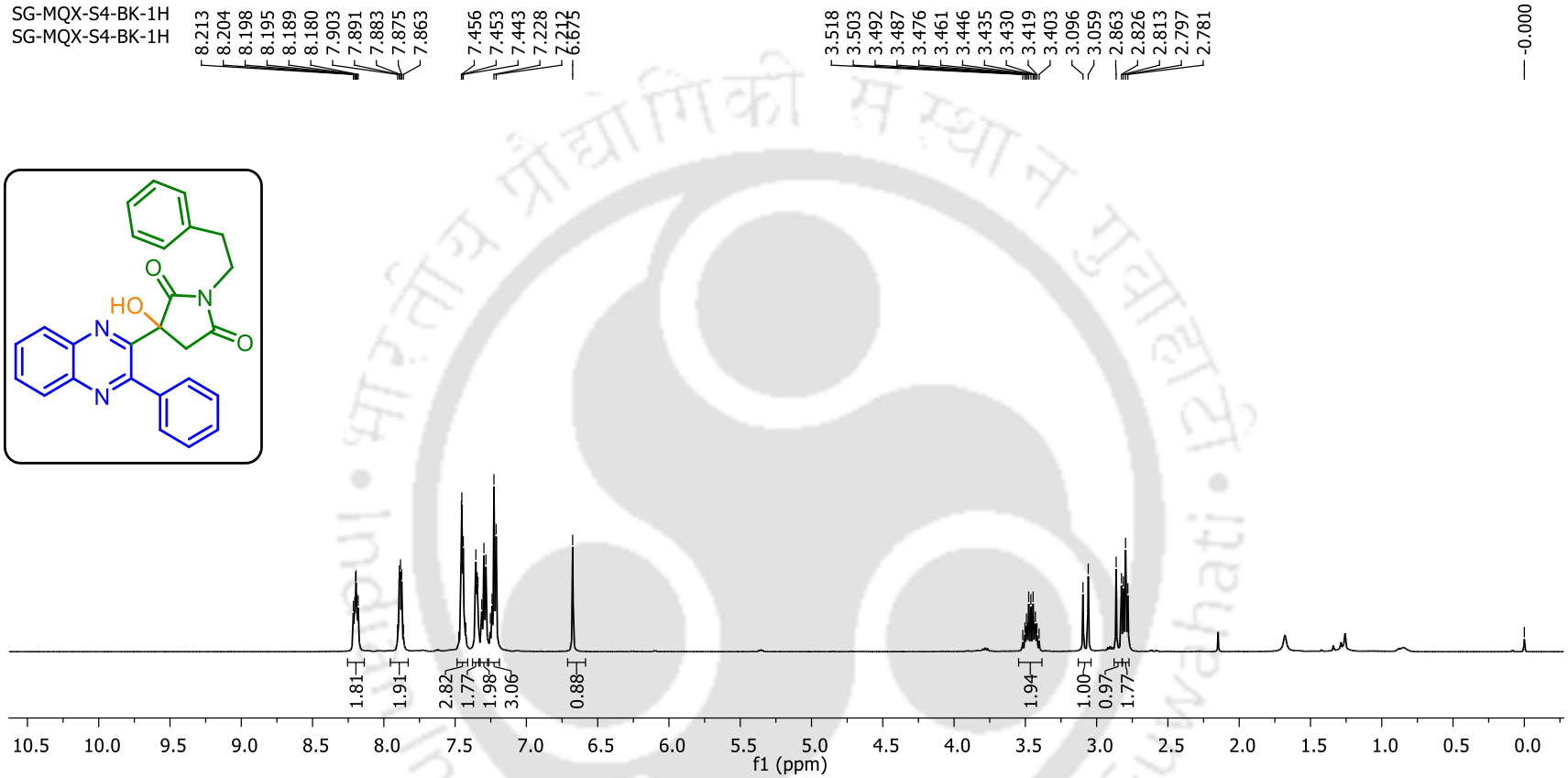

TH-3369_166122017

^{13}C {^{1}H} NMR of **3-Hydroxy-1-phenethyl-3-(3-phenylquinoxalin-2-yl)pyrrolidine-2,5-dione** (**29a**) ($CDCl_3$, 126 MHz)

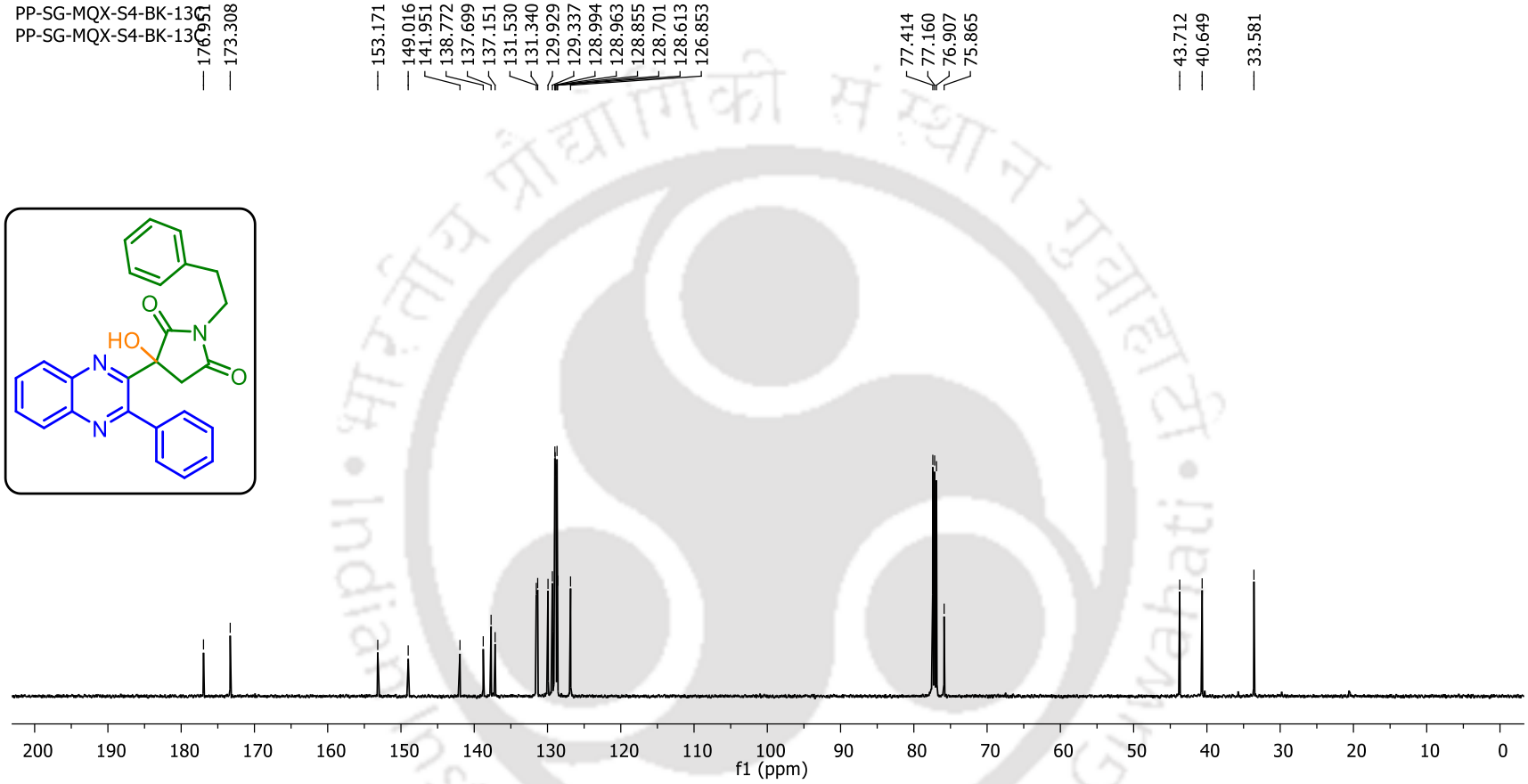

TH-3369_166122017

^{1}H NMR of **3-Hydroxy-3-(3-phenylquinoxalin-2-yl)-1-(2-(thiophen-2-yl)ethyl)pyrrolidine-2,5-dione** (**30a**) ($CDCl_3$, 500 MHz)

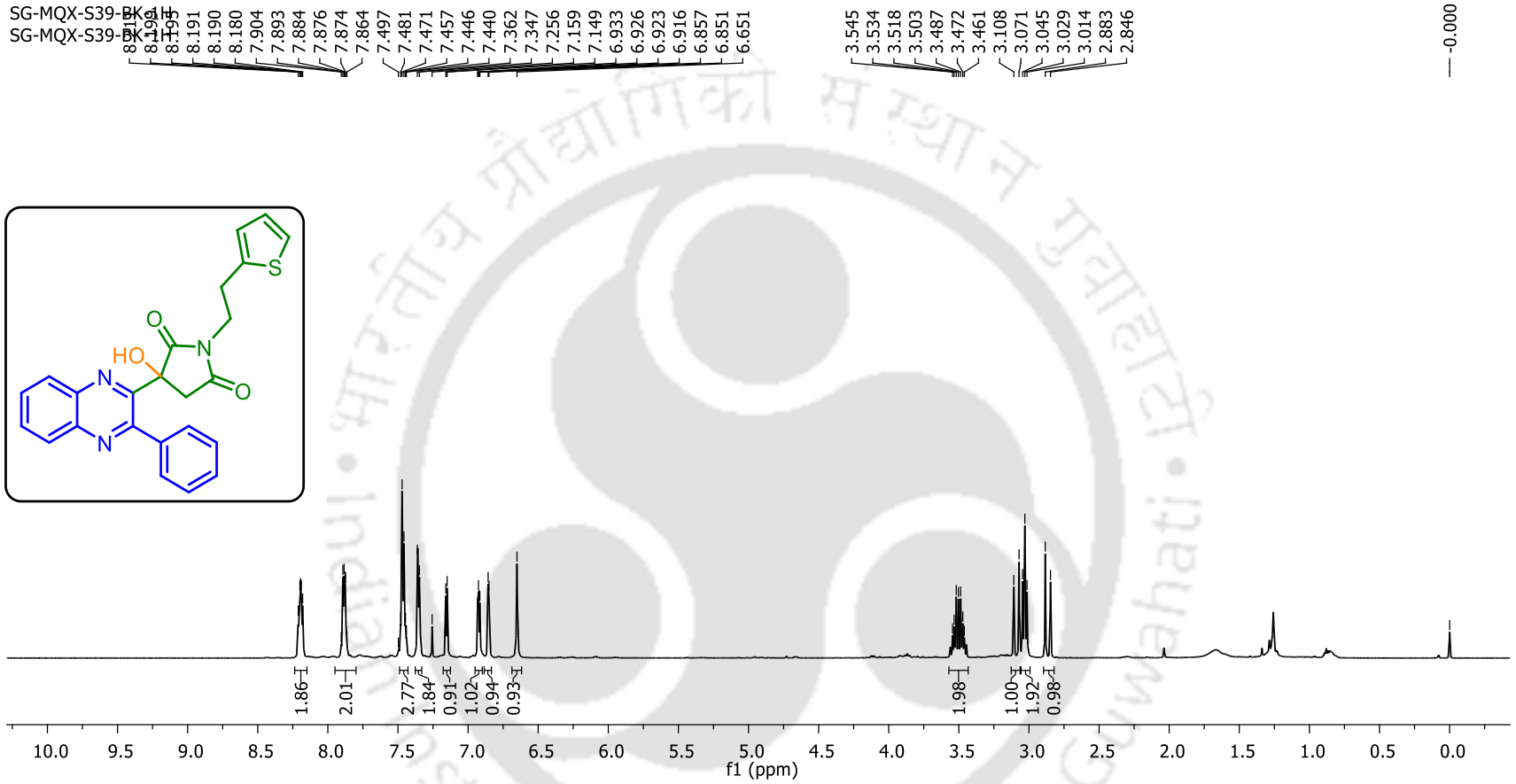

TH-3369_166122017

^{13}C {^{1}H} NMR of **3-Hydroxy-3-(3-phenylquinoxalin-2-yl)-1-(2-(thiophen-2-yl)ethyl)pyrrolidine-2,5-dione** (**30a**) ($CDCl_3$, 126 MHz)

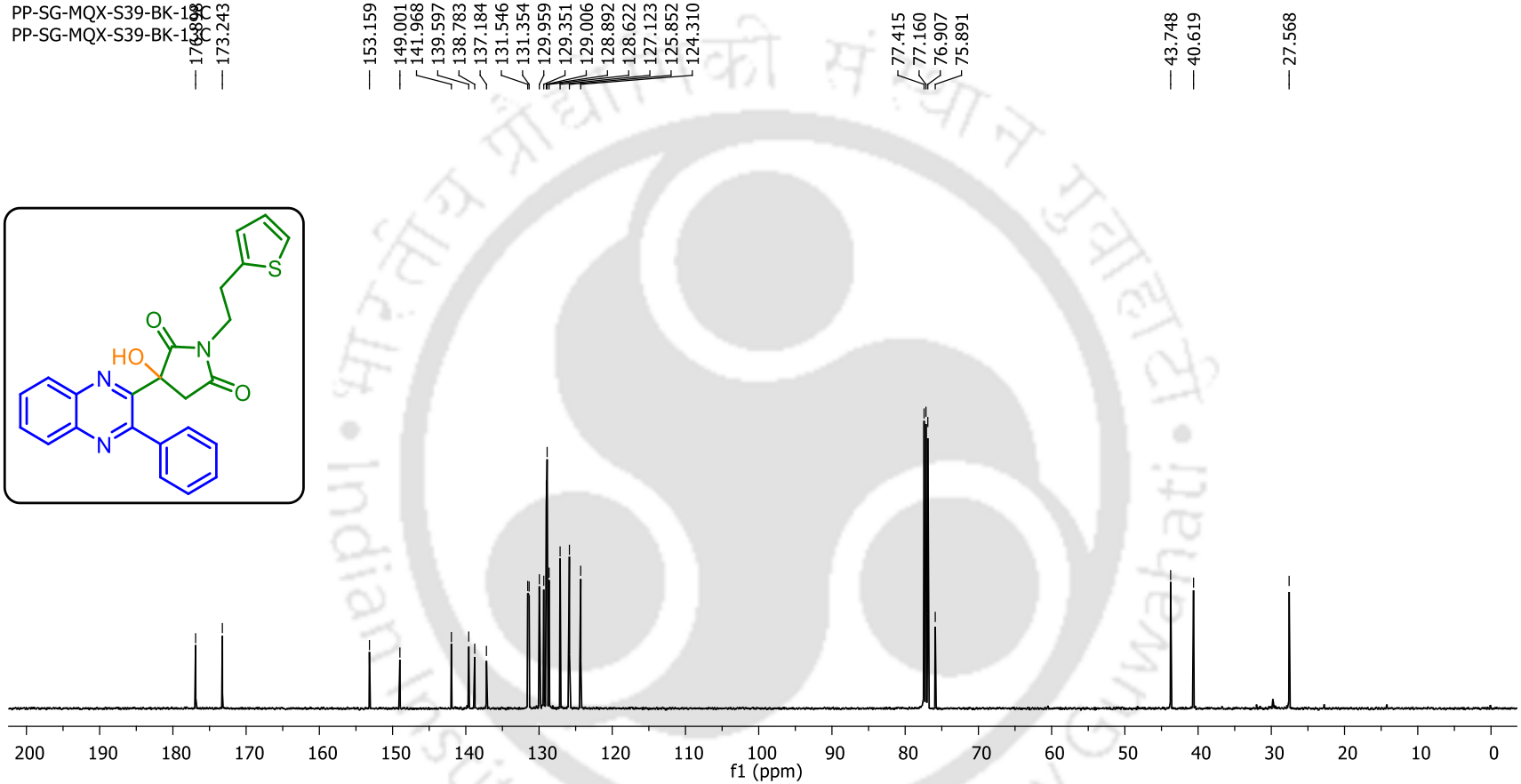

TH-3369_166122017

^{1}H NMR of **(1*S*,2*R*,5*S*)-2-isopropyl-5-methylcyclohexyl-4-(3-(3-hydroxy-2,5-dioxo-1-phenylpyrrolidin-3-yl)quinoxalin-2-yl)benzoate** (**31a**) ($CDCl_3$, 500 MHz)

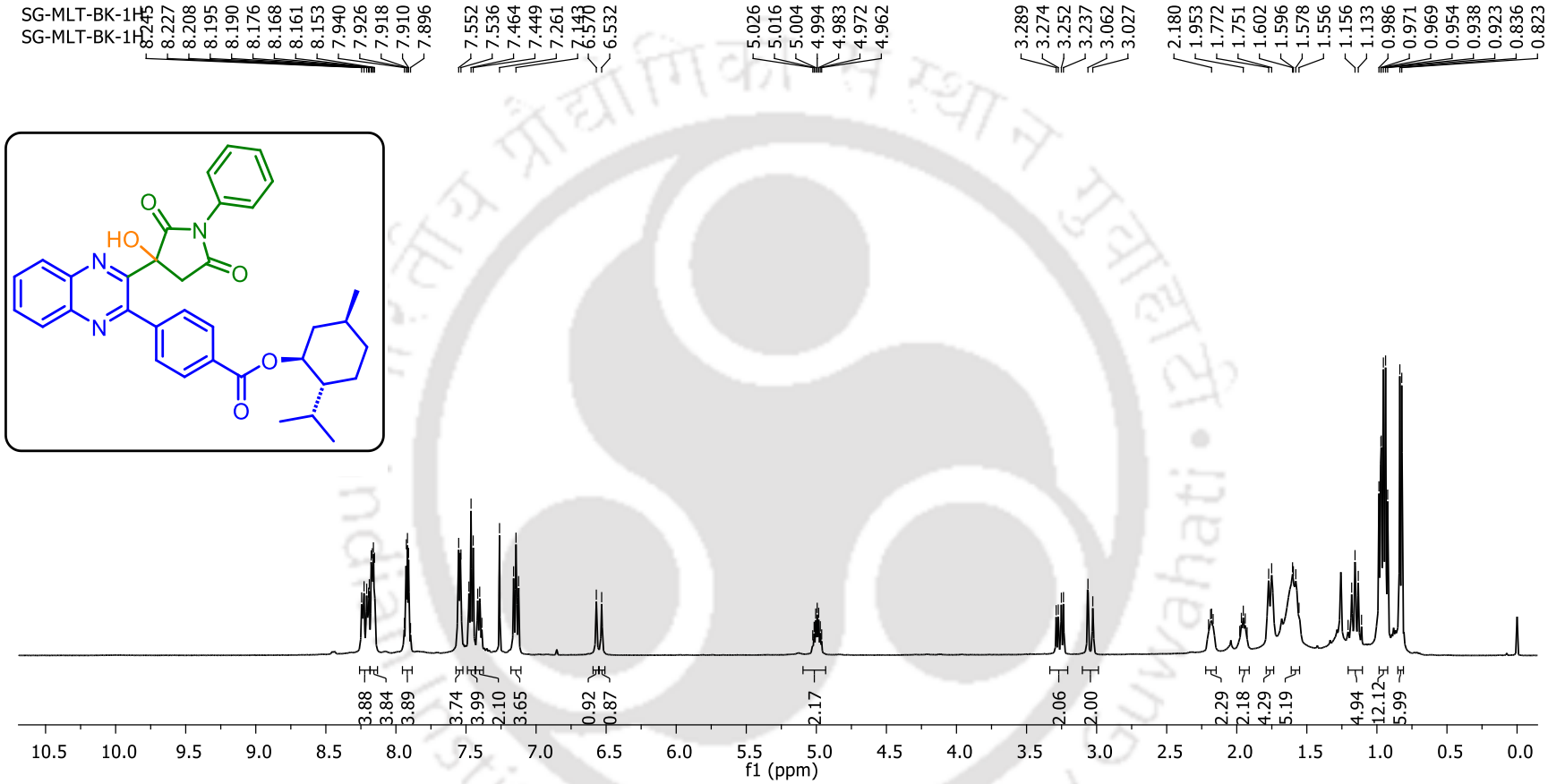

TH-3369_166122017

^{13}C {^{1}H} NMR of **(1*S*,2*R*,5*S*)-2-isopropyl-5-methylcyclohexyl-4-(3-(3-hydroxy-2,5-dioxo-1-phenylpyrrolidin-3-yl)quinoxalin-2-yl)benzoate** (**31a**) ($CDCl_3$, 126 MHz)

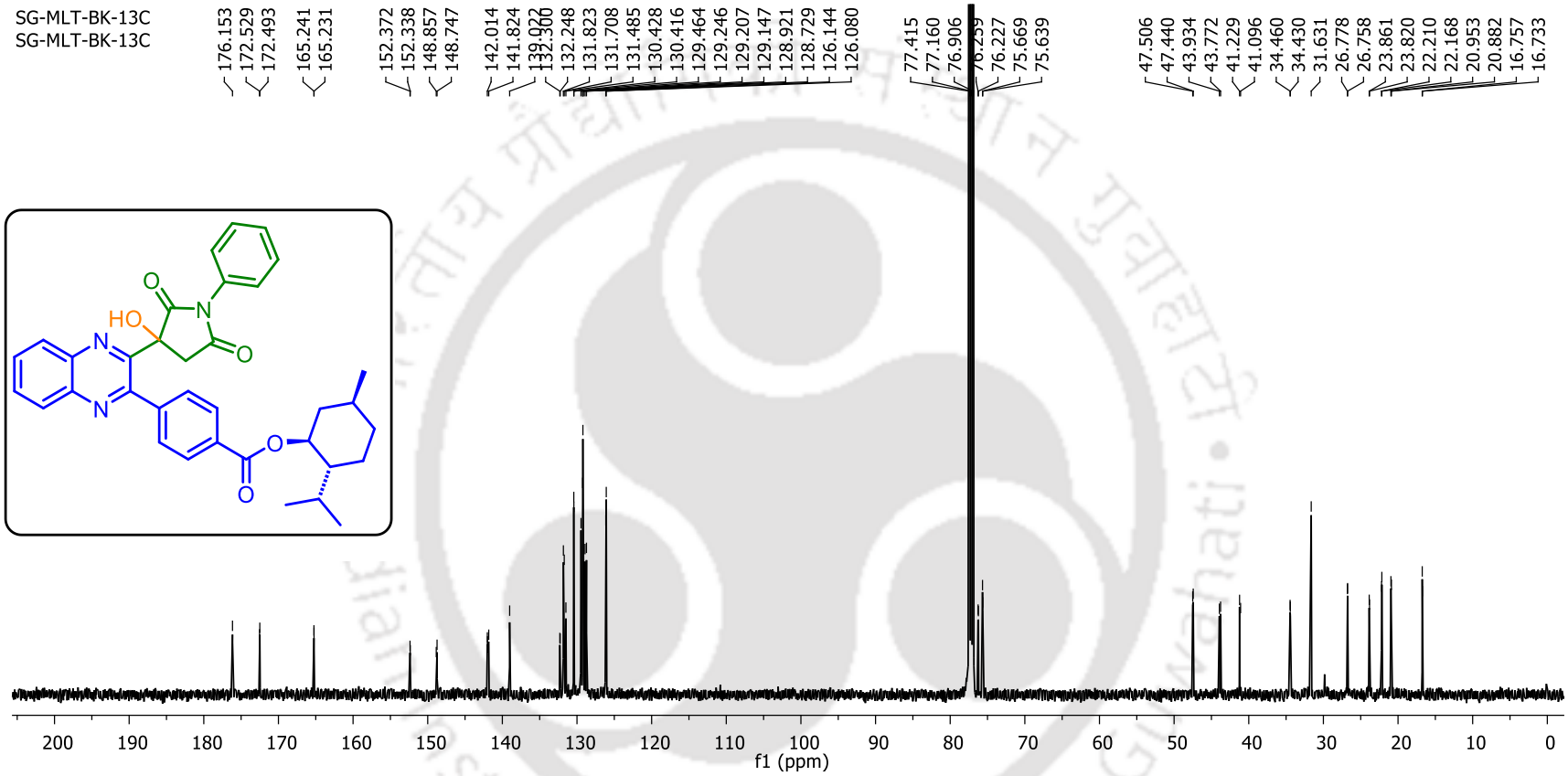

TH-3369_166122017

^{1}H NMR of **1,7,7-Trimethylbicyclo[2.2.1]heptan-2-yl-4-(3-(3-hydroxy-2,5-dioxo-1-phenylpyrrolidin-3-yl)quinoxalin-2-yl)benzoate** (**32a**) ($CDCl_3$, 500 MHz)

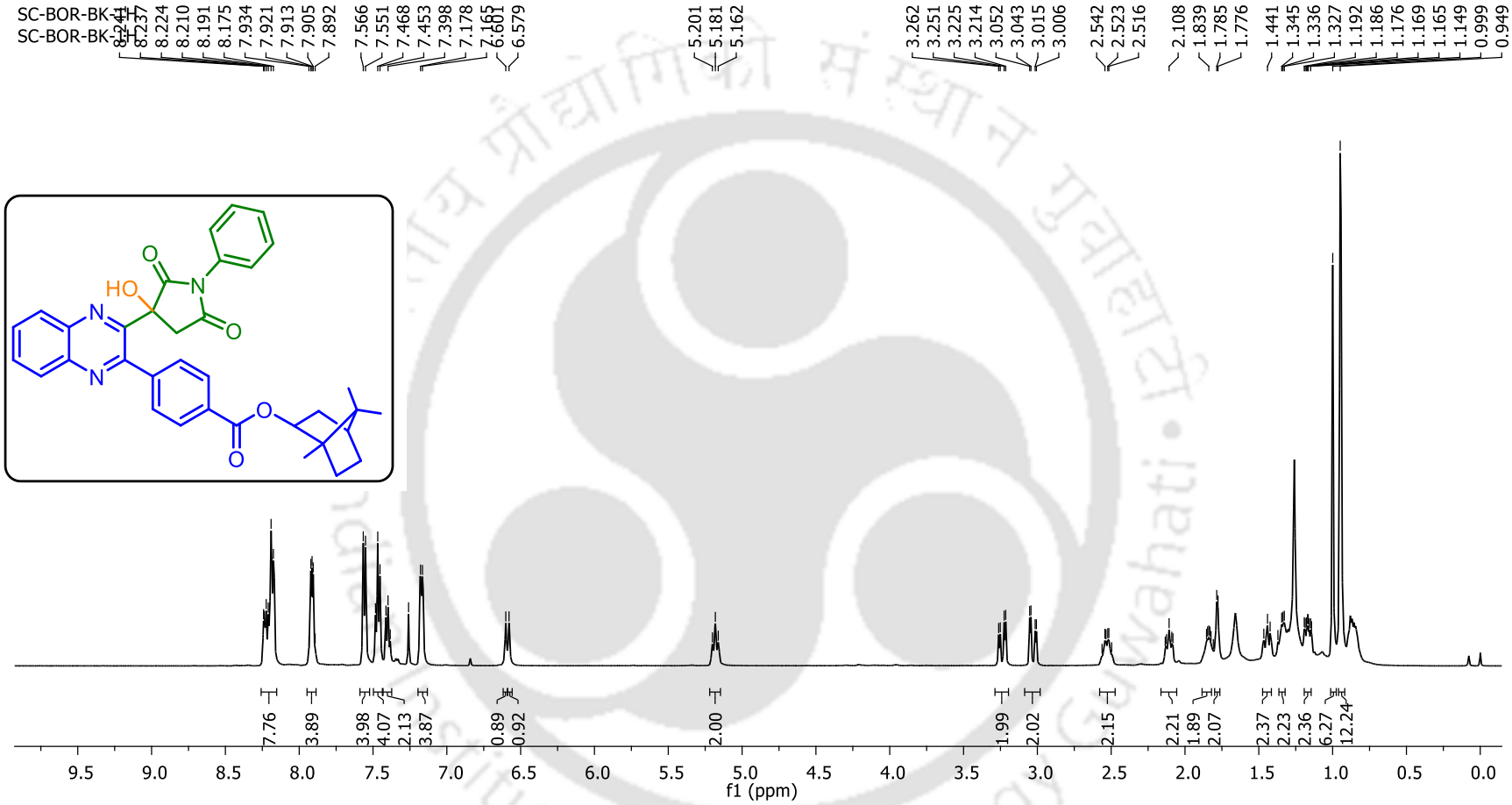

TH-3369_166122017

^{13}C {^{1}H} NMR of **1,7,7-Trimethylbicyclo[2.2.1]heptan-2-yl-4-(3-(3-hydroxy-2,5-dioxo-1-phenylpyrrolidin-3-yl)quinoxalin-2-yl)benzoate** (**32a**) ($CDCl_3$, 126 MHz)

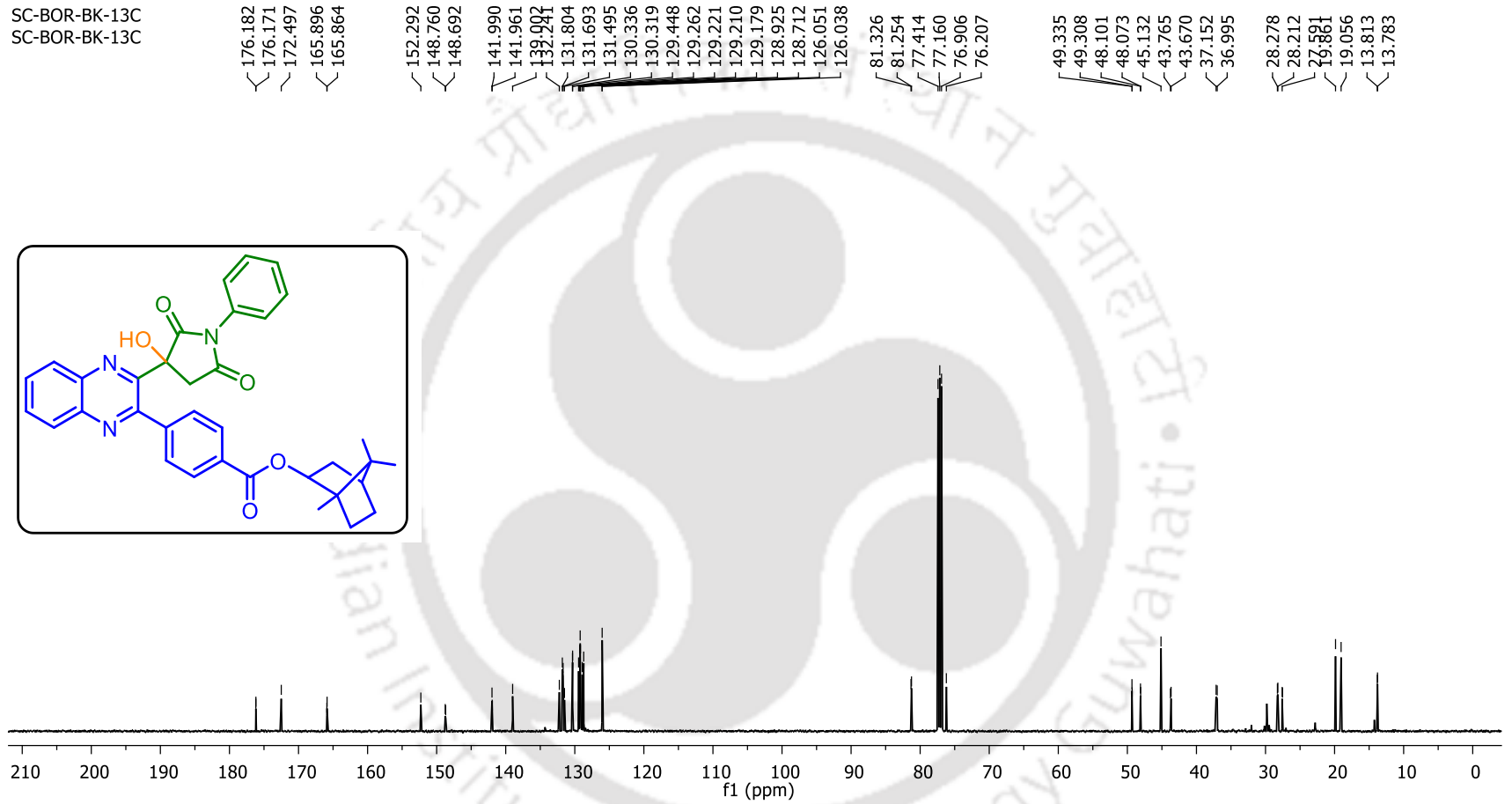

TH-3369_166122017

^{1}H NMR of **1'-Phenylspiro[chromeno[3,4-*b*]quinoxaline-6,3'-pyrrolidine]-2',5'-dione** (**1b**) ($CDCl_3$, 500 MHz)

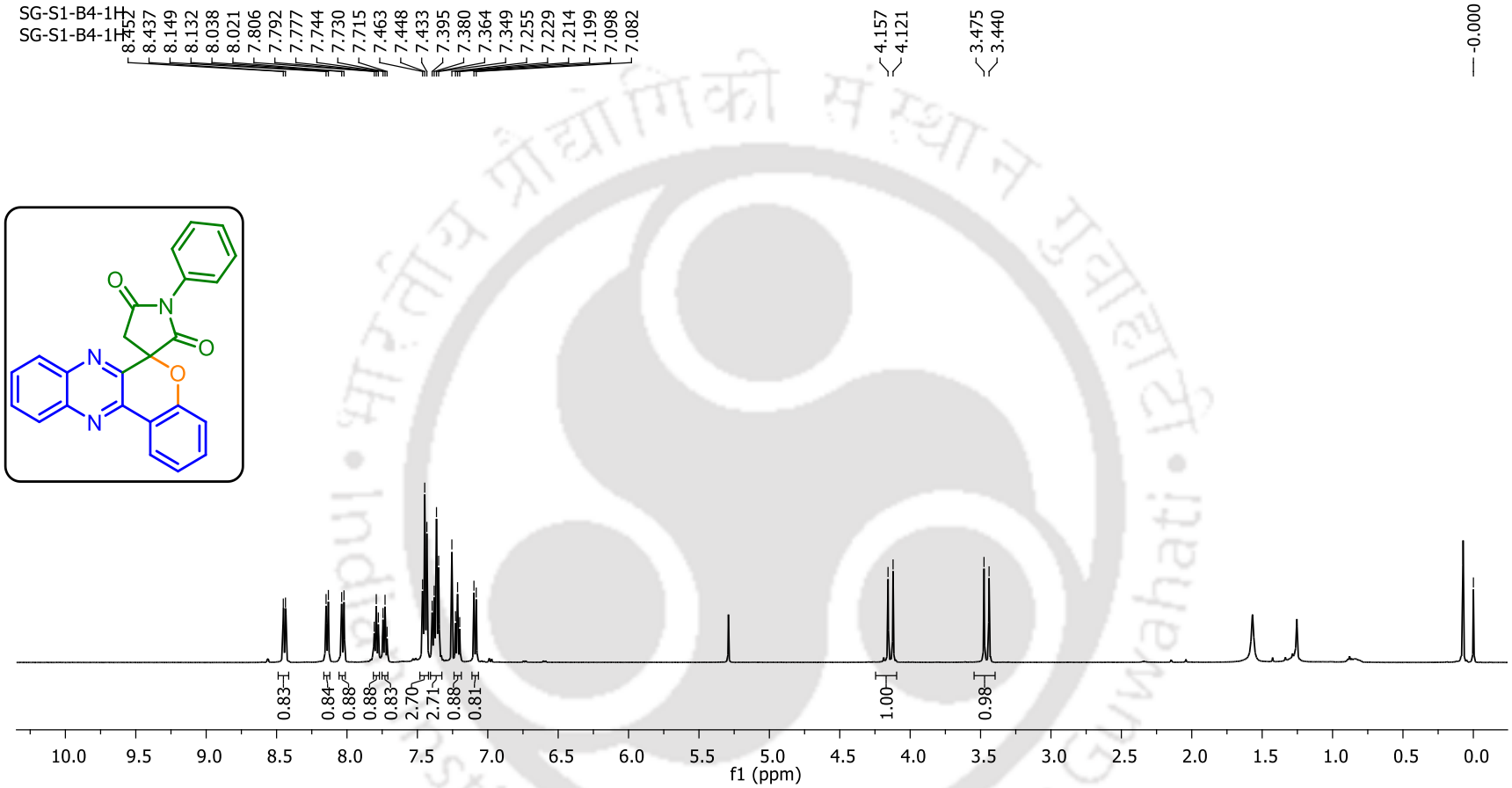

TH-3369_166122017

^{13}C {^{1}H} NMR of **1'-Phenylspiro[chromeno[3,4-*b*]quinoxaline-6,3'-pyrrolidine]-2',5'-dione** (**1b**) ($CDCl_3$, 126 MHz)

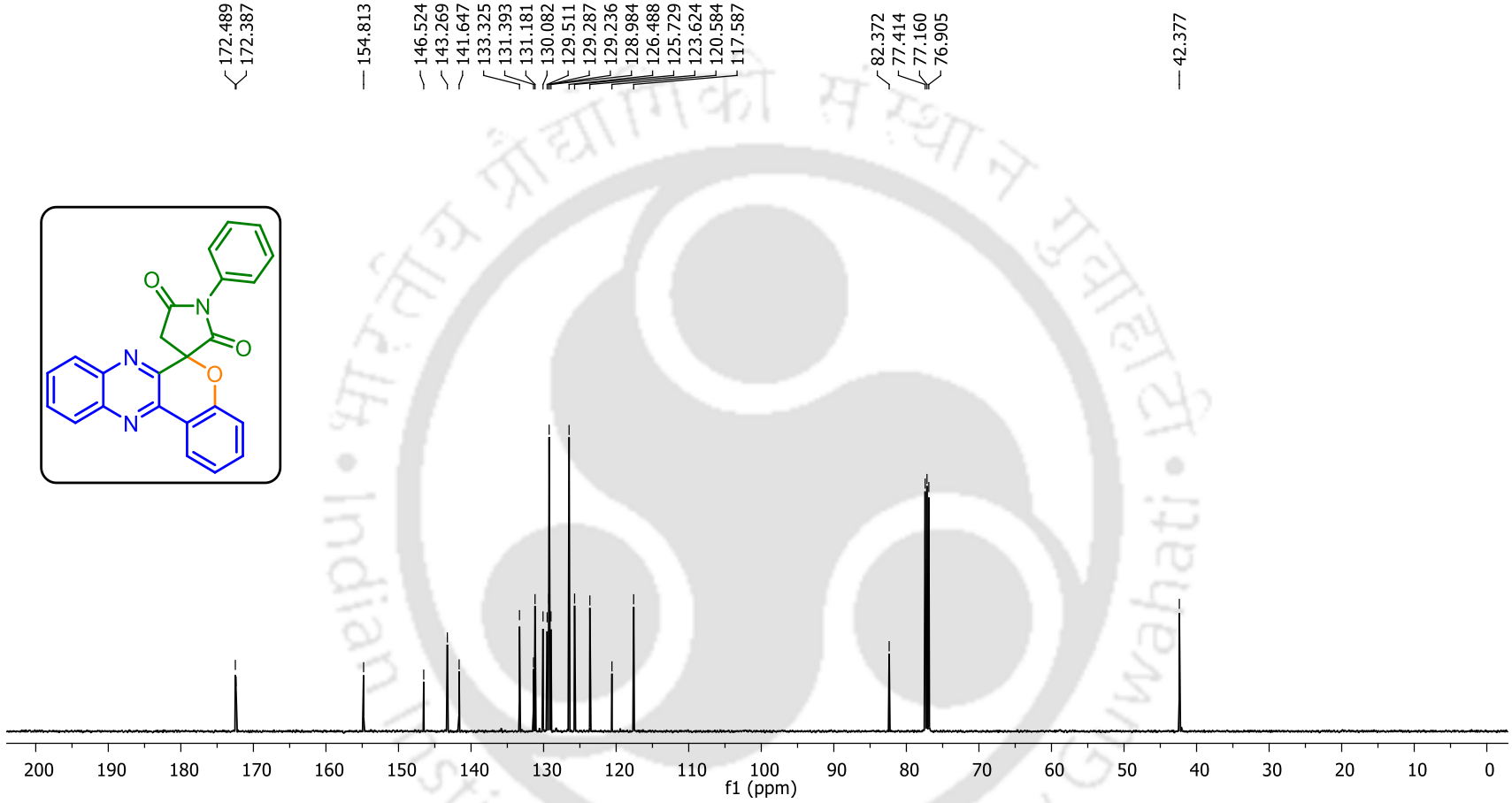

TH-3369_166122017

^{1}H NMR of **3-Methyl-1'-phenylspiro[chromeno[3,4-*b*]quinoxaline-6,3'-pyrrolidine]-2',5'-dione** (**2b**) ($CDCl_3$, 500 MHz)

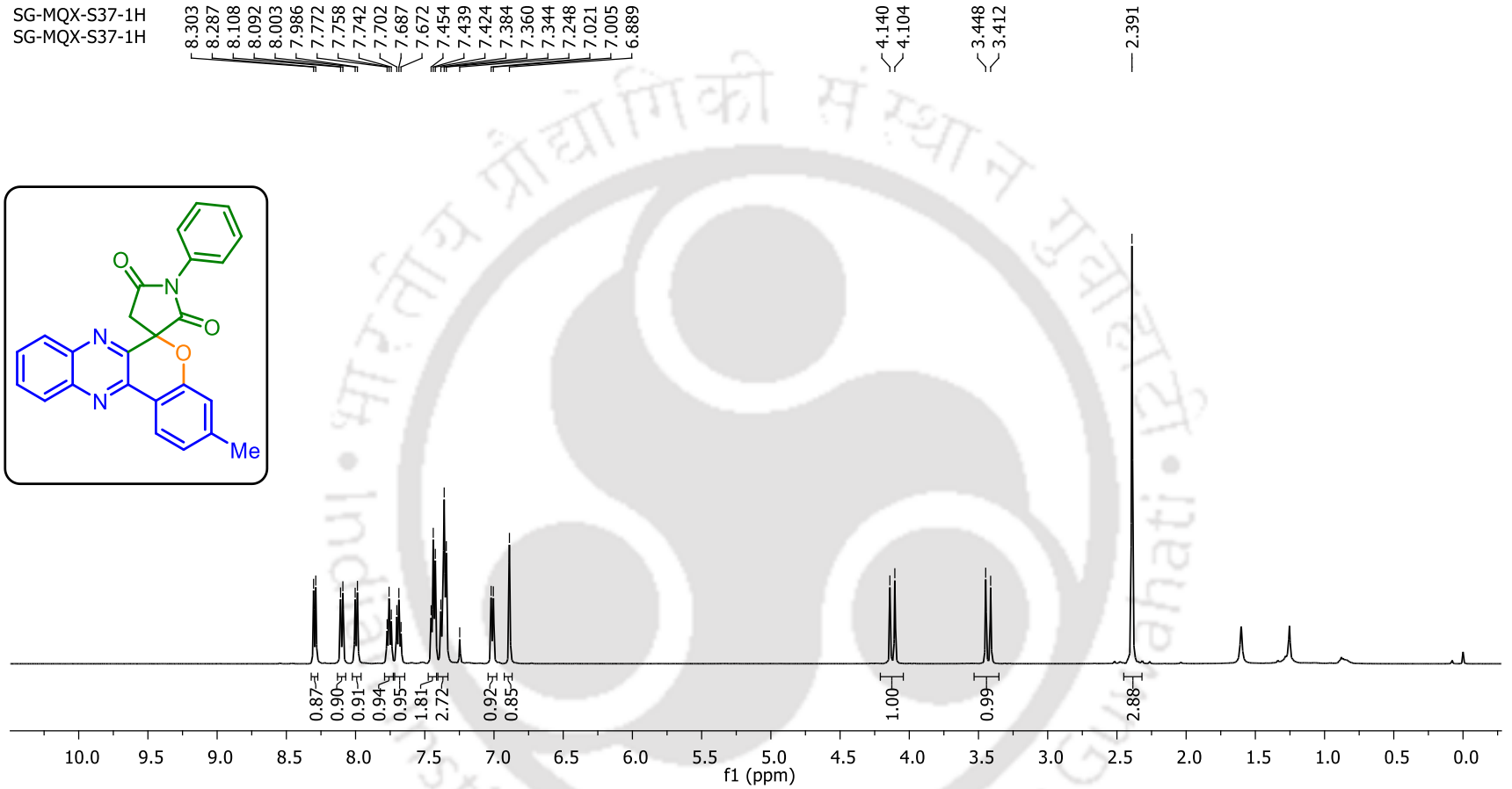

^{13}C {^{1}H} NMR of **3-Methyl-1'-phenylspiro[chromeno[3,4-*b*]quinoxaline-6,3'-pyrrolidine]-2',5'-dione** (**2b**) ($CDCl_3$, 126 MHz)

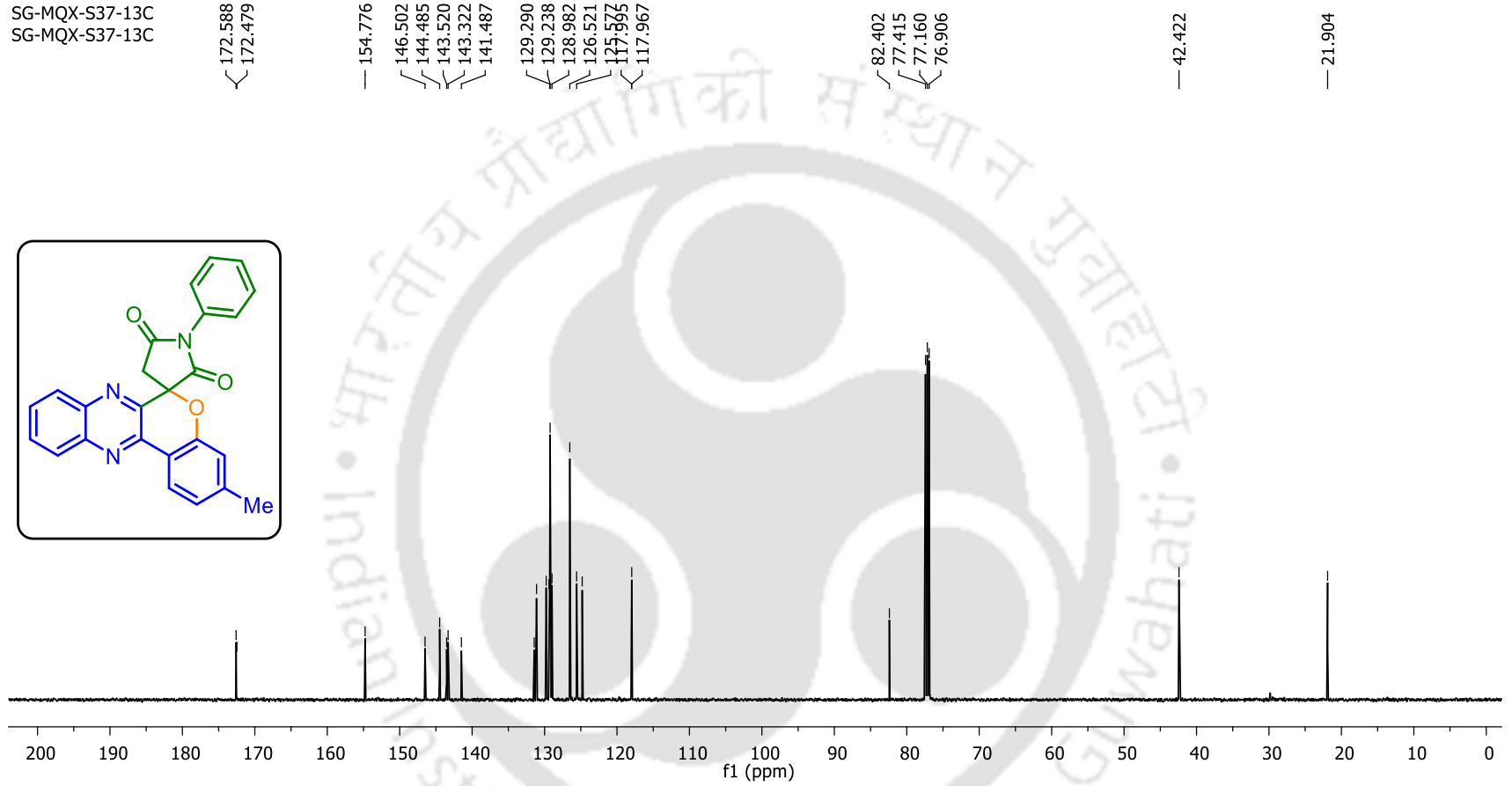

TH-3369_166122017

^{1}H NMR of **3-Fluoro-1'-phenylspiro[chromeno[3,4-*b*]quinoxaline-6,3'-pyrrolidine]-2',5'-dione** (**3b**) ($CDCl_3$, 500 MHz)

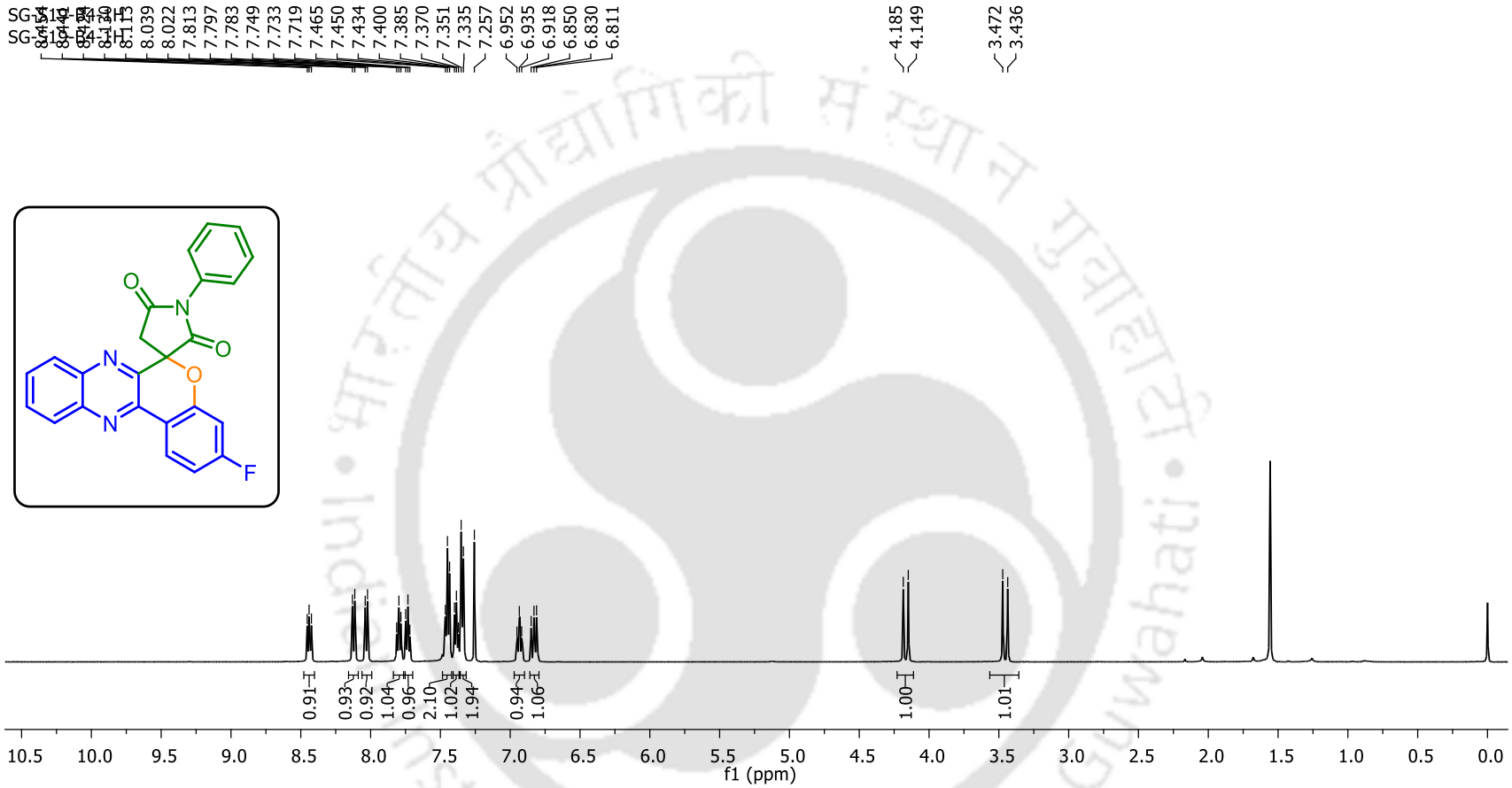

TH-3369_166122017

^{13}C {^{1}H} NMR of **3-Fluoro-1'-phenylspiro[chromeno[3,4-*b*]quinoxaline-6,3'-pyrrolidine]-2',5'-dione** (**3b**) ($CDCl_3$, 126 MHz)

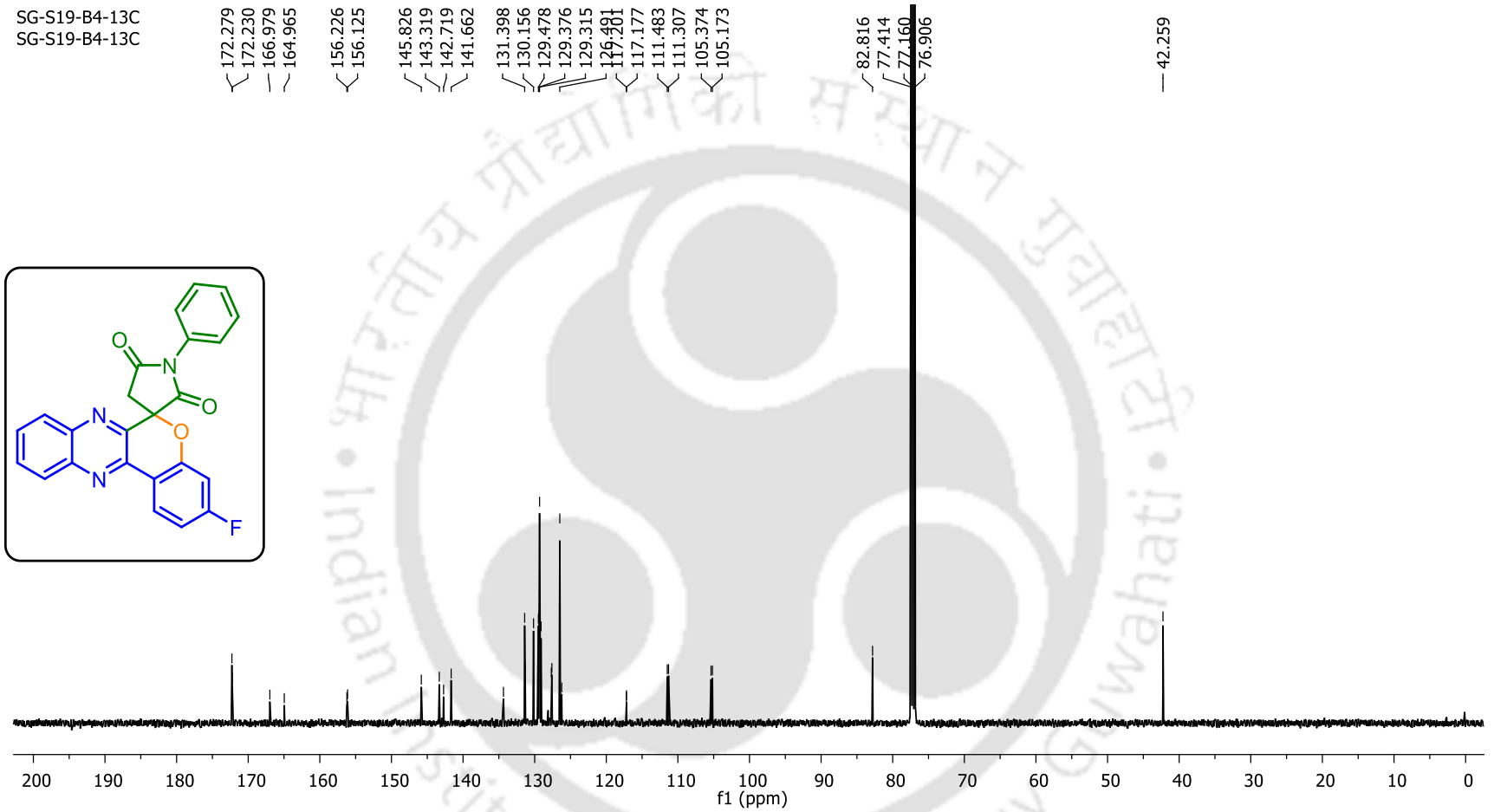

TH-3369_166122017

^{19}F NMR of **3-Fluoro-1'-phenylspiro[chromeno[3,4-*b*]quinoxaline-6,3'-pyrrolidine]-2',5'-dione** (**3b**) ($CDCl_3$)

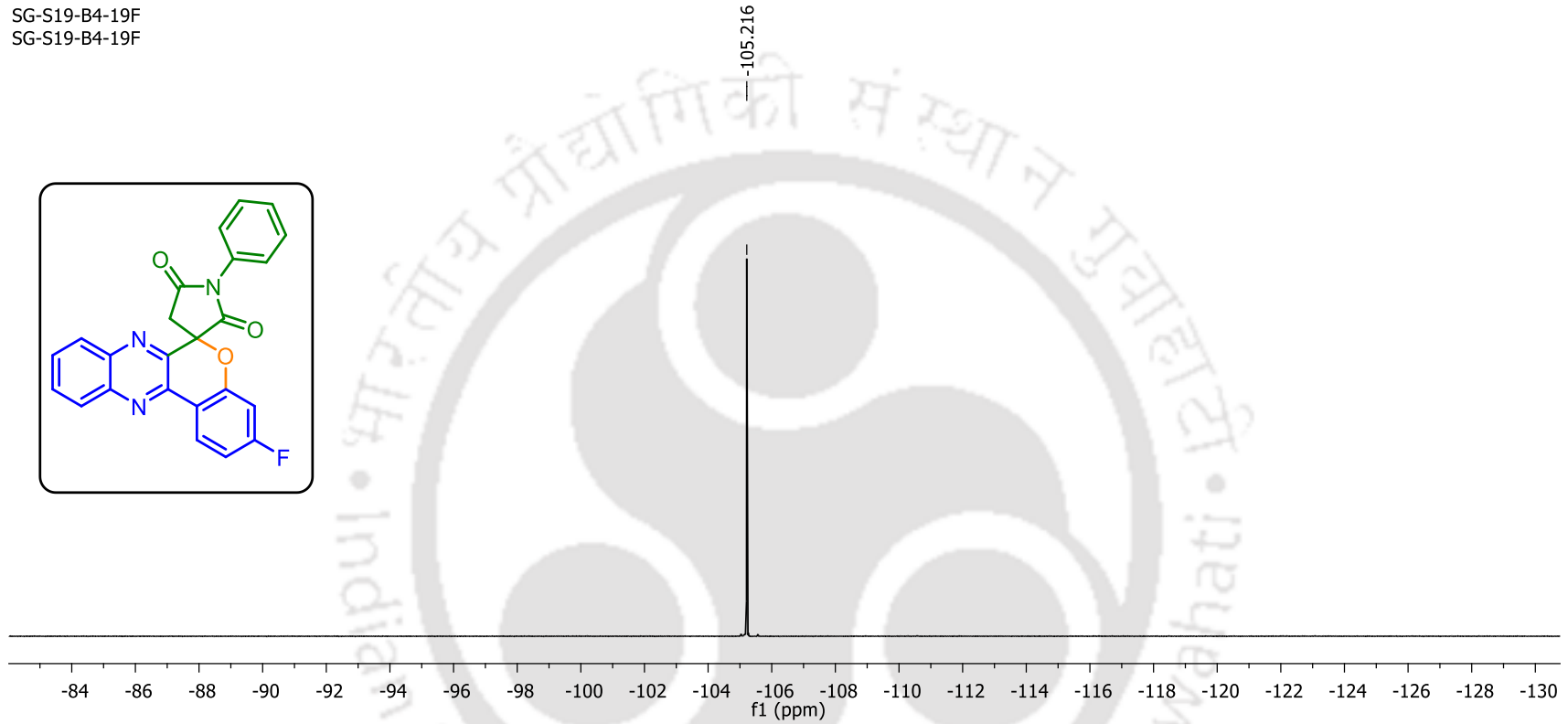

TH-3369_166122017

^{1}H NMR of **3-Bromo-1'-phenylspiro[chromeno[3,4-*b*]quinoxaline-6,3'-pyrrolidine]-2',5'-dione** (**5b**) ($CDCl_3$, 400 MHz)

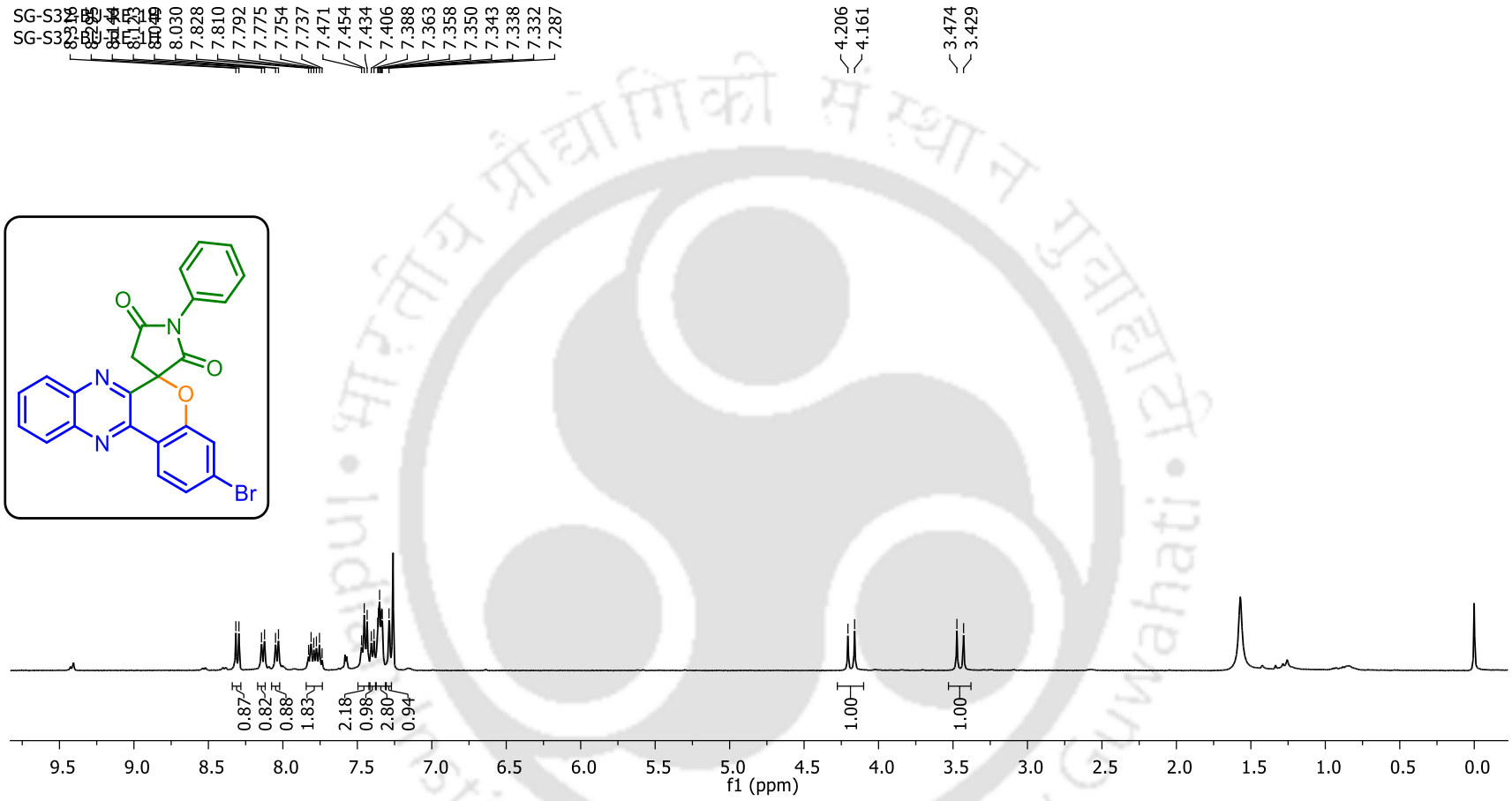

^{13}C {^{1}H} NMR of **3-Bromo-1'-phenylspiro[chromeno[3,4-*b*]quinoxaline-6,3'-pyrrolidine]-2',5'-dione** (**5b**) ($CDCl_3$, 126 MHz)

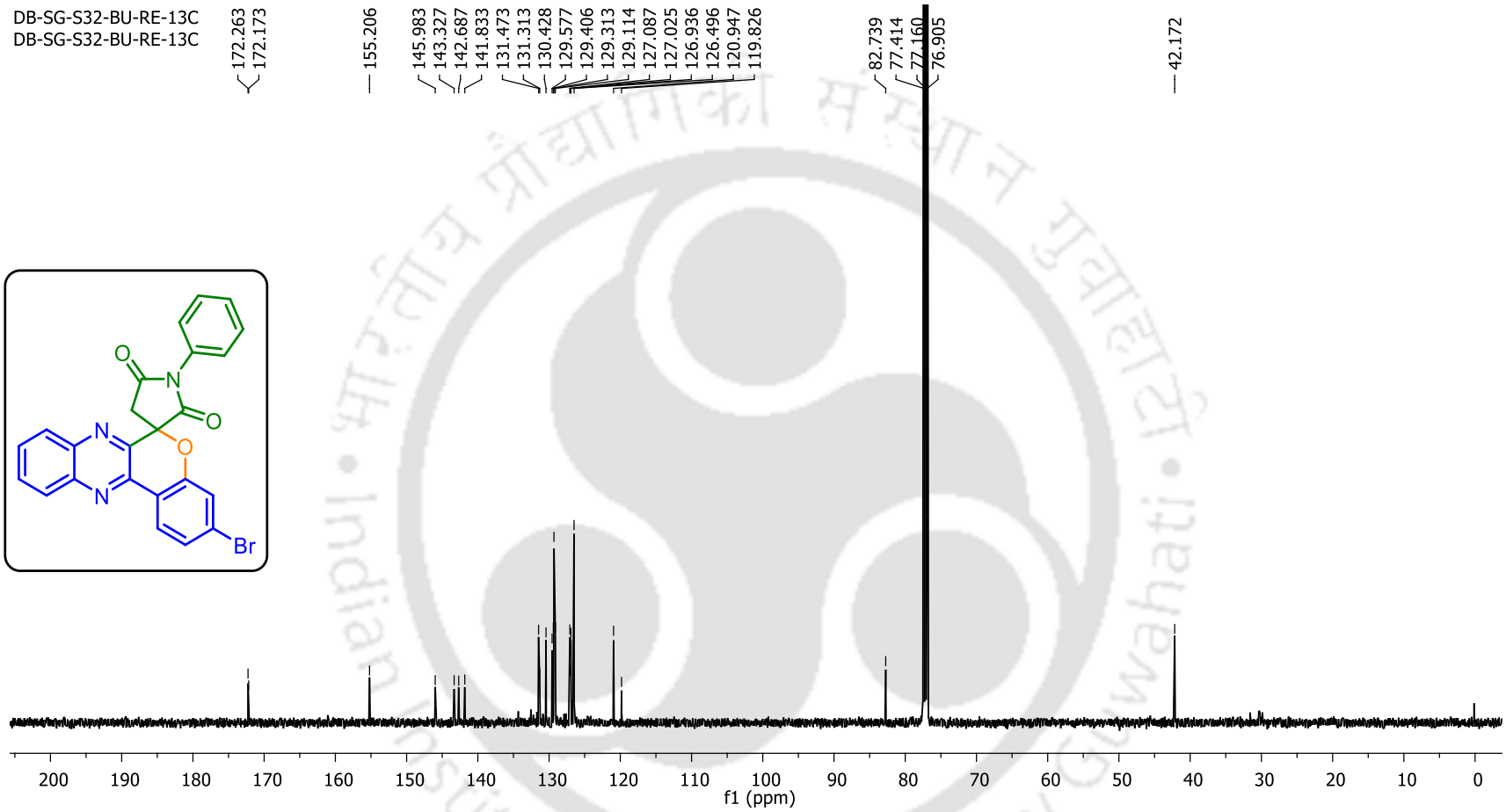

TH-3369_166122017

^{1}H NMR of **2-Methyl-1'-phenylspiro[chromeno[3,4-*b*]quinoxaline-6,3'-pyrrolidine]-2',5'-dione and 4-Methyl-1'-phenylspiro[chromeno[3,4-*b*]quinoxaline-6,3'-pyrrolidine]-2',5'-dione (8b)** ($CDCl_3$, 500 MHz)

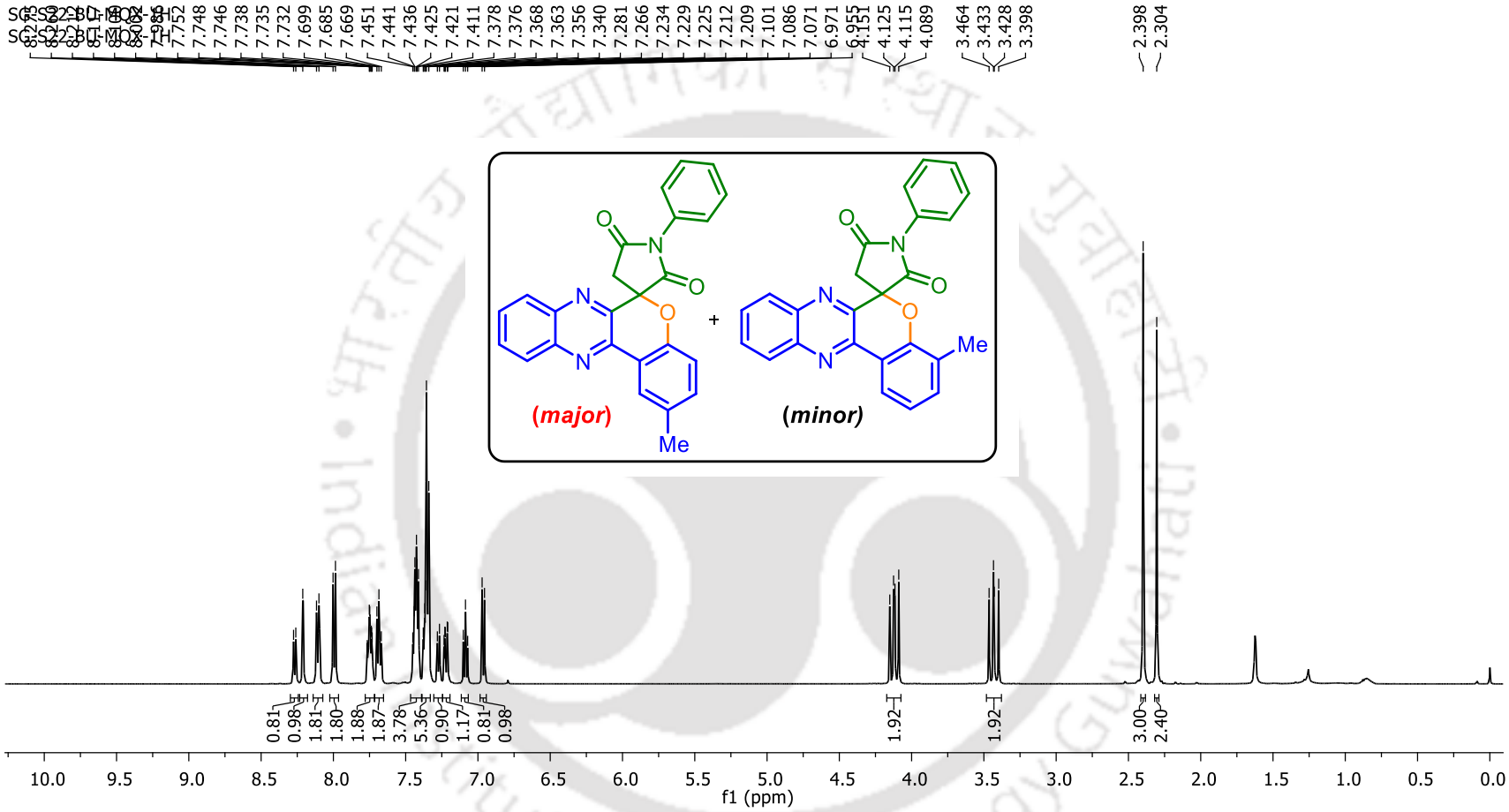

TH-3369_166122017

^{13}C {^{1}H} NMR of **2-Methyl-1'-phenylspiro[chromeno[3,4-*b*]quinoxaline-6,3'-pyrrolidine]-2',5'-dione and 4-Methyl-1'-phenylspiro[chromeno[3,4-*b*]quinoxaline-6,3'-pyrrolidine]-2',5'-dione (8b)** ($CDCl_3$, 126 MHz)

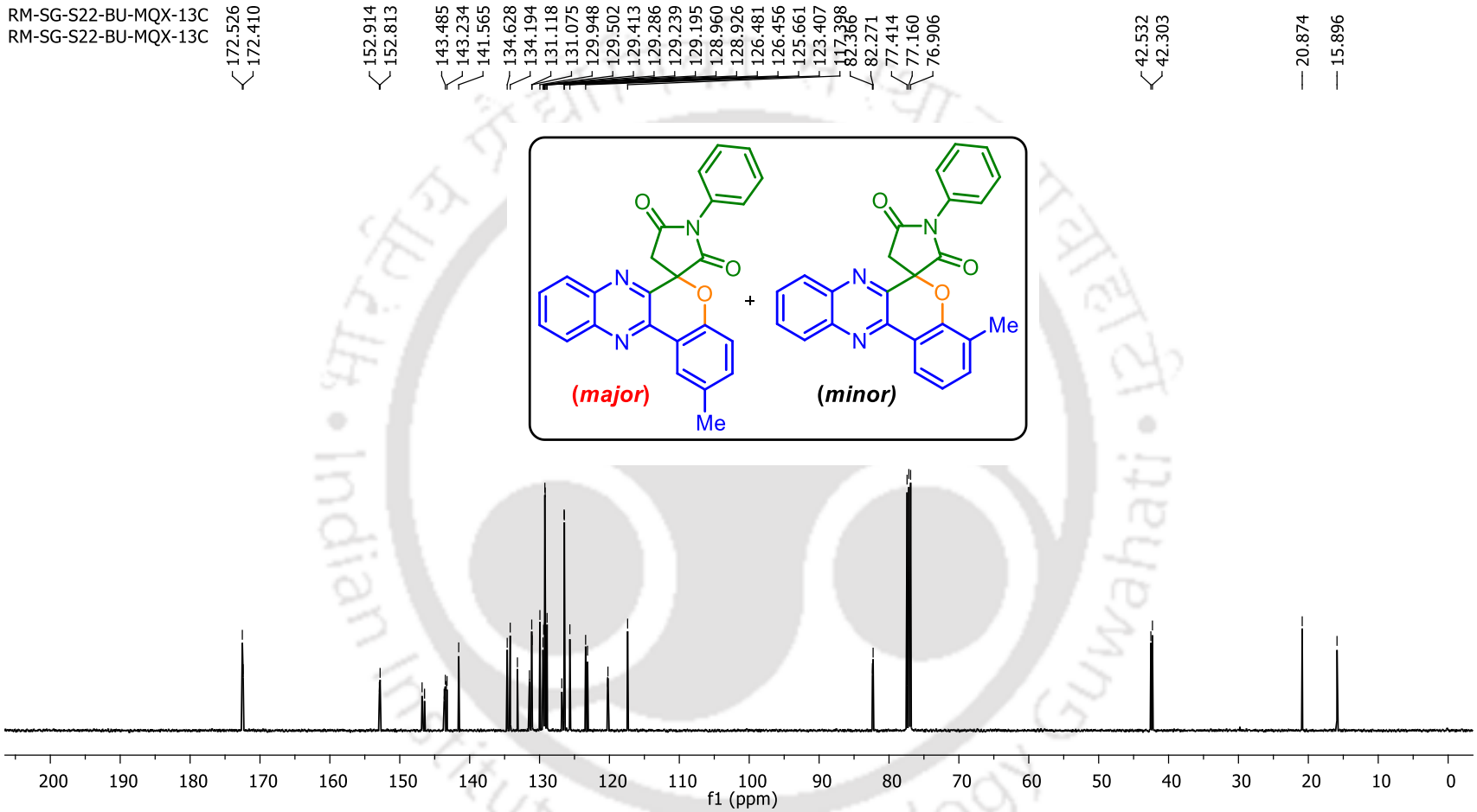

TH-3369_166122017

^{1}H NMR of **1'-Phenyl-2-(trifluoromethyl)spiro[chromeno[3,4-*b*]quinoxaline-6,3'-pyrrolidine]-2',5'-dione and 1'-Phenyl-4-(trifluoromethyl)spiro[chromeno[3,4-*b*]quinoxaline-6,3'-pyrrolidine]-2',5'-dione (9b)** ($CDCl_3$, 400 MHz)

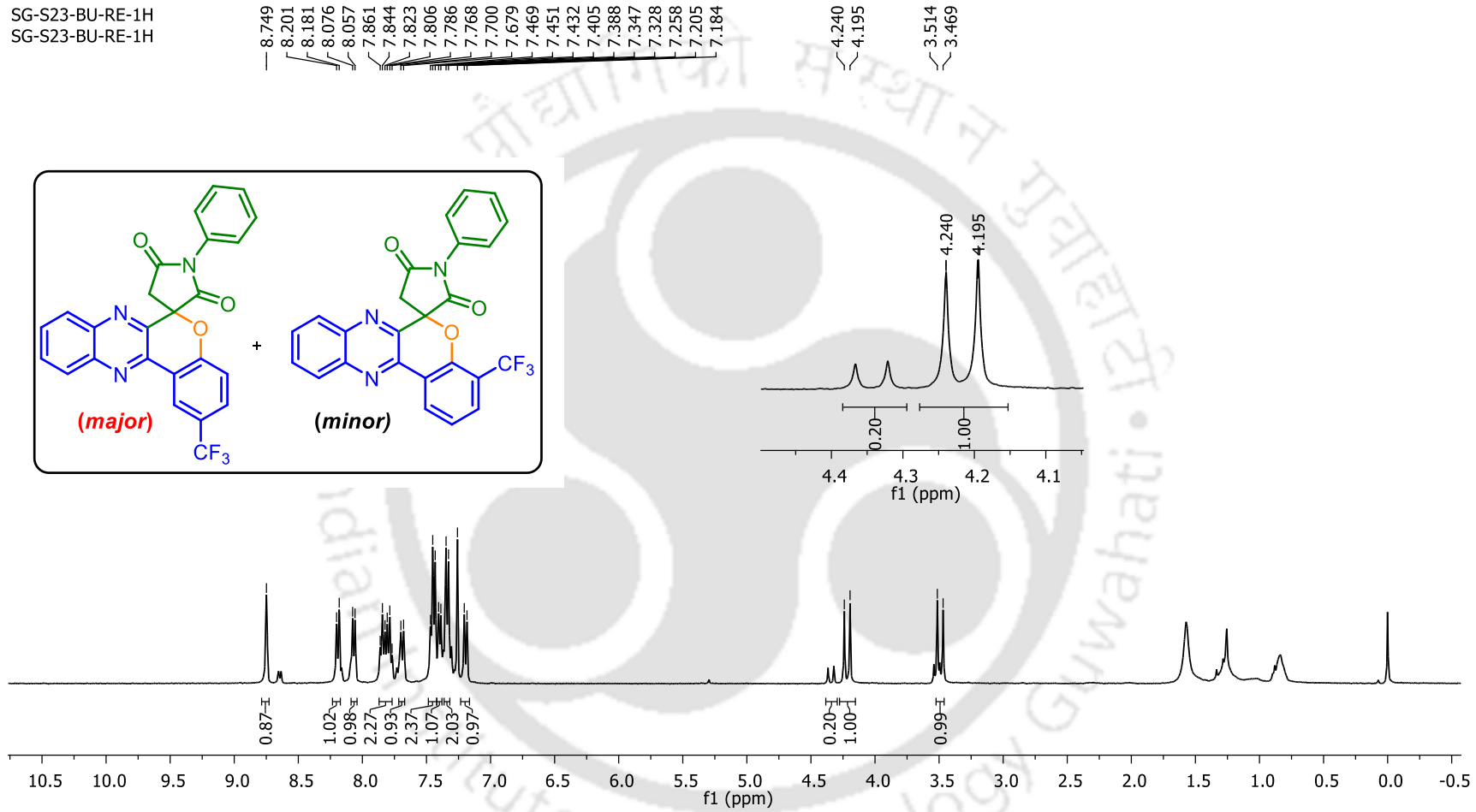

^{13}C {^{1}H} NMR of **1'-Phenyl-2-(trifluoromethyl)spiro[chromeno[3,4-*b*]quinoxaline-6,3'-pyrrolidine]-2',5'-dione and 1'-Phenyl-4-(trifluoromethyl)spiro[chromeno[3,4-*b*]quinoxaline-6,3'-pyrrolidine]-2',5'-dione** (**9b**) ($CDCl_3$, 126 MHz)

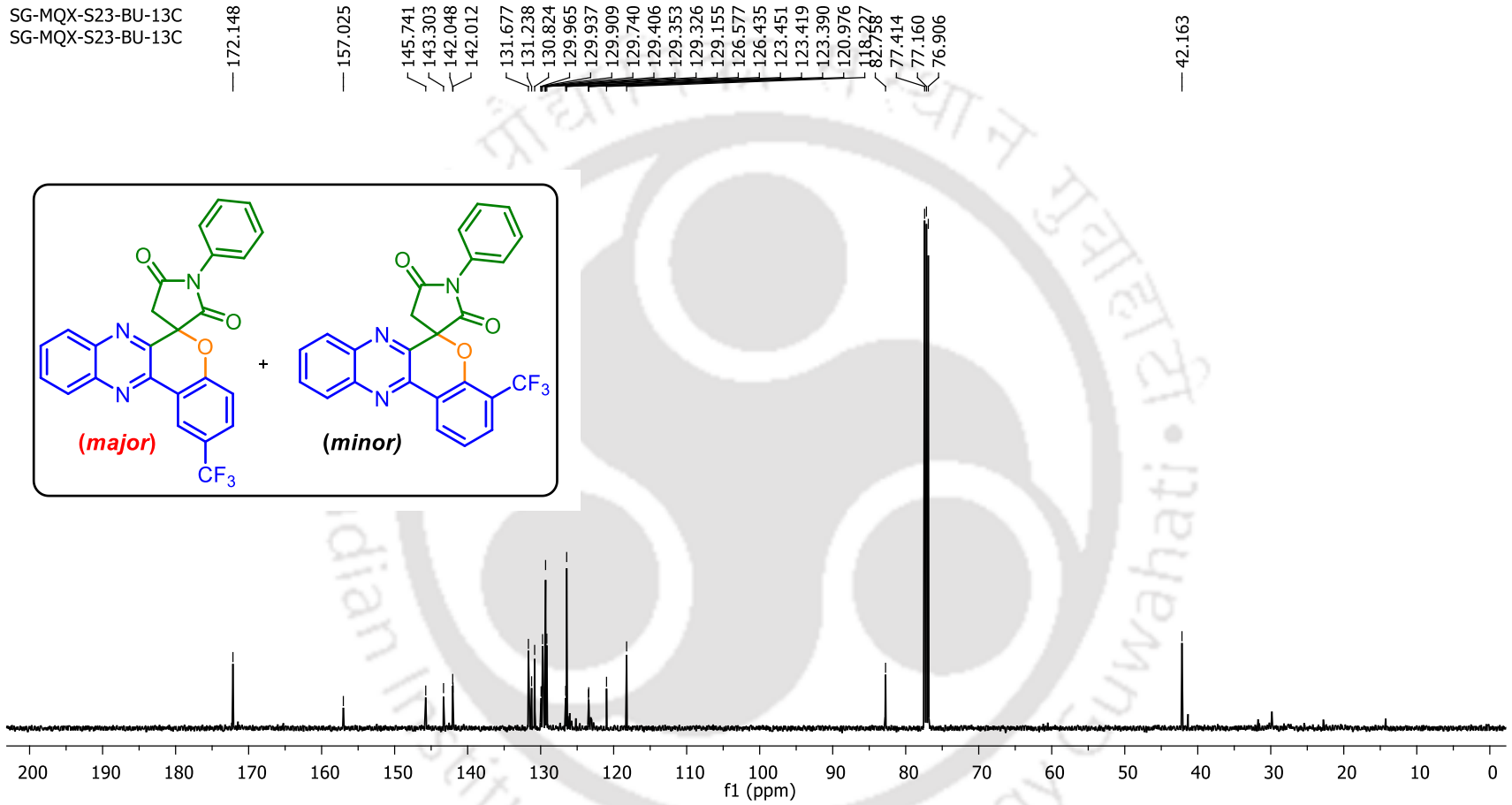

TH-3369_166122017

^{19}F NMR of **1'-Phenyl-2-(trifluoromethyl)spiro[chromeno[3,4-*b*]quinoxaline-6,3'-pyrrolidine]-2',5'-dione and 1'-Phenyl-4-(trifluoromethyl)spiro[chromeno[3,4-*b*]quinoxaline-6,3'-pyrrolidine]-2',5'-dione (9b)** ($CDCl_3$)

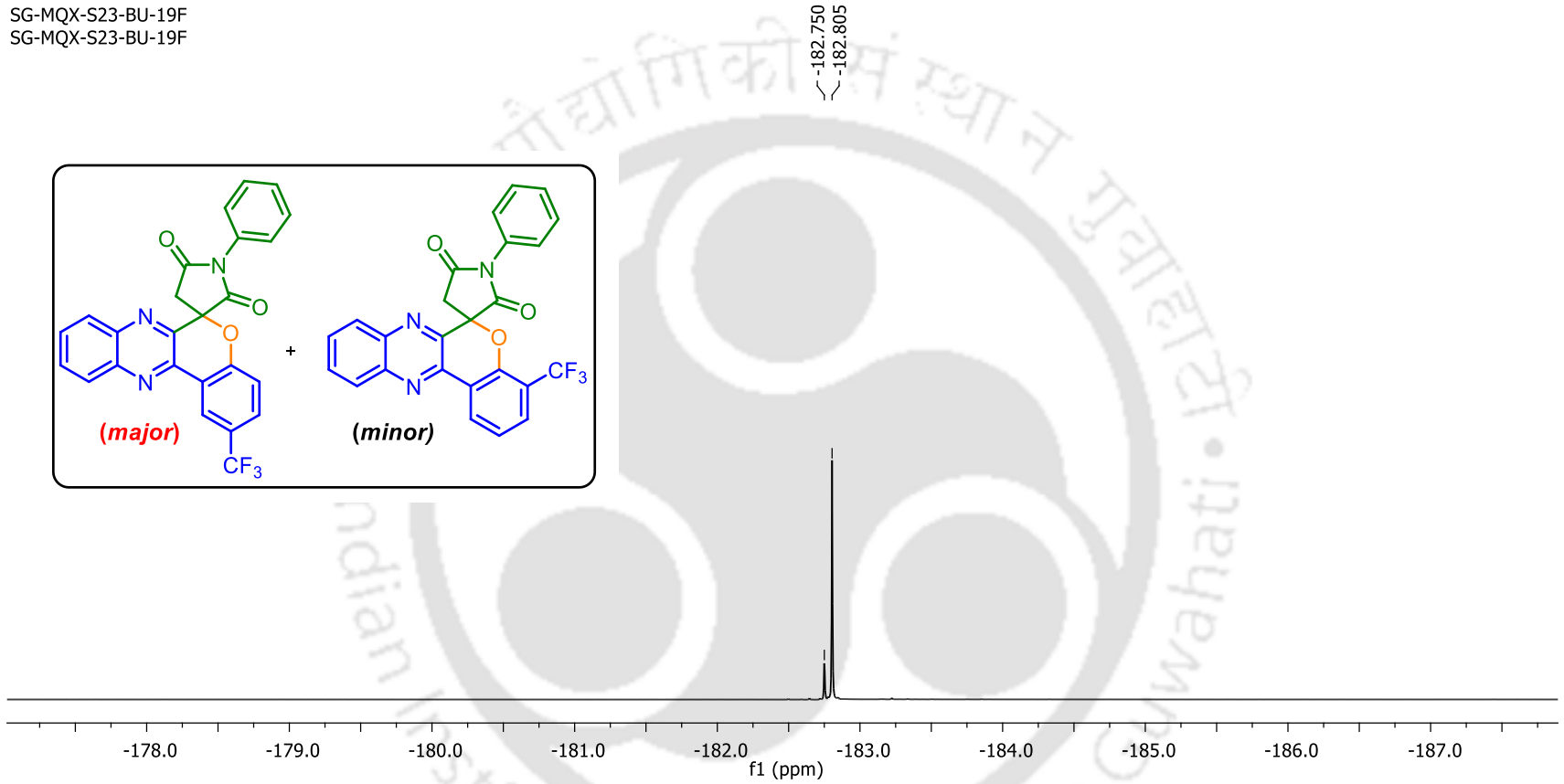

TH-3369_166122017

^{1}H NMR of **1'-Phenylspiro[benzo[7,8]chromeno[3,4-*b*]quinoxaline-6,3'-pyrrolidine]-2',5'-dione** (**13b**) ($CDCl_3$, 500 MHz)

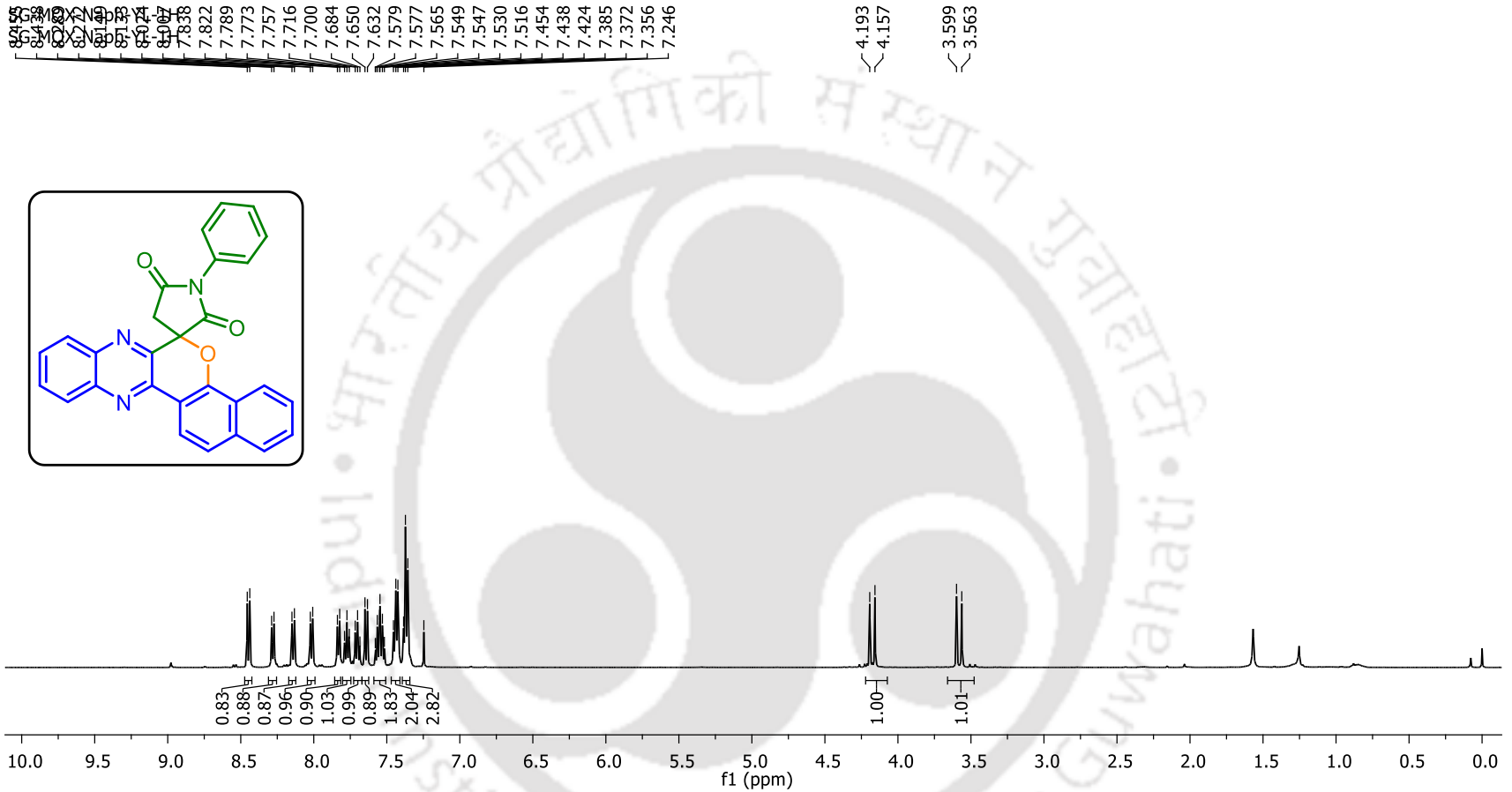

TH-3369_166122017

^{13}C {^{1}H} NMR of **1'-Phenylspiro[benzo[7,8]chromeno[3,4-*b*]quinoxaline-6,3'-pyrrolidine]-2',5'-dione** (**13b**) ($CDCl_3$, 126 MHz)

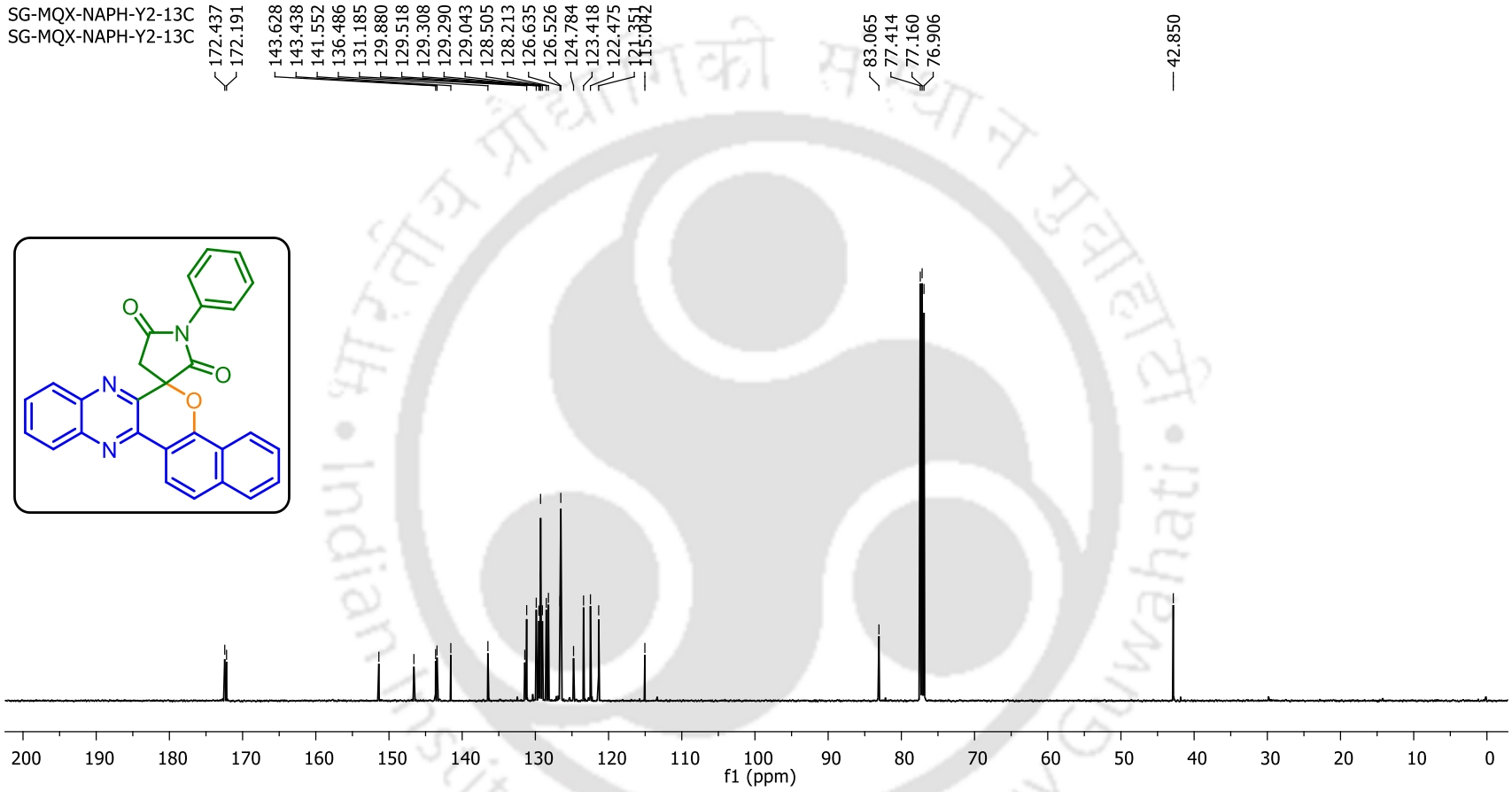

TH-3369_166122017

^{1}H NMR of **1'-Methylspiro[chromeno[3,4-*b*]quinoxaline-6,3'-pyrrolidine]-2',5'-dione** (**15b**) ($CDCl_3$, 500 MHz)

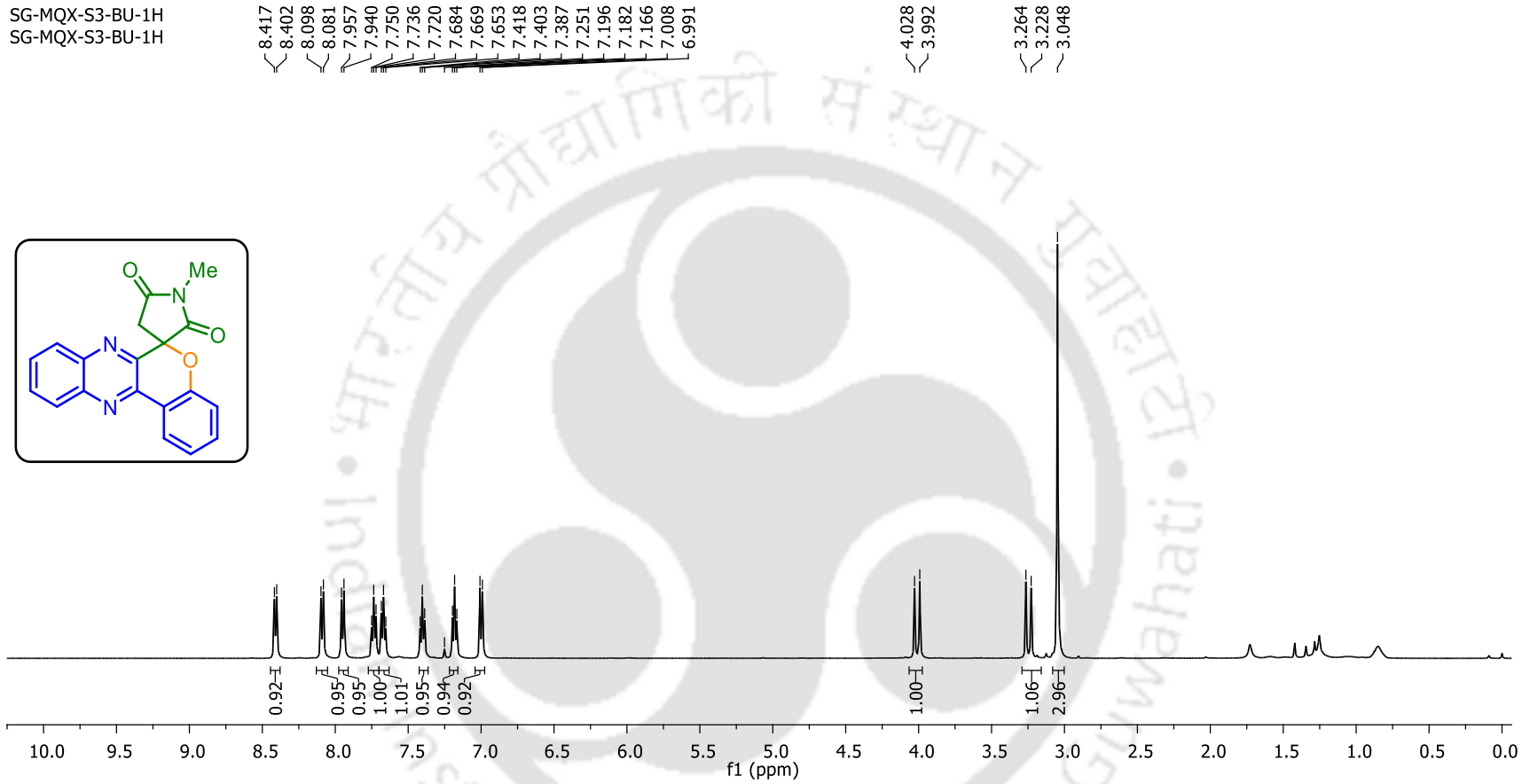

TH-3369_166122017

^{13}C {^{1}H} NMR of **1'-Methylspiro[chromeno[3,4-*b*]quinoxaline-6,3'-pyrrolidine]-2',5'-dione** (**15b**) ($CDCl_3$, 126 MHz)

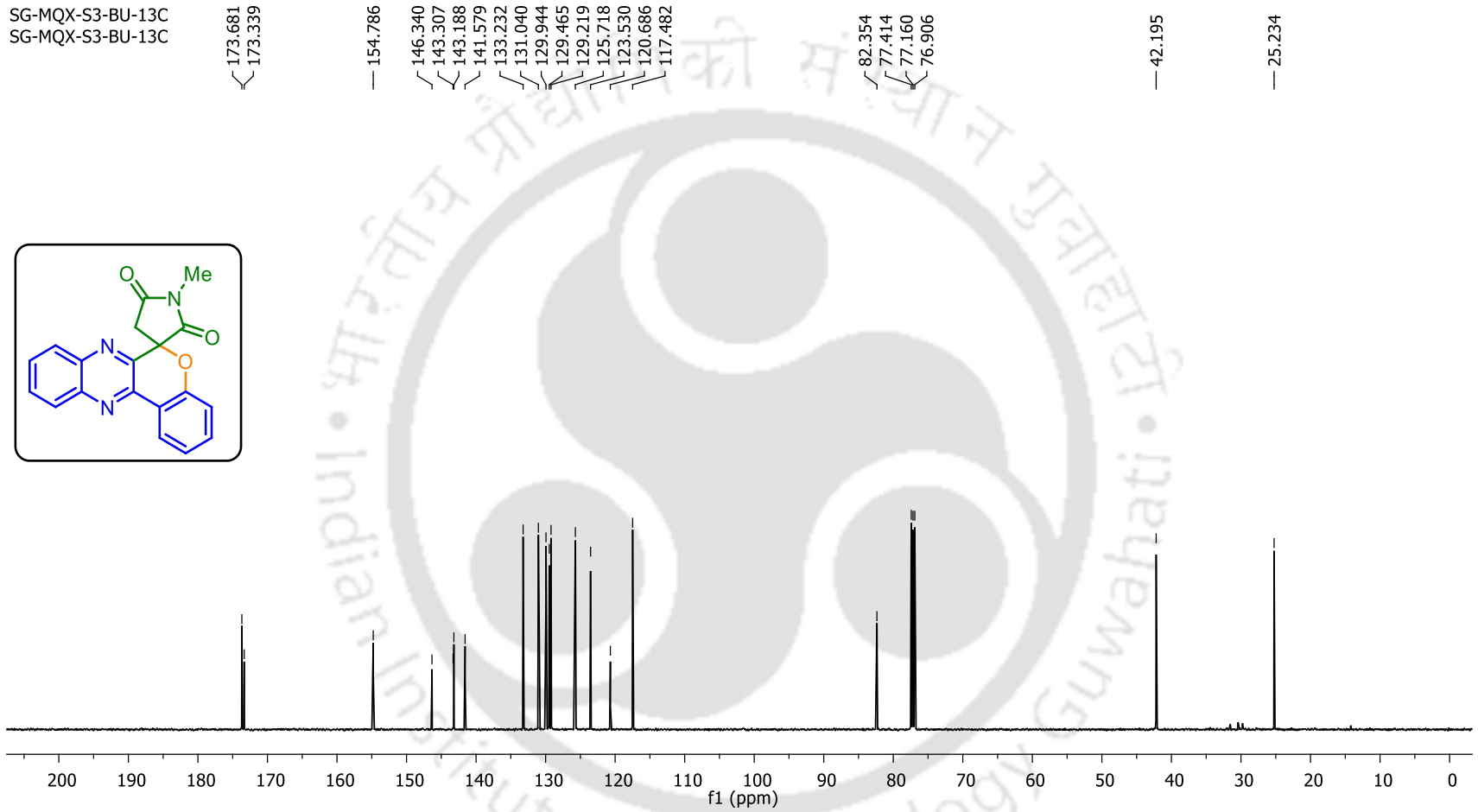

TH-3369_166122017

^{1}H NMR of **1'-Ethylspiro[chromeno[3,4-*b*]quinoxaline-6,3'-pyrrolidine]-2',5'-dione (16b)** ($CDCl_3$, 500 MHz)

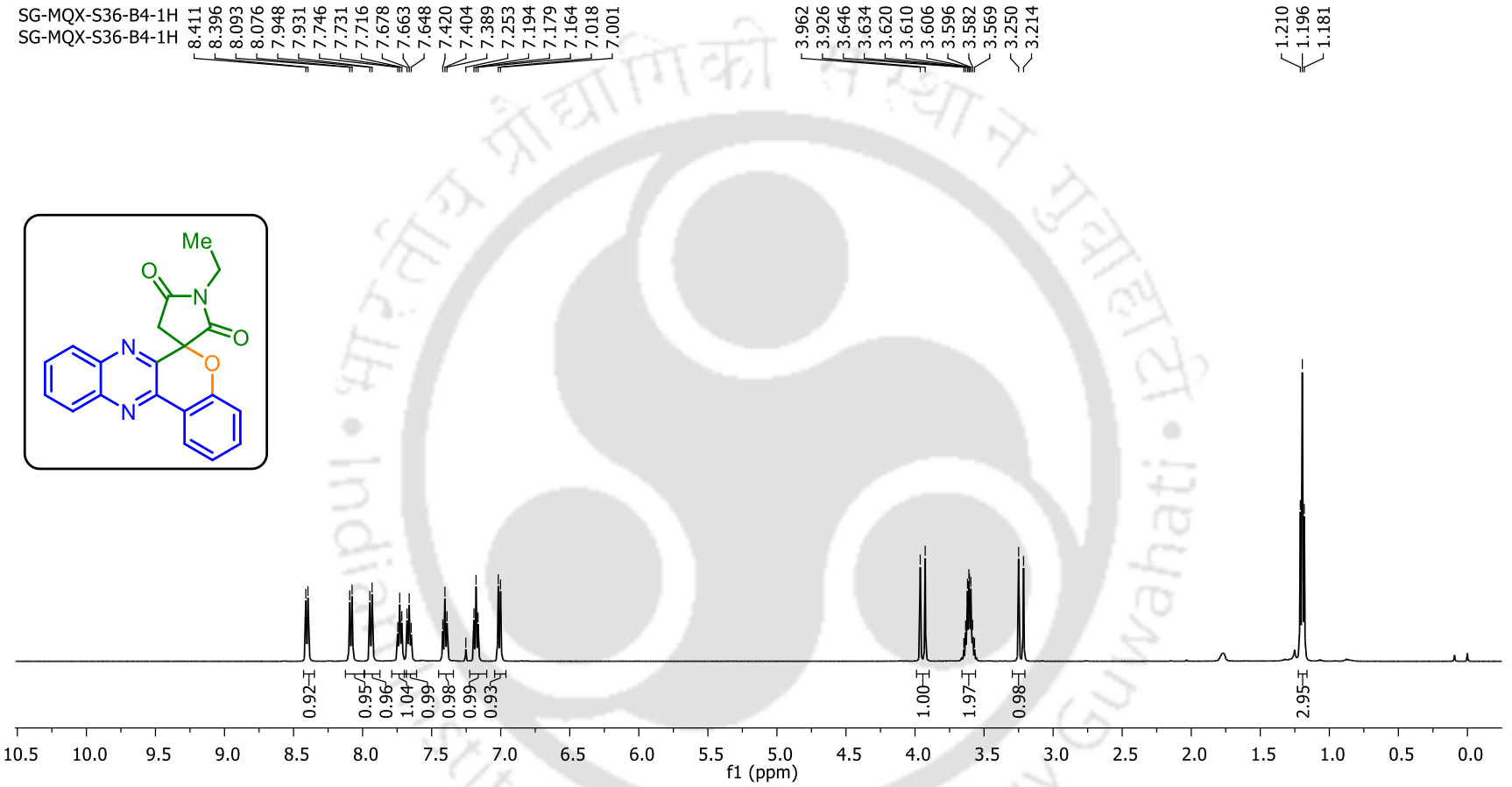

TH-3369_166122017

^{13}C {^{1}H} NMR of **1'-Ethylspiro[chromeno[3,4-*b*]quinoxaline-6,3'-pyrrolidine]-2',5'-dione (16b)** ($CDCl_3$, 126 MHz)

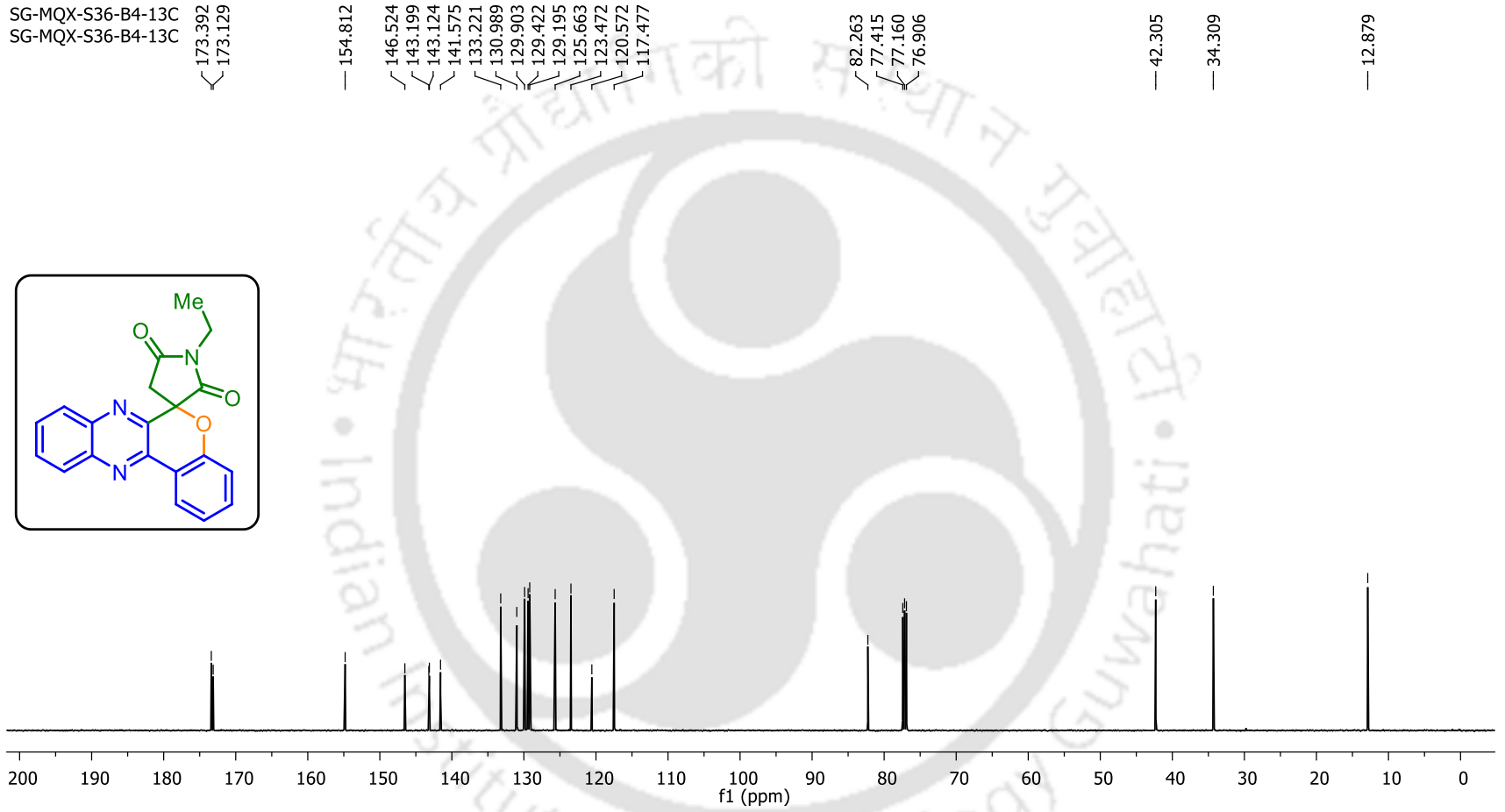

TH-3369_166122017

^{1}H NMR of **1'-Isobutylspiro[chromeno[3,4-*b*]quinoxaline-6,3'-pyrrolidine]-2',5'-dione (17b)** ($CDCl_3$, 500 MHz)

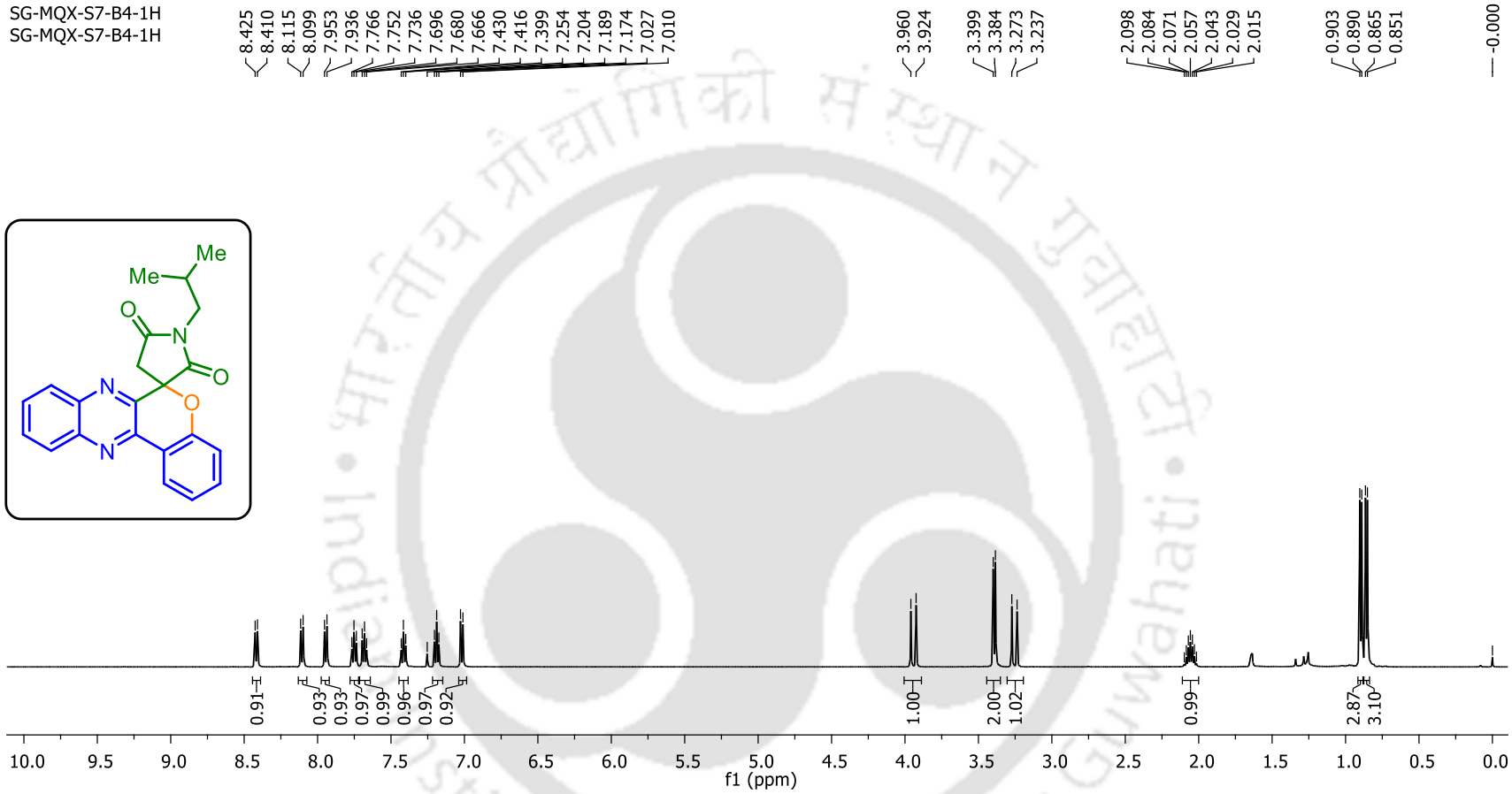

TH-3369_166122017

^{13}C {^{1}H} NMR of **1'-Isobutylspiro[chromeno[3,4-*b*]quinoxaline-6,3'-pyrrolidine]-2',5'-dione** (**17b**) ($CDCl_3$, 126 MHz)

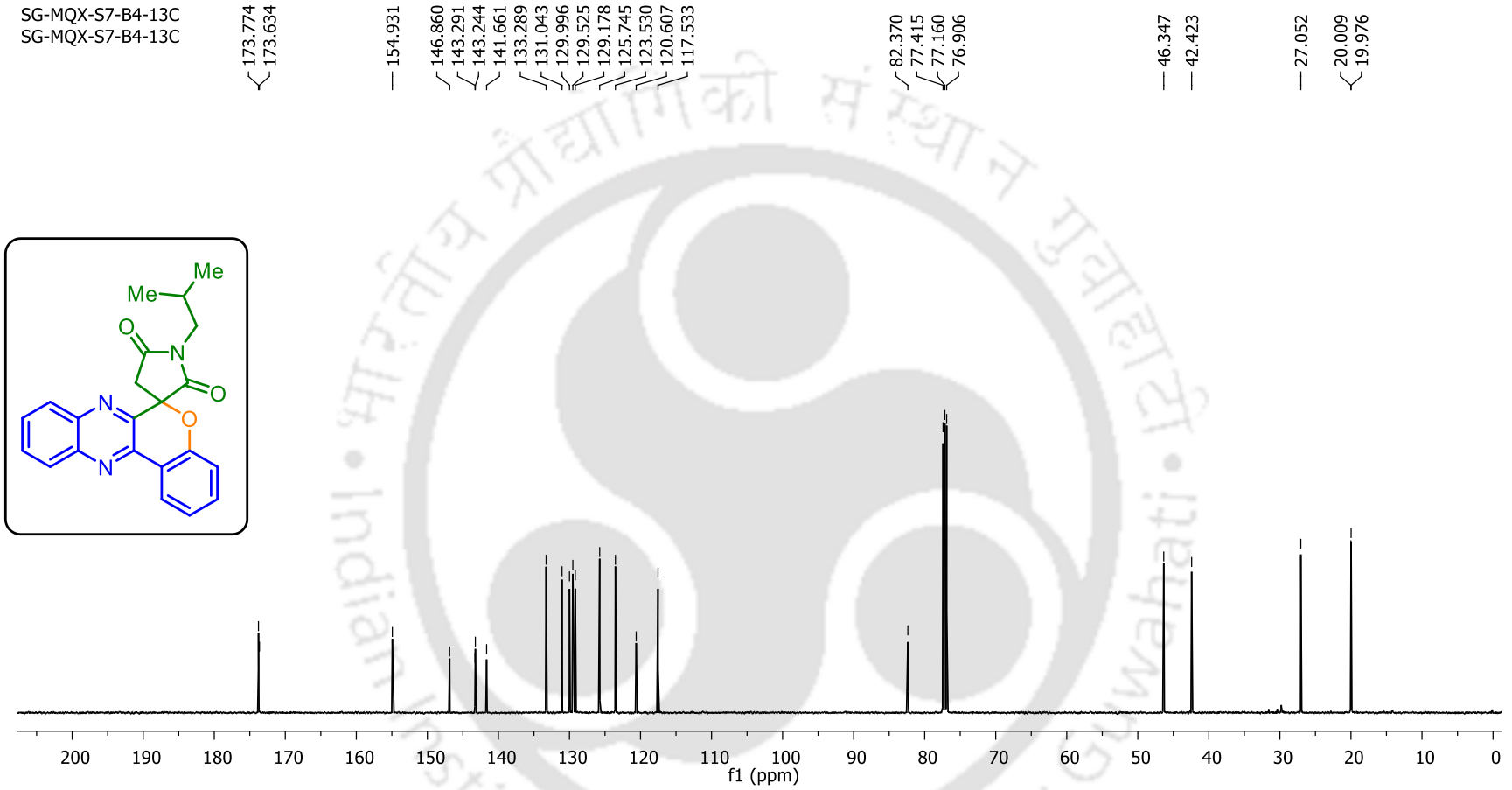

TH-3369_166122017

^{1}H NMR of **1'-Benzylspiro[chromeno[3,4-*b*]quinoxaline-6,3'-pyrrolidine]-2',5'-dione** (**18b**) ($CDCl_3$, 500 MHz)

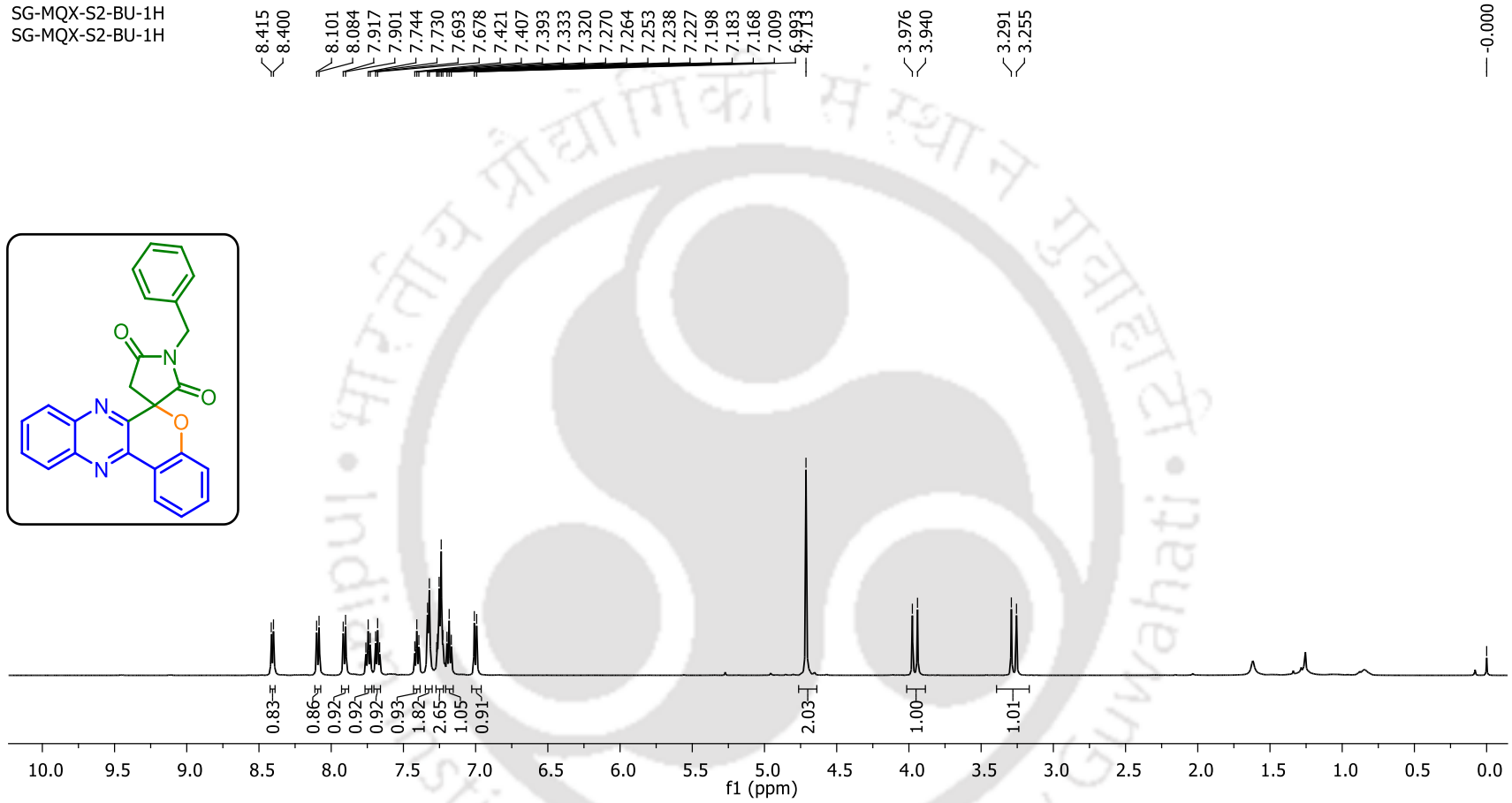

TH-3369_166122017

^{13}C {^{1}H} NMR of **1'-Benzylspiro[chromeno[3,4-*b*]quinoxaline-6,3'-pyrrolidine]-2',5'-dione** (**18b**) ($CDCl_3$, 126 MHz)

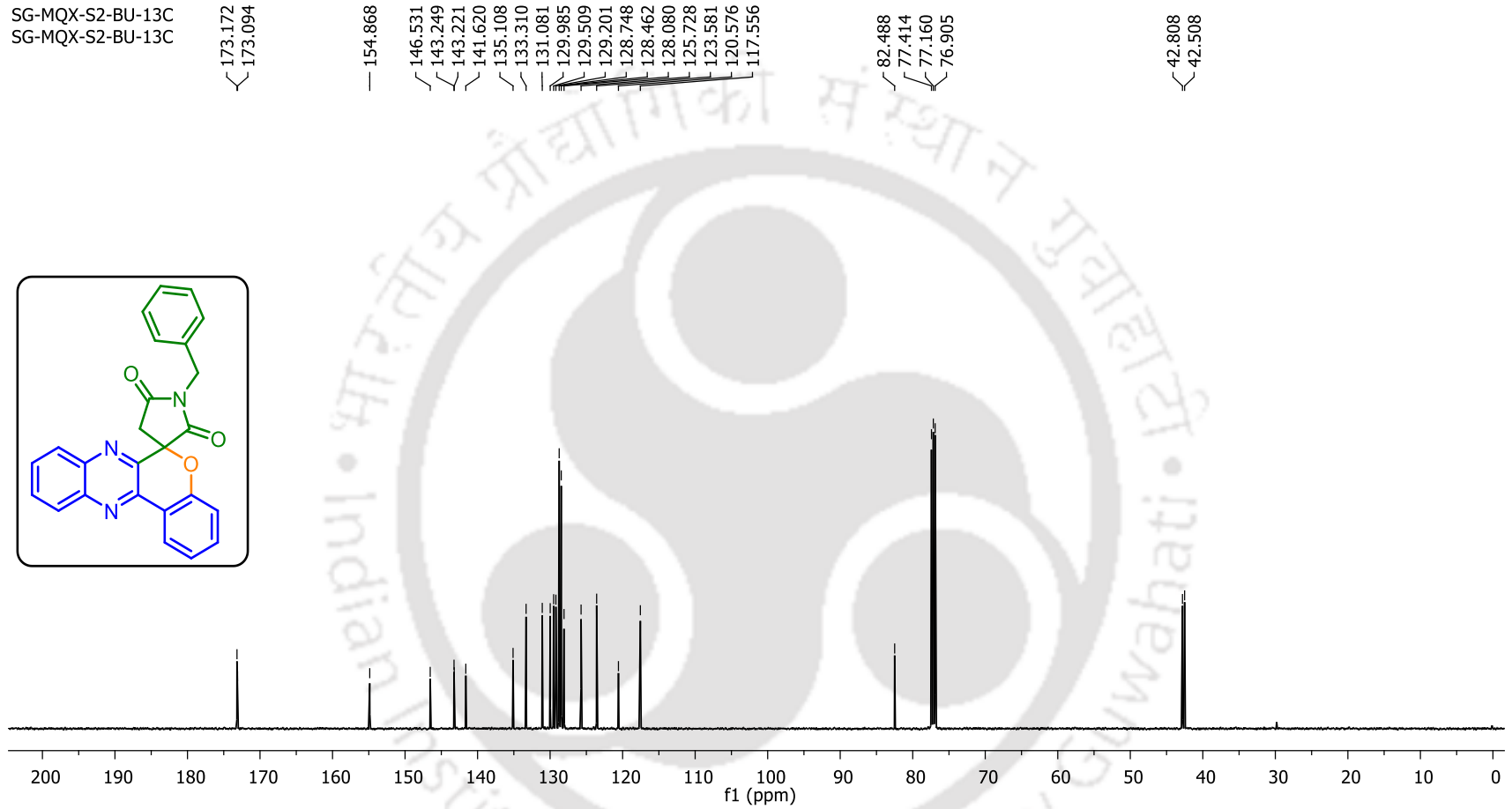

^{1}H NMR of **1'-(*p*-Tolyl)spiro[chromeno[3,4-*b*]quinoxaline-6,3'-pyrrolidine]-2',5'-dione** (**20b**) ($CDCl_3$, 500 MHz)

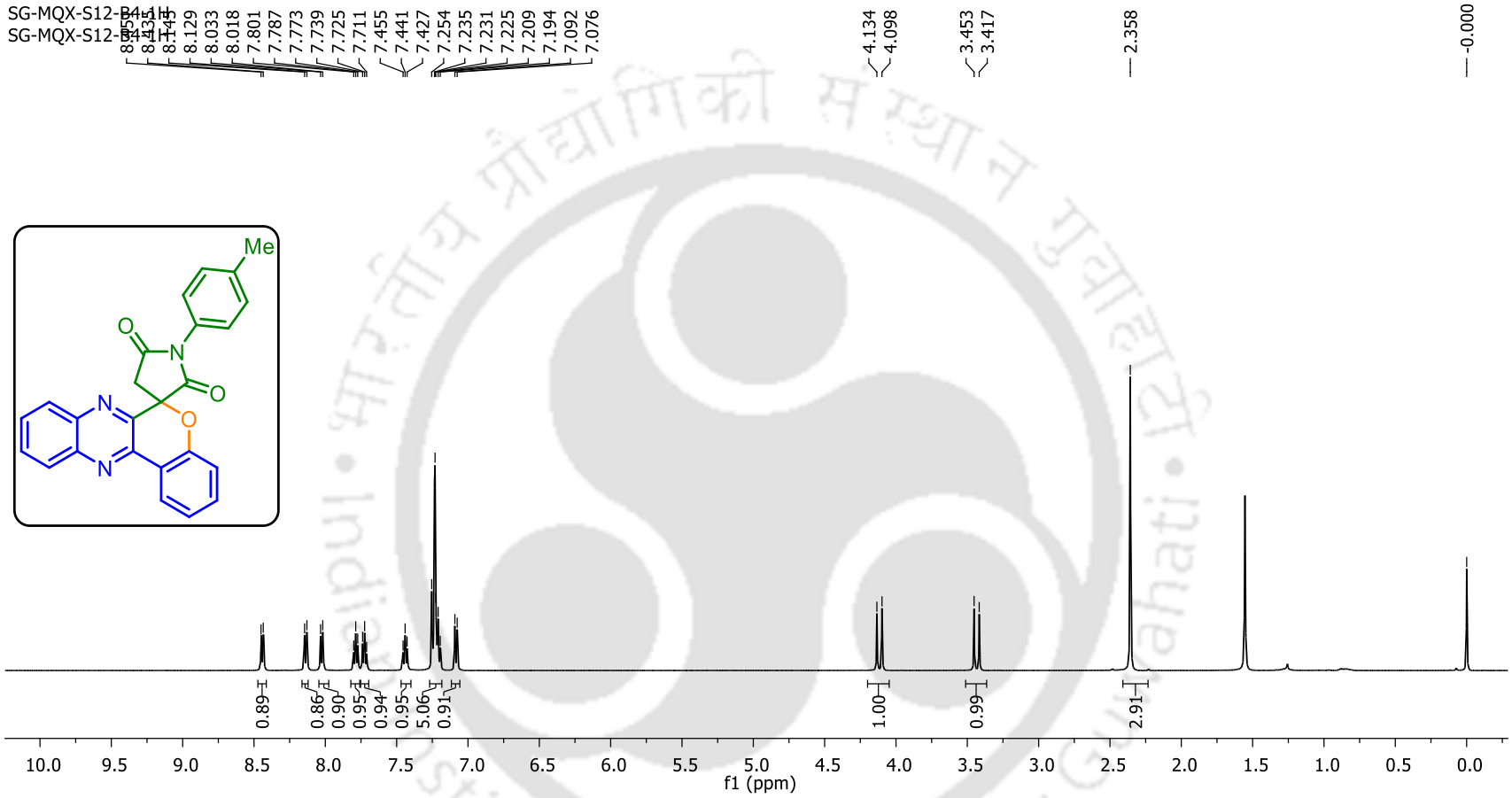

TH-3369_166122017

^{13}C {^{1}H} NMR of **1'-(*p*-Tolyl)spiro[chromeno[3,4-*b*]quinoxaline-6,3'-pyrrolidine]-2',5'-dione** (**20b**) ($CDCl_3$, 126 MHz)

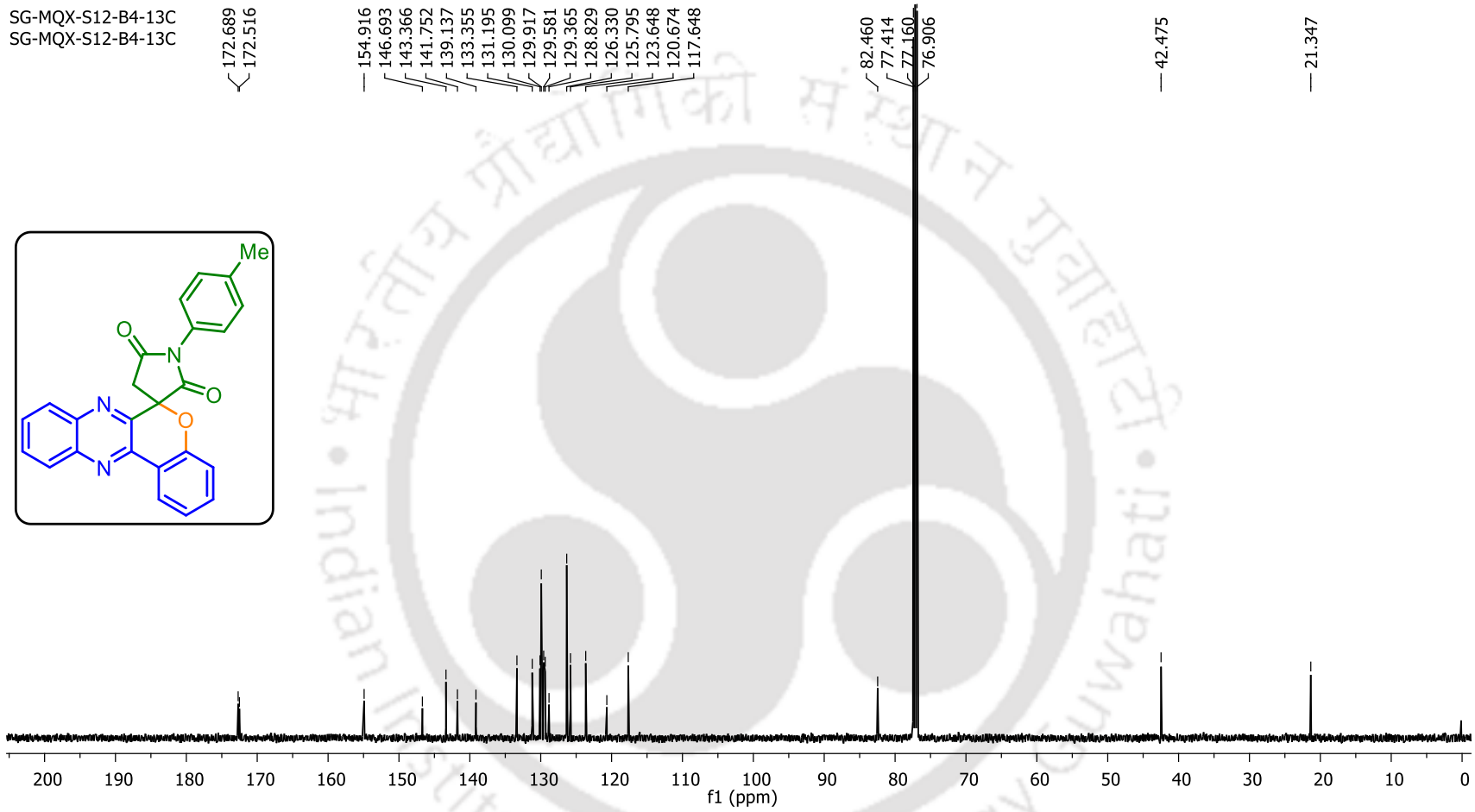

TH-3369_166122017

^{1}H NMR of **1'-(4-Fluorophenyl)spiro[chromeno[3,4-*b*]quinoxaline-6,3'-pyrrolidine]-2',5'-dione** (**21b**) ($CDCl_3$, 500 MHz)

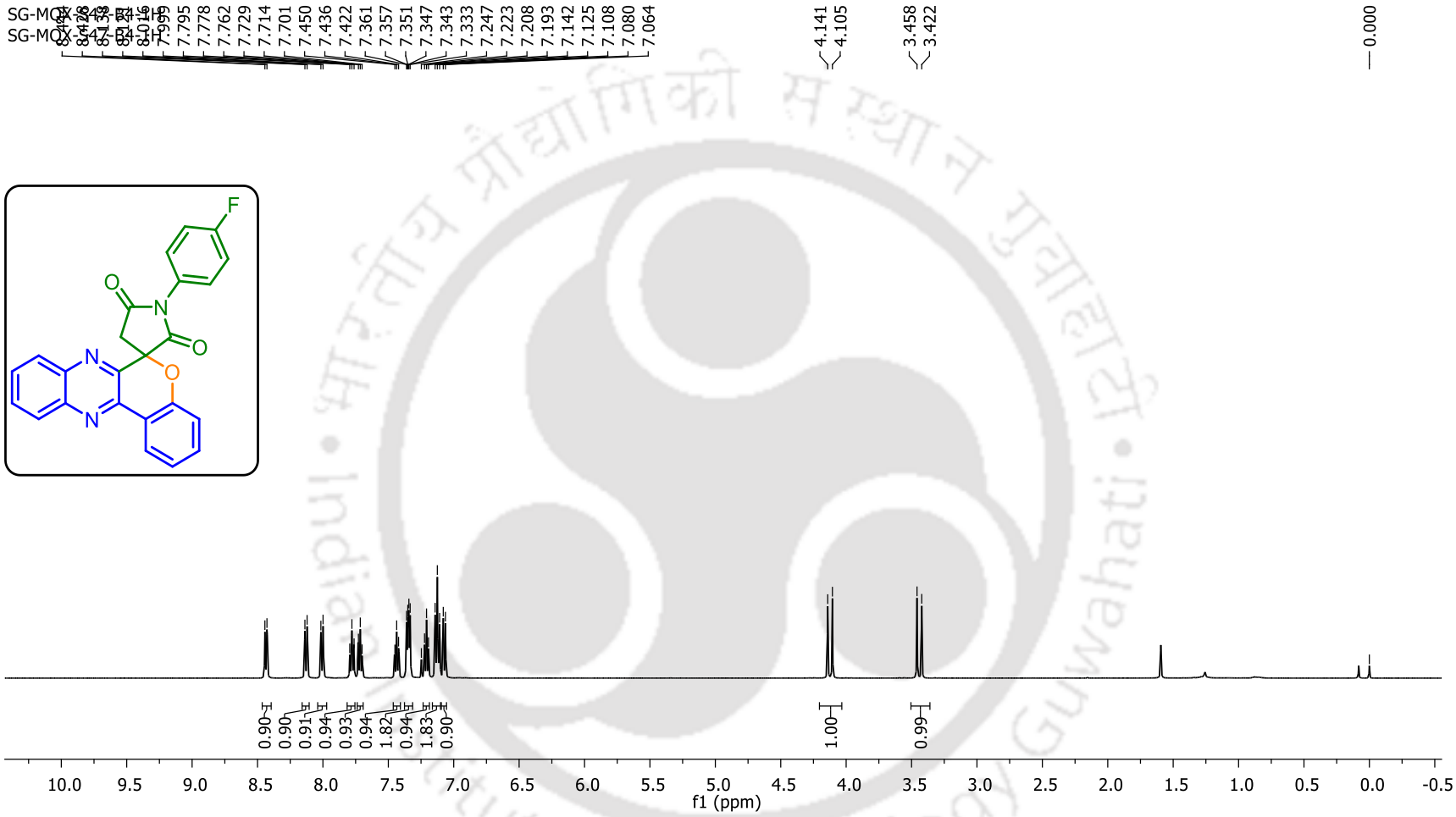

TH-3369_166122017

^{13}C {^{1}H} NMR of **1'-(4-Fluorophenyl)spiro[chromeno[3,4-*b*]quinoxaline-6,3'-pyrrolidine]-2',5'-dione** (**21b**) ($CDCl_3$, 126 MHz)

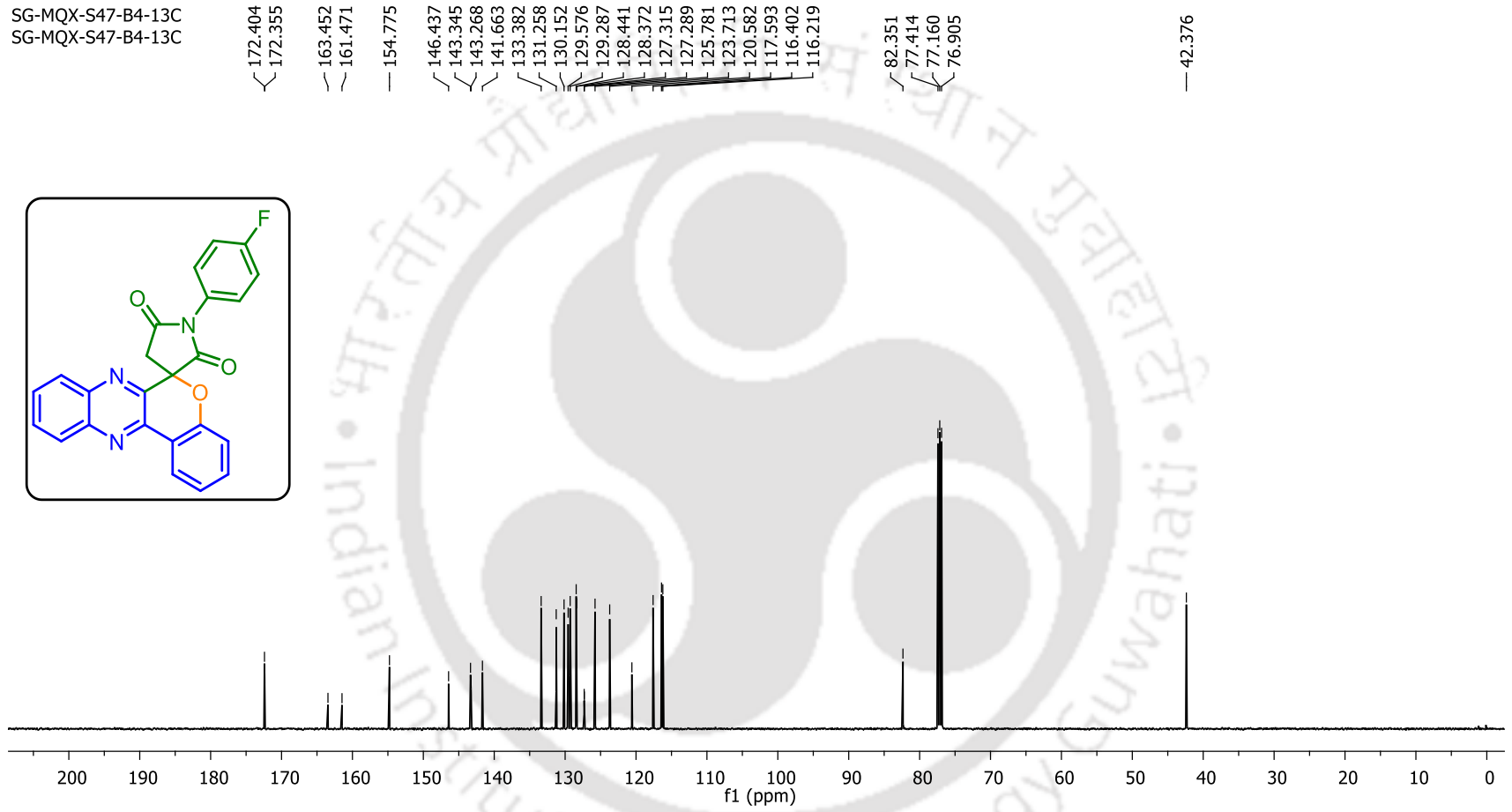

TH-3369_166122017

^{19}F NMR of **1'-(4-Fluorophenyl)spiro[chromeno[3,4-*b*]quinoxaline-6,3'-pyrrolidine]-2',5'-dione** (**21b**) ($CDCl_3$)

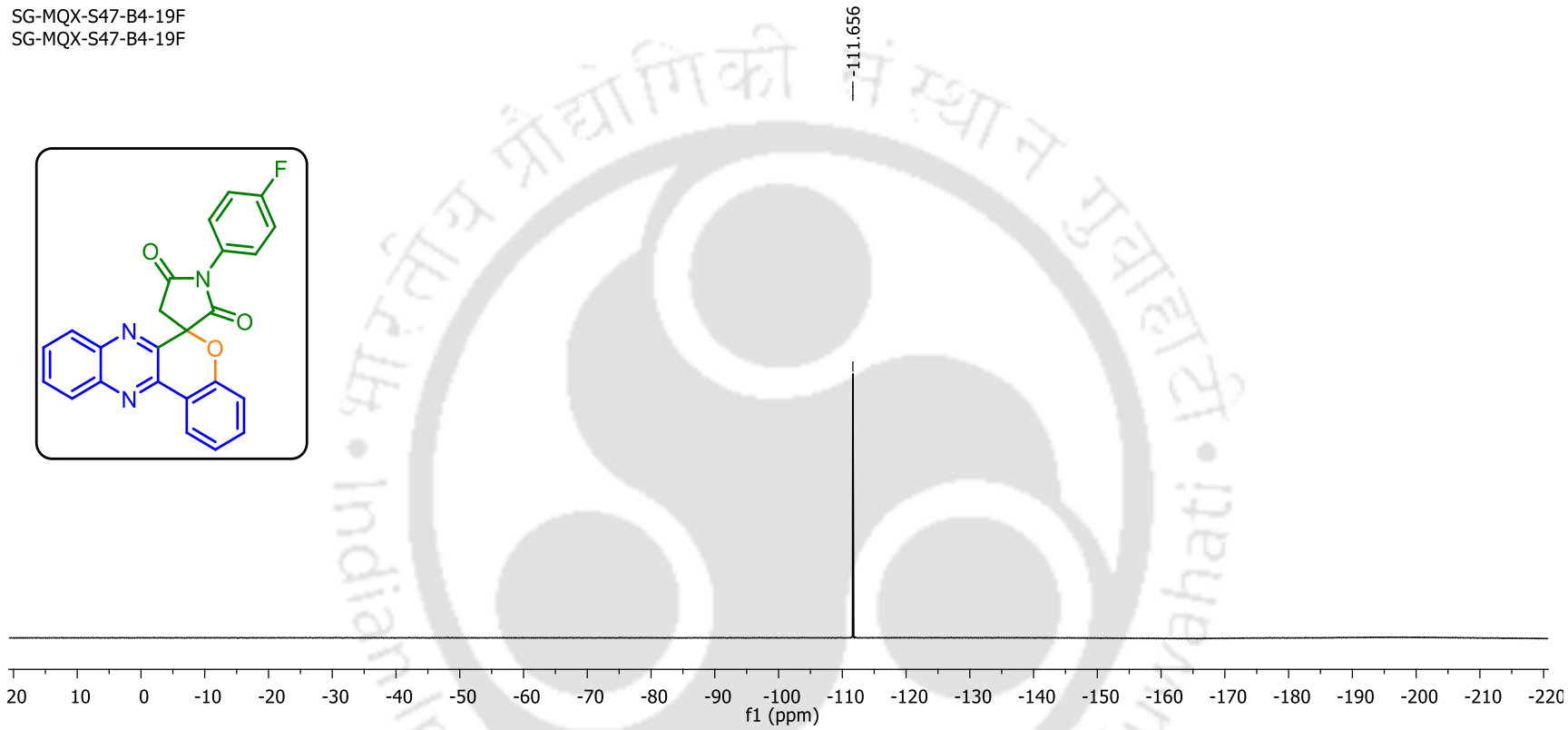

TH-3369_166122017

^{1}H NMR of **1'-(4-Methoxybenzyl)spiro[chromeno[3,4-*b*]quinoxaline-6,3'-pyrrolidine]-2',5'-dione** (**22b**) ($CDCl_3$, 500 MHz)

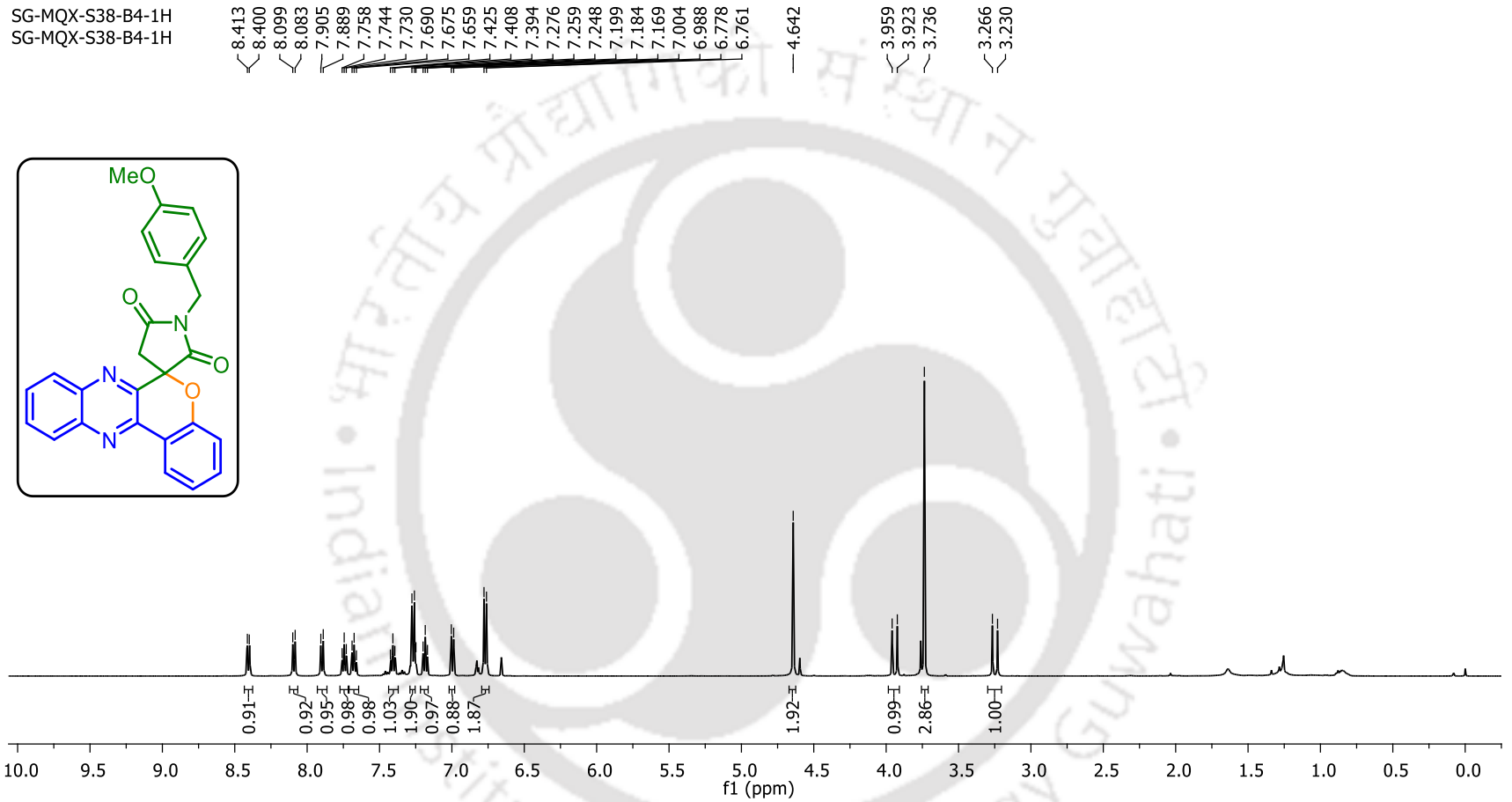

TH-3369_166122017

^{13}C {^{1}H} NMR of **1'-(4-Methoxybenzyl)spiro[chromeno[3,4-*b*]quinoxaline-6,3'-pyrrolidine]-2',5'-dione** (**22b**) ($CDCl_3$, 126 MHz)

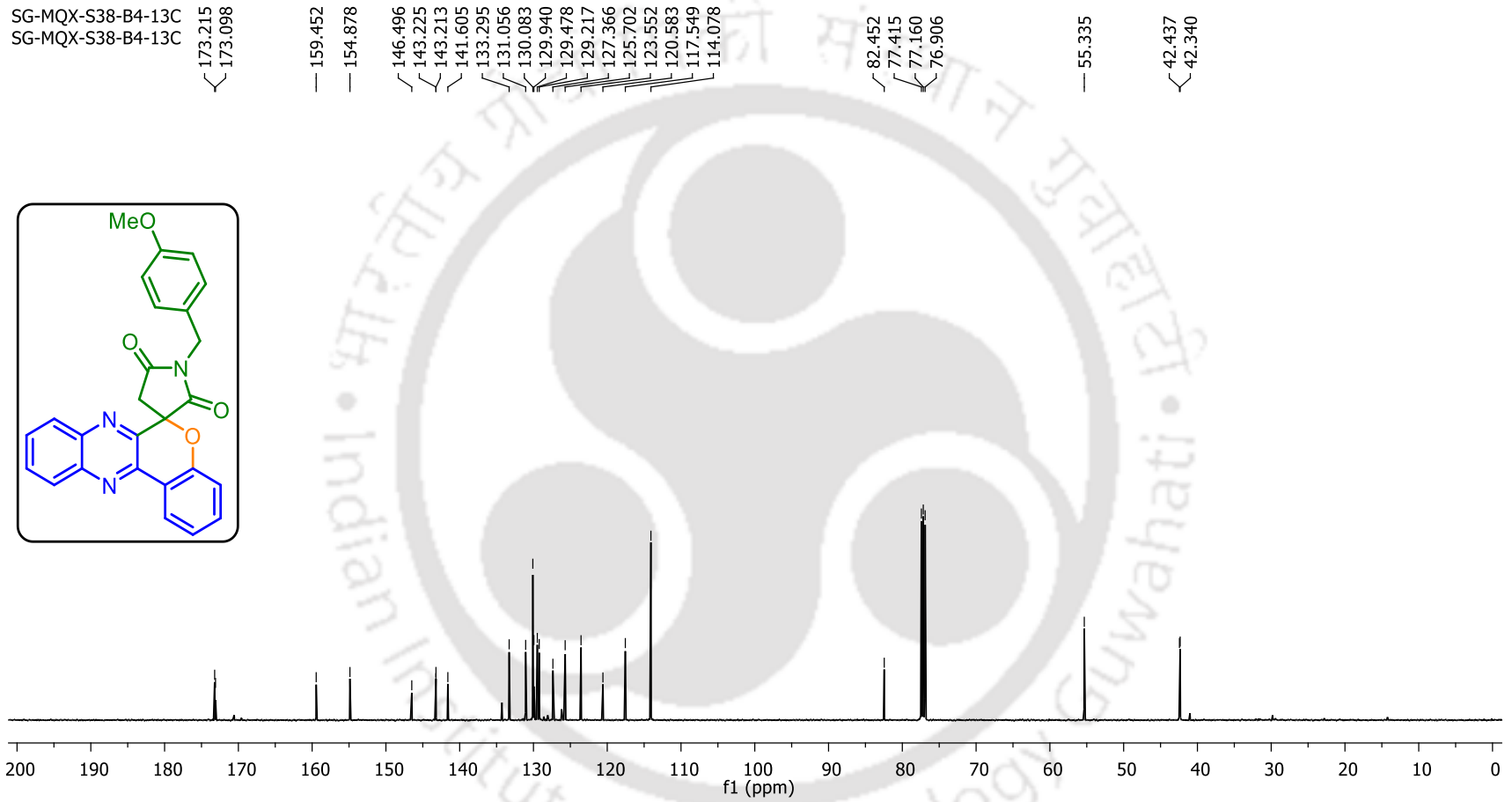

TH-3369_166122017

^{1}H NMR of **1'-(4-Phenylbutyl)spiro[chromeno[3,4-*b*]quinoxaline-6,3'-pyrrolidine]-2',5'-dione** (**23b**) ($CDCl_3$, 500 MHz)

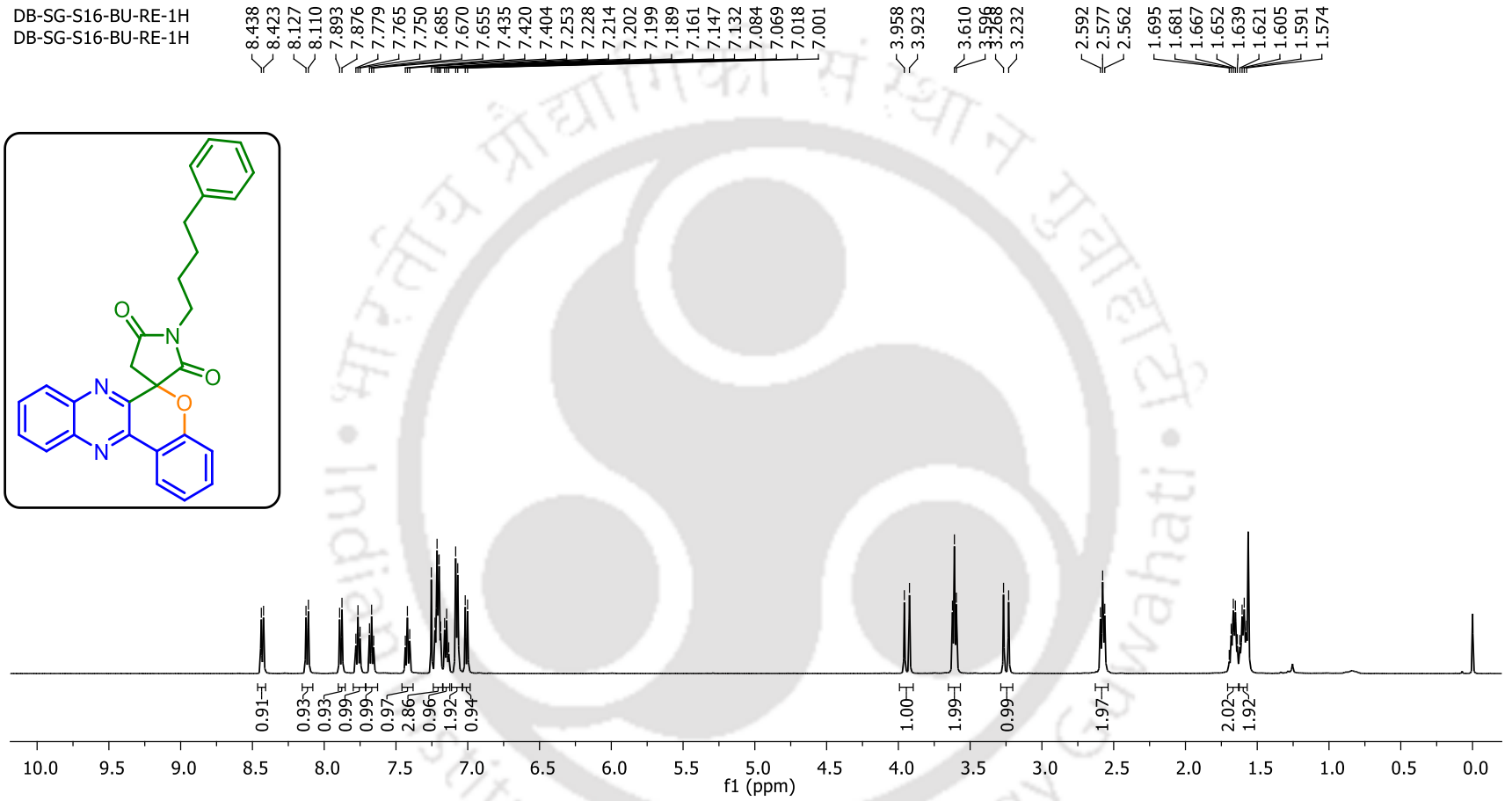

TH-3369_166122017

^{13}C {^{1}H} NMR of **1'-(4-Phenylbutyl)spiro[chromeno[3,4-*b*]quinoxaline-6,3'-pyrrolidine]-2',5'-dione** (**23b**) ($CDCl_3$, 126 MHz)

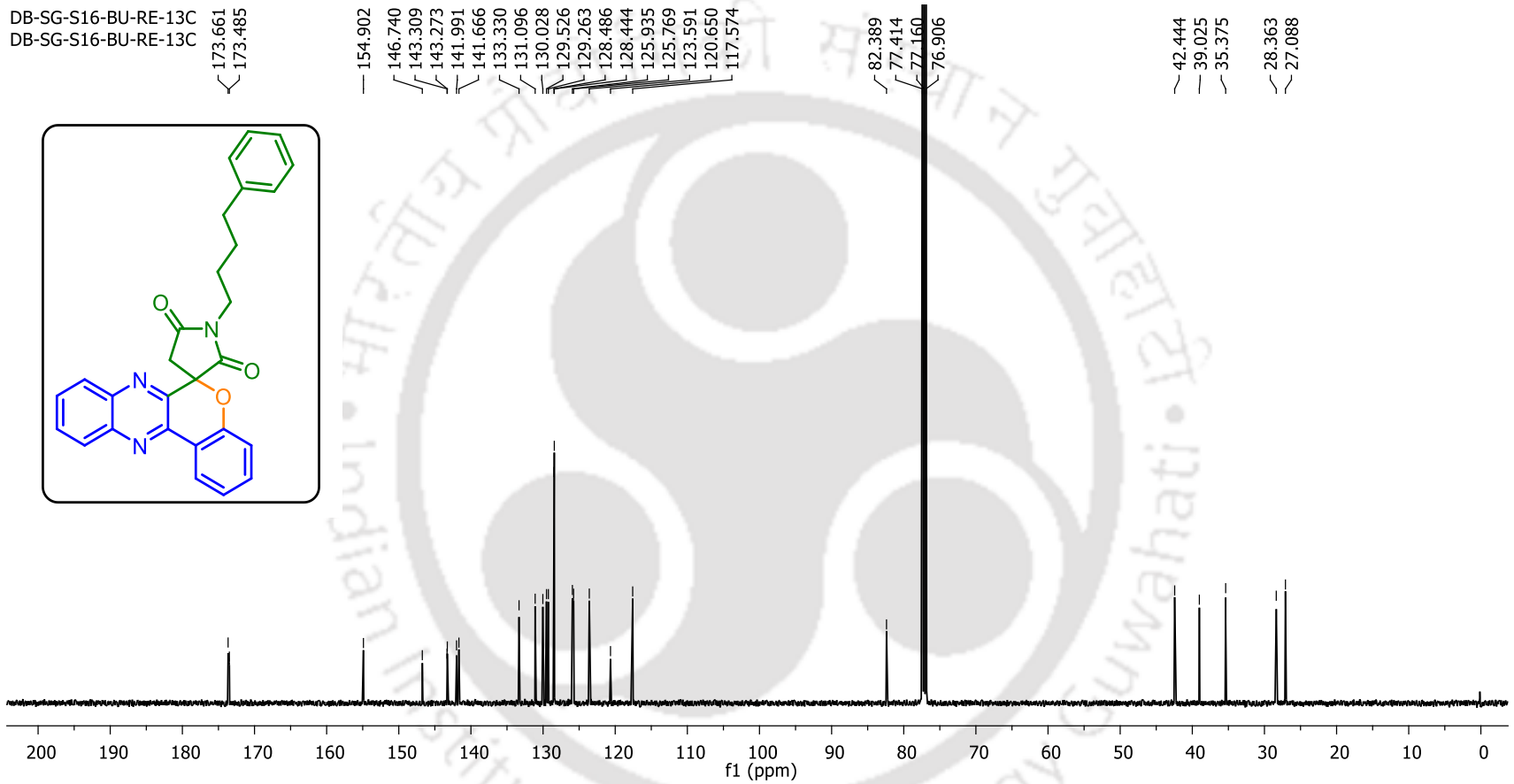

TH-3369_166122017

^{1}H NMR of **1'-Heptylspiro[chromeno[3,4-*b*]quinoxaline-6,3'-pyrrolidine]-2',5'-dione** (**24b**) ($CDCl_3$, 500 MHz)

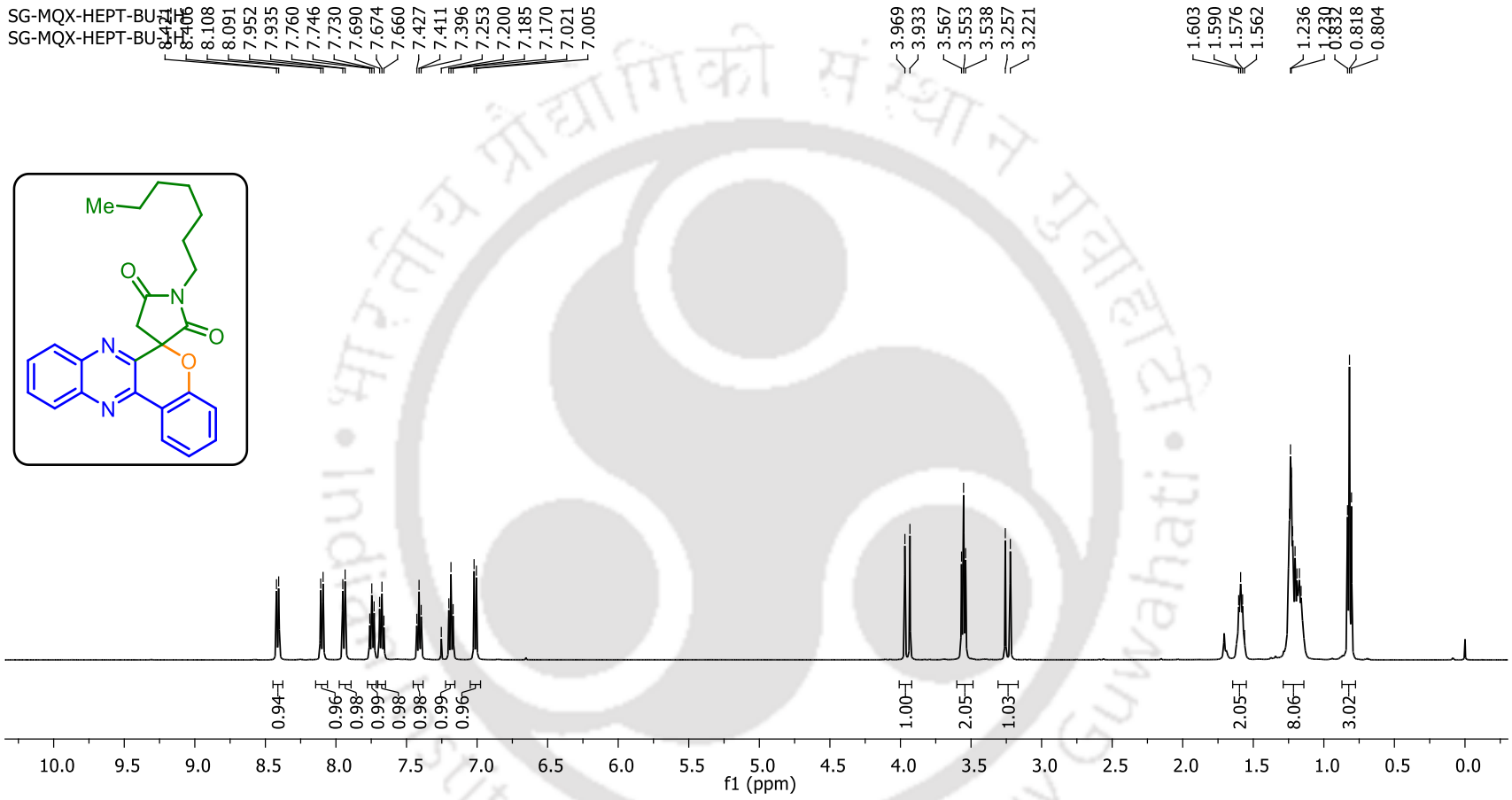

TH-3369_166122017

^{13}C {^{1}H} NMR of **1'-Heptylspiro[chromeno[3,4-*b*]quinoxaline-6,3'-pyrrolidine]-2',5'-dione** (**24b**) ($CDCl_3$, 126 MHz)

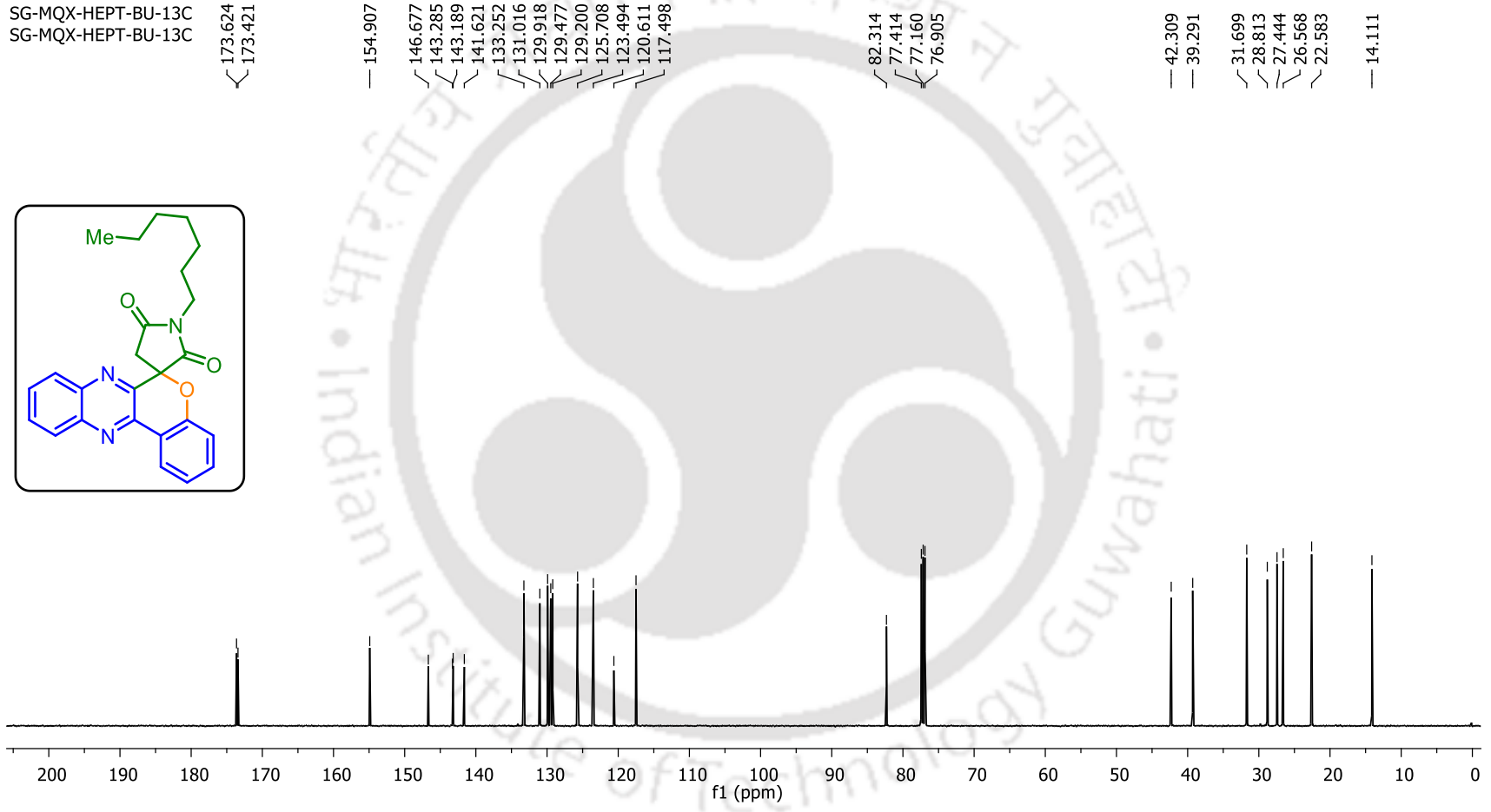

TH-3369_166122017

^{1}H NMR of **1'-Decylspiro[chromeno[3,4-*b*]quinoxaline-6,3'-pyrrolidine]-2',5'-dione (25b)** ($CDCl_3$, 500 MHz)

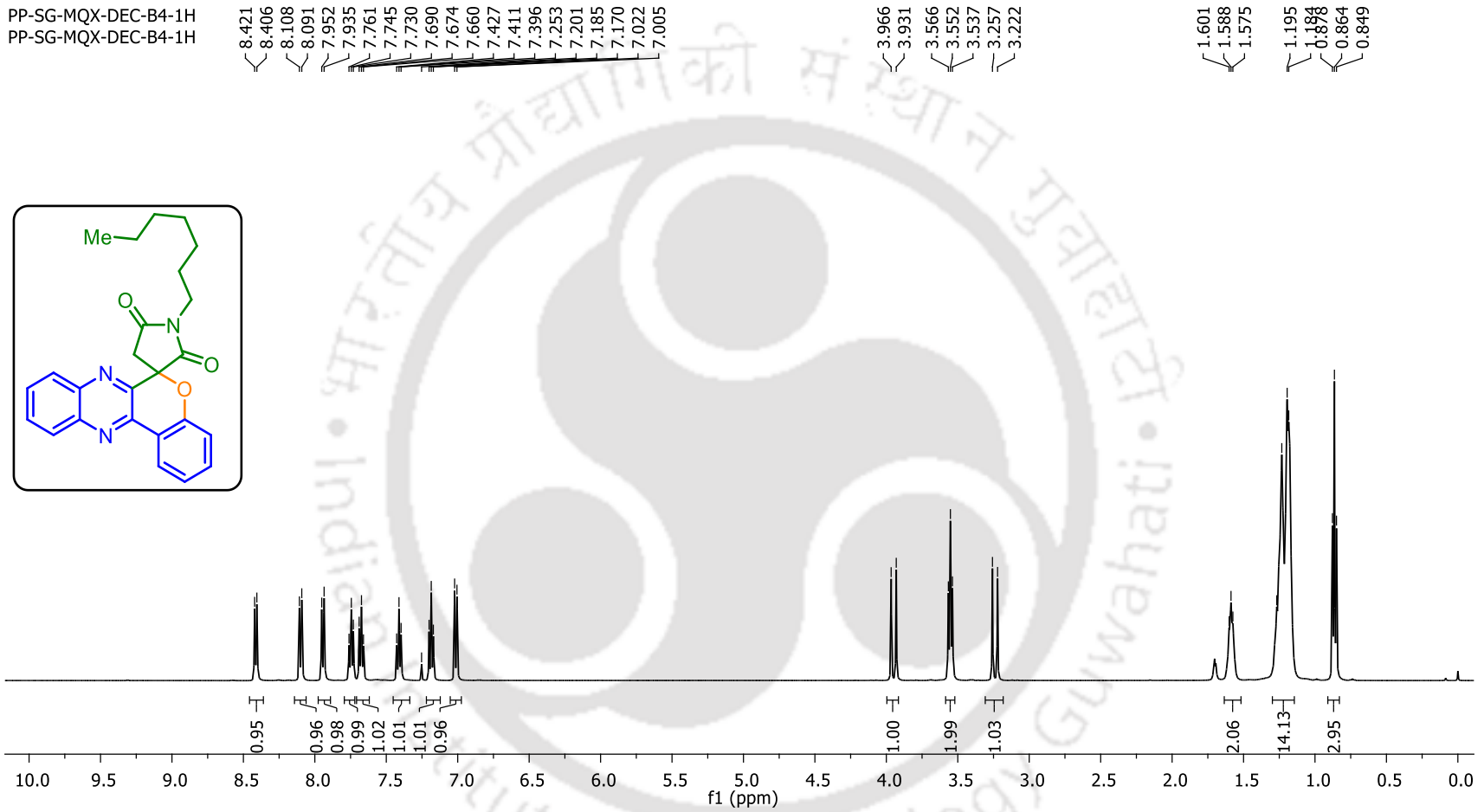

TH-3369_166122017

^{13}C {^{1}H} NMR of **1'-Decylspiro[chromeno[3,4-*b*]quinoxaline-6,3'-pyrrolidine]-2',5'-dione (25b)** ($CDCl_3$, 126 MHz)

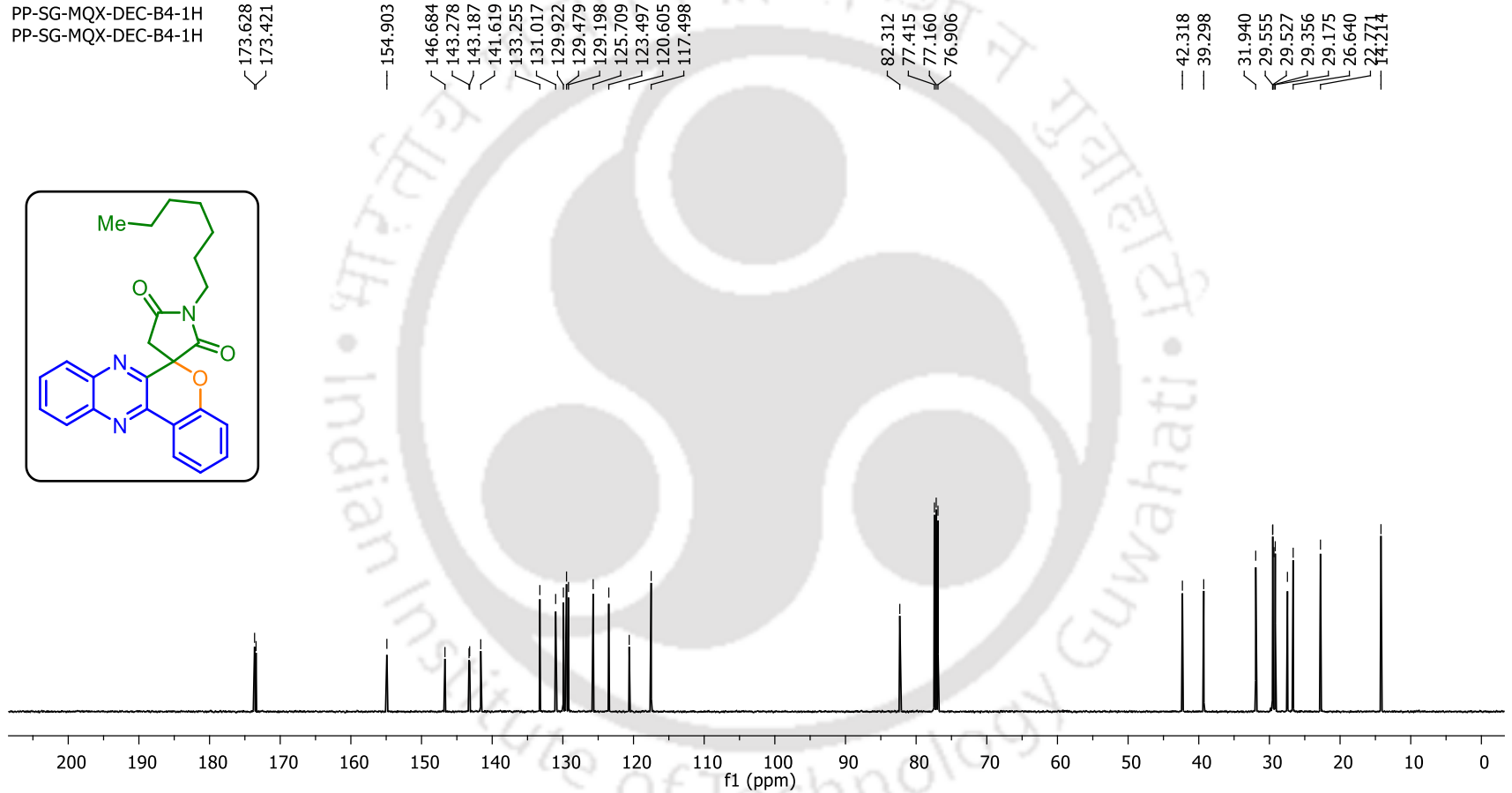

TH-3369_166122017

^{1}H NMR of **Spiro[chromeno[3,4-*b*]quinoxaline-6,3'-pyrrolidine]-2',5'-dione (26b)** (DMSO-d_6, 500 MHz)

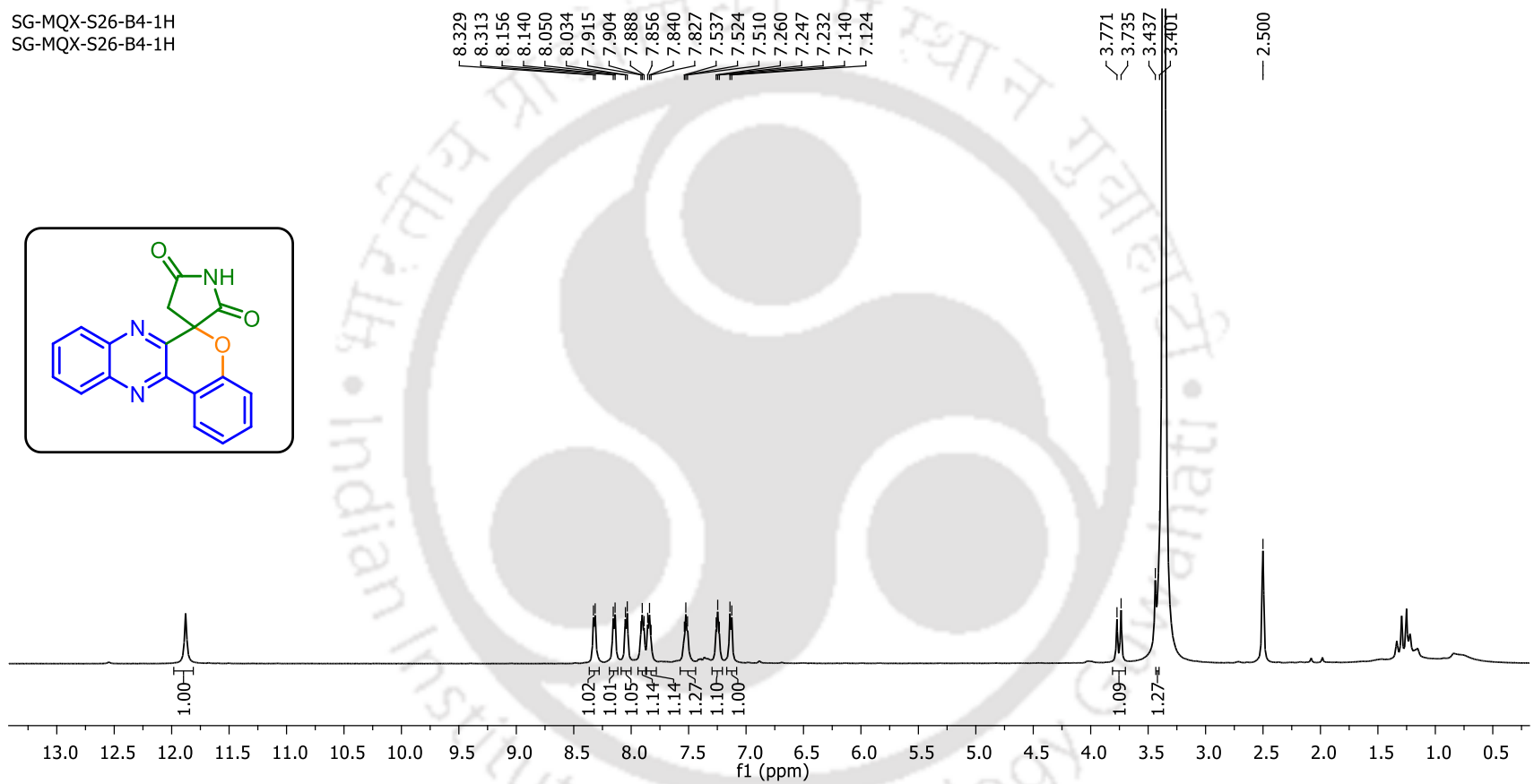

TH-3369_166122017

^{13}C {^{1}H} NMR of **Spiro[chromeno[3,4-*b*]quinoxaline-6,3'-pyrrolidine]-2',5'-dione** (**26b**) (DMSO-d_6, 126 MHz)

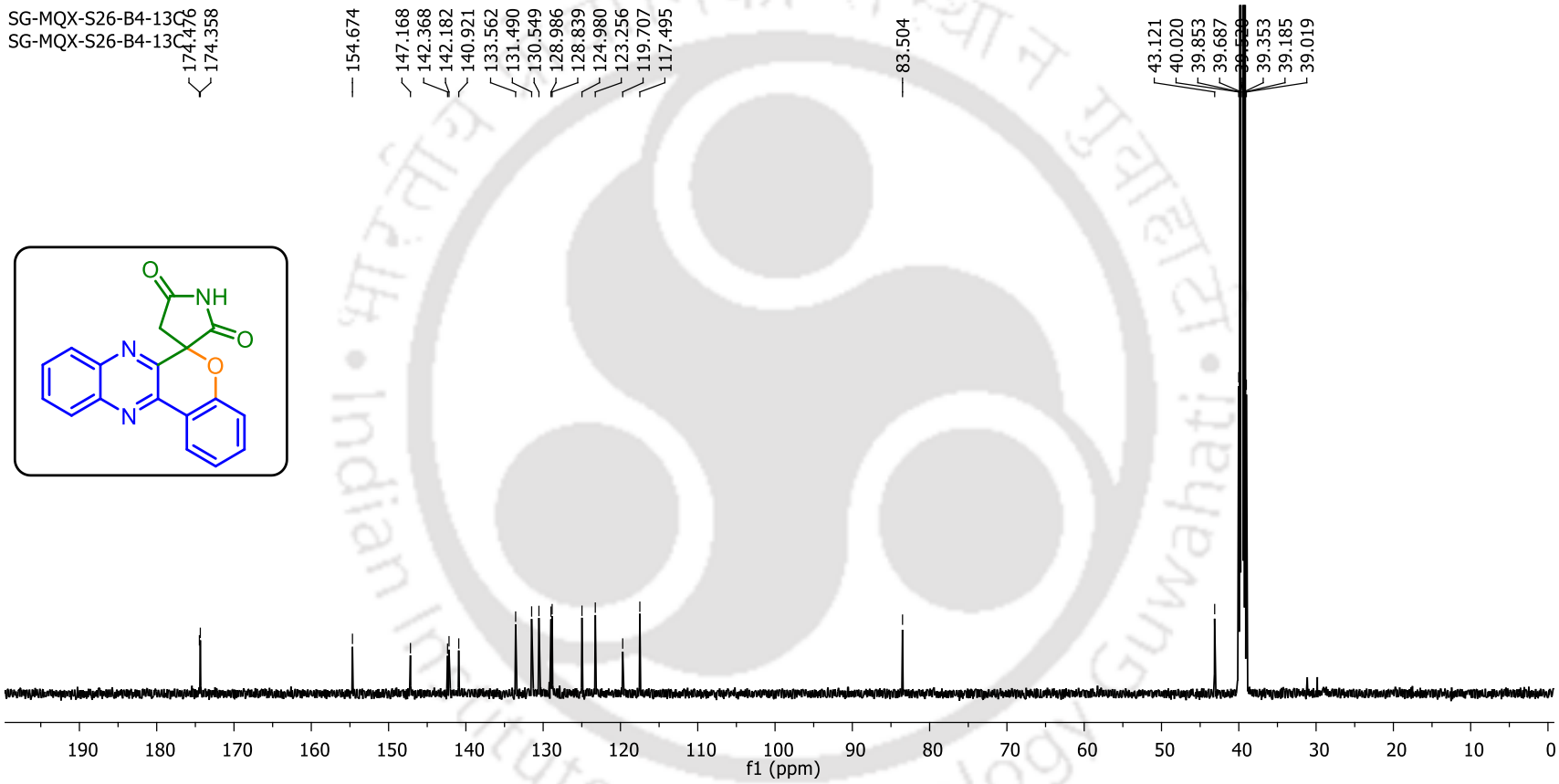

TH-3369_166122017

^{1}H NMR of **1'-((*S*)-1-(Naphthalen-1-yl)ethyl)spiro[chromeno[3,4-*b*]quinoxaline-6,3'-pyrrolidine]-2',5'-dione** (**27b**) ($CDCl_3$, 500 MHz)

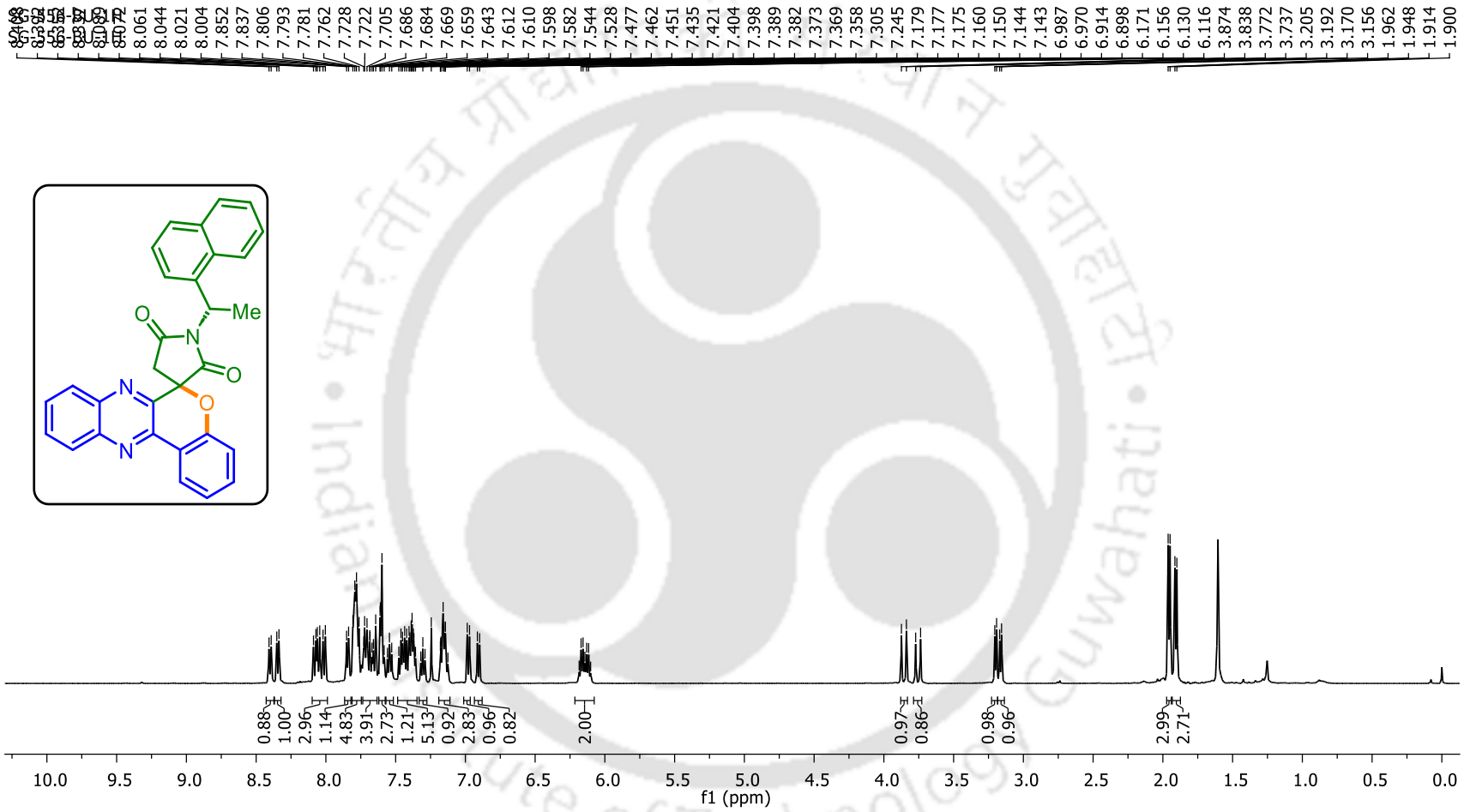

TH-3369_166122017

^{13}C {^{1}H} NMR of **1'-((*S*)-1-(Naphthalen-1-yl)ethyl)spiro[chromeno[3,4-*b*]quinoxaline-6,3'-pyrrolidine]-2',5'-dione** (**27b**) ($CDCl_3$, 126 MHz)

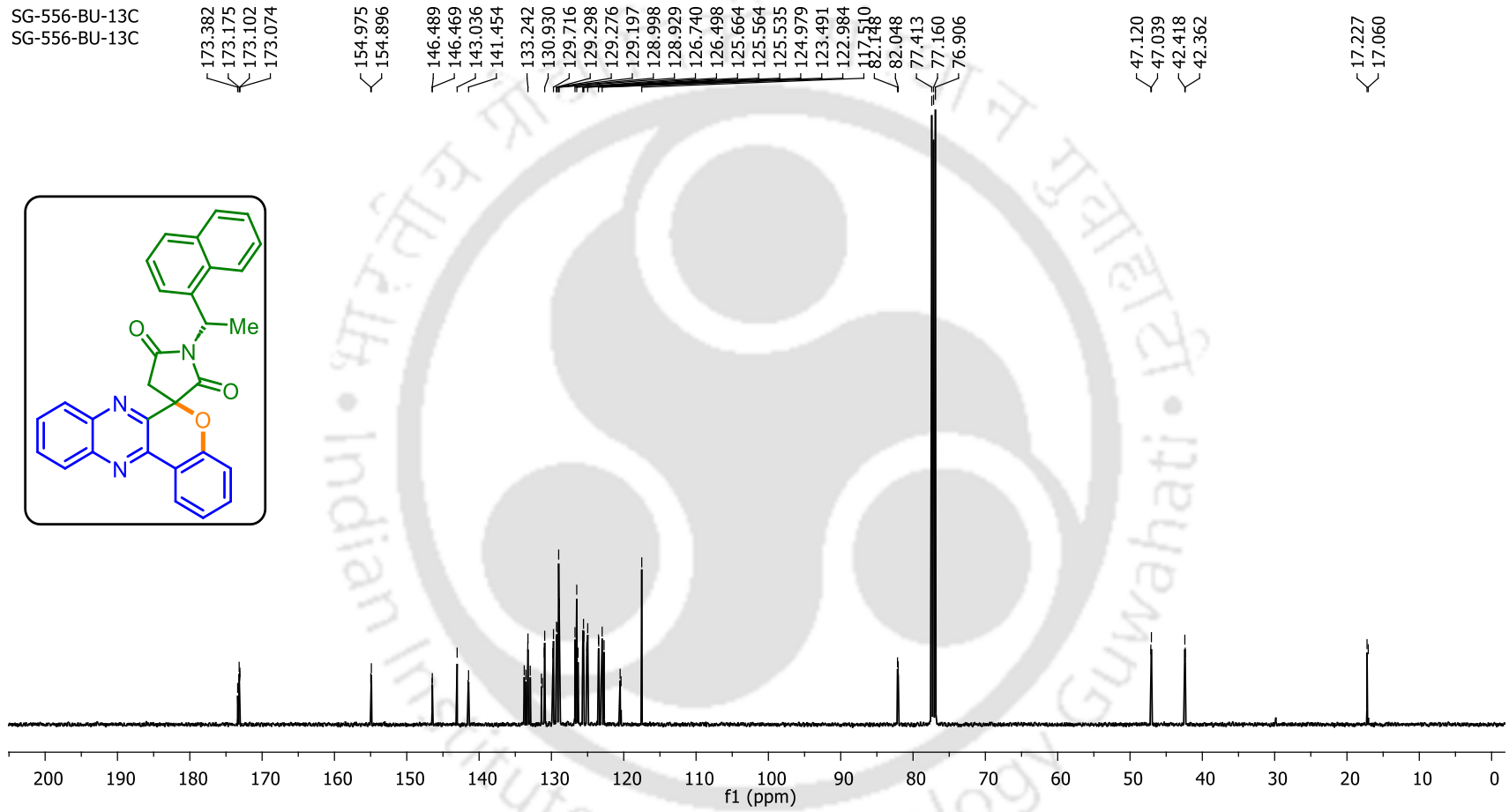

TH-3369_166122017

^{1}H NMR of **1'-((*S*)-1-Phenylethyl)spiro[chromeno[3,4-*b*]quinoxaline-6,3'-pyrrolidine]-2',5'-dione** (**28b**) ($CDCl_3$, 400 MHz)

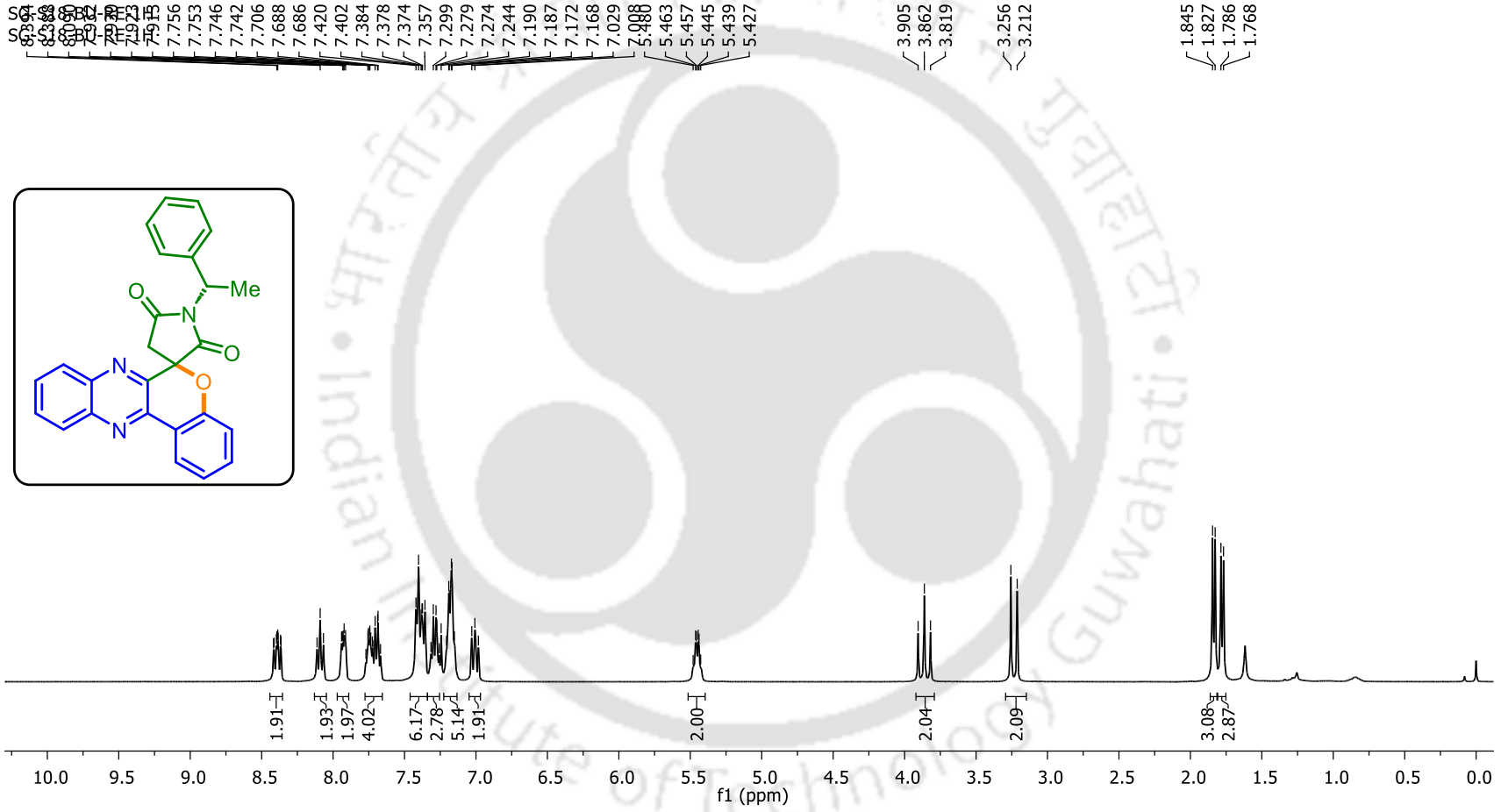

TH-3369_166122017

^{13}C {^{1}H} NMR of **1'-((*S*)-1-Phenylethyl)spiro[chromeno[3,4-*b*]quinoxaline-6,3'-pyrrolidine]-2',5'-dione** (**28b**) ($CDCl_3$, 126 MHz)

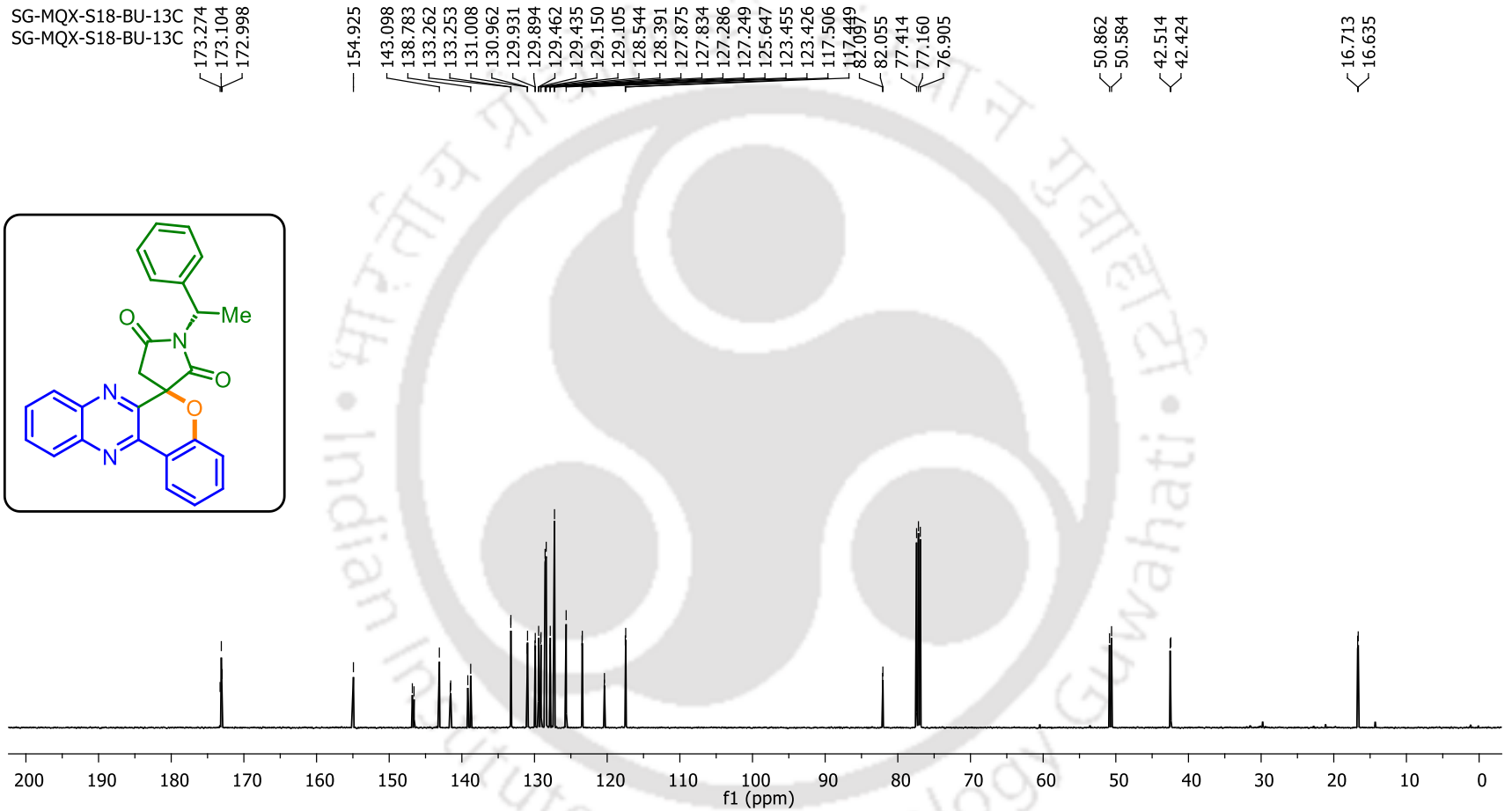

TH-3369_166122017

^{1}H NMR of **1'-Phenethylspiro[chromeno[3,4-*b*]quinoxaline-6,3'-pyrrolidine]-2',5'-dione** (**29b**) ($CDCl_3$, 500 MHz)

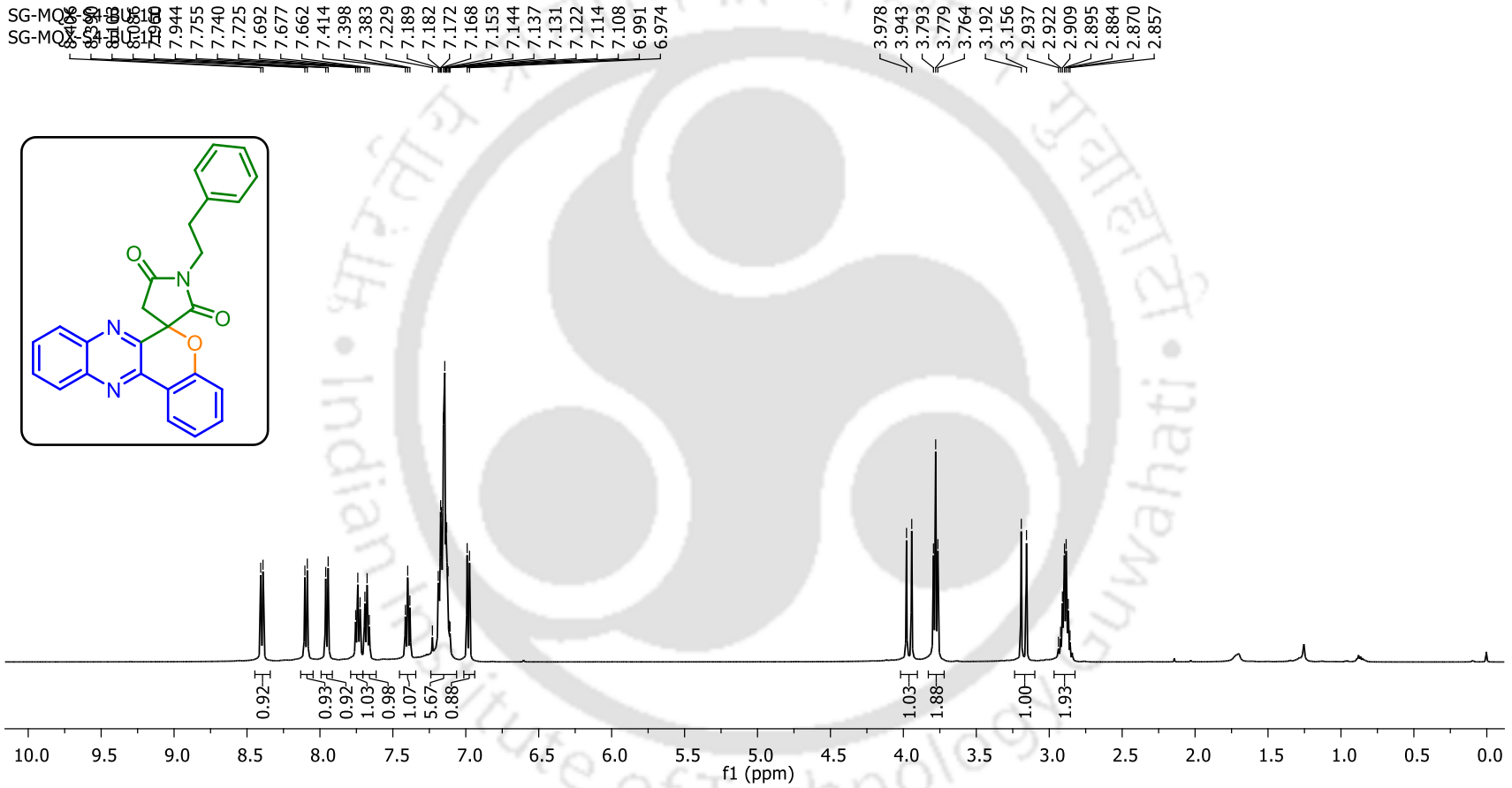

TH-3369_166122017

^{13}C {^{1}H} NMR of **1'-Phenethylspiro[chromeno[3,4-*b*]quinoxaline-6,3'-pyrrolidine]-2',5'-dione** (**29b**) ($CDCl_3$, 126 MHz)

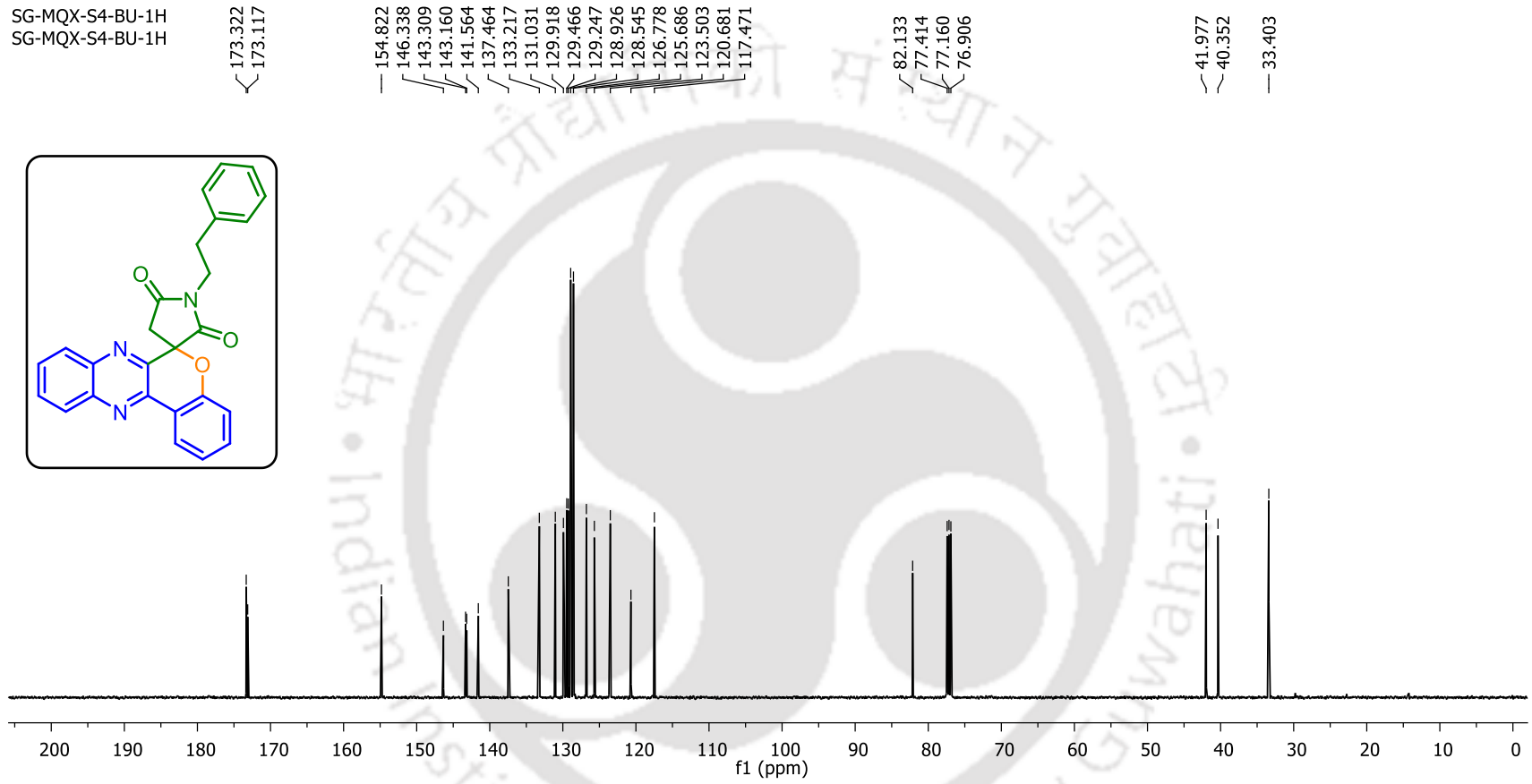

TH-3369_166122017

^{1}H NMR of **1'-(2-(Thiophen-2-yl)ethyl)spiro[chromeno[3,4-*b*]quinoxaline-6,3'-pyrrolidine]-2',5'-dione** (**30b**) ($CDCl_3$, 500 MHz)

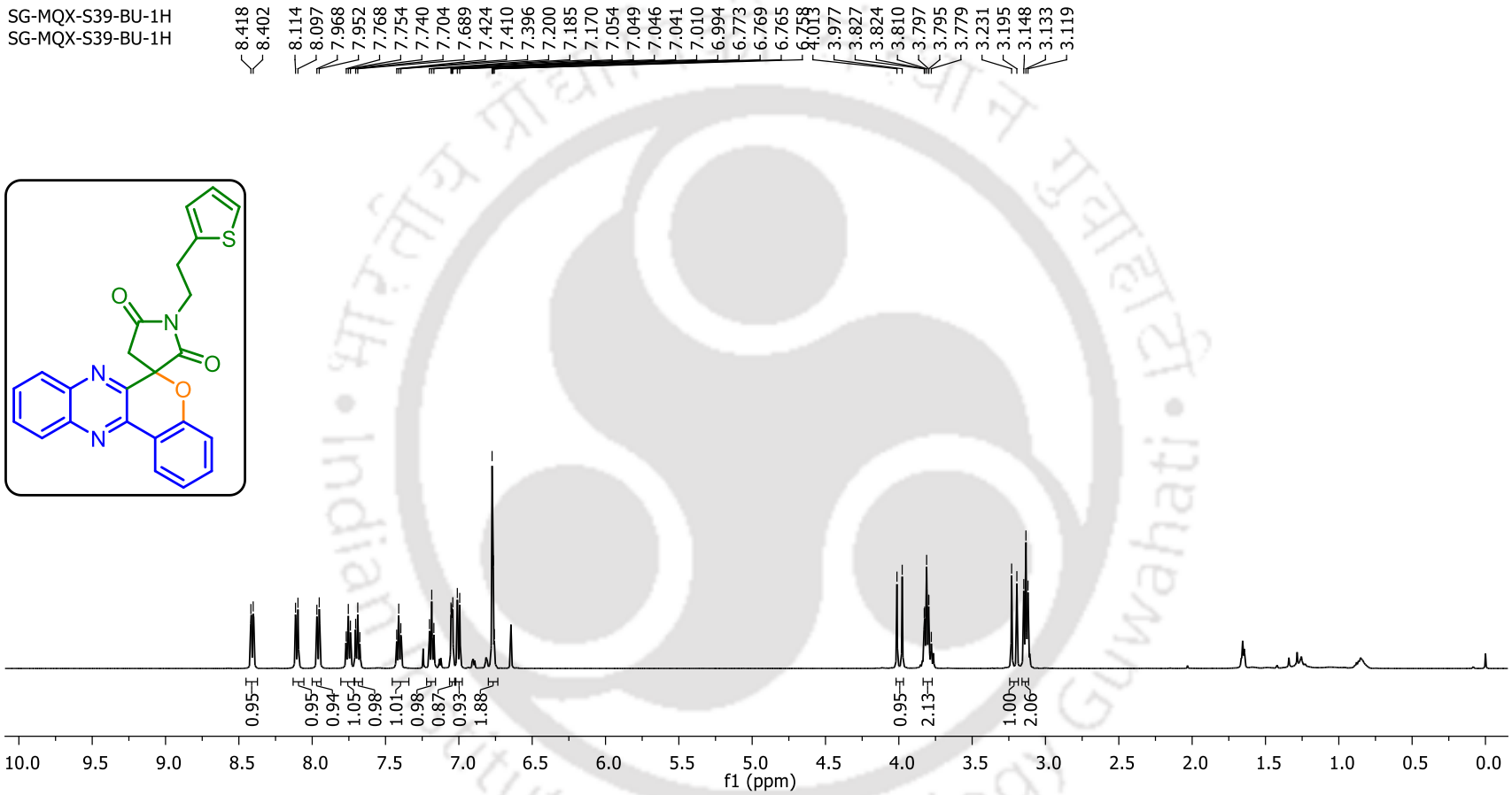

TH-3369_166122017

^{13}C {^{1}H} NMR of **1'-(2-(Thiophen-2-yl)ethyl)spiro[chromeno[3,4-*b*]quinoxaline-6,3'-pyrrolidine]-2',5'-dione** (**30b**) ($CDCl_3$, 126 MHz)

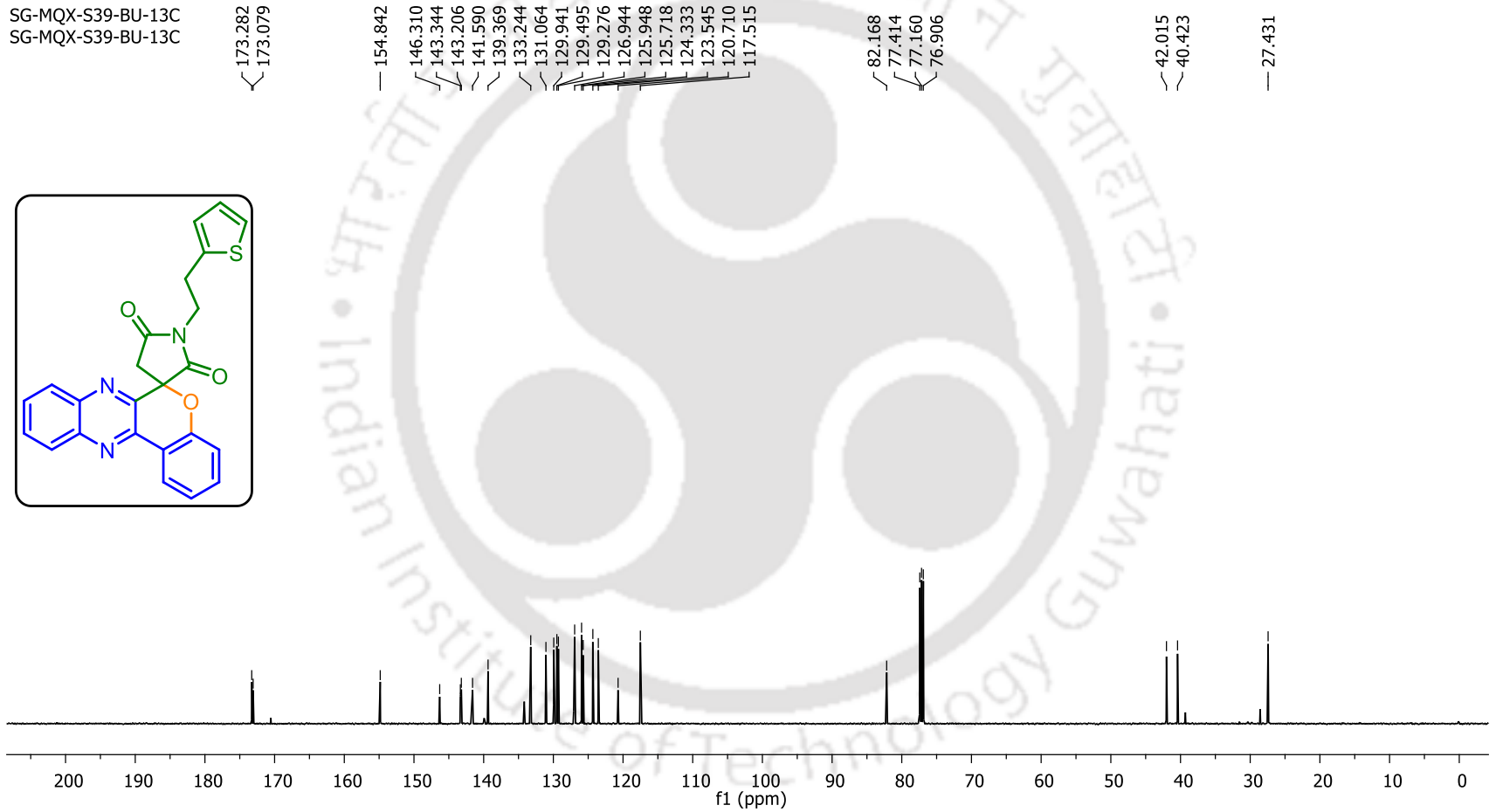

^{1}H NMR of **(1*S*,2*R*,5*S*)-2-isopropyl-5-methylcyclohexyl2',5'-dioxo-1'-phenylspiro[chromeno[3,4-*b*]quinoxaline-6,3'-pyrrolidine]-3-carboxylate** (**31b**) ($CDCl_3$, 500 MHz)

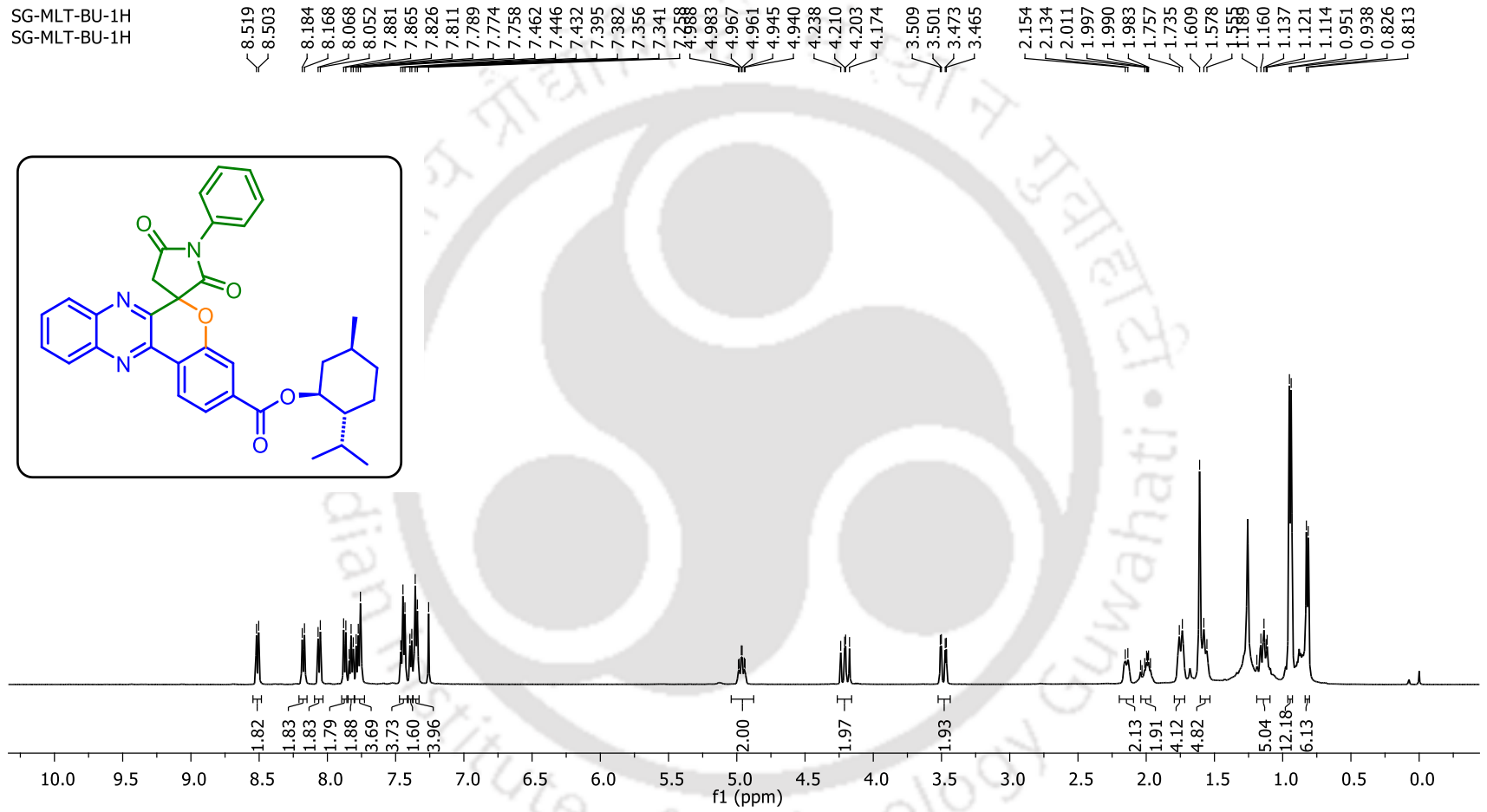

TH-3369_166122017

^{13}C {^{1}H} NMR of **(1*S*,2*R*,5*S*)-2-isopropyl-5-methylcyclohexyl2',5'-dioxo-1'-phenylspiro[chromeno[3,4-*b*]quinoxaline-6,3'-pyrrolidine]-3-carboxylate** (**31b**) ($CDCl_3$, 126 MHz)

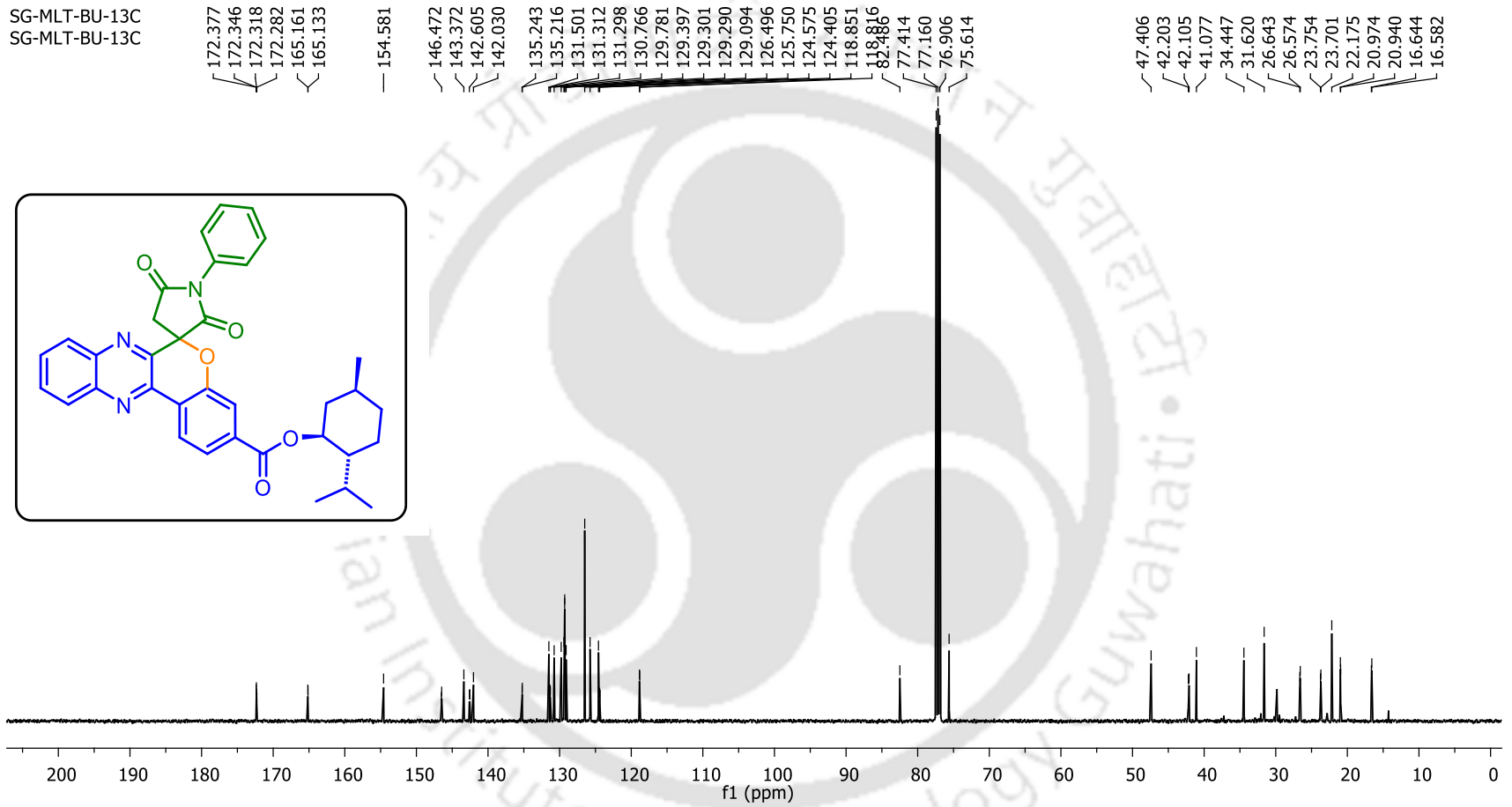

TH-3369_166122017

^{1}H NMR of **1,7,7-Trimethylbicyclo[2.2.1]heptan-2-yl2',5'-dioxo-1'-phenylspiro[chromeno[3,4-*b*]quinoxaline-6,3'-pyrrolidine]-3-carboxylate** (**32b**) ($CDCl_3$, 500 MHz)

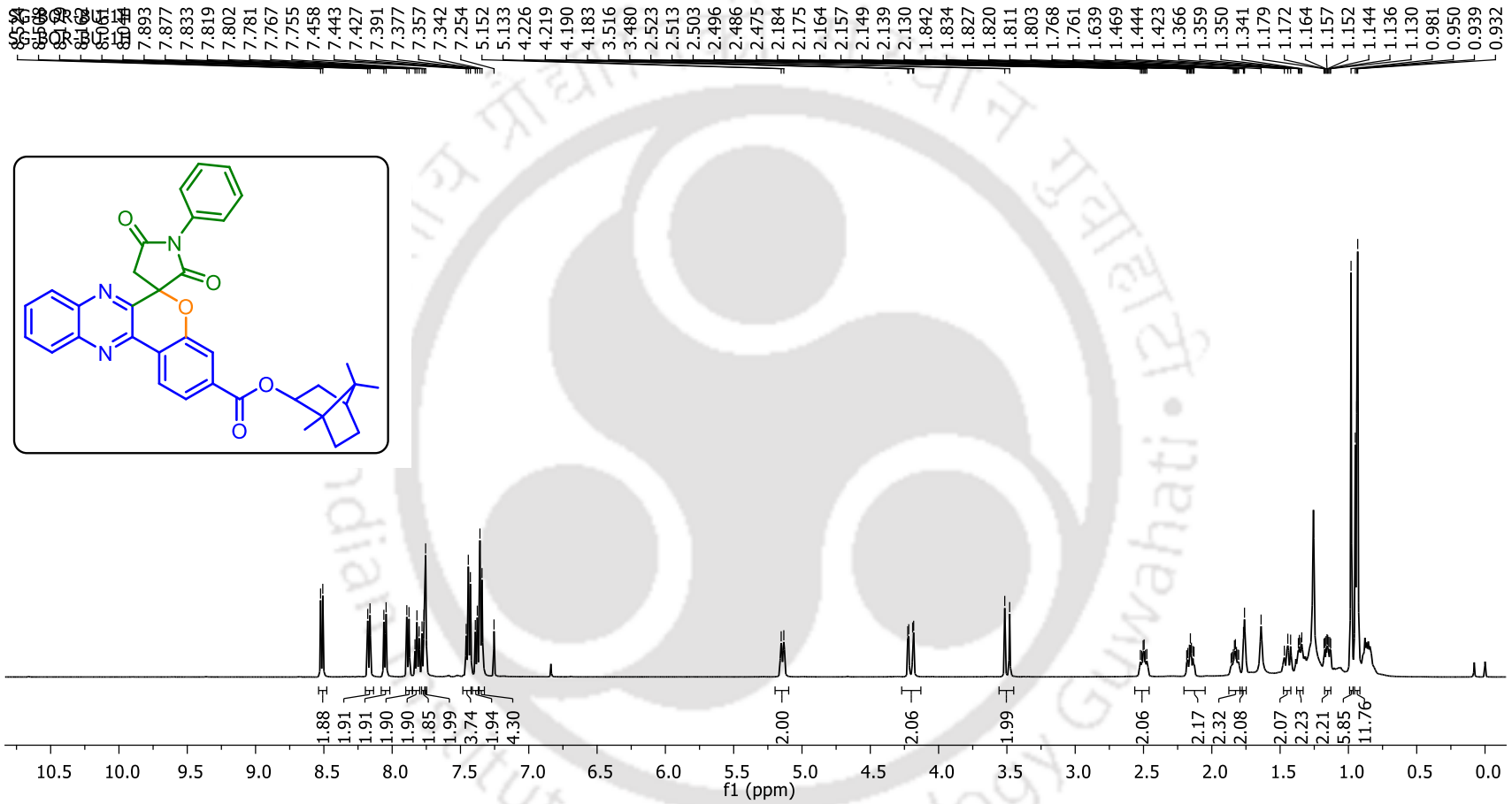

TH-3369_166122017

^{13}C {^{1}H} NMR of **1,7,7-Trimethylbicyclo[2.2.1]heptan-2-yl2',5'-dioxo-1'-phenylspiro[chromeno[3,4-*b*]quinoxaline-6,3'-pyrrolidine]-3-carboxylate** (**32b**) ($CDCl_3$, 126 MHz)

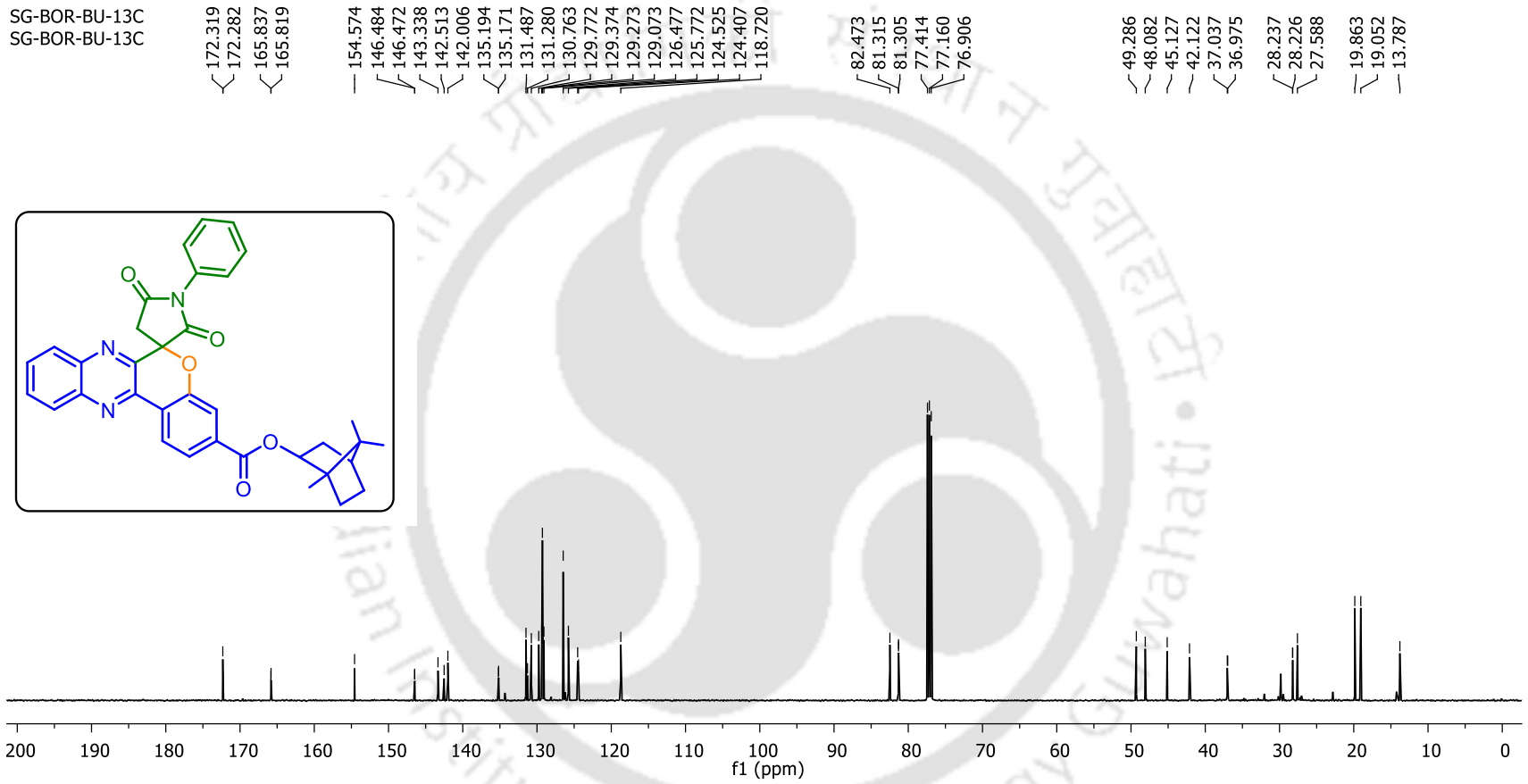

TH-3369_166122017

^{1}H NMR of **1'-(2-(1*H*-Indol-3-yl)ethyl)spiro[chromeno[3,4-*b*]quinoxaline-6,3'-pyrrolidine]-2',5'-dione** (**33b**) ($CDCl_3$, 500 MHz)

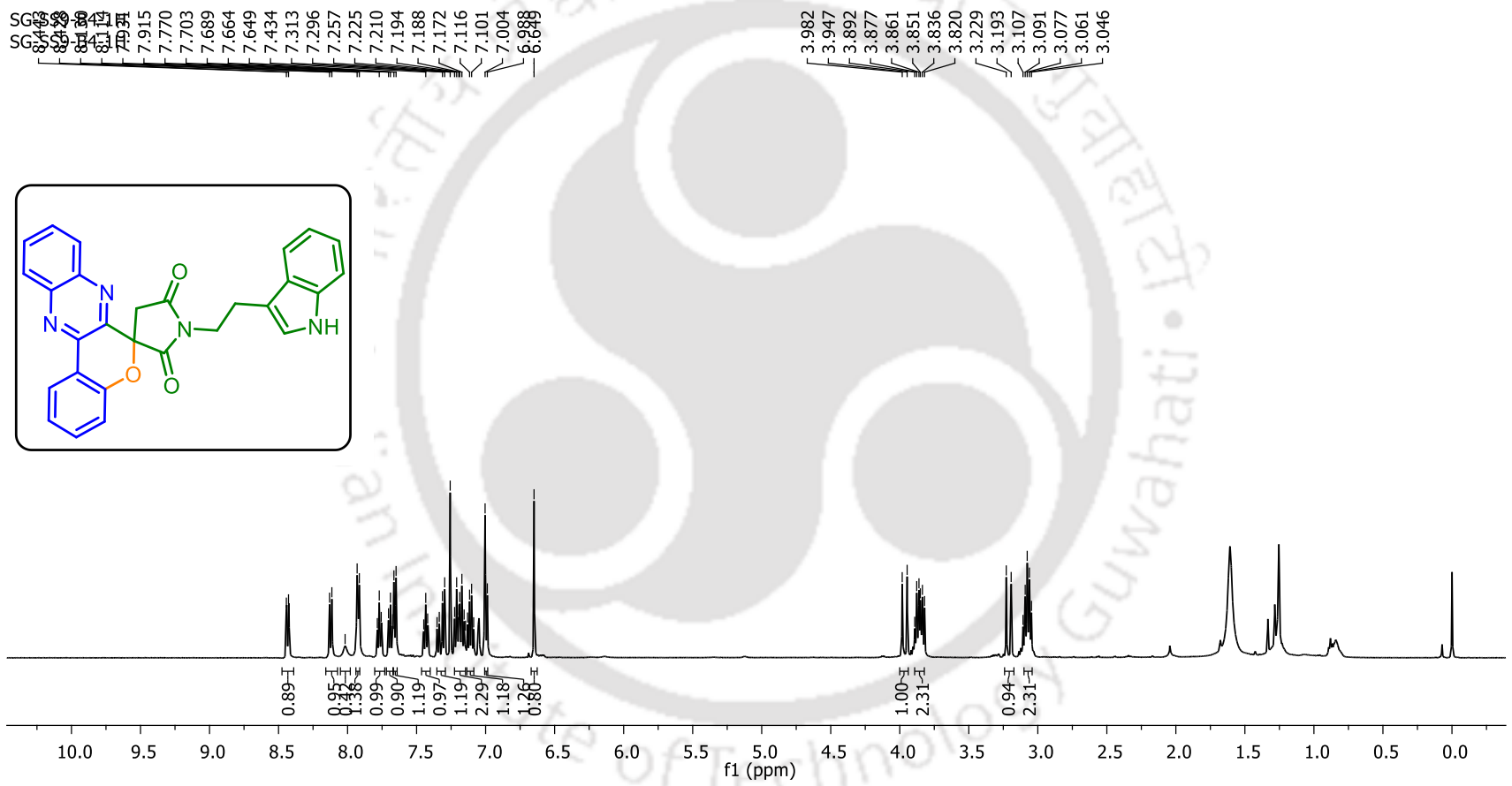

TH-3369_166122017

^{13}C {^{1}H} NMR of **1'-(2-(1*H*-Indol-3-yl)ethyl)spiro[chromeno[3,4-*b*]quinoxaline-6,3'-pyrrolidine]-2',5'-dione** (**33b**) ($CDCl_3$, 126 MHz)

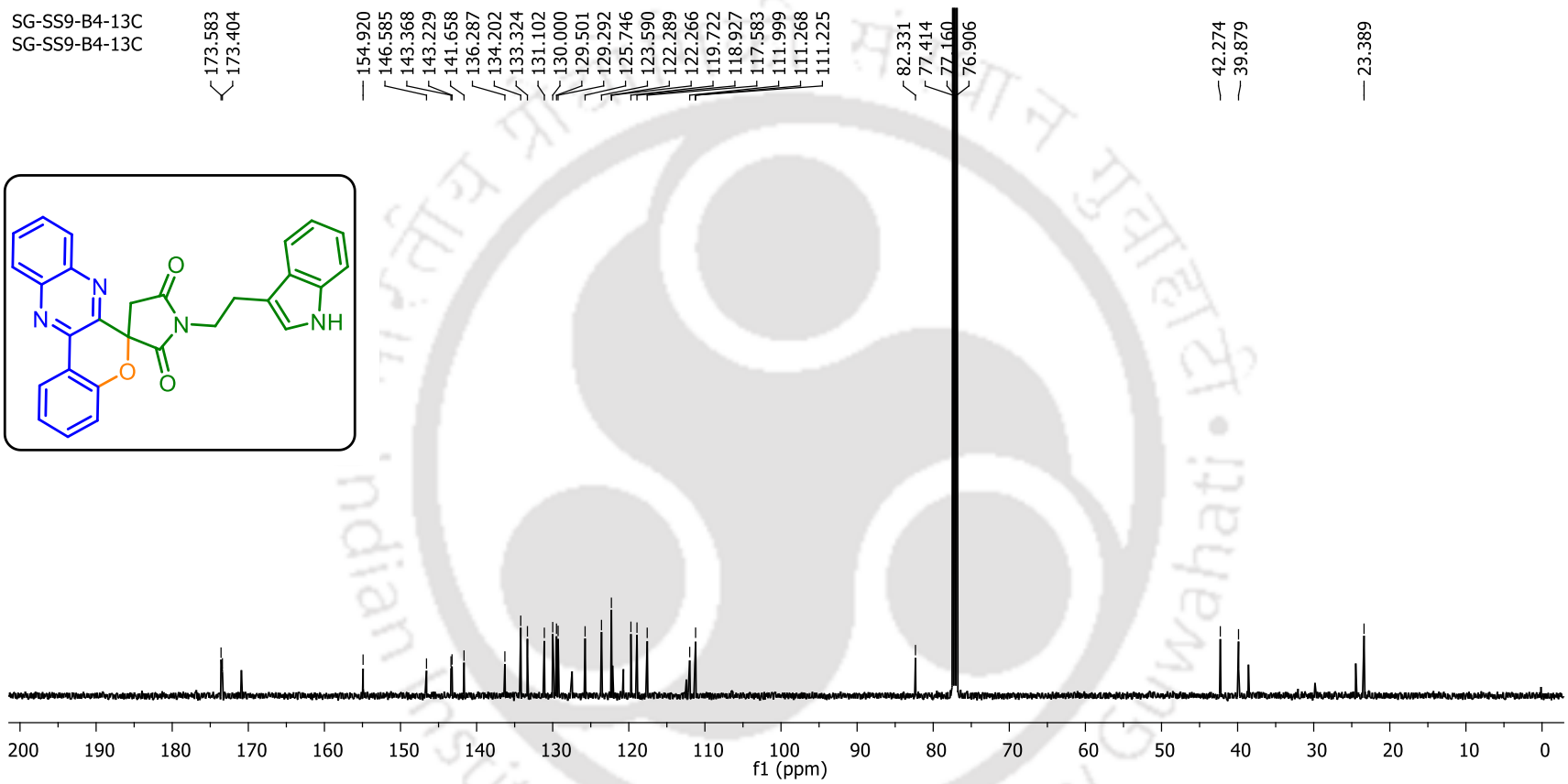

TH-3369_166122017

^{1}H NMR of **1',1'''-(1,3-Phenylene)bis(spiro[chromeno[3,4-*b*]quinoxaline-6,3'-pyrrolidine]-2',5'-dione)** (**34b**) ($CDCl_3$, 400 MHz)

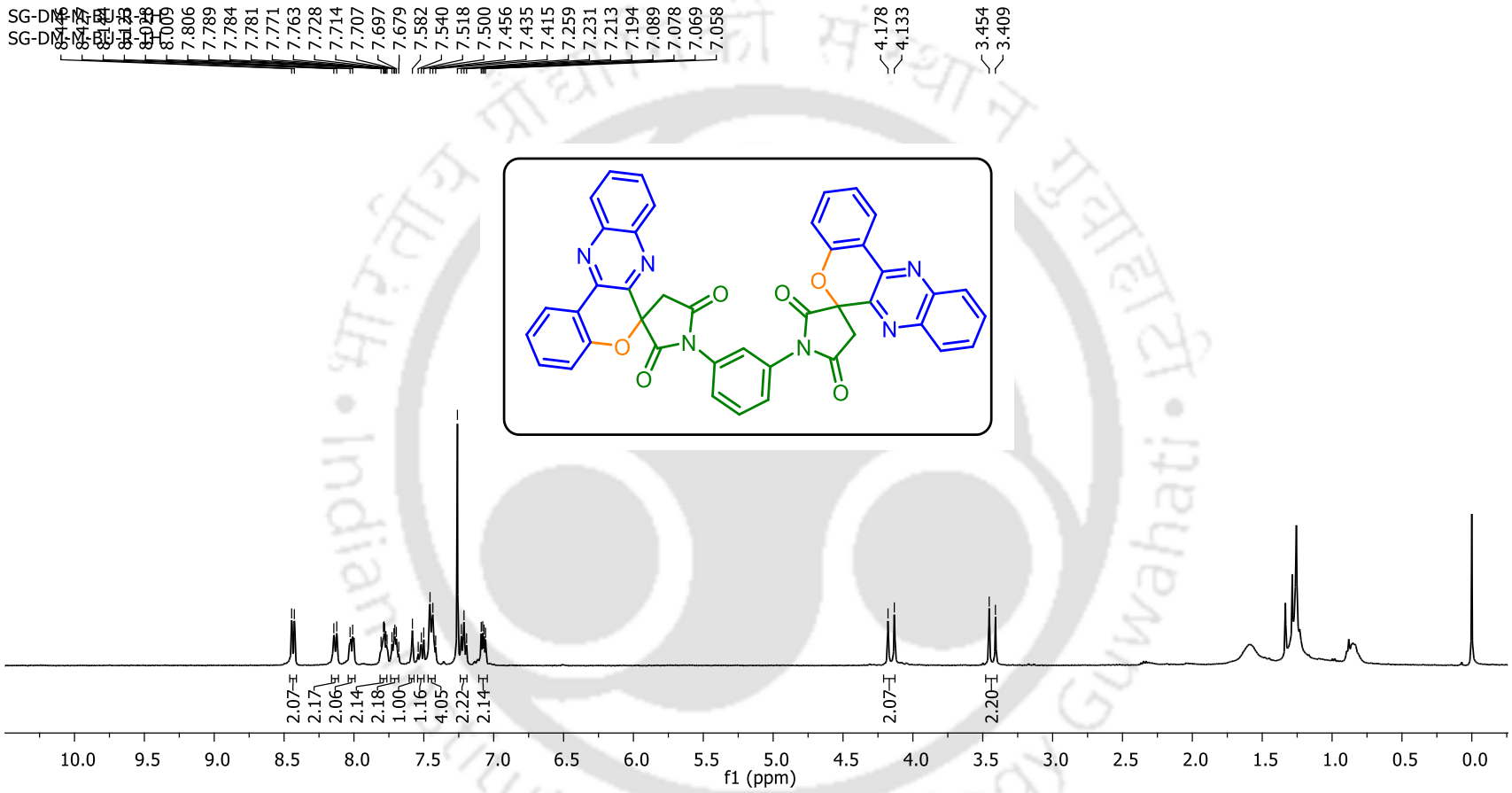

TH-3369_166122017

^{13}C {^{1}H} NMR of **1',1'''-(1,3-Phenylene)bis(spiro[chromeno[3,4-*b*]quinoxaline-6,3'-pyrrolidine]-2',5'-dione)** (**34b**) ($CDCl_3$, 126 MHz)

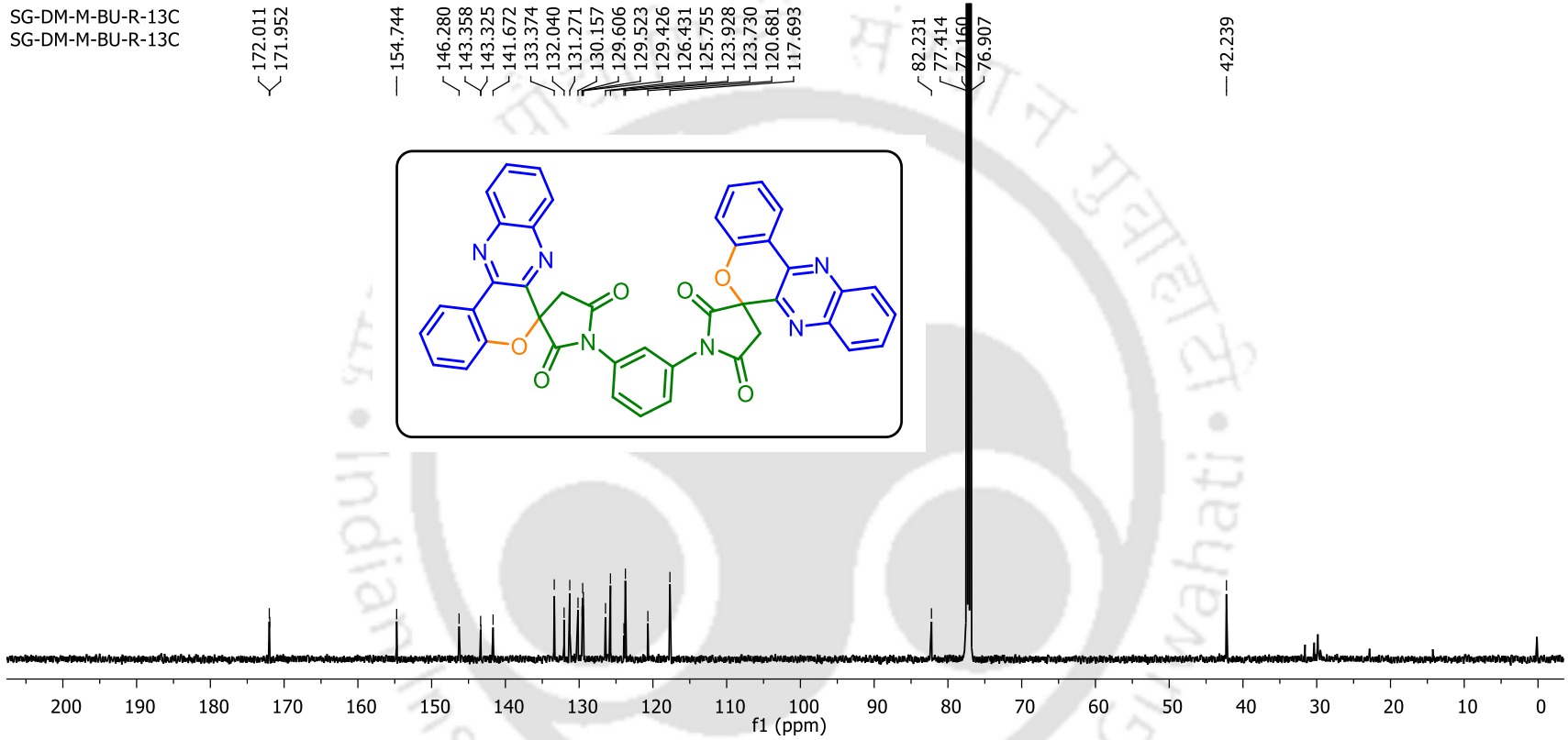

TH-3369_166122017

^{1}H NMR of **1-Fluoro-1'-phenylspiro[chromeno[3,4-*b*]quinoxaline-6,3'-pyrrolidine]-2',5'-dione** (**36b**) ($CDCl_3$, 500 MHz)

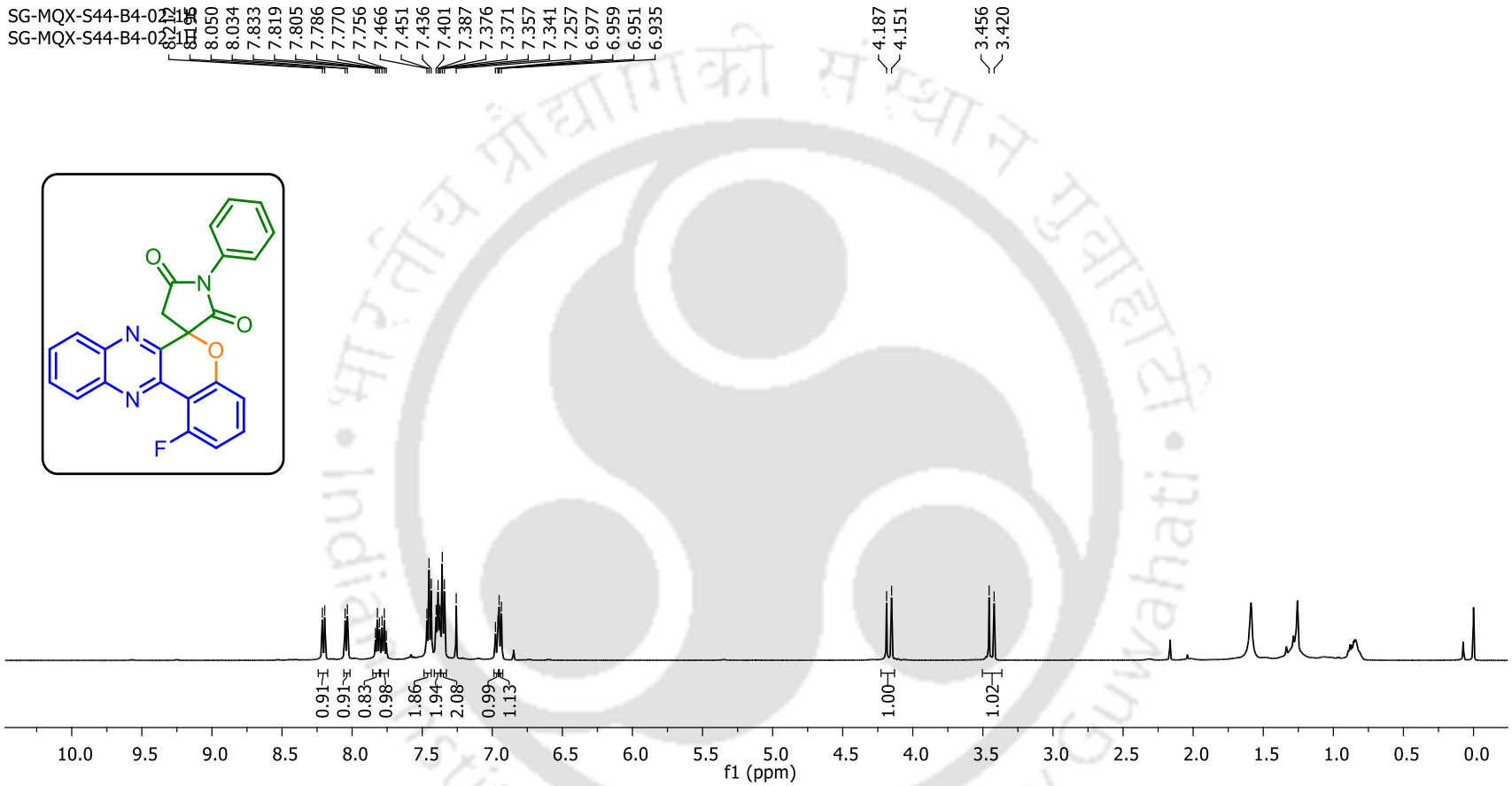

TH-3369_166122017

^{13}C {^{1}H} NMR of **1-Fluoro-1'-phenylspiro[chromeno[3,4-*b*]quinoxaline-6,3'-pyrrolidine]-2',5'-dione** (**36b**) ($CDCl_3$, 126 MHz)

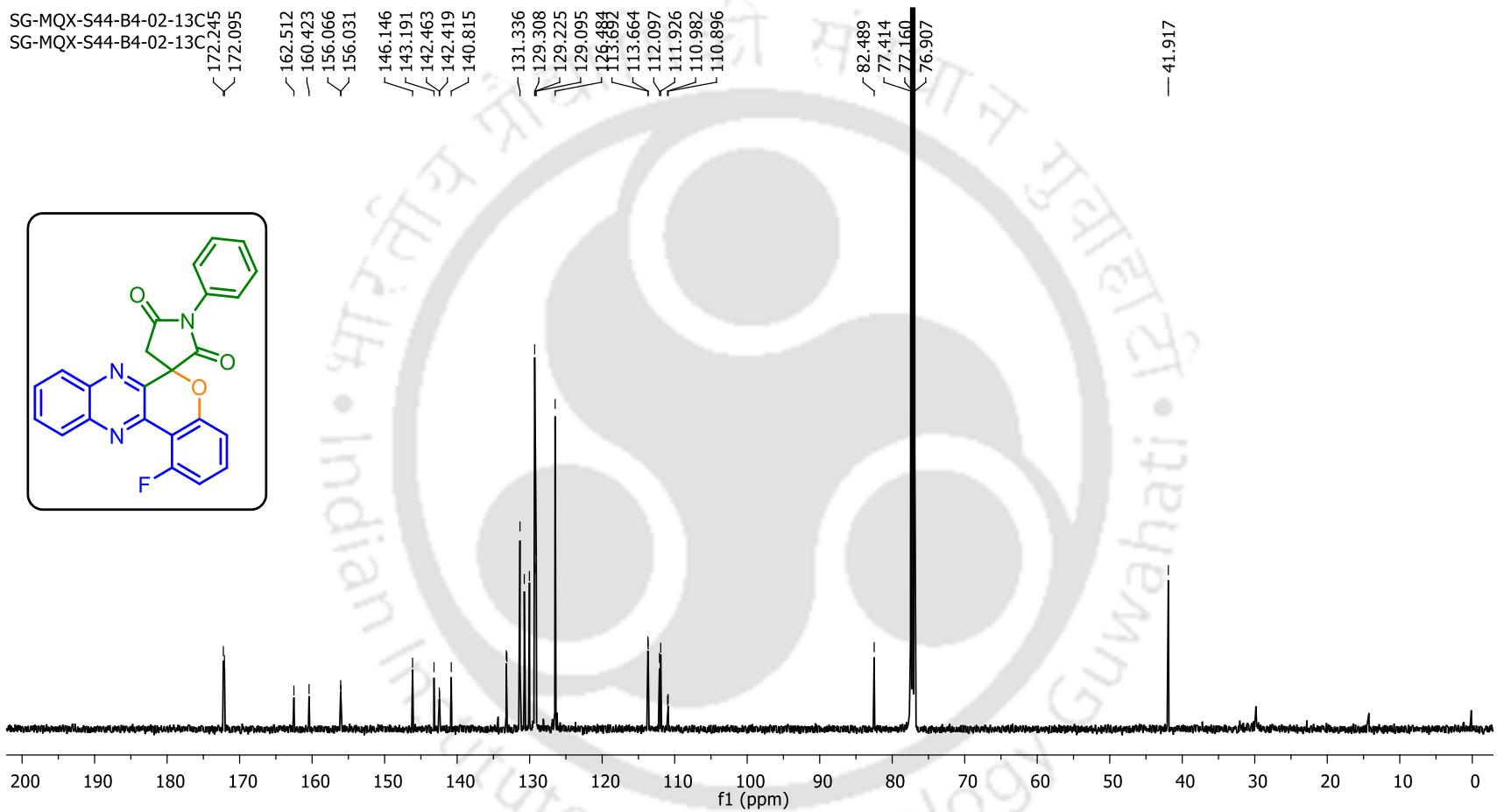

TH-3369_166122017

^{19}F NMR of **1-Fluoro-1'-phenylspiro[chromeno[3,4-*b*]quinoxaline-6,3'-pyrrolidine]-2',5'-dione** (**36b**) ($CDCl_3$)

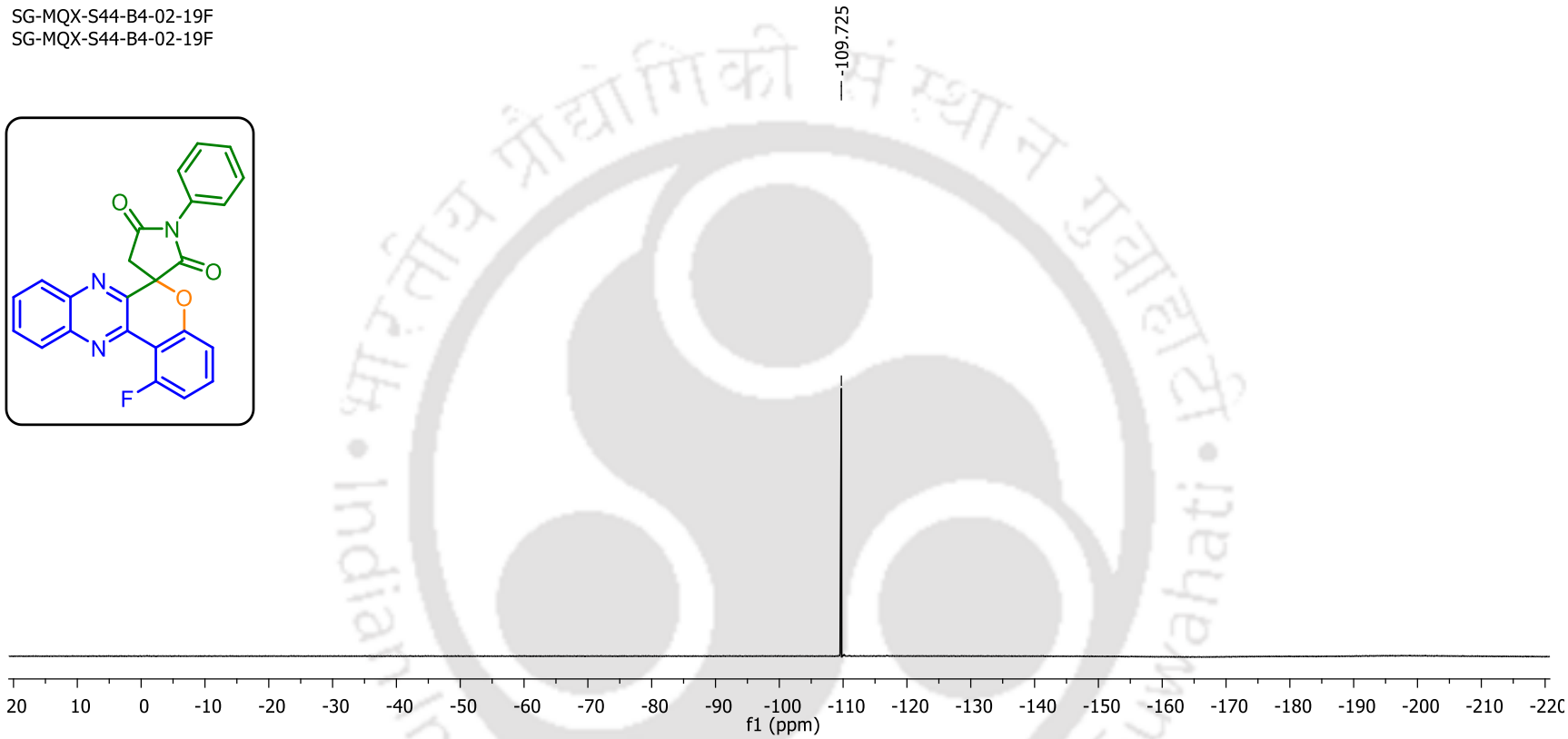

TH-3369_166122017

^{1}H NMR of **1-Chloro-1'-phenylspiro[chromeno[3,4-*b*]quinoxaline-6,3'-pyrrolidine]-2',5'-dione** (**37b**) ($CDCl_3$, 400 MHz)

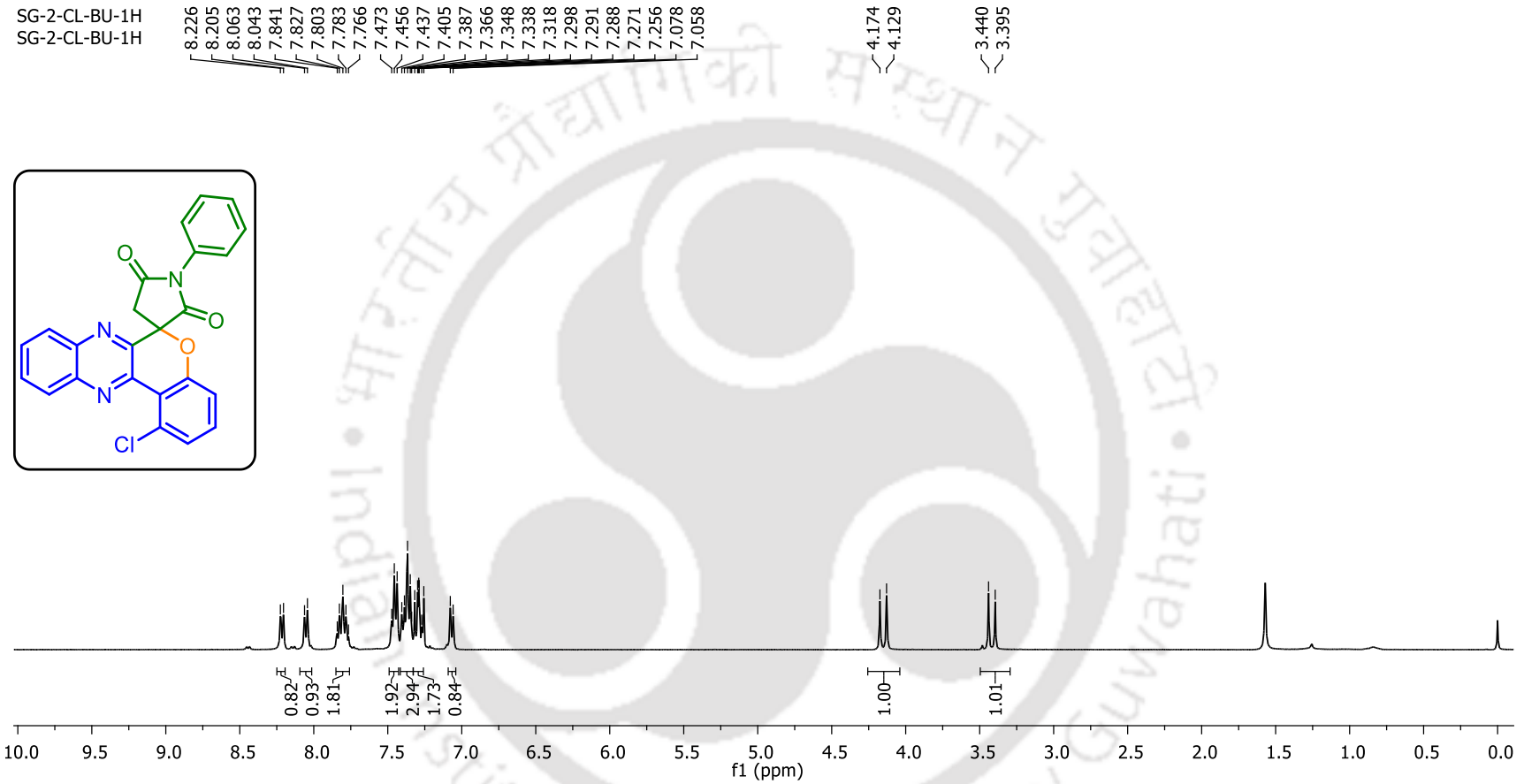

TH-3369_166122017

^{13}C {^{1}H} NMR of **1-Chloro-1'-phenylspiro[chromeno[3,4-*b*]quinoxaline-6,3'-pyrrolidine]-2',5'-dione** (**37b**) ($CDCl_3$, 126 MHz)

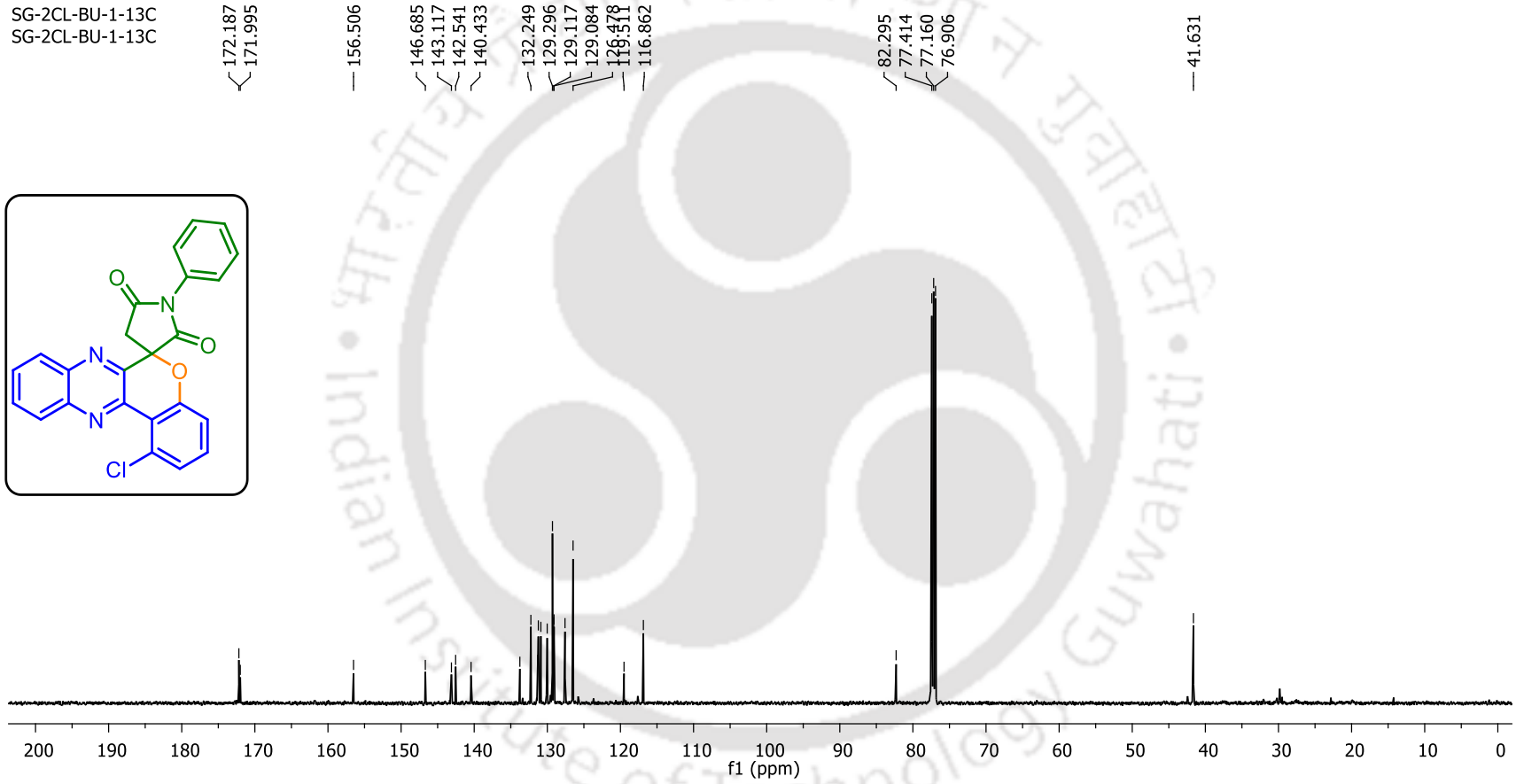

TH-3369_166122017

^{1}H NMR of **1-Bromo-1'-phenylspiro[chromeno[3,4-*b*]quinoxaline-6,3'-pyrrolidine]-2',5'-dione** (**11b**) ($CDCl_3$, 500 MHz)

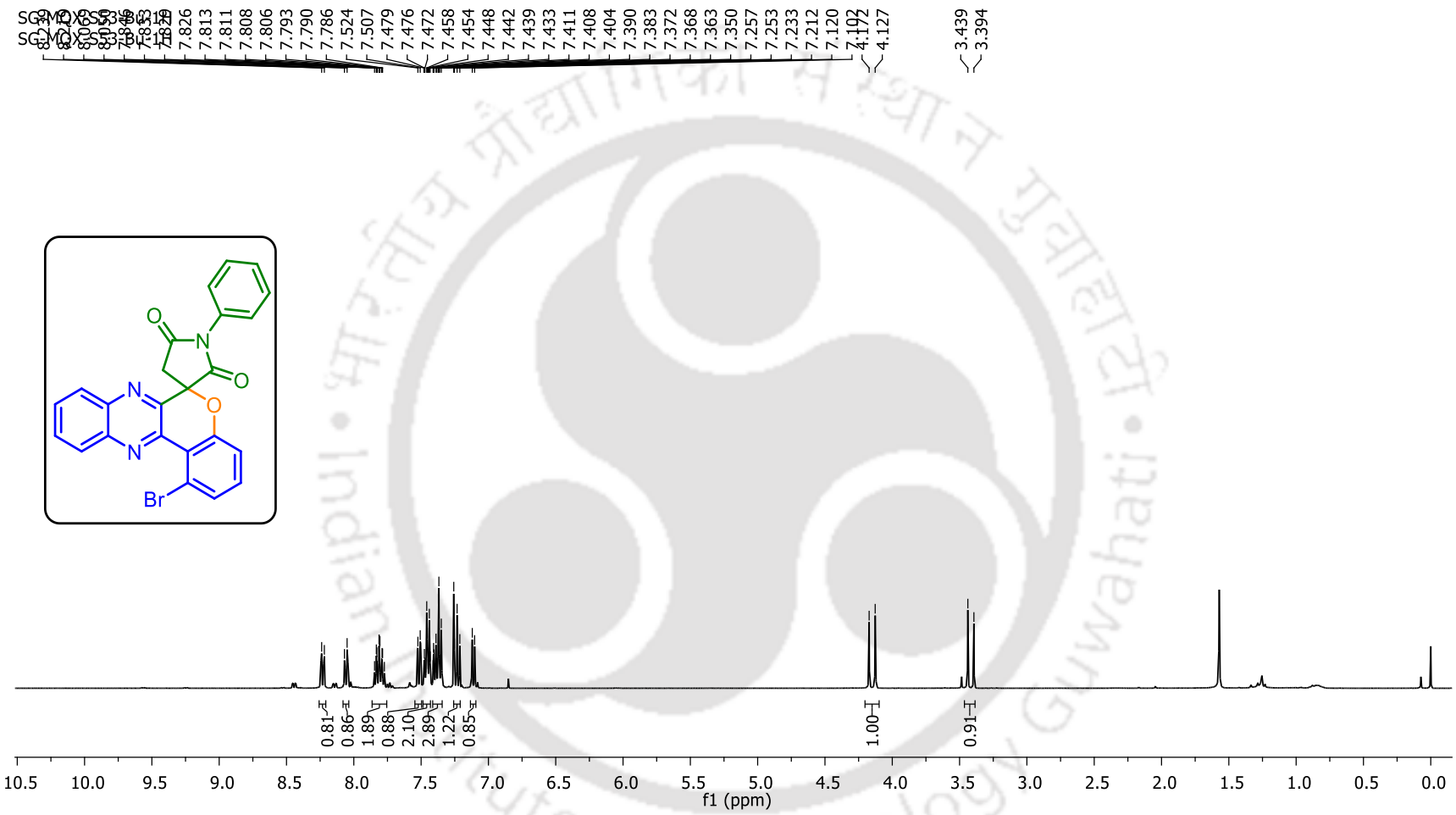

TH-3369_166122017

^{13}C {^{1}H} NMR of **1-Bromo-1'-phenylspiro[chromeno[3,4-*b*]quinoxaline-6,3'-pyrrolidine]-2',5'-dione** (**11b**) ($CDCl_3$, 126 MHz)

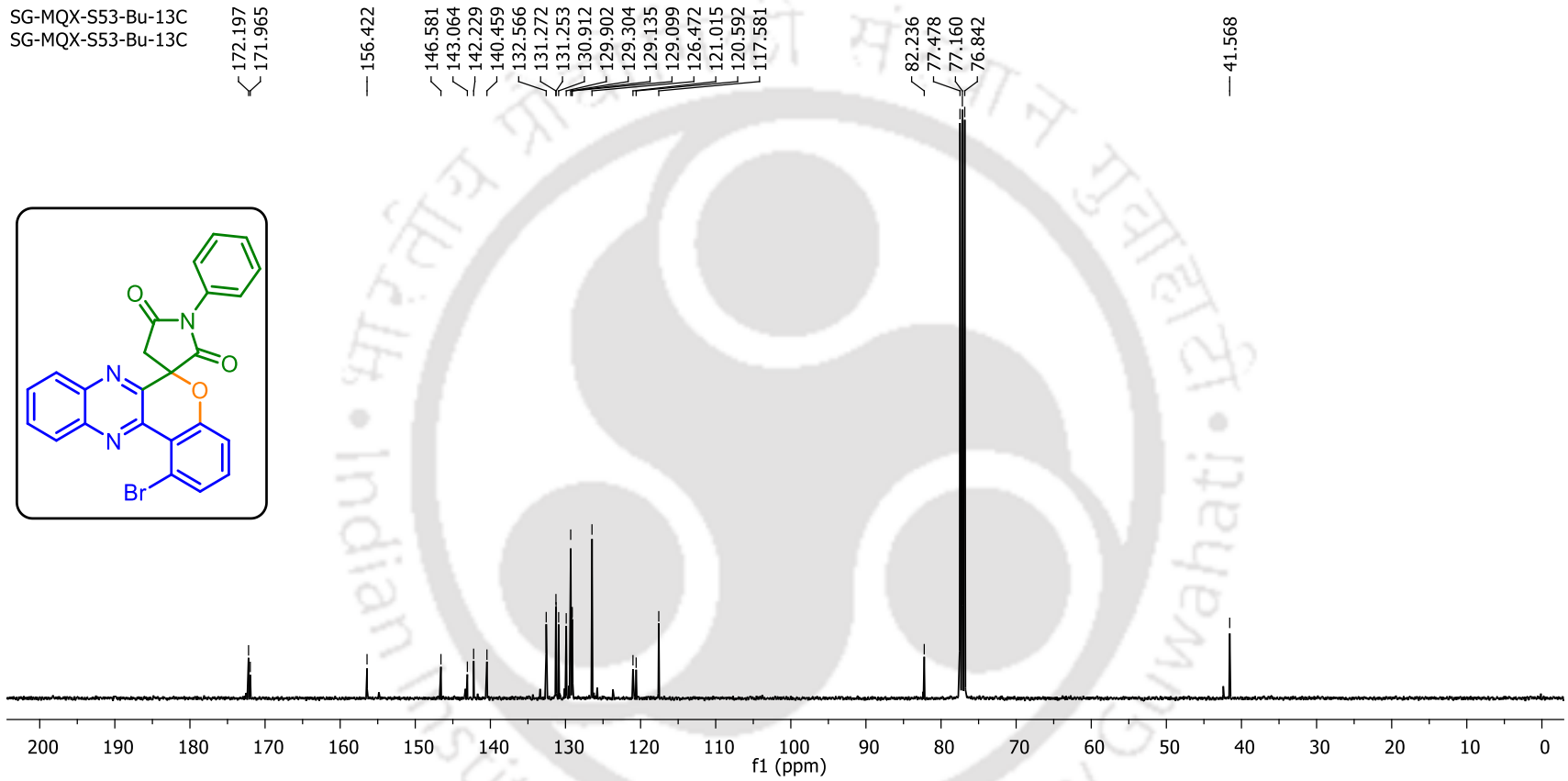

TH-3369_166122017

^{1}H NMR of **1'-(Prop-2-yn-1-yl)spiro[chromeno[3,4-*b*]quinoxaline-6,3'-pyrrolidine]-2',5'-dione (26bb)** ($CDCl_3$, 500 MHz)

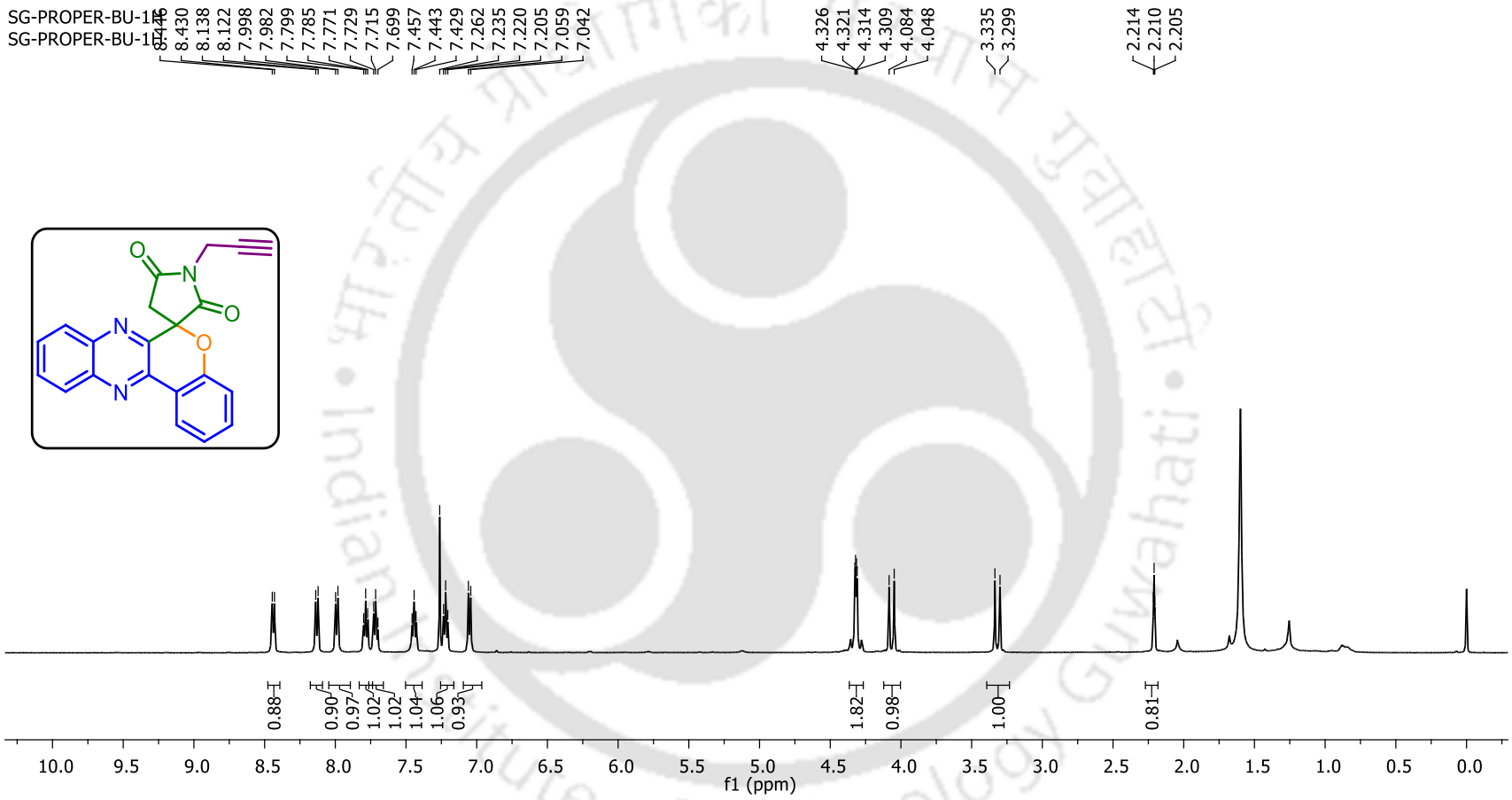

^{13}C {^{1}H} NMR of **1'-(Prop-2-yn-1-yl)spiro[chromeno[3,4-*b*]quinoxaline-6,3'-pyrrolidine]-2',5'-dione** (**26bb**) ($CDCl_3$, 126 MHz)

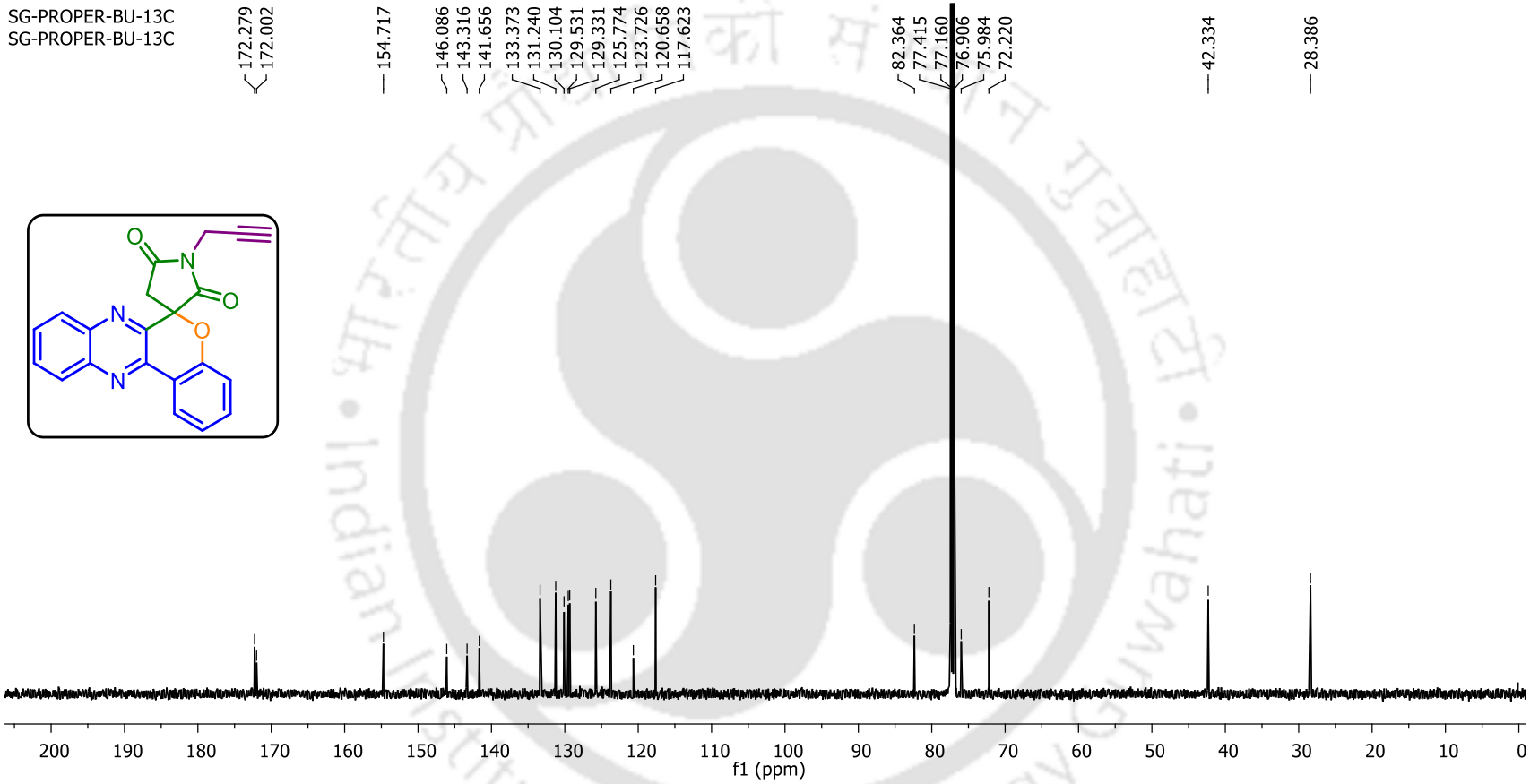

TH-3369_166122017

^{1}H NMR of **2',5'-Dioxo-1',11,12-triphenyl-4-oxa-6,10b-diazaspiro[benzo[*pqr*]tetraphene-5,3'-pyrrolidin]-1(12a),2,3a,5a,5a^{1}(10b),6a,8,10,11-nonaen-10b-ium** (**1bc**) ($CDCl_3$, 500 MHz)

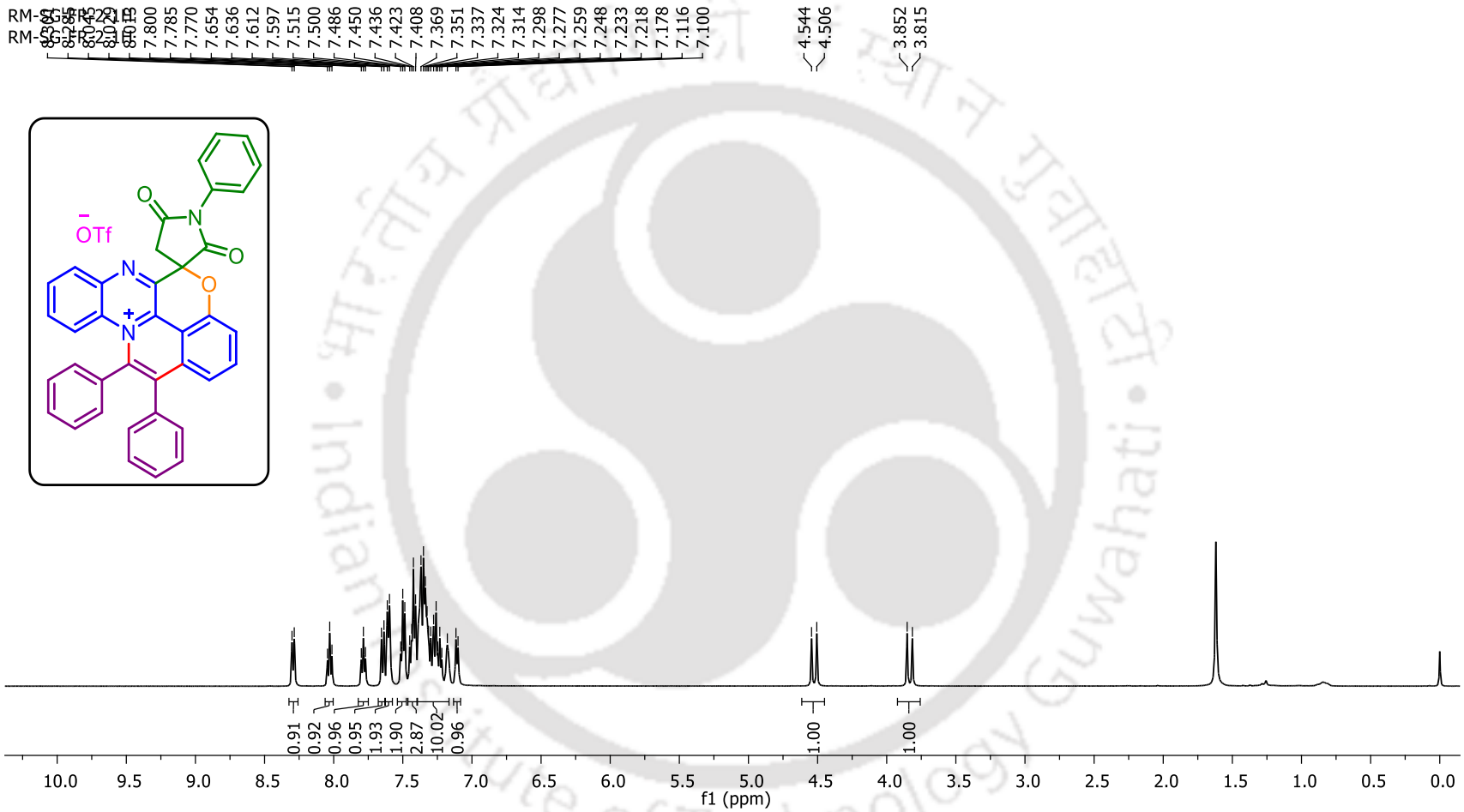

TH-3369_166122017

^{13}C {^{1}H} NMR of **2',5''-Dioxo-1',11,12-triphenyl-4-oxa-6,10b-diazaspiro[benzo[*pqr*]tetraphene-5,3''-pyrrolidin]-1(12a),2,3a,5a,5a^{1}(10b),6a,8,10,11-nonaen-10b-ium** (**1bc**) ($CDCl_3$, 126 MHz)

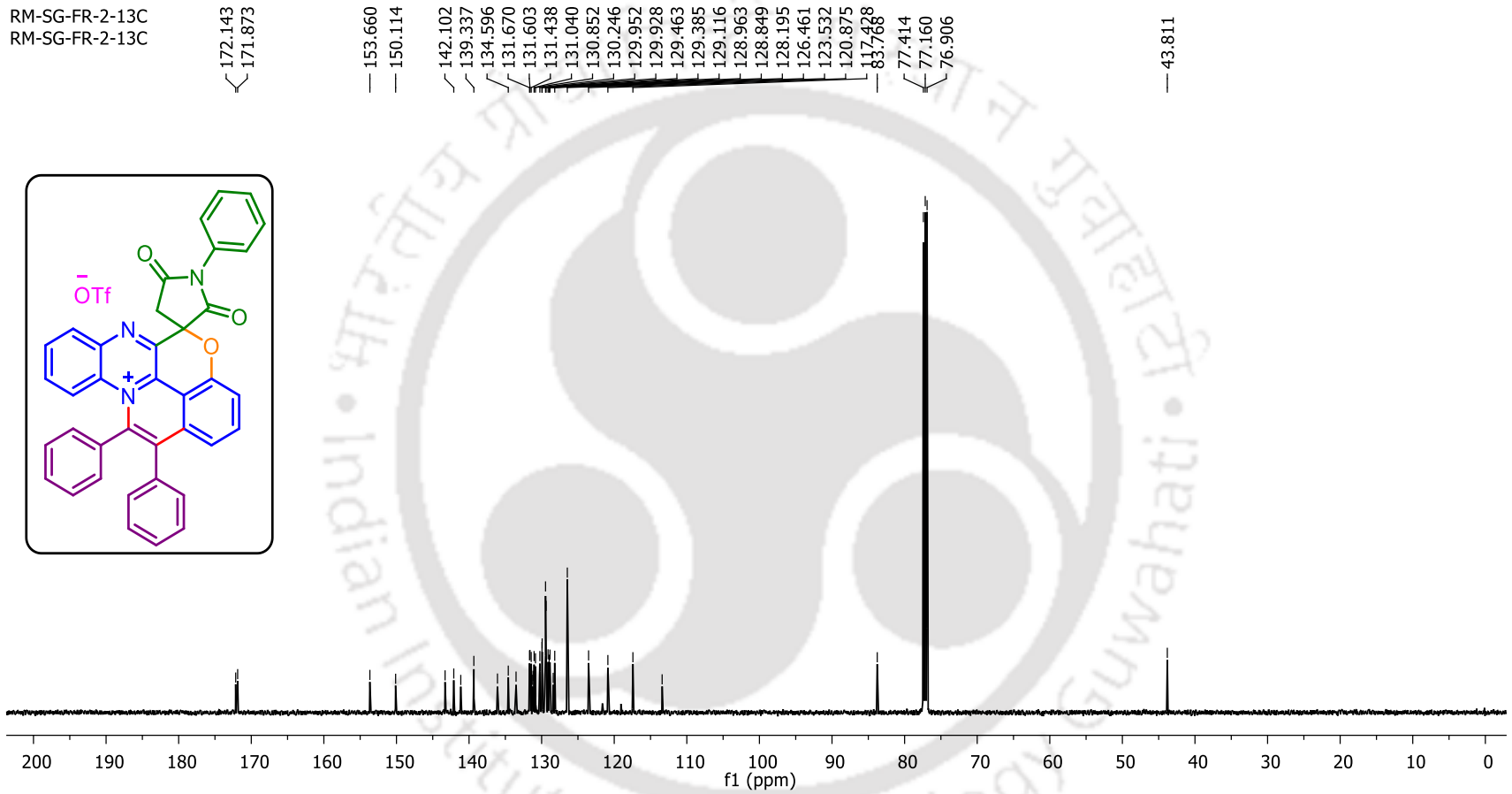

^{19}F NMR of **2',5'-Dioxo-1',11,12-triphenyl-4-oxa-6,10b-diazaspiro[benzo[*pqr*]tetraphene-5,3'-pyrrolidin]-1(12a),2,3a,5a,5a^{1}(10b),6a,8,10,11-nonaen-10b-ium** (**1bc**) ($CDCl_3$)

TH-3369_166122017

^{1}H NMR of **2-Bromo-1'-phenylspiro[chromeno[3,4-*b*]quinoxaline-6,3'-pyrrolidine]-2',5'-dione** (**1bd**) ($CDCl_3$, 500 MHz)

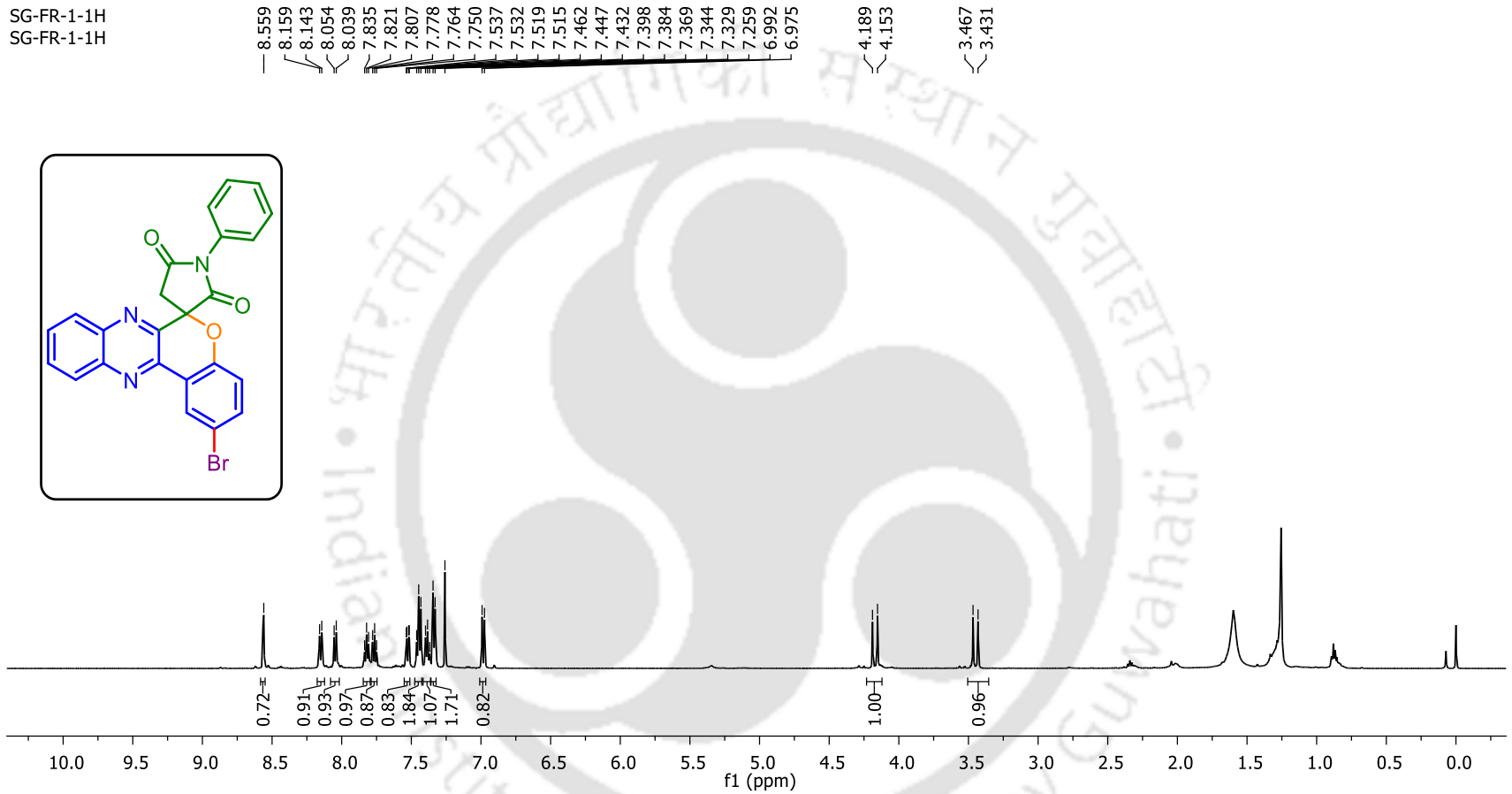

TH-3369_166122017

^{13}C {^{1}H} NMR of **2-Bromo-1'-phenylspiro[chromeno[3,4-*b*]quinoxaline-6,3'-pyrrolidine]-2',5'-dione** (**1bd**) ($CDCl_3$, 126 MHz)

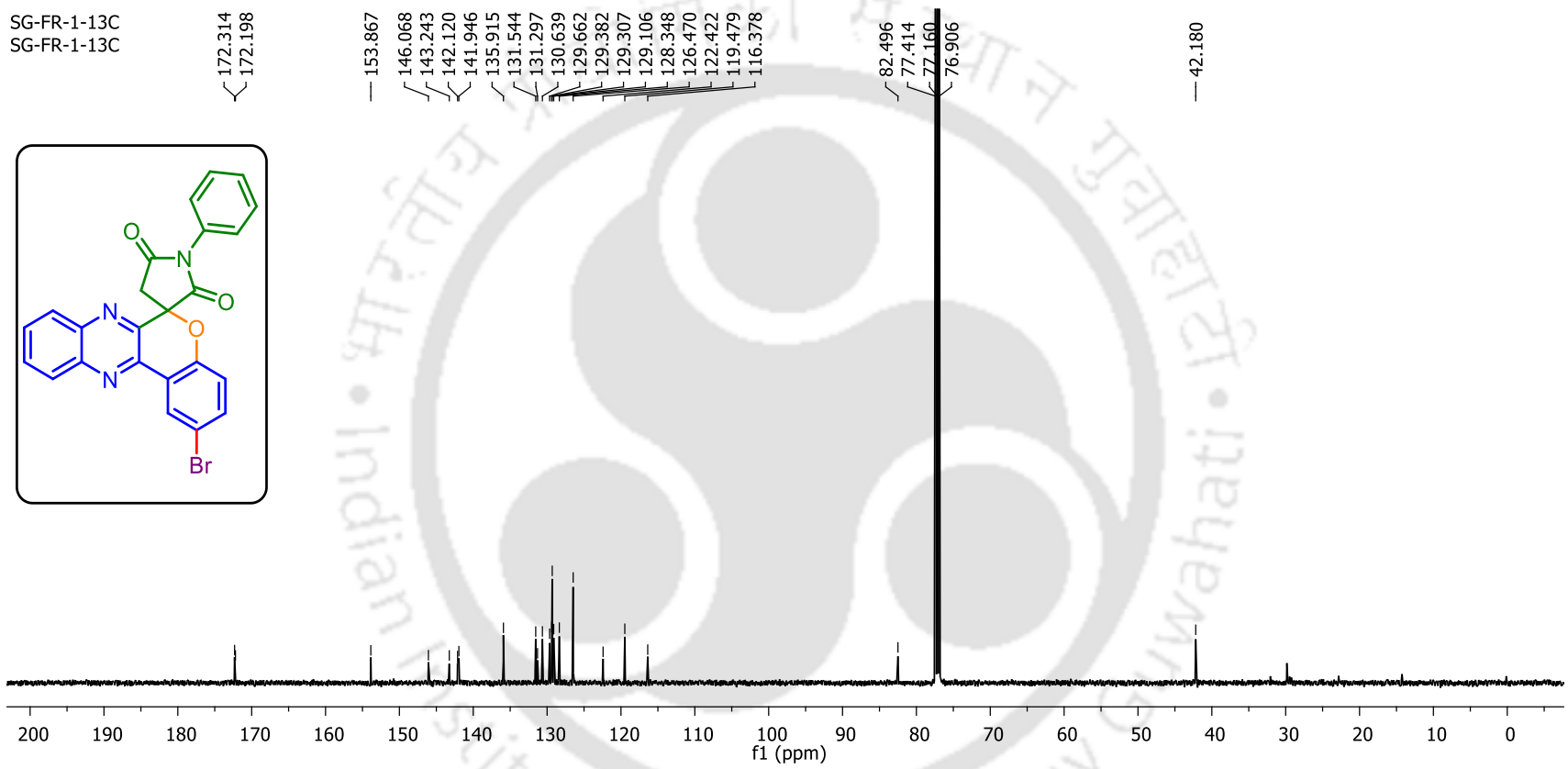

TH-3369_166122017

NEW FINDINGS and FUTURE PERSPECTIVE OF THESIS (UNDERGOING)

PART-I: Preferential Bis-alkenylation and [2+2+2] Annulation of Quinoxaline with Alkyne: A Substrate-Controlled Dual C-H Activation

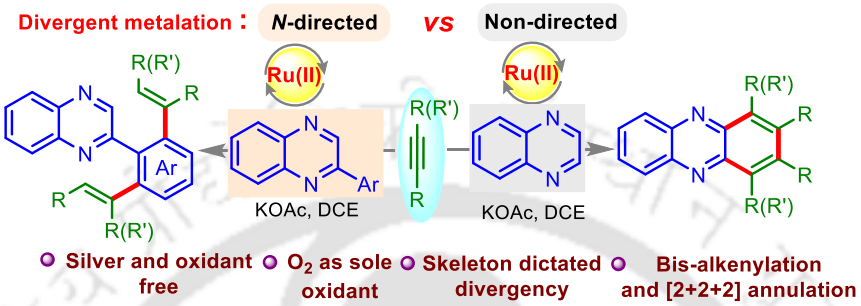

This section demonstrates a Ru(II) catalyzed substrate-controlled divergent access of bis-ortho alkenylation and [2+2+2] annulation of diversely substituted quinoxalines with various symmetrical and unsymmetrical internal alkynes to afford a library of bis-alkenylated and annulated extended quinoxalines. Herein, for 2-aryl quinoxaline system, the N-directed ruthenation was observed whereas for non-arylated quinoxalines, a non-directed ruthenation facilitates the annulation reaction under an identical set of conditions. Furthermore, the detailed mechanistic studies for fruitful implantation of the mechanism are currently undergoing.

PART-II: Intramolecular EnT Dictated Divergent Access of Oxidative Olefin Cleavage/Intramolecular Cyclization of Photochromic Bis-alkenylated Quinoxaline

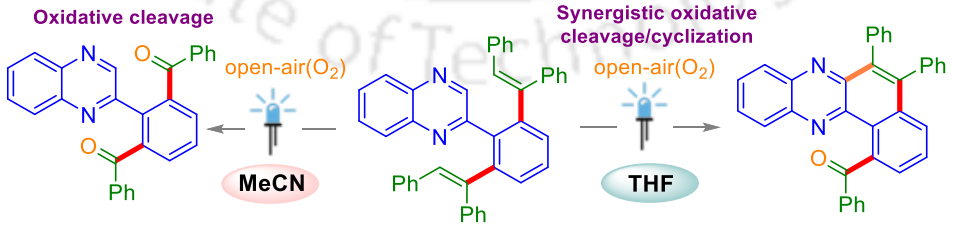

This section portrays a bis-alkenylated quinoxaline possess an intramolecular n-π^* charge-transfer mediated triplet energy transfer to facilitate the intramolecular oxidative cleavage and cyclization process of the appended olefins. Further, a set of control reactions along with derivations are currently being pursued.

TH-3369_166122017

Concluding Remarks

(***contribution towards synthetic community***)

❖ **Chapter IA** gives a concise overview of Transition-metal catalyzed C–H functionalization and oxidative annulation (cyclization). Whereas **Chapter IB** depicts the different photo-induced C–H functionalization and cyclization techniques. Besides these, in this section, their prior and present advancements are briefly illustrated.

❖ **Chapter II** demonstrates Ru(II)-catalyzed regioselective C–H/N oxidative annulation of 2-arylquinoxalines with internal alkynes. In this chapter, the synthesized quaternary annulated adducts are extensively scrutinized for the detailed photo-physical applications. ***Such donor-π-acceptor type molecules exhibits Aggregation Enhanced Emission (AEE) in DMF/water solvent system***. Apart from this, such annulated adducts possess reversible mechanochromism under external pressure. ***To the best of our knowledge for the first time, such small quaternary salts are utilized for Latent-fingerprint detection (up to 2nd level).*** Furthermore, such luminogens serves as a cellular imaging probes.

❖ **Chapter III** describes a solvent-switched regiodivergent C–H maleimidation on 2-arylimidazopyrdines under Mn(I)-catalysis. This protocol enables the selective C-H alkylation without the involvement of silver or oxidants. Before this work, $Mn(CO)_5Br$ is known for the directed C–H functionalizations. ***In this chapter, for the first time non-directed C–H metalation of $Mn(CO)_5Br$ apart from the directed strategy has been revealed***. This is further recognized by the review article from prof. García group (*ACS Omega* **2022**, *7*, 37008).

❖ **Chapter IV** offers ***the regioselective C–H functionalization at unattained C3–H site of 2-aryl quinoxalines***. ***Herein, the non-directed Mn-catalysis from chapter III enables the challenging C3–H activation over the usual ortho C–H activations***. Besides these, the synthesized C3-maleimidated quinoxalines exhibit PIFA-promoted electron-drifted Spirocyclization at room temperature, where the electrons are drifted from electron-rich

TH-3369_166122017

unperturbed C2-phenyl ring to succinimides. Also in presence of selectfluor, the C3-maleimidated quinoxalines undergoes dehydrogenation of succinimides ring.

❖ **Chapter V** represents a reagent-less photo-induced auto-catalyzed oxygenation at sterically hindered C(sp^3)–H site. ***This photochemical "reagent-less" solvent-dependent hydroxylation at Csp^3–H and spiro-etherification involving $C(sp^3)$–H/$C(sp^2)$–H are unparalleled. Herein, the N–H tautomer of C3-maleimidated quinoxalines acts as a triplet sensitizer and transfers its energy to a triplet oxygen ($^3O_2$) generating reactive singlet oxygen ($^1O_2$) which facilitates oxygenation reactions at the other $C(sp^3)$–H sites within the molecule making it a true auto-sensitized process***. This photo-oxygenation represents an illustration of a tautomer-assisted singlet oxygen uptake.

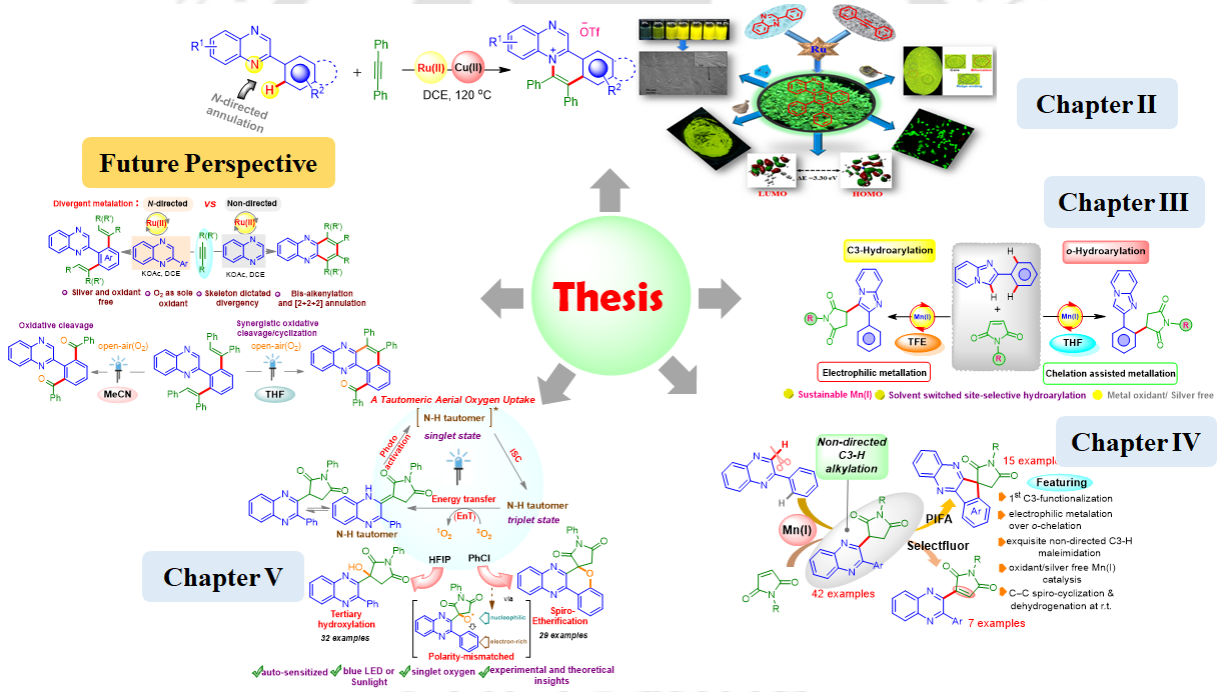

TH-3369_166122017

List of Publications (*Published*)

1. **Ghosh, S.**; Khandelia, T.; Mahadevan, A.; Panigrahi, P.; Kumar, P.; Mandal, R.; Boruah, D.; Venkataramani, S.; Patel, B. K. "Photo-Induced Generation of Oxygenated Quaternary Centers *via* EnT Enabled Singlet O_2 Addition to C3-Maleimidated Quinoxaline: A Reagent-Less Approach." (Under revision in *Chemistry: A European Journal*)

2. **Ghosh, S.**; Khandelia, T.; Panigrahi, P.; Mandal, R.; Patel, B. K. "Mn(I)-Catalyzed Preferential Electrophilic C3-Maleimidation in Quinoxaline Leading to Spirocyclization and Dehydrogenation of Succinimides." *Org. Lett*. **2023**, *25*, 3806. (IF: 5.2) https://doi.org/10.1021/acs.orglett.3c01350

3. **Ghosh, S.;** Khandelia, T.; Patel, B. K. "Solvent-Switched Manganese(I)-Catalyzed Regiodivergent Distal vs Proximal C–H Alkylation of Imidazopyridine with Maleimide." *Org. Lett*. **2021**, *23*, 7370. (IF: 5.2) https://doi.org/10.1021/acs.orglett.1c02536

4. **Ghosh, S.;** Pal, S.; Rajamanickam, S.; Shome, R.; Mohanta, P. R.; Ghosh, S. S.; Patel, B. K. "Access to Multifunctional AEEgens *via* Ru(II)-Catalyzed Quinoxaline-Directed Oxidative Annulation." *ACS Omega*. **2019**, *4*, 5565. (IF: 4.1) https://doi.org/10.1021/acsomega.9b00274

5. Khandelia, T.; **Ghosh, S.;** Panigrahi, P.; Mandal, R.; Boruah, D.; Patel, B. K. "Photo-Induced 1,2-Thiohydroxylation of Maleimide Involving Disulfide and Singlet Oxygen." *Chem. Commun*. **2023**, *59*, 11196. (IF: 4.9) https://doi.org/10.1039/D3CC03296E

6. Panigrahi, P.; **Ghosh, S.**; Khandelia, T.; Mandal, R.; Patel, B. K. "Isoxazole as Nitrile Synthon: En Routes to ortho-Alkenylated Isoxazole and Benzonitrile with Allyl Sulfone Catalyzed by Ru(II)." *Chem. Commun*. **2023**, *59*, 10536. (IF: 4.9) https://doi.org/10.1039/D3CC02996D

7. Khandelia, T.; **Ghosh, S.;** Patel, B. K. "Dearomative Bis-functionalization of Quinoxalines and Bis-*N*-arylation of (Benz) Imidazoles *via* Cu (II) Mediated Addition of Boronic Acids." *Chem. Commun*. **2023**, *59*, 2118. (IF: 4.9) https://doi.org/10.1039/D2CC06399A

8. Mandal, R.; **Ghosh, S.;** Khandelia, T.; Panigrahi, P.; Patel, B. K. "Base-Induced Decarboxylative 1,1-Alkoxy Thiolation and Hydrothiolation of Vinylene Carbonate."*J. Org. Chem*. **2023**, *88*, 16655. (IF: 3.6) https://doi.org/10.1021/acs.joc.3c02036

9. Khandelia, T.; **Ghosh, S.;** Panigrahi, P.; Shome, R.; Ghosh, S. S.; Patel, B. K. "Copper(I)-Mediated Cascade Annulation via Dual C–H/C–H Activation: Access to Benzo[*a*]carbazolic AEEgens." *J. Org. Chem*. **2021**, *86*, 16948. (IF: 3.6) https://doi.org/10.1021/acs.joc.1c02109

10. Rajamanickam, S.; Sah, C.; Mir, B. A.; **Ghosh, S.;** Sethi, G.; Yadav, V.; Venkataramani, S.; Patel, B. K. "Bu_4NI-Catalyzed, Radical-Induced Regioselective *N*-Alkylations and Arylations of Tetrazoles Using Organic Peroxides/Peresters." *J. Org. Chem*. **2020**, *85*, 2118. (IF: 3.6) https://doi.org/10.1021/acs.joc.9b02875

11. Mandal, A.; **Ghosh, S.;** Nath, B.; Patel, B. K. "Role of Non-Covalent Interactions to Dictate Chiral Selective Self-assembly in Ni (II), Cu (II) and Cd (II) Complexes of a Racemic 1, 2-

TH-3369_166122017

Dihydroquinazolinone Ligand." *Inorg. Chim. Acta.* **2020**, *503*, 119399. (IF:2.8) https://doi.org/10.1016/j.ica.2019.119399

12. Rakshit, A.; Sau, P.; **Ghosh, S.;** Patel, B. K. "One-Pot Sequential Synthesis of Fused Isoquinolines via Intramolecular Cyclization/Annulation and their Photophysical Investigation." *Adv. Synth. Catal.* **2019**, *361*, 3824. (IF: 5.4) https://doi.org/10.1002/adsc.201900543

List of Publications (*Submitted/Under preparation*)

1. **Ghosh, S.**; Patel, B. K. "Co(III)-Catalyzed Oxidative C–H/C–H Annulation Leading to Maleimide-fused Imidazopyridine AEEgen." (Under manuscript preparation)
2. Panigrahi, P.; **Ghosh, S.**; Khandelia, T.; Tripathy, G.; Mandal, R.; Patel, B. K. "Harnessing Reductive BF_2-Complexation *via* Ru(II)-Catalyzed N–O Cleavage of Isoxazoles." (Submitted)

Conferences

1. *Poster presentation* at **CRSI Symposium**, IIT Guwahati during March 25-27, **2022**.
2. *Oral presentation* at **XVII JNOST**, University of Hyderabad during January 6-9, **2022**.
3. *Poster presentation* at **ICCHD**, Heritage Institute of Technology Kolkata during January 9-11, **2020**.
4. *Poster presentation* at **ICANN**, IIT Guwahati during December 18-21, **2019**.

TH-3369_166122017

For *Figure IA.1.1.1*

ACS Publications
Most Trusted. Most Cited. Most Read.

Organocatalysis in Inert C–H Bond Functionalization

Author: Yan Qin, Lihui Zhu, Sanzhong Luo
Publication: Chemical Reviews
Publisher: American Chemical Society
Date: Jul 1, 2017

Copyright © 2017, American Chemical Society

PERMISSION/LICENSE IS GRANTED FOR YOUR ORDER AT NO CHARGE

This type of permission/license, instead of the standard Terms and Conditions, is sent to you because no fee is being charged for your order. Please note the following:

- Permission is granted for your request in both print and electronic formats, and translations.
- If figures and/or tables were requested, they may be adapted or used in part.
- Please print this page for your records and send a copy of it to your publisher/graduate school.
- Appropriate credit for the requested material should be given as follows: "Reprinted (adapted) with permission from {COMPLETE REFERENCE CITATION}. Copyright {YEAR} American Chemical Society." Insert appropriate information in place of the capitalized words.
- One-time permission is granted only for the use specified in your RightsLink request. No additional uses are granted (such as derivative works or other editions). For any uses, please submit a new request.

If credit is given to another source for the material you requested from RightsLink, permission must be obtained from that source.

For *Figure IA.1.1.2*

ACS Publications
Most Trusted. Most Cited. Most Read.

Bidentate Directing Groups: An Efficient Tool in C–H Bond Functionalization Chemistry for the Expedient Construction of C–C Bonds

Author: Supriya Rej, Yusuke Ano, Naoto Chatani
Publication: Chemical Reviews
Publisher: American Chemical Society
Date: Feb 1, 2020

Copyright © 2020, American Chemical Society

PERMISSION/LICENSE IS GRANTED FOR YOUR ORDER AT NO CHARGE

This type of permission/license, instead of the standard Terms and Conditions, is sent to you because no fee is being charged for your order. Please note the following:

- Permission is granted for your request in both print and electronic formats, and translations.
- If figures and/or tables were requested, they may be adapted or used in part.
- Please print this page for your records and send a copy of it to your publisher/graduate school.
- Appropriate credit for the requested material should be given as follows: "Reprinted (adapted) with permission from {COMPLETE REFERENCE CITATION}. Copyright {YEAR} American Chemical Society." Insert appropriate information in place of the capitalized words.
- One-time permission is granted only for the use specified in your RightsLink request. No additional uses are granted (such as derivative works or other editions). For any uses, please submit a new request.

If credit is given to another source for the material you requested from RightsLink, permission must be obtained from that source.

For *Figure IB.2.1*

ACS Publications
Most Trusted. Most Cited. Most Read.

Photoredox-Catalyzed C–H Functionalization Reactions

Author: Natalie Holmberg-Douglas, David A. Nicewicz
Publication: Chemical Reviews
Publisher: American Chemical Society
Date: Jan 1, 2022

Copyright © 2022, American Chemical Society

PERMISSION/LICENSE IS GRANTED FOR YOUR ORDER AT NO CHARGE

This type of permission/license, instead of the standard Terms and Conditions, is sent to you because no fee is being charged for your order. Please note the following:

- Permission is granted for your request in both print and electronic formats, and translations.
- If figures and/or tables were requested, they may be adapted or used in part.
- Please print this page for your records and send a copy of it to your publisher/graduate school.
- Appropriate credit for the requested material should be given as follows: "Reprinted (adapted) with permission from {COMPLETE REFERENCE CITATION}. Copyright {YEAR} American Chemical Society." Insert appropriate information in place of the capitalized words.
- One-time permission is granted only for the use specified in your RightsLink request. No additional uses are granted (such as derivative works or other editions). For any uses, please submit a new request.

If credit is given to another source for the material you requested from RightsLink, permission must be obtained from that source.

TH-3369_166122017

For *Figure IB.2.4 and IB.2.6*

1. Chemical Society reviews

Billing Status: Open

Article: Energy transfer photocatalysis: exciting modes of reactivity

Order License ID	1445513-1	**Type of Use**	Republish in a thesis/dissertation
Order detail status	Completed		
ISSN	0306-0012	**Publisher**	ROYAL SOCIETY OF CHEMISTRY, ETC.]
		Portion	Chart/graph/table/figure

0.00 USD
Republication Permission

LICENSED CONTENT

Publication Title	Chemical Society reviews	**Language**	English
Article Title	Energy transfer photocatalysis: exciting modes of reactivity	**Country**	United Kingdom of Great Britain and Northern Ireland
		Rightsholder	Royal Society of Chemistry
Author/Editor	CHEMICAL SOCIETY (GREAT BRITAIN)	**Publication Type**	Journal
Date	01/01/1972		

REQUEST DETAILS

Portion Type	Chart/graph/table/figure	**Distribution**	Worldwide
Number of Charts / Graphs / Tables / Figures Requested	2	**Translation**	Original language of publication
Format (select all that apply)	Print, Electronic	**Copies for the Disabled?**	No
		Minor Editing Privileges?	No
Who Will Republish the Content?	Not-for-profit entity	**Incidental Promotional Use?**	No
		Currency	USD
Duration of Use	Life of current edition		
Lifetime Unit Quantity	Up to 499		
Rights Requested	Main product		

NEW WORK DETAILS

Title	Thermal(Photo) Induced Selective C□H Bond Functionalization/Oxidative Cyclization in Di-Nitrogen Benzenoid Heterocycles	**Institution Name**	IIT Guwahati
		Expected Presentation Date	2024-02-05
Instructor Name	Bhisma K. Patel		

TH-3369_166122017

For *Figure IB.2.5*

1. Chemical Society reviews

Billing Status: Open

Article: Energy transfer catalysis mediated by visible light: principles, applications, directions.

Order License ID	1445515-1	**Type of Use**	Republish in a thesis/dissertation
Order detail status	Completed		
ISSN	0306-0012	**Publisher**	ROYAL SOCIETY OF CHEMISTRY, ETC.]
		Portion	Chart/graph/table/figure

0.00 USD
Republication Permission

LICENSED CONTENT

Publication Title	Chemical Society reviews	**Rightsholder**	Royal Society of Chemistry
Article Title	Energy transfer catalysis mediated by visible light: principles, applications, directions.	**Publication Type**	Journal
		Start Page	7190
		End Page	7202
Author/Editor	CHEMICAL SOCIETY (GREAT BRITAIN)	**Issue**	19
		Volume	47
Date	01/01/1972		
Language	English		
Country	United Kingdom of Great Britain and Northern Ireland		

REQUEST DETAILS

Portion Type	Chart/graph/table/figure	**Distribution**	Worldwide
Number of Charts / Graphs / Tables / Figures Requested	1	**Translation**	Original language of publication
Format (select all that apply)	Print, Electronic	**Copies for the Disabled?**	No
		Minor Editing Privileges?	No
Who Will Republish the Content?	Not-for-profit entity	**Incidental Promotional Use?**	No
		Currency	USD
Duration of Use	Life of current edition		
Lifetime Unit Quantity	Up to 499		
Rights Requested	Main product		

TH-3369_166122017